Schriftenreihe Baustoffe und Massivbau
Structural Materials and Engineering Series

Heft 3
No. 3

Ultra High Performance Concrete (UHPC)

Proceedings of the

International Symposium on
Ultra High Performance Concrete

Kassel, Germany
September 13-15, 2004

Series Editors

Prof. Dr.-Ing. habil. M. Schmidt
Universität Kassel
Fachbereich Bauingenieurwesen
Fachgebiet Werkstoffe des Bauwesens
Mönchebergstr. 7
34125 Kassel
Tel. +49 (561) 804 2601
Fax. +49 (561) 804 2662
baustk@uni-kassel.de
www.uni-kassel.de/fb14/baustoffkunde

Prof. Dr.-Ing. E. Fehling
Universität Kassel
Fachbereich Bauingenieurwesen
Fachgebiet Massivbau
Kurt-Wolter-Str. 3
34125 Kassel
Tel. +49 (561) 804 2656
Fax. +49 (561) 804 2803
bauing.massivbau@uni-kassel.de
www.uni-kassel.de/fb14/massivbau

Editor

Dipl.-Ing. Carsten Geisenhanslüke
Universität Kassel
Fachbereich Bauingenieurwesen
Fachgebiet Werkstoffe des Bauwesens
Mönchebergstr. 7
34125 Kassel
Tel. +49 (561) 804 2601
Fax. +49 (561) 804 2662
ghlueke@uni-kassel.de
www.uni-kassel.de/fb14/baustoffkunde

Preface

Ultra High Performance Concrete (UHPC) with a high compressive strength of more than 200 MPa and an improved durability marks a quantum leap in concrete technology. This high performance material offers a variety of interesting applications. It allows the construction of sustainable and economic buildings with an extraordinary slim design. Its high strength and ductility makes it the ultimate building material e.g. for bridge decks, storage halls, thin-wall shell structures and highly loaded columns.

Beside its improved strength properties, its outstanding resistance against all kinds of corrosion is an additional milestone on the way towards no-maintenance constructions.

UHPC has very special properties that are remarkably different to the properties of normal and high performance concrete. For complete utilisation of UHPC's superior properties, special knowledge is required for production, construction and design.

Worldwide this material is under detailed exploration. Several constructions or structural elements were already built utilizing UHPC. However, one of the first hybrid bridges consisting of precast UHPC elements and a steel construction will be built in Kassel in 2004. The bridge is designed as a foot and bike bridge with a total length of 150 m.

More than 75 experts from all over the world presented their research results and practical experiences with the new and outstanding material at the

International Symposium on Ultra High Performance Concrete

which took place in September 13 to 15, 2004. The symposium was organized by the Departments of Structural Materials and of Structural Engineering of the University of Kassel, Germany.

The experts gave a broad overview and a deep insight into all aspects of UHPC including raw materials, micro- and macro-structures, mechanical behaviour, durability as well as of construction and design specifications appropriate for this material.

The Conference Proceedings contain the conference papers and presentations. We hope that the conference and the excellent papers will promote further develop and exploitation of Ultra High Performance Concrete – the construction material of choice of the 21st century.

Kassel, September 2004

Prof. Dr.-Ing. habil. Michael Schmidt   Prof. Dr.-Ing. Ekkehard Fehling

Contents

Scientific Committee

Chairman

> **Prof. Michael Schmidt,**
> University of Kassel, D (chairman)

Vice-Chairmen

> **Prof. Ekkehard Fehling,**
> University of Kassel, D (vice-chairman)
> **Prof. Joost C. Walraven,**
> Delft University of Technology, NL (vice-chairman)

Members

> **Prof. Paul Acker,**
> Lafarge Company, F
> **Prof. Peter Bartos,**
> University of Paisley, GB
> **Prof. Ignasi Casanova,**
> Universitat Politecnica de Catalunya, E
> **Prof. Manfred Curbach,**
> Dresden University of Technology, D
> **Prof. Robert Day,**
> University of Calgary, CA
> **Dr. Frank Dehn,**
> University of Leipzig, D
> **Prof. Harald S. Müller,**
> Karlsruhe University of Technology, D
> **Prof. Peter Schießl,**
> München University of Technology, D
> **Prof. Ulrich Schneider,**
> Vienna University of Technology, A
> **Prof. Karen Scrivener,**
> École Polytechnique Fédérale de Lausanne, CH
> **Prof. Surendra P. Shah,**
> Northwestern University, USA
> **Prof. Man-Chung Tang,**
> T. Y. Lin International, USA
> **Prof. Nguyen V. Tue,**
> University of Leipzig, D
> **Prof. Gerd Thielen,**
> German Cement Work Association, D

Organising Committee

Symposium's Secretary

    Mr. Carsten Geisenhanslüke
    University of Kassel, D

Chairman of the Organising Committee

    Mr. Walter Schreiber
    Fehling & Jungmann,
    Structural and Material Consulting Engineers, Kassel, D

Members

    Prof. Ekkehard Fehling (vice-chairman)
    Prof. Michael Schmidt
    Mrs. Elvira Berndt
    Mr. Torsten Leutbecher
    Mr. Roland Bornemann
    Dr. Bernhard Middendorf
    Mrs. Ute Müller
    Mrs. Claudia Rebmann
    Mrs. Nadine Sonntag
    Mr. Thomas Teichmann

Sponsors

The University of Kassel provided essential support in infrastructure and administration for the Symposium. The following sponsors are thanked for their additional support:

fédération internationale du béton
Case Postale 88
CH-1015 Lausanne

American Concrete Institute
ACI International
PO Box 9094
Farmington Hills, MI 48333
USA

Deutscher Beton- und Bautechnik-Verein e.V.
Kurfürstenstraße 129
10785 Berlin

Deutscher Aussuss für Stahlbeton (DAfStb)
im DIN Deutsches Institut für Normung e.V.
Burggrafenstraße 6
10787 Berlin Tiergarten

Max Bögl Bauunternehmung
GmbH & Co. KG
Postfach 1120
92301 Neumarkt

Panalytical GmbH
Miriamstraße 87
34117 Kassel

STRATEC
Strahl- und Fasertechnik GmbH
An der Schleuse 3
58675 Hemer

HeidelbergCement AG
Berliner Straße 6
69120 Heidelberg

Part 1:

History and Experiences

Man-Chung Tang
Chairman of the Board and
Technical Director
T.Y. Lin International
San Francisco, USA

High Performance Concrete – Past, Present and Future

Summary

History shows that there is an interrelationship between a new material and the form of structures it is used for. Early arches were built with stones. Steel enabled trusses and long span girders. High strength wires made long span suspension bridges possible, etc. Ultra high performance concrete, with its extremely high strength and durability, is basically a new material, even though it is called concrete. Its application should not follow the path of regular concrete. It is anticipated that, with time, new structural concepts will be developed that can better utilize the superb properties of the UHPC.

Keywords: *concrete, high performance concrete, UHPC*

1   Introduction

Since ancient time, mankind has been searching for construction materials with higher and higher performance so they can build taller, longer and better structures. They probably started with mud, straw and wood because they were handily available. Mud brick and adobe structures are still being built by native people in many parts of the world. They can actually last a long time, given that the weather is favorably dry in these areas.

Fig. 1 Greek Parthenon

Fig. 2 Roman Pantheon

The Minoan started to use lime mortar around 2000 BC. The Greek used it too. But this material can dissolve itself in water and is therefore not very weather resistant. The Romans made a significant improvement on it by adding a volcanic ash from the town of Pozzuoli

(hence the name pozzolana). When tools became available, stone was widely used by the Greeks, Egyptians and Romans, Fig. 1.

The Romans were great builders who had left their mark in a vast portion of the world, spanning most of today's Europe and Middle East. They invented the arch, the vault and then the dome and they built many spectacular aqueducts to carry water from the mountain to the cities. The concrete at that time, a mixture of lime, sand, stone and water, is pretty much the same as that used in many areas of the ancient world, or even today in many under-developed countries. The high compressive strength of the ancient cement, in combination with brick and stone, allowed them to build large arches and great domes. A stone girder can hardly span 5 meters. An arch, on the contrary, can span over 50 meters. The Pantheon in Rome, built around 128 AD, has a dome that spans 43.3 meters, with stones and Roman concrete, which was the largest dome in the world for almost 1900 years.

Portland Cement was officially introduced by Josepf Aspdin in 1824 and reinforced concrete was first patented by W.B. Wilkinson in 1854. Accordingly, the history of reinforced concrete is only about 150 years.

2   Interrelationship between a material and structural form

There is a close relationship between the construction material available and the type of structures we build. Obviously, certain types of structures can only be built after we have developed the appropriate material for construction. In some rare occasions, engineers may have dreamed of specific structural concepts hoping that one day we can develop the required material to realize the construction.

Fig. 3 Space Elevator

This is the case, for instance, for the "Space Elevator", the idea of which was proposed by a Russian engineer back in the mid 1950s to transport people and material between the earth's station and the satelites. The idea is to tie a mass in the outer space to an earth station so the centrifugal force of the mass will keep the tying cable always in tension so that it can serve as a guide for an elevator to climb up and down between the space and the earth. The concept is feasible only if we have the ultra high strength material for the 25,000 km long cables, which we do not have, even today, not to mention in the 1950s. But, with further development of today's nanotechnology, which can now theoretically produce such high strength and long nanotubes, such a structure may one day materialize and the interest in such a concept has since increased.

This is an example where a concept is way ahead of its time. However, most engineers are conservative and more practical. Unlike scientists, who can spend whatever time is needed

4

to search for truth in nature, whether it is useful or not, engineers have to solve prevailing problems and produce what is needed at the present time. They have to make use of whatever is available, no matter how imperfect it is.

Stone, Roman concrete and brick are mainly compressive materials that are good for such structures as arch, domes and barrels. Iron has a much higher strength but is still weak in tension. With the introduction of iron we had arches with longer spans but the form was still similar. High tensile capacity of steel changed the landscape of construction. It allowed us to build long span girders and trusses, which led to rather long span bridges and tall buildings. The very high tensile strength of cold drawn wires made long span suspension bridges possible. High strength steel also serves as prestressing tendons for prestressed concrete. Prestressing is similar to providing concrete with a tensile capacity so that we can build much longer span concrete bridges.

Fig. 4 Telford's Iron Bridge Fig. 5 The Forth Bridge

Today, we are basically utilizing wood, concrete and steel in practically all of our construction. Composites and fiber-reinforced polymers are rather new introductions, they have yet to establish their empire of applications.

Similarly, ultra high performance concrete with strength in the range of 200 MPa is a new material. It is not really concrete anymore. It also has to establish its empire of applications.

3 Definition of High Performance Concrete

Construction materials have different designations in different countries. So is high performance concrete. In reality, today's world is rather small. We are using basically very similar materials in various parts of the world even though they may have different names.

Literally, the German term "Ultrahochfester Beton" is not really the same as "Ultra High Performance Concrete." "Hochfest" describes the internal condition of the concrete while "High Performance" refers to the external characteristics of the material. However, we are using them interchangeably.

In the United States, the definition of High Performance Concrete by the Federal Highway Administration includes eight performance characteristics: freeze-thaw durability, scaling

resistance, abrasion resistance, chloride penetration, compressive strength, modulus of elasticity, shrinkage, and creep.

4   Performance criteria for structures

For today's structures, we look for materials with four distinctive properties: strength, workability, durability and affordability. The first three properties basically include all the eight performance requirements listed above. Affordability is cost.

When we say high performance, we refer to the improvement in some or all of these properties. Sometimes, we have to give up a little in one to gain a little in the other. But, in general, with time, all these properties improve.

We will discuss these four properties one by one.

4.1   Strength

Higher strength offers savings in material. Weight, or the structural dead load, is a major loading in the design of structures. Consequently, higher strength usually gives us two advantages: less material and less weight. The reduction in weight in turn reduces the demand on material because it reduces the load the structure has to carry.

With strength of 200 MPa, the UHPC is almost like steel except its tensile capacity is still comparatively low so it can not be used like steel. But this is many folds higher than the regular concrete, the strength of which is around 50 Mpa.

4.2   Workability

A structure is not only designed, but it also must be constructed. Workability affects the cost and the time required to build the structure. Obviously time and cost are often the two fundamental determinants on whether a bridge or a certain type of structure will be built.

Workability also implies that a material is reliable and consistent. We need better equipment to achieve that in an industrial scale. A new material, such as UHPC, is inherently disadvantaged because construction methods need time to be developed.

4.3   Durability

When we look at some of the ancient structures of Roman and Byzantine eras that are still standing, we wonder how long our structures will last. Our ancient fellow engineers just built major structures based on their best knowledge and usually expected the structures to last forever. Today, we know that nothing will last forever and we become more humble and design our buildings and bridges to a defined design life. With the design life of major bridges usually being 100 to 150 years, we are in need of durable materials that will last a long time and are easy to maintain. UHPC does offer us good potential in this respect. However, in an

engineering world that values performance records, a certain amount of time will be needed to assure people that the long term performance of the material is what the laboratory tests have shown us.

4.4 Affordability

Cost is often a determining factor on whether a structure will be built. There are probably other good construction materials that can be used for construction except that their high cost may have prevented them from being used.

In this respect, it looks like a 'chicken and egg' question. A potentially good but expensive material may become affordable when its application is more widespread due to mass production, while its application can only get widespread if its cost is sufficiently low. Stainless steel, for example, is good for many applications in construction. However, the higher price of stainless steel is a hindrance to its widespread use.

5 UHPC Today

Obviously, "high" is a relative term. The term "ultra-high" is more so. The Laurentienne Building in Montreal, built in 1984, used a 106 MPa high performance concrete and the Two Union Square Building in Seattle, USA, built in 1988, utilized a 145 MPa high performance concrete. Going to a UHPC with strength higher than 200 MPa certainly is another big step forward.

Various tests have confirmed UHPC's performance in the laboratories. They show high strength and durability. Theoretically, we are able to use it for daily applications, wherever high strength and durability are beneficial. The basic principle is to use stronger aggregates, microsilica, and water reducing agents to raise its strength, steel fibers to prevent brittle failure and polypropylene fibers to increase its fire resistance, and so forth. In general, with steam curing, we are able to reach strength in the range of 200 Mpa or higher. The resulting concrete basically meets all eight performance criteria of the FHWA for high performance concrete. The material itself is therefore available. The problem is the ease of application and the price.

As a matter of fact, it is possible to produce concrete with a strength as high as 700 MPa in the laboratory many years ago. But to reproduce it in a jobsite will be difficult.

The Sherbrooke Pedestrain Bridge in Canada and the Seonyu Pedestrian Bridge in Korea are certainly showcase structures for UHPC.

Fig. 6 Seonyu Pedestrian Bridge
Seoul, Korea

There have been a few test construction of UHPC concrete for highway bridges in the United States. These are mainly precast beams based on the concept of existing AASHTO girders, Fig. 7. Other countries are also testing UHPC applications.

Fig. 7 FHWA UHPC-Girders   Fig. 8 Shear Failure
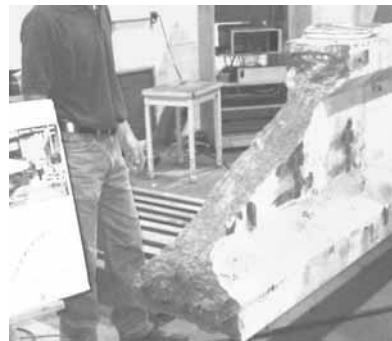
There are certainly applications where the higher strength of UHPC offers advantages, such as in a long span cable-stayed bridge. The predominantly compression structure can be made much lighter using UHPC. For cable-stayed bridges buckling is usually not a problem and shear force is relatively small. UHPC will provide savings in cables and foundations as result of a lighter superstructure. Prestressed UHPC may also be used for the deck of suspension bridges. Prestressing will be preferable because the deck of a suspension bridge is primarily a flexural member where tension and compression capacities are equally important.

Despite the fiber content, UHPC is still primarily a compression material. To improve it's tensile and shear capacity, UHPC may be combined with carbon fiber mats to form hybrid structural members, where the carbon fiber can resist all the tension. Or, if we can use carbon fiber as a mold to contain UHPC, we may be able to create very light weight and strong girders.

Because of its durability, UHPC may be used as a shell for large diameter precast concrete piles.

However, these ideas are still in the line of concrete. Generally speaking, due to the delicate nature of the production and handling process, a mass production of today's UHPC is still not

economical. The cost is rather high because if we use UHPC to replace regular concrete, such high strength may not offer sufficient advantage in most types of today's structures.

6   Outlook for UHPC

Since cost and workability are the two major obstacles, the future of UHPC depends on some breakthrough on these two fronts.

Apart from workability, the popularity of a material is affected by its cost. The less a material costs, the more it will be used. The Bessemer and Open Hearth Steel processing in the 1850s made the steel available in large quantities and at affordable prices. Its applications started to mushroom. That was also the time people started thinking of putting steel in concrete to improve its properties. UHPC probably needs a similar breakthrough in construction technology to push it into popular applications. At the present time, the high cost of material is a major hindrance to its widespread use.

On the other hand, if we think of UHPC as concrete, it must be able to work like concrete. This is another major constraint in actual applications. First, UHPC requires much more attention and special equipment to ensure its quality. Second, for today's construction, high strength is usually not very important because all concrete structural elements must have a certain minimum dimension to be workable.

Consequently, to fully utilize the capacity of UHPC, we must develop new applications. The very high strength of UHPC will not be necessary if we keep using it on existing types of structures. As indicated by the history, new forms of structures will be developed for a new type of material. This will require us to think "outside the box" to find more appropriate applications that are different from the prevailing forms, just like the application of high-strength wires for long span suspension bridges and prestressed concrete structures.

Let us be more innovative! It appears to be a good idea to think of UHPC not as concrete as we know it now. We should try to develop new structural concepts that can utilize the strength and superb performance of this material. With time, this will happen!

Paul Acker

PhD, Director of the Structured
Materials Department
Lafarge
Paris, France

Mouloud Behloul

PhD, Ductal® Technical Director

Lafarge
Paris, France

Ductal® Technology: a Large Spectrum of Properties, a Wide Range of Applications

Summary

A new formulation approach by using ultra-fines materials supported by strong development of new admixtures open the way over the last twenty years to amazing progresses in concrete technology. The range of performances and characteristics that are today covered by concrete have been expanded in various directions from ordinary concrete up to ultrahigh-performance concrete or selfcompacting concrete, etc. High-strength concrete, however, remains basically a brittle material requiring the use of passive reinforcement. A technological breakthrough took place at the turn the 90's with the development of the said Reactive Powder Concrete (RPC) [1], offering compressive strength exceeding 200 MPa and flexural strength over 40 MPa, showing some ductility. Based on the RPC initial research, the Ductal® technology was then developed [2]. Comprehensive physical analysis and experimental results have confirmed the ability to achieve and combine several properties, usually considered as contradictory. As a result of the ductility and very high compressive strength of such material, it is today possible to avoid passive reinforcements in structural elements. A range of formulations can be adjusted to meet specific requirements, contributing to the overall construction performances, reducing labor requirement, improving construction safety and durability, lowering maintenance need and increasing total life cycle. The Ductal® technology has been introduced as a first reference, in several countries, both in structural and architectural segments of construction and currently developing through innovative applications in large projects at various stages of development.

Keywords: *ultrahigh performance concrete, ductility, selfplacing concrete, applications, Ductal®.*

1   Introduction

Ductal®, the outcome of the research over the last 10 years in the area of concrete, is a new construction material technology belonging to UHPFRC family, with very high durability, compressive strength, flexural resistance with ductility and aesthetics.

The Ductal® technology product range was developed by the combined efforts of three companies, Lafarge, the construction materials manufacturer, Bouygues, contractor in civil and structural engineering and Rhodia, chemical materials manufacturer. With this joint effort

through intensive research and development, the material was patented, industrialised and commercialised.

There were more than 15 universities and 6 testing laboratories in different disciplines and countries which participated to the important research effort over several years.

In France, new recommendations for the use of ultrahigh strength concretes reinforced with fibres have been issued in May 2002 [3]. These recommendations were established by a BFUP working group (*Béton Fibré Ultra Performant*) coordinated by SETRA (Road and traffic governmental agency) and with representatives of construction industries (contractors, control agencies, suppliers, certification authorities).

Through the development period, several prototypes have been manufactured, prior to make an extensive use in civil works, structural and architectural various applications.

2   Ductal[®] technology: result of a decade of research

Ductal[®] refers to a simple concept, minimising number of defects such as micro-cracks and pore spaces, that allow to achieve a greater percentage of the potential ultimate load carrying capacity defined by its components and provide enhanced durability properties. To apply that concept, a concrete was proportioned with particle sizes ranging from a maximum of approximately 600 mm, down to less than 0.1 mm to obtain a very dense mixture which minimized void spaces in the concrete.

A Ductal[®] research program was conducted based on the following principles:
*   Enhancement of homogeneity by elimination of coarse aggregates,
*   Enhancement of density by optimization of the granular mixture,
*   Enhancement of the microstructure by post-set heat-treatment,
*   Enhancement of ductility by incorporating adequate size fibres,
*   Maintaining mixing and casting procedures as close as possible to existing practice.

By applying the first three principles, it was possible to define a concrete with very high compressive strength, but with not enough ductility compared to a conventional mortar. The inclusion of adequate fibres improves drastically tensile strength and provides a substantial level of ductility.

The various Ductal[®] formulations are all based on an optimised composition combining homogeneity and granular compacted density.

To enhance performances, especially mechanical ones, the option of heat treatment can be chosen. For each application according to technical and economical challenges, the Ductal[®] technology is adjusted to achieve the most adapted product to the customer requirements.

As described above, Ductal[®] is an Ultra High Performance Concrete reinforced with fibres. These fibres can be made of steel (Ductal[®]-FM), made of organic material (Ductal[®]-FO) or combination of both steel and organic material (Ductal[®] AF).

12

The fresh mix of all these ranges of material have very useful properties in term of fluidity and self placing. Most of the standard industrial batching facilities are able to mix Ductal® requiring only minors adjustments.

The Ductal® matrix is very fine and dense and shows outstanding capacity to replicate any kind of surface textures. By using adequate pigments a very wide range of colouring effects can be achieved. Thanks to these properties, Ductal® is a favoured material for architectural applications where most of the time high mechanical properties are not the major requirement.

In that case steel fibres could be replaced by organic fibres and reduced or even no heat treatment is applied. This range of material is named Ductal®-FO.

2.1　　Mechanical behaviour

2.1.1　　Mechanical properties and analysis

Ductal®-FM, the first developed mix, is designed for structural applications where high bending and direct tensile strengths are required. These mechanical properties are achieved by using short steel fibres. A content of 2 % by volume of 13-15 mm length　fibres with diameters around 0.2 mm emerged as the best optimum out of thousands of tests.

Figure 1 shows the compressive and bending behaviour of Ductal®. It can be observed that it has an ultimate bending strength which is over twice its first crack stress and more than ten times the ultimate stress of conventional mortar. Such very high strength and consequent ductility allows to design structures without any secondary passive reinforcement and no shear reinforcement.
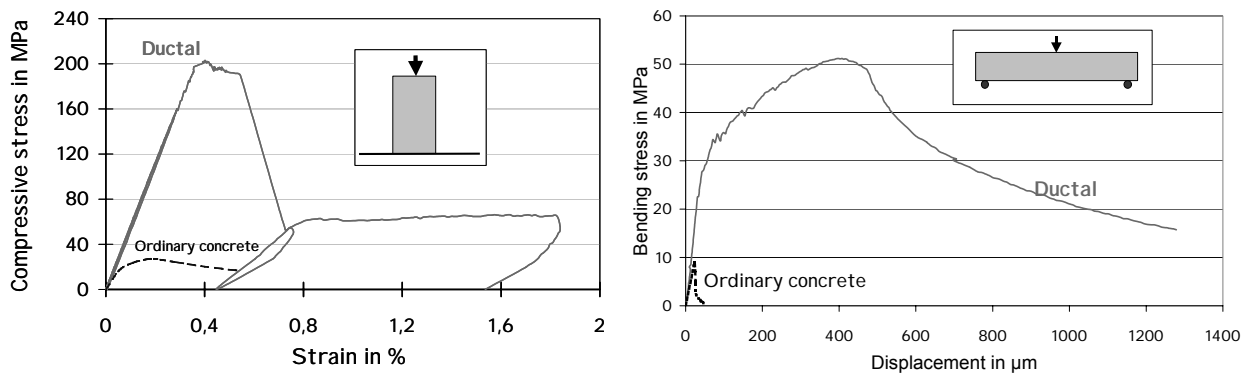
Figure 1: Ductal® behaviour in compression (left) and in bending (right).

The ductile behaviour observed in the bending test before the peak is characterised by a multiple cracking, without any localisation of a major crack, as shown in figure 2:
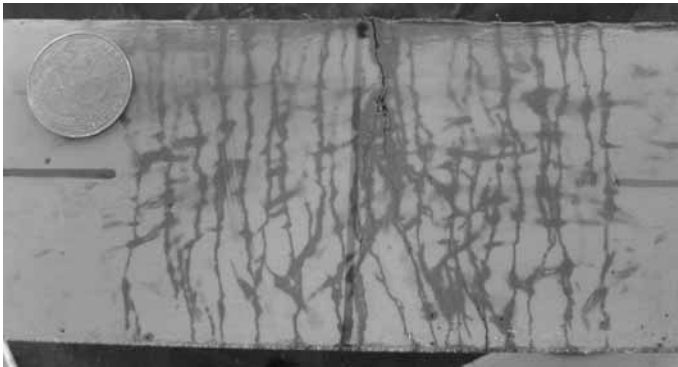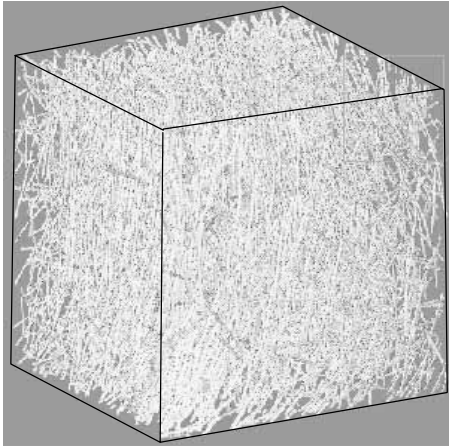
Figure 2: 3-D image (left), multiple cracking (right)

Figure 2 (left) shows an image obtained by X-ray scanning, where it can be observed the high density of fibres (2 % volume) of a 40x40x40 mm cube sawed out off a Ductal® beam (courtesy of TOMO-ADOUR). Figure 2 (right) shows multiple cracking (figure 2 right) in the tensile zone as observed after bending failure; it is noticeable that the crack openings are so small that they cannot be observed by naked eyes and the surface shall be wetted with alcohol to reveal the cracks; the apparition of the unique visible crack coincides with the peak load ("localisation" process).

Numerous full scale tests on beams, columns and shells have been performed [4, 5] (figure 3). These tests have accessible the validation of the calculation methodology which was then chosen as reference by the BFUP working group [1].
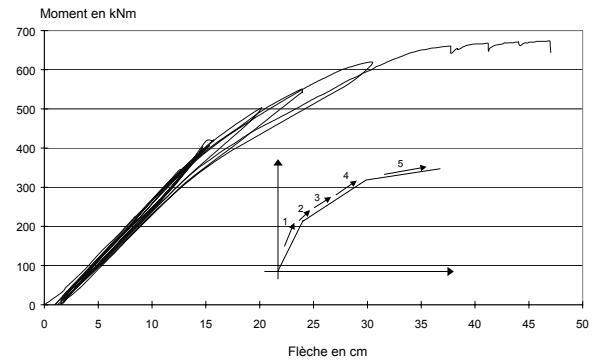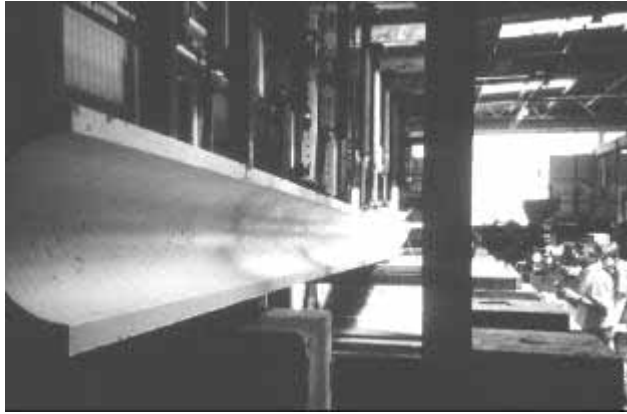
Figure 3: Full scale test on a prestressed beam, ENS Cachan [4]

2.1.2 Creep & shrinkage behaviour

Creep and shrinkage are probably the most outstanding characteristics of Ductal®. Creep was tested by ECN [7]. For normal concrete the so-called creep coefficient can reach up to 3 to 4, for high-performance concrete the creep coefficient is reduced, but the delayed strain is already higher than the elastic one. Creep coefficient of Ductal® is less than 0.8 and, when a thermal treatment is applied, the creep coefficient is as low as 0.2 (Figure 4) [8]. When using prestressing technology, the prestress losses are substantially reduced.

This very surprising result has been analysed [9], and this analysis will certainly impact our view on the creep mechanisms and theory.

As the water to cement ratio is very low, Ductal® does not exhibit any drying (no weight loss can be measured) nor drying shrinkage. A high autogenous shrinkage can be observed (300 to 400 microstrain) but when a heat treatment is applied, this shrinkage is completed at the end of the treatment and, when this treatment is over, absolutely no residual shrinkage occurs (Figure 5).
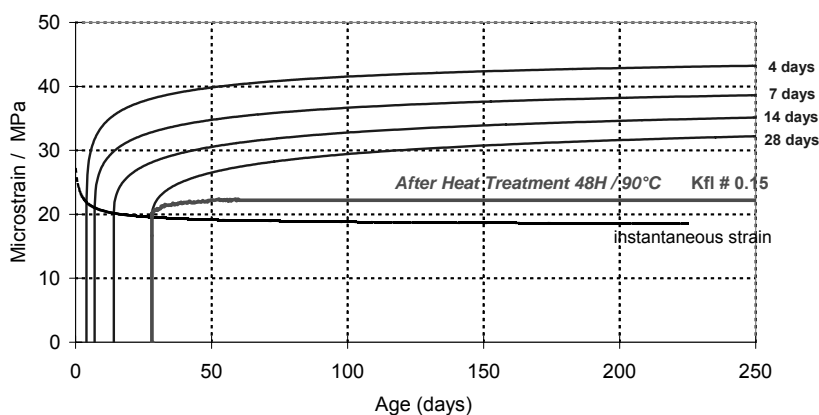
Figure 4: Ductal® basic creep [3]
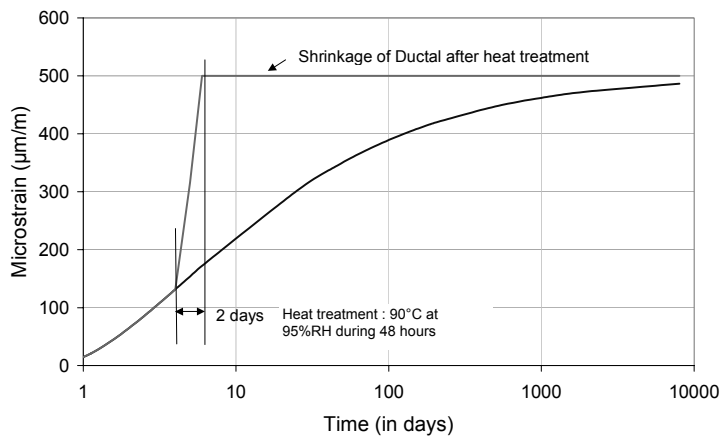
Figure 5: Ductal® shrinkage: after thermal treatment, no shrinkage is observed [3]

2.1.3 Fire and high temperature

Fire resistance is one of the main issues for developments in the building industry. For material developments like any concrete, Ultra High Performance Concretes are listed in M0 class of product (non-inflammable) that are slowing down the spread of fire. However, the very low porosity of UHPCs induces greater internal stresses. In these materials, the porosity is totally enclosed, which prevents water vapour (steam) to escape. By increasing the pressure within the material the spalling phenomenon occurs. Spalling has been almost suppressed by using adequate organic fibres. Above 150°C, such fibres begin to soften and melt, thereby provide escape routes for trapped steam. This approach was applied to a new Ductal®. As the matrix is completely closed when compared to HPC matrix a very important work was performed in order to up-grade Ductal® and to find the correct mix, geometry of fibres and the dosage when keeping the target of ultra high strength, very good workability and no spalling when submitted to fire.

Different kind of structures, loaded or unloaded columns, loaded and unloaded beams were tested, in France (CSTB) and Finland (VTT), under ISO fire with success. Also direct tensile hot tests were performed by the Politecnico di Milano [10].

The mechanical properties of this new Ductal® refered as Ductal®-AF are similar to Ductal®-FM.

16

before test	*after fire test*
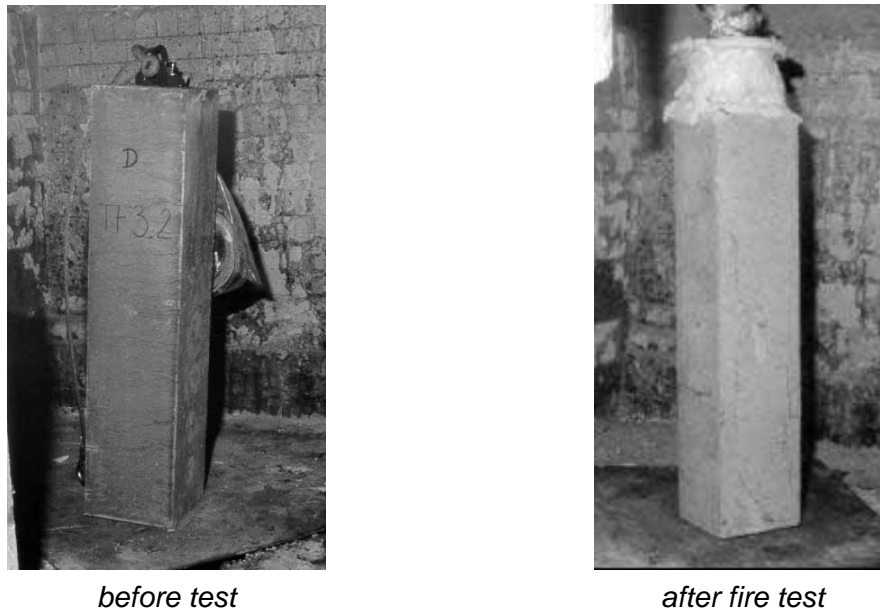
Figure 6: Ductal®-AF ISO fire test during 2 hours

2.2 Durability

The microstructure of Ductal® is completely closed and prevents the intrusion of any aggressive agent. Such characteristics provide to the material ultra high durability performance.

2.2.1 Durability properties and chemical stability

Full characterisation of the durability properties of the material were performed in different laboratories -INSA Toulouse, LCPC, EDF/CEMETE, ESPCI, Mines de Nancy, LERM- in which the porosity distribution, gas permeability, carbonation test, chlorine diffusion test, leaching test and the MNR microstructure characterisation tests were made. Also the chemical stability of the material was checked [11].

Freeze-thaw tests were performed on Ductal® samples at CEA [12] and also at CEBTP. The tests were performed until 300 cycles above the normative 100 cycles without any degradation.

2.2.2 Chemical attacks and ageing

UHPFRCs materials stand up to chemical conditions under which ordinary reinforced concretes are rapidly and severely damaged. Laboratory tests were performed out by CSIC (Spain) in which Ductal® was submitted to different chemical aggressive compounds (calcium sulphate, sodium sulphate, acetic acid, ammonium sulphide and nitrate and also sea water and distilled water). The results exhibit a very good resistance to the chemical attacks (see in [3]).

Other severe operating condition tests were performed at IFP in which Ductal® was submitted to different gas (CO_2, CH_4, H_2S), at high temperature (120°C) and high pressure (7MPa) showing again unexpected high resistance.

Ageing tests were also performed at CSTB in which the self sealing of Ductal® was demonstrated, see figure 7 [13].

Self-sealed micro-crack in a clinker grain
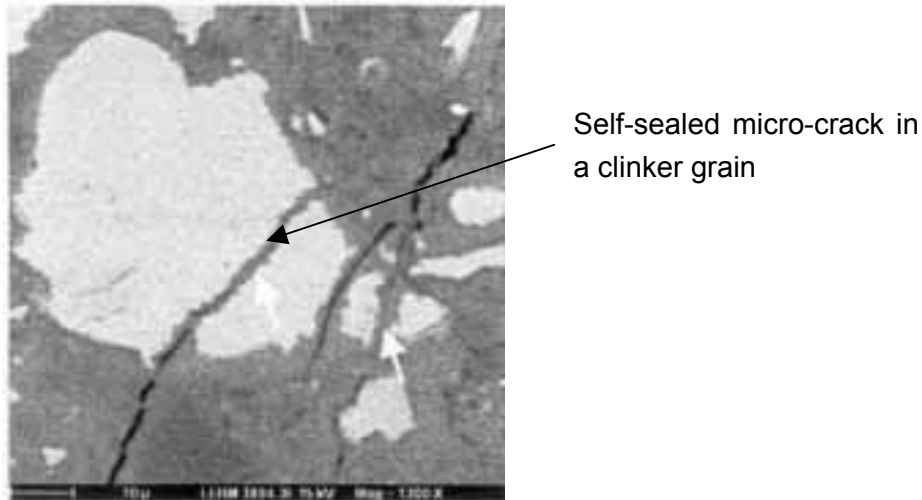
Figure 7: Self-sealing of micro-cracks by clinker hydration

3   Applications

The ultra high performance of Ductal® opens applications in different domains requiring at least :

- Ultra high strength
- The durability
- The architectural aspects

3.1   Mechanical strength

A material with such high ultimate compressive, and flexural-tensile strength offers interesting opportunities in the field of prestressed concrete. As might be expected, the high flexural tension capacity also gives rise to extremely high shear capacity.   This allows Ductal® to carry the shear load in the structure, without providing auxiliary shear reinforcement.

The elimination of passive reinforcement makes it possible to use thinner sections and a wider variety of innovative and acceptable cross-sectional shapes. The current structural precast shapes used for prestressed beams in bridges and buildings have been shaped for concretes with much lower strength properties. Their dimensions and design would not allow to take advantage of very high performances of Ductal®. In order to make the best use of the higher mechanical properties, there is several opportunities to introduce new shapes in prestressed beam design. Through such re-design approach of the elements the beam dead load can be reduced by a factor of three.

Among these kind of applications we can list the *Shepherds* Traffic Bridge erected in Australia [14], 5 footbridges: Sherbrooke footbridge in Canada (figure 8)– *Seonyu* footbridge

in Korea, figure 9 [15] – Sermaises footbridge in France- *Sakata Mirai* (figure 9) and *Akakura* footbridges in Japan and the canopies of LRT station of Shawnessy (figure10).

Figure 8 Sherbrooke footbridge, Canada,1997
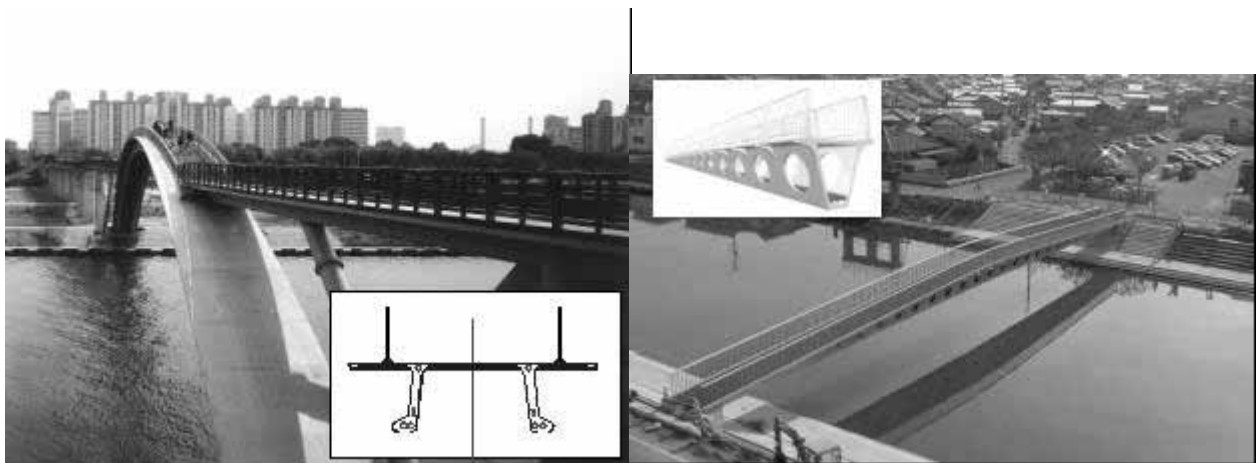
Figure 9. *Seonyu* footbridge, Korea,2002 (left) and *Sakata Mirai* footbridge, Japan, 2002 (right)

Figure 10. Ductal®-FO canopies - LRT Train Station, Shawnessy, Canada, 2003

An important work is performed in the US by the FHWA (Federal High-Way Administration) in order to design short span bridges made of Ductal® [16]. The shape and design was optimised by MIT using a new software they developed [17].
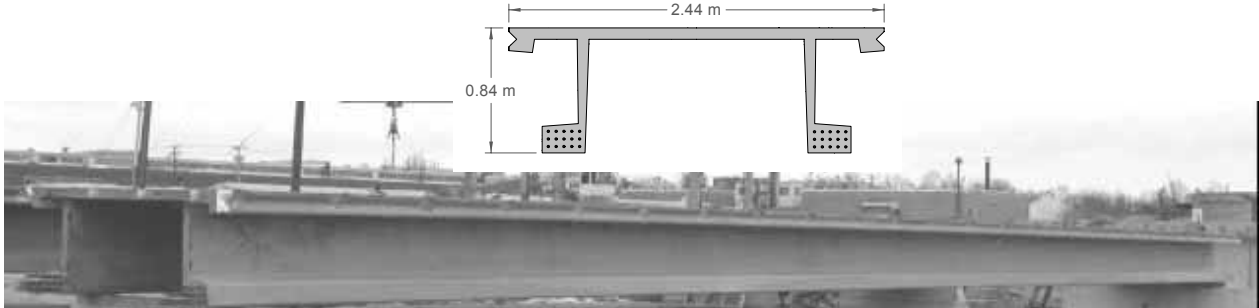
Figure 11 Traffic Bridge, Washington – π-shaped beams, 2004

3.2 Durability oriented applications

The durability of Ductal® is as important as the mechanical strength. Combining strength and durability, Ductal® can be an ideal solution for structures in severe environment. Also the durability of the material lowers the maintenance costs and makes the solution very competitive.

Ductal® was used in several durability /fire resistance oriented applications like the beams and girders (more than 2000) used for the Cattenom power plant cooling tower-France- (figure 12), the retained earth anchorages (more than 6000) used in Reunion Island (figure13) –France- and the Ductal®-AF used for the construction of composite columns in the *Reina Sofia* Museum in Madrid (Spain).
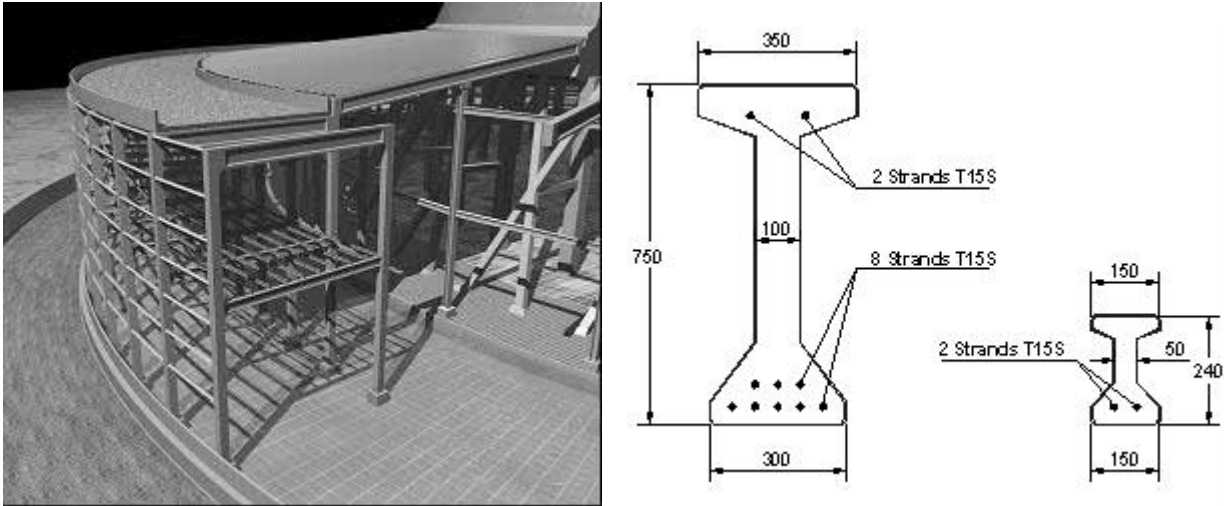
Figure 12. Cattenom cooling tower - Ductal® beams and girders (1997-1998)

Figure 13. Ductal® retained earth anchors – La Réunion Island (1999)

3.3 Architectural applications

The use of a concrete-like material but with almost unlimited possibilities of appearance, texture and colour has excited the architects by giving them access to unexpected new world of shapes and volumes. Ductal® was used in several architecturally oriented applications like the bus shelters in Tucson (USA), street furniture in Rennes (France), shower booths, sun shades, façade panels in Monaco (figure 14) and Kyoto clock tower in Japan.

Façade panels for Monaco railway station, 1999

Shower booths, France, 2000 →
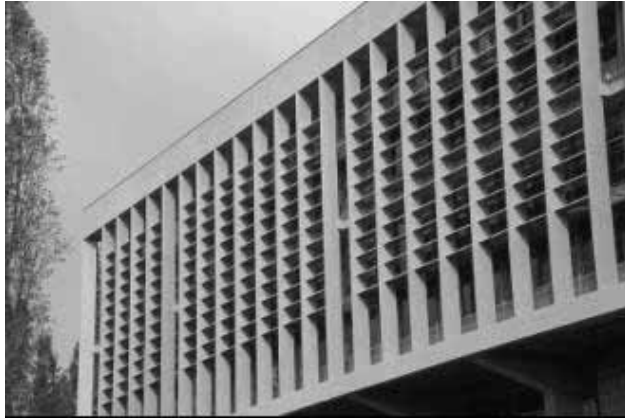
Sun shades, La Doua university Lyon, 2003   *Flower pots, Rennes, 2003*

Figure 14: Architectural application examples

4   Conclusion

Ductal® is a new technology of ultra high strength concretes that constitutes a breakthrough in concrete mix design. This family of products is characterised by a very dense microstructure and very high compressive strength achieving and possibly exceeding 200 MPa. Steel and organic fibres or combination of both are one of the major components of the material enhancing the bending strength, the ductility and fire resistance.

The three main categories of applications are :

- Mechanical strength : The very high mechanical properties combined with prestressing technology offer to engineers and architects lot of opportunities to design elegant structures by avoiding heavy steel reinforcement. Ductal® technology gives access to very thin slender and elegant structures like footbridges.
- Durability : the very dense microstructure of the Ductal® matrix offers a material which resist to very aggressive media and opens therefore a very wide range of applications.
- Architectural : a very wide range of textures and colours effects are accessible to Ductal®. Such properties provide architects with very high potential of innovative design in all elements that build up new architecture.

5   References

[1] Richard, P.; Cheyrezy, M.; Reactive Powder Concretes with high ductility and 200-800 MPa compressive strength, ACI SP144-24, 507-518, 1994.
[2] Orange, G.; Dugat, J.; Acker, P.; A new generation of UHP concrete : Ductal®. Damage resistance and micromechanical analysis, Proc. of the 3d Internat. RILEM Workshop, HPFRCC3, Mainz, 101-111, 1999.
[3] BFUP. AFGC, Ultra High Performance Fibre-Reinforced Concretes, Interim Recommendations, AFGC publication, France, 2002.
[4] Behloul,M. ; Analyse et modélisation du comportement d'un matériau à matrice cimentaire fibrée à ultra hautes performances. PhD thesis. Ecole Normale Supérieure de Cachan. 13 December 1996.

[5] Cuny, J. ; Essais de caractérisation de poteaux en matériau BPR. Rapport de DEA, Ecole Normale Supérieure de Cachan, Juin 1995.

[6] Adeline R., Chauvel D., Jacquemmoz C., Birelli G. First design rules for RPC beams. Proceedings of the International Symposium on High-Performance and Reactive Powder Concretes, August 1998, Sherbrooke, Volume 3, pp. 1-15.

[7] Loukili, A; Richard,P and Lamirault,J; A Study on Delayed Deformations of an Ultra High Strength Cementitious Material. Fourth CANMET/ACI/JCI Conference, Special Publication, American Concrete Institute SP-179, pp. 929- 950, juin 1998.

[8] Acker, P.; Why does Ultrahigh-Performance Concrete (UHPC) exhibit such a Low Shrinkage and such a Low Creep ?, Proceedings of: Autogenous Deformations of Concrete, ACI Fall Convention, Phoenix, USA, 2002.

[9] Acker, P.; Swelling, shrinkage and creep: a mechanical approach to cement hydration, Concrete Science & Engineering, Vol. 37, p.11-17, April 2004.

[10] Behloul, M.; Fire resistance of Ductal Ultra high Performance Concrete, Proc. Vol. 2., Session 7, pp 101-110. FIB 2002, Osaka, Japan, 2002.

[11] Vernet, C.; UHPC Microstructure and related Durability Performances - Laboratory Assessment and Field Experience Examples, PCI / FHWA 3rd International Symposium on HPC, Orlando, USA, 2003.

[12] Conteneur haute intégrité à base de liant hydraulique tenue aux cycles gel/dégel ". Rapport scientifique 1997-CEA, Direction du cycle du combustible- ISSN 0429-3460, pp152-159

[13] Pimienta, P.; Chanvillard, G.; Retention of the mechanical performances of Ductal specimens kept in various aggressive environments. fib Symposium, April 26-28, Avignon, France, 2004.

[14] B.Cavill and G.Chirgwin . "The worlds first Ductal road bridge Sherpherds gully creek bridge, NSW",. 21st Biennial Conference of the Concrete Institute of Australia, 17 – 19 July 2003. Brisbane.

[15] Behloul, M.; Lee, KC.; Ductal Seonyu footbridge. Structural Concrete. 2003, 4, N°4, pp195-201.

[16] Hartmann, J.; Graybeal, B.; Perry, V.; Durukal, A.; Early Results of the FHWA UHPC Research Program, International Conference on Advanced Materials for Construction of Bridges, Buildings and Other Structures, Davos, Switzerland, 2003.

[17] Chuang, E.-Y.; Ulm, F.-J.; Two-phase composite Model for high performance cementitious composites, M.ASCE Journal of Engineering Mechanics, p.1314-1323, 2002.

Peter Buitelaar
Technical Manager
Contec ApS
Højbjerg, Denmark

Heavy Reinforced Ultra High Performance Concrete

Summary

The use of a HPC and an UHPC in combination with large amounts of reinforcement (fibers, rebars and/or wire) and known under the name Compact Reinforced Concrete (C.R.C.) as original developed by Hans Henrik Bache in 1986, is extremely interesting in the case of the re-strengthening of existing constructions or to use as stand alone constructions. By adjusting the original concept and by developing a wide range of HPC and UPHC concretes the C.R.C. concept can be used for a wide range of applications from prefab till in-situ castings and pavements. The concept includes a philosophy and principles for structural design, especially against accidental overloading.

Keywords: *UHPC, CRC, Orthotropic bridge decks, Rehabilitation.*

1   Introduction

After the development of the D.S.P. mortars in 1978 [1, 2, 3 and 4] and the development of C.R.C. in 1986 [5, 6 and 7] the use of the HRUHPC was limited to applications in the security industry (vaults, strong rooms and special protective defense constructions) and the prefab industry (machinery parts, tooling, stairs, balconies, drain covers, etc.). More recent developments like for instance in France [8] are focussed on self compacting fibre reinforced UHPC with the objective to develop such a matrix with a blend of different fibers that additional reinforcement will not longer be necessary. This seems very interesting for particularly small sized constructions but is not yet to apply to medium and large sized constructions, here fore it will still be necessary to use additional reinforcement and/ or pre- or post stressing. Especially when we take fracture mechanics [9] in account, what is absolutely necessary for designing with brittle materials like UHPC, than medium- en large sized constructions will be much more brittle than small sized constructions and these problems can until now not be solved with only fibre reinforcement. Not only practical it seems to be very difficult to produce a self compacting UHPC with a large amount of fibers (mixing and casting, segregation and orientation of the fibers in the hardened matrix) but the addition of large amounts of special fibers is also from an economical point of view not always an attractive solution. In large structures like for instance beams the disorientation of the steel fibers will result in a large variation of the properties of the UHPC in the different locations of the beam and this will make it much more difficult for engineers to calculate and to design with the properties of the UHPC. It also seems that especially the large autogenous

- and chemical shrinkage, due to the high amount of cement and fine fillers combined with a low water/binder ratio, of self compacting fibre reinforced UHPC is reducing the effect of pre-tensioning. The C.R.C. principle makes it easier to design medium and large size constructions since the main reinforcement (traditional rebars, high strength rebars, carbon rebars, wire, etc.) can be exactly calculated and placed in the area where they are necessary. Different fibers added, even in very high amounts (steelfibers 0,15 x 6 mm v/v 10%), in the UHPC are much better orientated in the matrix due to the special properties of the UHPC, the main reinforcement will help to avoid segregation of the fibers and will also orientate the fibers much more efficient. The C.R.C. principle makes it possible to predict the behaviour of small, medium and large sized constructions under different loadings very accurate especially when scaling up from small models are used for modelling the actual construction. This makes it thus also possible to deal with high local stresses in constructions, accidental overloading and impact resistancy on any level. The HRUHPC seems to have extremely good fatigue resistance even under continuous high loads. Various research projects and applications are executed during especially the last 5 years for different applications of HRUHPC.

2   The Heavy Reinforced Ultra High Performance Concrete

The UHPC is consisting of a mixture designed for a certain application (workability, strength, density, shrinkage compensation, etc.) however due to the large experience of 20 years various standard mixes in different ranges and with different properties are available. For a HPC and an UHPC strength is not the only or necessary parameter to measure, other properties can be much more important than the compressive strength of a cube or cylinder. Especially when durability is important than this can not be related anymore to the compressive strength of the HPC/UHPC like in more traditional concrete. The durability (chloride penetration, frost /thaw resistance) in a HPC with a compressive strength of for instance 100 MPa can be equal to that of an UHPC with a compressive strength of for instance 300 MPa. The explanation for this is that the compressive strength in HPC/UHPC is depending mainly on the quality, size and composition of the aggregates and fibers used in the concrete and not on the binder. Various researches are made to investigate the durability of UHPC under different conditions during the last 25 years and of HRUHPC under different conditions during the last 14 years [10, 11, 12, 13, 14 and 22]. Further properties can be influenced by the type of binder, special fibers, and special additives to control shrinkage, internal curing compounds, etc. Especially for a self levelling HPC system for thin toppings (C110 -140, thickness 10 – 30 mm) on industrial floors shrinkage control and internal curing compounds are used and this technology will possible also be applied to the UHPC. The HRUHPC is a composite material which means that all the components (UHPC, fibers, reinforcement and other additional materials) are a part of the hardened matrix and its properties. Since thus the properties of the hardened matrix can be designed in a very wide range and are depending on the components used it is necessary to select these components very well for each application. Properties of the HRUHPC compared to HPC, UHPC and structural steel are shown in table 1.

Table 1: Properties of UHPC, HRUHPC and ductile high quality steel [7]

Properties	HPC	UHPC		HRUHPC	High quality steel
		0 - 2% fibers	4 – 12% fibers		
Compressive strength MPa	80	120 – 270	160 - 400	160 - 400	
Tensile strength MPa	5	6 - 15	10 - 30	100 - 300	500
Flexural strength MPa				100 - 400	600
Shear strength MPa				15 - 150	
Density kg/m^3	2.500	2.500 2.800	2.600 3.200	3.000 4.000	7.800
E-modules GPa	50	60 - 100	60 - 100	60 - 100	210
Fracture energy N/m	150	150 – 1.500	5.000 – 4.000	$2 \cdot 10^5 – 4 \cdot 10^6$	$2 \cdot 10^5$
Strength/ weight ratio m^2/sek^2				$3 \cdot 10^4$-10^5	$7.7 \cdot 10^4$
Stiffness/ weight ratio m^2/sek^2				$2 \cdot 10^7$- $3 \cdot 10^7$	$2.7 \cdot 10^7$
Frost resistance	Moderate/ good	Excellent	Excellent	Excellent	
Corrosion resistance	Moderate/ good	Excellent even with 5-10mm cover	Excellent even with 5-10mm cover	Excellent even with 5-10mm cover	Poor

3 Applications

One of the first large applications of the HRUHPC is as an overlay on damaged pavements and industrial floors and in cargo ships [15 and 16]. The unique properties of the HRUHPC makes it possible to place the overlay as an "independent" wearing course on a cracked and/ or polluted sub base or even an under dimensioned sub base made from different materials like asphalt concrete, concrete, wood, ceramics or steel. Due to the properties of the special composed HPC/UHPC is it possible to cast, compact and to finish the HRUHPC overlay like traditional monolithic concrete floors during several hours under different circumstances. HRUHPC is often used in Denmark, especially for slender and elegant prefab constructions like balconies and stairs. The HRUHPC is further used in the security industry for the production of prefab panels for large vaults and strong rooms (up to 10.000 m^3 volume!), safes and ATM's.

3.1 Rehabilitation and restrengthening of orthotropic bridge decks

In the Netherlands there are approximately 80 orthotropic steel bridges, most of them build in the seventies and eighties of the last century, around 10 of these are mayor bridges in the

infrastructure and are located in the main highway system. In the last 7 years fatigue cracks have been found in different locations and especially the cracks in the steel deck plate are very critical for the traffic security. During the last 6 years a very large research project, initiated by the Civil Engineering Division of the Ministry of Transport, Public Works and Water Management in the Netherlands, is carried out to investigate the reason for these fatigue cracks and to develop practical solutions for cost effective rehabilitation and renovation. The main reason for these fatigue failures are the high stress concentrations in combination with the local wheel loading and high traffic volume [17, 18 and 19]. Various methods were investigated to create a more rigid deck plate to reduce the stresses so much that a large extension of the total service life could be reached. A large research project is executed during the last 5 years to develop a new revolutionary HRUHPC wearing course which will also extend the service life of the total construction. More details about the HRUHPC and the application on orthotropic steel bridge decks can be found in several papers presented in the last 2 years [17, 20 and 21] and a part of the tests made with the HRUHPC are described in detail in several reports [22]. The research project is not finished yet and much more data is available and will be available in the next years when the research project is finished and larger orthotropic steel bridge decks (up to 32.000 m^2) will be resurfaced with an HRUHPC overlay. A short overview with the available research is given in table 2.

Table 2:   Description of the different tests made with the HRUHPC

Description test - research	Test made by parties involved	Period of testing - research
Adhesion tests on small Samples	Adhesion Institute Technical University Delft Contec ApS	November 1999 – May 2000
Fatigue tests on small Samples	Adhesion Institute Technical University Delft Contec ApS	November 1999 – May 2000
Placing 60 m^2 HRUHPC overlay on removed bascule	Civil Engineering Division Contec ApS B.Schipper Apeldoorn B.V.	October 2000
Placing 20 m^2 HRUHPC overlay on removed bascule	Civil Engineering Division Contec ApS B.Schipper Apeldoorn B.V.	July 2001
Removebility HRUHPC Overlay	Civil Engineering Division Contec ApS B.Schipper Apeldoorn B.V.	August 2001
Skid resistance HRUHPC overlay after shotblasting	DWW	August 2001
Compressive strength and	Stevin Lab. Technical	April – May 2002

modules of elasticity UHPC	University Delft	
Flexural strength UHPC	Stevin Lab. Technical University Delft	May – June 2002
Short term shrinkage and creep UHPC and HRUHPC	Stevin Lab. Technical University Delft	April – May 2002
Long term shrinkage and creep UHPC and HRUHPC	Stevin Lab. Technical University Delft	August – September 2002
Effect curing and power floating HRUHPC	Stevin Lab. Technical University Delft B.Schipper Apeldoorn B.V.	August – September 2002
Adhession UHPC on steel	Stevin Lab. Technical University Delft	August – September 2002
Frost/ thaw resistance UHPC CDF method	Stevin Lab. Technical University Delft	November – December 2002
Adhesion HRUHPC overlay on steel (-20°C - +20°C)	Stevin Lab. Technical University Delft	November – December 2002
Chloride penetration Nordtest	Stevin Lab. Technical University Delft	April 2002 – April 2004
Fatigue test HRUHPC overlay on part orthotropic bridge deck	TNO Building and Construction Research	June – July 2002
FEM calculations HRUHPC overlay on orthotropic bridge deck	Civil Engineering Division	May – April 2002
Extension of service life calculations on various orthotropic bridge decks	Civil Engineering Division	May – April 2002
Pilot project Caland bridge approx. 540 m^2	Civil Engineering Division Contec ApS Bruil-Ede B.V.	30 April – 3 May 2003
Stress reduction on Caland bridge after HRUHPC overlay	Civil Engineering Division	22 April 2003 (before placing) – 13 May 2003
Influence traffic on adhesion HRUHPC overlay on 2 orthotropic steel bridge decks	Civil Engineering Division Stevin Lab. Technical University Delft B.Schipper Apeldoorn B.V.	April – May 2004
Stress reduction after HRUHPC overlay placed on	Civil Engineering Division Technical University Delft	April – May 2004

part orthotropic bridge deck with un-repaired fatigue cracks	B.Schipper Apeldoorn B.V.	
FEM calculations HRUHPC overlay on different details orthotropic bridge deck	Civil Engineering Division	April – May 2004
Placing 300 m^2 HRUHPC overlay with slipform paver	Contec ApS Kirchhoff-Heine Strassenbau GmbH & Co. KG	May 2004

In the period from 29 April – until 4 May 2003 the Pilot project on a part (approx. 540 m^2) from the Caland bridge in the N15 (main route Rotterdam harbour) was executed to test the logistic aspects on an actual small sized project before other more complex and much larger projects will be executed. In the short available time the whole project had to be executed including rerouting the traffic, removal of the asphalt concrete wearing course, inspection and repair of the deck plate and the application, sufficient curing and shot blasting of the HRUHPC overlay. Any delay in one of the disciplines would have resulted in a delay of the other disciplines and, therefore, a team of skilled site manager and engineers was on site during the whole job. After the removal of the asphalt concrete wearing course a tent was placed over the whole area to exclude problems with the weather conditions and to have the possibility to heat up the area. Despite earlier instructions and attention there was some miscommunication about the way how to connect the reinforcement, the dense reinforcement should be welded but was in the first place only bonded together. This resulted in a bending in the upwards direction of the prefabricated welded mesh reinforcement mats at the crossings after some passages with the small crane which was used to place the reinforcement. This resulted in a delay and it was also necessary to accept a curve in the reinforcement in mainly the middle of the two traffic lanes. Casting and placing with the use of a double vibration screed over the whole width of 6,7 m went well. An accelerator was added to speed up the reaction of the UHPC, thus making both the finishing- and the shot blasting procedure earlier possible with the low temperature. The UHPC surface was floated with single power floats almost directly after compacting the mortar, a few hours later power trowels were used to obtain a smooth, dense and shiny surface. Hereafter the whole surface was covered with burlap sheets and wetted with water. A compressive strength of minimum 30 MPa was reached in much less than 24 hours after casting, the burlap sheets were removed and the surface was shot blasted to gain the required skid resistance of at least 52 SRT. Immediately after the shot blasting procedure details like the joints with the adjacent lanes were made, special trucks were used to remove the tent and the barriers were placed and connected. A special perforated water hose system was placed under the barrier to cure the HPC overlay during a period of 7 days independently and without disturbing the traffic streams. The whole execution of the pilot project from the first step until re-use of the new wearing course took less than 120 hours!

The problems with the reinforcement resulted in a thicker and unreinforced cover (3 – 4 cm) on the reinforcement in the middle of the bridge deck. This resulted in an insufficient curing because the water from the hose system couldn't pass the slope. Very fine transversal cracks (<0,02 mm), concentrated in the thicker applied middle part, are visible each 30 – 100 cm. Modelling and more investigation will be made but possible reasons are: thicker applied, less reinforcement in the layer itself but also in the longitudinal direction (only 50% compared to the transversal), insufficient curing in the first 7 days and movements in the orthotropic steel deck plate. There is no shrinkage visible at the steel profiles at the edges.

Much is learned from the pilot project and this experience and know-how will be very useful for larger projects which will be executed in the following years. Strain measurements on the re-surfaced Caland bridge are showing a stress reduction in the trough wall of 60% compared to the traditional asphalt concrete wearing course and a stress reduction in the deck plate of 80% compared to the traditional asphalt concrete wearing course. This equals the stress reduction factor of 4 – 5 measured on the small test samples in the Adhesion Institute of the Delft University of Technology and the computer simulations. All the tests proved that the intended application of a HRUHPC is a very promising solution to rehabilitate orthotropic steel bridge decks to elongate the service life of the total structure. Durability, strength and placebility are giving enough confidence for larger projects during the next years.

3.2   Prefab bridge deck for the Kaag bridges

A very good example of the use and the potential possibilities of the C.R.C. principle are the prefab panels placed on the bascule bridges in the motorway N 44 in the Netherlands [23]. To replace the existing wooden bridge decks different alternative solutions were investigated by the Civil Engineering Division of the Ministry of Transport, Public Works and Water Management in the Netherlands. A solution with HRUHPC prefab panels was chosen as the best solution concerning costs, maintenance and durability within the maximum weight tolerance of the operating machinery. Different tests were made with the producer of the panels, Hurks Beton at Veldhoven, to control the workability of the UHPC in combination with the densely placed reinforcement and the necessary angle of heel. Test samples [24] and a test panel were made to be tested at TNO Building and Construction Research. The UHPC was supplied in pre-weighted big bags as a premixed Binder, aggregates and steelfibers for a batch of 900 litres. The chosen mix design was based on a UHPC as used for the last 10 years in the security industry with a good workability and a C180 (cube strength) with a low amount (200 kg 0,4 x 12,5mm) of steel fibers. Large aggregates (calcinated bauxite 3 – 6 mm) were used to create, in combination with the fibers, very rigid bodies between the main reinforcement. Mixing took place in a stationary planet pan paddle mixer with a total mixing time of 5 minutes. The UHPC was transported in a large concrete batch from the mixer to the location of pouring. After spreading the UHPC in the mould the mould was vibrated for less than a minute to secure a good compaction around the dense reinforcement, thus even when the UHPC can not be described as self compacting it flows extremely well due to the good lubricating effect of the binder. After finishing the surface of the UHPC, necessary because of

the high demands on the tolerance of the panels, a curing-compound was applied. After 24 hours curing the panels were shot blasted for the necessary skid resistance and cured under plastic foil.

Testing of two small panels in the lab from TNO Building and Construction Research resulted in amazement by the engineers present: "If you want to see concrete flutter look to this" and "Amazing how flexible a plate with these dimensions can be, you see the plate clearly bulge under the load". This project demonstrates on a small scale what is possible to reach with the HRUHPC: light, thin and ductile constructions with strength possible as that from structural steel.

4   New applications

By combining the HRUHPC with other materials large ceramic/ metal-based hybride structures can be made that exhibit unique combinations of great strength in all directions; great hardness and extremely great fracture toughness. This make it not only possible to design and build gigantic structures and extremely slender, elegant and daringly designed structures but also to make non-brittle ceramics for medical (implants and bone replacements) and industrial applications (tooling, pumps, engines). In nearly future the use of HRHPC will not be focused only on applications in civil engineering because the composite is also offering new solutions for other fields of application. Especially when the HRHPC is used in combination with other materials to produce new composite materials there are interesting solutions and applications possible. New applications are possible based on the research and knowledge which is developed during the project rehabilitation and restrengthening of orthotropic steel bridge decks. This experience can not only be used for developing a new type of orthotropic bridge deck and bascule bridge but can also be used to develop new applications like special floor slabs in high rise buildings, protective structures and offshore constructions. For the offshore special HRHPC braces cast in-situ can be developed to restrength fatigue critical areas like jackets and tubulars from offshore platforms and offshore windmills. Practical tests are already made to restrength and to protect platform jackets made from concrete as well as made from steel. Decks of offshore platforms and supply vessels can be restrength and protected against corrosion and impact with an HRUHPC overlay bonded to the original deck plate. Very large offshore windmills with a high fatigue resistance and a large service life can be built in HRUHPC [25]. An other possible and very interesting application of UHPC and HRUHPC is the replacement of the sliding steel gates in the Eastern Scheldt Storm Surge Barrier in the Netherlands [26]. The 62 sliding steel gates are composed of a vertical plate construction, a main girder system and a vertical girder system and have a width of 41,0 m¹ and a height (depending on the location of the piers) between 5,9 and 11,9 m¹. The replacement of the sliding steel gates will maybe be necessary in the nearly future because of the very high maintenance costs and the repeated application under special conditions of a special coating to avoid corrosion. An internal research project initiated by the Civil Engineering Division of the Ministry of Transport, Public Works and Water Management in the Netherlands shows that it is possible to replace the

existing sliding steel gates with HPC/HRUHPC gates within the maximum weight tolerance of the existing gate-operating machinery. The present design for the HPC/HRUHPC sliding gates consists of a HPC concrete for the girders and a HRUHPC for the plate construction (75 mm thick and reinforced with 3 layers ø8 - 50mm). Possible more weight reduction and additional strength can be reached by the use of high strength steel and/ or the use of carbon fibre- or other fibre reinforcement in the plate construction. Because the expected service life of the HPC/HRUHPC sliding gates will exceed the 100 years without additional maintenance it seems both practical and economical a very interesting solution. The HRUHPC can also be used to restrength constructions like columns, bridge piles, piers and bridge decks in earthquake sensitive area's by replacing a part (concrete cover, wearing course) of the existing construction thus without adding to much weight on the total construction. With the use of woven fabrics made from high tech fibers very thin and ductile panels can be made for different purposes like cladding, permanent formwork, prefab constructions and protective shelter constructions.

5   New material developments

The strength and properties of an UHPC will go in an upwards direction in the nearly future. With the much better available research equipment and computer modelling the microstructure can be investigated much better than before what will result in new developments including the incorporation of much more additives to control and to influence the properties of the matrix. Heavy reinforcement in different materials and different forms will be used on all material levels thus also to reinforce the microstructure of the matrix. Future HRUHPC will thus incorporate a wide range of materials from different sources in both the binder part and the reinforcement part.

6 Conclusion

During the last 10 years new applications are found for the use of heavy reinforced ultra high performance concrete and it seems that the C.R.C. concept starts to find its way between other composite materials and composite structures. HRUHPC offers new and sometimes exiting possibilities: lighter structures, larger structures, hybride structures, new design and new products with a potential for a better economy and resource consumption than with more traditional concrete, steel and other building materials. When designers, architects, engineers and structural engineers are more open for the "new concrete" and the "new technology" and are more willing to investigate and to innovate with the existing knowledge than much more can be achieved. To make use of the large potential for HRUHPC there must be a change of direction and a break with conventional practice to be able to understand the material properties and possibilities. For this it will be necessary that the industry will cooperate in a much better way with Technical Universities, institutes, governments and end-users and that knowledge and practical experience will be much more exchanged between those parties.

7 References

[1] Bache H.H. Densified cement/ ultra fine particle based materials. The second International conference on superplasticizers in Concrete. Ottawa, Ontario, Canada June 10 – 12 1981.

[2] Bache H.H. High strength concrete development through 25 years. CBL report no. 17. Cement- and Concrete lab. Aalborg Portland.

[3] Buitelaar, P. Ultra High Strength Concrete, Congresso del Concreto 1995, AVICOPRE, Caracas Venezuela.

[4] Buitelaar, P. Densit high performance concretes for very strong and dense concrete. (in Dutch). Cement 1992 nr. 11.

[5] Bache H.H. Compact Reinforced Composite. CBL report no. 39. Cement- and Concrete lab. Aalborg Portland.

[6] Bache H.H. Concrete and Concrete Technology in a Broad Perspective. CBL reprint no. 26.

[7] Bache H.H. Ny Beton – Ny Teknologi Beton – Teknik 08.04.92 CtO Aalborg Portland.

[8] Rossi, P. Ultra-High performance Fibre-Reinforced Concretes. Concrete International December 2001.

[9] Bache H.H. Principles of similitude in design of reinforced brittle matrix composites. International Workshop "High Performance Fiber Reinforced Cement Composites" Mainz, Germany, June 24 – 26, 1991.

[10] Aarup,B. & Jensen, B.C. Bond Properties of High-Strength Fibre reinforced Concrete. ACI-publication SP-180, Bond and development of Reinforcement, 1998

[11] Andrade, M.C. & Frias, M. & Aarup, B. Durability of Ultra-High Strength Concrete: Compact Reinforced Composite. BHP96 Fourth International Symposium on Utilization of High-Strength/High-Performance Concrete, 29 – 31 May 1996, Paris, France.

[12] Klinghoffer,O. & Aarup, B. Effect of Microcracks on Durability of Ultra High Strength Concrete. 4th International Symposium on Corrosion of Reinforcement in Concrete Construction. Robison College, Cambridge, 1 – 4 July 1996.

[13] Jensen, B.C. & Aarup, B. Fire resistance of fibre reinforced silica fume based concrete. BHP96 Fourth International Symposium on Utilization of High-Strength/High-Performance Concrete, 29 – 31 May 1996, Paris, France.

[14] Juvas, K. & Jumppanen, U.M. & Aarup, B. High performance Concrete at High Temperatures. Proceedings of Nordic Concrete Research Meeting, 3 – 6 August 1999, Reykjavik, Iceland.

[15] Buitelaar P. Ultra thin white toppings using high strength high performance concretes. (in Dutch). Cement 1999 nr. 7.

[16] Buitelaar, P., 2002. Ultra Thin Heavy Reinforced High Performance Concrete Overlays. 6th International Symposium on Utilization of High Strength / High Performance Concrete, Leipzig, Germany.

[17] Boersma P.D., de Jong F.B.P. 2003. Techniques and solutions for rehabilitation of orthotropic steel bridge decks in the Netherlands. Proceedings Structural Faults and Repair.

[18] De Jong F.B.P.,Boersma P.D. 2003. Lifetime calculations for Orthotropic steel bridge decks. Proceedings Structural Faults and Repair.

[19] Wolchuk, R., 2002. Structural Behaviour of Surfacings on Steel Orthotropic Decks and Considerations for Practical Design. Structural Engineering International 2/2002.

[20] Braam, C.R., Kaptijn, N., Buitelaar, P., 2003. Hogesterktebeton als brugdekoverlaging. Technologische-, constructieve- en duurzaamheidsaspecten (in Dutch). Cement 1/2003.

[21] Braam, C.R., Buitelaar, P., Kaptijn, N., 2004. Reinforced high performance concrete overlay system for steel bridges. 5 [th]. CROW workshop Istanbul, Turkey.

[22] Braam, C.R. *et al.* Research Contec Ferroplan 2002 - 2004. Research reports Stevinlaboratory, Delft Technical University. By order of the Civil Engineering Division of the Ministry of Transport.

[23] Kaptijn, N., 2004. A new bridge deck for the Kaag bridges. International Symposium on Ultra High Performance Concrete. Kassel, September 2004.

[24] Braam, C.R. *et al.* Research Contec B250 2002. Research reports Stevinlaboratory, Delft Technical University. By order of the Civil Engineering Division of the Ministry of Transport.

[25] K.L. Hansen, 2001. Offshore wind turbine towers in high strength concrete. European Wind Energy Conference and Exhibition, Bella Center, Copenhagen, Denmark.

[26] F. Bockhoudt, 2003. Concrete gates in the flood barrier (in Dutch). Cement 4/2003.

Part 2:

Recent Applications

Ziad HAJAR
Senior Project Manager

Daniel LECOINTRE
Deputy Head of Large Bridges Division

Alain SIMON
Project Manager
Eiffage Construction
Neuilly s/ Marne, France

Jérôme PETITJEAN
Project Manager
SETRA
Bagneux, France

Design and Construction of the world first Ultra-High Performance Concrete road bridges

Summary

The two bridges described in this paper have been realized within the context of an "innovation charter" set up for engineering structures and represent a world first for road bridges, and were completed in 2001. Their decks are 12 m wide; each is an assembly of five π-shaped precast beams made of UHPFRC. The beams are longitudinally pretensioned with bonded strands and are stitched longitudinally and transversally with the same concrete (cast in place).

The concrete used has a compressive strength greater than 170 MPa and a characteristic direct tensile strength of 8 MPa with a 3 % of volume fiber incorporation. Except in keying areas, the steel fibers ensure non–fragility and replace the reinforcing steel, especially for transverse bending behaviour where only the UHPC takes part.

This application required to settle special calculation methods and design rules which are not currently covered by codes with the type of concrete employed. These rules where finalized in close collaboration with recommendations of a working group on UHPCs.

Keywords: *Fibre, Prestressed Concrete, Precast Beam, Direct Tensile Strength*

1 Background to the operation

The bridges discussed in this article are overpasses on the Bourg-lès-Valence bypass in France's Drôme region (south-east). They are road bridges made from ultra-high-performance fibre-reinforced concrete (UHPC), each with two spans of about twenty metres and completed in 2001.

These bridges are a world first, given that UHPC has previously been used only for footbridges and for beams in the cooling towers of two French nuclear power plants.

The Owner of the bridges is the French Government, represented by its Regional Department of Public Works for the Drôme district which also oversaw design and construction with the assistance of two more government agencies, the Service d'Etudes

Techniques des Routes et Autoroutes (SETRA) and the Centre d'Etudes Techniques de l'Equipement (CETE) of Lyon.

The bridges were built by contractor Eiffage Construction after a performance-based invitation to bid drawn up under an "Innovation Charter" signed by the National Roads Department and the National Public Works Federation. This charter aims to promote innovation in the field of bridges, cut-and-cover tunnels, and retaining walls.

2   Bridges description

2.1   Supports

Supports (pier and abutments) are of conventional design and are made from C30 reinforced concrete. The foundations are shallow (Figure 1). Each line of bearings has 10 blocks receiving tapered shims beneath the flanges of the beams in order to adjust the level of the deck. Each bearing block has a jacking base on either side to enable the bearings to be replaced by jacking against the crossbeams to raise the deck.
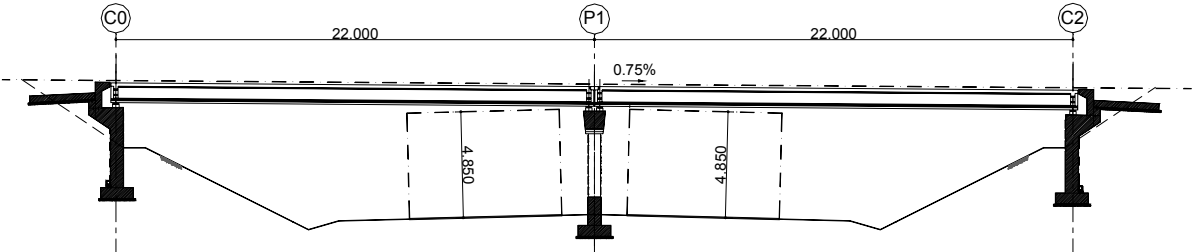
Figure 1:   Longitudinal cross-section of OA4

2.2   UHPC Decks

The structure is based on a conventional overpass design using prestressed beams with a continuity slab at central pier. Each deck supports a 9 m wide road pavement with 1 m and 2 m wide footways (Figure 2). Transversally both decks are identical; they are made from an assembly of five π-shaped precast beams made from Béton Spécial Industriel (BSI) concrete. The beams are cross-braced at the supports only.
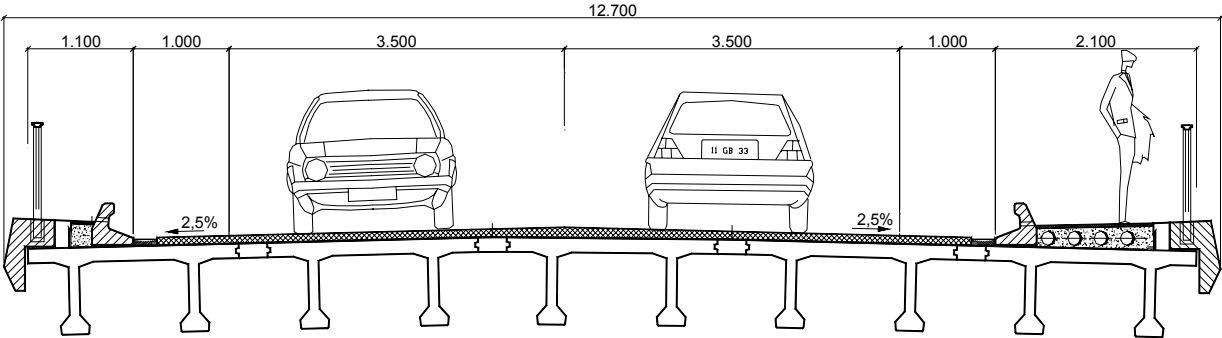
Figure 2:   Standard cross-section

Beams dimensions are :
- length : 20,50 m and 22,50 m
- height : 0,90 m
- width : 2.40 m
- web thickness : 11 cm
- weight : 37 tons

The π-shaped beams were also jointed together longitudinally with in situ UHPC. All the beams are prestressed by pre-tension, using very low relaxation T15 Super strands of strength class 1860 MPa. Each beam of the OA6 bridge has twenty-six strands, with thirty in the beams of the OA4 bridge. There is no transverse prestress.

In addition, the BSI beams have no passive reinforcement, except where components are jointed together transversally or longitudinally and where equipment (pavement joints and safety barriers) is attached.

The equivalent thickness of the deck is 0.25 m, compared to 0.75 m for a conventional prestressed slab bridge and 0.37 m for HPC decks. Use of UHPC therefore divides the selfweight of the beams by about 3.

3   BSI concrete

BSI concrete is a UHPC whose mix design is principally characterized by a high cement content, use of silica fume and small-diameter aggregate, and a low w/c ratio (Table 1).

Table 1:   Mix design

cement	kg/m³	1114
silica fume	kg/m³	169
0 - 6 mm aggregate	kg/m³	1072
fibres	kg/m³	234
superplasticizer	kg/m³	40
water	kg/m³	209
w/c ratio		0.19

Large quantities of steel fibres are used (3% by volume for the Bourg-lès-Valence bridges) in order to give the concrete good ductility under tensile stress and, in most cases, to dispense with the need for passive reinforcement.

The fibres used are straight (20 mm long, 0.3 mm diameter) and work by bonding with the cement matrix. They are made from high yield steel (σ_e = 1200 MPa).

The rheological behaviour of fresh BSI is rather special: it is a viscous fluid and is self-levelling, with slump flow of 64 cm with the DIN cone and no vibration of the table. This means no vibration is necessary to work the concrete into the forms.

Its practical working life can be adapted to suit the requirements of the works. For example, the BSI used for jointing the Bourg lès Valence bridges had to have a working life of at least one hour to cover the time for transport and placement.

After 28 days, without heat treatment, the BSI for this project had the following characteristics:

Table 2:   Characteristics of BSI

28-day characteristic compressive strength	175 MPa
28-day characteristic direct tensile strength of the matrix	8 MPa
28-day characteristic post-cracking direct tensile strength	9.1 MPa
Modulus of elasticity	64 GPa
Density	2.8 tons/m^3

This data was complemented by tests to characterize post-cracking tensile behaviour by measuring crack widths (direct tensile-strength test on notched cylinders or centre-point flexural tensile strength test with notched prisms) in order to determine a complete law for structural design purposes (Figure 3).
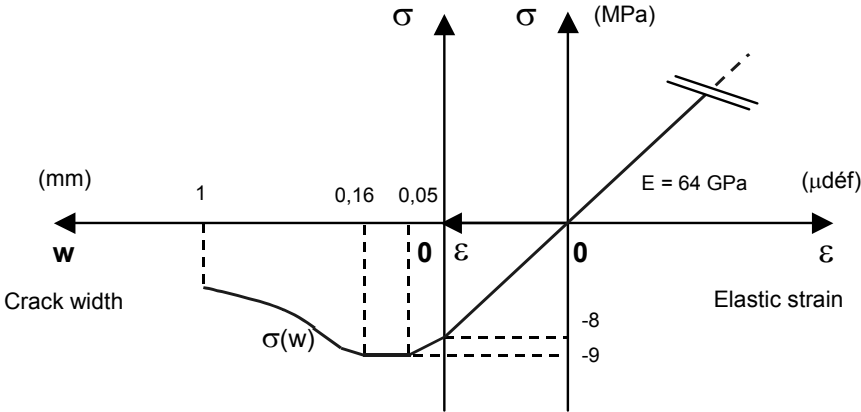
Figure 3:   BSI constitutive law

4   Design verifications

4.1   Longitudinal bending

For Serviceability Limit States (SLS) the verifications under normal stresses are similar to the french BPEL specifications [1], for conventional prestressed concrete.

For Ultimate Limit States (ULS) the ultimate resistant moment of cross-sections was calculated in accordance with the BPEL rules, with a conventional program for design of cross-sections, taking a perfect elastoplastic law for compression and overlooking the concrete's tensile strength.

4.2   Transverse bending

The verifications for transverse bending are somewhat different, given that in this case there is no passive or active reinforcement other than the steel fibres.
Tension in the concrete is limited to 8 MPa for rare SLS combinations, and to 6,4 MPa for frequent combinations. At Ultimate Limit States the resistance moment is calculated in accordance with the AFREM recommendations [2], taking account of the constitutive law of

the cracked concrete. This resistance moment of the cracked section is calculated with a special program using a discretized approximation of the constitutive law for the actual tensile behaviour of the material and reflecting the equilibrium of the cracked section.

4.3 Verifications for tangent loading

For the longitudinal behaviour of the prestressed beams, the verifications of SLS shear stresses were carried out in accordance with the BPEL rules.

For the transverse and longitudinal behaviour of the bridges, the verifications of ULS shear force were carried out with, in addition to the BPEL rules, the strength added by the fibres, calculated as per the AFREM recommendations.

4.4 Verification of prestressing transfer length

In order to limit bursting and general stress distribution effects in the beam end blocks, and to avoid any cracking in the prestress transfer length, the ends of some of the strands were sheathed. Three sheath lengths (2.2 m, 3.5 m, and 5.5 m) were used to allow a progressive transfer of prestressing forces.

5 Validation by testing

Before the bridges were built, a test campaign was undertaken to validate the assumptions used for deck design and to verify the behaviour of the concrete at the scale of the actual structure. This campaign comprised the following tests:

- Construction of a beam test component to check that there are no problems with prestress distribution and for new concrete characterization testing (flexural tests on sawn prisms taken from the actual structure, as recommended in [3]).

- Flexural tests on full-scale slabs in order to validate the transverse bending behaviour of the deck:
    - Flexural test on a monolithic slab,
    - Flexural test on a slab with a construction joint, to represent the longitudinal jointing between precast beams.

5.1 Test component

A 5 m long test component (Figure 4) was made in the same way as the beams made for the bridges.

Two arrangements for spreading out prestressing tendon anchorage were tested. The test was conclusive, in so far as no stress-distribution cracking was observed at the ends of the element. To study the combined effect of the form and concrete placement on the distribution

of fibres, test prisms were cut at different angles and at different locations in the web and upper flange of the test component. The prisms were tested in centre-point bending, with a notch downwards, with recording of mid-span crack width.

The mean curve for the tests carried out on prisms sawn from the flange of the beam was in perfect accordance with that given by theoretical calculation based on the constitutive law for the concrete, weighted by a coefficient reflecting the effect of sawing on the efficiency of fibres near the edges.

5.2   Flexural tests on slabs

Two flexural tests were carried out on slabs (Figure 5).   The dimensions of the slabs matched those of the flange of the beams: 15 cm thick, 1.15 m long (distance between the webs of the beams). They were made 40 cm long to limit edge effects on fibre distribution.

The third-point bending tests were displacement controlled (mid-span deflection) and taken to rupture of the test specimen.

Comparing these test results with the action effects taken into account in verifying the design of the bridges, it can be seen that there is a quite comfortable safety margin.

The bearing capacity of the monolithic slab and of the jointing zones were therefore more than adequate, and their behaviour were perfectly satisfactory.

Figure 4:   Test component
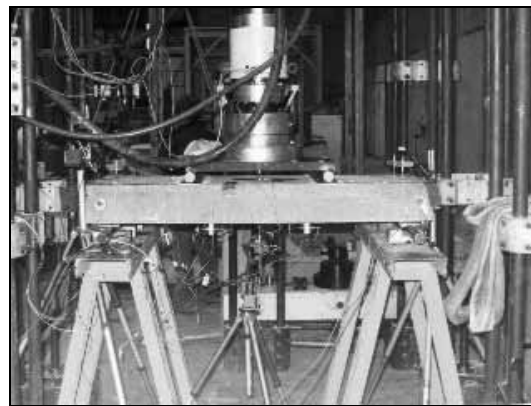
Figure 5:   third-point bending test

6   Precasting beams

The beams were cast at the plant of Dutch precaster Hurks Beton whose workforce had already built up sound experience with BSI concrete when making the beams for the Cattenom and Civaux power plants. The 20 π-beams were precast in 2 months (2-day manufacturing cycle for one beam).

BSI is completely self-compacting, even with a fibre content of 3%, so concreting is a simple, quiet operation (which is very appreciated by workforce in factory). The only condition of success is the control of the behaviour in a fresh state. The important duration (15 minutes) of mixing imposes a rigorous procedure of placement method.

Operations carried out after concrete placement were governed by maturity measurement: Setting is controlled under 20° saturated atmosphere, therefore without heat treatment. Full form removal and prestressing of the beam were made when the BSI was about 40 hours old, with a compressive strength of 120 MPa.

With these procedures, the level of reproducibility for the different beams was good; this was subsequently demonstrated by the fact that there was no significant deviation of mid-span deflection (< 5 mm).

7   Beam erection and jointing

The 20 beams for the two bridges were transported to the site by rail and road.

7.1   Beam erection

A truck-mounted crane was used to hoist the beams into place on top of the conventional concrete piers and abutments.

Placement of the 10 beams of the first bridge (OA4) took a little over 2 days whereas, benefiting from experience, those of the second bridge (OA6) were placed in just half a day (Figure 6).

The beams rest on concrete bearing blocks with neoprene bearing pads, on top of which are placed tapered shims to obtain the required crossfall.

7.2   Jointing

BSI joint slabs were cast between the main beams to make each deck as monolithic as possible. A ready-mix batching plant was chosen for making the "in situ" BSI.

The complete procedure for batching at the plant and transporting to the site by truck mixer (about 15 minutes) was validated before the works started. A campaign of suitability tests served to adjust the production parameters and check that the BSI produced met the stipulated requirements.

The stages in site production of the BSI were identical to those for precasting (cf. chapter 6.2). Because of the parameters of the mixer at the ready-mix plant, each batch was only 750 litres and the cycle took about 20 minutes.

The BSI was inspected (rheology, temperature, air content) and tracing samples taken before each truck mixer left for the site.

After verification of the conformity criteria, the concrete was transported to the site with the drum turning at a speed determined during the suitability tests. This was done to prevent segregation of the mix that might have been caused by too great a centrifugal effect.

The longitudinal joint slabs between the main beams were shuttered by panels suspended from the deck (Figure 7), which meant no scaffolding was necessary. Special attention was paid to the leaktightness of the forms.

Figure 6:   Erection of a precast beam   Figure 7:   Joint slab
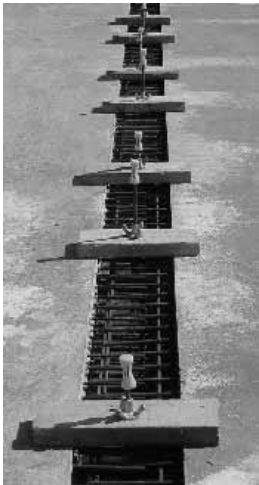
8   Conclusion and new applications

The innovative structures at Bourg-lès-Valence, the first road bridges built of UHPC, are already a reference allowing more general use of these new materials.

At the end of 2002, approximately two years after beams manufacture and one year after the opening to traffic, a detailed inspection of the bridges was carried out. No water seepage or cracks have been noticed on the beams.

The publication of the Interim Recommendations on UHPC [3] gives future Operating Authorities a reference to use in establishing their specifications and engineering firms a starting point for their design calculations.

Figure 8:   View of completed bridge

However, while these conventional bridges with small spans have served to validate the performance of the material, they have not yet revealed all the freedom and daring in design UHPCs make possible.

The toll-gate of the Millau Viaduct, currently under construction, which will have an elegant roof based on a thin Ceracem® (ex-BSI) shell, is the next step in the development of this new material.

This roof will look like an enormous twisted sheet of paper, 98 m long and 28 m wide, with a maximum thickness of 85 cm at centre (Figure 9). Its alveolate structure will be like an aircraft wing and will be made of match-cast prefabricated segments, 2 m wide, connected together by an internal longitudinal prestressing. In all, 1,000 m^3 of Ceracem® will be used, weighing a total of about 2,800 tons.

Figure 9:   View of Millau Viaduct toll-gate

9 References

[1] BPEL 91 révisé 99 (1999) Règles techniques de conception et de calcul des ouvrages et constructions en béton précontraint suivante la méthode des états limites. Fasc. 62 (Titre premier, section 2 du CCTG), avril 1999

[2] AFREM – BFM (1995) Recommandations sur les méthodes de dimensionnement, les essais de caractérisation, de convenance et de contrôle. Eléments de structures fonctionnant comme des poutres, décembre 1995.

[3] SETRA – AFGC (2002) Ultra High Performance Fibre-Reinforced Concretes. Interim Recommendations, January 2002

[4] G. BIRELLI, G. CADORET, F. DUTALLOIR, T. THIBAUX (2000) A new, very high performance concrete , International symposium on high-performance and reactive powder concretes, Sherbrooke (Canada), August 2000.

N. Kaptijn
Ing, senior research engineer
Ministry of Transport, Public Works and Watermanagement
Tilburg, The Netherlands

J. Blom
Ir, Project engineer
Ministry of Transport, Public Works and Watermanagement
Tilburg, The Netherlands

A new bridge deck for the Kaag bridges
The first CRC (Compact Reinforced Composite) application in civil infrastructure

Summary

An existing azobé wood bridge deck was replaced by ultra high strength concrete (cube strength 180 MPa) panels. This concerns 2 bascule moving bridges in the number 44 motorway near Sassenheim, The Netherlands. The longitudinal steel girders are 685 mm apart.

Each bridge deck consists of 4 panels 7,25 x 2,95 m. In order to keep the maximum weight under 170 kg/ m^2 the CRC principle was used. This means very slender ultra high strength concrete construction parts combined with a high percentage of reinforcement. In this case the panels are 45 mm thin with 3 layers Ø8-40 mm reinforcement (5.6 %). The edges are 65 mm thin with 10% reinforcement.

Keywords: *CRC, bridge deck, bascule bridge, prefabricated panels*

1   Introduction

In november 2002 the new bridge decks for the Kaag bridges were brought into use. It concerns the replacement of azobé wood bridge decks (115mm thick beams, 320 mm wide) by concrete panels (45 mm thick, 7,25 m wide and 2,95 m long at the most) of equal weight per square meter. The decks are mounted on the bascule moving bridges in the number 44 motorway over the Kaag near Sassenheim, The Netherlands.

Each bridge has 2 main longitudinal girders and 4 transverse girders. Longitudinal girders (axle distance 685 mm) are mounted on the transverse girders. The bridge deck is mounted on the longitudinal girders.

Since long wooden bridge decks are used for movable bridges.They are finished with an epoxy/ gravel wearing course.

Suitable wood is hard to get nowadays. It has to dry longer than 6 months to reduce unwanted shrinkage. A wooden bridge deck needs quite some maintenance; fastening bolts have to be checked and secured every year and wearing courses are damaged after a short period of time. The deck has to be replaced after not much longer than 15 years. This leads to traffic jams which are more and more unacceptable.

The Civil Engineering department investigated wether there are possible alternatives: an improved wood concept, aluminium, fiber reinforced plastics and Ultra High Strength Concrete C155/180 (prism/ cube strength). UHSC turned out to be the best solution concerning costs, maintenance, durability and sustainability.

In most cases UHSC is used without reinforcement [1]. This is costs saving and allows for the construction of very slender constructions. Large spans have to be pre or post tensioned. Bache [2] already showed in the nineteen eighties that special advantages can be gained by applying very dense reinforcements (up to 20%!) and high volume percentages of steel fibers (up to 6%). This principle is named CRC – Compact Reinforced Composite.

The strong matrix – together with the steel fibers – make a good cooperation with the reinforcement. This effect will even be stronger when using small bar diameters at small bars distances.CRC construction parts are very ductile, durable and slender. They are very impact and fatigue resistant.

High fiber and reinforcement percentages can deliver high equivalent bending strengths at ultimate limit state : up to more than 200 MPa.

2   Concrete

Because in this case the concrete structure had to be as light as possible, and because high demands were made on fatigue resistance, a CRC solution was the only possible one.

For the concrete Contec Secutec S9 was chosen, a mixture of CEM III 52,5, silicafume, bauxite 0-1 and 5-8 mm, steel fibers 0,4x12,5 mm, superplasticiser, air detraining agent and a water/ binder ratio wbr=0,18.

The concrete cube strength was over B180. This was sufficient to achieve the desired construction strength. B200 and higher can be gained by using more steel fibers and a lower water binder ratio. Hardening takes place under atmosferic pressure and at 20ºC. After 1 day the compression strength is about 90 MPa.

3   Production of the panels

Hurks Beton at Veldhoven was chosen to produce test specimen and bridge deck panels. This because of their provable experience with the production of UHSC prefabricated elements (BSI B180).

The mortar can be placed very easily (a 'thick yoghurt' like consistency) and it flows easily around the dense reinforcement (figure 1). The 45 mm thin panel is set up as follows (from bottom to top): a 9 mm concrete cover, 3 reinforcement layers ø8-40 and a 10 mm cover (3 layers ø8-40 need about 26 mm space, figure 2). The panels need stiffening along the joints in order to bear the edge moments. The thickness is 65 mm with a 5ø12-40 top reinforcement and a 5ø16-50 bottom reinforcement.

In order to get a good compaction of the concrete and good adhesion from the matrix on the reinforcement it was sufficient to vibrate the reinforcement for about 5 seconds and, after completing the moulding, to vibrate the mould for half a minute.
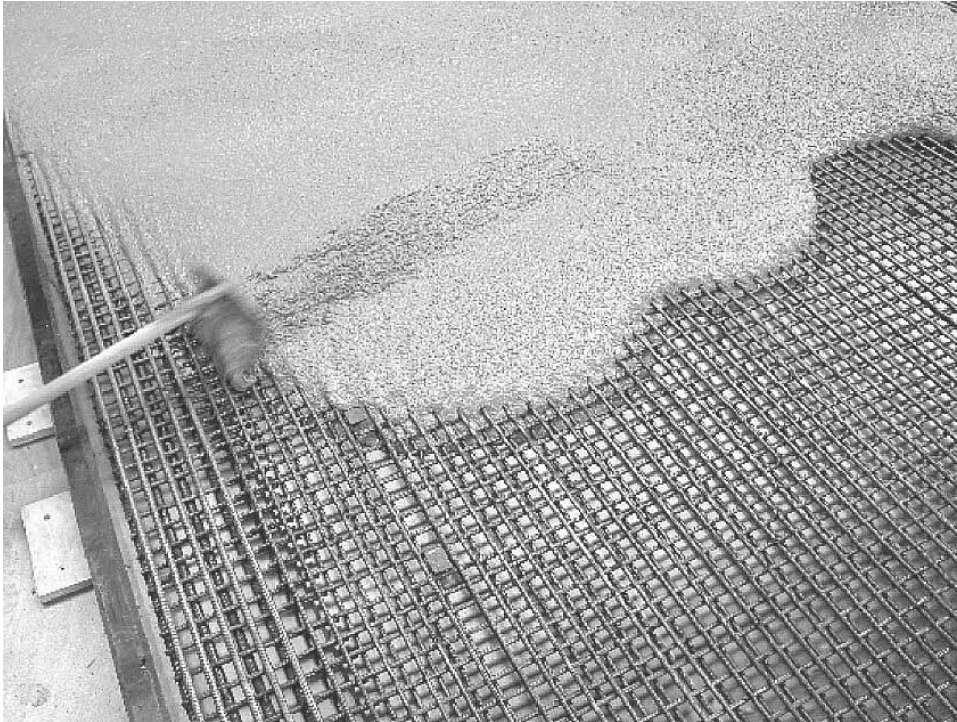
Figure 1:   casting of the bridge deck panels
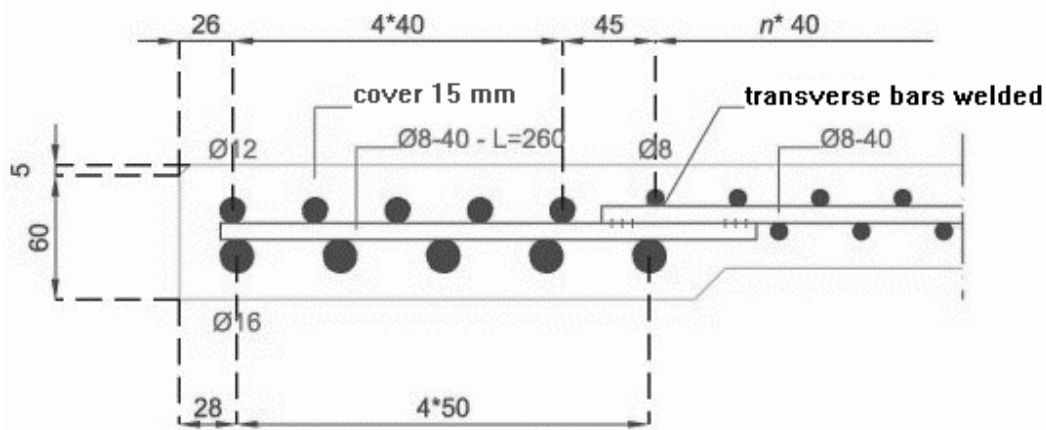
Figure 2:   reinforcement in the panel (5,6%) and in the edge stiffening (10%)

The top surface was leveled with a double pneumatic vibrating screed. It is often used to level high quality industrial floors. The desired skid resistance was achieved by shot blasting the top surface. No additional finishing will be applied (no wearing course).

It is clear that very high demands are made of the measurements of the concrete and the placing of the reinforcement. Tolerances are 2 mm at most.

The volumic weight of the concrete is 2850 kg/m^3. When including the reinforcement, the weight is 3350 kg/m^3. The panels weigh 170 kg/m^2.

4   Material properties

No material properties were available because there was no experience using the panels described. Because the possible mix compositions, the amount of steel fibers, the amount

and configuration of the reinforcement, the thickness of the panel, etc can vary depending of the application, it is difficult to determine a set of material properties before all these parameters are known. Properties can vary, depending upon the design of the section.

A test program was set up with Delft University of Civil Engineering [3] to determine the bending tensile strength of reinforced and unreinforced panels with different thicknesses (50, 100 and 150 mm). No thickness dependency was found. The RILEM test procedure was used [4].

The tests executed correspond with the experiments done for the Contec Ferroplan application described in [5]. The derived design strengths are reflected in figure 3.
The low tensile strength in the post cracked phase is a result of the large scatter in the test results. For the application described, the tensile strength is of minor importance. The reinforcement can easily carry all tensile forces. The steel fibers contribute only 7% towards the ultimate limit moment capacity. For applications where the tensile strength is of more importance, more steel fibers have to be used.
In this case the steel fibers contribute towards a good ductile behaviour of the compression zone, a denser cover, a smaller crackwidth and good fatigue resistance properties.

Stress MPa	Strain ‰
-128	-3,50
-128	-2,00
5,3	0,09
1,8	0,34
0,9	25,00
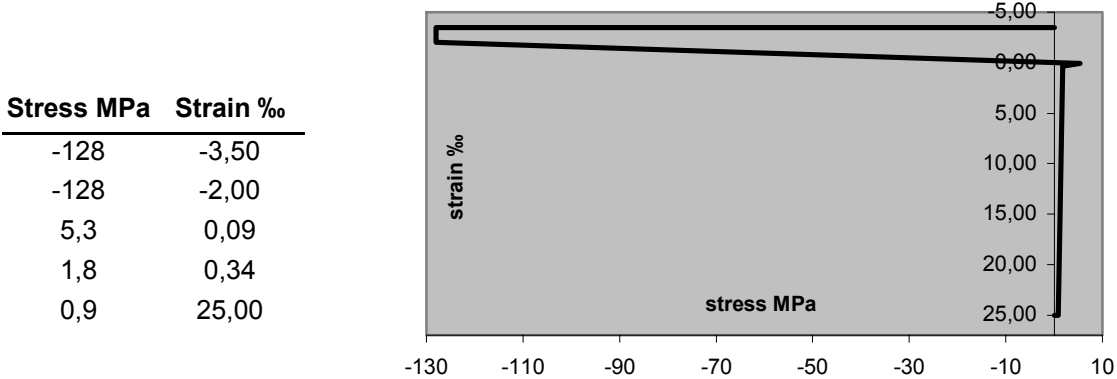
Figure 3;   stress/ strain diagram for concrete (design strength)

CRC does not work differently from ordinary reinforced concrete. Tension is carried in the reinforcement after cracking of the matrix. The crackwidths caused by the Eurocode model 3 loads are less than 0,03 mm in the 45 mm part and 0,05 mm in the edge stiffening. The crack distance is only 40 mm, one crack at every bar location.
Neglecting the post crack concrete tension strength causes a minor underestimation of the strength of the concrete part considered.
The mean equivalent tension strength is 112 MPa in ultimate limit state.

Shear tests were also performed. It was not possible to measure the ultimate limite state for shear. All panels collapsed in bending; the minimum shear force slenderness possible was 1,89. The mean shear tension was 17 MPa, the effective height was 31 mm.

The very small concrete cover is possible because of the extreme impermeability of the concrete. The diffusioncoefficient for chlorides for instance is a factor 50 smaller than that from a B55 blast furnace slag cement concrete, which in turn is a factor 50 smaller than that from a B55 portland cement concrete. Exposition tests of similar concretes in wetting/ drying cycles (3,5 % (volume) NaCl) during several years could not cause a chloride profile in the concrete cover apart from the outer 1 – 2 mm, even in permanently cracked concrete.

5 Loads

The wheel loads from the ENV 1991-3 *Traffic loads on bridges* were applied. This applies a 200 kN wheel load (wheel print 350x600 mm) anywhere on the panel.

Fatigue was dominant. The panels had to be tested for $125x10^6$ loadcycles in 50 years for wheelloads up to 90 kN, φ_{impact} = 1,3 included. This loading was derived from the actual traffic intensity (load model 5).

TNO BOUW did fatigue tests on two test panels. The second panel was supported similar to the situation on the bridge(figure 4).The behaviour was as predicted, more than $10x10^6$ cycles (0 <-> 78 kN), maximum stress in the reinforcement 151 MPa.
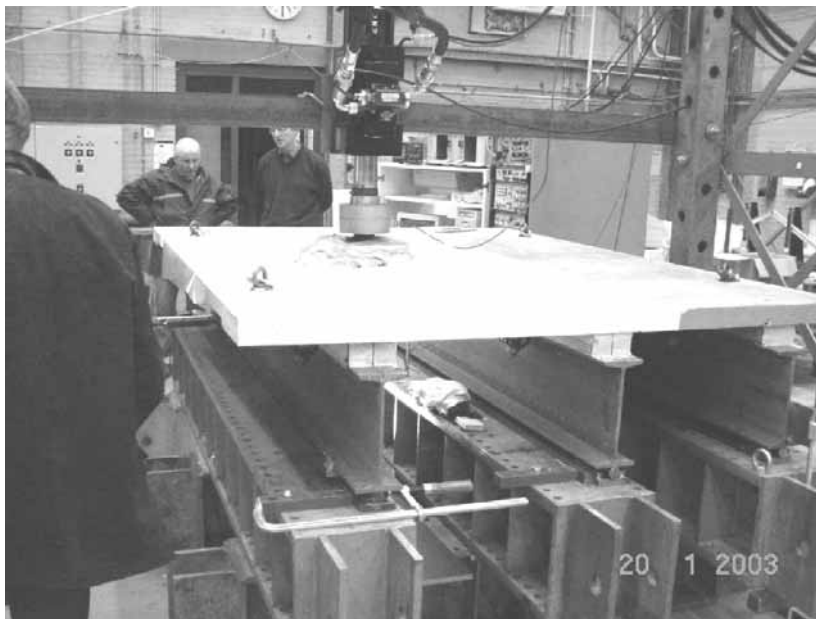
Figure 4:   fatigue testing at TNO BOUW

Figure 5:   laying down the panels with a vacuum lifting boom
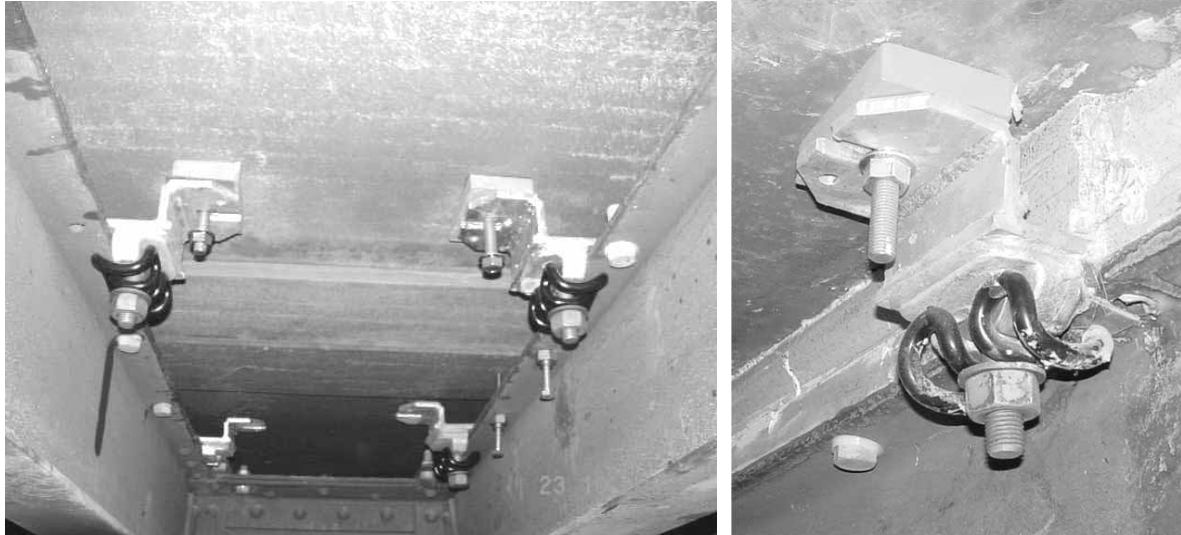
Figure 6: fixing of the panels on the steel girders. Note the bolts on the right(left photograph) for height adjustment of the panel edges. The right picture shows the gap between upper flange and the panel filled with polyurethane.

6 Assembly

The panels (maximum weight 3,5 tons, figure 5) were placed on the steel girders with a vacuum lifting boom. The exact height could be adjusted with 4 bolts in each (long) panel edge (figure 6). The space between the panels and the braces was filled with steel plates. The braces were then fixed with threaded bars screwed into the anchor sleeves that were cast in the panels. The braces are clamped to the steel flange with railway sleeper clamps. This ensures a more or less flexible connection.

Finally formwork was placed between the steel flanges and the panels. Polyurethane filled with cork particles was pumped into the formwork. This formed a good stiff support for the panels. The polyurethane filled up the spaces between bolt heads, iron connection plates, etc.

7 Life cycle costs

Table 1 shows an indication of the life cycle costs (price level 2002; discontinuity index 4%) over 50 years life. The wooden deck has to be replaced every 17 years. The wearing course has to be replaced every 7,5 years.

Concrete, fiber reinforced composite and aluminium have a 50 years lifespan.

The concrete has to be sandblasted every 17 years. The composite and aluminium get a new wearing course every 17 years.

Concrete proves to be the most economic alternative as for building costs as well as life cycle costs.

Table 1:   life cycle costs indication in €

	azobé wood	concrete	FRC	aluminium
Buildingcosts	930	910	1310	1430
Replacing deck	700	-	-	-
Replacing wearing course	200	30	60	60
Total	**1830**	**940**	**1370**	**1490**

8   Evaluation

The replacement of the decks was completed within a week. This is much faster than the time needed to replace a set of wooden decks (2-3 weeks).

The panels have been in use for 18 months (march 2004) and behave as expected.

The cost of the braces/ railway sleeper clamps and the pulyurethane filling was about 1/3 of the total building costs. It is possible to make a considerable cost saving here.
The PU filling could be replaced by hakorite or polyethene strips glued to the bottom of the panels. A good connection to the girder flange can be achieved by placing the strips on a 10 mm thick epoxy layer. This also speeds up the assembly of the panels.
The braces can be replaced by simple flat steel plates attached to PE blocks.
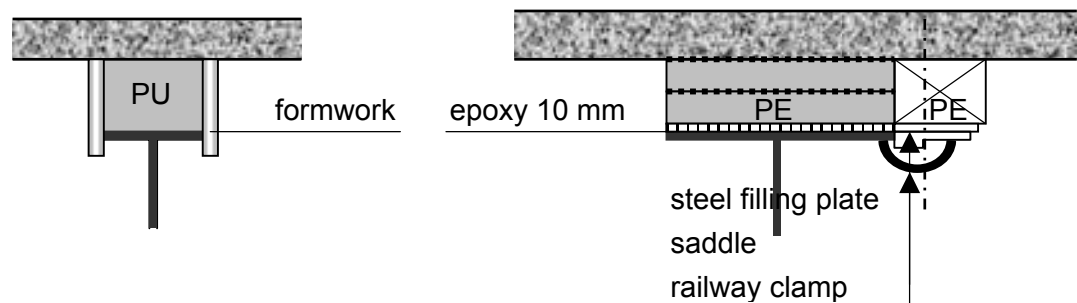
Figure 7:   the applied panel support (detail left); polyurethane pumped between (labour intensive) formwork. And the proposed alternative (right); polyethene strips glued to the bottom of the panel

Further cost savings (and a small weight reduction) can be achieved by using a C110/130 concrete instead of the C150/180 concrete used here.
Calculations for a bridge deck project with steel girders 900 mm apart (flange width 300 mm) showed that a panel thickness of 50 mm is possible for Eurocode loads (heavy traffic on a busy motorway).

Additional weight savings can be achieved by using fibre reinforced reinforcement; upto a maximum of 30 kg/m^2 bridge deck. Additional research is necessary because of the current lack of adequate experience. Better fatigue resistance can be expected because of the improved fatigue properties of fibre reinforced reinforcement.

9   Literature

[1]   Kaptijn, N., Future developments for ultra high strength concrete, Cement 2002/2 p 56 (in Dutch)

[2]   Bache, H.H., Ny beton - ny teknologi, Aalborg Portland, Aalborg Denemarken, 1992 (in Danish, English translation available)

[3]   Braam, C.R., A. Bosman, E. Horeweg, R. Mulder, A. van Rhijn, F. Schilperoort Contec B250, research reports Stevinlaboratory, Delft Technical University, summer 2002 (in Dutch)

[4]   RILEM TC 162-TDF: Test and design methods for steel fiber reinforced concrete, Materials and structures, end 2002.

[5]   Braam, C.R., Kaptijn, N, Buitelaar, P., Reinforced high performance concrete overlay system for steel bridges, Cement 2003/1 (in Dutch)

Dr. Urs Maeder
Product Technology Manager
Sika Technology AG
Zürich, Switzerland

Joel Chaignon
Technology Center Manager
Sika France
Gournay, France

Dr. Isabelle Lallemant-Gamboa
Research Engineer
Sika France
Gournay, France

Jean-Pierre Lombard
Lab Manager
Sika France
Gournay, France

Ceracem, a new high performance concrete: characterisations and applications

Abstract

Several years ago, a new generation of concrete, the ultra high strength fibre-reinforced concrete has been introduced. SIKA has developed a range of products based on such new technology, called CERACEM, in the frame of a partnership with the EIFFAGE company in Paris, France.

CERACEM has the advantage of being both self-compacting and ultra high-performance material. As it is self-compacting and as it does not need any further heat treatment, it bears several advantages on the job site, like faster setting and hardening, less noise and harmless to the workers due to the use of vibrators. With this type of concrete, it is possible to reduce or eliminate passive reinforcement and the thickness of the concrete elements can be reduced, which results in material and cost savings.

CERACEM is the result of an optimisation of the nature and the composition of different raw materials. It is composed of a premix, a new superplasticizer, fibres and water. The fibres can be either metallic or synthetic

A new type of Polycarboxylate-ether (PCE) of superplasticizer was found to combine strong water reduction with reduced set retardation and modifying the rheology of the paste in a way, that the fresh concrete becomes self-compacting.

Numerous investigations have been carried out with CERACEM such as plasticity, workability time, compressive strength, flexural strength, shrinkage, carbonation and porosity.

The CERACEM described in this paper was used for the casting of the tollgate roof of the viaduct at Millau, Southern France. This structure is part of the A71 motorway from Clermont-Ferrand to Montpellier. This shell with both structural and aesthetic properties is composed of about fifty precast elements of dimension equal to about 28 x 2 x 0.01 m, all made with CERACEM concrete.

1 Introduction

A new generation of concrete, the ultra high strength fibre-reinforced concretes have been introduced several years ago. The company EIFFAGE began to develop this type of concrete in 1996 under the name BSI. A French and an European patent was registered by EIFFAGE respectively in 1998 and in 1999 [1], [2], [3]. Since the year 2000, SIKA has developed in the frame of a partnership with EIFFAGE a range of products based on this new technology based on similar raw materials and with very similar mechanical and durability characteristics, called CERACEM. CERACEM is both ultra high performance fibre-reinforced concrete and self-compacting concrete. It does not need any further heat treatment to get it's design strenght. The CERACEM product range is the result of an optimisation of the nature and the composition of different raw materials. It is prepared out of a premix to which during the mixing the water, a specific Superplasticizer and fibres are added in well defined proportions. The premix is composed of a selected cement, silica fume, aggregates (0 to 7 mm) and admixtures. It is produced and controlled by SIKA.

A new type of CERACEM, and therefore notably a new premix, was developed in order to comply with the specifications for the tollgate roof of the viaduct at Millau, a project managed by EIFFAGE. In this paper, we present the technical characteristics and properties of this new material and its main application to date.

2 Materials

Premix

After carrying out feasibility and formulation studies to meet the contractor's requirements, extensive rheological, mechanical and shrinkage characterisations were carried out with this new material.

- Premix: 2355 kg/m^3
- Superplasticizer: 44.6 kg/m^3
- Water: 195 kg/m^3 (W/C = 0.22)
- Metallic fibres: 195 kg/m^3 IFT Unoloc 20/0.3

Superplasticizer

While concrete with normal requirements can be produced using traditional superplasticizers like Naphthalenesulfonate, Vinylcopolymers or Melamine sulfonate, the high requirements of special concretes and in particular SCC requires the use of special polymers.

Among these special polymers the polycarboxylate-type superplasticizers have become the most widely used within the last few years.

The molecular structure of the new polymers differs completely from conventional ones. [4].

The traditional polymers consist of long main chains carrying negatively charged side groups. These polymer adsorb strongly onto the surface of the cement grains and the ionic groups exert an electrostatic repulsion that prevents particles coming too close together.

The new polymers on the other hand typically feature short principal chains (backbone) containing ionic functions and very long polyether type side chains, that can separate particles by strong steric repulsion.

Considering the manifold properties of a polymer like molecular weight of the whole polymer, backbone or side chains, ionic strength, chemical composition or production conditions an extraordinary variety of special performing polymers is feasible. [5].

3 Properties

Plasticity

To characterise the behaviour of the fresh concrete CERACEM BFM-MILLAU, plasticity measurements were carried out in accordance with the European standard EN 12350-5 but without tapping (flow cone). The typical results are given below.
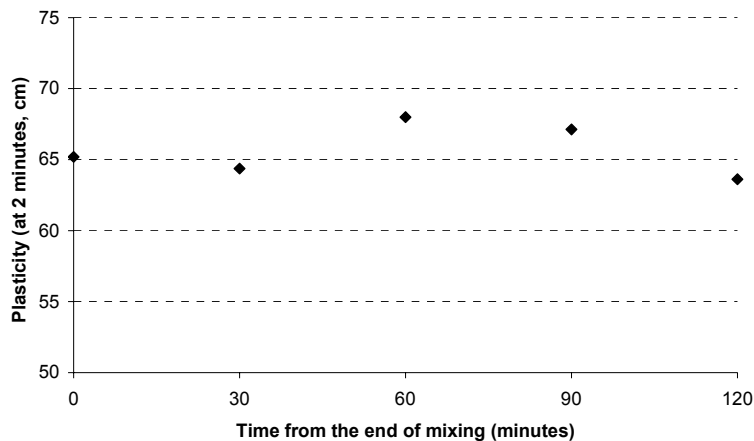
Figure 1:   Typical plasticity versus time

For the CERACEM BFM-MILLAU, the workability time is up to two hours. The nature and the content of the superplasticizers used allows to obtain an excellent workability time and to reduce the water dosage to obtain good mechanical strengths at the same time. The increase in workability with time is due to a specially designed polymer, which alters its functionality during the storage of the concrete . The air content of the material is less than 3.5 % and its density is equal to 2814 kg/m^3.

Compressive strength

Compressive strength measurements were carried out after 1, 2, 7 and 28 days respectively on cubs of 10 by 10 by 10 cm (three cubes per age). The samples were demoulded after 24 hours and were kept in water at 20 °C until they were crushed. The typical values obtained are illustrated in figure 2.

The compressive strength values after 2 and 7 days represent respectively 60 and 80 % of the

compressive strength value after 28 days. After 6 months, the compressive strength value is equal to 227 MPa which represents an increase of 13.5 % in comparison with the value after 28 days.
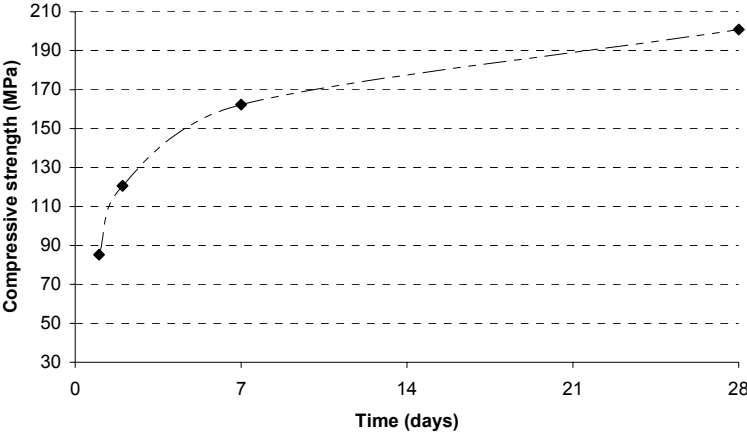
Figure 2:   Typical compressive strength versus time

To date, 2200 tons of the premix were produced. The quality control data for compressive strengths after 2 and 28 days were carried out regularly. The statistical QC data are given in table 1.

All these results are in accordance with those measured during the development of the product.

Compressive strength after	2 days	28 days
average (MPa)	122	199
standard deviation (MPa)	8	8
variation coefficient (%)	6	4
number of controlled batch	63	18

Table 1:   Statistical data

Flexural tensile strength

The four-point flexural strength and the centre-point flexural strength tests carried out do meet the Setra-AFGC recommendations on the ultra high performance fibre-reinforced concretes [4]. Consequently, the four-point flexural tests were carried out with deflection control (two external extensometers per sample); the rate used was 0.1 mm/min. The centre-point flexural tests were carried out on notched samples (notch depth: 0.5 x fibre length) with crack opening control (one extensometer bridging the crack); the rate used was 0.025

mm/min. At least twelve prismatic samples (10 by 10 by 40 cm) were tested for each type of test. Results are shown in figure 3 and 4.
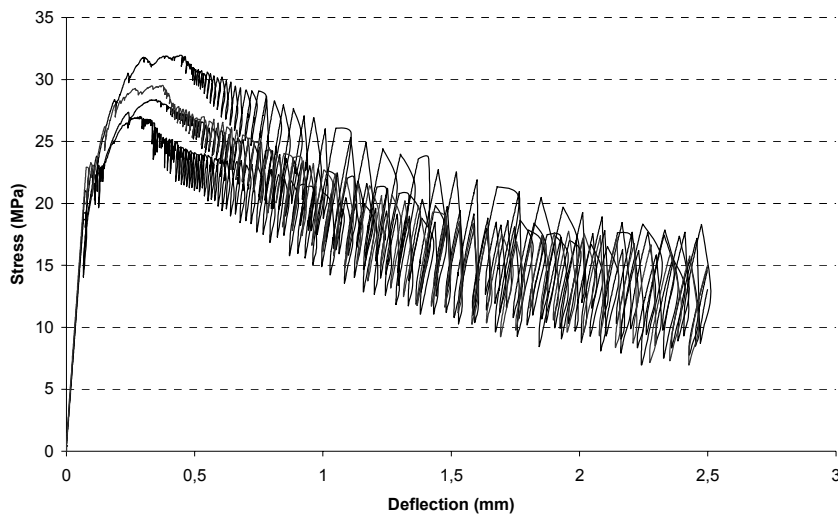
Figure 3:   Four-point flexural tests: stress versus deflection

From all the curves of the four-point flexural tests, the tensile strength of the cement matrix was determined (table 2). The maximum stress for each type of test was also determined (table 2). The metallic fibres allow to obtain a ductile concrete behaviour under tension which makes the use of passive reinforcement unnecessary.
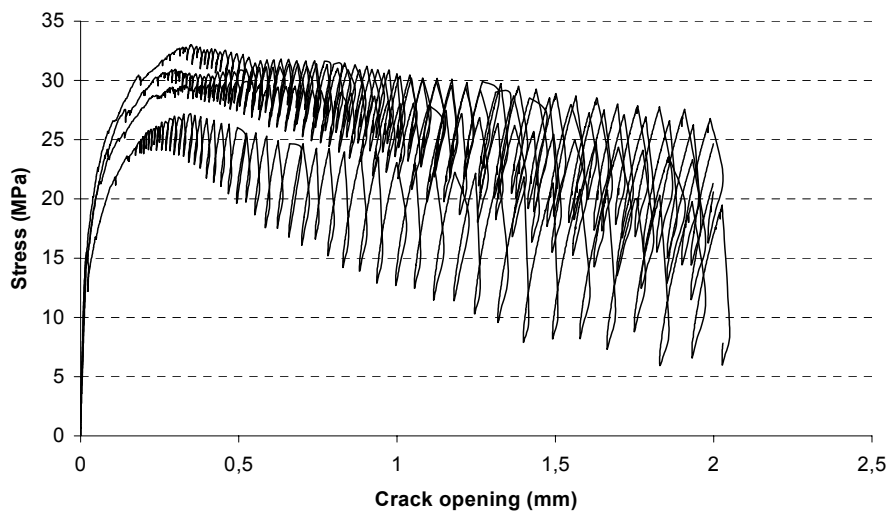
Figure 4:   Centre-point flexural tests: stress versus crack opening

	Maximum stress of the CERACEM BFM-MILLAU (MPa)	Tensile strength of the cement matrix (MPa)
Four-point flexural tests	29	8.8
Centre-point flexural tests	30	

Table 2:   Values of flexural tensile strength

Shrinkage

Cracks at the surface or in the concrete matrix have to be avoided because they can facilitate the penetration of aggressive agents into the matrix and consequently reduce the durability. Especially in binders with high cement content cracks formation can be a problem. Consequently, several studies were carried out to determine the total shrinkage, the autogeneous and the desiccation shrinkage. For the evaluation of the total shrinkage, the samples were demoulded after 24 hrs and then kept in a climatic chamber (50 % RH and 20 °C). The samples demoulded after 24 hours for the determination of the autogeneous shrinkage were wrapped in aluminium foil to avoid moisture transfer. The total shrinkage and the autogeneous shrinkage were carried out by linear measurements on prismatic samples (7 by 7 by 28 cm – 3 samples per type of shrinkage). The desiccation shrinkage has been calculated as the difference between the total shrinkage and the autogeneous shrinkage.
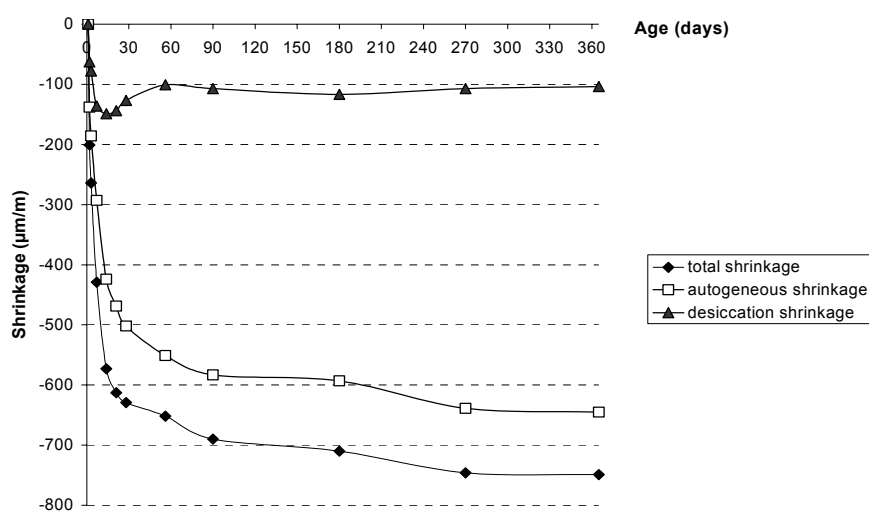
Figure 5:   Total, autogeneous and desiccation shrinkages versus time
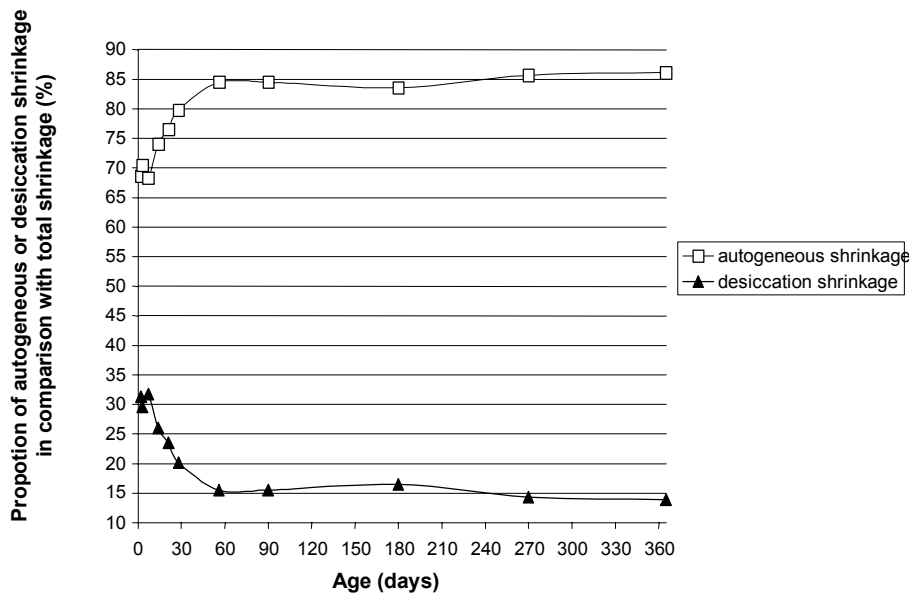
Figure 6:   Proportion of the autogeneous or desiccation shrinkage in comparison with the total shrinkage.

The proportion of the autogeneous shrinkage is higher than the one of the desiccation shrinkage (figure 5 and figure 6). This result is in accordance with the scientific literature [8], [9], [10]. Indeed, the autogeneous shrinkage increases when the water to cement ratio decreases; the autogeneous shrinkage is negligible for the ordinary concretes, but it is important for the high performance concretes and the ultra high performance concretes.

After 7 days, 50% of the the final shrinkage (1 year) is achieved, and about eighty percent is achieved after 28 days.

4   Applications

Before the SIKA-EIFFAGE co-operation started, several applications were carried out by EIFFAGE alone such as the renovation of cooling towers for several nuclear power stations and the building of two bridges [1], [2], [3]. In 2003 and 2004, EIFFAGE carried out the construction of the tollgate roof for the Millau's viaduct with CERACEM BFM-MILLAU (figures 7 to 13), the design and the structure calculations having been done also by EIFFAGE [8].

Figure 1: Picture of the tollgate roof – Architect: M. Herbert (source: Eiffage)

The length and the width of the roof are respectively 98 and 28 meters. This roof is composed of fifty-three precast elements without passive reinforcement. The element shell has a thickness equal to 10 centimetres. All these elements are supported by longitudinal pre-stressing.
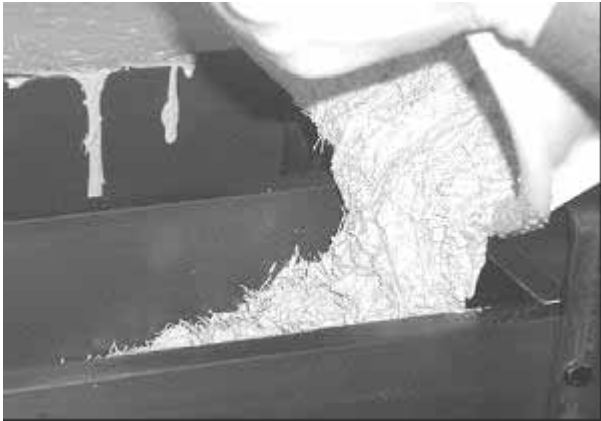
Figure 2: Fresh CERACEM BFM-MILLAU (source: Eiffage)

Figure 3: Element casting (source: Eiffage)

Figure 4: Mould (source: Eiffage)

Figure 5: CERACEM BFM-Millau element (source: Eiffage)
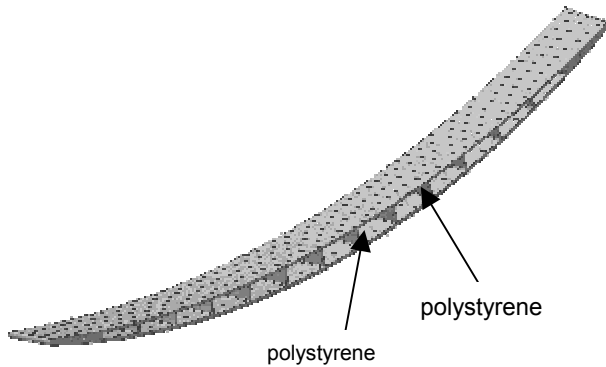
Figure 6: Picture of the element (source: Eiffage)   *Figure 7: Element (source: Eiffage)*

For the production of the precast elements, a site factory was established by EIFFAGE. SIKA was the supplier of the CERACEM BFM-MILLAU premix and the superplasticizer. No major problems in preparing the concrete were reported from the batching plant, however, the equipment and the mixing procedure had to be adapted (e.g. high energy mixer).

Additionally a concrete coating system for which the UV resistance was notably examined and an adhesive resin especially formulated for this job site, for which the bond strength properties with the CERACEM BFM-MILLAU concrete was studied.

5   Conclusion

The optimisation of the composition and the nature of the raw materials combined with the latest generation of a superplasticizer lead to the unique rheological, mechanical and durability properties of CERACEM. With its characteristics and properties, it can be used for on site placed concrete jobs as well in the precast concrete industry. With steel fibres-reinforced CERACEM, the thickness of the slabs can be reduced which leads to a decrease in weight of the structure. As CERACEM including steel fibres shows a ductile behaviour, the passive reinforcement is not longer necessary and therefore more freedom for the designer results (e.g complex shapes). The combination of high tech materials with proper design and workmanship allowed the construction of this futuristic toll gate with its elegant and unique shape.

1.   References

[1] Cadoret G. and Thibaux T., le BSI : un nouveau béton très hautes performances, Conférence de l'AFGC « bétons à hautes performances et bétons à ultra-hautes performances », Lyon, June 3rd 1998.

[2] Birelli G., Cadoret G., Dutalloir F. and Thibaux T., a new very high performance concrete, Conference in Sherbrooke, pp. 177-201, 1998.

[3] Semioli W. J., the new concrete technology, Concrete International, pp. 75-79, November 2001.

[4] Yamada K., Effects of the chemical structure on the properties of polycarboxylate-type superplasticizer, Cement and Concrete Research 30 (2000), 197 – 207

[5] Maeder U. , Schober I. , Performance of blends of polycarboxylate polymers in different cements, Proceedings of the11th International Congress on the Chemistry of Cement, May 2003, Durban, Editor Grieve, G. Owens

[6] Setra-AFGC, Ultra High Performance Fibre-Reinforced Concretes – Interim recommendations, 152 pp., January 2002.

[7] Baroghel-Bouny V., Caractérisations des pâtes de ciment et des bétons, Laboratoire Central des Ponts et Chaussées Paris, pp. 207-208, 226-227, 461-468, 1994.

[8] Détriché C.H., La maîtrise de la fissuration précoce : conditions de la durabilité des ouvrages in « La durabilité des bétons » (J. Baron/J.P. Ollivier), Collection de l'ATILH, Presses de l'École Nationale des Ponts et Chaussées, pp. 107-128, 1996.

[9] Aitcin P. C., Neville A. M. and Acker P., Integrated view of shrinkage deformation, Concrete International, vol. 19, n°9, pp. 35-41, September 1997.

[10] Hajar Z., Simon A., Thibaux Th. and Wyniecki P., Construction of an ultra high performance fibre-reinforced concrete thin-shell structure over the Millau viaduct toll gates, Conference FIB in Avignon, April 2004.

Ekkehard Fehling
Prof. Dr.-Ing.
Universität Kassel
Kassel, Germany

Kai Bunje
Dipl.-Ing.
Fehling + Jungmann GmbH
Kassel, Germany

Michael Schmidt
Prof. Dr.-Ing. habil.
Universität Kassel
Kassel, Germany

Walter Schreiber
Dipl.-Ing.
Fehling + Jungmann GmbH
Kassel, Germany

Ultra High Performance Composite Bridge across the River Fulda in Kassel
– Conceptual Design, Design Calculations and Invitation to Tender –

Summary

The following report shows the construction and the design of the first Ultra High Performance Composite Bridge in Germany. The bridge structure has 6 spans with a total length of 133.2 m and a maximum free span of 36 m. The bridge deck consists of precast prestressed UHPC slab elements. The longitudinal structure consists of a continuous truss girder system with triangular cross section. The truss girder consists of two upper chords of precast prestressed UHPC and a lower chord and diagonals made of tubular steel sections. Glued connections are used between the upper chords and the deck as well as between the deck plates.

Keywords: *pedestrian bridge, UHPC, Kassel, Conceptual Design, Design Calculations*

1   Introduction

Ultra High Performance Concrete has a compressive strength comparable with building steel as well as excellent load-capacity and toughness qualities, if it is produced with suitable steel or plastic fibres. Beyond this it offers an enormous high resistance to penetration of liquids and gases and therefore shows excellent durability qualities. This means quasi a quantum leap in the development of concrete building-materials.

Because of its high strength at low weight, such a new building-material makes it facilitates to build filigree and light bridge constructions. This was already shown by the construction of pedestrian bridges in Canada, Korea and Japan as well as a street bridge in France.

The departments of Concrete Strcutures (Prof. Dr.-Ing. Ekkehard Fehling) and Building Materials (Prof. Dr.-Ing. habil. Michael Schmidt) at the University of Kassel have worked for some years on the investigation and further development of Ultra High Performance

Concrete. On the one hand, questions of the mixture optimisation, the durability and the mechanical qualities of the material were examined and on the other hand design models for the ultimate limit state and the serviceability state were developed [1-3]. Therefore the time is ready to build the first greater bridge construction made of the new material in Germany.

It is intended as the first project of a UHPC-bridge in Germany to set up a pedestrian and cycle track bridge across the Fulda by the City of Kassel as client. The planed bridge is a hybrid construction made of steel and Ultra High Performance Concrete. This bridge shall replace an existing wood bridge which shows severe damage.

2   Conceptual design

The Gärtnerplatzbrücke is a pedestrian and cycle track bridge across the Fulda river, and is in addition to the neighbouring bridges (approx. 500 m in southerly direction the Damaschkebrücke as well as approx. 900 m in northeastern direction the Schwimmbadbrücke) connecting the area of the former National Garden Festival with the Karlsaue area specially for recreational traffic. The location of the Gärtnerplatzbrücke within the city area is shown in Figures 1 and 2.

Figure 1:   City map   Figure 2: Arial view

The new bridge construction which has to replace the existing wood bridge, completed in 1981 and having 7 spans and a total length of 147 m, shall use the available pillars as well as their foundations.

Figure 3:   Existing wooden bridge

Figure 4:   Damage in the beam

This is possible, because the support reactions of the filigree and light construction from the newly designed bridge are almost equal to the old wooden construction. Figure 5 shows the longitudinal section of the conceptual design of IBB Fehling + Jungmann consulting engineers, Kassel.
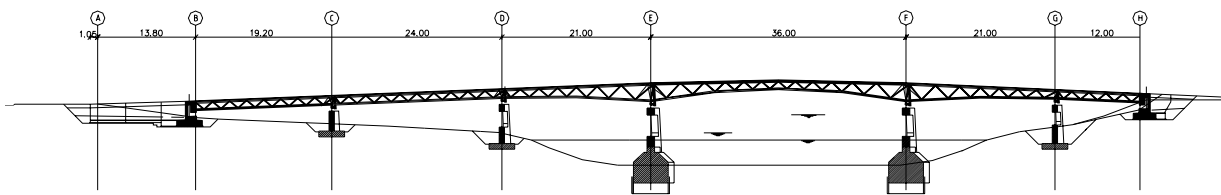
Figure 5:   longitudinal section

Due to some changes in the terrain profile, the new bridge is designed for 6-spans with a total length of 133.2 m in which the largest supporting distance in the river area is 36 meters. After extensive variant examinations, the following load-bearing structure was selected. The bridge girder is formed by a truss with three booms with variable building height, the top booms consist of UHPC while the sub boom is formed by a tubular steel. The diagonals also consist of tubular steel. The bridge deck consists of 5.00 m wide prestressed precast UHPC plates with 8 - 10 cm of thickness. The UHPC plates will be interlinked and connected to the top belts of the truss girder using epoxide resin glue. Figure 6 shows the new cross section.
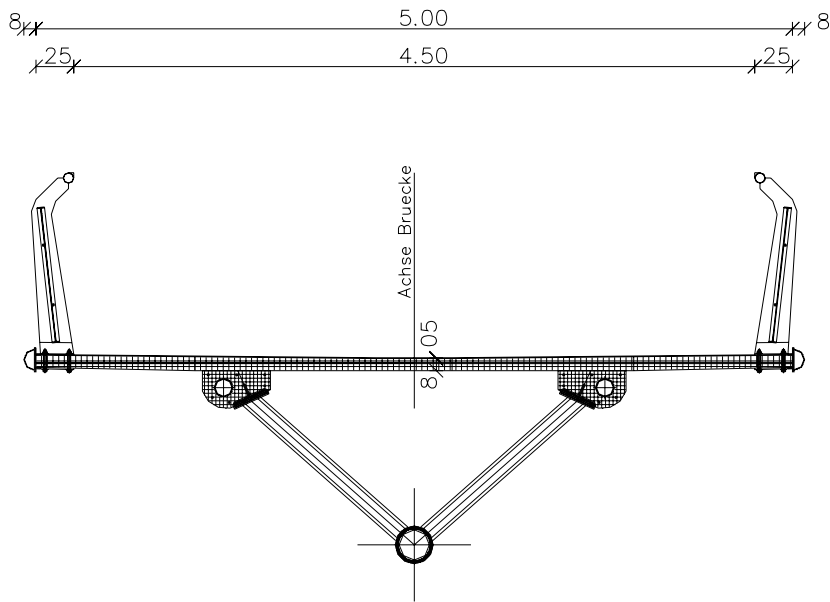
Figure 6:   cross section

The continuous girder shall be composed of single span girders. The single span girders consist of the UHPC top booms which are precast in a stressing bed and the steel parts of the truss girder (bottom boom and diagonals). The connection of the diagonals is carried out via end plate connections. The UHPC top booms also get steel end plates in order to establish the wedge anchorage of the prestressing strands and to link the booms with a bolted prestressed connection to obtain a continuous girder system.

In the end the prestressed precast UHPC deck plates will be mounted. A shear resistant connection in the composite joint between the plates and the top booms will be established by an epoxide resin glue. Simultaneously, the precast UHPC plates are also interconnected by glued connections. To ensure that there are no tensile stresses under permanent action in the bridge deck in longitudinal direction, the top booms will be equipped with tendons along the full length of the construction. The tendons which prestress both, the precast plates and the top booms will be anchored in the end cross beams.

For the continuous longitudinal prestressing, tendons suited for external prestressing shall be used. In this case, however, they will be led in additional conduits to the top booms. This allows to control the prestress forces over a period of time.

The old pillars are available for the intermediate support. With an expanse of 7 m they are very wide and do not suit architecturally the light bridge construction. Therefore the upper parts of the pillars will be removed and replaced by a more open looking reinforced concrete frame architecture (see Figure 7).
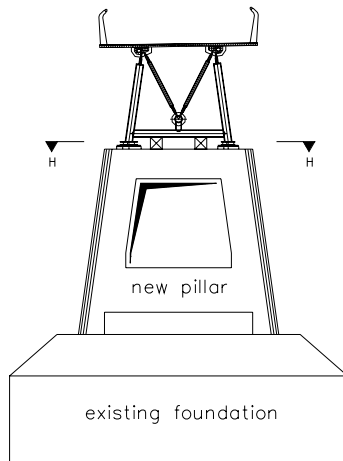
. Figure 7: new river pillar of the bridge

Figure 8:   3D-animation of the bridge design

3   Design Calculations

Using a Finite Element program, a three dimensional model of the bridge structure for the design calculations was set up. The calculations considered the process of construction on site and the effects due to creep and shrinkage. Tests on heat treated construction elements made of UHPC have shown, that the creep behaviour is very low and that there is almost no shrinkage left. Therefore a heat treatment of the precast elements is intended [3].
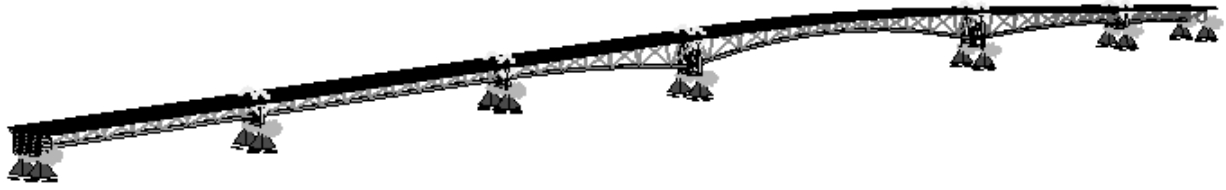
Figure 9:   3D-model of the bridge construction
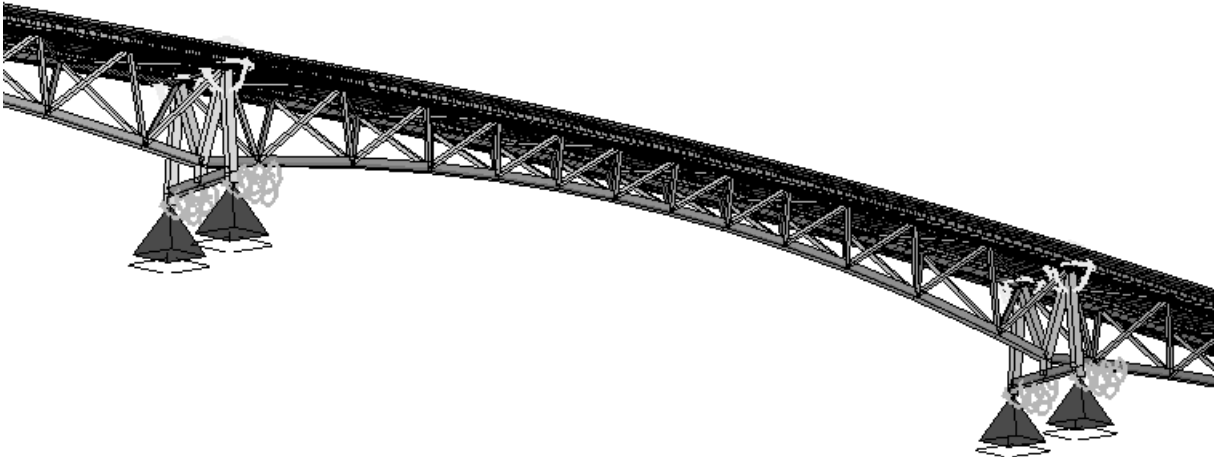
Figure 10:   3D-model of the bridge construction
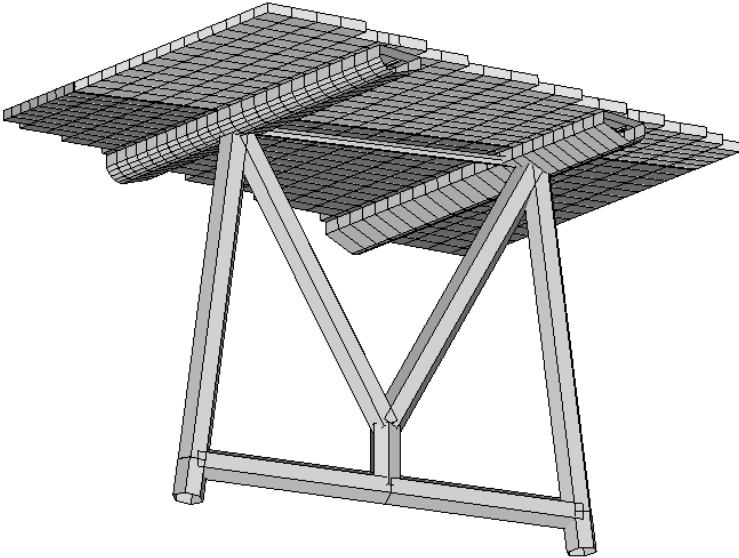
Figure 11:   3D-model of the bridge construction

Laboratory tests on gluing UHPC specimens to each other showed very positive results. Beyond, one can rely on long-standing experience in bridge-building in Switzerland. Nevertheless a failure of the glued connections is considered in design calculations for the ultimate limit state. To this it is proved that the load bearing safety of the complete system is

ensured also at failure of single slabs and that they can be exchanged if necessary. For further information on the gluing tests see [5].

4   Invitation to tender

Due to the use of new high tech materials and to the very specific construction, the invitation to tender will be limited. Interested contractors have to proof their experience with high strength or ultra high performance concrete in a prequalification process before the participation in the invitation of tender. Since precast elements, in-situ concrete and steel components are needed for the bridge, the suppliers must demonstrate there experience on all these subjects.

It is striven for to carry out the invitation to tender still in this year so that the erection of the new superstructure can be done in spring 2005.

5   Conclusions

The conception of the new Gärtnerplatzbrücke represents an ambitious design including several technical innovations. In addition to the use of Ultra High Performance Concrete (UHPC), a new application for unbonded external tendons as well as glued connections are proposed. Due to the extremely high compressive strength of UHPC and the ductile behavior also in tension, concentrated loads, such as e.g. anchoring forces of tendons, can be introduced easily. UHPC offers ideal conditions for glueing due to the high adhesion strength of this very dense concrete. These possibilities have been used to design a lightweight hybrid UHPC-Steel bridge.

6   References

[1] Bornemann, R., Fehling, E., Schmidt, M., Middendorf, B.: "Entwicklung und Verhalten von Ultrahochfestem Beton (UHPC)", In: Beton- und Stahlbetonbau, 2001.

[2] Schmidt, M., Fehling, E., Teichmann, T., Bunje, K., Bornemann, R.: "Ultra-Hochfester Beton: Perspektive für die Betonfertigteilindustrie", In : Betonwerk + Fertigteil - Technik, Heft 3 (2003), S. 16.

[3] Fehling, E.; Schmidt, M.; Teichmann, T.; Bunje, K.: Entwicklung, Dauerhaftigkeit und Berechnung Ultra-Hochfester Beton (UHPC), Forschungsbericht an die DFG, Universität Kassel, 2003.

[4] Schreiber, W.: Konstruktion und Ausführung der ersten europäischen Verbundbrücke mit UHPC in Kassel, Beitrag zu den 48. Ulmer Beton-Fertigteil-Tage.

Part 3:

Regulations and Recommendations

Jacques RESPLENDINO
Chief engineer
Head of the bridges and structures division
CETE Lyon
Lyon, France

First recommendations for Ultra-High-Performance Concretes and examples of application

Summary

This paper draws a short review of the use of UHPC, since the first research on Reactive Powder Concrete carried out by Bouygues from 1990 to 1995, to the most recent engineering structures completed in 2004.

Then this paper draws a brief sketch of the main features of French recommendations for Ultra-High Performance Concretes (UHPC), drafted by an AFGC-SETRA work group.

These recommendations were published in June 2002, in bilingual english – french version ; they are intended to constitute a reference document serving as a basis for use of UHPC in civil engineering applications. They deal with UHPC characterization and material properties, design and calculations methods for UHPC, durability aspects in comparison with Reinforced Concrete or HPC.

Keywords: *ultra high performance concrete; Fibre; reactive powder concrete; recommendations; durability; design methods…*

1   Introduction

UHPC refers to materials with a cement matrix and a characteristic compressive strength in excess of 150 MPa, possibly attaining 250 MPa. They are containing steel fibres in order to achieve ductile behaviour and, if possible, to dispense with the need for passive reinforcement.

The different UHPC currently marketed are :

- BSI "Béton Spécial Industriel" (special industrial concrete), which technology has evolved to come to Ceracem® concrete, developed by Eiffage in association with Sika.
- Different kinds of Ductal® concrete, including RPC (reactive powder concrete), resulting from joint research by Bouygues, Lafarge and Rhodia, and marketed by Lafarge and Bouygues,
- BCV® being developed by cement manufacturer Vicat and Vinci group.

Most cement manufacturers are developing products, and materials are being developed in the laboratories of EDF, LCPC (with CemTec Multiscale technology).

2 Short review of UHPC applications

2.1 Sherbrooke footbridge

First research carried out on UHPCs were led by Bouygues from 1990 to 1995 on Reactive Powder Concretes [2] [3] [4]. The world's first engineering structure designed with this UHPC was the Sherbrooke footbridge in Sherbrooke, Quebec, built in 1997 [5]. Spanning 60 m, this precast, prestressed pedestrian bridge is a post-tensioned open-web space RPC truss (Figure 1), with 4 access spans made of HPC. The main span is an assembly of six 10 m prefabricated match-cast segments.
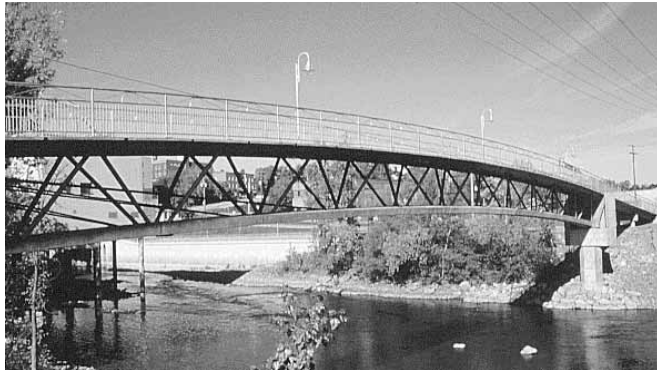
Figure 1: General view of Sherbrooke footbridge

The cross section is made of a ribbed slab 30 mm thick, with a transverse prestressing made of greased-sheathed monostrands. The truss webs are made of RPC confined in stainless steel tubes.

The structure is longitudinally prestressed by an internal prestressing placed in each longitudinal flange and an external prestressing anchored at the upper part of the end diaphragms and deviated in blocks placed at the level of the lower flange.

2.2 First industrial applications : beams of Cattenom and Civaux power plants

During years 1997 and 1998, the utility EDF carried out two important precasting sites using beams of UHPC, made of BSI and Ductal® [6] [7].These building sites consisted in replacing cooling towers steel beams in Cattenom (with BSI and Ductal®) and Civaux power plants (with BSI).

The extremely aggressive environment of the cooling towers induces important corrosion of the steel structures. UHPC with its outstanding qualities in terms of durability allows to replace steel beams with light elements with very long lifetimes without maintenance or repair.

2.3 The World first road UHPC bridges : Bourg-lès-Valence bridges

During years 2000-2001, the French Government, represented by its Regional Department of Public Works for the Drôme district with the assistance of the Service d'Etudes Techniques des Routes et Autoroutes (SETRA) and the Centre d'Etudes Techniques de l'Equipement

(CETE) of Lyon, realized the world first UHPC bridges, built by contractor Eiffage Construction with BSI on Valence bypass [10] [11] [12].

Each bridge has two isostatic spans of about 20 m. The road deck was made continuous by placing in situ UHPC between the two spans.

Each deck supports a 9 m wide road pavement with 1 m and 2 m sidewalks. Transversally both decks are identical; they are made from an assembly of five pi-shaped precast beams made from BSI, jointed together longitudinally with in situ UHPC (Figure 2).

All the beams are prestressed by pre-tension. There is no transverse prestress, and no transverse passive reinforcement, except where π-shaped beams are transversally jointed together.
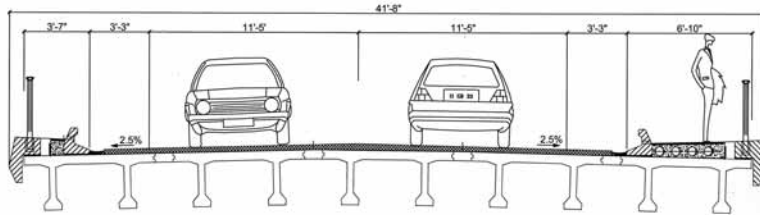
Figure 2: Bourg-lès-Valence bridges - Typical cross-section and view at central pier

The bridges were realized under an "Innovation Charter", and were designed and built in close collaboration with recommendations of a AFGC-SETRA working group on UHPCs.

This application also required to settle special calculation methods and design rules which are not currently covered by codes for the type of concrete employed. They were used to finalize some material characterization procedures and design calculation methods given by recommendations.

In 2001-2002, contractor Bouygues TP built a footbridge over the Han river running across Seoul in South Korea [13]. This foot bridge is made of an arch spanning 120 m, with two steel access spans (Figure 3).

Figure 3: General view of Seoul footbridge (left) and Sakata Miraï Footbridge (right)

The arch has a π-shaped cross-section, 1.30 m deep. The upper flange is a ribbed slab 30 mm thick, with a transverse prestressing made of greased-sheathed monostrands. The arch is an assembly of six 20 m prefabricated segments, connected on site by means of temporary supports. The elements are jointed together by an internal longitudinal prestressing placed in haunches in the lower and the upper parts of the webs.

We can also mention the Sakata Miraï footbridge which is the first Ductal® footbridge built in Japan with a span of 50 m. The deck is a simple beam 2.4 m wide with circular web holes. The structure is longitudinally prestressed by an external prestressing and has no passive reinforcement. This footbridge was completed at the end of 2002 (Figure 3).

The toll-gate of the Millau Viaduct, currently under construction, which will have an elegant roof based on a thin Ceracem shell, is the next step in the development of this new material.

This roof will look like an enormous twisted sheet of paper, 98 m long and 28 m wide, with a maximum thickness of 85 cm at centre (Figure 4). Its alveolate structure will be like an aircraft wing and will be made of match-cast prefabricated segments, 2 m wide, connected together by an internal longitudinal prestressing. In all, 1000 m3 of Ceracem® will be used, weighing a total of about 2800 tons.

Figure 4: General view of the roof of the Millau toll-gate and the Shawnessy tramway station.

We can also mention the Shawnessy tramway station in Calgary, Canada, which is completely made of Ductal®. Its roof is composed of very thin precast shells realized by injection (Figure 4).

At the end of 2003, began the construction of the Shepherds Gully Creek road Bridge in Croudace Bay, NSW, Australia, which has a deck made of precast prestressed I-girders beams connected to a traditional reinforced concrete slab.

Apart from these main civil engineering structures described above, some other applications have been realized with UHPC. Among these applications, we can make mention of these Ductal® ones:

- The construction of punched and thin accoustic sound panels for the underground Mocano railway station 1500 m2 of panels,
- The construction of architectural wall panels for Rhodia head office in Aubervilliers,
- The construction of 6300 anchor plates with polymer fibres and 200 plates with steel fibres for reinforced earth located on the sea-front on La Réunion island,

- A replica of the "Arbre Martel", a tree-shaped structure originally sculpted by brothers Martel,
- At the beginning of 2003, 30 m3 poured in steel tubes for making the pillars of the Keen Sofia Museum in Madrid (Span).

BCV concrete developed by cement manufacturer Vicat and contractor Vinci has been used in some applications:

- Construction of stays for a treatment reservoir of rainwater in Les Houches, France,
- Injection of curved saddles for stay cables in the pylons of Sungai Muar bridge in Malaisia,
- Construction of foundations blocks for the roof of the Cluses toll-gate on A40 motorway,
- UHPC flooring of the Lauterbrunnen footbridge in Swissland (Figure 5).

Figure 5: General view of Lauterbrunnen footbridge

3   The first recommendations on UHPC

The first French recommendations for Ultra-High Performance Fiber-Reinforced Concretes (UHPC) were published in 2002, in bilingual English-french version.

These recommendations integrates feedback from experience with the first industrial applications and experimental structures described below, as well as more than 10 years of laboratory research.

They are intended to constitute a reference document serving as a basis for use of this new material in civil engineering applications.

These recommendations are divided in three parts:

- A first part devoted to characterization of UHPC, giving specifications on the mechanical performance to be obtained and recommendations for characterizing UHPC. This part also deals with checks of finished products and of the concrete as it is produced.
- A second part deals with the design and analysis of UHPC structures, the particularity of which is to integrate the participation of fibres and the existence of non-prestressed and/or non-reinforced elements.
- A third part deals with the durability of UHPC.

3.1 Behaviour and mechanical characteristics of UHPC

After reminding the real compressive behaviour [3], the recommendations give a conventional constitutive law with a yield plateau which can be used for regulatory calculations regarding ULS bending.

The recommendations also give values of Poisson's ratio, thermal expansion coefficient, shrinkage strain and creep coefficient without or in case of heat treatment.

3.1.1 Effect of heat treatment

The recommendations remind the principal effects of heat treatment [2], which substantially reduces delayed shrinkage and creep effects, but must be carried out only after the concrete has set in order to avoid any risk of Delayed Ettringite Formation (DEF). Heat treatment therefore requires good knowledge of the setting time and a means of checking it.

3.1.2 Impact strength

The recommendations also account for the knowledge on UHPC behaviour under dynamic loading, which has been studied through impacts on radioactive-waste containers [1]. The recommendations enlight the principal concepts for UHPC calculations under dynamic loads defined and validated by experience.

3.1.3 Tensile behaviour

An important part of the recommendations deals with the tensile behaviour characterized by :
- An elastic stage limited by the tensile strength of the cement matrix f_{tj},
  - A post-cracking stage characterized by the tensile strength of the composite material reached after matrix cracking (Figure 6).
  -
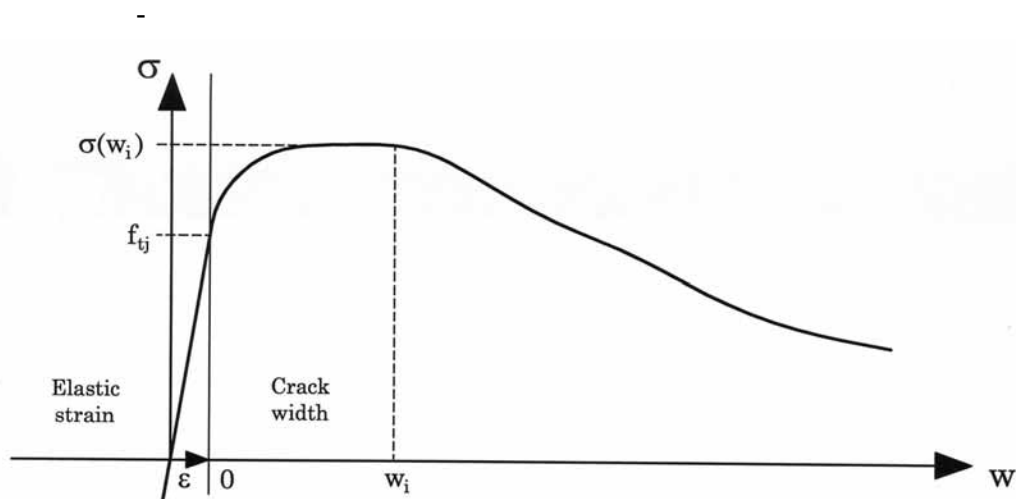
Figure 6: Example of a UHPC tensile constitutive law

The post-cracking behaviour is very important because it may dispense with the conventional reinforcement in the design of some structures.

On the other hand, it is quite difficult to characterize this behaviour because it depends very much on the mixing and placement process :

- Any flow during concrete placing tends to align fibres in the direction of flow,
- Fibres close to walls are naturally aligned parallel to the formwork. This phenomenon ceases beyond a distance from the formwork in excess of the fibre length. The closer component thicknesses are to the length of fibres, the greater is the effect on the effective tensile strength of the parts,
- Preferential gravitational orientation of fibres can sometimes occur, due to the natural behaviour of fibres in the viscous-liquid phase of concrete before it sets.

The methods outlined in the Recommendations take account of all these phenomena which are dissociated in two approaches.

Using characterization tests depending on the type of structure studied (thin slabs, thick slabs, beams, shells), and which can be of two types (direct tensile test or flexural tensile test), the Recommendations give for each proposed test procedure, the transfer factors to go from test results to an "intrinsic" curve for tensile behaviour which does not depend on test specimen size or on the type of test used.

Once the intrinsic curve for tension is determined, the recommendations give instructions for taking into account of the effect placement methods have on the real strength values to be considered in calculations. This correction of the intrinsic strength curves consists in applying a reduction coefficient 1/K representing the difference between the intrinsic curve and what would have been obtained on specimens taken from an actual structural element.

To determine this K factor, the recommendations impose suitability tests conducted on a representative models of the actual structure. The tensile strength measured on samples of the testing model allow to determine the K value which depends on the studied phenomena.

As for beams, the recommendations propose two values for this coefficient:

- A local value concerning designs, which propose to use fibre tensile strength in zones of material of reduced size in comparison with the piece size,
- A global value when justifications concern a sufficiently large zone so as to limit the effect of the local disparity in fibres orientation.

The principal results of this characterization process applied to the innovative Bourg-lès-Valence bridges [12] are enclosed with the recommendations.

3.2 Structural design methods

3.2.1 Generalities

The design methods proposed in the recommendations are based on the French codes for prestressed or reinforced concrete (BAEL [14], BPEL[15]) based on semi-probabilistic limit states verifications. The recommendations complete these design codes with specificity concerning UHPC which is essentially the strength provided from fibres which allows to design a structure without any conventional reinforcement.

For calculation, one may use an intrinsic law for characteristic tension drawn up assuming isotropic distribution of fibres throughout the structure.

In order to integrate the actual disparity in the fibre orientation due to placement, the various verifications are allocated an "orientation coefficient" 1/K determined by suitability tests as explained here above.

3.2.2 Normal stress verifications

For normal stress verification, the recommendations use the AFREM method [8] which concerns fibre concrete, and use a stress – crack width constitutive law $\sigma = f(w)$.

Moreover, in order to simplify calculation by using a traditional stress - strain law, the recommendations introduce the notion of characteristic length l_C , to go from crack width w to strain ε :

$$\varepsilon = \frac{f_{tj}}{E_{ij}} + \frac{w}{l_C}$$

The value of l_C depending on the sectional area.

Minimum fibre content and non-brittleness check

In order to guarantee sufficient ductility (in tension and compression), the recommendations consider a minimum fibre content and a non-brittleness check, which ensures that fibres can take tensile stress in case of matrix cracks.

Serviceability limit states

The analysis for standard sections is carried out considering that plane sections remain plane, and the concrete behaviour law detailed as below :
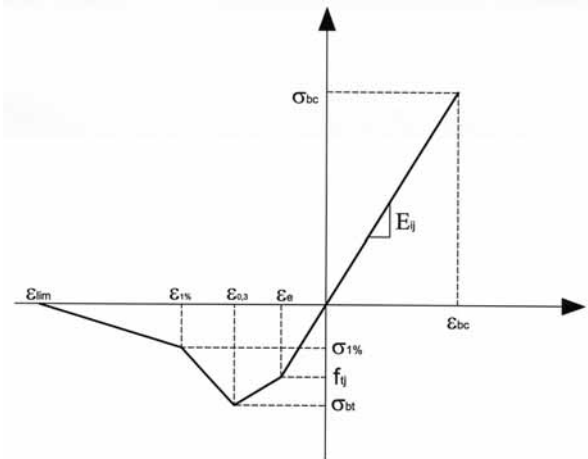
Figure 7: SLS strain hardening law

The limit stresses at the SLS are the same as a traditional concrete in case of a reinforced or prestressed structure (limitation of concrete compression, and steel under tension).

These checks are completed when there is no passive or active reinforcement by prescriptions concerning crack width :

- 0.3 mm for normal cracking, 0.2 mm for detrimental cracking and 0.1 mm for highly detrimental cracking.

Fatigue checks

In expectation of progress in this field of knowledge, the recommendations propose limits for tensile stress in case of parts subject to fatigue.

Ultimate limit states

Ultimate plastic strain of structure reinforced only with fibres are not very significant, so that recommendations do not allow non-linear calculation with plastic hinges if there is no passive or prestressing reinforcement capable of withstanding forces and moments when the participation of fibres is overlooked.

However, it may be possible to use a non-linear model using the constitutive law of the material.

For ultimate resistance calculation, recommendations propose a concrete behaviour law defined as below:
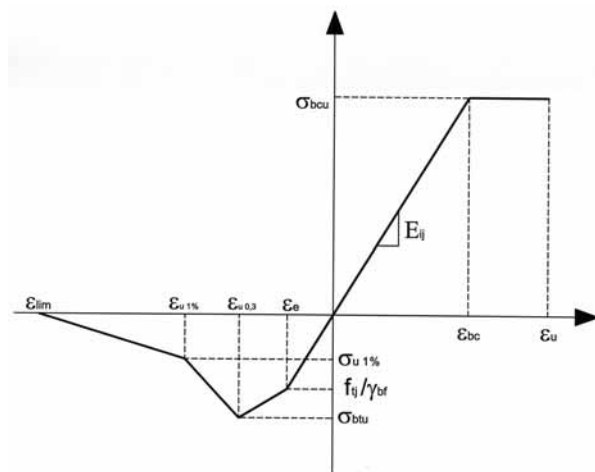
Figure 8: ULS strain hardening law

Moreover, the recommendations draw back that the methods which use ultimate strains to calculate ultimate resistance effects are valid only when there is passive or active reinforcement. In this case, this type of method gives pessimist results because it does not take all the fibres potential into account.

3.2.3 Shear stress verifications

At serviceability limit state, the recommendations propose to keep the shear stress limits of the French code for prestressed concrete.

At the ultimate limit state, the recommendations introduce fibre shear strength which complete resistance of the concrete and the potential active or passive reinforcements.

Moreover concrete shear strength of a UHPC must be taken different of a traditional concrete, because of aggregate interlock which increases quite less than the compression strength. Test results about this phenomenon are lacking for classical FRC. Hence the

recommendations limit concrete shear strength approximately at the value obtained with a C120 concrete.

3.2.4 Checks of zones submitted to concentrated forces

The recommendations complete actual regular prescriptions dealing with verifications of beam end blocks (equilibrium of bottom wedge, equilibrium of the compression strut), and verifications of the distribution of the prestressed concentrated forces. They account for complementary resistance brought by fibres.

3.3 Durability of UHPC

3.3.1 Conventional aggressions and specific features of UHPC

The recommendations provide the main UHPC durability indicators proposed by the AFGC working group "durability indicators".
The following table shows that the values obtained for UHPC indicate a clear improvement in durability, compared to any other types of concrete [9] :

	OC	HPC	VHPC	UHPC
Water porosity (%)	14 - 20	10 - 13	6 – 9	1.5 – 5
Oxygen permeability (m^2)	10^{-16}	10^{-17}	10^{-18}	$<10^{-19}$
Chloride-ion diffusion factor (m²/s)	2.10^{-11}	2.10^{-12}	10^{-13}	2.10^{-14}
Portlandite content (kg/m^3)	76	86	66	0

Table 1: Durability indicators for UHPC, traditional concrete and HPC

Moreover, the recommendations deal with specific indicators to UHPC (stability of the admixtures, possible rehydration, corrosion of steel fibres, chemical aggression of polymer fibres).
So far all the available research and published results show that there is no real problem with any of these phenomena.

3.3.2 Fire performance of UHPC

At the moment, there is insufficient data about the loss of strength depending on the temperature rise versus time so as to establish general design rules.
All the manufacturers nowadays are eager to search about these phenomena so as to be able to bring out a formula, which can respond to detailed specifications (they generally incorporate polymer fibres).
Considering the present knowledge, a formula validation needs tests carried out using standardized specimens in the case of a UHPC not subject to scaling, using representative specimens of structural elements in other cases.

4   Conclusion - prospects

The "Interim recommendations on Ultra High Performance Fibre-Reinforced Concretes (UHPC)" constitute the first reference document serving as a sure basis for use of this new material in civil engineering applications.

The different applications built with this kind of material have demonstrated UHPC's great qualities, making particularly durable parts with outstanding mechanical performance.

Several projects in progress should make the technique going forward and contribute to the development of the material.

The publication of the AFGC-SETRA recommendations reinforced interest of foreign countries, and a UHPC Bridge is going to be built in United States on behalf of FHWA.

Within the framework of National Project MIKTI led by IREX, a feasibility study of UHPC slabs for composite bridges should demonstrate the interest of this material which presents little delayed shrinkage and creep effects.

5   References

[1] Toutlemonde F. , "Résistance au choc des structures en béton. Du comportement du matériau au calcul des ouvrages", *thèse de l'Ecole Nationale des Ponts et Chaussées*, Paris, 16 décembre 1994. Publiée en rapport de recherche du LCPC, hors collection, juillet 1995. 348 pages, 197 réf., résumé anglais.

[2] Richard P., Cheyrezy M., "Les Bétons de Poudres Réactives" , *Annales de l'ITBTP*, n°532, Mars-Avril 1995, série Béton 320 pp. 85-102

[3] Behloul M., "Analyse et Modélisation du comportement d'un matériau à matrice cimentaire fibrée à ultra-hautes performances (B.P.R.). Du matériau à la structure", Ph. D. Thesis, ENS Cachan, 13 décembre 1996.

[4] Behloul M., Bernier G., Cheyrezy M., "Tensile behavior of reactive powder concrete (RPC)", *Proc. of the 4th Int. Symp. on utilization of HSC/HPC, BHP'96*, Paris, Presses de l'ENPC, vol. 3, pp. 1375-1381.

[5] Adeline R., Cheyrezy M., "La passerelle de Sherbrooke : premier ouvrage d'art en BPR / The Sherbrooke footbridge : the first RPC structure", *La technique française du Béton*, AFPC-AFREM, XIII° congrès de la FIP, Amsterdam 1998, pp. 343-348.

[6] Birelli G., Chauvel D., Dugat J., Adeline R., Bekaert A., "Industrialisation du BPR. Utilisation dans les réfrigérants à courants croisés et premières règles de calcul / RPC Industrialization. Using in cross flow air cooling towers and first design rules", in *La technique française du Béton*, AFPC-AFREM, XIII° congrès de la FIP, Amsterdam 1998, pp. 203-213.

[7] Dutalloir F., Thibaux T., Cadoret G., Birelli G., "Un nouveau béton très hautes performances : le BSI – Première application industrielle / B.S.I. : A new, very high performance concrete. Initial industrial application", in *La technique française du Béton*, AFPC-AFREM, XIII° congrès de la FIP, Amsterdam 1998, pp. 25-32.

[8] AFREM – BFM (1995) Recommandations sur les méthodes de dimensionnement, les essais de caractérisation, de convenance et de contrôle. Eléments de structures fonctionnant comme des poutres, décembre 1995

[9] Recommandation AFGC décembre 1997 Durabilité des bétons : Méthodes recommandées pour la mesure des grandeurs associées à la durabilité (L.M.D.C. INSA-UPS, Toulouse).

[10] Resplendino J., Roy J.M., Petitjean J., Blondeau P., Hajar Z., Simon A., Thibaux T., "Ouvrages innovants de Bourg-lès-Valence", *Revue Travaux*, No.783, pp. 42-47

[11] Thibaux T., Tanner J.A., "Construction des premiers ponts français en béton fibré à ultra hautes performances/construction of the first french road bridges in ultra high performance concrete", in *La technique française du Béton*, AFGC, The first fib congress 2002, Osaka 2002.

[12] Hajar Z., Simon A., Lecointre D., Petitjean J., "Construction of the first road bridges made of UHPC", 3rd International Symposium on HPC, Orlando *2003*.

[13] Behloul M, Causse G, Etienne D, "Passerelle en Ductal® de Séoul/Ductal® footbridge in Seoul", in *La technique française du Béton*, AFGC, The first fib congress 2002, Osaka 2002.

[14] BAEL 91 révisé 99, "Règles techniques de conception et de calcul des ouvrages et constructions en béton armé suivante la méthode des états limites", Fasc. 62 (Titre premier, section 1 du CCTG), avril 1999.

[15] BPEL 91 révisé 99, "Règles techniques de conception et de calcul des ouvrages et constructions en béton précontraint suivante la méthode des états limites", Fasc. 62 (Titre premier, section 2 du CCTG), avril 1999.

Part 4:

Binders and Fillers

L. Elfgren
Luleå University of Technology
Sweden

J.-E. Jonasson
Luleå University of Technology
Sweden

V. Ronin
Luleå University of Technology
Sweden

High Performance Concretes with Energetically Modified Cement (EMC)

Summary

The demands of the modern building industry require development of new types of binder materials with improved properties for high and ultra high strength concretes and with significantly improved durability. They will provide new potential possibilities for the controlling of high performance concrete technology.

In the Department of Civil Engineering at Luleå University of Technology a study of energetically modified cement (EMC) indicates that it is possible to obtain much more rapid hardening cement than the original cement used. As an example the strength of EMC-concrete increases about 100 per cent at the age of one day compared with a conventional high strength concrete.

A new type of the cement gives possibilities to obtain required workability of the concrete mixtures with low water to binder ratios (w/B < 0.24) and achieve the strength levels up to 200 MPa with binder content not exceeding 550 kg/m^3.

The modification process used in this study means a special mechanochemical treatment in vibrating milling equipment of the blend containing Ordinary Portland Cement (OPC) and silica fume (SF), which increases the surface energy and the chemical reactivity of the newly obtained binder. This results in an accelerating effect, which maintains at least for nine months.

According to ongoing investigations the energetically modified cement appears to give a considerable acceleration effect in the whole range of studied temperature. Concretes produced with EMC cement demonstrated very high durability at very severe testing conditions, including drying, saturation in sodium chloride solution and freezing-thawing. These results are very promising and it might be used in a lot of applications as winter concreting, precast element production, special structural elements, repair of buildings, rehabilitation, topping of concrete, floors, roads, etc.

1 Background

Energetically Modified Cement (EMC) is produced by high intensive grinding/activation of ordinary Portland cement (OPC) together with different types of fillers. Mechanical activation of mixtures containing different types of fillers involves the dispersion of solids and their plastic deformation. These processes cause the generation of defects in solids; they accelerate the migration of defects in bulk, increase the number of contacts between particles, and renew the contacts. All these factors provide the chemical interaction between solids initiated by the highly efficient mechanical treatment that takes place in the milling devices, where impact and shear stresses are applied to the solid phase (planetary mills, vibrating mills, etc.). The following could be achieved by the milling process: (i) improved binding capacity of Portland cement fraction in combination with (ii) increased pozzolanic activity of fly ash, and/or (iii) improved chemical reactivity of blast furnace slag, and/or (iv) creation of hydraulic activity of recycled concrete due to opening of Portland cement unhydrated grains. The mentioned example is an illustration of nanostructuring of composite materials with use of special milling devices.

The EMC process was developed at Luleå University of Technology and at EMC Development AB, Sweden from 1994. Studies on the performance of EMC have been published by Ronin et al [1, 2, 3], Jonasson et al [4], Rao et al [5], Groth et al [6], Hedlund et al [7], Johansson et al [8], Elfgren et al [9], and Justnes et al [10-13].

This paper presents properties of high strength and ultra high strength cement pastes and concretes obtained by the use of energetically modified cements (EMC) developed in the department of Civil Engineering at Luleå University.

2 Experimental Details

In these experiments the main types of cement commercially produced in Sweden were used. They are ordinary Portland cement (Std P), rapid hardening Portland cement (SH P), and moderate heat liberating Portland cement (Std P Anl, or Anl for simplicity). Silica fume used in this investigation was produced by Elkem A/S in Norway and used as a pozzolanic additive. We used Mighty 100, a naphthalene type of superplasticizer, to the amount of 3 % of weight of the cement/binder in all the cement pastes and concrete mixtures.

EMC cements have been produced by intergrinding of the mentioned OPC and SF in a Humboldt Palla 20U vibrating mill. The blends of 2 kg material were subjected to milling for 30 min with porcelain cylindrical grinding media. EMC cements characterized by the fineness of 5500-6000 cm^2/ g (Blaine).

All the types of cement mentioned above were subjected to energetically modification, and in this paper this treatment is referred to by abbreviation "EMC", which stands for Energetically Modified Cement, e. g. EMC (Std P) means the energetically modification of cement type Std P.

In these experiments the amount of silica fume was 5 to 20 % by weight of the cement. The water to binder ratio (w/B) for cement pastes was in the interval 0.16 to 0.20. All EMC pastes prepared for the strength tests had w/B equal to 0.16.

Concrete mixtures were produced with type Std P Anl both modified and non-modified. The cement content was 480 to 550 kg/m^3. Fine aggregate (0-8 mm) and coarse aggregate (12-16 mm) were used. The amount of silica fume (SF) was 10 to 20 %, and the amount of superplasticizer was 3 % by weight of the binder. The water to binder ratio (w/(C+SF) = w/B was from 0.19 to 0.27.

The cement pastes and concrete samples were cast at room temperatures (+ 20 °C) in 20x20x20 mm and 100x100x100 mm steel moulds, respectively. After casting the samples were put in water. The cement paste samples were for compressive strength tested in an Dartec testing machine ± 200 kN, ± 50 mm, deformation rate 0.01 mm/s. The concrete samples were tested on the hydraulic testing press, SEGER 2000 kN.

The porosity of the cement pastes was examined with the use of mercury intrusion porosimeter Pore Size - 9310 (Micrometrics) with capacity of 30 000 psi. The samples were dried at 105 °C before testing.

The temperature effect on the hardening process was studied by measurements of strength growth at different hardening temperatures (5, 20, 35, and 50 °C, respectively). The test samples were cubes 100x100x100 mm stored in water.

The liberated heat at hydration of the concrete was calculated from measurements of the temperature development during adiabatic and semi-adiabatic conditions. Each test specimen was about four litres of concrete placed in a bucket of thin walled steel.

3   Results

3.1   Strength of cement paste and concrete

The results obtained show that the usage of EMC increases the strength of the cement paste hardened at +20 °C in comparison with non-modified cements, see table 1 for comparison of compressive 28 days strength and figure 1 for comparison of strength developments. This effect is especially profound at an early age (1, 3, and 7 days), where the value of the compressive strength of EMC pastes surpasses the strength of reference mixes in 1.8 - 2.0 times. This drastic rate of the strength was registered approximately at an equal level for all the types of cements used for both amounts of silica fume content. The main cause of this effect is probably the modification of the hydration products morphology, effective package of the calcium silicate hydrates and significant reduction of the cement paste porosity. An additional cause of this increase in this case is the reduction of w/B ratio from 0.18 to 0.16.

The use of EMC in concrete mix also significantly changes the rate of strength development. In this case for all levels of w/B ratios from 0.19 to 0.24, see figure 2, where very intensive hardening was observed in the early age - from 1 to 7 days. So, for an enough wide interval of water to binder ratio (from 0.19 to 0.24) and workability (slump from 7 to 110 mm), EMC can be an effective tool for high performance technology.

Table 1.   Compressive 28 days strength of cement paste for non-modified and EMC cements, respectively. Hardening temperature is about +20°C.

Amount of silica fume by per cent of cement weight	Compressive strength (MPa) for					
	Non-modified cement			Modified cement (EMC) based on		
	OPC	RHPC	Anl*	OPC	RHPC	Anl*
0	89.5	88.7	94.7	-	-	-
5	96.7	94.1	105.0	170.0	154.0	165.4
10	98.4	96.3	108.0	180.5	164.0	172.3
20	-	-	-	-	-	205.0

*) "Anl" here means a moderate heat liberating Portland cement.
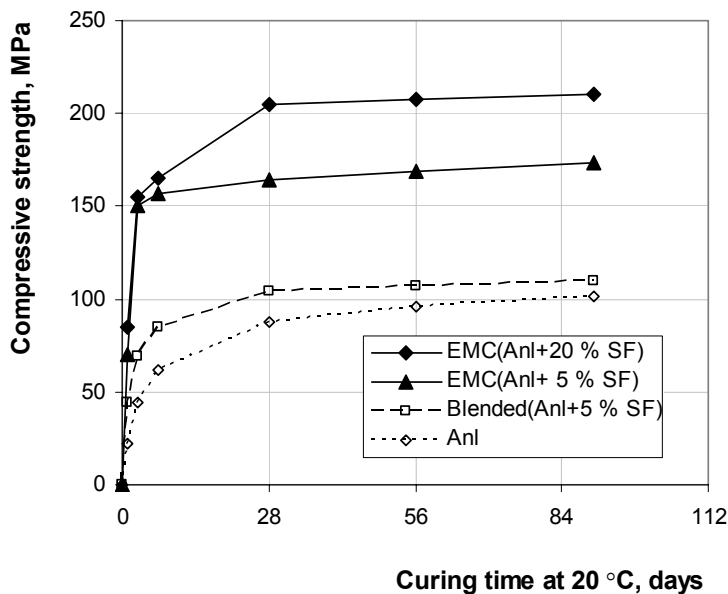
Fig 1.   Strength development at 20 °C curing for cement paste with water-to-binder ratio 0.16 with and without use of the EMC technology. "Anl" stands for a moderate heat liberating Portland cement.
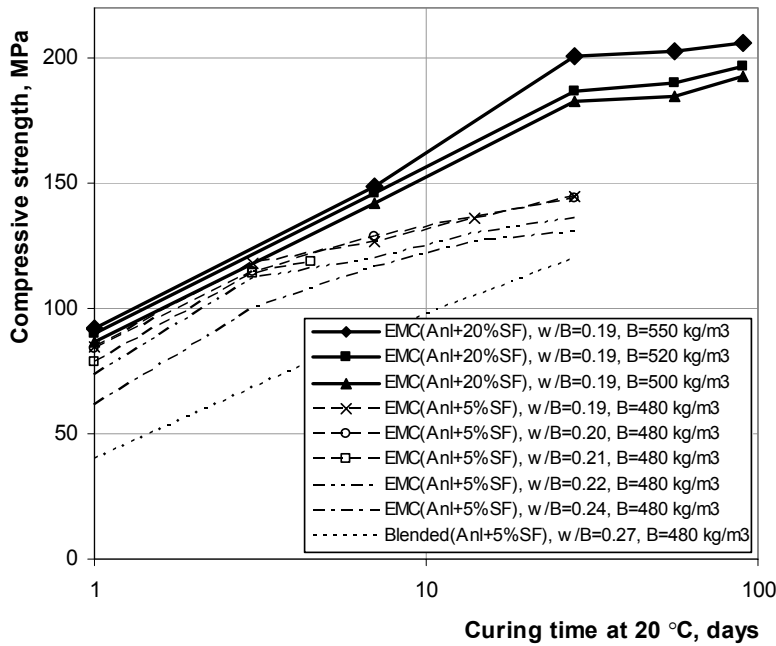
Fig 2. Strength developments for EMC concrete mixtures with water to binder ratios from 0.19 to 0.24, and for concrete with non-modified cement at w/B equals 0.27. All samples cured in water at about 20 °C.

3.2 Structure of the cement paste

The mercury porosity results of cement paste samples with w/B = 0.2 cured at room temperature in water for 28 days are presented in figure 3. As can be seen in the figure, the introduction of silica fume acted to refine the pore structure of the paste, and the usage of EMC shows an additional significant influence on the pore structure of the matrix. This influence is reflected in a decrease in total porosity as well as a decrease in the average diameter of the pores.

The examination of the EMC concrete fracture surface after strength testing of the samples showed an improved paste-aggregate bonding. The EMC concrete transition zone appears to be very dense without any visible microstructural gradients.

Properties mentioned above are expected to be favourable from the point of view of concrete durability. Long-term durability factors need to be studied to obtain EMC concrete performance parameters for durability design
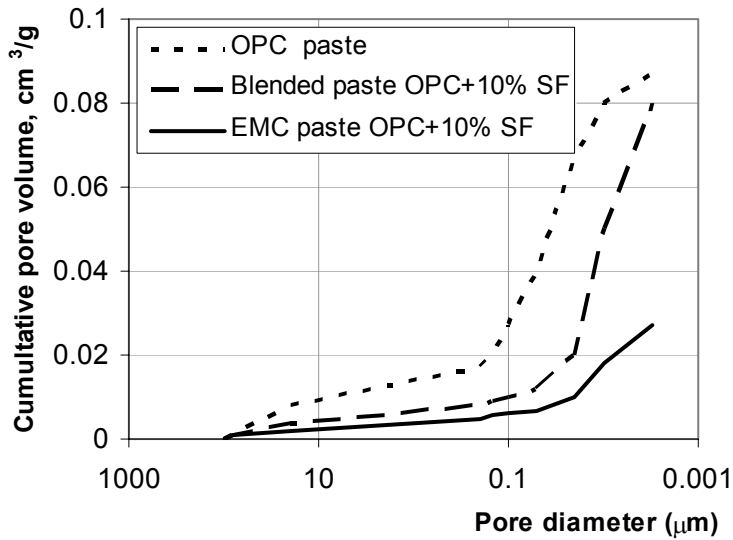
Fig 3.   Pore size distribution

3.3   Maturity development

Measurements of strength growth at different temperatures for two types of concrete results in the relative maturity rates are shown in figure 4. The lower rate factor for the EMC concrete at temperatures above 20 °C is probably an effect of a reduction in the pore humilities due to self-desiccation.

As can be seen from figure 4, the scatter of the test data for each strength curve is rather small. This means that the concept of maturity rate only depending on the temperature works in a simplified model to take into account variable curing temperatures for early age concrete, see figure 5.

Resulting hydration heat for the two studied concretes is shown in figure 6, where it is obvious that the EMC concrete is significantly more rapid than the concrete made with non-modified cement.
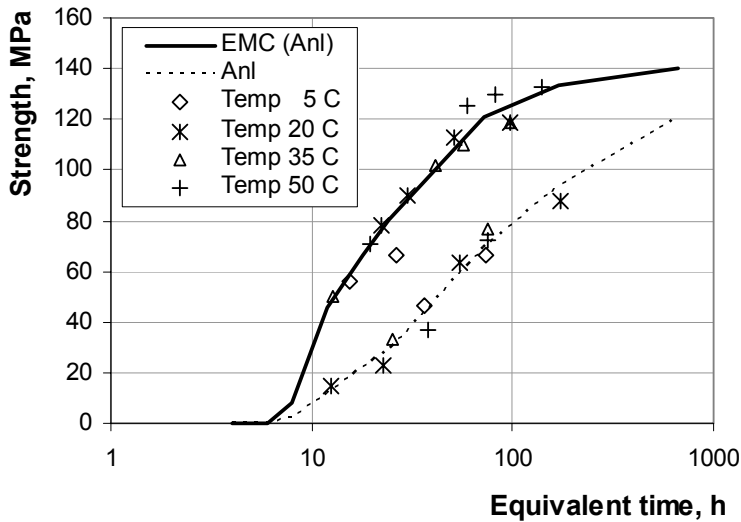
Fig 4.   Compressive strength as a function of temperature-equivalent time
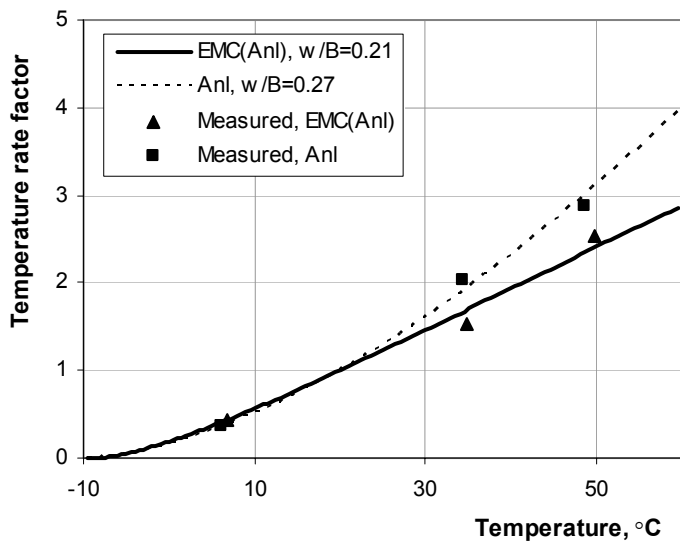
Fig 5.   Temperature rate ratios as a function of time

One way to compare the hydration heat for these two concretes is to study the liberated heat per developed strength unit. This has been done by dividing the heat values from figure 6 with the strength values of figure 4. The result is presented in figure 7, where evidently the EMC concrete has a significantly lower heat production per strength unit than the concrete with non-modified cement. Furthermore, as the curve for the EMC concrete in figure 7 is almost horizontal it means that the liberated heat in this case is directly related to the strength growth for the whole range studied.
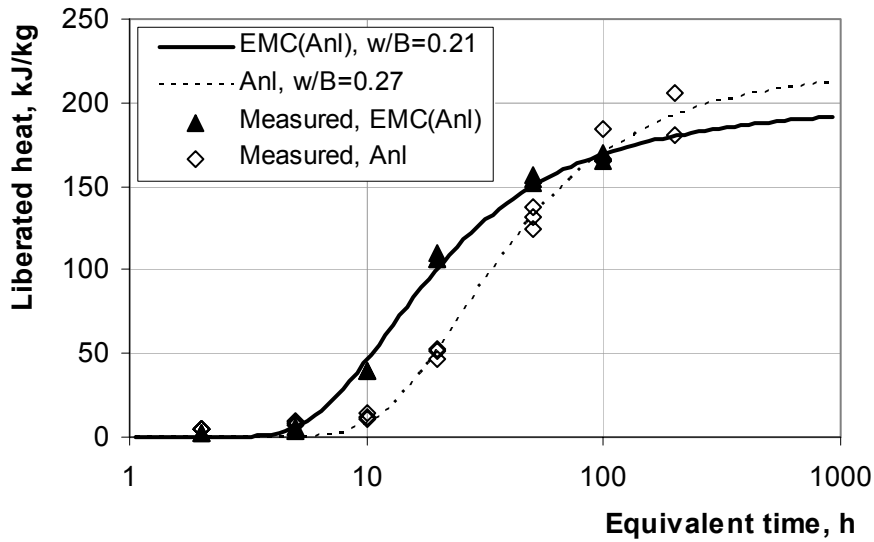
Fig 6.   Liberated heat as a function temperature-equivalent time
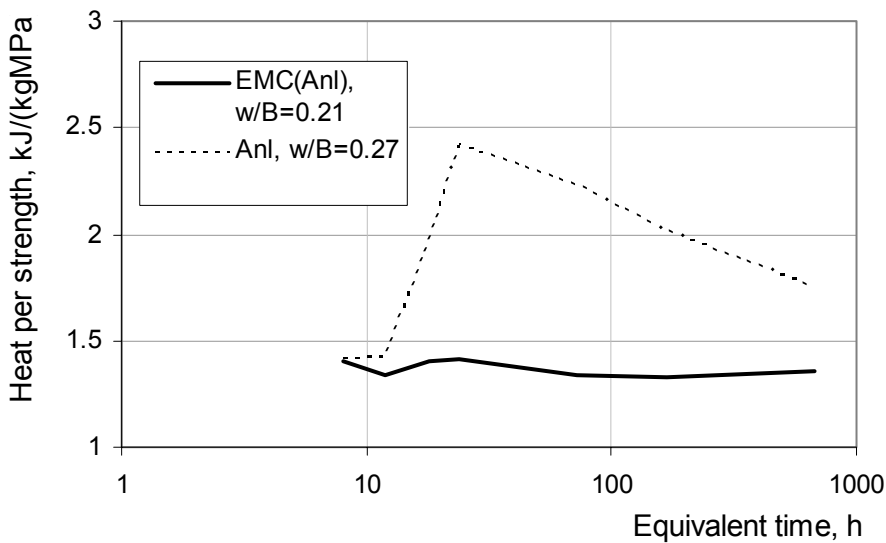
Fig 7.   Liberated heat per strength unit as a function of temperature-equivalent time

3.4   Durability

Durability tests has been performed according to Bache [14], see scheme for one testing cycle in figure 8.

We should point out that this is one of the most severe testing procedures for concrete, which includes the sequence saturation by sodium chloride, drying and freezing. All steps mentioned in figure 8 are performed during 24 hours and is considered as 1 cycle.

EMC concrete and OPC concrete with, after 28 days of curing, compressive strengths 180.3 and 128.4 MPa, correspondingly, have been tested. Mass losses have been determined as a durability characterization.
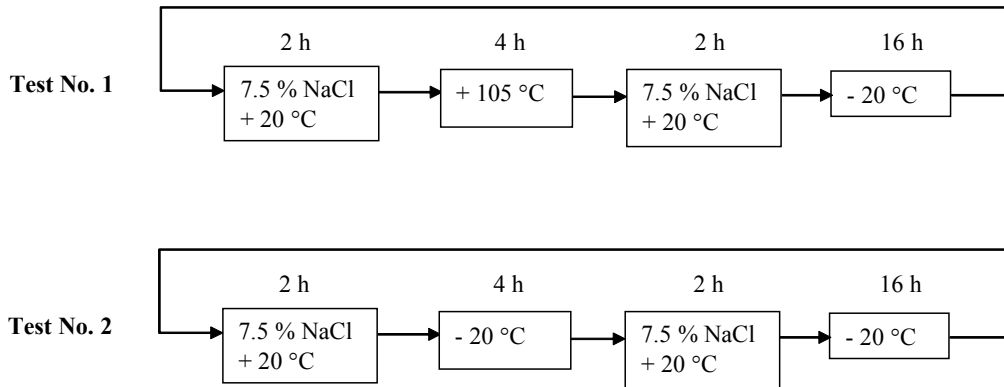
Fig 8.   Test cycle scheme of durability tests.

EMC concrete showed rather high durability level during all testing period. Practically no scaling of the concrete has been observed. At the same time reference OPC concrete was totally destructed after about 16 cycles. This is in line with Bache's observations for high strength concrete with water-to-binder ration 0.25 subjected to similar testing procedure [14].
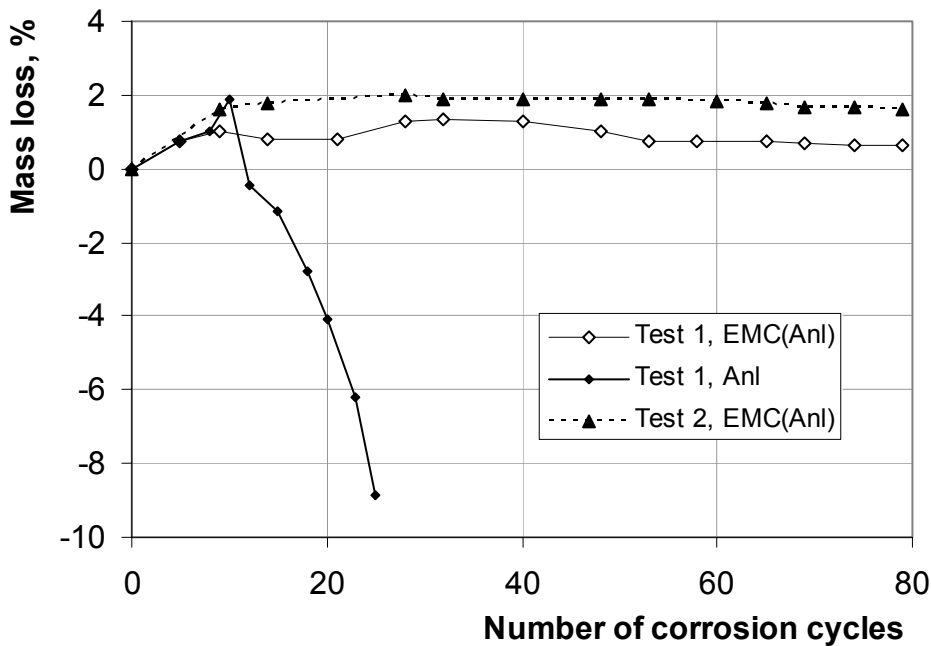
Fig 9.   Mass loss of the concrete versus number of corrosion cycles

4   Conclusions

EMC cement has an important influence on the strength and structure of the hardened product:

- ultra high rate of strength development in wide range of curing temperatures
- higher absolute values of strength of the cement paste and concrete, which exceed 200 MPa
- EMC pastes have much lower porosity and more finer pore size distributions
- the liberated heat are rapid, but it is lower per strength unit compared with the use of non-modified cement
- the amount of total liberated heat per cement weight for EMC concrete is approximately the same as for the concrete with non-modified cement
- EMC concrete demonstrated extremely high durability in very severe testing conditions

5   References

[1]   Ronin, V. and Jonasson, J.-E. (1994): Investigation of the effective winter concreting with the usage of energetically modified cement (EMC) - material science aspects. Report 1994:03, Div of Struct Eng, Luleå Univ of Techn, Luleå 1994, 24 pp.

[2]   Ronin, V, and Jonasson, J-E. (1995): High strength and high performance concrete with use of EMC hardening at cold climate conditions, Proceedings of International Conference on Concrete under Severe Conditions, Sapporo, Japan, August 1995.

[3]   Ronin, V., Jonasson, J.-E., and Hedlund, H (1997): Advanced modification technologies of the Portland cement based binders for different high performance applications. Proceedings of the 10th International Congress on the Chemistry of Cement (Ed. by H. Justnes), Gothenburg, June 1997. Inform Trycket AB, Gothenburg, 2ii077, 8pp. (ISBN 91-630-5496-5).

[4]   Jonasson, J.-E., Ronin, V. and Hedlund, H. (1996): High strength concretes with energetically modified cement and modeling of shrinkage caused by self-desiccation, Proceedings of the 4th International Symposium on the Utilization of High Strength/High Performance Concrete, Paris, France, August 1996, Presses Pont et Chaussees, Paris, 1996, pp 245-254.

[5]   Rao, K. H., Ronin, V. and Forssberg, K. S. E. (1997): High performance energetically modified Portland blast-furnace cements, Proceedings of the 10th International Congress of the Chemistry of Cement (Ed. by H. Justnes), Gothenburg, June 1997. Inform Trycket AB, Gothenburg, 3ii104, 9 pp. (ISBN 91-630-5497-5).

[6]   Groth, P. and Ronin, V. (1999): Influence of Energetically Modified Cement on Interfacial Bond and Fracture Toughness in Cement-Based Fiber Reinforced Composites, 5th International Symposium on Utilization of High Strength/High Performance Cement, Sandefjord 20-24 June 1999, Ed. by I. Holand and E. J. Sellevold, Norwegian Concrete Association, Oslo 1999, pp 1114-1123, ISBN 82-91341-25-7.

[7]   Hedlund, H., Ronin, V. and Jonasson, J.-E. (1999).: Ecological Effective High Performance Cement Based Binders, 5th International Symposium on Utilization of High Strength/High Performance Cement, Sandefjord 20-24 June 1999, Ed. by I. Holand and E. J. Sellevold, Norwegian Concrete Association, Oslo 1999, pp 1144-1153, ISBN 82-91341-25-7.

[8]   Johansson, K., Larsson, C., Antzutkin, O. N., Forsling, W., Rao, K. H. and Ronin V. (1999): Kinetics of the hydration reactions in the cement paste with mechanochemically modified cement 29Si magic-angle-spinning NMR study, Cem Concr Res 29 (1999) 1575-1581

[9]   Elfgren, Lennart and Jonasson, Jan-Erik (2000): Energetically Modified Cement (EMC) and Ordinary Portland Cement (OPC) – A Comparison. Report. Division of Structural Engineering and the Centre for High Performance Cement, CHPC, Luleå University of Technology, Luleå 2000, 45 pp.

[10] Justnes, Harald (2002): EMC Mechanism. SINTEF Civil and Environmental Engineering, Report STF22 A02612, Trondheim, 2002, 41 + 20 pp. ISBN 82-14-02575-3.

[11] Justnes H, Elfgren L and Ronin V (2003): Mechanism for Performance Energetically Modified Cement (EMC) versus Corresponding Blended Cement. Accepted for publication to Journal "Cement and Concrete Research" May 11, 2004, 19 pp.

[12] Justnes H, Elfgren L, Ronin V and Jonasson J-E (2003): Performance of Concrete Made with Energetically Modified Cement (EMC) Containing Quartz Filler in Comparison with Ordinary Portland Cement. To be submitted for publication in Journal "Cement and Concrete Research", 11 pp.

[13] Justnes H, Dahl P A, Ronin V and Elfgren L (2003): Microstructure and performance of energetically modified cement (EMC) with high filler content. Proceedings of the 6th CANMET/ACI International Conference on Recent Advances in Concrete Technology, Compiled by Maria Venturino, June 8-11, 2003. Bucharest, Romania, pp. 15 – 29.

[14] Bache, M (1983): Densified cement/ultra fine particle-based materials. Proceeding of the Second International Conference on Superplasticizers in Concrete.

N. B. Singh
Department of Chemistry
D. D. U. Gorakhpur University
Gorakhpur. INDIA

Highly reactive ß-Dicalcium silicate for ultra high performance concrete

Summary

Belite rich cement has been widely recognized to be suitable for high flowing and ultra high performance concrete as well as for low heat concrete. The major problem with belite cement is that it reacts very slowly and gives very little strength during early hours of hydration. Therefore attempts have been made to prepare belite cement in such a way that it becomes highly reactive. Highly reactive β-dicalcium silicate has been prepared at low temperature by using hydrothermal method. The material was characterized by different experimental techniques. The hydration studies were made by determining the non-evaporable water contents , free lime and specific surface area of the hydrated samples. X-ray diffraction and SEM studies on the hydrated samples were also made. The results showed that β-dicalcium silicate prepared is highly reactive. Possible causes of high reactivity have been discussed. Fluidity measurements of the mortar made from highly reactive β-dicalcium silicate in the presence of fly ash and polycarboxylate type superplasticizer have also been made.

1   Introduction

Ultra high performance concrete (UHPC) finds wide use in tall buildings, bridges, airports, power plants etc. The most important feature of UHPC is its superior durability in widely fluctuating adverse environmental conditions[1]. UHPC may be one of the most promising concrete of 21st century. It must have high strength, high modulus of elasticity, low permeability, excellent durability characteristics, very low heat of hydration (in order to minimize cracks due to thermal stresses) and high fluidity. There are certain basic criteria for production of UHPC: (i) use of proper aggregate (ii) cement quality in terms of rheology and strength (iii) use of suitable pozzolanic material and (iv) cement compatibility with superplasticizer[2,3]. High belite cements have been one of the highlights in the area of cement since the 1970's energy crisis. In the 1980's it had become one of the high performance cements for preparing high performance concrete because the cement had such advances as required for UHPC.[4]

The belite rich cement has been widely recognized to be suitable for high flowing concrete and UHPC as well as for low heat concrete. The major problem with the belite cement is that it reacts very slowly and gives very little strength during early hours of hydration. Further, it is

widely known that better fluidity is achieved by the additions of suitable pozzolanic materials and superplasticizers.

Attempts have been made to prepare β-dicalcium silicate of high reactivity at low temperature.[5-8] Suitable superplasticizers have also been used to reduce the water requirement and to increase the early strength and at the same time produce highly flowable concrete.

In this paper hydrothermal method has been used to prepare β-dicalcaium silicate and polycarboxylate type superplasticizer has been used to increase the flowability in the presence of fly ash. β-dicalcium silicate prepared hydrothermally has been characterized and its hydration properties studied. Flow area of the β-dicalcium silicate mixed with fly ash in the presence of polycarboxylate type superplasticizer at different w/c ratio have been measured.

2 Experimental

2.1 Materials

Calcium carbonate (Merck) and Aerosil 200 (Merck) were used as the starting material.

Fly ash was obtained from Bokaro plant, India. Chemical composition of the fly ash is given in Table 1 and its specific surface area was 3.2 m^2/g.

Polycarboxylate-based superplasticizer (PC) having molecular weight of 36000 and the following structure was used as a dispersing component.
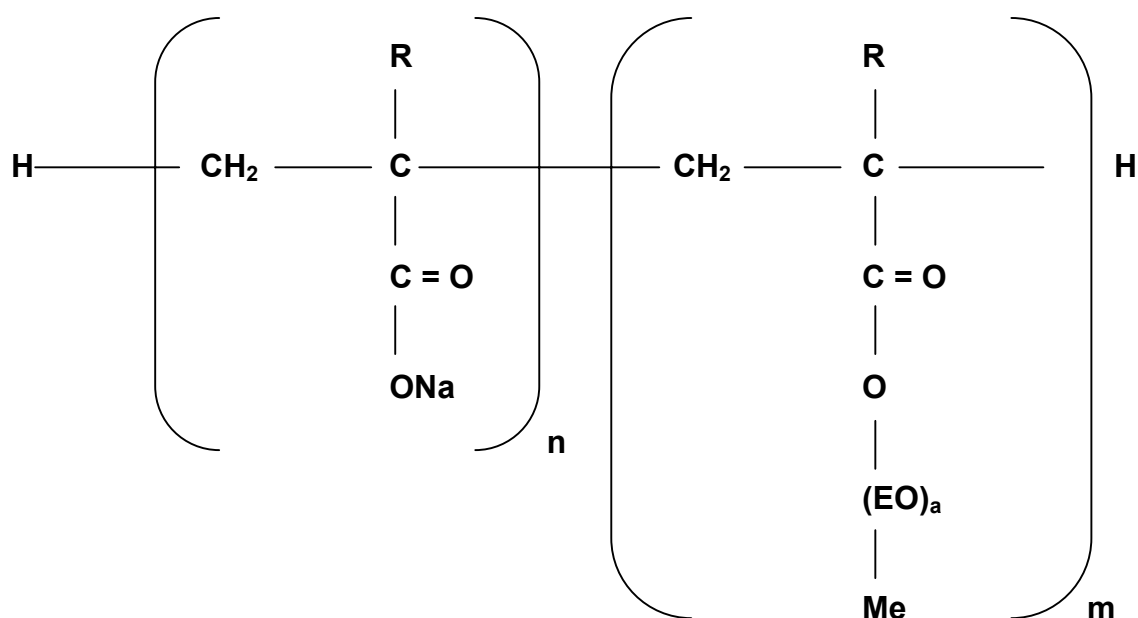
R = H, Me

EO – Ethylene Oxide

Me – Methyl

Standard grade sands 1, 2 and 3 were used. The mortars were made with 1:3 β-dicalcium silicate to sand ratio, where equal part of each sand grade was mixed. β-Dicalcium silicate was already mixed with 10% fly ash.

2.2 Methods

Freshly prepared Calcium oxide was mixed with aerosil 200 in a stoichiometric ratio (C/S=2.0). The dry mix was then thoroughly homogenized in a plastic bottle by shaking on a roller for 24h. Water was added to have w/s=10. This was again shaken well on the roller for 2h. the entire mass was placed in a beaker and kept in an autoclave at ≈200°C for 24h at a pressure of about 20 bar. The hydrated mass was then heated at 105^0C for 2h to remove excess of water. This was further heated at different temperatures (700-1200^{0}C) each for 1h in order to have β-dicalcium silicate. The β-dicalcium silicate obtained at 800^{0}C was used for detailed investigations. The product of hydrothermal reaction was analyzed by X-ray diffraction and TG-DTG-DTA techniques. β-Dicalcium silicate obtained at 800^{0}C was characterized by X-ray diffraction technique. This β-dicalcium silicate is designated as highly reactive β-dicalcium silicate (HRDS) and was used for detailed investigations.

Surface areas of β-dicalcium silicate obtained at different temperatures (700-1200^{0}C) were determined by BET apparatus. Free lime values were determined by modified Franke method.

β-Dicalcium silicate was also prepared in a conventional way at 1450^{0}C using 0.5 wt.% B_2O_3 as a stabilizer for control experiment.

FTIR spectra of β-dicalcium silicate prepared at 800^{0}C and that prepared in a conventional manner at 1450^{0}C using boron trioxide as stabilizer (control) were recorded with Perkin Elmer FT IR spectrometer in KBr phase.

Pellets of HRDS (thickness-0.124 cm, area-1.2733cm^2) and control (thickness-0.135 cm, area-1.2733cm^2) were prepared by applying a pressure of 10 Pa with a hydraulic press. Current and voltage across the pellets were measured at temperatures 303-383 K by using Keithley meter model 236 and platinum electrodes. From current and voltage values, the electrical conductivities were calculated.

Hydrations of HRDS was carried out at a w/c=1.5 (because of high surface area larger amount of water was required to make a paste) at room temperature (20^{0}C). The hydrations were stopped at different intervals of time. Boron trioxide stabilized β-dicalcium silicate was also hydrated as a control sample at a w/c=0.5.

CH content in the hydrated samples was determined by modified Franke method. The non-evaporable water contents (W_n) were determined by measuring the weight loss at 1000^{0}C.

Specific surface area of the hydrated samples was determined by area meter (BET). X-ray diffraction patterns of the hydrated samples and scanning electron microscopic picture of HRDS hydrated at 14 days were also recorded.

Mortars of HRDS mixed with fly ash were mixed in a Hobert mixer. Flow was measured by pull out spread of the mortar from a cone of top diameter 35 mm, bottom diameter 50 mm

and height 30 mm. The spread (F) was the average of two perpendicularly crossing diameters. From the spread (F), relative flow area A was calculated by eq. (1)

$$A = (F/r_0)^2 - 1 \qquad\qquad\qquad (1)$$

Where r_0 = 25 mm, bottom cone radius. Flow measurements were studied in the presence of 0.5% PC sperplasticizer at different w/c ratio.

3   Results and Discussion

Hydrothermal reaction product was characterized by X-ray diffraction and TG-DTG-DTA techniques. The studies revealed that during hydrothermal reaction hillebrandite (C_2SH_x) is obtained. When this compound is heated at 700^0C for 1h, gave β-dicalcium silicate associated with small amounts of wollastanite as an impurity. Since in the TG experiment weight losses in C_2SH_x continued upto 800^0C, β-dicalcium silicate was prepared by heating C_2SH_x at 800^0C. The β-dicalcium silicate thus obtained was also contaminated with small amounts of wollastanite as indicated by X-ray diffraction pattern.

Scanning electron microscopic studies revealed that the morphology of C_2SH_x is needle shaped and when it is heated at 800^0C to give HRDS, the morphology remained unchanged (Fig.1). This showed that HRDS is formed from C_2SH_x topotactically.

β-Dicalcium silicate obtained by heating dicalcium silicate hydrate (C_2SH_x)at different temperatures, contain varying amounts of free lime and possess different specific surface area. Both the surface area and the free lime decreased with the increase of temperature as usually expected.

In order to have an idea about the symmetric nature of $[SiO_4]^{4-}$ tetrahedron in HRDS and the control, IR spectra were recorded. The frequencies of vibrations of the two β-dicalcium silicate are given in Table 2.

The peaks in the spectra of HRDS are sharp and more in number as compared to that of control. The peak positions are also different. These observations show that probably $[SiO_4]^{4-}$ tetrahedron is less symmetric or distorted in HRDS than in control.

The variation of electrical conductivities with temperature for the HRDS and control are shown in figure 2. The results indicate that the values of electricall conductivities at all the temperatures are higher for the control than that of HRDS. Since surface area of HRDS is much higher than that of control, a large number of grain boundaries will be present in the HRDS. This will lower down the electrical conductivities of HRDS.

Because of high specific surface area of HRDS (4.0 m^2/g), the paste could be prepared at a w/c ratio of 1.5. There is a very little increase in the W_n values upto 3 days of hydration but after that there is a rapid increase upto 28 days (the time of investigation) (Fig. 3). A nucleation and growth mechanism is suggested in which the dormant period is characterized by the formation of critical size nuclei of hydration products. Thereafter, hydration proceeds at a much higher rate. Such mechanisms have been described for tricalcium silicate hydration by Ludwig and Singh[9]. As the hydration progressed, the amount of hydration

product increased.   Probably the hydration products are colloidal in nature as indicated by increased surface area (Fig. 4). The surface area of hydrated HRDS increased significantly upto 28 days. Further it appears that the hydration products are porous in nature and do not hinder much the approach of water molecules to the fresh surface of β-dicalcium silicate and as a result the reaction continued. If we consider the following stoichiometry for the hydration reaction

$$2\ C_2S + 5H \rightarrow C_3S_2H_4 + CH$$
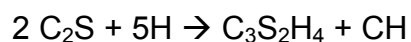
the non-evaporable water content for complete hydration will be 26.12%. In the present case, W_n value is 24.0 % and this gives the degree of hydration of 92% at 28 days of hydration. The W_n and specific surface area values in the case of control are much lower indicating lesser degree of hydration as compared to that of HRDS.

X-ray diffraction patterns of HRDS hydrated at different intervals of time are shown in Fig. 5. At 1 and 2 days of hydration, there is a very little change in the intensities of the X-ray peaks indicating that the hydration is very slow but at 7 days, the extent of hydration is increased as indicated by the decrease of the intensities of the peaks of HRDS and an enhanced peak at $2\theta = 18^0$ (d=4.9 Å) due to CH formation. Further at 14 days of hydration the intensities of the peaks due to HRDS are decreased considerably and the intensity of the peak due to CH formation is increased significantly. This indicates that the extent of hydration is much high. This has been supported by SEM photograph (Fig. 6). The results are in conformity to the results obtained by non-evaporable water contents and CH determinations on the hydrated samples of HRDS. At 28 days of hydration the intensity of the peaks due to HRDS are almost negligible but not vanished completely indicating that the hydration is still not complete. However the intensities at $2\theta=29.16$, 31.82, 49.895^0 (d=3.06, 2.81, 1.8263 Å) are appreciable. This may be due to the formation of C-S-H. The intensity of the CH peak at $2\theta=18^0$ is lower than that of the sample hydrated at 14 days. There may be two possibilities (i) a part of CH is amorphous or (ii) a part of CH has reacted with C-S-H gel. The possibility of CH being amorphous in nature is more because the extraction method gives higher values of free lime at 28 days as compared to that at 14 days.

From the results it is inferred that the reactivity of β-C_2S prepared by hydrothermal method is much higher than that of the control and following factors may be responsible for higher reactivity:

(i)   high specific surface area

(ii)   imperfections

(iii)   molecular geometry of silicate tetrahedra

(iv)   nature of hydration products and

(v)   high water/solid ratio.

Higher specific surface area generally accelerates the reaction since larger number of particles come in contact to other reactant molecule. In this case the other reactant is water which is in considerably higher amounts and so the molecular interaction becomes much higher resulting into higher degree of hydration. Since highly reactive β-C_2S is of high surface area, the particle size will be small. As a result it may contain large number of imperfections especially grain boundaries. Since in the present system larger number of grain boundaries

are expected to be present and the silicate $[SiO_4]^{4-}$ tetrahedral are distorted, the energy of activation for the hydration reaction is expected to be lower and the reaction will be faster as compared to that of control. Further porous nature of the reaction product permits continued reaction of water molecules over fresh surface of β-C_2S and the reaction does not become diffusion control.

In order to make a paste of standard consistency high water to solid ratio (w/s=1.5) is required because of high specific surface area. Therefore fly ash and polycarboxylate type superplasticizer were used. The fluidity of the mortar in presence of 10% FA and 0.5 % PC sperplasticizer with different w/c ratio is given in Fig. 7. As the w/c ratio increased, the fluidity is increased. Due to increase in fluidity, it is expected that compaction will increase resulting into an increase in density, which in turn will give high compressive strength. It appears that in the presence of FA and PC sperplasticizer the increase in fluidity is due to decrease in internal friction between particles. The FA particles increase the fluidity by increasing the lubricating effect. Further, the superplasticizers if present are adsorbed at the surface giving higher dispersion. This further increases fluidity.

4   Conclusions

Highly reactive β-dicalcium silicate (HRDS) could be prepared at low temperature by hydrothermal method which if mixed with suitable pozzolanic materials like fly ash in the presence of a polycarboxylate type superplasticizer will have high fluidity. This type of material can be used for the preparation of ultra high performance concrete.

5   References:

[1] Jain, A: High Performance Concrete Research and Practice, Proc. Construction Management and Materials, I.I.T., Kharagpur, Jan 9-11, 450-560, 2003.

[2] Khurana,R; Admixtures for ready mixed high strength and durable concrete ERMCO, 12th European Congress, June, 1998.

[3] Aitcin, P.C.: High Performance Concrete, E and FN. Spon, London, 1998.

[4] A. K. Chatterjee, A.K.; 'High Belite Cement-present status and future technological options, Cement and Concrete Research, 26, 1227-1223, 1996

[5] Ghosh, S.N.; Mathur, V.K; and Chopra, S.K.; Low temperature OPC-type cement containing superhydraulic dicalcium silicate phase, Cem. Concr. Res., 14 (3), 437-,1984.

[6] Ishida, H; Yamazaki, S; Sasaki, K; Okada, Y; and Mitsuda, T; α-dicalcium silicate hydrate: Preparation, decomposed phase & its hydration, J. Am. Ceram. Soc. 76 (7), 1707-1712 ,1993.

[7] A.K.Chatterjee, A.K.; High Belite Cements-present Status and Future Technological Options : Part 1, Cem.Concr.Res, 26(8), 1213-1225 ,1996

[8] N. B. Singh, N.B.; Rai, Sarita and Singh Neelam; Highly Reactive β- dicalcium silicate, J.Amer.Ceram.Soc., 85(9)2171-76,2002.

[9] Ludwig, U.; and Singh, N.B.; Kinetics and mechanism of alite hydration, Zement-Kalk-Gips, 39 (12),688-692 ,1986.

Table 1   Chemical composition of fly ash

Oxides	MgO	Al_2O_3	SiO_2	P_2O_5	*CaO*	Fe_2O_3	K_2O	Na_2O	SO_3
Composition (%)	0.19	21.75	38.42	0.21	*0.51*	4.10	0.94	0.15	1.60

Table 2   Vibration frequencies

β- Dicalcium silicate(HRDS) ν (cm^{-1})	β- Dicalcium silicate (control) ν (cm^{-1})
979.93 with a shoulder	997.29 with a small shoulder
929.77	875.76
902.77 with a shoulder	844.90
846.83	
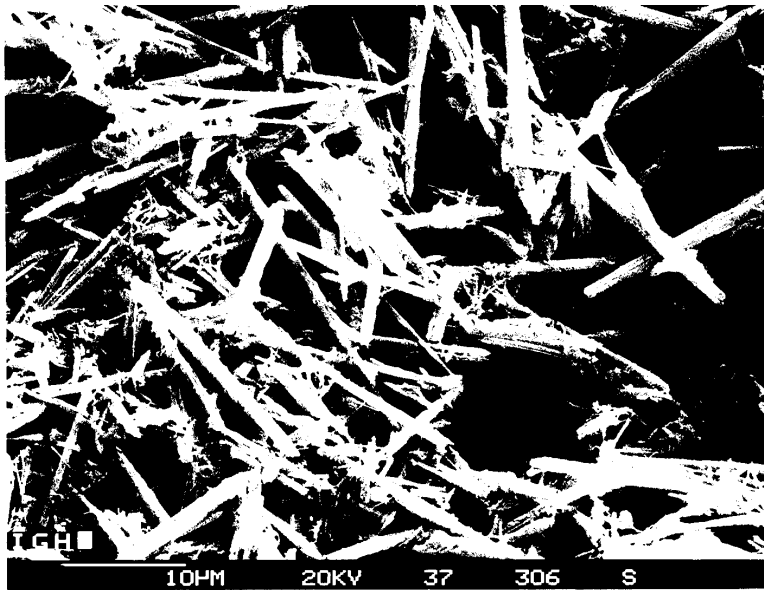
(a)
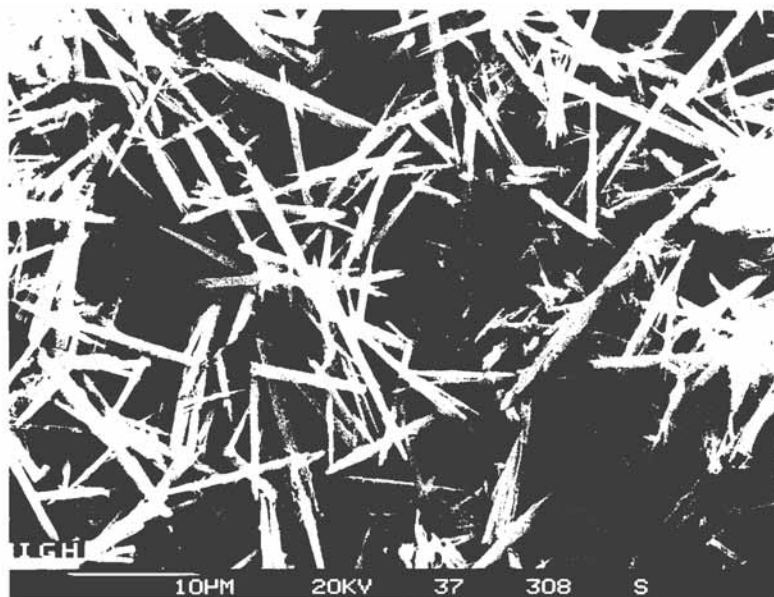
(b)

Fig. 1: (a). SEM picture of hydrothermally prepared calcium silicate hydrate.
(b). SEM picture of highly reactive -dicalcium silicate obtained at 9000C.
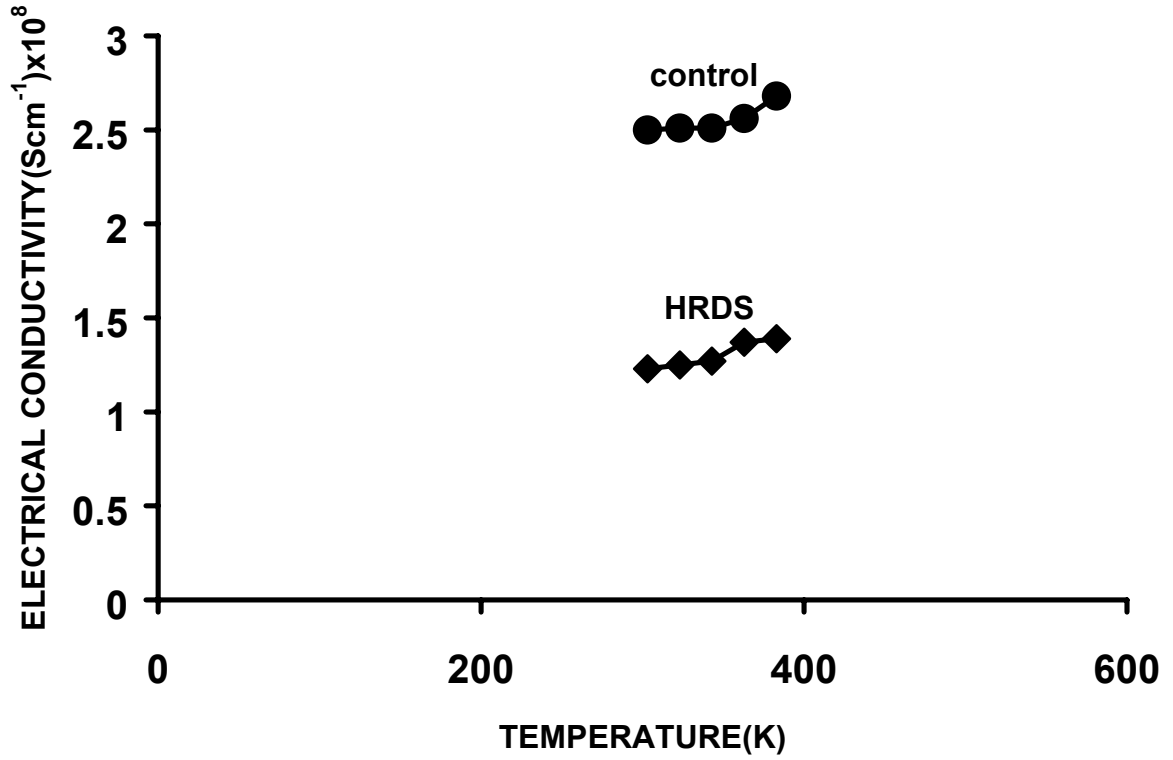
Fig.2   Variation of electrical conductivity with temperature of solid HRDS and control sample
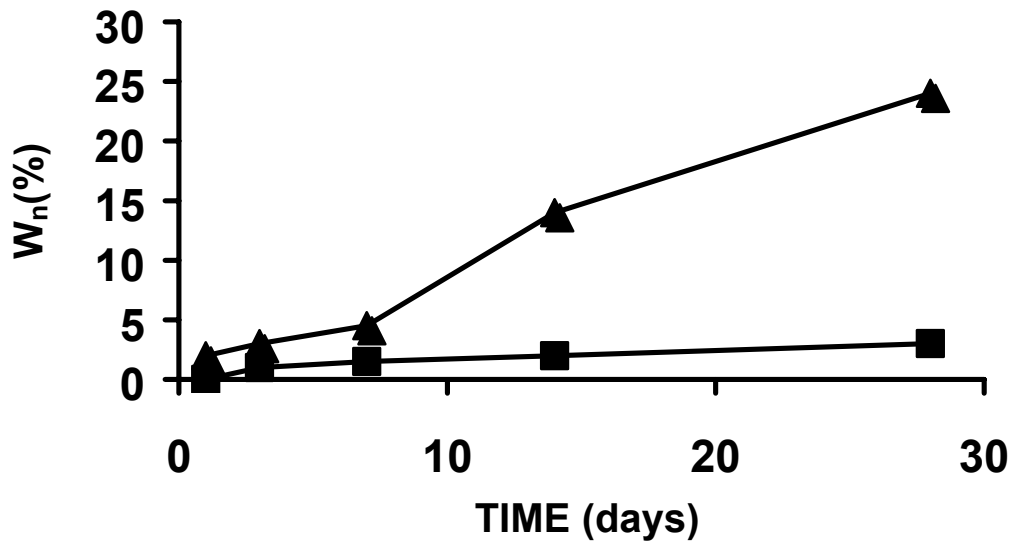
Fig.3   Variation of non evaporable water contents with hydration time
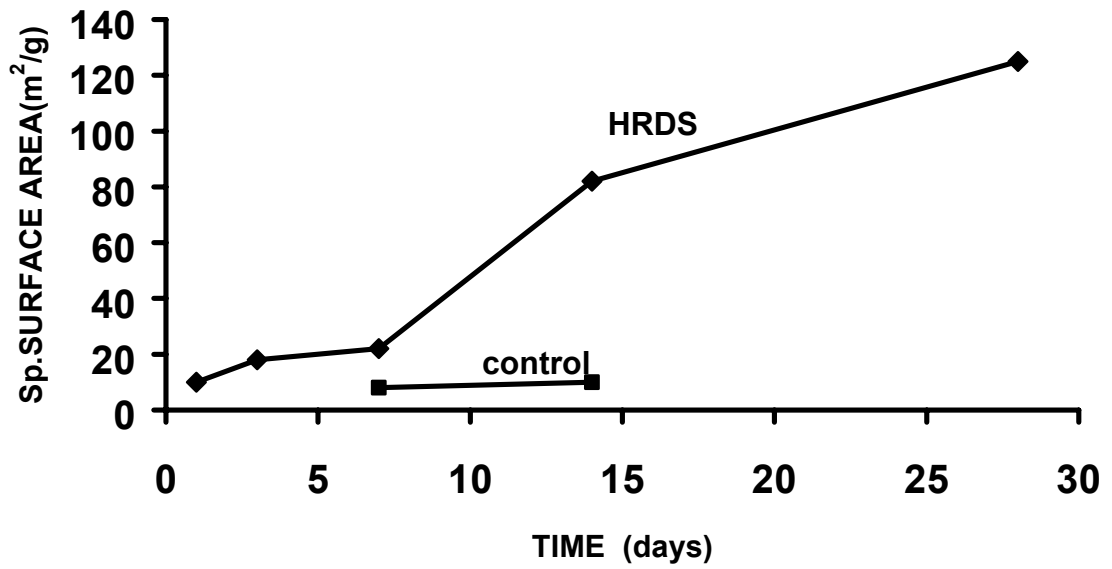
Fig.4   Variation of specific surface area with hydration time
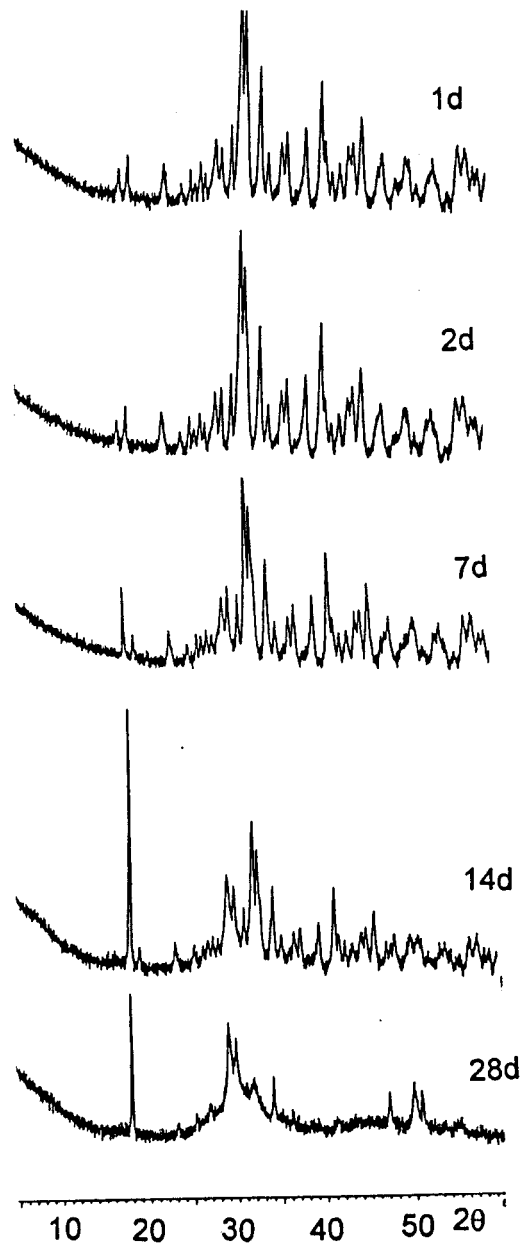
Fig.5 : X-ray diffraction patterns of highly reactive β-dicalcium silicate hydrated at different intervals of time (w/s=1.5).
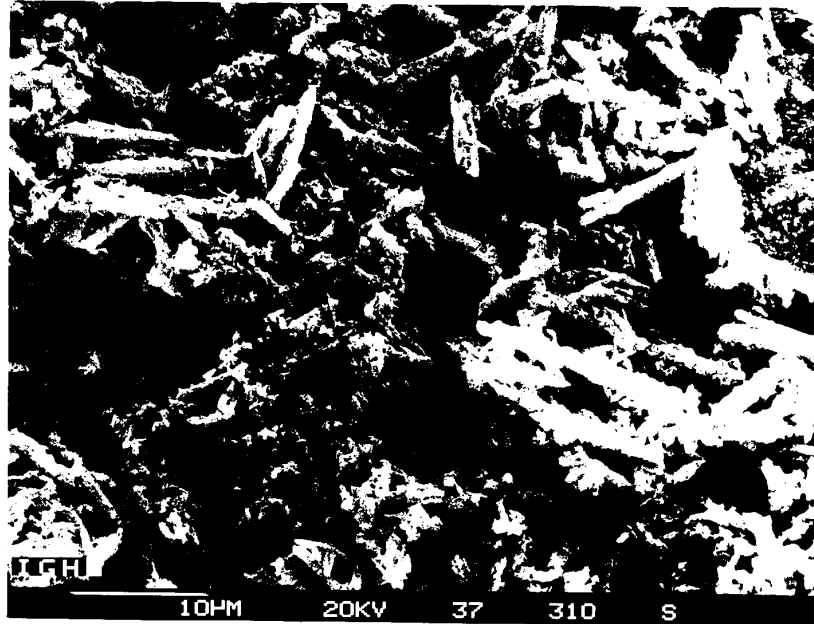
Fig.6   SEM of hydrated HRDS for 14 days
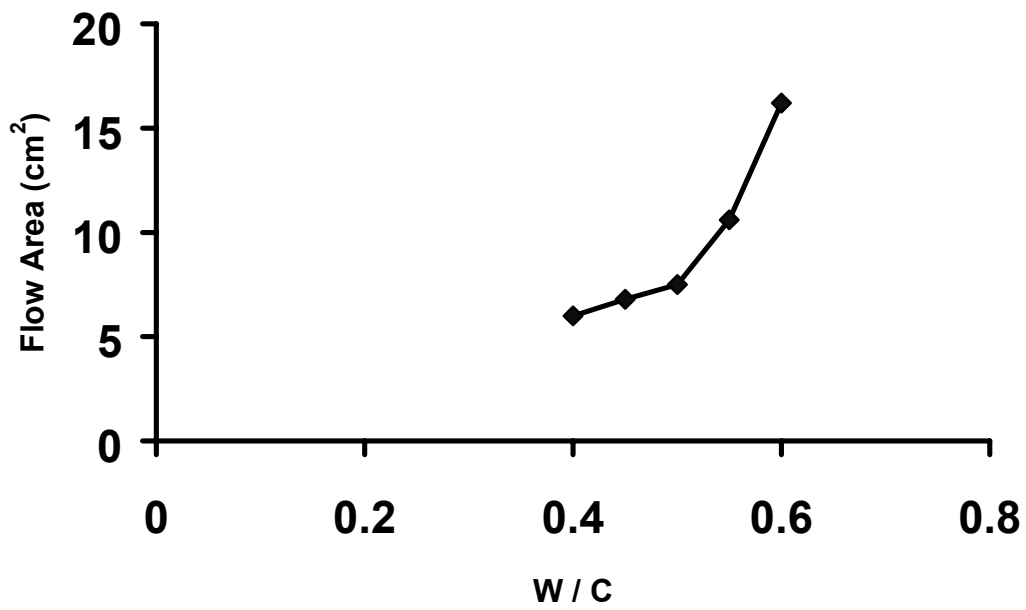
Fig.7   Variation of flow area with w/c in the presence of 0.5 wt% polycarboxylate type superplasticizer

J. F. Martirena
Prof. Dr. habil.
Universidad Central de las Villas
Santa Clara. Cuba

Robert L. Day
Prof. Dr. Dept. of Civil Engineering
University of Calgary
Calgary, Canada

Bernhard Middendorf
Dr. Senior scientist
University of Kassel
Kassel, Germany

Matthias Gehrke
Eng.
University of Kassel
Kassel, Germany

Lesday Martínez
Dr.
Universidad Central de las Villas
Santa Clara. Cuba

Juan M. Dopico
Eng.
Universidad Central de las Villas
Santa Clara. Cuba

Lime-pozzolan binder as a very fine mineral admixture in concrete

Summary

The very high concrete strength and durability achieved in high and ultra-high-performance concrete is associated with a very dense matrix, accomplished through the use of high volumes of very fine mineral additions, such as fly ash, silica-fume, metakaolin and ground quartz sand. The paper reports on a study where a finely ground lime-pozzolan binder (LPB) is used as active mineral addition in concrete. The very fine lime particles, having size between 0.1-10 μm, can fill the gaps between cement grains, while the larger pozzolan particles, having size between 10-100 μm, can fill the gaps between fine aggregate grains; this results in a much denser matrix. The addition of lime during concrete mixing also increases the Ca^{2+} and OH^- ion concentration, which results in a better and faster hydration of both ordinary portland cement (OPC) and pozzolanic reaction products. The use of LPB as an active addition in some ultra-high performance concretes could contribute to lowering the cost of the product for equivalent strength and durability performance, through the use of less cement, thus improving the ecologic profile of the material. Results from an initial series of tests are examined; further testing is required to establish the benefits of the use of LPC in UHP concrete. Examples of applications of this work in normal and high-performance concrete are presented.

1   Introduction

Although portland cement has contributed substantially to the development of our modern society and economy, its manufacture is based on the intensive use of non-renewable resources, and the production process produces large quantities of greenhouse gases. World cement production grows at spectacular rates. In 2002 it was 1.75 x 10^9 tons, with an

average yearly growth of 3.5%, measured since 1970. These production figures will continue to increase in the coming years as large segments of the world's population move to a higher level of industrialization. Cement production growth is estimated to range between 120-180% in 2020 [1].

Measures to decrease the rate of CO_2 emissions during cement manufacture can be classified in two main groups: a) attaining a higher efficiency in the production process, by decreasing fuel consumption; b) reducing the rate of clinker production by using mineral replacements, added during manufacture or directly through cement replacement at the building site [1,2]. The contribution of any of these measures to the reduction of energy consumption and emissions are small in comparison to the projected production increase. Although the goal is to replace 50% of fossil fuel by alternative fuels, in practical terms only 15% has so-far been achieved [3]. Moreover, the reported use of mineral additions has produced only a 22% emissions reduction. The technological improvements depend on the economy of the country where the production takes place [3].

In order to have the same levels of energy consumption and emissions in 2014 than those existing in 2004, the cement industry is challenged to reduce emissions by more than 50%. This implies a change of paradigms in production and use of portland cement, to make it comply with environmental requirements. Any solution of the problem includes the reduction of the amount of portland cement in the binding materials used to make concrete.

Progress in our knowledge of the science of concrete, the use of modern techniques to investigate the chemistry and microstructure, as well as the dynamic developments in the chemical-admixture industry, has opened new perspectives for the use of concrete as a modern construction material. These developments have revealed new routes towards the development of high strength, high durability, concretes that contain reduced quantities of portland cement. The use of less cement and larger amounts of pozzolanic minerals and other wastes, combined with highly active dispersing agents seems to be an attractive way to improve the environmental profile of concrete.

There are now a wide variety of blended cements available [4-7]. The inorganic materials that are used to reduce cement quantities can be blended and/or ground intimately with clinker and/or cement during manufacture, or blended while preparing the concrete or mortar. The most commonly used minerals are fly ash, granulated slag, micro silica (silica fume) and various natural and calcined pozzolans [4-7]. The nature of the product formed during the pozzolanic reaction in blended cements depends on the properties of the pozzolan and the clinker used to manufacture concrete. The main reaction products are calcium silicate hydrate (CSH), and smaller amounts of ettringite, hydrogarnet and hydrated aluminates; the relative proportions of the product depends upon details of the chemistry and mineralogy of the pozzolan used [4, 7].

Little is known about reactions and reaction rates in CH supersaturated solutions that may exist when using either lime-pozzolan binders or in blended cements. Apparently, the excess, undissolved, CH creates additional nucleation sites mainly because of its high specific surface. The early presence of CH in the mix seems to accelerate the pozzolanic reaction, probably because of the high amount of Ca^{2+} ions immediately available in the solution [8].

1.1   The use of mineral admixtures in concrete

Fine-grained mineral additions can help improve many qualities of concrete. There can be physical effects such as increased packing, or chemical-physical effects such as new reaction products formed during the pozzolanic reaction. In both cases the end effect is similar: the concrete porosity decreases and pore size distribution shifts towards smaller size fractions. The use of pozzolans can modify any or all rheological, mechanical and durability properties of concrete.

In regular-strength concrete, pozzolans are added to reduce cost and to improve the longer-term strength and durability of the hardened mass. In such cases the pozzolan helps to improve the packing density of the solids, but the primary role of the pozzolan is to provide additional calcium-silicate-hydrate through reaction with water and the calcium hydroxide contributed by the reaction of portland cement. This pozzolanic reaction is slow for most pozzolans that are used in high proportion; thus, the benefits of the pozzolan are seen within the time-frame of a week to several weeks after casting. Some of the finer, more highly reactive pozzolans (such as silica fume) are added in smaller proportion and help to improve early strengths as well as durability at later ages [9, 10].

In high and ultra-high performance concrete, the primary aim is to optimize the grain size distribution, especially of the fine particles. The use of superplasticizers and high-quality aggregates permits fluid mixes with very low water to cementing-materials ratio. The resulting concrete has a very high strength and density and very low porosity. In many of these mixes, however, the replacement by mass of portland cement is less than 15% [5, 11-13]. Conversely, in "high volume fly ash concrete" (HVFAC) the mass of mineral addition is higher than that of ordinary portland cement (OPC), and the water/binder ratio is very low (under 0.35). Twenty-eight days strength is in the range of 60-90 MPa, far higher than the control series manufactured with 100% OPC [14,15,16].

The pozzolan or mineral admixture plays a double role in these cases. The pozzolanic particles fill the empty spaces between cement grains and between other pozzolanic particles and improve packing. Only a small part of the added pozzolan, less than 20%, reacts. The compressive strength, however, does not correspond to the low level of hydration achieved. Some have attributed the strength increase to the contribution of electrical interaction between the smallest fly ash particles [15-17)

The pozzolanic reaction in most pozzolans becomes significant after the seventh day, when enough cement reaction products already exist and the alkali concentration is high enough to break chemical bonds and enable the formation of cement reaction products. In most cases, and depending on the reactivity of the pozzolan, most of the reaction is finished in the first 60 days [5, 9, 18]. However, the use of large volumes of pozzolanic additions increases the risk of self-neutralization because of excessive consumption of CH during the pozzolanic reaction. A significant drop in pH can result in the dissolution of the other reaction products and destruction of the cementing matrix [19].

1.2   Lime-pozzolan blends as fine mineral admixture in concrete

The properties of concrete with large volumes of pozzolan can be improved by replacing cement with lime-pozzolan blends (LPBs) rather than with pozzolan alone. The excess lime available immediately upon mixing reduces the risk of self-neutralization, even for large replacement volumes. The early presence of lime increases the Ca^{2+} concentration; it is hypothesized that this contributes to a faster formation of the reaction products. The presence of lime brings about an increase in OH^- ions, whose task is to break the silica bonds in the pozzolan; this can accelerate the start of the pozzolanic reaction.

The effect of lime can be seen in three different stages:
  a) During mixing the very fine particles of lime occupy the empty spaces between the cement grains and limit the flow of water, thus helping to increase water retention in the fresh mix. The smallest particles with high specific surface can adsorb on the surface of cement grains, thus acting as a dispersing agent that prevents flocculation and increases mix plasticity [5, 6].
  b) At early age the lime helps increase concrete packing, as the small lime grains with size between 1-30 µm, have not yet been completely dissolved and fill the gaps between cement grains.
  c) At later ages the 2-5 µm hexagonal plates occupy spaces between the reaction products. Fig 1 presents an SEM picture of a sample of a 28 days paste where 60% of the OPC has been replaced by an LPB. The hexagonal plates are quite visible, very close to the CSH phases.

A pozzolan for use in an LPB must be highly reactive and finely ground. Many authors state that using natural pozzolan and agriculture ashes brings about an increase in water demand in the mix, because of the irregular shape of the particles and the high internal porosity. However, when these particles are ground to fine powder, the internal structure is destroyed and the grains become more regular in shape and the internal porosity is thus reduced [20].
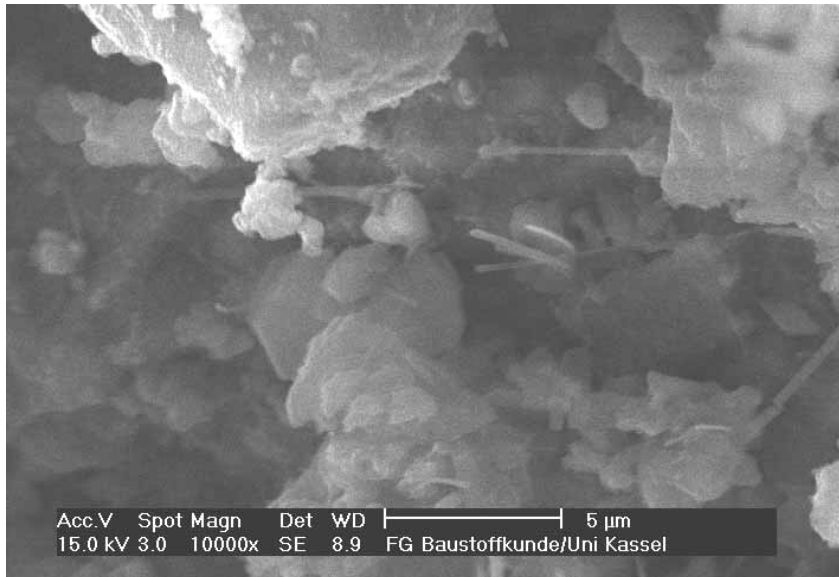
Fig. 1: Lime hexagonal plate crystals observed on the SEM on a 28 days OPC-LPB paste

Figure 2 shows a sugar-cane straw ash (SCSA) grain ground to an average particle size of approximately 10-µm. It has a cubic to spherical morphology with fewer visible internal pores, presumably because they were destroyed at grinding. The LPBs used in the present study consist of an interground blend of 20% lime and 80% pozzolan. The pozzolan used was either sugar can straw ash or a natural pozzolan (zeolite) found in Cuba. There was no significant difference in engineering performance between equivalent mortars and concretes made with these two pozzolans.

Mixing and grinding the pozzolan with lime should be done until the fineness of the powder equals that of OPC. This fineness level can be accomplished after only one-hour grinding in a batch ball mill. Through grinding, the size distribution of the pozzolan is improved, thus compensating for the effect of the irregular shape of the grains. The interaction between pozzolan and lime during grinding is also of great interest. Being softer, lime is more finely ground than the pozzolan. Figure 3 presents a typical grain size distribution for the pozzolan the CH and a portland cement. The resulting grain size of the lime particles lies between 1 - 30 µm. The pozzolan fraction has a larger grain size -- between 10-100 µm [21].
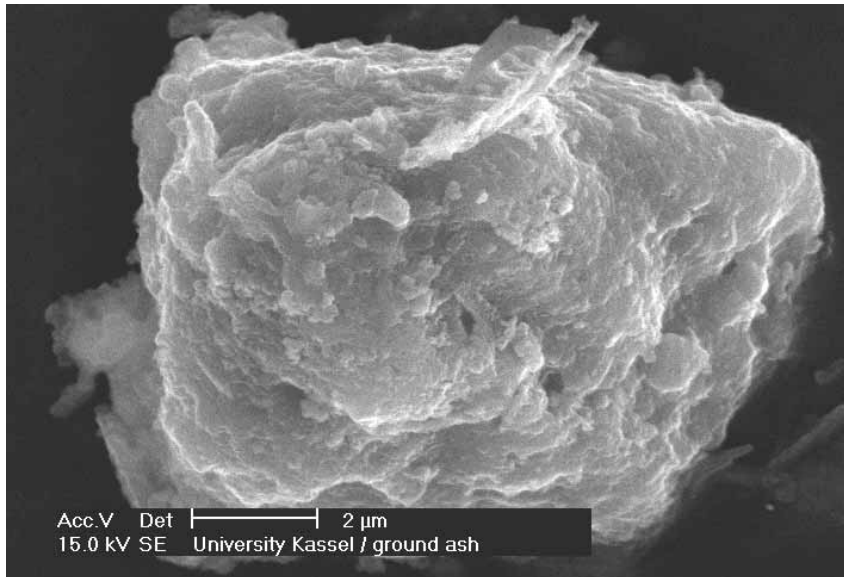
Fig. 2: Sugar Cane Straw Ash particle after grinding
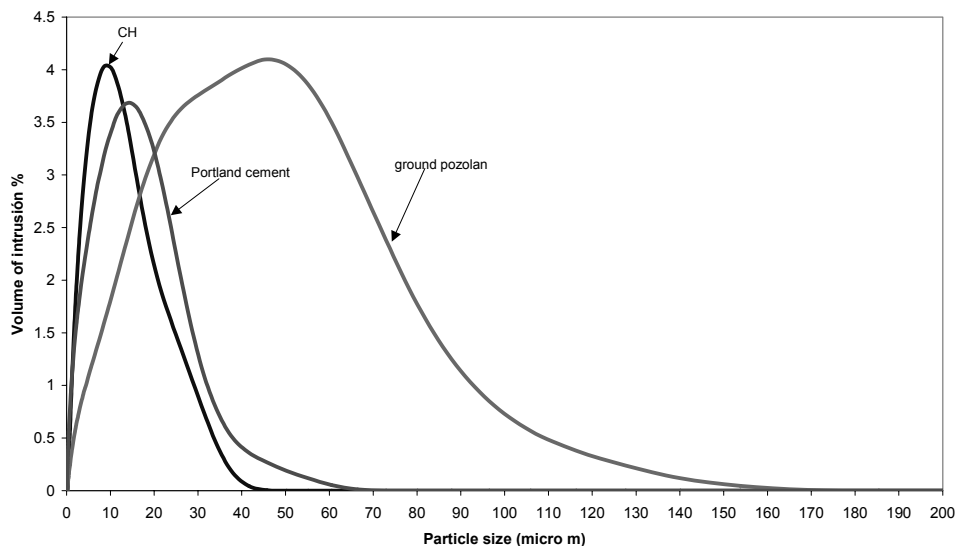
Fig. 3: Particle size distribution for CH, OPC and ground pozzolan

1.3 Concrete with high volumes of lime-pozzolan blend (LPB)

In order to optimize consumption of OPC in concrete, the relationship between compressive strength and cement content and fines in concrete must be thoroughly understood. A denser and stronger matrix cannot be achieved by only increasing the amount of OPC, since this implies an increase of the water demand in the mix -- which implies an increase in the porosity and microcracking in the hardened matrix. Instead, one can use very fine, low water-demand mineral additions that partially replace OPC and combine these with superplasticizers in order to manufacture concrete mixes with a lower water to fines ratio. This should produce a decrease in shrinkage and thermal microcracking, and provide a better hydrating condition for the OPC used. Also, the fine grains of the LPB complement the

particle size distribution of the cement by filling the voids between cement grains, and potentially those existing between the smaller grains of aggregate. This principle can be applied to any type of concrete, just as it has been applied to SCC and UHPC with the advantage of achieving excellent mechanical properties and durability with a very low OPC consumption.

To assess how much OPC can be replaced without varying the rheological properties of the mix, the authors propose a method that allows a correction to the traditional mix proportion to incorporate large volumes of LPB. The process has two stages. The first stage is to determine the maximum volume of cementing fines (volume of OPC + LPB, hereafter termed "fines") that a mix can assimilate without changing rheological properties significantly. To do this, a series of experimental trials is performed, where a given mass of OPC is replaced by the same mass of LPB at different replacement levels – for example, starting with 20% OPC replacement and increasing. The water is adjusted for each mix in order to remain within a target slump range. For each mix, strength of test cylinders at early age is measured. The optimum mix is the one with the highest replacement level but in which the water/fines ratio has not increased significantly (less than 20%) and there is an acceptable fall in the early compressive strength (less than 40%). The volume of fines at this point is considered to be the maximum volume of fines that the mix can assimilate for a given consistency.

Once the maximum volume of fines is determined, stage 2 adjustments are made. The total volume of cementing materials (OPC + LPB) and the amount of water used is kept constant – thus, the volumetric ratio of water/fines is constant – and the optimum volume ratio between OPC and LPB is determined [22, 23]. Usually, the proportion of LPB to OPC is increased until the target property, say 28-day strength, and a given consistency starts to show a significant change. The minimum amount of OPC to use is established in this way.

The use of a large volume of LPB results in a change in the aggregate/paste ratio, since the LPB has lower density than OPC. As the proportion of LPB increases, the volume of paste increases and the average spacing between aggregate grains increases. A thin section (Figure 4), clearly shows that in mortars where 40% of OPC is replaced, the aggregate grains separate from each other because of the increase of the volume of paste.
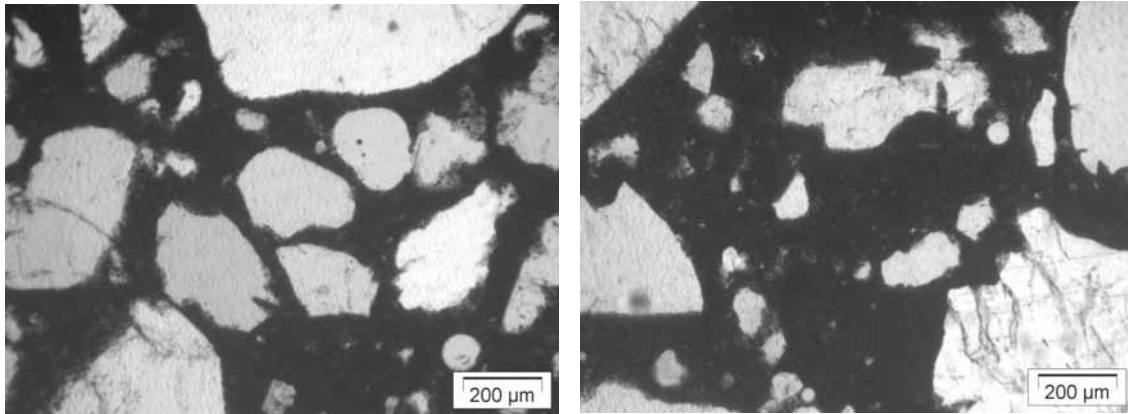
Figure 4: Mortars made with OPC (left) and with 40% lime-pozzolan addition (right)

1.4　　　Example of Optimum OPC-LPB Determination

To demonstrate the principles outlined here, a concrete was designed for the Cuban construction industry. The concrete has a 30 MPa target strength at 28 days. A traditional mix design requires 515 kg/m^3 of OPC because of the very poor quality limestone aggregate common in Cuba. The mix was designed for a target slump between 100-150 mm.

Stage 1: from 0 – 80% of the cement was replaced by the same mass of LPB. Table 1 tabulates the components of the mixes prepared and Fig. 5 shows the results of the compressive strength tests. OPC replacement always produces a lower compressive strength than the control at all ages. The mix prepared with 40% LPB (mass) proved to be able to assimilate the maximum volume of fines, while still maintaining an acceptable consistency. Above 40% replacement, 3 d and 7 d compressive strength fell significantly in comparison with the control series, and the water to fines ratio increased approximately 20% compared to that of the control series.

Table 1: Components of the mixes prepared in stage 1 (LPB Density = 2170 kg/m^3)

Material	unit	Proportion between LPB/OPC (mass)				
		0%	20%	40%	60%	80%
cement	kg/m^3	515	412	309	206	103
LPB	kg/m^3	0	103	206	309	412
Volume of "fines"	l/m^3	166	178	193	209	223
Fine aggregate	kg/m^3	737	737	737	737	737
Coarse aggregate	kg/m^3	737	737	737	737	737
superplasticizer	l/m^3	6.2	6.2	6.2	6.2	6.2
Water	kg/m^3	175	183	210	213	275
Water to OPC ratio (mass)	-	0.34	0.44	0.68	1.03	2.67
Water to fines ratio	-	0.34	0.36	0.41	0.41	0.53
Slump	mm	156	151	128	152	120
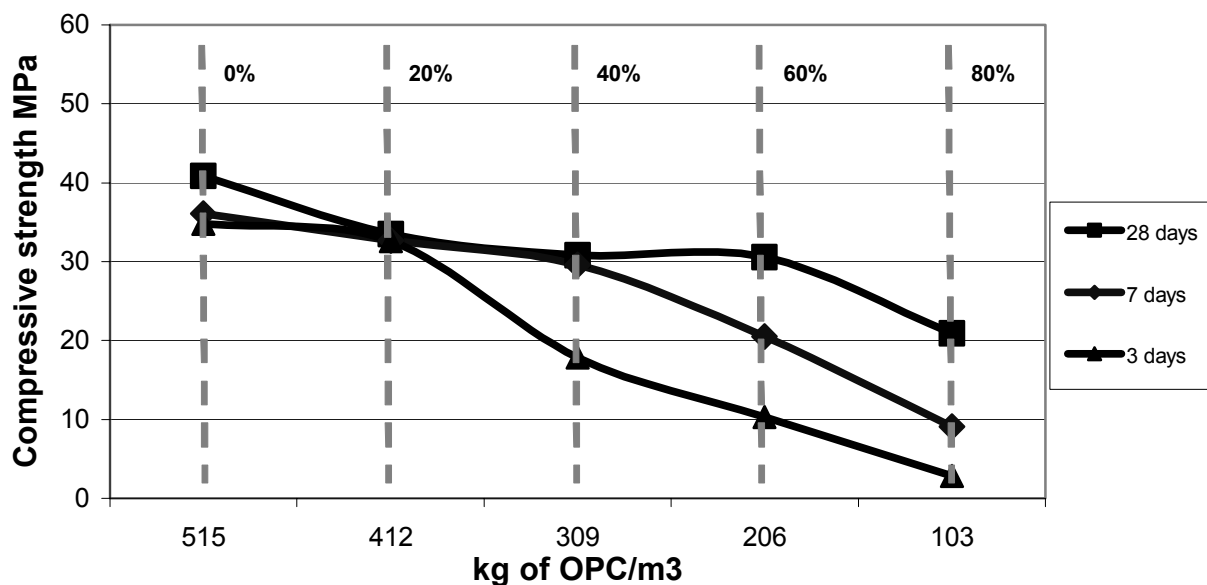
Fig. 5: Results of Stage I Strength Tests

Stage 2: the volumetric proportion between OPC and LPB was varied while keeping the total volume of fines and the water content constant (thus keeping the volumetric water to fines ratio constant), in order to assess the limits of OPC replacement. Table 2 presents the components of the mixes and Fig. 6 shows the results of compressive strength. The differences in compressive strength between the control series and that with 60% OPC volume replacement for mixes prepared with the maximum volume of fines are under 15%, while a 20% replacement of OPC with LPB appears to give optimum strength at 7 and 28 days.

The testing confirms that large amounts of OPC in a given mix can be replaced by LPC without serious reduction in the 28 days compressive strength and without significant variations in consistency, provided the volumetric ratio water to fines is kept constant and the

mix is prepared with the maximum volume of fines that it can assimilate. The samples tested in stage 2 show improvement in the compressive strength between 15-20% compared with samples prepared in stage 1 having similar mass of OPC per cubic meter.

1.5 Influence of lime-pozzolan admixture on pore structure

As concrete is a porous material, many aspects of its durability are associated with liquids transport within the pore structure of the concrete. In cold climates the water retained in the capillary pores can expand at temperatures below freezing and destroy the matrix. During chemical attack, pore water becomes a medium for reaction of various expansive compounds.

In the absence of cracking, impermeability is generally related to the volume of the capillary pore fraction. The definition of the boundary between capillary and the smaller pore fraction is a matter of some controversy. Here, we adopt the definition of capillary pores as those between 0.03 and 10 microns. Figure 7 shows the cumulative volume of mercury intruded for one OPC paste at 2 ages, and one 60:40 OPC:LPB paste at the same two ages. These pastes were water cured for 28 days and 60 days.

Table 2: Components of the mixes prepared for stage 2

| | | LPB/OPC proportion (vol.) | | | | |
	unit	0%	20%	40%	50%	60%
cement	kg/m^3	626	501	376	313	250
LPB	kg/m^3	0	81	163	203	244
Total LPB + OPC	kg/m^3	626	582	538	516	494
Water	L/m^3	210	210	210	210	210
Volume of "fines"	L/m^3	202	199	196	195	193
Fine aggregate	kg/m^3	737	737	737	737	737
Coarse aggregate	kg/m^3	737	737	737	737	737
superplasticizer	L/m3	7.5	7.0	6.5	6.2	5.9
Slump	mm	160	130	115	110	92
Water to OPC ratio (mass)	-	0.34	0.42	0.56	0.67	0.84
Water to fines ratio (mass)	-	0.34	0.36	0.39	0.41	0.42
Volumetric water to fines ratio		0.40	0.40	0.40	0.40	0.40
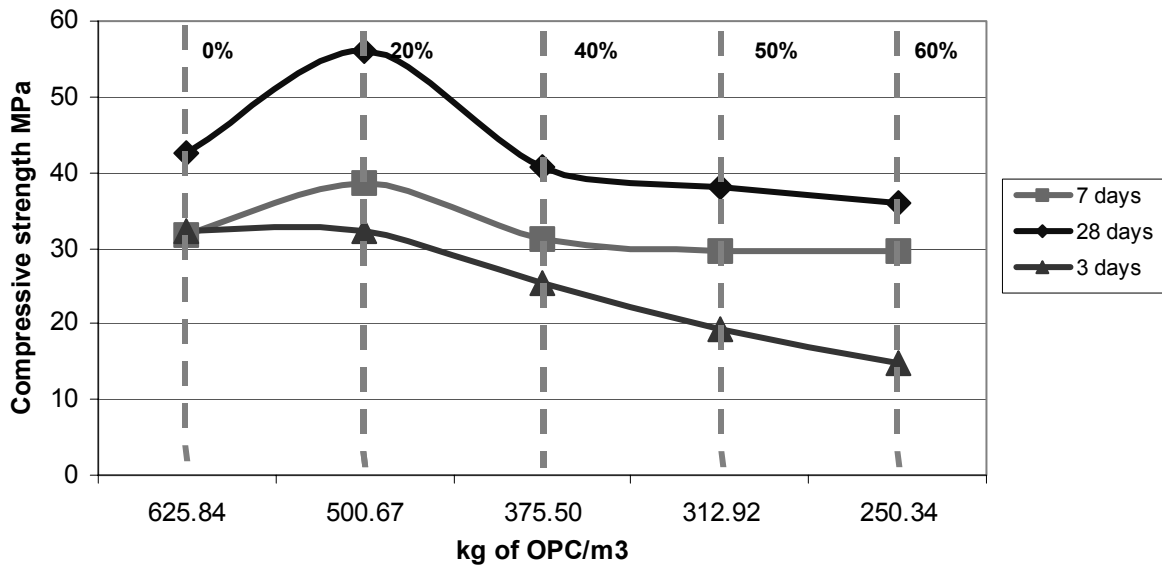
Fig. 6: Results of the experimental test carried out in stage 2

The refinement of pore structure in the OPC:LPB blend with age is a result of OPC hydration and continuing pozzolanic activity – additional confirmation of this is given below. However, Figure 7 clearly shows that the OPC:LPB paste has a significantly larger volume of capillary pores when compared to the OPC paste. One might expect a concrete made from the OPC:LPB blends to have a higher permeability than its OPC equivalent. This is not certain, however, since the effect on mass transport properties of optimizing the mix design – as described above – has yet to be determined.

The larger capillary porosity of pozzolan blended pastes that refines more quickly with time than OPC pastes is a common phenomenon for many types of pozzolans. In all cases additional testing of concretes made with these pastes under a wide range of exposure conditions is necessary.
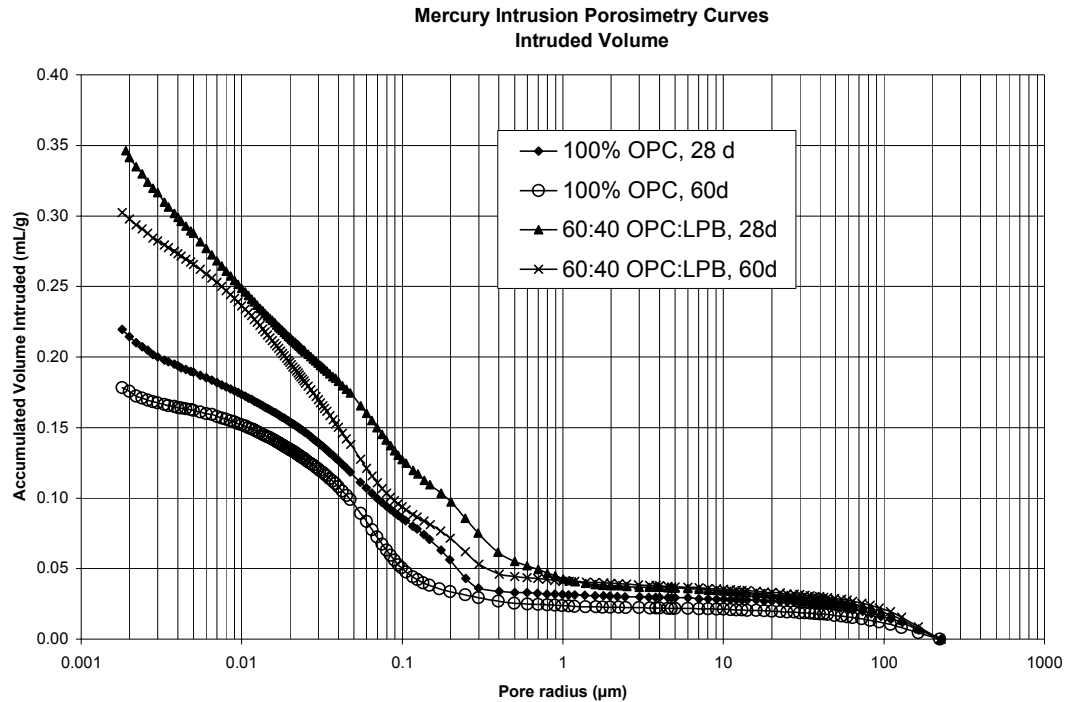
Figure 7: Pore-size distribution determined using mercury porosimetry. All pastes water cured for the time shown.

Fig. 8 shows the XRD traces of pastes made with different OPC/LPB blends. It can be observed that the higher the amount of LPB admixture, the lower the intensity of the CH peak, which suggests a considerable amount of pozzolanic activity in the OPC/LPB blends during the first 28 days of hydration.

The pozzolanic activity suggested by the XRD traces was confirmed by performing TGA on an OPC paste, and on 80:20 and 60:40 OPC/LPB pastes. Pastes were manufactured and then cured in sealed glass vials for 28 days, at which point TGA analysis was performed. The weight-loss vs. temperature curve allows one to determine the water lost from CH dehydroxylation during heating in the range from 470 to 550 ºC. Since the material proportions are known, one can calculate the theoretical CH content of the pastes assuming no pozzolanic activity. This value can then be compared to the estimated CH content from the measured weight loss. Thus, the following table was calculated:

OPC (g)	LPB (g)	Theoretical mass of CH present	Calculated mass of CH present, determined from measured water loss	CH consumed	CH consumedper g pozzolan
100	0	8.34	8.34	0	0
80	20	10.67	8.75	1.92	0.12
60	40	13.00	5.34	7.66	0.24

The TG analysis confirms the presence of pozzolanic activity. It also indicates that pozzolanic activity is higher when higher proportions are used – the 60:40 OPC:LPB blend consumes 0.24 g of CH per g of pozzolan, which the value is 0.12 for the paste containing only 20% LPB.
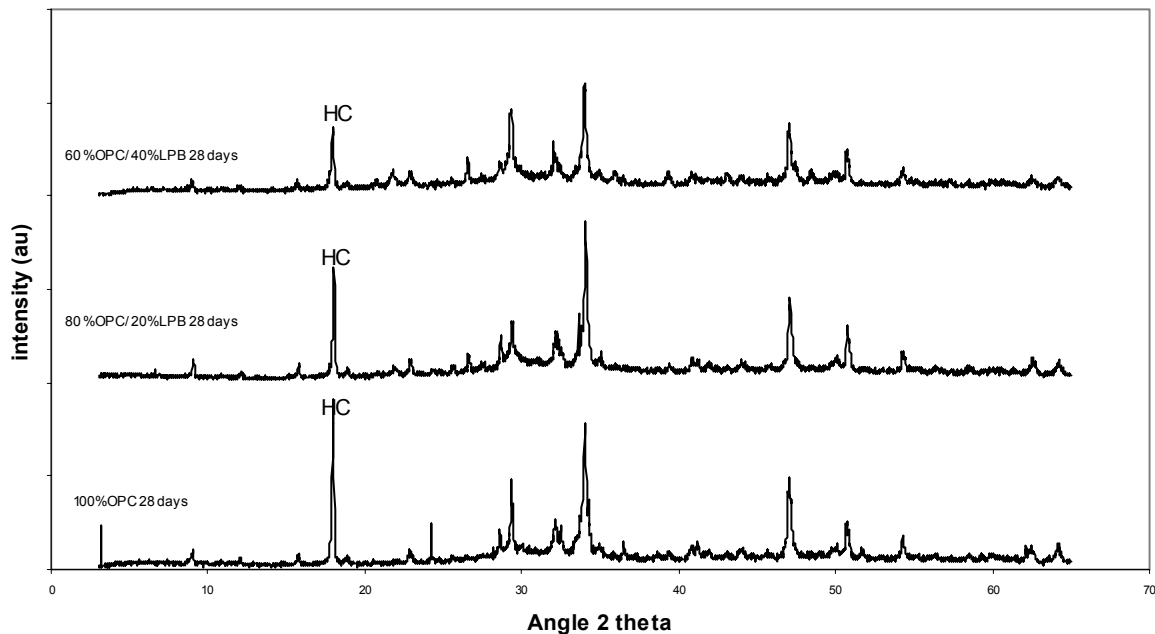
Figure 8. X-ray diffraction traces of hydrated cement paste and OPC:LPB pastes.

2 Conclusions

The use of lime-pozzolan binder (LPB) to reduce the amount of cement used in high and ultra-high performance concrete is an attractive proposition from an ecological viewpoint. Tests reported here have concentrated on regular-strength concrete, but the principles are expected to also apply to higher strength mixes. Results suggest that the quantity of cement can be reduced while maintaining equivalent strength by using a systematic procedure that optimizes the OPC/LPB ratio while maintaining a constant water/fines ratio and constant consistency.

From the standpoint of durability, the use of high levels of free-lime in a fresh concrete mix is a concern. Preliminary tests on pore structure and mineralogy indicate that this concern may not be founded, since chemical reaction between the pozzolan and lime reduces the amount of lime and also refines the pore structure of the concrete. However, for full-scale implementation of the proposed technology, additional engineering testing to establish mass transport properties and volume stability of OPC/LPB concretes under a wide range of exposure conditions is required.

3 Literature

[1] Vanderley M. John. On the sustainability of the Concrete. Extended version of the paper commissioned by UNEP Journal Industry and Environment. 2002.

[2] Price Lyan, Worrel Ernst, Phylipsen Dian. Energy Use and Carbon Dioxide Emissions in Energy-Intensive Industries in Key developing Countries. Proceedings of the 1990 Earth Technologies Forum, Washington, DC, September 27-29, 1999.

[3] Schmidt, M. Secondary Fuels and Raw Materials for Cement. Benefit for the environment and cost reduction. Keynote presentation at IV Simposium on Structures and Materials, november 2002. Santa Clara. Cuba.

[4] Day Robert L. Pozzolans for use in low cost housing: state of the art report. Department of Civil Engineering. Universidad de Calgary. Report No. CE92-1. January 1992.

[5] Malhotra V.M, Mehta P.K. Pozzolanic and cementitious materials. Published by Gordon and Breach. UK. 1996.

[6] Swamy R.N, Cement replacement materials. Series "Concrete technology and Design", Volume 3. Surrey University Press. UK 1986.

[7] Taylor H.F.W.: Cement Chemistry. Academic Press. London, 1993.

[8] Williams P. Jason, Biernacki Joseph J, Walker Larry R, Meyer Harry M, Rawn Claudia J, Jianming Bai. Microanalysis of alkali-activated fly ash-CH pastes. Cement & Concrete Research Vol. 32, pp 963-972, 2002. USA.

[9] Shannang M.J, Yeginobali A. Properties of pastes, mortars and concretes containing natural pozzolans. Cement & Concrete Research Vol. 25, No. 3, pp 647-657, 1995. USA.

[10] Singh N.B, "Hydration of bagasse-ash blended Portland cement", Cement & Concrete Research Issue No. 9, Vol. 30, 2000 pp: 1485-1488.

[11] Aitcin Pierre-Claude, "Cements of yesterday and today. Concrete of tomorrow", Cement & Concrete Research Issue No. 9, Vol. 30, 2000, pp: 1349-1359.

[12] Taylor M.R. et al, "Mix proportions for high strength concrete", Construction and Building Materials No. 6, Vol. 10, 1996, pp: 445-450.

[13] Zhang M.H. et al, "Rice-husk ash paste and concrete: some aspects of hydration and the microstructure of the interfacial zone between the aggregate and paste", Cement & Concrete Research Issue No. 6, Vol. 26, 1996 pp: 963-977.

[14] Bouzoubaa, N. et al, "Laboratory-produced high-Volume fly ash blended cements: physical properties and compressive strength of mortars", Cement & Concrete Research Issue No. 11, Vol. 28, 1998 pp: 1555-1569.

[15] Lam L. et al, "Degree of hydration and gel/space ratio of high Volume fly ash/cement systems", Cement & Concrete Research Issue No. 5, Vol. 30, 2000 pp: 747-756.

[16] Poon C.S. et al, "A study on high strength concrete prepared with large Volumes of low calcium ash", Cement & Concrete Research Issue No. 3, Vol. 30, 2000 pp: 447-455.

[17] Qualin Niu, Naiqian Feng, Jing Yang, Xiaoyan Zheng. Effect of superfine slag powder on cement properties. Cement & Concrete Research Vol. 33, pp 615-621, 2003. USA.

[18] Jamal Shannag M, "Properties of pastes, mortars and concrete containing natural pozzolana", Cement & Concrete Research Issue No. 3, Vol. 25, 1995 pp: 647-657.

[19] Groves G.W, and Richardson I.G.: Microcrystalline Calcium Hydroxide in Pozzolanic Cement Pastes, Cement and Concrete Research, Vol. 24, pp 1191-1196, 1994.

[20] Erdogdu K, "Effect of fly ash particle size on strength of Portland cement fly ash mortars", Cement & Concrete Research Issue No. 9, Vol. 28, 1998 pp: 1109-1117

[21] Martirena J.F.: The Development of Pozzolanic Cement in Cuba, Journal of Appropriate Technology, Vol. 21, No. 2, September 1994, Intermediate Technology Publications, U.K.

[22] Bornemann, R. The role of powders in concrete. 6th international Symposium on utilization of high strength / high performance concrete. Leipzig 2002.

[23] Schmidt, M. Ultra-Hochleistungsbeton- Ausganstoffe, Eigenschaften und Leistungsfaehigkeit. Proceedings of the conference Ultra-Hochfester Beton University of Kassel, September 2003. Germany.

Iman Talebinejad

MSc students of structural engineering

University of Tehran

Tehran, Iran

Amirhossein Iranmanesh

MSc students of structural engineering

University of Tehran

Tehran, Iran

Seyed Asadollah Bassam

MSc students of structural engineering

University of Tehran

Tehran, Iran

Mohammad Shekarchizadeh

Assistant professor

University of Tehran

Tehran, Iran

Optimizing mix proportions of Normal Weight Reactive Powder Concrete with Strengths of 200-350 MPa

Summary

In this paper, the effect of super plasticizer amount, water/cement ratio and the cement and silica fume content is studied on the ultimate compressive strength of the new generation of Ultra High Strength Concrete (UHSC) known as Reactive Powder Concrete (RPC). In this kind of concrete, the strength can reach to 200-800 MPa depending on the curing type and the manufacturing process. The emphasis is on the RPC with the strength range of 200-350 MPa. Also, the effect of curing temperature is observed on the ultimate compressive strength of RPC and finally, the effect of confinement on the ultimate compressive strength is evaluated. Based on the data of testing more than 38 different mix proportions and curing procedures, an optimized mix proportion with a density of about 2400 kg/m^3 and strength of more than 300 MPa is designed.

Keywords: *super plasticizers, cement, silica fume, Reactive Powder Concrete, strength*

1   Introduction

The term Reactive Powder Concrete (RPC) has been used to describe a fiber-reinforced, super plasticized, silica fume-cement mixture with very low water-cement ratio (W/C) characterized by the presence of very fine quartz sand (0.1-0.5 mm) instead of ordinary aggregate [1, 2]. In fact, it is not a concrete because there is no coarse aggregate in the cement mixture. The absence of coarse aggregate was considered by the inventors to be a key aspect for the microstructure and the performance of the RPC [1, 2] in order to reduce the heterogeneity between the cement matrix and the aggregate. However, due to the use of very fine sand instead of ordinary aggregate, the cement factor of the RPC is more than 1000 kg/m^3. Another characteristic of RPC is its high density which is usually more than 2600 kg/m^3 due to the pressure applied before its setting. When the concrete is pressed before setting, the entrapped air and most of the chemical contraction accompanying hydration reaction can be eliminated. It is shown in [3] that pressing fresh concrete during setting can

improve its strength. Finally, the use of steel micro fibers in the RPC mixture improves the ductility of the material.

Also, it has recently been shown [4, 5] that confining RPC in thin steel tubes presents several advantages: it drastically increases concrete compressive strength and ductility.

The main purpose of the present investigation is to modify RPC by taking into account all of the effective parameters in RPC production, so that without increasing the concrete density, an optimum mix proportion with the maximum possible compressive strength could be obtained.

2   Scope of study

Experimental work conducted as part of this study included: producing appropriate powder aggregate in the laboratory, mixing trial batches to determine appropriate mix proportions under laboratory condition, testing hardened samples to determine which mix proportions and manufacturing method provided good properties for RPC, and establishing basic material properties.

Most experimental work including sieve analysis, cement and silica fume grounding, compressive tests on cubic samples and curing of the RPC specimens was conducted at the University of Tehran.

3   Material detail

The aggregates used are crushed quartzite with maximum size of 1 mm with the same grading of ASTM. The cement is type 5 cement produced by Tehran Cement Co. and the Super Plasticizer (SP) is polymer based. Chemical specifications of the cement and silica fume used in this study are shown in table 1.

Table 1: Chemical Specifications of Cement and Silica Fume (%)

	CaO	SiO_2	Al_2O_3	Fe_2O_3	MgO	SO_3	K_2O	Na_2O	Lol
Cement Type 5	63.78	20.59	3.66	6.10	0.95	2.13	0.48	0.26	2.05
Silica Fume	2	90	1.5	1.5	0.8	---	---	---	---

The main reason for using type 5 cement is the lack of C_3A in this kind of cement which results in the better effect of super plasticizer, and therefore, one needs less W/C ratio and can reach to higher strengths. Micro steel fibers with yielding strength of 2500 MPa, 12 millimeters long and equivalent diameter of 0.1 mm are used which are manufactured by VTI, Germany.

4   Mix proportions

Several mix proportions are tested to study the effective parameters. These mix proportions are shown in table 2.

5   Curing methods

Four curing methods are used to study the effect of curing on the ultimate strength of the specimens. The reason of high temperature curing (with temperatures of more than 200 $^{\circ}$C) is the formation of a new generation of C-S-H known as xonolite with the formulation of C_6-S_6-H [1]. It is believed that this hydration product is the reason of gaining strengths of more than 200 MPa in RPC. Also, all of the specimens are cured in cold (room-tempered) water. Curing of the concrete in cold water in its early age leads to a better and stronger formation of silicate hydrates while continuing of curing in higher temperatures accelerates the silicate hydrates formation [6]. The curing methods are shown in figure 1.
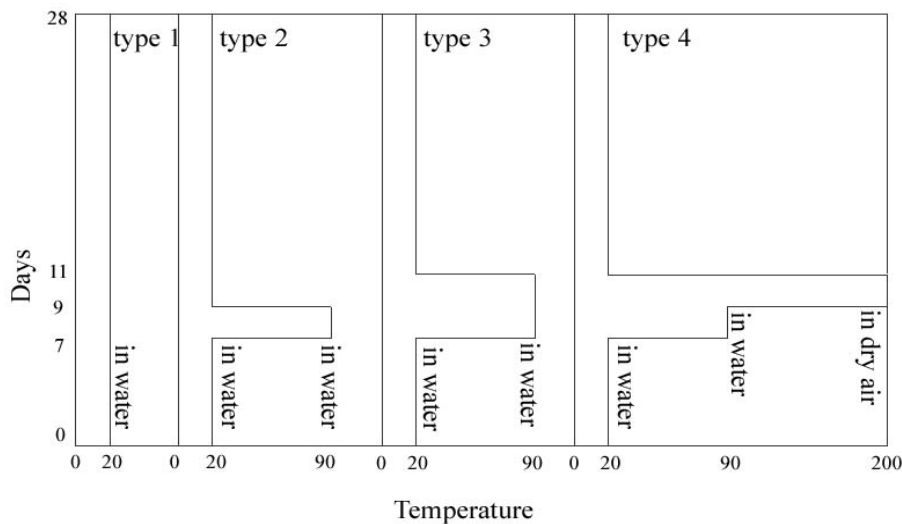
Figure 1: Curing methods

6   Test program

6.1   Specimen details

For each of the mix proportions, 3 samples are made by casting RPC in a 3-cell 5x5x5 cm cubic mold and pressing the mold cells by applying a 2-ton load on the upper surface of the cubes. The lateral walls of the mold exerts a lateral pressure on the fresh concrete and therefore, a 3 directional pressure, compacts the RPC by removing all of the entrained air. The pressure remains constant on the mold for 10 hours and then, the specimens are demolded and the curing processing starts. After the curing processing finishes, all of the 3 specimens are tested in compression and the average compressive strength is recorded as the ultimate strength of that mix proportion.

Table 2: Mix proportions of RPC specimens and their applied curing type

Specimen	W/C (%)	Cement (Kg/m^3)	Silica Fume (%)	Steel Fiber (%)	Type of Curing
s_1	11.5	1300	25	1	4
s_2	11.5	1500	25	1	4
s_3	11.5	1750	25	1	4
s_4	11.5	1900	25	1	4
s_5	11.5	2105	25	1	4
s_6	13	1300	25	1	4
s_7	13	1500	25	1	4
s_8	13	1750	25	1	4
s_9	13	2105	25	1	4
s_{10}	17	1300	25	1	4
s_{11}	17	1500	25	1	4
s_{12}	17	1750	25	1	4
s_{13}	17	2105	25	1	4
s_{14}	11.5	1900	20	1	4
s_{15}	11.5	1900	30	1	4
s_{16}	11.5	1900	35	1	4
s_{17}	12	1900	20	1	4
s_{18}	12	1900	25	1	4
s_{19}	12	1900	30	1	4
s_{20}	12	1900	35	1	4
s_{21}	13	1900	20	1	4
s_{22}	13	1900	25	1	4
s_{23}	13	1900	30	1	4
s_{24}	13	1900	35	1	4
s_{25}	17	1900	20	1	4
s_{26}	17	1900	25	1	4
s_{27}	17	1900	30	1	4
s_{28}	17	1900	35	1	4
s_{29}	10	1900	25	1	4
s_{30}	11	1900	25	1	4
s_{31}	20	1900	25	1	4
s_{32}	11.5	1900	25	1	4
s_{33}	13	1900	25	1	4
s_{34}	17	1900	25	1	4
s_{35}	20	1900	25	1	4
s_{36}	11.5	1900	25	1	3
s_{37}	11.5	1900	25	1	2
s_{38}	11.5	1900	25	1	1

6.2 Testing device

The specimens are tested under compression applied uniaxially by a 200-ton hydraulic jack. The load is applied at a rate of 300 KN/min. The maximum load achieved prior to failure is recorded as the load capacity.

7 Results

In this part, we discuss on the effect of some of the parameters on RPC strength. The results are shown in table 3. The numbers of mix proportions shown in this table are in accord with the numbers shown in table 2.

Table 3: Compressive strength obtained for different RPC compositions and curing methods

Specimen	S_1	S_2	S_3	S_4	S_5	S_6	S_7	S_8	S_9	S_{10}	S_{11}	S_{12}
f_c (Mpa)	261	274	307	325	241	230	255	295	212	163	187	230
Specimen	S_{13}	S_{14}	S_{15}	S_{16}	S_{17}	S_{18}	S_{19}	S_{20}	S_{21}	S_{22}	S_{23}	S_{24}
f_c (Mpa)	156	288	308	291	270	309	292	280	253	289	262	237
Specimen	S_{25}	S_{26}	S_{27}	S_{28}	S_{29}	S_{30}	S_{31}	S_{32}	S_{33}	S_{34}	S_{35}	S_{36}
f_c (Mpa)	185	228	209	195	224	270	173	248	243	203	160	249
Specimen	S_{37}	S_{38}										
f_c (Mpa)	233	152										

7.1 Cement factor

To study on the effect of cement factor, we limit ourselves to the 4th curing method shown in figure 1. The silica fume content for such study is 25 %. The result of testing different RPC compositions with the above characteristics is shown in Figure 2.

In what follows, we use the cement factor of 1900 kg/m^3 for the sake of comparison.

7.2 Silica fume content

To study on the effect of silica fume content, we made RPC with different W/C ratios, and made the specimens with the optimum cement content observed in section 7.1. The results are shown in figure 3.

As can be seen, the optimum silica fume content for RPC with strengths of 300-350 MPa is about 25% of the cement weight.

7.3 W/C ratio

As we expect, the ultimate compressive strength of RPC is increased by reducing the W/C ratio. To study on the effect of W/C ratio, we keep the silica fume content to 25% of the cement weight. The results are shown in figure 4.

7.4 Curing effect

With the optimized mix proportion obtained by now, we study the effect of curing methods on the ultimate compressive strength of RPC. The effect of curing is shown in table 4.
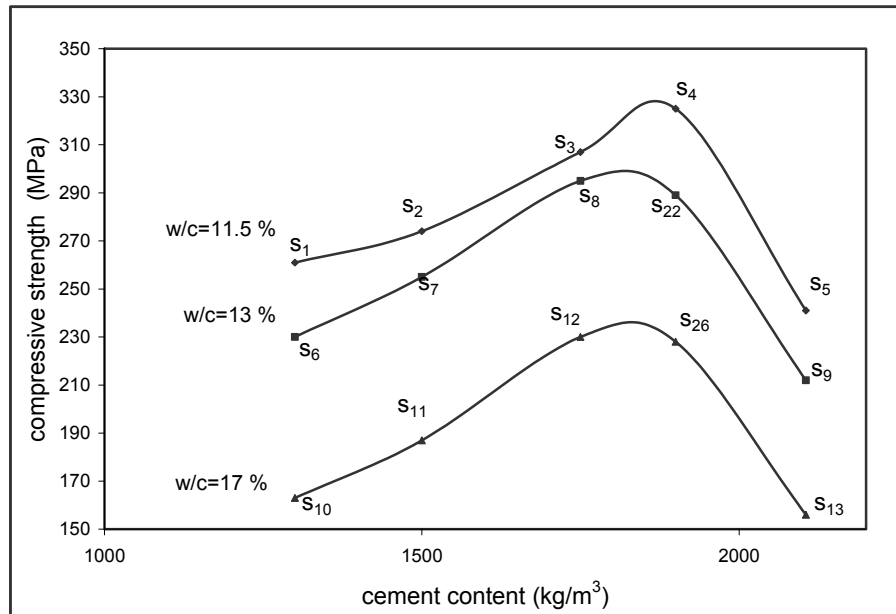
Figure 2: Cement factor vs Compressive strength of RPC
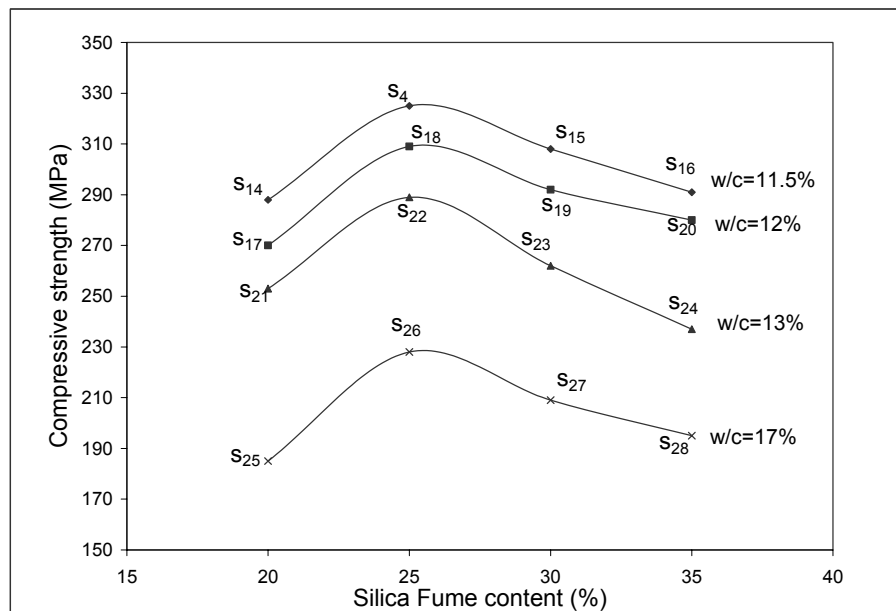
Figure 3: The effect of silica fume content on the compressive strength of RPC
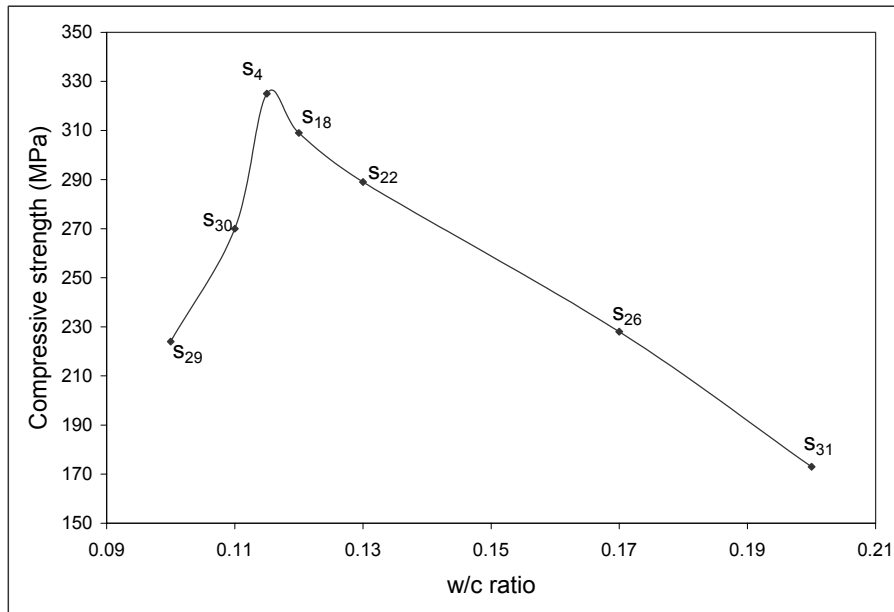
Figure 4: The effect of W/C ratio on the compressive strength of RPC

Table 4: The effect of curing on the Compressive strength

Specimen	S_{38}	S_{37}	S_{36}	S_4
Type of Curing	1	2	3	4
f_c (Mpa)	152	233	249	325

7.5   Confinement effect

As mentioned in the previous sections, a confining pressure is applied on the final specimen. The strengths obtained with and without this pressure are shown in figure 5.

In figure 5, one can note that the confining pressure of 8 MPa can increase the ultimate compressive strength of RPC to 25%.

8   Conclusions

From the results of this study, following conclusions can be drawn:

It can be shown that a cement factor range of 1700 to 2000 kg/m3 results in highest compressive strengths. Although it seems that the strengths should increase with increasing the cement factor, after a certain value of cement factor, the strength drops. The reason of this phenomenon is in the fact that with increasing the cement factor, the aggregates can not participate in RPC compaction. Therefore, RPC with high cement factor does not have a good grading and can not reach to its optimum compaction. Also, by reducing the cement factor to amounts of less that the optimum range, the compressive strength of the aggregates takes a major role in the overall strength of RPC and since the compressive strength of the aggregates are far less
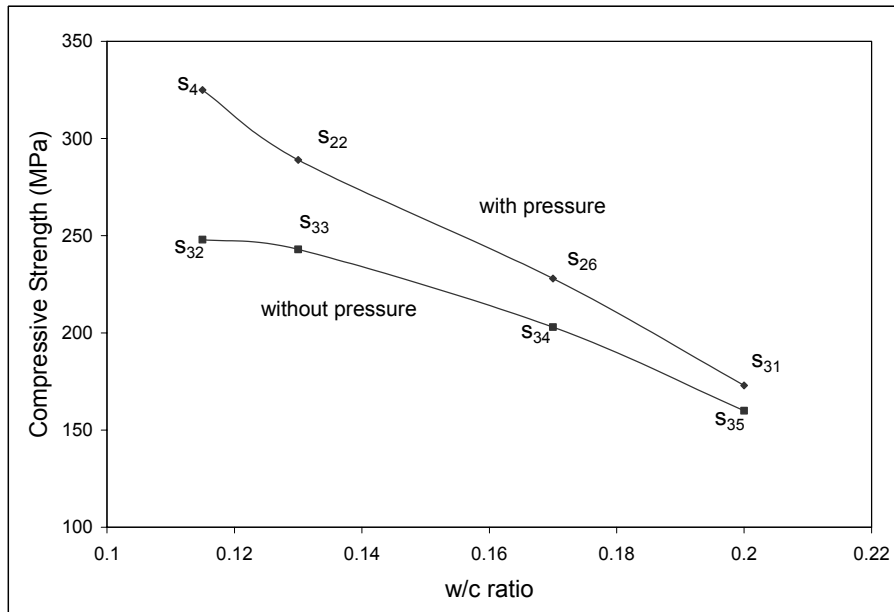
Figure 5: The effect of confining pressure on the strength

than the strength of RPC, the overall strength of RPC decreases with reducing the amount of cement factor to less than the optimum value.

From table 4, one can note that the 4th curing type leads to the best results. As it is mentioned in section 5, the reason of this deference is the formation of xonolite in high temperatures (Higher than 200 $^{\circ}$C) which is a very high strength type of C-S-H family. Second and third type of curing result in higher ultimate compressive strengths due to the effect if hot-water curing on increasing pozzolanic activity of the concrete. Also, hot-water curing accelerates the hydration of cement and leads to higher early-age strengths of concrete.

The main role of silica fume is that by the chemical reaction occurred during the curing processing, the low strength C-H made in concrete is combined with Silica fume and the product is the well known high-strength C-S-H. The optimum amount of silica fume in concrete is highly dependent to the amount of W/C ratio. According to [7], the optimum silica fume content is 30-35% of the cement weight in RPC with strength of 200 MPa. But, in this study, the desired compressive strength is more than 300 MPa, and a lower amount of W/C ratio is necessary to reach to such strengths. Therefore, lower amount of C-H is produced during the curing and lower optimum silica fume content is observed in our study.

The test results shown in figure 5 indicate that the water to binder ratio is the most important factor affecting the strength of RPC. With the same mix proportions and curing method, the reduction of W/C ratio from 20% to 11.5% increase the compressive strength approximately 46%. Also, figure 5 shows that for the W/C ratios of less than 10%, compressive strength substantially decreases. This can be because of the lack of water for completing the chemical reactions. It is also seen that for a W/C ratio of about 10%, workability of concrete is not enough, and the confining pressure can not be applied appropriately.

Confining and pressing RPC at the time of casting result in an outstanding new very high strength concrete which has a compressive strength around 350 MPa.

9   **Acknowledgement**

10   **References**

[1] Richard, P. and Cheyrezy, M.H. "Reactive Powder Concretes with High Ductility and 200-800 MPa Compressive Strength", Concrete Technology: Past, Present, and Future, Proceedings of the V. Mohan Malhotra Symposium, ACI SP-144, S. Francisco 1994, pp. 507-518. Editor: P.K. Mehta.

[2] Coppola, L., Troli, R., Collepardi, S., Borsoi, A., Cerulli, T. and Collepardi, M. "Innovative Cementitious Materials. From HPC to RPC. Part II. The Effect of Cement and Silica Fume Type on the Compressive Strength of Reactive Powder Concrete", L'Industria Italiana del Cemento, 707, 1996, pp. 112-125.

[3] Freyssinet, M.E. "Cement and Concrete Manufacture." vol. 9, 1936, p. 71.

[4] Lahlou, K., Aïtcin, P.-C., and Chaallal, O. "Behaviour of High Strength Concrete under Confined Stress." *Cement and Concrete Composites,* 14(3), 1992, pp. 185-193.

[5] S. Collepardi, L. Coppola, R. Troli, M. Collepardi. "Mechanical Properties of Modified Reactive Powder Concrete".

[6] A. M. Neville. "Properties of concrete", 4th edition, Longman Publishing Co, 1995.

[7] Youhua Yang. "Manufacturing Reactive Powder Concrete using common new Zealand materials", Master of engineering thesis, university of Auckland, July 2000.

[8] P. Richard. "Reactive Powder Concrete: A new Ultra High Strength Cementitious Material" Fourth Intl Symposium on the Utilization of High Strength Concrete, Vol 3, 1996, pp. 1343-1349.

Vellmer, Carsten
Dr.; Postdoctoral Research Fellow
University Kassel
Kassel, Germany

Gehrke, Matthias
Research Assistant
University Kassel
Kassel, Germany

Middendorf, Bernhard
Dr.; Senior Scientist
University Kassel
Kassel, Germany

Seeing at the nanoscale: Hydration of pozzolanic and cementitious materials

Summary

Nowadays concrete is the most utilized building material for civil engineering and infrastructure projects. However, we are still far from an understanding of what happens in detail during setting and hydration of concrete. This period is of mayor importance since it determines the physico-mechanical characteristics of concrete, especially its microstructure as well as the morphology of hydration products. While SEM gave some inside into hydration mechanisms it failed to visualize the hydration processes in-situ under characteristic conditions (temperature, pressure, pore solution). However, atomic force microscopy (AFM) provides a resolution at nanometer scale and allows in-situ observation at atmospheric condition and characteristic environments.

AFM studies provide the necessary information on complex hydration processes which are required to design ultra-high-performance concrete with a defect-free microstructure which will result in an enhanced long-term performance.

Keywords: *microstructure, porosity, microsilica, super plasticizers, hydration products, calorimetry, AFM technique, nanoscale*

1   Introduction

Normal strength concrete according EN 206 is a porous media with a high content of capillary pores. Particularly the transition zone between aggregate particles and cement paste is characterized by a high capillary porosity. Due to its porosity normal strength concrete is susceptible to deterioration in severe service environments. Taking this into account European standard EN 206 defines exposure classes. Additionally, application rules for EN 206 (DIN 1045) give the range of cements suitable for use in defined exposure classes as well as the appropriate concrete specification (water/binder ratio, minimum cement content, minimum compressive strength, etc.). However, EN 206 (DIN 1045) only covers strength classes of concrete up to C100/115.

For advanced civil engineering and infrastructure projects like reinforced concrete structures exposed to chlorides (e.g., bridge decks), sulfates (e.g., marine environments) and a variety of chemicals (e.g., industrial plants) an advanced construction material with enhanced long-term performance is required [1, 2]. As consequence concretes with high-strength (±100 MPa, HSC) and ultra-high strength (±200 MPa, UHSC) were developed. Since a high strength generally is correlated with low permeability that itself is associated with an enhanced long-term performance [3], these concretes usually also referred to as high- and ultra-high-performance concretes (HPC, UHPC). The basic concept of HPC and UHPC mix design is the utilization of superplasticizers to obtain workable concretes at low water/cement ratios and the incorporation of microsilica to achieve an optimal packing density of the cementitious materials [4, 5]. Additionally, due to the pozzolanic reaction microsilica maximizes strength properties and impermeability of the hardened concrete (Fig 1, 2).
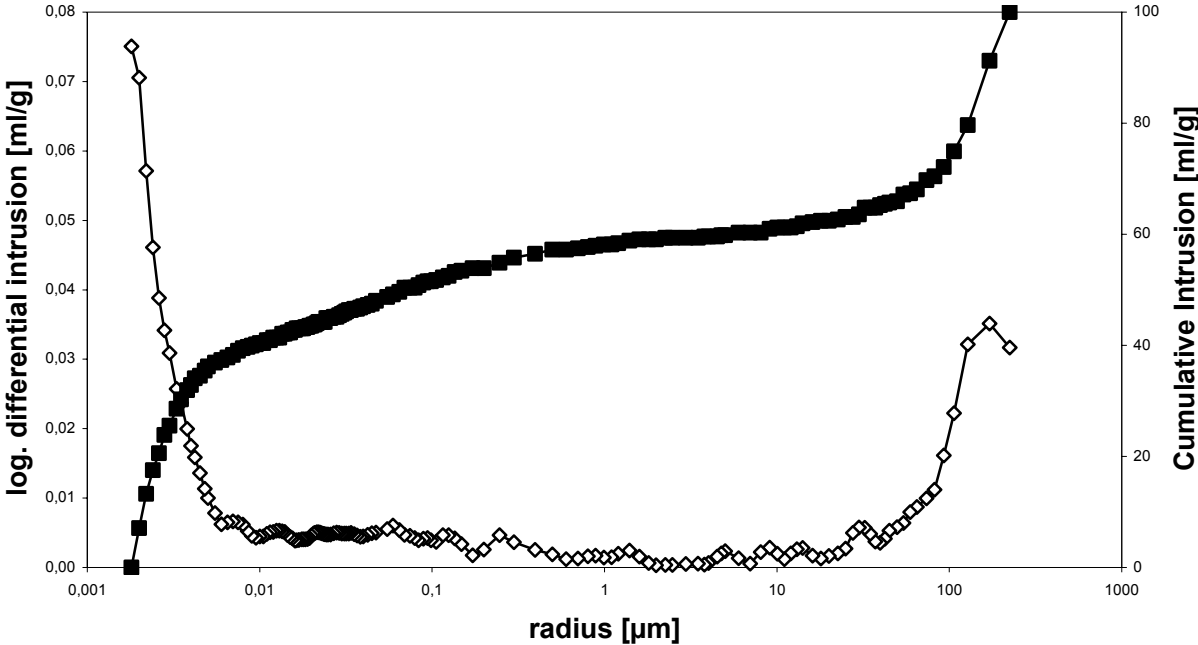
Figure 1:   Pore-size distribution of the internal UHPC mixture M1Q. The low total porosity and particularly the very low amount of capillary pores are the reasons for UHPC's enhanced long-term performance.
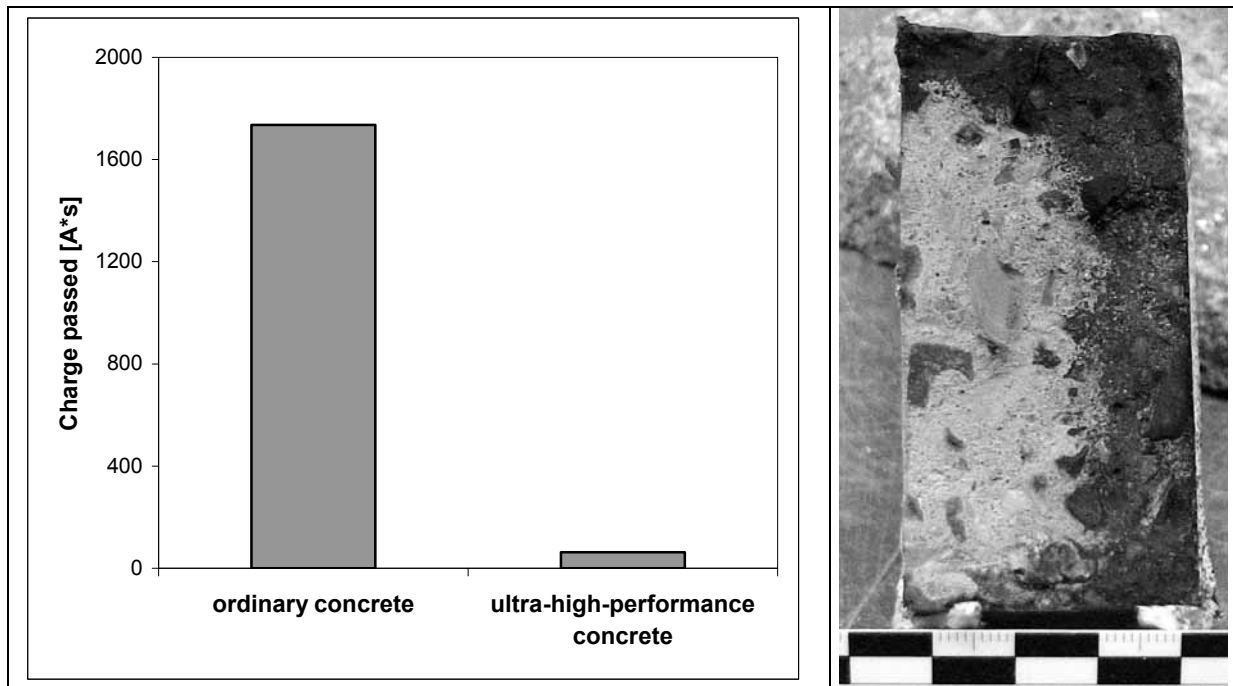
Figure 2: Rapid chloride permeability test [6] results for the internal UHPC mixture M1Q and normal concrete acc. EN 206. Additionally, the 'diffusion' front of chloride ions was visualized using a special staining method [7]. The bright and dark areas of the split sample (right picture) are caused by the interaction of the sample (chloride ions) with the indicator solution and the subsequent formation of silver chloride and silver oxide, respectively.

2   Setting and hydration of cement

The hydration of cement is an exothermic process. As function of time the heat evolution goes through a number of stages [8]. To examine the hydration behavior of cements and the effect of mineral and chemical additives on the setting and hydration, isothermal conduction calorimetry is a suitable technique [9]. The setting behavior of cement pastes generally corresponds to the location of the large peak in the heat evolution curves that is related to formation of calcium silicate hydrate (C-S-H phases) and calcium hydroxide in the course of C_3S hydration.

Beside a CEM I cement and a natural sand the UHPC M1Q mix contains both microsilica and quartz powder as mineral additive (Fig. 3). Additionally a polycarboxylate comb polymer [10] is used as water reducing admixture.

| CEM I 52.5 R NA/HS | Quartz powder W12 |
| Elkem microsilica grade 983 | |
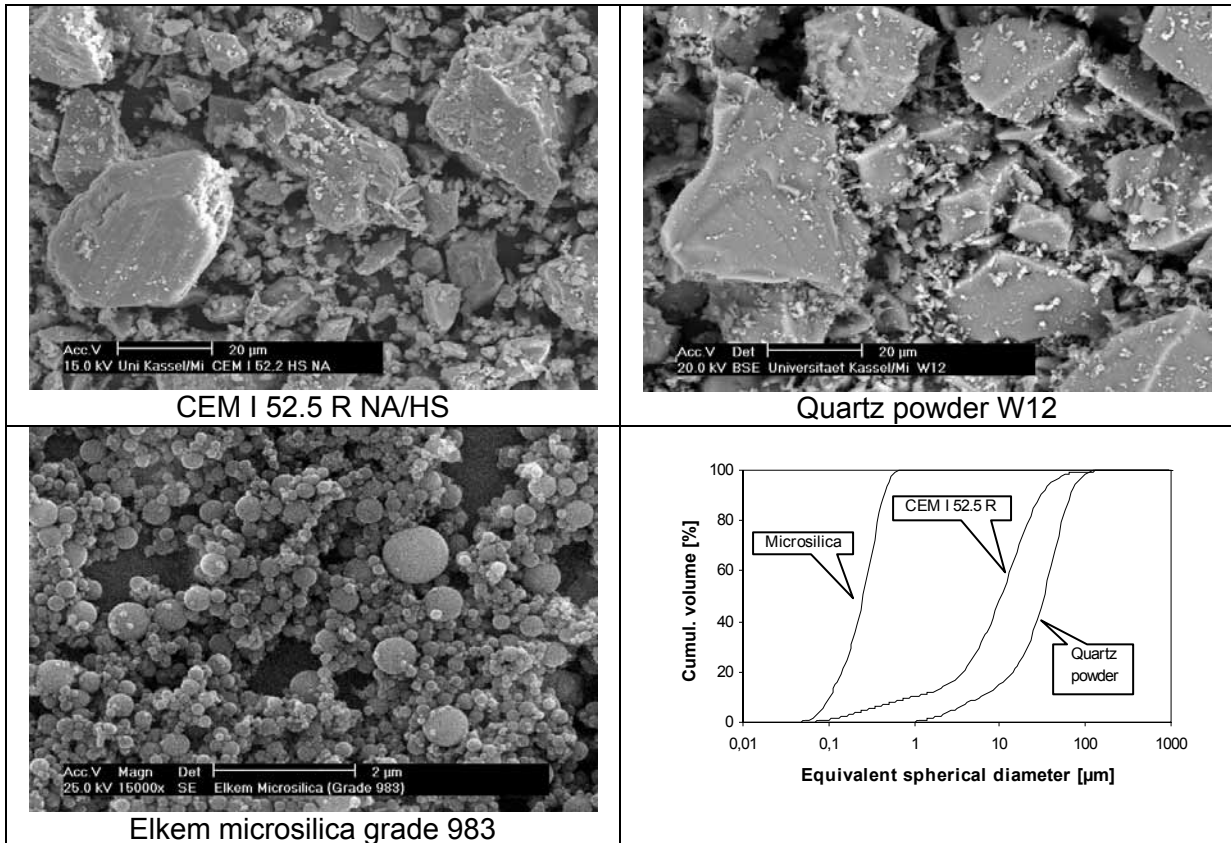
Figure 3:   SEM images and particle size distribution (PSD) of selected UHPC M1Q constituents (PSD data by courtesy of the UHPC chain gang Kassel).

Since it is well known that mineral and chemical additives affect the setting and hydration of cements and concretes the heat evolution of 5 g CEM I hydrating at 30°C with and without mineral and chemical additives was examined (Fig. 4). In case of CEM I the large peak in the heat evolution curve appears at about 10 hours; adding 1 % water reducing admixture shifts the peak to about 29 hours. In the presence of 1 % water reducing admixture the peak in the heat evolution curve of cement pastes containing 0.5 g and 1.0 g microsilica occurs at about 16 and 22 hours, respectively. Fine grained quartz powder has no substantial effect on the setting and hydration of CEM I containing 1 % water reducing admixture.
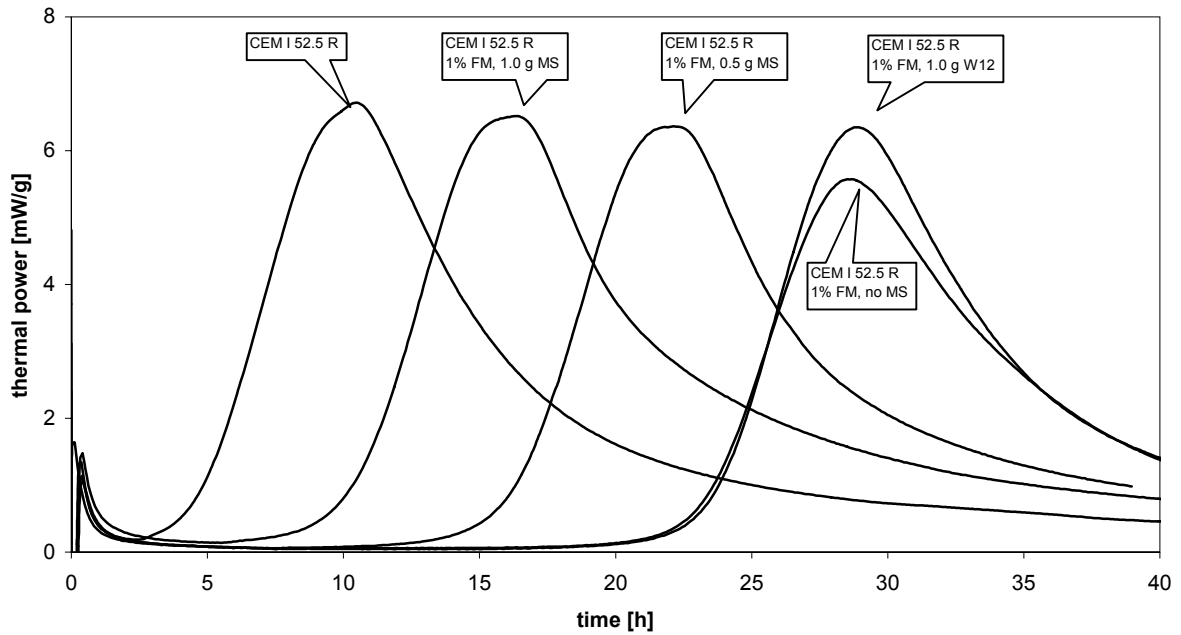
Figure 4:   Heat evolution curves of CEM I 52.5R NA / HS hydration at 30°C with and without mineral and chemical additives utilizing isothermal conduction calorimetry.

SEM images of hardened heat-treated cement pastes containing microsilica and quartz powder W12 may explain the isothermal conduction calorimetric results. There is no indication that quartz grains reacted with the pore solution of the cement paste (Fig. 5). The marked transition zone around the quartz grains is the weakest link in the paste. Even relatively small grains still exhibit surfaces derived from grinding.
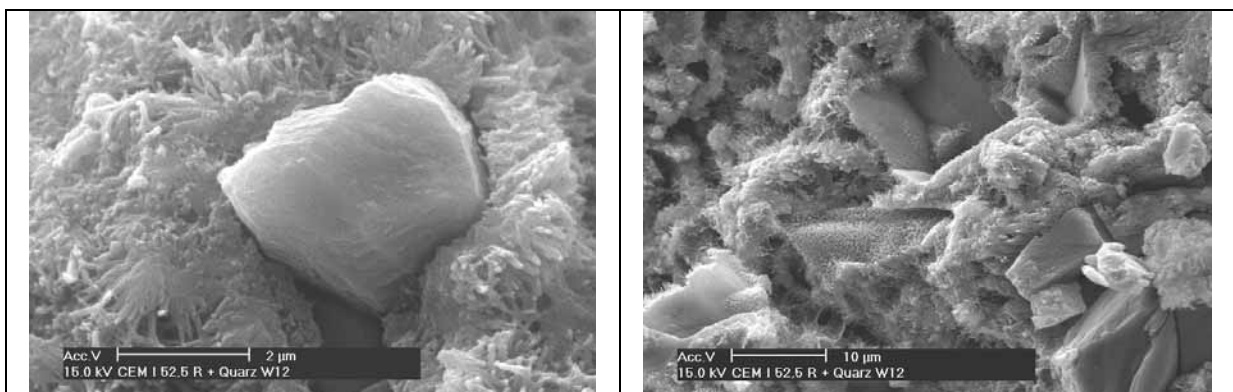
Figure 5:   SEM images of heat-treated cement paste containing quartz powder W12.

Microsilica with higher surface area and amorphous nature is highly reactive. In an alkaline pore solution microsilica experiences a rapid dissolution. As a consequence the pore solution is supersaturated with respect to a silica-rich phase. This may promote the formation of C-S-H phases while the nucleation and growth of calcium hydroxide is reduced. Relict microsilica

particles in heat treated cement pastes suggest that the consumption of microsilica due to the pozzolanic reaction is a continuous process. Moreover, microsilica may act as a silica depot for the formation of calcium silicate hydrates (Fig. 5, 6).
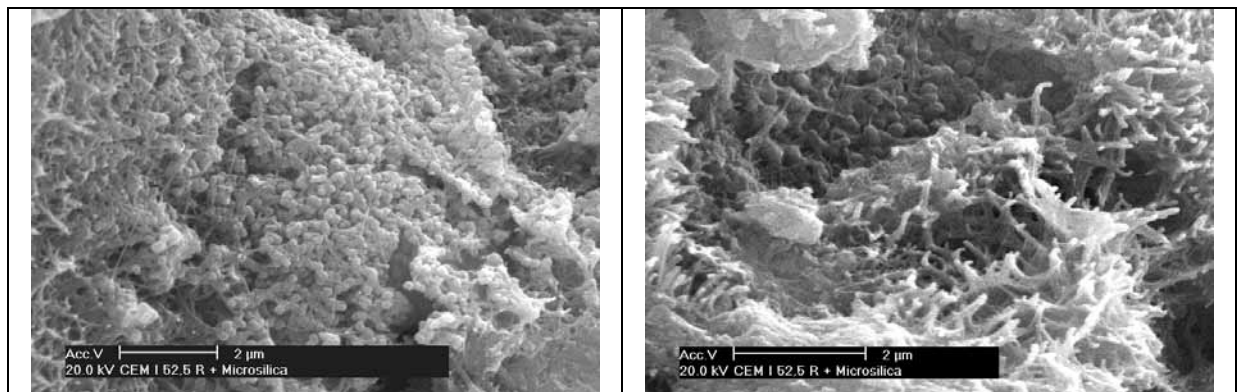
Figure 6: SEM images of heat-treated cement paste containing microsilica. C-S-H phases dominate the fracture surface. Calcium hydroxide fully disappeared and transformed into C-S-H phases.
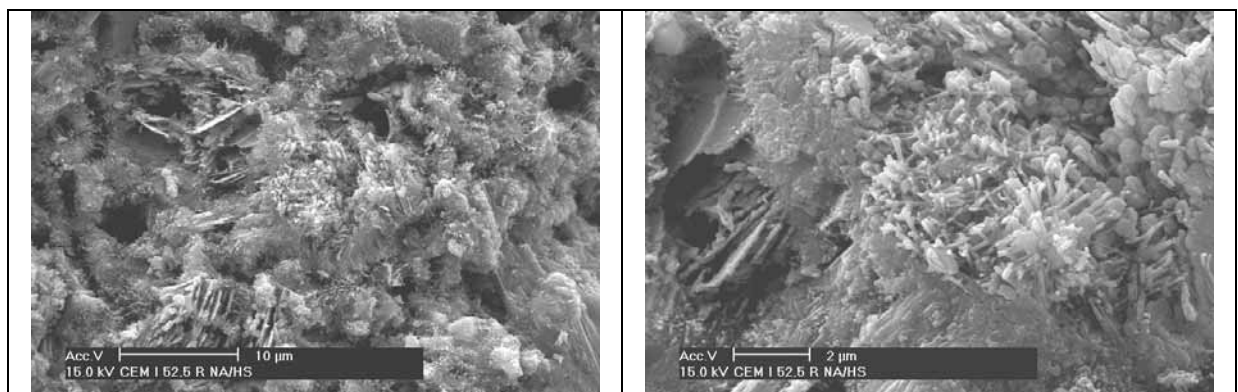
Figure 7: SEM images of heat-treated cement paste. The fracture surface exhibits C-S-H phases and calcium hydroxide deposits. The latter are well known to weaken the bonds between C-S-H phases as well as between cement and aggregates.

Without microsilica both major hydration products C-S-H phases and calcium hydroxide are formed. Calcium hydroxide deposits are a disadvantage since they weaken the bonds between C-S-H phases as well as between cement and aggregates. This demonstrates that the use of materials with pozzolanic and cementitious properties are beneficial in concretes for technical and also for economic reasons. State of the art concrete technology already exploits a variety of industrial by-products among them are fly ash, granulated blast furnace slag and microsilica. Detailed knowledge of the reaction mechanism of these materials in concrete are limited, because the materials itself and/or the instant reaction products are too small to be observed in detail by SEM. Atomic force microscopy (AFM) provides a resolution at nanometer scale and allows in-situ observation at atmospheric condition and characteristic environments like artificial concrete pore solutions [11 - 13].

3.   Visualization of cement hydration at the nanoscale

In order to study the cement hydration by AFM a flat sample was prepared from a clinker granule. In a first step the roughness of small regions (1µm*1µm) of a fresh fracture surface of a cement clinker were determined using AFM. In case of untreated cement clinker the difference between the measured and the projected surface area is in general about 10%.
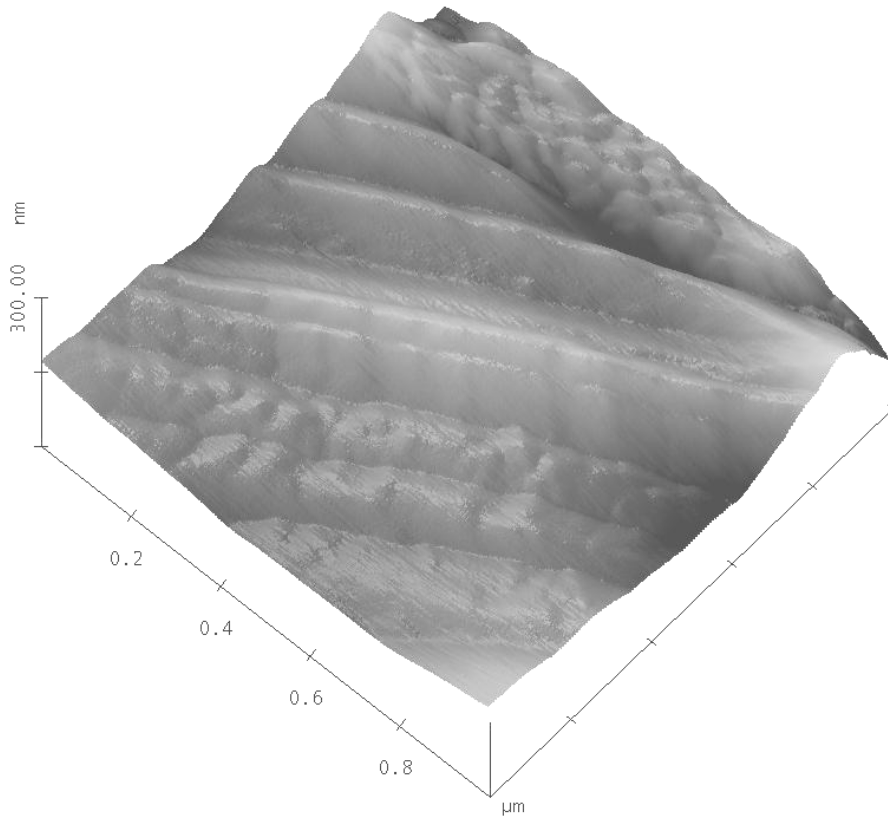
Figure 8:   AFM image (1µm*1µm) of a fresh fracture surface of a cement clinker. The surface structure may reflect its complex phase composition.

In a next step the clinker surface was treated with water for 20 minutes. Due to the interaction between the clinker and the water the surface structure became more pronounced. In comparison to the untreated sample the vertical distance between the peaks as well as the horizontal distance between the peaks and the troughs increased.
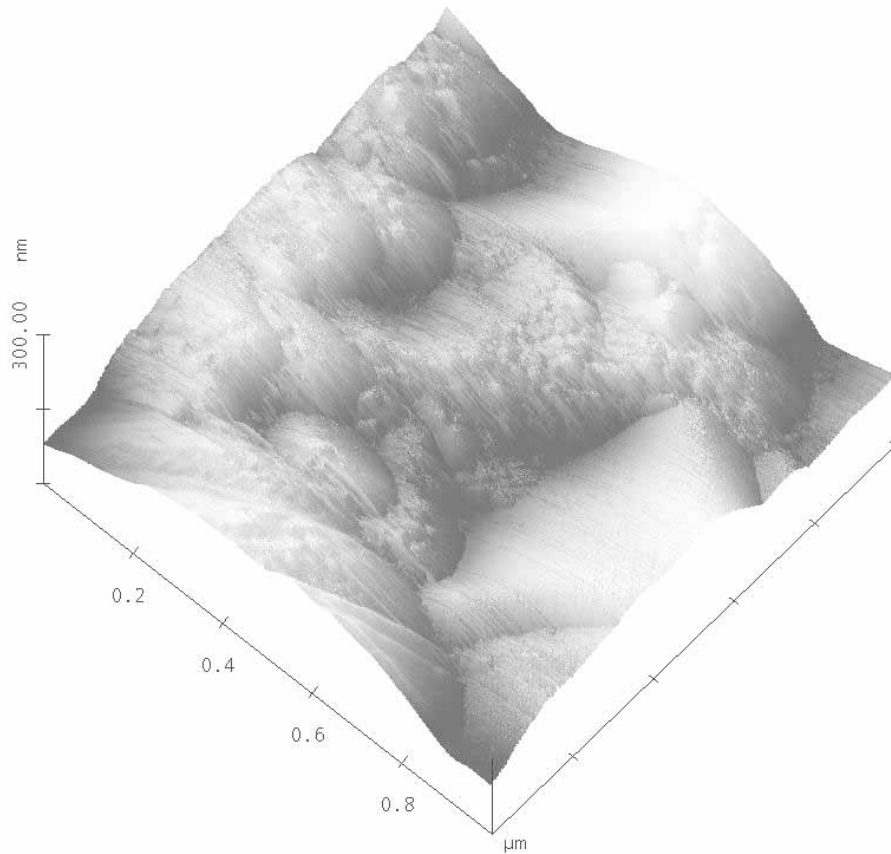
Figure 9:   AFM image (1µm*1µm) of a fracture surface of a cement clinker treated with water. Compared to Fig.8 the surface structure is more pronounced.

Image Statistics	
Img. Z range	129.04 nm
Img. Mean	-0.00002 nm
Img. Raw mean	-0.00002 nm
Img. Rms (Rq)	21.486 nm
Img. Ra	17.388 nm
Img. Rmax	129.04 nm
Img. Srf. area	1.168 µm²
Img. Prj. Srf. area	999999 nm²
Img. Srf. area diff	16.750 %
Img. SAE	1.023
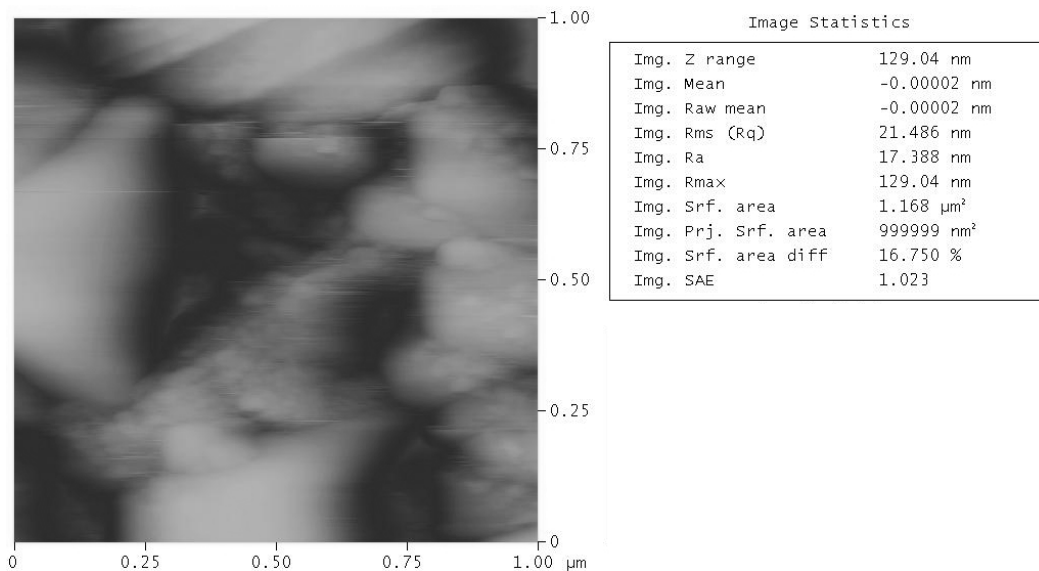
Figure 10: Roughness analysis of cement clinker fracture surface from Fig. 9. The difference between the measured and the projected surface area is about 16 %. Due to the interaction with demineralized water the surface of the fracture surface increased by about 60 % within 20 minutes.
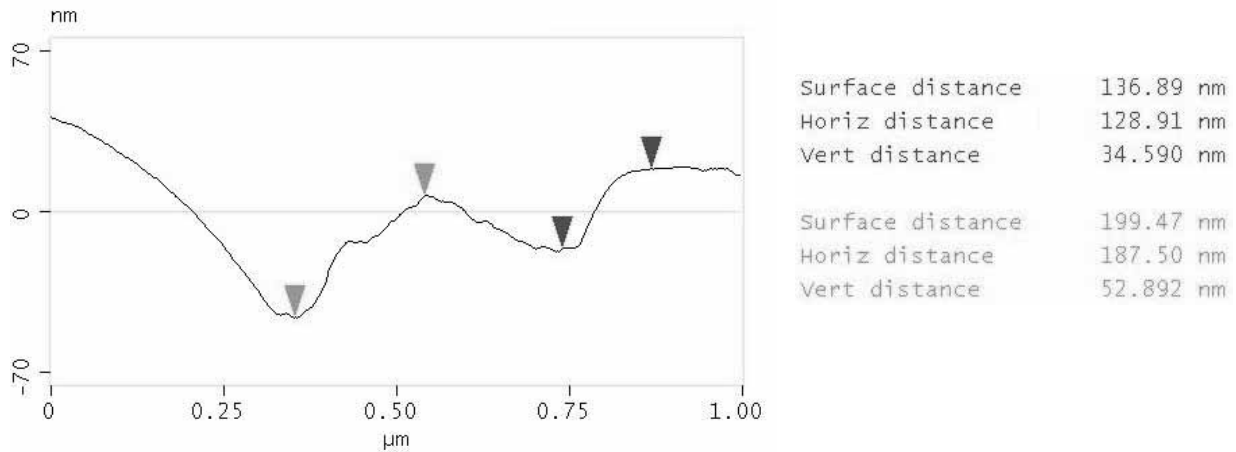
Figure 11: Section analysis of cement clinker fracture surface from Fig. 9. The vertical distances between the peaks as well as the horizontal distances between the peaks and the troughs are larger than in the case of the untreated sample.

4.   Discussion

The macroscopic properties of UHPC are related to its microstructure, i.e. porosity, pore-size distribution as well as morphology of hydration products. Knowledge of these parameters is the key to optimize the high-tech construction material UHPC especially in respect of strengths and durability. In the past SEM or ESEM studies provided a wealth of knowledge on cement hydration and the microstructure of concrete. However, this techniques do not allow to study cement hydration reactions under characteristic conditions. Furthermore, in-situ measurements in fluids at nanoscale are not possible. AFM technology in combination with a fluid cell allows this type of measurements at atmospheric conditions. Formation of hydration products can be quantified.

AFM studies reveal that the surface of clinker increases considerably due to the interaction with demineralized water. In our example the surface of the clinker increased by about 60 % within 20 minutes. The vertical distances between the peaks as well as the horizontal distances between the peaks and the troughs are larger than in case of the untreated sample. This type of investigation also allows to characterize the interaction between clinker phases and chemical additives during hydration. This will provide fundamental knowledge on hydration processes in the presence of chemical additives which may lead to enhanced building materials

5.   Acknowledgement

6. References

[1] Mehta P.K.: Durability: critical issues for the future. In: Concrete International 19, 27-33, 1997.

[2] Mehta P.K.; Burrows, R.W.: Building durable structures in the 21st century. In: Concrete International 23, 57-63, 2001.

[3] Bentur A.: High-strength concrete for long-term durability performance. In: The Construction Specifier, 66 – 72, 2004.

[4] Richard, P.; Cheyrezy, M.: Composition of reactive powder concrete. In: Cement and Concrete Research 25, 1501-1511, 1995.

[5] Bornemann, R.; Schmidt, M.; Fehling, E.; Middendorf, B.: Ultra-Hochleistungsbeton UHPC – Herstellung, Eigenschaften und Anwendungsmöglichkeiten. In: Beton- und Stahlbetonbau 96, Heft 7, 458-467, 2001.

[6] Tang, I.; Nilsson, L.O.: Rapid determination of the chloride diffusivity in concrete by applying an electrical field. In: ACI Materials Journal 89, 49-53, 1992.

[7] Collepardi, M.; Marcialis, A.; Turriziani, R.: La cinetica die penetrazione degli ioni cloruro nel calcestruzzo In: Il Cemento 67, 157-164, 1970.

[8] Young, J.F.: Hydration of Portland cement. In: Instructional modulus in cement science. (ed) D.M. Roy: Materials Education Council, Materials Research Laboratory, University Park, PA, USA, 1985.

[9] Bensted, J.: Some applications of conduction calorimetry to cement hydration. In: Advances in Cement Research 1, 35 – 44, 1987.

[10] Sakai, E.; Yamada, K.; Ohta, A.: Molecular structure and dispersion-adsorption mechanisms of comb-type superplasticizers used in Japan. In: Journal of Advanced Concrete Technology 1, 16 – 25, 2003.

[11] Uchikawa, H.; Hanehara, S.; Shirasaka, T.; Sawaki, D.: Effect of admixture on Hydration of cement, adsorptive behaviour of admixture and fluidity and setting of fresh cement paste. In: Cement and Concrete Research 22, 1115 – 1129, 1992.

[12] Papadakis, V.G.; Pedersen, E.J.; Lindgreen, H.: An AFM – SEM investigation of the effect of silica fume and fly ash on cement paste microstructure. In: Journal of Materials Science 34, 683 – 690, 1999.

[13] Mitchel, L.D.; Prica, M.; Birchall, J.D.: Aspects of Portland cement hydration studied using atomic force microscopy. In: Journal of Materials Science 31, 4207 – 4212, 1996.

Part 5:

Silica Fume and Additives

Arjan Korpa
Dipl.-Chem.
University of Siegen
Siegen, Germany

Reinhard Trettin
Prof. Dr.
University of Siegen
Siegen, Germany

The use of synthetic colloidal silica dispersions for making HPC and UHPC systems, preliminary comparison results between colloidal silica dispersions and silica fumes (SF)

Abstract.

A comparison of the mechanical properties (flexural and uniaxial compressive strengths) between some mix formulations referred to the conventional reactive powder concrete systems (RPC) is done on this work.

The comparison is done between mix formulations containing only silica fume (SF), (microsilica) at the optimal contents for the best mechanical properties and mix formulations containing only synthetic silica dispersion, or combination of silica dispersion with fly ash, SF, cristobalite or quartz powder.

The results show that even though silica fume can be used at much higher percentages (20-30% referred to the cement content) with the mix formulations, adequate formulations containing only colloidal silica dispersions at much lower contents (1-7%), or silica dispersions combined with other pozzolanic additives can give the same results and even better ones.

Hardened specimens of adequate formulations give mechanical properties that are well at the initial border of the zone of mechanical properties for UHPC systems (150-165 MPa), actually without including any fibres or applying special setting or post-setting treatment (pressure, temperature programme) etc. Although the higher specific surface area of the silica dispersions increases the water demand and worsen somehow the workability, still adequate mixture proportioning may give fresh concretes having self flowing abilities in addition to the superior mechanical properties in the hardened state. The early strength development for some of the mixtures with silica dispersions is also generally faster and a little better than for those specimens casted only with SF.

Additionally a microstructure investigation is done for the hardened specimens in order to see the similarities and differences between them

The use of adapted synthetic colloidal silica dispersions for cement systems, combined with other pozzolans, is very promising for HPC or UHPC applications.

Keywords: *Silica fume; Synthetic colloidal silica; Reactivity; Ultra high performance; Microstructure*

1   Introduction

Silica fume (SF) or microsilica is the principal constituent of the new generation high and ultra-high performance concretes (HPC and UHPC) in combination with superplasticizer [1]. Due to its known superior properties, the most important being; filling ability, enhancement of rheological characteristics by lubrification and production of secondary hydrates by pozzolanic reaction with the lime and C-S-H phases resulting from primary hydration, it is now possible to produce concretes with outstanding properties [2].

Silica fume is an industrial by product from ferro-silicium alloys producing units, and hence its availability is limited. It also sometimes gives dark colour to the concrete, which is due to the unburnt coal contained in it, and is an aesthetical problem. However, specially treated silica fumes are available, but they are expensive. Beside this, being an industrial by-product, homogeneity of the product can vary [3].

Therefore we are testing adequate synthetic amorphous silicas (fumed silica oxides) adapted for use with cement systems and comparing their performance with that of the silica fumes, and since their particle sizes are smaller and specific surface areas are considerably larger than for the silica fumes, better results are to be expected theoretically as those obtained by using the last mentioned ones.

Other authors have also used different synthetic colloidal silicas in the past for improving the rheological properties such as bleed and segregation for self-compacting concretes and an improvement of mechanical properties was also observed [4].

We used the silica dispersions supplied by Degussa (Germany) under the trade name AERODISP® in this comparison work. AERODISP® dispersions of fumed oxides under the new brand name AERODISP® cover a wide range of pH-values and solid contents designed to meet the requirements of the different applications. Dispersing media are either water or ethylene glycol and various dispersing techniques are applied for making them. Special additives can change the Zeta-potential of the dispersion. The solids contents of those dispersions can vary from 12 to 50%. The characteristics of AERODISP® dispersions are:

- dust free
- easy to handle
- ready to use
- high quality particle size distributions
- requires less storage space

2   Experimental and results

Two commercial non-compacted silica fumes (microsilicas) were used; SF_1- Elkem microsilica G 983 with BET = 17 ± 1.5 m^2/g and SF_2- Microsilica Elkem 971-U with BET = 22 ± 1.5 m^2/g and their SEM pictures are shown in fig.1 and fig.2.

The quantity of the SF used with the adapted mix formulations based on RPC mix formulations (ref 1) was 25 wt % referred to the cement content (in the mix formulations where the SF^{-s} were used alone). The fumed silica AERODISP® dispersions used were; W 1714 (14 %, $d_{50aggreg.}$=0.16), W 1226 (26 %, $d_{50aggreg.}$=0.20) and W 7520 (20 %, $d_{50aggreg.}$=0.12) concentration by weight. They were progressively diluted until around 1 % concentration and were included at the same adapted mix formulations as the silica fumes or at mix formulations containing AERODISP® dispersions together silica fume or other pozzolans.
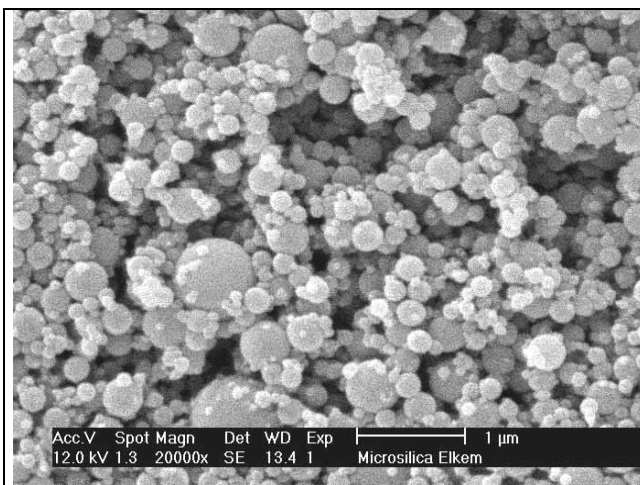
Fig. 1. SEM picture of SF_1 (Elkem microsilica G 983)	Fig. 2. SEM picture of SF_2 (Microsilica Elkem 971-U)
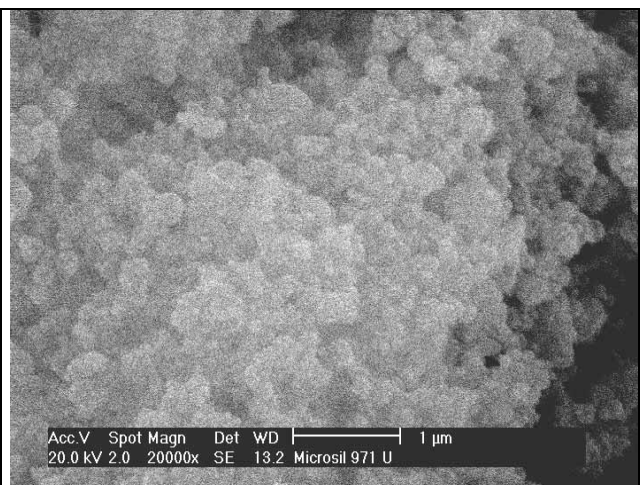
The water-cement (w/c) ratio was kept below 0.25 and the SP varied between 1.5-2.5 % wt versus cement. The superplasticizer (SP) used was of the polycarboxylate type produced in Germany. The cement used was PC I 52.5R with Blaine fineness around 4500 ±100 cm^2/g.

After mixing and molding into prism-shaped specimens (1.5 x 1.5 x 6 cm) the forms were vibrated at a vibration table. No special way of curing was applied.

Mechanical properties were tested after the specified hydration times and the results are compared and shown at figs 3-12.
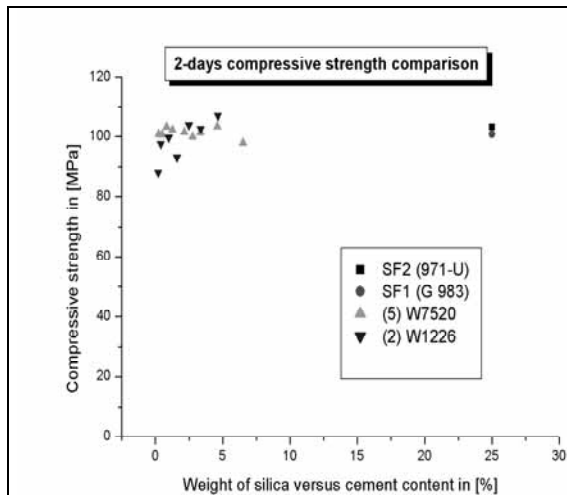
Fig. 3. 2-days compressive strength comparison
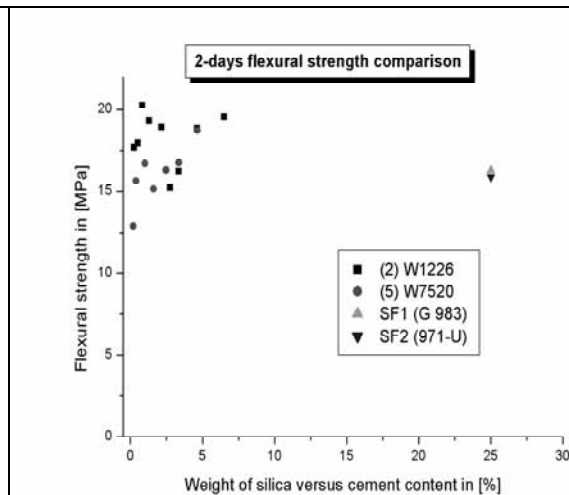
Fig. 4. 2-days flexural strength comparison comparison

Some of the 2-days mechanical properties for the specimens shown in fig. 3 and fig. 4 seems to be comparable or slightly better (more pronounced with flexural strengths) than for the specimens casted with only SF_1 and SF_2. In other words there is a faster early strength development for specimens casted with fumed silica dispersions than for those casted with silica fumes which is also supported by the hydration behaviour as shown at figures 17 and 18. Also the represented mechanical properties performance as it was observed are result of a competition between rheological behaviour and quantity of silica coming from dispersion, still it exists a trend of better mechanical properties for higher quantities of silica for the specimens casted with aerosil dispersions inside around 1-7 wt% silica. The best mechanical properties result for specimens that flow relatively easily and contain silica at around 4-5 wt%. The same comments can be done for the mechanical properties of the 7 days old specimens and the results are shown at figures 5 and 6.

After 28 days there are already specimens casted with silica fumes that represent slightly better mechanical properties that those casted with fumed silica dispersions.

It may be assumed at that hydration time that the pozzolanic reaction of larger silica fume particles that exist also in larger quantity (25% wt) has attained a considerable degree to contribute remarkably at the mechanical properties performance as shown at figures 7 and 8 together with their filling ability.
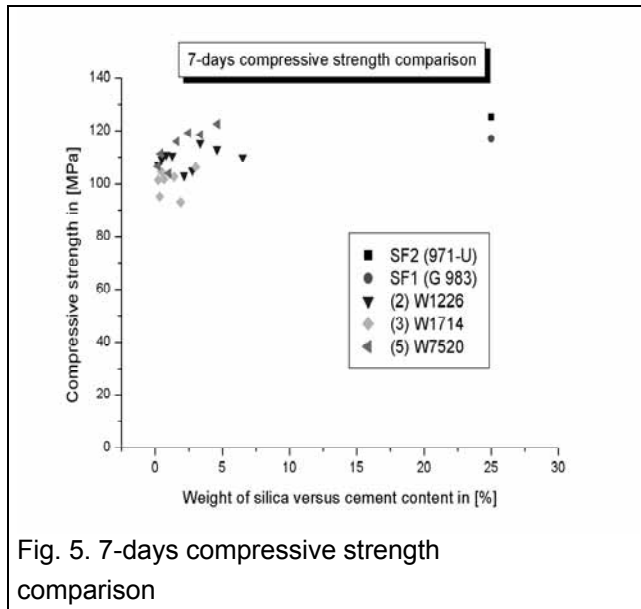
Fig. 5. 7-days compressive strength comparison
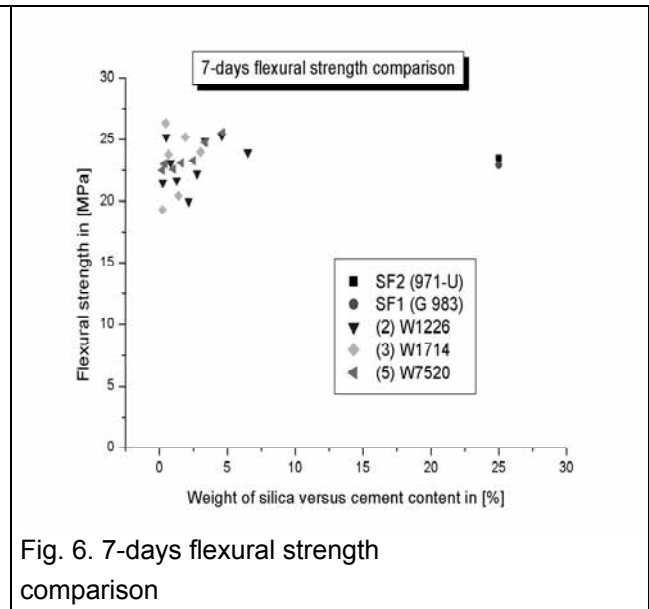
Fig. 6. 7-days flexural strength comparison

In figures 9 and 10 are shown some mechanical property results for specimens casted with the W1226 aerosil dispersion (the fresh mixtures casted with W1226 showed better flow ability than mixtures casted with W1714 and W7520) together with other pozzolans namely; fly ash (FA SWF), cristobalite powder (SF6000) and also SF_1 or SF_2. These results are compared with the results for specimens casted with only SF_1 or SF_2.

Again here the mechanical properties of mixtures including aerosil dispersion W1226
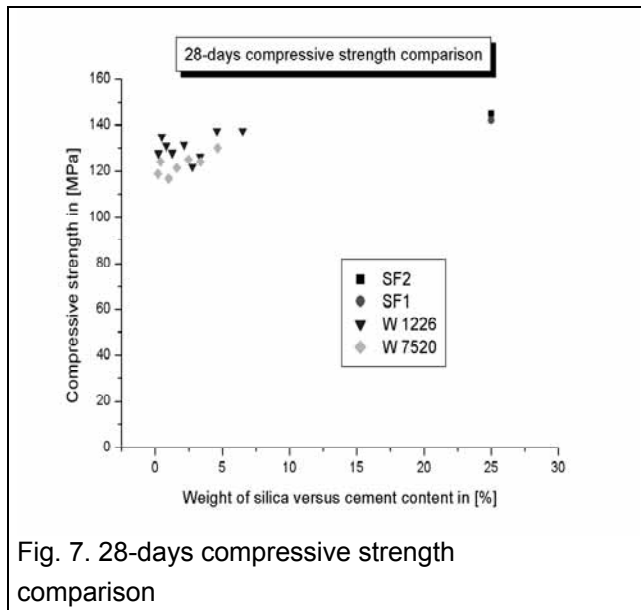
Fig. 7. 28-days compressive strength comparison
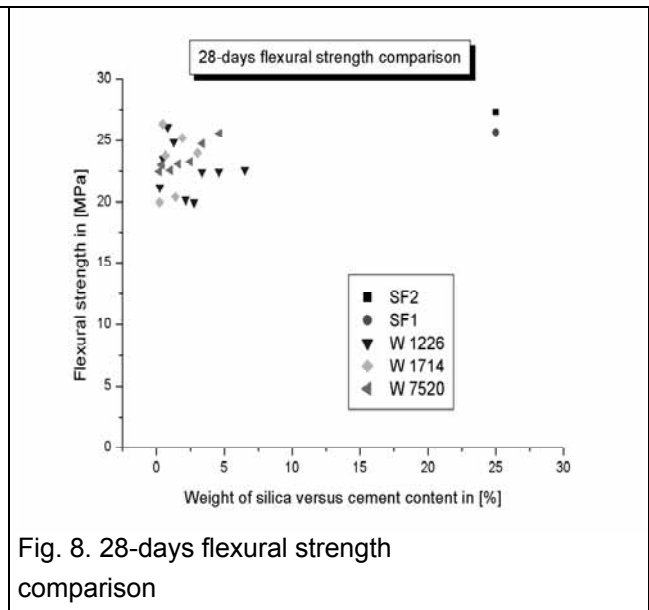
Fig. 8. 28-days flexural strength comparison

together with FA or cristobalite powder SF6000 represent values that are well compared with those of mixtures casted only with SF_1 (G 983) or SF_2 (971 U) being at around 150 MPa (28 days compressive strength and 25-26 MPa (28 days flexural strength) for curing at 20°C and >90% rel. humidity. Some of the values for the specimens casted with W1226 together with SF_1 or SF_2 (being at around 160 MPa and 26-27 MPa after 28 days) are a little superior to the mechanical property values of those specimens casted with only SF_1 or SF_2 (fig 9 and 10).
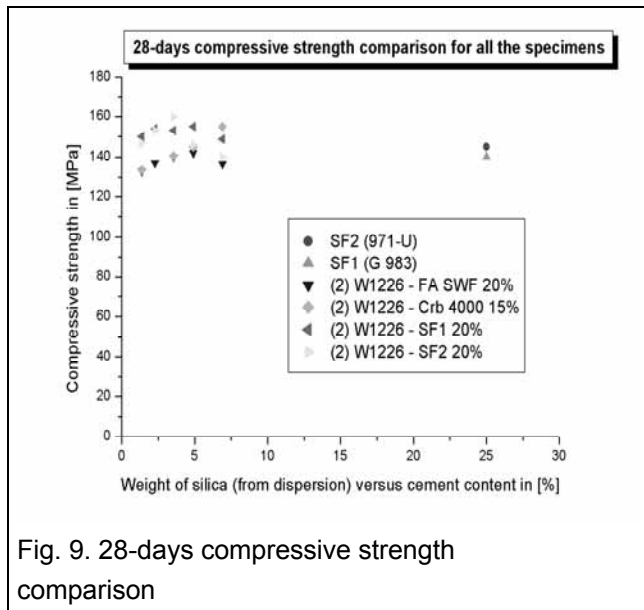
Fig. 9. 28-days compressive strength comparison
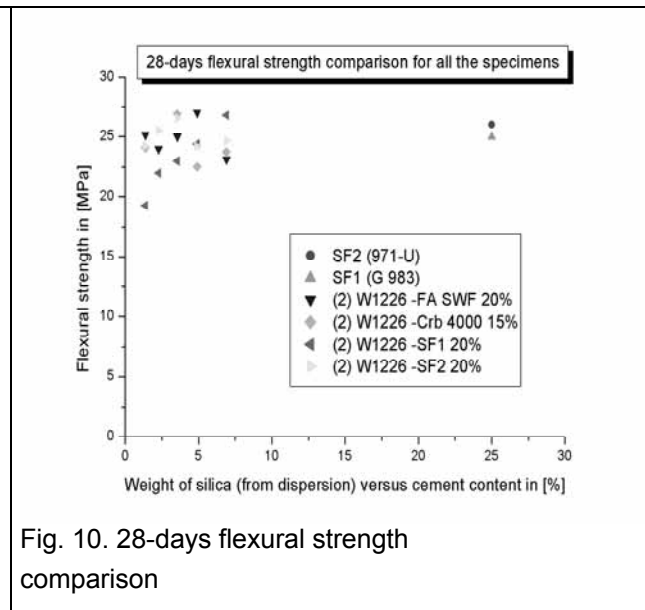
Fig. 10. 28-days flexural strength comparison

In fig 11 and fig 12 are shown the mechanical properties after 28 days for specimens casted with a combination of SF_1, FA (SWF) and W1226 used at various concentrations. The mechanical properties of such systems lies at around 160-165 MPa compressive strength and 23-24 MPa flexural strength for specimens cured under water at 18°C. There is a little decrease on flexural strength values as compared with those from the above-mentioned mixtures, even though the compressive strength values are improved. It is not very clear whether this is due to the curing under water or to any other reasons. Here again the mechanical performance is a competition between rheological behaviour (easy flow or not) and quantity of aerosil dispersion (as large as possible for better mechanical performance). The best values are attained for aerosil quantity at around 4% wt versus cement content.

In figures 13 and 14 are also shown the denser microstructure of a specimen casted with SF_1 and W1226 as compared to a normal concrete system (w/c=0.45 and maximum aggregate size around 1mm) by means of SEM pictures. There are also shown the different morphologies of their C-S-H phases and the clearly visible C-H crystals for the normal concrete specimen, as well as silica fume and fumed silica (from aerosil dispersion) particles for the high performance specimen casted with silica fume and aerosil dispersion. For the high performance specimen there is not a visible zone of C-H crystals which might be present as very fine crystals or even in amorphous phase and in very small quantity.
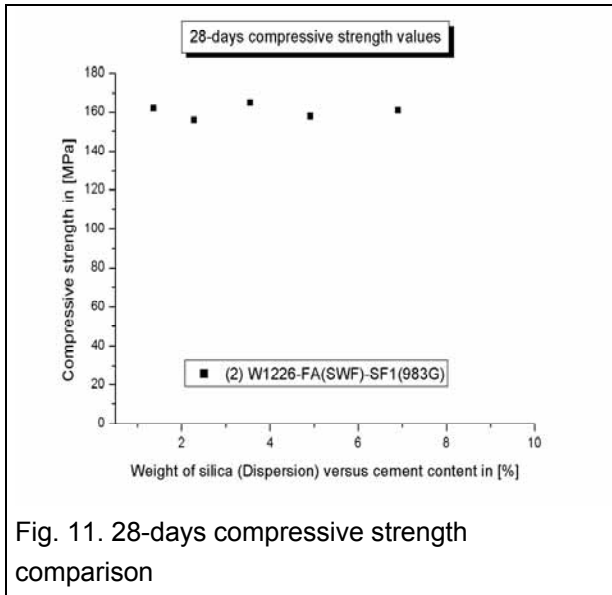
Fig. 11. 28-days compressive strength comparison
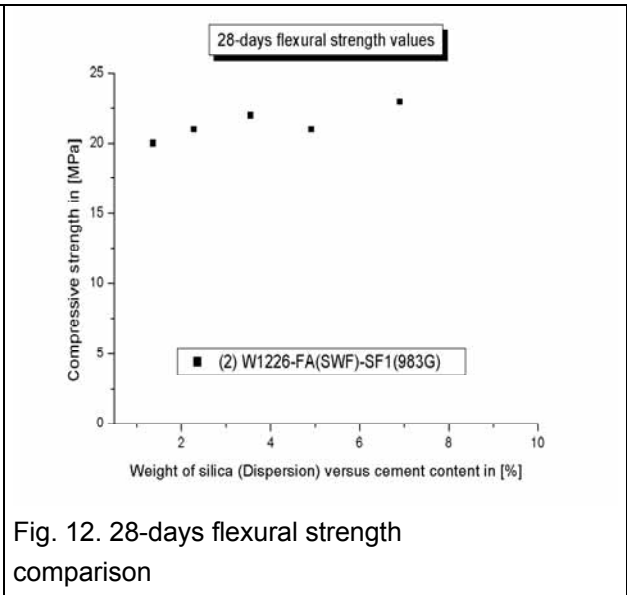
Fig. 12. 28-days flexural strength comparison
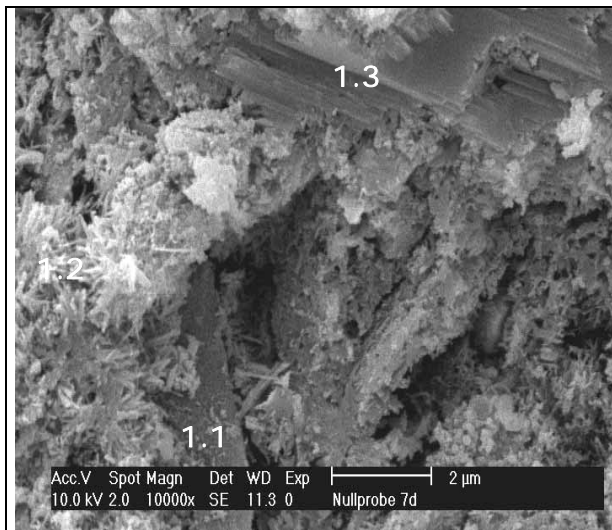
Fig. 13. SEM picture of normal concrete system (max aggregate size = 1mm, w/c=0.45)
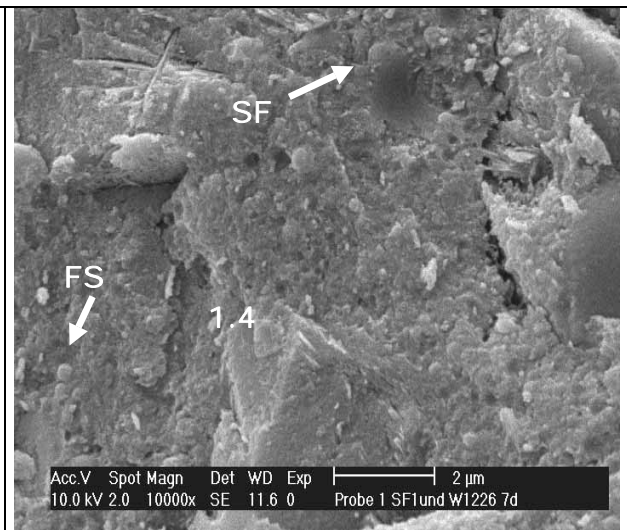
Fig. 14. SEM picture of a specimen casted with SF_1 20% and W1226 3.55%

The surface area and porosity measurements done on the normal strength concrete as well as the specimen casted with only silica fume (25%) and the specimen casted with the combination of silica fume together with aerosil dispersion (fumed silica) confirm also the conclusion of a denser and finer structure for the last mentioned one as shown at figures 15 and 16. The most probable explanation would be that the finer and more reactive (pozzolanicaly) fumed silica particles contribute somehow at a certain extent to obtain a denser microstructure resulting also on improved mechanical properties.

The hydration behaviour of various mixtures is shown at figures 17 and 18. It is to be observed an acceleration of the hydration for the mixtures containing aerosil dispersions as compared to mixtures containing silica fumes or other pozzolans.
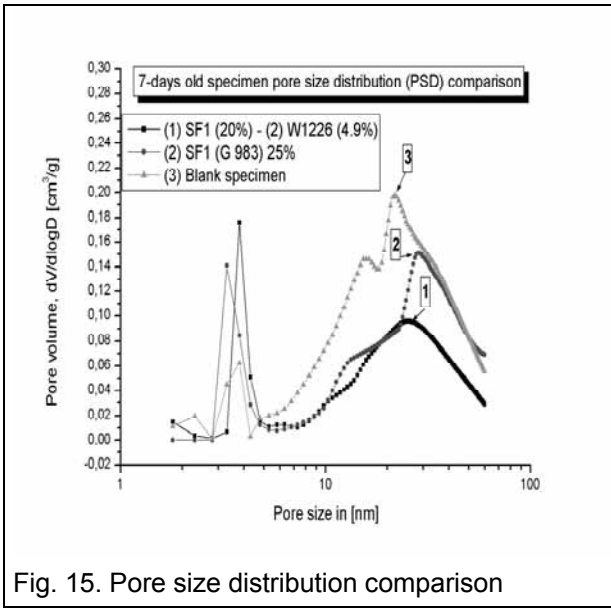
Fig. 15. Pore size distribution comparison
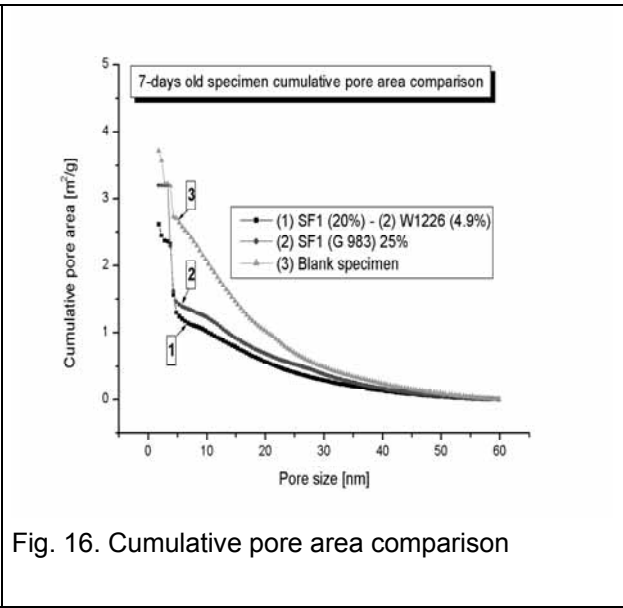
Fig. 16. Cumulative pore area comparison
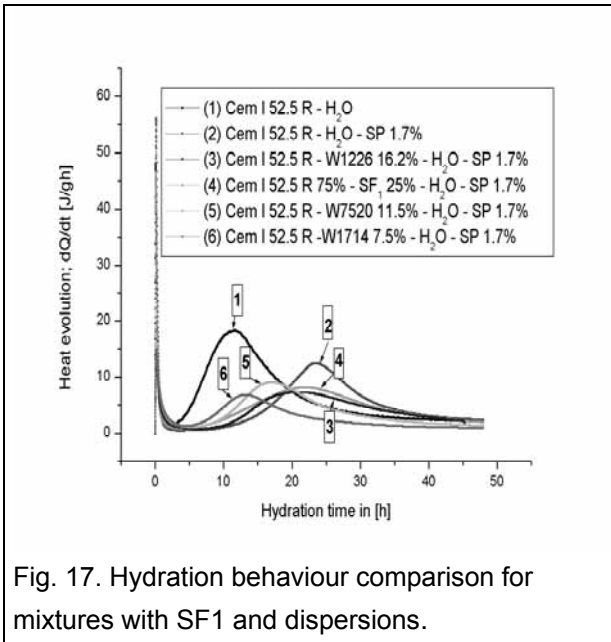
Fig. 17. Hydration behaviour comparison for mixtures with SF1 and dispersions.
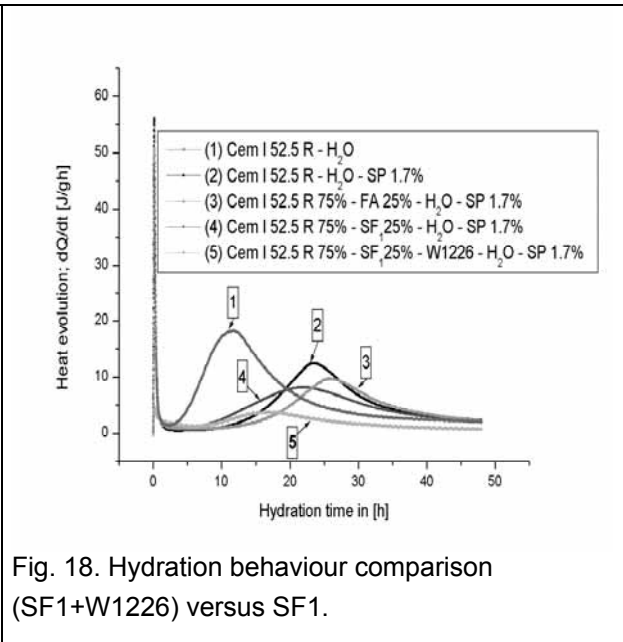
Fig. 18. Hydration behaviour comparison (SF1+W1226) versus SF1.

The sample casted with the aerosil dispersion W7520 (which has the smallest aggregate size) represent the shortest induction period, comparable with that of blank sample (the mixture containing only cement and water) even though the first mentioned one contains also superplasticizer.

For the aerosil dispersions (cement – aerosil – superplasticizer mixtures) there exist a dependence of the hydration behaviour depending on the particle size as shown at fig. 17. Smaller particle size introduce a shorter induction period for the mixtures containing aerosil particles together with superplasticizer molecules.

Additionally there exist a reduced heat of hydration peak for the mixtures containing the smallest size fumed silica dispersion, as well as for the other aerosil fumed silica dispersions.

The same can be said also for the first peaks of hydration curves even though it is not shown here. The mixture containing fly ash FA (SWF) represents the longest induction period as compared to mixtures containing other pozzolanic additives.

The mixture containing silica fume together with aerosil dispersion represents a slightly shorter induction period (3-4 hours) than the mixtures containing only silica fume or only aerosil as shown at fig. 18. Also this mixture is characterised by a much lower heat of hydration peaks shown again at fig. 18.

3 Conclusions

We showed some preliminary work results concerning the possibility of making HPC systems by including only fumed silica aerosil dispersions (in much smaller quantities) at mixture formulations which are refered to the conventional RPC systems. The best mixture proportions give hardened specimens that could attain around 100 MPa after 2 days of hydration and around 135-140 MPa after 28 days of hydration without applying special curing methods (curing at 20°C and >90% rel. humidity).

Compared to the mixture formulations containing only silica fumes the previous ones are characterised by a slightly worsened workability due to the larger specific surface area of the aerosil fumed silica particles.

The 28 days mechanical properties for the specimens casted with only silica fumes are a little superior compared to those casted with only fumed silica due to a larger silica particles quantity and to somehow a better flow ability.

Appropriate combinations of fumed silica dispersions with other pozzolans can be used to cast specimens with comparable mechanical performance to the systems casted with silica fume. Furthermore in the cases when silica fumes are used as "other" pozzolans and combined with adequate fumed silica dispersions, specimens with improved mechanical properties can be produced. This can be explained as a further densifying of the microstructure and is supplied by porosity and surface area measurements.

Also ternary combinations of fumed silica with silica fumes and fly ashes can produce specimens that are well at the UHPC zone of mechanical properties performance (160-165 MPa) by applying only normal casting, processing and curing methods and without including any fibres.

Ongoing work intending further improvement also by including fibres and other ways of processing and curing, as well as a rheological characterisation for some mixture formulations is beeing carried out at our laboratory.

4   References

[1]   Khayat K.H. and Aitcin P.C., Silica fume in concrete: an overview, Fourth CANMET/ACI International Conference on Fly ash, Silica fume, slag and natural pozzolans in concrete, SP-132, V.2 (1992), 835. Guide for use of silica fume, 234R-96 ACI Publications (1996).

[2]   Pierre Richard, Marcel Cheyrezy, Composition of reactive powder concretes, Cement and Concrete Research, vol. 25, No. 7, pp. 1501-1511, 1995

[3]   Chandra, S, Bergqvist, H, Interaction of silica colloid with Portland cement, Proc. Int. Congr. Chem. Cem. Vol. 3 (1997), 3ii106, 6pp.

[4]   Carl Bigley, Peter Greenwood, Using silica to control bleed and segregation in self-compacting concrete, Concrete, february 2003, pp 43-45.

KARTHIKEYAN JAYAKUMAR
POST GRADUATE STUDENT IN STRUCTURAL ENGINEERING
V.L.B.JANAKIAMMAL COLLEGE OF ENGG & TECHNOLOGY
COIMBATORE, INDIA

Role of Silica fume Concrete in Concrete Technology

Summary

This paper highlights an experimental investigation on the strength characteristics of UHPC mixes, with different replacement levels of cement with Condensed Silica Fume (CSF). The compressive strength of 76.5MPa at 28 days with 7.5 percent replacement of OPC by CSF and 60.75MPa at 28 days with 5 percent replacement of PPC with CSF was achieved. Also a maximum compressive strength of 89.25 MPa at 90 days with 7.5 percent replacement of OPC by CSF and 75.75 MPa at 90 days with 5 percent replacement of PPC by CSF was observed for a water cementitious material ratio of 0.32. Split tensile, flexural strength and modulus of elasticity was found to be greater than that of conventional concrete. Micro structural studies like sorptivity test, saturated water adsorption test and porosity were also studied to check the impermeability of UHPC. Condensed silica fume concrete is more resistance to acids, where a significant damage is observed in plain concrete mix. Ultrasonic pulse velocity test has been carried out in order to check the concrete quality. The pulse velocity for the concrete mixes was found to be greater than 4570 m/s that falls under the excellent category.

Keywords: *Ultra High performances Concrete (UHPC) - Condensed Silica fume (CSF) - Ordinary Portland Cement (OPC) - Portland Pozzolanna Cement (PPC) - Super plasticizers – Bureau of Indian Standards (BIS).*

1   Introduction

Condensed Silica Fume (CSF) is a by-product of the ferrosilicon alloy industries and contribute significantly to compressive strength development of concrete because of the microfiller effect and excellent pozzolanic properties of the material. The use of CSF in concrete increases the calcium silicate hydrate (C-S-H) gel formation that is mainly responsible for the high strength, high durability of concrete structures and reduction of pore sizes in the transition zone [2].

Table 1: Properties of Condensed Silica Fume

Components	Percentage (%)
Chemical properties	
SiO_2	90-96
Al_2O_3	0.5-0.8
MgO	0.5-1.5
Fe_2O_3	0.2-0.8
CaO	0.1-0.5
Na_2O	0.2-0.7
K_2O	0.4-1
C	0.5-1.4
S	0.1-0.4
Loss of Ignition (LOI)	0.7-2.5
Physical properties	
Specific gravity	2.2
Surface area	20,000 m^2/Kg
Size	0.1 micron
Bulk density	576 Kg/ m^3

2   Scope of Investigation

A water-cementatious ratio of 0.32 was adopted. The effect of different percentage of CSF replacements of cement were 2.5, 5, 7.5, 10 and 12.5 percent with CSF, was studied with OPC and PPC. The quantity of fine aggregate was suitably adjusted for the different replacement levels with CSF. Concrete cube specimens of size 100 x 100 x 100mm, cylinder specimens of size 100 x 200mm and beam specimen of size 100 x 100 x 500mm were cast as per specifications. Three specimens were tested for each variable considered. The compressive strength, split tensile strength and flexural strength of the mixes were investigated as per the BIS specifications in the laboratory. Also, Durability and microstructural studies has been carried out. Nondestructive test – Ultrasonic pulse Velocity is carried out to check the quality of the concrete.

3   Materials Used

Cement: (I) Ordinary Portland Cement (OPC) 53 Grade refers to 28 days compressive strength
        (II) Portland Pozzolana Cement (PPC) Flyash based 20% replacement level.
Coarse aggregate: 12.5 mm down size. Fineness Modulus = 5.9
Fine aggregate: River sand of fineness Modulus =2.75[3]
Chemical admixture – Super Plasticizer (Sulphonated Naphthalene based)
Mineral admixture: Condensed Silica fume, (Imported SiO_2 more than 90%)
Water: Potable water as per BIS 456:2000

Table 2: Mix Design Details[6]

Ingredients		M₁	M₂
Cement	kg/m³	500	487.8
Sand	kg/m³	698.12	696.38
Coarse aggregate	kg/m³	1075.37	1072.7
Silica fume	kg/m³	0	12.2
Silica fume replacement level	%	0	2.5
Superplasticizer	lit/m³	10.42	10.16
Unit water content	lit/m³	160	160
Ingredients		**M₃**	**M₄**
Cement	kg/m³	476.2	465.1
Sand	kg/m³	695	693.15
Coarse aggregate	kg/m³	1070	1067.71
Silica fume	kg/m³	23.8	34.9
Silica fume replacement level	%	5	7.5
Superplasticizer	lit/m³	9.92	9.69
Unit water content	lit/m³	160	160
Ingredients		**M₅**	**M₆**
Cement	kg/m³	454.54	444.44
Sand	kg/m³	691.65	690.2
Coarse aggregate	kg/m³	1065.4	1063.17
Silica fume	kg/m³	45.45	55.56
Silica fume replacement level	%	10	12.5
Superplasticizer	lit/m³	9.47	9.26
Unit water content	lit/m³	160	160

The absolute volume method of mix design was used to determine the quantities of different ingredients. Air content for concrete was assumed as 1%.

4   Test Results and Discussions – Compressive Strength

The compressive strength of CSF concrete with OPC and PPC at the ages of 1,3,7,14,28,56 and 90days were given in tables 3 and 4. When CSF is added as additional admixture, there

is a significant improvement in the strength of concrete because of its high pozzolanic nature to form more CSH gels. It is seen from the tables 3 and 4, that the compressive strength at the early age (1 day) for the CSF based UHPC is marginally higher for OPC than PPC because of due to slow pozzolanic reaction. It is observed that the compressive strength increases with increasing age of curing. The maximum cube compressive strength can be seen from table 3 for a mix of 7.5 percent CSF for 28 days that is 76.5MPa and at 90 days is 89.25MPa for OPC concrete. Whereas it is observed in table 4, the maximum cube compressive strength for PPC concrete for 28 days is 60.75MPa and at 90 days is 75.75MPa. The maximum compressive strength of concrete in combination with CSF is based on two parameters that are the replacement level and the age of curing. The optimum replacement of CSF for achieving maximum strength in OPC and PPC are 7.5 % and 5% for all the ages of curing.

4.1 Split tensile strength

Tests were carried out according BIS 5816-1970 to obtain the splitting tensile strengths for various concrete mixes. The tensile strength of concrete a property that affects both resistance to cracking at prestress release and shear capacity are important with respect to the appearance and durability of concrete structural members. The rate of increase of tensile strength is less for high strength concrete (75-100MPa) than observed for low strength concrete (22-55MPa). The relationship between the tensile strength and compressive strength at 28 days were studied and concluded that at low compressive strength the tensile strength is as high as 10% of the compressive strength but at higher strength this was about 5%. The split tensile strength of mixes are given in table no. 3 and 4. The split tensile strength at the age of 28 days for OPC varies from 4.46 to 5.47MPa, whereas in case of PPC the tensile strength varies from 3 to 3.82MPa. It can be seen that for mix of M_4 shows higher tensile strength for OPC, whereas for PPC the mix is M_3. It is observed that the tensile strength of about 7% of compressive strength for OPC and 6% of compressive strength for PPC.

4.2 Flexural strength

Tests are carried out according BIS 516-1959 to obtain the flexural strength for various concrete mixes used. Three beams were cast for each mix tested using two-point loading. The experimental results of flexural strength of OPC and PPC are shown in table 3 and 4. The flexural strength at the age of 28 days for OPC varies from 6.36 to 7.63MPa, whereas in case of PPC the flexural strength varies from 4.32 to 5.16MPa. It can be seen mix of M_4 shows higher flexural strength for OPC, whereas PPC the mix is M_3. It is observed that the flexural strength is about 10% of compressive strength for OPC and 8.5% of compressive strength for PPC.

Table 3 Properties of HPC mixes of OPC[6]

Properties	M_1	M_2	M_3	M_4	M_5	M_6
Compressive strength (MPa) 1 day	12.25	15.25	19.50	26.50	20.25	15.75
3 days	35.75	40.00	41.75	44.50	41.00	38.50
7 days	42.25	43.25	45.00	47.50	46.00	44.25
14 days	51.25	53.25	57.00	63.75	53.75	47.75
28 days	55.25	58.50	59.75	76.50	61.25	59.00
56 days	68.50	70.00	74.75	83.50	78.00	70.75
90 days	72.75	74.50	79.75	89.25	81.50	76.25
Split tensile strength (MPa) 28 days	4.46	4.52	4.65	5.47	4.71	4.52
Flexural strength (MPa) 28 days	6.42	6.49	6.90	7.63	6.51	6.36
Young's modulus (GPa) 28 days	37.17	38.26	38.65	43.73	39.13	38.41
Workability (CF)	0.85	0.83	0.825	0.81	0.78	0.73
Vee-Bee (seconds)	17	19	20	21	23	28

Table 4 Properties of HPC mixes of PPC[6]

Properties	M₁	M₂	M₃	M₄	M₅	M₆
Compressive strength (MPa)						
1 day	8.00	9.50	11.25	10.75	8.50	7.50
3 days	14.75	22.00	29.25	26.25	21.00	17.50
7 days	34.50	40.75	45.25	40.25	31.50	29.25
14 days	42.00	49.25	51.75	46.50	40.75	36.25
28 days	54.50	57.25	60.75	48.50	44.25	40.50
56 days	60.75	62.25	62.50	55.75	48.75	45.00
90 days	62.00	65.25	75.75	70.50	65.50	60.75
Split tensile strength (MPa) 28 days	3.00	3.12	3.82	3.44	3.37	3.21
Flexural strength (MPa) 28 days	4.48	4.61	5.16	4.96	4.77	4.62
Young's modulus (GPa) 28 days	36.91	37.83	38.97	34.82	33.26	31.82
Workability (CF)	0.84	0.82	0.805	0.75	0.72	0.70
Vee-Bee (seconds)	16	18	23	30	34	38

4.3   Durability

When Concrete is exposed to aggressive environment containing chlorides, sulphates and chemicals, leads to deterioration of concrete and are measured in terms of loss of weight of concrete. To study the acid resistance of concrete, the cube specimens of concrete is cured for 28 days and then immersed in 2.5% of HCl and 2.5% H_2SO_4 of solution up to 90 days. It is observed in table no 5 that the increase in percentage of CSF decreases the loss of weight in concrete.

Table 5 – Durability- Acid Resistance Test Results[6]

CSF (%)	Loss of weight in % 2.5% HCl soln.	Loss of weight in % 2.5% H_2SO_4 soln.
0	3.51	3.07
2.5	2.09	1.92
5	1.85	1.73
7.5	1.78	1.58
10	1.64	1.35
12.5	1.43	1.18
15	1.30	1.01

4.4   Micro structural Properties

The micro structural properties of UHPC like saturated water absorption, porosity and sorptivity was studied. According to BIS and ASTM specifications, the sorptivity results were compared with Taywood engineering (1993) to check the quality of concrete. The UHPC mixes show good quality[4].

Table 6 Micro Structural Related Properties – OPC[6]

CSF (%)	Saturated water absorption (%)		Porosity (%)		Sorptivity ($mm^3/mm^2/\sqrt{min}$)	
	28 days	90 days	28 days	90 days	28 days	90 days
0	4.12	3.58	3.95	3.42	0.143	0.089
2.5	3.67	3.23	3.54	3.09	0.122	0.076
5.0	3.33	2.98	3.22	2.89	0.122	0.069
7.5	1.002	0.94	0.992	0.85	0.0304	0.028
10.0	1.242	1.12	1.23	1.06	0.0456	0.035
12.5	1.43	1.26	1.41	1.18	0.0687	0.056

Table 7 Micro Structural Related Properties – PPC[6]

CSF (%)	Saturated water absorption (%)		Porosity (%)		Sorptivity (mm^3/mm^2/√min)	
	28 days	90 days	28 days	90 days	28 days	90 days
0	2.986	2.44	2.9	2.21	0.054	0.045
2.5	2.46	2.29	2.19	2.01	0.0396	0.0358
5.0	1.85	1.78	1.82	1.69	0.0243	0.0212
7.5	2.88	2.35	2.78	2.21	0.0912	0.083
10.0	2.98	2.67	2.8	2.52	0.1	0.094
12.5	3.14	2.86	3.1	2.67	0.1065	0.109

Table 8 Quality of concrete suggested by Taywood engineering[6]

Concrete quality	Sorptivity (mm^3/mm^2/√min)
Good	<0.1
Acceptable	0.1 to 0.2
Poor	>0.2

4.5   Ultra Sonic Pulse Velocity test (NDT):

The ultrasonic pulse velocity test is used to check the quality of the HPC cubes. Tests were carried out for both OPC and PPC, HPC cubes. A maximum and minimum pulse velocity of 5780.35 m/sec and 5555.56 m/sec was observed for OPC. But for PPC, it was 5586 m/sec and 4784.69m/sec, which falls under the excellent category. Table 9 gives the pulse velocity ratings as suggested by Leslie and Cheesman.

Table 9 Suggested Pulse Velocity of Concrete by Leslie & Cheesman[6]

Pulse Velocity m/sec	General Conditions
> 4575	Excellent
3660 – 4575	Good
3050 – 3660	Questionable
2135 – 3050	Poor
< 2135	Very Poor

Table 10 Pulse Velocity of the HPC cubes[6]

CSF (%)	Distance traveled (m)	Time taken to travel (t x 10^{-6} secs)		Pulse velocity (m/sec)	
		OPC	PPC	OPC	PPC
0.0		18.0	20.9	5555.56	4784.69
2.5		17.5	18.2	5714.29	5494.51
5.0		17.4	17.9	5747.13	5586
7.5	0.1	17.3	18.9	5780.35	5291
10.0		17.8	19	5618.00	5263.16
12.5		18.6	19.5	5376.34	5128.21

5   CONCLUSION

Based on the experimental investigation, the following conclusions are drawn within the limitation of test results.

Compressive strength

- The use of CSF is necessary for the production of HPC. The cube compressive strength studies indicate that the optimum percentages of CSF are 7.5% and 5% for OPC and PPC concrete.
- The compressive strength of CSF concrete increases with increase in age of curing.
- The use of CSF in concrete improves the early strength for OPC concrete.

Split tensile strength

- The rate of increase of split tensile strength with compressive strength is less.
- The ratio of tensile strength to compressive strength decreases with increase in compressive strength.
- The tensile strength does not increase significantly with increase CSF content.

Flexural strength

- OPC concrete with CSF attains greater flexural strength than that of PPC concrete.
- The flexural strength calculated, using IS 456:2000 is found always lower compared to the test results.

Durability-acid resistance test

- The durability of silica fume concrete are more resistance to H2SO4 and HCl where a significant damage is observed in plain concrete mix, the addition of silica fume has shown a significant improvement.

Micro structural studies

- This test is carried out to identify the impermeable nature of the silica fume concrete for 28days & 90 days.
- A very low SWA percentage obtained for 7.5% of silica fume for OPC was 1.002% for 28 days &1.35% for PPC, for 90 days OPC was 0.94% & for 90 days PPC was 1.78 %.
- The porosity of concrete for OPC of 28 days is 0.992%, whereas for PPC is 1.82%, for OPC of 90 days 0.85%, whereas for PPC 1.69 %.
- Sorptivity of concrete for OPC of 28 days is 0.0304 mm/$\sqrt{}$min, whereas for is PPC 0.0243 mm/$\sqrt{}$min. For OPC 90 days is 0.028 mm/$\sqrt{}$min, whereas for PPC is 0.0212 mm/$\sqrt{}$min.

Non- destructive test

- The ultrasonic pulse velocity test is used to find the quality of concrete.
- Leslie & Chessman specified the suggested pulse velocity of concrete as pulse velocity of > than 4575 m/sec then that concrete comes under excellent category.
- The high pulse velocity of concrete for 7.5% of silica fume for OPC was 5780.35 m/sec & for 5% of silica fume for PPC was 5494.51 m/sec. this falls under the excellent category.

6   References

[1] BIS 456 – 2000.; "Plain & Reinforced Concrete Code of Practice" 4th Edition.

[2] Chinnappa,B.; "High performance concrete", Proceedings of the advanced in concrete technology with emphasis on HPC, Pondicherry-India 2001.

[3] Rajamane.N.P,; Gopalakrishnan,S,;, "HPC- part II Selection Ingredients", the national seminar on HPC (NSHPC – 98), Chennai-India 1998.

[4] Adam Neville,; "Properties of Concrete" fourth and final edition, Pearson Education Asia Ltd 2000.

[5] BIS 5816 – 1970,; "Concrete Testing Code of Practice".

[6] KarthikeyanJayakumar,; "Effect of partial replacement of cement with silicafume on properties of high performance concrete", Project Report for the Bachelors degree in Engineering 2002, Kumaraguru College of Technology, Coimbatore- India.

Ivailo Terzijski
Associated professor
Brno University of Technology, Faculty of Civil Engineering
Brno, Czech Republic

Compatibility of Components of High and Ultra High Performance Concrete

Summary

The article describes aspects of compatibility and efficiency of components frequently used in HSC and UHPC concretes mix compositions. Extended technique of binder components compatibility measurement was used. For tests model suspensions and model mortars were used. Large set of different polycarboxylate superplasticizers, micro fillers and nano fillers was tested. Non-standard behaviour of several polycarboxylate formulations was observed. Strong influence of polycarboxylate superplasticizer formulation on rheological properties, amount of entrapped air and strength is documented. Tough impact of silica fume form on its dispersion in concrete and on concrete strength was recognized.

Keywords: *concrete, UHPC, HSC, HPC, mix design, component, compatibility, superplasticizer, polycarboxylate, micro filler, colloid.*

1   Introduction

By production of UHPC, HPC or HSC it is necessary to use in their mix composition miscellaneous additives and admixtures. Usage of relatively great number of components makes mix design of these kinds of concrete distinctly more difficult comparing to regular ones. On each used component are high demands, there. But usually more troubles can be obtained form the fact that even high quality components cannot from time to time effectively act together. This problem of non-effective concurrency can be observed even by the components which parameters, as single substance, are fully satisfactory. In such case we have obtained *non-compatible* combination of the components. In opposite case we have analogically obtained *compatible* combination of the components.

2   Compatibility measurement of concrete components

Nowadays is still impossible to find i.e. optimal combination of cement and superplasticizer by looking at their data sheets. The situation is even more complicated by UHPC, HPC or HSC as their binder composition consists from more components. Minimally, reactive micro filler as additional component is used. Therefore, as a minimum, experimental prediction of concrete rheological behaviour is usually necessary. As performing real concrete trial batches is exacting, several simplified and easier to repeat techniques have been developed [1]. These are generally based on studying the rheological behaviour of plasticized water-

cement suspension. The prediction by using this method is not utterly accurate, but in the range of regular superplasticizers and regular concretes it is relatively safe. By our previous tests [2] was found out that nowadays the compatibility test have to be extended to respect the different behaviour of the new generation of polycarboxylate superplasticizers.

The major principles of extension are as follows:

- Economically weighted dosage of superplasticizers: as the plasticizers are produced in various concentrations of effective basis and in various prices, the dosage with respect to comparable price is important.
- Additional minislump test on the model mortar prepared from tested binder components and standardized quartz aggregate.
- Additional strength test of the model mortar.
- Observation of the amount of air entrapped into water/cement/plasticizer suspension and mentioned model mortar.

The principles mentioned above were used as the base for another extension of compatibility testing technique, suitable for UHPC, HPC and HSC design. Report on this extended technique and found out basic principles for designs of these concretes are the main content of the paper.

3　　　Compatibility tests for HSC design

3.1　　　Tested HSC binder components

Cements

Two cements of class CEM I 42,5 R and two cements of class CEM I 52,5 R from two cement works in the Czech Republic have been used.

Plasticizers (superplasticizers)

By referred tests preferably superplasticizers of the new generation were used. These new superplasticizers are commonly called polycarboxylates or polycarboxylate polymers. The new chemistry is being referred to as comb polymers because their structure which involves a backbone consisting of a polycarboxylate polymer to which has been grafted polyoxyalkylene pedant group [3]. The main polymer is frequently condensation product of polyacrylic acid and polyetheramin – so the designation polycarboxylethers in such case can be observed, too. It is comprehensible that properties and effects of such widely defined substances are very variable. Moreover, produced commercial products consist usually of a mix of molecules with different molecular weight and character.

In presented tests 16 different superplasticizers produced by Addiment, Chryso, Mapei, Peramin, Sika, Schepens, SKW-MBT and Woermann were used. For correct action instead of commercial markings common marking "PCx" in the paper is used (where "x" is a number of the sample). In spite of used test technique each product was represented by the sample and price, both given by its official distributor.

Micro fillers

Micro filler is nowadays-regular part of HSC. Mostly in this role is silica fume used. Therefore four different silica fume based products from Addiment, Sika and Woermann were tested.

Two products were in powdered form (marking in diagrams "Px") and two products were in suspension form (marking "Sx"). As in the previous case "x" is here a number of the sample.

3.2   Technique of compatibility tests

The technique continuously developed at BUT, Faculty of Civil Engineering, consists of two basic phases:

1. Set of tests executed on the suspension level (suspension of binder components).
2. Set of tests executed on the mortar prepared from the suspension and standardised quartz sand.

Tests on the suspension level

Basic water-cement-superplasticizer-micro filler suspension was prepared by usage of standardised work-sequence by help of medium-shear mixer. Dosage of all components by all tests was constant except of superplasticizer, which dosage was price-constant. Basic parameters of the model suspension for HSC were:

- Water/(cement + silica fume) ratio: 0,27.
- Dosage of the silica fume (solid mass):   10% of the cement dosage.
- Price-weighted dosage of superplasticizers in the interval (0,8; 1,4)% of the cement content.

By test on the model suspension particularly changes of its apparent viscosity in time interval from 10 to 120 minutes has been measured. The apparent viscosity here is expressed with a spread of the suspension run out from minicone with the volume of 177 cm^3. Larger spread indicates lower viscosity of the suspension and better efficiency of used cement-superplasticizer-micro filler combination.

The principal theory for compatible cement-superplasticizer combination [1,2] presumes zero or minimal slump loss of the suspension spread with time – see Figure 1. By some polycarboxylate superplasticizers special "overcompatible" behaviour was observed [2].
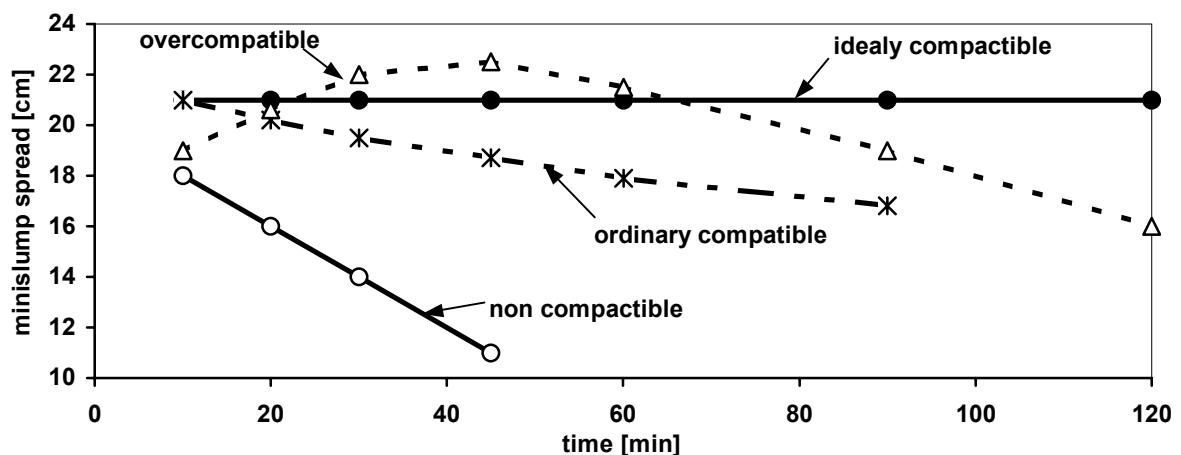
Figure 1: Examples of typical compatibility measurements results

Tests on the mortar level

For maximum simplicity and repeatability this test technique was derived from the standard procedure for cement strength testing [5]. The only important difference is substitution of the standard volume of water-cement paste (binder) with the same volume of water-cement-superplasticizer-silica fume suspension. For this task suspension prepared in previous test stage was used. By prepared mortar flow-table spread according to Haegermann was measured. Standard specimens of mortar for strength test was prepared and tested in the age of 2 and 28 days. From accurately measured density of mortar and known specific weight of components amount of entrapped air into mortar was calculated.

3.3 Results of compatibility tests for HSC design

In spite of big number of tested components and their possible combinations very large set of test results was obtained. Their complete presentation exceeds limits of this paper. Therefore the major trends and basic obtained knowledge are presented only.

3.3.1 Influence of the silica fume form

It was observed that the form (powder or suspension) of silica fume has distinct impact to the binder properties both in the fresh and hardened stage. In the fresh stage the powder form of silica fume increases the viscosity of model suspension and model mortar. As an example results of the apparent viscosity changes in time, obtained with one cement, two plasticizers (PC1 and PC2) and three silica fume products (two in suspension form - S1, S2 and one powdered - P1) are shown on figure 2.
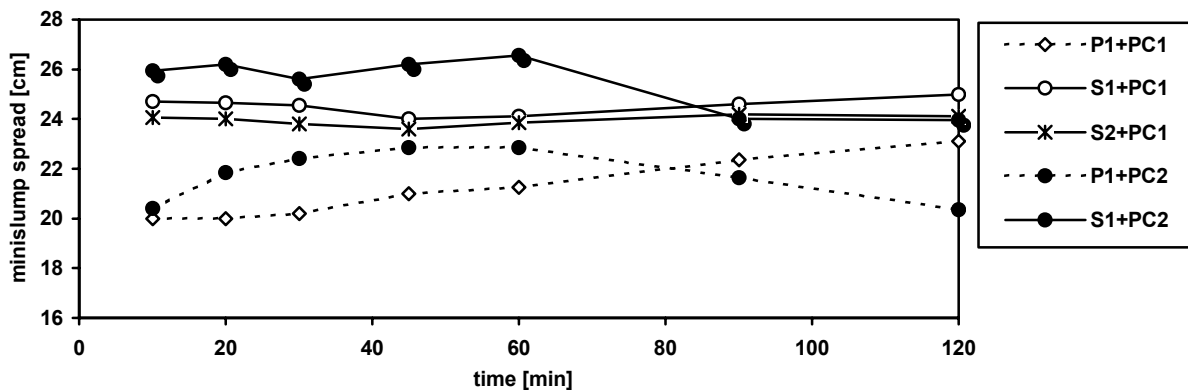
Figure 2: Influence of the silica fume form on the apparent viscosity of model suspension

Perhaps, more important for concrete mix design is the impact of the silica fume form on the final strength of the model mortar or concrete. Here has been observed clear advantage of the suspension form of silica fume over the powdered one. Comparison of the strength results achieved with the suspension form (S1) and the powdered form (P1) of silica fume from the same producer is on figure 3. The difference is in the range from 8 to 15% in favour of the suspension form. This difference has been explained and verified with help of

microstructure analysis. On typical photos on figure 4 taken with electron microscope is obviously seen the significant difference in dispersion of both forms of silica fume. On the micro photo of hardened cement paste with the powdered form of silica fume are clearly visible only partially reacted agglomerates of not fully dispersed silica fume particles. In the opposite way, on photos of hardened cement paste with the suspension form of silica fume dense structure of CSH phases can be seen only, without agglomerates.
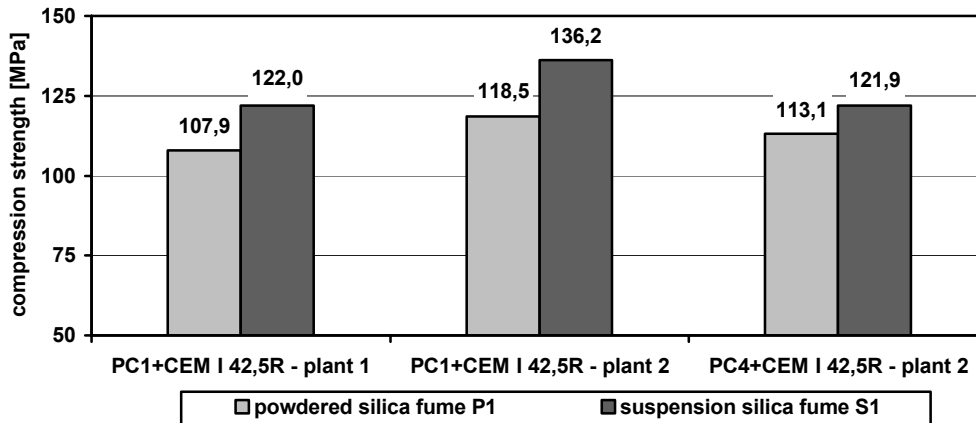
Figure 3: Influence of the silica fume form on the compression strength of the model mortar
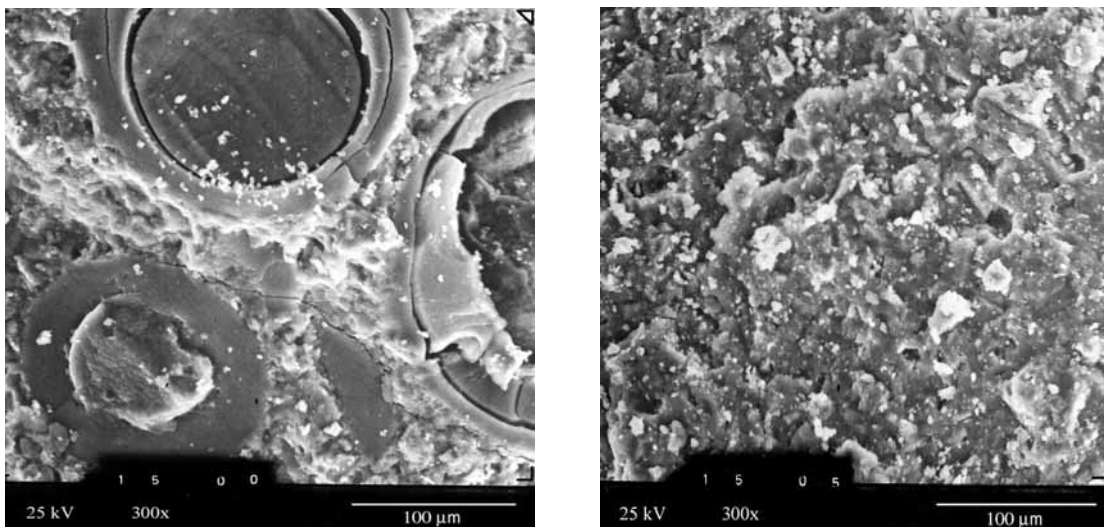
Figure 4:   Agglomerate powdered silica fume particles (left) and dense structure of cement paste with suspension silica fume form (right).

3.3.2   Influence of the type of superplasticizer

In this field presumption of relative large variability of polycarboxylate superplasticizer was verified. Economically weighted dosage has this fact accented. By the superplasticizer is the most important property the ability to plasticize concrete. This ability was represented in displayed tests by observation of the apparent viscosity of model suspension and mortar. As an example are on figure 5 curves of changes of the apparent viscosity of model suspension presented. All results for different superplasticizers have been obtained with the same

cement and silica fume product. The figure demonstrates great differences between diverse superplasticizers. It is evident that based on the "classical theory" – see [1], almost all of tested polycarboxylate superplasticizers are compatible. In the same time it is evident that this fact is not sufficient for evaluation of cement – plasticizer compatibility, now. It is because their efficiency is very variable.
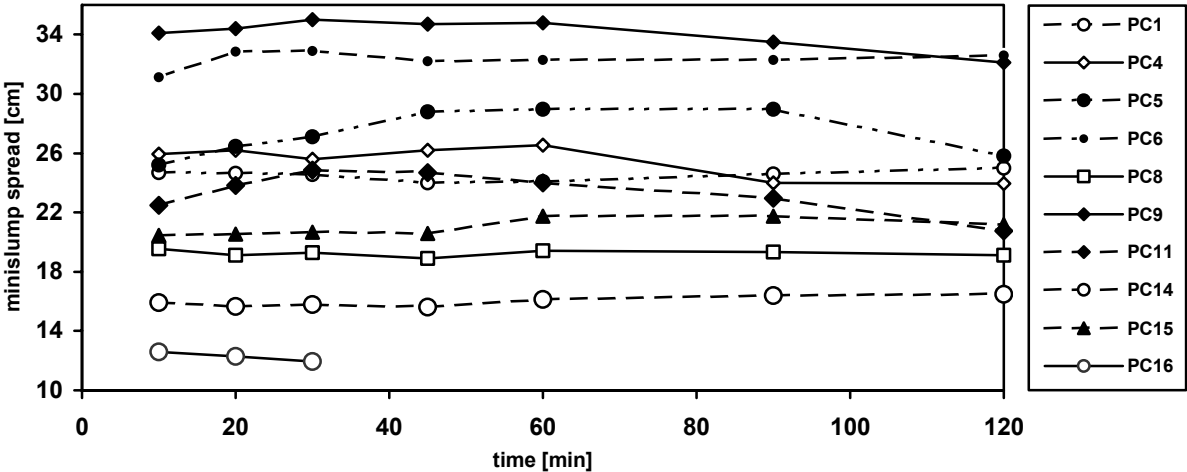
Figure 5: Influence of superplasticizer on the apparent viscosity of model suspension

Similar range of the plasticizers properties can be observed on figure 6. On this figure are simultaneously plotted spreads of model mortars and relevant base model suspensions measured in the same time (30 min) after mixing. As in the previous figure the impact of different plasticizers on the apparent viscosity is very variable. Interesting is the fact that better (=lower) spread of the suspension does not lead automatically to better spread of the mortar prepared from the same suspension and standardised sand. It was observed that the magnitude of difference between these two readings indicates sensitivity of the superplasticizer to lose of water (i.e. due to adsorption on the surfaces of particles of HSC binder and aggregate). In the same time this difference indicates the degree of superplasticizer ability to stabilize concrete mix – with decrease of the difference grows usually stabilizing effect of the superplasticizer. (Notice: Strongly stabilizing polycarboxylate superplasticizers are not suitable for HSC and UHPC as they by low water/cement ratio produce "gummy" concrete mix.)

Further important information were obtained by the tests of compression strength and tests of amount of entrapped air by the model mortar. Was detected that entrapped air overruns in more then half of cases content 2%. In the extreme case the content of entrapped air was 11,7%. Consequences for strength and its decrease in mentioned case are evident. Very illustrative from this point of view is following figure 7 that shows strength and air content data obtained for 16 different polycarboxylate plasticizers and equal rest components. On figure 7 is for better readability the air content value multiplied by 10.
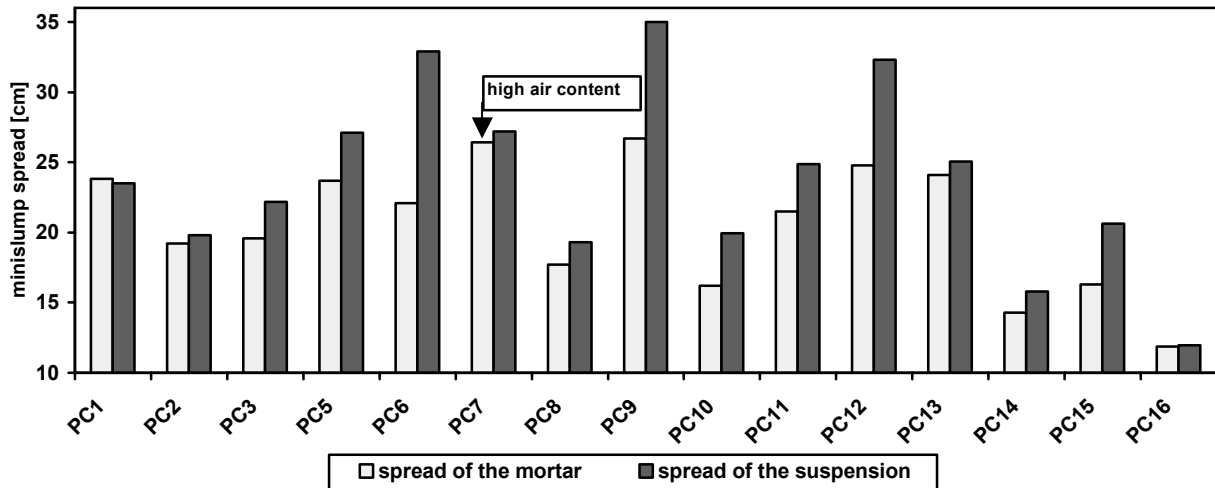
Figure 6: Impact of the superplasticizer type on the suspension and mortar viscosity
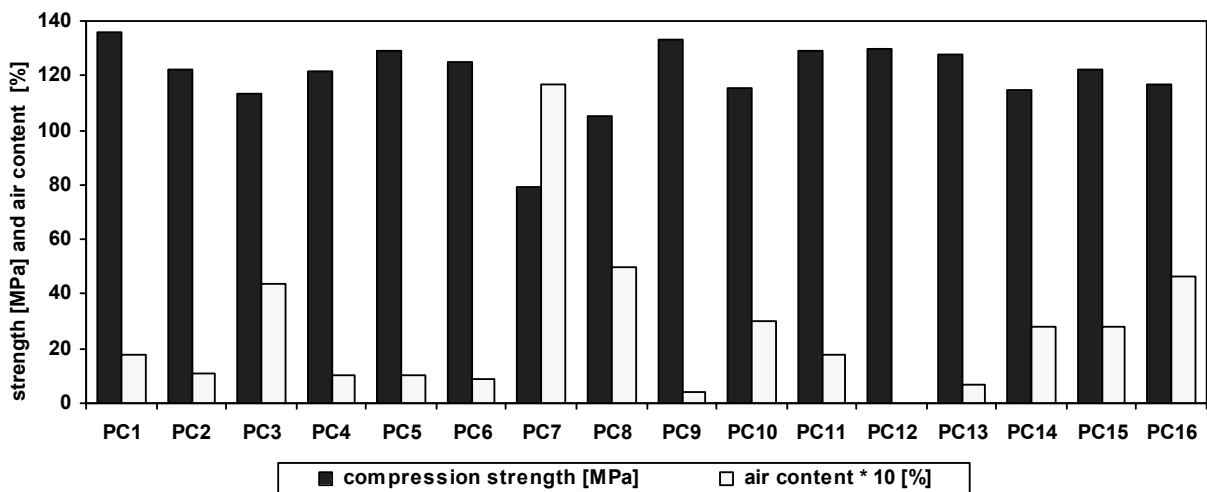
Figure 7: Influence of the superplasticizers on the compression 28-days strength and air content

3.3.3 Influence of the Portland cement class

The main task here was to check if the usage of relatively fine grinded cements of the class 52,5 is really effective for HSC. On the following figure 8 is demonstrated the influence of cement class on the apparent viscosity of model suspension. Presented data was obtained with cements from the same cement work and 3 different superplasticizers.

Not as unambiguous as by viscosity is cement class impact on strength. It is documented on figure 9, which shows the influence of used Portland cements and their classes on the 28-days strength of the model mortar. For plotted comparison the results obtained with 5 different superplasticizers were used. It can be recognised that some cements of 42,5 class

reach the same or better strength then cements of 52,5 class, without negative influence on the workability.
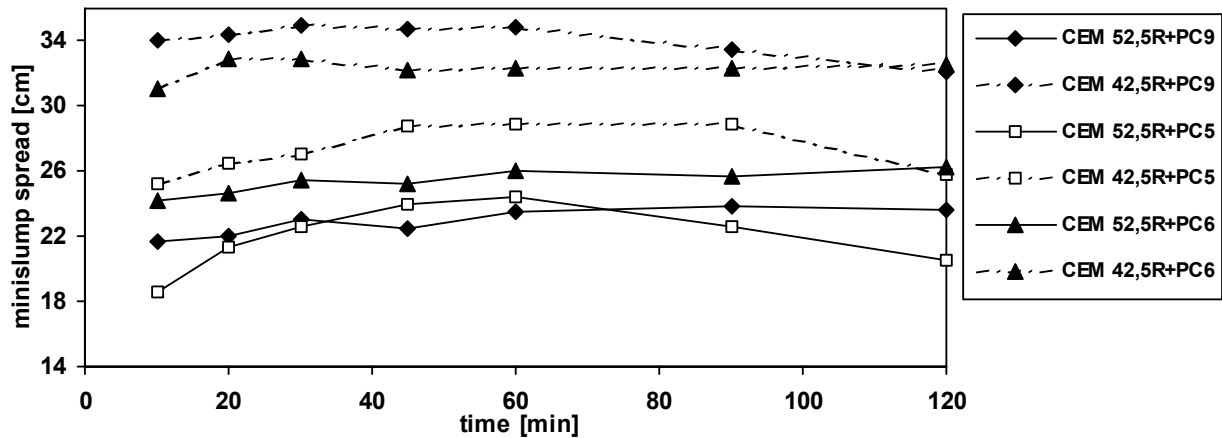
Figure 8: Influence of the cement class on the apparent viscosity of the model suspension
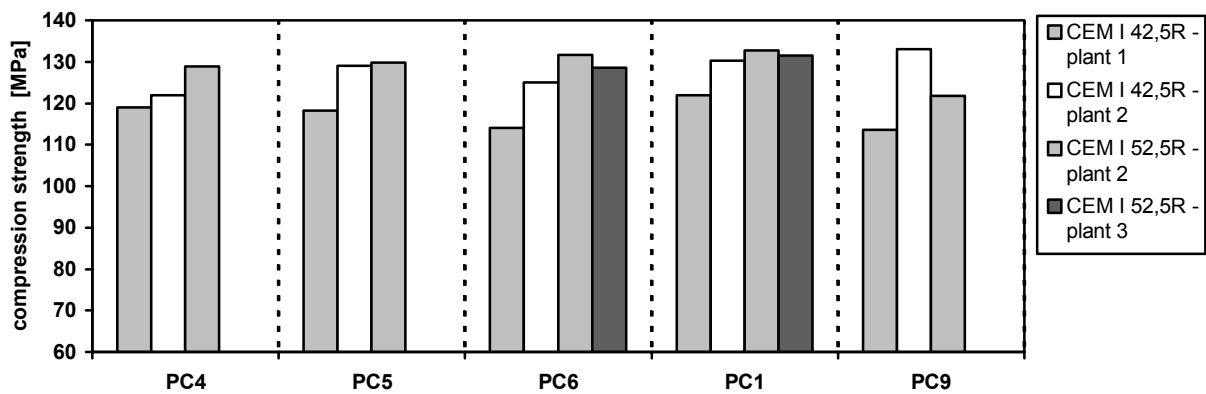
Figure 9: Influence of the cement class on the compression 28-days strength of model mortar

4　　　Compatibility tests for UHPC design

4.1　　　Tested UHPC binder components

Cements

One cement of class CEM I 42,5 R and two cements of class CEM I 52,5 R from two cement works in the Czech Republic have been used.

Plasticizers (superplasticizers)

By referred test selection of the most efficient polycarboxylate superplasticizers tested in the rank of HSC compatibility test were used – for more see article 3.1

Micro fillers and nano fillers

Proven silica fume in a suspension form was primarily used. As an alternative to silica fume relatively unknown product GT – Lasto-Crete F was tested. It is powdered product based on aluminium silicate. Its fineness is 24,1 – 100,2 $m^2 . g^{-3}$ and it is comparable with regular silica

fume. Furthermore two products based on the colloidal SiO_2 form as a supplement to the silica fume was tested. Both product were in liquid form, with 30% respectively 40% of SiO_2 content. This kind of products is frequently called "nano silica" as their colloidal particles are finer and specific surface larger when compared to regular silica fume (micro silica). In the average the specific surface of nano silica is 10 to 20 times greater. Of course, amorphous SiO_2 is very reactive with alkali lime phases of cement paste, so the marking "filler" is not very correct. (In similar way it holds true for the silica fume.)

4.2 Technique of compatibility tests

In the principle the same technique of compatibility test as by HSC tests was used – see article 3.2. Possible differences are mentioned in the following test.

Tests on the suspension level

Basic parameters of the model suspension for UHPC were:
- Water/(cement + silica fume) ratio: 0.20
- Dosage of the silica fume (solid mass):   15% of cement dosage
- Alternative dosage of nano silica (solid mass):   5% of cement dosage
- Price-weighted dosage of superplasticizer in the interval (2,2 to 3,3)% of cement content.

Tests on the mortar level

In the principle the same technique of compatibility test, as by HSC tests was used – see article 3.2. When compared to this, relative amount of model suspension was increased to 50% of the mortar volume only and 15% of standardized sand weight was substituted with quartz powder.

4.3 Results of compatibility tests for UHPC design

4.3.1 Influence of the micro and nano filler type

Substitution of the silica fume with Lasto-Crete was tested. Full substitution was not really applicable due to high request for rheological water content. Finally, substitution of 1/3rd of the silica fume content (5% dosage of Lasto-Crete to the cement content) in combination with superplasticizers PC1 and PC3 was tested. Negative impact on the apparent viscosity of model suspension of such dosage was not too great – see curves marked with 5%L on figure 10. Impact on the strength of model mortar was also not too great, but definitely negative – see figure 11.
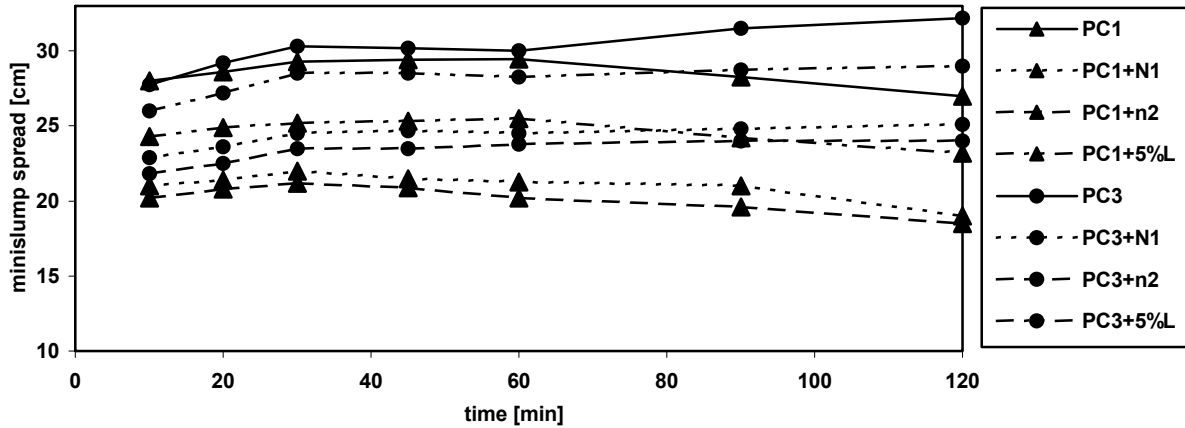
Figure 10: Influence of used micro and nano filler on the apparent viscosity of model suspension
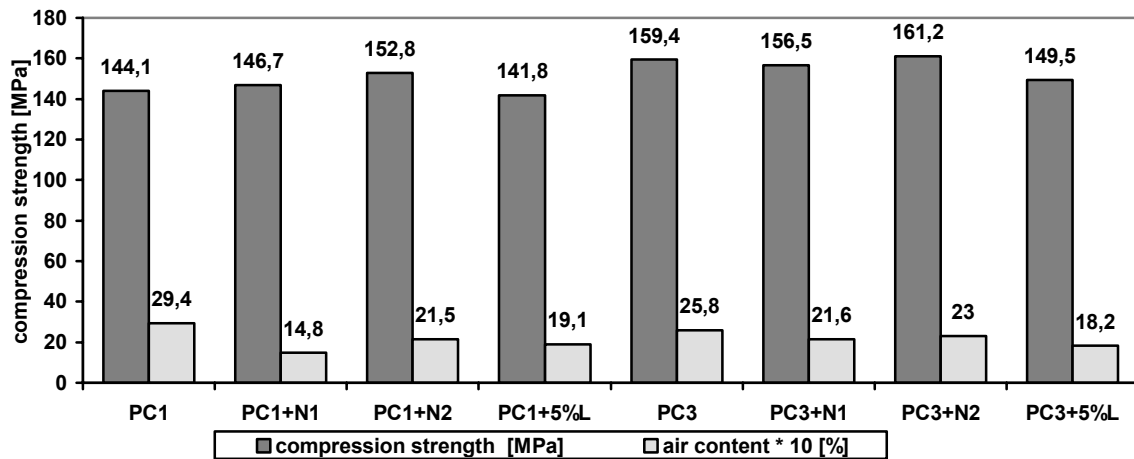
Figure 11: Influence of used micro and nano filler on the 28-day strength of model mortar

Addition of both nano silica products (marking N1 and N2 on figures 10 and 11) into model suspension has approximately the same effect – increase of the apparent viscosity. The effect was a little bit greater for product N2 with greater fineness of colloidal SiO_2 particles. The impact on the model mortar strength is not fully approved in spite of the small strength differences, but light tendency to the strength increase (esp. for the product N2) is visible.

4.3.2   Influence of the superplasticizer type

As proven and efficient polycarboxylate superplasticizers from the HSC compatibility tests were used, the impact of superplasticizer type on the apparent viscosity of the model suspension and model mortar was not to great and without any surprise. Therefore, relevant curves of minislump-spread changes in time are not presented. On the other hand, one interesting fact was obtained by the strength tests of model mortar: one from six used superplasticizer (which works excellent by HSC) retards by high UHPC dosage heavily

increase of the strength. The relevant mortar was 3 days in gummy consistence and even the 28-days strength was about ½ of the comparable one – see item PC2 on figure 12.
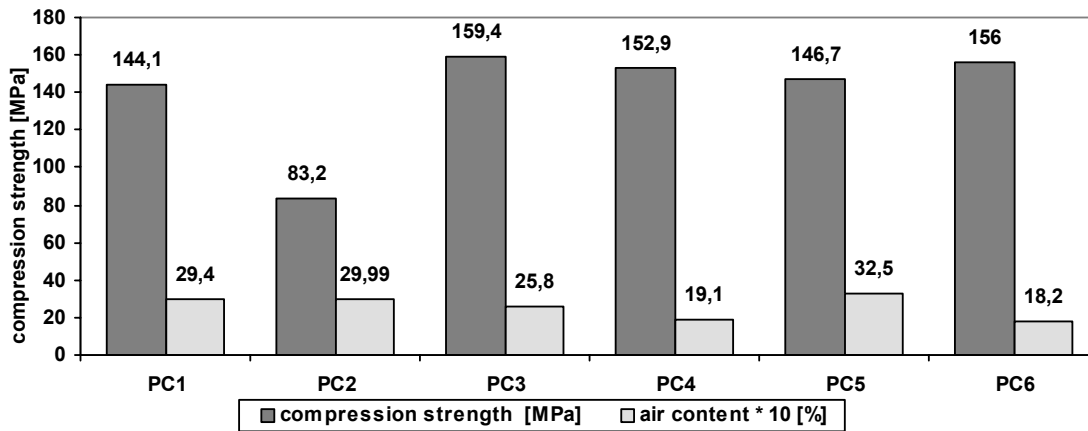
Figure 12: Influence of the superplasticizer on the compression 28-days strength and air content

By the rest mixes the strength results were relatively on equivalent level with differences based mainly on the content of entrapped air.

4.3.3   Influence of the cement type and class

Experimental works needed for assessment of cement type influence have been not finished yet; therefore relevant experimental data are not presented. But it is evident that not all cements can reach by low water/cement ratio the level of strength needed for UHPC. (Perhaps this is the reason why higher strengths were not reached.) This problem, with consideration to the production in the country of origin, has to be researched in the near future.

5   Conclusions

The contribution of presented works can be seen in two main areas:
1. In the development of extended methodology suitable for testing of compatibility and efficiency of binder components used for HPC, HSC and UHPC mix design.
2. In acquiring knowledge about behaviour of large set of binder components, which are or can be used in HPC, HSC and UHPC mix composition.

Concerning to point 1: extended methodology of compatibility testing has been successfully used for optimised mix design of NSC and HSC concretes used for bridge structures elements in the Czech Republic. Practical application of UHPC has been not reached, yet.

Concerning to point 2: basic knowledge can be summarised into following items:

- Nowadays is produced large set of polycarboxylate or polycarboxylate based superplasticizers with wide spread of properties, concentration and prices. If combined with distinct cement, it can be from the price/performance ratio point of view obtained very efficient or very inefficient couple.

- Important is the impact of superplasticizer/cement combination on the long-term strength of concrete. In some cases of incompatible combinations can the large amount of entrapped air lead to significant lost of potential concrete strength (and modulus of elasticity, too).

- By UHPC design can be by some superplasticizers reached critical dosage with detrimental consequences to concrete strength.

- Dispersion of the silica fume (and probably also of others micro fillers) in concrete is much better if they are used in suspension form. Better dispersion improves significantly the positive impact of the silica fume on concrete final strength.

- Tested micro filler based on aluminium silicate powder appears to be not efficient for usage in UHPC. Its role is presumed chiefly as concrete mix stabiliser.

- Colloidal silicon dioxide "nano fillers" can improve UHPC strength a little bit. Others possible and probable improvements of concrete properties have to be checked (e.g. freeze-thaw resistance, permeability, etc.).

- Not all nowadays produced Portland cements are suitable for usage in HSC or UHPC. It depends mostly on the mineralogical composition (what has been not discussed in the paper), fineness of grinding and on the type of used regulator of cement setting.

Finally, in the future the methods for optimal UHPC, HPC or HSC concrete mix design should be improved in mainly to embrace the fracture properties of concrete and durability problems.

6   Acknowledgements

7   References

[1]   Aïtcin, P. -C.: High Performance Concrete, E & FN Spon, London, 591 p., 1998.

[2]   Terzijski, I.: Cement - Plasticizer Compatibility of Polycarboxylate Superplasticizers. In: Proc. Non-traditional Concrete 2002, Brno 2002.

[3]   V.M. Malhotra, "Fifth CAMET/ACI international conference on Superplasticizers and Other Chemical Admixtures in Concrete", ACI Special Publication, SP-173-4, 1997.

[4]   Kantro, D.L.: Influence of water-reducing admixtures on properties of cement paste – a miniature slump test. Cement, Concrete and Aggregates. Vol.2, 1980, p. 95-108.

[5]   EN 196-1 Methods of testing cement. Part 1: Determination of strength.

Rudolf Hela
Doc. Dipl., Ing. CSc.
University of Technology Brno,
Faculty of Building Engineering,
Brno, Czech Republic

Jiri Zach,
Dipl.-Ing. Ph.D.
University of Technology Brno,
Faculty of Building Engineering,
Brno, Czech Republic

Petr Kubicek
Dipl.-Ing.
University of Technology Brno,
Faculty of Building Engineering,
Brno, Czech Republic

Utilization of Chemical Admixtures in High Performance Concretes (HPC)

Summary

At the stage of design of ultra high performance concrete (UHPC) we have to take in respect the requests posed for both fresh and for hardened concrete. At present there is a wide scale of chemical admixtures at the building market that are being added into UHPC for their quality improvement. The verification of the compatibility of chemical admixtures and used binders and also the suitability of given chemical admixture is often essential with respect to specific requirements posed for both fresh and hardened concrete. This paper describes the procedure for checking the suitability of chemical admixtures for UHPC by means of chosen testing methods performed on cement pastes. The unavoidable parts of UHPC are the active or passive admixtures (micro silica, finely ground slag, ashes from electricity supply industry, etc.) that significantly act in the whole process and effect both rheological properties of fresh composite materials and physical-mechanical properties of hardened composite materials. The verification of suitability of chemical admixtures and their effective compatibility in the whole system cement-admixture-additive-water is also essential in this case.

Keywords: HPC, hydration heat, cement, admixture, additives, thermal dilatation

1 Problems of HPC Sensitivity to Cracks Formation in Initial Stage of Hydration

The High Performance Concrete (HPC) with higher workability and better durability is one of very important building materials. Therefore it is necessary to investigate the properties of this material. The hardening process is one of non-negligible concrete characteristics during the hardening of concrete stone.

Significant volume changes take place in the structure of concrete during hydration. These changes can be divided as follows:

a) Thermal dilatation – **TD** – is caused primarily by the exothermic effect of clinker minerals hydration reactions with water. The rate of hydration heat liberation is given by the intensity of ongoing hydration reactions and it depends in particular on the type of used binder (chemico-mineralogical composition, grain fineness), on temperature, water/cement ratio, admixtures and additives. In concrete structure temperature gradients are formed, which become evident by the formation of negative internal tensions. (The quick temperature change of concrete in dependence on time, which causes cracks in concrete as the result of concrete brittleness – incapability of concrete to relax quick temperature changes, can be characterized as negative too).

b) Autogenous deformation - **AD** – this effect takes place as the result of new internal structure formation. The autogenous deformation is often termed as self-desiccation, because it is first of all chemical shrinkage connected with hydration (bound of water molecules into the structure of CSH gels). In the case of HPC is this deformation higher than in the case of common concrete types, because the low water/cement ratio affects the formation of smaller capillary pores and in this way it increases the self-drying effect.

c) Evaporation of physically bound water. Capillary pores are formed on the surface of the composite as the effect of water evaporation. During the loss of batch water as the result of desiccation under elevated temperature, overpressure is formed in the internal structure of concrete which needs not to be in relation with the tensile strength of concrete at the moment.

It is necessary to know how to quantify these changes and primarily to know how to predict them on the base of knowledge concerning the typical behaviour of binders in combination with chemical admixtures and fine-grained fractions.

One of methods which can manage the description of the binder mix behaviour during the hydration phase is the calorimetric method. This method can be used for the prediction of TD and partially even for the prediction of AD. It is the calorimetric determination of the intensity of hydration heat liberation. This method is relatively quick, exact and on the base of it we can determine the size of chemical admixtures and additives effect on the change of binder reaction kinetics in concrete.

2   Process of Cement Hydration

The cement hydration is a very complicated process, which is influenced by many variables. The hydration of cement becomes evident by strength increase in concrete, in dependence on technological parameters and on surroundings conditions in which the hydration takes place. From the quantitative point of view the course of hydration reactions can be followed by means of calorimetry. A system of isoperibolic calorimeters for hydration heat determination of silicate materials was developed in the Brno University of Technology. The hydration takes place in a calorimeter. The heat characteristics of this calorimeter are known

under exactly defined conditions. The temperature of the tested sample in the calorimeter during the period of hydration and the surrounding temperature are monitored and recorded. The intensity of heat liberation is determined according to the following formula:

$$I_i = \frac{\dfrac{m \cdot c \cdot (\theta_i - \theta_{i-1})}{\tau_i - \tau_{i-1}} + \Phi_{zi}}{m_{cem}} \qquad (1)$$

where :   I   intensity of hydration heat liberation (in relation to 1kg cement) [J.s^{-1}.K^{-1}],

         m   mass of the sample [kg],

         c   specific heat capacity of the sample [J.kg^{-1} . K^{-1}],

         Θ temperature of the sample [°C],

         τ time [s],

         Φ_z heat flow by heat transmission through the calorimeter body [W],

         m_{cem} mass of cement [kg].

Figure 1: Photography of isoperibolic calorimeter body

In the case of comparison measurements we can proceed directly from measured temperature courses, from which the following comparing quantities are determined:

- The time to reach the maximum temperature τ_{max}
- The temperature increase – the achieved maximum temperature - Θ_{max}

Graph 1:   Schematic representation of monitored quantities
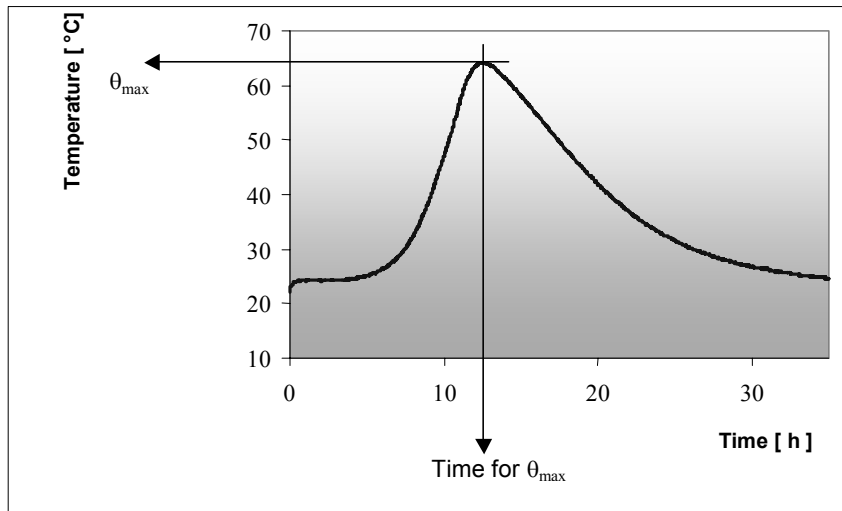
3   **Utilization of chemical admixtures in HPC**

The High Performance concretes are nowadays prepared from cements of practically all classes. Self Compacting Concrete is for instance designed from cements of class CEM III and in spite of some adverse aspects (increased tendency to bleeding) which are connected with the utilization of these cements, it is possible to prepare often concrete with higher utility properties than with utilization of classical cements class CEM I.

Graph 2:   Course of hydration temperatures of different types of cements at the
               surrounding temperature +20 °C
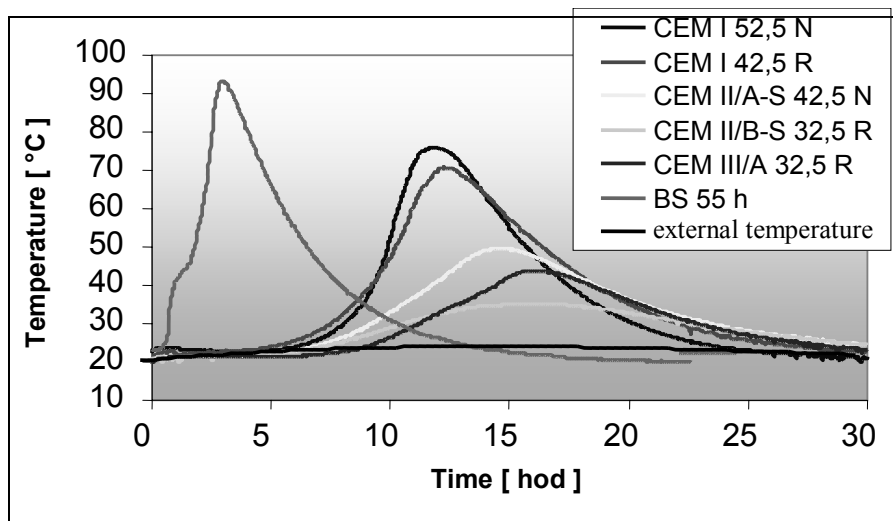
From the point of view of the fact that in most cases a great quantity of super-plasticizing admixtures is used for HPC (mostly admixtures of new generation), we have oriented the research primarily on of hydration reactions course study of concretes modified by higher quantities of super-plasticizing admixtures.

For the comparative measurement additives based on polycarboxylates were used. The measurements were realized with two types of cements:

- CEM I 42,5 R from plant Mokrá
- CEM II/A 32,5 R from plant Radotín.

The results of measurements are in following graphs.

Graph 3:   The hydration temperature course of cement CEM III/A 32.5 R (w/c= 0,34) with the addition of a superplasticizer based on polycarboxylate (1,1%) at the surrounding temperature +20°C.
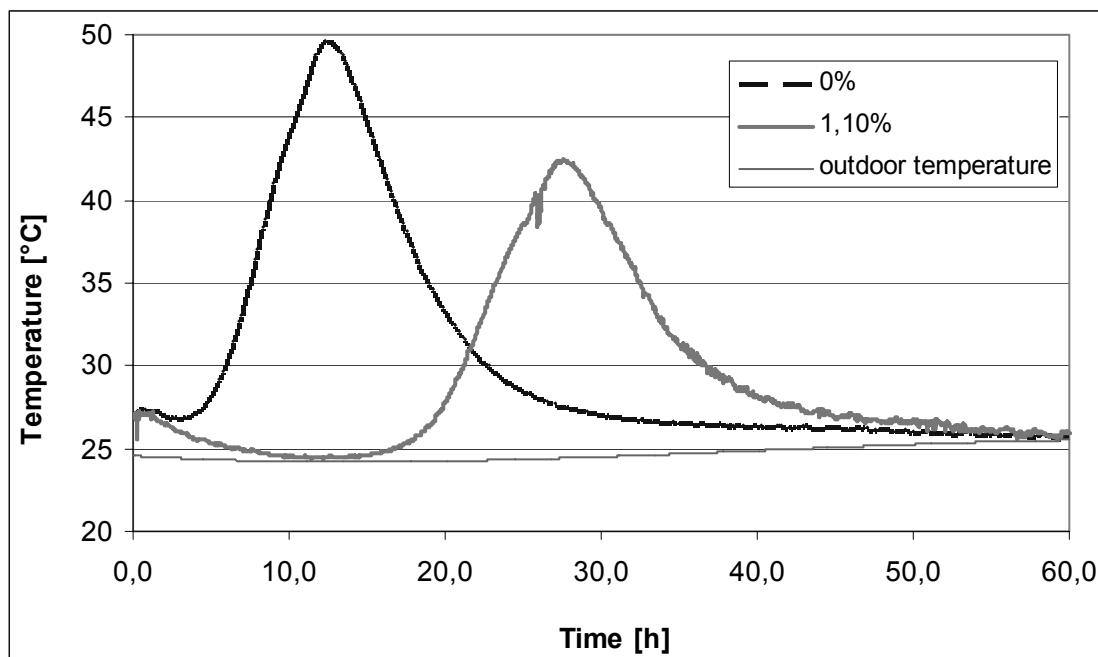
Further we examined the Portland cement of class CEM I 42.5R from plant Mokrá, with different quantities of superplasticizer based on polycarboxylate. The dose was chosen in a way to secure identical rheological properties of the cement paste.

The applied formula: CEM I 42.5 R Mokrá,

water (water/cement ratio)   w = 0,38

addition in doses 0,5 % - 2,0 % (mass) of binder

$\Theta_{surroundings} = +20\ °C$

Graph 4:   The hydration temperature course with addition of superplasticizer based on polycarboxylates.
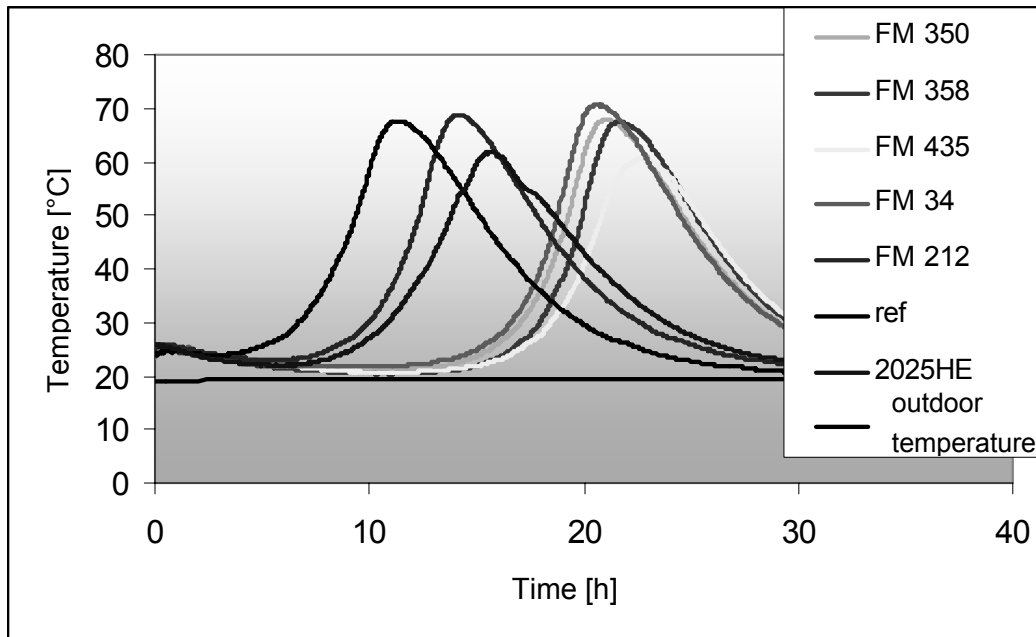
Graph 5:   Effect of different superplasticizing additives on achieved maximum temperature Θ_{max} .
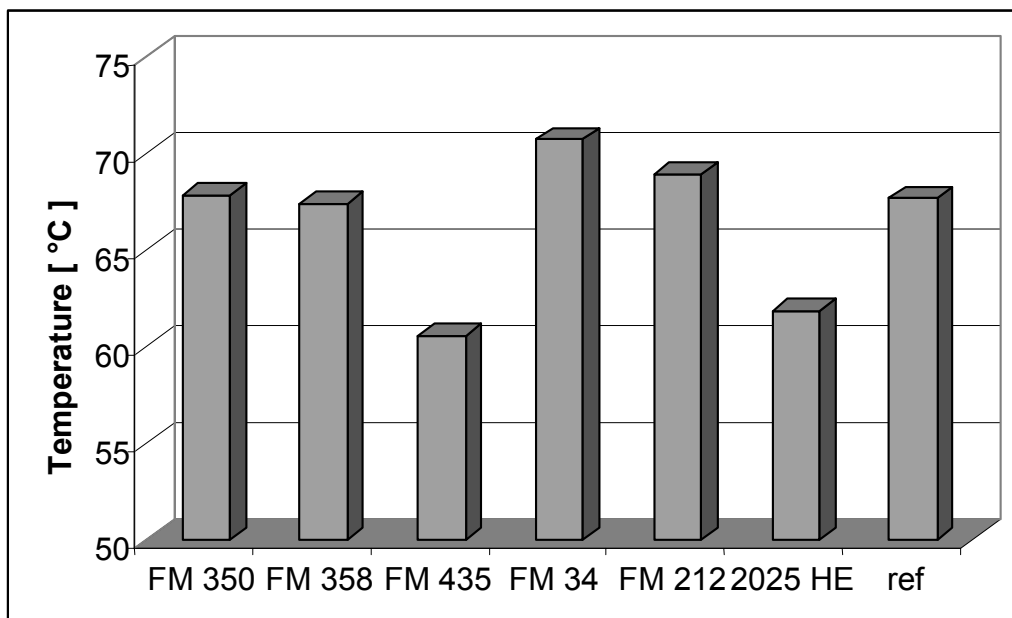
Graph 6:   Effect of different superplasticizing additives on the time
            period necessary to reach Θ_{max} .
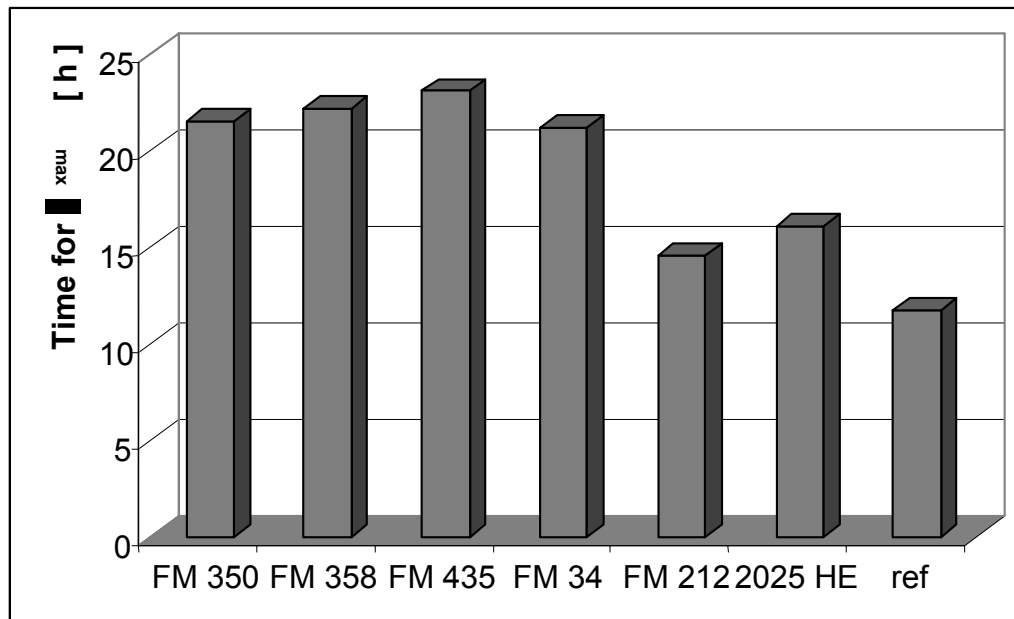
4   Conclusion

In laboratory measurements using selected formulae we provided documentary evidence of super-plasticizers strong effect on the change of hydration kinetics of resulting binder mixture. Based on these obtained results a temperature course effective prediction in hydrating masses is possible and in this way it is possible to determine the negative TD and partially even the AS. On the base of AS and TD prediction of hydrating masses effective measures can be taken, to reduce the negative influences of these actions and to secure the good final parameters and durability of final concrete structure.

Further we found, that the macromolecules shape and composition of super-plasticizing agents based on polycarboxylates have a very strong influence on the hydration process. Therefore a suitable selection of super-plasticizing additive is necessary in dependence on particular demands. In particular we must respect the possible retardation of the hydrating process, which in the case of massive structures can be positive, but on the contrary it is in the manufacture of prefabricated elements harmful.

Torsten Kowald
Ph.D. student
University of Siegen
Siegen, Germany

Influence of surface-modified Carbon Nanotubes on Ultra-High Performance Concrete

Summary

The improvement of the mechanical properties of the worldwide most important building material, the composite concrete, is mainly reached by the use of volume-filling additives like micro- and nano-silica or carbon fibres. As a consequence the use of carbon based nanostructures like carbon nanotubes is very promising. Their unparalleled mechanical properties could be of use for the development of new ultra-high performance composites. First experiments show the influence on the mechanical properties of cement-based building materials by the incorporation of surface-modified multi-walled nanotubes.

Keywords: *carbon nanotubes, composites, mechanical strength, functionalization*

1 Introduction

The mechanical characteristics of the composite concrete can be significantly improved by the use of micro- and nanoscale volume-filling additives. Recently, due to their outstanding mechanical properties, carbon-based nanostructures (CNSs) have been utilized to reinforce concrete [1, 2]. Nevertheless, there are still two key issues that need to be addressed: 1) dispersing the CNSs and 2) linkage between the CNSs and the concrete matrix.

With respect to the complexity of this task a cooperation between the institute of materials engineering and the institute for building and materials chemistry has been initiated at the University of Siegen.

Multi-walled nanotubes (MWNTs) are the most promising CNSs with respect to reinforcement of building materials, as they show more surface defects than any other CNSs. These defects lead to an improved linkage between the MWNTs and the cement matrix [2]. By the use of MWNTs within pure cement pastes the 14 d compressive strength could be improved by 30% with respect to the plain cement paste whereas the incorporation of single-walled nanotubes (SWNTs) only lead to an increase of 6% [2]. Additionally the defects allow a functionalization of the nanotube's surface.

The used MWNTs purchased from Sun Nanotech Co Ltd. are synthesized by the chemical vapour deposition (CVD) method with a typical diameter between 10 and 30 nm and a length of some microns.

There are different possibilities of modifying the inert surfaces of the MWNTs. Without changing the nanotube's surface itself, polymers can be wrapped around these and enhance the dispersibility of the CNTs in water [3]. By means of oxidation it is possible to add surface defects and functional groups to the inert surfaces of the MWNTs [4]. The modifications should simplify the dispersion of the CNSs within the building material and improve the linkage between CNSs and cement matrix.

1.1   Properties and surface modification of carbon nanotubes

Iijima was the first who reported about the occurrence of carbon nanotubes (CNTs) in 1991 [5]. Since then the unique physical properties of these nanostructures had been investigated intensely [6].
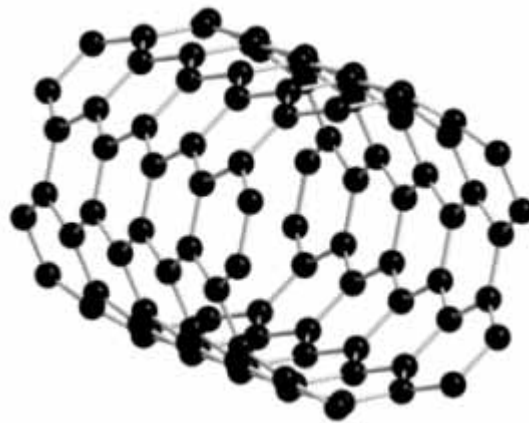
Figure 1:   Exemplary structure for a SWNTs

CNTs can be imagined as graphite modifications with one or more graphite layers rolled into a tube (Figures 1). The resulting tubes are called single-walled nanotubes (SWNTs) consisting of
only one rolled graphite sheet (Figure 1) or multi-walled nanotubes (MWNTs) with multiple rolled sheets (Figure 2). CNSs exhibit a large variety of properties depending on their structure. Their high tensile strength of ~30 GPa [7] and their high aspect ratio are making them very interesting as ideal reinforcing fibres for developing new composite materials.

Figure 2:   TEM-image of MWNTs, SUN Nanotech Co Ltd. [8]

The used MWNTs were purchased from Sun Nanotech Co Ltd. The MWNTs were grown by the CVD method having a purity of >80%. Their diameter is between 10 and 30 nm and their length between 1 and 10 µm.

A bundling of the individual CNTs is caused by Van-der-Waals-Forces. Figure 3 shows an

Figure 3:   Bundle of CNTs imaged by AFM on HOPG

AFM-image of such a CNTs-bundle. To get a homogenous composite these bundles must be broken into the individual nanostructures. This can be done by sonification of the CNTs within the mixing water. The superplasticizer (SP) should wrap around the dispersed CNTs thus preventing a bundling after the sonification is stopped.

After Hirsch there are four different possibilities of modifying the CNTs surface. An exohedral modification can be reached by defect group functionalization, covalent sidewall functionalization, non-covalent functionalization by tensides and non-covalent functionalization by polymers [9]. A defect group functionalization can be obtained by oxidizing the CNTs [10]. The additionally generated surface defects are decorated by carboxylic (-COOH), carbonyl (-C=O) and hydroxyl (-COH) groups with approximate proportions of 4:2:1 [11]. As a result of the surface modifications a better dispersion of the oxidized CNTs within the mixing water is possible.

1.2   Experimental

All prisms were made from the same main compounds CEM I 52.5 R, sand and silica fume. A polycarboxylate based SP was used to get a better workability at the low water to cement ratio of 0.22 and for dispersing the MWNTs. Different amounts of untreated or modified MWNTs were dispersed in the mixing water using sonification for 15 minutes. The SP was then added and the mixture sonificated in addition for 2 minutes. The pastes were moulded into prism-shaped forms (8 mm x 8 mm x 30 mm) and compacted by vibration. Due to the bad workability of the pastes including the oxidized MWNTs these samples were compacted by applying a pressure of 125 MPa for 45 minutes. The prisms were demoulded after 1 day of storage at a relative humidity of >90% and 20°C. The mechanical strength tests took place after 7 d, 14 d and 28 d of water curing at 20°C.

To enhance the surface defect concentration of the MWNTs by oxidation 500 mg were refluxed in 160 ml of nitric or sulphuric acid for 2 h. Than the acids were distilled off and the MWNTs were repeatedly washed with distilled water and centrifuged at 3000 rpm until a pH-value of 7 had been reached.

1.3   Results

First the influence of different amounts of untreated MWNTs covered by SP on the flexural and compressive strength were observed. The 7-day strength tests are showing an increase of the compressive strength if 0.5 wt % referred to the cement amount had been used (Figure 4). The 0.5 wt % sample showed a compressive strength increase by 8% after 7 d and by 12% after 14 d. The addition of 1.0 wt % of MWNTs made an increase of the water to cement ratio from w/c = 0.22 to 0.26 necessary. Otherwise a processing of the pastes having this composition was impossible. As a result of the higher water to cement ratio the 7-day compressive strength test results of these samples were lower compared to the prior ones.
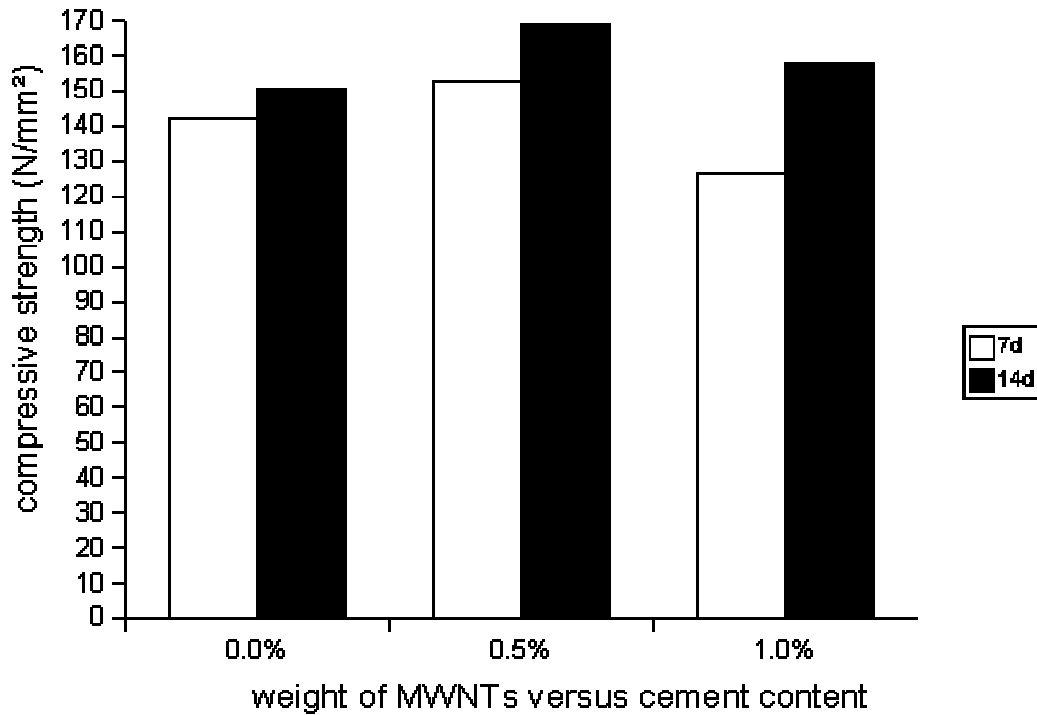
Figure 4:   Compressive strength with varying MWNTs content

The high improvement in compressive strength of the 1.0 wt % samples after 14 d is pointing to a slower hydration rate compared to the samples with lower and 0.0 wt % MWNTs content. Here an improvement of 5% compared to the 0.0 wt % sample could be observed.

Figure 5 is showing how the MWNTs amount is influencing the 7-day compressive strength of pastes at a water to cement ratio of 0.39. This was the minimum ratio for processing the pastes without compacting them by pressure. The samples contained 0.0 wt %, 0.5 wt %, 1.0 wt %, 2.5 wt % and 5.0 wt % of MWNTs with respect to the cement amount.

After 7 d the change of the MWNTs amount seems to have nearly no influence on the compressive strength of the samples (Figure 5). Only the samples containing 2.5 wt % MWNTs showed a decrease in the compressive strength of 19 % compared to the samples containing 0.0 wt % MWNTs. Further experiments have to show whether this was a preparation problem or if there is a reproducible decrease in the compressive strength at this MWNTs amount.
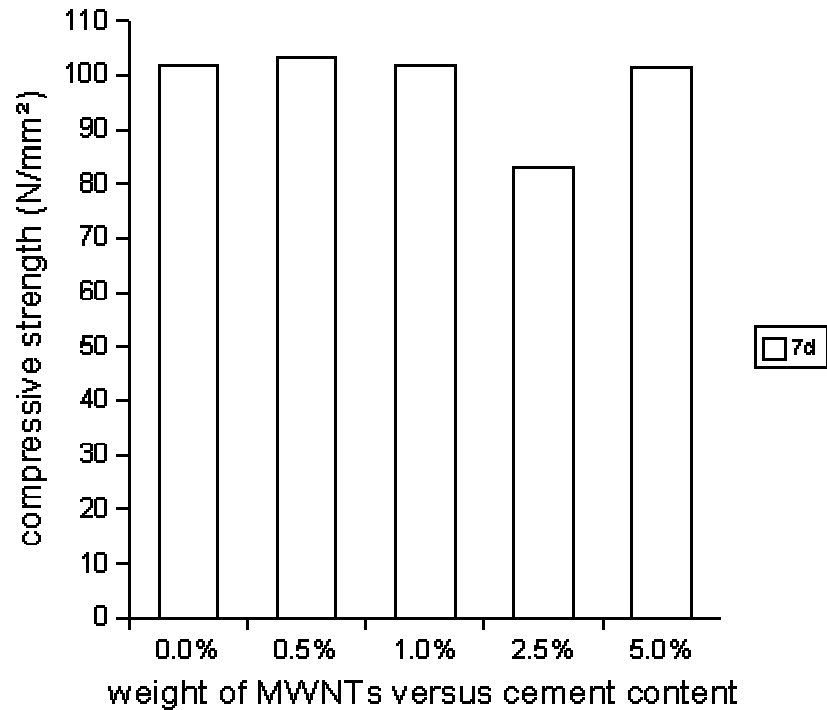
Figure 5:   Compressive strength with varying MWNTs content, w/c = 0.39

The results of the compressive strength tests with SP-wrapped and oxidized, SP-wrapped MWNTs are shown in figure 6. These samples were containing 0.5 wt % of differently
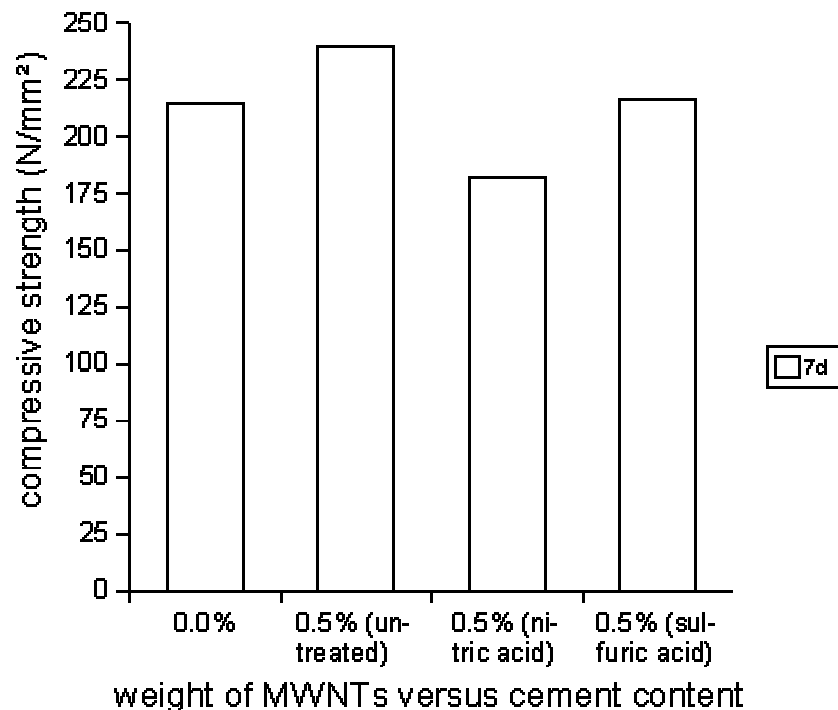
Figure 6:   Compressive strength with untreated and oxidized MWNTs, w/c =0.22

modified MWNTs referred to the cement weight and were compared to a MWNTs-free sample. These samples were moulded into a special prism-shaped form and compacted

applying a pressure of 125 MPa for 45 minutes. Afterwards these samples were handled like the samples mentioned above.

An improvement of 12 % in the compressive strength of the samples with the untreated MWNTs could be achieved. The samples containing the MWNTs oxidized in nitric acid showed a very bad workability which is, even though the samples were compacted by applying a pressure of 125 MPa, leading to a loss in the mechanical strength of the composite. The samples with the MWNTs oxidized in sulphuric acid showed no in- or decrease in their compressive strength compared to the samples without MWNTs.

1.4   Conclusions

We showed some first results about the incorporation of carbon nanostructures into ultra-high performance concrete. The compressive strength could be increased by 7% after 7 d to 153 MPa and 12% after 14 d to 169 MPa if 0.5 wt % of superplasticizer wrapped multi-walled nanotubes had been used (figure 4). At higher water to cement ratios (w/c = 0.39) there seems to be no effect on the 7-day compressive strength of the samples by the incorporation of multi-walled nanotubes (figure 5). The 7-day compressive strength of the pressure-compacted samples increased by 12% to 239 MPa by the usage of polymer wrapped multi-walled nanotubes (figure 6). The 14-day compressive strength tests (figure 4) are pointing to a retardation of cement hydration. This effect is to be proven by differential heat-flow calorimetry and by ultrasonic experiments in future works.

At higher carbon nanotube-concentrations the workability of the pastes was getting worse. This is mainly due to the higher water-demand of the pastes because of the carbon nanotube's high specific surface and additionally due to the wrapping of the carbon nanotubes by the superplasticizer. Thus a higher concentration of superplasticizer is needed to decrease the water-demands of these cement pastes. The workability grew even worse by the use of oxidized multi-walled nanotubes.

To ensure further improvements in the mechanical properties of carbon nanotube reinforced UHPC ongoing experiments exploring the influence on the micro- and nanostructure of these composites have to be done. New functionalized carbon nanotubes with a better linkage between them and the cement matrix and also providing a better handling of the cement pastes could lead to high performance cement based nano-composites.

2   References

[1] Makar, J.M.; Beaudoin, J.J.: Carbon Nanotubes And Their Application In The Construction Industry. In: Proceedings of the 1st International Symposium on Nanotechnologie in Construction, p. 246-258, Paisley 2003.

[2] Campillo, I.; Dolado, J.S.; Porro, A.: High-Performance Nanostructured Materials For Construction. In: Proceedings of the 1st International Symposium on Nanotechnologie in Construction, p. 110-121, Paisley 2003.

[3]   O´Connell, M.J.; Boul, P.; Ericson, L.M.; et al.: Reversible water-solubilization of single-walled carbon nanotubes by polymer wrapping. In: Chemical Physics Letters 342, p. 265-271, 2001.

[4]   Ebbesen, T.W.; Hiura, H.; Bisher, M.E.; Treacy, M.M.J.; Shreeve-Keyer, J.L.; Haushalter, R.C.: Decoration of Carbon Nanotubes. In: Advanced Materials, 8, p. 155-157, 1996.

[5]   Iijima, S.: Helical microtubules of graphitic carbon. In: Nature, 345, p. 56-58, 1991.

[6]   Ajayan, P.M.; Ebbesen, T.W.: Nanometre-size tubes of carbon. In: Reports on Progress in Physics, 60, p. 1025-1062, 1997.

[7]   Yu, M.-F.; Files, B.S.; Arepalli, S.; Ruoff, R.S.: Tensile Loading of Ropes of Single Wall Carbon Nanotubes and their Mechanical Properties. In: Physical Review Letters, 84, p. 5552-5555, 2000.

[8]   Sun Nano Co Ltd., http://www.sunnano.com.

[9]   Hirsch, A.: Funktionalisierung von einwandigen Kohlenstoffnanoröhren. In: Angewandte Chemie, 114, p. 1933-1939, 2002.

[10] Satishkumar, B.C.; Govindaraj, A.; Mofokeng, J.; Subbanna, G.N.; Rao,.C.N.R.: Novel experiments with carbon nanotubes: opening, filling, closing and functionalising nanotubes. In: J. Phys. B, 29, p. 4925-4934, 1996.

[11] Ebbesen, T.W.; Hiura, H.; Bisher, M.E.; Treacy, M.M.J.; Shreeve-Keyer, J.L.; Haushalter, R.C.: Decoration of carbon Nanotubes. In: Advanced Materials, 8, p. 155-157, 1996.

Part 6:

Fillers and Aggregates

J. Ma
Dipl.-Ing.
University of Leipzig
Leipzig, Germany

M. Orgass
Dipl.-Ing.
University of Leipzig; MFPA Leipzig
Leipzig, Germany

F. Dehn
Dr.-Ing.
University of Leipzig; MFPA Leipzig
Leipzig, Germany

Dr. Detlef Schmidt
Bilfinger+Berger AG
Mannheim, Germany

N. V. Tue
Prof. Dr.-Ing. habil.
University of Leipzig; König, Heunisch Leipzig
Leipzig, Germany

Comparative Investigations on Ultra-High Performance Concrete with and without Coarse Aggregates

Abstract

In the present paper UHPC was produced with crushed basalt with the particle size from 2 to 5 mm. The compressive strength has reached the same magnitude as reactive powder concrete (RPC) in which the maximal aggregate size is smaller than 1.0 mm. The use of the coarse aggregates led not only to the decrease in cementitious paste volume fraction, but also to some changes in mixing process and in mechanical properties. UHPC containing coarse aggregate was easier to be fluidised and homogenized. The mixing time can be shorter than that for RPC. The both tested UHPC exhibited a similar behaviour under compressive stresses, except somewhat different modulus of elasticity and strain at peak stress, which related to the stiffness of the used aggregates. The lower paste volume fraction and the hindrance of the stiffer basalt split resulted in a lower autogenous shrinkage of UHPC containing coarse aggregates.

Keywords: *ultrahigh performance concrete, reactive powder concrete, coarse aggregate*

1   Introduction

Ultra-high performance concrete (UHPC) is one of the latest developing in concrete technology. Depending on its composition and the treating temperature its compressive strength ranges between 150 N/mm² and up to 800 N/mm² [1]. Some basic principles improving the properties of concrete were suggested in [1], e. g. the optimisation of the granular skeleton, the densification of the cementitious matrix through lowing water to binder ratio and post set heat treatment, as well as the elimination of coarse aggregates. In [1] it was emphasized that the difference in thermal and mechanical properties between

aggregate and cementitious matrix is one of the main reasons for the micro cracking in the interface zone, and that the length of the micro cracks is proportional with the grain size of aggregates. Therefore, the grain size of aggregate should be limited to 0.6 mm. The ultrahigh performance concrete produced in such a way is called as reactive powder concrete (RPC). However, the smaller the aggregates, the larger is the aggregate surface to be enveloped with cementitious paste. This leads to a high paste volume in reactive powder concrete to get a sufficient flowing ability for manufacture. The cement content ranges often from 700 up to 1000 kg/m³ [2, 3], which indicates some disadvantages in concrete properties, e.g. high autogenous shrinkage.

Experiments in this paper showed that concrete with coarse aggregates can also reach the compressive strength of reactive powder concrete. The behaviour of UHPC with and without coarse aggregates during mixing process and the concrete properties in fresh and hardened state were comparatively investigated.

2   Materials and concrete compositions

In both UHPCs the powder was composed of ordinary Portland cement CEM I 42,5 R, white silica fume and quartz powder. The fineness of this quartz powder is between the silica fume and the cement and was used as a micro filler to optimise the packing density of the powder mixture. According to the suggestions in [1] coarse aggregate was eliminated in UHPC1 (Table 1). Only quartz sand in the range of 0.3 to 0.8 mm was used as aggregate. So UHPC1 is comparable to a RPC. In UHPC2 basalt splits with particles from 2 to 5 mm were used as coarse aggregate, and the same sand in UHPC1 as fine aggregate. Superplasticizer (SP) on the basis of polycarboxylateether ensured the both UHPC a high fluid ability as self-compacting concrete.

Table 1:   Proportion of self-compacting UHPC with and without coarse aggregates

Materials	UHPC1 (RPC)	UHPC2
Cement CEM I 42.5 R (c)	1.0	1.0
Water to cement ratio (w/c)	0.268	0.302
Water to binder ratio (w/b)	0.206	0.232
Volumetric water to powder ratio	0.431	0.487
Quartz sand (0.3-0.8 mm)	1.532	0.811
Basalt split (2-5 mm)	0.0	1.830
Paste volume fraction	60%	50%
$f_{c,cyl.100*200}$ (N/mm², 28d/20°C)	150-160	150-165
$f_{c,cyl.100*200}$ (N/mm², 90d/20°C)	165-180	165-175

The volume fraction of the cementitious paste (water + powder) in both UHPCs is higher than that in conventional HPC and SCC, as shown in Fig. 1. This can be reasoned by the fact that the superplasticizer content in the UHPC was almost the saturation dosage. A higher superplasticizer dosage could not significantly increase the paste fluidity. In this case the concrete consistency depends mainly on the paste volume fraction and the grain size of the

aggregates. In UHPC1 the aggregate surface to be enveloped with cementitious paste was so large that the paste volume fraction had to be increased up to 60% to get the sufficient fluid ability, while it was 50% in UHPC2 containing coarse aggregates (Fig. 1).
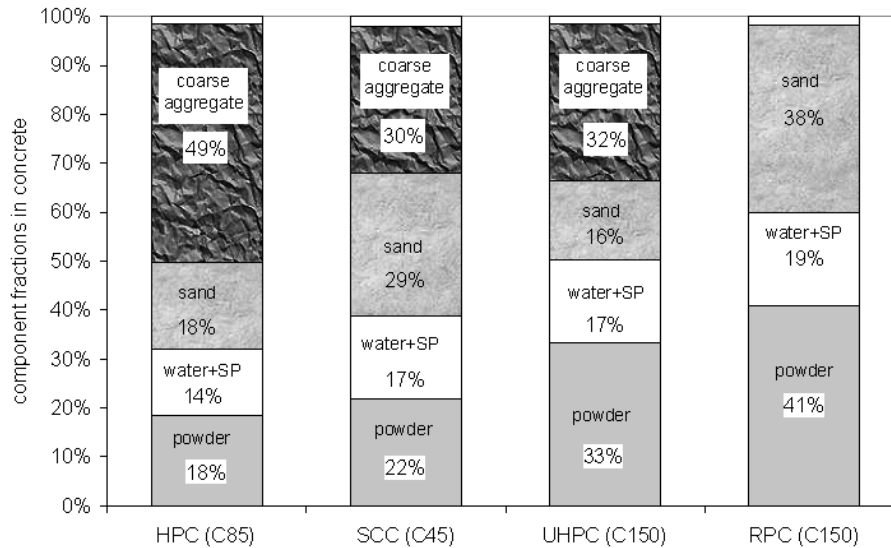
Fig. 1:   Component volume fractions in HPC, SCC and UHPC

3   UHPC in mixing process

In the mixing process all particles of solid components are repositioned through relative movement and rotation. Smaller particles fill progressively the voids between coarser particles. Mixing water fills the remained voids between all solid particles and facilitates their movement as a lubricant. The dispersing process of the particles and the feature of the power consumption during mixing are shown in Fig. 2 (left). The time at which the power-time curve reaches the asymptote is defined as stabilisation time [4]. Generally it is also the mixing time.
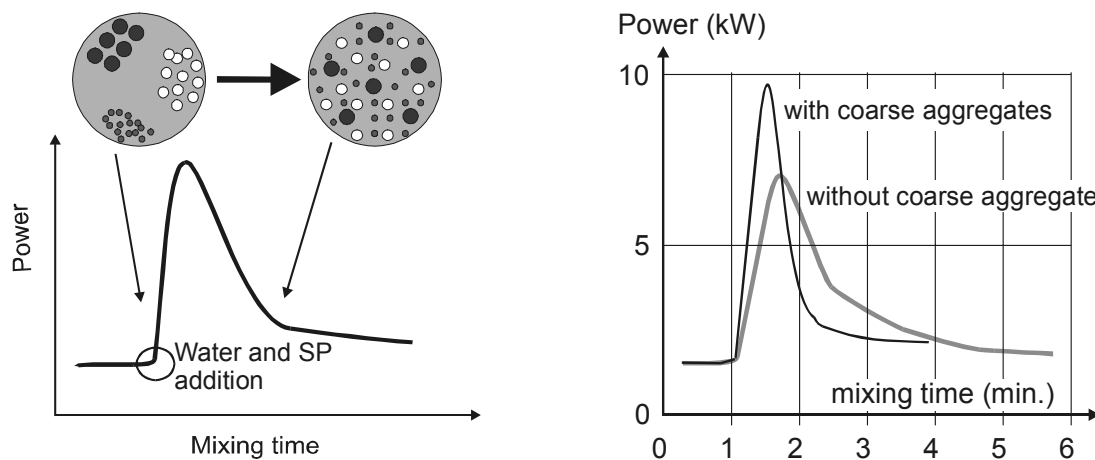
Fig. 2:   Power consumption during mixing process

Fig. 2 (right) shows the power consumption of both UHPC mixtures produced in a forced mixer R08 at Maschinenfabrik Gustav Eirich GmbH & KG. The power consumption peak for UHPC2 containing coarse aggregates is high and narrow, while for UHPC1 without coarse aggregate low and wide. The stabilisation time for UHPC2 was approx 2 minutes. The total time from dry mixing to discharging was approx 3.5 minutes. For UHPC1 the stabilisation time and the total time was about 3,5 and 5.5 minutes, respectively.

The power consumption feature and the different mixing time can be attributed to the friction between solid particles. In fact, the friction depends on the particle surface feature and the thickness of the water layer enveloping the particles. The thicker the water layer, the lower the friction. In the first seconds after water addition some mixing water was enclosed in agglomerates of fine particles (cement, silica fume and quartz powder). This part of water did not contribute to fluidise the concrete. After these agglomerates had been destroyed by the dispersing effect of the superplasticizer and the friction between solid particles, the enclosed water was released and thickened the water layer around solid particles. The concrete became more and more fluid, leading to the decrease in power consumption. In UHPC1 without coarse aggregate the friction between solid particles is obviously reduced. More time is needed to destroy the agglomerates.

The reduced friction in UHPC1 leads not only to a slower fluidisation, but also to a slower homogenisation of the whole concrete mixture. After 4 minutes mixing in a laboratory forced pan mixer there were still some lumps (10-15 mm) swimming in the fluid concrete. More 3 minutes mixing was needed to destroy these lumps. In the case of UHPC2 such lumps thoroughly disappeared after 2 minutes mixing.

4   The properties of fresh ultra high performance concrete

Some properties of fresh UHPC were investigated with the experimental apparatus, which are usually used to determine the properties of self-compacting concrete. Details of these apparatus are described in [5].

From table 2 it could be seen that both UHPCs satisfied the demands on self-compacting concrete. Compared with conventional SCC no principle difference has been observed. Due to the very low w/b-ratio and the very high fineness of silica fume and quartz powder the viscosity of the UHPC is obviously higher than that of conventional SCC. The air content is therefore somewhat higher than in conventional SCC.

Table 2:   Properties of fresh self-compacting UHPC

	Without coarse aggregate	With coarse aggregate
Slump flow (mm)	790	765
t_{500} (sec.)	4.0	7.0
V-funnel test (sec.)	8.6	15.6
L-box-test (H_1/H_2)	0.9	0.92
U-box-test (Δh)	0	0
Air content	4.0-5.5%	2.5-3.5%

5 Mechanical properties of hardened concrete

The grain size of the aggregate has no significant affect on the achievable compressive strength. The both non-fibre reinforced self-compacting UHPC presented here have the cylinder strength in the range of 150-165 N/mm² after 28d water curing at about 20°C and approx 190 N/mm² after heat treatment at 90°C, respectively. In [10] UHPC containing coarse aggregates with a maximal grain size of 8 mm showed a comparable strength. Upper limits of grain size of coarse aggregate used for UHPC should be studied in future work.

The stress-strain curve of the both non-fibre reinforced UHPC subjected to compressive stress showed almost a same characteristics. Due to the perfect interface zone between aggregate and cementitious matrix the stress-strain curve keeps almost linear up to the stress level of about 80% peak stress. Compared with high strength concrete UHPCs exhibit higher brittleness. At peak stress they failed explosively. A descending branch could not be observed. The only obvious difference is the strain at peak stress. It is about 3.400 µm/m for UHPC2 and 4.400 µm/m for UHPC1, respectively. This can be related to the higher stiffness of UHPC2.

In principle the elastic modulus of UHPC is higher than that of conventional concrete with a same type of aggregates. Its magnitude depends on the type of aggregate and the paste volume fraction. For instance, UHPC without coarse aggregate contains normally quartz sand smaller than 1 mm. Its modulus of elasticity is about 48.000 N/mm², lower than UHPC containing basalt split (ca. 58.000 N/mm²). The UHPC composed of bauxit split can even reach the value over 70.000 N/mm² [6].

The relationship between modulus of elasticity and compressive strength is similar as that supposed in CEB-FIP Model Code 1990 [11], regardless of the grain size. However, due to the high paste volume the modulus of elasticity of UHPC is about 12% lower than that predicted with the equation in CEB-FIP Model Code 1990 (Fig. 3).
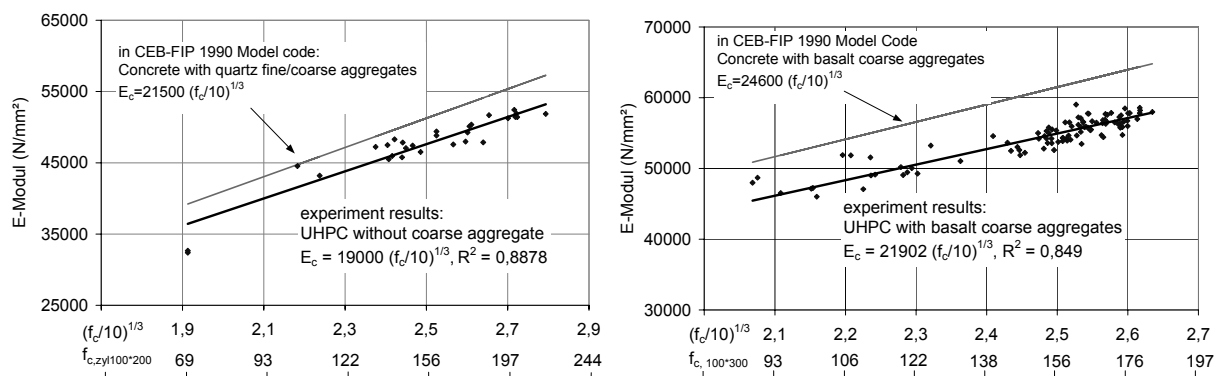
Fig. 3: Relationship between modulus of elasticity and compressive strength of UHPC

6 The autogenous shrinkage of ultra high performance concrete

The autogenous shrinkage is the macroscopic volume reduction of unloaded cementitious materials when cement hydrates after initial setting. It is the combination of chemical

shrinkage and volumetric contraction caused by self-desiccation under sealed isothermal conditions [7]. The autogenous shrinkage of the both investigated UHPC were tested on specimens of 150×150×700 mm³. The total deformation vs. time curves are shown in Fig. 4, in which the total deformation is the sum of autogenous shrinkage and thermal dilation caused by temperature rise during cement hydration. The autogenous shrinkage was calculated by subtracting the thermal dilation from the measured total deformation. Theoretically autogenous shrinkage occurs when concrete begin to set. However, the thermal dilation coefficient of concrete at very early age is not a certain value. It is much higher than that of hardened concrete and decreases rapidly with concrete age. The experiments in [8, 9] indicated that, it begins to become constant approximately at the time of the highest temperature in concrete. So the autogenous shrinkages of the both UHPC in this paper were considered after the highest temperature and denoted in Fig. 5.

The experimented UHPC exhibited quickly developing and very high autogenous shrinkages. This can be resulted from the accelerated self-desiccation due to the very low water to cement ratio and the very fine capillary pores, the intensified volume contraction caused by puzzolanic reaction at high silica fume content, as well as the high paste volume in UHPC.

A comparison of the two UHPC shows that three weeks after casting the autogenous shrinkage of the UHPC2 containing basalt split as coarse aggregate is about 40% lower than that without coarse aggregate. Except for the slightly higher w/c and the lower cementitious paste volume, which are advantageous for the reduction of autogenous shrinkage, the higher modulus of elasticity of UHPC2 can also make a certain contribution to decrease the autogenous shrinkage.
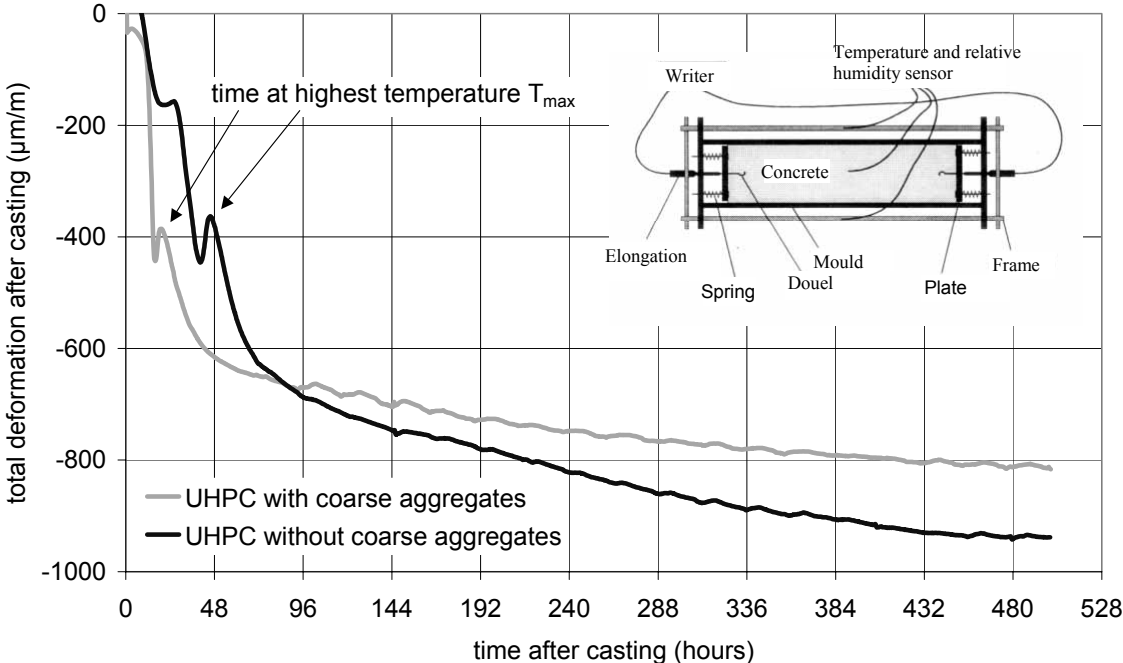
Fig. 4:   Total deformation of UHPC with and without coarse aggregates
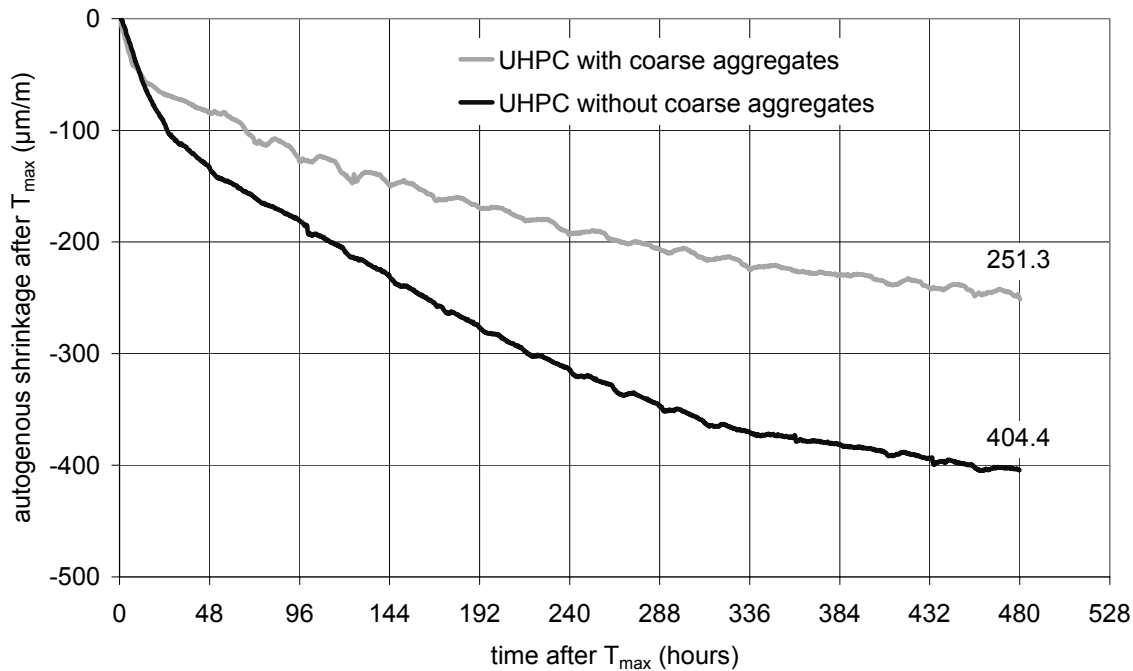
Fig. 5   Autogenous shrinkage of UHPC with and without coarse aggregate

The high autogenous shrinkage and its quickly developing indicate a high risk of micro cracking at early ages, if a construction element made of UHPC is restrained. From this point of view, the restrained UHPC without coarse aggregate is more sensitive to cracking than UHPC containing coarse aggregate.

7   Conclusions

In this paper some comparative investigations on two UHPC were carried out. The UHPC containing coarse aggregates differs from the classic UHPC without coarse aggregate (RPC) mainly in the concrete proportion, mixing time, and in the autogenous shrinkage. The cementitious paste volume fraction in UHPC containing basalt split (2-5 mm) as coarse aggregate is about 20% lower than that in RPC possessing similar compressive strength and fluid ability. The cement content in UHPC can be then lower than 550 kg/m³, while in RPC it ranges often between 700 kg/m³ and 1000 kg/m³. During mixing the UHPC containing coarse aggregate is easier to be fluidised and homogenized. A shorter mixing time can be expected. Both UHPC showed a high and quickly developing autogenous shrinkage. In UHPC containing coarse aggregates the lower cementitious paste volume and the stiffer basalt split result in a noticeable decrease in autogenous shrinkage. The autogenous shrinkage of UHPC containing coarse aggregates is about 60% of RPC experimented in this paper.

The both non-fibre reinforced UHPC in hardened state showed no distinct difference in mechanical properties under compressive stress, except the higher modulus of elasticity and lower strains at peak stress for UHPC containing basalt split, which can be attributed to the higher stiffness of the basalt split used.

8 Acknowledgements

9 References

[1] Richard, P.; Cheyrezy, M.: composition of reactive powder concrete. In: Cement and Concrete Research 25, No. 7, S. 1501-1511, 1995

[2] Olivier Bonneau, Mohamed Lachemi, Éric Dallaire et al.: Mechanical properties and durability of two industrial reactive powder concretes. In: ACI Materials Journal, July-August 1997, S. 286-290

[3] J. Dugat, N. Roux, G: Bernier: Mechanical properties of reactive powder concretes. In: Materials and Structures, Vol. 29, S. 233-240, May 1996

[4] David Chopin, F. de Larrard, Bogdan Cazacliu: Why do HPC and SCC require a longer mixing time? In: Cement and Concrete Research 2004, article in press,

[5] Peter Grübl, Christoph Lemer: Anforderung an die Frischbetoneigenschaften von SVB. In: Selbstverdichtender Beton, Innovationen im Bauwesen, Beiträge aus Praxis und Wissensschaft, Bauwerk Berlin, 2001

[6] Frank Mathiesen, Morten Mork, Jesper Tychsen: General Jacket design and reassessment conditions, Background document on Densit Grout Materials, Maersk Olie og Gas AS, January 2000

[7] Ei-ichi Tazawa, Ryoichi Sato, et al: Work of JCI committee on autogenous shrinkage. In: Shrinkage of concrete. Proceedings of the International RILEM workshop, Paris, France, 16-17 October 2000, Edited by V. Baroghel-Bouny and P. C. Aïtcin

[8] Ahmed Loukili, David Chopin et al.: A new approach to determine autogenous shrinkage of mortar at an early age considering temperature history. In: Cement and Concrete Research 30, S. 915-922, 2000.

[9] H. Kada, M. Lachemi, N. Petrov, O. Bonneau, P. C. Aïtcin: Determination of the coefficient of thermal expansion of high performance concrete from initial setting. In: Materials and Structures, Vol. 35, S. 35-41, January 2002

[10] Roland Bornemann, Michael Schmidt, Ekkehard Fehling, Bernhard Middendorf: Ultra-Hochleistungsbeton UHPC. In: Beton- und Stahlbetonbau, Heft 7, S. 458-467, 2001

[11] Comité Euro-International du Béton : CEB-FIP Model Code 1990, Design Code, 1993

Patrick ROUGEAU
Head of the Material Division
CERIB (Study and Research Centre for the
French Concrete Industry)
Epernon, France

Béatrice BORYS
CERIB (Study and Research Centre for the
French Concrete Industry), Epernon, France
Now at COFRAC (French Committee for
Accreditation)
Paris, France

Ultra High Performance Concrete with ultrafine particles other than silica fume

Summary

Several ultrafines were used to produce Very High Performance Concrete (VHPC) and Ultra High Performance Concrete (UHPC). The ultrafine powders used were metakaolin (MK), pulverized fly ash (PFA), limestone microfiller (LM), siliceous microfiller (SM) and micronized phonolith (PH). This paper deals with the performances obtained with these ultrafines: compressive and tensile strength, porosity, water absorption and resistance to carbonation. The results show that other ultrafines than silica fume can be used in VHPC and UHPC.

Keywords: *UHPC, ultrafine, silica fume, metakaolin, pulverized fly ash, limestone microfiller, siliceous microfiller, phonolith*

1   Introduction

Very High Performance Concrete (80 to 150 MPa) and Ultra High Performance Concrete (up to 150 MPa) present a great interest for precast concrete industry. They allow new designs for the precast products which cannot be done with usual concrete. By using these new materials, it is possible to produce lighter products with thinner section. VHPC and UHPC are made using a very low mixing water amount and large quantities of superplasticizer and ultrafine powders. Ultrafine content is typically between 10 to 15 % of the cement content for VHPC and 20 to 30% for UHPC. Nowadays, most of these concretes are made with silica fume. It is well known that silica fume improves the particle packing density of cementitious matrices, its mechanical properties and durability. However, silica fume has some disadvantages: the available quantity is limited, the variability of carbon content can decrease the fluidity of VHPC and UHPC, the concrete surface colour obtained with grey silica fume is dark. For these reasons it is necessary to enlarge the choice of ultrafine. Other ultrafines are available on the market. Many studies have been done on the use of ultrafine particles for high performance concrete [1 to 6]. It has been showed that pulverized granulated blast furnace slag and pulverized fly ash can also be used to make very high performance concrete [7].

The objective of the study is to determine the potential interest of several ultrafines: metakaolin, pulverized fly ash, limestone microfiller, siliceous microfiller and micronized phonolith for VHPC and UHPC. Properties of VHPC and UHPC with these ultrafines are compared to silica fume concretes. The influence of ultrafine on rheological properties in fresh state, pore network, mechanical properties, water absorption and carbonation was studied.

2   Characteristics of ultrafines

The characteristics of the ultrafine powders used in this study are shown in Table 1 and Table 2. Silica fume containing 95% SiO_2 and having a BET (Brunauer, Emmette and Teller – a nitrogen adsorption method to determine specific surface area) specific surface area of 18.6 m^2/g was used. The pozzolanic activity of the silica fume is 688 mg CaO/g sample.

Pulverized metakaolin is made by thermal treatment of natural clay. The crystalline clay minerals are dehydroxylated. Metakaolin powder has the higher pozzolanic activity (756 mg CaO/g sample). The calcining temperature of clay affects the pozzolanic reactivity of the resulting product. The clay is in its most reactive state when the calcining temperature leads to loss of hydoxyls and results in a collapsed and disarranged structure [8]. The calcining temperature producing the active state is usually in the range 600-800°C. Metakaolins are well known for their benefits to concrete properties: early strength enhancement, refinement of the pore structure, improvement of the concrete resistance to aggressive solutions, reducing alkali silica reaction [8, 9].

Pulverized phonolith is made from a volcanic rock which contains about 45% of zeolite. Like metakaolin, silica fume and pulverised fly ash, micronized phonolith has pozzolanic properties (412 mg CaO/g sample). Originally the term pozzolana was associated with naturally formed volcanic ashes and calcined earths, which react with lime at ambient temperatures in the presence of water. In recent times the term has been extend to cover all siliceous/aluminous materials which, in finely divided form and in the presence of water, will react chemically with calcium oxide to form compounds that possess cementitious properties [8].

Fly ashes are man-made, finely divided amorphous silicas and aluminas. The fly ash used in this study has a low calcium content (Table 2). The pulverized fly ash particles have the higher average diameter (11.7 µm).

Limestone microfiller has a low average diameter (1.6 µm). This powder contains 99.3% of calcite. The tint of the limestone microfiller is particularly clear. This is also the case for siliceous microfiller. The siliceous microfiller used in these study was a mix between micronized natural quartz sand and synthetic silica fume. One can note that its specific surface area is higher than those of silica fume: 25 m^2/g instead of 18.6 m^2/g for silica fume.

Table 1:   Characteristics of ultrafines

Ultrafine		Silica fume	Metakaolin	Phonolith	Pulverized fly ash	Limestone microfiller	Siliceous microfiller
Particle size	D_{50} µm	1.0	6.7	3.3	11.7	1.6	nd*
	D_{90} µm	8.4	16.2	8.1	50.1	4.3	nd*
Pozzolanic activity (mg CaO/g sample)		688	756	412	314	0	nd*
Specific area (m^2/g)		18.6	6.8	9.4	7.0	6.0	25.0
Density (kg/m^3)		2 200	2 200	2 600	2 690	2 650	2 450
Colour		Grey	White	Grey	Beige	White	White
Disponibility** (t/year)		40 à 50 000	10 000	> 100 000	> 100 000	> 100 000	100 to 1000

* nd : no determinate   ** in France

Table 2:   Chemical compositions (%) of ultrafines

Oxyde	Silica fume	Metakaolin	Phonolith	Pulverized fly ash	Limestone microfiller	Siliceous microfiller
Al_2O_3	--	40	18	19.4	--	--
SiO_2	95	55	49	50.8	--	> 99
Fe_2O_3	--	1.2	4	6.3	0.03	--
MgO	--	< 0.3	1	2.4	0.9	--
CaO	0.5	< 0.3	7	5.6	54.9	--
$Na_2O + K_2O$	0.6	1.9	12	4.9	--	--
SO_3	--	--	--	3.5	--	--
TiO_2, MnO, P_2O_5	--	0.4	< 1	1.3	--	--
Ignition loss	> 2.5	< 1	8	5.8	43.7	--

Figure 1 shows the particle size distributions of ultrafine. Silica fume contains the higher proportion of particle for which diameter is lower than 1 µm. It can be noted that limestone microfiller, phonolith and metakaolin have narrowed particle size distribution. For these ultrafines, most of the particle are over 0.1 µm and under 12 µm. The particle size distributions of by-products, silica fume and pulverized fly ash, are larger.

Figure 1 : Particle size distribution of ultrafines
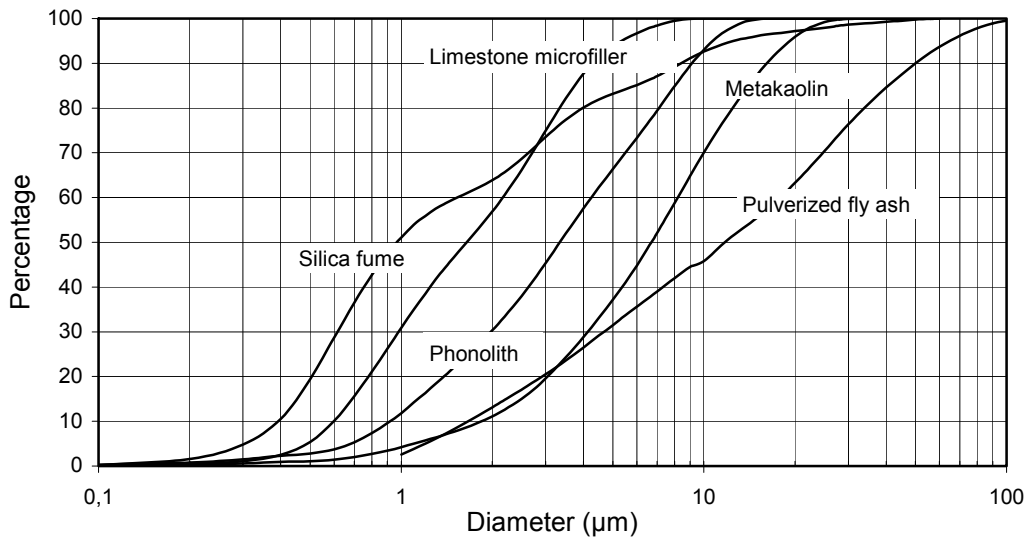
The particle morphologies were characterized using a scanning electron microscope. Silica fume is characterized by numerous agglomerates which size is between 40 to 50 μm. The shape of elementary particles is spherical (Figure 2a). The limestone microfiller has a regular particle size distribution with little or none particle above 10 μm. The grains are more angular. Limestone microfiller has low particle packing (Figure 2b). The particles of metakaolin have a typical structure like sheet (Figure 2c). The phonolith grains appear with different facies: spheres, prisms, and other angular shapes. The pulverized fly ash shows pseudo-spherical particles and sometimes structures like sheet.

Figure 2 : Scanning electron microscopic observations of the ultrafine particles
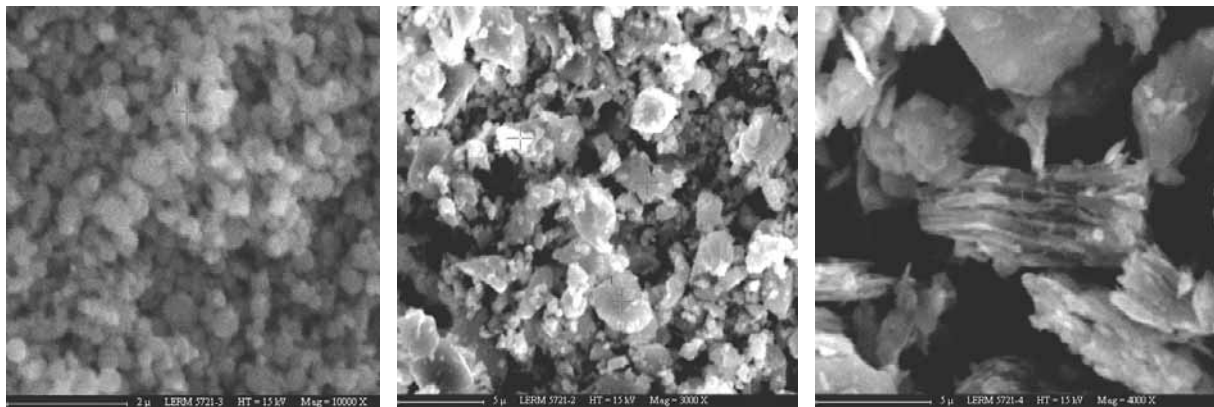
a) Silica fume
spheres

b) Limestone microfiller
particles

c) Typical structure
of metakaolin

3 Materials and methods

3.1 Design mix of concretes

Concrete mixture proportions are given in Tables 3 and 4. The VHPC and UHPC were made respectively with a dosage of ultrafine equal to eleven and twenty percent by weight of cement. For each kind of concrete, the content of cement and ultrafine was maintained constant. The dosage of superplasticizer was adjusted for each mix in order to reach the same fluidity: a slump around 21 cm for the VHPC and a value for the flow test around 20 cm for the UHPC. One can note that the water content was also adjusted in the case of UHPC to achieve the required fluidity.

The following steps of the mixing procedure used for UHPC were :
- mixing of dry constituents for 2 min
- progressive incorporation of water containing the superplasticizer with phosphonate, mixing for 4 min
- addition of the second superplasticizer (polyacrylate) and mixing for 4 min.

The concrete were casted into stainless molds and immediately stored in room at 20°C. The specimens were demolded after 24 hours and then placed in fog room until tests.

Table 3: Concrete mixture proportions of Very High Performance Concretes

Ultrafine	Silica fume	Metakaolin	Phonolith	Pulve-rized fly ash	Lime-stone micro-filler	Siliceous micro-filler
Cement CEM I 52,5 PM ES	405	405	405	405	405	405
Ultrafine	45	45	45	45	45	45
Siliceous sand 0/5	788	788	801	801	801	801
Siliceous gravel 2/6 siliceux	263	263	267	267	267	267
Siliceous gravel 5/12 siliceux	700	700	712	712	712	712
Superplasticizer* (phosphonate)	3.04	2.73	2.73	2.62	2.13	2.73
Total water	120	121	122	122	121	122
Slump test (cm)	21	22	21	21	21	21

* dry content

Table 4: Concrete mixture proportions of Ultra High Performance Concretes

Ultrafine	Silica fume	Metaka olin	Phonolit h	Pulve-rized fly ash	Lime-stone micro-filler	Siliceou s micro-filler
Cement CEM I 52,5 PM ES	903	903	903	903	903	903
Ultrafine	181	181	181	181	181	181
Siliceous sand 0.2/0.5	767	767	767	767	767	767
Siliceous filler	271	271	271	271	271	271
Metallic fibers ($\varnothing$ 150 µm, L = 13 mm)	79	79	79	79	79	79
Superplasticizer* (phosphonate)	7.04	12.46	7.04	13.84	7.04	10.59
Superplasticizer* (polyacrylate)	1.01	4.88	2.32	4.88	1.14	4.87
Total water	174	197	185	203	184	189
Flow table test (cm)	21	17	23	21	22	22

* dry content

3.2 Test methods of physico-chemical and mechanical properties of concretes

Compressive strengths of concrete were determined on 40 x 40 x 40 mm cubes. Flexural strengths of concrete were carried on 70 x 70 x 280 mm prisms.

Mercury Intrusion Porometry measurements were performed on discs (3.2 cm in diameter, 1cm thick) drilled from blocks. The treatment of samples consists of a drying period at 45°C in the presence of a silica gel during 7 to 14 days. The choice of this temperature is an optimum between preserving the nature of the hydrates contained in the cement paste and removing the free water. Samples were considered as "dry" when their relative loss of mass did not exceed 0.5% for 24 hours.

Water absorptions were measured according EN 13369 standard. After conditioning to 20 ± 3 °C the test specimen was soaked to constant mass and then dried (105 ± 5) °C. The water absorption corresponds to the loss in mass expressed as a percentage of the mass of the dry test specimen.

Accelerated carbonation tests was carried under a controlled gas mixture (50 ± 5% CO_2 and 50 ± 5% air) using an analyst - regulator (Siemens Ultramat 21) at a constant temperature of 20 ± 2°C. The use of a saline solution in the enclosure guaranted a relative humidity of 65 ± 5%. The carbonation test was carried during four months. Carbonation depths were determined using a solution of phenolphthalein.

4 Results and discussion

4.1 Influence of ultrafine on fluidity of VHPC and UHPC

It is well known that there is often a compatibility problem between superplasticizer, cement and other fine particles. The better the compatibility, the lower the dosage of superplasticizer needed.

For the VHPC the results show that a lower dosage of superplasticizer is needed with limestone microfiller (Table 3). With the same dosage of superplasticizer used for silica fume,

it would be possible with this ultrafine to reduce the water/cement ratio without disturbing the workability.

For the UHPC, limestone microfiller and micronized phonolith lead to a good fluidity. The UHPC with metakaolin, pulverized fly ash and siliceous microfiller need more superplasticizer and water to achieve the same workability. Despite a significant higher dosage of superplasticizer in comparison of those with silica fume, the UHPC with metakaolin shows poor workability (17 cm for the flow table test). The lack of fluidity of concrete or pastes with metakaolin has been noted by other authors. The fluidity of metakaolin blended cement became poorer than that of Portland cement at the same dosage of superplasticizer and the same water/cement ratio [9].

UHPC with pulverized fly ash required significant higher water content (water/cement ratio equal to 0.22 instead of 0.19 with silica fume). The rheological properties of cement pastes containing fly ashes are influenced by both physical and chemical properties of the ash [10]. The spherical shape of fly ash particles as well as the presence of glassy phase on the fly ash surface improve significantly the structure of paste. Therefore the paste is effectively densified and the water content can be reduced while the fluidity is kept constant. The effect of chemical properties depends on the chemical and mineral composition. Therefore the high-calcium fly ashes exhibit hydraulic properties. The phases which are susceptible to the hydration process affect the setting of fly ashes and thus the rheological properties of the cement-fly ah pastes. A high-calcium fly ash admixture to cement results in a decrease of pastes (higher yeld value and plastic viscosity). The authors have also shown that additional grinding of the high calcium fly ash increases the fluidity of pastes.

The constrating behaviours of various pozzolans with respect to strength development and workability have led some investigators to examine ternary blends containing metakaolin with a view to use the beneficial properties of the different pozzolans. Some investigators have noted that when both metakaolin and ultrafine slag are incorporated into cement Portland paste, the compressive strength of the blended paste and also the fluidity are improved compared to metakaolin blended cement paste [10].

4.2 Pore structure

Pore size distribution obtained for the VHPC and UHPC are respectively shown in Figure 3 and 4.

For VHPC the total porosies measured by intrusion mercury porometry are similar, in the range of 5.1 to 6.6%. For each VHPC, most of the pore have a diameter under 0.1μm which is a specific characteristic for this kind of concrete. The MIP measurements reveal a finer pore network for UHPC made with silica fume, siliceous microfiller and metakaolin. Silica fume fills the voids between cement grains and modifies the microstructure of the transition zone, making it denser and stronger [2]. Previous studies have clearly shown that the pore structure of metakaolin blended pastes is finer than that in plain cement paste [8]. With metakaolin, the rate of pore refinement was very rapid up to 14 days curing after which pore size changed very little. According to the authors, though pozzolanic activity continues

beyond 28 days, a significant proportion of the reaction occurs within the first 14 days when maximum relative strength is also achieved.

In the case of UHPC, the pore network is finer than those of VHPC. Pore diameters are under 0.03 µm for each UHPC. Meanwhile, there are significant differences between UHPC made with silica fume, for which total porosity is very low (2,2%), and other UHPC. One can note the important value obtained with pulverized fly ash, phonolith and limestone microfiller, respectively 9,0 ; 8,8 and 7,6%. To compare the total porosity of VHPC and UHPC, it is important to take into account that the proportion of paste is significantly higher in the case of UHPC compared to the VHPC. The pore diameters of the UHPC with silica fume are under 0.01 µm. This porosity corresponds to the intercrystallite space [11]. UHPC with other ultrafine contain much more pores in the range 0.01 to 0.03 µm which correspond to crystallite packing defect.

The reaction mechanism involve by ultrafines in cement paste can be divided into physical and chemical aspects. The physical effect is that ultrafine particles fill the voids in cement, which makes the microstructure of cement paste denser. The physical filling of voids with ultrafines depends on the particle size distribution. The chemical effect is the reaction of ultrafine particles with the cement hydrates. Pozzolanic ultrafines can react with portlandite released by cement clinker hydration to produce secondary C-S-H gel which improves the microstructure of cement paste matrix.

Figure 3: Pore size distribution and total porosity of VHPC at the age of 90 days.
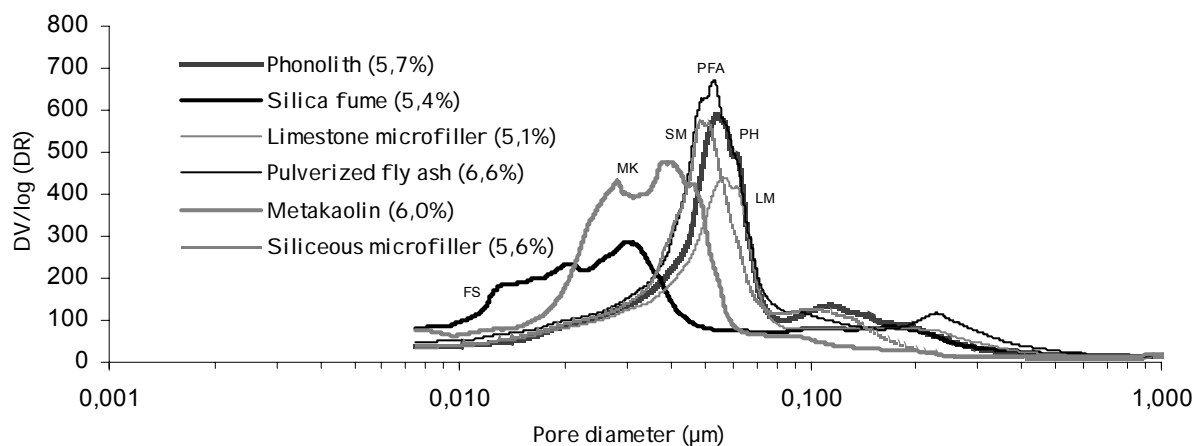
Figure 4:   Pore size distribution and total porosity of UHPC at the age of 90 days.
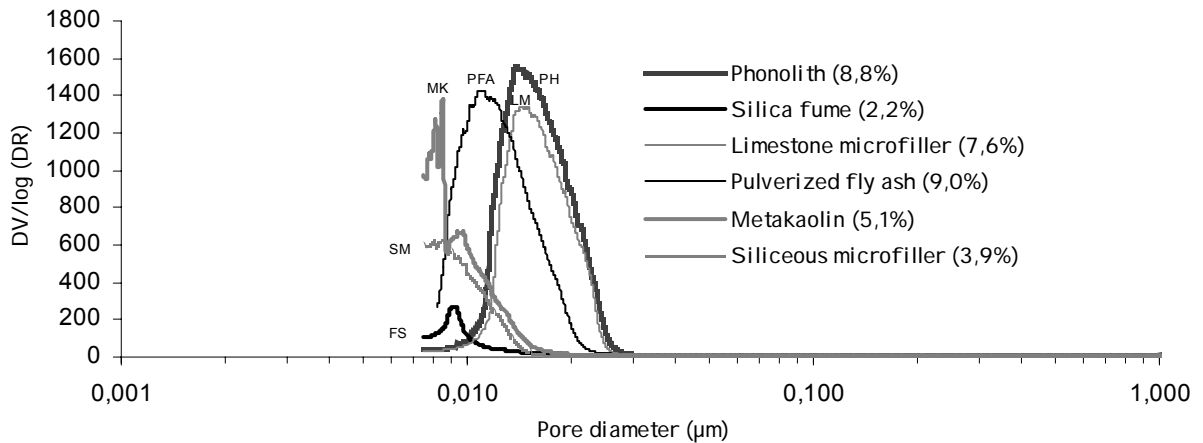
4.3   Compressive and flexural strengths

The results show that the ultrafines used allow the making of VHPC and UHPC, excepted for pulverized fly ash. At the age of 28 days, the compressive strengths of VHPC are similar excepted for those with limestone microfiller for which the resistance was lower (Figure 5). At the age of 90 days, silica fume leads to the higher compressive strength (119.7 MPa). There is a significant increase of the resistance for the VHPC with limestone microfiller between 28 and 90 days. For each ultrafine, flexural strengths do not exhibit important evolution between 28 and 90 days.

All the compressive strengths of UHPC are over 150 MPa at the age of 28 days excepted for those with pulverized fly ash (Figure 6). The higher performances are obtained for the UHPC with silica fume. The higher increase between 28 and 90 days have been noted with silica fume, metakaolin and siliceous microfiller. Most of the flexural strengths are over 25 MPa, excepted for pulverized fly ash.

Figure 5:   Compressive and flexural strength of VHPC at the age of 28 and 90 days
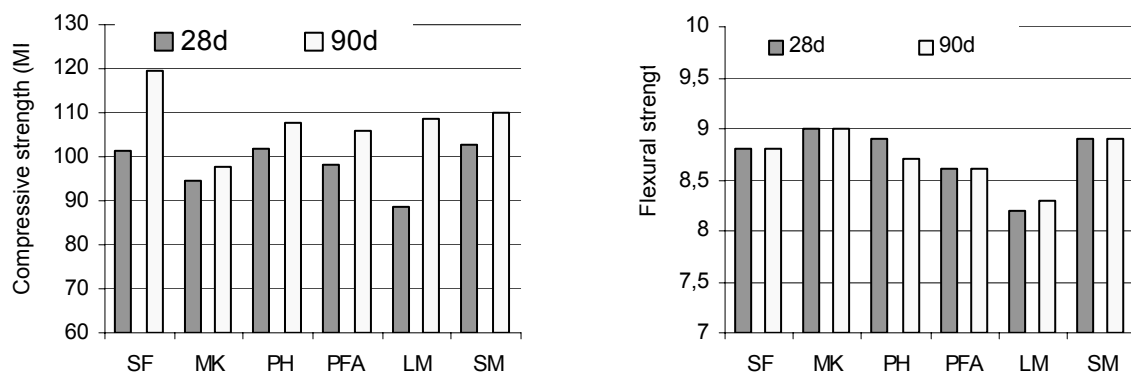
Figure 6:   Compressive and flexural strength of UHPC at the age of 28 and 90 days
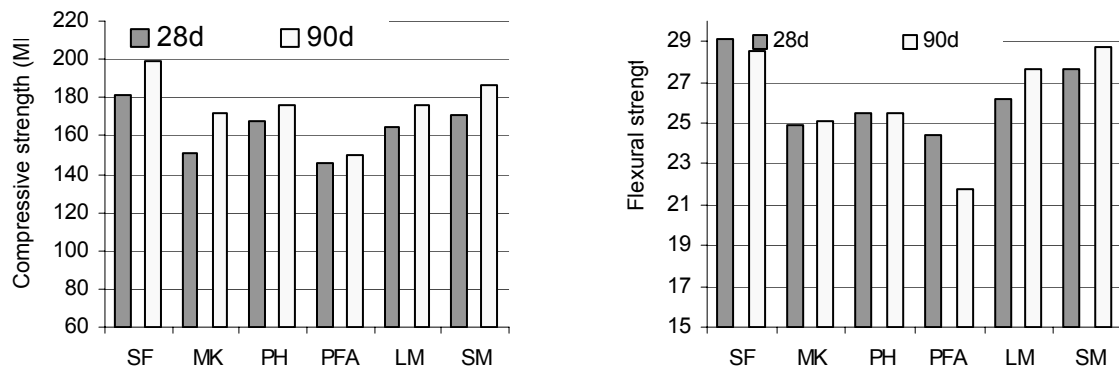
There are three elementary factors which influence the contribution that ultrafine particles makes to concrete strength. These are the filler effect, which is immediate, the influence on the Portland cement hydration which occurs within the first 24 hours, and the eventual pozzolanic reaction. MIP measurements showed significant differences of the pore network of UHPC. Silica fume leads to a much more denser matrix.

It is known that limestone fillers cause a good packing of cement granular skeleton and a large dispersion of cement grains [12]. These ultrafine acts as the crystallisation nucleus for the precipitation of portlandite. These simultaneous effects produce an acceleration of the hydration of cement grains. Authors have shown that there is a higher degree of hydration in very low water/cement ratio paste when the limestone filler content is increased [12]. For a given cement, the optimum filler content for different water/cement ratios can be obtained by using the gel-space ratio concept. According to the gel-space ratio concept, the compressive strength of concrete depends on the effective water/cement ratio and the degree of hydration of cement. The addition of an ultrafine creates changes in both gel-space ratio terms.

There have been several studies on the strength development of concrete containing metakaolin. Metakaolin prompts the hydration of cement and shortens the setting time [9]. The very early strength enhancement is due to a combination of the filler effect and accelerated cement hydration. The authors have shown that when metakaolin and ultrafine slag are used in cement at the same time, there is a synergistic effect, also called compounding effect. Metakaolin is a high active pozzolanic mineral admixture and slag is a latent hydraulic mineral. Both metakaolin and ultrafine slag can react with portlandite released by cement clinker hydration to produce secondary C-S-H gel, making the microstructure denser.

For the UHPC, the pulverized fly ash leads to the lower compressive strength. This is due to the higher W/C required. The activity of fly ash in cement matrix can be enhanced by chemical treatment of the ultrafine [13].

It is important to see that for each kind of concrete (VHPC and UHPC), the ultrafine/cement proportion has not been optimised in this study. Because the physico-chemical properties

(particle size, shape, pozzolanicity activity,…) of ultrafine are not the same, there is an optimum ratio for each ultrafine and concrete.

4.4   Water absorption and carbonation

The water absorption measured according to the EN 13369 standard are presented in Table 5. VHPC and UHPC have low water absorption due to their high compactness. This behaviour is due to the rapid reduction of the capillary pores connectivity and to the increase of tortuosity by formation of a dense structure. Silica fume gives the lower value (3.3% for the VHPC and 0.7% for the UHPC). For the UHPC, pulverized fly ash, limestone filler and phonolith give the higher water absorption values. These results are in good agreement with MIP measurements which point out the higher porosity with these ultrafines.

Table 5:   Water absorption of VHPC and UHPC at the age of 90 days

Ultrafine	Silica fume	Metakaolin	Phonolith	Pulverized fly ash	Limestone microfiller	Siliceous microfiller
VHPC	3.3	4.0	4.2	4.3	4.2	4.1
UHPC	0.7	1.9	2.2	3.2	2.8	1.6

After four months of accelerated carbonation test, no carbonation has been detected for each VHPC and UHPC. The carbonation depths are under the limit detection of the method which is around 0.5 mm.

The kinetic of carbonation is essentially linked to the cement matrix compactness and the volume of portlandite liberated by cement hydration. When the water/cement ratio is very low, the capillary pores become discontinuous relatively early. Moreover, the precipitation of calcite induces a significant decrease of the porosity which is initially low. Both mechanisms explain the excellent resistance to carbonation of VHPC and UHPC.

It is well known that silica fume and pulverized fly ash are quite useful in improving the durability of concrete. Numerous studies have also shown that metakaolin can have benefit effect in controlling alkali aggregate reaction, reducing risk of chloride-induced corrosion of embedded steel, reducing the rate of water absorption and increasing the resistance of concrete to aggressive solutions [8]. The utilisation of pozzolanic ultrafines results in added technical advantages manifested in reductions in temperature rise and improvements strength enhancement, although in some cases strength develops more slowly. Pozzolanic ultrafines particles are also interesting to increase the durability of concrete. The portlandite liberated by the hydration of Portland cement does not make a significant contribution to strength and can be harmful to concrete durability, in the case of some chemical aggressive environment for example. Pozzolanic ultrafines can react with portlandite released by cement clinker hydration to produce secondary C-S-H gel inside the cement paste. The secondary formed C-S-H gel improves the compactness of microstructure of cement paste. The reduction of portlandite can result in greatly enhanced durability and strength.

5   Conclusion

Potential interests of ultrafines other than silica fume for very high performance concrete and ultra high performance concrete were studied. The powders investigated in this study are metakaolin, pulverized fly ash, limestone microfiller, siliceous microfiller and micronized phonolith. The experimental results point out the good ability of these ultrafines to realize these new kinds of concrete. From a technical point of view, it appears that other ultrafine than silica fume can be used to produce concrete with very high compactness. The performances of the VHPC obtained are nearest to those of materials with silica fume. For the UHPC, silica fume leads to the highest performances. Nevertheless, limestone microfiller, siliceous microfiller, metakaolin and phonolith can be used to achieve compressive strength over 150 MPa.

The discussion in this paper has focused on the good behaviour of the limestone microfiller for which it is possible, in the case of VHPC, to reduce the superplasticizer dosage without disturbing the rheology.

Some of the ultrafine allow white surface tint. This is particularly the case with the limestone microfiller, the micronized metakaolin and the siliceous microfiller. Compared to the usual dark tint of concrete with grey silica fume, this is an important advantage.

Further investigations are needed to increase the potential benefits of ultrafines in VHPC and UHPC: knowledge on early compressive and flexural strength, creep, shrinkage, resistance to freeze/thaw cycles, chemical attacks,… Another promising way is the possibility to use several ultrafines together to optimise fluidity and compressive strength.

6   References

[1]   De Larrard, F.: Ultrafine particles for the making of very high strength concretes. In: Cement and Concrete Research, vol. 19, 161-172, 1989.

[2]   Goldman, A. and Bentur, A.: Effect of pozzolanic and non-reactive microfillers on the transition zone in high strength concretes. In: Interface in Cementitious Composites, RILEM Proceeding, 18, 53-61, 1992.

[3]   Gruber, K.A.; Ramlochan, T.; Boddy, A.; Hooton, R.D. and Thomas, M.D.A.: Increasing concrete durability with high-reactivity metakaolin. In: Cement and Concrete Composites, vol. 23, 479-484, 2001.

[4]   Naiqian, F.: The properties of zeolite mineral admixture concretes. In: Mineral Admixture in Cement and Concrete, ABI Books Private Limited, 396-447, 1993.

[5]   Uchikawa, H.; Hanehara, S. and Hirao, H.: Influence of microstructure on the physical properties of concrete prepared by substituting mineral powder for part of fine aggregate. In: Cement and Concrete Research, vol. 26, 101-111, 1996.

[6]   Zhang, M.H. and Malhotra, V.M.: Rice-husk ash paste and concrete : Some aspects of hydration and the microstructure of the interfacial zone between the aggregate and paste. In: Cement and Concrete Research, vol. 26, 963-977, 1996.

[7]   Long, G.; Wang, X. and Xie, Y.: Very high performance concrete with ultrafine powders. In: Cement and Concrete Research, vol. 32., 601-605, 2002.

[8]   Sabir, B.B.; Wild, S. and Bai, J.: Metakaolin and calcined clays as pozzolans for concrete: a review. In: Cement and concrete Composites, vol. 23, 441-454, 2001.

[9]   Li, Z. and Ding, Z.: Property improvement of Portland cement by incorporating with metakaolin and slag. In: Cement and Concrete Research, vol. 33, 579-584, 2003.

[10] Grzeszczyk, S.. and Lipowski, G.: Effect of content and particle size distribution of high-calcium fly ash on the rheological properties of cement pastes. In: Cement and Concrete Composite, vol. 27., 907-916, 1997.

[11] Vernet, C.; Lukasik, J.; and Prat, E.: Nanostructure, porosity, permeability and diffusivity of Ultra High Performance Concretes. In: Proceedings of International symposium on High Performance and Reactive Powder concretes, 1998.

[12] Bonavetti, V.; Donza, H.; Menendez, G.: Cabrera, O. and Irassar, E.F.: Limestone filler cement in low w/c concrete: A rational use of energy. In: Cement and Concrete Research, vol. 33, 865-871, 2003.

[13] Fan, Y.; Yin, S.; Wen, Z. and Zhong, J.: Activation of fly ash and its effects on cement properties. In: Cement and Concrete Research, vol. 29., 467-472, 1999.

Dr. Ing. Hans-Werner Röth
Head of OMYA Concrete Minerals
OMYA GmbH Köln
Germany

Production of Calciumcarbonate based fine fillers for UHPC

Summary

Calcium carbonate ($CaCO_3$) is a very common mineral that can be found in abundant masses within the Earth's crust and other geological environments. It exists in all parts of the world and in all three classifications of rocks. Calcium carbonate is most commonly taken from limestone and ground up into it's pure form. However, it is also naturally found as chalk, marble, aragonite and calcite.

A large number of industries, from ceramics to cosmetics, food to paints and coat-ings, papers to plastics and of course the wide range of building materials - rely on powdered calcium carbonate fillers to optimize their products.

The world´s largest calcium carbonate supplier to these industries is OMYA. OMYA has extensive production capacity consisting of approximately 140 plants located in more than 30 countries worldwide. Beside the classical fields OMYA has become an important partner of the cement- and concrete industry. Their demand in high-quality fine and ultra-fine fillers for special applications (e.g. UHPC) is growing steadily.

1   What is Calcium Carbonate ($CaCO_3$) ?

1.1   Chemical aspects

Calcium is one of the seven most common elements of the earth. It appears in 700 different minerals and in the earth`s crust it has got a share of 3,36 % which means the fifth common element in this part.

$CaCO_3$ is a mineral built as a chemical salt through the reaction of carbon acid with burnt or slaked lime:

$$CaO + H_2CO_3 \qquad \leftrightarrow \qquad CaCO_3 + H_2O \text{ (burnt lime)}$$

$$Ca(OH)_2 + H_2CO_3 \qquad \leftrightarrow \qquad CaCO3 + 2\,H_2O \text{ (slaked lime)}$$
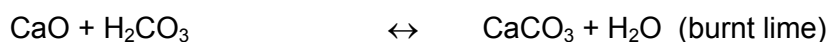
Every carbonate is very sensible throughout acids and acid waters:

$$CaCO_3 + 2\,HCl \qquad \leftrightarrow \qquad CaCl_2 \;+ CO_2 + H_2O$$
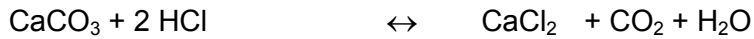
In pure destillated water it can hardly be solved (max. 13 mg/l).

There is a great influence of the hydrostatic pressure rising the amount of $CaCO_3$ in water. The more carbonacid is dissociated in water by rising pressure the more lime will be solved in it. Therefore a fallout of lime can be seen for instance at springs or waterfalls, due to the sudden decline of pressure.

The influence of temperature on the solubility of $CaCO_3$ is even well known. When water is heated up lime falls out because carbonacid escapes. We can see it daily in our coffee maker or water cooker.

The third way to come to a $CaCO_3$ fallout are evaporation (shown in stalactite caves), vaporation and frost.

1.2 Cristallic forms

Three different mineralogical modifications of $CaCO_3$ can be distinguished:

Calcite , Aragonite and Vaterite

Figure 1 shows Calcite which cristallizes as

a: rhombohedron

b: scalenohedron

c: prism
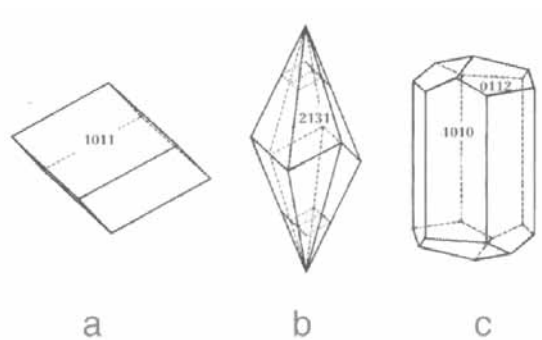
Figure 1: Calcite

Calcite is one of the most frequent minerals of the earth`s crust varifying to several hundred different forms. Pure calcite is transparent and without colour. Natural deposits are milky white.

Aragonite (figure 2) appears more seldom than calcite. It is not stable in geological ages because it changes to calcite. Aragonite can be seen in individuals like mussels and coralls when they are alive - but when building sedimentary rocks it gets trans-formed to calcite.

a: orthorhombic single crystal

b: orthorhombic twins

c: hexagonal triplets
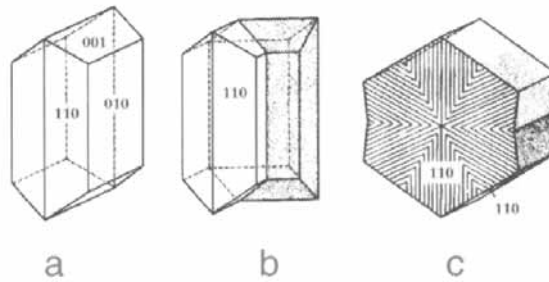
Figure 2 : Aragonite

Vaterite is a variety of $CaCO_3$ produced only chemically. It is instable and it`s occurence in nature is an exception and therefore it has got no industrial meaning.

2 Sorts of Limestone Rocks

There are three sorts of $CacO_3$-built rocks due to their origin.

Limestone	= sedimentary rock
Carbonatite	= magmatic rock
Marble	= metamorphic rock

2.1 Limestone

During the formation of sedimentary limestone organic material like shells of mussels, ammonites, algae and monocellulars or riffs of coralls are stored on the ground of a warm ocean bassin. After consolidation they form layers and deposits
with thicknesses up to 100 m and more (figure 3).

Figure 3: Limestone deposit

If there is low diagenetic consolidation with few binding material within the particles the resultant rock is called "chalk". It is a soft-rock which can easily be scratched and destroyed and which has got a high absorbance to water. It reacts like a sponge.

Higher diagenetic consolidation with calcite binding material within the sedimentary particles causes a "limestone". It is a hard rock which must be blown up in quarries without the ability to collect water because the interspace is filled with binding material.

2.2 Carbonatite

Carbonatites which are of magmatic origin occur rather seldom and have no meaning for the mineral industries. Meanwhile the other described sorts of calcite rocks build up the OMYA deposits and businesses.

2.3 Marble

If a rock is exposed to increasing temperatures (> 500 ^{o}C) and/or increasing pressure due to submission to deeper parts of the earth`s crust in times of orogenesis the minerals of the rock melt up. After relaxation the minerals crystallize again and the rock now has changed from limestone into marble which is geologically called "metamorphic limestone".

For example the Carrara-Marble (figure 4) got its metamorphic character throughout the orogenesis of the Alps.

Figure 4: Carrara marble

3 Production of Calciumcarbonate-Fines

Most of the worldwide OMYA-plants are based on opencast-operations. In only very few cases the calciumcarbonate is being won in underground mines.

Calcium carbonate fillers and coating pigments are tailor-made products with highly specific property profiles. It is no wonder that the quarries of the past are now pro-duction facilities with the latest technology. Almost everything - from extraction and processing through to packing ready for dispatch - is done automatically.

This chapter shall give a short survey of such a typical factory.

The single process steps are the following ones:

- Blasting of the rock
- Pre-crushing
- Transport to the factory by truck or conveyor belt
- Storage of the raw material
- Milling
- Flotation
- Dewatering
- Micro-Milling/Drying
- Sizing

3.1 Blasting

There are four main categories of commercial high explosives:

- Dynamite
- Slurries
- ANFO (Ammonium Nitrate + Fuel Oil)
- Two-component explosives

The first three are the most common explosives for borehole charges. OMYA prefers to blast with ANFO explosives, because the detonation efficiency can be controlled very flexibly and easily. It is free flowing and can be blown or augered from the bulk trucks directly into the blastholes (figure 5). Figure 6 shows the quarry blasting.

ANFO does not chemically pollute the raw-material and has no negative influence on the light colour of the stone. ANFO explosives are comparably safe to handle and to store. A wet surrounding is no problem for them.

Figure 5 : Filling the blasthole

Figure 6 : Blasting

3.2   Pre-Crushing

During this step the big and lumpy stones (up to 2,5 m) are being destroyed and broken down to a max. size of 50 mm. In most OMYA open pits this is being done by semi-mobile jaw- or hammer-crushers (figure 7). Big wheel loaders are carrying the

blasted material to the crushing station and dump it into the mill-hole. The crushers have an average capacity between 500 and 750 t/h. Special attention has to be spent to the quality of the crusher tools to avoid any pollution of the raw material with metallic particles. High resistance to abrasion can be reached with tools consisting of special alloys (chrome-vanadium, tungsten-carbide).

Figure 7 : Semi-mobile hammer-crusher

3.3 Transport

The pre-crushed run-of-mine material has to be transported to the preparation plant. Depending on the distance two different transportation systems are being used in the OMYA pits. The most common ones are continously operating conveyor belts (figure 8). They are very flexible regarding to the topography as well as the weather conditions. Their width lays between 1000 and 2000 mm, the maximum length comes to approx. 5 km.

Figure 8 : Conveyor belt

If the distance is longer, it´s more feasible to carry the material discontinously by big dumpers (figure 9). Their haulage capacities vary between 15 and 35 cbm. With a max. speed of 55 - 70 km/h they can be used in a distance range of 3 - 20 km.

Figure 9: Dumpers

Other systems like trains, cable-ways a.o. don`t play any role at OMYA.

3.4 Storage of the raw-material

The raw-material gets stockpiled ina storehouse. The typical capacitiesmove between 6.000 and 10.000 t. It remains there for 24 hours. Mainpurposes are to lower the surface moisture during rain periods, to homogenize the stone quality as well as to have an emergency stock in case of some technical difficulties in the quarry.

The material is removed by a reclaimer as shown in figure 10.

Figure 10: Portal Reclaimer

3.5   Milling

The next step is to mill the Calciumcarbonate down to a top-cut of max. 1,0 mm.
This happens in large grate rod-mills (figures 11 and 12).
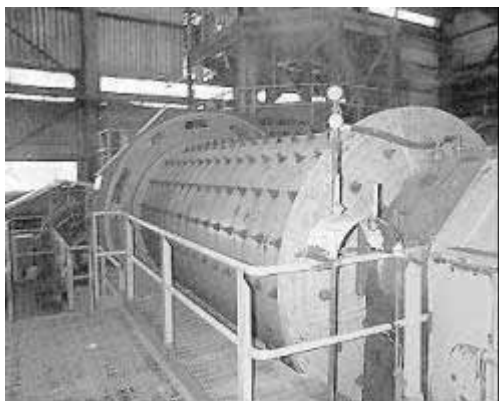
Figure 11: Grate rod-mill

Figure 12: opened mill

This type of mill is filled with long rods, parallel to its rotating axis. They fill approx. 35% of the total inner space of the mill. The whole system is circulating with a moderate speed (<1 rps). The cascading rods break the stones and the crushed material leaves the mill at the end.

3.6   Flotation

It occurs when the density of particles is artificially decreased to allow particles to float. This is based on the capacity for certain solid particles to link up with air bubble to form « particle-gas » with a density lower than the liquid. Special chemical addi-tives (collectors, frothers, pressing agents) improve the selectivity.

The calciumcarbonate flotation is an in-direct one. That means, that the tailings (soil, clay, organics etc.) are being flotated and the calciumcarbonate is pressed. Tailings are everything, which might reduce the $CaCO_3$-content.

The Flotation takes place in a number of serial flotation cells (figure 13). The ground material coming from the rod-mill is being given to the initial cell battery. A stirring system and injected air bubbles lead to a stable foam on the surface, which carries the tailings. They are taken out by specially designed paddles and deposited.

The valuable is the pre-concentrated $CaCO_3$-pulp, which is the feed for the next cell battery. After three flotation stages the final concentrate has reached nearly 100% $CaCO_3$.

Figure 13: Flotation cells

3.7 Dewatering

The liquid $CaCO_3$ pulp - coming from the flotation - has to be dewatered. This happens in a "Filter Vacuum Rotary Drum" (figure 14). The end-product is an earthdry filtercake with a residual moisture of approx. 8-10 %.

Figure 14: Filter Vacuum Rotary Drum

3.8 Micro-Milling and Drying

The filtercake is given to a combined milling and drying system. In most cases
vertical roller mills are put to use (figures 15 and 16). Roller mills feature an efficient grinding mechanism ensuring a high fine-grinding efficiency and an operational stability as well as a classification mechanism permitting the flexible adjustment of particle size distribution in products, thereby offering various advantages in actual plant operation.

The heating gas is being generated indirectly in external burner systems, which can be fired alternatively with oil or gas. The ground, extremely fine particles are trans-ported from this point pneumatically together with the air, which leaves the mill at its top.

Figure 15: Vertical roller mill   Figure 16: Vertical roller mill (principle)
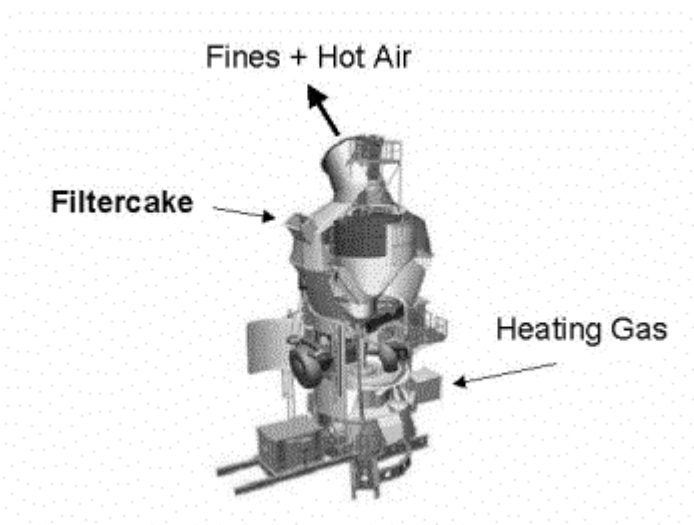
3.9 Sizing

The whole size distribution of the dried and milled high-concentrated calciumcarbo-nate ranges from 0 to 90 micron. The separating into the different size-fractions is
done in cyclons (figure 17).

Figure 17: air-separator

Air enters through a tangential inlet generating a swirling flow that forces entrained solids radially outward. The solids drop out through the bottom of the separator while the air plus the ultrafines (for example < 12 micron) exit through the top.

A good example for this is the OMYACARB 2-GU from the OMYA-plant Gummern in Austria:

Chemical analysis: $CaCO_3$ > 98   %
                       Fe_2O_3 < 0,15 %

Sizing: > 45 μm   < 0,1   %
                D_{98} 12 μm
                D_{50} 2,5 μm
                < 2 μm   40   %

Physical properties: H_2O < 0,2 %
                         R_y 94,5   %
                         Density   2,7 g/cm^3

Figure 18: Size distribution of OMYACARB 2-GU

4   Fields of application for OMYA Fillers

There are only very few products of the daily life worldwide which have no direct relationship to OMYA fines. The most important fields are the following industries:

- Paper

- **Plastics**

- Paints

- Others:

glass, asphalt, drinking-water, power-plants, fertilizer, lake-liming, electric cables, rubber, wooden chip boards, ceramics, cosmetics, food, cement, concrete

Powdered Calciumcarbonate Fines optimize these products individually.

P. Haleerattanawattana
Ph.D. Student
Chulalongkorn University
Bangkok, Thailand

E. Limsuwan
Professor Dr.
Chulalongkorn University
Bangkok, Thailand

Strength-Based Gradation of Coarse Aggregates for Ultra-High-Strength Concrete

Summary

For producing ultra-high-strength concrete, selection of very strong aggregate with appropriate gradation to become effective skeleton transferring internal forces is necessary. In this paper, the physical and mechanical properties of coarse aggregate with different types and sizes are discussed. Afterwards, the idea of *strength-based gradation* (*SBG*) is presented as an attempt to render both packing density and strength index of coarse aggregate to be a single parameter indicating its potential for making such concrete. From the experiment, the dependence of concrete strength on this parameter is shown. Further, the application of this concept to determine the optimum quantity of binder is described.

Keywords: *aggregates, gradation, strength, ultra-high-strength concrete*

1   Introduction

Generally, aggregate is relatively inexpensive and strong concrete-making material. It is treated customarily as an inert filler. The primary concerns of aggregate in mix design for high-strength concrete are gradation, maximum size, and strength. Providing that concrete is workable, the gradation is usually composed as dense as possible, i.e. with maximum packing. That forms the most intense structure for load carrying and minimizes the necessary amount of binder, filling the cavities between aggregate particles. Different ideal grading curves were recommended [1]. In addition, the optimization of aggregate with packing calculation was elaborated [2-3].

The large particles of aggregate are undesirable to produce high-strength concrete. Although smaller maximum size of aggregate leads to higher water demand, the larger total surface area of the aggregate with smaller maximum size is resulted in the lower stress at interface. Thus, the concrete is prevented from bond failure [4].

Strength of aggregate becomes significantly more important as concrete strength increases. It is pleasing that aggregate particles have no weak planes that would cause the aggregate to fail in a brittle manner when the concrete is loaded [5]. It was also reported that concrete strength seems to be proportion to the aggregate parent rock [6-7]. The quantitative influence of rock intrinsic strength on concrete compressive strength was proposed [8]. Nevertheless,

the quality of aggregate is uncertain. It considerably varies from one area to another, depending on the geological conditions. Moreover, strength of aggregate seems to be contrary to its size. From rock mechanics, the energy required for size reduction of crushed rock is an inverse function of the particle size [9-10]. Providing that the input energy is not excessive, defects or microcracks in the internal structure may be removed along the comminution process.

However, the variation of aggregate properties with its size is usually overseen. Only regarding to the packing, the particle distribution of aggregate mixture is optimized. The advantages of aggregate may be not adopted completely. Therefore, this study aims at applying the aggregate properties to take part in the determination of its gradation. The strength parameter is combined with the packing density to establish *strength-based gradation* (SBG) of aggregate. SBG index represents the effective volume of strong aggregate particles in the mixture. Increase in such volume possibly enhances the performance of concrete. This study is a part of works intended to develop mix design for ultra-high-strength concrete (28-day compressive strength exceeding 150 MPa) with the common available materials and conventional practice.

2   Properties of Aggregate

Three types of crushed rock, i.e., limestone, basalt and granite, were investigated. Each of them had derived from two quarries in the same area. They were classified into four classes, regarding to their size, i.e., 1" (25.40 mm), 3/4" (19.05 mm), 1/2" (12.70 mm), and 3/8" (9.53 mm). Samples from each class were tested for their physical and mechanical properties. List of the properties and test methods are shown in Table 1.

Table 1: List of properties and test methods

Category	Properties	Test Method
Physical	Specific Gravity and Water Absorption	ASTM C127
	Unit Weight and Void Content	ASTM C29
	Flakiness Index	BS 812: 105.1
	Elongation Index	BS 812: 105.2
Mechanical	Aggregate Crushing Value	BS 812: 110
	Aggregate Impact Value	BS 812: 112
	Los Angeles Abrasion Value	ASTM C131
	Point-Load Strength Index	ISRM [11]
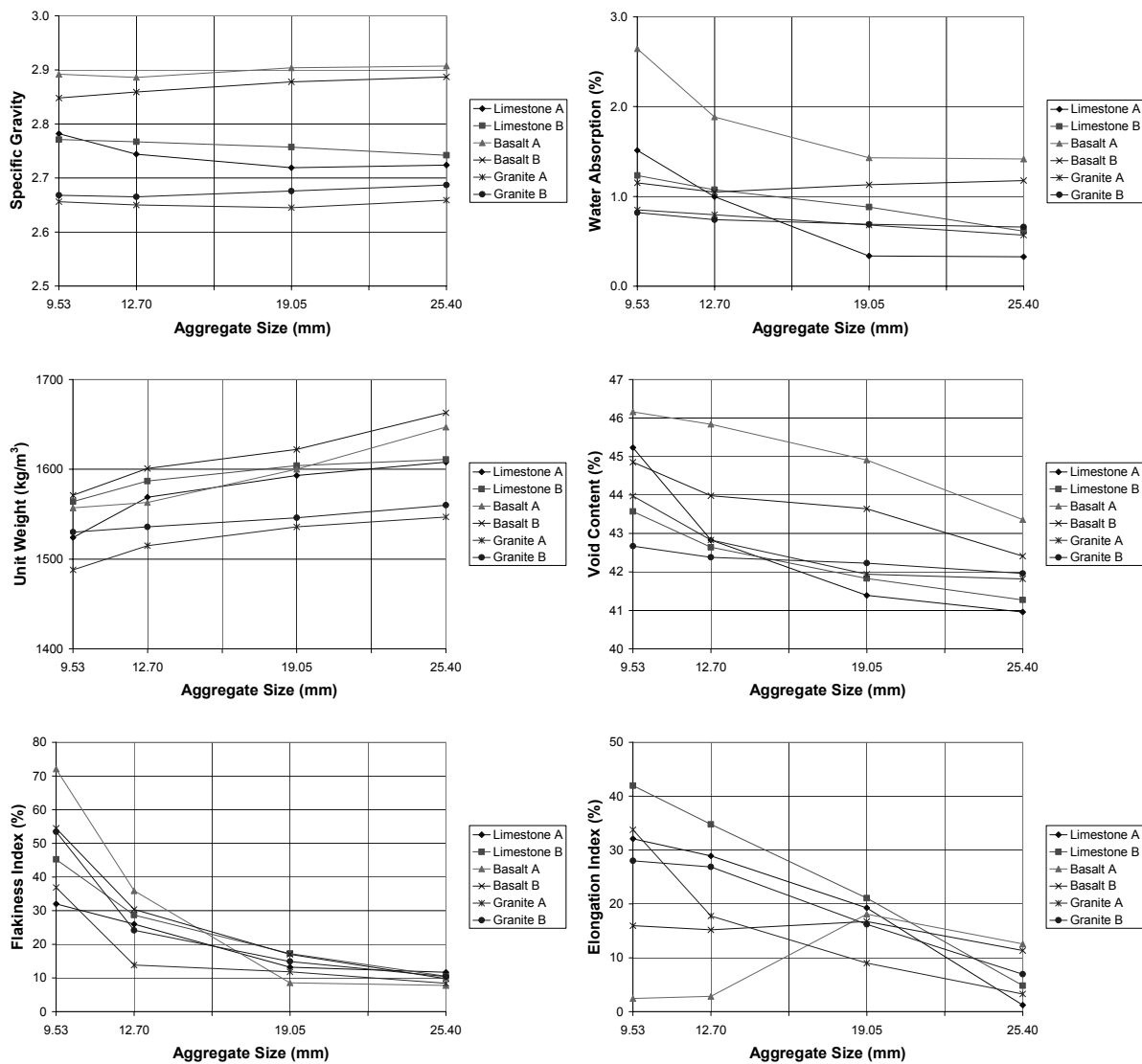
Fig. 1 Mechanical properties of aggregates with various sizes and shapes

Plots of the test results with aggregate sizes are shown in Fig. 1 and 2. It can be observed that the specific gravity of all crushed rocks is constant. It is about 2.75, 2.88 and 2.66 for limestone, basalt and granite, respectively. For all aggregates, the water absorption tends to increase with size reduction. In addition, when the aggregate size decreases, the unit weight of the mixture decreases as well, but the void content between particles increases. The worse packing may be due to the undesirable shape of smaller aggregate, which is reflected from the significantly high values of flakiness and elongation index. As strength parameters, the aggregate crushing value (ACV) and the aggregate impact value (AIV) decreases with decreasing size of aggregate. But, it is not in the case of the Los Angeles abrasion (LAA). It is possibly resulted from using a single sieve (no. 8), according to the standard, to screen the remains from abrasion for all aggregate sizes. The probability of small aggregates to become particles passing the prescribed sieve is higher than that of the larger. Thus, in this study, the sieve size was varied depending on the sample size, in the same manner that ACV and AIV

were evaluated. This abrasion value is named as *modified Los Angeles abrasion* (MLAA). Like ACV and AIV, MLAA decreases with decreasing aggregate size. It means that smaller aggregate tends to be stronger than the larger one. This is also confirmed by the point-load
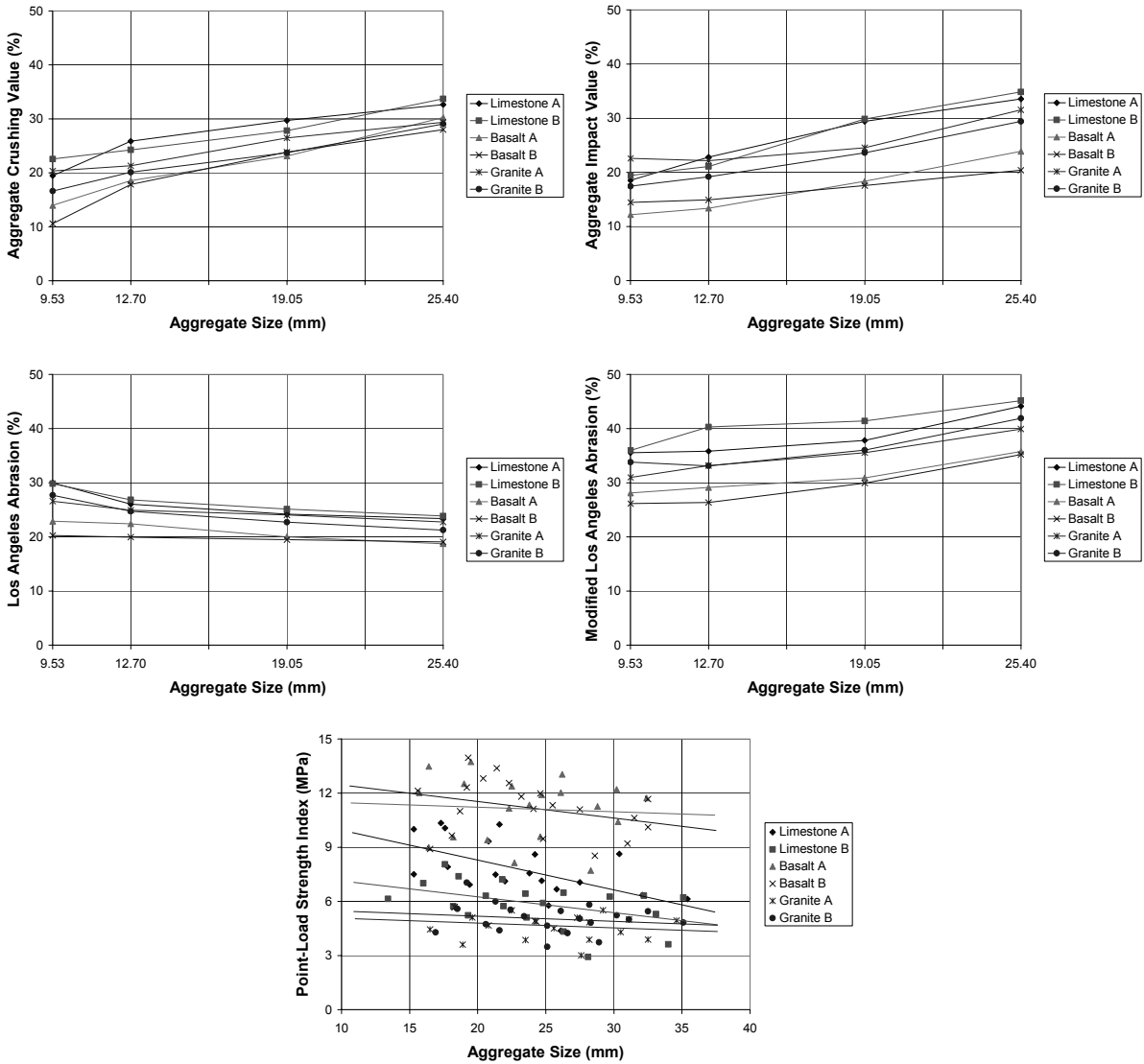
Fig. 2 Mechanical properties of aggregates with various sizes and shapes

strength index. Although the deviation of the index is rather high, the linear relation between point-load strength index and size of aggregate can be pointed out. As expected, basalt aggregate is the strongest, following by granite and limestone.

Even the number of quarries is small; some observations can be drawn from the experimental results. That is, the input energy for size reduction process, i.e., blasting or crushing, breaks down the aggregate particles by destroying internal weak planes, microcracks or any defects. This makes the aggregate stronger, thus providing higher degree of the resistance for crushing, impact and abrasion. Consequently, it is required more energy to reduce aggregate size further. Unfortunately, using high amount of energy can not control

the aggregate shape satisfactorily. Moreover, the surplus energy may induce the artificial microcracks in the particles and reduce their intrinsic strength. Therefore, the aggregate gradation should be composed with paying attention to this concern, so that it is beneficial to concrete performance.

3   Packing Density

Because there are unlimited numbers of possibility for composing aggregate gradation, and, in practice, it is impossible to evaluate the effect of all these possibilities, packing density is raised to facilitate this inconvenience. Packing density is defined as the volume of particles in relation to the total volume, or mathematically as one minus porosity. Packing of aggregate mixtures depends on shape of particles, interaction among particles with different sizes, and degree of compaction. De Larrard [12] proposed the implicit expression to determine packing density (ϕ) of n-class aggregate as

$$K = \sum_{i=1}^{n} \frac{y_i / \beta_i}{\dfrac{1}{\phi} - \dfrac{1}{\gamma_i}} \tag{1}$$

K is the compaction factor, depending on the process of packing. The value of K is about 4.5 for sticking the aggregate mixture with a rod. y_i and β_i are the volume fraction and the residual packing density of class-i aggregate, respectively. And, γ_i is the packing density when class-i aggregate is dominant, and can be determined from

$$\gamma_i = \frac{\beta_i}{1 - \sum_{j=1}^{i-1} \left[1 - \beta_i + b_{ij}\beta_j\left(1 - 1/\beta_j\right)\right]y_i - \sum_{j=i+1}^{n} \left(1 - a_{ij}\,\beta_i/\beta_j\right)y_j} \tag{2}$$

where a_{ij} and b_{ij} are the parameters representing interaction between each class of particles, i.e. loosening and wall effect, respectively. Both parameters are functions of the ratio between the diameter of class-i and -j particle.

The calculation above can be easily implemented in the computer program. Then, the variation of the packing density of n-class aggregate mixtures with various patterns of gradation can be figured out. The aggregate gradation with maximum packing density will be determined.

4   Strength-Based Gradation

It is an objective of this study to introduce the strength parameters into the determination of aggregate gradation. Thus, while packing density is the total fractional volume of aggregate in the concrete mixture, strength-based gradation (SBG) index is defined as the summation of the products between fractional volume and strength index of each class of aggregate. For n-class aggregate mixture, SBG index can be derived as

$$SBG = \sum_{i=1}^{n} \left(\text{fractional volume}\right)_i \cdot \left(\text{strength index}\right)_i$$

$$= \sum_{i=1}^{n} \left(\phi y_i \right) \left(S_i^c \right)$$

$$= \phi \sum_{i=1}^{n} y_i S_i^c \tag{3}$$

ϕ is packing density of the overall mixture, which can be calculated from eq. (1) as a function of the volume fraction (y_i), whereas S_i are the strength index of class-i aggregate. Because there are many strength parameters, strength index can be represented by 1-ACV, 1-AIV, or 1-MLAA. PLS is not proper to be strength index because it is much larger than unity. c is the magnifying coefficient of the strength index. It is raised due to the different sensitivity of the strength indices and packing density to the SBG index, and can be evaluated from the experiment.

In laboratory, portland cement type I and ordinary river sand with fineness modulus of 2.74 were used for making four standard mortars. The water/cement ratio was 0.20 and 0.24, whereas the sand/cement ratio was 1.5 and 2.0. These parameters can undoubtedly apply in the production of high-strength concrete. The standard mortars were blended with the three types of coarse aggregate used in the previous study. The coarse aggregates had been classified regarding to their size before re-combining them to achieve the given gradation patterns, which are tabulated in Table 2. All gradation patterns are in the recommendation of ASTM C33. The maximum size of aggregate was varied in the first four patterns, whereas in the rest all sizes of aggregate were included with a dominated size, which its amount was double of the others. The ratio of paste volume to void content of compacted aggregate mixture (γ) was about 1.10. The polymer-based superplasticizer was applied to guarantee 110% ±10% of flow value, following the test method of DIN 1048, Part 1, Chapter 3.1.2. The concrete specimens were manufactured by using the conventional practice and cured under water until the day of testing. They were tested for their compressive strength, according to ASTM C39 at 28 days.

SBG indices, which calculate from various types of strength index, were expected to be linear functions of concrete compressive strength. Thus, the magnifying coefficient c was evaluated by performing nonlinear regression analysis. The concept of the least square method was applied on the residual between the measured normalized compressive strength by the compressive strength of standard mortar and the calculated one. It has been found that the best value of c for the correlation is 2.53, 1.89, and 2.09 for strength index computed from ACV, AIV, and MLAA, respectively. The significance of strength indices on SBG index is approximately twice that of packing density.

Table 2: Gradation patterns of coarse aggregate

Sieve Size		Cumulative Percentage Passing							
Metric	ASTM	Gradation Patterns							
(mm)	No.	No. 1	No. 2	No. 3	No. 4	No. 5	No. 6	No. 7	No. 8
25.40	1"	100	0	0	0	100	100	100	100
19.05	3/4"	75	100	0	0	60	80	80	80
12.70	1/2"	50	67	100	0	40	40	60	60
9.53	3/8"	25	33	50	100	20	20	20	40
4.75	No. 4	0	0	0	0	0	0	0	0

Table 3: Packing density and SBG indices of coarse aggregates

Limestone A	Gradation Patterns							
	No. 1	No. 2	No. 3	No. 4	No. 5	No. 6	No. 7	No. 8
Packing Density	0.6271	0.6115	0.5894	0.5677	0.6338	0.6281	0.6193	0.6195
SBG Index: ACV	0.2861	0.2971	0.3085	0.3281	0.2780	0.2808	0.2841	0.2977
: AIV	0.3561	0.3690	0.3807	0.3854	0.3465	0.3504	0.3573	0.3656
: MLAA	0.2291	0.2375	0.2393	0.2416	0.2227	0.2300	0.2350	0.2365

Basalt A	Gradation Patterns							
	No. 1	No. 2	No. 3	No. 4	No. 5	No. 6	No. 7	No. 8
Packing Density	0.5929	0.5766	0.5562	0.5384	0.5973	0.5893	0.5863	0.5900
SBG Index: ACV	0.3136	0.3338	0.3457	0.3592	0.2980	0.3075	0.3156	0.3284
: AIV	0.3972	0.4090	0.4130	0.4058	0.3860	0.3916	0.3999	0.4051
: MLAA	0.2629	0.2683	0.2690	0.2706	0.2570	0.2613	0.2630	0.2664

Granite A	Gradation Patterns							
	No. 1	No. 2	No. 3	No. 4	No. 5	No. 6	No. 7	No. 8
Packing Density	0.6174	0.6034	0.5820	0.5603	0.6201	0.6150	0.6120	0.6136
SBG Index: ACV	0.2927	0.3025	0.3104	0.3137	0.2838	0.2870	0.2963	0.2992
: AIV	0.3288	0.3405	0.3452	0.3507	0.3185	0.3286	0.3317	0.3317
: MLAA	0.2409	0.2484	0.2487	0.2489	0.2340	0.2387	0.2415	0.2458

With these magnifying coefficients, the SBG indices of aggregate mixture with different patterns of gradation can be computed. The packing density and SBG indices are tabulated in Table 3. SBG index calculated from ACV is in the range of 0.27 and 0.36, while that from AIV and MLAA is about 0.31-0.42, and 0.22-0.28, respectively. In contrast to packing density, SBG indices of all aggregate types increase when the maximum size of aggregate is reduced, or when the amount of large aggregate is lessened. It is because smaller aggregate particles seem stronger than the larger ones. This may be one of the reasons for the requirement of smaller maximum aggregate size to produce high-strength concrete in the mechanical viewpoint.

Although the packing density of basalt aggregate is the least owing to its undesirable particle shape, basalt aggregate, which is the strongest aggregate in this study, provides the best SBG indices. The linear relations between the normalized concrete compressive strength by the compressive strength of standard mortar at 28 days and the SBG indices are shown in Fig. 4. The concrete compressive strength varies from 1.15 to 1.43 times that of the standard mortar. The variation from the regression is less than 5% for SBG calculated from ACV, 6% from MLAA, and 7% from AIV.
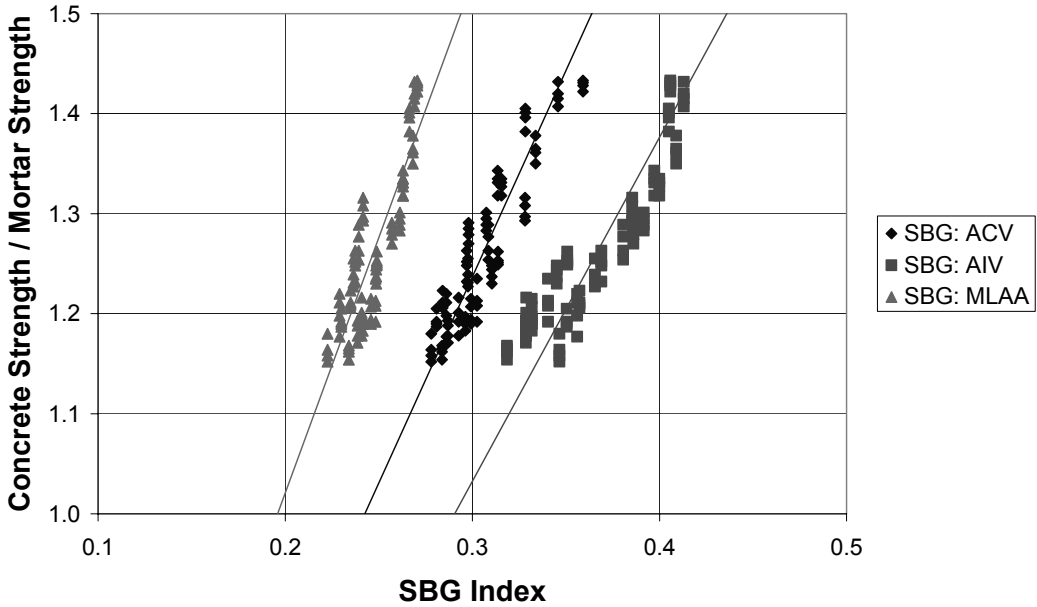
Fig. 3 Normalized concrete compressive strength against SBG indices

5   Application to Mix Design

SBG index integrates both physical features and mechanical properties via the parameters of packing density and strength index. With the magnifying coefficient, its relation to the ratio of concrete strength to mortar strength is linear. Therefore, it can be a parameter indicating the potential of aggregate for producing high-strength concrete. Selection of aggregate source or quarry can be done by using this basis.

Furthermore, SBG index can be applied as a tool for concrete mix design. Regarding to strength of aggregate, the aggregate gradation is determined readily. The amount of mortar or binder can be determined so that it corresponds to the cavities between the aggregate. However, such amount must be typically increased by 5% for covering every aggregate particle with a layer of binder, and providing workability of concrete mixture [13]. So, to account on this offset, another experiment was performed. The concrete mixes in section 4 were reproduced by varying the ratio of paste volume to void content of compacted aggregate mixture (γ) from 0.89 to 1.56. The relation between concrete strength divided by mortar strength and γ could be obtained. Fig. 4 is the interaction diagram for SBG index computed from ACV. It can be seen that the optimum γ is about 1.18 when SBG index is

0.280. It shifts gradually and becomes 1.07 when SBG index is 0.370. This change may be because the aggregate mixture with high value of SBG index will form an effective skeleton to transfer the internal forces when the concrete specimen is loaded. And the required amount of binder to coat around aggregate particles is then reduced. Similar interaction diagrams were achieved for SBG index computed from AIV and MLAA. These charts are useful to determine the amount of mortar or binder when one of SBG indices is specified.
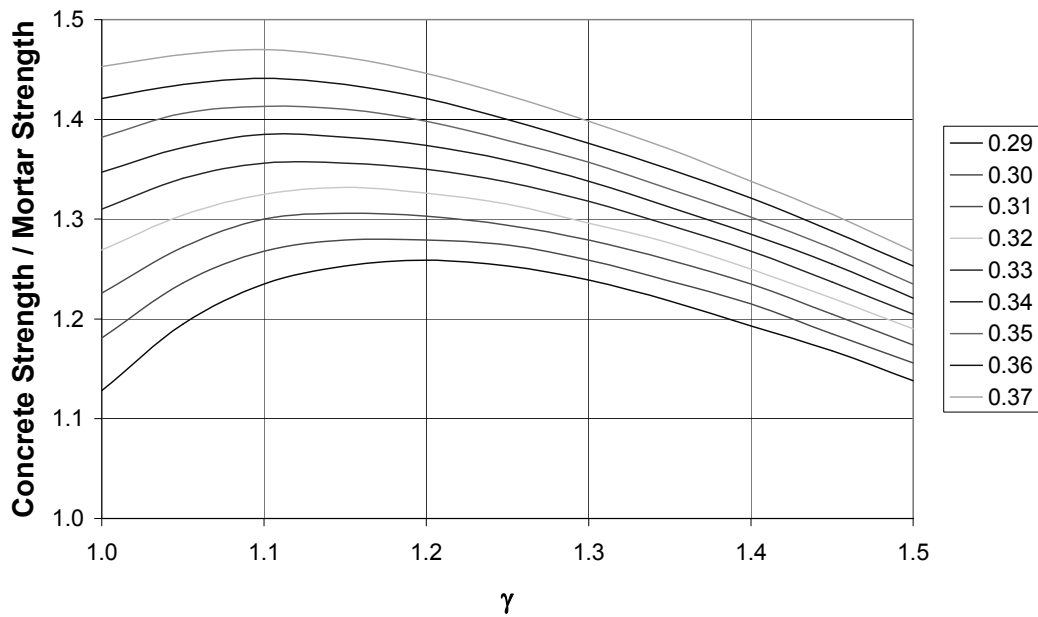
Fig. 4 Interaction diagram for SBG index computed from ACV
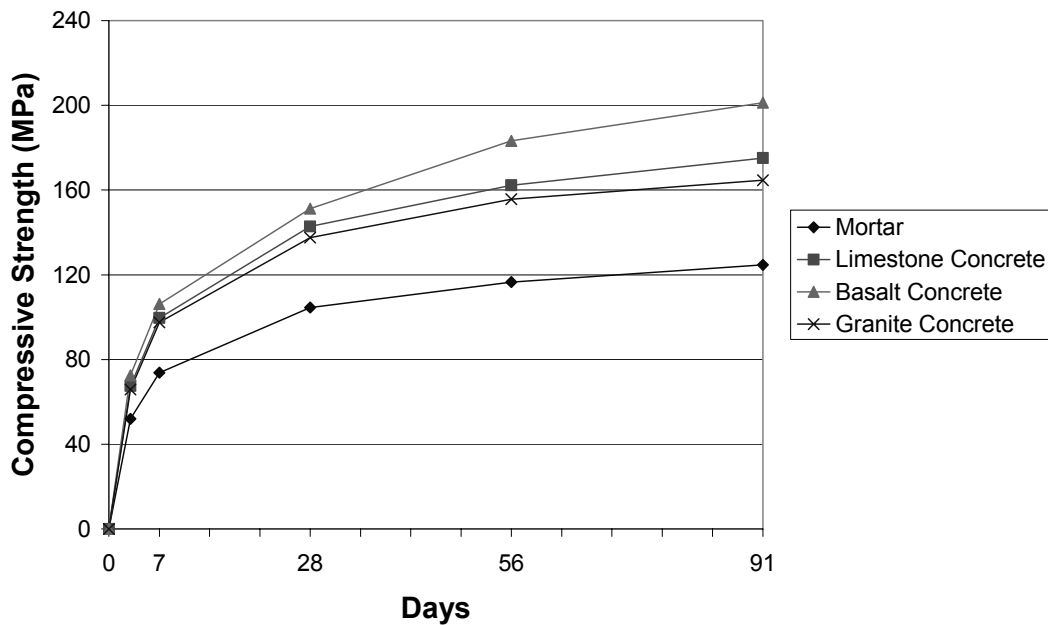
Fig. 5 Strength development of ultra-high-strength concrete and mortar

To be an example for mix design of ultra-high-strength concrete, an ultra-high-strength mortar had been proportioned with water/cement ratio of 0.16, sand/cement ratio of 1.5, and 10% silica fume. By using the conventional practice, the mortar compressive strength at 28 days was 104.6 MPa. This mortar was mixed with limestone, basalt and granite aggregate with the SBG index calculated by using ACV equal to 0.3416, 0.3627 and 0.3248, respectively. The strength development is shown in Fig. 5. It can be seen that all of them provided compressive strength higher than 100 MPa after 7 days. Compressive strength of concrete with basalt aggregate reaches 150 MPa at 28 days and exceeds 200 MPa at 91 days.

6   Conclusion

In this paper, the idea of a new parameter reflecting the effective volume of strong aggregate particle in concrete mix, called *strength-based gradation* (SBG), has been presented. Based on the work accomplished, the following conclusion can be drawn:

1)   The properties of aggregates with different size are not uniform. Aggregate strength increases with size reduction due to the removal of internal defects along process. However, small aggregate particle tends to be flat and elongated, causing low value of packing density.

2)   SBG index is defined as sum of the products between packing density and strength index of each class of aggregate. With the magnifying coefficient, SBG index relates linearly to concrete compressive strength.

3)   The SBG concept is useful for selection of aggregate source as well as for concrete mix design. The aggregate gradation is composed based on strength concern. And, the optimum amount of mortar or binder can be determined.

4)   With this concept, ultra-high-strength concrete with compressive strength higher than 150 MPa at 28 days and exceeding 200 MPa at 91 days can be obtained by using the conventional practice.

8   References

[1] Lecomte, A.; Thomas, A.: Caractere fractal des melanges granulaires pour betons de haute compacite. In: Materials and Structures 25, No. 149, pp. 255-264, 1992.

[2] de Larrard, F; Sedran, T.: Optimization of ultra-high-performance by the use of a packing model. In: Cement and Concrete Research 24, No. 6, pp. 997-1009, 1994.

[3] Goltermann, P; Johansen, V.; Palbol, L: Packing of aggregates: an alternative tool to determine the optimal aggregate mix. In: ACI Materials Journal 94, No. 5., pp. 435-443, 1997.

[4] Neville, A.M.: Aggregate bond and modulus of elasticity of concrete. In: ACI Materials Journal 94, No. 1, pp. 71-74, 1997.

[5] Baalbaki, M; Baalbaki, W.; Sarker, S.L.: A comparative study of mechanical properties and microstructure of high performance concretes containing natural and artificial aggregates. In: Proc. of symposium on utilization of high strength concrete, Vol. 2, Norway, 1993.

[6] Giaccio, G.; Rocco, C.; Violini, D.; Zappitelli, J.; Zerbino, R.: High-strength concretes incorporating different coarse aggregates. In: ACI Materials Journal 89, No. 3, pp. 242-246, 1992.

[7] Chang, T.P.; Su, N.K.: Estimation of coarse aggregate strength in high-strength concrete. In: ACI Materials Journal 93, No. 1, pp. 3-9, 1996.

[8] de Larrard, F.; Belloc, A.: The influence of aggregate on the compressive strength of normal and high-strength concrete. In: ACI Materials Journal 94, No. 5, pp. 417-426, 1997.

[9] Nagahama, H.; Yoshii, K.: Fractal dimension and failure of brittle rocks. In: International Journal of Rock Mechanics, Mining Science and Geomechanics Abstracts 30, No. 2, pp. 173-175. 1993.

[10] Revnitsev, V.I.: We really need a revolution in comminution. In: Proc. of the 16th International Mineral Processing Congress, 1988.

[11] ISRM: Suggested method for determining point-load strength test. In: International Journal of Rock Mechanics, Mining Science and Geomechanics Abstracts 22, No. 1, pp. 51-60, 1985.

[12] de Larrard, F.: Concrete Mixing Proportioning, E&FN Spon, London, 1999.

[13] Domonem, P.L.J.; Soutsos, M.N.: An approach to the proportioning of high-strength concrete mixed. In: Concrete International 39, No. 10, pp. 26-31, 1994.

Part 7:

Material Modelling and Prediction

K. van Breugel
Prof.Dr., Full professor and director
Micromechanical Lab.
Faculty of Civil Engineering and Geosciences,
TU Delft
Delft, The Netherlands

Y. Guang
Dr.Msc, Senior Researcher
Magnel Laboratory for Concrete Research
Ghent University
Ghent, Belgium

Analyses of hydration processes and microstructural development of UHPC through numerical simulation

Summary

Mixtures for Ultra High Performance Concrete are generally made with a very low water-cement ratio (w/c), even as low as 0.2. The lower the w/c, the lower the percentage of cement that can react with water. In spite of a low degree of hydration, very high strength values can be achieved. What counts is the intensity with which hydrating particles are clued together. In this paper it will be shown how the evolution of the strength can be correlated to the total contact area between solid particles. This correlation was recently established for traditional mixtures with the numerical simulation program HYMOSTRUC3D. The main features of the model will be explained. The model shows how high strength values can be obtained at a low degree of hydration of the cement. This (well-known) fact will be discussed in view of optimisation of UHPC mixtures. The potential of advanced numerical simulation programs in optimisation studies will be outlined as well.

Keywords: *Microstructure, numerical simulation, ultrasonic pulse velocity*

1   Introduction

In the past high performance concrete has often been the synonym for high strength concrete. In line with that perception ultra high performance concrete became the synonym for ultra high strength concrete. Strength, however, is only one of the characteristics that determines whether a concrete can be called a high performance concrete. Besides mechanical properties, like strength and stiffness, also other parameters determine the performance of the concrete like workability, durability, recycleability and energy consumption. Concrete is a high performance concrete if a particular set of pre-defined criteria can be fulfilled within narrow limits. These criteria may include high or ultra high strength. But a concrete with a moderate strength, but at the same time a high resistance against aggressive agents, can also be denoted as high performance concrete. From the materials science and concrete technology point of view the discussion about terminology boils down to the more fundamental question how a predefined performance of the concrete can be accomplished. In the past the answer to this question required a lot of experience and

a tedious experimental process of trial-and-error. Many developments in concrete technology have been realised in this traditional way. It was well understood at that time that the basis of materials performance goes back to the properties of the microstructure, or even nano-structure of the material. However, the complexity of cement-based systems was so high that experience, engineering judgement and experiments played a key-role in new developments. More recently it has been endeavoured to develop a more fundamental research strategy whereby the engineering properties are directly related to the microstructural properties of the material. Both advanced experimental techniques and the increasing computation power of modern computers have given this new strategy an enormous push. In this contribution the potential of microstructural models for understanding and optimisation of cement-based materials will be demonstrated. The focus of attention will be on the modelling of the microstructure and the correlation between typical properties of a virtual microstructure and the experimentally obtained information of the real microstructure.

2   Evolution of materials properties - Traditional concepts

In the past the evolution of materials properties has always been expressed as a function time. From the engineering point of view this is understandable. The site engineer is interested in the time at which the scaffolding can be removed or the prestress can be applied. For a given mixture the evolution of the materials properties can be described mathematically quite accurately, provided that the curing temperature does not deviated too much from an arbitrary chosen reference temperature (for example 20°C or a semi-adiabatic temperature regime). In the practice the actual curing temperature almost always deviates from such a reference temperature. To allow for the effect of the actual curing temperature on the evolution of the materials properties, the maturity concept was launched [1]. The maturity of the concrete is often expressed in "degree-Celsius-hours". It represents the area below the temperature curve, measured from a certain reference temperature. The idea behind the maturity concept is: same maturity = same strength. In the last two decades a number of maturity rules have been proposed. The basis of the maturity concept is, in essence, strongly phenomenological, and does not deal directly with the origin of the evolution of material properties. An exception must be made for the maturity concepts presented by Powers [2] and Hansen [3]. In their concepts maturity is identical to *degree of hydration*.

Precursors of microstructural models for strength development are the strength-porosity models and the gel-space ratio concept. In the porosity models the strength is related to the capillary porosity of the cement paste. With increasing hydration the capillary porosity decreases and the strength increases. It is noticed that the capillary porosity P_{cap} can be represented as a function of the degree of hydration α according to:

$$P_{cap}(\alpha) = \frac{\left(\dfrac{\omega - 0.3375\,\alpha}{\rho_w}\right) C + V_{air}}{\left(\dfrac{\rho_w}{\rho_{ce}} + \omega\right) C + V_{air}} \qquad (1)$$

with ω the water-cement ratio, C [gr] the cement content, ρ_w and ρ_{ce} the specific mass [gr/cm^3] of the water and the cement, respectively, and V_{air} the initial air content (v/v). From eq. (1) it can easily been seen that the capillary porosity is a linear function of the degree of hydration α.

According to Powers [4] the strength of cement paste, mortar and concrete can be related to the gel-space ratio. The gel-space ratio $X(\alpha)$ is defined as the quotient of the volume of the gel, V_{gel}, and the total volume of the paste *minus* the volume of the still unhydrated cement. In formula form:

$$X(\alpha) = \frac{V_{gel}(\alpha)}{V_{air}(\alpha) + V_{capw}(\alpha) + V_{gel}(\alpha)} \tag{2}$$

In the gel-space ratio concept the strength $f_c(\alpha)$ is related to the gel-space ratio $X(\alpha)$:

$$f_c = f_0 * X(\alpha)^3$$

(3)

where f_0 is the intrinsic strength of the paste. The intrinsic strength f_0, i.e. the strength of the capillary pore-free cement paste, varies from about 200 MPa for ordinary cement [5] up to 600 MPa for hot pressed cement pastes [6]. For the intrinsic strength of mortar a value of $f_0 = 180...342$ MPa is applicable with a mean value of 290 MPa and a standard deviation of 68 MPa [7].

In both the strength-porosity concept and the gel-space ratio concept the parameters to which the strength is related can be described as a function of the degree of hydration. For the relationship between strength and degree of hydration follows the general format hold [8]:

$$f_c(t) = f_{max} \frac{\alpha(t) - \alpha_0}{1 - \alpha_0} \tag{4}$$

in which f_{max} is the fictitious maximum strength in case of complete hydration ($\alpha = 1.0$) and α_0 the critical degree of hydration below which the strength is zero. The parameter f_{max} in eq. (4) is comparable with the parameter f_0 in the gel-space ratio concept in the sense that the parameter represents a typical intrinsic strength of the cement paste.

The concepts for describing the evolution of the materials properties presented in this section are all based on changes in *volume concentrations* of individual components in the cement paste. They do not consider the evolution of the microstructure *explicitly*. For that reason these models are not suitable for in-depth research of the microstructure and of the correlation between the microstructure and the material properties. For that purpose *microstructural models* are required.

3   Microstructural models

3.1   Main features of recent microstructural models

On reaction of cement with water hydration products are produced. These hydration products, viz. ettringite, calcium silicate hydrates and calcium hydroxide, are the structural elements of a spatial network that fixes the position hydrating cement particles within the hydration cement paste. Typical pictures of a cement paste in the early stage of hardening are shown in Figure 1. The strength of the paste can be assumed to be a function of the number of contact points between elementary species [9,10]. Quantification of these contact points through numerical modelling is, in essence, what microstructural models are actually aiming for. Microstructural models that are of interest in this respect are the NIST model [11], the model developed by Navi et al. [12], the DUCOM system launched by researchers from Tokyo University [13] and the HYMOSTRUC model [14]. The last three mentioned models have in common that they consider the cement particles as spheres between which contacts gradually form with progress of the hydration process. After a short presentation of the NIST model the HYMOSTRUC model will be discussed in more detail.
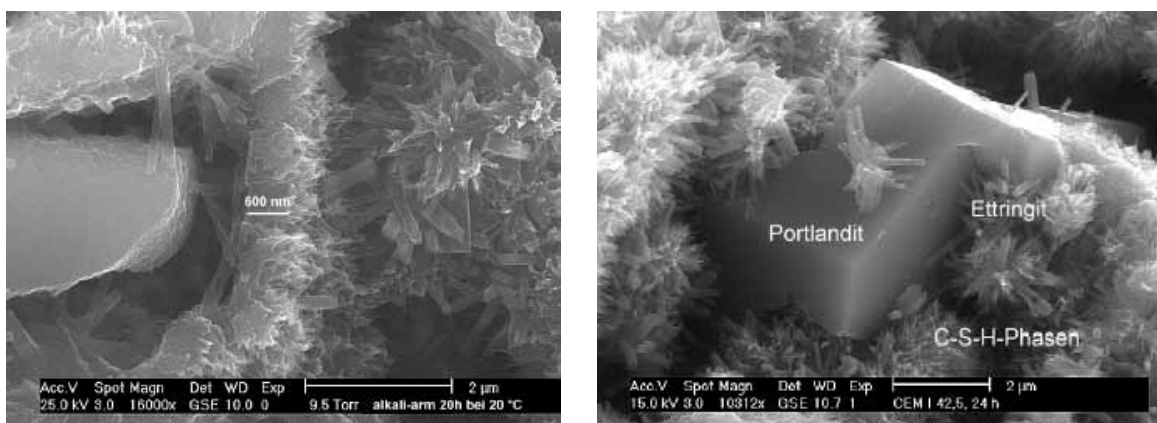
Figure 1:   Microstructure hydrating cement paste after 20 hours (left) and 24 hours
              (right) hydration *(courtesy M.R. de Rooij).*

3.2   Pixel model - NIST

In the NIST model the formation of interparticle contacts is accomplished through continuous precipitation of reaction products in the form a unit cells, or pixels. The size of one pixel is 1 μm^3. For a representative volume of cement paste a volume of about 200^3 μm^3 is needed. Adopting smaller pixels would result in a substantial increase of the computation time, which might be undesirable from the practical point of view. It has been shown that with the NIST model the evolution of the hydration process and of the porosity can be predicted quite accurately. Either the degree of hydration or the porosity can subsequently be used for predicting the evolution of the mechanical properties. More complicated is the prediction of the permeability, since the latter quantity strongly depends on the connectivity of the pores. This connectivity and the size of the smallest pore that can be simulated depend on the

256

adopted pixels size. This means that the size of the smallest pore is of the same order of magnitude as the pixel size.
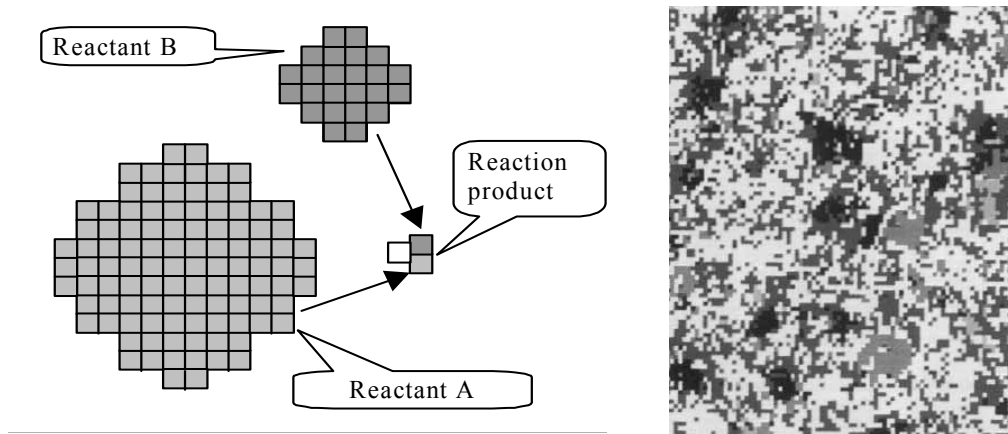
Figure 2: Basic idea of the pixel model (left) and a typical microstructure composed of 1μm^3 pixels (right) *(Courtesy: D.P. Bentz)*

3.3 The Delft model - HYMOSTRUC

In the Delft model, called HYMOSTRUC, the acronym for Hydration, Morphology and Structure formation, cement particles are considered as spheres. Particles are assumed randomly distributed in the cell (Figure 3, left). On reaction with water the cement particles growth in outward direction, while making contact with adjacent particles. The adjacent particles, which might still
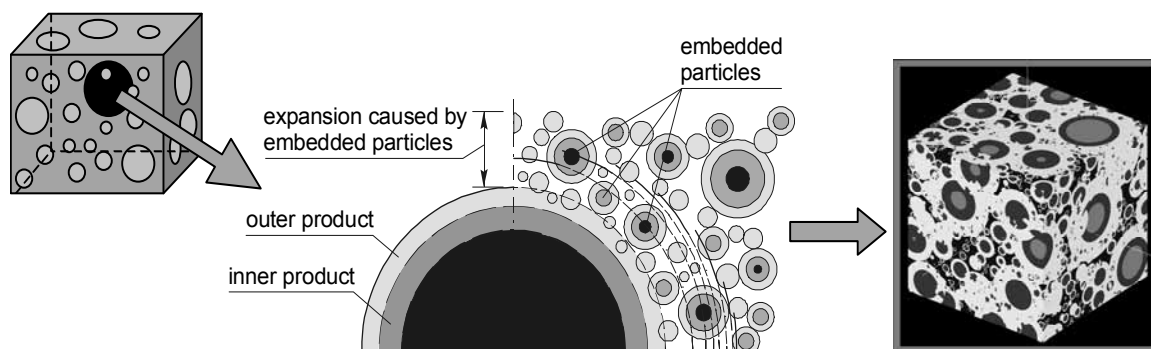
Figure 3: Simulated microstructure of cement paste. Left: cell. Middle: growth process and embedding of cement particles. Right: Cube with 200 μm rib size. W/c = 0.3. α = 0.75.

be hydrating themselves, will gradually become embedded in the outer shell of the growing particles. The resulting growth process is described with a mathematical series [14]. Figure 3

shows a microstructure, simulated with the latest version of the HYMOSTRUC3D program. From this microstructure the pore structure has been deduced by removing the solid phase, i.e. the still anhydrous cement cores and the gel. The resulting pore structure exhibits typical features, of which its irregularity is the most obvious one. The main features of the model have been presented extensively elsewhere [15].

4 From microstructure to mechanical properties

4.1 Evolution of interparticle contacts versus ultrasonic pulse velocity

One possibility to check the reasonable of microstructural development through formation of interparticle contacts between growing spheres exists in a comparison of the calculated degree of connectivity between hydrating particles and the measured ultrasonic pulse velocity. In a fresh paste an ultrasonic signal has to travel through a volume of water in which cement particles are dispersed. In that stage the speed of the sound will be determined predominately by the liquid phase. As soon as the particles become connected the speed of the sound through the system will change. A sharp increase of this speed is to be expected when the particles form a continuous path from one side of the sample to the other. Schematically this is shown in Figure 4. The picture represent a cement paste, w/c = 0.45, at a degree of hydration α = 0% (left) and α= 2.7% (right). The latter value was calculated to be the smallest degree of hydration for which a fully connected path of solid particles was formed. Figure 5 shows a more complete picture of the evolution of the calculated fraction of total solid and connected solid, respectively, and of the measured ultrasonic pulse velocity. The evolution of the total capillary porosity is presented as well. The trends of the calculated connected solid and the measured USPV correlate quite well. From this it can be inferred that the concept of microstructural development through a mechanism of growing spheres seems to make sense. Furthermore it is
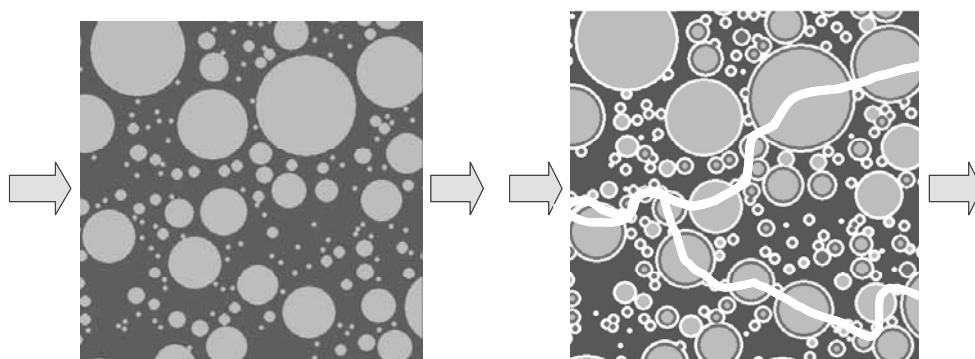
Figure 4:   Development of a connected path of solid particle. Degree of hydration a = 0% (left) and 2.7% (right) (after Ye Guang [15]).
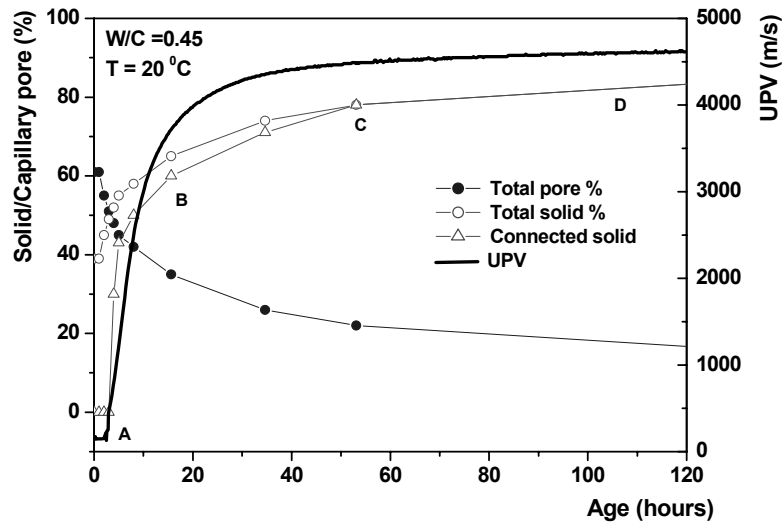
Figure 5: Evolution of the calculated amount of total solid and connected solid and capillary porosity (left axis) and of the measured ultrasonic sound velocity (right axis) (after [15]).

noticed that what actually counts in view of reaching solid percolation is the *formation of contacts between solid particles*. The *nature* of the solid particles as such, i.e. whether it is reactive cement particle or inert material, is not relevant.

4.2   Mechanical properties

4.2.1   Strength as function of "bridge volume"

Since the increase of the calculated interparticle contacts correlates well with the increase of the ultrasonic pulse velocity, it was considered conceivable that these interparticle contacts would also correlate well with the increase in strength. Figure 6 shows schematically the evolution of the interparticle contacts as assumed in the HYMOSTRUC model. Shortly after the initial stage particles become connected and form clusters (Figure 6b). After this the clusters become connected by bridge particles (Figure 6c). With progress of the hydration process the clusters become more intensively connected. From this concept of gradual formation of interparticle contacts two microstructural parameters can be deduced, viz. the *embedded cement volume* and the *bridge volume*. The embedded cement volume is defined as the amount

of reaction products and unreacted cement that is located inside the outer products of larger particles. The bridge volume is the total volume of bridge particles in the paste.
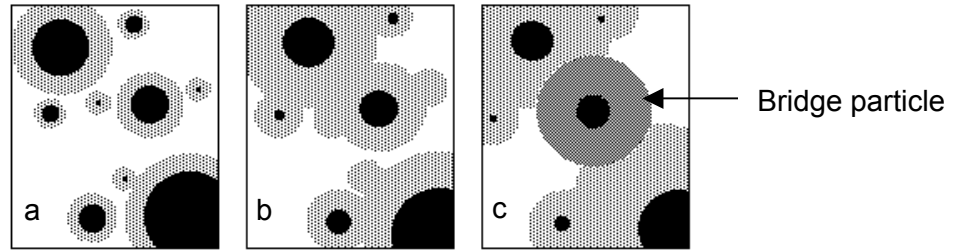
Figure 6: Subsequent stages in the formation of the microstructure (after Lokhorst [16])

In order to act as a bridge, a bridge particle should be larger than a certain minimum size. This size is related to the thickness of the outer shell of the "free" particle (Figure 7). The *bridge criterion* states that the diameter D of the bridging particle must be b times the thickness S of the outer shell of the free particle. The factor b is called the *bridge length factor.* Based on an extensive parameter study Lokhorst [16] found that a bridge particle should have a diameter of about 1 to 3 times the shell thickness of the free particle. Thus the bridge length factor ranges between 1 and 3.
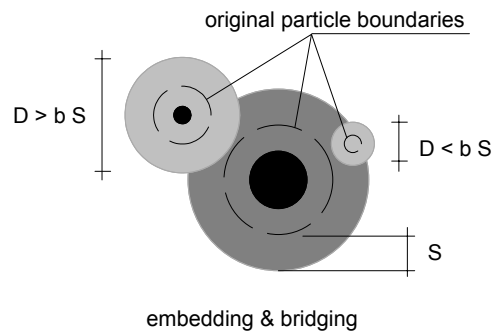
Figure 7: Schematic presentation of bridge criterion principle. A particle can act as a bridge if its diameter D is larger than the product of the bridge length factor b and the thickness of the outer shell of the free particle [16].

Both the embedded cement volume and the bridge volume are indicators of the intensity with which growing spheres are connected with each other. Assuming that more interparticle contacts imply a higher strength, these parameters are considered to exhibit a correlation with the evolution the strength of cement paste and concrete. This hypothesis has been put to the test by van Breugel et al. [14,17] and Lokhorst [16]. Figure 8 shows the compressive strength of concrete mixtures made with w/c = 0.36 to 0.7 as a function of the degree of hydration (left) and of the calculated bridge volume (right). The figure shows that, whereas the relationship between strength and degree of hydration still exhibits a significant effect of the water-cement ratio, the effect of the water-cement ratio is much less pronounced in the relationship between strength and bridge volume. From the latter finding it is inferred that the bridge volume is a more or less unique strength parameter.
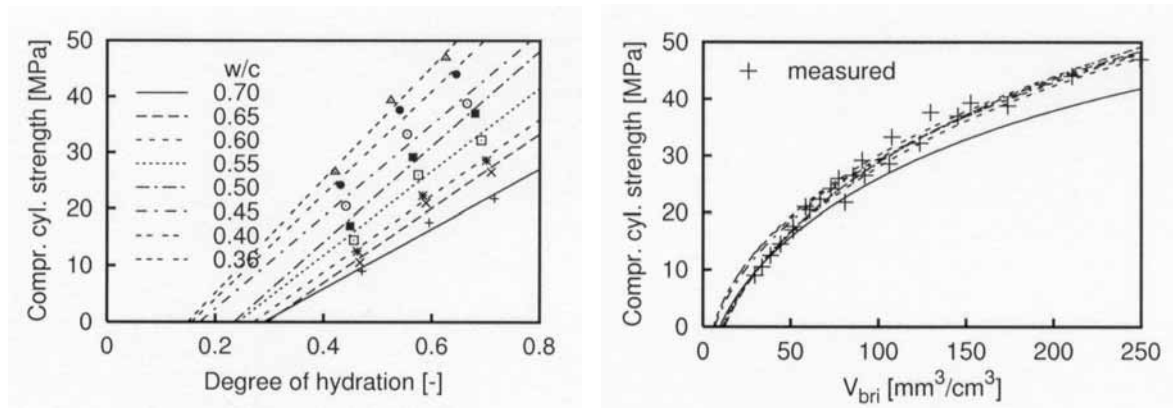
Figure 8: Compressive cylinder strength as a function of the calculated degree of hydration (left) and, for the same concrete mixtures, the bridge volume V_{bri} (right) [17].

4.2.2 Shear modulus as function of interparticle contact area

From the virtual microstructure simulated with the HYMOSTRUC model an even more universal microstructural parameter can be deduced, viz. the interparticle contact area. An interparticle contact area is defined as the smallest disk-shape area by which two particles are connected. Schematically this is shown in Figure 9-left. With the HYMOSTRUC model the summarized contact area per unit of paste volume can be determined. The hypothesis is that this summarised contact area is correlated to the strength and stiffness of the cement paste. To check the reasonableness of this hypothesis the shear modulus G of mixtures with w/c 0.35, 0.5 and 0.6 has been measured and presented as function of the calculated contact area. Figure 9, right, shows that there is a strong correlation indeed between the contact area and the shear modulus. The correlation seems to be hardly effected by the water-cement ratio. This indicates that the contact area is a more or less unique microstructural parameter to which mechanical properties can be related.
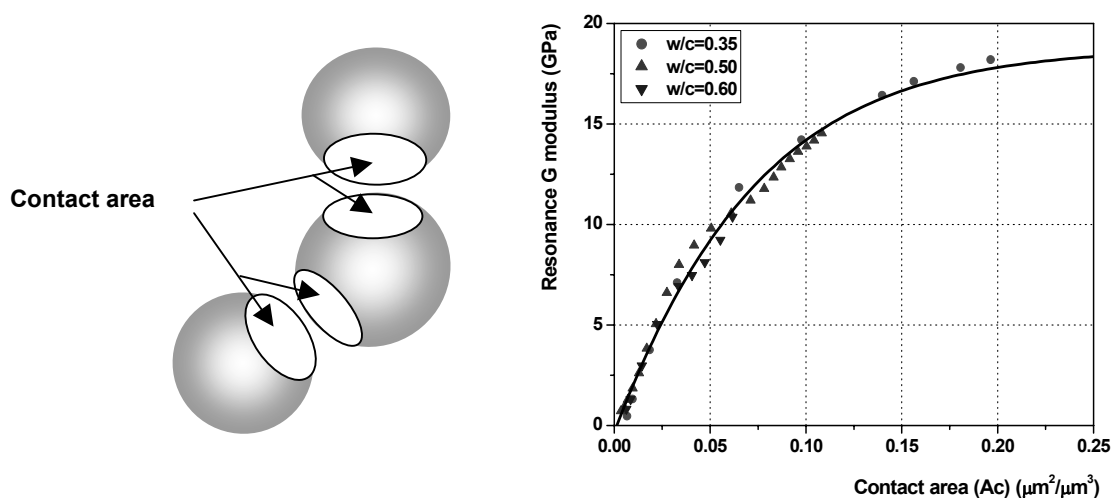
Figure 9: Concept of interparticle contact area (left) and relationship between calculated contact area and resonance G modulus (right).

5 Discussion, Comments and Conclusions

5.1 Mechanical properties as function of microstructural parameters

The microstructure of cement-based materials is the basis for the materials properties. With advanced microstructural models it is possible to generate virtual microstructures, which mimic some features of the real microstructure. In this contribution the reasonableness of the assumption that the mechanical properties of cement-based systems are a function of the intensity with which cement particles are mutually connected was investigated. This intensity of interparticle contacts is determined by the w/c, the degree of hydration and the particle size distribution of the powder. In case of a low w/c and a dense packing of the particles, the volume of hydration product needed to "glue" the particles is less than in case of a poor particle packing. Microstructural models, like the HYMOSTRUC model presented in this paper, allows us to quantify microstructural parameters with the engineering properties like ultrasonic pulse velocity, compressive strength and resonance shear modulus. From the good correlation between the properties of the virtual microstructure and the real microstructure it was concluded that representing the microstructure as a system of growing and connected spheres makes sense.

5.2 Predicting the performance of blended powders

It is noticed that the microstructural parameters that were deduced from the virtual micro-structure are geometric in nature. In the model the strength and stiffness are supposed to be determined by the "glue" with which the solid particles are connected with each other, but not by the nature of the solid particles. From the geometrical point of view unreacted cement particles may be replaced by inert particles, as long as there is enough reactive material for production of the required volume of "glue". In this context it is remarked that in low w/c mixtures a large amount of cement will remain unhydrated. Figure 10 shows indicatively the maximum degree of hydration that is reached under practicles circumstances as a function of the w/c. Even in traditional mixtures with w/c between 0.4 and 0.5 up to 30% of the cement will remain unhydrated.
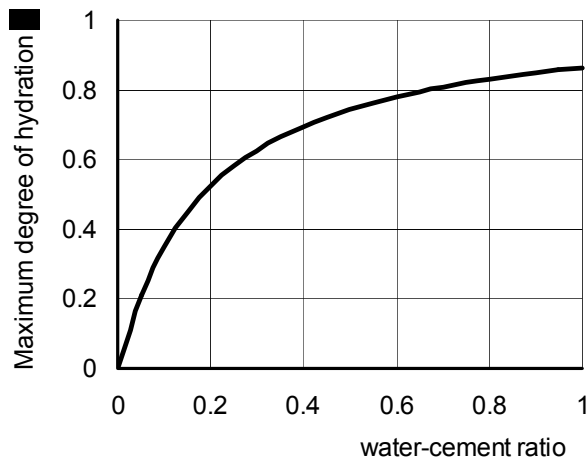
Figure 10: Indicative values for the maximum degree of hydration as function of w/c (after [18])

The lower the w/c, the more cement will remain unhydrated. In these mixtures there is room for replacement of the relative expensive cement by other, may be inert, powders. Microstructural models can be used for optimisation of these blended cements.

5.3 Towards multi-parameter judgement of high performance concrete

The qualification "Ultra High Performance" does not only refer to the strength and stiffness of the material, but also to the durability, the economy and energy consumption of the raw materials. Advanced microstructural models allow us to perform multi-criteria optimisation studies of cement-based systems in which all these parameters are addressed. The focus of this paper was on the modelling of mechanical properties. In another study it was shown that the HYMOSTRUC3D model could also be used for predicting the pore structure and the permeability of cement pastes [15]. This option is crucial for predicting transport phenomena and durability-related processes. Estimations of the effect of inert fillers on the mechanical and physical properties can be supported with numerical simulation of the performance of virtual microstructures. Thus the mixture can be optimised in view of its technical performance on the one hand and its ecological and economic performance on the other hand, supposed that ecological and economic data of the individual mixture components are available.

6   References

[1] Carino, N.J.; Maturity functions for concrete. Proc. RILEM-Symposium on Concrete at Early Ages, Paris, Vol. I, pp. 123-128, 1982.

[2] Powers, T.C.; Properties of cement paste and concrete. Proc. 4th Int. Symp. on the chemistry of Cements, Washington, pp. 577-609, 1960.

[3] Hansen, T.C.; Physical composition of hardened Portland cement paste. ACI-Journal, pp. 404-407, 1970.

[4] Powers, T.C.; Studies of the physical properties of hardened Portland cement paste. Part 1-9, ACI Journal, 1946-1947.

[5] Locher, F.W., Richartz, W., Sprung, S.; Erstarren von Zement - Teil I: Reaktion und Gefugeentwicklung. Zement-Kalk-Gips, Nr. 10, pp. 435-442, 1976.

[6] Roy (1973)

[7] Fagerlund, G.; Relations between the strength and degree of hydration or porosity of cement paste, cement mortar and concrete. Research Report, Lund, 51 p., 1987.

[8] Laube, M.; Werkstoffmodell zur Berechnung von Temperaturspanningen in massigen betonbauteilen im jungen Alter. Braunschweig, Germany, Technischen Universität Carolo-Wilhelmina: 251 p., 1990.

[9] Budnikov, P.P., Strelkov, M.I.; Some recent concepts on Portland cement hydration and hardening. In: Structure of Portland cement paste and concrete. ACI SP 90, pp. 447-464, 1966.

[10] Bache, H.H.; Model for strength of brittle materials built up of particles joined at points of contact. In: Journal of American Ceramic Society, Soc. 53 (12), 654-658, 1970.

[11] Bentz, D.P.; Three-Dimensional computer simulation of Portland cement hydration and microstructure development. In: Journal of American Ceramic Society, 80 (1) (1997) 3-2 1997

[12] Navi, P., Pignat, C.; Simulation of effects of small inert grains on cement hydration and its contact surfaces. In: The modelling of microstructure and its potential for studying transport properties and durability, Eds. Jennings et al., NATO ASI Series E, 304, 227-241, 1996.

[13] Meakawa, K., Chaube, R., Kishi, T.; Modelling of concrete performance – Hydration, microstructure formation and mass transport. E&FN SPON, London, 1999.

[14] Breugel, K. van; Simulation of hydration and formation of structure in hardening cement based materials. Delft University Press, Delft, 1991.

[15] Guang, Y.; The microstructure and permeability of cementitious materials. PhD Thesis, Delft University Press, Delft, 186 p. 2003.

[16] Lokhorst, S.J.; Deformational behaviour of concrete influenced by hydration-related changes of the microstructure. Research Report TU Delft, 1998.

[17] Breugel, K. van, Guang, Y., Smilauer, V.; Numerical Modelling of Microstructure Development and Strength of Cementitious Materials. In: Finite Elements in Civil Engineering Applications, Ed. Max. A.N. Hendriks et al., Tokyo, pp. 141-148, 2002.

[19] Mills, R.H.; Factors influencing cessation of hydration in water cured cement pastes. In: Structure of Portland cement paste and concrete. ACI SP 90, pp. 406-424, 1966

Jürgen Adolphs,

Porotec GmbH

Hofheim, Germany

Andreas Schreiber

Porotec GmbH

Hofheim, Germany

Microstructural Characterisation of Ultra-High Performance Concrete

Summary

In this paper an ultra-high performance concrete (UHPC) provided by Department of Structural Engineering University of Kassel is investigated regarding its microstructural features. In particular porosity measurements with mercury porosimetry, surface area determination with nitrogen sorption, density with helium pycnometry and finally water vapour sorption were conducted. Compared to normal hardened cement paste porosity is strongly reduced and specific surface area is very low. Compared to a fully hydrated cement paste of OPC with w/c =0.4 there are almost no pores observed in the nanoporous range with pore sizes up top 100nm. During the density measurement the kinetics were recorded. Most surprising are the water vapor sorption results, since they exhibit an isotherm whith a triangular hysteresis shape which can be attributed to the presence of tobermorite like csh gel with pore widths of approx. 2nm.

Keywords: *ultra-high performance concrete, hardened cement paste, porosity, mercury intrusion, specific surface area, nitrogen sorption, density, helium pycnometry, water vapor sorption*

1   Introduction

Ultra-high performance concrete (UHPC) exhibits outstanding mechanical features with a compressive strength around 180 to 230 N/mm². UHPC can be processed in the over a wide range from earth-moist to self-compacting. It is produced in conventional mixing plants like precast plants with sufficient mixing effect. Although the production is time and cost intensive, the final product is a high tech material of highest strength and durability. The investigated UHPC specimen was the M1Q provided by the Department of Structural Engineering University of Kassel. The composition and properties are published in [1], with the difference that no steel fibres were incorporated. The composition data are: cement CEM 52,5R HS-NA (733 kg/m³), sand (1008 kg/m³), microsilica (230kg/m³), quartz I (183 kg/m³), vol.% of fines < 0.125mm (405 l/m³), plasticiser (28.6 kg/m³), water (161 l/m³). The water cement ratio was w/c = 0.23, considering the water content of the plasticiser the water binder ratio is w/b = 0.19,. and the slump value was 55cm. The published values for the compressive strength were determined with steel fibres and reach values between 148 and 163 MN/m² and were enhanced after 2 days heat curing at 90°C to values between 184 and

206 MN/m². Due to the composition and carefully manufacturing process no capillary pores are formed. This reduced transport capability leads to improved resistance against chloride diffusion, carbonization, frost and frost/de-icing salt attack features.

2   Experimental

The provided UHPC M1Q was crashed in small particles down to a size of millimetres. The employed equipment in the POROTEC lab consists of mercury intrusion porosimeter low pressure PASCAL 140 and high pressure PASCAL 440 (Thermo Electron), working with pressures up to 400 Mpa. Further a SORPTOMATIC 1990 (Thermo Electron) was used for the nitrogen sorption measurements and a Pycnomatic 200 (POROTEC) for the Helium density measurements. At least the water vapor sorption isotherm was measured with a dynamic vapor sorption apparatus DVS1 (SMS Ltd).

The PASCAL porosimeters work pressure – volume controlled, that means a next mercury intrusion step is only proceeded when the volume is in equilibrium with constant pressure, which is different to older techniques when the pressure drops while the volume is increased. The helium pycnometer is temperature controlled within 0.01°C. The pressure transducer measures the absolute pressures and corrects automatically every measurement with respect to the atmospheric pressure. In this instrument the helium is first introduced to the reference chamber and then released to the sample chamber, avoiding any contamination of the reference chamber and providing a preferable one-way penetration of the helium gas. In this case the helium needs only to diffuse into the porous sample in order to determine the displaced volume from the equilibrium pressure. On the other hand the path from the sample to the reference chamber always needs diffusion into the material at higher pressure and then in the final state diffusion out of the sample. Particular for this investigated UHPC this is no longer to neglectable, since the diffusion rates are slow. The pycnomter is connected to a computer and a special software allows to record the pressure data. By this way the kinetics of the diffusion of helium can be observed and studied.

The water vapor sorption apparatus DVS1 rapidly measures uptake and loss of moisture by flowing a carrier gas at a specified relative humidity (RH) over a sample (1mg - 1.5g) suspended from the weighing mechanism of a Cahn D-200 ultra-sensitive recording microbalance. A schematic of a DVS automated gravimetric sorption system is shown in Figure 1.
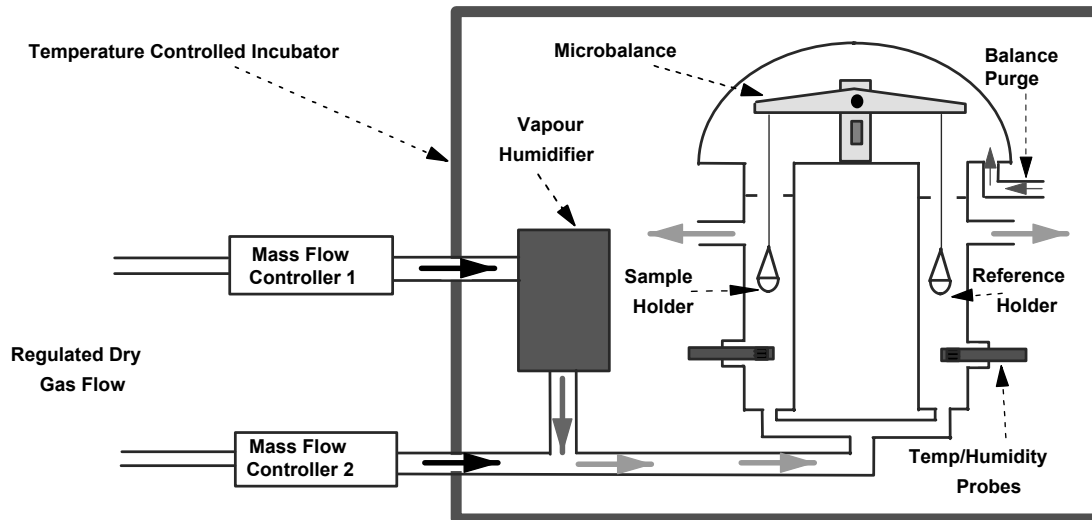
Figure 1:   Schematic of the water vapor sorption analyser DVS 1 from SMS Ltd..

The main DVS instrument systems are therefore housed in a precisely controlled constant temperature incubator with a temperature stability of ±0.1°C. This ensures a good instrument baseline stability as well as accurate control of the relative humidity generation. The required relative humidities are generated by accurately mixing dry and saturated vapour gas flows in the correct proportions using mass flow controllers. Humidity and temperature probes are situated just below the sample and reference holders to give independent verification of system performance. The microbalance mechanism is very sensitive to sorption and desorption of moisture, therefore a constant dry gas purge to the balance head is provided to give the best performance in terms of baseline stability.

Samples were broken in small pieces of mm and cm size, bigger pieces were tested with the pycnometer, the smallest ones with 54mg with the DVS.

3   Results

In Figure 2 the water vapor sorption isotherm is plotted as the percentage of adsorbed water related to the dry mass. The starting point was chosen at 50%RH. There is still a hysteresis to observe down to low relative humidity like in normal hardened cement paste [2]. The triangular shape of the isotherm is similar to these of tobermorite like calcium silicate hydrate (CSH) gel. From theoretical considerations and computer simulation [3] the morphology of this material must be of sheet like structure, which supports also the latest assumption about the morphology of CSH [4]. The pore width is about nm where water can already form capillary condensate at ca. 30% RH, indicated with steep decrease in the desorption branch. [5]

In Figure 3 the poresize distribution from mercury intrusion porosimetry (MIP) is shown, where r denotes the half width between two plates, since the pore model based for the calculations is a plate model, a better assumption for the CSH morphology of this material. Two maxima can be

detected, one at around 10 nm the other at 2 nm. Latter can be related to the mentioned CSH

Water Vapor Sorption on UHPC at 25°C
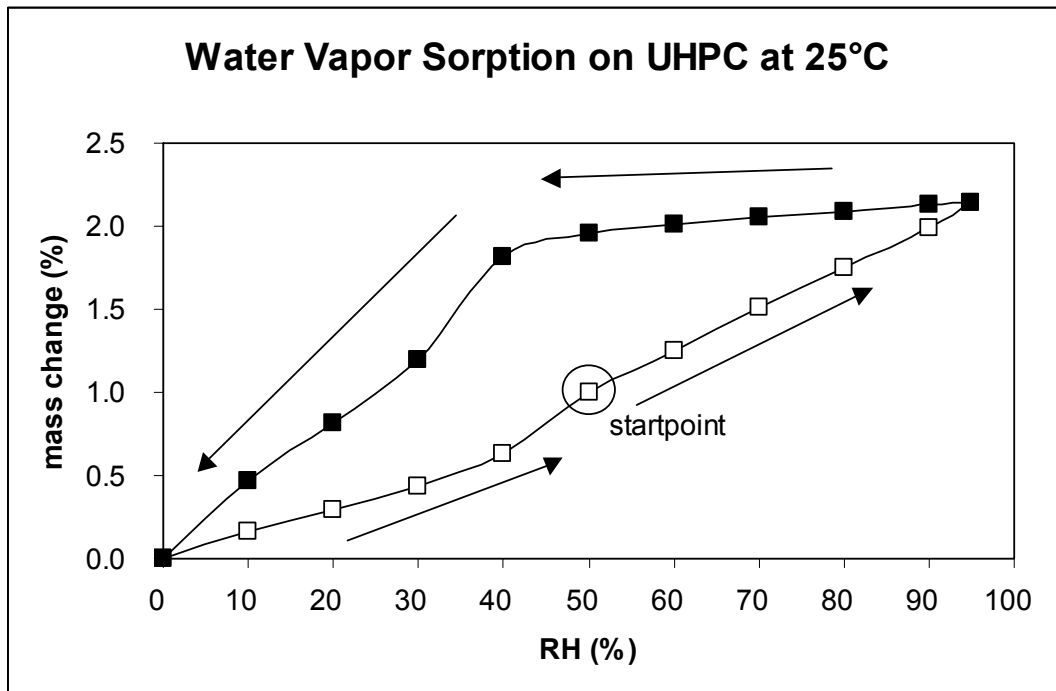
Figure 2:   Water vapor sorption isotherm of UHPC at 25°C, measured with a DVS1.

MIP Poresize Distribution of UHPC
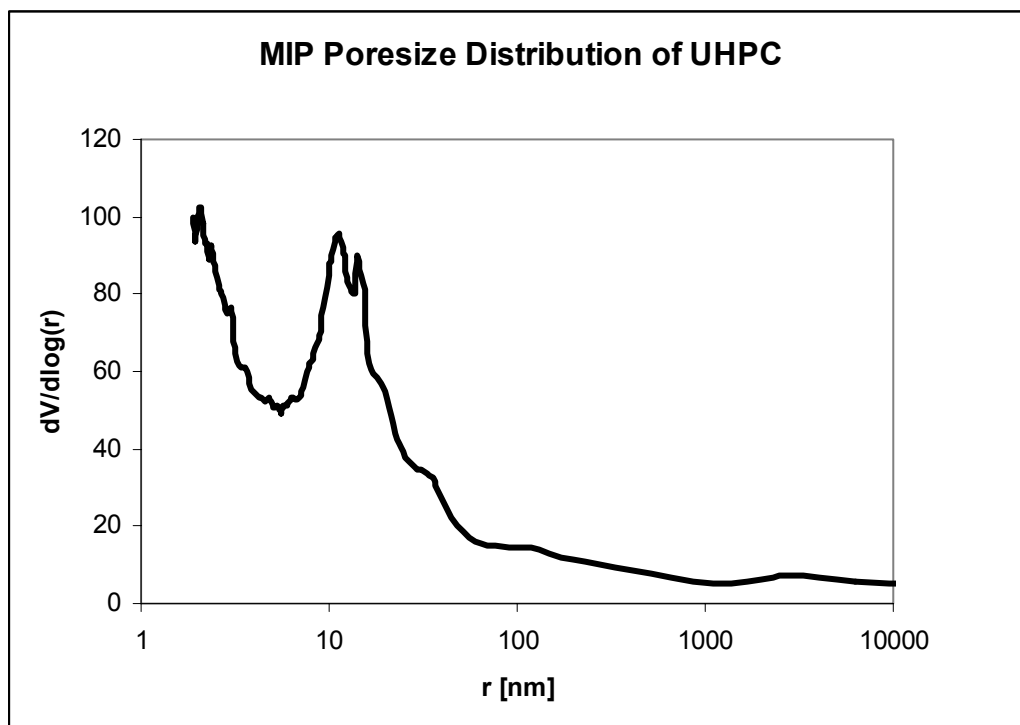
Figure 3:   Poresize distribution obtained with PASCAL porosimter with two pore half widthmaxima at 2nm and 10nm. Total number of intrusion data points was 910.

nanopores. The bulk density is 2.298 cm³/g and the apparent density including the pores is 2.439 cm³/g. The surface area was 7.04 m²/g and the porosity 5.781%.

The helium pycnometer measurements were proceeded with a sample mass of 67.6371g with the large sample and reference cells of 60ccm at 25°C. A series of various atmospheric equilibrium times were tested, ranging from 25 s, 45 s and finally 90 s. In Figure 4 is shown the development of the pressure over the time during such an experiment. In section A the pressure was released from the reference to the sample chamber. Between A and B the system was opened to atmospheric pressure and then closed. The following pressure build up, although very low of about 2 mbar respectively 200 Pa, may be caused due to helium release of the sample. Thus for the final experiment an extended atmospheric pressure equilibrium time of 90 seconds was chosen.

The density varies then from 2.4008 +/- 0.00044 ccm/g to finally 2.4173+/-0.00099 ccm/g. These values correlate very well with those of the apparent density obtained from mercury intrusion porosimetry.

From nitrogen sorption measurements very low specific surface areas were measured, compared to normal hardened cement paste [6].

For the sample preparation 4 different pre-treatments were chosen: a) 30 min evacuated at room temperature, b) 24 hrs evacuated at 70°C, c) 2 days evacuated at 150°C, d) 2 days evacuated at 250°C. The sample masses for each pre-treatment and experiment varied between 12 and 12.7 gm. In particular in the high temperature pre-treatment d) the formation of condensate on the glass walls of the sample holder was observed. This might be due to the evaporation of some organic constituents, since the condensate appeared to be in an oily consistence.

The specific surface areas according BET were for each pre-treatment are listed in Table 1:

Table 1

Pre-treatment	a) 30min evac.	b) 24hrs 70°C	c) 2d 150°C	d) 2d 250°C
Spec. surface area BET	0.86 m²/g	1.12 m²/g	1.50 m²/g	1.98 m²/g

At all the values are low, in particular they are lower than the specific surface area measured and computed from the mercury intrusion porosimetry. However, from the relatively low water vapor uptake a low specific surface area had to be expected. Although a specific surface from water vapor sorption measurements is not very meaningful, a number for comparison will be given: 16.04 m²/g according BET. This is by a factor 8 to 10 smaller compared to values of normal hardened cement paste. Interesting is that due to the extension of pre-treatment time and increase of the temperature an increase of the specific surface area was achieved.
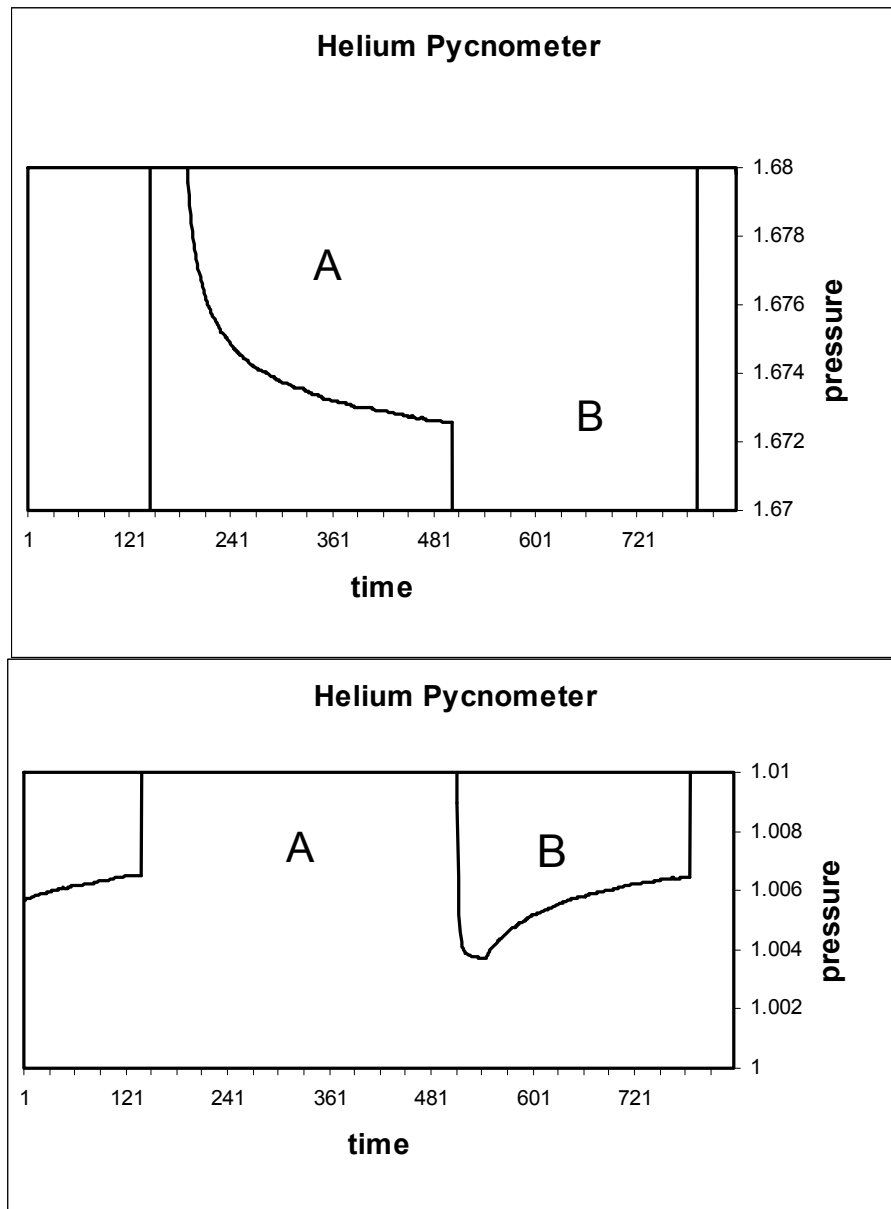
Figure 4: Pressure (bar) over time diagram (seconds) of the Helium Pycnometer measurement with an atmospheric equilibration time of 45 seconds shown in two parts of the pressure region. In A pressure is released from reference chamber into sample chamber. In B the pressure is released to atmospheric pressure and then the sample chamber is closed. Pressure increases.

4 Discussion

The presented results of the ultra-high performance concrete reveal that this material is compared to normal hardened cement paste much denser and a material with less porosity and a very specific surface area. Nevertheless, the material is porous and exhibiting pores in the 10nm region as well as CSH 2nm gel pores. The access to these pores by gas diffusion is restricted. Therefore this needs to be considerate in the preparation of experiments like sorption or diffusion, where standard time conditions may not be sufficient for the

achievement of data at equilibrium. The kinetic behaviour plays a dominant role in the microstructural investigation of UHPC. At all the microstructural data give support to a promising durability behaviour.

5　Acknowledgment

The authors appreciate gratefully the provision of the UHPC MQ1 material and discussions with Prof. Schmidt and Dipl.-Ing. Teichmann from the Department of Structural Engineering University of Kassel.

6　References

[1] Bornemann, R.; Schmidt, M.; Fehling, E.; Middendorf, B.: Ultra-Hochleistungsbeton UHPC – Herstellung, Eigenschaften und Anwendungsmöglichkeiten. In: Beton- und Stahlbetonbau 96, Heft 7, S. 458-467, 2001.

[2] Adolphs, J., Heine, P., Setzer, M.J.: Changes in Pore structure and Mercury Contact Angle of Hardened Cement Paste Depending on Relative Humidity. In: *Materials and Structures* Vol. 35, 477-486 2002.

[3] Churaev, N.V., Starke, G., Adolphs, J.: Description of Sorption including Capillary Condensation Hysteresis in Porous Bodies: I. Cylindrical and Slit Pores. In: *J. Colloid Interface Sci.* 221, 246-253 2000.

[4] Discussion with E. Gardener at Hal Taylor Symposium, Les Diblerets, Switzerland, June 2004.

[5] Adolphs, J. : The role of Nanopores in Concrete. In: Proceedings of the International RILEM Workshop 'Frost Resistance of Concrete' (eds. Setzer, Auberg, Keck), 45 – 52 (2002).

[6] Thomas, J.J., Jennings, H.M., Allen, A.J.: The Surface Area of Hardened Cement paste as Measured by Various Techniques. In: Concrete Sci. & Eng. Vol. 1, 45-64, 1999.

H. Taghaddos

M.Sc student Structural Engineering

University of Tehran,

Tehran, Iran

A. Pourmoghaddam

M.Sc student Structural Engineering

University of Tehran,

Tehran, Iran

F. Mahmoudzadeh

M.Sc student Structural Engineering

University of Tehran,

Tehran, Iran

M. Shekarchizadeh

Assistant Professor Structural engineering

University of Tehran,

Tehran, Iran

Prediction of Compressive Strength Behaviour in RPC with applying an Adaptive Network-Based Fuzzy Interface System

Summary

Intelligent computing tools such as artificial neural network (ANN) and fuzzy logic approaches are proven to be efficient, when applied individually to a variety of problems. Recently there has been a growing interest in combining both these approaches, and as a result, neuro-fuzzy computing techniques have evolved. This approach has been tested and evaluated in the field of signal processing and related areas. This paper presents the application of an adaptive neuro fuzzy inference system (ANFIS) to predict compressive strength behaviour of ultra high strength(UHSC) concrete specially Reactive Powder Concrete (RPC) considering mix design and curing conditions.

Keywords*: Ultra High Strength Concrete (UHSC), Reactive Powder Concrete (RPC), Adaptive Network-Based Interface Fuzzy System (ANFIS), Sugeno first order*

1 Introduction

Concrete with strength higher than 42 MPa is named High Strength Concrete (HSC). However, these days the technology of manufacturing Ultra High Strength Concrete (UHSC) improved the advantageous of HPCs. One of the most approachs of using UHPC is designing of smaller sections, which leads to lower dead weight allowing large pans.

Reactive Powder Concrete (RPC) represents concrete with a significant production procedure leading to produce UHSC. This type of concrete mostly has compressive strength 200-300 MPa. Sometimes this kind of concrecte has a non-structural application.

The high brittleness of UHSC is a most problem. The increase in the compressive strength decreases the ductility. This matter reduces the use of UHSC in structures. RPC increases the ductility of UHSC simultaneously. The homogeneity and isotropy of concrete is obtained by addition of Steel Micro Fibers(SMF). On the other hand improvement of microstructure is

obtained by a specific high heat treatment, which leads to the changing the nature of hydrated pruducts. However using an external pressure while the specimens are cured, the entrapped air is eliminated. These factors encourage the use of RPC in specified projects. The high cost of this concrete still is a weakness point in using RPC and as it is mentioned before this kind of concrete is used mostly in some non-structural projects.[1,2]

In this research, effect of different parameters on UHSC and specially RPC is investigated by using a new method named as Adaptive Network Based Fuzzy Interface System (ANFIS). And finally the effect of different parameters on the compressive strength trend is investigated.

2   Experimental works

The focus of our research is based on using RPC technology. In this kind of concrete, homogeneity is improved by using a powder concrete in which aggregates and traditional sand are replaced by ground quartz less than 300 microns in size. The high cement content of type 5 ordinary Portland cement, with different amount is used to achieve higher strength. Type 5 is used, to obtain wokability that occurs from

 Another significant characteristic is applying low water-cement ratio in the range of 0.11-0.20. Different amount of chemical admixtures are used to improve the workability of the fresh concrete in so low water-cement ratio. Moreover, High volume silica fume (SF) more than 20 percent, is used to work as the filler, increase the density. In addition some chemical reaction in the special curing condition occur.

In the present research, the cubic specimens are cured in a specific time duration and conditions. 7 days room temprature curing in the $20C^0$ water, 4 days steam curing in hot humid conditions ($90C^0$), 1 day in high pressure steam curing in hot-dry condition($200C^0$). The effect of compacting pressure applied during the molding stage to increase the density is investigated. Stainless steel micro fiber less than 3 mm length which are straight and smooth are also added to prevent the brittle behavior. The effect of different types of grading is investigated (Table1). As it's indicated in the table 1 no aggregate is used in type1. In some specimens polymer fiber is added to find their effect on the strength and the diffrent percentag of microfiber is also used. Briefly, all of these parameters can be seen in table 2.

Table1-Type of grading Aggraegate

	0- .125	.125-.250	0.25-0.5	0.5-1	1-2	2-4	4-5.6	5.6-6.3	6.3-8	8-9.5
type1	0.00	0.00	0.00	-----	-----	-----	-----	-----	-----	-----
type2	0.18	0.57	0.25	-----	-----	-----	-----	-----	-----	-----
type3	0.06	0.12	0.22	0.27	0.20	0.13	-----	-----	-----	-----
type4	0.02	0.05	0.09	0.11	0.00	0.05	0.22	0.00	0.24	0.21

Table 2- Mix properties and obtained strength

Mix no.	Cement	SF	W/CM	SP	MF	Polymer	Pressure	Grading	f (14 day)
	kg/m^3	%	%	%	kg/m^3	gr	Y/N	type	MPa
1	900	20	14	1.5	0	0	0	4	167
2	900	20	15	1.5	0	0	0	4	172
3	900	25	15	2.5	0	0	0	4	98
4	900	20	17	2.5	0	0	0	4	154
5	900	25	17	2.5	0	0	0	4	154
6	900	20	18	2.5	0	0	0	4	149
7	900	25	18	2.5	0	0	0	4	105
8	900	22.5	19	2.5	0	0	0	4	160
9	900	20	19	2.5	0	0	0	4	132
10	900	25	19	2.5	0	0	0	4	123
11	1750	20	10	1.5	0	0	0	3	200
12	1750	25	11	3	150	0	1	3	303
13	1750	30	11.5	3	150	0	0	3	136
14	1765	30	11.9	3	0	0	0	3	158
15	1900	25	11	3	75	0	0	2	218
16	1900	30	11	3	0	0	0	2	216
17	1900	30	11.5	3	75	0	0	2	228
18	1900	30	11.5	3	75	0	1	2	244
19	1900	30	11.5	3	75	0.9	1	2	231
20	1900	25	11.5	3	0	0	1	2	288
21	1900	30	11.5	3	75	0.95	1	2	259
22	1900	30	12	3	0	0	0	3	189
23	1900	30	13	3	0	0	0	2	262
24	1900	25	13	3	75	0	0	2	238
25	1900	25	13	3	75	0	1	2	273
26	1900	25	13	3	0	0.6	1	2	183
27	1900	30	17.5	3	75	0.6	1	2	209
28	1900	25	20	3	75	0.6	0	2	173
29	2008	30	12	3	150	0.9	0	1	247
30	2008	30	12	3	150	0	0	1	252
31	2010	30	12	3	150	1	0	1	249
32	2017	25	11.5	3	150	0	0	1	219
33	2017	30	11.5	3	150	0.9	0	1	200
34	2027	25	11	3	150	0	1	1	241
35	2055	30	13	3	75	0.6	1	1	258
36	2105	25	10.5	3	75	0	1	1	259
37	2113	25	10	3	75	0	0	1	222
38	2182	30	10	2.5	0	0	0	3	146

3   Neuro-fuzzy model

Neuro-fuzzy modeling refers to the way of applying various learning techniques developed in the neural network literature to fuzzy modeling or to a fuzzy inference system (FIS). The basic structure of a FIS consists of three conceptual components: a rule-base, which contains a selection of fuzzy rules; a data-base which defines the membership functions (MF) used in the fuzzy rules; and a reasoning mechanism, which performs the inference procedure upon the rules to derive an output (Figure. 1). FIS implements a nonlinear mapping from its input space to the output space. This mapping is accomplished by a number of fuzzy if-then rules, which each describes the local behavior of the mapping. The parameters of the if-then rules (antecedents or premises in fuzzy modeling) define a fuzzy region of the input space, and the output parameters (also consequents in fuzzy modeling) specify the corresponding output. Hence, the efficiency of the FIS depends on the estimated parameters. However, the selection of the shape of the fuzzy set (described by the antecedents) corresponding to an input is not guided by any procedure (Ojala, 1995[3]). But the rule structure of a FIS makes it possible to incorporate human expertise about the system being modeled directly into the modeling process to decide on the relevant inputs, number of MFs for each input, etc. and the corresponding numerical data for parameter estimation. In the present study, the concept of the adaptive network, which is a generalization of the common back-propagation neural network, is employed to tackle the parameter identification problem in a FIS.[4]
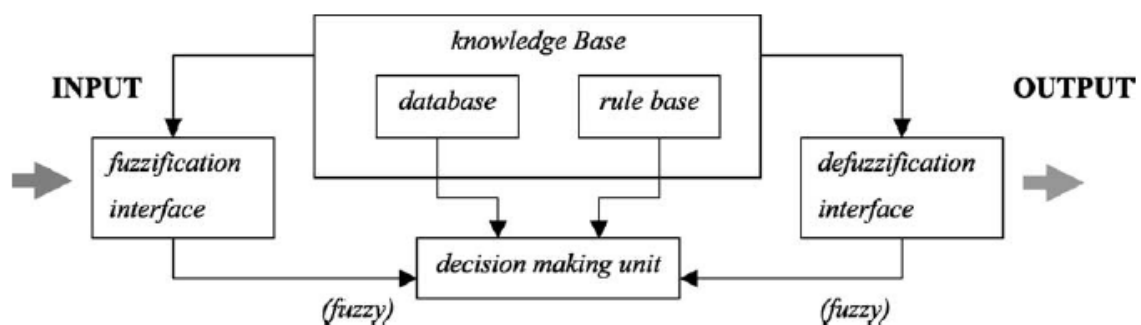
Figure1. Fuzzy Inference System with crisp output.

An adaptive network is a multi layered feed forward structure whose overall output behavior is determined by the value of a collection of modifiable parameters. More specifically, the conFigureuration of an adaptive network is composed of a set of nodes connected through directional links, where each node is a process unit that performs a static node function on its incoming signal to generate a single node output. The node function is a parameterized function with modifiable parameters. It may be noted that links in an adaptive network only indicate the flow direction of signals between nodes and no weights are associated with these links. Readers are referred to Brown and Harris (1994)[7] for more details on adaptive networks. Jang (1993)[7] introduced a novel architecture and learning procedure for the FIS that uses a neural network learning algorithm for constructing a set of fuzzy if-then rules with appropriate MFs from the stipulated input–output pairs. This procedure of developing a FIS

using the framework of adaptive neural networks is called an Adaptive Neuro Fuzzy Inference system (ANFIS).[4]

3.1 ANFIS architecture

The general structure of the ANFIS is presented in Figure. 2. Selection of the FIS is the major concern when designing an ANFIS to model a specific target system. Various types of FIS are reported in the literature (e.g. Mamdani and Assilian, 1975[7]; Tsukamoto, 1979[8]; Takagi and Sugeno, 1985[9]) and each are characterized by their consequent parameters only. The current study uses the Sugeno fuzzy model (Takagi and Sugeno, 1985[9]; Sugeno and Kang, 1988[10]) since the consequent part of this FIS is a linear equation and the parameters can be estimated by a simple least squares error method.

| (a) | (b) |
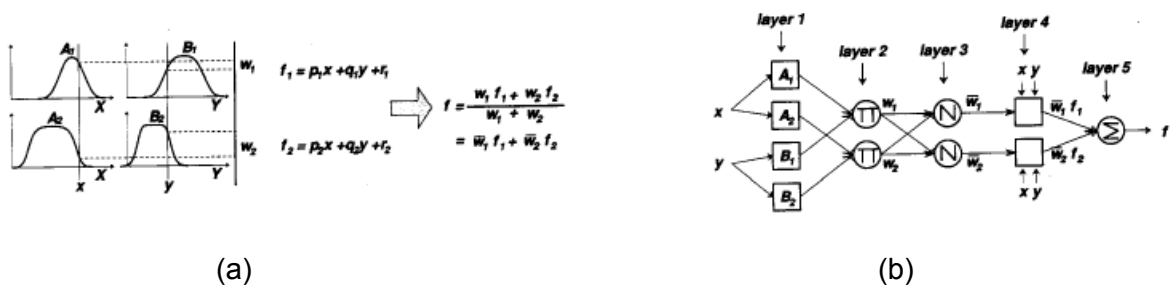
Figure. 2. (a) Fuzzy inference system. (b) Equivalent ANFIS architecture.

For instance, consider that the FIS has two inputs x and y and one output z: For the first order Sugeno fuzzy model, a typical rule set with two fuzzy if-then rules can be expressed as:

Rule 1: If x is A_1 and y is B_1; then $f_1 = p_1 x + q_1 y + r_1$

Rule 2: If x is A_2 and y is B_2; then $f_2 = p_2 x + q_2 y + r_2$

Where;

A_1, A_2 and B_1, B_2 are the MFs for inputs x and y respectively.

p_1, q_1, r_1 and p_2, q_2, r_2 are the parameters of the output function.

Figure. 2(a) illustrates the fuzzy reasoning mechanism for this Sugeno model to derive an output function (f) from a given input vector [x, y]. The corresponding equivalent ANFIS architecture is presented in Figure. 2(b), where nodes of the same layer have similar functions. The function of the ANFIS is as follows:

Layer 1: Each node in this layer generates membership grades of an input variable. The node output OP_i^1 is defined by:

$$OP_i^1 = \mu_{Ai}(x) \qquad for \ i = 1,2 \qquad or \qquad OP_i^1 = \mu_{Bi-2}(y) \qquad for \ i = 3,4 \qquad (1)$$

where x (or y) is the input to the node; Ai (or Bi_2) is a fuzzy set associated with this node, characterized by the shape of the MFs in this node and can be any appropriate functions that are continuous and piecewise differentiable such as Gaussian, generalized bell shaped, trapezoidal shaped and triangular shaped functions. Assuming a Gaussian function as the MF, the output OP_i^1 can be computed as,

$$OP_i^1 = \mu_{Ai}(x) = \exp(-(\frac{x - c_i}{a_i})^2) \tag{2}$$

where {ai, ci} is the parameter set that changes the shapes of the MF with maximum equal to 1 and minimum equal to 0.

Layer 2: Every node in this layer multiplies the incoming signals, denoted as Q, and the output OP_i^2 that represents the firing strength of a rule is computed as,

$$OP_i^2 = w_i = \mu_{Ai}(x)\mu_{Bi}(y), \qquad i = 1,2 \tag{3}$$

Layer 3: The ith node of this layer, labeled as N, computes the normalized firing strengths as,

$$OP_i^3 = \overline{w_i} = \frac{w_i}{w_1 + w_2}, \qquad i = 1,2 \tag{4}$$

Layer 4: Node i in this layer computes the contribution of the ith rule towards the model output, with the following node function:

$$OP_i^4 = \overline{w_i} f_i = \overline{w_i}(p_i x + q_i y + r_i) \tag{5}$$

where w is the output of layer 3 and {pi; qi; ri} is the parameter set.

Layer 5: The single node in this layer computes the overall output of the ANFIS as:[4]

$$OP_1^5 = Overal\ output = \sum_i \overline{w_i} f_i = \frac{\sum_i w_i f_i}{\sum_i w_i} \tag{6}$$

3.2 Estimation of parameters

The parameters for optimization in an ANFIS are the premise parameters {a_i; c_i}; which describe the shape of the MFs, and the consequent parameters {p_i; q_i; r_i}; which describe the overall output of the system. The basic learning rule of an adaptive network, the back-propagation algorithm (Rumelhart et al., 1986[11]), which is based on the gradient descent rule, can be successfully applied to estimate these parameters. However, Jang (1991)[12] argues that the gradient descent method is generally slow and is likely to get trapped in local minima. Jang has proposed a faster learning algorithm, which combines the gradient descent method and the least squares estimate (LSE) to identify parameters, as described below: The adaptive network has one output and is assumed to be

$$output = F(\vec{I}, S),$$

(7)

where $\vec{I}$ is the set of input variables and S is the set of parameters. If there exists a function H such that the composite function H+F is linear in some of the elements of S; then these elements can be identified by the least squares method. More formally, if the parameter set S can be decomposed into two sets

$$S = S_1 \oplus S_2,$$

(8)

(where $\oplus$ represents the direct sum) such that H+F is linear in the element S2; then applying H to Eq. (10),we have

$$H(output) = H \circ F(\vec{I}, S)$$

(9)

which is linear in the elements of S2: Now given values of elements of S1; the P training data can be plugged into Eq. (12) to obtain the matrix equation:

$$AX = B$$

(10)

where X is the unknown vector whose elements are parameters in S2: Let IS2I = M; then the dimensions of A; X and B are P * M; M * 1 and P * 1; respectively. Since P (number of training data pairs) is usually greater than M (number of linear parameters), this is an over-determined problem and generally there is no exact solution to Eq. (13). However, a LSE of X can be sought that minimizes the squared error $\|AX - B\|^2$.

From the ANFIS architecture presented in Figure. 2 it is observed that given the values of the premise parameters, the overall output can be expressed as linear combinations of consequent parameters. More precisely, the output f can be rewritten as,

$$f = \overline{w_1} f_1 + \overline{w_2} f_2 = (\overline{w_1} x) p_1 + (\overline{w_1} y) q_1 + (\overline{w_1}) r_1 + (\overline{w_2} x) p_2 + (\overline{w_2} y) q_2 + (\overline{w_2}) r_2$$

(11)

which is linear in the consequent parameters (p1; q1;r1; p2; q2 and r2). As a result, the total number of parameters (S) in an ANFIS can be divided into two such that S1 = set of premise parameters and S2 = set of consequent parameters. Consequently the hybrid learning algorithm, which combines the back-propagation gradient descent and least squares method, can be used for an effective search of the optimal parameters of the ANFIS. More specifically, in the forward pass of the hybrid learning algorithm, the node output goes forward until layer 4 and the consequent parameters are identified by the least squares method. In the backward pass, the error signal propagates backwards and the premise parameters are updated by gradient descent. As mentioned earlier, the consequent parameters thus identified are optimal under the condition that the premise parameters are fixed. Accordingly, the hybrid approach converges much faster since it reduces the dimension of the search space of the original back-propagation method. A detailed description of this algorithm can be found in Jang and Sun (1995)[13].

3.3 Defuzzification

It may be noted that the basic ANFIS takes either fuzzy inputs or crisp inputs, but the overall outputs are fuzzy sets. Therefore, a defuzzification strategy is needed to convert a fuzzy set to a crisp value. The crisp output is generally obtained using different defuzzification strategies (Brown and Harris, 1994[7]).The Takagi-Sugeno approach (Takagi and Sugeno,1985[9]) that is used in the current investigation, however, does not have an explicit Defuzzification procedure (Xiong et al., 2001[14]), or rather, it amalgamates two procedures, the logic decision and defuzzification procedures into one composite procedure.[4]

3.4 Modeling

There are no fixed rules for developing an ANFIS, even though a general framework can be followed based on previous successful applications in engineering. The goal of an ANFIS is to generalize a relationship of the form:

$$Y = f(X^n)$$

(12)

where X_n is an n-dimensional input vector consisting of variables $x_1, \ldots, x_n$ and Y is the output variable: In the present model, values of x_i include water-cement ratio and seven other investigated parameteres and the value of Y is the concrete compressive strength.

In the ANFIS development, the selection of appropriate input variables is very important since it provides the basic information about the system being modeled. The selected parameters in this model are water-cement ratio, percentage of super plasticizer and silica fume, amount of cement and polymer and steel micro fiber, type of grading, and whether fresh concrete is maintained under pressure at the molding stage or not.

Two important factor should be considered in assigning MFs to each input variable: data number and the importance of each parameter. For instance, three different values for the silica fume percentage (20%, 25%, 30%) are tested, thus a linear relationship in the silica fume-compressive strength space is assumed (figure 3(b)).

following equations should be satisfied if a linear relationship between one of the inputs and the output variable is assumed.

(13)

$$\frac{\partial C^*}{\partial x_i} = Cte$$

And we also know that:

$$C_r = P_{ri} \times x_i \qquad\qquad (14)$$

$$C^* = \overline{W}_r \times C_r$$

Where; x_i represents the ith input, $\overline{W}_r$ weight function of the rth rule, P_{ri} represents their correspond consequent parameter, C_r is the output of the rth rule, and C^* the final obtained output of the ANFIS, C indicates the real output.

By using chain rule following equations obtained:

(15)

$$\frac{\partial C^*}{\partial x_i} = \frac{\partial C^*}{\partial C_r} \cdot \frac{\partial C_r}{\partial x_i} + \frac{\partial C^*}{\partial \overline{W}_r} \cdot \frac{\partial \overline{W}_r}{\partial W_r} \cdot \frac{\partial W_r}{\partial \mu_{jr}} \cdot \frac{\partial \mu_{jr}}{\partial x_i} = \frac{\partial C^*}{\partial C_r} \cdot P_{ri} + \frac{\partial C^*}{\partial \overline{W}_r} \cdot \frac{\partial \overline{W}_r}{\partial W_r} \cdot \frac{\partial W_r}{\partial \mu_{jr}} \cdot \frac{\partial \mu_{jr}}{\partial x_i}$$

$$\Rightarrow \quad \frac{\partial \mu_{jr}}{\partial x_i} = 0 \qquad \Rightarrow \quad \mu_{jr} = Cte \qquad\qquad\qquad (16)$$

(a)   (b)
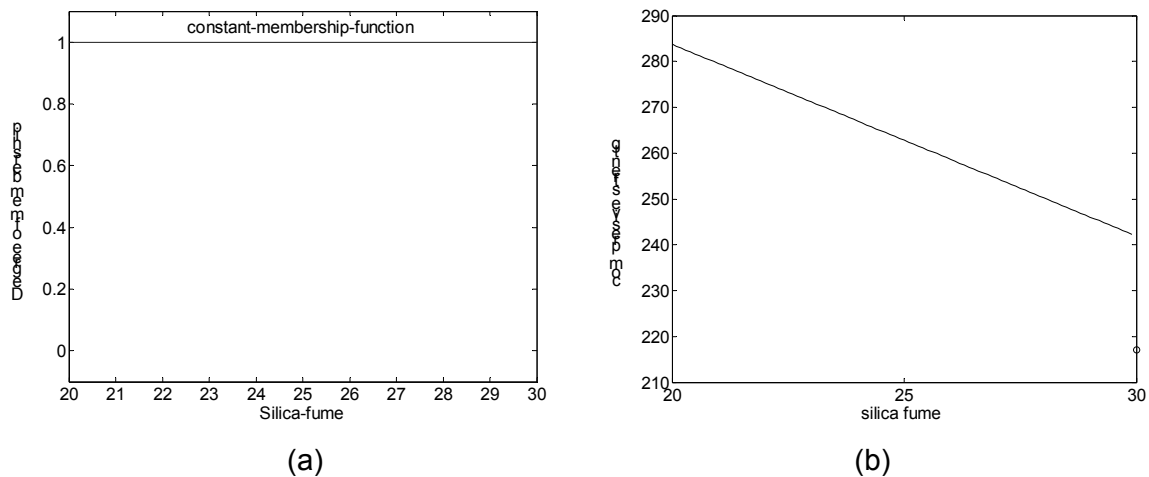
Figure 3- A constant membership function of a input variable (a)

and its linear relationship with the output variable (b)

So for a linear relationship between one of the inputs and the output variable, the input variable's membership function should be constant(figure 3 a and b).

Because of importance of water-cement ratio in relation to the other parameters and lack of data number; only water-cement ratio is partitioned and assumed a constant membership function and a linear relationship for seven other properties.

4   Results and discussions

An ANFIS method is used to optimize UHSC mix design which leads to approximate strength prediction. The effect of 8 investigated parameters in the trend of compressive strength in two cases of Very Low Water Cement Ratio (VLWCR) and Low Water Cement Ratio (LWCR) could be found from the consequence parameters (table 3). The value of this parameters for each input parameters, indicated it's influnces on compressive strength, Thus with this parameters , prediction of effect of input vriable is done.

Rule 1:   If w/c is low (VLWCR)   ;   then $f_1 = A_1$ (Cement) + A_2(SF)+ A_3(W/C)+
             A_4(SP)   + A_5 (MF)+ A_6 (Polymer)+ A_7 (Pressure)+ A_8 (Grading) +A_9

Rule 2:   If w/c is low (LWCR)   ;   then $f_2 = B_1$ (Cement) + B_2(SF)+ B_3(W/C)+
             B_4(SP)   + B_5 (MF)+ B_6 (Polymer)+ B_7 (Pressure)+ B_8 (Grading) +B_9

Table 3- Consequence parameters of laws in ANFIS

	Cement	SF	W/C	SP	MF	Polymer	Pressure	Grading	Constant coefficient
A	-0.3605	-15.15	-112.9	253.1	-0.8492	233.1	119.3	56.51	1707
B	-0.02128	-1.164	-1.139	-29.31	-0.0083	-80.73	5.305	-75.09	573.5

VLWCR and LWCR are defined by training initial membership function of water cement ratio(figure 4). Each of these cases corresponds to a law in ANFIS model. For instance, the degree of memebrship of W/C = 0.11 to VLWCR is about 0.35 and to LWCR is about 0.25.
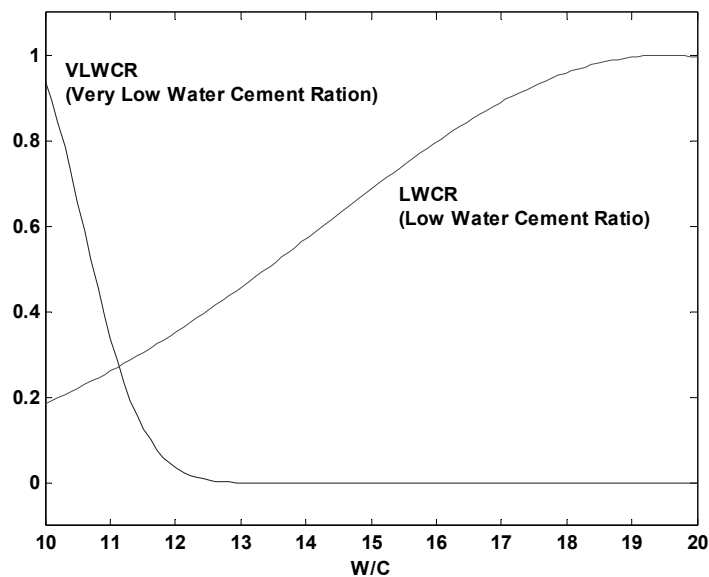
Figure 4: Degree of Membership of w/c (partitionining to low and very low W/C)

According to the obtained results, following conclusions are derived:

1. Decreasing of cement amount increases the compressive strength in VLWCR but it doesn't change the compressive strength in LWCR so much. So the optimum cement amount must be about 900 until 1200. Although the behavior of concrete is different in low and high volume cement, the Cement-Strength space has been devided only to one partition like 7 other parameters because lack of data. So the behavior of concrete in low and high volume cement can not be distinguished and it might make some numerical error in our prediction.

2. In VLWCR the strength rate is decreased by adding Silica fume more than LWCR. So the optimum amount of silica fume might be 20% or 25%.

3. In VLWCR decreasing of water cement amount increase the compressive strength much more than in LWCR.

4. Adding super plasticizer has a considering effect on improvement of compressive strength in VLWCR but in LWCR it has negative effect to some extent.

5. Albeit adding Steel micro fiber in VLWCR decreases the compressive strength, it nearly doesn't change the compressive strength in LWCR.

6. In VLWCR, using polymer fibers increase the compressive but in HWCR it is vise versa.

7. In VLWCR using compacting pressure has much more positive effect on the compressive than LWCR.

8. In VLWCR, increase of maximum size of aggregate has positive effect on compressive strength increase, but it has negative effect in LWCR.

It should be noted that this work is valid for UHSC and specially RPC. And because of lack of a linear realtionship is assumed that couldn't be percise thus, some error may be occured in the conclusions. To confirm and generalize these results, much more exprimental works should be conducted.

5   Acknowledgment

6   Reference

[1] Richard, P. and Cheyrezy, M.H. "Reactive Powder Concretes with High Ductility and 200-800 MPa Compressive Strength", Concrete Technology: Past, Present, and Future, Proceedings of the V. Mohan Malhotra Symposium, ACI SP-144, S. Francisco 1994, pp. 507-518. Editor: P.K. Mehta.

[2] Olivier Bonneau, Claude Poulin, Jerome Dugat, Pierre Richard, and Pierre-Claude Aitcin. "Reactive Powder Concrete: From Theory to Practice", Concrete International, Vol. 18, No. 4, April 1996, pp. 47-49.

[3] Ojala, T., 1995, "Neuro-Fuzzy systems in control". M Sc. Thesis, Tempere Univeristy of Technology, Tampere, Finland.

[4] P.C. Nayaka, K.P. Sudheerb, D.M. Ranganc, K.S. Ramasastrid,"A neuro-fuzzy computing technique for modeling hydrological time series", Journal of Hydrology 291 (2004) 52–66

[5] Brown, M., Harris, C., 1994. "Neuro-fuzzy Adaptive Modeling and Control", Prentice Hall.

[6] Jang, J.-S.R., Sun, C.-T., 1995. "Neuro-fuzzy modeling and control". Proceedings IEEE 83 (3), 378–406.

[7] Mamdani, E.H., Assilian, S., 1975. "An experiment in linguistic synthesis with a fuzzy logic controller", International Journal of Man-Machine Studies 7 (1), 1–13.

[8] Tsukamoto, Y., 1979. "An approach to fuzzy reasoning method". In: Gupta, M.M., Ragade, R.K., Yager, R.R. (Eds.), Advances in Fuzzy Set Theory and Application, North-Holland, Amsterdam, pp. 137–149.

[9] Takagi, T., Sugeno, M., 1985. "Fuzzy identification of systems and its application to modeling and control". IEEE Transactions on Systems, Man and Cybernetics 15 (1), 116–132.

[10] Sugeno, M., Kang, G.T., 1988. "Structure identification of fuzzy model". Fuzzy Sets and Systems 28, 15–33.

[11] A Rumelhart, D.E., Hinton, G.E., Williams, R.J., 1986. "Learning representations by back-propagating errors". Nature 323, 533–536.

[12] Jang, J.-S.R., 1991. "Rule extraction using generalized neural networks". In Proceedings of the fourth IFSA World Congress 4, 82–86.Volume for Artificial Intelligence.

[13] Jang, J.-S.R., Sun, C.-T., 1995. "Neuro-fuzzy modeling and control". Proceedings IEEE 83 (3), 378–406.

[14] Xiong, L.H., Shamseldin, A.Y., O'Connor, K.M., 2001. "A nonlinear combination of the forecasts of rainfall-runoff models by the first order Takagi-Sugeno fuzzy system". Journal of Hydrology 245 (1–4), 196–217.

Dr. Klaus Droll
Wilhelm Dyckerhoff Institut
Dyckerhoff AG
Wiesbaden, Germany

Influence of additions on
ultra high performance concretes – grain size optimisation

Summary

Inerte and reactive finely ground additions are particularly important for the performance in fresh (rheology, water demand) and in hardened ultra high performance concretes (mechanical and durability properties). The effects are primarily based on 3 fundamental mechanisms: Physical packing density optimisation, chemical structure optimisation (improvement of the binder matrix), optimised adhesion between cement matrix and aggregates (improvement of the interfacial transition zone).

The packing density was optimised by modelling and selection of suitable additions.

These optimisation mechanisms are demonstrated by electron microscopy of the interfacial transition zone, the reduction of water demand, and compressive strength development of ultra high performance concretes using different addition/cement mixes.

The production of concrete pipes is shown as an example for the practical use of ultra high performance concrete.

Keywords: *Ultra high performance concrete, addition, grain-size optimisation, modelling*

1   Introduction

The technology of ultra high performance concretes is based on the fundamental investigations on "reactive powder concretes" developed in the 1980s and 1990s in France/Canada [1] [2] [3]. The maximum grain size of these fine-grained concretes is smaller than 1 mm. The principles for these high performance concretes are optimised grain packings of the fine reactive and the non-reactive components as well as the harmonized hydraulic and puzzolanic processes. In the 1990s, the technology of ultra high performance concretes was expanded to coarser grain sizes [4], [5]. In principle, all ultra high performance concretes contain a high content of fine powder <250 µm and fitting coarse grains. The crucial optimisations are taking place in the fine grain size area only.

In this talk, the optimisation possibilities of concretes in the fine grained area by additions will be described (without consideration of fibers).

Firstly, some basic statements concerning the optimisation of grain packets, particularly the fine grain size distributions are being made. Secondly, some additions are presented contributing to the optimisation of the structure development of ultra high performance concretes. Finally, the effect of such optimisation procedures in the fine grain size area by reactive and non-reactive additions are presented by showing rheological properties of the fresh concrete as well as the performance of the hardened ultra high performance concrete.

2 Effects of additions

The fine components play an important role in high performance concretes. In particular, the fine powder - water matrix is responsible for the performance of the concrete system, both in the fresh concrete (workability = rheology, water demand of the concrete) and in the hardened concrete (structure, porosity, mechanical properties, durability).

Ultra high performance concretes have a dense microstructure which can be optimised at a very low water content. The following fundamental effects are responsible for this:

- High packing density particularly in the fine grain size area (physical optimisation)

- Hydraulic and pozzolanic reactions in the powder area (chemical optimisation)

- Improvement of the interfacial transition zone between cement stone matrix and aggregates (adhesion optimisation)

A dense, non-porous solid structure attains a high performance very rapidly due to the short diffusion paths at hydration, pozzolanic reactions and other physico-chemical reactions.

EN 206 covers two types of inorganic additions:

- Inert additions (type I): Suitable rock meals, pigments according to EN 12878 or inert powders with a European or national approval.

- Reactive, pozzolanic or latent-hydraulic additions (type II): Fly ashes according to EN 450, trass, microsilica, finely ground blast furnace slag, as well as other reactive additions with a European or national approval.

2.1 Applied meals - literature overview

In the literature many designs of ultra high performance concretes with various meals and their contribution to the performance of the concrete are described. Descriptive characteristic properties are the specific surface area and granulometry of the powders determined by laser scattering. Especially microsilica and quartz powders are used in ultra high performance concretes, recently other additions like fine fly ashes and finely ground blast furnace slag powders are also applied.

Table 1: *Overview of the most common additions in ultra high performance concretes - chemical and physical properties of the meals - completes [7]*

	Portland cement	Pit coal fly ash	Microsilica	Finely ground granulated blastfurnace slag CEM III/C-Microcement	Quartz meal
Content	[M.-%]	[M.-%]	[M.-%]	[M.-%]	[M.-%]
SiO_2	18 ... 24	40 ... 60	80 ... 99	30 ... 39	95 ... 100
Al_2O_3	4 ... 8	23 ... 24	0,5 ... 3,0	9 ... 18	0 ... 3
Fe_2O_3	1 ... 5	2 ... 16	0,1 ... 5,0	0,1 ... 1	---
CaO	61 ... 69	0,6 ... 8,5	0,7 ... 2,5	33 ... 48	0 ... 3
Average particle size [µm]	10 ... 25	10 ... 30	0,1 ... 0,5	0,1 ... 10	0,1 ... 100
Absolute density [kg/dm²]	3,0 ... 3,15	2,15 .. 2,45	2,22 ... 2,40	Ca. 2,9	2,63
Spec. Surface area [m²/g]	0,3 ... 0,6	0,3 ... 0,8	16 ... 22	0,8 ... 1,5	0,1 ... 10
Physical state	Powder	Powder	Powder	Powder	Powder

2.1.1 Microsilica (MS)

Finely dispersed silica, particularly microsilica, an addition obtained from the production of silicon and silicon alloys at high temperatures in the electrical arc is the best known fine addition with highly pozzolanic properties in high performance concretes. In most of the mixes being published microsilica and quartz powders are predominantly applied. Cement contents in the range von 700 to 950 kg/m³ and microsilica contents of about 10 to 15% rel. cement are very high.

In general, the protection against rebar corrosion by the reduction of calcium hydroxide reacting with microsilica is neglectible. The very high heat development in the early age of the concrete, particularly at very high microsilica contents by the pozzolanic reaction could be more problematic since microcracks can develop by thermal tensions in the structure together with low tensile strength of the young concrete. [8], [9]

2.1.2 Finely ground blast furnace slag powder (GGBS)

In some recent publications the use of finely ground blast furnace slag powder (higher grinding fineness than cements) in high performance concretes has been reported [10] [11]. Basic work on this topic was already carried out in the 1990s, and the optimisation of the granulometry of cement and finely ground blast furnace slag powder mixes, the influence on the cement stone structure as well as the transition zone cement matrix - aggregates were described [8] . - Some explanations are given for the performance of finely ground blast furnace slag in section 4 and 5. Since no finely ground blast furnace slag is available on the German market but defined powder finenesses are needed for the specific use CEM III/C microcement (Mikrodur[®] R) was used in the tests .

2.1.3 Pit coal fly ashes (SFA)

Fly ashes react with the during cement hydration forming calcium and alkali hydroxides to CSH phases. They cover approximately the grain size distribution of cement, i.e. they can substitute the cement physically. Very fine fly ashes (d_{95} < 10 μm) are described in some publications, i.e. fly ashes which are ground to particular finenesses . They partly complete the grain size spectrum between cement and microsilica and can substitute cement and microsilica resulting in concretes with comparable compressive strengths.

2.1.4 Other meals

The most frequently used rock meals in ultra high performance concretes are quartz and basalt meals.

In particular, quartz meals are frequently used for optimisation of the packing density [12], [13] as an addition between the grain size distributions of microsilica and cement or cement and sand. They can react on large fresh surfaces with calcium and alkali hydroxides resulting from the cement hydration to CSH phases ("etching effect") and thus also densify structure and improve cohesion. - Since inhalation of quartz dusts contains the risk of a silicosis illness, the appropriate regulations and guidelines for working with quartz powders with regard to use and protection of health should be taken into account.

Limestone meals are described in some basic investigations on the packing density and rheologic properties of concretes in the literature. However their suitability for use in ultra high performance concretes is controversial due to their mechanical properties.

2.2 Reduction of the porosity by high packing density in the fine grain size area (physical optimisation)

The specific granulometry of fine substances in order to obtain high packing densities in cement-based building materials has been described in many publications, e.g. [14], [15]. In the following, some fundamentals as well as the practical application in powder systems of ultra high performance concretes is being described.

The granulometric optimisation of high performance concretes includes the complete grain size spectrum. The problem can be treated by 2 fundamental approaches:

- Analysis of the grain size distribution, consisting of discrete monodispersions according to FURNAS [16], or

- Resulting from similarity considerations from a continuous grain size distribution after ANDREASEN et al. [17].

The theory of the continuous dispersions by ANDREASEN et al. is proving best for the optimisation considerations in ultra high performance concretes [17] (see equation 1). This model is based on a limited grain size distribution showing a maximum grain size. FUNK et al. [18] modified this model by restricting the grain size distribution also to small grain sizes (see equation 2).

288

A. ANDREASEN model [17]:

$$\frac{CPFT}{100\%} = \frac{D^n}{D_{Max}{}^n}$$

(Equation 1)

B. Extension by FUNK et al. [18] – lower limit of the grain size distribution:

$$\frac{CPFT}{100\%} = \frac{D^n - D_{min}{}^n}{D_{Max}{}^n - D_{min}{}^n}$$

(Equation 2)

CPFT	=	cumulative percent finer than
D	=	grain size
D_{Max}	=	maximum grain size
D_{min}	=	minimum grain size
n	=	distribution exponent, for spatial distribution = 0.37

From the considerations and the experiments of ANDREASEN et al. [17], FUNK et al. [18] and WESTMAN et al. [19] it results that for inert grain distributions

- an optimal packing density and therefore a minimum porosity is achieved for a distribution exponent of 0.37,

- the porosity is minimized by a broad grain size distribution (and a distribution exponent of 0.37),

- the cavities between the coarse particles are filled only to some extend by the finer particles - for a square-root grain size classes distribution only approx. 12 vol.% of the next finer class fill the coarser class,

- the packing in the fine grain size as well as the smallest grain size are primarily responsible for the complete porosity,

- porosity of ultra high performance concrete is mainly determined by the packing density of the fine particles.

Note:

The grain size distribution according to FULLER et al. [20] is similar to the Andreasen function, using a distribution exponent of 0.5. The distribution curve is steeper, i.e. the coarse particles - aggregates in the concrete - form a framework in which a maximum of possibly smaller grain size particles are packed. In practice of the fine powders wall effects and "slip grain" (fine particles which can "slip" into the gaps of framework of the coarser particles) play an important role, however, so that the FULLER and THOMPSON approach is in principle less suitable. A distribution exponent of 0.37 is therefore approved for fine powders.

Consequences of a high packing density of the fine powders in ultra high performance concretes are:

- reduction of the water demand and thus very low water cement ratios,

- reduction of the diffusion distances / better substance transports for chemical reactions

- with spheric fine substances so-called "ball bearing"-effects, resulting in better rheologic properties of the fresh concrete.

2-D packing of spheres in a rectangular room with particle hindrance:

Slip gaps between neighbouring large spheres are too small so that sufficiently smaller spheres can not be packed in the gaps.

= particle hindrance
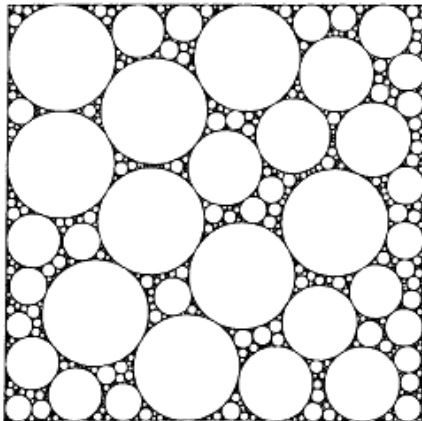
Optimal packing density of a 2-D packing of spheres in the a rectangular room:

Slip gaps between neighbouring large spheres are big enough that an adequate number of small spheres is able to be packed in the gaps.

= no particle hindrance
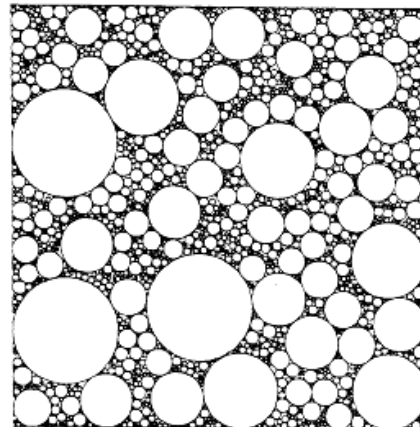
Figure 1: Grain structure model for spheres with continuous grain size distribution (from FUNK et al. [18])

2.3 Hydraulic and pozzolanic reactions of the additions (chemical optimisation)

Not only the physical filler effects mentioned above cause an optimisation of the microstructure. Crystal chemistry and hydraulic / pozzolanic reaction effects of the additions e.g. microsilica, fly ashes, or ground granulated blast furnace slags result in a high packing density of the microstructure and a reduction of defects.

When using pozzolanes (microsilica, fly ashes), a part of the calcium hydroxide resulting from the cement hydration reacts to CSH phases. Weak zones in the concrete = portlandite crystals are stabilized and changed into strength-increasing CSH phases. Depending on the additions these reactions take place at various rates.

Using ground granulated blast furnace slags as a substitution of cement reduces the calcium hydroxide content in concrete developing from cement hydration.

Moreover, reactive and non-reactive fine fillers can work as seed crystals and cause a growing of CSH phases epitaxially due to their size and their surfaces.

These reactions are particularly important for the third effect described below.

2.4   Improvement of the interfacial transition zone (adhesion optimisation)

The interfacial transition zone cement matrix/aggregates is a weak zone in the concrete [21]. Cement stone with an increased water cement ratio around the aggregates and a higher porosity is formed by "inner bleeding" [22]. This porous zone with reduced strength can show a gap around the aggregates up to 70 µm accumulating orientated calcium hydroxide and ettringite crystals. The interfacial transition zone can remain as a gap, however, then the aggregates are isolated to the binder matrix. By use of very fine filler additions this weak zone rich in calcium hydroxide is almost eliminated and the solid and stable CSH phases are in direct contact with the aggregates.

3   Modelling of the packing density in the fine grain-size area

Based on the principles described in section 2.2, calculations to minimize the porosity = optimisation of the packaging density were carried out in the system CEM I 42.5 R HS - Mikrodur® R (fine ground granulated blastfurnace slag cement = CEM III/C) - microsilica. - The selection of C_3A-free cement results from our own experiences and from the literature: Particularly Portland cements poor and free in C_3A, e.g. CEM I 42.5 R HS or oil well cements "Black label" gave good rheological and mechanical results particularly in interaction with high performance superplasticizers [23], [24].
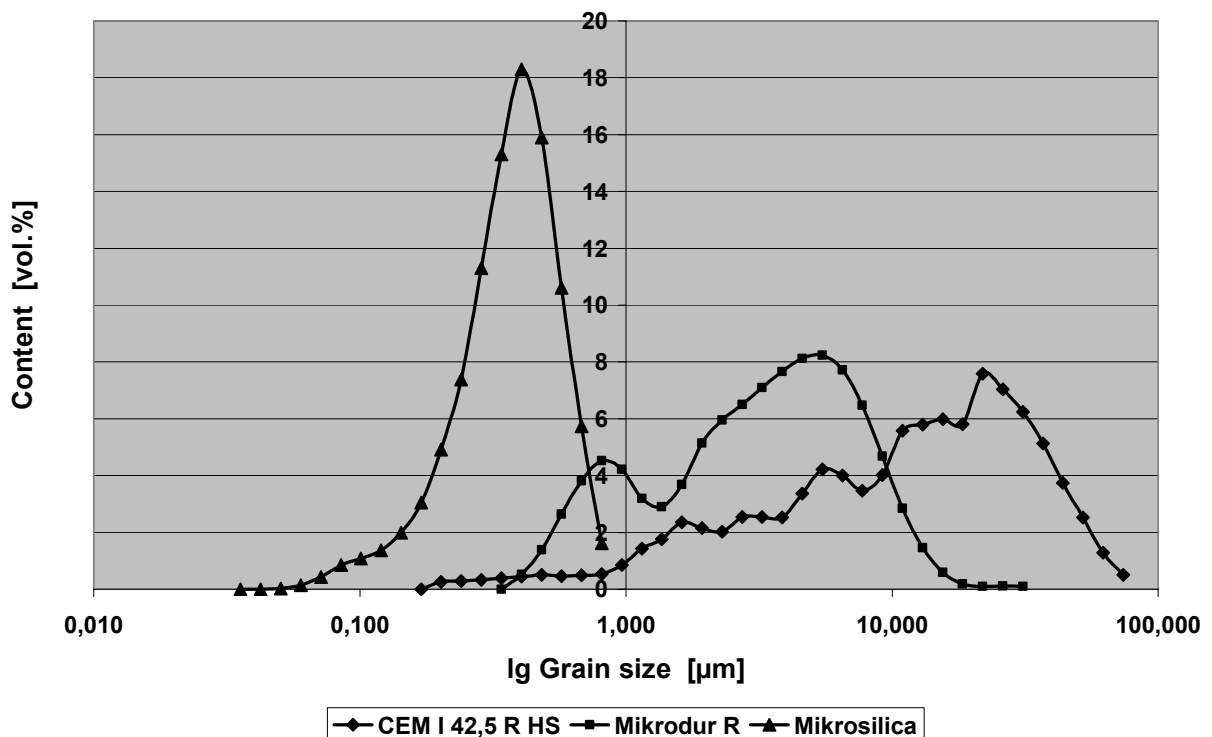
Figure 2: Grain-size distribution of the starting materials

A program based on the equation of FUNK et al. [18] was installed at the Wilhelm Dyckerhoff institute and is being used for packing optimisation. Basis for the selection of the raw materials is a grain size distribution in the complete grain size spectrum (see figure 2).

The calculations were carried out on the basis of the idealized model of inert sphere packets and without taking into account chemical reactions or changes of the single components by the hydration. The porosity minimization without consideration of the grain form and chemical effects can show fundamental optimisation possibilities. The calculated porosities are relative values.

In the sub-frames CEM I 42.5 R HS - Mikrodur$^®$ R or CEM I 42.5 R HS - microsilica a porosity minimum can be calculated at approx. 10 percent of the fine substance each (see figure 3). The relative porosities at the minimum are approx. 15% and 20% less than the pure cement CEM I 42.5 R HS, respectively.

CEM I 42,5 R HS - Mikrodur® R   **CEM I 42,5 R HS - Mikrosilica**
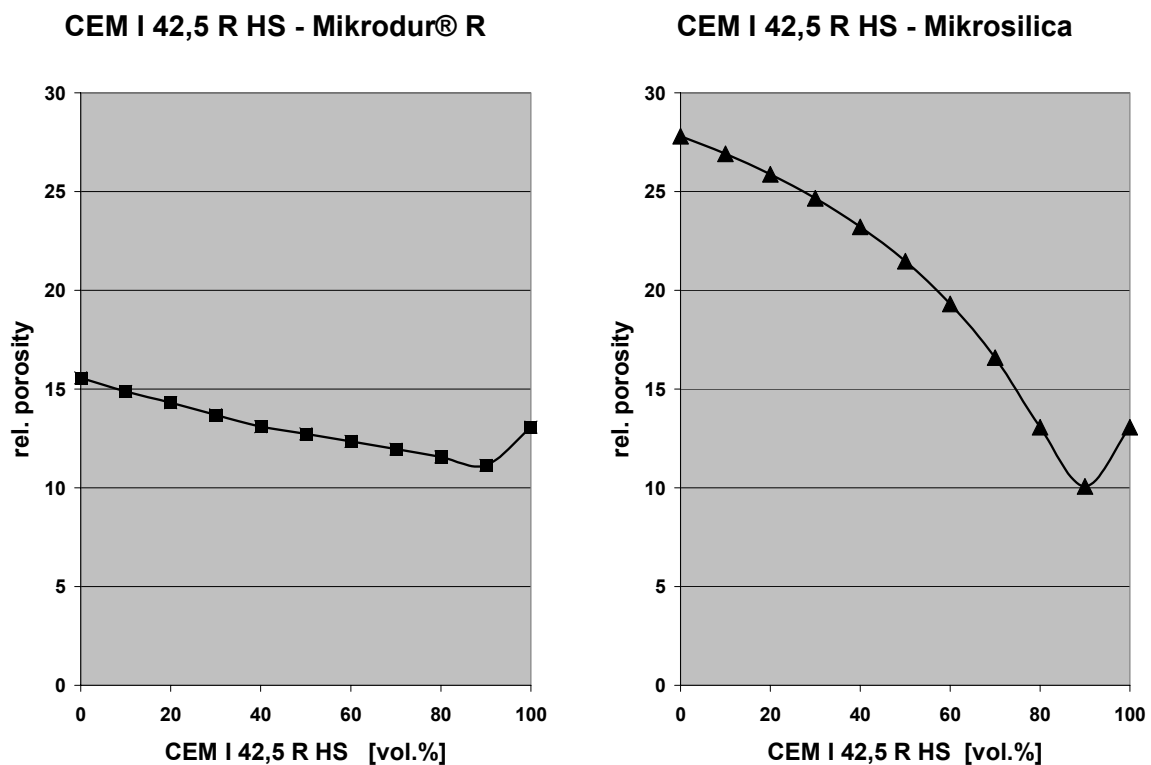
Figure 3:   Relative porosities in the sub-systems CEM I 42,5 R HS – Mikrodur$^®$ R and CEM I 42,5 R HS -Microsilica

In the 3-component-system a relative porosity minimum at about 80 vol.% CEM I 42.5 I R HS + 10 vol.% Mikrodur® R + 10 vol.% microsilica can be calculated (see figure 4). A packing density optimisation of about 36% relative to pure CEM I 42.5 R HS is found.
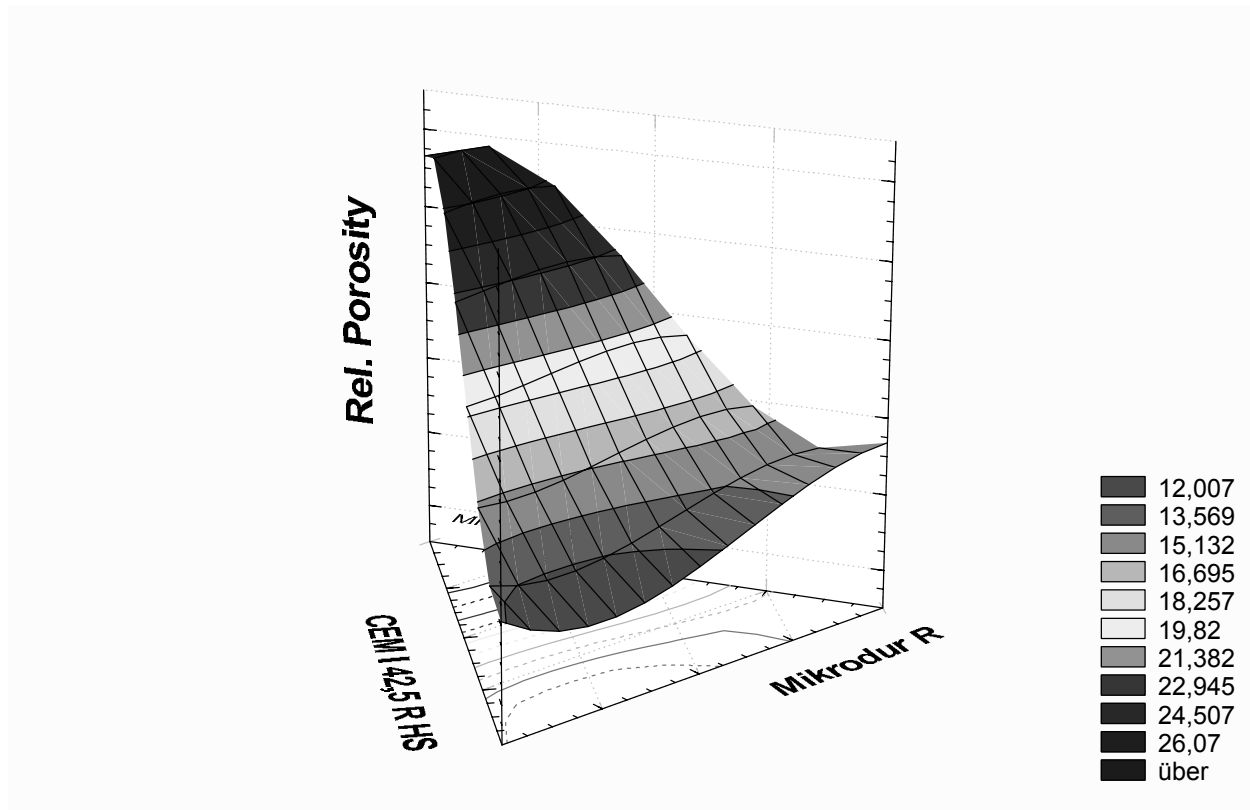
Figure 4 :   Relative porosities in the system CEM I 42,5 R – Mikrodur® R - microsilica

4   Investigations of the influence of fine additions on the fresh concrete properties of ultra high performance concretes

Ultra high performance concretes, both fine concretes as well as concretes with a grain size up to 16 mm, in principle contain a high, granulometric carefully selected fine powder content (< 0.125 mm) of > 1000 kg/m³ (cement and fine additions). Glue contents with w/c ratios of 0.08 to 0.30 are > 450 dm³/m³. The performance of superplasticizers and the high packing density in the fine size area result in good (glutinous) flowing properties without vibrating. - The use of fibers is not be taken into account.

Ultra high performance concretes are very sensitive to batching faults like self-compacting concretes. When mixing ultra high performance concretes weighing-out of the starting materials as well as mixing sequence, mixing intensity and mixing duration are to be kept exactly to avoid inhomogeneities and a too strong warming of the concrete during mixing.

But also water loss by evaporating deteriorates the workability of these concretes. An "elephant skin" arises from drying up from the surface making a flowing of the concrete difficult or leading to inhomogeneities in the concrete structure later. By covering the mixer, application of a surface curing agent or using water spray such a water loss can be avoided.

As described in section 3, the raise of the packing density of the fine powder mixture causes minimum porosity and thus also a reduction of the water demand although the specific surface of the powder can rise strongly. This effect is investigated in the system CEM I 42.5

R HS – Mikrodur® R by a substitution of the cement with granulated blast furnace slag powders (figure 5).

By adding 10 to 15 Vol.% Mikrodur® R, the water demand of the cement is reduced by around 5% although the specific surface rises significantly (approx. 800 to 1000 cm of ²/g).
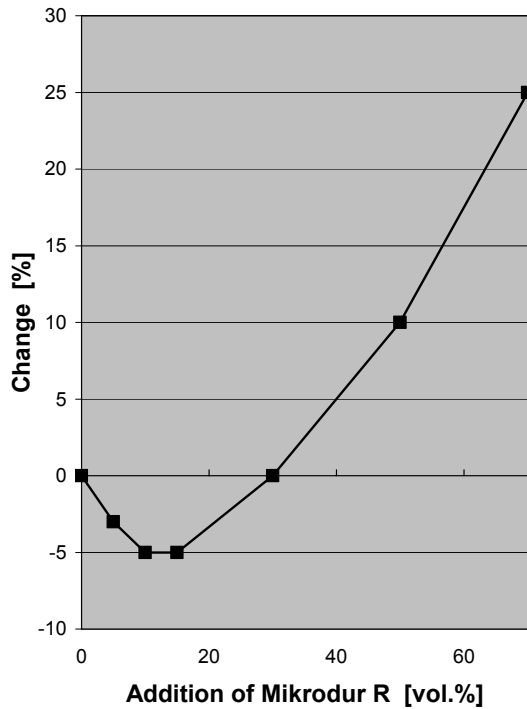
Figure 5:   Percentage change of the water demand by addition of Mikrodur® R to CEM I 42.5 R HS (improvement of the packaging density)

In the 3-component system CEM I 42.5 R HS - Mikrodur® R - microsilica a porosity minimum was calculated at 80-10-10. A 15%-decrease of the water demand could be shown experimentally despite an increase of the specific surface of the mixture.

The high glue contents in ultra high performance concrete result in special rheological properties, because the coarse particles cannot be hindered in their movability avoiding "antiblocking"-effects. These rheological properties can be determined by the methods for self-compacting concretes [25]:

- Relative viscosity from the flow velocity by the flowing funnel - influenced primarily by water addition

- Relative yield value from the slump - influenced primarily by the choice and amount of the superplasticizer

Ultra high performance concretes are usually clearly tougher, they flow more slowly, can be to mix, to condense and to ventilate worse, though. The reasons are extremely lower water-powder ratios as well as the higher grain fineness frequently causing an increase in the

dilatant behavior of the binder glue (= excessive increase of the shear stress with increase of shear rate) or a change from intrinsically viscous to dilatant behavior.

Bornemann et al. [4] investigated the influence of microsilica and quartz meals on the viscosity of ultra high performance concretes. In their concrete system the lowest viscosity was obtained at a micosilica addition of 13 % (rel. cement content), i.e. the best processing consistency of the concrete.

KAUFMANN et al. [26] found a positive influence on the rheological properties, resulting in an improvement of the processing properties by the optimated admixture of fine fly ashes, microsilica, and finely ground granulated blast furnace slag (CEM III/C microcements).

5 Influence on the solid concrete properties

Most investigations on the influence of additions in ultra high performance concretes published in the literature are dealing with the improvement of the performance of the hardened concrete, i.e. mechanical and durability properties of the new building material.

Here the improvement of the adhesion between cement matrix (interfacial transition zone) and aggregates and the strength development depending to the packing density of the concrete is shown exemplarily.

5.1 Adhesion of cement matrix and aggregates / interfacial transition zone

The basis for the performance of ultra high performance concretes are high density, defect-free and interlocked structures and an excellent adhesion between cement matrix and aggregates.

In figure 6 transition zones of different concretes are shown by electron microscopy (SEM, extension 1000x):

Figure 6a shows a C45/55 concrete. Broad gaps between the cement matrix and aggregate grains up to 20 µm are clearly visible. A direct adhesion takes place only at a part of the complete contact surface. The adhesion between the matrix and aggregates is almost perfect in the ultra high performance concretes (figure 6b and 6c).

The principles for this in ultra high performance concretes are (see sections 2.2 and 2.4):

- High packing density of the structure with low porosity

- Reduction of the cement structure-weakening phases calcium hydroxide and ettringite by pozzolanic reactions to strength increasing CSH phases

- Etching of fresh quartz surfaces by the alkaline pore solutions and production of strength increasing CSH phases

- Precipitation of CSH phases in the pore solutions of the interfacial transition zone.

Comparable effects of the interfacial transition zone can also be produced without microsilica by optimised quartz and finely ground granulated blastfurnace slag powders.
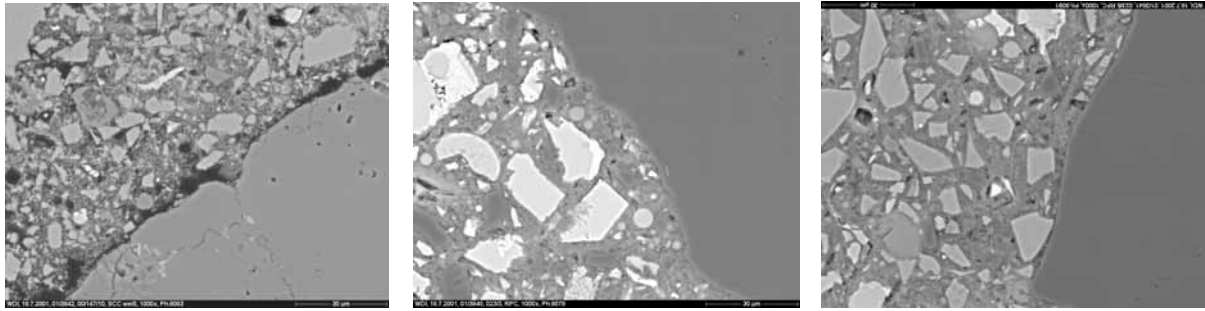
| *a. C45/50* | *b. UHPC with quartz powder + MS* | *c. UHPC with quartz powder + GGBS* |

Figure 6:   Interfacial transition zone in a „normal" concrete C45/55 and in ultra high performance concretes (REM,ext.1000x)

5.2   Strength development

The mechanical properties of the concrete are also influenced by the fine powders. In our investigations the effect of various additions on the compressive strength development was exemplarily checked on prisms of 4x4x16 cm³. A coarse sand 0.1-0.8 mm, cement CEM I 42.5 R HS, microsilica, finely ground granulated blast furnace slag powders (Mikrodur® R) and a quartz powder as fine and with a simular grain size distribution as the cement were used (see figure 7). For the broad distribution of the complete grain size area optimisation models introduced in section 3 were used.

Aim of the investigations was the optimisation of a reference mix from literature comparable by powder grain variations with

- variable cement contents and

- variable addition contents: Microsilica - granulated blast furnace slag powders (Mikrodur® R) and fine quartz powder.

Ultra high performance concretes were produced with a slump of 18 to 20 cm and equivalent water-cement ratios of 0.15 to 0.25 adding a PCE-based superplasticizer. Mixes are summarized in table 2. Storage of the samples was carried out at 20° C under water until the examination. For the reference mix a 6-days heat treatment at 90° C (in water, starting after 24 hours) was carried out.
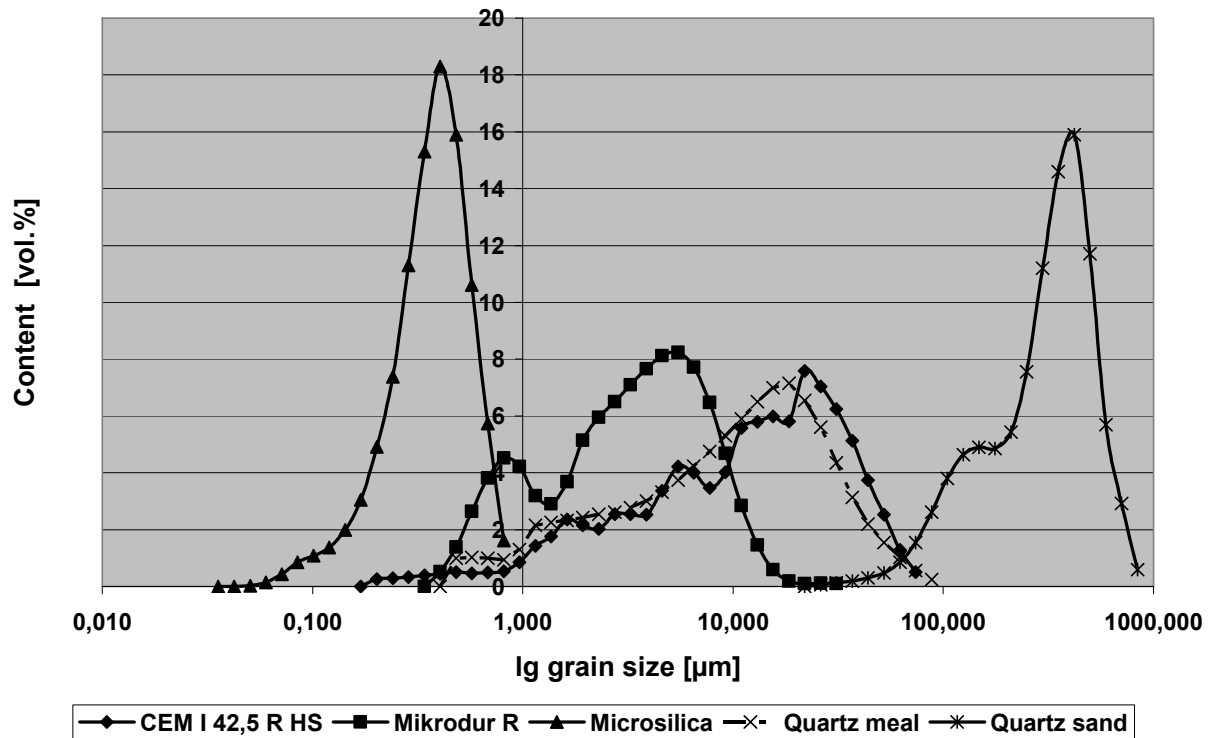
Figure 7:   Grain size distribution of the starting materials

Table 2:   Concrete mixes

	cement	micro-silica	Mikrodur ® R	quartz-powder fine	quartz-sand	water	
I.	750	250	---	220	1020	146	reference mix (compare literature)
II.	820	50	110	400	790	228	partly substitution of microsilica by Mikrodur® R
III.	830	---	110	400	810	234	without microsilica, with Mikrodur® R
IV.	610	50	250	410	840	223	reduced cement content, partly substitution of microsilica

The results are presented in figure 8:

- Reference mix (I) has a compressive strength of approx. 170 MPa after 28 days at 20°C. An additional strength gain could not be shown.

- By an additional 6-days heat-treatment a compressive strength of approx. 200 MPa is reached already after 7 days. - In principle, for high early strengths a heat-treatment is necessary.

- Use of fine granulated blast furnace slag and quartz powders substituting cement and microsilica reduces the final strength insignificantly comparing the reference mix (I) to 155 to 165 MPa (without heat treatment) after 56 days. Compressive strengths after 7 and 28 days are significantly lower. A clear strength increase is ascertainable between 28 and 56 days.
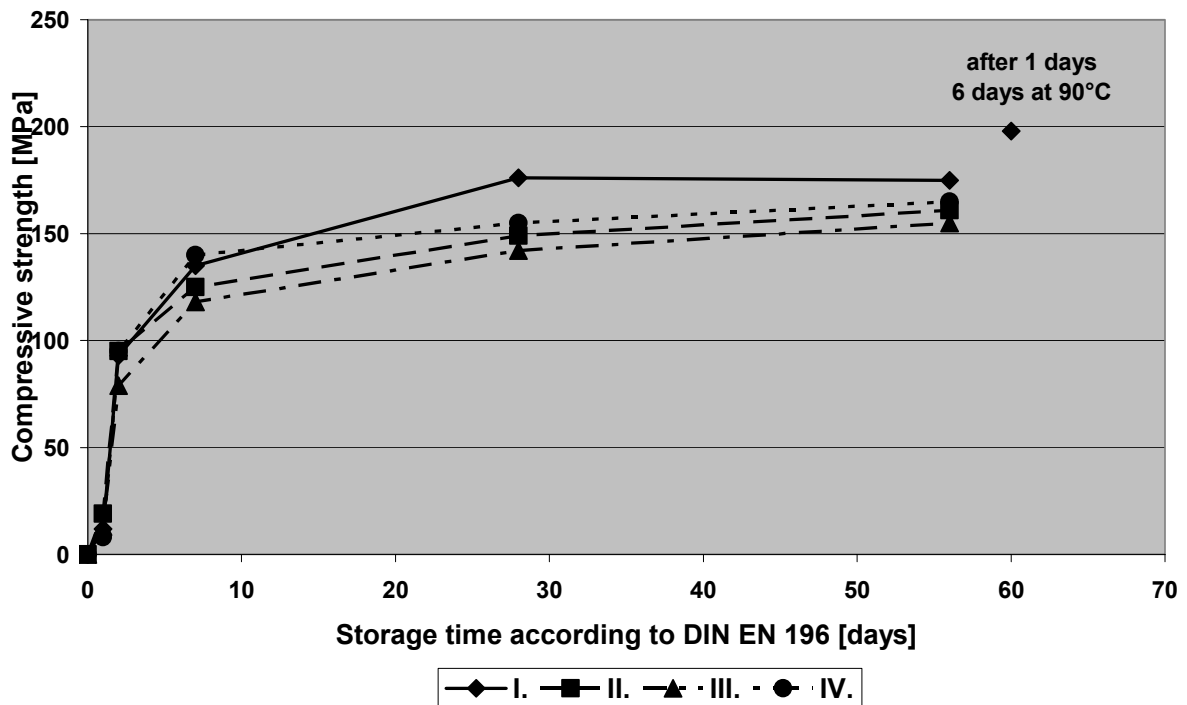
Figure 8: *Strength development of ultra high performance concretes (mixes are presented in table 2)*

6   Summary and outlook - additions for ultra high performance concretes

Finely ground additions are particularly important for ultra high performance concretes. Inerte and reactive fine additions are fundamentally responsible for the performance in the fresh concrete (rheology, water demand) and in the hardened concrete (mechanical and durability properties). Their effects are primarily based on 3 fundamental mechanisms:

a. <u>Physical packing density optimisation:</u> Ultra high performance concretes have a high glue content consisting of cements + additions + water the coarse aggregates are "floating" inside and thus being responsible for the workability. The flowable consistency at low water powder ratios is being controlled by the specific choice of the additions (+ cements), water dosage and admixtures.

The granulometric optimisation in the fine powder area taking wall effects and "slip" grain effects into account requires a careful choice of the used fine powders for reaching flat grain size distributions in a broad grain size area for modelling after ANDREASEN et al. [17] and FUNK et al. [18]. Thereby, low porosities = high packing densities can be gained with the practical consequences of a reduction of the water demand, rheological

optimisation (lower viscosity) and, if necessary, also a reduction of the superplasticizer demand.

The material diffusion paths are shortened in the cement glue, a thick solid structure is built up and pores are reduced in the structure by moving the solid substances closer together.

With examples of the rheological and mechanical optimisations by specific use of additions, microsilica, finely ground granulated blastfurnace slag powder (in the form of CEM III/C microfine cements) and quartz powders are shown.

b. Chemical structure optimisation: Particularly reactive pozzolanic fine powders produce a dense structure of the concrete by eliminating the weak positions in the cement matrix structure e.g. calcium hydroxide produced during cement hydration by changing into a structure consolidating CSH mineral phases. During the hydration of finely ground latently hydraulic granulated blast furnace slag powder only few calcium hydroxide is produced.

c. Optimised adhesion between cement matrix and aggregates: Selected finest additions improve the interfacial transition zone by reactions described in b. The growth of CSH phases occurs by high surface strengths forces in this zone and an epitaxially growing up of CSH phases on the fine particles.

This optimisation mechanism in the interfacial transition zone is demonstrated by electron microscopy, comparing a C45/55 concrete with ultra high performance concretes.

The result of this structure optimisation by reduction of weak concrete structures and the improvement in the interfacial transition zone are dense, strong concrete structures with mechanical properties like ceramic materials.

Although the use of ultra high performance concretes in construction is in the beginning, there are some companies using these materials in the market. A new material technology can be taken to success only by experiences.

Today, there already are sufficient application fields for the use of this new technology. Pipes with extraordinary properties can be produced using ultra high performance concrete (see figure 9). These concrete pipes can be produced with the same mechanical performance but a higher shape accuracy than ceramic pipes. In comparison with normal concrete the material deployment can be reduced to less than a third.
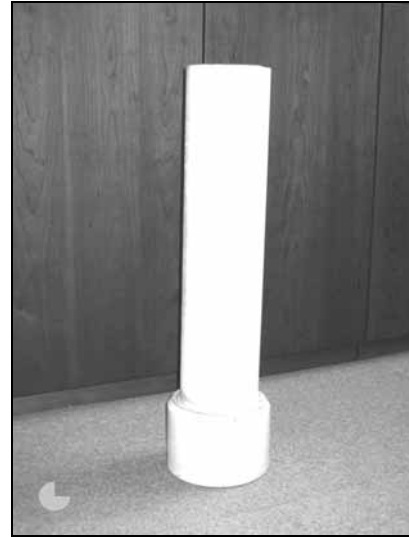
Figure 9:   *Use of ultra high performance concretes in sewage pipes*

7   References

[1]   Richard, P. ; Cheyrezy, M.: Composition of reactive powder concretes. In: Cement and Concrete Research 25 (1995), H. 7, S. 1501-1511

[2]   Cheyrezy, M. ; Maret, V. ; Frouin, L.: Microstructural analysis of RPC (Reactive Powder Concrete). In: Cement and Concrete Research 25 (1995), H.7, S. 1491-1500

[3]   Bonneau, O. ; Poulin, C. ; Dugat, J. ; Richard, P. ; Aitcin, P.-C.: Reactive Powder Concretes - From Theory to Practice.In: Concrete International (1996), H. 4, S. 47-49

[4]   Bornemann, R.; Schmidt, M.; Fehling, E.; Middendorf, B.; Ultrahochleistungsbeton   UHFB – Herstellung, Eigenschaften und Anwendungsmöglichkeiten. In: Beton und Stahlbetonbau 96 (2001), H. 7, S. 458 - 467

[5]   Bornemann, R.; Fehling, E.: Ultrahochfester Beton - Entwicklung und Verhalten. In: 10. Leipziger Massivbau-Seminar (2000), S. 1-15

[6]   Deutscher Ausschuss für Stahlbeton: Sachstandbericht Ultrahochfester Beton. In Vorbereitung

[7]   König R., Wagner J.P.: Mikrosilica – Baustoff aus der Zukunft. Handbuch der Fa. Woermann 2000

[8]   Lange F.: Gefügeuntersuchungen und Eigenschaften von Hüttensand enthaltenden Zementen, Dissertation Univ. Erlangen, 1996

[9]   Metha P.K., Monteiro P.J.M.: Concrete: Microstructure, Properties and Materials – Kap.4 McGraw-Hill Comp. Inc., 2nd ed. 1993

[10] Long G., Wand X., Xie Y.: Very-high-performance concrete with ultrafine powders. Cement and Concrete Research 32 (2002), S. 601-605

[11] Niu Q., Feng N., Yang J., Zheng X.: Effect of superfine slag powder on cement properties. Cement and Concrete Research 32 (2002), S. 615-621

[12] Richard, P. ; Cheyrezy, M.: Composition of reactive powder concretes. In: Cement and Concrete Research 25 (1995), H. 7, S. 1501-1511

[13] Richard, P.; Cheyrezy, M.; Dugat, J.: Mortier à très haute performance, bétons obtenus à partir de ce mortier et les éléments fabriqués avec ce mortier ou béton. Publikationsnummer: 0 518 777 A1, Europäisches Patentamt, München/Paris 1992

[14] Reschke T.: Der Einfluß der Granulometrie der Feinstoffe auf die Gefügeentwicklung und die Festigkeit von Beton. Dissertation Bauhaus-Universität Weimar, Weimar 2000.

[15] Geisenhanslücke C., Schmidt M., Fehling E., Teichmann T.: Ultrahochfester und selbstverdichtender Beton – Ergebnis optimal dichter Kornpackungen. IBAUSIL 2003.

[16] Furnas C.C.: Grading Aggregates, I. Mathematical relations for beds of broken solids of maximum density. Ind. & Engng Chemistry 23 (1931), 1052-1058

[17] Andreasen A.H.M., Andersen J.: Über die Beziehung zwischen Kornabstufung und Zwischenraum in Produkten aus losen Körnern (mit einigen Experimenten). Kolloid-Zeitung 50 (1930), 217-228

[18] Funk J.E., Dinger D.R.: Predictive process control of crowded particulate suspensions - applied to ceramic manufacturing. Kluver Academic Pulishers - Boston/Dordrecht/London 1994, 786 S.

[19] Westman A.E.R., Hugill H.R.: The packing of particles. J.Am.Cer.Soc. 13 (1937), 127-129

[20] Fuller W.B., Thompson S.E.: The laws of proportioning concrete. Proc.Am.Soc.Civil Engr. 22 (1907)

[21] RILEM Second International Conference on the Interfacial Trabsition Zone in cementitious composites, Haifa, Israel (1998), Proceedings edited by Katz A., Bentur A., Alexander M., Arliguie G., F & FN Spon, London and New York

[22] Rudert V., Strunge J., Wihler H.D.: Beton aus anderer Sicht – Filigranes Mikrogefüge. Betonwerk- und Fertigteil-Technik BFT, Heft 9, 1984

[23] Siebel E., Müller C.: Geeignete Zemente für die Herstellung von UHFB. 3. Leipziger Fachtagung „Ultrahochfester Beton (UHFB)", Leipzig 27./28.Nov.2003

[24] Kleen E.: Zusatzmittel für Ultrahochleistungsbeton. 3. Leipziger Fachtagung „Ultrahochfester Beton (UHFB)", Leipzig 27./28.Nov.2003

[25] Deutscher Ausschuss für Stahlbeton: DAfStb-Richtlinie Selbstverdichtender Beton (SVB-Richtlinie), Ausgabe Juni 2001

[26] Kaufmann J., Matschei T., Hesselbarth D.: Effect of the addition of ultrafine cement on the properties of fiber reinforced composites. Int.Cem.Chem.Conferenz, Durban 2003

[27] Droll K.: Einfluss von Zusatzstoffen auf die rheologischen und mechanischen Eigenschaften von UHFB. 3. Leipziger Fachtagung „Ultrahochfester Beton (UHFB)", Leipzig 27./28.Nov.2003

Carsten Geisenhanslüke
Dipl.-Ing.; PhD student
Department of Structural Materials
University of Kassel
Kassel, Germany

Michael Schmidt
Professor
Department of Structural Materials
University of Kassel
Kassel, Germany

Methods for Modelling and Calculation of High Density Packing for Cement and Fillers in UHPC

Summary

The hardened concrete matrix of Ultra-High Performance Concrete (UHPC) is very dense and shows extraordinary strength and durability properties. These features are the result of the use of fine powders to increase the packing density of the matrix. The properties of fresh UHPC like viscosity and resistance against sedimentation are improved as well. Hence, the homogeneity, the density and the deformation resistance of the hardened concrete can be increased.

The low water-cement-ratio (w/c) of about 0.20 is one reason for the high compressive strength higher than 200 N/mm². Another reason is the optimization of different fine and finest materials up to a particle size of 0.5 mm. The selective choice of these materials result in a high packing density, a decrease of porosity of the concrete matrix and almost self-compacting concrete properties. One way to describe the packing design of the materials is the specific solid volume of the binder matrix, specified as the volumetric ratio of water to solid volume including cement and all other fine particles (w/F_v). The other way is the application of models and computer simulations covering all necessary variables of the mixture and the raw materials like particle size distribution, particle shape and particle density. In this study, a packing procedure is presented for mixture proportioning of UHPC to be produced with locally available materials and the influence of the packing density on different properties of fresh and hardened concrete.

Keywords: *modelling, calculation, packing, high density, packing design, particle shape, particle size distribution*

1   Impact of Packing Density for Concrete

Investigations on the optimum composition of aggregates for concrete and their impact on the hardened concrete were already made by *Fuller and Thompson* at the beginning of the 20th century [1]. Their fundamental experience were followed subsequently by different authors (e.g. [2]). Mostly coarse aggregates were investigated. Each particle was represented by a circle. This simple assumption limits the time needed for calculating of packing density.

But these two dimensional circle-models are not sufficient for the calculation and optimisation of the packing density of UHPC and other high performance concretes, e.g. self-compacting concrete. The increasing amount of fine grained materials (Figure 1) can cause practically important changes of workability and the density will not be sufficiently considered. A better approach for the composition of aggregates was described by *Schwanda* and improved by *Krell* and *Reschke* [3-5]. *Krell* used an algorithm to calculate the water demand of aggregates and fines in correlation to the air-void-volume. *Reschke* investigated the influence of the granulometry of fine materials on the properties of fresh and hardened concrete. He used mineral additives and cement with different particle size distributions and calculated their packing density. Furthermore some mathematical models for the optimization of mixtures of different grains were described in [6-9].
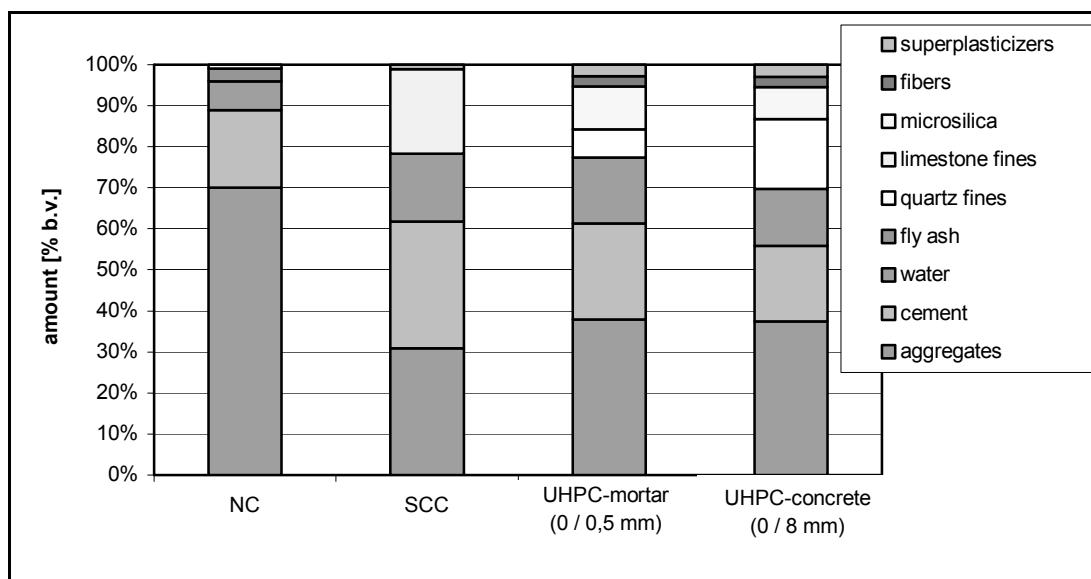
Figure 1: Examples of compositions of Normal Concrete (NC), Self-Compacting Concrete (SCC) and two mixtures of Ultra-High Performance concretes

Different computer algorithms are also known for the simulation of the packing process of cement and mineral additions. *Stroeven and Stroeven* developed a computer code to position spheres randomly and with high packing density [10]. In the next step they used such an optimal structure as the starting point to simulate the hydration process of cement [10]. Other simulations included mineral additions, their chemical composition, the w/c-ratio, and the temperature of hydration in the simulation and calculation processes [11, 12]. Miscellaneous investigations dealt with the possibility to enhance the accuracy of models for aggregates and fine materials. The characterisation of these particles can be improved by representing the real shape in three dimensions instead of simplifying shapes as circles (2D) or spheres (3D). Two dimensional pictures of the shape can be made with optical systems (microscope) combined with an image analysis system [13-15]. High-resolution images in three dimensions can be generated with computer tomography (CT) [16, 17]. A resolution up to 2 µm is possible with the micro-computer tomography (µCT). Herewith, finest mineral particles can be detected and described.

Mathematical methods are used to do computer simulations with real shaped particles. The irregular particle shape of aggregates and cement particles was described using "spherical harmonic coefficients" [16]. An increase of the coefficients represents an increase in the precision of the image of particle shape. Nevertheless, the necessary computer capacity also increases.

Fractal calculation methods had been also developed [18] or the surface was described with Fourier-descriptors [19].

With all these mathematical methods and computer simulations, it will be possible to establish concretes for special applications in a faster and more efficient way by using suitable models and calculation methods. If a precise modelling is possible, UHPC can be made with locally available materials and without an extensive experimental program. In the following first results of this investigation program are presented.

2 Calculation Methods for High Density Packing

The used materials for the calculations and the experiments are summarised in Table 1.

Table1: Properties and packing density of the raw materials used

material	specific surface area (Blaine) [cm^2/g]	position parameter d' [µm]	slope parameter n [-]	packing density (calculated) [Vol.-%]	packing density after Puntke [15][*] [Vol.-%]
cement CEM I 32,5	3,255	20.8	0.87	53.7	51.7
cement CEM I 52,5R HS-NA	4,530	12.0	1.00	51.6	-
quartz filler Q1	18,000	2.92	1.44	47.0	50.4
quartz filler Q2	3,590	42.0	1.29	48.6	50.8
limestone filler K1	18,000	2.60	1.44	47.1	49.8
fly ash F1	2,946	30.0	0.73	54.3	38.5
sand 0 / 0.125 mm	100	320	3.10	45.0	-

 * measured with water mixed with 2 % retarder

Grading curves based on DIN EN 1045-2 are utilized in normal concrete to obtain the standard of an exposition class. This procedure can be specified as the one to get usual packing density for concrete mixtures. As mentioned before, this method is not usable for high performance concrete and other special types of concrete. Therefore, some advancements and variable compositions are essential with an extension of the amount of materials and their adjustment to each other.

One calculation scheme to get the packing density of a material or a mixture is based on the particle size distribution. The material is classified into more than 120 grain size fractions [22]. Each fraction is compared with each other regarding the ability to fill the free spaces in between the grains of the next coarser fraction. In addition the porosity of all individual fractions and of the grain mix is calculated [5, 21, 22].

In Figure 2 the accordance of the particle size distribution and the packing density is shown. As a siplified example two quartz fines Q1 and Q2 were mixed in different volume proportions (see Table 1). The density was calculated for every proportion on the basis of the particle size distribution of the mixture. In this case the maximum density was achieved at a proportion finer to coarser quartz of 30 : 70.
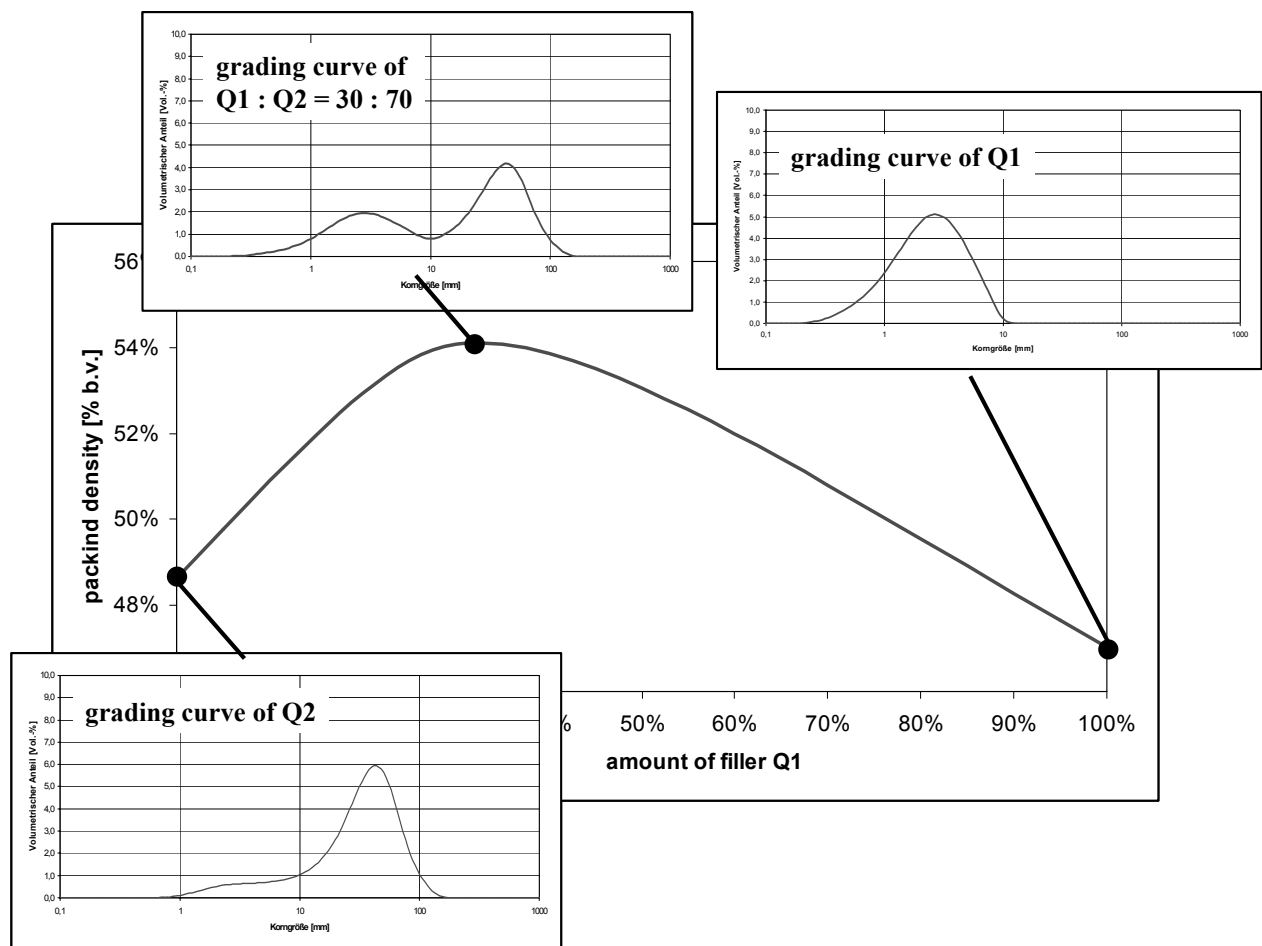
Figure 2:   Influence of particle size distribution on the calculated packing density

Theoretical calculations are also available to get maximum packing density. A new method is under development at the University of Kassel. Its initial point is the characterisation of aggregates as 3-dimensional spheres arranged in the edges of a tetrahedron. The hollow space inside this tetrahedron will be filled with other smaller spheres by computer calculations. The algorithm firstly identify the position, the size and the shape of the filling spheres [23]. In a second step a grading curve is calculated which provides the highest possible packing density considering these basic informations (Figure 3).
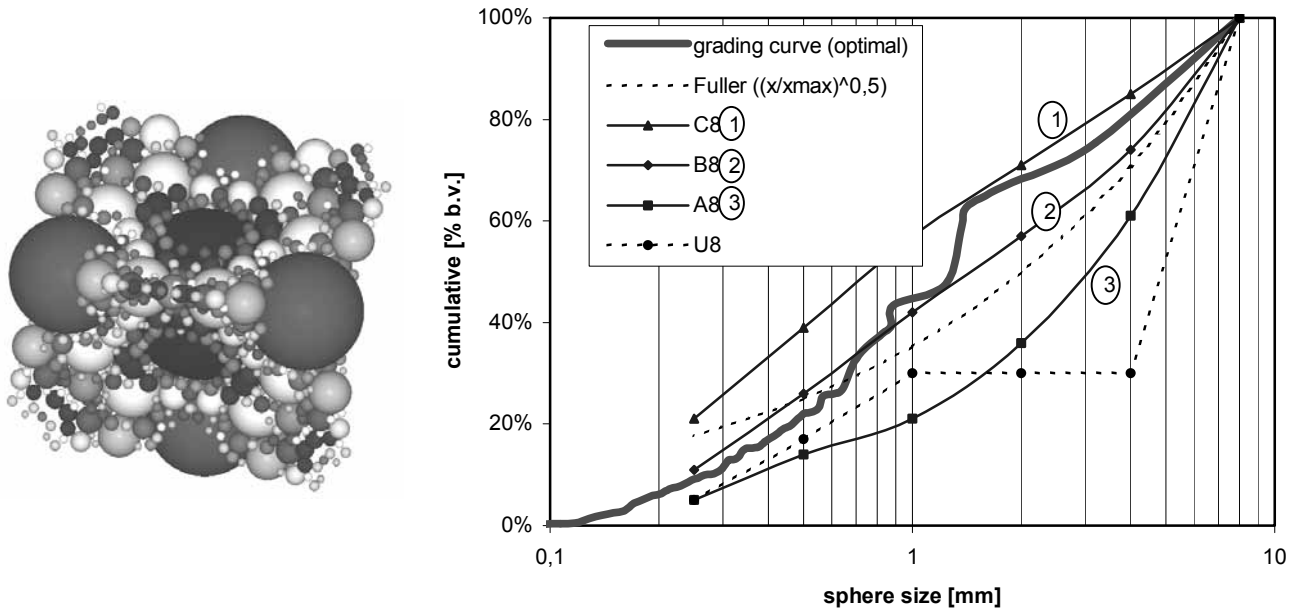
Figure 3:   Optimal position and size of filling particles for a rhombohedra
             sphere arrangement [23]

3   Experimental Methods for High Density Packing

The maximum packing density of a dense randomly packing of mono-sized grains is 63.7 % b.v. That means that a certain unit volume of those grains contains a minimum hollow space volume of 36.3 % b.v. However, concretes with mono-grained aggregates and/or fines are not very efficient. As a rule the low packing density causes a higher water demand and a higher cement content. By using multi-grained-fines the amount of cement can be reduced and the workability, the strength and the durability of ordinary concrete, high performance concrete and of UHPC can be increased. The effect of filling free space between the cement particles is shown in Figure 4 where two fillers are mixed with cement (CEM I 32,5R) separately. The maximum in packing density (about 54 % b.v.) is achieved at around 30 % addition of one of the fillers. If the amount of fillers is increased, the packing density is decreasing below the value of pure cement (about 51.5 % b.v.) because of the higher fineness. Starting from the mixing proportion of cement : filler = 70 : 30 the remaining free space in the system has to be filled with cement lime or coarser aggregates. A further increase of packing density can be made by inserting additional fillers. In Figure 7 the

grading curve for UHPC containing five different fines is shown. A packing density of around 80 % b.v. was achieved.
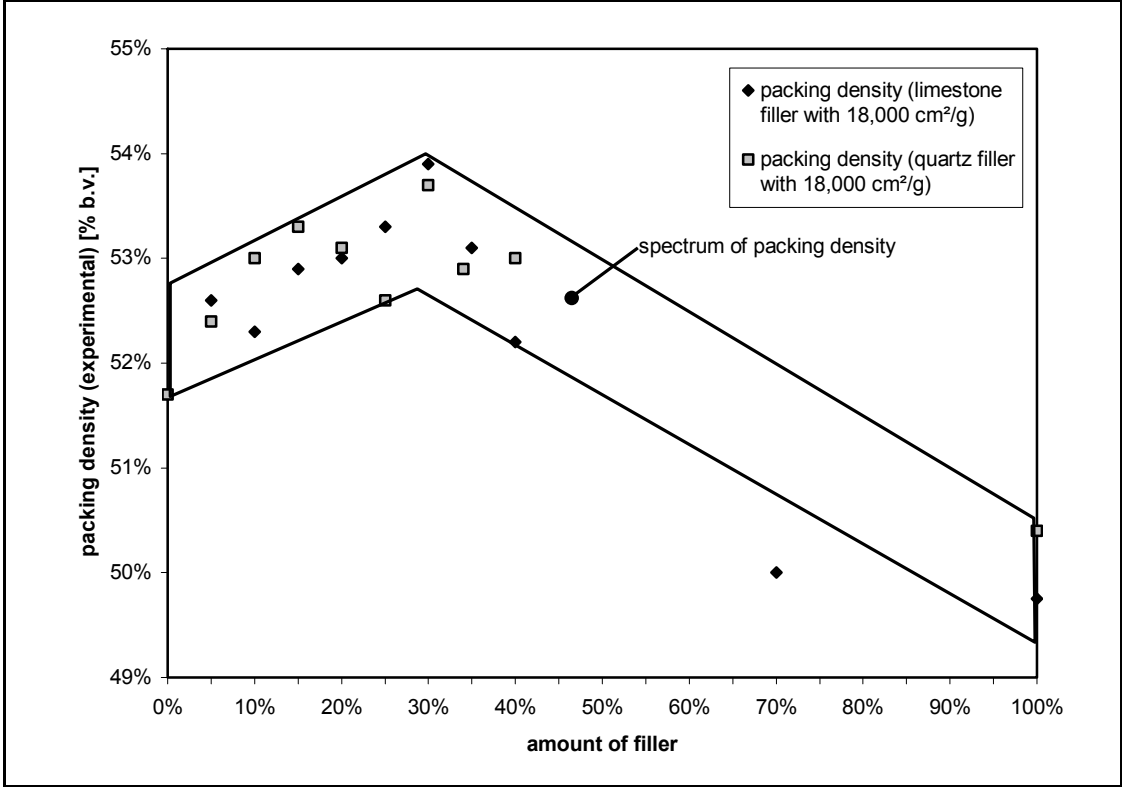
Figure 4: Increase of packing density using fine powders as filler for cement (2,800 cm²/g) (measured after method of Puntke [20])

As mentioned before the packing density is directly correlated to the viscosity of the fresh concrete. Figure 5 as an example shows the calculated packing density of two quartz fines with different particle size distributions and the viscosity of pastes produced with these fines. The maximum packing density correlates with the minimum in viscosity. That means the viscosity sufficiently reflects the results gather by the calculation model used.

The next step to further improve the calculation model is to implement the particle shape. For example, limestone particles have smoother edges compared to quartz particles. Therefore the same amount of those differently shaped fines would result in different packing densities and at least in different viscosities of the fresh matrix (Figure 6).
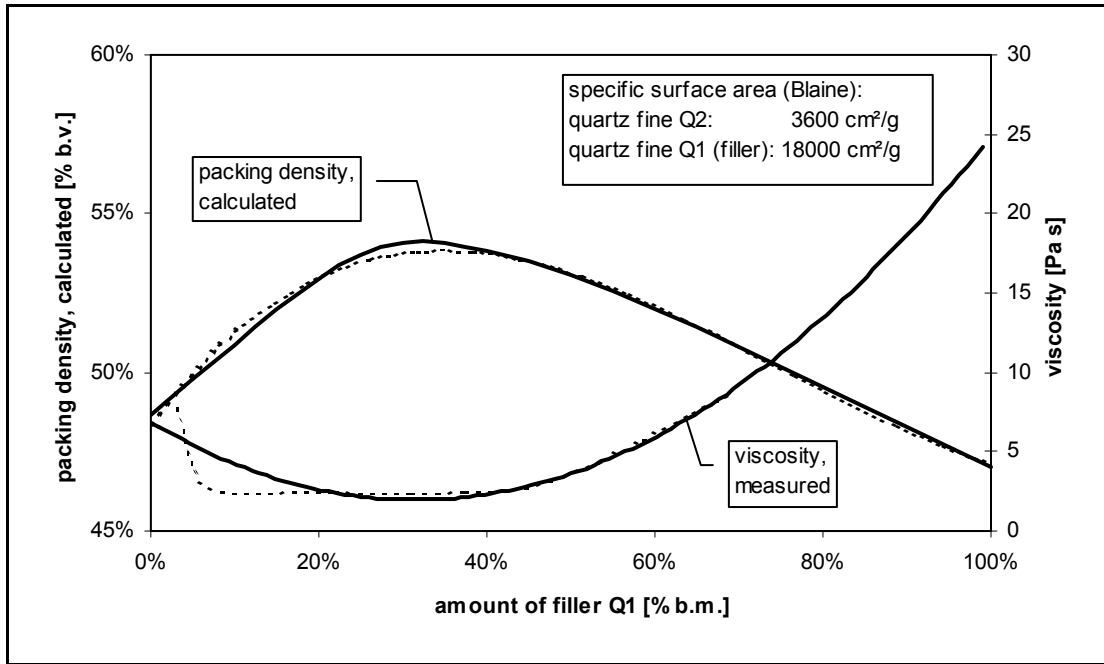
Figure 5: Correlation between packing density and viscosity of pastes with two different quartz fines (Q1, Q2) and 1.5 % b.m. superplasticizer (w/F$_m$ = 0.26)
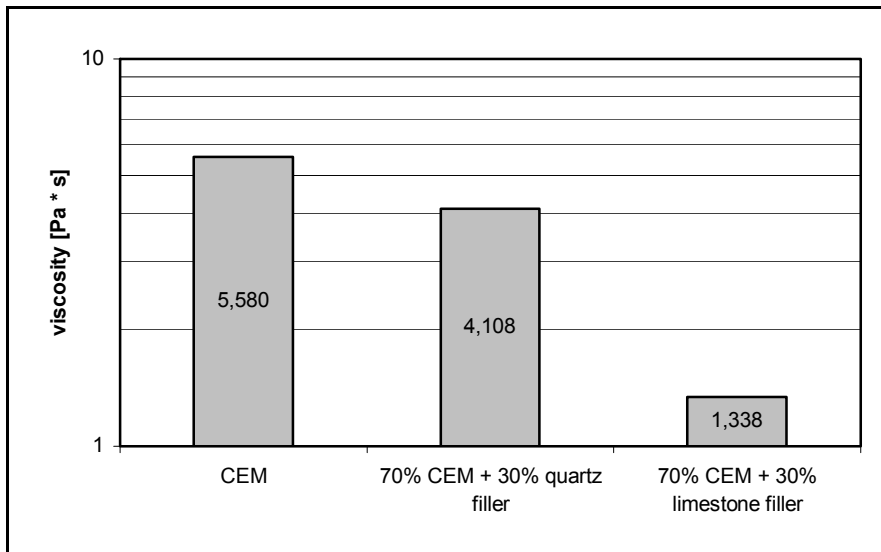
Figure 6: Decrease of viscosity of mixtures consitsting of cement (CEM I 32.5R) and quartz (Q2) or limestone fillers (K1)
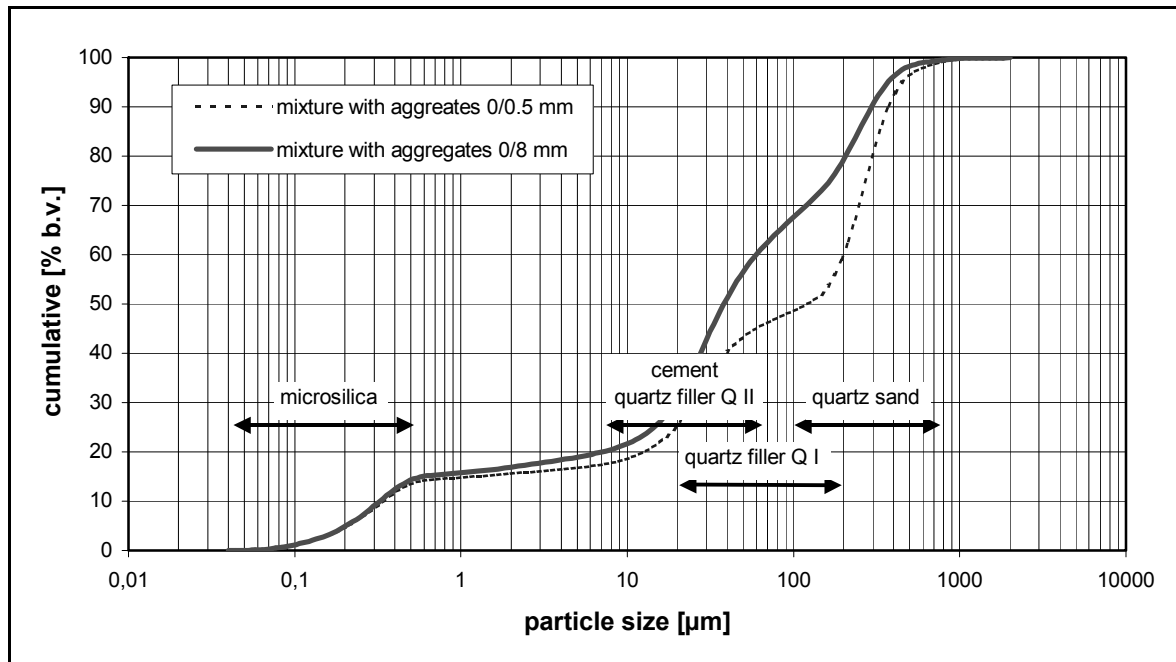
Figure 7:   Particle size distribution of UHPC with high packing density of mixture of all
materials (raw materials: see Table 1)

If all essential properties of mineral additions are known and implemented in e.g. an expert system or database, then concrete can be composed for special applications with an optimum of workability, highest strength and durability properties. These are main topics for further research at the University of Kassel.

4   Conclusions

Modelling, simulations, and computer aided calculation methods for the packing density of fine and coarse aggregates for concrete allow to achieve high and highest packing densities. In Figure 7 as an example the optimum grading curve of two mixtures of UHPC containing fine and coarse aggragates are shown. They are based both on experiments and on calculations using the methods explained above. The differences in the results were almost small but nevertheless significant. By further improving the structural model and the calculation method it might be possible to compose optimized mixtures based on the specific material data of the raw materials only.

5   References

[1]   Fuller, W. B.; Thompson, S. E.: The laws of proportioning concrete. American society of civil engineers Vol. 33 (1907); S. 223-298.

[2]   Andreasen, A. H. M.; Andersen, J.: Ueber die Beziehung zwischen Kornabstufung und Zwischenraum in Produkten aus losen Koernern (mit einigen Experimenten). Kolloid-Zeitschrift 50 (1930); S. 217-228.

[3]   Schwanda, F.: Der Bestwert der Kornzusammensetzung von Betonzuschlagstoffen. Der Bauingenieur Vol. 31 (1956); S. 41-46.

[4]   Krell, J.: Die Konsistenz von Zementleim, Mörtel und Beton und ihre zeitliche Veränderung. Schriftenreihe der Zementindustrie Vol. 46 (Forschungsinstitut der Zementindustrie, Düsseldorf, 1985).

[5]   Reschke, T.: Der Einfluss der Granulometrie der Feinstoffe auf die Gefügeentwicklung und die Festigkeit von Beton. Schriftenreihe der Zementindustrie Vol. 62 (Verein Deutscher Zementwerke e.V., Düsseldorf, 2001).

[6]   de Larrard, F.; Sedran, T.: Mixture-proportioning of high-performance concrete. Cement and Concrete Research 32 (2002); S. 1699-1704.

[7]   Stovall, T.; de Larrad, F.: Linear Packing Density Model of Grain Mixtures. Powder Technology Vol. 48 (1986); S. 1-12.

[8]   de Larrad, F.: Concrete mixture proportioning: a scientific approach. Modern Concrete Technology Series Vol. 9 (E&FN Spon, London, 1999).

[9]   de Larrard, F.; Sedran, T.: Optimization of ultra-high-performance concrete by the use of a packing model. Cement and Concrete Research Vol. 24 (1994); S. 997-1009.

[10] Stroeven, M.; Stroeven, P.: SPACE system for simulation of aggregated matter application to cement hydration. Cement and Concrete Research Vol. 29 (1999); S. 1299-1304.

[11] Bentz, D. P.: CEMHYD3D: A Three-Dimensional Cement Hydration and Microstructural Development Modelling Package. in: (US Department of Commerce, 2000).

[12] van Breugel, K.: Simulation of hydration and formation of structure in hardening cement-based-materials. PhD-thesis; Delft University of Technology, 1991.

[13] Unland, G.; Folgner, T.: Automatische Kornformbestimmung durch photooptische Partikelanalyse. Naturstein-Industrie (1997); S. 20-28.

[14] Brzezicki, J. M.; Kasperkiewicz, J.: Automatic image analysis in evaluation of aggregate shape. Journal of computing in civil engineering (1999); S. 123-128.

[15] Kwan, A. K. H.; Mora, C. F.; Chan, H. C.: Particle shape analysis of coarse aggregate using digital image processing. Cement and Concrete Research 29 (1999); S. 1403-1410.

[16] Garboczi, E. J.: Three-dimensional mathematical analysis of particle shape using X-ray tomography and spherical harmonics: Application to aggregate used in concrete. Cement and Concrete Reseach 32 (2002); S. 1621-1638.

[17] Williams, R. A.; Jia, X.: Tomographic imaging of particulate systems. Advanced Powder Technology 14 (2003); S. 1-16.

[18] Li, L.; Chan, P.: Quantitative analysis of aggregate shape based on fractals. ACI Materials Journal (1993); S. 357-365.

[19] Bowman, E. T.; Soga, K.; Drummond, W.: Particle shape characterisation using Fourier descriptor analysis. Geotechnique 51 (2001); S. 545-554.

[20] Puntke, W.: Wasseranspruch von feinen Kornhaufwerken. beton (2002); S. 242-248.

[21] Schwanda, F.: Der Hohlraumgehalt von Korngemischen. Beton (1959); S. 12-17.

[22] Geisenhanslüke, C.: Computergestützte Modellierung und Berechnung zur Ermittlung der Packungsdichte von Schüttgütern. in: (Kassel, unveröffentlicht, 2002).

[23] Geisenhanslüke, C.: Herleitung eines dreidimensionalen Partikelverteilungsmodells zur Entwicklung verbesserter UHPC - Mischungen. Universität Kassel, Diplomarbeit (2002).

[24] Scott, G. D.: Packing of spheres. Nature 188 (1960); S. 908-909.

Thomas Teichmann

Dipl.-Ing., PhD Student

University of Kassel

Kassel, Germany

Michael Schmidt

Prof. Dr.-Ing. habil.

University of Kassel

Kassel, Germany

Influence of the packing density of fine particles on structure, strength and durability of UHPC

Summary

Ultra-High Strength Concretes or better known as Ultra-High Performance Concrete (UHSC/UHPC) are made using a very low amount of water and a high amount of cement and fines. These materials are characterized by a dense microstructure, obtained by the particle packing improvement, combined with the very low water cement ratio. The sufficent workability is obtained by using superplastizisers in combination with the low water demand of the fresh concrete due to the high packing density of the fines. The particle packing is improved using sub-micron particles which extend the particles size range and allows to fill the hollow spaces in between the cement grains.

The mechanical performance and the durability of Ultra-High Strength Concretes are conditioned by the packing density as well. That means, the view at the micrometer and nanometer scale is necessary to really understand the very special nature of UHPC.

This paper shows some of the fundamental research results, focused on the structural properties of Ultra-High Strength Concrete and on its influence on the strength and durability.

Keywords: *microstructure, particle densitiy, permeability coefficient, water absorption coefficient, chloride diffusion, durability, reactive powder concrete, ultra-high performance concrete*

1   Introduction

Ultra-high strength concrete consists of different fine materials. The high strength, density and durability of utra-high strength concrete do not depend only on the cement and silica fume but mainly on the dense packing of the fines. While on high performance concrete silica fume is added to improve strength and workability only, at ultra-high perfomance concrete silica fume and other ultrafine particles will be added based on a grain-graded sieveline. In this way, gaps, that originate through the pacingt of a fine-material, should be filled by the next-smaller fine-material. This causes an increasing of the packing density (table 1) and the water demand decreases at the same workability [1,2]. As a result the volume-rated water-ultrafines value (w/f-ratio) is less than that of high strength concrete, shown in table 1. This leads to a decreased capillary porosity which reduces the capillary suction of water or solutions very effectively. The packing densities calculated after Schwanda [3,4] for ordinary,

high performance and ultra-high performance concretes are shown in table 1. The very high packing density of 0.87 of the reactive powder concrete RPC C500 can achieved only through a high compression compacting of the fresh concrete and is shown as the relative density $k_{rel} = d_0/d_s$ [5].

With UHPC it is therefore no longer sufficient to base the mix composition on relationship between the w/c-ratio and the compressive strength, as is the case with normal or high performance concrete. Of relevant influence is also the volume-rated water-ultrafines value w/f of the binding agent (all particles ≤ 0.125 μm), presented in table 1.
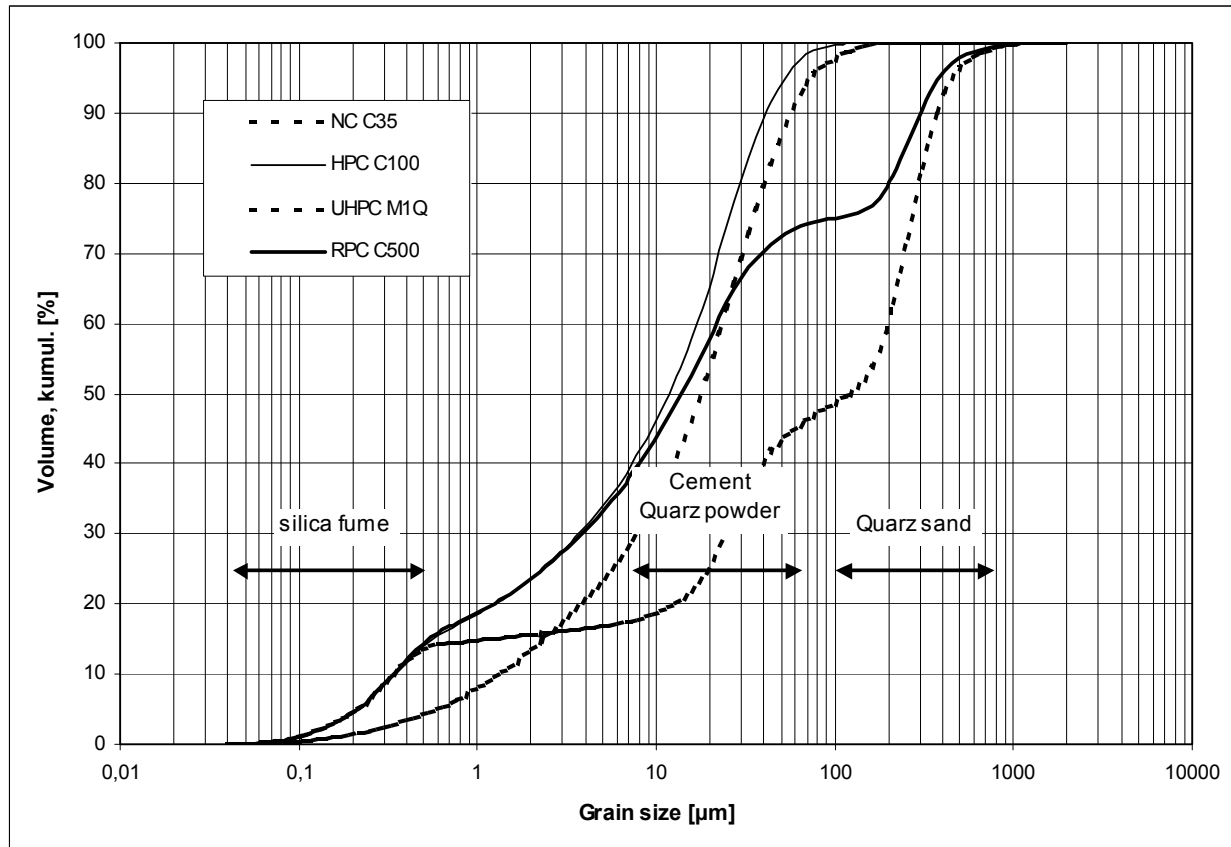
Figure 1:   kumul. sieveline of the fines < 500 µm, NC C35, HPC C100, UHPC C200, RPC C500

2   Concrete Investigations

Investigations of the structure and durability of UHPC were achieved in the university of Kassel. In this paper some results of the structure investigations of a UHPC were compared with these of ordinary and high performance concrete.

Beside the compressive strength, structure was also evaluated by investigating the microstructure aided by porosity, chloride diffusion, water adsortion, permeability of nitrogen and different microscopic investigations. With the RPC C500 compressive strength and structure by microscope were investigated only, cause it was not possible to produce suitable

specimens. The RPC C500 as a example for a laboratory concrete should be shown which densities are possible with a maximum packing density.

2.1 Mixing and Curing Regime

Four concretes were investigated (see table 1). The NC C35 is a ordinary concrete with a cement content of 350 kg/m³ und a maximum aggregate size of 16 mm. The HPC C100 is a High Perfomance Conrete with a cement content of 450 kg/m³ and 45 kg/m³ silica fume. The maximum aggergate size is 16 mm also. The UHPC C200 is a powder concrete with a maximum aggregate size of 0.5 mm, consisting of quartz sand and 733 kg/m³ cement. The RPC C500 is a reactive powder concrete concrete with a maximum aggregate size of 0.5 mm, consisting of quartz sand and 1000 kg/m³ cement. Only the RPC C500 was reinforced with steel fibres.

Table 1: Mixing proportions [4,5,6]

concrete		NC C35	HPC C100	UHPC C200	RPC C500
cement	kg/m³	350	450	733	1000
silica fume	kg/m³	-	45	230	230
quarz powder	kg/m³	-	-	183	390
quarz sand	kg/m³	562	634	1008	500
coarse aggregates	kg/m³	1338	1228	-	-
steel fibres	kg/m³	-	-	-	630
w/c-ratio		0.50	0.33	0.24	0.17
w/f-ratio		1.55	0.91	0.44	0.24
resulting w/c-ratio		-	-	-	0.14
calc. packing density for 0-125 μm		0.68 (Schwanda)	0.71 (Schwanda)	0.76 (Schwanda)	0.87 (Richard)
curing		water	water	1. 90°C for 2d	250°C for 7d
		-	-	2. water only	-

For the NC C35 and HPC C100 a CEM I 32,5 R respectively a CEM I 42,5 R was used. The cement used for the UHPC C200 was a CEM I 52,5 R HS/NA, being advantageous for UHPC because of its low C_3A and alkali content. For the RPC C500 a CEM I 52,5 R was used. The reactive powder concrete was produced according to Richard [5]. At mixing the fresh concrete water-cement ratio was 0.17. Directly after mixing the fresh concrete was filled in a steel cylinder and compacted with 200 kN load over a 7 cm diameter rod, shown in figure 2 and 3. This results in 50 N/mm² compression stress and was hold for 4 hours. The out-pressed water was measured. This reduced the water-cement ratio from 0.17 to 0.14.
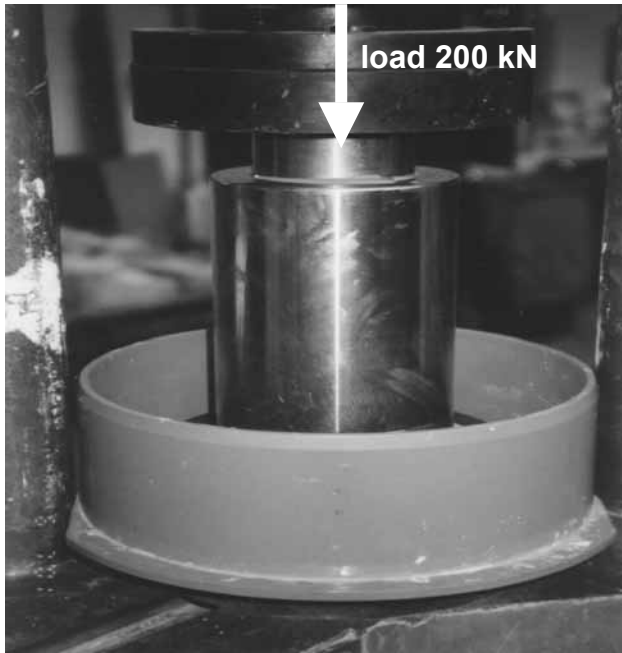
Figure 2: compression of the fresh concrete (RPC C500) with a load of 200 kN

Figure 3: out-pressed water

Specimens of the NC C35 and HPC C100 were cured under water. The Specimens of the UHPC C200 were cured in two different ways: After compaction the concretes were cured in moulds at room temperature (20°C) for exactly 24 hours. Thereafter they were demoulded and one half of the samples was soaked in water (20°C) and cured until they were taken out for standard storage at 20°C and 65% rel. humidity (in table 2: UHPC C200 water cured). The other part was heat treated at 90°C two days after demoulding for 48 hours with a heat rate of 10 K/min. After heat treating the concretes were taken out for standard storage (in table 2: UHPC C200 heat cured). The specimens the RPC C500 were demoulded after two days and then cured at 20°C/65% rel. humidity for two days. After that the specimens were heat treated at 250°C for 7 days with a heat rate of 10K/hour.

2.2   Strength

The compressive strengths of all concretes was tested after 28 days, according to DIN 1048 and EN 196 (table 2). The specimens were cylinders (D/L = 150/300 mm) for the NC, HPC and UHPC. The specimen of the RPC C500 was a smaller cylinder (D/L = 70/100 mm).

Table 2: compressive strength and spec. density

Table		NC C35	HPC C100	UHPC C200 water cured	UHPC C200 heat cured	RPC C500
compr. Strength after 28d	N/mm²	40	109	162	213	487
spec. density	g/cm³	2.36	2.48	2.39	2.39	2.76

2.3   Structure

Table 3 and figure 4 present the results of the investigation of the pore-size distribution. The normal concrete has a total porosity of 15 vol.-%, while the high performance concrete and ultra high performance concrete have a total porosity of 8.2 vol.-% respectively 6 vol.-%. The total porosity of the reactive powder concrete is 2 vol.-%.
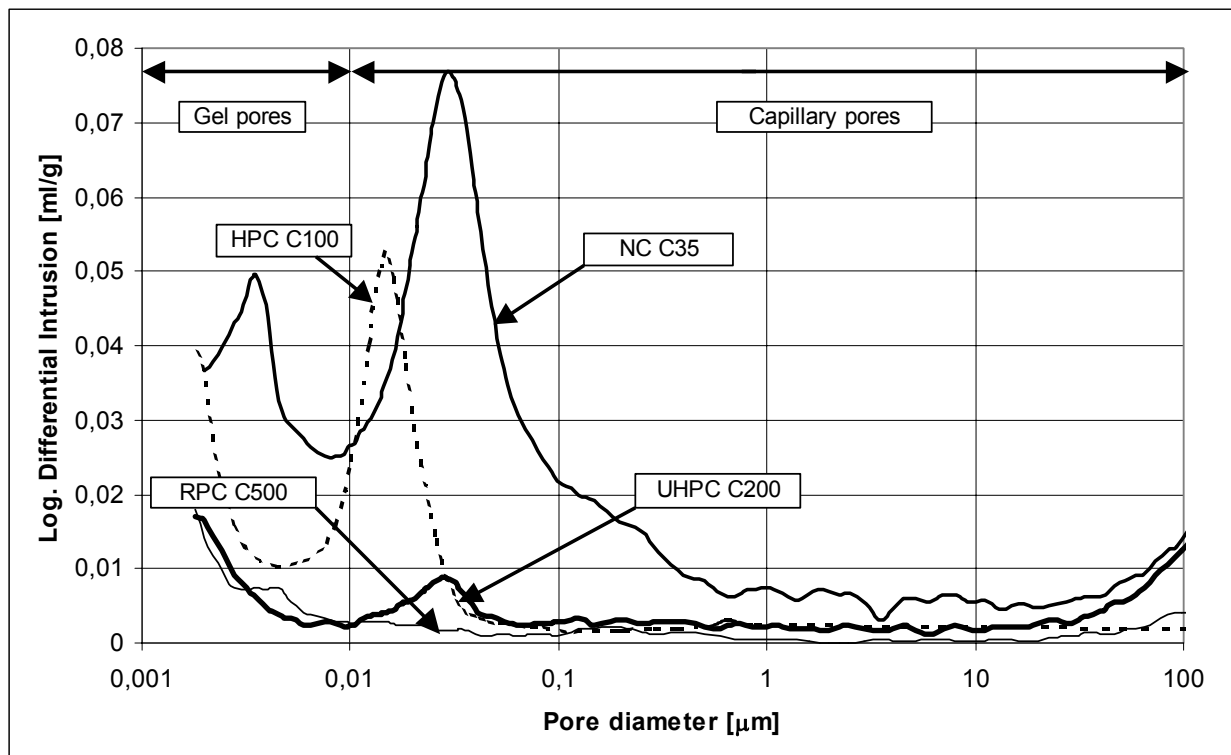
Figure 4: pore-size distribution

The most important aspect of durability of concrete is the capillar-pore content. While normal concrete and HPC have a capillar-pore content of 8.3 vol.-% and 5.2 vol.-%, UHPC has a capillar-pore content of 1.5 … 1.8 vol.-% only. Because of the very low capillar-pore value of

the UHPC, the capillary suction of water and de-icing salt solutions is very effectivly reduced. The capillary-pore content of the RPC is 0.8 vol.-% only.

Table 3: total porosity and capillar pores

Table		NC C35	HPC C100	UHPC C200	RPC C500
total porosity	vol.-%	15.0	8.3	6.0	2.0
capillary pores	vol.-%	8.3	5.2	1.5	0.8

Figure 5, 6 and 7 shown the microstructur of HPC C100 in comparision with UHPC C200 and RPC C500 at the same scale, observed by scanning electron microscope (SEM). Cause the defined void filling the density of the matrix of the UHPC increases, presented in figure 5 and 6. Oppsite the HPC at the UHPC the value of capillary pores is reduced very effectively.
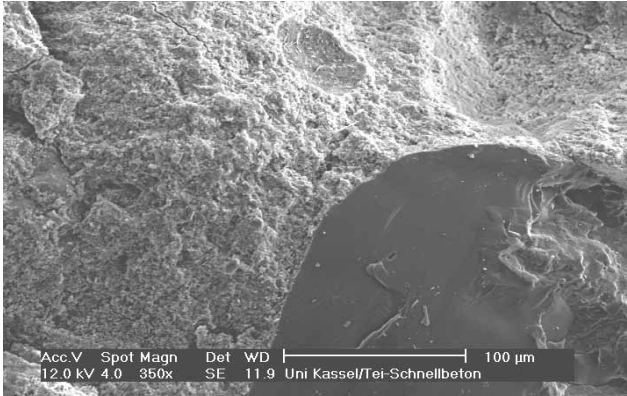
Figure 5: microstructure of HPC C100
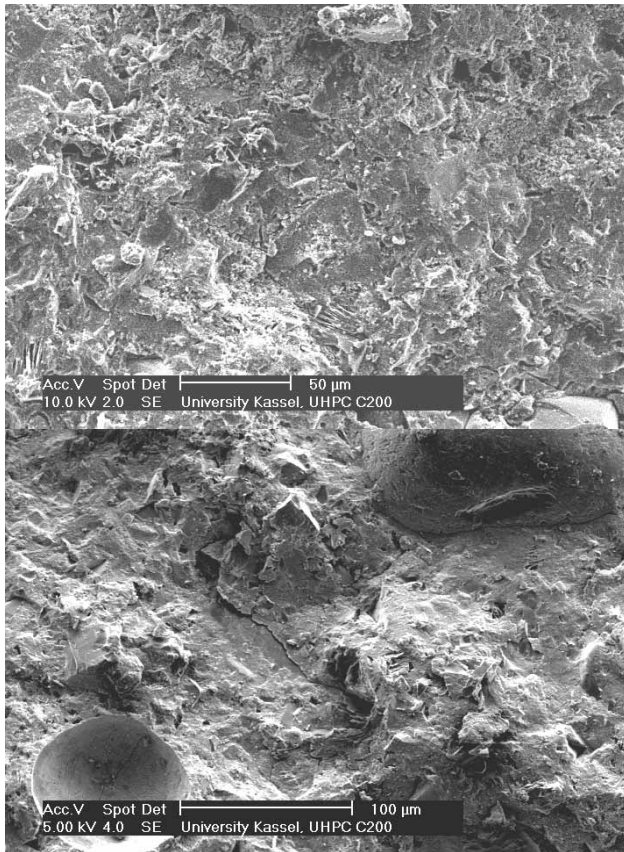
Figure 6: microstructure of UHPC C200

Due to the farthermore packing and compaction of RPC C500 the density arised (table 1), shown in figure 7. The matrix of this concrete seems very homogenous and voidless.
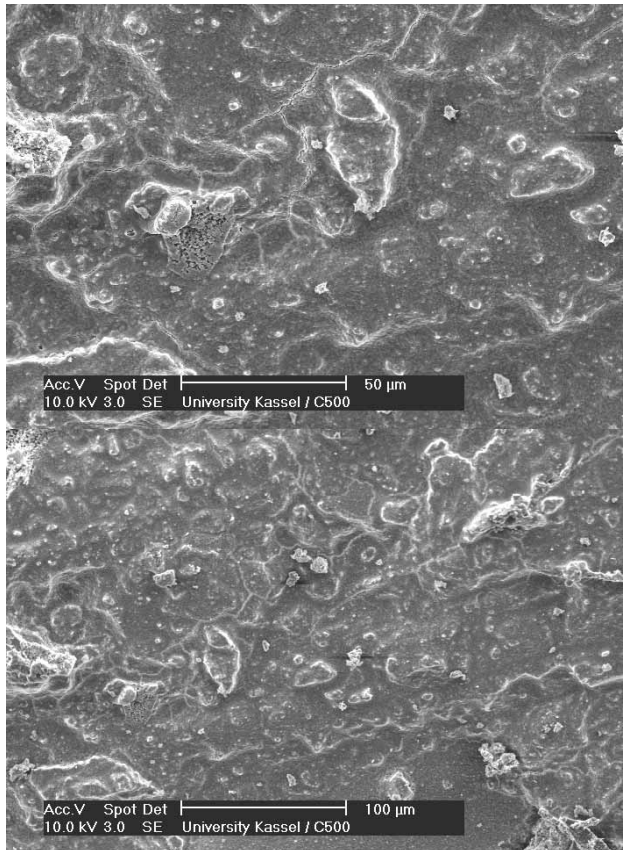
Figure 7: microstructure of RPC C500

2.4 Durability

The transport of water and solutions, transporting harmfull materials as chlorides, is occured by capillary pores. As the value of capillary pores decreases the resistance to transport of harmfull materials improves.

Figure 8 and 9 shows the results of the permeability coefficient and the water-absorption coefficient according to DIN 52617. The expression gas permeability can be understand as the performance of the material against a gas, which passes under pressure through the material. The gas permeability presents a important material parameter which characterizes structure and durability of the concrete. It essentially depend on the open porosity of the cement lime, the aggregates and the proportion of these two components in the mix. The specific permeability coefficient K was evaluated by the inert gas nitrogen (N). [7]
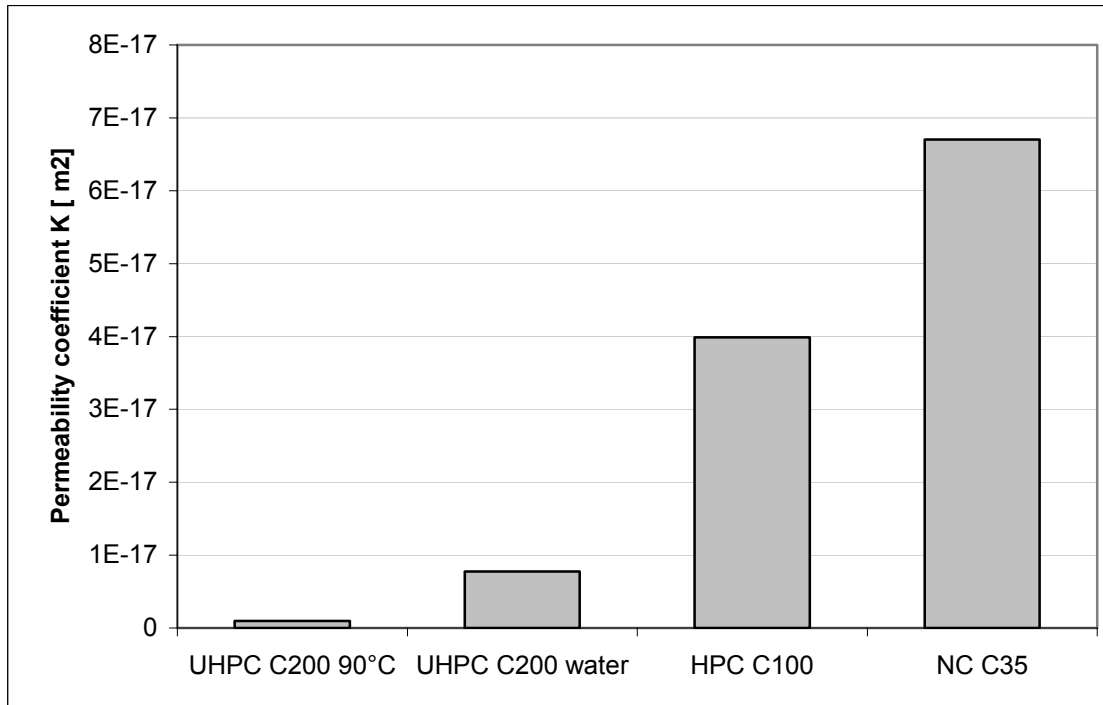
Figure 8: Permeability coefficient

The results of permeability of UHPC C200, HPC C100 and NC C35 are 0.01^{-17} …0.08^{-17}m², 4^{-17}m² and 6.7^{17}m². This illustrates that the permeability of UHPC is much lower than the two concretes, figure 8.

Similar trend was found for water absorption.
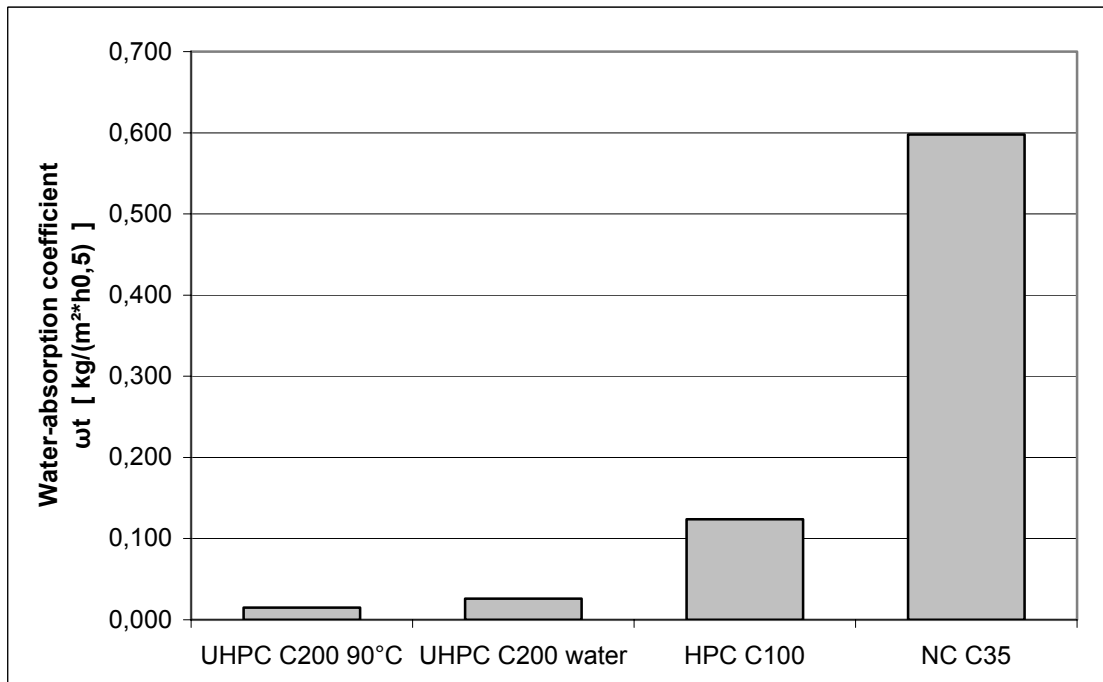
Figure 9: Water-absorption coefficient

The water-absorption coefficients of all investigated concretes were under the value of 0.6 kg/(m²*h^{0,5}). With 0.12 kg/(m²*h^{0,5}) the water-absorption coefficient of HPC C100 is 20% of ordinary concrete NC C35. The water-absorption coefficient of sand stone ranges from 1 to 2 kg/(m²*h^{0,5}). The water-absorption coefficients of water cured and heat treated UHPC are 0.02 and 0.01 kg/(m²*h^{0,5}), which are very small and similar to the error of the results of other concrete.

For the durability of concretes or mortars the influence of chlorides is very effectively. The entry of chlorides in concrete is one of the essential causes for damage of concrete-constructions through steel corrosion. The chlorides can penetrate a water-saturated concrete due to diffusion only. The resistance to the diffusion of chloride ions was measured with a quick-migration test [8]. Concrete plates of 3.5 cm thickness were installed between two chambers. One chamber is filled with water, the other contains a 10% chloride solution. Chloride diffusion is accelrated by applying a DC voltage of 40V over a period of 6 hours. The load transferred during this time is measured and the penetration depth of the chloride ions established upon completion of the diffusion.
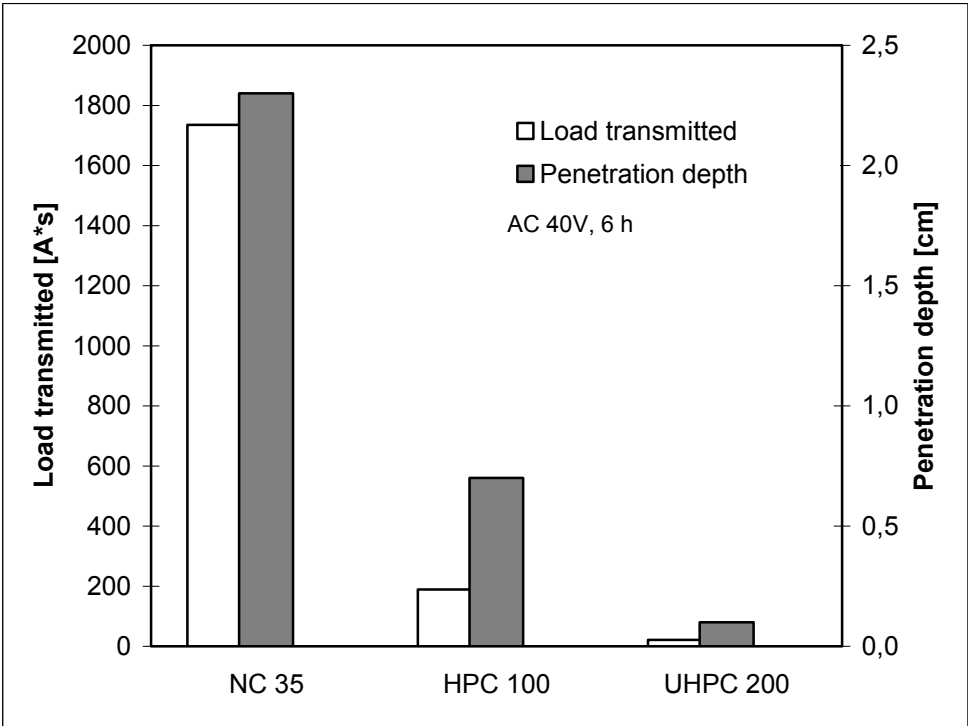
Figure 10: Transmitted loads and penetrations depths

The NC C35, as expected, experienced at 2.3 cm the highest penetration depth. With 0.7 cm the penetration depth of chlorides was decreased very effectivly in the HPC C100. In the heat treated UHPC, the chlorides penetrated less than 0.1 cm into the concrete. Also the amount of chlorides transferred in the UHPC indicated a very high resistance to chloride attacks.

3   Concluding Remarks

The technology of ultra-high performance concretes depend mainly on the increased matrix packing density – expressed through the volume-rated water-ultrafines value w/f-ratio – improved bond between aggregates and cement lime matrix. In combination with very low watercement ratio and defined fine materials with a low water demand are concrete compressive strengths over 200 N/mm² achievable. The increased packing density leads not only to high compressive strengths, but also to a high matrix density. The high density increase the resistance of concrete to entrance of gases and fluids, compared to ordinary and high performance concretes.

4   References

[1]   Kessler, H.-G.: Kugelmodell für Ausfallkörnungen dichter Betone; Beton, 1984, Heft 11, S. 63-76

[2]   Geisenhanslüke, C.: Diplomarbeit: Herleitung eines dreidimensionalen Partikelverteilungsmodells zur Entwicklung verbesserter UHPC-Mischungen; Universität Kassel, Diplomarbeit, Kassel 2002; Betreuer: T. Teichmann

[3]   Reschke, T.: Der Einfluss der Granulometrie der Feinstoffe auf die Gefügeentwicklung und die Festigkeit von Beton; Schriftreihe der Zementindustrie, Heft 62/2000, Bau+Technik Verlag, Düsseldorf 2001

[4]   Schwanda, F.: Das rechnerische Verfahren zur Bestimmung des Hohlraumes und Zementleimanspruches von Zuschlägen und seine Bedeutung für den Spannbetonbau;Zement und Beton 37, 1966, S. 8-17

[5]   Richard, P.; Cheyrezy, M.: Composition of reactive powder concrete. In: Cement and Concrete Research 25, No. 7, S.1501-1511, 1995.

[6]   Teichmann,T., Bunje, K., Schmidt, M., Fehling, E.: Durability of Ultra-High Performance Concrete (UHPC). Proceedings of the 6th International Symposium on Utilization of High Strength/High Performance Concrete, Leipzig 2002

[7]   Gräf, H.; Grube, H.: Einfluss der Zusammensetzung und der Nachbehandlung des Betons auf seine Gasdurchlässigkeit; Beton, 1986, Heft 11, S. 426-429 und Heft 12, S. 473-476

[8]   Tang, L.; Nilsson, L.-O.: Rapid determination of the chloride diffusivity in concrete by applying an electrical field; ACI Materials Journal 89, S.49-53, 1992

Part 8:

Design Specific Material Aspects

Ekkehard Fehling
Prof. Dr.-Ing.
Universität Kassel
Kassel, Germany

Kai Bunje
Dipl.-Ing.
Fehling - Jungmann GmbH
Kassel, Germany

Torsten Leutbecher
Dipl.-Ing.
Universität Kassel
Kassel, Germany

Design relevant properties
of hardened Ultra High Performance Concrete

Summary

Ultra High Performance Concrete (UHPC) offers a great spectrum of favourable material properties. The structural behaviour of UHPC differs from normal- or high-strength concrete, particularly for a supplement of fibres. In most countries valid design rules for this new material do not yet exit. In Germany a work group of the German Commission on Reinforced Concrete (Deutsche Ausschuss für Stahlbeton DAfStb) has presented a state of the art report on UHPC [1]. Chapter 6 of this report describes the knowledge about the properties of hardened UHPC. This paper summarises some of the main aspects dealt with there.

Keywords: *material properties, shrinkage, creep, fatigue behaviour, bond, fire resistance*

1   Introduction

The properties of hardened Ultra High Performance Concrete (UHPC) [2] are determined by the very dense structure of this material. The microstructure of UHPC differs significantly from normal- and high-strength concrete. With respect to the mechanical behaviour, UHPC with fibres shows, depending on the type and quantity of fibres contained in the mix, ductile behaviour under compression as well as in tension. In contrast to this, UHPC without fibres behaves brittle, if no additional measure such as confinement is chosen. Since the pre-peak behaviour does not show significant differences, the elastic properties of UHPC with and without fibres can be described in common whereas the influence of fibres has to be described separately.

As one consequence of the dense structure of UHPC, the porosity of UHPC is much lower than for normal- and even for high-strength concrete. Another consequence is the improvement of the contact zones between the cement matrix and the aggregates as well as the fibre reinforcement which allows a short length of fibres.

This is illustrated by Figure 1 showing the good bond between the different components (a and b). Figure 1c shows a situation which can often be found in normal-strength concrete. The dense structure is also responsible for the very low permeability for gases and fluids and

hence superior durability of this material. The low permeability has an adverse effect with respect to fire resistance. This, however, can be compensated as shown in chapter 8.
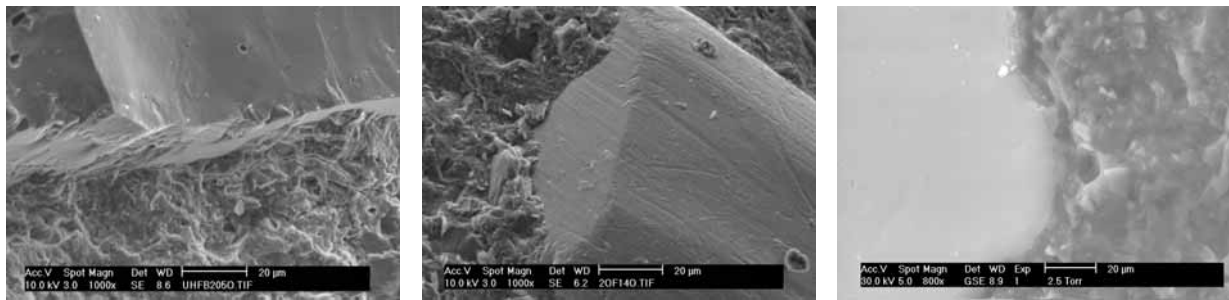
a) good bond between cement matrix and quartz sand particles (left)
b) exceptional bond between matrix and steel fibre
c) less satisfactory bond between matrix and quartz sand particle (right)

Figure 1:   Contact zones in UHPC between matrix and aggregates or fibres

2   Behaviour under Compression

The typical compressive strength of UHPC is in the range of 150 to 220 MPa. Until about 70 to 80 % of the compressive strength, UHPC shows a linear elastic behaviour (Figure 2). According to experimental evidence as obtained until now, this holds true for UHPC regardless of the maximum   aggregate size. The failure of UHPC without fibres is of explosive nature. No descending branch in the stress-strain-diagram does exist. This, however, can also be observed for HSC with f_c > 90 MPa.
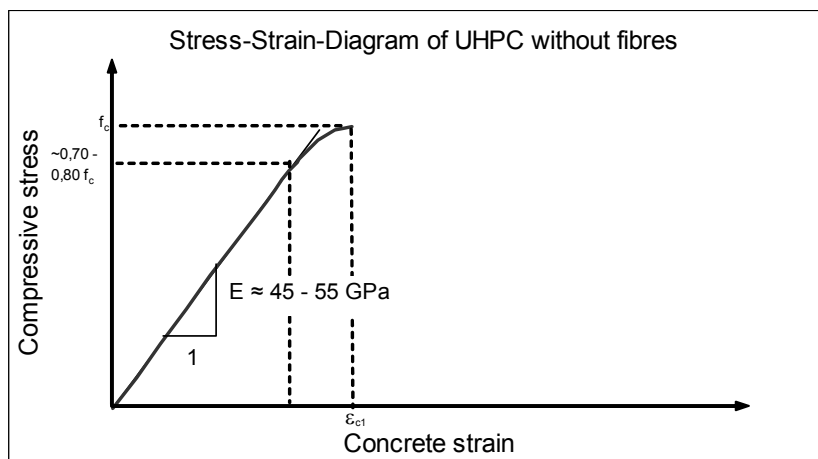
Figure 2:   Stress-strain-diagram of UHPC without fibres

Due to the dense structure, the elastic modulus of UHPC is higher than for normal- and high-strength concrete when using identical aggregate types. Figure 3 shows typical results as obtained at Leipzig University [1].
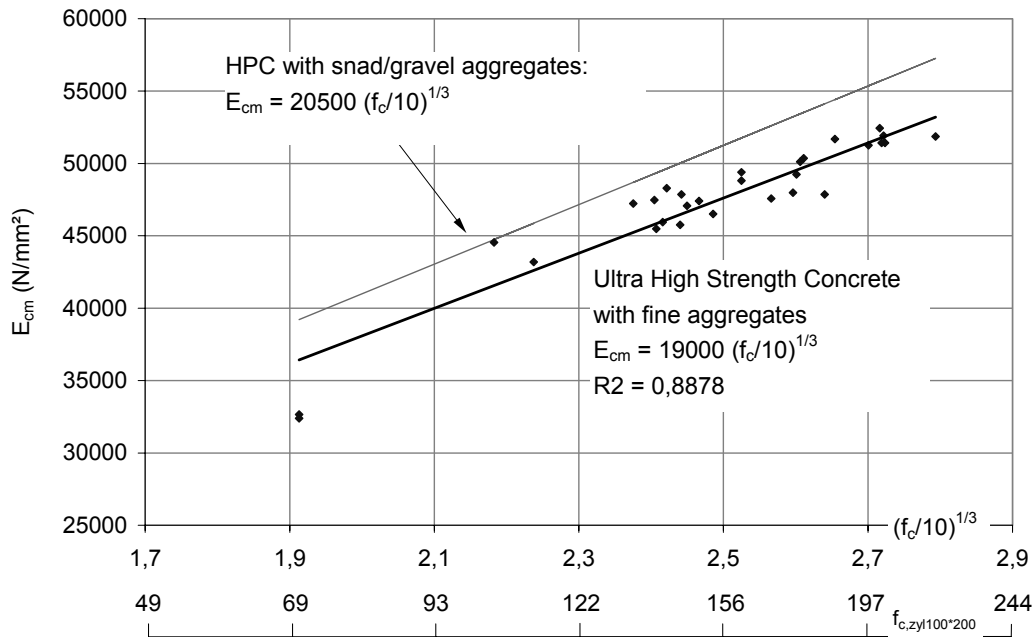
Figure 3: Elastic modulus versus compressive strength

The Poisson ratio in general has been determined to be about 0.2 in the linear elastic range.The strain at peak stress for UHPC with fine aggregates amounts to approximately 4.4 ‰. For basaltic aggregates or e. g. DENSIT-UHPC using bauxite, lower values have to be expected.

For UHPC with fibres (UHPFRC), a pronounced descending branch can be developed by the effect of the fibres (Figure 4). The slope of the descending branch depends on

- fibre content,
- fibre geometry (length, diameter),
- fibre length in relation to maximum aggregate size,
- fibre stiffness (in case of fibre cocktails) and
- fibre orientation.

Although in general the influence of fibres on the compression strength is low. Due to 2.5 vol.-% of fibres, an increase of the compressive strength of about 15 % has been noted [3].

For UHPC, the geometry of test specimens seems to have less influence on the compressive strength. However, contradictory results from different sources exist with respect to this question.

Heat treatment can speed up the development of the compressive strength. At 250 °C, a significant increase of the strength can be obtained, since the high temperature does not only accelerate the chemical reaction but also leads to an improvement of the microstructure. According to [1 ,3], even at 90°C heat treatment lasting 48 hours will enable higher compressive strength values than for the case of curing 28 days in water.
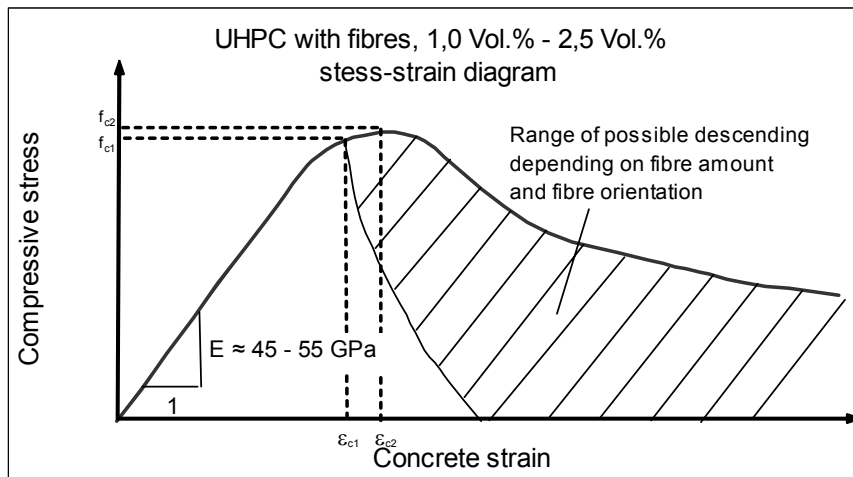
Figure 4:   Typical stress-strain-diagrams of UHPFRC

3   Behaviour in Tension

The tensile strength can be determined experimentally using prismatic or cylindrical specimens. It may be advantageous to use probes sawn out of plates. In principle, it is possible to use specimens with or without notches.

Direct tension tests on UHPC without fibres have delivered tensile strength values between 7 and 10 MPa. According to results obtained at the Universities of Kassel and Leipzig, there are only small differences between UHPC with fine or coarse aggregates. The failure is rather brittle, hence without a significant descending branch.

Depending on the amount, type and orientation of fibres, the tensile strength of UHPFRC can be increased beyond the matrix strength. Values in the range between 7 and 15 MPa [3] have been recorded. Due to the effect of fibres, the behaviour becomes ductile. After onset of cracking, the material may be characterised by the stress-crack-opening-diagram. The typical behaviour is depicted in Figure 5. It should be noted, that the slope of the descending branch can be very different, depending on the fibre orientation and the content and type of fibres.
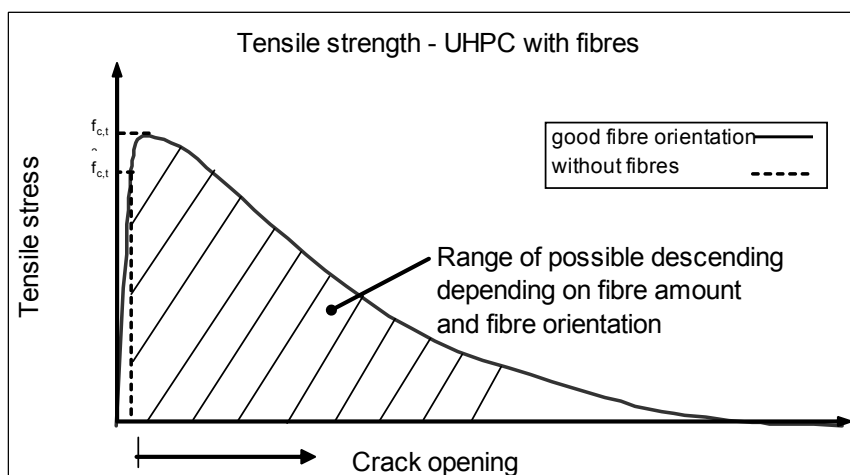
Figure 5:   Typical stress-crack-opening-curve for UHPC

In [1], a formula for the estimation of the splitting tensile strength in dependency on the compressive strength is given. Furthermore, the axial tensile strength may be derived from the bending tensile strength considering the size effect.
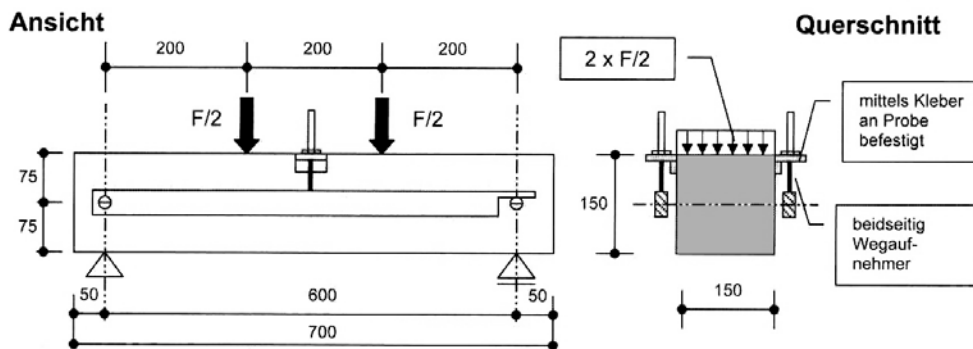
Figure 6:   Standard bending test according to DAfStb-Guideline on Steel-Fibre Concrete [4]

In order to simplify the testing procedure for tensile properties, the DAfStb-Guideline on Steel-Fibre Concrete [4] defines a test setup which allows the determination of the tensile strength as well as a stress-crack-opening-relationship. This is possible, since in general only one crack opens significantly so that the bending deformation is concentrated there and the crack opening is almost proportional to the deflection. Furthermore, a method to transform the stress-crack-opening-relationship into a stress-strain-relationship is presented in these guidelines. Figure 7 shows the typical result as obtained from bending tests, see [1].
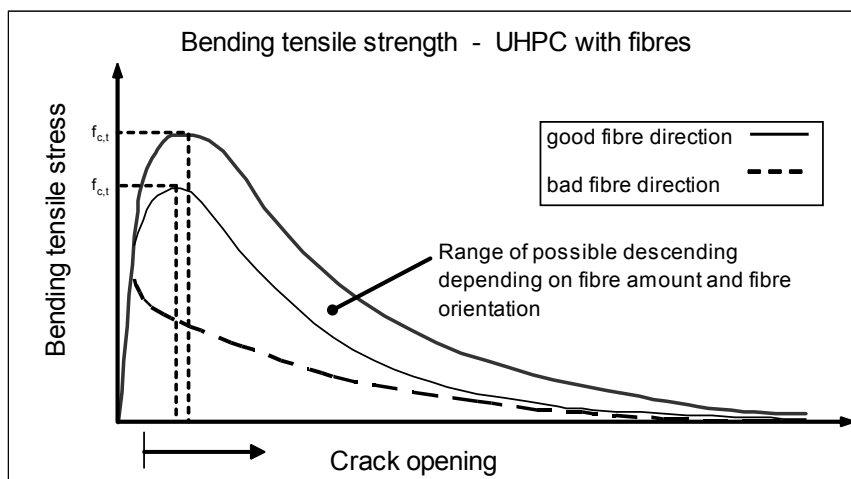
Figure 7:   Typical results from bending tensile tests

The influence of the fibre orientation has been studied by Bernier und Behloul [1], see Figure 8.
The influence of the fibre orientation is also picted in Table 1, where different types of specimens with vertical and horizontal pouring direction are compared.
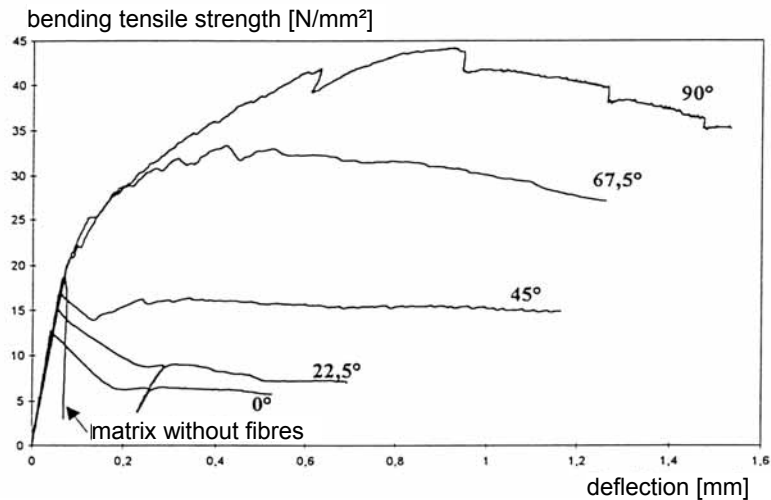
Figure 8: Influence of the fibre orientation on the bending behaviour

Table 1: Influence of casting direction on tensile strength and fracture energy

Test specimens	Age	Axial tension			Bending tension						
		F (specimen)		F (specimen)	Prism 160 * 40 *40		Beam 700 * 150 * 150				
Concrete		M1Q		B3Q	M1Q		M1Q			B3Q	
Curring		90°		90°	90°		WL	90°		WL	90°
Pouring direction		horizontal	vertical	horizontal	horizontal	vertical	horizontal		vertical	horizontal	
Fracture energy $G_{F,10\%}$ [N/m]	7d	16757	9993	-	20100	15097	-	20355	14543	-	-
	28d	14555	-	12932	18052	-	-	19892	-	-	-
	28d*	17014	-	-	19820	-	-	-	-	-	-
Tensile strength f_{ct} [N/mm²]	7d	14,2	7,9	-	34,0	22,5	11,1	22,1	17,6	18,3	18,0
	28d	13,3	-	7,0	35,7	-	13,3	22,2	-	20,4	17,9
	56d	17,7	-	-	36,3	-	16,2	22,1	-	24,2	18,1

Tests at TU Delft show, that especially the flow direction during the casting process affects the fibre orientation highly and thus, the tensile strength and ductility properties. The fracture energy of UHPC without fibres has been investigated e. g. at Leipzig University. Results are shown in Table 2. Figure 9 shows the decrease of the characteristic length with the compressive strength for NSC, HSC and UHPC.

Table 2:   Fracture parameters of UHPC for different mix designs

	Mortar 1	Mortar 2	Mortar 3	selfcompacting fine-grained concrete	compacted fine-grained concrete	UHPC with basalt grain
Cylinder compressive strength [N/mm²]	40	81,2	106,6	149,1	196,3	145,0
Fracture energy G_F [(N/m]	53,7	65,1	66,5	62,8	54,7	95,0
Tensile strength [N/mm²], $f_{ct}=0,9f_{ct,sp}$	3,2	6,1	8,0	9,4	11,9	8,3
Characteristic length l_{ch} [mm]	133,5	61,3	44,7	32,6	20,1	80,6
Softening function	bilinear	bilinear	Linear	linear	linear	bilinear
Limit crack width [µm]	79,2	65,6	15,1	13,2	9,8	127,2
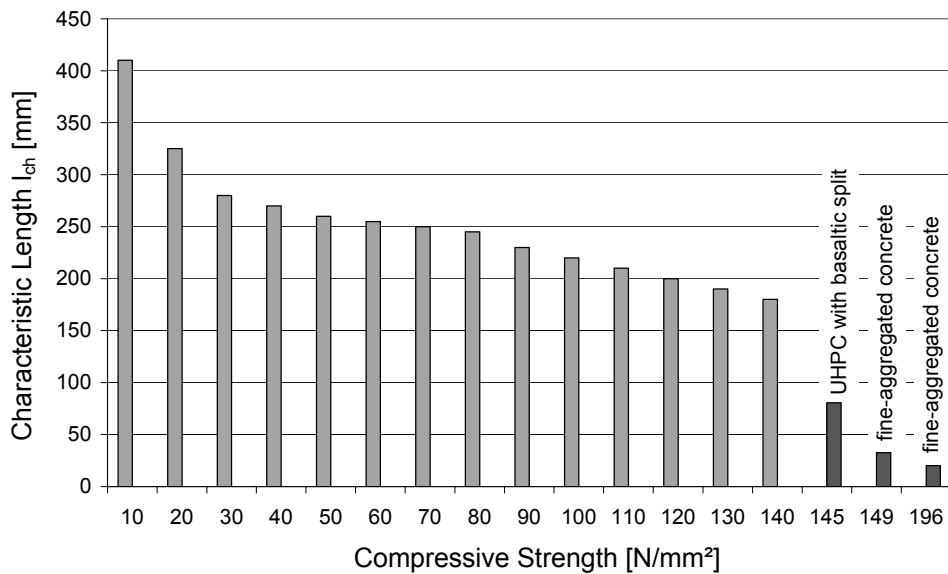
Figure 9:   Characteristic length l_{ch} versus compressive strength

4   Time dependant Properties

4.1   Shrinkage

According to data from Kassel and Leipzig [1, 3], the total shrinkage of sealed UHPC with fine aggregates amounts to 0.7 mm/m under isothermal conditions in the first seven days after pouring. Until an age of 28 days, the total shrinkage increases to about 0.9 mm/m. The influence of steel fibres on the autogenous shrinkage is of minor importance. Figure 10a and b give examples for the development of shrinkage versus time.
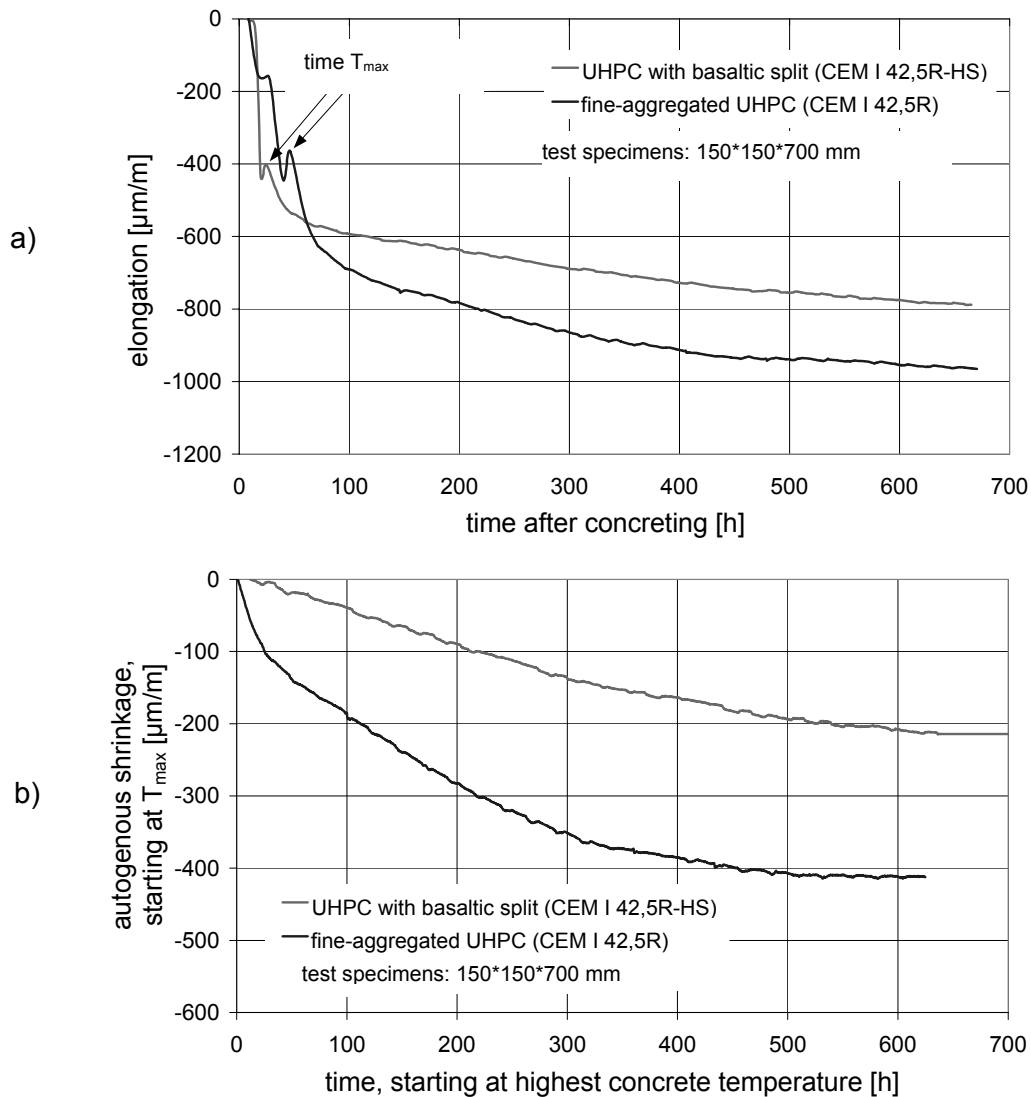
Figure 10: Development of shrinkage versus time

The development of drying shrinkage of UHPC is similar as of HPC. Due to the high density of the matrix structure, however, the amount of drying shrinkage is reduced in comparison to HPC. For heat treated UHPC, drying shrinkage can practically be neglected after the end of the heat treatment.

4.2   Creep

Creep of UHPC is generally less than for concrete with lower strength. Table 3 shows the results according to [5] and [1]. A strong dependency on the concrete age at the start of loading becomes evident.

Table 3:   Results of investigations on creep of fine-aggregated-UHPC [6]

Age at Start of Loading [days]	Amount of Creep (10^{-6}/MPa)	Creep-Number ϕ (-)
1	46,9	2,27
4	37,2	1,80
7	32,5	1,57
28	22,2	1,08

(Age at Start of Loading = 7 d, Loading Duration = 135 d)

Degree of Utilisation	Amount of Creep (10^{-6}/MPa)	Creep-Number ϕ (-)
45%, sealed	37,2	1,613
45%, free	42,1	1,787
53%, sealed	34,0	1,378

5   Coefficient of thermal expansion

As for NSC, the coefficient of thermal expansion is age-related. For UHPC with fine aggregates, 12 µm/mK have been recorded in [7]. This value is in the same range as for NSC (about 11,0 µm/mK). For very young UHPC (less than 3 days), further research is necessary.

6   Fatigue Resistance

For fatigue loading under compression, tests performed at the University of Kassel for UHPFRC have shown a rather good-natured behaviour. S-N-curves for UHPC and NSC are compared in Figure 11. The (relative) stress range of UHPFRC for a large number of load reversals (> 2 million) is similar high as for NSC, while the absolute stress level is much higher than for NSC. Thus, it can be said, that in contrast to other high strength materials, the high strength of UHPC with fibres does not lead to disadvantages with regard to fatigue.

Currently, fatigue tests in bending are conducted at Delft University of Technology. Since a paper on this topic is given to the conference, the subject is not to be discussed here.
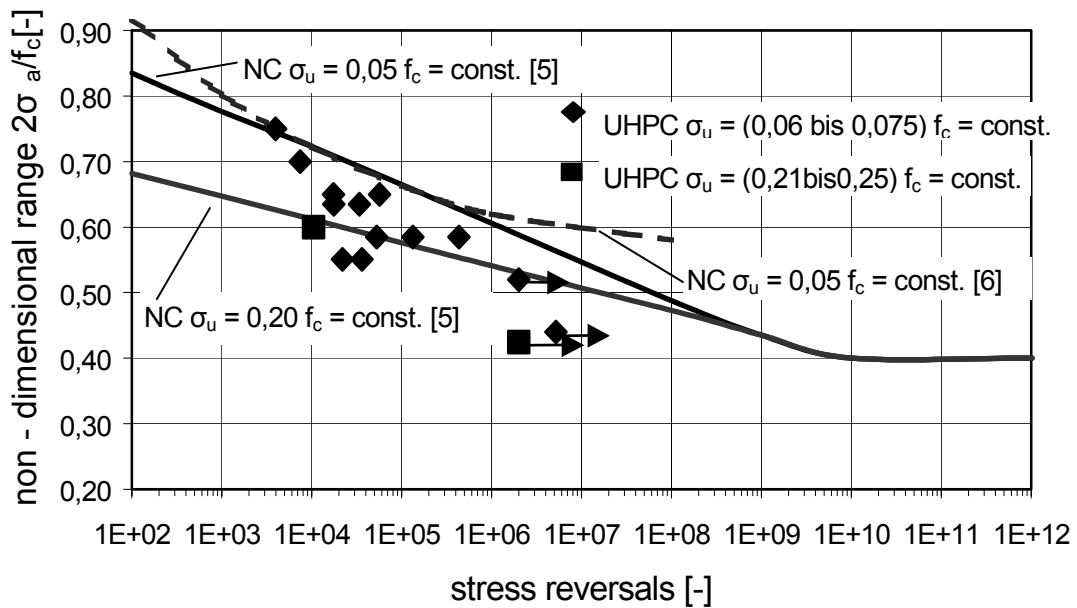
Figure 11: S-N-curves for UHPC in comparison to NSC

7 Bond of Reinforcement

Due to the high compressive strength and the high density, UHPC enables very high bond stresses. For smooth fibres (l = 13 mm, Ø = 0.15/0.2 mm), Behloul [1] reports a value of f_b = 11.5 MPa for BPR (DUCTAL). For prestressing wires and strands, the maximum bond stress depends on the concrete cover (see Figure 12)
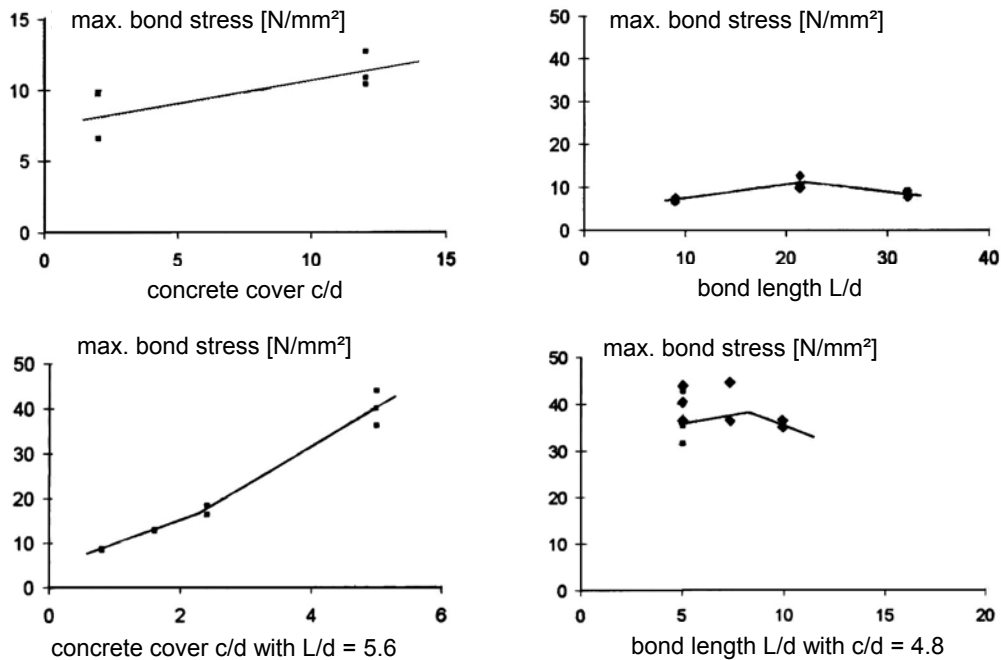
Figure 12: Bond strength for prestressing strands (Ø 12,5 mm) depending on contact length to diameter according to [Cheyrezy, Roux, Behloul, Ressicaud and Demonte (1998)]

For ribbed reinforcing bars, test results are available from Weiße in Leipzig and Greiner/Reineck (University of Stuttgart, Figure 13). Very high bond stresses in the range of 40 to 70 MPa have been reported. In tests on rebars with 10 mm diameter, Weiße observed splitting failure in the concrete cover for a cover less than 25 mm. Due to the high bond stresses, the bond length in the standard RILEM pull-out specimen has to be reduced to 2 $\varnothing$ instead of 5 $\varnothing$ (see Figure 14). Otherwise, no pull-out would be feasible before the yielding of steel. Weiße used 1.5 $\varnothing$ for his tests.
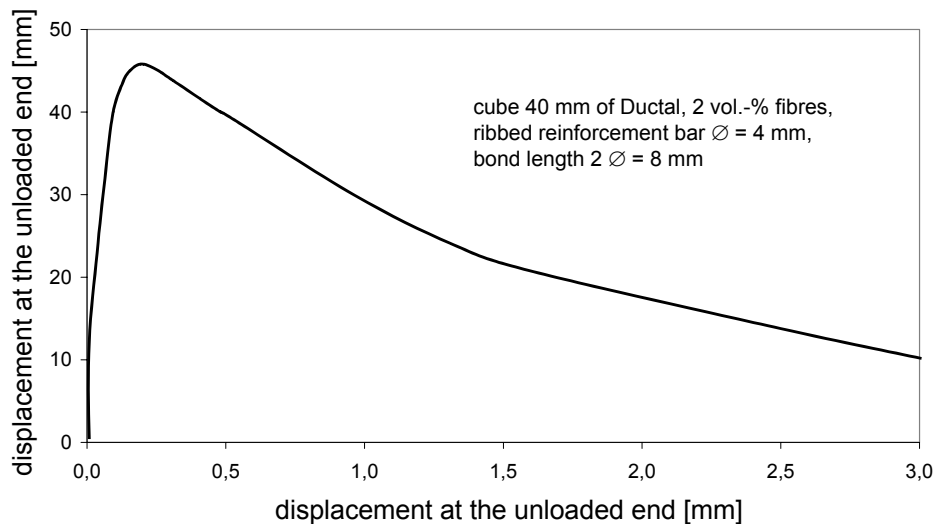
Figure 13: Bond-stress-slip-relationship of UHPC according to Reineck and Greiner [1]
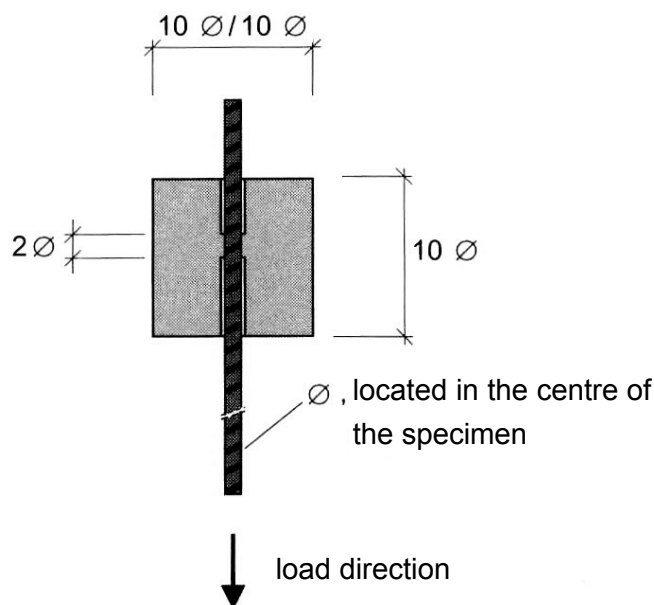
Figure 14: Modified RILEM pull-out test

8 Fire Resistance

Due to the extremely high density of UHPC, high water pressure can arise when UHPC is exhibited to fire. This can lead to deterioration of the concrete structure. The problem can be overcome by the use of fibres, e. g. polypropylene fibres. One effect of the fibres is that they create capillary pores due to melting and burning. Furthermore, around the fibres transition zones to the cement matrix are formed. By this, the existing transition zones between aggregates and matrix are interlinked so that the permeability increases and the steam pressure is reduced. Experiments have shown the effectivity of adding polypropylene fibres [8, 9, 10, 11].

Another problem is associated with the anomaly of quartzitic compounds with respect to the volumetric expansion occurring at 573 °C due to the change of crystal phases (α-quartz to β-quartz). Good results could be obtained by replacing quartz by basalt [12].

9 References

[1] Sachstandsbericht Ultrahochfester Beton - Betontechnik und Bemessung - in preparation, Deutscher Ausschuss für Stahlbeton im DIN Deutsches Institut für Normung e. V., 2004.

[2] Bornemann, R.; Schmidt, M.; Fehling, E.; Middendorf, B.: Ultra-Hochleistungsbeton UHPC – Herstellung, Eigenschaften und Anwendungsmöglichkeiten. Beton- und Stahlbetonbau 96, No. 7, p. 458-467, 2001.

[3] Fehling, E.; Schmidt, M.; Teichmann, T.; Bunje, K.: Entwicklung, Dauerhaftigkeit und Berechnung Ultra-Hochfester Beton (UHPC), Forschungsbericht an die DFG, Universität Kassel, 2003.

[4] DAfStb-Richtlinie Stahlfaserbeton (10. Entwurf), Ergänzungen zu DIN 1045-1, Teile 1 bis 4, March 2003, Deutscher Ausschuss für Stahlbeton im DIN Deutsches Institut für Normung e. V.

[5] AFGC Groupe de travail BFUP: wissenschaftliche und technische Berichte über Ultra High Performance Fibre-Reinforced Concretes, Zwischenbericht, Frankreich, January 2002.

[6] Ma, J; Schneider, H.: Creep of ultra-high performance concrete under compressive stresses, Leipzig Annual Civil Engineering Report, No. 8, 2003.

[7] Ma, J.; Dehn, F.; König G.: Autogenous shrinkage of self-compacting ultra-high perfomance concrete, in Proceeding "International Conference on Advances in Concrete and Structures", May 2004, Xuzhou, P.R. China.

[8] Diederichs, U.: Hochtemperatur- und Brandverhalten von hochfestem Stahlfaserbeton. In: Betonbau Forschung, Entwicklung und Anwendung, No. 142, p. 67-76, TU Braunschweig 1999.

[9] Schneider, U.; Horvath, J.; Dehn, F.: Abplatzverhalten von ultrahochfestem Beton (UHPC) unter Brandbeanspruchung, Leipzig Annual Civil Engineering Report (LACER), No. 6, Universität Leipzig 2001.

[10] Schneider, U.; Horvath, J.; Dehn, F.: Faserbewehrte ultrahochfeste Betone, in: König, G.; Holschemacher, K.; Dehn, F. (Eds.): Faserbeton - Innovationen im Bauwesen, Bauwerk-Verlag, Berlin 2002.

[11] Dehn, F.; König, G.: Fire Resistance of different Fibre Reinforced High-Performance Concretes, In: Naaman, A; Reinhardt, H.-W.: Workshop HPFRCC 4, Ann Arbor (USA), June 2003.

[12] Bornemann, R.; Schmidt, M.; Vellmer, C.: Feuerwiderstand ultra-hochfester Betone, Beton 52, No. 9, p. 418-422, 2002.

Tue, Ngyen Viet
Prof. Dr.-Ing. habil.
Leipzig University
Leipzig, Germany

Simsch, Gert
Dr.-Ing.
Bilfinger | Berger AG
Mannheim, Germany

Schneider, Holger
Dipl.-Ing.
Leipzig University
Leipzig, Germany

Schmidt, Detlef
Dr.-Ing.
Bilfinger | Berger AG
Leipzig, Germany

Bearing Capacity of Stub Columns made of NSC, HSC and UHPC confined by a Steel Tube

Summary

The contribution gives an overview of a series of tests on stub composite columns under centric loading. The filling consists of concretes of a wide strength range. Normal strength concrete (NSC, 36 MPa), High Strength Concrete (HSC, 96 MPa) and Ultra High Performance Concrete (UHPC, 160 MPa) are used. The load is applied in this series exclusive on the concrete section so that the load bearing behaviour of the confined concrete core can be tested. Comparatively the carrying behaviour of a UHPC-stub column is presented during load application on the entire section.

The ultimate forces and the mechanical behaviour of the different specimens are compared. In general, the bearing capacity of columns is lower when the load is applied on the entire cross-section than when the load is applied on the concrete. Columns made of NSC and HSC filling are able to activate the steel confinement after a low cycling pre-loading, where columns made of UHPC need a higher stress level to excite a sufficient lateral strain to compensate the shrinking gap between the concrete core and the steel casing.

Keywords: *Confinemend effects, stub columns*

1   Introduction

Within the Bilfinger | Berger AG research project conducted at the institute for structural concrete and building materials at the Leipzig University, hybrid elements with high bearing capacity and sufficient ductility consisting of Ultra High Performance Concrete (UHPC) shall be developed. The concrete without fibres has compression strength of approximately 160 MPa. Because of the brittle behaviour of UHPC without fibres, steel tubes are used to increase the ductility. This leads to a hybrid element.

Basing on test results on stub columns of the slenderness l / D = 4, which are loaded exclusively at the concrete area, in the context of this contribution the potential and the characteris-tics of the UHPC are shown, in contrast to the well known HSC and NSC.

The perceptions that can be derived are required for the development of calculation models for hybrid elements made of UHPC.

2   Geometry of the specimens

Figure 1 shows the experiment setup of the presented series. The loading was applied alternatively on the entire and/or only on the concrete section. In the tests two levels of measurement (centre and D/2 of the edge of the cross section) with three 90°-strain gauge rosettes were arranged for each specimen monitoring the steel strains. Additionally, the integral deformations of the specimens over the centre area (measuring length 300mm) and over the overall length are recorded. At the series denoted as 'concrete cross section', shown in figure 1, the concrete deformations were measured directly over a length of 300 mm. This could be achieved by an arrangement of drillings in the steel tube and cast-in measuring mounting bars.

The geometry of the specimens is almost identical. Only the wall thickness of the steel tube was varied. Cold formed welded and industrially manufactured pipes were used exclusively, due to better dimensional accuracy. The cross section of the series presented here is a pipe with a di-ameter of 168.3 mm and a wall thickness of 4.5 mm. The strength of the pipe material can be indicated for the relevant strain ranges at approximately 350 MPa. (fig. 3). Due to practical con-siderations, the application of high strength steel was waived although this is generally favour-able for the bearing behaviour.
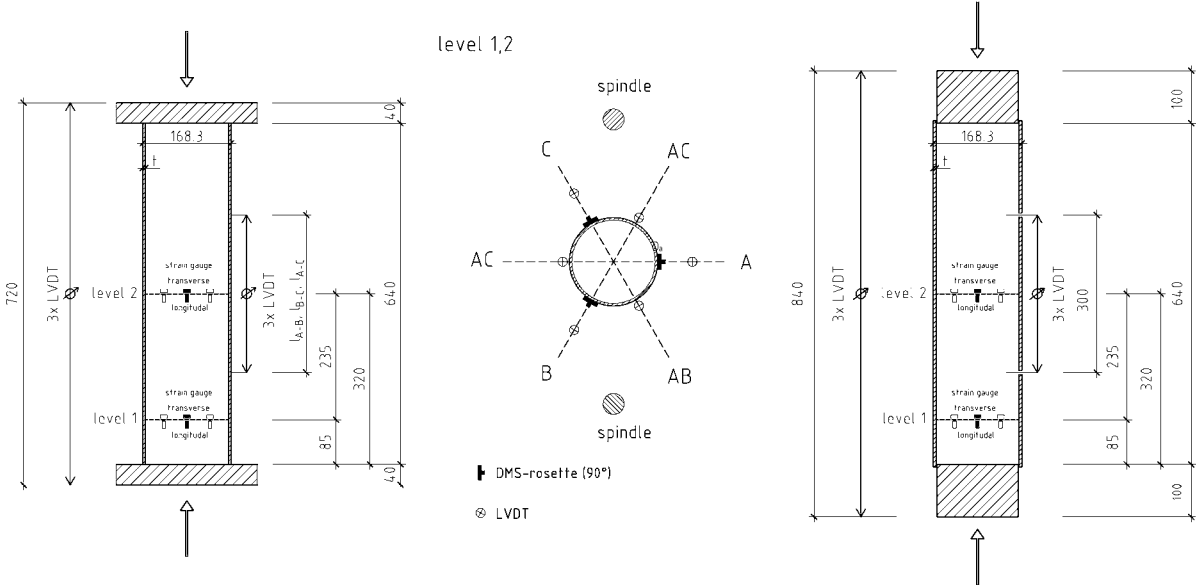
Figure 1:   Setup of the experiments

3   Material properties

3.1   Properties of the filling material UHPC in comparison to HSC und NSC

UHPC without fibres differs fundamentally from normal-strength concrete (NSC) and high-strength concrete (HSC). For this investigation, coarse aggregate (basalt) UHPC with compara-tively low cement content and self compacting characteristics, which ensures a

340

characteristic 28-days strength of at least 150 MPa, and without thermal treatment was used. Table 1 shows the mixture of the tested concrete.

Table 1:   Mixture of the tested concrete

Materials	UHPC	HSC	NSC
Cement CEM I 42.5 R (c)	1.0	1.0	1.0
Water to cement ratio (w/c)	0.302	0,316	0,519
Water to binder ratio (w/b)	0.232	0,276	0,519
Lime powder / to water	- -	- -	0,481
Quartz sand (0.3-0.8 mm) / water	3,003	- -	- -
Basalt split (2-5 mm) / water	6,778	- -	- -
Sand 0/2 to water	- -	5,389	4,356
Coarse Aggregate 2/8 to water	- -	3,170	1,448
Coarse Aggregate 8/16 to water	- -	6,643	4,69
$f_{c,cyl.100*200}$ (N/mm², 28d/20°C)	150-165	96	36

In accompanying tests the stress-strain correlation and the lateral extension behaviour of the filling materials were determined. Fig 2 shows a typical stress-strain curve of the UHPC compared with normal strength concrete (36 MPa) and high strength concrete (96 MPa) as well as the development of the Poisson's ratio in relation to the relative compression stress (fig. 3)
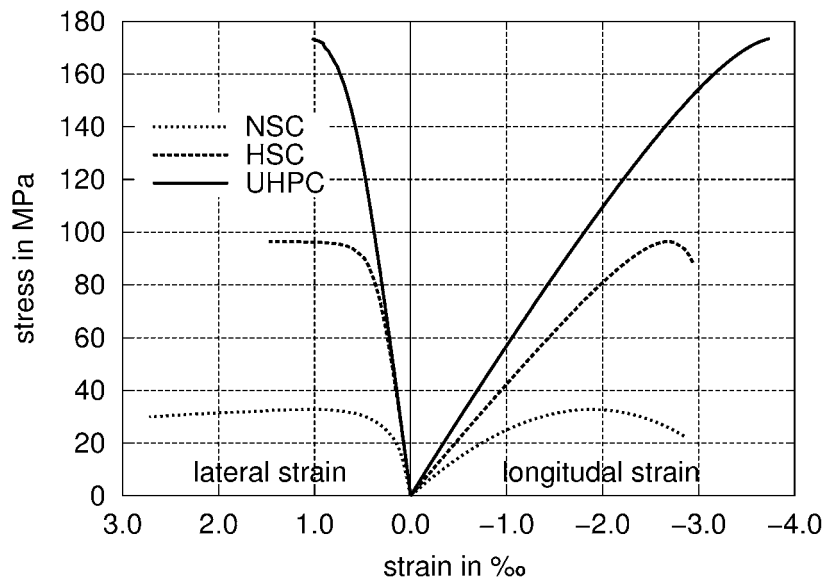
Figure 2:   Concrete stress vs. strain
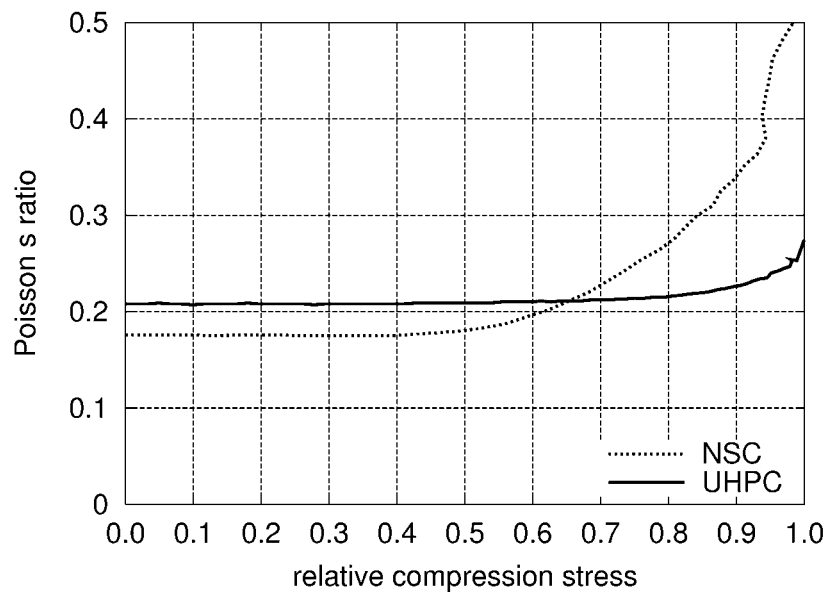
Figure 3:   Poisson's ratio vs. relative compressive stress

The UHPC differs significantly from NSC according to the following critical aspects for the description of the bearing behaviour:

· high modulus of elasticity of approximately 55000 MPa
· linear gradient of stress-strain curve below stresses of approximately 70% of the strength
· almost no micro cracking and no increase of the material volume
· constant Poisson's ratio from approximately v=0,21 below 0,7 f_{ck}, increase up to max. v=0,32 above 0,7 f_{ck}
· extremely brittle material failure
· almost no short time creeping at stresses below 0,6 f_{ck} measurable
· comparatively high autogenous shrinkage [1]

3.2   Properties of the tube

The constitutive law of the steel under tensile stresses was determined in accompanying strain gauge equipped tension-coupon tests. In order to derive the constitutive law under compression within the relevant strain range, short pieces of pipes were compressed, see fig. 4.

Due to the cold transforming process of the tubes during the production, both the solidification effects under tensile stress and a slight Bauschinger effect under compression stress occurred. For the following investigations, however, it is acceptable to use the same constitutive law under compression and tensile stresses, which can be computed as an average value between the compression and tensile constitutive law.
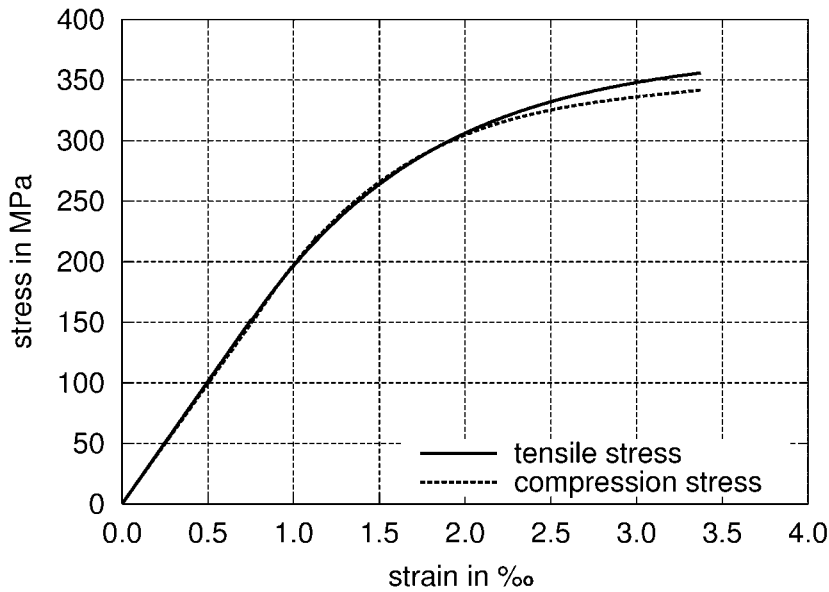
Figure 4:   Constitutive law of the tube material under compression and tensile stress

4   Investigational procedure and selected results

4.1   Load history

The tests were performed generally with the load path according to figure 5. Each test specimen received a pre-loading from 100 load-cycles with maximum amplitude from approximately 40% of the theoretical longitudinal yielding force of the entire section. This alternating stress was followed by a 15 minute shutdown period. After the application of the cyclic loading, stress the specimen was loaded until failure controlled by deformation.
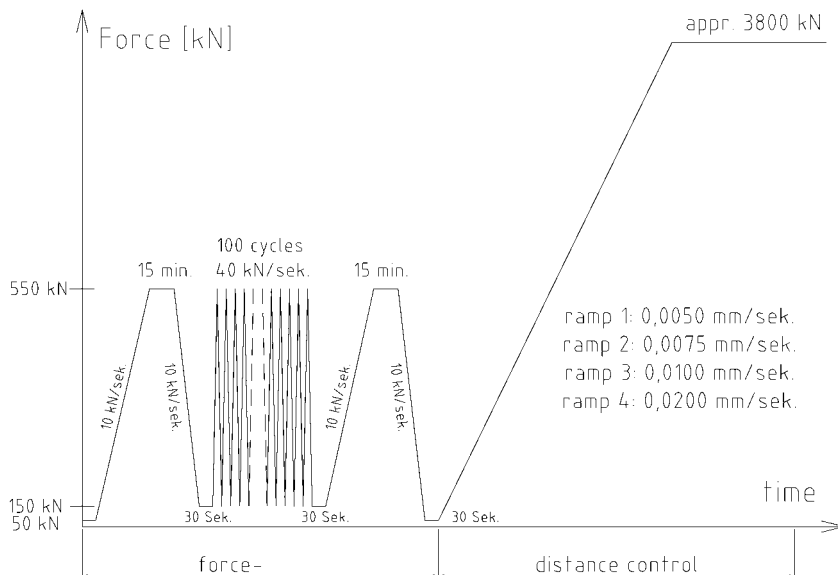
Figure 5:   Load history

4.2   Load-deformation relationship of the specimens

Figure 6 shows curves of the last load branch and the post peak behaviour of the examined specimens. The specimen with NSC filling shows a remarkable ductile deformation capacity. Due to extensive micro cracking, a horizontal load plateau on a load level of approximately 1750 kN was detected showing large deformations. The plastic load capacity (steel + concrete) was exceeded by 15 %.

An HSC filling of the tube is able to almost double the load. The increase of the load path is clearly steeper compared to the NSC, which is caused by the higher modulus of elasticity. After reaching the peak load, the load drops continuously with increasing deformation. The load decrease is, however, very moderate. The failure is induced by the formation of a shear plane. After the separation of the concrete core, both shear plane surfaces slide relatively to each other, whereby the steel tube, which is yielding in tangential direction, provides a holding force.

The presented curve of the UHPC filled specimen is similar to the HSC curve, however, with a more distinctive characteristic. The increase in force is steeper due to the higher modulus of elasticity. The failure characteristic is also more brittle. Regarding safety aspects, it has to be mentioned that a load level of approximately 66% of the plastic load capacity is reached when the shear plain occurs.

The plastic normal force of the specimen loaded at the concrete (UHPC) and the tube section is indicated by the peek of the ES-curve in Fig. 6. Due to the early activation of the steel cross section, this curve proceeds more steeply compared to the corresponding function of the specimen loaded only at the concrete cross section (CS-curve); however, the load level of the CS-curve cannot be achieved. This behaviour is caused particularly by the low lateral strain of the UHPC at high stress level. This effect leads to lower - propitious - lateral pressure; hence, for this load arrangement the confinement effect of the UHPC is small and both the steel and the concrete cross-section act separately until failure.
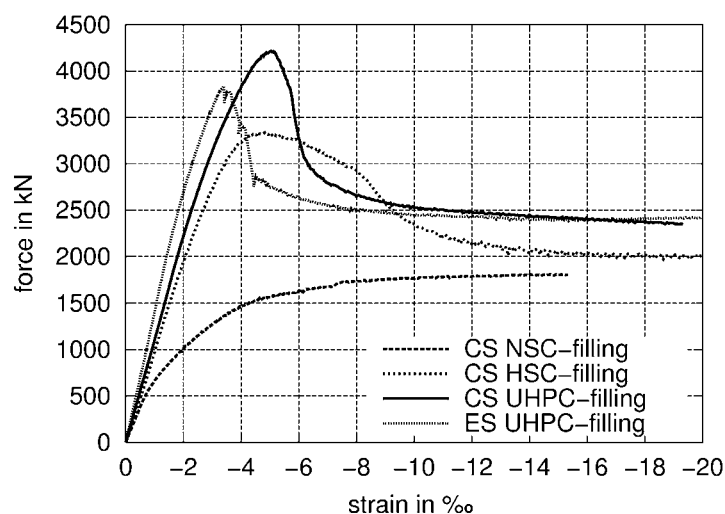
Figure 6:   Force-strain-relationship of the specimen with different concrete grades and load arrangements

From the presented tests the potential of the HPC and UHPC can be derived. Substantial effects of a confinement are the increasing strength and ultimate compression strain due to the multi-axial stress state. The ultimate uniaxial compression strain of the unconfined UHPC is identical to that of the entire loaded cross section specimen. The confinement effects as a function of the wall thickness are one main part of the above mentioned research project.

4.3 Identification of certain parameters

Apart from the global point of view, during the evaluation of the force deformation relations, the important parameters must be defined for a structural model and be extracted from the measured data.

Following parameters are important:

- Stress state of the steel in the two levels of measurement in radial and longitudinal direction
- Contact zone between steel and concrete (friction coefficient, shrinking gap)

In Fig. 7 a comparison of the strain states of level 2 is shown, varying the strength of the filling material (series 'concrete section loaded').
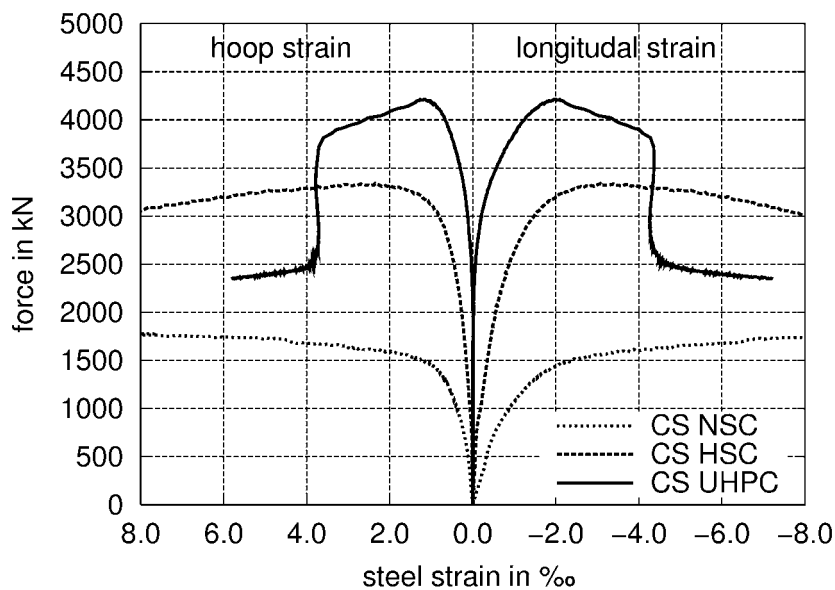
Figure 7: Strain states of the measurement level 2 for different concrete fillings

The NSC shows a distinctive potential on deformation capacity with enormous member ductility. Filling concretes of this strength grade are capable of large redistribution of stress, which enables plastic resistance capacity. This approach was the basis for normative calculation models using the entire plastic capacity since many years.

The specimen with HSC filling behaves – at a high load level, but below a strain of approximately 6 ‰ - similarly to the NSC filling.

The separation of the material occurs moderately and finally results in a strain range beyond the shown curve range ending with formation of a shear plain. This behaviour is not compatible - particularly under the aspect of an additional bending load - with the basic assumptions that are implemented for a plastic calculation model. For this reason, these strength grades are not con-sistent to the current calculation standards like EC4 [2] and DIN 18805 [3].

Focusing on the UHPC filling, the failure process is characterised by a greater brittleness. Be-yond that it is remarkable that steel strains at the UHPC specimen are measurable above a load level of approximately 2500 kN, while at the remaining specimens steel strains are measurable directly after beginning of loading. Since within the elastic range the Poisson ratio of all applied concretes is always about 0.2, this phenomenon leads to perception that a gap between the concrete core and the steel casing must exist; this gap is being closed with increasing lateral extension of the specimens that are loaded exclusively at the concrete section. It is evident that such a gap can only result from a strong autogenous and plastic shrinkage of the UHPC, which can be indicated as 0.5 ‰ for this concrete [1]. Of course, also HSC tends to plastic and autogenous shrinkage, which should not be neglected. However, these are no longer recognizable at the last load branch since due to the preloading of these concretes the shrinking gap is already closed by plastic deformation of the material. Thus, a complete contact between wall and core already exists when applying the ultimate load.

The following rough calculation may clarify the correlations.
Concrete stress while starting contact

$$\sigma_c = \frac{2500 \cdot \pi \cdot 4}{\left(168{,}6 - 2 \cdot 3{,}94\right)^2} \cdot 100 = 122 \ \text{MPa} \ \approx \ 0{,}79 f_c$$

attained lateral strain

$$\varepsilon_{quer} = \frac{\sigma_c}{k \cdot E_c} \cdot \mu = \frac{122}{0{,}95 \cdot 56.000} \cdot 0{,}21 = 0{,}48 \ \text{‰}$$

with correction factor modulus of elasticity at $0{,}8 \cdot f_c$: $k = 0{,}95$

The UHPC, therefore, exhibits only such small plastic deformation – also under cycling loading – that the developing shrinking gap cannot be closed.

Table 2 shows an overview of the theoretical concrete stresses during the preloading phase assuming that the load is applied exclusively on the concrete cross section. Therefore, the stress level of all tests is about 50 % of the uniaxial cylinder strength. At this stress range for the NSC as well as for the HSC, portions of plastic deformation in evidence appear, which are responsible for closing the gap that is smaller for these types of concrete.

Table 2:   Stress level of the concrete core during the cyclic loading

test	force [kN]	stress [MPa]	σ/f_c [--]
NSC	365	18	0,55
HSC	975	48	0,49
UHPC[1)]	1550	76	0,49

[1)] Parallel test with entire section loaded f_c=154 MPa

Therefore, if the effect of the shrinking gap for NSC and HSC can be excluded, this influence must be considered for the modelling and design of the components with UHPC filling.

In the following, the proceeding of the evaluation for the UHPC series is described in details. If the contact between stele and concrete exists due to the increasing lateral extension of the concrete core, the steel strains increase continuously and lead to steel stresses. Fig. 8 and 9 show the applied load and the developing of steel stress vs. concrete strains for the particular specimens under pure loading of the concrete. The stresses of the steel occurring in longitude and radial direction were determined iteratively on the basis of the uniaxial constitutive law with the program system ABAQUS.
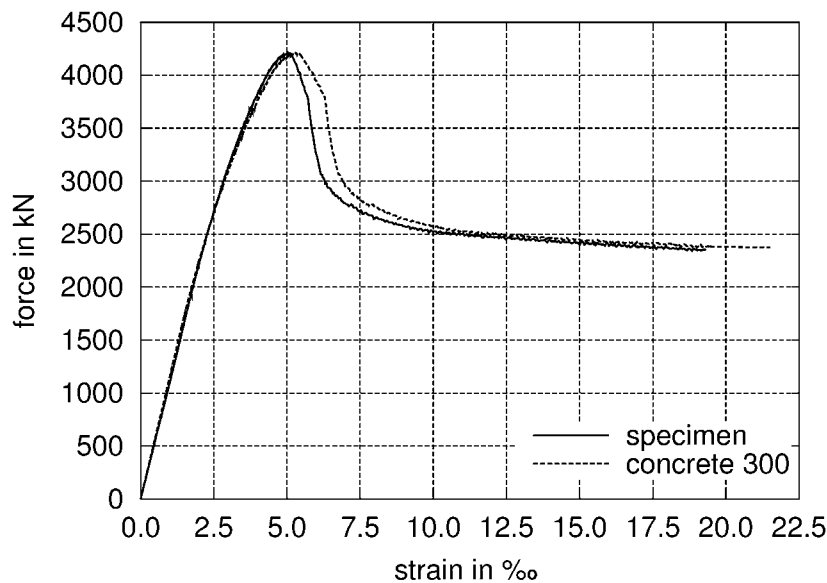
Figure 8:   Load vs. concrete strain
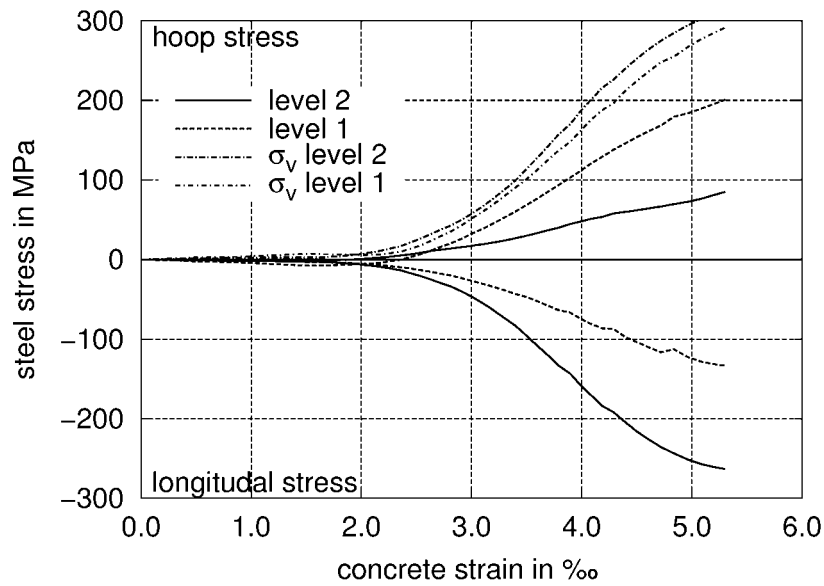
Figure 9:   Steel stress vs. concrete strain

If the stresses are known within the steel cross-section in both levels of measurement, the stresses can be converted into forces and the internal force equilibrium can be formulated for each level of applied loading. On this basis, the associated concrete stresses in longitudinal and radial direction can be determined for the different levels. Fig. 10 shows the corresponding curves in dependence of the longitudinal concrete strain for the levels directly at the load stamp, at the level 1, and at the level 2 in the centre of the specimen. The differences result from friction effects in the contact zone between the steel wall and the concrete core. As comparison the curve for the unconfined concrete shown additionally, which was extracted from the test with loading on the entire section. The effect of increasing stresses and associating strains due to the confinement effect is obvious.
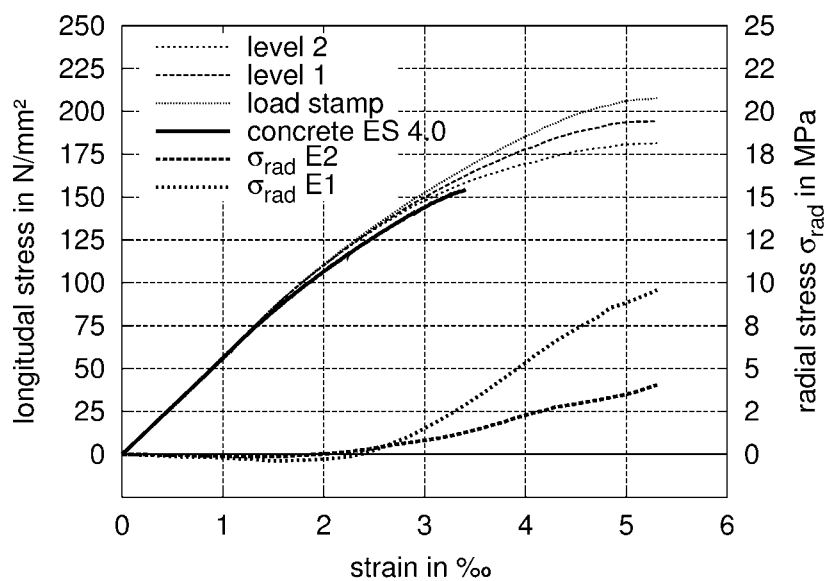
Figure 10:   Longitudinal and radial stress vs. strain

force in kN
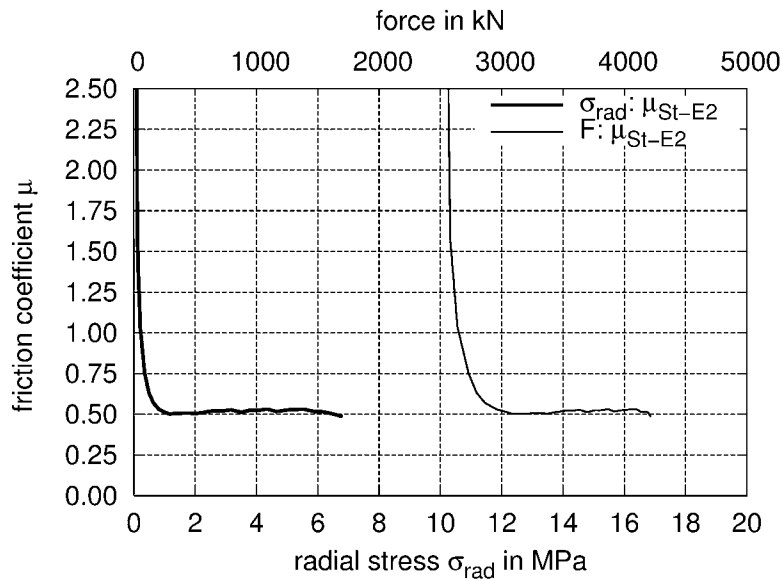
Figure 11:   Coefficient of friction vs. applied loading and radial stress

Figure 11 shows the computed friction coefficient, which is necessary for the equilibrium within the steel tube as mean value of the radial tension in the levels 1 and 2 assuming a constant value over the inducing length. The coefficient of friction plotted vs. the mean radial stress and the applied force. It can be found that for the precisely manufactured pipes the coefficient is $\mu=0,5$.

5   Summary

The investigations on stub, centrically loaded columns with a wide range of concrete strengths show clear differences regarding the load bearing behaviour. Fillings of normal strength concrete have an extensive deformation capacity when appropriately confined which is an decisive premise for an horizontal load plateau. Due to its higher stiffness, the more brittle HSC exhibits a clearly steeper inclination at the ascending branch of the load-deformation relationship. The application of UHPC can increase further the stiffness of the construction.

Assuming a uniformly distributed utilisation ratio for steel and concrete the required areas for steel and concrete can be reduced by using UHPC, while the ultimate load and the deformation behaviour compared to a HSC remain the same.

Therefore, this allows the application of cross-sections made of UHPC on columns, which were reserved previously to composite columns.

For the design of cross-sections, the high stiffness of the UHPC filling must be considered. The small plastic deformation of the material leads almost exclusively to reversible deformations, including cyclic loading within an upper range of the service load. This characteristic in combination with a rather intense shrinkage of the UHPC results in a lasting gap between the concrete core and the confining material, which is only closed when the stresses exceed the service level and lateral strain increases.

Acknowledgment

6   References

[1]   Ma, Jianxin: Comparative Investigations on Ultra-High Performance Concrete with and without Coarse Aggregates, Proceedings, International Symposium on Ultra-High Performance Concrete, Kassel, Germany, 2004

[2]   Eurocode 4: Design of Composite Steel and Concrete Structures

[3]   E-DIN 18800, Teil 5 – Verbundtragwerke aus Stahl und Beton; Bemessung und Konstruktion. 01/1999

Josef Hegger
Prof. Dr.-Ing.
RWTH Aachen University
Aachen, Germany

Dirk Tuchlinski
Dipl.-Ing.
Consulting Engineers Neff, Hirsch, Dr. Mahr
Köln, Germany

Boris Kommer
Dipl.-Ing.
RWTH Aachen University
Aachen, Germany

Bond Anchorage Behavior and Shear Capacity of Ultra High Performance Concrete Beams

Summary

The use of UHPC (UHPC = Ultra High Performance Concrete) opens up new possibilities for bridge- and high-rise building construction, and offers economic advantages through savings in the reinforcing steel, smaller cross-sectional dimensions and lower transport costs. In addition, the high compressive strength and the considerable high load-carrying capacity of UHPC, opens up new areas of application for prefabricated construction units, currently still reserved to other building materials.

In order to investigate the bond anchorage behavior and shear capacity the of pre-tensioned UHPC beams, several tests were carried out at the Institute of Structural Concrete at the RWTH Aachen University.

Keywords*:   Ultra High Performance Concretes (UHPC), Reactive Powder Concretes (RPC), High Performance Concrete (HPC), bond anchorage behavior, pretensioned tendons, shear bearing capacity.*

1   Introduction

The investigations performed at the Institute of Structural Concrete at RWTH Aachen University - on the basis of the mix designs documented in [3 to 8] - show that UHPC with a strength of f_c = 200 MPa can be reliably manufactured without additional heat curing. When these concretes are cured at temperatures of up to 250° C, a further increase in compressive strength of up to f_c = 360 MPa with flexural tensile strengths of $f_{ct,fl}$ = 40 MPa can be achieved [9]. Requisite for the attainment of these strengths, in addition to an optimal packing density of the aggregates, is a low water-binder ratio, which can be achieved with superplasticizing admixtures. The addition of wire fibers will ensure a sufficiently ductile behavior. Due to the performance behavior of UHPC, which differs from high strength concrete (HSC), the

concrete's significantly higher tensile strength and the omission of steel reinforcement, the verification concepts given in DIN 1045-1 cannot be applied to members made of UHPC [10 to 12]. For this reason, first investigations on the effect of heat curing on the development of strength, the transfer of prestressing force and the behavior of members made of UHPC under shear loading, were carried out.

2 Effect of Heat curing

A considerable increase in the compressive strength of concrete can be achieved with heat curing, with only a slight increase in the modulus of elasticity. Table 1 contains the material characteristics obtained in the experiments under different types of heat curing.

Table 1:   Concrete strength and modulus of elasticity for different types of heat curing

				Type of heat curing	
			-	90° C H_2O 24 h	250° C 24 h
Compressive concrete strength	$f_{c, cube\ 100}$	MPa	202	260	360
Tensile strength of concrete fiber length 6 mm	$f_{ct, fl}$	MPa	34,6	42,2	43,3
Tensile strength of concrete fiber length 13 mm	$f_{ct, fl}$	MPa	52,2	-	56,4
Modulus of elasticity	E_c	MPa	50 000	-	57 000

With heat curing at 250° C, a compressive strength within the range of the compressive strengths of steel can be achieved. The value of the concrete's tensile strength is influenced by the fiber length and the fiber content and is largely independent of heat curing. A comparison of the modules of elasticity shows that additional heat curing has only little influence on the magnitude of the modulus of elasticity. Therefore, it may be assumed that concrete cured at a temperature of 250° C would have to achieve a significantly higher elongation at failure. Figure 1 shows the elongations at failure undergone by a specimen not subjected to curing, and that of a specimen cured at 250° C. In addition, the development of the compressive strength as a function of the elongation of a concrete of C 100/115 is presented.
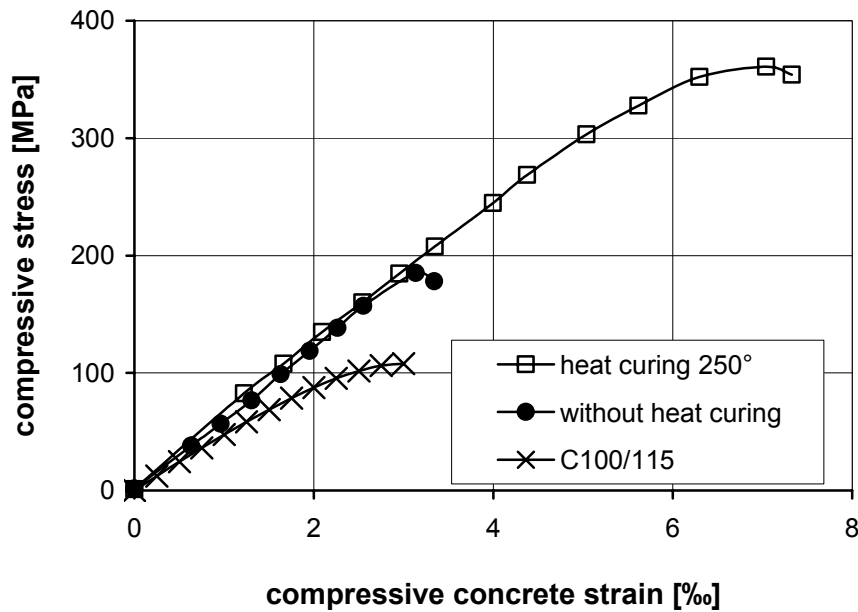
Figure 1: Comparison of the elongation at failure of UHPC and HSC (High Strength Concrete)

3 Bond Anchorage Behavior

3.1 General

Over the past years, several pull-out tests, tests on the transfer of prestressing force and tests of pretensioned beams made of High Performance Concrete (HPC) have been carried out [14]. Based on these tests, the bond properties of 7-wire strands (d_p = 0,5 in = 12.5 mm) and ribbed wires Ø 12 mm were investigated. Especially the lateral strain-dependent bond properties for the different types of concrete and the behavior in the transfer and anchorage zone were determined. The objective of the tests was to develop the basic information needed for code specifications, regulations and standards for the use of bond anchorages of pretensioned tendons, which are so far lacking.

The dimension of the bond anchorage zone can positively influence the cost-effective design of prestressed concrete girders. However, a minimum concrete cover has to be ensured to avoid splitting cracks. Splitting cracks in the transmission zone of the prestressing force yield to an uncontrolled increase in the transmission length and can cause an early failure induced by anchorage fracture.

The bond forces can be increased with special effectiveness with strands by the stress dependent lateral strain in the transmission zone of the prestressing forces. Therefore, an increase of the bond forces (especially for strands) can be expected (Fig. 2). This is attributed to the high radial pressure in the contact zone between prestressing tendon and concrete, called the Hoyer effect or Poisson's ratio effect [13].
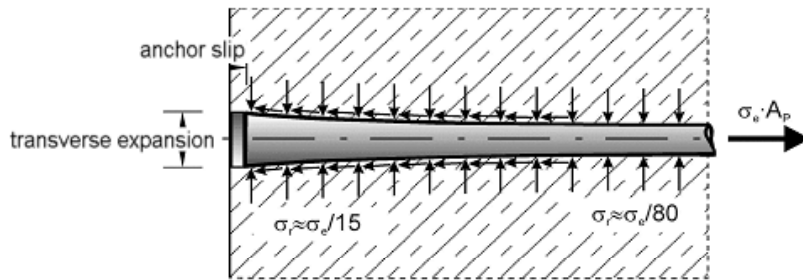
Figure 2:   Schematic view of the Poisson effect [13]

3.2   Tests of the Introduction of prestessing forces

The specimen used for the introduction of prestressing forces was dimensioned by varying the concrete covering and the clear spacing. The objective was here to establish the minimum concrete cover and the clear spacing required to prevent splitting. The test specimen models the transmission zone of prestressed girders as illustrated in Figure 3. The specimens have a rectangular cross-section with two or four 7-wire strands (d_p = 12.5 mm).
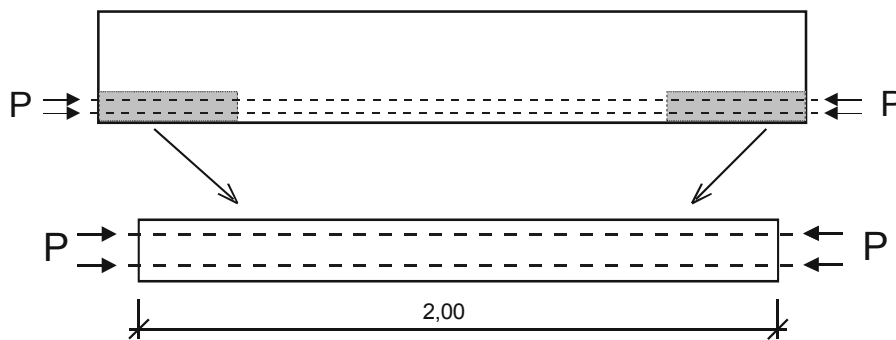
Figure 3:   Specimen modeling the transmission zone of the prestressing force

The first series contained two 7-wire strands to investigate the minimum concrete cover to prevent splitting. Subsequent specimens with four 7-wire strands were used to investigate the minimum clear spacing between the tendons to prevent splitting. The test specimens were manufactured on a prestressing bed.

For the transmission of prestressing forces according to DIN 1045-1 for 7- wire strands [15], the following dimensions are sufficient to guarantee a split-free anchorage zone.

> For s $\geq$ 2.5 d_p: c $\geq$ 2.5 d_p or
> For s = 2.0 d_p: c $\geq$ 3.0 d_p

Where s = clear spacing; c = concrete covering; d_p = nominal diameter of the 7-wire strands

The evaluation of HSC shows that these values are not dependent on the concrete strength. In Figure 4, dependence of the development of splitting cracks as a function of concrete cover and clear spacing of the 7-wire strands are described for HLC (High Strength Lightweight Concrete), and for SCC (Self Compacting Concrete). The results show that, for

HLC, the minimum concrete cover have to be increased to 3.0 d_p. For SCC, the specified minimum concrete cover and clear spacing are sufficient.
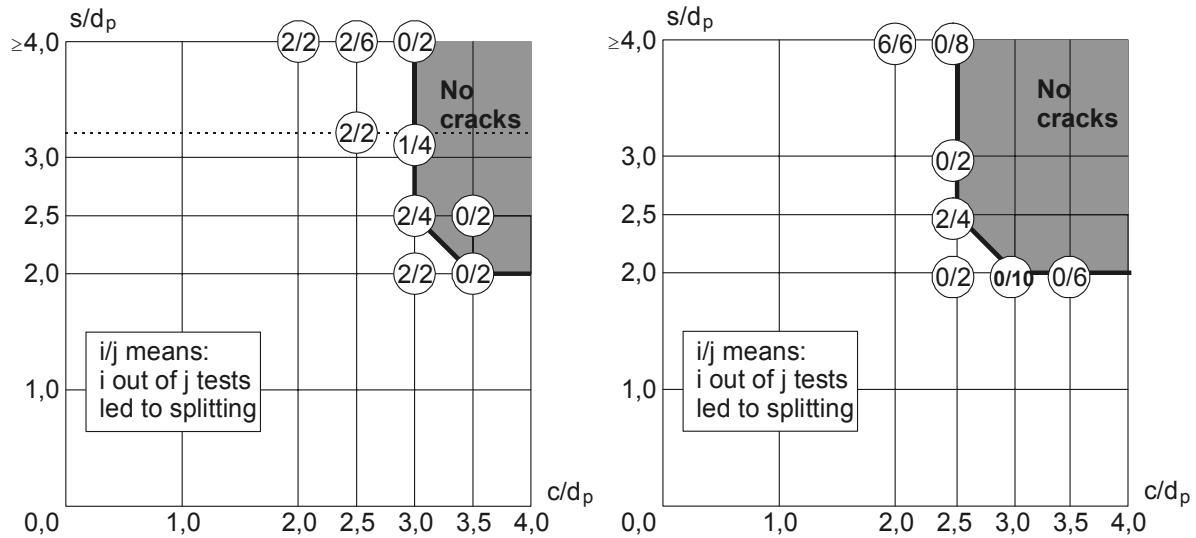
Figure 4: Development of splitting cracks as a function of concrete cover c and clear spacing s to the nominal diameter d_p of the 7-wire strands using HLC (left side) and SCC (right side)

These results are reasonable, considering the lower tensile strength of HLC and the higher tensile strength of SCC in comparison to NSC (Normal Strength Concrete). Because UHPC has a very high tensile strength, due to its fibre reinforcement, we can expect for a UHPC a smaller concrete cover and clear spacing preventing splitting. In order to investigate the bond anchorage behavior of pretensioned UHPC beams, several tests were carried out. In addition to the investigation of the minimum concrete cover and the clear spacing required to prevent splitting, the transmission lengths of the prestressing forces were measured on the test specimens. The measurement of the elongations of the concrete in the area of transmission was carried out by attaching stretch strobes (SDM) to both sides of the specimen (Figure 5). In order to investigate the slip at the end of the body, inductive displacement gauges were used.
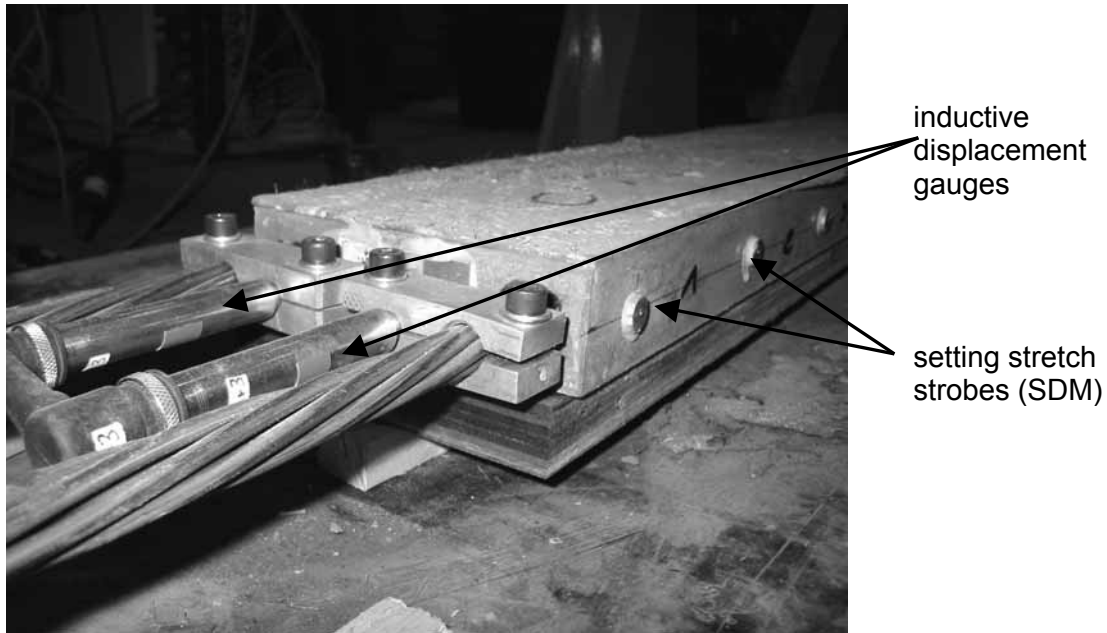
Figure 5: Test specimen with attached stretch strobes (SDM) and inductive displacement gauges for investigating the slip

First experiments have shown that the concrete cover required by the high tensile strength generated through the application of the prestressing forces and the minimum required clear spacing between the tendons can probably be reduced to 1,5 d_p to 2,0 d_p, compared to the values required for members made of HSC and SCC (Figure 6).

a) Introduction of prestressing forces

b) Strand slippage
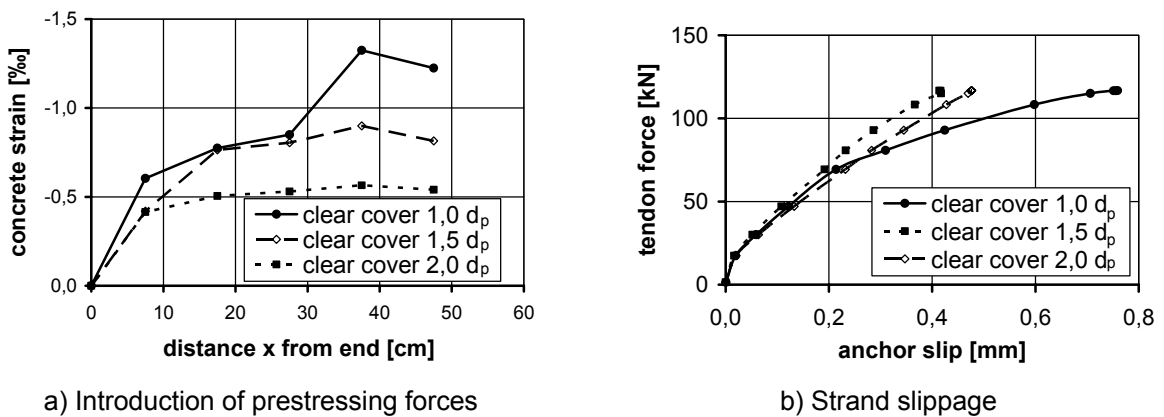
Figure 6: a) Comparison of concrete strain due to prestressing and b) anchor slip for different clear covers

By reducing both, the clear spacing between the tendons and the concrete cover, the size of the member required for introducing the prestressing force into the tensile chord is significantly reduced.

4   Shear Resistance

Several tests were performed to investigate the specimens behavior under shear loading. Based on the findings gained with the anchorage tendons, the clear spacing s and the concrete cover c was determined to be $s = c = 2{,}0 \cdot d_p$. The essential test parameters are summarized in Table 2.

Table 2:   Shear test data

Compressive concrete strength	$f_{c, cube\ 100}$	MPa	202
Modulus of elasticity	E_c	MPa	50100
Steel fibers	Length/diameter	mm	13/0,16
Fiber content	By volume	%	2,5
Cross-section of tendons	A_p	mm²	150
Prestressing force of the tendon	V_p/strand	kN	150
Total prestressing force	V_p	kN	1200
Failure moment	M_u	kNm	366
Ultimate shear strength	V_u	kN	273

The UHPC was manufactured in a conventional concrete mixer and had nearly self-compacting properties. Figure 7 shows the consistency of the fresh concrete.

Figure 7:   Fresh UHP concrete

A prestressing force $V_p = 1{,}2$ MN could be transmitted into the specimen without causing recognizable cracks. The dimensions of the specimen and a view of its cross-section are shown in Figure 8.
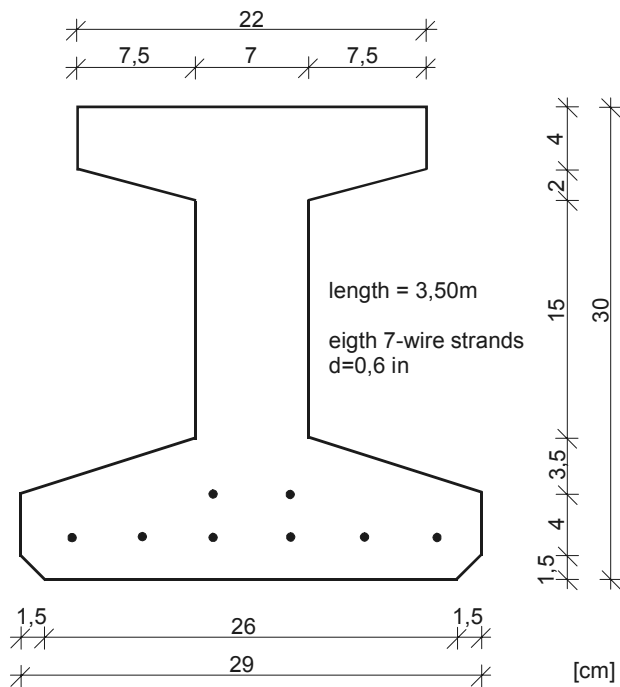
a) X-section of the specimen   b) View of the specimen

Figure 8:   Girder tested to determine its behavior under shear loading

The girder has a length of l = 3,5 m and a shear slenderness of a/d = 135/26 = 5,1 (Figure 9). The failure loads determined corresponded to the design loads of a steel girder of comparable dimension and weight.
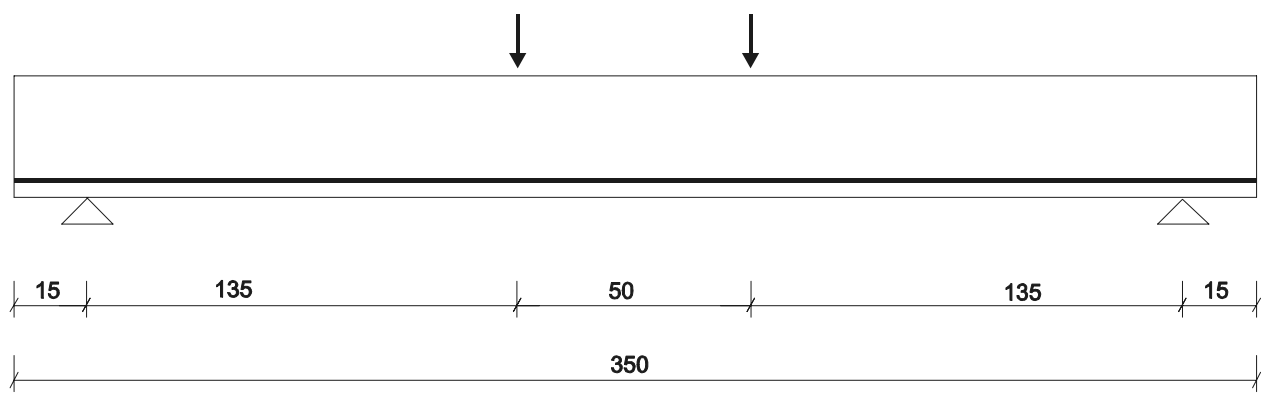
Figure 9:   Test setup for the shear tests

The beams failed in shear as shown in Figure 10. In comparable tests performed on specimens made with high-strength concrete, brittle failure occurred in much the same way as with UHPC specimens.

Figure 10: Test specimen in a state of failure

The degree of utilization of the tendons at the time of failure was approx. 80 %. A further increase of the shear resistance seems to be possible by reducing the number of tendons (without changing the prestressing force), by optimizing the cross-section of the specimen and by using a combination of short and long fibers.

5 Conclusions

In order to investigate the shear bearing capacity and the bond anchorage behavior of pre-tensioned UHPC beams, several tests were carried out at the Institute of Structural Concrete at the RWTH Aachen University.

At this point of time, the following conclusions can be drawn:

- UHPC with a compressive strength of $f_{c,cube100}$ = 200 MPa can be produced with a conventional concrete mixer.
- The concrete cover necessary for the anchorage zone of pre-tensioned elements made of UHPC and the necessary clear spacing of the tendons are considerably less in comparison with other types of concrete.
- The load carrying capacity is comparable to steel girders of the same dimensions.
- For practical load cases the shear capacity of pretensioned UHPC beams is sufficient; no additional shear reinforcement is required.

6   References

[1]   Simon, A.; Hajar, Z.; Lecointre, D.; Petitjean, J.: Realization of two road bridges with Ultra-High-Performance Fibre-Reinforced Concrete, 6th International Symposium on High Strength / High Performance Concrete, Proceedings Leipzig 2002.

[2]   Jovanovic, L.; Paatsch, A.; Durukal, A.: Ductal®: a New Generation of Ultra High Performance Concrete, 6th International Symposium on High Strength / High Performance Concrete, Proceedings Leipzig 2002.

[3]   Richard, P., Cheyrezy, M.:Composition of Reactiv Powder Concretes. Cement and Concrete Research, Vol. 25, No. 7, 1995, S. 1501-1511.

[4]   Pfeiler, A., Schneider, U., Horvath, J.: Auswirkungen der Nachbehandlung bei höheren Temperaturen auf die Druckfestigkeit von Reactive Powder Concrete, Diplomarbeit, Technische Universität Wien, 2000.

[5]   Dehn, F.: Ultrahochfeste Betone. In: König, G., Tue, N., Zink, M.: Hochleistungsbeton - Bemessung, Herstellung und Anwendung, Berlin 2001.

[6]   Bornemann, R., Schmidt, M., Fehling, E., Middendorf, B.: Ultra-Hochleistungsbeton UHPC - Herstellung, Eigenschaften und Anwendungsmöglichkeiten, Beton- und Stahlbetonbau 96, Heft 7, 2001, S. 458-467.

[7]   Richard, Pierre; Cheyrezy, Marcel H.: Reactive Powder Concretes with High Ductlity and 200-800 MPa Compressive Strength, American Concrete Spring Convention, ACI SP 144-24, San Francisco, März 1994, S. 507-518.

[8]   Schmidt, M., Bornemann, R.: Möglichkeiten und Grenzen von ultrahochfestem Beton. IBAUSIL - 14. internationale Baustofftagung, Band 1, 2000, S. 1083-1091.

[9]   Hegger, J.; Tuchlinski, D.: Voruntersuchungen zum Tragverhalten von ultrahochfestem Beton. (unpublished)

[10]   DIN 1045-1 Tragwerke aus Beton, Stahlbeton und Spannbeton. Juli 2001

[11]   Associatiation Francaise de Genie Civil: Betons fibres a ultra-hautes performances – Recommandations provisoires-, Paris, Januar 2002.

[12]   BPEL 91 revise 99, Regles techniques de conception et de calcul des ouvrages et constructions en beton precontraint suivante la methode des etats limites, 1999.

[13]   Hoyer, E.: Der Stahlsaitenbeton. Otto Elsner Verlagsgesellschaft, 1939.

[14]   Kommer, B: Bond anchorage behavior of pretensioned tendons in high performance concrete (HPC). 5th International PhD Symposium in Civil Engineering, 16-19 June 2004, Delft, The Netherlands; Tagungsband S. 833-840, ISBN 90 5809 676 9.

[15]   Nitsch, A.: Spannbettfertigteile aus hochfestem Beton unter Berücksichtigung der teilweisen Vorspannung; Dissertation RWTH Aachen, 2001.

Karl-Heinz Reineck
Prof. Dr.-Ing.
(Assoc. Prof. University of Sarajevo)
University of Stuttgart
Stuttgart, Germany

Stefan Greiner
Dipl.-Ing.
University of Stuttgart
Stuttgart, Germany

Tests on ultra-high performance fibre reinforced concrete designing hot-water tanks and UHPFRC-shells

Summary

Hot-water tanks serve for the seasonal storage of solar heat. This paper summarizes the results of a research program on ultra-high performance fibre reinforced concrete (UHPFRC), which should prove that UHPFRC is so dense that the expensive inner steel liner may be omitted for such tanks. The results of material tests and tests on a shell element are reported and some design proposals presented for hot-water tanks respectively UHPFRC-shells.

Keywords: *hot-water tanks, UHPFRC, size effect, pull-out-tests, design rules for UHPFRC*

1 Seasonal storage of solar energy

Much of the energy demand in Middle and Northern Europe is due to heating and warm water supply of buildings, and this fact poses a great challenge for civil engineers to replace oil by solar energy. Throughout the last 15 years a concept of "Central Solar Heating Plants with Seasonal Storage" for housing in Germany has been developed by Hahne, Fisch and Kübler [1,2] as well as Fisch et al. [3]. The "heart" of such a plant is a water tank, which stores the energy in hot water gained in summer by means of solar water collectors on the roofs of the buildings. So in winter the heat can be made available for heating and hot water supply of buildings. Such plants may provide between 50% and 75% of the annual heat demand of residential areas with properly insulated buildings. Further details see [3, 4, 5 ,6].

The designing engineer faces the task of achieving the optimum structure and shape for the tank depending on various conditions [7, 8]. The integration into the landscape respectively, low costs concerning construction as well as maintenance and repair, and especially low heat losses are of major importance. This goal can only be reached if the designer is consulted already in the early planning phases, if all specialists fully support this concept, and if sufficient time is allotted for the design and tender and for the discussions between all those involved.

These tanks have to be built underground because they should be located as closely as possible to the residential area they have to supply with heat. Therefore, much attention has to be paid that the tank harmonises with the surroundings, and this determines the possible height of the tank over the surrounding area.

A major portion of the costs for heat storage is caused by the concrete structure itself. Therefore, the optimum solution has to be obtained for a small surface and low specific costs for it as well as for the excavations. Since heat loss mostly occurs at the surface its reduced size provides another advantage. Therefore, a rather helpful value is the ratio between the surface and the volume, and the optimum ratio 3/r is obtained with a sphere (r = radius of the sphere). However, a sphere is not the optimum shape for a storage tank because the formwork would be very expensive and its great height would require deep and thus costly excavations. Consequently the tank was polygonally approximated to the sphere by different shells, as shown in Fig. 1 [7, 8].

Apart from the usual load cases such as dead load, the loads due to the infill and the water, high temperature gradients occur in hot-water tanks for long-term storage. For example, a temperature difference of 32 K has to be assumed over the height of only 1,0 m of the wall, and the temperature drops 17 K respectively 11 K across the wall thickness. Therefore, a non-linear analysis has to be carried out for the concrete structure in order to achieve realistic results for the inner forces at the ultimate limit state as well as the serviceability limit state and to avoid uneconomic amounts of reinforcements.

2   Brief survey on the hot-water tanks already built in Germany

In Germany a first pilot tank with a volume of about 600 m³ was built in Rottweil in 1995, which served as a short time storage tank. In 1996 the first two large tanks made of prestressed concrete with inner stainless steel liners were built, and both were built under earth, because they had to be integrated in newly built housing areas. The first tank in Hamburg had a storage capacity of 4.800 m³ and the second in Friedrichshafen 12.000 m³ (Fig. 1). The tank in Friedrichshafen was designed by Reineck and Lichtenfels [7], and it consists out of a combination of a cylindrical shell with two conical shells and slabs as roof and floor. The design and the building of this tank represent a milestone in the development of this concept.
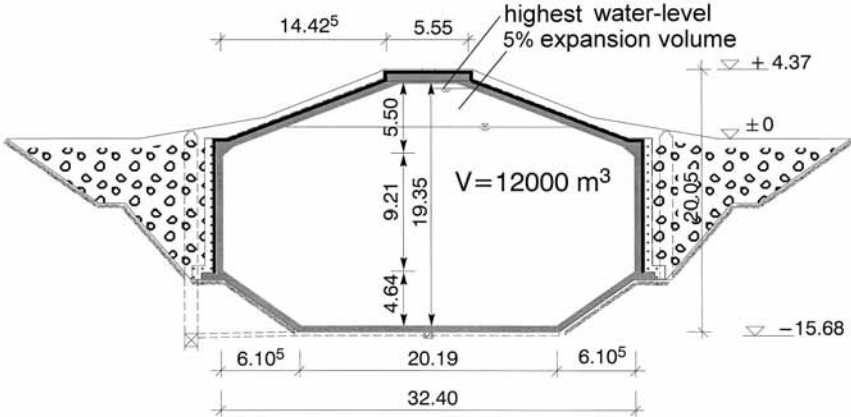
Figure 1:   The hot-water tank in Friedrichshafen made of normal concrete with an inner steel liner [7]

The aim of further research and of further pilot projects sponsored successively by the BMBF, BMWi and BMU via BEO, Jülich, was to investigate the technical possibilities to further reduce the costs for such tanks. The next step was to prove that the expensive inner liner out of stainless steel can be omitted, and it was investigated whether high-performance concrete (HPC) could serve as density barrier apart from carrying the loads. The hot-water tank in Hannover-Kronsberg built for the EXPO 2000 with a water volume of 2.750 m^3 proved that a solution out of HPC without steel inner liner works, and it is probably the first shell out of HPC (Fig. 2).
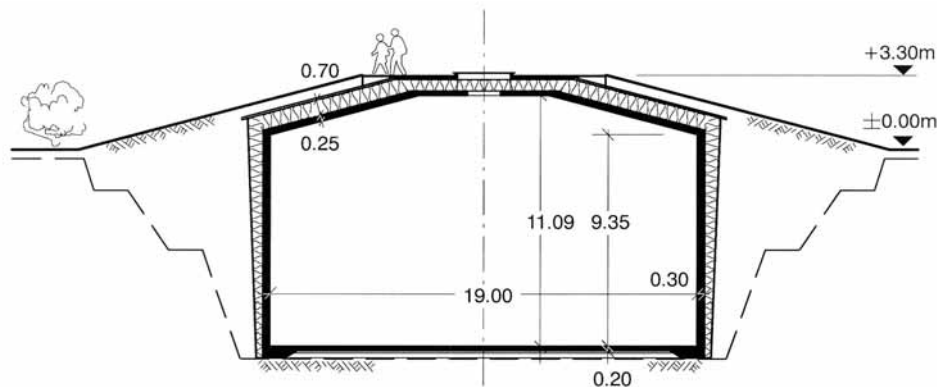
Figure 2: Hot-water tank in Hannover for the Expo 2000 out of HPC (V = 2.750 m^3) [4]

However, more efforts are necessary to reach an economical level, and therefore ultra-high performance fibre-reinforced concrete (UHPFRC) with its higher (water) density and strengths appears to be the most promising material. Yet it should not be forgotten either, that already these tanks contribute to the urgently required reduction of carbon dioxide emission, as e.g. pointed out by Hahne, Fisch and Kübler [2] as well as by Schlaich [9, 10].

3 Material properties of UHPFRC

3.1 Density of UHPFRC

The main purpose of UHPFRC is to serve as a density barrier for the hot-water tank, and therefore, density tests were carried out by Reinhardt and Jooß [11, 12] resp. Jooß [13] using BPR resp. Ductal® developed by Bouygues, Lafarge and Rhodia. These tests comprised the water absorption, the permeability and the diffusion of normal, high performance and ultra-high performance concrete. The results showed that the density of UHPFRC is about 15-times higher than a special water tight normal concrete and about 7-times higher than the density of HPC. In terms of water loss this means about 1,5 m^3/ per year for a tank of 12.000 m^3 (Fig. 3a), and this is a quite acceptable value concerning the heat loss. Since so far no density tests on HPC and UHPFRC were carried out for high temperatures, the density tests were carried out for 20, 50 and 80 °C, and in Fig. 3b the results for the diffusion coefficient are plotted versus the temperature for NC, HPC and UHPFRC. The reduction of the density with increasing temperature was to be expected, but it remained low for HPC with an increase of only about 20 %. Therefore, already HPC may serve as a density barrier if the insulation is not too sensitive against moisture. For UHPFRC the permeability and diffusion

could almost not be measured (Fig. 3b), so that UHPFRC is a most appropriate material for hot-water tanks.
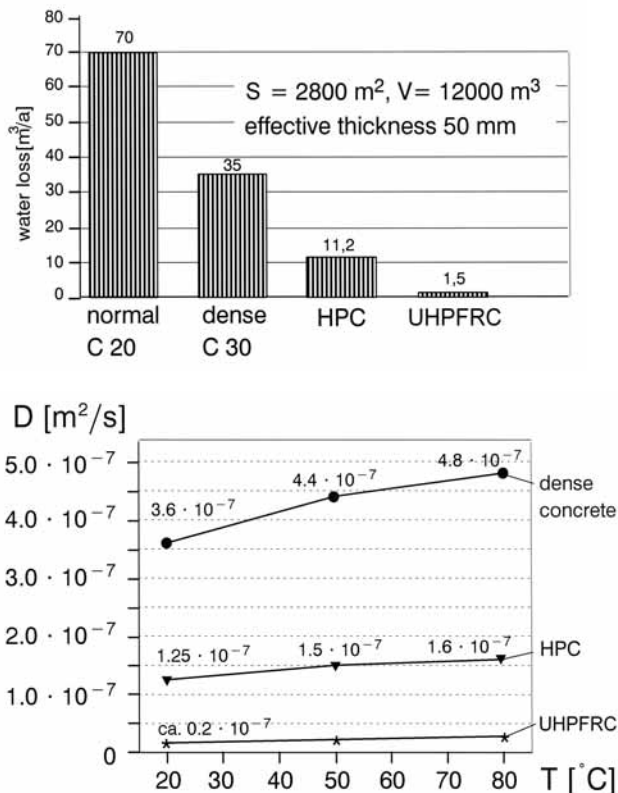
a) water loss per year for a hot-water tank   b) diffusion coefficient versus temperature

Figure 3: Density of UHPFRC compared to HPC and normal strength concrete [11, 12, 13]

3.2 Compressive, tensile and flexural tensile strength of UHPFRC

Own material tests [14] were carried out on standard specimens of Ductal® with 2 Vol-% steel fibres. For the compressive strength values of about 180 MPa were attained, and the axial tensile strengths were about 9 to 10 MPa. These values comply well with results published by other researchers: Behloul and Lee [15] stated an characteristic tensile strength of 8 MPa and a post-peak strength of 5 MPa for the Ductal® used for the Seonyu Bridge in Seoul, and Chanvillard und Rigaud [16] reported a mean value of 15,1 MPa.

The axial tensile tests were carried out with flat bone-shaped specimen with a cross section of 30 · 90 mm (Fig. 4b). This flat shape is better suited than prisms or cylinders to determine this important material characteristic for UHPFRC used for shells and tanks. Fig. 4a shows the deformational behaviour of such an axial tensile test, whereby this has to be regarded as an ideal curve.

a) stress-strain-relationship

b) bone-shaped specimen

c) crack pattern
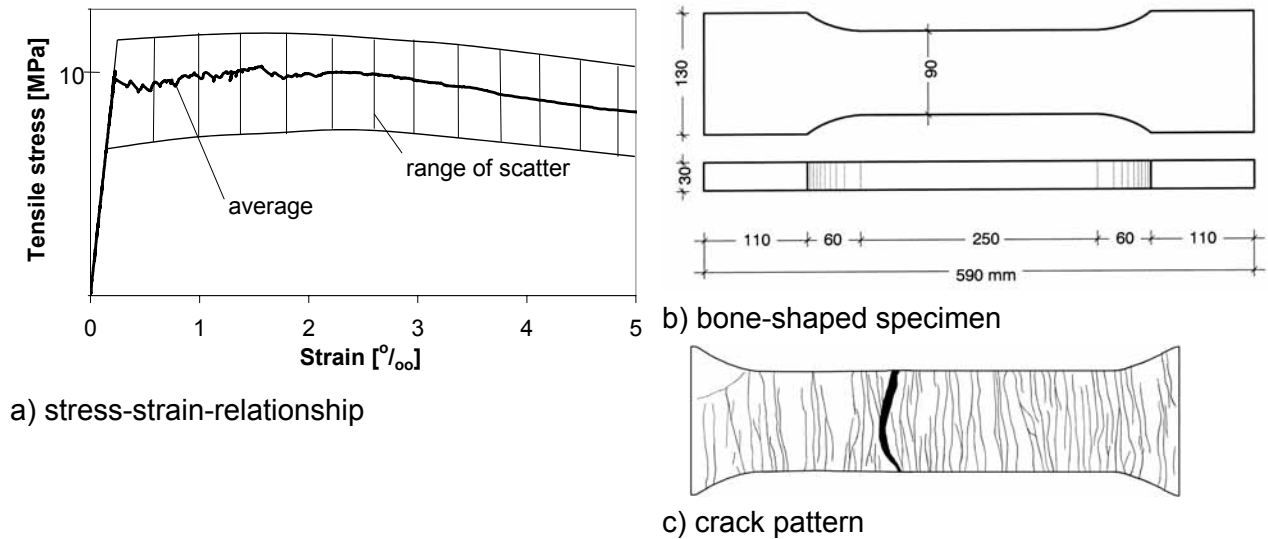
Figure 4: Results of the axial tensile tests [14]

In most tests, no or only a slight increase of the load could be measured after first cracking. Mostly a decrease of the load occurred, and in some cases it was so drastic that it obviously was a specimen with a weak cross section where the fibres were mostly orientated perpendicularly to the load direction due to mistakes in concreting. Therefore, utmost care must be paid on the concreting and the quality assurance in general.

For the flexural tensile strength values of 25 to 40 MPa were reported [17]. These values were conformed in own tests, see Fig. 5a, but the flexural tensile strength clearly decreases with increasing depths of the prisms, and this means that there is a distinct "size effect". Therefore, the size of the prism must always be mentioned when such values are reported. One main cause for this size effect is the orientation of the fibres, which leads to a preferred orientation of the fibres parallel to the surface respectively to the formwork, and this is of greater influence for small dimensions.

The Fig. 5b shows the relationship between the flexural tensile stress and the deflection, whereby the possible scatter is indicated, which again depends on the size of the prism respectively on the fibre orientation. The Fig. 5b shows as a typical example that a distinct load increase occurs after the first cracks appear. However, as mentioned before for the axial tensile tests, unfavourable fibre distributions due to faults during concreting may result in a low cracking level and no increase of the load after appearance of the first cracks (not shown here).
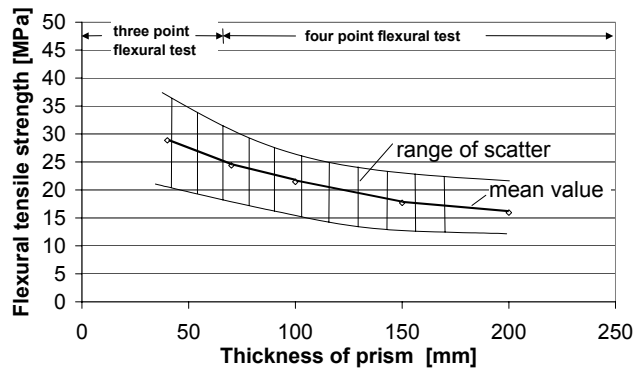
a) size effect
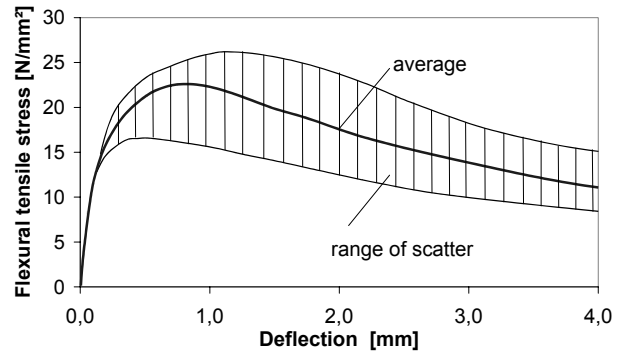
b) flexural tensile stress versus deflection for prisms 100·100·530 mm

Figure 5: Results of the flexural test for prisms with different thicknesses [14]

3.3 Pull-out-tests

Some pull-out-tests were carried out to determine the anchorage length of reinforcing bars in UHPFRC. The pull-out-tests were carried out with specimens according to RILEM, but the embedment length had to be reduced from 5 Ø to 2 Ø of the reinforcement bar (Fig. 6a), because due to the high bond strength the bars always yielded. A typical bond stress - slip - relationship is shown in Fig. 6b for a bar diameter of Ø = 4 mm. A bond strength of about 40 to 50 MPa could be reached. Because of that anchorage lengths between 3 Ø to 5 ∅ should be sufficient.
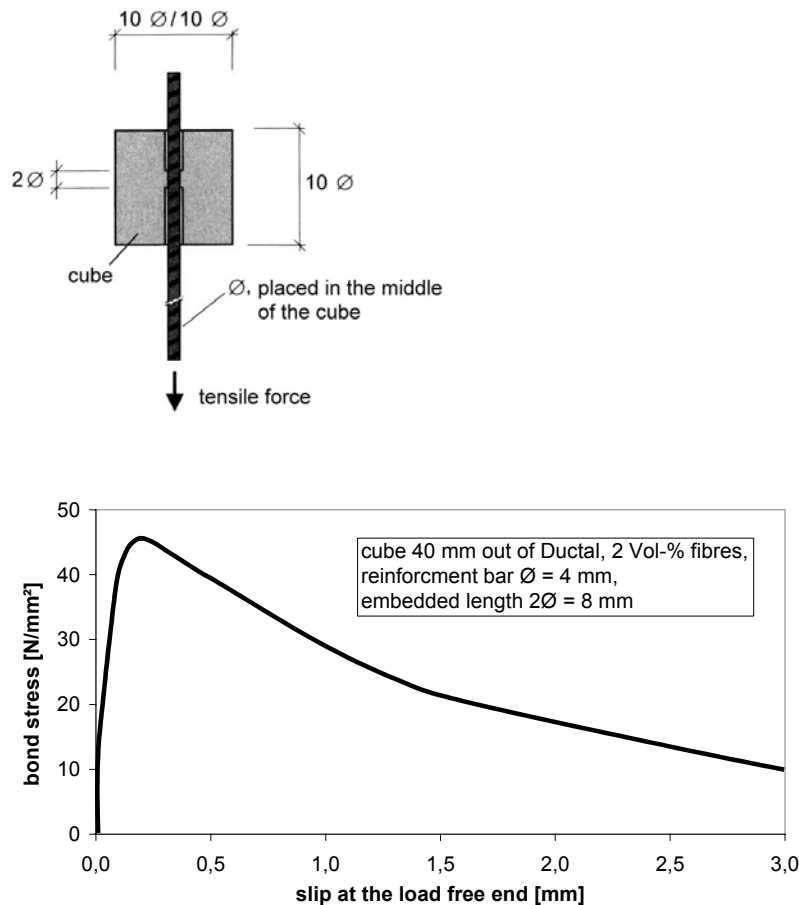
a) specimen for pull-out-test   b) typical bond stress - slip - relationship

Figure 6: Pull-out-test for UHPFRC [14]

4   Hot-water tanks out of UHPFRC

4.1   Design

A series of designs of hot-water tanks out of UHPFRC was performed and apart from redesigning the tank of Friedrichshafen (Fig. 1) the focus was on designing smaller tanks which could possibly be produced as standard types. The Figure 7 shows two possible designs for a tank volume of 1.000 m^3 where the wall thicknesses are only about 60 mm.
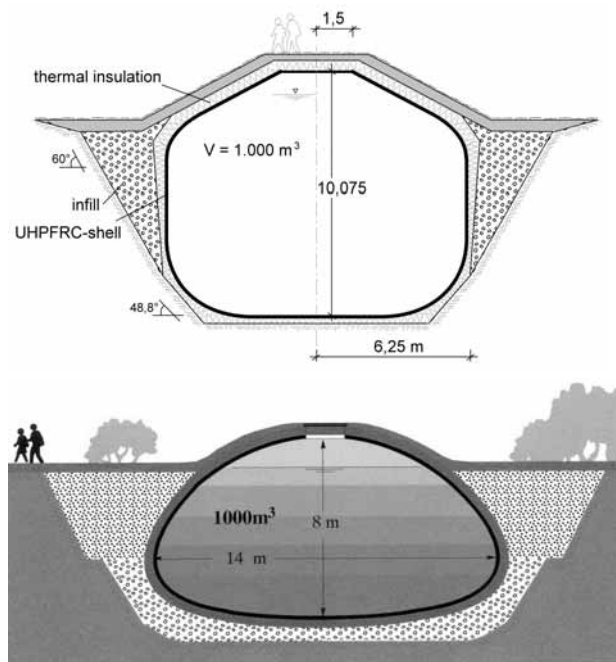
Figure 7: Possible shapes for hot-water tanks out of UHPFRC (standard type, V = 1.000m^3) [14]

For such a standard type the transition region from the cylindrical to the conical shells is smoothly curved in order to reduce unfavourable moments. However, since different load cases occur there are still some bending moments in addition to axial forces which determine the thickness of this region. This means that this region has to be designed for the combined loading of normal forces and bending moments and thereby the size effect has to be considered as explained before, i.e. there must be a transition between the axial tensile stress for pure tension and the higher flexural tensile stress under pure bending.

4.2   Test on a shell element out of Ductal®

In order to check some theoretical considerations a few pilot tests were carried out on specimens representing the transition region from the upper conical to the cylindrical shell. The test specimen had a cross-section of 60 · 200 mm (Fig. 8b) and is designed such that it is only uniaxially pushed or only pulled, as shown in Fig. 8a. The relation between the axial force and the bending moment is given by the curvature of the specimen (Fig. 8b).

The moments and forces depend on whether the tank is placed completely under earth or above ground. The following two extreme load cases were examined. In the first case the hot-water tank is mainly above the ground and filled with water; this leads to axial tension in the transition region combined with moments. In the second case the hot-water tank is empty and completely covered with earth; this leads to axial compression combined with bending in the transition region. A wall thickness of 60 mm was selected, which is sufficient for a 1.000 m^3 prestressed tank. The two extreme load cases of the hot-water tank are represented by a

tensile force of about F = 13 kN and a compressive force of about F = - 14 kN, which lead to tensile stresses of +10,5 MPa and -9,0 MPa in the extreme fibre.

In the testing program first load cycles were carried out between values of + 13 kN and - 14 kN. Then the (tensile) load was increased until visible cracks occurred and a clear decrease of the stiffness was observed in the load-deformation-diagram. At this load level further load cycles were carried out. Finally the load was increased until the ultimate tensile or the maximum compressive force was reached. Altogether only 2 specimens could be tested and the result of specimen No. 1 is given in Fig. 9.
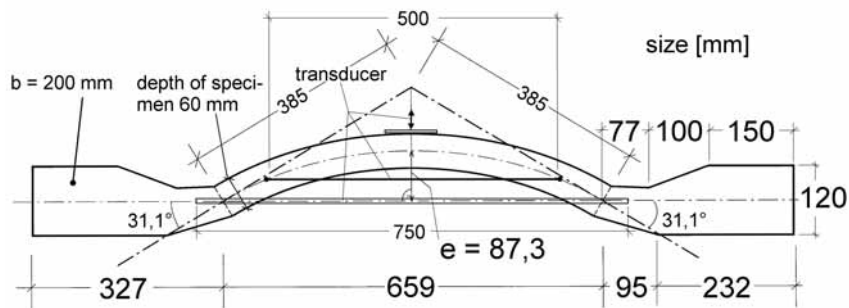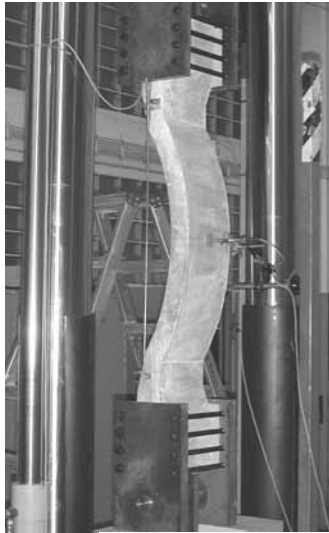
a) test rig   b) main dimensions of the test specimens

Figure 8: Test on a shell element representative for the transition region of a hot-water tank
         [14]
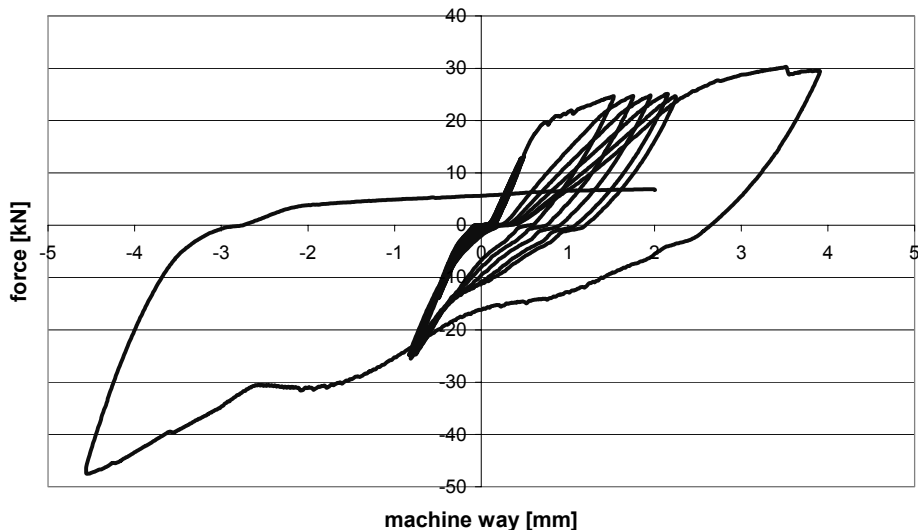
Figure 9: Relationship between load and machine way [14]

Specimen No. 1 was loaded up to a tension load of 30,3 kN giving a stress of +24,6 MPa for the outer fibre for the loading case bending moment combined with an axial tensile force. The load could have been increased further, but only with large deformations and further widening of the cracks. Before the cracks became too wide the load was reversed and the specimen was loaded with a compressive load up to failure at 47,5 kN giving a tensile stress of +30,6 MPa for the extreme fibre for the load case bending moment combined with a compressive force. These values are close to the flexural tensile strengths previously reported. This result was to be expected, because the axial stresses were low with only +2,5 MPa respectively –4,0 MPa.

4.3   Proposals for design rules

The first guideline for the design of UHPFRC („Interim Recommendations") was published 2002 in France by AFGC and SETRA [18], and they reflect the experiences with the two French products Ductal® resp. BPR and BSI („Béton Spécial Industriel"). These recommendations consist of general rules, design rules and proposals for tests to determine the material strengths. The design value of the tensile strength is defined by the post-peak-strength, for which a safety factor of 1,3 is considered. Furthermore these recommendations propose to carry out tests on structural members in the original size because the fibre orientation depends on the concreting process. For cases where it is not possible to test real-size specimens, the recommendations propose a correction factor.

In Germany a state-of-the-art report will be published in 2004 by the German Concrete Association DAfStb, in which one chapter [19] deals with the design of structural members out of ultra-high performance concrete (UHPC). This report refers in some parts to the German guidelines for steel fibre reinforced concrete [20, 21]. Correction factors for different sizes of the structural members are also included in the German guidelines for steel fibre reinforced concrete which underlines the importance of this "size-effect".

The influence of an unfavourable fibre orientation is considered in the French recommendations by a correction factor K which is 1,25 for general loading and 1,75 for local effects. The influence of this correction factor or kind of safety factor γ_f is shown in a simplified design proposal for tension in Figure 10a.

Figure 10b shows a proposal by Behloul [22] who proposed an analytical expression for determining the relationship between the tensile stress and the crack width w from the basic parameters of the materials, i.e. the length L_F and the diameter $\varnothing$ of the fibre, the fibre content ρ, the orientation of the fibres α and the bond stress τ.
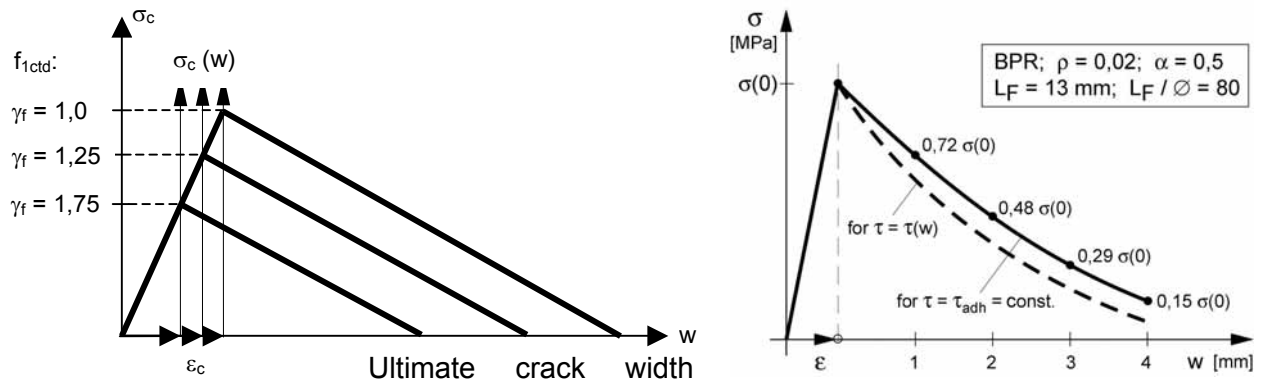
a) influence of the fibre orientation on the tensile strength   b) stress-deformation-relation

Figure 10: Constitutive laws for UHPFRC under tension [19, 22]

The axial tensile strength may also be determined directly from e.g. bone-shaped specimens, but most guidelines or recommendations give a constitutive law in order to derive the tensile strength from the flexural tensile test, normally the 4-point loading test. Thereby the German DAfStb guidelines for fibre reinforced concrete use a prism with a depth of 150 mm and a span of 600 mm.

In the German code DIN 1045-1 [23] an additional safety factor γ'_c is applied to determine the design value for the compressive strength of HPC because of the higher scatter, the higher brittleness of the material and the higher sensitivity to any difference in the mixture:

$$f_{cd} = 0,85\, f_{ck} / (\gamma_c \cdot \gamma'_c) \qquad \text{with: } \gamma'_c = 1 / (1,1 - f_{ck}/500) \geq 1,0 \qquad (1)$$

In [19] it is proposed to use this relationship also for UHPC up to f_{ck} = 150 MPa leading to a maximum value of 1.25, because the above reasons still apply.

Of course, it may be discussed whether this increase for γ'_c for very high strengths is also necessary for fibre reinforced UHPFRC, which is less brittle and which is well supervised, especially in case of prefabrication. In [19] it is proposed to use the value of γ'_c = 1,11 for a C 100, and Figure 11 shows the consequences for the design diagram.

Figure 11: Design proposal for the stress-strain-relation for UHPFRC under compression [19]

The factor 0,85 for the design value of the compressive strength considers in case of NC and HPC (up to C100) the reduction from the cylinder to the wanted uniaxial strength, i.e. the prism strength (by a factor 0,95) and the long duration of the load (by a factor 0,90). In case of UHPC both reduction factors are still disputed or not yet known, so that for simplicity the factor 0,85 is kept to. The ascending branch of the stress-strain curve is elastic whereby the design value E_{cd} considers the long term duration of the load corresponding to the factor 0,85. Further research is still needed on the creep behaviour of UHPC to confirm the influence of long duration loading on these design values.

The descending branch of UHPFRC depends on the fibre content and Figure 11 gives a first proposal, whereby the curve for a fibre content of 2% is based on own tests. It is proposed to define a minimum value for the fibre content in order to apply the design rules for UHPFRC.

5 Conclusions

After a brief review on the development of hot-water tanks for solar heat, the results of a research project are reported, which proved that UHPFRC can fulfil the requirements for hot-water tanks especially with respect to the density. The design and calculations of some typical tanks revealed that despite higher costs for the material itself UHPFRC offers chances for further cost reductions considering new fabrication techniques.

Tests on the material properties were reported with respect to the density as well as to the strengths. For the compressive strength values of about 180 MPa were attained, and for the axial tensile strength values of around 10 MPa were tested with flat specimens of 30 · 90 mm

cross-section. The flexural tensile tests exhibited a distinct size effect. The pull-out tests on bars Ø 4 mm yielded bond strengths of 40 to 50 MPa so that short anchorage lengths between 3 Ø to 5 Ø are possible. Two pilot tests were carried out on curved shell elements representing the transition region between a cylinder and a conical shell in order to test the flexural tensile strength under combined axial force and bending moment. Finally some proposals for design rules are given.

Acknowledgments

References

[1] Hahne, E.; Fisch, M.N. (1992): Einsatz von solarunterstützten Nachwärmeversorgungssystemen mit saisonalem Wärmespeicher. Forschungsbericht zum BMFT-Vorhaben 0328867A, Institute of Thermodynamics and Thermal Engineering (ITW), University of Stuttgart, June 1992 (in German)

[2] Hahne, E.; Fisch, M.N. (1995): Solarunterstützte Nahwärmeversorgung mit und ohne Langzeit-Wärmespeicherung. Forschungsbericht zum BMFT-Vorhaben 0328867C, Institute of Thermodynamics and Thermal Engineering (ITW), University of Stuttgart, June 1995 (in German)

[3] Fisch, N.; Möws, B.; Zieger, J. (2001): Solarstadt: Konzepte, Technologien, Projekte. W. Kohlhammer, Stuttgart, 2001 (in German)

[4] Reineck, K.-H.; Lichtenfels, A.; Greiner, S. (2001): Seasonal storage of solar energy in hot-water tanks made out of high performance concrete. in: Session A6: Energy and Conservation, Environmental Aspects in Operation, Aspects of Health and Working Environment, Proceedings fib Symposium "Concrete and Environment"Berlin 2001, 3-5 October. Ed. by: DBV - Deutscher Beton- und Bautechnik Verein E.V. Berlin, 2001 (in English)

[5] Reineck, K.-H.; Lichtenfels, A.; Greiner, S. (2002): HPC hot-water tanks for the seasonal storage of solar heat. p. 739 - 752 in: V. 1 Proceedings 6th International Symposium on Utilization of High strength / High Performance Concrete, Leipzig June 2002. (Edtrs. König, G.; Dehn, F.; Faust, T.). Leipzig University, Institute for Structural Concrete and Building Materials, 2002 (in English)

[6] Reineck, K.-H.; Greiner, S.; Lichtenfels. A. (2003): Wasserspeicher aus UHFB - Bemessung. S. 257 - 268 in: König, G.; Holschemacher, K.; Dehn, F. (Hrsg.): Ultrahochfester Beton - Innovationen im Bauwesen, Beiträge aus Praxis und Wissenschaft. Bauwerk Verl., Berlin 2003 (in German)

[7] Reineck, K.-H.; Lichtenfels, A. (1997): Entwurf und Bemessung von Heißwasser-Wärmespeichern aus Konstruktionsbeton, study within the research project BMBF 0329606C, Institute for Structural Design II, University of Stuttgart, 1997 (in German)

[8] Lichtenfels, A. (2004): Schalentragwerke und Wärmespeicher aus Ultra-Hochleistungs-Beton. Doctor thesis, University of Stuttgart (in German, in preparation)

[9]   Schlaich, J. (1982): Neue und erneuerbare Energiequellen. Festschrift 75 Jahre DAfStb. DAfStb H. 333, 115-130, 1982 (in German)

[10] Schlaich, J. (1997): Bauen für eine solare Energieversorgung. Vortrag in Fachsitzung 2, Deutscher Betontag. 10. April 1997, Berlin. DBV-Tagungsband, 306-321, Wiesbaden, 1997 (in German)

[11] Reinhardt, H.-W.; Jooß, M. (2000): Untersuchungen zur Dichtigkeit von Hochleistungsbeton. Abschlußbericht zu den Materialuntersuchungen. Institute for Materials, University of Stuttgart, 2000 (in German)

[12] Reinhardt, H.-W.; Jooß, M. (2003): Wasserspeicher aus UHFB – Technologie. S. 239-255 in: Ultrahochfester Beton. Innovationen im Bauwesen. Beiträge aus Praxis und Wissenschaft (Herausgeber: König, G.; Holschemacher, K.; Dehn, F.). Bauwerk Verlag GmbH. Berlin, November 2003 (in German)

[13] Jooß, M. (2001): Dichtheit von Heißwasser-Langzeitspeichern aus Hochleistungsbeton, Doctor thesis, Institute for Materials, University of Stuttgart, July 2001 (in German)

[14] Reineck, K.-H.; Greiner, S. (2004): Dichte Heißwasser-Wärmespeicher aus ultrahochfestem Faserfeinkornbeton. Forschungsbericht zum BMBF-Vorhaben 0329606 V. Institut für Leichtbau Entwerfen und Konstruieren (ILEK), Universität Stuttgart, 2004 (in German)

[15] Belhoul, M.; Lee, KC. (2002): Innovative Footbridge in Seoul – Seonyu Footbridge; The first fib Congress 2002 – Concrete Structures in the 21st Century, Osaka 2002 (in English)

[16] Chanvillard, G.; Rigaud, S. (2003): Complete characterisation of tensile properties of Ductal® UHPFRC according to the French Recommendations, HPFRCC4 Workshop, pp. 21-34, Ann Arbor, USA, 2003 (in English)

[17] Lafarge Zement (2001): Ductal®, mehr als ein neuer Baustoff – ein Durchbruch in der Werkstofftechnologie. Firmenbroschüre, Stand 06/2001 (in German)

[18] AFGC, SETRA (2002): Bétons fibrés à ultra-hautes performances. Recommandations provisoires. Documents scientifiques et techniques. Association Française de Génie Civil, Setra, Bagneux Cedex, janvier 2002, 152 pp (in French and English)

[19] Reineck, K.-H.; Greiner, S. et al. (2004): Bemessung und Konstruktion. Abschnitt 7 in: Sachstandsbericht „Ultrahochfester Beton" des DAfStb-UA UHFB. Entwurf 20. Februar 2004 (in German)

[20] DBV (2001): Merkblatt Stahlfaserbeton, Fassung: Oktober 2001 (in German)

[21] DAfStb (2004): DAfStb-Richtlinie „Stahlfaserbeton" (16. Entwurf). 1. März 2004 (in German)

[22] Behloul, M. (1996): Les micro-bétons renforcés de fibres. De l'éprouvette aux structures. XIVèmes Journées de l'AUGC, Clermont-Ferrand. Prix Jeunes Chercheurs «René Houpert», 1996 (in French)

[23] DIN 1045-1 (2001-07): Plain, reinforced and prestressed concrete structures - Part 1: Design and construction. 122 pp. Normenausschuss Bauwesen (NABau) im DIN Deutsches Institut für Normung e.V. . Beuth Verl. Berlin, Juli 2001 (in German)

Klaus Holschemacher

Prof. Dr.-Ing.

Leipzig University of Applied Sciences

(HTWK Leipzig)

Leipzig, Germany

Dirk Weiße

Dipl.-Ing.

Leipzig University of Applied Sciences

(HTWK Leipzig)

Leipzig, Germany

Sven Klotz

MSc. Dipl.-Ing.

Leipzig University of Applied Sciences

(HTWK Leipzig)

Leipzig, Germany

Bond of Reinforcement in Ultra High Strength Concrete

Summary

Ultra high strength concrete (UHSC) is undoubtedly an engineered high-tech material, which can be seen as the latest step in the concrete technology development. Because this concrete type is a quite young one, the structural behaviour in the ULS as well as in the SLS is not fully investigated and understood, as little as the bond behaviour of reinforcement. This paper outlines an experimental programme and its results on the bond behaviour of conventional rebars in ultra high strength concrete. In this study, the hardened concrete properties and the bond behaviour were investigated at a concrete age of 3, 7, 28 and 56 days. Varying parameters in this programme were rebar diameter, size of the concrete cover and the loading rate.

Keywords: bond behaviour, concrete cover, splitting, reinforcement, static loading, tensile strength, ultra high strength concrete (UHSC), reactive powder concrete (RPC)

1 Introduction

One of the most important influences on the bearing capacity of reinforced concrete members is the bond between concrete and reinforcement. In this context, the anchorage of the reinforcing bars, lapped splices, crack width control (minimum amount and distribution of the reinforcement) and the rotation capacity of concrete structures are mentionable. The scale for the quality of the bond is the bond stress-slip-relationship. The force transfer between the rebar and the concrete is characterised by the different states adhesive bond, shear bond and friction bond. Figure 1 shows the bond stress-slip-relationship for deformed and plain reinforcing bars. The basic mechanisms of the force transfer in each state will not be described in detail, in this context a valuable overview is given in [1] - [3].
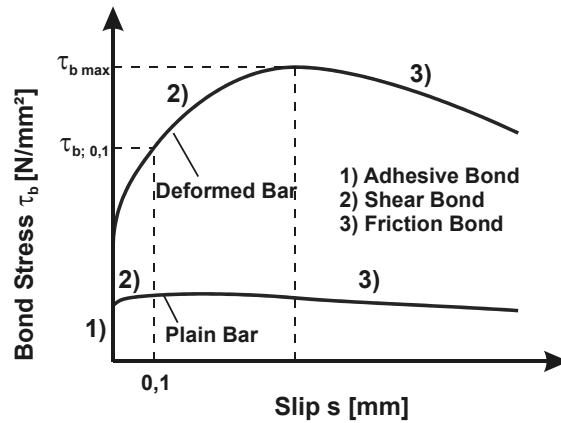
Figure 1: Bond stress-slip-relationship for deformed and plain reinforcing bars according to Will [4]

The shear bond is of prime importance, because in this state the highest bond stresses will be reached. In this curve area (sector 2 in Figure 1) the force transfer takes place only by the ribs of the rebar and the concrete keys in between. Therewith large compressive stresses occur on the contact points. These compressive stresses direct inclined outwards and cause in the concrete cross-section around the rebar radial tensile stresses (spatially displayed in Figure 2). If the radial tensile stresses exceed the concrete tensile strength before the concrete keys are sheared-off, cracking will occur by generating longitudinal cracks perpendicular to the radial tensile stresses. That means, the concrete cover rips along the reinforcing bar or spalles respectively. In this case the bearing capacity, e.g. through friction (see Figure 1), is nonexistent or very low. Consequently a brittle failure of the anchorage or the lapped splice is imaginable. The type of bond failure (splitting or pulling-out), and therefore the performance is decisively influenced by the compressive strength and the modulus of elasticity, yet again especially by the concrete tensile strength.
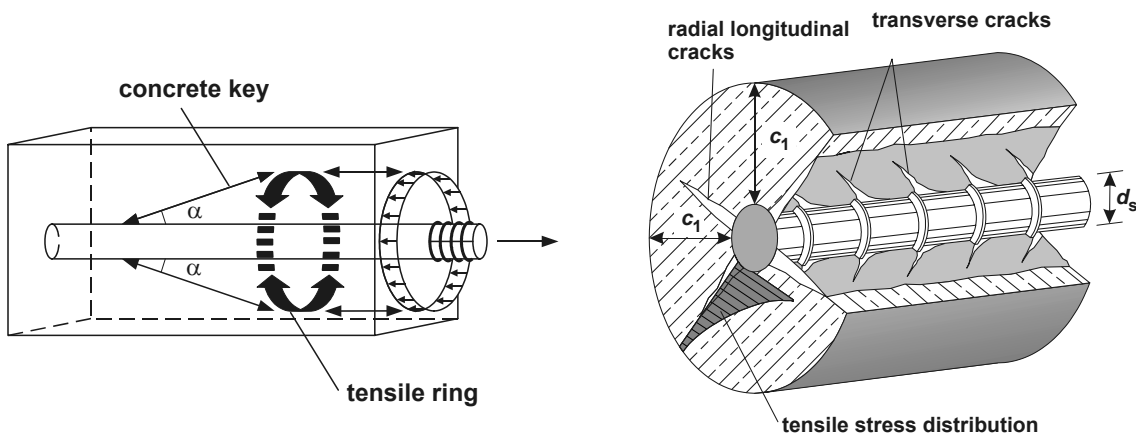
Figure 2: Spatial model of the force transfer at the rebar according to Tepfers [5]

Figure 3: Longitudinal and transfers crack development due to the bond (Tepfers [5])

Generally the parameter influencing the bond can be divided into 4 groups:

- ➢ concrete
  - concrete composition, e.g. grading curve of the aggregates, binder content
  - fresh concrete properties, e.g. flow and slump, compactibility
  - hardened concrete properties, e.g. compressive and tensile strength, modulus of elasticity, fracture characteristic (brittleness)
- ➢ properties of the reinforcement
  - rebar diameter
  - rib geometry and its arrangement, e.g. high- or deep-ribbed, orientation and number of rows of the ribs
  - relative rib area
- ➢ loading regime
  - short or long term monotonic (static) loading, e.g. loading rate
  - dynamic loading, e.g. frequency, amplitude
- ➢ system parameter
  - concrete cover, confinement (e.g. due to traverse reinforcement, fibres)
  - position of the rebar during casting
  - orientation of the rebar relative to the direction the concrete is placed

For these reasons it becomes apparent, how complex the bond between reinforcement and concrete is, and the spectrum can be an extremely wide area through the influencing variables, the boundary conditions and its interaction. In the following only parameters and their possible effects especially for high and ultra high strength concrete will be discussed.

2   Particularities of UHSC for the Bond Behaviour

Ultra high strength concrete is characterised by its high compressive strength, but also the tensile strength is raised. In this context two points have to be assessed critically: first the tendency of splitting of the concrete cover (the risk of longitudinal cracking - see paragraph 1), because the tensile strength increases not proportionally in comparison to the compressive strength. And second the minimum required reinforcement for the crack width control.

The modulus of elasticity increases under proportionally in the same manner as for high strength concrete. Regarding the bond this will certainly have an influence on the ascending branch (Figure 1) in the bond stress-slip-relationship, so on the bond stiffness.

Just as the hardened concrete properties, great importance must be attached to the fact of an accumulated brittleness of the material. Here, impact and impulse loading are mentionable, that means at high loading rates the bond properties could be changed.

As a last point the modified mix design may affect the bond behaviour. The concrete matrix is more homogeneous due to smaller maximum grain sizes of the aggregates, a higher binder content and micro filler. The reinforcement is therefore better enclosed. Nevertheless the aggregate interlock is definitely lower because of the reduction in the maximum grain size.

3 State of the Art

Only a few investigations can be found in the literature about „Bond in ultra high strength concrete". Hansen [6] reported on bond tests using Densit Joint Cast[®] with different rebar diameters. The main series was carried out with Ø 16 mm, whereby the bond length was 170 mm. It must be mentioned, that Densit Joint Cast[®] is a fibre reinforced ultra high strength concrete with a fibre content of 6 Vol.-% (about 480 kg/m³), and therefore splitting failure is nearly impossible. Furthermore the bond length was chosen quite high, so that the descending branch of the bond stress-slip-relationship (pull-out of the rebar) could not be measured. At all pull-out specimens steel failure was observed.

Also first results about the "Bond Performance between Ultra-High Performance concrete and Prestressing Strands" are available [7]. Different strand diameters were applied on normal strength concrete and different UHSC mixes. For the same embedment length, the transferable bond stresses increased, but not proportional with the compressive strength. The depth of the embedment required to anchor the strands could be decreased to about 50 – 66% of those values required for normal strength concrete.

In consequence of the few experimental investigations, with the performed test programme basic knowledge about the bond behaviour in UHSC is to gather. In the following the achieved results and the conclusions will be presented.

4 Test Programme

4.1 Used Materials

Three different mix designs were used for ultra high strength concrete, which varied in the composition as well as in the basic concept. Whereas the principle of a „classic" reactive powder concrete (RPC) was chosen for the UHSC 2 (Table 1), crushed aggregates with a maximum grain size of 5 mm were applied for the two other UHSC mixes. In order to class the results for the UHSC used, two reference concretes with natural round and crushed aggregates were cast. Within all mixes a cement CEM I 42,5 R was chosen, moreover fly ash and/or silica fume as reactive filler in order to ensure a similar strength development. The relevant mix designs of all concretes are presented in Table 1.

Within the test programme the fresh concrete properties for each mix were determined in order to ensure resembling workability. In the hardened state the mechanical properties (compressive and splitting tensile strength, modulus of elasticity) were measured at a concrete age of 3, 7, 28 and 56 days for evaluating the performed bond tests.

Table 1:   Mix designs

			Reference 1	Reference 2	UHSC 1	UHSC 2	UHSC 3
Sand 0/2 mm			1.86	2.42	0.92	-	-
Gravel 2/8, 8/16 mm			3.46	-	-	-	-
Crushed aggregates 2/5 mm			-	0.49	1.68	-	2.06
Crushed aggregates 5/8 mm			-	2.15	-	-	-
Cement CEM I 42,5 R			1.00	1.00	1.00	1.00	1.00
Fly ash	Content of Cement [mass-%]		0.21	0.27	0.20	-	-
Silica-slurry 50/50			-	-	0.13 (solids)	-	-
Silica-fume			-	-	-	0.30	0.18
Quartz sand			-	-	0.30	1.53	0.88
Quartz powder			-	-	-	0.43	0.54
Water			0.53	0.52	0.30	0.25	0.27
Superplasticizer			0.01	0.02	0.04	0.03	0.04

4.2   Pull-out Specimen

The bond properties were determined with pull-out tests applying the RILEM-specimen [8]. Within the programme mainly rebars with d_s = 10 mm were used, in some test series additionally the diameter 8 mm. In this report only the results of the Ø 10 mm rebar are presented, the others are described detailed in [13]. Because of the two different rebar diameter the dimensions of the pull-out specimens were also diverse, so for Ø 10 mm analogue Figure 4 (rebar in vertical orientation), and smaller magnitudes for the Ø 8 mm. The rebar was placed in the concrete in two different directions, that means horizontal (at a right angle to the casting direction) and vertical (parallel to the casting direction). The vertical rebar orientation has to be distinguished between loading in and against concrete placing direction Table 2.

Besides the rebar diameter the concrete cover is a further crucial parameter. According to the RILEM-recommendation [8] for a rebar Ø 10 mm the concrete cover results in 4.5 cm (Figure 4). This is indeed required only for extreme exposures (XD and XS [9]) and for abrasion (XM [9]) according to the German Standard DIN 1045-1 [10]. Therefore for one series the cover thickness was gradually decreased in order to choose a lower, in the construction practice common cover, and on the other hand to provoke splitting failure of the concrete cover. This failure type occurred at values of 2.5 cm and less, so that 2.5 cm were defined for the following test series (Figure 5).

The bond length between concrete and reinforcement measures 5-times the reinforcing bar diameter d_S according to the RILEM-recommendation [8]. This recommendation was admittedly released for normal strength concrete. Since the bond strength increases with the compressive strength, the bond length must be reduced for high and ultra high strength concrete. This change is necessary because of the high transferable bond forces, otherwise the rebar would yield beyond the bond length. After some pre-tests, the bond length was

defined by 1.5-times the rebar diameter d_S for ultra high strength concrete, i.e. 1.5 cm for Ø 10 mm.

Except for one series (see paragraph 5.2.3) the pull-out specimens were loaded path-controlled with a loading rate of 0,005 mm/s by means of a servo-hydraulic testing machine. The slip between rebar and concrete was measured at the unloaded end of the specimen with three rotation-symmetrically around the rebar fixed LVDT's (Figure 6 and 7).

Table 2:   Overview about the pull-out tests

Age at testing	Reference 1	Reference 2	UHSC 1	UHSC 2	UHSC 3
	rebar diameter 10 mm, bond length 15 mm, concrete cover size 4.5 cm or 2.5 cm				
	rebar orientation – variant 1: vertical, loaded in casting direction; variant 2: horizontal; variant 3: vertical, loaded against casting direction				
3 days	-	-	cover 4.5 cm, variants: 1, 2, 3	cover 4.5 cm, variants: 1, 2, 3	-
7 days	cover 4.5 cm, variants: 2	cover 4.5 cm, variants: 1, 2	cover 4.5 cm, variants: 1, 2, 3	cover 4.5 cm, variants: 1, 2, 3	-
28 days	cover 4.5 cm, variants: 2	cover 4.5 cm, variants: 1, 2	cover 4.5 cm variants: 1, 2, 3	cover 4.5 cm, variants: 1, 2, 3	cover 4.5 cm, variants: 1, 2, 3
56 days	-	-	cover 4.5 cm, variants: 1, 2, 3	cover 4.5 cm, variants: 1, 2, 3	-
3 days	-	-	-	cover 4.5 cm, variants: 1, 2, 3	-
7 days	cover 2.5 cm, variants: 2	cover 2.5 cm, variants: 1	-	cover 4.5 cm, variants: 1, 2, 3	-
28 days	cover 2.5 cm, variants: 2	cover 2.5 cm, variants: 1	cover 2.5 cm, variants: 1, 2, 3	cover 2.5 cm, variants: 1, 2, 3	cover 2.5 cm, variants: 1, 2, 3
56 days	-	-	-	cover 2.5 cm, variants: 1, 2, 3	-
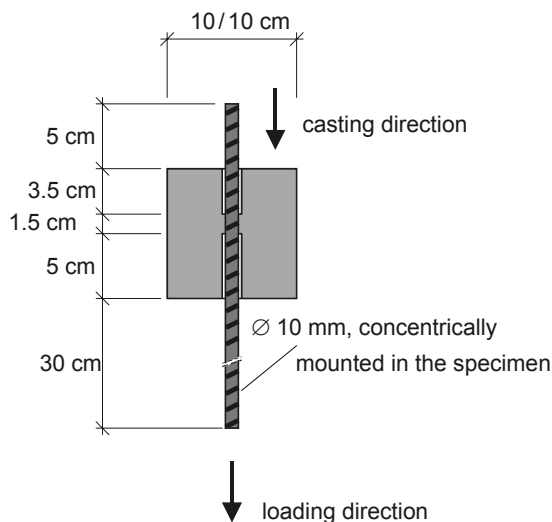
Figure 4:   Pull-out specimen with vertical
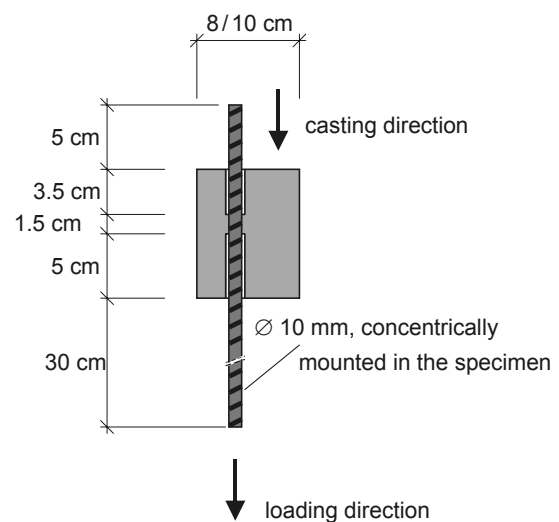
Figure 5:   Pull-out specimen with vertical

orientated rebar and concrete cover
according to RILEM

orientated rebar and reduced
concrete cover

elastic pad

steel plate

direction of loading
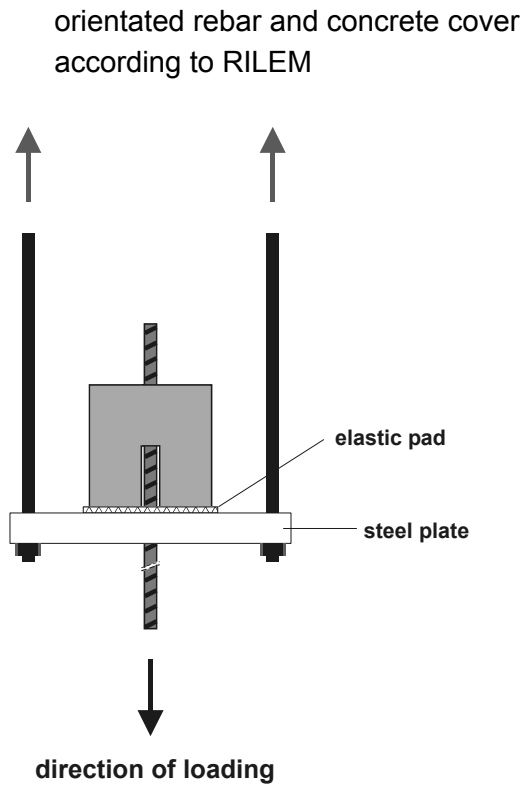
Figure 6: Loading of the specimen in
principle
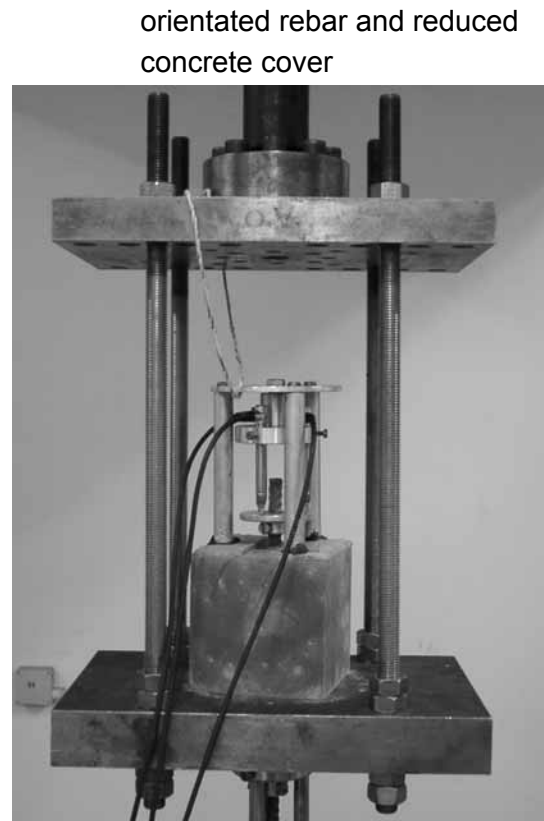
Figure 7: Specimen arrangement in testing
machine

5   Results

5.1   Hardened Concrete Properties

All tested specimens for the hardened concrete properties were cured under water until the test (concrete ages of 3, 7, 28 and 56 days). The values for the cylinder compressive strength and the E-modulus were determined on cylinders ($Ø$ 100/h = 200 mm), the cube compressive and the splitting tensile strength on cubes measuring 100 × 100 × 100 mm³ corresponding to DIN EN 12390 [11]. The chosen smaller dimensions of the specimens compared to those used in DIN 1045-2 [9] to categorise the concrete in compressive strength classes were necessary, because of the capacity of available testing machines. In Table 3 the determined hardened concrete properties after 28 days are shown as a mean out of 3 values each.

The time development was also measured for all hardened properties in order to evaluate the bond properties. Typically for UHSC are not only the high compressive strengths after 28 days, but also the high early age strength is quite remarkable. So, 80 - 120 N/mm² after 3 days are easily possible (Figure 8). Therefore this concrete type is fairly interesting for prestressed reinforced concrete members, because the pretensioning can be applied earlier. Figure 8 indicates the time development of the cylinder compressive strength, the curves for the other properties are summarised in [12].

Table 3: Hardened concrete properties after 28 days

Material property [N/mm²]	Reference 1	Reference 2	UHSC 1	UHSC 2	UHSC 3
Cylinder compressive strength $f_{c,cyl}$	53	62	135	147	144
Cube compressive strength $f_{c,cube}$	63	66	133	148	144
Splitting tensile strength $f_{ct,sp}$	4.4	5.1	9.5	12.2	10.9
Modulus of elasticity E_c	33,700	33,300	49,800	47,100	52,900
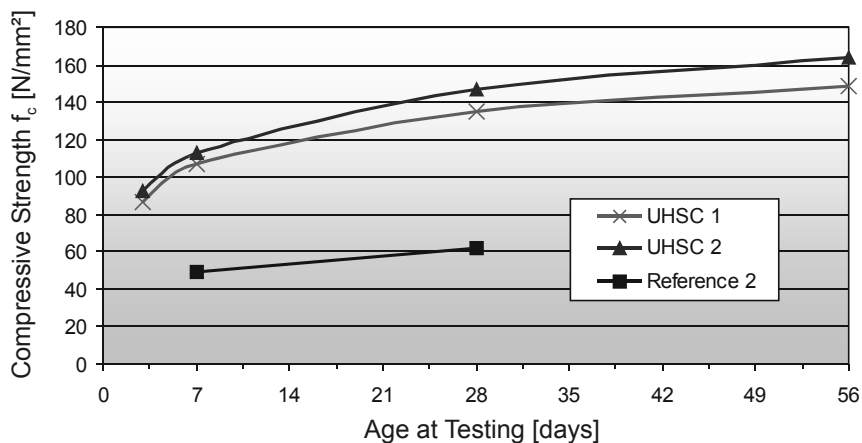
Figure 8: Time development of cylinder compressive strength

5.2 Bond of Reinforcement in UHSC

The bond stress-slip-relationships for the different concrete types were determined on RILEM-specimens [8] (see paragraph 4.2) At each tested concrete age 3 pull-out specimens per rebar orientation were experimentally analysed, so that the displayed curves represent the mean out of 3 corresponding pull-out tests. Altogether 155 bond tests were performed for rebar Ø 10 mm.

5.2.1 Time Development of the Bond Properties

The time development of the mean bond stress-slip-relationships is illustrated separately for 3 of the tested concretes in Figure 9 – 12. It is clearly visible, that the bond strength as well as the bond stiffness at an age of 3 days is quite high for UHSC. The further increase of the maximum reachable bond stress until 28 days reaches from 50% for the UHSC 1 and nearly 100% for the UHSC 2. In addition the increase after 28 days is rather small for the UHSC 2 (Figure 10), but the increment for the UHSC 1 is still remarkable. The reason for this fact is the effect of the fly ash, which reacts definitely later than silica fume and therefore it contributes later to the strength too. The bond stiffness increases over the time too. Positive to mention is the ductile bond behaviour of the tested UHSC and Reference 2, characterised by level descending branch of each curves. Despite of the reached high bond stresses (for UHSC) only a few splitting failure occurred. In comparison to Reference 2 higher values of the bond stresses relative to the compressive strength were investigated (Figure 12). In this figure also the different bond stiffnesses of the concrete types used are visible.
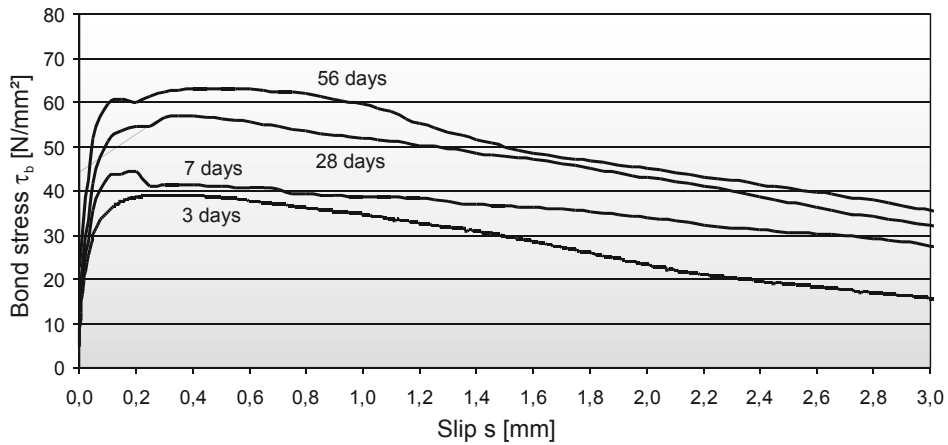
Figure 9: Time development of the bond stress for the UHSC 1 – variant 1: vertical rebar orientation, loaded in casting direction, Ø 10 mm, concrete cover 4.5 cm, bond length 1.5 cm
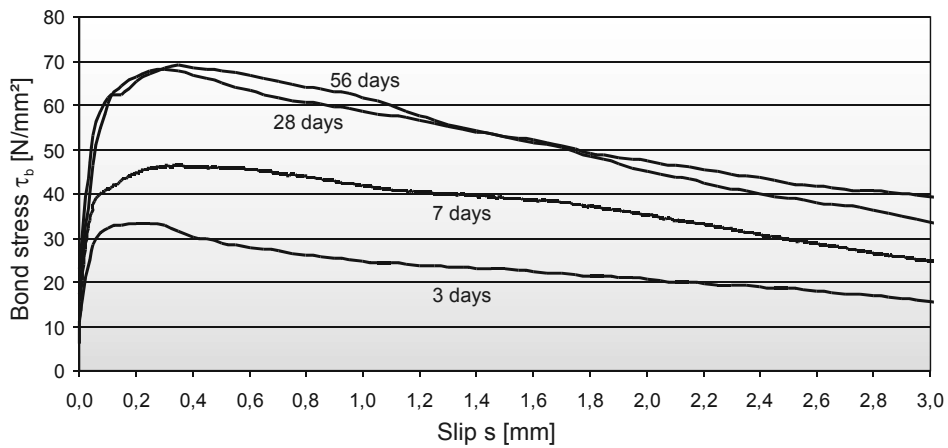
Figure 10: Time development of the bond stress for the UHSC 2 – variant 1: vertical rebar orientation, loaded in casting direction, Ø 10 mm, concrete cover 4.5 cm, bond length 1.5 cm
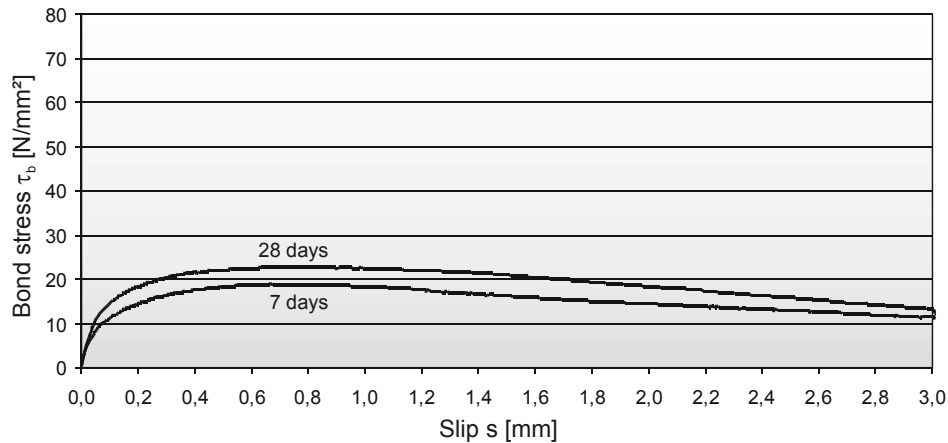
Figure 11: Time development of the bond stress for the Reference 2 – variant 1: vertical rebar orientation, loaded in casting direction, Ø 10 mm, concrete cover 4.5 cm, bond length 1.5 cm
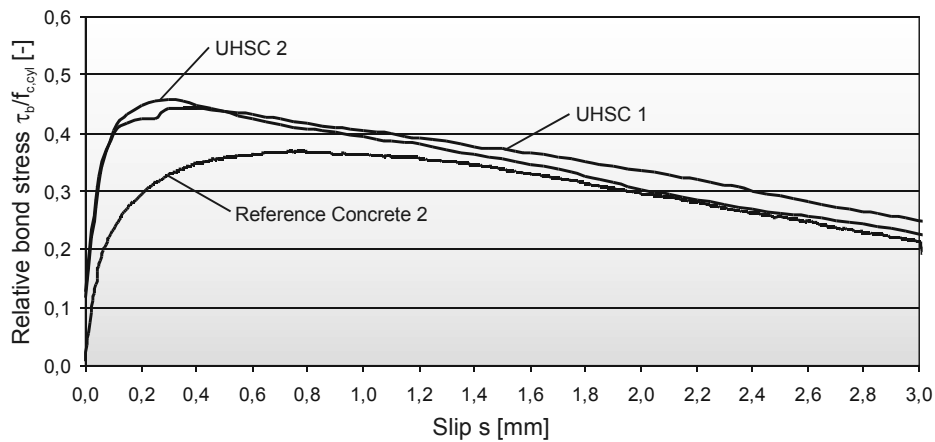
Figure 12: Relative bond stress-slip-relationship for UHSC 1, UHSC 2 and Reference 2 after 28 days – variant 1: vertical rebar orientation, loaded in casting direction, Ø 10 mm, concrete cover 4.5 cm, bond length 1.5 cm

5.2.2 Influence of the Concrete Cover Size

In order to determine the size of the concrete cover, two main principles must be borne in mind:

➢ a sufficient mechanical anchorage of the rebar as well as

➢ the protection of the reinforcement against environmental attacks like chlorides, acids or carbon dioxide in order to prevent corrosion.

The splitting of the cover or the bond degradation due to corrosion and for both cases the associated loss of bond strength must be avoided. The effect of concrete cover and corrosion level on splitting and bond strength has been examined in other research, e.g. [14] - [16]. In this context also the permeability of UHSC has been investigated. It has been shown that the resistance against ingress of ions like chloride is very high [17]. From this point of view it may be possible to reduce the required cover size, so the values stated in [9]

for different exposures. Nevertheless the mechanical anchorage plays the major role for UHSC, because the changed relations of the hardened concrete properties (see paragraph 2) may dominate the general bond behaviour. Engström et al. presented results about the influence of confinement and cover on bond in high strength concrete [18]. A reduction of the concrete cover to 16 mm (same as rebar diameter) resulted in a drop of the maximum bond stress of about 25% in comparison to well confined concrete. When applying stirrups or a cover of 32 mm, the load level was the same as for well confined concrete. However, the post-peak behaviour was brittle due to longitudinal cracking.

In the study presented here, the cover size was reduced from 4.5 cm to 2.5 cm (see Table 2). At a concrete age of 3 days there was no influence: the maximum bond stresses were at the same level and no splitting occurred. Beginning from 7 days splitting failure came about for the smaller cover for UHSC 2. The measured results at an age of 28 days differ for the concretes used. Whereas both UHSC with a maximum grain size of 5 mm (UHSC 1 and 3) showed no negative effect due to the reduction of the cover in terms of splitting or bond stress, for UHSC 2 the splitting risk increased. One third and two thirds of the specimens cracked by longitudinal splitting after 28 days and 56 days, respectively. For the large cover size this failure mode was less significant. It has to be mentioned that UHSC 2 showed high shrinkage rates, and some specimens were pre-damaged due to small surface cracks.

5.2.3   Influence of the Loading Rate

Within a small test series the influence of the loading rate was investigated. Five different loading rate levels (1/1000, 5/1000, 10/1000, 50/1000 and 100/1000 mm/sec loading rate) were applied path-controlled. It is displayed in Figure 13, that the loading rate influences the shape of the bond stress-slip-curves. At the lowest loading rate (1/1000 mm/sec) the descending branch is flatter than the other ones. Other interesting points are the maximum bond stress and the slip values at maximum bond stress. The faster the loading rate (especially 50/1000 and 100/1000 mm/sec), the higher the bond stress values as well as the larger the displacement at maximum bond stress are (Figure 13). The third remarkable aspect is the ascending branch of the bond stress-slip-relationship. The lower the loading rate the steeper the increase, so the higher the bond stiffness.
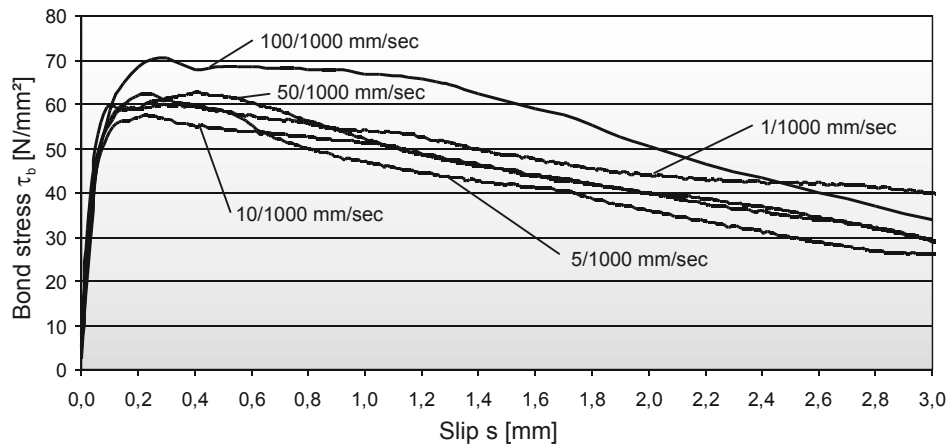
Figure 13: Influence of the loading rate on the bond stress-slip-relationship for the UHSC 2 after 28 days – variant 1: vertical rebar orientation, loaded in casting direction, Ø 10 mm, concrete cover 4.5 cm, bond length 1.5 cm

6 Conclusions

With the performed test programme could be shown, that the bond behaviour of reinforcement in ultra high strength concrete is not negatively influenced by the high brittleness of the material. The bond stiffness is increased due to the high compressive strength and modulus of elasticity, the bond stresses relative to the compressive strength are in the same range as the Reference mixes. Regarding the time development of the bond stresses, the mix design has a major influence on UHSC. In further studies lapped splices should be investigated.

Acknowledgement

7 References

[1] Bond of reinforcement in concrete. State-of-art report. fib-bulletin 10, Switzerland, 2000.

[2] Rehm, G.: Über die Grundlagen des Verbundes zwischen Stahl und Beton. Deutscher Ausschuß für Stahlbeton, Booklet 138, 1961.

[3] Martin, H.; Noakowski, P.: Verbundverhalten von Betonstählen. Untersuchung auf Grundlage von Ausziehversuchen. Deutscher Ausschuß für Stahlbeton, Booklet 319, 1981.

[4] Will, N.: Zum Verbundverhalten von Spanngliedern mit nachträglichem Verbund unter statischer und dynamischer Dauerbeanspruchung. Published by RTWH Aachen, 1997.

[5] Tepfers, R.: A theory of bond applied to overlapped tensile reinforcement splices of deformed bars. Report 73-2, Chalmers University of Technology, Göteborg, 1973.

[6] Hansen, L. P.: Building system with joints of high-strength reinforced concrete. Proceedings of the 2nd International Conference on Structural and Construction Engineering: System-based Vision for Strategic and Creative Design. Rome 2003, Vol. 2, pp. 1097 - 1102, A.A. Balkema Publishers, Lisse.

[7] Lubbers, A. R.: Bond Performance between Ultra-High Performance concrete and Prestressing Strands. Master Thesis, College of Engineering and Technology, Ohio University, 2003.

[8] RILEM: Technical Recommendations for the Testing and Use of Construction Materials: RC 6, Bond Test for Reinforcement Steel. 2. Pull-out Test, 1970.

[9] DIN 1045-2: Tragwerke aus Beton, Stahlbeton und Spannbeton - Teil 2: Beton: Festlegung, Eigenschaften, Herstellung und Konformität. Deutsche Anwendungsregeln zu DIN EN 206-1. (Concrete, reinforced and prestressed concrete structures - Part 2: Concrete . Specification, properties, production and conformity. German Application rules for DIN EN 206-1). July 2001.

[10] DIN 1045-1: Tragwerke aus Beton, Stahlbeton und Spannbeton - Teil 1: Bemessung und Konstruktion. (Concrete, reinforced and prestressed concrete structures - Part 1: Design). July 2001.

[11] DIN EN 12390-1: Prüfung von Festbeton - Teil 1: Form, Maße und andere Anforderungen für Probekörper und Formen. (Testing hardened concrete - Part 1: Shape, dimensions and other requirements for specimens and moulds). February 2001.

[12] Weiße, D.; Ma, J.: Mechanical Properties of Ultra High Strength Concrete. Leipzig Annual Civil Engineering Report No. 8 (2003), pp. 175 - 184.

[13] Weiße, D.: Verbundverhalten der Bewehrung in UHFB. In: König, G.; Holschemacher, K.; Dehn, F. (eds.): Ultrahochfester Beton, pp. 199 - 214. Bauwerk Verlag Berlin, 2003.

[14] Ghandehari, M.; Zulli, M.; Shah S. P.: Influence of Corrosion on Bond Degradation in Reinforced Concrete. Proceedings EM2000, 14th Engineering Mechanics Conference, ASCE, Austin, USA.

[15] Andrade, C.; Alonso, F.; Molina, F. J.: Cover Cracking as a Function of Bar Corrosion. Part I-Experimental Test . Materials and Structures, Vol. 26, October 1993, pp. 453 - 464.

[16] Amleh, L.; Mirza, S.: Corrosion Influence on Bond Between Steel and Concrete. ACI Structural Journal, Vol. 96, May-June 1999, pp. 415 - 423.

[17] Ludwig, H.-M.; Thiel, R.: Dauerhaftigkeit von UHFB. In: König, G.; Holschemacher, K.; Dehn, F. (eds.): Ultrahochfester Beton, pp. 89 - 107. Bauwerk Verlag Berlin, 2003.

[18] Engström, B.; Magnusson, J.; Huang, Z.: Pull-Out Bond Behaviour of Ribbed Bars in Normal and High-Strength Concrete with Various Confinements. In: Bond and Development of Reinforcement. A Tribute to Dr. Peter Gergely. ACI Special Publication, SP-180, 1998, pp. 215 - 242.

Katrin Habel

Dr sc. techn., civil engineer;
post doctoral researcher
Swiss Federal Institute of Technology (EPFL)
Lausanne, Switzerland

Emmanuel Denarié

Dr sc. techn., civil engineer;
senior research engineer
Swiss Federal Institute of Technology (EPFL)
Lausanne, Switzerland

Eugen Brühwiler

Dr sc. techn., civil engineer; professor
Swiss Federal Institute of Technology (EPFL)
Lausanne, Switzerland

Structural response of composite "UHPFRC-concrete" members under bending

Summary

Rehabilitation projects aim to enhance durability and to ensure structural safety. Ultra-High Performance Fibre Reinforced Concretes (UHPFRC) may fulfil these requirements when used as conservation materials. The structural response of composite "UHPFRC-concrete" elements under 4-point-bending was studied by means of experiments and an analytical model with the UHPFRC layer being under tension. Different depths of the UHPFRC layer were tested and rebars were placed in the UHPFRC layer in order to enhance the structural response. The results demonstrate the outstanding mechanical properties of UHPFRC in terms of structural response in composite elements. The addition of rebars in the UHPFRC layer enhances significantly resistance and stiffness and delays crack formation. An original analytical model allows to predict the moment-curvature relationship of composite "UHPFRC-concrete" elements.

Keywords: *UHPFRC, rehabilitation, conservation, composite elements, structural response*

1   Introduction

The properties of Ultra-High Performance Fibre Reinforced Concretes (UHPFRC) in terms of strength and permeability are outstanding when compared to normal strength concrete [1, 2]. UHPFRC materials are well adapted for the improvement of strength and durability of structural elements. In composite structural elements formed of existing ordinary reinforced concrete and new concrete, these UHPFRC offer a high potential in view of the protective and load carrying function of the new layer.

The basic conceptual idea for the improvement of existing reinforced concrete structures consists in applying high performance cementitious materials in zones of severe exposure. In the case of bridges, such zones of severe exposure include the top surface of the deck slab and the curbs when the bridge is exposed to de-icing salts (Figure 1). The deck slab obviously may also be subjected to higher mechanical loading when traffic loads are increased, and the load carrying capacity has to be enhanced accordingly and possibly without increasing the dead weight of the structure in order not to trigger strengthening interventions on other structural elements and the foundation.
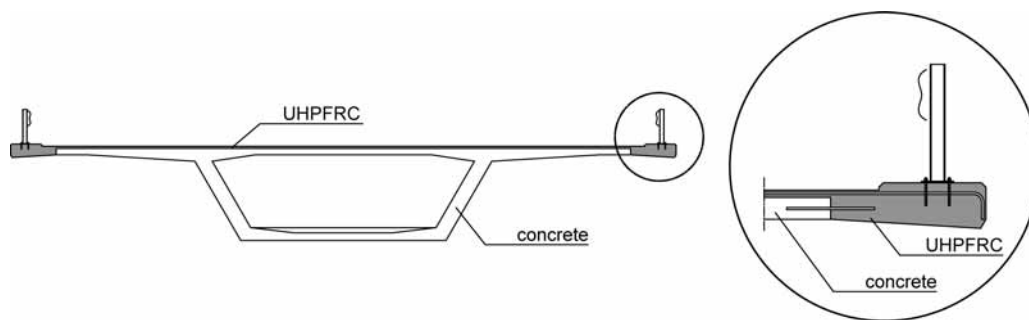
Figure 1:   Composite "UHPFRC-concrete" bridge deck

The structural behaviour of such composite elements has been investigated with respect to early age and long term behaviour as well as at ultimate limit state [3]. Experimental and analytical investigations have been conducted to study the composite behaviour of composite structural elements consisting of UHPFRC and normal strength concrete. The study shows that the structural response and the durability relevant properties of such composite elements are significantly improved when compared to elements consisting of ordinary reinforced concrete alone. The performance of such composite elements will be described and discussed in terms of load carrying capacity, stiffness, cracking behaviour and energy dissipation.

Based on this comprehensive research project an analytical model for the prediction of the bending structural response of composite elements has been developed in [3]. The objective of this paper is to discuss the structural response of composite "UHPFRC-concrete" elements by means of the experimental results and the analytical model with regards to potential applications.

2   Experimental program

The fracture behaviour of composite "UHPFRC-concrete" elements was studied by means of 4-point bending beams (Figure 2). The upper UHPFRC layer was under tension (negative bending moment) in order to investigate the tensile behaviour of this material under a constant bending moment. The behaviour of composite "UHPFRC-concrete" elements was investigated on 15 full-size bending beams with a length of 5.40 m. The beams consisted of a substrate of reinforced concrete that was between 8 and 15 months old and a layer of UHPFRC that was 90 days old at testing. Prior to the fracture tests, early age and long-term behaviour was investigated over a period of 3 months. The contact zone of the concrete was prepared by hydrojetting.

The concrete layer was identical for all beams with a reinforcement $A_{s,cc}$ = 1010 mm^2 and $A_{s,ct}$ = 339 mm^2 (corresponding to a reinforcement ratio of ρ = 0.83 % for a negative bending moment). The parameters of the experimental campaign were the thickness of the UHPFRC layer and its reinforcement ratio. Three beams had a thickness h_U = 3 cm and six beams each had h_U = 5 cm and 10 cm. Rebars ($\rho_{s,U}$ = $A_{s,U}/A_U$ = 2 %) were placed in the UHPFRC layer of half of the beams with h_U = 5 cm and 10 cm.
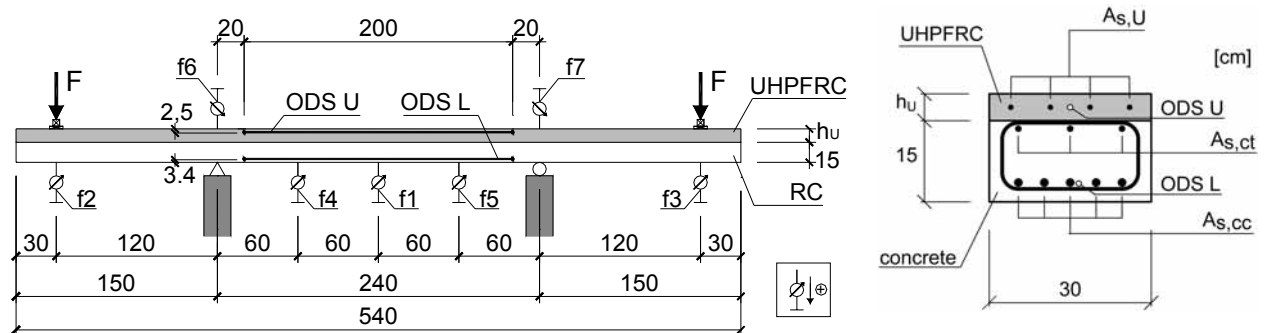
Figure 2:   System of the beam tests

The tests were displacement-controlled by imposing the displacement of one of the two hydraulic jacks. The forces were kept equal in the two jacks. The speed of the controlled jack was 0.4 mm/min.

Deflections were measured with LVDTs f1 to f7, and the mid-span deflection was deduced by f1 + 0.5 (f6 + f7). Internal deformations were measured with two optical deformation sensors (ODS) in the central span of the beams. The widths of localized macrocracks were followed with Ω-gages that were placed on the top surface of the beams. Cracks that were visible with the naked eye were traced on the beams during testing in order to follow the crack evolution. Here, only the composite beams with reinforcement in the UHPFRC layer are presented. The results for the beams without reinforcement are discussed in [3].

3   Materials

The UHPFRC was a self-compacting CEMTEC$_{multiscale}$® with one fibre type, developed at the LCPC [4]. 6 Vol.-% of steel fibres (l = 10 mm, $\varnothing$ 0.2 mm) were incorporated in the mix.

Considering an isotropic fibre distribution, the reinforcement ratio of the steel fibres corresponded to $\rho_{f,U} = 0.5 \cdot 6$ Vol.-% = 3 Vol.-%. The UHPFRC matrix consisted of cement, silica fume, fine sand, superplasticizer and water (water/binder = 0.14). Its maximal aggregate size was 0.5 mm. The normal strength concrete had a maximal aggregate size of 16 mm and a w/c = 0.40. The compressive strength (f_{cc}) and the elastic secant modulus at 30 % (E_{cc}) were determined on cylinders (UHPFRC: $\varnothing$ 11 cm, concrete: $\varnothing$ 16 cm) (Table 1). Tensile behaviour and strengths were investigated on notched plates ($5 \cdot 20 \cdot 50$ cm^3) with a uniaxial tensile test described in [3].

Table 1: Mechanical properties at 28 days (mean values)

		UHPFRC	NSC
f_{cc}	[MPa]	168	51
E_{cc}	[GPa]	48	38
f_{ct}	[MPa]	-	3.4
$f_{Ut,1st}$	[MPa]	9.1	-
$f_{Ut,max}$	[MPa]	11.0	-
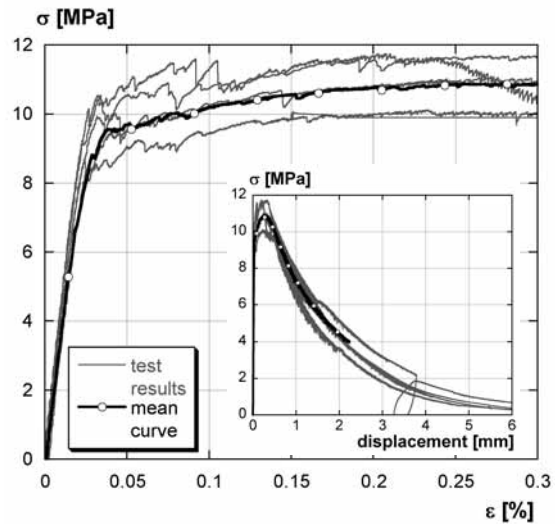
Figure 3: Uniaxial tensile behaviour of UHPFRC

The uniaxial UHPFRC tensile behaviour at 28 days is shown in Figure 3. The hardening branch is transformed into deformation. The displacements were measured with LVDTs over a base of 10 cm. Four test results and the mean curve are represented. Reference values are distinguished at the end of the linear-elastic zone ($f_{Ut,1st}$) and the end of the hardening zone ($f_{Ut,max}$) (see Figure 5a). The detail shows the complete curves with the abscissa in displacements. The tensile behaviour was exclusively determined by uniaxial tensile tests, since bending tests are not appropriate to determine material properties of UHPFRC.

4   Analytical model

The flexural behaviour of composite "UHPFRC-concrete" elements is determined with an analytical cross-sectional model. The moment-curvature relationship is established for a section with the UHPFRC layer in tension (Figure 4). The analytical model is based on an extension of the commonly used bending model for reinforced concrete and considers the tensile behaviour of UHPFRC. It is based on the following hypothesis:

1. Plane sections remain plane (hypothesis of Bernoulli). This means that the adherence between the cementitious materials (concrete and UHPFRC) and the reinforcement is perfect and that the adherence at the interface between concrete and UHPFRC is perfect (monolithic behaviour).
2. The behaviour of steel and cementitious materials is described with material laws.

3. The cross-section is in equilibrium, i.e. the equilibrium of forces and moment is stated.
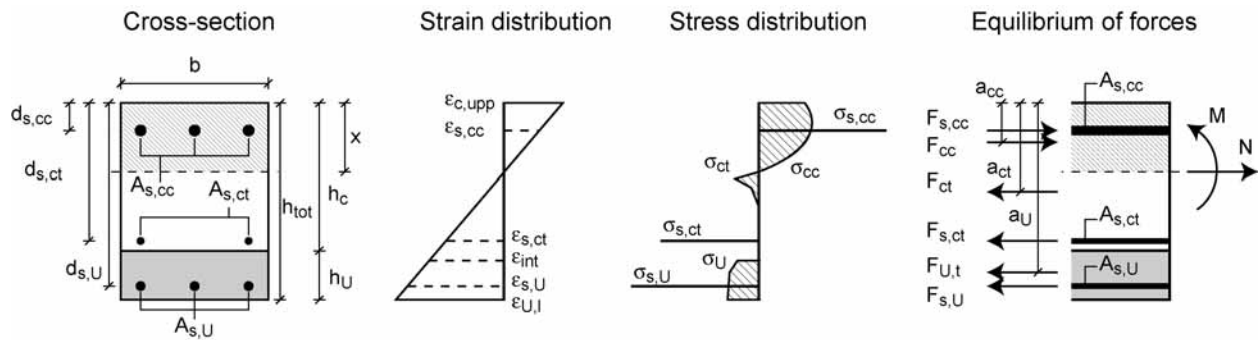
Figure 4: Definition of the model (UHPFRC in tension on the bottom)
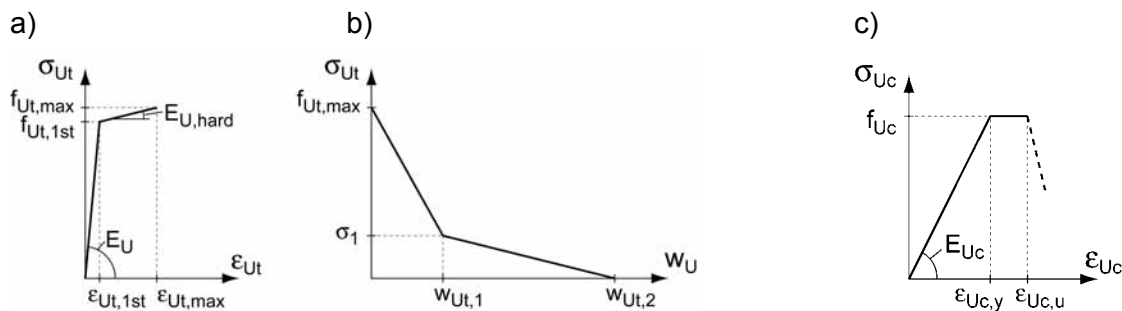
Figure 5: Material laws of UHPFRC

The tensile behaviour of the UHPFRC is modelled in two parts: The material is considered as a continuum according to a bi-linear relation for strains smaller than $\varepsilon_{Ut,max}$ (Figure 5a). Beyond hardening at $f_{Ut,max}$, the formation of a fictitious crack with an opening w is assumed following a bi-linear softening law (Figure 5b). The compressive behaviour of UHPFRC is modelled with a tri-linear diagram as proposed in [5] (Figure 5c). The compression of the concrete is modelled by a parabola diagram and its tensile behaviour by a linear-elastic part and a bi-linear softening diagram. A bi-linear material law is assumed for the steel reinforcement, symmetric in tension and compression.

The strain and stress states in a section of a flexural "UHPFRC-concrete" element are calculated with the model given in Figure 4. The linear strain distribution allows to calculate the curvature κ and the stresses in the cross-section using material laws.

5 Composite "UHPFRC-concrete" beams with reinforcement in the UHPFRC layer

5.1 Experimental results

Figure 6 shows the test results of the composite "UHPFRC-concrete" beams with reinforcement in the UHPFRC layer. The beams with a thickness of the UHPFRC layer of h_U = 5 cm are called R5, those with h_U = 10 cm R10. The behaviour of the original reinforced

concrete section (RC) with h/b = 17/30 cm and of composite RC beams with the same geometry as the composite "UHPFRC-concrete" beams are determined by the analytical model and added to the figure in order to be able to evaluate the contribution of the reinforced UHPFRC layer with respect to elements consisting of normal strength concrete.
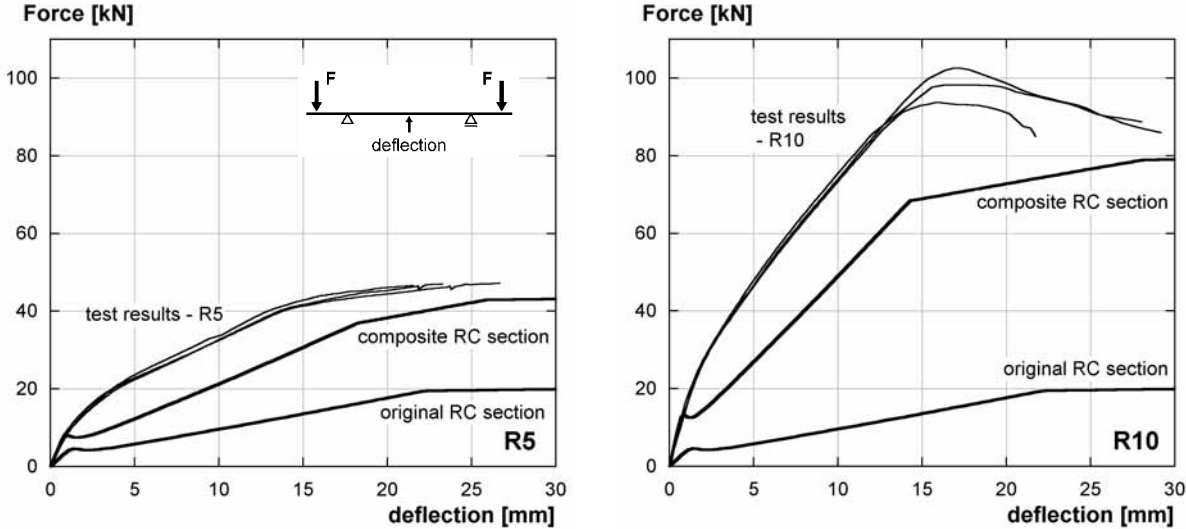
Figure 6:   Force-deflection curves for beams R5 and R10

The addition of a reinforced UHPFRC layer increases dramatically the resistance of the element: the maximum force is two times higher for beams R5 and five times higher for beams R10 than for the original concrete beam without UHPFRC. The maximum force is also significantly increased when compared to composite RC element: 10% for R5 and 20% for R10. Furthermore, the stiffness of the composite element is considerably higher than for the composite RC element. The stiffness of composite "UHPFRC-concrete" elements decreases more smoothly until the maximum fore is reached, while the stiffness of composite RC elements is significantly reduced for deflections higher than 2 mm due to the formation of discrete cracks in the concrete.

The advantageous behaviour of composite "UHPFRC-concrete" elements is explained by the tensile properties of the UHPFRC: The strength $f_{Ut,1st}$ is significantly higher than for normal strength concrete. Densely distributed fine macrocracks in the UHPFRC layer lead to strain-hardening and the macroscopic deformation in the UHPFRC layer is still uniform in axial direction in the central span of the beams. In comparison, discrete bending cracks form in reinforced concrete members, significantly reducing the stiffness of the structural member. Distributed macrocracks in the UHPFRC after complete exploitation of the strain-hardening capacity could be observed visually: at the maximum force, distributed macrocracks had formed every 1 to 5 cm (Figure 7).
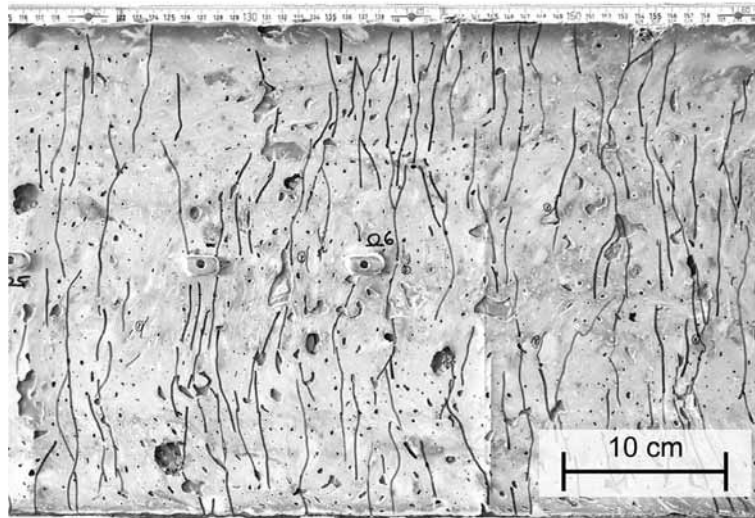
Figure 7:   Distributed macrocracks at maximum force (beam R10)

One to three localized macrocracks formed in the composite "UHPFRC-concrete" beam at a mid-span deflection of 15 cm (l/160). When these cracks reached the interface, interface cracks propagated in axial direction, however, these interface cracks remained small (crack width < 0.5 mm [3]) and did not alter the structural response of the composite elements, i.e. no local debonding occurred and the structural behaviour remained monolithic. Afterwards, the width of the localized macrocracks increased rapidly, and final failure of the beam occurred in one of these bending cracks.

On the basis of the test results and the analytical model, the structural response of the composite "UHPFRC-concrete" beams may be described following five stages (Figure 8a and b)

I.   At small forces, i.e. in the beginning of the test, the beam shows quasi linear-elastic behaviour. No visible cracks occur in the UHPFRC.

II. Microcracks develop into densely distributed macrocracks of small openings (< 50 μm). The deformations of the UHPFRC are still considered to be homogeneously distributed over the beam.

III. Localized macrocracks develop out of distributed fine macrocracks at a mid-span deflection of l/160 when the maximum force is reach. When the localized macrocracks arrive at the interface, interface cracks occur.

IV. The force transferred in the macrocracked UHPFRC layer decreases, and more and more stresses are deviated into the tensile reinforcement in the UHPFRC and the concrete layer. The tensile rebars start to yield and one to three hinges develop.

V.   The composite beam finally fails by fracture of the tensile reinforcement and by concrete crushing in one of the hinges.
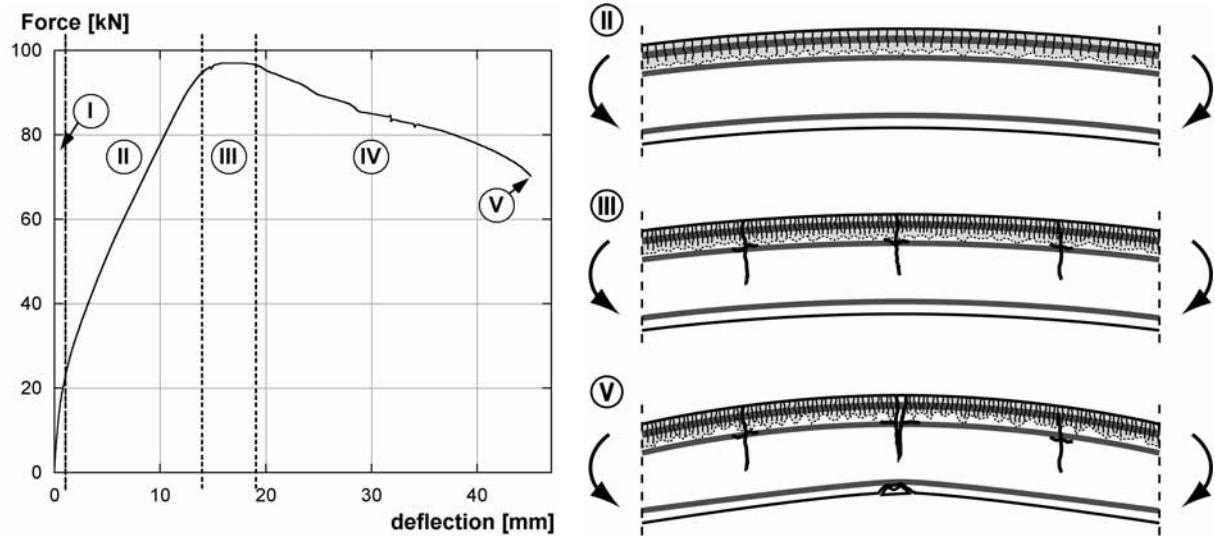
Figure 8: Structural response of beam R: typical force-deflection diagram (R10) and evolution of the crack pattern

5.2 Comparison with the analytical model

The analytical model is used to determine the UHPRFC tensile behaviour by inverse analysis. The results of the analytical model are transformed into force-deflection curves by assuming a constant curvature over the entire central span of the beams. They are first fitted to the results of the beam tests by adapting the UHFPRC tensile properties (Figure 9a). The bi-linear tension law resulting from the best fit is then compared to the uniaxial tensile test results (Figure 9b).
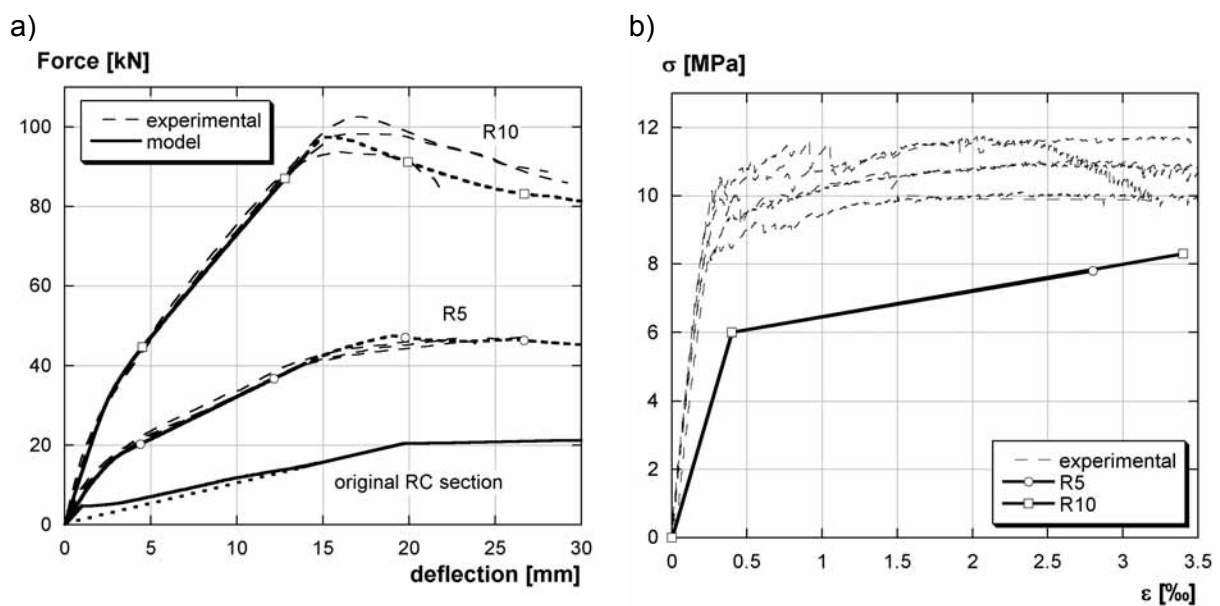
Figure 9: Comparison between test results and analytical model

The force-deflection curves of R5 and R10 are reproduced with an error smaller than 5 % (Figure 9a) by considering the corresponding tensile input values of Figure 9b. The strengths $f_{Ut,1st}$ and $f_{Ut,max}$ are approximately 33 % lower than the mean experimental values in uniaxial tension. The apparent secant modulus is lower than the secant modulus observed in the tests (reduction of 50 %). However, the initial stiffness - for deflections smaller than 2 mm - is underestimated by the analytical model. This indicates non-linearity of the UHPFRC tensile behaviour before the deformation $\varepsilon_{Ut,1st}$. The strain in the UHPFRC layer at the formation of localized macrocracks $\varepsilon_{Ut,max}$ is equal or even higher than indicated by the tensile test results. The significant difference between the UHPFRC tensile behaviour and the tensile behaviour determined by inverse analysis on the basis of the beam tests has several reasons:

- In the tensile test, the notch concentrates the fracture process into a given cross-section - not the weakest one, while in the bending beams, the weakest sections fracture first. As a consequence, the tensile test tends to overestimate tensile properties.

- The reduction of the tensile strength of the UHPFRC of the beams may be due to fibre segregation in the UHPFRC. Fewer fibres were found near the top surface of the beams. This segregation was more pronounced for thicker UHPFRC layers.

- The lower apparent secant modulus and the steeper hardening modulus $E_{U,hard}$ of the tensile properties found by inverse analysis may be due to the formation of microcracks in the UHPFRC layer due to the time-dependent behaviour of the composite elements during the 90 days prior to the fracture tests [3]. This may also explain the non-linearity in the UHPFRC tensile behaviour for deformations smaller than $\varepsilon_{Ut,1st}$.

The differences between the tensile test results and the tensile properties, determined from the beam tests by inverse analysis, show that the material test results cannot be directly applied to structural elements. There is a need for further research into the deduction of UHPFRC tensile parameters for the analysis of composite "UHPFRC-concrete" elements demands further research.

Moreover, the UHPFRC tensile properties, obtained by the inverse analysis, indicate the beneficial effect of rebars in the UHPFRC layer: In addition to the enhancement in load carrying capacity and stiffness, this reinforcement increases significantly the magnitude of hardening, i.e. the deformation at the maximum strength $f_{Ut,max}$, that is 1‰ for the beams without reinforcement in the UHPFRC layer (see [3]) and 2.8 and 3.4‰ for the beams with reinforcement in the UHPFRC layer.

The results show that the tensile behaviour, in particular the strain-hardening, improve the structural response of composite "UHPFRC-concrete" elements in terms of load carrying capacity and stiffness compared to composite RC elements.

6   Conceptual design

Three different cross sections are deduced from the comprehensive study of composite "UHPFRC-concrete" elements [3] (Figure 10) and are discussed in [6]:
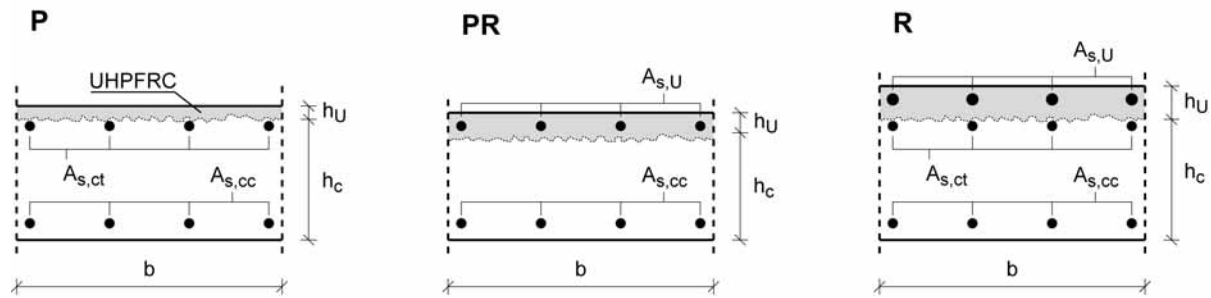
Figure 10: Three types of cross-sections for composite "UHPFRC-concrete" elements

(1) *Cross section (P)* with a thin UHPFRC layer is designed for protection purposes. The tensile reinforcement in the existing concrete is situated near the interface between the two concretes. Such cross-sections are obtained when the tensile reinforcement of the existing RC structure (As,ct) is not or only slightly deteriorated and the load carrying capacity is sufficient.

(2) *Cross section (PR)* represents the case when additional tensile reinforcement is placed into the UHPFRC layer to replace and/or to complement the existing strongly deteriorated rebars. This configuration provides both an improved protection function and an increase in load carrying capacity.

(3) *Cross section (R)* is designed primarily to increase significantly the load carrying resistance of the structural element. The cross-section consists of the original reinforced concrete section which is complemented by the reinforced UHPFRC layer which can be seen as an externally bonded additional reinforcement. Also, the UHPFRC provides the protection function for the structural element which is beneficial to durability of the element.

7   Conclusions

1. Three basic composite "UHPFRC-concrete" configurations are proposed for the functions of protection and resistance of new and existing concrete structures.

2. The outstanding mechanical properties of UHPFRC are demonstrated in terms of improved structural response of composite "UHPFRC-concrete" elements. This is attributed to the high strengths and the pronounced strain-hardening behaviour of UHPFRC under uniaxial tension.

3. The stiffness of composite "UHPFRC-concrete" elements is significantly increased under service conditions and no localized macrocracks form until the maximum force is reached.

4. Rebars in the UHPFRC layer increase resistance and stiffness of the elements. Moreover, the apparent magnitude of hardening is increased by a factor of 3 and the formation of localized macrocracks is delayed.

5. The suggested analytical model allows to predict the moment-curvature relationship of composite "UHPFRC-concrete" bending elements of different geometric and material configurations.

8   Acknowledgements

9   References

[1]   Rossi, P.: Ultra-high performance fibre reinforced concretes (UHPFRC): an overview, BEFIB'2000, Proceedings of the Fifth International RILEM Symposium on Fibre-Reinforced Concretes (FRC), Ed. by P. Rossi and G. Chanvillard, Lyon, France, p. 87-100, 2000.

[2]   Charron, J.P.; Denarié, E.; Brühwiler, E.: Permeability of UHPFRC under high stresses. Proceedings, RILEM Symposium, Advances in Concrete Through Science and Engineering, March 22-24, 12 p., Chicago, USA, 2004.

[3]   Habel, K.: Structural behaviour of composite "UHPFRC-concrete" elements, Doctoral thesis, Swiss Federal Institute of Technology, Lausanne, Switzerland, 2004, to be published.

[4]   Rossi, P.: Development of new cement composite material for construction, Innovations and Developments In Concrete Materials And Construction, Proceedings of the International Conference, University of Dundee, Ed. by R. K. Dhir, P. C.Hewlett, L. J. Csetenyi, pp 17-29, Dundee, Scotland, September, 2002.

[5]   AFGC: Bétons fibrés à ultra-hautes performances (Ultra high performance fibre-reinforced concretes), SETRA, AFGC, France, 152 p., 2002.

[6]   Brühwiler, E.; Habel, K.; Denarié, E.: Advanced reinforced concrete for the improvement of bridges, Second International Conference on Bridge Maintenance, Safety and Management (IABMAS'04), Kyoto, Japan, 7 p., October, 2004.

Kai Bunje
Dipl.-Ing.
Fehling + Jungmann GmbH
Kassel, Germany

Ekkehard Fehling
Prof. Dr.-Ing.
Universität Kassel
Kassel, Germany

About shear force and punching shear resistance of structural elements of Ultra High Performance Concrete

Summary

An extensive research program was started in 2001 at the University of Kassel in order to study the durability and mechanical properties of the new material Ultra High Performance Concrete and the structural behaviour of construction elements built of UHPC. This report includes results about the shear force load carrying behaviour of UHPC beams and the punching shear load carrying behaviour of thin UHPC plates.

Keywords: *UHPC, shear force, punching shear, steel fibre reinforcement*

1   Introduction

In the following, test results concerning the shear force resistance behaviour of UHPC beams and the punching shear load carrying behaviour of thin UHPC plates are shown. The results of both types of tests are important to provide a safe design of building constructions like the Gärtnerplatzbrücke.

2   Shear force

The German design code DIN 1045-1 for concrete structures distinguishes between plates and beams in the design calculations for the shear load capacity. Due to their spatial load bearing capability, plates have the possibility to redistribute force peaks to other areas. Therefore it is allowed to build plates without shear force reinforcement, whereas for beams a minimum shear reinforcement has to be placed. Tests on UHPC beams with steel fibres have shown, that it is very effective to use steel fibres as a shear force reinforcement instead of stirrups.

2.1   UHPC without fibres and without shear force reinforcement

Tests on beams of UHPC without steel fibres have been performed at the University of Kassel [1]. Figure 1 shows the longitudinal reinforcement of the test specimens.
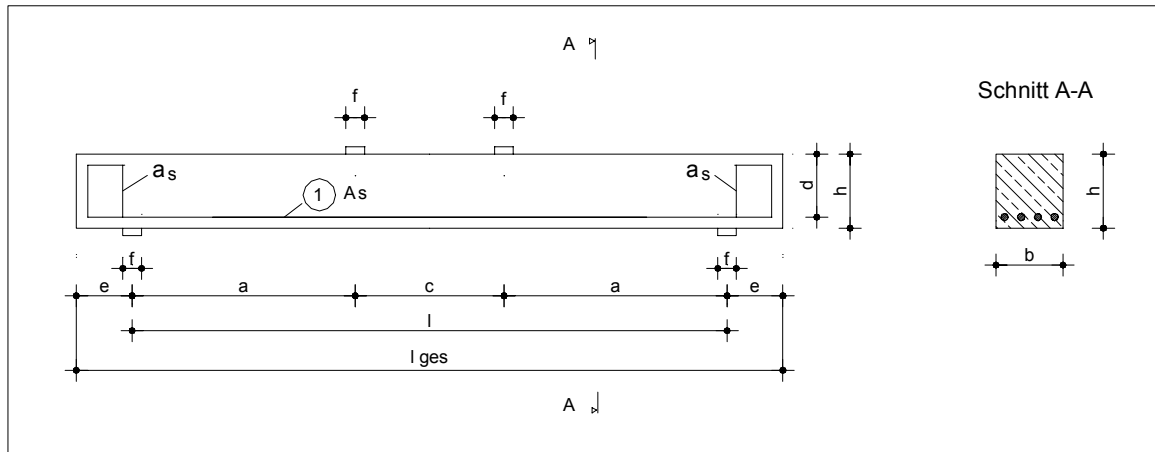
Figure 1: Longitudinal reinforcement of the test specimens
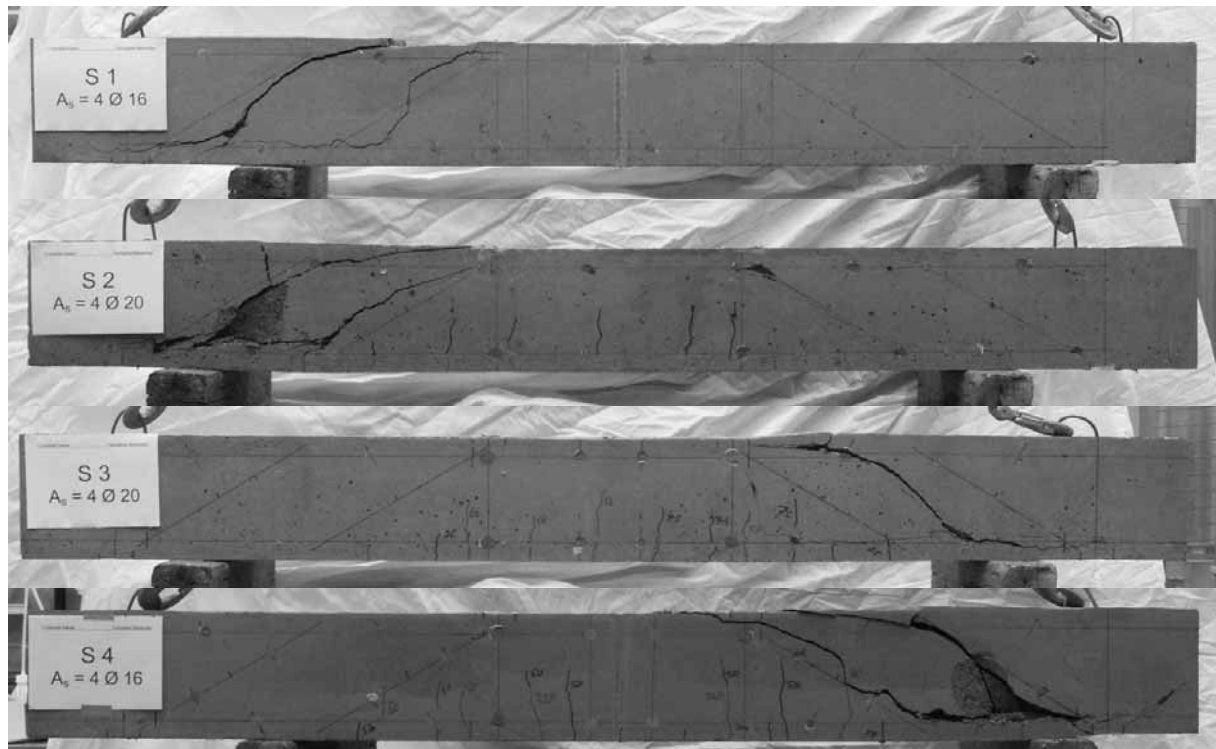
Figure 2: Failure pattern of the test specimens

A model for the shear force capacity of HPC-beams without shear reinforcement (stirrups) has been proposed by Zink [2]. According to this model, the main shear force load carrying mechanism is given by the capacity of the compressive zone of the structural element in shear (Figure 3).

Limiting case: shear carrying proportion
in the tension zone negligible
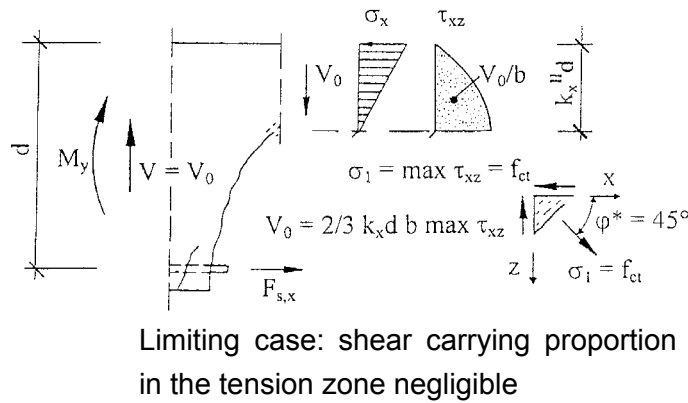
Figure 3:   Shear stress distribution in the compressive zone [2]

According to this model, the following formula for the determination of the shear force carrying capacity $V_{u,ct}$ also takes into account the fracture mechanical influence due to the transfer of tensile stresses near the crack tip and the influence of the shear slenderness a/d :

$$V_{u,ct} = V_{u,ct} = \frac{2}{3} \cdot b_w \cdot k_x \cdot d \cdot f_{ct} \cdot \left(\frac{4 \cdot d}{a}\right)^{1/4} \cdot \left(\frac{5 \cdot l_{ch}}{d}\right)^{1/4}$$

with $l_{ch} = \dfrac{E_c \cdot G_f}{f_{ct}^2}$ as the characteristic length as a fracture mechanics parameter of the

concrete. In accordance to the investigations by Remmel [3] and Grimm [4] on material properties of HPC, the fracture energy of the coarse aggregate UHPC used was estimated to G_f = 143 N/m.

Figure 4 shows the good correspondence of the ultimate loads predicted by the model with the test results. The abscissa in Figure 4 shows the longitudinal reinforcement ratio ρ_l as an indicator for the compressive zone height.

Similar to the model by Zink, the design value of the shear force from flexural reinforced structures without shear force reinforcement according to DIN 1045-1 [5] is as follows:

$$V_{Rdt,ct} = \left[0{,}10\kappa \cdot \eta_1 \cdot \left(100\rho_1 \cdot f_{ck}\right)^{1/3} - 0{,}12\sigma_{cd}\right] \cdot b_w \cdot d$$

with

$$\kappa = 1 + \sqrt{\frac{200}{d}} \le 2{,}0$$

η_1 = 1,0 for normal concrete

ρ_1 longitudinal reinforcement ratio

$$\rho_1 = \frac{A_{sl}}{b_w \cdot d} \le 2.0 \%$$

A_{sl} area of the reinforcement for bending

b_w smallest sectional width in the tensile zone

d   efficient height of the longitudinal reinforcement

f_{ck} characteristic compressive strength

σ_{cd} design value of the normal concrete stress in the centre line
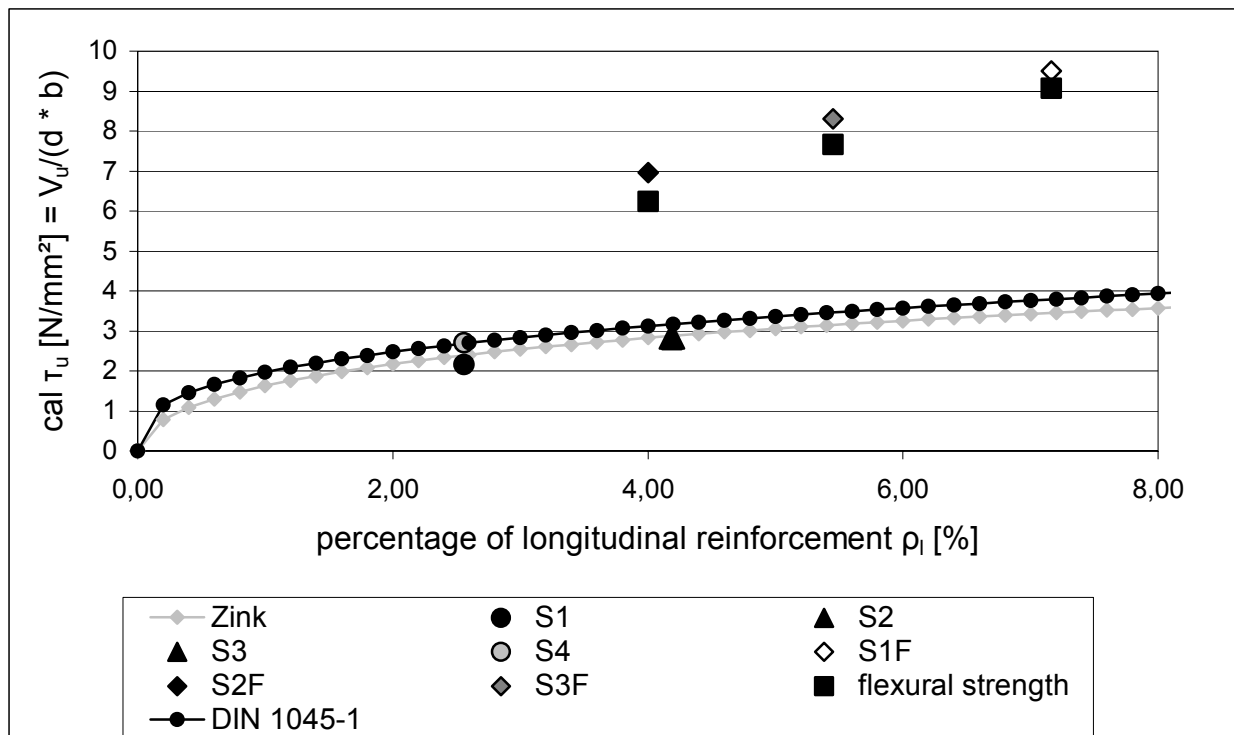
Figure 4:   Load carrying capacity depending on the longitudinal reinforcement ratio ρ_l

In DIN 1045-1 the applicable reinforcement ratio of the longitudinal reinforcement is limited to 2 %. However, the test results show that a higher percentage of the longitudinal reinforcement beyond this limit has a positive influence on the shear force load carrying capacity of UHPC elements.

2.2   UHPC with fibres and without shear force reinforcement

The tested beams of UHPC with steel fibres showed a shear force capacity which was significantly higher than that of beams without steel fibres. All beams reached the full flexural load carrying capacity. The failure was very ductile. Only the test specimen S1F with a very high percentage of the longitudinal reinforcement of ρ_l = 7,2 % has shown a combined flexural and shear failure (see Figures 5 - 7).
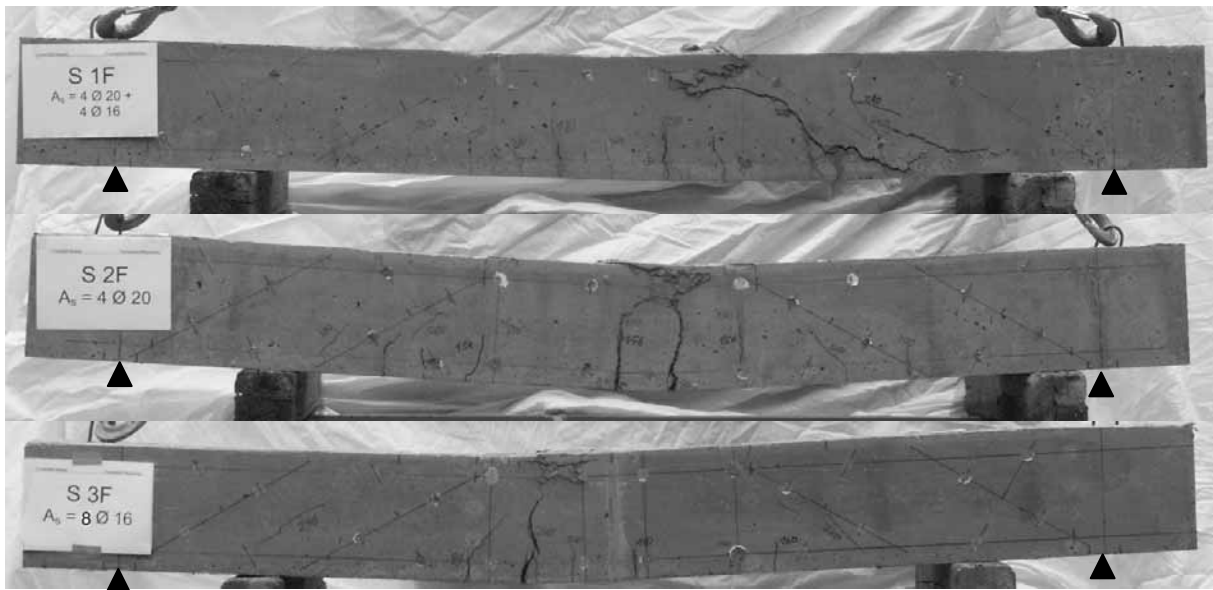
Figure 5:   Test specimens S1F – S3F of UHPC with steel fibres
            (2, 5 Vol.-%, Fibres 9 mm / 0,15 mm)[1]

Figure 6: Failure S1F   Figure 7: Failure S2F

The reached ultimate load fits very well to the calculated ultimate flexural strength. In [6] and [7] proposals for design assumptions to calculate the shear load capacity of UHPC beams with steel fibres following DBV–Merkblatt Stahlfaserbeton [8] are given. Further research in Kassel investigates if the basis of design for normal fibre concrete can also be used for design of UHPC with fibres.

3   Punching shear

For thin UHPC bridge decks of pedestrian bridges, as they shall be used for the Gärtnerplatzbrücke project in Kassel, it is required, that a rescue vehicle can pass. Therefore it is interesting to know the punching shear force load capacity of steel fibre reinforced plates.

At the University of Kassel two types of plates have been tested.

- Plates with the dimensions 200 * 200 * 3 cm with 3 different load arrangements
- Plates with the dimensions 100 * 100 cm with 4 different heights.

Test arrangements are shown in Figures 8 and 9.
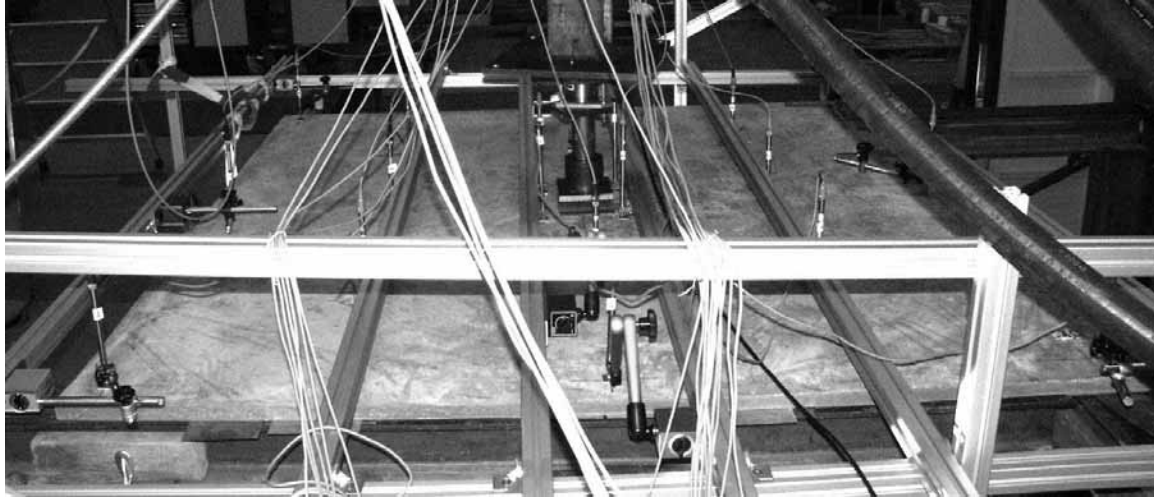
Figure 8: 200 * 200 * 3 cm test plate with measurement devises
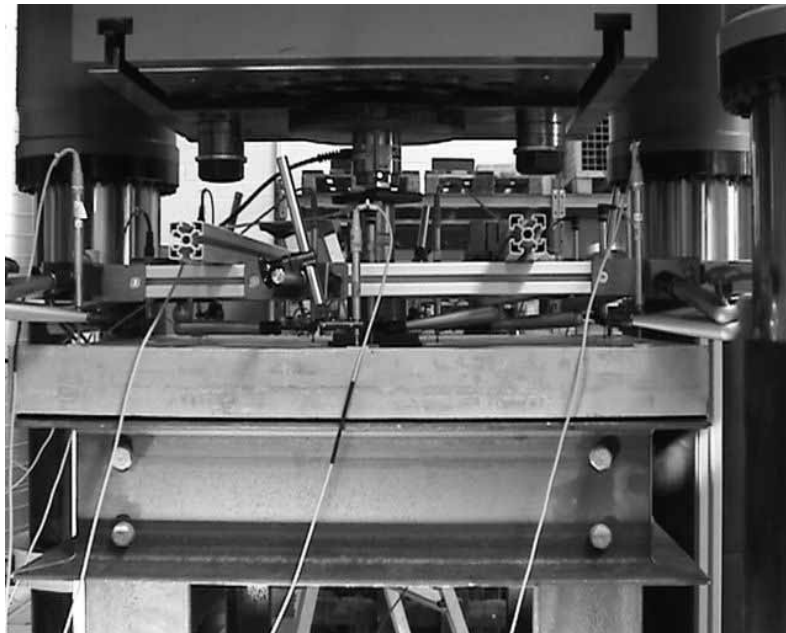
Figure 9: 100 * 100 * 8 cm test plate with measurement devises

3.1 Test results

The tested plates, made of UHPC with steel fibres, showed a very ductile behaviour. In all cases a flexural failure occurred; no plate showed a sudden punching shear failure. The crack in the 200 * 200 * 3 cm plates went from the point of load application in radial direction to the supporting frame (see Figures 10 and 11).
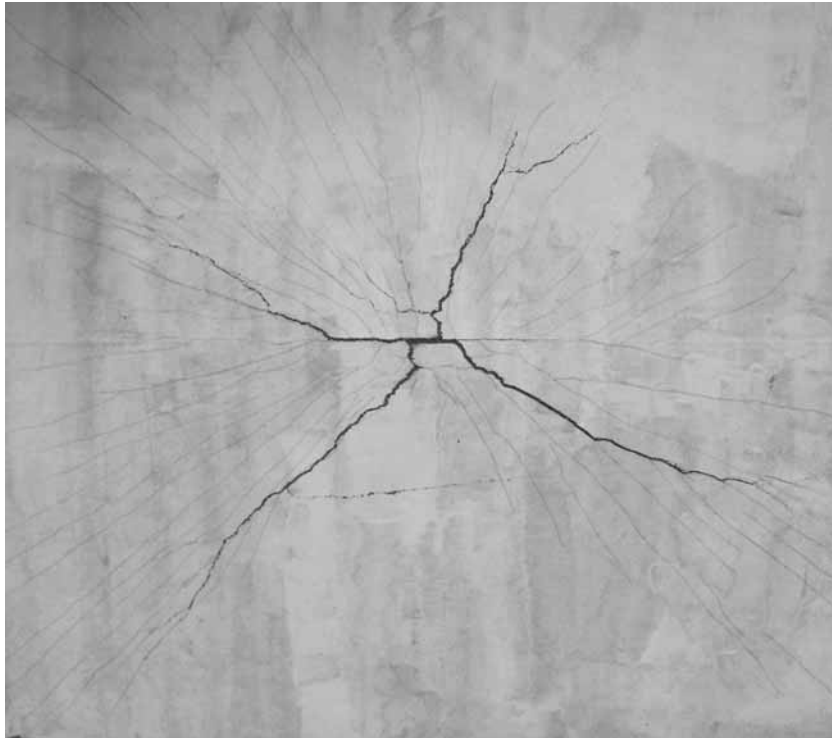
Figure 10: crack pattern in plate 1.2 (200 * 200 * 3 cm) centre load

Figure 11: crack pattern in plate 2.1 (200 * 200 * 3 cm) edge load

The same behaviour could be observed at the 100 * 100 * 3 cm plates (see Fig. 12) and even at the plates with 8 cm thickness (see Fig. 13).

Figure 12: crack pattern in plate 2 (100 * 100 * 3 cm) centre load

Figure 13: crack pattern in plate 5 (100 * 100 * 8 cm) centre load

After reaching the maximum load capacity, the loading has been continued until significant cracking due to bending could be observed on the top side of the plate. The cracks opened just before the collapse tangentially around the point of loading (see Figure 13).

Figure 14: crack pattern in the plate 2.1 (200 * 200 * 3 cm) on the top side

The ultimate loads and cracking loads are given in Table 1 and Table 2. It is interesting, that for both geometries with a thickness of 3 cm the first cracks occured at almost equal loads.

Table 1: Test results of plates 200 cm by 200 cm 3 cm thick

Point of load application at Pos. X / Plates Nr.		Ultimate load [KN]	Deformation at point of load application [mm]	Crack load [kN]	Deformation at point of load application [mm]
Mixture 1 loading center	1.1	-25,3	59,1	-7,3	5,0
	1.2	-31,5	62,0	-9,1	6,1
Mixture 2 loading edge	2.1	-37,9	42,5	-12,1	4,7
	2.2	-39,9	46,4	-10,2	4,8
Mixture loading corner	3.1	-34,7	34,1	-10,1	2,9
	3.2	-43,2	36,6	-12,2	3,1

Table 2:   Test results of plates 100 cm by 100 cm

Plates Nr.	Thickness [cm]	Ultimate load [KN]	Deformation at point of load Application [mm]	Crack load [kN]	Deformation at point of load application [mm]
1	3 cm	-22,4	21,8	-11,3	3,6
2	3 cm	-27,9	21,2	-12,5	2,37
3	4 cm	-41,2	19,9	-20,2	2,56
4	5 cm	-57,0	14,8	-40,3	3,22
5	8 cm	-131,4	10,1	-68,3	3,20
6	8 cm	-132,2	10,5	-63,8	2,785

For required thickness of a UHPC deck of pedestrian bridges which also have to be designed for the wheel loads of a rescue vehicle with a total weight of six tons and three tons per axle can be determined as follows:

Vehicle wheel load V_{wheel} = 15 kN, γ_F = 1,5, γ_C = 1,5

V_{wheel} = 15 kN *1,5 * 1,5 = 33,75 kN < V_{crack} ➔ 5 cm plates.

To confirm the results of this pre tests further tests are required.

4   Conclusions

The following conclusions concerning the shear force load carrying behaviour of UHPC beams and the punching shear load carrying behaviour of thin UHPC plates can be drawn:

- The UHPC beams without steel fibres had a shear failure. With the model by Zink or the formulas of DIN 1045-1 the ultimate load can be very well predicted.
- The shear failure of the beams made of UHPC without fibres was sudden.
- Beams made of the same UHPC but with steel fibres had a bending failure. The steel fibres worked very well as shear reinforcement, further investigations are required to develop a design model for the shear load capacity of UHPC beams with steel fibres.
- The beams with steel fibres showed a very ductile behaviour.
- The thin UHPC plates did not show a punching shear failure.
- The failure of the plates started with a flexural failure in the bottom and ended with bending cracks on the top of the plates
- The plates showed a ductile behaviour

5   References

[1] Fehling, E.; Schmidt, M.; Teichmann, T.; Bunje, K.: Entwicklung, Dauerhaftigkeit und Berechnung Ultra-Hochfester Beton (UHPC), Forschungsbericht an die DFG, Universität Kassel, 2003.

[2] Zink, M.: Zum Biegeschubversagen schlanker Bauteile aus Hochleistungsbeton mit und ohne Vorspannung. Dissertation, Universität Leipzig, 1999.

[3] Grimm, R.: Einfluss bruchmechanischer Kenngrößen auf das Biege- und Schubtragverhalten hochfester Betone. DAfStb, Heft 477, Beuth Verlag, 1997.

[4] Remmel, G.: Zum Zug- und Schubtragverhalten von Bauteilen aus hochfestem Beton, Dissertation, DAfStb, Heft 444, Beuth Verlag, 1994.

[5] DIN 1045-1: Tragwerke aus Beton, Stahlbeton und Spannbeton. Teil 1: Bemessung und Konstruktion. Entwurf September 2000.

[6] Tue, N.; Schneider, H.: Besonderheiten bei der Bemessung und der konstruktiven Ausbildung von Bauteilen aus UHPC im Rahmen der Zulassung im Einzelfall. In der Schriftenreihe Baustoffe und Massivbau, Heft 2, Universität Kassel, Sep. 2003.

[7] Deutscher Ausschuss für Stahlbeton: Hochfester Beton – Sachstandsbericht. DAfStb, Heft 436, Berlin, 1994.

[8] DBV-Merkblatt Stahlfaserbeton, Deutscher Beton- und Bautechnik Verein E.V., Oktober 2001.

Janis Brauns
Dr habil. Sc. Eng., Professor
Riga Technical University
Riga, Latvia

Karlis Rocens
Dr habil. Sc. Eng., Professor
Riga Technical University
Riga, Latvia

Stress State Optimization in Steel-Concrete Composite Elements

Summary

Composite columns and beams are a combination of concrete and steel elements realising the advantages of both types of materials. According to codes for concrete-filled column, the plastic resistance of the cross-section is given as a sum of the components and taking into account the effect of confinement in the case of circular sections. In this study the stress state in composite column is determined taking into account non-linear relationship of the modulus of elasticity and Poisson's ratio on the stress level in the concrete core. It is determined that the effect of confinement occurs at a high stress level when structural steel acts in tension and concrete works in lateral compression. The stress state and load bearing capacity of section in bending is determined taking into account non-linear dependence on position of neutral axis. Because the ultimate limit state of material is not attained for all the parts simultaneously, to improve the stress state of a composite element and to prevent the possibility of a failure the appropriate strength of concrete and steel should be used. The safety of high-stressed composite structures can be achieved by using ultra-high-performance concrete (UHPC).

Keywords: *composite columns and beams, stress state, non-linear deformation, ultra-high-performance concrete*

1   Introduction

Composite columns and beams, formed as hollow steel sections filled with concrete have advantages in different architectural and structural solutions. The composite structure characterises with higher ductility than the concrete column and advantages of steel may be successfully used in connections. The concrete filling and reinforced bar increase rigidity and load-bearing capacity of the hollow steel section with no changing in external dimensions of column. The filling improves the fire resistance as well. Composite column with a corresponding content of reinforcement can provide at least 90-minutes of fire-resistance rating [1].

According to EC4 [2] to determine the resistance of a section against bending moment, a full plastic stress distribution in the section has been assumed. The internal bending moment resulting from the stresses is the resistance of the section against acting moment. In order to increase the plastic bending capacity reinforcement can be included.

EC4 gives a simplified ultimate limit state design method for the composite structures, which is applicable for practical purposes. The method is based on consumption that ultimate strength of material is attained simultaneously in all parts of the section.

In previous decades investigations regarding interaction between steel shell and concrete core has been performed [3-7]. In general, it is concluded that for service load practically no bond exists and that the core and shell act as two independent materials. In the early stages of loading, the Poisson's ratio for concrete is lower than that for steel and the steel tube has no restraining effect on the concrete core. As the longitudinal strain increases, Poisson's ratio of concrete can remarkably increase. Therefore, the lateral expansion of unconstrained concrete gradually becomes greater than that of steel. A radial pressure develops at the steel-concrete interface thereby restraining the concrete core and setting up a hoop tension in the tube. At this stage, the concrete core is stressed triaxially and the steel tube biaxially. Interaction between steel tube and concrete is the key issue to understand the behaviour of this kind of column. It is shown [8] that concrete compaction affects the properties of the core and also may influence the interaction between the steel tube and its concrete core, and thus influences the behaviour of the composite columns.

The original lies mainly in the use of concrete, especially UHPC, in the form o slender composite elements for bridges rather than massive elements more commonly associated with concrete structures [9, 10].

In this study stress analysis of the composite column and beam is performed with purpose to obtain the maximum value of load-bearing capacity and enhance the safety of the structure using components with the appropriate strength properties and taking into account the composite action. The effect of UHPC on the stress state and load carrying capacity of composite elements is analysed.

2 Analytical model for stress analysis

The behaviour of short straight concrete-filled steel column under axial loading is considered. The term "short column" refers to a compression member that can attain its ultimate capacity without overall buckling. Disregarding the local effects at the ends, the stress state in the cross-section of the middle part of the column is analysed. A reinforced concrete core with radius R_0 is included in steel tube of thickness t (Figure 1). The reinforcement consists of symmetrically arranged longitudinal steel bars and circumferential reinforcing wire located at radius R_s from axis z.

For radial displacements w and circumferential displacements u on the contact surface concrete-structural steel ($r = R_0$) and concrete-reinforcement surface ($r = R_s$) the following equalities are valid:

$$w^a = w^c; u^a = u^c; \tag{1}$$

$$w^s = w^c; \quad u^s = u^c. \tag{2}$$

Here and below, the indices *a*, *c* and *s* refer to the steel tube, concrete and reinforcement. In the axial direction of the column, the cross-section area of the reinforcement is A_z^s, but in the circumferential direction - A_θ^s, placed with the given step. It is taken into account that the reinforcement is "spreaded" throughout the cross-sectional area, in result of that the anisotropic column is formed.
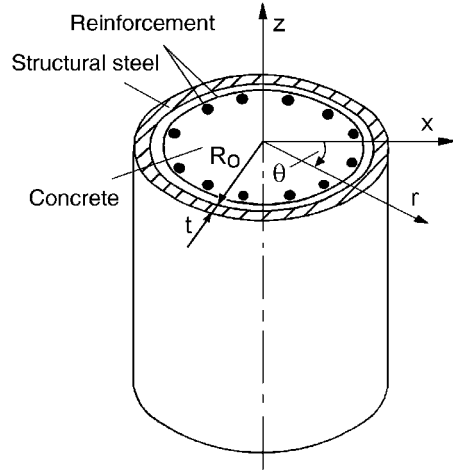
Figure 1:   Concrete-filled hollow column with reinforcement

The following relationships should be written assuming throughout the steel tube an in-plane membrane stressed state:

$$\frac{\partial \sigma_z^a}{\partial z} = 0 \, ; \tag{3}$$

$$\sigma_\theta^a = \frac{p_c R_o}{t} \, ; \tag{4}$$

$$\varepsilon_z^a = \frac{\partial w^a}{\partial z} = \text{const}; \ \varepsilon_\theta^a = \frac{u^a}{r} \, , \tag{5}$$

where p_c – the contact pressure on the boundary surface steel tube-concrete, σ_z^a, σ_θ^a, ε_z^a and ε_θ^a – stresses and strains of the steel tube in the axial and circumferential direction. It is assumed the existing equality of stresses in the radial and circumferential direction ($\sigma_r^c = \sigma_\theta^c$) in concrete core.

Taking into account the compatibility relationships (1) and (2), four equations can be written:

$$\frac{1}{E^a} \sigma_z^a - \frac{\nu^a}{E^a} \sigma_\theta^a = \frac{1}{E_z^c} \sigma_z^c - \frac{\nu_{zr}^c}{E_r^c} \sigma_r^c - \frac{\nu_{z\theta}^c}{E_\theta^c} \sigma_\theta^c \, ; \tag{6}$$

$$\frac{v^a}{E^a}\sigma_z^a - \frac{1}{E^a}\sigma_\theta^a = \frac{v_{zr}^c}{E_z^c}\sigma_z^c - \frac{1}{E_r^c}\sigma_r^c + \frac{v_{z\theta}^c}{E_\theta^c}\sigma_\theta^c \;; \tag{7}$$

$$\frac{1}{E_z^s}\sigma_z^s = \frac{1}{E_z^c}\sigma_z^c - \frac{v_{zr}^c}{E_r^c}\sigma_r^c - \frac{v_{z\theta}^c}{E_\theta^c}\sigma_\theta^c \;; \tag{8}$$

$$\frac{1}{E_\theta^s}\sigma_\theta^s = \frac{1}{E_\theta^c}\sigma_\theta^c - \frac{v_{r\theta}^c}{E_r^c}\sigma_r^c - \frac{v_{z\theta}^c}{E_z^c}\sigma_z^c \;, \tag{9}$$

were v^a – is Poisson's ratio of the steel tube, v_{ij}^c – Poisson's ratio values of the reinforced concrete ($i, j = r, z, \theta$; $i \neq j$). Equations (6) – (9) have been written taking into account the transverse deformation. The equilibrium equations in the z and θ directions are as follows

$$\frac{A_\theta^s}{R_s}\sigma_\theta^s + \frac{t}{R_0}\sigma_\theta^a + \sigma_\theta^c = 0\;; \tag{10}$$

$$A^c\sigma_z^c + A^a\sigma_z^a + A_z^s + q(A^a + A^c) = 0\;, \tag{11}$$

where A^c and A^a – the cross-sectional area of the concrete and structural steel accordingly, E^a – modulus of elasticity of the steel tube, E_z^c, E_r^c and E_θ^c – moduli of elasticity of the reinforced anisotropic concrete core in the directions z, r and θ, E_z^s and E_θ^s – moduli of elasticity of the reinforcement in directions z and θ, q – a uniformly distributed axial load. It is assumed the load is applied to the entire section.

The load carrying capacity of composite elements in bending can be characterised by plastic deformation of structural steel in tension, by cracking of concrete in compression or by both. At the same time, the stresses in reinforcement can be less or more of the yield limit of steel. The stress analysis of composite elements in bending has been performed with certain assumptions: 1) the hypothesis of flat sections has been used; 2) the concrete lying in the tension zone of the section is assumed to be cracked and is therefore neglected; 3) the conditions of deformation continuity of structural steel and concrete fulfil in the compression zone; 4) relationship for the stress distribution in the compression zone of concrete has been assumed in following non-linear form:

$$\sigma^c{}_z = \sigma^c{}_f (z/x)^{n_c}\;, \tag{12}$$

where $\sigma^c{}_z$ – stresses in concrete at distance z from neutral axis; $\sigma^c{}_f$ – stresses in concrete in more compressed fiber; x – height of the compressed zone of concrete; n_c – characteristic of the stress diagram form. The cross section of reinforced composite beam and the stress-strain distribution diagrams are shown in Figure 2.
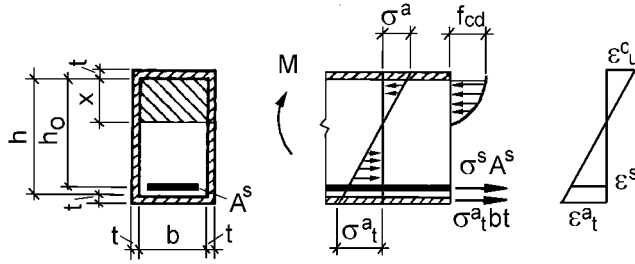
Figure 2: Stress and strain distribution in composite beam

Based on the equilibrium conditions of the internal forces and taking into account the hypothesis of flat sections, the position of neutral axis can be determined by using non-linear equation:

$$x^2\left[\frac{f_{cd}b}{(1+E^c{}_u/E^c)\varepsilon^c{}_u}-t(E^a-E^a{}_t)\right]+x\left[E^a(bt+2t^2)+E^a{}_t(bt+2ht+t^2)+E^sA^s\right]-$$
$$-E^a{}_t\left(hbt+h^2t+ht^2\right)-E^sA^sh_0=0,$$

(13)

where $E^c{}_u$ and E^c – tangent and initial modulus of the concrete, $E^a{}_t$ – modulus of constructional steel in tension, $\varepsilon^c{}_u$ – ultimate deformation of concrete in compression. The ultimate bending moment M_u was determined by using the condition of equality of the moments in section of the beam

$$M_u=b\int_0^x \sigma^c_f(z/x)^{n_c}\,zdz+\sigma^a btx+\frac{2}{3}\left[\sigma^a btx(x+t)+\sigma^a_t t(h-x)(h+t-x)\right]+$$
$$+\sigma^sA^s(h_0-x)+\sigma^a_t bt(h-x).$$

(14)

where b, h and h_0 – width, height and effective height of concrete section; z – distance from neutral axis.

3   Numerical solution and analysis

In order to perform the stress analysis in composite column the system of six linear equations (6) – (11) was solved. In matrix form it is written as

[A] **X =B**.   (15)

The components of the unknown vector **X** are stresses in the steel tube, concrete, longitudinal and spiral reinforcement, i.e.,

$$\mathbf{X}=\left[\sigma^a_z,\sigma^a_\theta,\sigma^c_z,\sigma^c_\theta,\sigma^s_z,\sigma^s_\theta\right]^\mathsf{T}.$$

(16)

The matrix of system [A] and vector of constants **B** is determined from the stress-strain relationships and equilibrium equations as follows:

$$
A = \begin{bmatrix}
\dfrac{1}{E^a} & -\dfrac{\nu^a}{E^a} & -\dfrac{1}{E_z^c} & \dfrac{\nu_{zr}^c}{E_r^c}+\dfrac{\nu_{z\theta}^c}{E_\theta^c} & 0 & 0 \\[3mm]
\dfrac{\nu^a}{E^a} & -\dfrac{1}{E^a} & -\dfrac{\nu_{rz}^c}{E_z^c} & \dfrac{1}{E_r^c}-\dfrac{\nu_{r\theta}^c}{E_\theta^c} & 0 & 0 \\[3mm]
A^a & 0 & A^c & 0 & A_z^s & 0 \\[3mm]
0 & 0 & \dfrac{1}{E_z^c} & -\left(\dfrac{\nu_{zr}^c}{E_r^c}+\dfrac{\nu_{r\theta}^c}{E_\theta^c}\right) & -\dfrac{1}{E_z^s} & 0 \\[3mm]
0 & \dfrac{h}{R_0} & 0 & 1 & 0 & \dfrac{A_\theta^s}{R_s} \\[3mm]
0 & 0 & -\dfrac{\nu_{z\theta}^c}{E_z^c} & -\dfrac{\nu_{r\theta}^c}{E_r^c}+\dfrac{1}{E_\theta^c} & 0 & -\dfrac{1}{E_\theta^s}
\end{bmatrix} ; \tag{17}
$$

$$
\mathbf{B} = \left[0,0,-q(A^a+A^s),0,0,0\right]^{\mathsf{T}} . \tag{18}
$$

The following geometrical parameters were chosen for the analysis: diameter of circular hollow section $d = 21.9$ cm, thickness of the steel tube section $t = 0.5$ cm, reinforcement content $\mu = 4$ % of the concrete section, distance from the central axis to the reinforcement bar axis $R_s = 8.0$ cm, cross-sectional area of the longitudinal reinforcement $A_z^s = 14.5$ cm^2 and secondary reinforcement $A_\theta^s = 0.01$ cm^2 (per 1 cm of the column length). The modulus of elasticity for the reinforcement is $E^s = 200\,000$ MPa, for structural steel – $E^a = 210\,000$ MPa and Poisson's ratio $\nu^a = 0.25$.

In order to determine real mechanical characteristics of conventional concrete under compression stresses, prisms of conventional concrete were tested in uniaxial compression. The development of lateral strain ε_l and axial strain ε_a fixed in the test is shown in Figure 3. In the first part of the loading phase, the stress-strain relation shows an almost linear response. Due to the heterogeneity of the concrete, a uniform uniaxial stress applied to a concrete specimen results in locally non-uniform. At a stress, corresponding approximately to 40 % of the peak stress, obviously due to the difference in lateral deformation of material constituents the stress-strain relation exhibits visible non-linear response. Approximately at 85 % of the peak stress, the response is marked non-linear.

Similar situation was observed in case of UHPC [11]. With increasing compressive strength, the initial slope corresponding to the modulus of elasticity increases and the linear part extends to higher stress levels. Furthermore, the ultimate strain, i.e. the strain at maximum stress, increases with increasing compressive strength of UHPC. During loading of cylindrical specimens 300 mm high and 100 mm in diameter stress-strain curves were investigated. Initial Poisson's ratio of UHPC was about 0.18. This value kept constant till 75% of compression strength. After compressive stress exceeded this level, the Poisson's ratio raised abruptly and tended to 0.3.

In the initial stage of composite column loading, the Poisson's ratio of concrete core is lower than for steel. Therefore, the steel tube expands faster in the radial direction compared with

the concrete core; hence, the steel tube does not restrain the concrete core. As a result, columns centric loaded on the entire section are affected by the difference between the values of Poisson's ratio of the steel tube, v^a, and the concrete core, v^c.
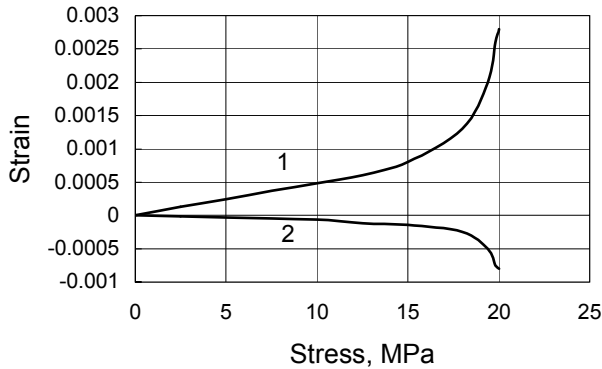
Figure 3:   Stress-strain relation for concrete prism in uniaxial compression: 1 - ε_a; 2 - ε_l

In analysis the initial modulus and tangent modulus at the given stress level has been used as the modulus of elasticity of the concrete. Based on experimental results the Poisson's ratio of the concrete changes in accordance to the stress level, starting with v^c = 0.2 in the initial stage [12, 13]. The moduli of elasticity of a reinforced anisotropic concrete core E_z^c, E_r^c, and E_θ^c as well as Poisson's ratio values are found on the basis of the reinforcement theory [14] taking into account the content of the reinforcement µ and mechanical properties of the constituents.
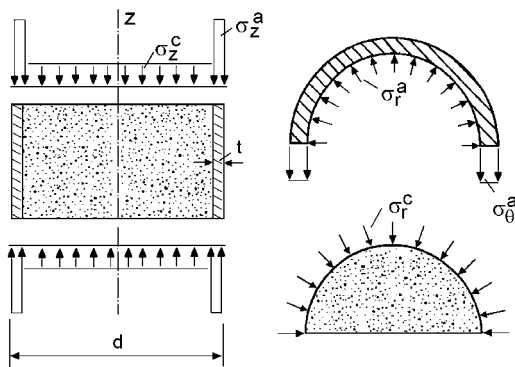
Figure 4:   Stress distribution in the section of composite column

The stress in material components with applied force *N* for conventional concrete and UHPC are given in Table 1. In the case of conventional concrete stresses in steel section, concrete and reinforcement exceed strength of materials. By using UHPC as column filling the load carrying capacity keeps enough.

According to EC 4, for the concrete-filled circular hollow sections, the load-bearing capacity of the concrete is increased due to the prevention of transverse strain. This effect is shown in

Figure 4. The transverse compression of the concrete (σ_r^c) at high stress levels leads to three-dimensional effects, which promotes increase of the column resistance. At the same time, the circular tensile stresses (σ_θ^c) arise on the cylindrical surfaces reducing its normal stress capacity. Circular tensile stresses σ_θ^c in the concrete core of the column change into compression stresses due to behaviour of steel tube and mentioned above features of concrete deformation process.

Table 1:   Stress values (MPa) in constituents of composite column for ratio $d/t = 44$

Strength of concrete, MPa	Axial force N, kN	σ_z^a	σ_θ^a	σ_z^c	σ_z^c	σ_z^s	σ_θ^s
30	3200	− 332	− 4.3	− 47	− 0.1	− 316	94
180	3200	− 255	− 2.0	− 58	− 0.2	− 243	73

According to [2], the plastic resistance of the cross-section of a composite column with axial loading is given as the sum of the components:

$$N_{pl.Rd} = A^a f_{yd} + A^c f_{cd} + A_z^s f_{sd}, \tag{19}$$

where A^a, A^c and A_z^s are the cross-sectional areas of the structural steel, concrete and reinforcement in the axial direction, and f_{yd}, f_{cd} and f_{sd} are design strength values of the materials mentioned above.

Refined analysis of the load bearing capacity of the composite column is performed taking into account the design strength of steel and conventional concrete as well as limit ratios of the circular hollow sections. The results are shown in Figure 5. It is determined that the main load limiting factors are concrete design strength f_{cd} and diameter thickness ratio d/t. Using concrete of the strength class C35/45 and steel of grade Fe235 the load bearing capacity of the composite column increases by 18 % in comparison with concrete of class C30/37. For a thin wall hollow section ($d/t = 90$) instead of section with $d/t = 46$ the steel economy is for 50 %.

The results of the stress analysis of the composite beam are shown in Figure 6. By using non-linear approach the position of neutral axis of reinforced concrete element depends on ultimate deformation of concrete in compression ε_u^c. Taking into account this peculiarity the stresses in structural steel σ^a in tension zone tends to yield limit f_y (steel grade Fe235) when $\varepsilon_u^c < 1{\cdot}10^{-3}$. The ultimate bending moment M_u in this case is 40% less than plastic moment $M_{pl.Rd}$ determined according to EC4.
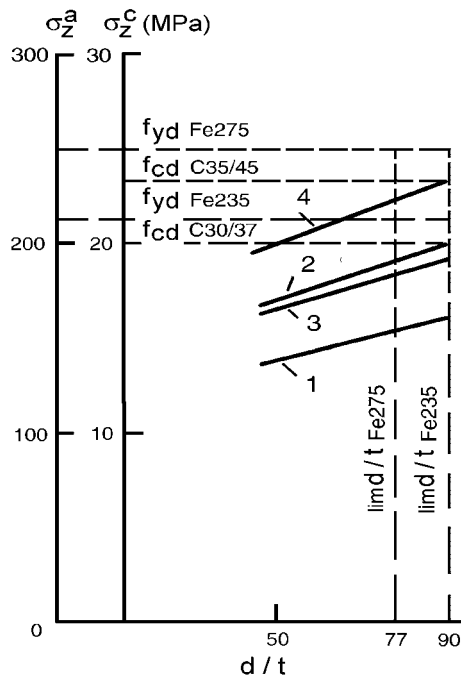
Figure 5: Variation of stresses in structural steel and concrete in relationship of ratio *d/t*: 1, 2 σ_z^a and σ_z^c for axial force $N = 4000$ kN; 3, 4 – σ_z^a and σ_z^c for $N = 5000$ kN

The concrete filling leads to the increase of the load-bearing capacity that is much higher than that of steel elements and promotes the fire resistance as well. The concrete is contained within a circular steel profile and cannot split away, even if the ultimate strength of concrete is reached. Nevertheless, in order to prevent the possibility of a failure, especially, in the case of small thickness of the structural steel and fire, the appropriate strength classes of concrete and steel have to be used. The effect depends on the type of concrete because the strength of core affects the point at which confinement can take place.

Table 2: Comparison of composite beams with conventional concrete and UHPC

Ultimate concrete deformation, $\varepsilon_{cu} \cdot 10^3$	Compressive strength of concrete, MPa			
	30		180	
	Relative compressive depth, *x*/*h*	Ultimate moment M_u, kNm	Relative compressive depth, *x*/h	Ultimate moment M_u, kNm
1	0.42	92.7	0.27	186.8
2	0.47	155.4	0.34	271.8
3	0.49	248.0	0.39	383.4
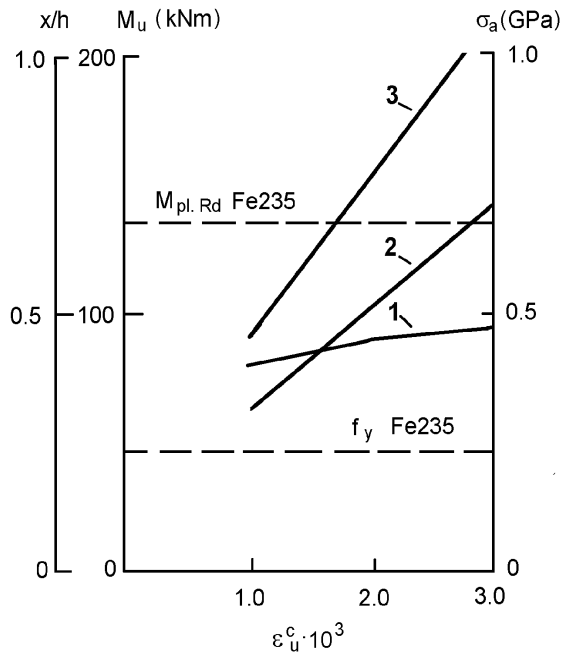
Figure 6:   Influence of ultimate concrete deformation in compression on position of neutral axis, stresses in structural steel and ultimate bending moment: $1 - x/h$, $2 - \sigma^a$, $3 - M_u$

4   Conclusions

1. On the basis of constitutive relationships for material components, the stress state in a composite column is determined, taking into account the dependence of the modulus of elasticity and Poisson's ratio on the stress level in the concrete. It is proved that the effect of confinement acts at a high stress level when the structural steel behaves in tension and the concrete in compression. The main load limiting factors are concrete design strength f_{cd} and d/t ratio. By using higher concrete strength (steel grade Fe235) the load bearing capacity of the composite column increases by 18-20%. In the case of a thin hollow section ($d/t = 90$), the steel economy can be for 50 %.

2. By using non-linear approach, the position of neutral axis of composite beam depends on the ultimate deformation of concrete in compression ε^c_u. When $\varepsilon^c_u < 1 \cdot 10^{-3}$ the ultimate bending moment M_u is 40% less than plastic moment $M_{pl.Rd}$ determined according to EC4 but the stresses in structural steel σ^a_t in tension zone reach yield limit.

3. The optimization of working conditions and cross section area of the composite structure as well as the prevention of the possibility of a failure in the case of small thickness of structural steel and fire can be realized by using appropriate strength of concrete and steel. By using UHPC as steel element filling the increase of load carrying capacity can be significant.

5   References

[1] Bergman R., Matsui C., Meinsma C. & Dutta D. Design guide for concrete filled hollow section columns under static and seismic loading, Köln: Verlag TÜV Rheinland GmbH, 68 p., 1995.

[2] Eurocode 4: Design of composite steel and concrete structures, Part 1.1: General rules and rules for building. ENV 1994-1-1, 33 p., 1994.

[3] Johansson M. Composite action and confinement effects in tubular steel-concrete columns. Thesis for the degree of Doctor of Philosophy, Göteborg: Chalmers University of Technology, 77 p., 2002.

[4] Kvedaras A.K., Sapalas A. Research and practice of concrete-filled steel tubes in Lithuania. Journal of Constructional Steel Research, Vol. 49, No 2, 189-196, 1999.

[5] Brauns J. Analysis of stress state in concrete-filled steel column. Journal of Constructional Steel Research, Vol. 49, No 2, 197-212, 1999.

[6] Lakshmi B., Shanmugan N.E. Non-linear analysis of in-filled steel-concrete composite columns. Journal of Structural Engineering, Vol. 128, No. 7, 922-933, 2002.

[7] O'Shea M.D., Bridge R.Q. Design of circular thin-walled concrete filled steel tubes. Journal of Structural Engineering, Vol. 126, No. 11, 1295-1303, 2000.

[8] Han Lin-Hai, H.; Guo-Huang, Y. Influence of concrete compaction on the strength of concrete-filled steel RHS columns. Journal of Constructional Steel Research, Vol. 59, No 6, 751-768, 2003.

[9] Zilch, K.; Hennecke, M. Anwendung hochfesten Betons im Brűckenbau, Forschungsbericht 99. Massivbau TUM, Műnchen, 1999.

[10] Dowd, W.M.; Dauriac, Ch.E. Reactive powder concrete. The Construction Specifier, 48-52, 1996.

[11] Ma, J.; Schneider, H. Properties of Ultra-High-Performance Concrete. LACER, No 7, 25-32, 2002.

[12] Neville, A. M. Properties of concrete, London: Pitman Publishing, 1981. 409 p.

[13] Eurocode 2: Design of concrete structures, Part 1.1: General rules and rules for building, ENV 1992-1-1, 1992. 109 p.

[14] Malmeister, A.K.; Tamuz, V.P.; Teters, G.A. Strength of polymer and composite materials (in Russian). Riga: Zinatne, 1980. 571 p.

Josef HEGGER

Professor

RWTH Aachen University

Aachen, Germany

Sabine RAUSCHER

Research engineer

RWTH Aachen University

Aachen, Germany

Claus GORALSKI

Research engineer

RWTH Aachen University

Aachen, Germany

Push-Out Tests on Headed Studs embedded in UHPC

Summary

In composite construction the shear load in the interface between steel and concrete is transferred by headed studs. Besides a high ultimate load the headed stud has to feature a high initial stiffness and a high ductility to allow an economic design. At the Institute of Structural Concrete at RWTH Aachen University numerous push-out tests have been performed to investigate the load carrying behavior of shear connectors and headed studs. Several modifications have been applied to the headed stud among them a cover made of ultra-high performance concrete (UHPC). This modification leads to an increase in the load carrying capacity as well as to an improvement in the ductility. The test program included studs with a diameter of 19 and 22 mm in normal strength (NSC) as well as in high strength concrete (HSC). This paper presents the main results of the experimental investigations.

Keywords: *composite construction, headed stud, ultra-high performance concrete*

1 Introduction

Composite structures made of structural steel and concrete maximize the advantages of the two components. The interaction of the two materials is guaranteed by shear connectors. The strength of headed studs does not only depend on the stud details (strength, diameter and height) but also on the concrete environment. Numerous tests performed at the Institute of Structural Concrete indicate that the load carrying behavior of headed studs in high strength concrete (HSC) is different from that in normal strength concrete (NSC) [1, 2, 3 and 4]. In NSC ($f_{ck} \leq 50$ MPa) the load carrying capacity is governed by the concrete strength. Hereby, failure is initiated by concrete crushing. Due to the lower stiffness of the normal strength concrete the stud's shaft is deformed completely over its height. In HSC ($f_{ck} > 50$ MPa) the shaft is tightly held in the surrounding concrete, the stud's deformation is concentrated on the stud's base directly above the welded collar. This leads to a high ultimate load but a significantly reduced ductility. Covering the shaft of headed studs with UHPC leads to a higher initial stiffness and an increase in the load carrying capacity in NSC. In HSC the UHPC cover improves the ductility of the headed stud. In the following the results

regarding the increased load carrying behavior of headed studs embedded in UHPC are presented.

2 Test set-up for push-out tests

The Push-Out Standard Test (POST) according to EC 4 [5] simulates the shear transfer in the composite joint of composite girders (Figure 1, left). A total of eight studs are tested. Due to the eccentricity of the action lines of the forces the studs are not stressed equally such as the lower studs are subjected to both shear and tension. This may lead to a reduction of the load carrying capacity of the headed stud. Therefore, the Single Push-Out Test (SPOT) has been developed at the Institute of Structural Concrete (Figure 1, right). Here, the load-slip relation of a single stud under virtually pure shear load can be determined [1, 2, 3, and 6]. Because of its small dimensions it is an appropriate test set-up for shear connectors in HSC, but also suitable for NSC. It consists of a steel frame embracing the reinforced concrete block, where the bending moment resulting from the eccentricity of the applied loads is balanced by an upper horizontal cross beam and a lower horizontal steel frame. The specimen is easy to fabricate and lower testing loads are required. Due to the virtually pure shear loading, the load carrying capacity of headed studs is approximately 15% higher compared to the POST [2].
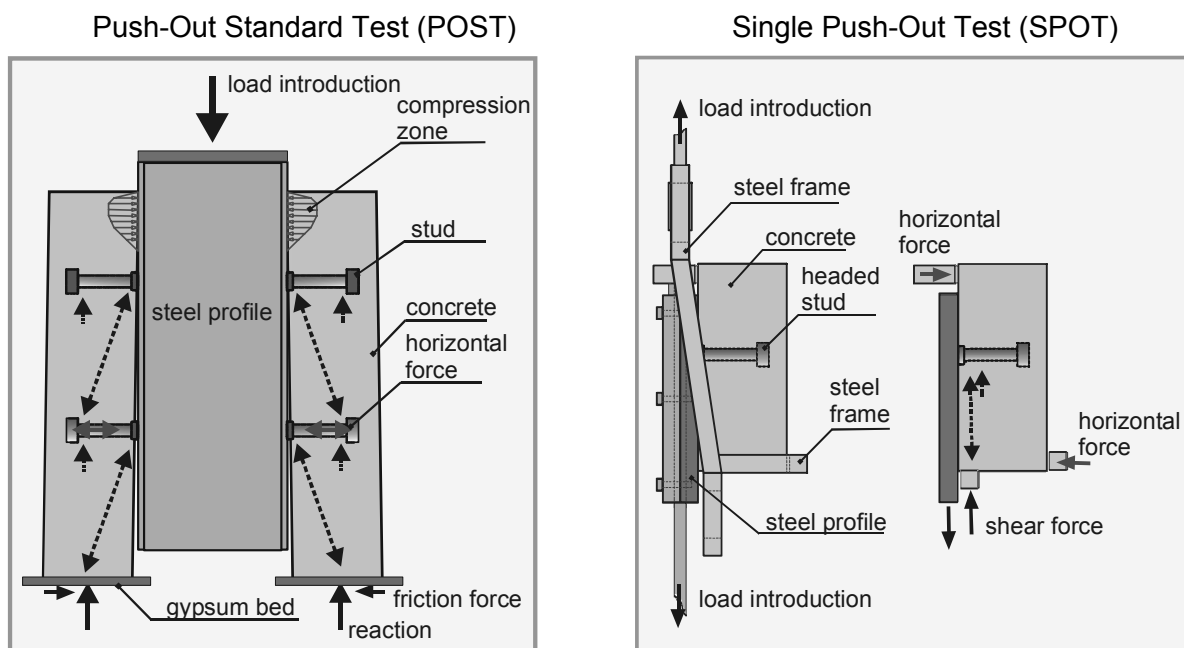
Figure 1: Test set-ups for push-out tests

3 Load carrying behavior of headed studs

3.1 Headed studs in NSC

The load carrying behavior of headed studs in NSC was investigated by Lungershausen [7] conducting push-out tests (Figure 2). In the beginning of testing the shear force T is basically carried by the welded collar (force P_W). With increasing shear load, the concrete plasticizes

in this area due to the concentrated load introduction. The shear force is transferred into the stud's shaft which is principally subjected to bending stress P_B. Underneath the stud's head compressive struts P_C are developing and the shaft experiences a tensile stress P_T. Due to the compressive struts friction forces P_F are activated in the composite joint between steel and concrete. With increasing load the stud plasticizes and the failure occurs due to shearing of the stud or concrete failure whichever shows the smaller resistance.
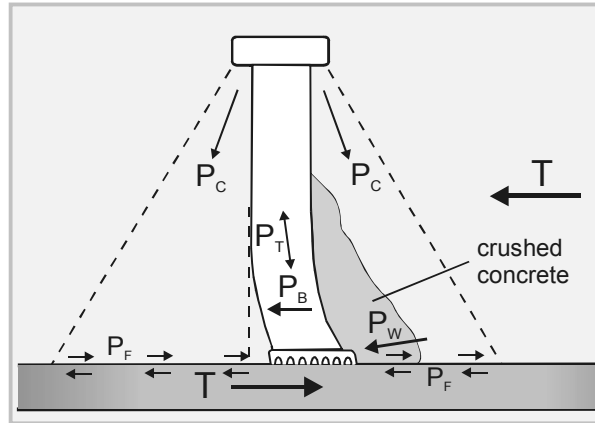
Figure 2:   Load carrying mechanism of headed studs in NSC [7]

3.2   Headed studs in HSC

Within three research projects [2, 3, 4] the load carrying behavior of shear connectors in HSC has been investigated. High strength materials increase the load carrying capacity of structural members. Thus, the shear connectors have to be capable of transferring higher shear forces in the composite joint. The load carrying behavior of headed studs in HSC (f_c >50 MPa) is different from that in NSC [1, 2, 3, 4, 6 and 8]. Due to the rigid restraint the stud is subjected to pure shearing and fails directly above the welded collar. Döinghaus [1] described the failure mechanism of headed studs in HSC as follows:

In the beginning compression forces P_w are concentrated directly in front of the welded collar (Figure 3). When the load arises the compression forces concentrate within a compressive concrete wedge (b). The main part of the load is carried by the welded collar. Subsequently the force in front of the welded collar moves upwards and the stud's shaft starts to deform directly above the welded collar since it is subjected to shear force P_S. The concrete body slides over the concrete wedge (c). Due to this uplift there is no full three-axial stress condition in the compressive wedge which starts to plasticize at approximately 150% of its uni-axial compressive strength. Friction forces P_F are generated in the interface between the concrete wedge and the concrete body which lead to further compression of the concrete wedge. Finally, the stud plasticizes directly above the welded collar and fails due to shearing.
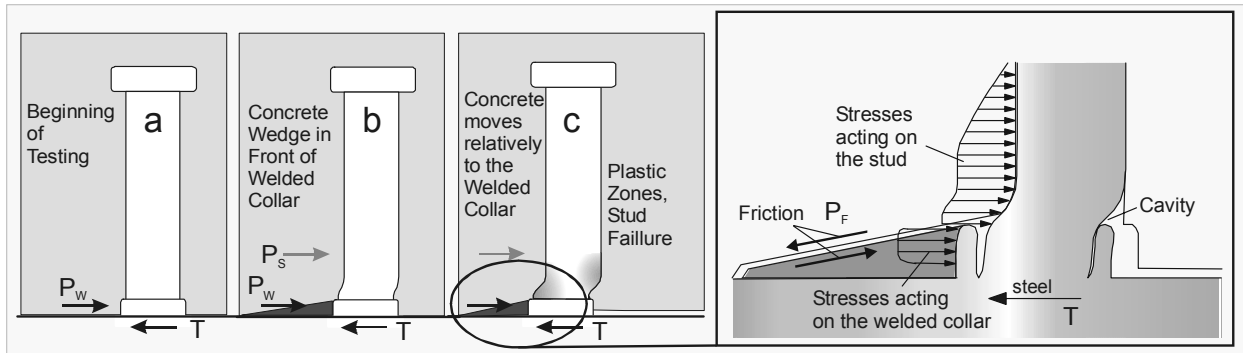
Figure 3: Load carrying mechanism of headed studs in HSC [1]

4 Headed studs embedded in UHPC

To optimize the load carrying behavior of headed studs a cover made of ultra-high performance concrete (UHPC) has been developed (Figure 4). The concrete recipe of the UHPC used for the concrete cover has been developed at the Institute of Structural Concrete. The main characteristics are a high compressive and tensile strength as well as a high durability compared to ordinary concrete. The UHPC shows a compressive strength of more than 150 MPa without thermal treatment. The high performance of UHPC is based on the following vital factors: a low water-cementitious materials ratio (w/cm) of 0.18, a high density which is achieved by a high content of cement, fine sands (mainly quartz) and silica fume. This is essential to fill the cavities between the solid particles. The silica fume functions as a superplasticizer. To guarantee a sufficient ductility thin steel fibers are added. Hereby, a tensile splitting strength of 23 MPa and a flexural strength of up to 50 MPa could be achieved. Due to the steel fibers UHPC not only features a high compressive strength but also a linear-elastic behavior until a high ultimate strain (Figure 4, left). A thermal treatment leads to a further increase in compressive strength, for this application, however, it is neither suitable nor economical.
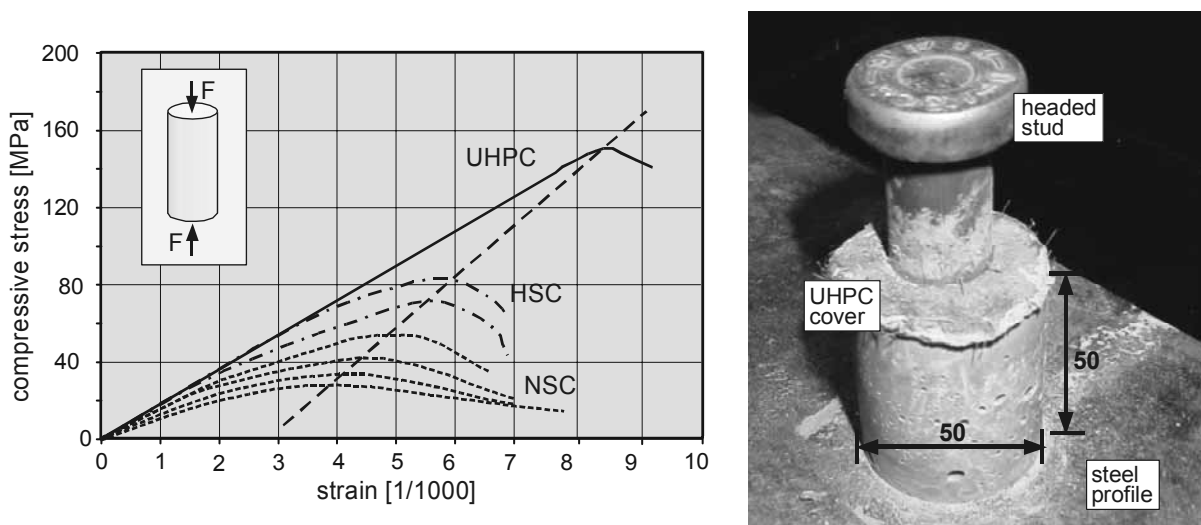
Figure 4: Stress-strain diagram of UHPC (left) and dimensions of the UHPC cover (right)

The dimensions of the concrete cover were chosen 50 x 50 mm (Figure 4, right). The cover was concreted after welding the stud to the steel profile to guarantee a proper fitting without any cavities.

5   Experimental investigation

5.1   Experimental program

The experimental program is presented in Figure 5. For reference reasons ordinary studs with a diameter of 19 and 22 mm were tested in HSC (Series A). Headed studs embedded in UHPC (f_c = 150 MPa) were investigated in Series B in NSC (C20/25). In Series C headed studs with UHPC cover were tested in HSC (C70/85). All tests were conducted as a SPOT including 25 load cycles between 5 and 40% of the expected failure load.
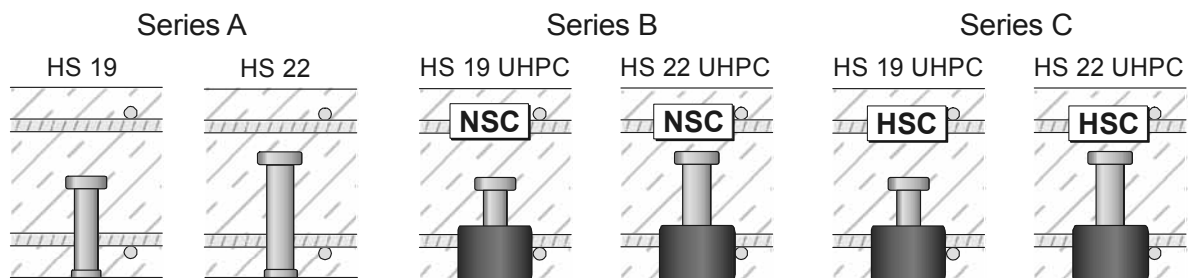
Figure 5:   Experimental program

The material properties, the characteristic loads and corresponding slips according to EC 4 [5] are presented in Table 1. The characteristic loads and slips are listed in column 6 and 7 of the table. The material properties of the stud (tensile strength $f_{u,avg}$) and the concrete body (concrete compressive cube strength $f_{c,avg}$) are presented in column 4 and 5.

Table 1:   Characteristics of experimental tests

Series	Test set-up	Description	$f_{c,avg.}$	$f_{u,avg.}$	P_{Rk}	δ_{uk}
A	SPOT	19 mm stud HSC	115.4	557	151.3	4.19
A	POST	19 mm stud HSC	110.1	-	125.8	4.51
A	SPOT	22 mm stud HSC	109.3	546	169.7	5.56
A	POST	22 mm stud HSC	112.6	531	171.8	5.98
B	SPOT	19 mm stud NSC + UHPC	28.8	513	119.9	7.61
B	SPOT	22 mm stud NSC + UHPC	25.7	519	154.8	9.59
C	SPOT	19 mm stud HSC + UHPC	86.3	513	141.6	6.37
C	SPOT	22 mm stud HSC + UHPC	87.0	519	166.1	6.29

5.2 Test results

The load-slip diagrams are presented in Figure 6. For each configuration only the maximum and minimum curve is plotted. Thus, the scatter in the test results is reflected by these two curves in the following diagrams.
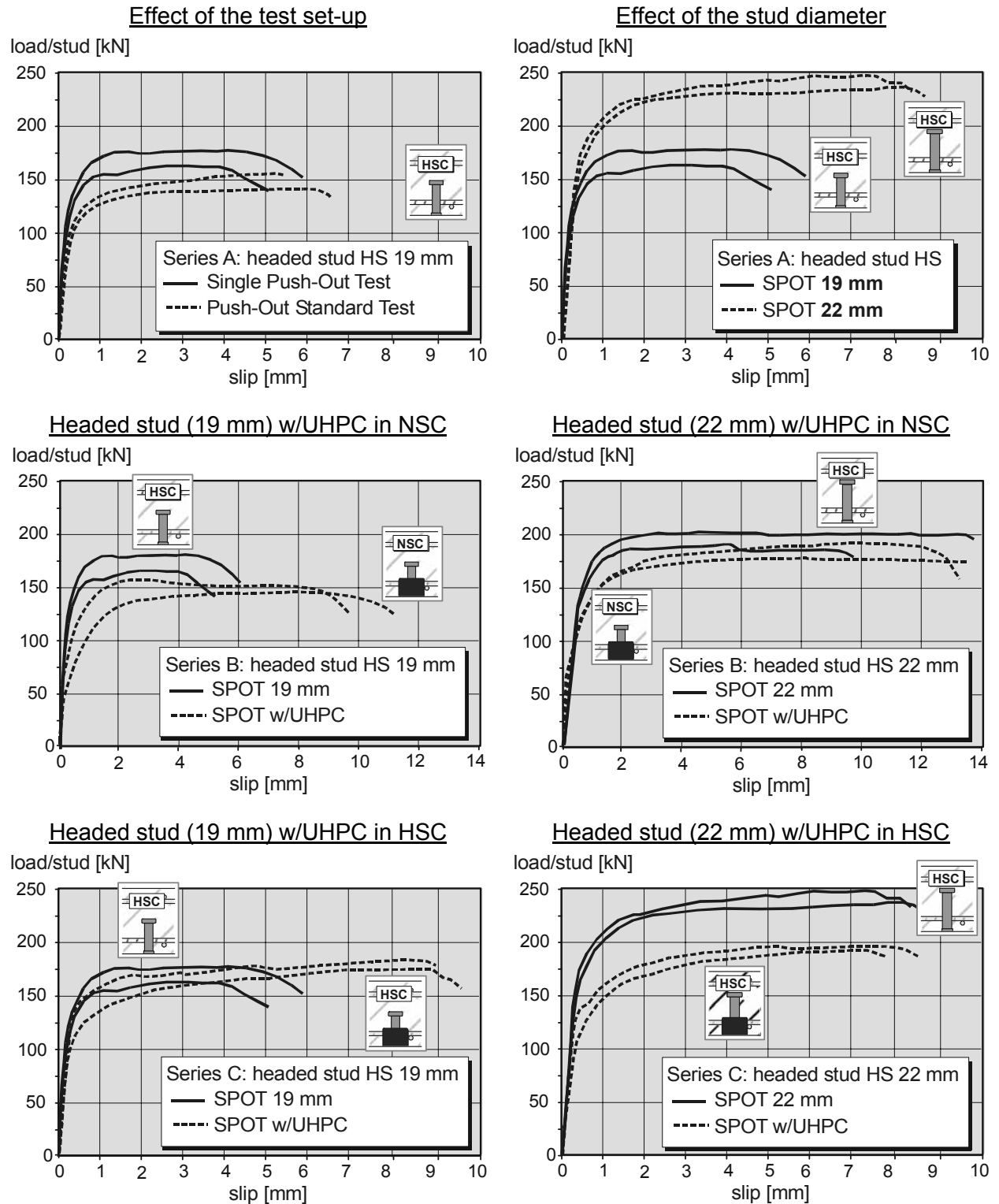
Figure 6: Load-slip diagrams of the tested headed studs

<u>Effect of the test set-up</u>

Due to the virtually pure shear loading in the SPOT the ultimate load was increased by approximately 15% compared to the results obtained in the POST. However, the ductility was decreased slightly.

<u>Effect of the stud diameter</u>

It is obvious that a greater diameter results in an increase of both, the shear carrying capacity and the ductility. The shear resistance of the stud arises nonlinear compared to the activated concrete area in front of the stud. The concrete is subjected to higher stresses and thus, it plasticizes to a higher degree. Nevertheless, the EC 4 [5] ductility requirements (δ_{uk} = 6 mm) could not be fulfilled.

<u>Headed studs with UHPC cover in NSC</u>

In Series B the effect of the UHPC cover on the load carrying behavior of headed studs in NSC has been investigated. In most tests, steel failure could be achieved. For comparison reasons only the tests with steel failure are evaluated in the following.

The UHPC cover provides a certain stiffness due to its high compressive strength and thus strengthens the concrete shaft. As intended, the ultimate load of the headed studs could be increased. With the UHPC cover the ultimate load of the 19 mm stud was about 80% of the load achieved in HSC with the same diameter and the initial stiffness was comparably high. The characteristic slip, however, could be increased significantly. The ductility criterion according to EC 4 [5] could be fulfilled. The 22 mm stud achieved 75% of the 22 mm stud without UHPC cover in HSC, but also here, the ductility could be increased noticeably. Corresponding to the behavior in HSC the failure of the headed stud occurred directly above the welded collar (Figure 7). The concrete wedge consists of compressed NSC and UHPC. The steel fibers in the UHPC are orientated in direction of the load transfer.
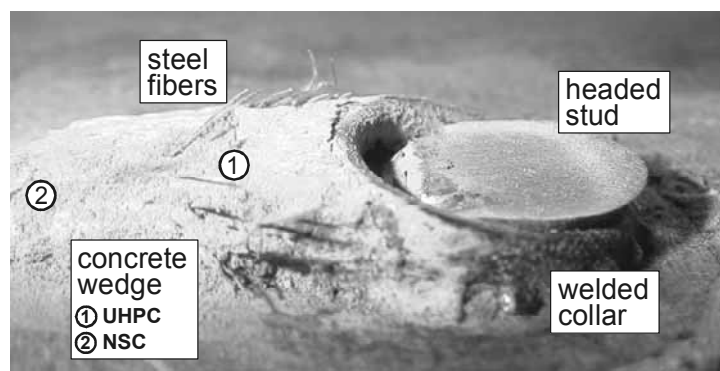
Figure 7: Headed stud after failure

Headed studs with UHPC cover in HSC

In HSC all the headed studs failed due to shearing of the stud's shaft. For the 19 mm headed stud there was hardly any difference in the initial stiffness and ultimate load, but the characteristic slip was increased noticeably. The load carrying capacity of the 22 mm headed stud with UHPC cover was extremely low. So far, no reason could be found why the ultimate load is about 20% lower than the headed stud without a cover, but further investigations are ongoing.

6 Application areas of headed studs with UHPC cover

Due to the improved load carrying behavior of headed studs with UHPC cover their application is very promising. In the following the possibilities of headed studs with UHPC cover are discussed.

Partial shear connection:

In composite beams the shear connectors are arranged according to the curse of the shear forces in the composite joint (Figure 8). When using shear connectors that fulfill the ductility criterion according to EC 4 [5] a partial shear connection can be performed, for example, a systematically partial shear connection or an equal distribution of the shear connectors (e.g. in composite beams with profiled sheets). Headed studs with UHPC cover would be an appropriate shear connection for areas subjected to high shear stresses.

$$n_i = \frac{F_i}{P_{Rd}}$$

$$N = \sum n_i$$
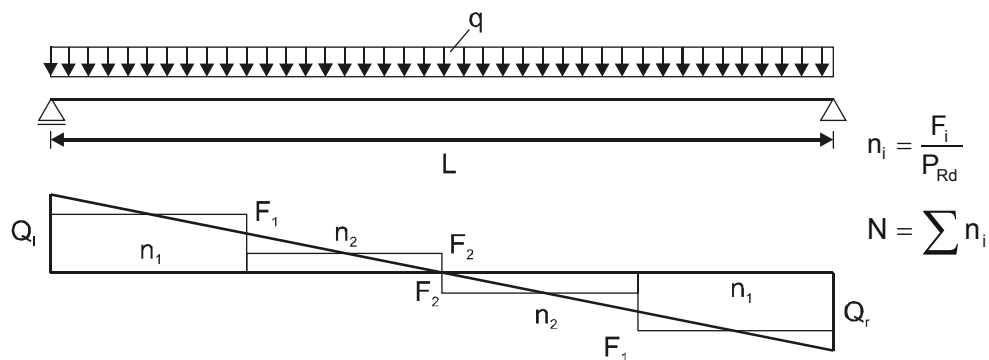
Figure 8: Shear forces in the composite joint

Also, when advanced requirements have to be met for design and ductility behavior (e.g. in earthquake regions) headed studs embedded in UHPC are a proper solution.

In NSC an economic design can be performed using headed studs, for example, approximately 30% less headed studs are required using headed studs embedded in UHPC.

Connection beam-column

The load carrying behavior of a composite structure is influenced by the characteristics of the connection between the beam and column. Due to their high ultimate load headed studs with UHPC cover are advantageous in areas of concentrated load introduction when using NSC (Figure 9).

432
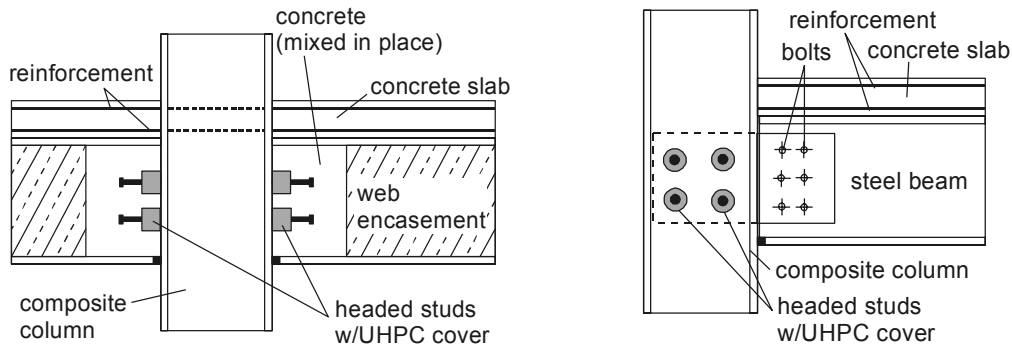
Figure 9: Detail: connection beam-column

Connection column-footing

Vertical loads are transferred into the ground via solid footings. The resistance against horizontal loads can be provided using headed studs with UHPC cover as presented in Figure 10. Thus, a simply support (Figure 10, left side) as well as a clamped support (Figure 10, right side) for the column can be performed. Especially for prefabricated columns this is a promising solution.
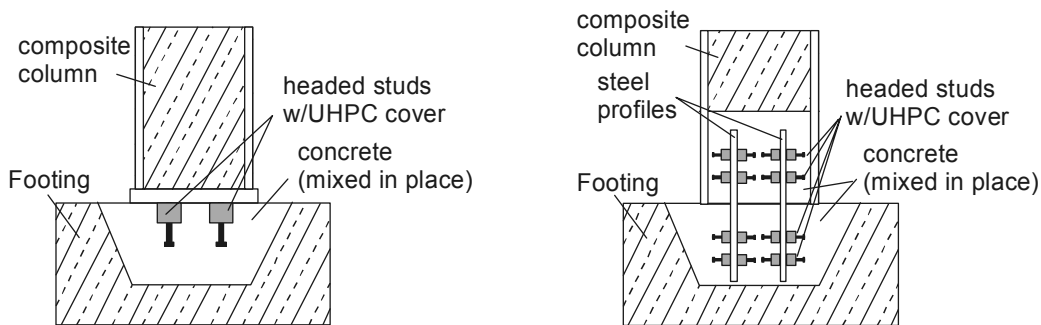
Figure 10: Detail: connection column footing

7   Summary and conclusions

A cover made of UHPC was applied to headed studs in order to increase the load carrying capacity in NSC. In HSC it was intended to improve the ductility behavior to obtain the characteristic slip of 6 mm according to EC 4 [5]. Numerous push-out tests have been performed to investigate the effect of the UHPC cover. The results can be summarized as follows:

- In NSC the ultimate load arises while a high initial stiffness and a sufficient ductility is ensured. The load carrying behavior of the headed studs with UHPC cover in NSC is comparable to the behavior in HSC without UHPC cover.
- In HSC there was no increase in ultimate load but the ductility behavior could be improved.
- There are many application areas for headed studs with UHPC.
- In order to confirm the test results further research is required which is ongoing in the future.

- Concluding it has to be mentioned that an appropriate production method has to be developed to enable a simple and economic application of the UHPC cover. Here, any cooperation of the industry is appreciated.

8 References

[1] Döinghaus, P., 2001, "Zum Zusammenwirken hochfester Baustoffe in Verbundträgern", Doctoral thesis, RWTH Aachen University, Germany.

[2] AiF, 2000, "Untersuchungen zur Duktilität der Verbundmittel bei Anwendung von hochfestem Stahl und hochfestem Beton", AiF-Research Project No. 12124 N/P 486/25/99, RWTH Aachen University, Germany.

[3] AiF, "Untersuchungen zum Trag- und Verformungsverhalten von Verbundmitteln unter ruhender und nichtruhender Belastung bei Verwendung hochfester Werkstoffe", current AiF-Research Project No. 13867 N/P 621, RWTH Aachen University, Germany.

[4] ECSC, 2000, "Use of High Strength Steel S460", Research Project No. 7210-SA/129, 130, 131, 325, 524, RWTH Aachen, Germany.

[5] prEN 1994-1-1, 2003, "Design of composite steel and concrete structures Part 1.1 – General rules and rules for buildings", Brussels.

[6] Döinghaus, P.; Will, N. and Goralski, C., 2001, "Design Rules for Composite Structures with High Performance Steel and High Performance Concrete", UEF – International Conference on High Performance Materials in Bridges and Buildings, Aston Keauhou Beach Resort, Conference Center, Kailua-Kona, Hawaii, USA, July 29 - August 3, 2001.

[7] Lungershausen, H., 1988, "Zur Schubtragfähigkeit von Kopfbolzendübeln", Technisch-wissenschaftliche Mitteilung Nr. 88-7, Institut für konstruktiven Ingenieurbau der Ruhr-Universität Bochum.

[8] Roik, K. and Hanswille, G., 1989, "Background report on EC 4", Ministerium für Raumordnung, Bauwesen und Städtebau, reference number: RSII 1-674102-8630, Bochum, Germany.

9 Conversion factors

1 in.	=	25.4 mm
1 ft	=	0.3048 m
1 kip	=	4.448 kN
1 ft-kip	=	1.356 kN-m
1 psi	=	6.89×10^{-3} MPa

Torsten Leutbecher
Dipl.-Ing.
University of Kassel
Kassel, Germany

Ekkehard Fehling
Prof. Dr.-Ing.
University of Kassel
Kassel, Germany

Structural Behaviour of UHPC under Tensile Stress and Biaxial Loading

Summary

An extensive test programme on Ultra High Performance Concrete (UHPC) has been started at the Chair of Structural Concrete of Kassel University in summer 2004. The purpose of these investigations is to analyse the interaction of steel fibres and conventional bar reinforcement under tensile stress as well as the influence of cracking on the compressive strength of UHPC. The tests are conducted on panel-shaped structural members and on tensile members with different cross-sections. The objective of these tests is to develop constitutive models for cracked UHPC under tension and under compression. Based on this, calculation methods for ultimate limit state (ULS) as well as for serviceability limit state (SLS) shall be derived (calculation of crack width and deflections, ultimate limit state design).

Keywords: *tensile stress, biaxial loading, crack width, tension stiffening, concrete design*

1   Introduction

Ultra High Performance Concrete [1] is a very dense structured, fine- or coarse-aggregated concrete. A low water/cementitious binder ratio < 0.35, high effective concrete admixtures and the use of cement and mineral admixtures which are selected in aggregate composition and aggregate form (low hollow space) lead to compressive strengths near to the yield strength of structural steel (approx. 150 to 230 N/mm²). Because of the compressive strength, this kind of concrete is named Ultra High Strength Concrete (UHSC). However, UHSC offers not only a high compressive strength but also a great spectrum of several other favourable characteristics.

As an example the high resistance against each form of physical or chemical attack, resulting from the dense structure, is to be mentioned. The whole of these favourable material properties is described by the term Ultra High Performance Concrete (UHPC).

From the structural point of view, the behaviour under tensile stress is of substantial interest as well. The tensile strength of UHPC attains a magnitude of 1/25 to 1/20 of the compressive strength. Compared with normal strength concrete, tensile strength increases less than proportionally with increasing compressive strength. The failure at crack initiation is brittle. To increase the tensile strength and the flexural tensile strength respectively, and to attain a ductile behaviour in cracking and post-cracking, high-strength fibres, usually steel fibres, are

added (UHPFRC). In this way the tensile strength of concrete is systematically usable for structural design calculations in ultimate limit state.

However, the load-carrying capacity of exclusively fibre-reinforced UHPFRC beams is limited by the (flexural) tensile strength. An utilisation of the compressive strength of UHPC can be achieved by adding bar reinforcement. As already examined at normal- and high-strength concrete, a combination of fibres and bar reinforcement affects the structural and deformation behaviour, both in the working load range and in ultimate limit state. By interaction of fibre reinforcement and bar reinforcement the crack width can be diminished, the crack propagation can be prevented or at least reduced and a good bond between the reinforcement and the surrounding concrete can be achieved [2, 3]. Moreover, a more uniformly distributed crack formation is possible [4]. In a test programme, the structural and deformation behaviour of UHPC and UHPFRC under tensile stress shall be investigated, using panel-shaped structural members and tensile members. In the following, the preparation of this series and the results of some preliminary tests will be presented.

Apart from the investigations under tension, the effects of cracking on the compressive strength of UHPC and UHPFRC are to be examined at panel-shaped test specimens. This biaxial loading, which occurs very frequently on panels or shells, leads to a decrease of the compressive strength in comparison with the uniaxial strength measured at cylinders. For more than three decades, experimental investigations were conducted on this topic at panel-shaped structural members of normal-strength concrete. However, the results differ a lot.

During last year, a test series on panels of normal strength concrete was executed at Kassel University. For the first time the effects of fibre addition on the biaxial strength were investigated [5]. On the basis of the results and the experience attained by these tests, a similar test program with test specimens of UHPC and UHPFRC is carried out at present. Chapter 3 deals with this topic.

2   Tension tests on reinforced UHPFRC

2.1   Determination of tensile strength of UHPFRC

The tensile strength of fibre reinforced concrete can be determined by a centric tensile test, e.g. at notched prisms. Due to the difficult load introduction, the determination of the tensile strength from a bending tensile test is preferred. However, the tensile strength obtained by this procedure depends on the height of the test specimen as well as on the placing direction and on the fibre orientation respectively. According to the DBV data sheet "steel-fibre concrete" [6], the flexural tensile strength of normal- and high-strength concrete is to be attained by a four-point-bending test (Fig. 1). Afterwards, a stress-strain-relationship is derived, using the stress-displacement-diagram of these tests (Fig. 2).

According to Teutsch [7], the test specimen, shown in Figure 1, can also be used for UHPFRC. Figure 3 shows the results of such kind of test.
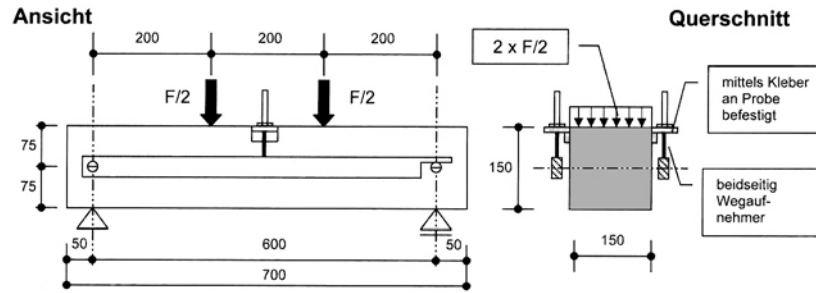
Figure 1: Four-point-bending test according to the DBV data sheet "steel fibre concrete" [6]
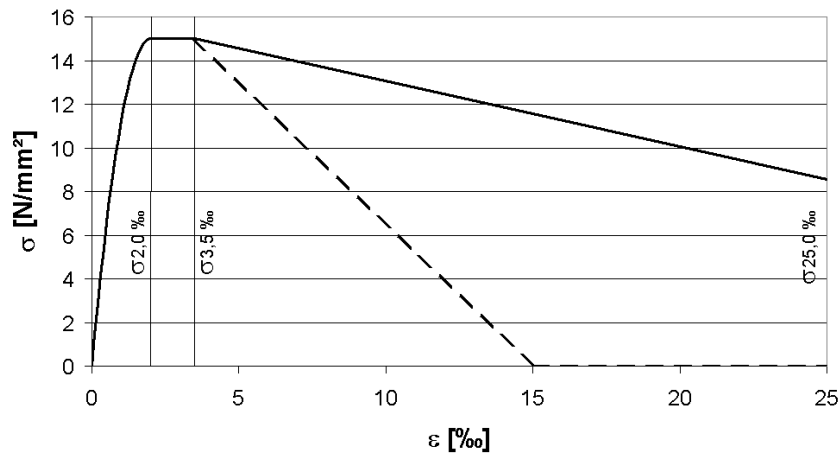
Figure 2: Stress-strain-relationship for steel fibre reinforced normal-/high-strength concrete and for UHPFRC [7]
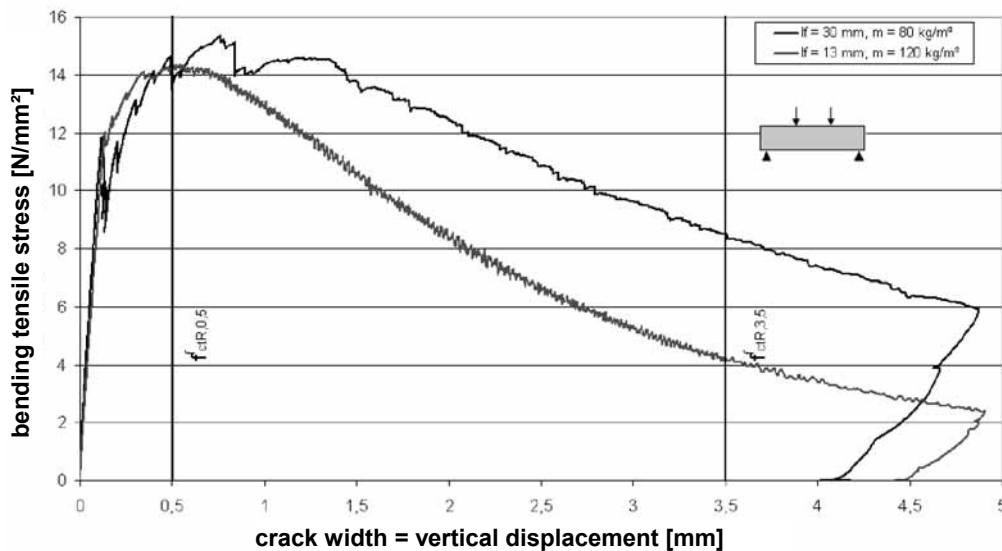
Figure 3: Results of bending tests on UHPFRC carried out by Teutsch [7]

According to Figure 3, with increasing crack width the sustainable load of short fibres decreases fast because of the pull out of the fibres. In contrast, long fibres are still able to carry high stresses even for large crack widths. Formulating a design model, this effect has to be considered, in order not to overestimate the effect of fibres. In the DBV data sheet [6]

and the outline of the code for steel-fibre concrete [8] a limitation of strain is defined at $\varepsilon_u = 25$ ‰. However, in the progress report on UHPC [7] of the German Committee for Reinforced Concrete (DAfStb) it is suggested to use an ultimate strain ε_u and an ultimate stress $\sigma_u = f_{3,5} \cdot \beta$ as a function of the ratio $f_{3,5}/f_{0,5}$ (Fig. 4). The coefficient β is determined by recalculating several test results.
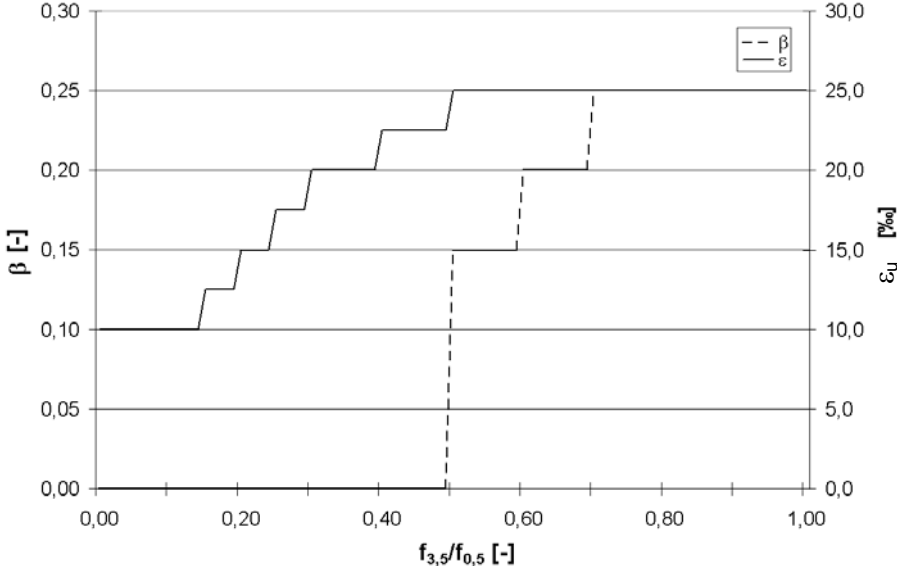
Figure 4: Ultimate strain ε_u and coefficient β to convert bending tensile strength in centric tensile strength according to [7]

2.2 Interaction of fibres and bar reinforcement

The systematic utilisation of the compressive strength of UHPC in structural members predominantly loaded in bending requires an additional reinforcement in the tension zone, using ordinary or prestressed reinforcement. However, for economic reasons, it is desirable to consider steel fibres (used for ductility reasons anyway) for the calculations in ultimate and serviceability limit state as well.

The consideration of the fibres for the ultimate limit state design requires knowledge concerning the fracture-mechanic relations. [6] and [8] contain models for the interaction of fibres and bar reinforcement for normal- and high-strength concrete.

On the one hand, for a systematic limitation of crack width under working load conditions, the consideration of discrete cracks is necessary. On the other hand design models based on smeared cracking should be developed to describe the stiffening influence of the fibres compared to non-fibred members, e. g. for a realistic calculation of deformations.

The intention of the testing programme on tensile members of UHPFRC, initiated by Kassel University, is to develop a constitutive model to describe the interaction of fibre reinforcement and bar reinforcement under tensile stress. Hence, models based on discrete cracking as well as on smeared cracks (calculation of crack width, ultimate limit state design) for reinforced UHPFRC are supposed to be developed.

2.3 Description of the tensile tests

Test specimens

The interaction of fibres and conventional bar reinforcement will be tested at approx. 30 panel-shaped structural members (Fig. 5), fabricated with and without fibres. Additionally, small tensile members with different cross sections are tested (Fig. 6).
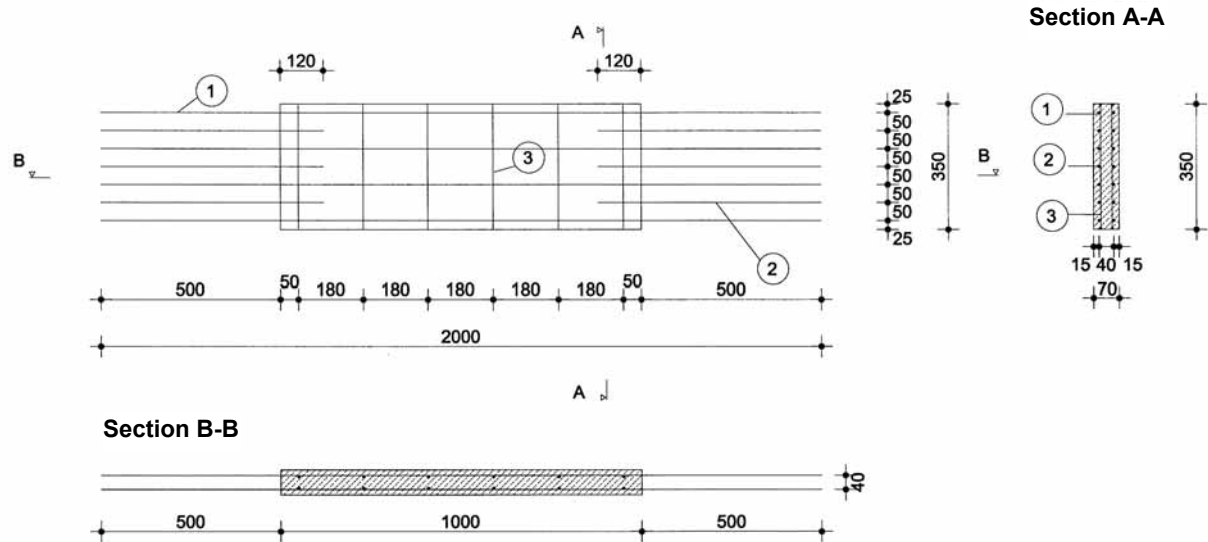
Figure 5:   Panel-shaped structural members for the investigations on tensile stress (type L)

(a)   (b)
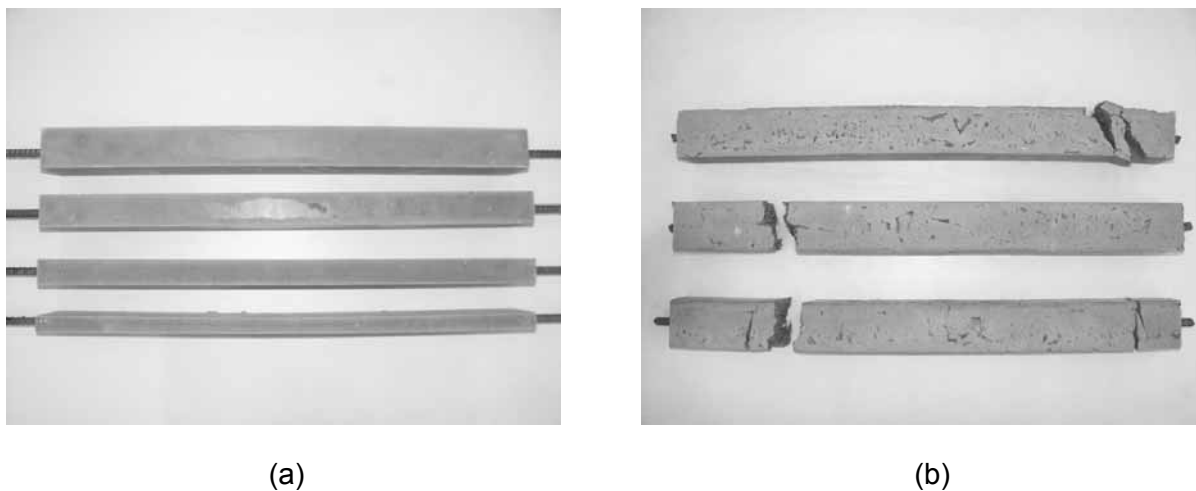
Figure 6:   Tensile members with different cross sections for the investigations on tensile
            stress (a) and results of preliminary tests (b)

The panels are 1000 mm long (load direction), 350 mm high and 70 mm thick. They are reinforced in two directions with two layers of high-strength rebars in each direction, SIGMA prestressing steel St 1420/1570, diameter $\varnothing$ 8 mm. In order to avoid an early failure at the junction points to the load device, reinforcing bars with rolled-up threads are used.

The tensile members are reinforced centrically with one SIGMA prestressing steel St 1420/1570. Both, the cross sections of the tensile member and the diameter of the reinforcement bar ($\varnothing$ 8, 10 and 12 mm) will be varied.

For reinforcing steel BSt 500 commonly used today, the reinforcement ratio becomes unsatisfying high. Otherwise the steel stresses at crack initiation reach very high values near to the yield strength. For this reason high-strength reinforcement (prestressing steel type) was selected for the test series.

The panel-shaped test specimens are poured vertically in a rigid steel formwork. The top side of the panels is flattened with a smoothing trowel after concreting. The mix composition is selected in a way that allows a fabrication of the panels without or with just a small mechanical compaction (quasi-selfcompacting concrete). Through this, the danger of an unintentional alignment of the steel fibres, e. g. by using an internal vibrating machine, and a segregation of the fluid mix (settlement of the fibres) is avoided. After taking out of the formwork at an age of 2 days, the test specimens are heat treated at approx. 90°C for 48 hours. Afterwards they are stored under normal climate (20°C). In this way, the specimens reach their final strength already after 4 days.

Mix compositions

Table 1 shows the mix compositions of the UHPC and the UHPFRC. The percentage of steel fibres of the UHPFRC is 0.95 vol.-%. The high-strength steel fibres used are sized 17 mm long with a diameter of 0,15 mm. The consistency of the concrete mixtures is capable of flowing.

Table 1:   Mix composition

Mix Composition		UHPC	UHPFRC
cement CEM I 52,5R HS-NA	kg/m³	733	733
quartz sand 0,125/0,5	kg/m³	1008	1008
silica fume	kg/m³	230	230
steel fibres (17 mm/0,15 mm)	kg/m³	-	74,6
quartz powder	kg/m³	183	183
superplasticiser	kg/m³	28,6	28,6
water	kg/m³	161	161

Preliminary tests

In some preliminary tests, tensile members of UHPFRC, reinforced centrically with one reinforcement bar $\varnothing$ = 10 mm, BSt 500, were loaded until failure of the steel occurred. The tests were carried out path controlled. Figure 7 shows the force-displacement-relationship of two tensile members with different cross section and the characteristic curve of the plain steel.

Because of the larger (concrete) cross section, the influence of the steel fibres is greater for smaller reinforcement ratio. Starting with the first crack, the contribution of concrete (tension stiffening and effects of steel fibres) is nearly constant until reaching the yield strength of steel. Figure 7 shows as well, that the ultimate load capacity of the tensile members is approximately attained at the yield point of the bar reinforcement. This can be explained by the fact, that the tensile stress transferred by the fibres is still remaining on a high level for

small and middle crack widths (see Fig. 3). The sustainable load in a crack results from the sum of reinforcement and steel fibre loads.
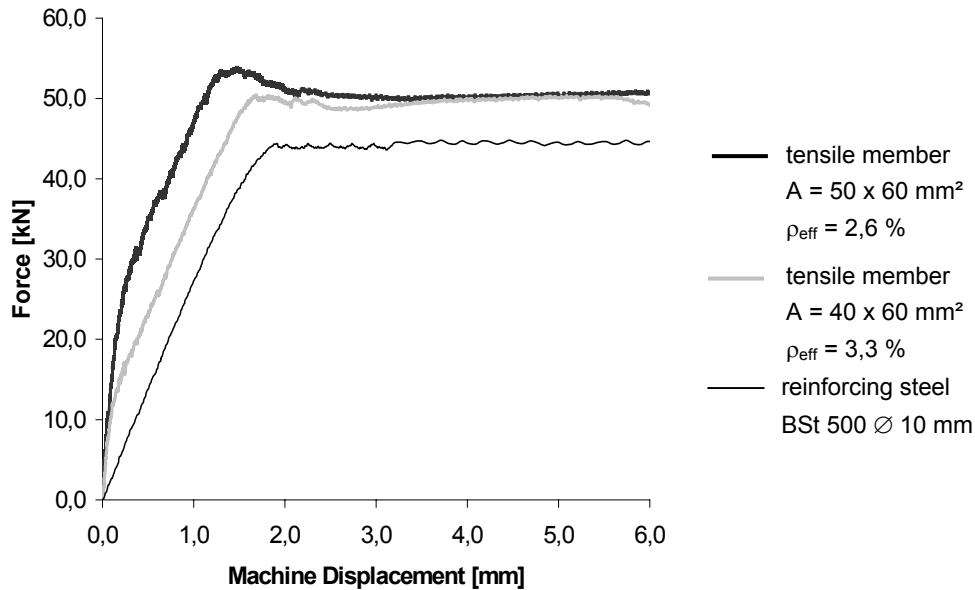
Figure 7:   Results of two preliminary tests on tensile members of UHPFRC

Coincidentally or affected by concreting/compacting the distribution and the alignment of the fibres vary over the length of the tensile member. Therefore the load distribution between fibres and bar reinforcement is different in each crack. The bar reinforcement in the crack with the most unfavourable fibre distribution/alignment reaches the yield strength first. A further load increase in this cross section would have to be sustained exclusively by the fibres. However, with increasing crack width, the destabilisation of the fibre-reinforced concrete (fibre pull-out and/or yielding of the steel fibres) is starting. Hence, the load-carrying capacity of the tensile member decreases gradually to the pure load-carrying capacity of the hardening reinforcing steel. By the hardening of the steel the load-carrying capacity of one specimen was increasing a little bit. Thus it was possible to generate steel yielding in a second crack (Fig. 6).

A similar deformation behaviour could be observed at specimens, tested in the context of the biaxial compression-tension tests on panels of normal strength concrete. Over the whole length of the panel (1000 mm), the bar reinforcement was reaching the yield strength only in one crack, even at high strain. The other cracks retained their crack widths (Fig. 8). With the opening of the crack the load-carrying capacity decreased.

Recapitulating it is to be stated that the maximum load-carrying capacity of the tensile members was obtained for a relative small strain still within the elastic range of the reinforcing steel. The crack widths were still at a level of serviceability at this time (w < 0,2 mm). After unloading these cracks closed almost completely.

For the ultimate limit state design, the influence of the fibres has to be considered not only to achieve an adequate safety but also to attain a ductile behaviour with an announcement of failure by excessive cracking.

Figure 8:   Opening of only one crack in the middle of the panel at a strain of 5.5 ‰

3   Biaxial compression-tension tests on UHPC-panels

3.1   Influencing variables on the compressive strength of cracked concrete

In the literature, the crack width and the crack spacing (Schlaich/Schäfer [9]), the tensile stress (Kollegger/Mehlhorn [10]), the main tensile strain and the load path (Belarbi/Hsu [11]), the main tensile strain (Vecchio/Collins [12]) or the tensile stress and the crack initiation (Tanabe/Wu [13]) are mentioned as major influences on the decrease of the uniaxial compressive strength due to biaxial loading.

Due to the cracking of the concrete member, a partitioning into several compression struts occurs. The dimensions of the struts are defined by crack spacing and thickness of the panel. Affected by the crack initiation the compression struts are shaped irregularly.

There are many parameters influencing the crack growth and final crack spacings. A special dependence exists regarding the direction and the stress of the tensile reinforcement. The direction of the reinforcement affects considerably the crack direction. Cracks, which do not run parallel to the main compression stress direction, represent a disturbance of the load path and reduce the load-carrying capacity of the compression struts. For the reinforcement, reaching the yield strength means a crucial border. Above this border, the tensile strain can serve as a suitable size to describe the cracking.

Affected by the crack opening under very large tensile strain, the damage of the panel is increasing strongly. Interaction between the compression struts by aggregate interlock at inclined cracks (Fig. 9a) is not possible anymore. Also the dowel effect of the reinforcement (Fig. 9b), which causes a mutual support of the slim compression struts, is almost lost beyond the yield point. Besides this, very high bond stresses near to the cracks appear, which contribute to a further destruction of the grain structure. For this reason the stresses have to be redistributed from the edges to the centre of the compression struts.

Due to small crack spacings, for small compression struts the risk exists, that they are already destroyed by tensile stress or split up along the reinforcement from bar to bar by compression stress. If the panels are reinforced in two directions, as common for concrete

structures, the reinforcing bars can buckle in compression direction, effected by an insufficient concrete cover and missing support respectively. This may cause a premature failure of the whole structure. A detailed theoretical investigation on the topic of biaxial loading is given by Roos [14].

(a)   (b)
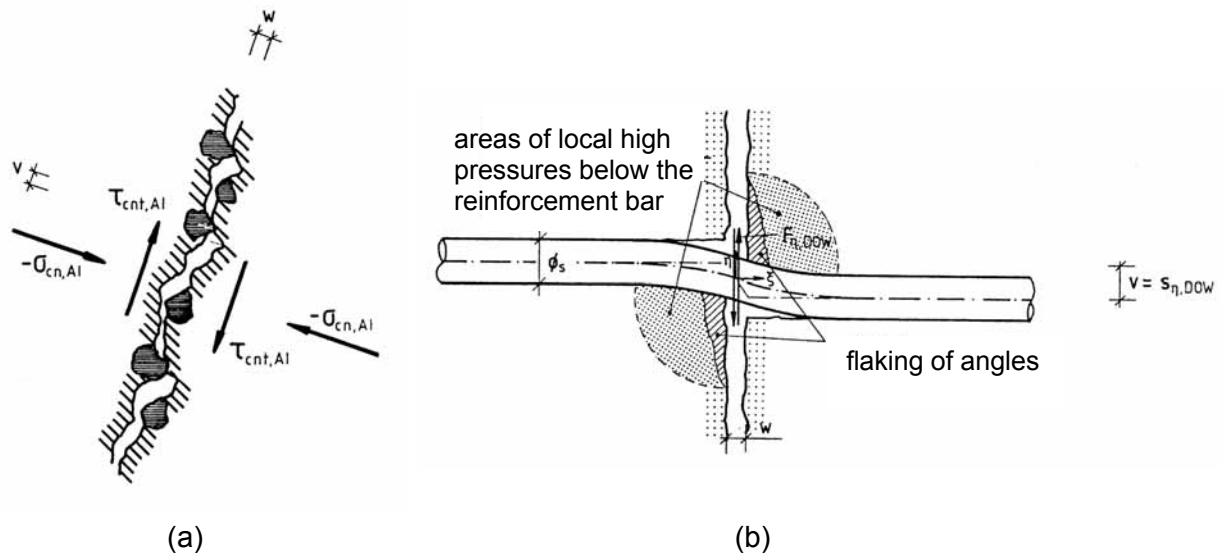
Figure 9:   Aggregate interlock (a) and dowel effect of the reinforcement (b) [14]

3.2   Description of the biaxial compression-tension tests

Test programme

In the context of the test series concerning the structural behaviour of reinforced UHPFRC panels under tensile stress also the biaxial compressive strength is to be investigated. The panels of UHPC and UHPFRC are tested in the Laboratory of Civil Engineering at Kassel University (Fig. 10). Thereby the influences of tensile strain, crack orientation and steel fibres on the compressive strength of UHPC are analysed.

Test specimen

The dimensions and the reinforcement of the tested panels (type K) are represented in Figure 11. Due to the limitation of the vertical force of the load device on 5.5 MN, compared to Figure 5 (type L), the dimensions of the panel had to be reduced. The panels used are 500 mm long (tension), 350 mm high (compression) and 70 mm thick. In this way compressive stresses up to 157 N/mm² can be obtained. In case of a distinct decrease of the compressive strength of UHPC due to the applied transverse strain, the longer type of panels (type L) may also be used within this test series.

The test specimens are fabricated as described in chapter 2.3. For the determination of the modulus of elasticity, the tensile splitting strength and the compressive strength several cylinders of the same concrete mix are fabricated. The test can be scheduled very flexibly, because the final strength is reached after only 48 hours of thermal treatment with approx. 90° C. To ensure an approximately uniformly distributed load over the length of the panel, on the top side and on the bottom side of the panel a very thin levelling layer of UHPC is applied one day before the test.
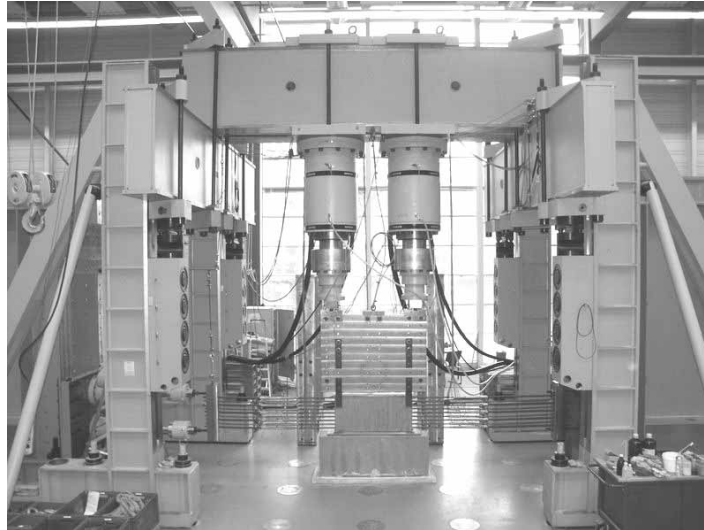
Figure 10: Test setup for the biaxial compression-tension tests on concrete-panels
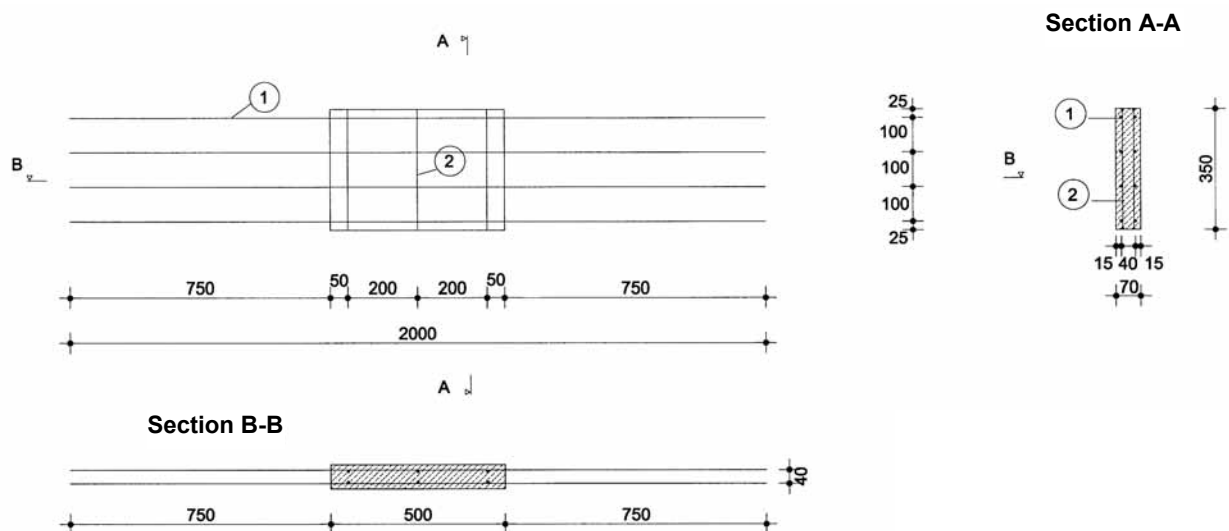
Figure 11: Panels for the investigations on biaxial compression-tension loading (type K)

Mix composition

For the investigations on the biaxial compression-tension strength of UHPC, the compressive strength of the test specimens has to be adapted to the maximum force of the load device. For this purpose, the compressive strengths of the UHPC mixtures, designed at Kassel University reach too high values. In order to reduce the compressive strength systematically without affecting the grain structure substantially, parts of the quartz sand 0.125/0.5 contained in the mixture according to table 1 are replaced by adding glass foam adapted in grain size and volume. This leads to an increased air content, which reduces the compressive strength to an objective of 150 N/mm².

Performance of tests

First the appropriate strain in horizontal direction is applied. Subsequently, the test specimens are loaded in vertical direction at failure (sequential load applying).

In the context of the investigations on panels of normal-strength concrete a preliminary test on a panel of UHPC reinforced exclusively with bar reinforcement was carried out, too. The characteristic cylinder compressive strength of the mixture used was approx. 160 N/mm². The panel was extended in horizontal direction at a strain of 25 ‰ before applying the compressive load. In contrast to the fibre reinforced panels, as described in chapter 2.3 (Fig. 8), the yield strength of the reinforcement was reached in almost every crack (Fig. 12). Even after reaching the yield point successive crack propagation was recognized. Finally, the crack spacing was in the range of 30 to 50 mm.
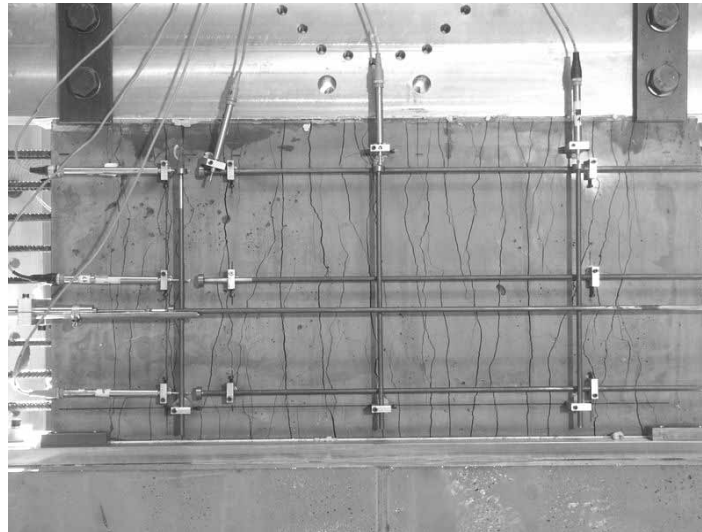
Figure 12: Test specimen of UHPC (without fibres) after
applying the horizontal strain (25 ‰)

As expected, the very narrow and irregularly shaped concrete compression struts had only a minor remaining load-carrying capacity. The reduction of the uniaxial compressive strength was significantly more pronounced than the maximum reduction attained in the tests on normal-strength reinforced concrete panels (without fibres). The average crack spacing measured at specimens of normal-strength concrete was approximately 100 mm. This result points out the great influence of the crack pattern on the reduction of the compressive strength. For the fibre-reinforced panels of UHPFRC the reduction is expected to be less due to the different crack development (cp. chapter 2.3).

4   Conclusion

In the context of this paper the investigations on the structural behaviour of UHPC under tensile stress und under biaxial compression-tension loading, that have been initiated at the Chair of structural Concrete of Kassel University, were presented. The first preliminary tests show the necessity of these investigations in the sense of an economic and safe design of structural UHPC- and UHPFRC-members. The results refer to both, common features and differences existing in these topics between normal- or high-strength concrete on the one hand and Ultra High Performance Concrete on the other hand.

5 References

[1] Bornemann, R.; Schmidt, M.; Fehling, E.; Middendorf, B.: Ultra-Hochleistungsbeton UHPC – Herstellung, Eigenschaften und Anwendungsmöglichkeiten. Beton- und Stahlbetonbau 96, No. 7, p. 458-467, 2001.

[2] Weiler, B., Grosse, C. & Reinhardt, H. W.: Debonding Behaviour of Steel Fibers with Hooked Ends; Proceedings of the Third International RILEM Workshop [Eds.: Reinhardt, H. M. & Naaman, A. E.], RILEM Publications, 1999, p. 423-433.

[3] Jensen, B. C.: Application of Steel-Fibre-Reinforced Ultra-High-Strength Concrete; Structural Engineering International 2/99, 1999, p. 143-146.

[4] Shah, S. P.: Fiber Reinforced Concrete, Handbook of structural Concrete. [Eds.: Kong, F. K., Evans, R. H., Cohen, E. et al.], Pitman Books Limited, London, 1983, p. 6.1-6.14.

[5] Fehling, E.; Leutbecher, T.; Röder, F.-K.: Versuche zur Druck-Querzugfestigkeit von gerissenem stahlfaserverstärkten Stahlbeton in scheibenförmigen Bauteilen; Forschungsbericht aus dem Fachgebiet Massivbau - in preparation, Fachbereich Bauingenieurwesen, Universität Kassel, 2004

[6] Merkblatt Stahlfaserbeton, Deutscher Beton- und Bautechnik Verein E.V., October 2001

[7] Sachstandsbericht Ultrahochfester Beton - Betontechnik und Bemessung - in preparation, Deutscher Ausschuss für Stahlbeton im DIN Deutsches Institut für Normung e. V., 2004

[8] DAfStb-Richtlinie Stahlfaserbeton (10. Entwurf), Ergänzungen zu DIN 1045-1, Teile 1 bis 4, March 2003, Deutscher Ausschuss für Stahlbeton im DIN Deutsches Institut für Normung e. V.

[9] Schlaich, J.; Schäfer, K.: Zur Druck-Querzug-Festigkeit des Stahlbetons. Beton- und Stahlbetonbau 78, p. 73-78, 1983

[10] Kollegger, J.; Mehlhorn, G.: Experimentelle Untersuchungen zur Bestimmung der Druckfestigkeit des gerissenen Stahlbetons bei einer Querzugbeanspruchung, Heft 413 DAfStb, Beuth-Verlag, Berlin, 1990

[11] Belarbi, A.; Hsu, T. T. C.: Constitutive Laws of Reinforced Concrete in Biaxial Tension-Compression, Research report UHCEE 91-2, University of Houston, 1991

[12] Vecchio, F.; Collins, M. P.: The Response of Reinforced Concrete to In-Plane Shear and Normal Stresses, Publication No. 82-03. University of Toronto 1982

[13] Tanabe, T.; Wu, Z.: Strain Softening under Bi-Axial Tension and Compression. IABSE Colloquium Stuttgart 1991, p. 623-636. Zürich: ETH-Hönggerberg 1991

[14] Roos, W.: Zur Druckfestigkeit des gerissenen Stahlbetons in scheibenförmigen Bauteilen bei gleichzeitig wirkender Querzugbeanspruchung. Berichte aus dem Konstruktiven Ingenieurbau 2/95. Technische Universität München, 1994

Eleni S. Lappa
Dipl.-Ing, Junior researcher
Delft University of Technology
Delft, The Netherlands

C. René Braam
dr. ir. drs., Associate Professor
Delft University of Technology
Delft, The Netherlands

Joost C. Walraven
Prof. dr. ir., Head of section
Delft University of Technology
Delft, The Netherlands

Static and fatigue bending tests of UHPC

Summary

The flexural behaviour, as observed under static and fatigue loading, is an essential aspect in the design of structures such as bridges. Beams of steel fibre reinforced ultra high strength concrete have been tested with a four point bending test at a 750 mm span. The static tests were deformation-controlled, the deflection was the control parameter. The fatigue tests were performed at a frequency of 10 Hz with a constant load ratio of 0.2. The actual value of the upper load level in the fatigue test was first assumed as a percentage of the previously determined static flexural strength, and later corrected. Two methods were used for the correction: a remaining half of the tested beam was tested again in a three point bending test, and the number of fibres and their orientation in a cross section close to the fracture surface was determined by image analysis.

Keywords: *UHPC, steel fibres, fatigue, fibre orientation, image analysis*

1   Introduction

Fatigue can lead to severe crack growth and even failure of structures subjected to cyclic or repeated loading, such as high traffic loads, wind or temperature changes. Failure can occur even if the acting loads lead to stresses which are much lower than the static material strength. In metals fatigue cracks are easily recognised through their characteristic fracture surface. In concrete this is not the case: fatigue cracks cannot be distinguished from other types of cracks. Therefore fatigue was not recognised as a possible failure mode until the early seventies [1]. The Model Code 90 [2] was one of the first regulations that included detailed fatigue verifications, which were adopted afterwards in recent national codes and in the new Eurocode 2 [3].

Since the recognition of fatigue as a possible failure mode for concrete structures, many experimental and theoretical studies have been performed. The first ones that focused on the mechanisms of fatigue crack growth and failure were the studies of Gylltoft [4] and Hordijk [5]. Recently these studies have been extended to fatigue of fibre reinforced concrete. A good overview is given Lee and Barr [6]. However, only a few studies exist on

the fatigue behaviour of ultra high performance fibre reinforced concretes (UHPC) [7, 8]. This is due to the fact that these materials have only been developed recently and research in that field is still in progress. One of the main applications refers to bridges, thus structures subjected to frequent and high cyclic loading due to traffic loads. It should be noted that structures nowadays have to be designed to resist much higher traffic loads due to the traffic increase in the past decades. Knowledge of the fatigue behaviour of UHPC materials is therefore of great importance for a safe design and a long service life of structures.

In this paper, first results of static and fatigue bending tests are presented. Focus is set to the accurate estimation the value of the upper load level as a percentage of the static material flexural strength for the fatigue tests. With this approach, the scatter in fatigue results is tried to be kept as low as possible.

2   Materials and methods

The UHPC used was the CERACEM, developed and delivered by Eiffage. The concrete mixture consists of 2355 kg/m^3 of a premix containing cement, aggregates and microsilica, 44.6 kg/m^3 of superplasticiser SIKA 5400 F, 195 kg/m^3 steel fibres and 195 kg/m^3 of water. The premix contains 47 % Portland cement, 45% aggregates with a maximum aggregate size of 7 mm, and 7% microsilica. The steel fibres are straight, 20 mm long, 0.3 mm thick, resulting in an aspect ratio of 67. Their tensile strength is above 1250 MPa.

The concrete mixture is self-compacting so no vibration is needed for the compaction of the test specimens. It is mixed in a forced pan mixer with a total mixing time of 11 minutes. After mixing, the fresh state properties of the mixture are controlled by the slump spread and air content. The slump spread is measured with a 20 cm high cone with 13 cm diameter at the top and 20 cm diameter at the bottom. The diameter of the slump spread measured two minutes after the removal of the cone should be approximately 60 cm. The air content should be less than 3 % by volume.

For each cast batch of concrete, the compressive strength and splitting tensile strength were determined at an age of 28 days on three cubical specimens with a rib length of 100 mm. The mean value of the compressive strength was 217.1 MPa, the splitting tensile strength was 28.16 MPa on average.

The beams for the bending and fatigue tests had dimensions of 125/125/1000 mm and were tested with a four point bending test at a 750 mm span. They were not provided with a notch. The concrete was cast into steel moulds. For the static tests, two different methods of casting were applied to examine if there is a preferable way that keeps the scatter of the strength as low as possible. Therefore, the beams were either cast by pouring the concrete from one end into the mould (method A), or by placing the concrete in small pours at different places into the mould, by moving the bucket along it (method B). The beams were demoulded one day after casting and kept in a fog room at 99% relative humidity until the age of 28 days.

2.1   Experimental program and set-up

The static tests were performed in a deformation controlled way with the deflection as the control parameter. The beams were loaded at their third points. Two linear variable

displacement transducers (LVDT's) measured the deflection at midspan at the bottom fibre of both sides of the beam. The crack openings were measured indirectly by a set of eight LVDT's that were placed at the bottom of the beam between the loading points in order to measure the longitudinal displacement. The test was stopped when a deflection of 8 mm was reached.

The fatigue tests were performed in the same set-up. The tests were performed at a frequency of 10 Hz with a sinusoidal load. The ratio of the lower to the upper load level, R, was kept constant at 0.2. The upper load level was fixed to a certain percentage of the previously determined static mean load. The testing was stopped at failure of the beam or, if the beam did not fail, when 10 million load cycles were reached.

Fatigue experiments often show a large scatter, which is mainly related to the scatter in the material's strength. In order to reduce the scatter and correct the value of the initially assumed upper load level, the tested beams were sawn into two halves close to the fracture surface. At least one of the two remaining halves was then tested in a three point bending test, once again deformation controlled via the deflection, at a 400 mm span. The flexural strength of the three point bending test could be related to the flexural strength of the four point bending test through a relation that was determined by additionally testing the halves of the statically tested beams as well.

A second method used for correcting the initially assumed upper load level was through counting the number of fibres and their orientation in the sawn cross-section of the beam close to the fracture surface. Pictures were taken of the beams tested by both the static and fatigue four point bending tests. Since the concrete absorbed the flashlight while the fibres reflected it, the fibres can be distinguished and counted with appropriate image analysis software. Figure 1 shows the picture of one of the tested beams and the fibres present in it.
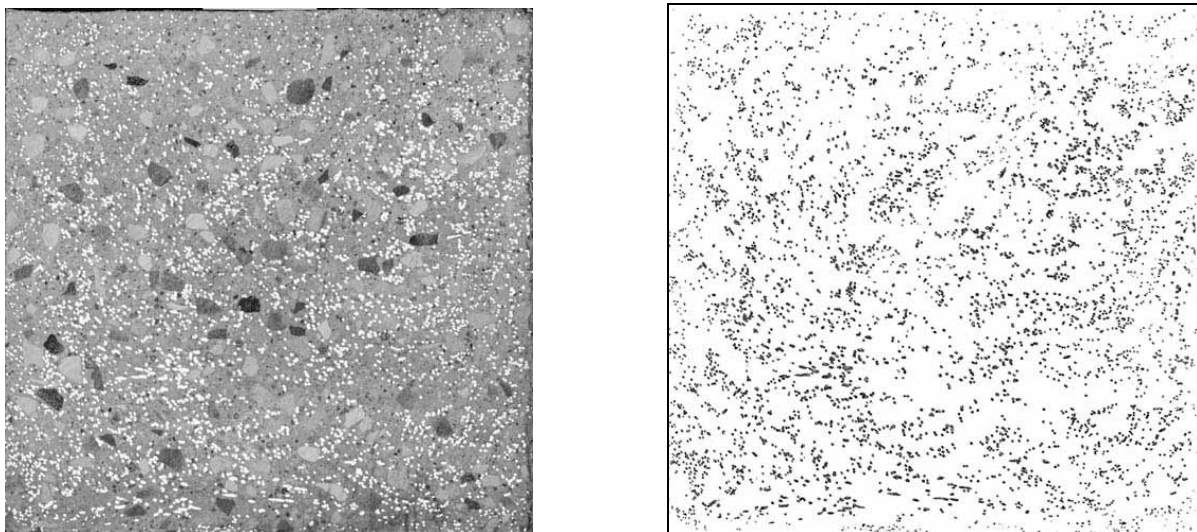
Figure 1:   Picture of a beam cross-section close to the fracture surface and the fibres present in the same cross-section.

The shape of the fibre on the image will only be a full circle when it is oriented at an angle of 90 degrees to the fracture surface [9]. At any other angle, the fibre will be displayed as an

ellipse. The length of the smaller major axis corresponds to the fibre diameter, while the fibre diameter divided by the length of the longer major axis indicates the angle φ in which the fibre is orientated in the fracture surface. A total orientation number η_φ, that gives a general impression about the overall orientation of all fibres in the beam, was determined with the following equation [9]:

$$\eta_\varphi = \frac{1}{N} \cdot \sum_i^N \cos\varphi \qquad (1)$$

Here, N represents the number of fibres in the beam's cross-section, and φ the angle between the direction of the applied tensile force and the steel fibre (cos φ = d_F / d_E; d_F diameter of the fibre, d_E length of the major axis of the ellipse).

The pictures of the beams tested statically were used to obtain a relation between the number of fibres in the fracture cross-section and the flexural strength of the four point bending test. The relation was used to correct the initially assumed value of the upper load level of the fatigue test.

3 Results

3.1 Static four point bending tests

Figure 2 shows the equivalent bending stress at the bottom fibre of the beam versus the deflection. Eleven beams were tested; six of them were cast according to method A and five according to method B. The mean value for all beams together was 24.96 MPa with a standard deviation of 6.61 MPa. The coefficient of variation, which is the standard deviation divided by the mean value and is a parameter often used to express the scatter in results, is quite high with a value of 26.5%. That is a high value even for fibre reinforced concrete, which is known to show values up to 20%. The weakest beam had a flexural strength of 14.5 MPa, while the strongest one had a twice as high strength of 30 MPa.
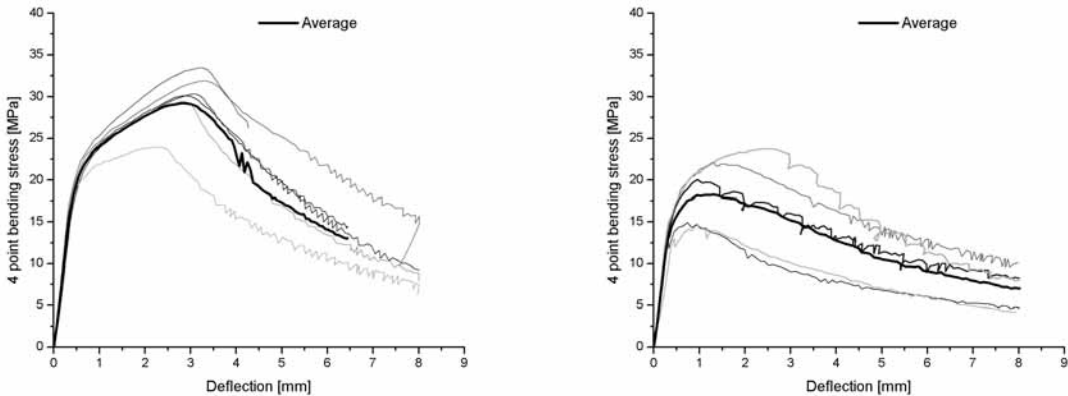
Figure 2:   Results of the static four point bending tests. Left the beams and their average curve cast according to method A, right the ones according to method B.

3.2   Fatigue four point bending tests

A typical cyclic creep curve, showing all three characteristic stages during a fatigue experiment, is presented in Figure 3. After the initial stage, where the deformations increase rapidly, the process is stabilised and the deformations increase slowly at a constant rate. These first two stages normally correspond to 80% of the total fatigue life of the test specimen. Before failure the deformations then again increase rapidly. The beam that corresponds to the given curve was tested at an assumed load level of 50% of the static flexural strength and showed 30559 cycles to failure.
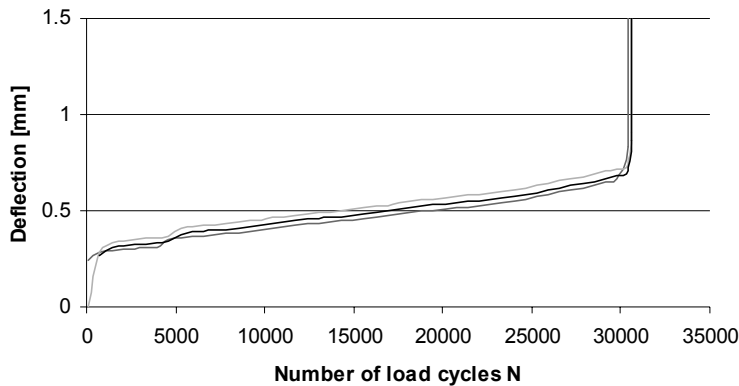
Figure 3:   Typical cyclic curve of the deflection increase and number of load cycles during a fatigue test. The deflection at both sides of the beam at midspan and their average value are shown.

The main aim of the fatigue tests is to establish relations between the upper stress level S and corresponding number of cycles to failure N, the so-called S-N or Wöhler curves. Not enough test specimens have been tested up to this point in order to show such curves yet, the testing will be continued in future work. However, the beams tested so far clearly state the main difficulty in establishing the curves: the exact determination of the upper stress level as a percentage of the beam's static flexural strength. Two beams that were supposed to be tested at an 80% stress level failed immediately, indicating that the actual flexural strength of the beam had been reached or even surpassed. With the two following test methods this problem is expected to be overcome. The initially assumed upper stress level will be corrected after the fatigue test is performed, by trying to trace back the actual value of the beam's flexural strength by means of three point bending tests on beam halves and image analysis on a plane just 2 cm behind the fracture surface.

For the determination of the S-N relation only the tests on the 75% stress level has been finished so far. Four beams were successfully tested and showed 29295, 124003, 163931 and 170771 cycles to failure. Three point bending tests on their halves and image analysis on a section close to the fracture surface are still to be performed in order to verify or correct the assumed 75 % stress level.

3.3 Three point bending tests on beam halves

Twenty-two beam halves were tested with the three point bending test, fourteen of them originated from statically tested beams and eight were tested under fatigue loading. The mean value of the flexural strength was 35.87 MPa with a standard deviation of 4.72 MPa, so the coefficient of variation was 13.2%.

Figure 4 shows the relation between the flexural strength of the whole beam tested with the static four point bending test and the flexural strength of the corresponding beam half tested in a three point bending test. Beams cast according to both methods were taken into account. This relation can be used to predict the actual value of the static strength of a four point bending test of a whole beam tested under fatigue loading.
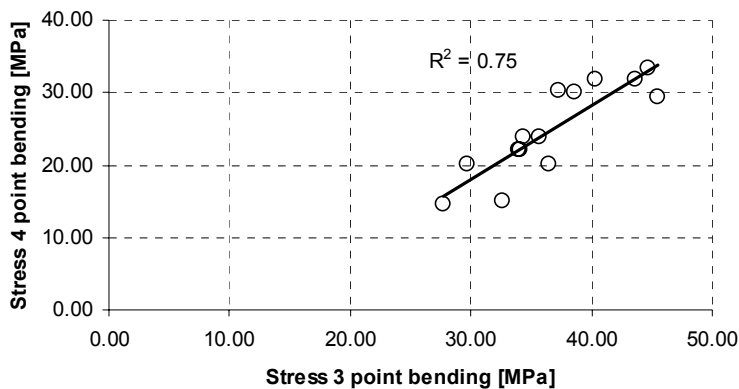
Figure 4: Relation between the four point bending flexural strength of a whole beam and its corresponding three point bending stress of a beam half.

3.4 Fibre count by image analysis

Image analysis was used to count the fibres in the beam cross-section close to the fracture surface since with an average of 15.6 fibres / cm^2, it would have been almost impossible to count all fibres by hand.

The relation obtained between the number of fibres / cm^2 in the cross-section of the tensile zone of the beam and its corresponding static flexural strength from the four point bending test is shown in Figure 5.

No such relation could be derived for the orientation number, determined with equation (1), and the flexural strength of the four point bending stress. The orientation number was, for all beams, in accordance with both casting methods on average 0.56.
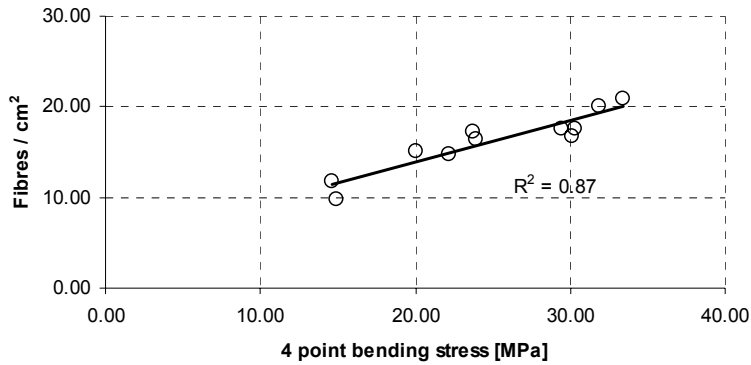
Figure 5: Relation between the four point bending stress and the number of fibres / cm^2 in a cross-section close to the fracture surface for the statically tested beams.

4 Discussion

The results of the static bending tests show that the production method influences the bending behaviour and its scatter. In order to get comparable results, an identical production method should be applied between separate batches of concrete. The scatter is significantly reduced when each of the two production methods is regarded separately. For the beams cast with method A, the mean value of the flexural strength was 29.83 MPa with a standard deviation of 3.23 MPa, resulting in a relatively low coefficient of variation of 10.8%. The beams cast with method B had an average flexural strength of 19.10 MPa with a standard deviation of 4.17 MPa, showing a larger scatter compared to method A and a coefficient of variation of 21.8%.

Comparing the individual results of beams cast in separate batches of concrete but with the same production method one can see that comparable average flexural strengths are obtained for each batch. The six statically tested beams produced with method A were cast in two batches of three beams The average of the first set of three was 30.99 MPa, while the same value of the second set was 28.72 MPa. In good agreement were also the averages of each one of the two batches of the beams produced with method B. The average of the first set of three was 17.23 MPa and the average of the second set of two 21.90 MPa.

Image analysis serves as well as an indication of the segregation of the fibres in the matrix. The fibres were also counted separately for the bottom and top half of the beam surface. The top surface is the top of the beam during the casting, which also corresponds to the top surface of the beam during the four point bending test. Fibres in steel fibre reinforced concrete have been reported to concentrate more in the bottom part of the beam due to gravity. This effect might even be more pronounced when vibration is used for compaction. The beams cast with method A had on average 54% of their fibres concentrated in the bottom part and the remaining 46% in the top part. The segregation was less visible for the beams cast with method B. 53% of the fibres were present in the top half of the beams and 47% in the bottom. It has to be noted that the main difference in the average flexural strength between the two cast methods is not related to this difference in the fibre concentration along

the height of the beam, but only to the total number of fibres present in the beam's cross-section.

Determining the orientation number with equation (1) has the disadvantage that it is very sensitive to the reflection of the light by the fibres. In larger cross-sections it can be very difficult to equally distribute the flashlight on the entire cross-section. In the beams examined here, often in the corners the fibres were not able to reflect the light, or only partly. The orientation number can also be determined with the following equation, which states the theoretical number of fibres in the cross-section as obtained from the fibre volume fraction of the mixture [10]:

$$N_F = \frac{V_F}{A_F} \cdot \eta_\varphi \qquad (2)$$

With N_F [1/cm^2] the number of fibres in the cross-section, V_F the fibre volume fraction, A_F [cm^2] the area of a single fibre and η_φ the orientation number in the direction perpendicular to the crack surface. Determining the orientation number with equation (2) has the disadvantage that the same fibre content is assumed for each beam, which is not necessarily the case. Even if the same amount of fibres is present in all beams, it cannot be assumed that they are equally distributed in each cross-section across the beam's length. The orientation number according to equation (2) can be determined as well after determining the number of fibres in the cross-section N_F from the photographs. Figure 6 shows the orientation number as obtained with both equations. It can be seen that in general higher orientation numbers were obtained with equation (2). The average orientation number was 0.562 according to equation (1) and 0.693 with equation (2). However, since the numbers determined with the first equation are independent of the actual content of steel fibres in the cross-section, they can be considered more realistic. In the future, a few beams will be sawn on different sections along their length, to examine whether the steel fibres tend to concentrate on one end of the beam or uniformly along its length, especially when cast with method A.
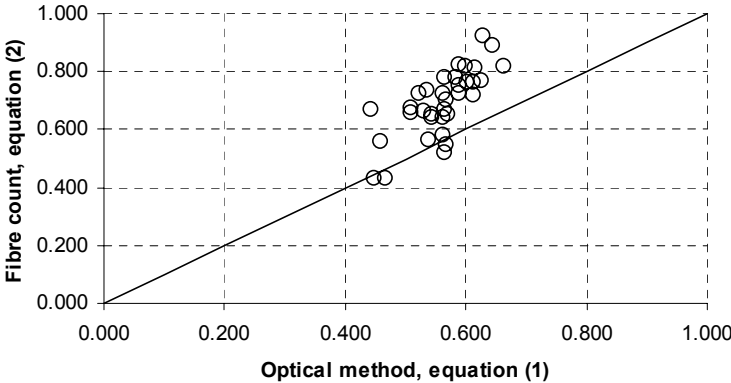
Figure 6:   Orientation number of all examined beams corresponding to equation (1) and (2).

Not enough experiments are performed so far to present S-N lines for this mixture. The relations found between the four and three point bending strength (Figure 4) and the four

point bending strength and number of fibres present in the cross-section (Figure 5) promise to estimate the actual material flexural strength and therefore correct the first assumed load level, thus enabling a better estimation of the S-N relation. As a start, the flexural strength's of five beams subjected to fatigue was determined according to both methods, and are listed in Table 1. Two of those were subjected to an assumed upper level of 80%, the other three to 50%. The first two failed immediately, indicating that the beams had a lower strength than assumed. The set upper load level had already reached or even surpassed the static flexural strength. This is verified by both methods. One of the three beams tested at 50% failed after only 30559 load cycles, indicating that also this beam was significantly weaker than the average of the statically tested ones. For this particular beam, both methods correct the upper load level to 64%. The remaining two beams tested at 50% did not show failure after 2 million load cycles, indicating that the actual strength might be close to the assumed value.

Table 1:   Correction of the upper load level with the two presented methods

Assumed load level	Predicted strength with 3 point bending and corrected upper load level	Predicted strength with image analysis and corrected upper load level
Beam 1: 80%	22.15 MPa (108%)	21.73 MPa (110%)
Beam 2: 80%	15.54 MPa (154%)	23.58 MPa (101%)
Beam 3: 50%	23.52 MPa (64%)	23.40 MPa (65%)
Beam 4: 50%	24.31 MPa (62%)	26.40 MPa (57%)
Beam 5: 50%	24.25 MPa (62%)	46.7 MPa (47%)

These first results indicate that the image analysis might estimate higher values for the flexural strength than the three point bending tests. Since the correlation between the number of fibres in the cross-section and the flexural strength of the four point bending test was better, the estimations with image analysis should be more realistic, provided that the quality of the photographs is adequate. Especially all fibres in the bottom part of the cross-section should reflect the flashlight.

5   Final comments and conclusions

Fatigue experiments often show a high scatter, which is often related to the scatter in the material strength. The main difficulty in determining S-N relations is to accurately set the value of the upper load level as a percentage of the static flexural strength. The latter cannot be predicted beforehand. With two methods presented here, three point bending tests on beam parts and image analysis of pictures of beam cross-sections close to the fracture surface it is possible to estimate the actual material strength. With this knowledge, the initially assumed upper load level can later be corrected.

The scatter in the material strength can be controlled by the casting process. Test specimens were produced with two different casting methods. Method A proved to be beneficial regarding the scatter and the number of fibres present in the critical cross-section close to the fracture surface. It has also the further advantage that the test specimens are easier to

cast in that way. Therefore it was chosen to cast all test specimens for the fatigue experiments with this method.

Image analysis showed that the fibre orientation number did not vary to a great extent in the examined beams. Even though the fibres were oriented in a similar way in all beams, the number of fibres present in the cross-section did differ. The static flexural strength was found to be in direct relation with the number of fibres present in the bottom part of the critical cross-section.

6 Acknowledgements

7 References

[1]   Comité Euro-International du Béton: Fatigue of concrete structures; State of the art report. CEB Bulletin No 188, 1988.

[2]   Comité Euro-International du Béton: CEB-FIP Model Code 1990. CEB Bulletin d'information, No 203, Lausanne, 1993.

[3]   prEN 1992: Eurocode 2; Design of concrete structures. Final draft, September 2001.

[4]   Gylltoft, K.: Fracture mechanics models for fatigue in concrete structures. PhD-Thesis, Lulea University of Technology, 1983.

[5]   Hordijk, D.A.: Local approach to fatigue of concrete. PhD-Thesis, Delft University of Technology, 1991.

[6]   Lee, M.K. and Barr, B.I.G.: An overview of the fatigue behaviour of plain and fibre reinforced concrete. In: Cement and Concrete Composites, article in press, accepted 26-11-2002.

[7]   Mouquet, D., Bernier, G. and Behloul, M.: Etude du comportement a la fatigue du BPR fibre. In: Proc. 5th RILEM symposium on Fibre-Reinforced Concretes (FRC), Lyon, France, 13-15 September 2000, pp. 769-779.

[8]   Schmidt, M., Fehling, E., Teichmann, T. and Bunje, K.: Durability of ultra high performance concrete (UHPC). In: Proc. 6th International symposium on utilization of High Strength / High Performance Concrete, June 2002, Leipzig, Germany, pp. 1367-1376.

[9]   Schönlin, K.: Determination of the orientation, the content and the distribution of the fibres in fibre reinforced concrete. In: Beton- und Stahlbetonbau 83, Heft 6, pp. 168-171, 1988 (in German).

[10] Krenchel, H.: Fibre spacing and Specific Fibre Surface. Fibre reinforced cement and concrete, edited by Neville, The Construction Press, UK, pp. 69-79, 1975.

Sebastian Ortlepp
Dipl.-Ing.
Dresden University
Dresden, Germany

Manfred Curbach
Prof. Dr.-Ing.
Dresden University
Dresden, Germany

Research into high-strength concrete at high rates of loading

Summary

High-strength concrete shows an increasing in the tensile strength at high rates of loading, but with a substantial smaller factor than plain concrete. Due to the minor strength dispersion of the material components of high-strength concrete and the good bond between aggregate and cement paste, the influence of the aggregate interlock on the force transfer after the cracking is smaller. This leads to relatively smooth crack surfaces and to a low ductility of high strength concrete. Researches on the crack surface of fast loaded specimen have shown a higher fragmentation of this area compared to surfaces of the quasi-static tests, so that the real crack surface increases. Due to this fact, the ultimate bearing force increases too, because it is dependant on the ultimate tension stress and the size of the fracture surface.

Keywords: *high-strength concrete, impact, surface analysis*

1   Introduction

Figure 1 shows that high rates of loading may act on buildings in different kinds of events. For example: a sudden loading on a bridge as a result of a vehicle driving over an expansion joint of a bridge, an aircraft crashing into a high-risk building or a gas explosion in a bunker.
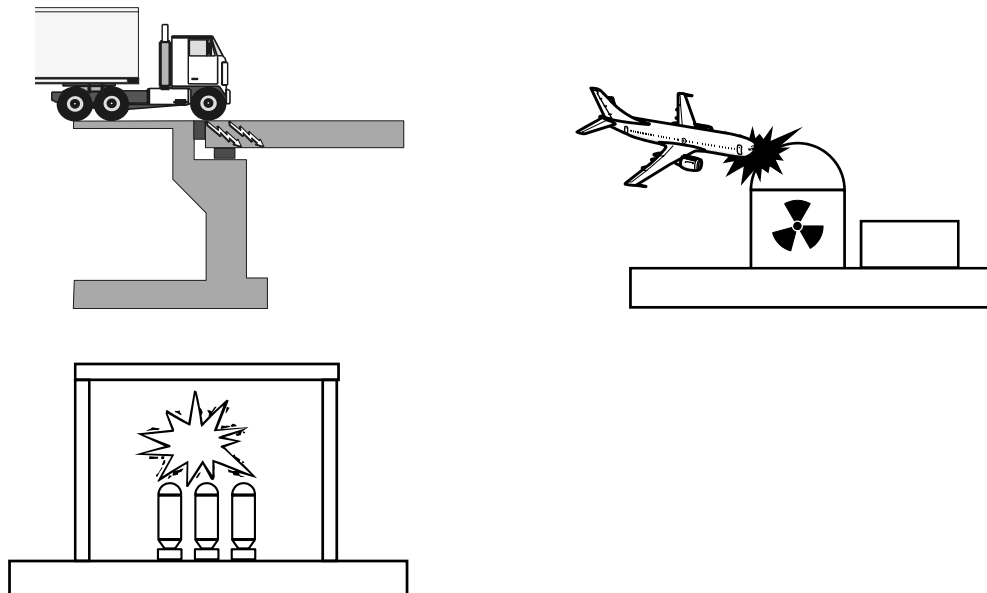
Figure 1:   Impact loads on various structures

Table 1:   Typical strain rate for various types of loading, according to CEB [1]

type of loading	strain rate ($\dot{\varepsilon}$) [s^{-1}]		
Simulation of a static loading	10^{-6}	–	$3 \cdot 10^{-5}$
Impact of cars and ships	10^{-6}	–	10^{-4}
Gas explosions	$5 \cdot 10^{-5}$	–	$5 \cdot 10^{-4}$
Earthquake	10^{-2}	–	$5 \cdot 10^{0}$
Pile driving	10^{-2}	–	10^{0}
Impact of airplane	$5 \cdot 10^{-2}$	–	$5 \cdot 10^{-0}$
Hard impact	10^{0}	–	$5 \cdot 10^{1}$
Hypervelocity impact	10^{2}	–	10^{6}

Table 1 shows some approximate values of typical strain rates, that buildings can experience in different kinds of events. These data are reference values and present a simple overview of dynamic effects on buildings.

Relatively large ranges of the maximum strain rate are suggested for the individual types of loading. The typical strain rate for the simulation of a static load of concrete is maximum $3 \cdot 10^{-5}$ s^{-1} and is fixed by the DIN 1048 [2] for example.

2 Concrete behaviour at tensile stress

In Germany, the standards for high-strength concrete were regulated by the DAfStb guideline "Hochfester Beton" [3] till the introducing of the new DIN 1045-2 [4]. In this standard, the high-strength concrete starts at the compression strength class of C 55/67. According to the CEB/FIB – report [5], concrete with a cylinder compression strength of more than 60 N/mm² is classed as high-strength concrete.

As a basis for the description of the dynamic material behaviour of concrete, a summary of the experimental results concerning plain concrete behaviour at high rates of load application are given at this point. Nearly all investigations on the dynamic characteristics of concrete are focused on uniaxial tensile tests. Figure 2 shows a summary of the material behaviour of plain concrete at high rates of loading from different publications.
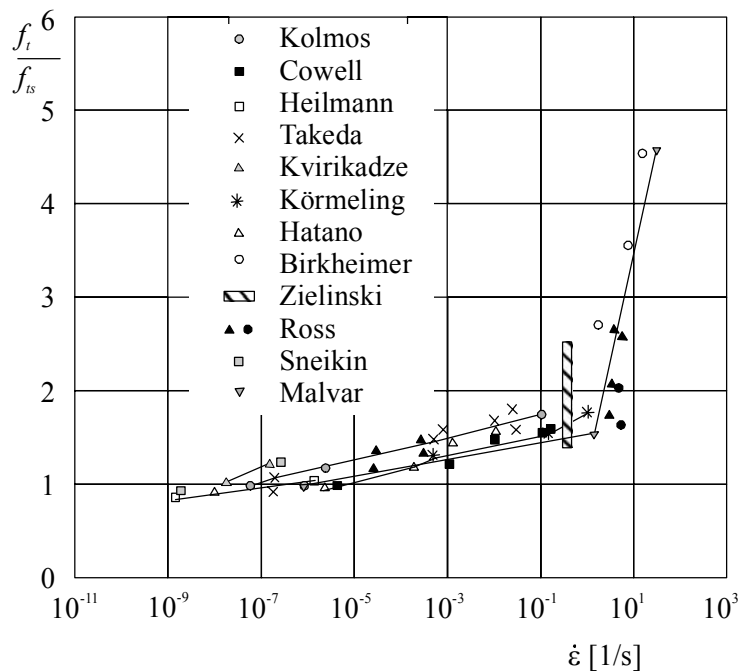
Figure 2: Tensile strength of plain concrete subject to the strain rate, taken from Bachmann [7]

Obviously, a solidification of the material can be registered at increasing rates of loading. As already known, the strength increase versus the strain rate can be divided into two parts. The first part reaches a strain rate at approx. 1 s^{-1}. The factor between the dynamic and static tensile strength at this point is approx. 2.0. From this value, the factor increases suddenly up to a value more than 4.0 at a strain rate of 10 s^{-1}. An exact investigation of the fracture area shows that after a dynamic loading in proposition more aggregates are cracked, instead their pullout. Therefore, it was assumed that the cement paste could transmit a higher tensile stress during a fast loading, without its destruction. Therefore, in situation with high rates of loading, an increase in the strength of the concrete appears here.

A change of the material properties of the concrete can be observed at high dynamic loading. Both, the elastic modulus and the maximum tensile strength are influenced by the kind of loading. A general tensile stress-strain-relationship is represented in equation (1)

$$\sigma = E\left(\varepsilon, \dot{\varepsilon}\right) \cdot \varepsilon \leq \sigma_{max}\left(\dot{\varepsilon}\right) \quad (1)$$

Due to the minor strength dispersion of the material components of high-strength concrete and the good bond between aggregate and cement paste, the influence of the aggregate interlock on the force transfer after the cracking is smaller than the aggregate interlock of plain concrete. In addition, the roughness of the fracture surface decreases as the compression strength increases (Koenig et al.[6]). This leads to relatively smooth crack surfaces and to a low ductility of high-strength concrete.

The cement paste already exhibits an enormous tensile strength at high strength concrete and is also a better bond to the aggregate. Thus, the aggregate will get a higher force during the static tensile loading. That means that during the developing failure of the specimen, the crack runs predominantly through the aggregates and not around them, in contrast to the observation at plain concrete. Impact tensile tests show a strength increase of the high strength concrete, so if this is assumed in this case then a solidification of this material will only have a small effect on the total strength, because the aggregates in this case will also fail. Now the question arises, whether the cement paste and the bond to the aggregates solidify at high strain rates.

3   Results

In the year 2000, an impact machine for the investigation of dynamic material properties of concrete was developed at the institute of concrete structures at the Technische Universität Dresden. Details of this device are previously presented in Curbach / Ortlepp [8].

Figure 3 shows the findings of the dynamic behaviour, gained from impact tensile tests. In this overview, the increase of the tensile strength is plotted against the strain rate. In the figure, different results of with different ultimate cube strength in compression of the respective sample are represented.
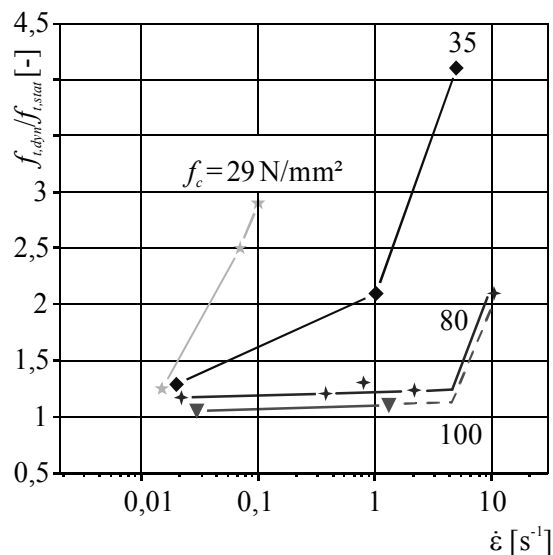
Figure 3:   Ultimate tensile strength ratio subjected to strain rate and cube strength

These Investigations can confirm the two-part strength increase of normal concrete. As can be seen from the graph, the increase of the ultimate tension strength of high-strength

concrete is less than that of the normal concrete. There seems to be a difference between the cracking process of quasi-static and the cracking process of dynamic loading. The surface of the fracture area was observed more closely to analyze this difference.

4   Investigation of the crack surface

4.1   General remarks

One possibility of evaluating picture data arrays is the description of periodic signals in the frequency range. Periodic signals can be generally represented as Fourier series. The signals are divided into their harmonious components. The Fourier transformed signal accurately contains the same information in the frequency range, as the associated signal in the time range. They only differ in the kind of representation of the information. This permits the view for a function from another point of view, i.e. within the transformed range (frequency range). The signals are analyzed with the FFT-algorithm (Fast Fourier Transformation) from COLLEY [9].

In the following, some examples of special signal forms are demonstrated (see Figure 4). The frequency analysis of a sine curve, which is illustrated in Figure 4 a) is well known. Because of the fact that the superposition law is applicable to the frequency analysis, only a partial oscillation is shown in Figure 4 b) and c). Both signal impulses have a length of t = 100.0 ms and a scanning rate of 160 values/ms. The frequency spectrum of the square-wave impulse in Figure 4 c) shows zero points at frequencies of 10, 20 and 30 Hz. These values can be calculated by means of the impulse length τ with the help of the equation $f = 1 / (\tau \cdot n)$. The parameter n is an integer and must have a value of not less than one. Between the points of zero, the frequency spectrum still reaches considerably local peaks. On the other hand, substantially lower local maxima develop in the frequency spectrum in Figure 4 b) between the points of zero. Hence one can draw the conclusion that a larger deviation from a harmonious signal leads to higher amplitudes of the higher frequency parts in the frequency spectrum.
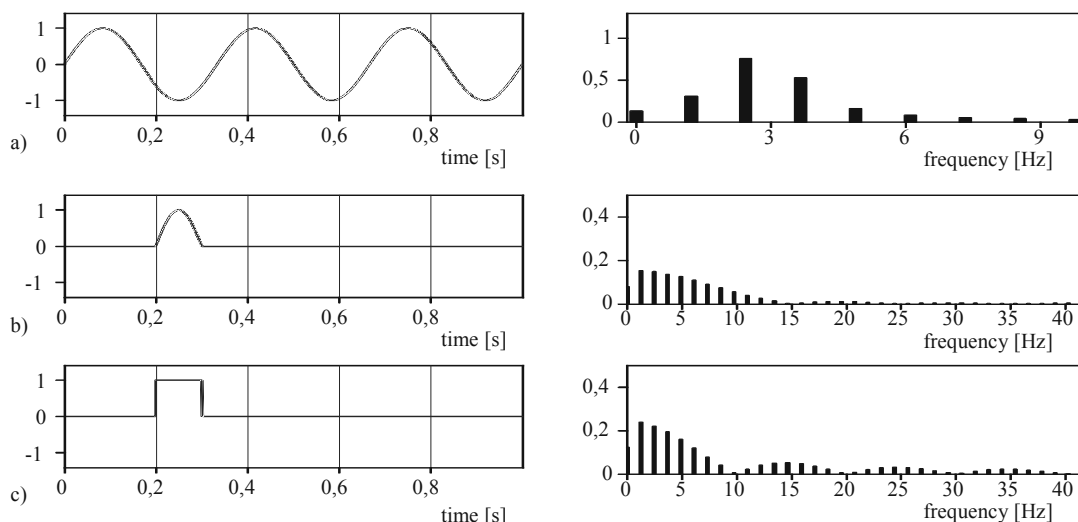
Figure 4:   Signals in the frequency range

4.2 Examination of the fracture surface

Two-dimensional arrays, which consist of a number of individual signal components, can only analyzed problematically with the help of an x-y-representation, like a normal two dimensional diagram. Analysis and synthesis of linear signals can be transformed by a temporal dependence into frequency dependence. Also pictures with the local spatial coordinates x and y can be transformed into spatial frequency pictures with the spatial frequencies f_x and f_y. Generally, the transformation from the time range (spatial range) into the frequency range is also called Fourier transformation.

The calculation of the spatial frequency pictures of the fracture surfaces proceeds via the analysis of the altitude profile. For this investigation, a so-called unidimensional FFT is used. Here, the fracture surface is scanned line-by-line. A separate frequency spectrum is generated for each series of measurements for each line. This frequency spectrum is written back to the same line of the data array. The result is a data array, which consists of many parallel frequency spectra. Thus, a line-by-line evaluation of the spatial frequencies along the fracture surface is possible. Figure 5 descriptively shows the arithmetic operation.
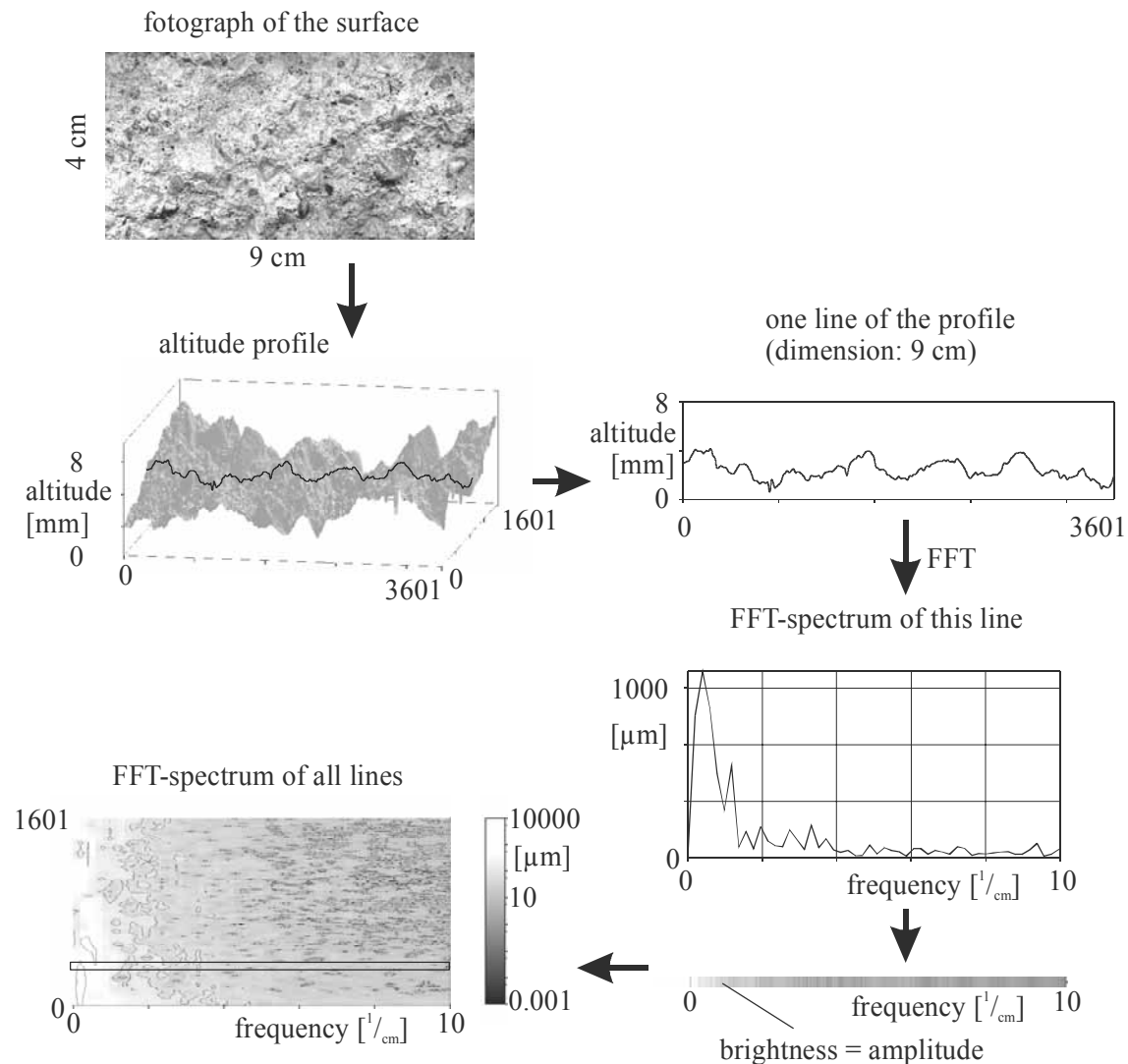
Figure 5:   Scheme of determination of spatial frequency spectra

The fracture surface of a high-strength concrete essentially consists of broken aggregates and of broken cement paste. Unbroken aggregates are hardly present. Special attention is drawn here, to the general condition of the fracture surface. Two cuts for different parts of the surfaces with different loading histories are represented in Figure 6.
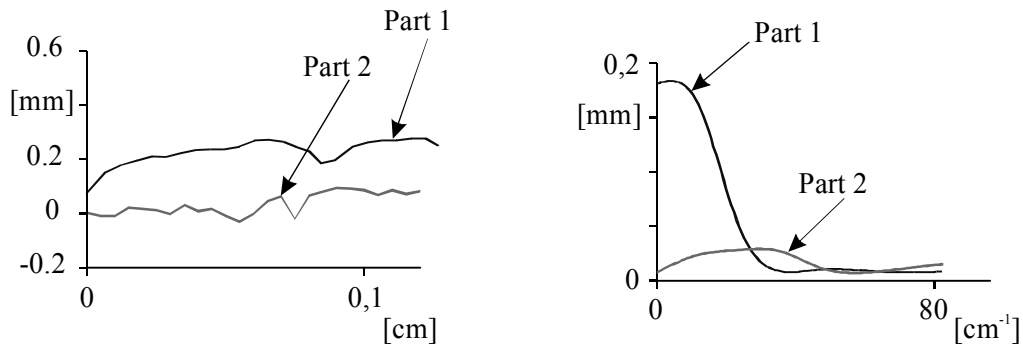
Figure 6:   Cuts of surfaces of different load history

As already seen from the optical impression, a relatively smooth surface produces a larger oscillation period than a rougher surface. This characteristic oscillation appears as a local maximum in the frequency spectrum.

4.3   Results of the spatial frequency spectrum

The tested fracture surfaces have dimensions of 4 cm × 9 cm. These fracture surfaces were scanned at intervals of 25 μm by means of a laser beam. Due to this, the developed surface array has the dimensions of 1601 × 3601 values. Figure 7 shows the examined surface profiles.
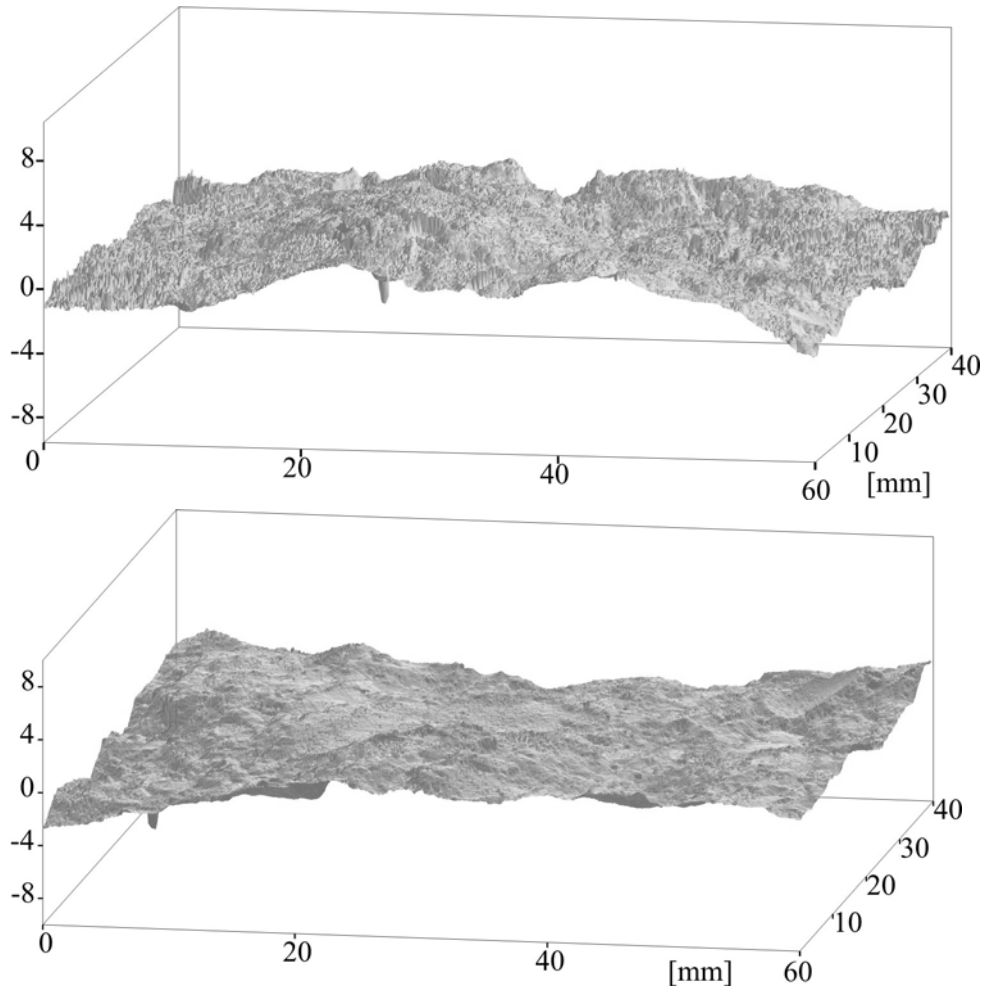
Figure 7: Typical fracture surfaces of a high (top) and a low (bottom) loading rate

The surface of the low loading rated concrete seems to be smoother. This impression can be confirmed by calculating spatial frequency spectrum. The study of the fracture surfaces for quasi-static loading and dynamic loading leads to the following spatial frequency spectra (Figure 8 and Figure 9).
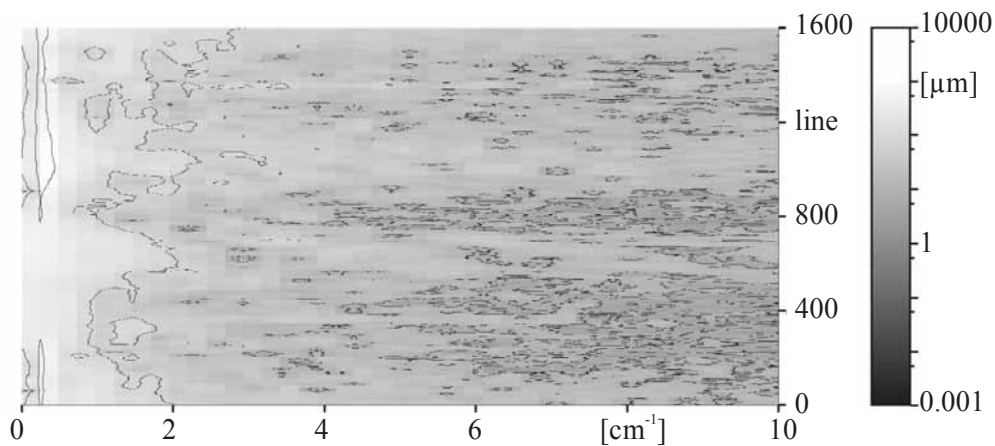
Figure 8: Spatial frequency spectra of high strength concrete at quasi-static loading
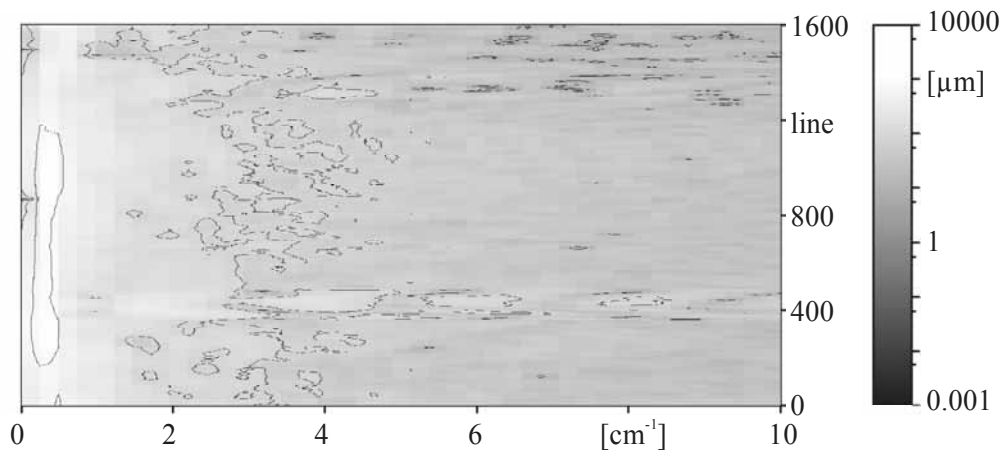
Figure 9: Spatial frequency spectra of high strength concrete at dynamic loading

The brighter ranges in the previous mentioned Figures refer to larger amplitudes of the frequency in each case. Here, the frequency displacement can be clearly recognized in both spectra. At the fracture surface of the quasi-statically loaded specimen, the deep frequencies are dominant. In contrast, the frequency spectrum of the dynamically loaded fracture surface shows higher frequencies. The distribution of the frequency is also very irregular over the width of the examined fracture surface, which is charted along the y-axis.

5 Conclusions

Higher spatial frequencies represent an increase of the roughness or fragmentation of the fracture surface. A higher fragmentation leads to an increasing of the total fracture area. In contrast to the smooth surface of slow loaded specimen, the ultimate tensile stress of the concrete material increases too, due to the additional force transmission of the larger area. This effect leads to an increase of the tensile strength at high rates of loading even on high-strength concretes.

6 References

[1] CEB-FIB Model Code 1990. Bulletin d'Information No 203-205, Lusanne, 1991

[2] Deutsches Institut für Normung e. V. (DIN): Prüfverfahren für Beton DIN 1048 Teil 5: Festbeton, gesondert hergestellter Probekörper, Juni 1991

[3] Deutscher Ausschuß für Stahlbeton (DAfStb): Richtlinie für hochfesten Beton – Ergänzung zu DIN 1045/07.88 für die Festigkeitsklassen B 65 bis B 115, August 1995

[4] Deutsches Institut für Normung e. V. (DIN): Tragwerke aus Beton, Stahlbeton und Spannbeton DIN 1045-2 Teil2: Beton – Festlegung, Eigenschaften, Herstellung und Konformität; Juli 2001

[5] CEB: Concrete structures under impact and impulsive loading. Bulletin d'Information No 187, Lusanne, 1988

[6] König, G.; Tue, N.V.; Zink, M.: Hochleistungsbeton Bemessung, Herstellung und Anwendung. Ernst & Sohn, Berlin 2001

[7] Bachmann, H.: Die Masseträgheit in einem Pseudostoffgesetz für Beton bei schneller Zugbeanspruchung. Dissertation und Heft 19 der Schriftenreihe des Instituts für Massivbau und Baustofftechnologie, Universität Karlsruhe, 1993

[8]   [Curbach, M.; Ortlepp, S.: Dynamische Untersuchungen an hochfestem Beton. In: 2. Symposium Experimentelle Untersuchungen von Baukonstruktionen, Ehrenkolloquium zum 65. Geburtstag von Herrn Prof. Dr.-Ing. habil. Heinz Opitz. Institut für Tragwerke und Baustoffe, TU-Dresden (Hrsg.), Dresden, Eigenverlag, 2002

[9]   Cooley, J. W.; Tukey, J. W.: An Algorithm for the Machine Computation of the Complex Fourier Series. Mathematics of Computation, Vol. 19, April 1965, pp. 297-301

Klaus Holschemacher

Prof. Dr.-Ing.

Leipzig University of Applied Sciences
(HTWK Leipzig)

Leipzig, Germany

Sven Klotz

MSc. Dipl.-Ing.

Leipzig University of Applied Sciences
(HTWK Leipzig)

Leipzig, Germany

Frank Dehn

Dr.-Ing.

MFPA Leipzig GmbH

Leipzig, Germany

Dirk Weiße

Dipl.-Ing.

Leipzig University of Applied Sciences
(HTWK Leipzig)

Leipzig, Germany

Ultra High Strength Concrete under Concentrated Loading

Summary

In order to investigate the load bearing capacity and the failure behaviour of ultra high strength concrete (UHSC) under concentrated loading an experimental programme was implemented. Thereby specimens made of plain and reinforced concrete using helical reinforcement as well as different specimen heights were tested. The results should be compared with an extrapolation of an existing design rule established for normal and high strength concrete. In this context, 3 different concretes were investigated in order to recognise the influence of concrete strength and composition on the load bearing behaviour as well as capacity under concentrated load.

Keywords: concentrated loading, ultra high strength concrete (UHSC), helical reinforcement,
reactive powder concrete (RPC), transversal tensile stress

1   Introduction

Ultra high strength concrete is characterized by a very homogeneous composition. Due to the application of highly efficient superplasticizers a reduction of the water-binder-ratio is possible. The achievable strength and the modified composition of the UHSC lead to different properties compared to conventional concrete. A brittle behaviour at failure is caused by the limited working capacity. Furthermore, the tensile strength increases under-proportionally with the compressive strength [1]. These mentioned bearing and failure properties should be investigated before the application of UHSC in practice, so also the state of concentrated loading. Existing design rules, which were established for normal and high strength concrete, must be verified for UHSC.

2   State of Concentrated Loading

Concentrated loads occur in the end zone of prestressed concrete members as well as under bridge supports and in the junction of column and ceiling. Thereby only a part of the available cross section is loaded and this affects stress concentration in the structural member.
For normal and high strength concrete the bearable concentrated load F_{Rdu} is calculated with equation (1) according to the German standard DIN 1045-1 [2].

$$F_{Rdu} = A_{c0} \cdot f_{cd} \cdot \sqrt{A_{c1}/A_{c0}} \leq 3{,}0 \cdot f_{cd} \cdot A_{c0} \qquad (1)$$

with

f_{cd} design value of concrete compressive strength

A_{c0} loaded area

A_{c1} arithmetical distribution area

Furthermore, the compliance with some geometrical agreements according to Figure 1 is required for the design of the concentrated load.

$$h \geq d_2 - d_1$$
$$h \geq b_2 - b_1$$
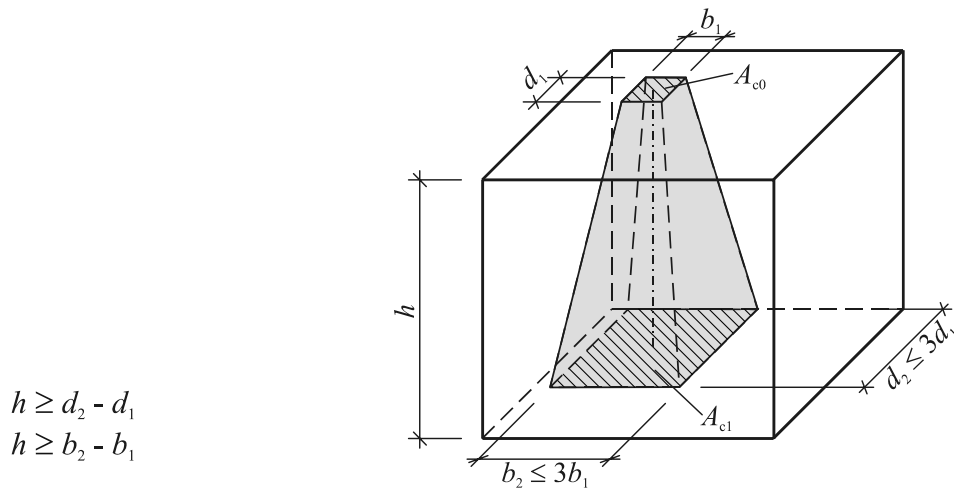
Figure 1:   Geometrical requirements according to DIN 1045-1 [2]

The transversal tensile force Z due to the concentrated loading can be approximately determined from equation (2) using a strut and tie model for simplified representation (Figure 2).

$$Z = 0{,}25 \cdot F_{Rdu} \cdot \left(1 - \frac{a}{b}\right) \qquad (2)$$

with

F_{Rdu} bearable concentrated load

a dimension of the loaded area

b dimension of the structural member.
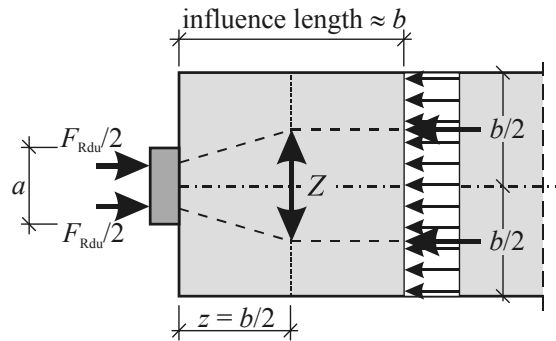
Figure 2:   Strut and tie model

Transversal tensile stresses due to the concentrated loading lead to splitting forces in the concrete member. These forces must be absorbed with suitable reinforcement, whereby stirrups or helical reinforcement are mainly in use. It is also possible to apply steel fibres as confined reinforcement ([3], [4], [5]).

3   Test Programme

3.1   Building Material

In order to take into account the concrete composition 2 different ultra high strength concretes were investigated. UHSC 1 was a classical reactive powder concrete (RPC) and for UHSC 2 crushed aggregates (maximum grain size 5 mm) were applied, both with a target compressive strength of 150 N/mm². A high strength concrete (HSC) was used for comparison and for classificationTable 1.

Table 1:   Concrete mix compositions

		UHSC 1	UHSC 2	HSC
Sand 0/2 mm		-	-	2.42
Crushed aggregates 2/5 mm		-	2.06	0.49
Crushed aggregates 5/8 mm		-	-	2.15
Quartz sand (0.3 – 0.8)		1.53	0.88	-
Cement CEM I 42.5 R	Content of cement (mass-%)	1.00	1.00	1.00
Fly ash		-	-	0.27
Silica fume		0.30	0.18	-
Quartz powder		0.43	0.54	-
Water		0.25	0.27	0.52
Superplasticizer		0.03	0.04	0.02

The specimens were made of plain as well as reinforced concrete whereby a helical reinforcement and longitudinal rebars were used. The helical reinforcement had a diameter of 8 mm and a pitch of 42 mm. The diameter of the main reinforcing bars was 12 mm.

3.2 Specimens and Test Set-up

For the determination of the bearable concentrated load 2 different specimens height were applied, whereby dimensions of 200 × 200 × 400 mm³ and 200 × 200 × 200 mm³ were chosen (Figure 3). In order to apply the stress on the specimens, cylindrical loading stamps with diameters of 30 and 50 mm were used.

The stamp push-in and the transversal strain were determined as deformation of the specimens due to the loading. For these purposes 2 vertically arranged LVDT´s measured the stamp push-in and 4 circumferential horizontal LVDT´s detected the initial cracking development mainly by the reinforced specimens. The tests were performed in a hydraulic testing machine with a path-controlled load increase.
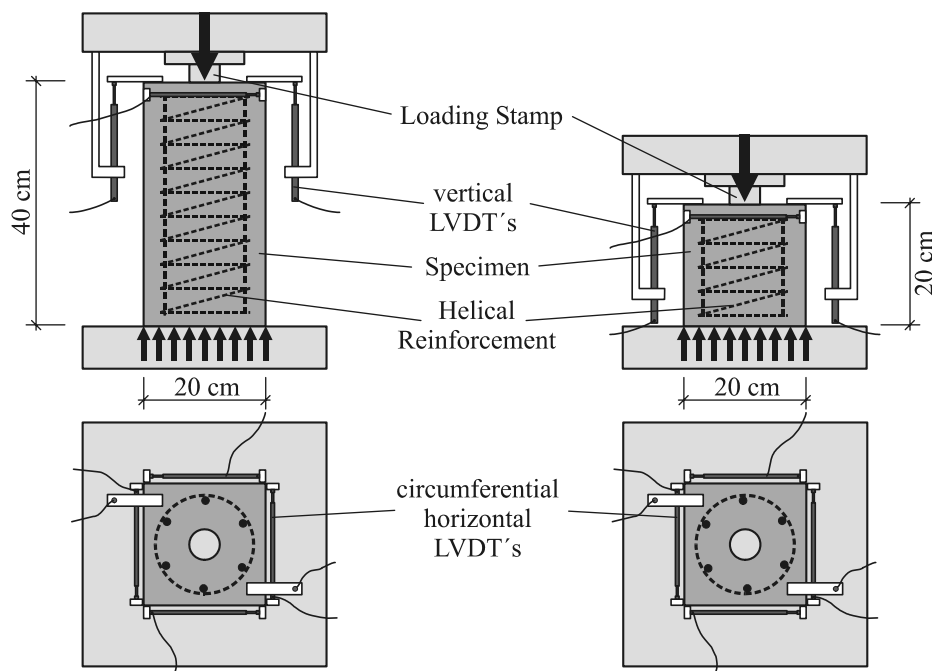
Figure 3: Specimens in the test set-up

4 Test Results

4.1 Hardened Concrete Properties

Because of the available testing machines, the concrete properties (Table 2) were determined using cubes with 100 mm edge length and cylinders ∅100/200 mm according to DIN 12390 [6]. All specimens were cured under water until the tests.

Table 2: Hardened concrete properties (after 28 days)

		UHSC 1	UHSC 2	HSC
cylinder compressive strength $f_{c,cyl}$		147	144	62
cube compressive strength $f_{c,cube}$	N/mm²	148	144	66
splitting tensile strength $f_{ct,sp}$		12.2	10.9	5.1
modulus of elasticity E_c		47,100	52,900	33,300

4.2 Concentrated Loading

4.2.1 Plain Concrete

Due to the mentioned transversal tensile stresses the specimens made of plain concrete failed by splitting. Depending on the dimension of the applied loading area 2 different kinds of splitting appeared. The specimens loaded with the small loading area ($\varnothing$ 30 mm) split up abruptly at failure (Figure 4). In contrast a loading core was formed (Figure 5) caused by the large loading area ($\varnothing$ 50 mm). After the drop of the load the specimens could bear up a small part of the load. In both cases a concrete wedge was shaped under the loading stamp (Figure 6), which was visible after the test.
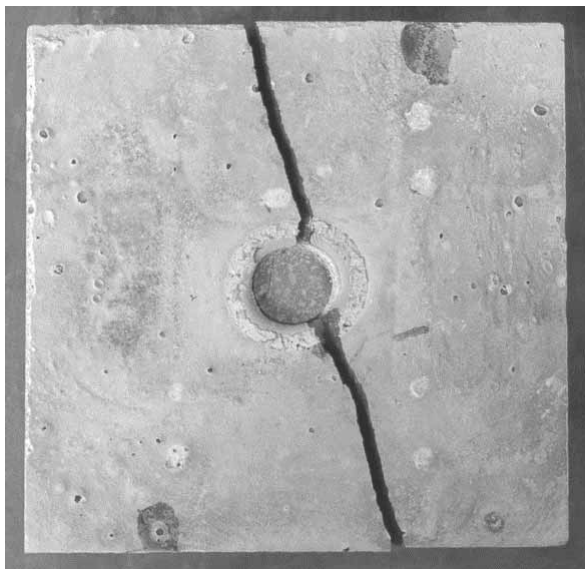
Figure 4:   Splitting up of the specimens   Figure 5:   Loading cone

Figure 6:   Concrete wedge under the loading area

4.2.2 Reinforced Concrete

The confinement due to the reinforcement led to several radial cracks with a homogenous distribution starting from the loading area (Figure 7). From this radial cracks longitudinal ones developed over the height of the specimens. The above-mentioned strut and tie model and accordingly its effect were visible with a cascaded shape between the windings of the helical reinforcement (Figure 8). Thereby the concrete compressive struts were formed between the loading area and the several windings of the reinforcement. The tensile stresses of the tie were absorbed by the helical reinforcement.
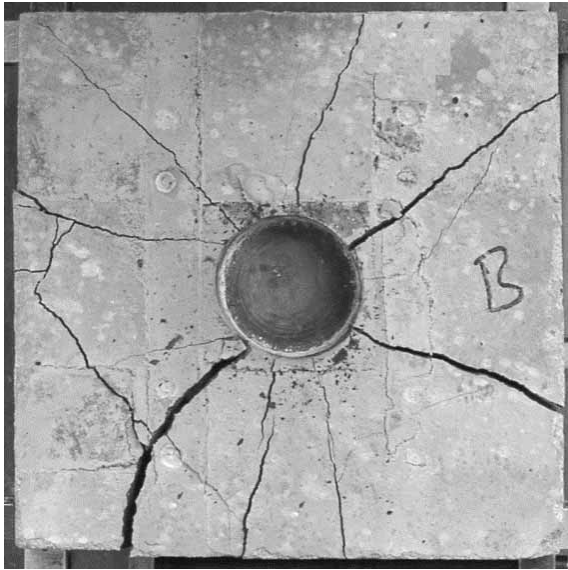
Figure 7:   Radial cracks
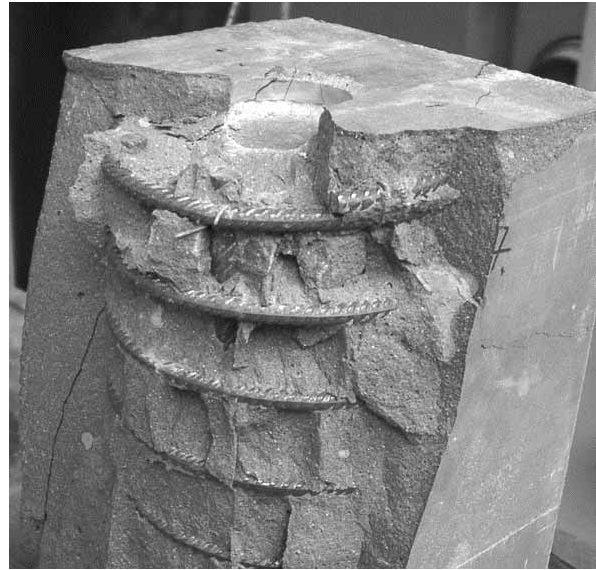
Figure 8:   Confinement effect of the reinforcement

4.2.3 Comparison between Plain and Reinforced Concrete

The applied helical reinforcement affected a more ductile behaviour at failure compared to the plain concrete. Furthermore there was an extended load increase after the crack development, which was detected with the horizontally arranged LVDT´s. This higher load level was obtained because of the confinement of the reinforcement, which also hampered the splitting of the concrete. The load level of the initial crack development and the ascending branch of the curve are very similar for the plain and reinforced concrete (Figure 9). The represented stress–stamp push-in–relationships of the loading area run approximately proportional before the initial crack development.
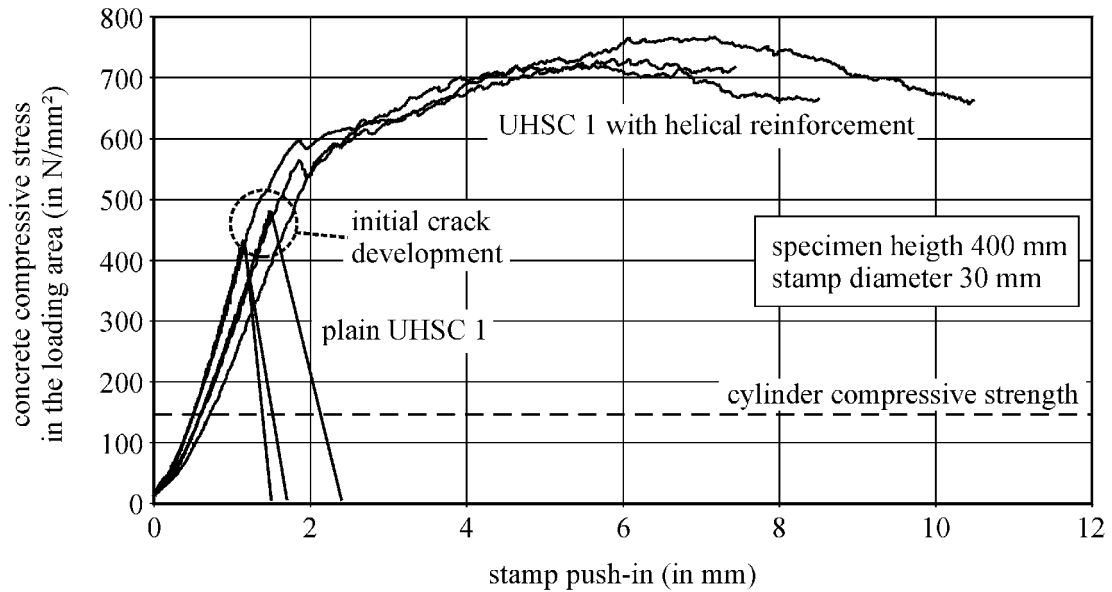
Figure 9: Comparison between plain and reinforced concrete

Even for plain concrete the achievable stresses could exceed the corresponding cylinder concrete compressive strength. The surrounding concrete as well as the applied reinforcement obstruct the transversal strain. Whereby the helical reinforcement had no visible influence on the initial crack load and on the stiffness of the specimens before cracking (Figure 9).

Figure 10 shows the effect of the diameter of the loading stamp. The bearable concentrated stresses increase with a reduction of the loading area. These higher values are possible due to the increased obstruction of the transversal strain through the surrounding concrete.
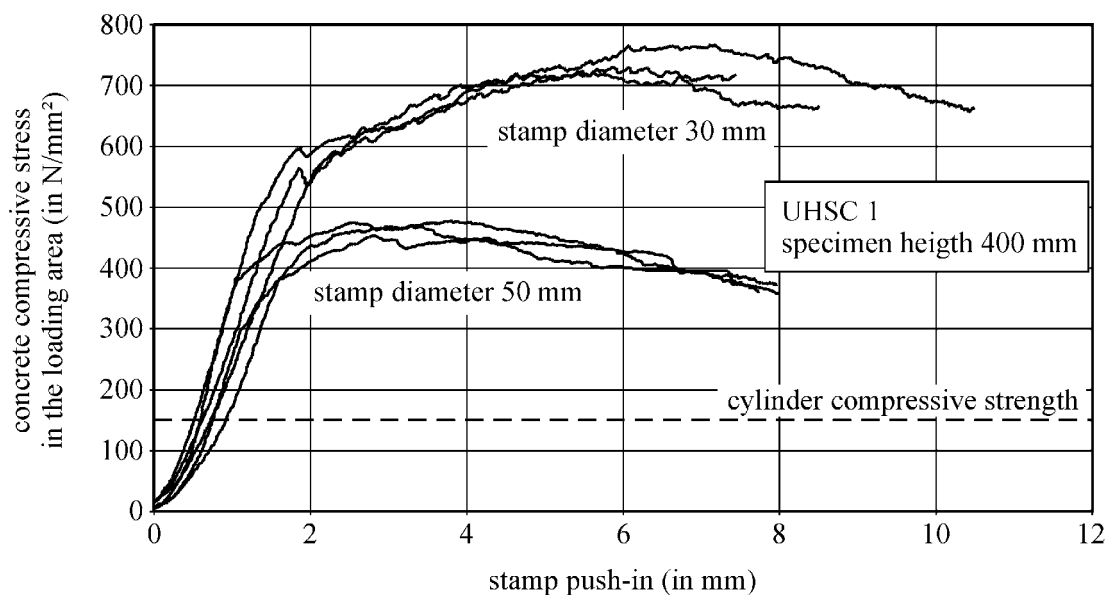
Figure 10: Effect of the stamp diameter

The influence of the concrete compressive strength on the concentrated load is obvious (Figure 11). The achieved stiffness of the high strength concrete (HSC) was lower compared to UHSC, due to the lower modulus of elasticity .
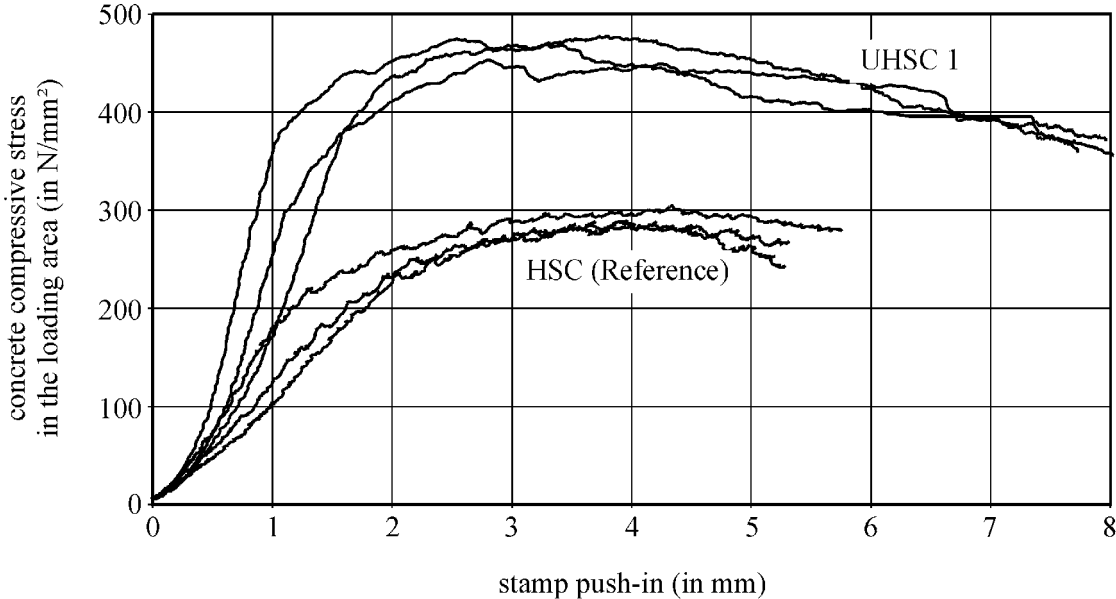
Figure 11: Comparison between HSC and UHSC

The applied HSC presented a higher concentrated load referring to the compressive strength (ratio σ_{c0} / $f_{c,cyl}$ in Table 3). The dependence of the concentrated load on the tensile strength, which increases under-proportionally with the compressive strength [1], leads to lower values for UHSC.

Table 3 shows the results of the implemented test programme. The value σ_{c0} is the achieved concentrated stress in the loading area complied for all investigated test parameters.

Table 3: Test results (average of 3 single tests)

	Diameter of loading stamp	Height of specimen		Stress in the loading area	
				Plain	Reinforced
UHSC 1	30 mm	200 mm	stress σ_{c0}	501.3 N/mm²	751.9 N/mm²
			σ_{c0} / $f_{c,cyl}$	3.7	5.5
		400 mm	stress σ_{c0}	447.3 N/mm²	758.5 N/mm²
			σ_{c0} / $f_{c,cyl}$	2.9	4.9
	50 mm	200 mm	stress σ_{c0}	303.7 N/mm²	445.2 N/mm²
			σ_{c0} / $f_{c,cyl}$	2.0	3.0
		400 mm	stress σ_{c0}	288.1 N/mm²	475.4 N/mm²
			σ_{c0} / $f_{c,cyl}$	2.0	3.3
UHSC 2	50 mm	400 mm	stress σ_{c0}	322.6 N/mm²	494.6 N/mm²
			σ_{c0} / $f_{c,cyl}$	2.2	3.4
HSC	50 mm	400 mm	stress σ_{c0}	158.0 N/mm²	303.9 N/mm²
			σ_{c0} / $f_{c,cyl}$	2.5	4.9

5   Conclusions and Outlook

The German standard DIN 1045-1 [2] specifies an equation for concentrated loading, which is established for normal and high strength concrete. Reinhardt and Koch recommended the application of a reduction factor of 0.8 for the bearable concentrated load F_{Rdu} according to equation (1) based on former investigations with high strength concrete under concentrated loading [7]. This factor takes into account the mentioned under-proportional increase of the tensile strength compared to the compressive strength.

The own test results of the applied concrete with crushed rock as part of the aggregates (UHSC 2 and HSC), approximately agree with an extrapolation of this mentioned approach. Thereby the UHSC 2 reached slightly lower values, so that the factor would have to be chosen to about 0.75. UHSC 1 (reactive powder concrete - RPC) shows definite lower values, which could be ascribed to the lower influence of aggregate interlock because of the fine grained concrete matrix.

Figure 12 represents a comparison between the design rule according to DIN 1045-1, the design recommendation after [7] and own test results of the unreinforced specimens using the large loading area ($\varnothing$ 50 mm).
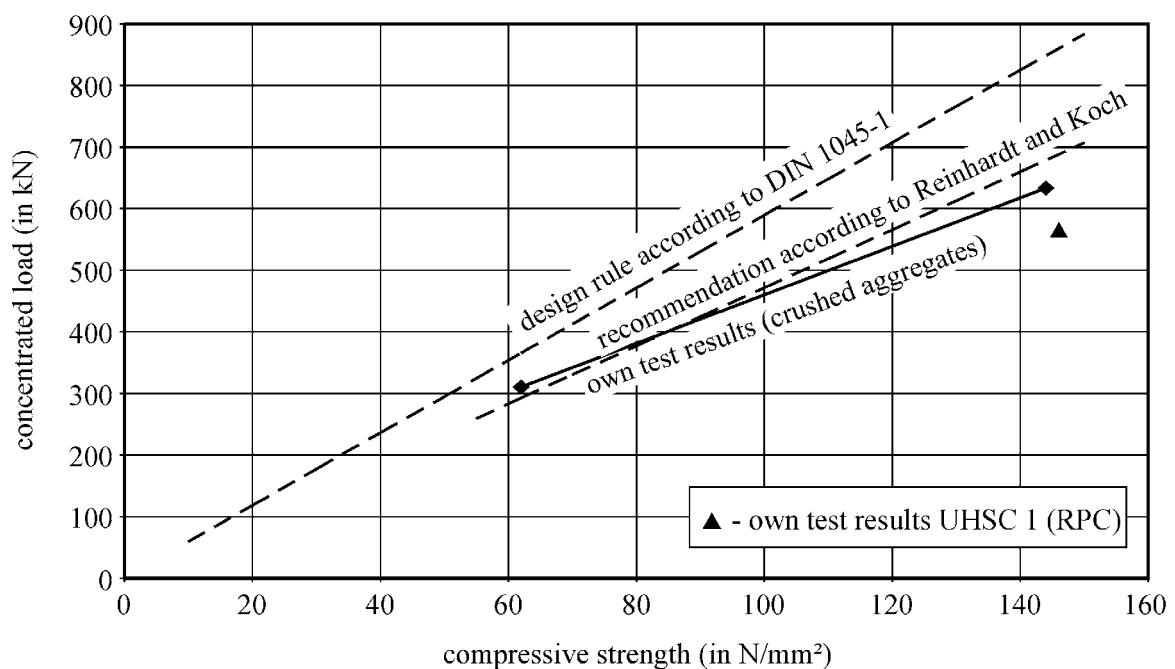
Figure 12: Comparison between the design rule according to DIN 1045-1, the
            recommendation of Reinhardt and Koch [7] and the own test results

The implemented test programme shows, that the performance of the UHSC under concentrated load is influenced by the concrete matrix and the used aggregates (see the results of UHSC 1). Due to this fact and the mentioned dependence of the tensile strength, it

is not recommended to apply the design rule according to DIN 1045-1 for UHSC without a modification. The recommendation of Reinhardt and Koch with the reduction factor of 0.8 shows a possible solution, but a final determination demands further tests.

The transversal tensile forces due to concentrated load are mainly absorbed through stirrups and helical reinforcement. During the implemented tests the concrete cover spalled in the range of the maximum load, which also appeared during a similar investigation with high strength concrete [3]. A reasonable alternative to the conventional reinforcement is the application of steel fibres as complete or partial replacement. Fibres are also existing and effective respectively in the near-to-surface zone and in the statically ineffective concrete cover of structural members.

The implemented test programme and the described results can be regarded as pre-tests because of the limited number of single tests per series. The influence of the concrete composition on the behaviour under concentrated load will be investigated in further tests. The aim is a design recommendation for this state of loading using UHSC. For the clarification of the influence of fibres on the load bearing behaviour different contents of fibres also in combination with helical reinforcement will be applied.

6   References

[1]   Weiße, D.; Ma, J.: Mechanical Properties of Ultra High Strength Concrete. Leipzig Annual Civil Engineering Report 8 (2003), pp. 175 - 184.

[2]   DIN 1045-1: Tragwerke aus Beton, Stahlbeton und Spannbeton: Bemessung und Konstruktion. (Concrete, reinforced and prestressed concrete structures: Design). 2001, (in German).

[3]   Boulay, C.: Experimental study on reinforced VHSC prism under concentrated loading. Proceedings of the 6th International Symposium on High Strength/High Performance Concrete, Leipzig 2002, pp. 177 - 192.

[4]   Yazdani, N.; Spainhour, L.; Haroon, S.: Application of Fiber Reinforced Concrete in the End Zone of Precast Prestressed Bridge Girders. Technical Report of the Florida Department of Transportation. Florida A & M University – Florida State University, College of Civil Engineering, 2002.

[5]   Bétons fibrés à ultra-hautes performances (Ultra High Performance Fibre-Reinforced Concrete). Association Française de Génie Civil, 2002.

[6]   DIN EN 12390-1: Prüfung von Festbeton: Form, Maße und andere Anforderungen für Probekörper und Formen. (Testing hardened concrete: Shape, dimensions and other requirements for specimens and moulds). 2001, (in German).

[7]   Reinhardt, H.-W.; Koch, R.: Hochfester Beton unter Teilflächenbelastung. (High strength concrete under concentrated loading). (in German), Beton- und Stahlbetonbau 93 (1998), No. 7, pp. 182 - 188.

Tobias Stiel
Dipl.-Ing., Student
Universität Kassel / Cardiff University
Kassel, Germany / Cardiff, UK

Bhushan L. Karihaloo
Professor
Cardiff University
Cardiff, UK

Ekkehard Fehling
Professor
Universität Kassel
Kassel, Germany

Effect of Casting Direction on the Mechanical Properties of CARDIFRC[®]

Summary

The orientation of the small steel fibres plays a crucial part in their effectiveness in fibre-reinforced concrete. In this study tests were performed to investigate the effect of fibre orientation and any unintentional grading over the specimen size of CARDIFRC[®] on its mechanical properties. CARDIFRC[®] is an UHPC reinforced with steel fibres of two different lengths and a compressive strength of about 200 MPa. Beams were cast horizontally and vertically and tested in three-point bending. In addition, two 1 m tall slabs were cast and sawn into cubes. The cube splitting strength, compressive strength and Young's modulus were determined by varying the loading direction and the location of the cube in the slab. It was found that the mechanical properties of vertically-cast beams are up to five times lower than for horizontally-cast beams, caused by the alignment of fibres along layers normal to the casting direction. For the slab, however, the fibres were found not to be aligned along layers normal to the casting direction. [1]

Keywords: *fibre orientation, fracture energy, flexural strength, splitting strength,* CARDIFRC[®]

1   Introduction

1.1   CARDIFRC[®]

CARDIFRC[®] is a class of materials which generally contains no coarse aggregates and is characterised by both high strength and high toughness. The design of CARDIFRC[®] followed rigorous optimisation strategies to balance the intrinsic competition between tensile/flexural strength and ductility, in contrast to the traditionally applied trial and error procedure.

The constitutive behaviour of CARDIFRC[®] was modelled by Karihaloo and co-workers using micromechanical principles to identify the mechanisms responsible for the mechanical behaviour and to relate the mix variables (water-to-binder ratio w/b, maximum size of coarse aggregate g, volume fraction of aggregate V_a, superplasticiser to water ratio sp/w, fibre length L, fibre diameter d and fibre volume fraction V_f) to the measurable mechanical

properties (modulus of elasticity E, tensile/flexural strength f_t, compressive strength f_c and the fracture energy G_F) [2]. Mathematical optimisation strategies were used for the development of the mix, where the constitutive equations appeared as constraints.

The most important steps necessary for the manufacture of CARDIFRC[®] were patented (GB 0109686.6) and the class of materials produced in that way were registered under the trademark CARDIFRC[®]. The maximisation of the dry density through optimisation and the even and random distribution of short steel fibres are the two most important steps.

Details of the constitution of CARDIFRC[®] mix I and II are given in Table 1.

Table 1: Mix constituents of CARDIFRC[®] mix I and II for 1 m[3] [1]

		CARDIFRC[®] mix proportions	
Constituents	**Unit**	**mix I**	**mix II**
Portland Cement 42,5 N	[kg/m^3]	855	744
Microsilica	[kg/m^3]	214	178
Quartz Sand 9-300 μm	[kg/m^3]	470	166
Quartz Sand 250-600 μm	[kg/m^3]	470	-
Quartz Sand 212-1000 μm	[kg/m^3]	-	335
Quartz Sand 1-2 mm	[kg/m^3]	-	672
Steel fibres 6 mm	[kg/m^3]	390 (5 vol.-%)	351 (4.5 vol.-%)
Steel fibres 13 mm	[kg/m^3]	78 (1 vol.-%)	117 (1.5 vol.-%)
Water	[kg/m^3]	188	149
Superplasticiser	[kg/m^3]	34	55
Water/cement	[-]	0.22	0.20
Water/binder	[-]	0.18	0.16
Superplasticiser/water	[-]	0.18	0.18

The following mixing procedure was developed for CARDIFRC[®]. First, the coarsest constituent is mixed with the finest (microsilica). Next, the second coarsest aggregate is added and mixed, then the second finest and so on. This ensures that each addition was well spread over the dry mix and lumping is avoided – microsilica in particular tends to lump. In previous studies [3, 4] it has been observed that microsilica was not always uniformly distributed. The procedure described above allows this problem to be overcome. The short steel fibres are added to the dry constituents through vibrating apertured surfaces, in order to ensure that the fibres do not clump together, but fall into the rotating mixer in an even manner so they are distributed randomly in the dry mix.

The use of two fibre lengths is a consequence of the constitutive modelling, which shows that short fibres are necessary for increasing the tensile/flexural strength, whilst long fibres increase the toughness. The use of superplasticiser enables a good workability of the mixes.

The fibre distribution was checked by using computerised tomography (CT) imaging technique and it was found that the fibres are generally uniformly distributed in CARDIFRC[®], irrespective of the shape of the specimen [4].

1.2   Fracture Energy of Concrete

The specific fracture energy G_F is one of the most important material parameters in the analysis of cracked concrete structures [5]. In the well-received fictitious crack model, the strain-softening concept of concrete under tension is introduced with G_F being equal to the area under the cohesive stress–crack-opening softening curve.

According to the RILEM recommendations [6], the specific fracture energy G_f is the average energy given by dividing the total work of fracture by the initially uncracked area. Therefore, for a initially notched specimen, the fracture energy is given by

$$G_F = \frac{1}{(W-a)B} \int P d\delta \tag{1}$$

where B is the specimen thickness, W is the depth, a is the notch length, P is the applied load and δ is the displacement of the load point.

The fracture energy determined in three-point bend tests is size-dependent, i.e. an increase of fracture energy is measured with increasing beam size [7].

Following Hu and Wittmann [8], G_f is used exclusively for the size-dependent fracture energy and G_F is used for the size-independent fracture energy in this study. G_F is the asymptotic value of G_f when the specimen size is very large.

As stated in the fictitious crack model (FCM), ahead of a traction-free crack there is a damage zone or fracture process zone (FPZ) where cohesive or bridging stresses are transferred and energy is dissipated. Therefore, the FPZ is directly related to the fracture energy G_f. Any size effect in G_f must be related to some variation in the FPZ, either its length or width [8].

Duan et al. [9] developed a boundary effect model, which takes into account the effect of the FPZ. They assumed a bilinear distribution of the fracture energy along the uncracked ligament and derived the following relationship between size-dependent fracture energy G_f and size-independent G_F

$$G_f \left(\frac{a}{W} \right) = \begin{cases} G_F \left[1 - \frac{1}{2} \cdot \frac{a_l/W}{1-a/W} \right] & 1-a/W > a_l/W \\ G_F \frac{1}{2} \cdot \frac{(1-a/W)}{a_l/W} & 1-a/W \le a_l/W \end{cases} \tag{2}$$

where a is the notch depth, W the depth of the beam and al the transition ligament size, which gives the distance from the backface of the specimen to the point where the fracture energy starts to decrease from the value G_F to zero. Using this equation the size-independent fracture energy can be determined from three-point bend tests of beams with several different notch-to-depth ratios. Abdalla and Karihaloo [10] verified this equation and found that G_F can also be determined by testing only two beams, providing their notch-to-depth ratios are well separated. They recommended notch-to-depth ratios of 0.05 and 0.5 for three-point bend specimens. This procedure was used in this study.

1.3   Fibre Orientation

Fibres are used for different reasons in concrete structures. In ordinary fibre-reinforced concrete, the fibres are basically used for crack control. For fibre-reinforced UHPC the fibres

are used to achieve a ductile response and the tensile strength is improved by the very good bonding between fibres and matrix.

The efficiency of fibres in concrete depends, among other things, on their orientation relative to the direction of stress. Therefore, the orientation of fibres has a significant influence on the bridging action and on the mechanical properties of fibre-reinforced concrete. If the fibres are randomly distributed, the strength and fracture energy are expected to be isotropic; but if the fibres are aligned, the mechanical properties can vary significantly along different axes of a structural member.

Investigations on conventional fibre-reinforced concrete have shown a significant effect of the casting direction on the fibre orientation [11-14]. It was found that the fibres try to align perpendicular to the casting direction. This effect increased significantly with increasing workability of the mix [14].

Stiel and Pfeiffer [3] performed bending and tension tests on two ultra-high performance concrete mixes, a powder mix (M1Q) and a mix containing also coarse aggregate (B3Q). The mix M1Q was also tested with 1.5 vol.-%. They tested beams (150/150/700 mm) in four-point bending, prisms (40/40/160 mm) in three-point bending and notched prisms (40/40/160 mm, 2 x 1 mm notch) in uniaxial tension with pinned ends. All tests were performed for both horizontally- and vertically-cast specimens. The specimens were compacted through vibrating.

The results of their investigation are summarised in Table 2. Their findings showed a strong effect of casting direction on both the flexural/tensile strength and the fracture energy. For the coarser B3Q mix the effect of casting direction was only noticed in the small prisms, but not in the beams.

Table 2:   Test results of Stiel and Pfeiffer [3] for fibre reinforced UHPC

Beams bending	Flexural strength [MPa]		Size-dependent fracture energy [N/m]	
	vertically cast	horizontally cast	vertically cast	horizontally cast
M1Q-2,5%	17.58	22.11	14543	20355
M1Q-1,5%	10.07	17.72	9726	18006
M1Q-0%	7.24	7.17	–	–
B3Q-2,5%	22.75	21.98	16064	16465
Prism bending	Flexural strength [MPa]		Size-dependent fracture energy [N/m]	
	vertically cast	horizontally cast	vertically cast	horizontally cast
M1Q-2,5%	22.51	30.03	15097	21280
M1Q-1,5%	22.47	30.87	15120	23577
M1Q-0%	14.48	13.93	–	–
B3Q-2,5%	15.15	24.25	4864	16247
Prism tension	Tensile strength [MPa]		Size-dependent fracture energy [N/m]	
	vertically cast	horizontally cast	vertically cast	horizontally cast
M1Q-2,5%	7.86	12.59	9993	17084
M1Q-1,5%	7.93	9.68	8980	14578
M1Q-0%	7.27	7.86	–	–
B3Q-2,5%	–	11.57	–	14121

2 Experimental Procedures

2.1 Objective

The experimental investigations had two main objectives: To study 1. the influence of the casting direction on the mechanical properties, namely the specific fracture energy G_F, the flexural strength f_{cf}, the splitting cube strength f_{spl}, the compressive strength f_c and Young's modulus E of CARDIFRC® and 2. the variation over the height, i.e. unintentional grading, of the splitting cube strength f_{spl}, the compressive strength f_c and Young's modulus E of CARDIFRC® of cubes cut from a large vertically-cast slab.

The mixing procedure was as explained above. The moulds were filled in thin layers and compacted with a vibrating table, which did not allow the orientation of the fibres to be affected by magnetism. Each layer was vibrated at a frequency of 70 Hz. The specimens were cured at 90°C in a water tank for seven days.

2.2 Three-point bend tests

The tensile response and the size-independent specific fracture energy G_F were determined in three-point bend tests on notched beams with a span to depth ratio of 4. The beam shape, dimensions and the direction of casting are shown in Figure 1.
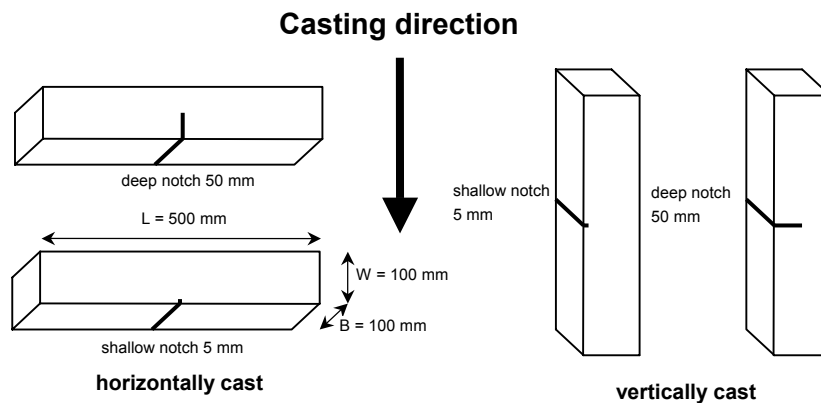
Figure 1: Casting direction, shape and dimensions of the beams for the three-point bend tests[1]

According to the method developed by Karihaloo et al. [15], the true specific fracture energy G_F can be determined from TPB-tests on beams with a central edge notch and only two different notch-to-depth ratios, provided that these ratios are well separated. Consequently, the notch-to-depth ratios $\alpha = 0.5$ and $\alpha = 0.05$ were chosen. Thus, 5 and 50 mm deep notches were introduced centrally with a diamond saw. The beams were tested in three-point bending with a closed loop servo hydraulic testing machine. The tests were performed under displacement controlled using an LVDT with a slow rate of 0.002 mm/sec.

2.3 Cube tests

As one of the objectives was to investigate the variation over the specimen size, a large specimen (a slab) was cast and sawn into cubes. The cutting arrangement, loading and casting direction is shown in Figure 2. Splitting (Brazilian test), compression and static

modulus of elasticity tests were performed on the cubes to determine the indirect tensile strength, compressive strength and Young's modulus.

The loading alignment of the splitting cubes was chosen as shown in Figure 2. Although the loading direction was varied between horizontal and vertical, the crack plane was the same. That was done in order to obtain a crack surface straight through the whole slab and thus a view into the CARDIFRC® specimen.
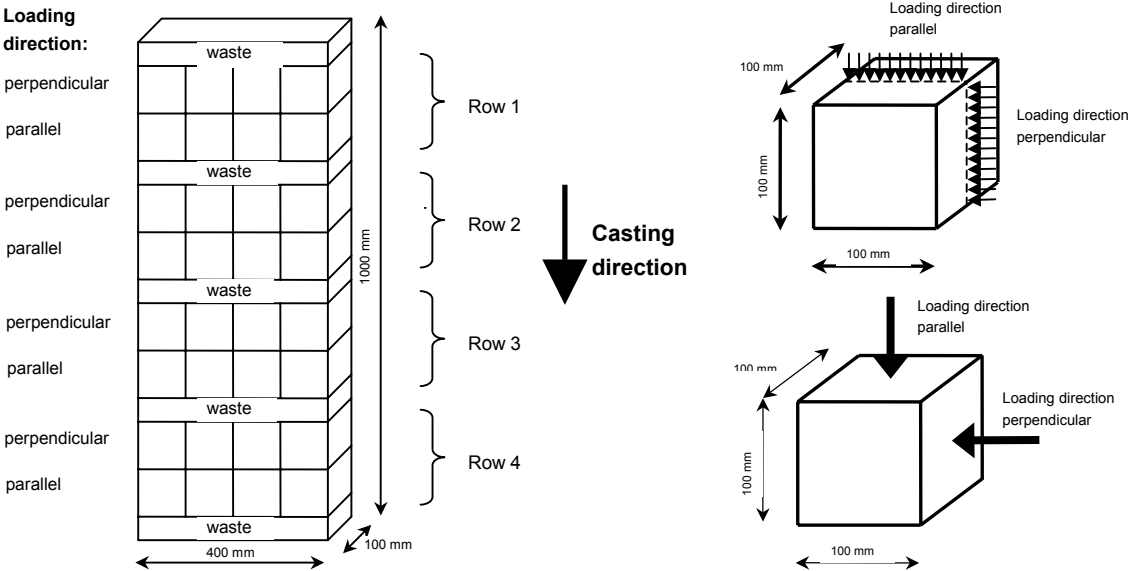
Figure 2:   Cutting arrangement, casting and loading direction of the test cubes [1]

For comparison, eight cubes were sawn from the halves of the beams previously tested in three-point bending and tested in splitting. Four cubes were sawn from the vertically-cast beams and four from the horizontally-cast. The loading arrangement was chosen in such a way that the failure plane was perpendicular to the casting direction. When the splitting test was finished, the cubes were broken in halves and assembled in the same order in which they were cast to obtain an overview of the fibre orientation over the whole specimen.

3   Results

3.1   Three-point bend tests

Table 3 summarises the results of the three-point bend beam tests: load P, flexural strength f_{cf}, size-dependent fracture $G_f (\alpha)$ with their standard deviation; size-independent fracture energy G_F and transition ligament length a_l. The data is distinguished by the casting direction and the notch-to-depth ratio α.

The influence of casting direction is clearly visible in the averaged P-δ curves (Figure 3) for both notch-to-depth ratios.

Table 3:   Results of the three-point bend tests [1]

Number of beams	Casting direction	α	Mean P [kN]	Mean f_{cf} [MPa]	Std. dev. [MPa]	Mean $G_f(\alpha)$	Std. dev. [N/m]	G_F [N/m]	a_l [mm]
6	Horizontal	0.05	58.4	38.4	9.3	25443	8004		
8	Horizontal	0.50	21.0	49.6	7.3	27396	5565	29708	27.4
2	Vertical	0.05	19.8	12.9	1.1	5324	1028		
8	Vertical	0.50	5.2	11.7	4.3	5371	1618	6325	30.2

Beams with a shallow notch (= 0.05)

Beams with a deep notch (= 0.5)
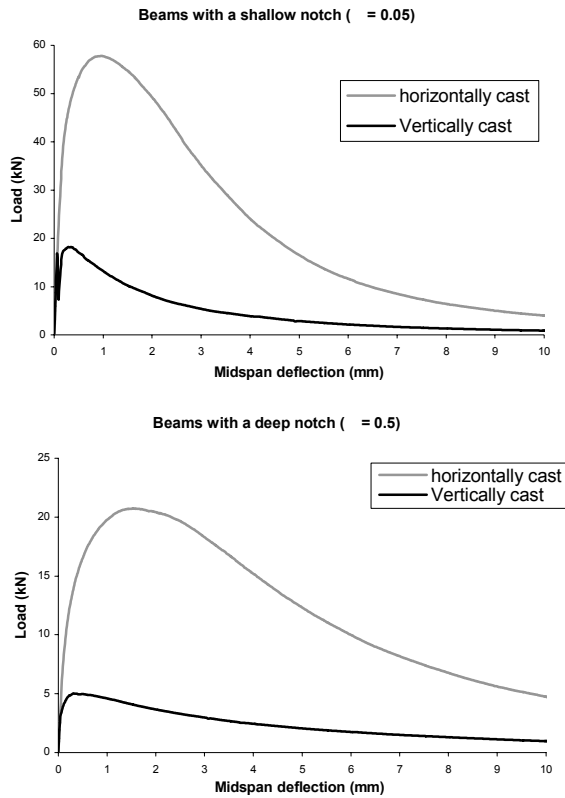
Figure 3:   Comparison of the vertically and horizontally cast beams by averaged P-δ curves [1]

Beams with a shallow notch (= 0.05)

Beams with a deep notch (= 0.5)
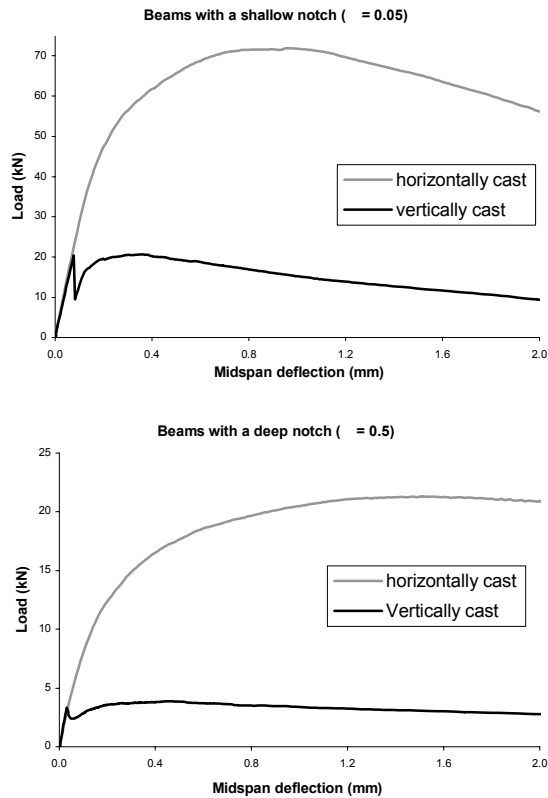
Figure 4:   Illustration of the diverse behaviour in the pre-peak section of horizontally and vertically cast beams exemplified by four characteristic test results for both notch-to-depth ratios [1]

The difference in the behaviour and the shape of the $P\text{-}\delta$ curves in the pre-peak section is seen in Figure 4. The diagrams show the peak load and the shape. The slope at the beginning of the curve is almost the same, but at a specific load level, the curve of the vertically-cast beams drops abruptly, whereas that of the horizontally-cast beams continues to rise. The slope of the latter decreases gradually to zero until the peak is reached. However, after the drop, the curve of the vertically-cast beams also continues to rise to its peak, although the peak is no higher than the load at the instant of drop.

The steel fibres of CARDIFRC$^{®}$ were orientated perpendicular to casting direction. Figure 5 shows the different orientations of the steel fibres in the crack surface. For the horizontally-cast beams the fibres were mostly orientated normal to the crack surface and therefore poked out of the concrete matrix (Figure 5(a)). The fibres of the vertically-cast specimens were orientated in layers parallel to the crack surface and protruded only slightly from the matrix (Figure 5(b)). Moreover, the crack surface of the vertically-cast beams was more or less smooth, whereas that of the horizontally-cast beams was rough and craggy.
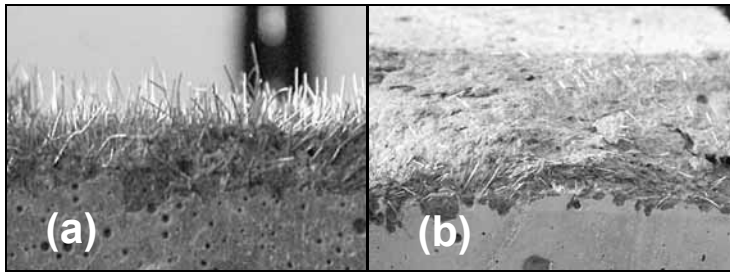
Figure 5: Illustration of the different fibre alignments in the crack surfaces for (a) horizontally and (b) vertically cast beams [1]

3.2 Cube tests

Table 4: Mean of cube splitting strength of the sawn cubes, shown in terms of different cube locations from top to bottom (1 to 4) and loading direction, perpendicular and parallel with respect to the casting direction [1]

Cube location, Row	Number of cubes	Loading direction	Mean Load P [kN]	Mean f_{spl} [MPa]	Std. dev. (COV) [MPa]
1	4	perpendicular	290	19.3	2.04 (10.6%)
1	4	parallel	288	19.4	2.35 (12.1%)
2	4	perpendicular	303	20.4	3.35 (16.4%)
2	4	parallel	303	20.0	4.43 (22.2%)
3	4	perpendicular	316	20.4	2.39 (11.7%)
3	4	parallel	282	18.3	1.46 (8.0%)
4	4	perpendicular	316	20.4	2.00 (9.8%)
4	4	parallel	349	22.5	3.15 (14.0%)
Mean	32	perp./parall.	306	20.1	2.71 (13.5%)

The results of the splitting test on the cubes are summarised in Table 4. The cube location from top to bottom is represented by the numbers 1 to 4. Besides the loading direction, the mean of the maximum load P and the mean of the corresponding compressive strength f_c with its standard deviation are shown for each row.

No regularity could be identified in the fibre orientation in the fracture surface of the specimens. In other words the fibres were not aligned in any one specific direction; however they were also not always randomly orientated in all directions. The most likely orientation that occurred was a vertical alignment of the fibres.

The average results for the eight cubes sawn from the beams are shown in Table 5. The values for the horizontally-cast specimens were significantly higher than for the vertically-cast ones.

Table 5:   Mean of cube splitting strength of the sawn cubes, shown in terms of casting direction

Cube	Number of cubes	Loading direction	Mean Load P [kN]	Mean f_{spl} [MPa]	Std. dev. (COV) [MPa]
Sawn from horizontally cast beams	4	parallel	400	25.36	2.09 (10.8%)
Sawn from vertically cast beams	4	perpendicular	307	19.27	2.13 (8.4%)

The results of the compression tests of the cubes are summarised in Table 6. The cube location from top to bottom is represented by the numbers 1 to 4. Besides the loading direction, the mean of the maximum load P and the mean of the corresponding compressive strength f_c with its standard deviation are shown for each row.

Table 6:   Mean of cube compressive strength of the sawn cubes, shown in terms of different cube locations from top to bottom (1 to 4) and loading direction, perpendicular and parallel with respect to the casting direction [1]

Cube location, Row	Number of cubes	Loading direction	Mean Load P [kN]	Mean f_c [MPa]	Std. dev. (COV) [MPa]
1	4	perpendicular	1973	192.3	11.76 (6.1%)
1	4	parallel	1907	193.4	10.62 (5.5%)
2	4	perpendicular	2019	197.4	12.72 (6.4%)
2	4	parallel	1867	184.8	6.46 (3.5%)
3	4	perpendicular	1904	185.1	9.48 (5.1%)
3	4	parallel	1880	186.7	6.94 (3.7%)
4	4	perpendicular	1866	181.6	18.47 (10.2%)
4	4	parallel	1918	188.8	9.81 (5.2%)
Mean	32	perp./parall.	1917	188.8	11.16 (5.9%)

The results of the static modulus of elasticity tests are shown in Table 7.

Table 7:   Static modulus of elasticity of the sawn cubes, distinguished by different cube locations from top to bottom (1 to 4) and loading direction, perpendicular and parallel with respect to the casting direction [6]

Cube location	Loading direction	Static modulus of elasticity E [MPa]
1	Perpendicular	45372
1	Parallel	44060
2	Perpendicular	45301
2	Parallel	41646
3	Perpendicular	45070
3	Parallel	43203
4	Perpendicular	44864
4	Parallel	41697
Overall mean		43902
Overall std. dev. (COV)		587 (1.3%)

Statistical analyses of the results were undertaken, which indicate that neither the loading direction nor the cube location has a significant influence on the splitting cube strength, compressive strength and static modulus of elasticity.

4   Discussion

The fibre orientation was found to be influenced by the casting direction. An unintentional grading of the mechanical properties of CARDIFRC® was not detected in large vertical pours. For all the mechanical properties of CARDIFRC® investigated, namely the splitting cube strength, the compressive strength and the modulus of elasticity, no significant variation – unintentional grading – over the specimen size was identified.

Horizontally- and vertically-cast beams differed distinctly in both flexural strength and fracture energy. For horizontally-cast beams, the fibres lead to an extended strain-hardening behaviour, whereas for the vertically-cast beams no, or very slight, strain-hardening was noticed and an abrupt decrease often occurred after the matrix cracked. Fibres in the vertically-cast beams appeared to align in layers normal to the casting direction. This is supported by results from other investigations for both conventional FRC [11-14] and UHPC [3]. By way of contrast, for the 1 m tall specimen no alignment in layers normal to the casting direction was observed.

Thus, there must be other factors influencing the orientation of the fibres than the casting direction itself. It is to be surmised that the workability has an influence on the fibre orientation. The stiffer a mix is, the more difficult it is for the fibre to rotate in the mix and to align. Therefore, it can be conjectured that in a loose mix the effect of casting direction is stronger or more relevant. This tendency was also noticed by Stiel and Pfeiffer [3], who observed no fibre alignment for a coarser mix (B3Q); and Toutanji and Bayasi [14] who achieved a stronger effect of fibre alignment with increasing workability. Moreover, the

aspect ratio and the size of the specimen is likely to have an effect on the fibre orientation. Due to different inertia, the large slab and the beams experience different compaction under vibration. Furthermore, the stiffness and therefore the vibration behaviour of the moulds, namely the large mould made of wood and the small steel moulds, was very different, which could have a decisive influence on fibre orientation.

Most specimens that are tested in a Laboratory are cast horizontally and the mechanical properties of fibre reinforced concrete are determined according to these specimens. Thus, there exists a risk of overestimating the capacity of the material and of assuming mechanical properties for design that can lead to a reduced safety margin. Accordingly, investigations of the fibre orientation under similar conditions need to be undertaken before using a fibre-reinforced concrete for practical applications. To put this anisotropic material behaviour to good effect, it is recommended to arrange the compaction procedure so that the fibres are aligned in the most beneficial direction relative to the expected stress field, which means casting slender specimens horizontally.

The mean splitting strength of cubes sawn from the large slab is of the same order as that of the cubes sawn from the vertically-cast beams. This suggests that the fibres were aligned parallel to the fracture surface. That is in accordance with the mostly visually observed fibre orientation. This needs to be further verified. However, the compressive strength is not much influenced by the fibres and therefore the fibre orientation is not as important as it is for the tensile strength and fracture energy. For example, Stiel and Pfeiffer [3] found a difference of only 13% in the compressive strength between a mix (M1Q) with 2.5% fibre content and the same mix without fibres.

5 Conclusions

Tests were performed to investigate the effect of fibre orientation and the unintentional grading over the specimen size of CARDIFRC®. The following conclusions can be drawn:

1. A significant difference between horizontally- and vertically-cast beams was observed in three-point bend tests. The size-independent fracture energy for the vertically-cast beams was only 21.3% and their splitting and flexural strengths were only 23.6% and 33.6% of the corresponding values for the horizontally-cast beams.

2. The fibres in the vertically-cast beams were aligned in layers normal to the casting direction which results in a large reduction in their bridging action across crack faces.

3. The fibres in the 1 m tall slab were not aligned in layers but were orientated randomly as was revealed by placing split half cubes in the order in which they were cast.

4. No significant unintentional grading of the cube splitting strength, Young's modulus and the compressive strength of CARDIFRC® was observed.

5. Some factor(s) other than the casting direction must influence the fibre orientation, such as the size of the cast specimen and mix workability.

6. A fracture energy of up to 40,000 N/m; a flexural strength of up to 54 MPa; a splitting cube strength of up to 28 MPa; compressive strength of up to 215 MPa; and a modulus of elasticity of 44 GPa were achieved with CARDIFRC®.

7. It is recommended to cast slender specimens in a horizontal position to utilize the material's potential fully.

8. Extensive studies are required to further quantify the effect of fibre orientation. For example it is necessary to study the effects of the following: specimen size or aspect ratio, different casting procedures and vibration methods, degree of workability, fibre content and type of fibre and the type of mould used for casting.

9. Investigations for self-compacting fibre-reinforced concretes are needed to analyse if fibre alignment also takes place without vibration.

6   References

[1] Stiel, T.: Fracture Mechanics Parameters of CARDIFRC[®], Diplomarbeit, Cardiff / Kassel University, 2004.

[2] Benson, S.D.P. and Karihaloo, B.L.: CARDIFRC[®] – Manufacture and Constitutive Behaviour, In: High Performance Fiber Reinforced Cement Composites (HPFRCC4), Proc. 4th International RILEM Workshop, Ann Arbor, USA, Ed. by A.E. Naaman and H.W. Reinhardt, 2003, S. 65-79.

[3] Stiel, T. and Pfeiffer, U.: Einfluss der Betonierrichtung auf Stahlfaserbewehrte UHPC Bauteile, Projektarbeit, Kassel University, 2003.

[4] Benson, S.D.P.: CARDIFRC[®] – Development and Constitutive Behaviour, PhD Thesis Cardiff University, 2003.

[5] Karihaloo, B.L.: Fracture Mechanics and Structural Concrete, Addison Wesley Longman, London, 1995.

[6] RILEM Committee FMC 50: Determination of fracture energy of mortar and concrete by means of the three-point bend tests on notched beams, Materials and Structures, 1985, 18, 285-290.

[7] Elices, M., Guinea, G.V. and Planas, J.: Measurement of the fracture energy using three-point bend tests: part 3 – Influence of cutting the P–δ tail, Materials and Structures, 1992, 25, 327-334.

[8] Hu, X.Z. and Wittmann, F.H.: Fracture energy and fracture process zone, Materials and Structures, 1992, 25, 319-326.

[9] Duan, K., Hu, X.Z. and Wittmann, F.H.: Boundary effect on concrete fracture and non-constant fracture energy distribution, Engineering Fracture Mechanics, 2003, 70, 2257-2268.

[10] Abdalla, H.M. and Karihaloo, B.L.: Determination of size-independent specific fracture energy of concrete from three-point bend and wedge splitting tests, Magazine of Concrete Research, 2003, 55, 133-141.

[11] Edgington, J. and Hannant, D.J.: Steel fibre reinforced concrete. The effect on fibre orientation of compaction by vibration, Materials and Structures, 1972, 5, 41-44.

[12] Bonzel, J. and Schmidt, M.: Verteilung und Orientierung von Stahlfasern im Beton und ihr Einfluß auf die Eigenschaften von Stahlfaserbeton, Beton, 1984, 463-470.

[13] Soroushian, P. and Lee, C.-D.: Distribution and Orientation of Fibers in Steel Fiber Reinforced Concrete, ACI Materials Journal, 1990, 87, 433-439.

[14] Toutanji, H. and Bayasi, Z.: Effects of Manufacturing Techniques on the Flexural Behaviour of Steel Fiber-Reinforced Concrete, Cement and Concrete Research, 1998, 28, 115-124.

[15] Karihaloo, B.L., Abdalla, H.M. and Imjai, T.: A simple method for determining the true specific size-independent fracture energy of concrete, Magazine of Concrete Research, 2003, 55, 471-481.

Lars Kraft

PhD, MSc, Research Engineer

Doxa AB

Uppsala, Sweden

Leif Hermansson

Professor, Scientific Coordinator

The Ångström Laboratory

Uppsala University and Doxa AB

Uppsala, Sweden

Deformation Characteristics in Various Calcium Aluminate Cement Admixtures Investigated With Three Different Methods

Summary

The dimensional stability in various Ca-aluminate-based materials was investigated using three different methods; split-pin expander technique, digital micrometer and an automatic laser radial micrometer. The influence of degree of compaction, sample size, cement composition, grain size and storage condition on the deformation with time was evaluated. Two different types of specimens, pre-pressed and prepared hand-compacted specimens were used in the different methods. Two variants of the pre-pressed specimens were used, namely, pins and tablets. Also two different types of hand-compacted specimens were used, namely tablet-compacted specimens and wet-pressed compacted specimens. The deformation is micro-structurally controlled. The main factors controlling the deformation are grain size, cement composition, and additives that affect the basic cement system. Other factors controlling the dimensional stability are compaction degree, preparation process and the general surrounding environment. Furthermore, caution must be used in interpreting experimental data since the test methods may differ from each other, mainly with regard to the different boundary conditions applied for each measurement technique. Precipitation upon free surfaces and surface-initiated growth contribute to the dimensional change detected, particularly in small samples. Depending on what application the deformation studies aim at and what type of material is tested, different test equipment may be considered. The split-pin expander technique is validated further and, if properly used, is deemed to be a reliable method in the evaluation of deformation of small samples of the Ca-aluminate-system for dental filling applications. It is concluded that the long-term free expansion, in the wet cured small samples of Ca-aluminate based materials, is in the interval 0.2-0.6 %, including surface growth. That is for different sample preparation and measurement methods.

Keywords: *Deformation, methods, calcium aluminates, expansion controlling factors.*

1 Introduction

The development of high strength and high performance concretes (HSC/HPC) - which are characterised by low porosity, high strength and a low w/c ratio – has revealed problems associated with dimensional changes. This lack of robustness in these new types of concretes raised questions about the durability of the HSC/HPC, and has later represented a major stumbling block for introducing HSC/HPC on the market [1].

Factors such as degree of compaction, filler grade, cement type, composition, grain size and the environment influence the dimensional behaviour of cement-based materials during hydration and long-term performance. The degree of compaction, or bulk density, controls both porosity and the w/c ratio, thus having a profound influence on the physical boundaries of hydration mechanisms [2-4]. In compositions with a low w/c ratio there is a possibility over time of a slow continuous hydration of anhydrous cement grains, which also might affect the dimensions of the material in a long-term perspective. Questions of the influence of specimen size on deformation in cement materials have been raised in civil engineering research [5]. These may be related to surface phenomena and differential shrinkage [6].

The surrounding environment, temperature and humidity greatly influence the outcome of the hydration process for all cements and thereby the properties of the resulting material. Especially for Calcium aluminate cements (CAC) the surrounding temperature during the hydration process is crucial, since different temperatures give different hydration products, which determine the properties of the material. This is most significant at normal or lower hydration temperatures (10-25°C). The initial strength of CAC is high, but strength decreases significantly with time due to the conversion of the meta-stable hydrates CAH_{10} and C_2AH_8 [7]. In particular, this conversion process becomes detrimental to higher temperatures and with higher humidity, which speed up the process. Conversion can decrease the compressive strength by as much as 50 % and can contribute to a more porous material, making it more vulnerable to all kinds of deterioration processes like acid or sulphate attack, carbonation, alkali-silica reactions or alkaline hydrolysis [8,9]. In applications of CAC in warm and humid milieus, which increase the rate of conversion, the materials must be cast at higher temperatures to avoid conversion. Thereby a more secure long-term performance is achieved [10].

In October 2000, a calcium aluminate cement (CAC)-based dental filling material, called Doxadent®, was launched on the Swedish market. The material was delivered as small tablets, or powder compacts, which were immersed into a hydration liquid before insertion. Due to insufficient aesthetics and too complicated handling properties the material was withdrawn from the market in spring 2003. The hardened material can be characterized as a chemically bonded ceramic and as an ultra-high performance micro-concrete with a compressive strength of 180 MPa [11]. This work is part of the efforts in the development of this dental filling product [10].

Basically this paper describes findings concerning the long-term dimensional changes of prototypes of this material and other experimental CAC mixes, aimed for biomaterial applications at 37°C [12,13]. The dimensional stability of Doxadent® is evaluated and the influence on the results from different measurement methods is also discussed.

2　　　　Materials

The majority of deformation measurements presented were conducted on specimens from experimental powders with a chemical composition similar to that of the commercial product Doxadent®. Different compositions and particle size distributions were investigated. All prepared specimens had a compaction degree over 50%.

2.1　　　　CAC admixtures

Mixtures of CAC with additions of silica fume, Portland cement or alumina or combinations thereof were investigated (Table I). Some mixes had an addition of 28vol% of alumina, a volume fraction which was calculated from a theoretical model [10], to increase the w/c ratio and thereby the degree of hydration in the cement.

2.2　　　　Experimental Doxadent® powder

The dental filling material Doxadent® is based on Secar 71®, a calcium aluminate cement produced by Lafarge Aluminates. Zirconium dioxide is added as filler to achieve radio opacity of the material. The typical chemical composition expressed as oxides in the cured material is presented in Table II. Distilled water with a dosage of 71 mMol Lithium cloride, added as accelerator, was used as hydration liquid in all mixes.

Table I: Composition of the admixtures studied, quantitatively.

Mix nr.	Secar 71 (Lafarge AB)	Microsilica additives	Portland cement addition	Filler fraction (Alumina)
1	Coarse S71 (milling 24 h)	0	0	28 vol%
2	Fine S71 (milling 70 h)	0	0	28 vol%
3	Fine S71 (milling 70 h)	<10%	<10%	0

Table II. Chemical composition of Doxadent® material by weight %.

Oxide	Fraction (%)
Al_2O_3	43
CaO	19
H_2O	15
ZrO_2	19
Others: (Si-, Fe- Mg-, Ti- and alkali-oxides)	<4
Total	100

3　　　　Methods

Different measurement methods require different types of specimens of different geometries. Therefore different techniques were used for the preparation of specimens.

3.1 Specimen Preparation

Two different types of specimens, pre-pressed and prepared/compacted specimens were used in the different studies. All prepared specimens, made from tablets or from wet-pressed powders, were stored in water at 37˚C.

3.1.1 Pre-pressed specimens

Two variants of pre-pressed specimens were used, *pins* and *tablets*. Pre-pressed tablets were either machine-pressed or hand-pressed uni-axially with a pressure of approximately 150 MPa. The pre-pressed pins was manufactured by cold isostatic pressing (CIP) and carefully sawn and ground by hand to a cross-section dimension of 3-4 mm and a length between 10 and 25 mm. *Pins* of different degrees of compaction, different compositions and different lengths were made. Specimens of different lengths were used to investigate whether there was an influence of differential surface hydration by comparing the relative deformation.

3.1.2 Prepared (compacted) specimens

Two different types of the raw materials were used – uni-axially pressed tablets or wet-pressed material (See 3.1.3). In the preparation of specimens in the split-pin expanders the tablets are very practical. For preparation of larger specimens, wet-pressed material was usually employed.

3.1.3 The wet-press method

Fig. 1 shows the procedure used in the wet-press method. To achieve a complete and isotropic wetting of all cement grains in the material, the cement powder is thoroughly blended in a small pot (A, B) with an excess of water (w/p ~ 1.5) for one minute. The mix is poured onto a porous ceramic plate in a cylindrical hole of a plastic ring (B). By pressing on top of the paste with a wooden knob, excess water is soaked into the ceramic plate (C, D) and the wooden knob. Likewise, more water is pressed out from the paste in the press using a wooden plate and wooden disc (E, F). Thereby a highly compacted disc of cement paste, with a low w/c ratio (w/c ~ 0.2) is produced without any use of water-reducing additives. The damp paste is subsequently inserted into any mould or cavity selected. The knobs, discs and plates were made of beech, a very fine-porous wood.

A)   B)   C)

D)   E)   F)
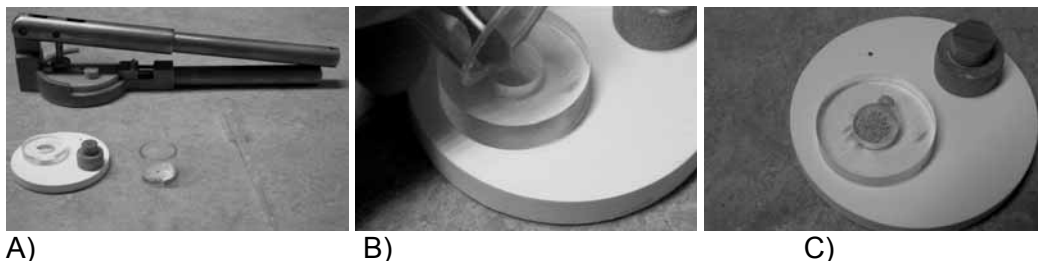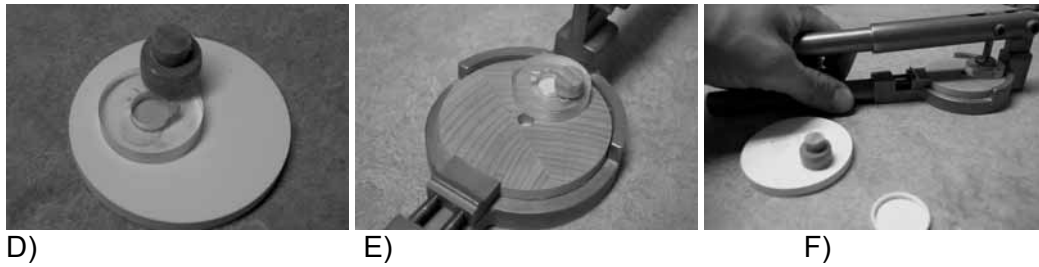
Figure 1: The wet-press method generates a low w/c ratio material without WR agents.

3.2   Measurement Techniques

Free expansion and restrained expansion of the different test materials were evaluated by three different methods: a split-pin expander technique (restrained expansion), digimatic micrometer and a laser beam scanner (free expansion). The methods are described briefly below.

3.2.1   Split-pin expander technique

Acrylic split-pin expanders work both as a sample holder and as a movement gauge. The technique is presented in detail elsewhere [10, 14]. The measurement error is estimated to ±0.05%.

3.2.2   The digimatic indicator

A Mitutoyo digimatic indicator with a sensitivity of 1µm and an accuracy of ±1.5µm (at 0-40°C) was used for dimension change measurements in the materials studied (Fig. 2). The specimens were placed upon cylindrical rods for perfect alignment at every measurement [15].

3.2.3   The Automatic Laser Scan Radial Micrometer

The measuring device consists of a laser-scan micrometer, also made by Mitutoyo (Figure 3), which is positioned horizontally on a table. The laser scan measurements were conducted at

Figure 2. The digimatic Mitutoyo micrometer.   Figure 3. The Mitutoyo Laser Scan micrometer.

the Department of Clinical Engineering, University of Liverpool, with a set-up constructed by Jedynakiewicz and Martin [16]. The accuracy of the measurements is dependent on the surface roughness of the periphery. Five laser scans over two coins with a smooth and a ribbed periphery respectively, gave a discrepancy of the standard deviation of the mean values. The variation coefficient (the relative error) was 0,002% and 0,029% respectively. Thus, measurements on samples with a low surface roughness are very accurate.

4   Results

All results presented is the average from two specimens, except in Fig. 5A (three expanders) and in Fig. 10 (four or five expanders). In Fig 6B the results presented are from single specimens to illustrate the accuracy of the digimatic micrometer method as well as the spread of the results obtained.

From Fig. 4 it is concluded that mix 1, with a larger grain size particle distribution, has a far greater expansion than mix 2 that was ground for 70 hours. Also an almost zero expansion was detected with the split-pin expanders for mix 3. The same relative difference between the mixes was found with the laser beam micrometer. After ~1½ years the long-term restrained linear expansion of Doxadent® is ~0,3% for specimens prepared from tablets (Fig. 5A). From wet-pressed "doxadent"-powder the corresponding expansion is about 0,1% larger (Fig. 5B). Thereafter no further expansion takes place. Fig. 6 shows that with filler particles the linear expansion decreases, at least in the case where the expansion is restrained, i. e. when measured with the split-pin expanders. No significant difference between the compositions can be seen in Fig. 6B. Instead a spread of the material expansion is detected, since the measurement error in the digimatic micrometer is as low as 0.02% [15]. In Fig. 7A it is seen that larger specimens give larger (relative) linear expansion. In Fig. 7B the opposite was found. Again, in Fig. 8A, the linear expansion detected is higher in shorter pins compared to in longer pins. Fig. 8B shows an influence on the expansion due to what type of storage medium that was used. Finally Fig. 9 shows that a higher degree of compaction gives a lower linear expansion.
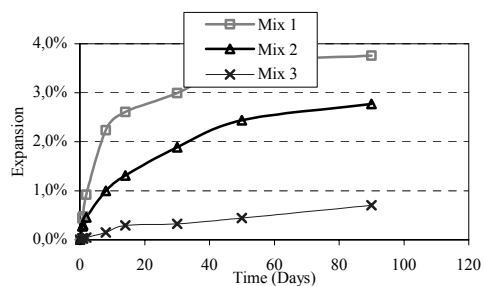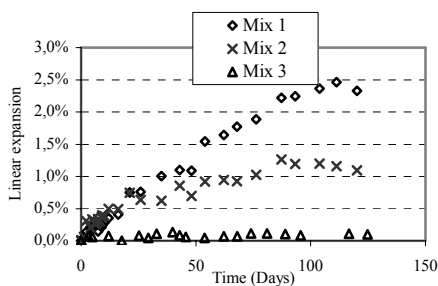
A)   B)

Figure 4. The grain size influence and the cement composition influence on the linear expansion. Measured with split-pin expanders (A) and the laser scan micrometer (B), respectively. All specimens were prepared from wet-pressed powder.
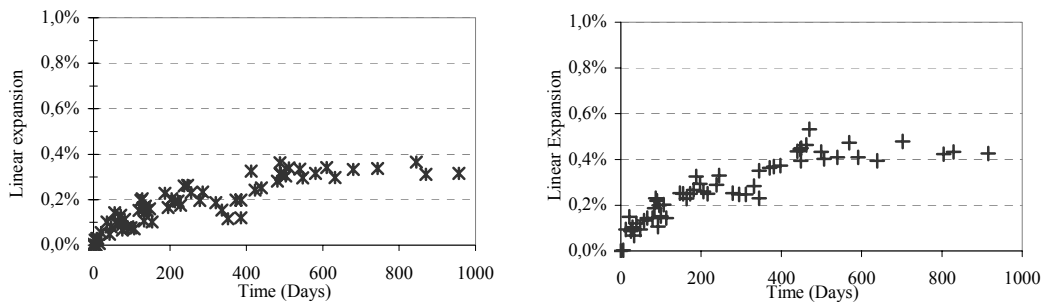
A)   B)

Figure 5. The linear expansion in experimental Doxadent® measured with split-pin expanders. Specimens prepared from tablets in (A) and from wet-pressed powder in (B), respectively.
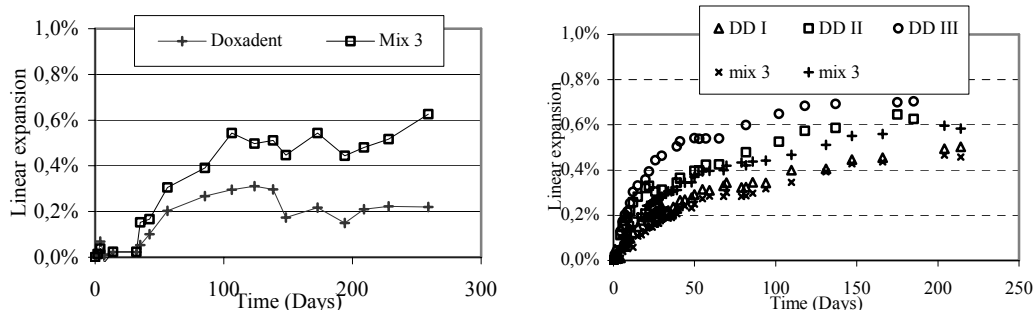
A)   B)

Figure 6. Influence of filler content (wet pressed samples) measured with split-pin expanders (A) the digimatic micrometer (B), respectively. In (A) three samples per composition with different specimen sizes of 3, 4 and 6 mm in diameter were used. All specimens were prepared from wet-pressed powder. (DD = Doxadent powder.)
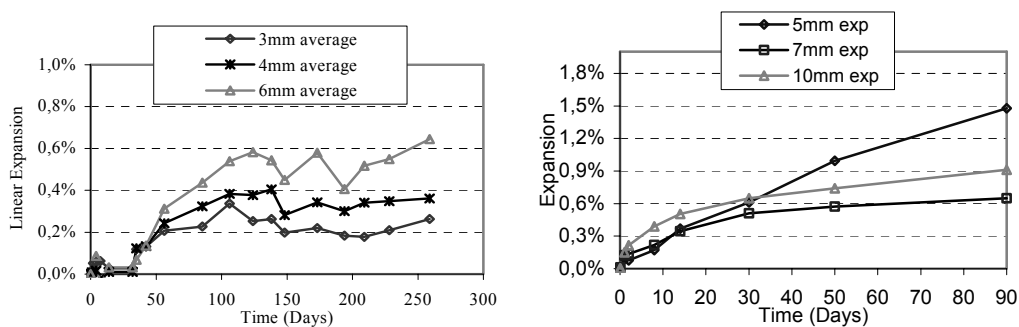
A)   B)

Figure 7. The influence of different sample sizes on the expansion, wet-pressed samples evaluated by split-pins (A) and laser-beam scanning (B), respectively.
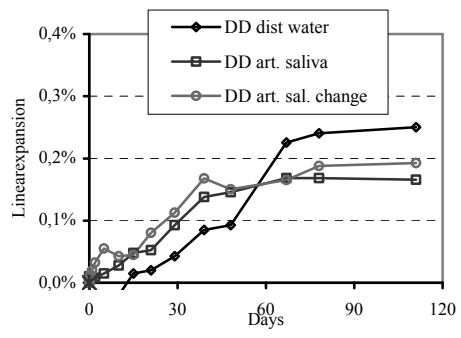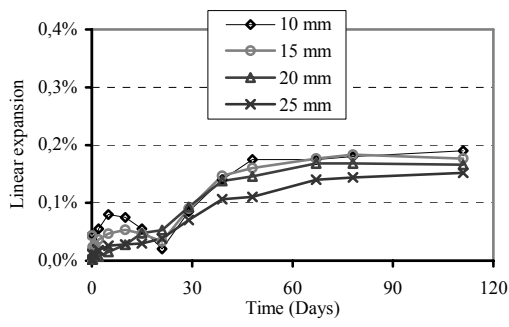
A)   B)

Figure 8. The free linear expansion of pre-pressed experimental Doxadent® pins of different lengths stored in artificial saliva (A), and the free expansion of pre-pressed experimental Doxadent® stored in different environments (B), measured with the digimatic micrometer. In one of the series the storage solution – artificial saliva – was exchanged at every measurement.
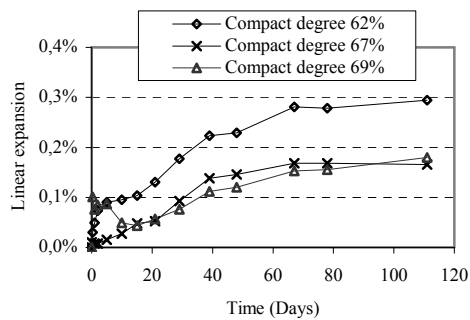
Figure 9. The free expansion for Doxadent® pins of different degrees of compaction stored in artificial saliva. Measured with the digimatic micrometer.

5   Discussion

The deformation development during curing of CAC-based cements is dependent on a large number of factors. Conducting few experiments only will give an inaccurate answer to the question of deformation in the system, due to uncertainty in the measurement techniques and to variations in specimen preparation.

5.1   Influence of Physical and Chemical Characteristics

The most important physical characteristics to achieve strength in cement-based materials are the degree of compaction, the w/c ratio, the grain size and the homogeneity of the powders. These properties also deeply affect the deformation characteristics of the curing material.

Generally, it is the w/c ratio that controls the performance of cement-based materials. However, all of the tested specimens in this report must be regarded as cement compacts. Therefore the degree of compaction is as essential to discuss, since it controls how much water is activated. Thus, the lower the degree of compaction is, the higher the w/c ratio gets.

502

5.1.1   The Degree of Compaction and the w/c ratio

There is a tendency that higher degrees of compaction reduce the expansion, at least for very high degrees of compaction (Fig. 9). Half the cross-section in the 69% compacted pins was still anhydrous when studied under microscope. However, this was not the case in the 67% compacted specimens. Thus the practical maximum degree of compaction lies between 67-69%. Furthermore, the preparation technique with which samples, or fillings, are produced will influence the degree of compaction and/or the w/c. Prepared specimens from tablets result in a higher degree of compaction and somewhat lower expansion (Fig. 5) compared with samples prepared from wet-pressed powders, having a compact degree of 59 and 53 % respectively.

From the literature [1] it is proved that the shrinkage increases with lower w/c ratio. This is particularly the case in measurements of autogenous shrinkage, which are performed under sealed conditions [1, 17]. Also in wet curing the same tendency has been found, but as the water content reaches a certain ratio an expansion can be detected. Tazawa et al observed this for a w/c ratio above 0.30 for a Portland cement paste if the samples were small enough [5]. Since the compaction increases when the w/c decreases in hydraulic cement, analogously the expansion decreases in the cement compacts studied here.

However, swelling or expansion at higher w/c ratios is only true up to a certain limit. For example, Lobo and Cohen [18], found decreasing expansion with increasing w/c ratio in expansive cements.

5.1.2   Grain Size

The factor with the greatest single influence on the deformation detected was the grain size distribution (Fig. 4). Smaller grains result in lower linear expansion in these particle size regimes, which were 0.01 – 30 microns. A fine-grained microstructure will keep the different possible expansion factors locally at low levels.

5.1.3   Chemical Composition

The second most important single factor influencing deformation is the addition of silica and/or silica-containing phases. In experiments with different high performance concrete blends, it has been shown that the addition of silica fume into concrete mixes increases the shrinkage [5,23]. From Fig.4 it is obvious that silica at low concentrations decreases the expansion for CAC based materials that are stored in water [17,18,19].

5.1.4   Filler Ratio

The filler content (inert fillers) will decrease the expansion related to the hydration in the cement. The higher the fraction of fillers in concrete mixes is, the lower the resulting expansion becomes (Fig 6A).

5.2   Influence of the Measuring Technique on Deformation Results

In Fig. 4A-B, 6A-B and 7A-B, we have the same type of specimens measured with two different methods respectively. The reason for the expansion-detected discrepancies is either

influence from the differential hydration mechanisms (bulk, in-surface, on-surface) to different extents or influence of free or partly restrained expansion (as with the acrylic split-pin expanders). Restrained measurements will induce creep and change the net deformation in the hydrated cement. Therefore the sample position and measurement technique play a crucial role.

5.2.1 Sample Position And Specimen Size

The sample position may restrict the direct contact of the material with the surrounding solution or provide direct contact with the external solution. Due to the general hydration mechanism involving dissolution of the cement raw materials and precipitation, the formation of new hydrates occurs within the material bulk in the originally water-filled pores, but also in the surface region and on the surface. The hydrate formation in the surface region and the possibility of direct precipitation from the surrounding solution contribute to the deformation. Since the samples are positioned in different ways in the tests, these different deformation mechanisms will affect the overall deformation detected to different extents. From Fig. 8 the existence of a hydrated surface layer is proven. SEM studies have confirmed a layer of precipitated calcite on samples stored in distilled water and a in-surface layer of apatite on samples stored in phosphate buffer solution [10]. Loose surface layers explain the larger expansion found in Fig. 4B.

5.2.2 Expansion detected by the split-pin expanders

Also the difference in expansion detected by either water-saturated or dry split-pin expanders, as well as the influence of an initial pre-stress applied upon the specimens were investigated. Therefore identical specimens were prepared in wet-saturated with and without pre-stress and in dry specimens with initial pre-stress applied. FEM calculations estimated the pre-stress in the experiments to about ~ 7 MPa. This stress exerted by the split-pin expanders upon the cement specimens corresponds to a stress present after a linear expansion of 1% in the expanders [10].

Four or five split-pins per test series were used and the result is presented in Fig. 10. It is seen that dry expanders underestimate the expansion by 0.1%. Furthermore, the initial pre-stress induces creep in the specimens which result in approximately 0,15% lower net expansion compared with the expansion recorded without pre-stress. Therefore all long-term split-pin expander data recorded, in this paper and in papers presented earlier, not using water-saturated expanders, is underestimated by 0,10%. For comparison of split-pin expanders data with free expansion data a further ~0,15% or more should be added due to creep. Then agreement is achieved with the discrepancies between test results for restricted and free expansion in this study (Fig. 5 and 6). It is important to emphasize that the boundary conditions in the different tests affect the material. Therefore the final long-term deformation will depend on whether the expansion was measured free or under pre-stress, i. e. if creep will take place or not. Dental fillings in cavities will be influenced in a similar manner due to the boundary conditions present.
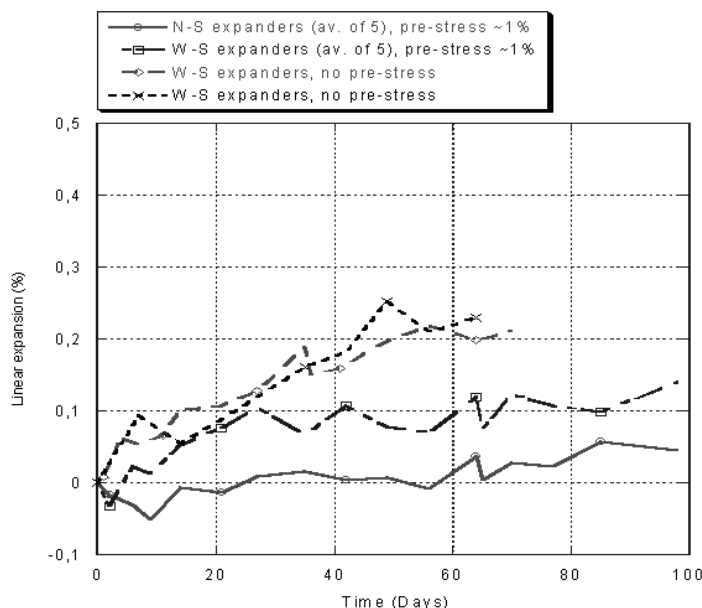
Figure 10: The different in measured expansion between water saturated and dry acrylic expanders. (N-S = non-saturated, W-S = water-saturated)

6   Conclusions

The dimensional change of the Ca-aluminate based materials studied can be controlled by material and preparation modifications to be in the interval 0.2-0.6 %. Compacted experimental Doxadent® have a long-term final linear expansion of 0.4% in restrained water saturated split-pin expanders.

The main factors controlling the deformation (microstructure developed) are grain size, composition (filler contents), and additives that affect the basic cement system. Other factors that control the dimensional stability are compact degree, preparation technique, and the general environment. These factors are important when optimising the dimension changes close to zero-expansion.

Caution must be exercised in interpreting experimental data since different test methods may differ from each other, mainly with regard to the different boundary conditions applied for each measurement technique. Precipitation upon free surfaces and surface-initiated growth will contribute to the dimensional changes detected. The split-pin expander method is deemed to be a reliable method in the evaluation of dimensional changes in the CAC based dental materials, if used properly.

Digimatic micrometry and laser beam scanning show high accuracy in the measurements, but is more influenced by external factors such as on-surface precipitation.

7   Acknowledgements

8   References

[1]   Baroghel-Bouny, V.; Aitcïn, P.-C.; Eds. In: Shrinkage 2000. RILEM Proceedings Pro 17. Paris, RILEM, 2000.

[2]   Powers, T.C.; Brownyard, T.L.; Studies of the physical properties of hardened Portland cement paste. Chicago, Research Laboratories of the Portland Cement Association, 1948.

[3]   Jensen, O.M.; Hansen, P.F.; Water-entrained cement-based materials I: Principles and theoretical background, Cement and Concrete research Vol. 31, No. 4, S. 647-654, 2001.

[4]   Frigione, G.; Marra, S.; Relationship between particle size distribution and compressive strength in Portland cement. In: Cement. & Concrete Research, 6, S.113-128, 1976.

[5]   Tazawa, E.; Sato, R.; Sakai, E.; Miyazawa, S.; Work of JCI Committee on Autogenous shrinkage. In: V. Baroghel-Bouny, P-C. Aïtcin (Eds.), Shrinkage of Concrete - Shrinkage 2000, Pro 17 RILEM, 16-17 October, Paris, S. 21-40, 2000.

[6]   Neville, A.M.; Properties of concrete. John Wiley & Sons, 1996

[7]   Neville, A.M.; High Alumina Cement Concrete, John Wiley & Sons, 1975.

[8]   Scrivener, K.L.; Capmas, A.; Calcium Aluminate Cements, Lea's Chemistry of Cement and Concrete, Edited by P.C. Hewlett, Arnold, S. 1998.

[9]   Technical Report, Calcium Aluminate Cements in Construction, a Re-Assessment, The Concrete Society, UK, 1997.

[10] Kraft L.; Calcium Aluminate Based Cement as Dental Restorative Materials. Ph D Thesis, Uppsala University, Sweden, 2002.

[11] Lööf, J.; Engqvist, H.; Ahnfelt, N.O.; Hermansson, L., Mechanical properties of a permanent dental restorative material based on calcium aluminate. In: Journal of Materials Science: Materials in Medicine, 1033-1037, 2003.

[12] Engqvist, H., Schulz-Walz, J.E.; Lööf, J.; Botton, GA.; Mayer, D.; Pfaneuf, MW.; Ahnfelt, N.O.; Hermansson, L.; Chemical and biological integration of a mouldable bioactive ceramic material capable of forming apatite in vivo in teeth. In: Biomaterials, 25(17): S. 2781-2787, 2004.

[13] Axén, N.; Persson, T., Björklund, K., Engqvist, H.; Hermansson, L.; An injectable bone void filler cement based on ca-aluminate. In: Key Engineering Materials, 254-256: S. 265-268, 2004.

[14] Kraft, L.; Hermansson, L.; Gomez-Ortega, G.; A Method for the Examination of Geometrical changes in a CAC Based Cement Paste. In: V. Baroghel-Bouny, P-C. Aïtcin (Eds.), Shrinkage of Concrete - Shrinkage 2000, Pro 17 RILEM, 16-17 October 2000, S. 401-413, 2000.

[15] Kraft, L.; Engqvist, H.; Hermansson, L.; Early-age dimensional changes, drying shrinkage and thermal dilation in a new type of dental restorative material based on calcium aluminate cement. In: Cem Con Res,; 3: S. 439-446, 2004.

[16] Jedynakiewicz, N.; Martin, N.; Expansion behaviour of compomer restoratives, Biomaterials 22, S. 743-748, 2001.

[17] Mejlhede Jensen, O.; Freiesleben Hansen, P.; Autogenous deformation and change of the relative humidity in silica fume-modified cement paste. In: ACI Materials Journal. No. 93-M61, S. 539-543, 1996.

[18] Lobo, C.; Cohen M.D.; Effects of silica fume on expansion characteristics of expansive cement pastes. In: ACI Materials Journal. No. 89-M51, S. 481-490, 1992.

[19] Rao, G.A.; Influence of silica fume replacement of cement on expansion and drying shrinkage. In: Cem. & Conc. Res 28 (10), S. 1505-1509, 1998.

Part 9:

Design and Construction

Brameshuber, W.
Prof. Dr.-Ing.
Institute of Building Materials Research (ibac)
Aachen University, Germany

Brockmann, T.
Dipl.-Ing.
Institute of Building Materials Research (ibac)
Aachen University, Germany

Banholzer, B.
Dipl.-Ing.
Institute of Building Materials Research (ibac)
Aachen University, Germany

Textile reinforced ultra high performance concrete

Summary

Within the collaborative research centre SFB 532 "Textile reinforced concrete - basic developments of a new technology" at Aachen University investigations on serviceability of thin structured textile reinforced concrete elements have shown potential for optimisation. In order to enlarge the loading capacity for serviceability ultra high performance concrete matrices (UHPC) have been developed. The objective of the presented investigations is to show the influence on the loading capacity of textile reinforced elements of the newly developed mixtures with and without adding short fibres in comparison to the reference mixture used so far. Mechanical, fracture mechanical and deformation properties of the high performance mixtures like e.g. compressive and flexural strengths, the Young´s modulus, shrinkage, fracture energy are determined. Furthermore the interactions with different textile materials are investigated by means of tensile tests on textile reinforced elements. Finally structural members used as e.g. permanent formwork are tested under flexural loading.

Keywords: *textile reinforced concrete, ultra high performance concrete, mechanical properties*

1 Introduction

Within the scope of the collaborative research centre SFB 532 "Textile reinforced concrete - basic developments of a new technology" financed by the German Research Foundation and carried out at Aachen University, fine grained concrete matrices are developed. Typically, they show a highly flowable consistency which offers full penetration of the technical textiles and a suitable bonding behaviour. These special properties are achieved by using a small maximum grain size (d_{max} = 0.6 mm), high binder content, and adding different pozzolanic additives and plasticizers [1].

As previous investigations on serviceability of thin structured textile reinforced concrete elements have shown potential for optimisation, further ultra high performance concrete matrices have been developed. In order to enlarge the loading capacity for serviceability

increased binder contents, reduced water/binder ratios and different amounts of short AR-glass fibres have been used, which offer increased tensile strengths and a high ductility. The use of short fibres leads to an increase of loading capacity, a finely distributed crack formation and a continuously increasing loading with increasing deformations [2].

The objective of the presented investigations is to show the influence of newly developed ultra high performance mixtures with and without adding short fibres in comparison to the reference mixture used as matrix for textile reinforced elements so far. Mechanical, fracture mechanical and deformation properties of the high performance mixtures like compressive and flexural strengths, the Young´s modulus, shrinkage, and fracture energy are determined. Furthermore the interactions with different textile materials are investigated by means of tensile tests on textile reinforced elements. Finally structural members used as e.g. permanent formworks are tested under flexural loading.

2   Materials and testing methods

2.1   Mixture compositions

For the following investigations, the mixture R0 (PZ-0899-01) is used as reference mixture to the newly developed ultra high performance mixtures R1 to R4 as shown in Table 1. Due to the application as textile reinforced concrete, these mixtures differ from typical mixture compositions of ordinary UHPC like e.g. in maximum grain size, binder or water content. The ultra high performance mixtures R1 to R4 mainly differ from the reference mixture R0 in a significant lower water-binder ratio, a higher binder content as well as the content of silica fume.

Table 1:   Composition of fine grained concrete mixtures

Materials		Mixtures				
		R0	**R1**	**R2**	**R3**	**R4**
cement, c	kg/m³	490	980	970	951	980
fly ash, f		175	210	208	204	210
silica fume, sf		35	210	208	204	210
siliceous fines		500	118	117	115	118
siliceous sand		714	168	166	163	168
plasticizer	% of binder	1.5	2.5	2.4	2.3	2.4
polymer dispers.		-	-	-	-	5.0
AR-glass fibres	Vol. %	-	0.0	1.0	3.0	-
w/c		0.57	0.36			
w/b = w / (c + f + sf)		0.40	0.25			

Despite a small w/b ratio, highly flowable consistencies as well as high strengths of the hardened concrete are expected for these mixtures. Mixtures R2, R3, and R4 only differ from

mixture R1 by adding short AR-glass fibres (1 - 3 Vol.-%), or a polymer dispersion respectively, and hence are designed for higher tensile strengths and a ductile cracking behaviour. For comparison it was intended to add 1 to 3 Vol.-% of AR-glass fibres to the reference mixture R0, but this did not lead to satisfying consistencies. All mixtures are mixed in a mortar mixer for 5 minutes [3]. All test specimens are cured for 24 hours at a temperature of 20 °C and 95 % R.H., and then until testing, a sealed storage at a temperature of 20 °C is chosen, if not quoted otherwise.

2.2 Determination of fresh and hardened concrete properties

2.2.1 Fresh concrete properties

Air content and density of the fresh concrete are determined according to German Standard DIN 18555-2 [4]. The consistency of the mixtures is determined with slump flow and flow time according to testing procedures also used for self compacting concrete. Both testing procedures are described in detail in [1].

2.2.2 Hardened concrete properties

In order to determine the loading capacity and deformation behaviour of the hardenend concrete the compressive strength, flexural and splitting strength as well as the Young´s modulus and shrinkage are determined at a testing age of 28 days.

Compressive strength and flexural strength are determined according to German Standard DIN 18555-3 [5] using specimens with the dimensions 40 x 40 x 160 mm³.

The Young´s modulus is determined according to German Standard DIN 1048 [6] using cylindrical specimens with a diameter of d = 50 mm and a height of h = 100 mm.

The splitting strength also is determined according German Standard DIN 1048 [6] but using prismatic specimens with the dimensions 40 x 40 x 160 mm³.

Shrinkage is measured also using prismatic specimens with the dimensions 40 x 40 x 160 mm³ according to German Standard DIN 52450 [7]. These specimens were stored continuously at a temperature of 20 °C and 65 % R.H..

2.3 3-point bending test on concrete specimens

Concrete specimens (without textile reinforcement) with the dimensions 40 x 40 x 240 mm³ and a notch depth a = 10 mm as shown in Figure 1 are used for the 3-point bending test carried out to determine the load-displacement curve and the corresponding fracture energy G_f. Before testing, the notches are sawn using a diamond saw with a thickness of 2 mm. The displacement controlled (displacement u in the mid-section, Figure 1) 3-point bending tests

are carried out using a universal testing machine (INSTRON 5566) at a rate of 0.015 mm/min.
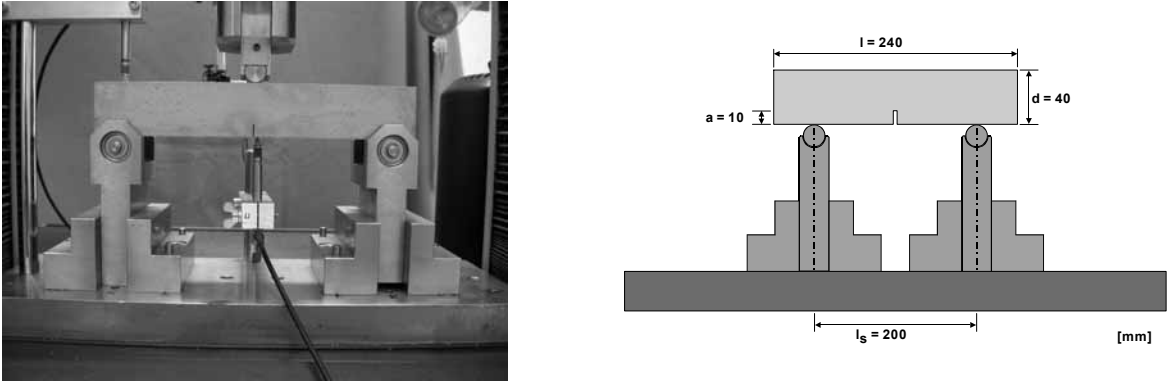
Figure 1: 3-point bending test of fine grained concrete specimens

2.4 Tensile test on textile reinforced elements

The tensile test as shown in Figure 2 is carried out on textile reinforced elements to determine the load carrying capacity and development of cracking patterns. For production of the textile reinforced elements, the fine grained concrete mixtures as shown in Table 1, are used and as reinforcement technical textiles made of carbon rovings (MAG-04-03) produced within the research project SFB 532, or made of AR-glass rovings (Bi-AR-SA-N, a bi-directional woven 2400 tex roving with a 8 mm spacing (500 g/m²)) and subsequently saturated with epoxy resin are used. The textile is fixed to the moulding in two layers with a concrete cover of about 3 mm as shown in Figure 2. The amount of reinforcement then sums up to 178,44 mm²/m for both textile materials. Finally the fresh concrete is poured into the moulding, levelled off and covered with a glass plate. The specimens are cured for 24 hours at a temperature of 20 °C and 95 % R.H. and stored in water at a temperature of 20 °C (carbon textile), or at 20 °C and 65 % R.H. respectively (AR-glass textile) until testing.
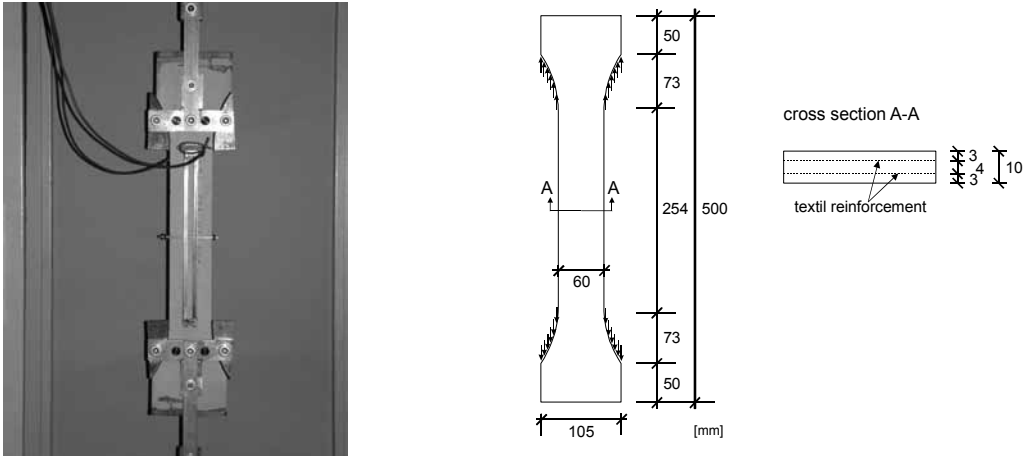
Figure 2: Tensile test on textile reinforced elements

The specimens are tested at 7 days. The tensile test is carried out controlled by crosshead displacement at a rate of 0.1 mm/min and measuring the strain by two inductive position encoders with a measuring length of 250 mm.

2.5 4-point bending test on permanent formwork elements

In the present study, so called permanent formwork elements are tested under flexural loading in a 4-point bending test to investigate whether the information gained in the previously mentioned tensile tests can be adopted to infer on the load carrying capacity of a structural member. These elements consist of a flange reinforced with a single layer of epoxy-saturated textile (Bi-AR-SA-N) in the tensile zone and of a bi-directional arrangement of concrete ribs with a uniform spacing of d_{rib} (waffle slab) in the compressive zone. This complex geometry of the structural members demands a high effort in preparation as the two major sides of the elements have to be shaped, i.e. the front side has to be casted in fair-faced concrete and the rear side of the system has to show the bi-directional rib arrangement. To guarantee a high concrete quality at the exposed side, the paling-board for the flange is coated with a synthetic material. The rib or waffle arrangement on the opposite side is shaped by rectangular forming elements of height h_{rib} attached to the rear paling board. All other four sides are also planked to obtain a tongue and groove joint system. Small concrete spacers are used to keep the textile centric in the slab in position. An injection technique is used for casting the elements. A complete permanent formwork element is shown in Figure 3.

1. load introduction
2. load introduction in the intenders
3. formwork element
4. support
5. gauges
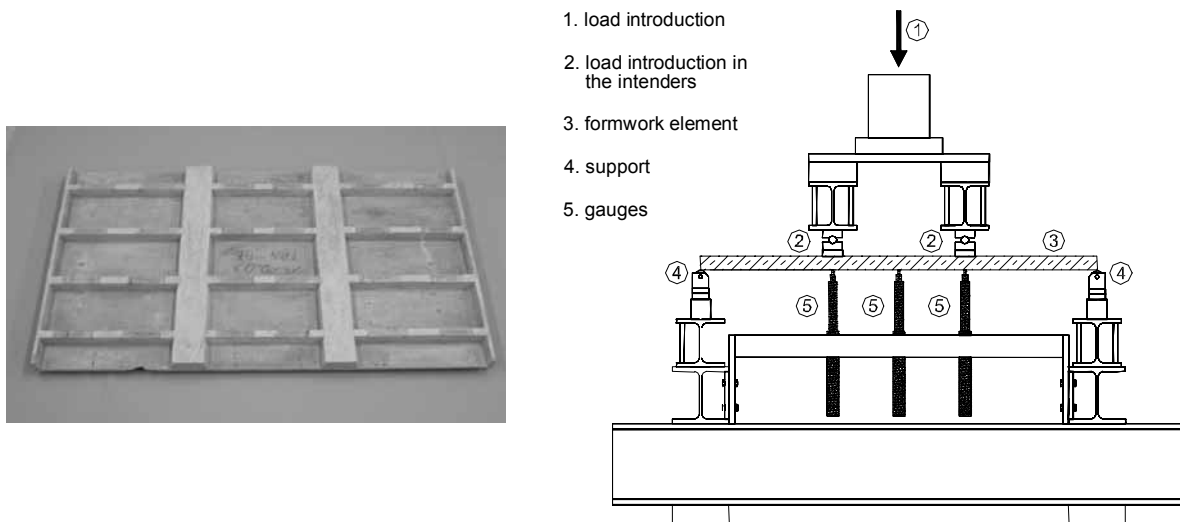
Figure 3:   Permanent formwork element and test set-up for 4-point bending test.

The test set-up to investigate the flexural behaviour and the load carrying capacity of the permanent formwork elements is presented also in Figure 3. The element rests upon two supports within a 1000 mm distance and is loaded using a two-point loading 333 mm apart. The mid-span load is applied gradually until the ultimate load carrying capacity is reached. The deflections in mid-span and under the load introduction points are measured by gauges and recorded simultaneously with the load at equal intervals.

3 Results

3.1 Fresh and hardened concrete properties

The fresh concrete properties of the different fine grained concrete mixtures are listed in detail in [7]. All investigated mixtures show a suitable consistency for the production of textile reinforced elements as the slump flow and flow time were measured to be within the limits of 250 – 350 mm for slump flow and 3 - 11 sec for flow time. Previous investigations on the workability of the different mixtures used as matrix for textile reinforced elements already have shown that the consistency of a fine grained concrete within these limits can be classified as suitable, regarding to fluidity.

Table 2 shows the mechanical properties of the mixtures R0 to R4, i.e. the compressive, flexural and tensile strength, the Young´s modulus, and shrinkage at a testing age of 28 days. Also, the calculated tensile strength $f_{ct} = 0,9 * f_{ct,sp}$ [8], which is needed as input parameter to determine the characteristic length l_{ch} as fracture mechanical parameter is shown (see Eq. 1).

Table 2: Mechanical properties of UHPC mixtures at a testing age of 28 days

Mechanical properties		Mixtures				
		R0	R1	R2	R3	R4
compressive strength f_c	N/mm²	74.2	97.9	96.5	94.4	86.1
flexural strength $f_{ct,fl}$		7.6	8.1	7.9	19.4	5.8
Young´s modulus E_{stat}		35,000	26,500	-	25,100	21,200
splitting strength $f_{ct,sp}$		5.9	4.8	8.7	8.8	5.8
calc. tensile strength f_{ct}		5.3	4.4	7.7	7.9	5.2
shrinkage	mm/m	0.84	1.04	1.43	1.40	1.88

The compressive strengths of the ultra high performance mixtures R1 to R3 are f_c = 94.4 - 97.9 N/mm² and hence exceed the compressive strength of the reference mixture R0 of f_c = 74.2 N/mm². At this stage the development of the ultra high performance mixtures did not focus on higher compressive strengths (usually typical for UHPC) but rather on investigation of use of these mixtures on the loading capacity and deformation behaviour of the composite material in principal. Mixture R4, containing a polymer dispersion as additive, shows a lower increase in strength compared to the other high performance mixtures, and regarding the flexural strength even a reduction in strength compared to the reference mixture R0. A comparison of mixtures R2 and R3 shows that an AR-glass fibre content of 3 Vol.-% leads to a significant increase in the flexural strength to $f_{ct,fl}$ = 19.4 N/mm², while an AR-glass fibre content of 1 Vol.-% only leads to a flexural strengths comparable to mixture R1 without any AR-glass short fibres. Regarding the splitting strength, already a AR-glass fibre content of 1 Vol.-% leads to an increase of the splitting strength compared to mixtures R0, R1, and R4, and is not enhanced any more by a higher fibre content of 3 Vol.-% as for mixture R3.

The Young´s modulus of all investigated UHPC mixtures R1 to R4 shows relatively low values of about 21,200 - 26,500 N/mm² due to the high content of cement paste, while the reference mixture shows a Young´s modulus of E_{stat} = 35,000 N/mm².

In general, there are observed lower compressive strengths for the chosen sealed storage compared to a storage under water. Water storage mixtures R1 to R4 show compressive strengths of about 120 - 130 N/mm², i.e. the newly developed mixtures are classified in the lower range regarding strength criteria of UHPC.

3.2　　　3-point-bending test on concrete specimens

Figure 4 (left) shows the load-displacement curves for mixtures R0, R1, R2 and R4 as result of the 3-point bending tests.
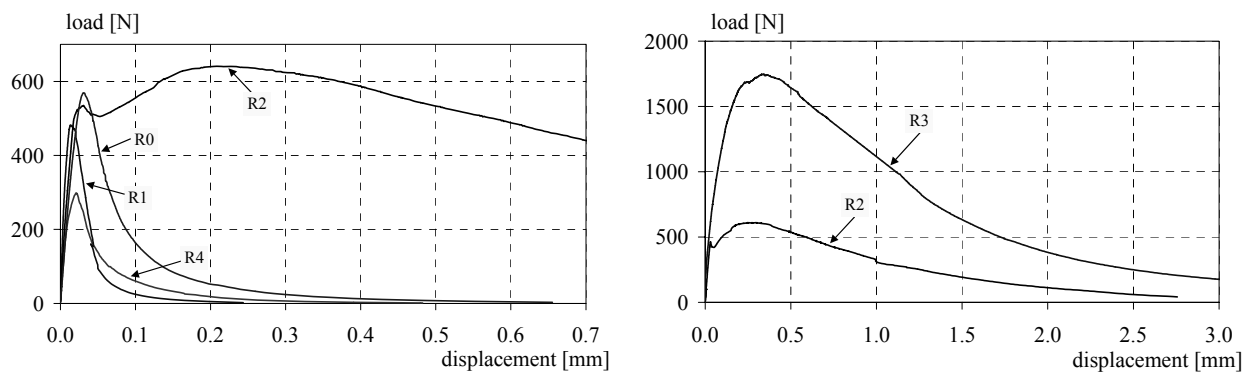
Figure 4:　Load-displacement curves – UHPC in comparison to the reference mixture

Mixtures R1 and R4 show a slightly or significantly lower maximum load compared to the reference mixture R0. Still the curve progression is similar for all these mixtures. Only mixture R2 with 1 Vol.-% AR-glass fibres shows a different loading behaviour with a distinctive ductility. After a first peak at a load of about 520 N, first cracks occur but the AR-glass fibres take a crack-bridging function and start carrying the load. This change in load carrying capacity leads to an ascending branch of the load-displacement curve and hence again to an increase in load up to a maximum load of about 650 N (Figure 4, left). Afterwards there is a ductile failure with displacements of about 2.7 mm (Figure 4, right). The influence of a higher AR-glass fibre content on the loading characteristics is shown in Figure 4, right. A higher amount of AR-glass fibres (mixture R3 with 3 Vol.-% AR-glass fibres compared to 1 Vol.-%) leads to a continuous increase of the ascending branch of the load-displacement curve up to the maximum load of about 1740 N (no first peak). This can be explained by the short AR-glass fibres which directly take the load at crack initiation. Similar to mixture R2 there follows a ductile failure of the testing specimens with displacements of about 18 mm and a residual load of about 2 N (not shown in the Figure).

For a more detailed evaluation of the brittleness and failure mechanisms of the fine grained concrete mixtures the fracture energy G_f and the characteristic length l_{ch} are also determined. The area under the load-displacement curve gives the fracture energy, related to the

projected cross-section, which is required to split the concrete specimen completely. The characteristic length l_{ch} is used to evaluate the brittleness of the material, and according to Eq. 1 a small value of l_{ch} represents a high brittleness.

$$l_{ch} = \frac{E \cdot G_f}{f_t^2} \quad [\text{mm}] \tag{1}$$

The results for the fracture energy G_f and the characteristic length l_{ch} are shown in Table 3, where the Young´s modulus and the tensile strength from Table 2 are used as input parameters to determine l_{ch}.

Table 3:   Fracture mechanical properties of the fine grained concrete mixtures

Fracture mechanical properties		Mixtures				
		R0	R1	R2	R3	R4
fracture energy G_f	N/m	49.9	20.8	> 750[1)]	> 2250[1)]	20.8
characteristic length l_{ch}	mm	62.2	27.9	> 328	> 905	16.3

1)   Integration up to a displacement of 2.5 mm

As expected, the ultra high performance mixtures R1 and R4 without short fibres show a smaller fracture energy compared to the reference mixture R0, due to a high binder content and a low w/b ratio. These ultra high strength concrete mixtures show a brittle behaviour also shown by small values of l_{ch}. The brittleness of the unreinforced UHPC R1 and R4 in comparison to mixture R0 is shown in Figure 5, which shows a straight continuous crack development for the brittle mixture R1 (Figure 5, left), while the less brittle reference mixture R0 shows an energy consuming development of overlaps and branches of the crack, which explains the higher values of the fracture energy.
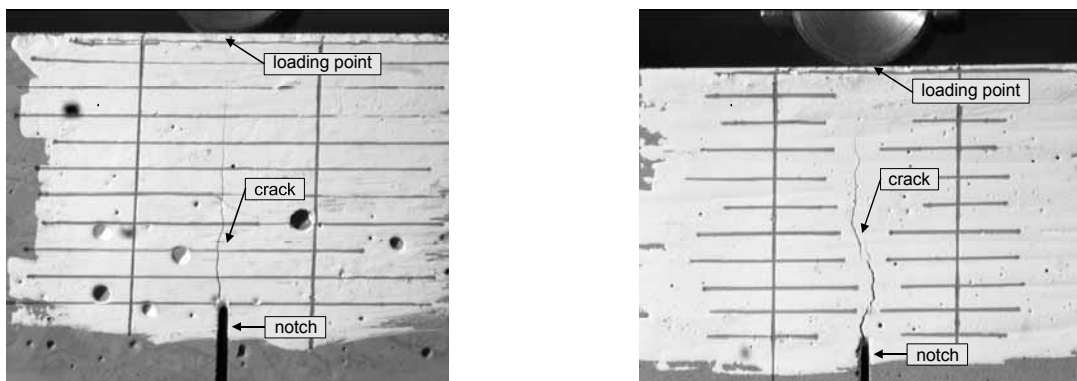
Figure 5:   Crack development of concrete specimens during 3-point bending tests at a displacement of 2 mm, mixture R1 (left) and reference mixture R0 (right)

3.3   Tensile test on textile reinforced elements

The results of the tensile test on textile reinforced elements are taken as mean curve of three tests each and are shown as load-displacement curves to evaluate the loading behaviour of the composite. Figure 6 (left) shows a comparison of the different mixtures (Table 1) after 7 days of water storage at 20 °C with carbon textiles as reinforcement. The testing specimens

of mixtures R0, R1, and R4, produced without any short fibres all show a similar loading behaviour. After reaching a service load of about 2.4 kN the phase of crack initiation starts, where all test specimens show a similar stiffness, until finally the textile reinforcement dominates the load carrying behaviour. The observed service loads correspond with the tensile strengths (Table 2), which are in a similar range for the considered mixtures. Adding short AR-glass fibres by 1 – 3 Vol.-% leads to a higher degree of reinforcement and hence, to a considerable increase in service load as observed for mixtures R2 and R3. Also the loading behaviour of the textile reinforced elements is influenced by the addition of short fibres which leads to a finely distributed crack formation. Especially the high amount of short fibres (3 Vol.-%) of mixture R3 leads to a continuous loading. In contrast to mixture R2 the crack development does not go along with a significant reduction in stiffness after crack initiation as the short fibres take the occurring loads. Therefore higher loads are achieved at same displacements. Finally only the textile reinforcement dominates the load carrying behaviour and leads to failure loads in a similar range as for mixtures R2, and R4. Mixtures R2, and R3, show a higher level of failure load due to a higher volume of reinforcement (carbon textile + AR-glass short fibres) compared to mixtures R0, and R1 (carbon textile, no short fibres). The relatively high failure load observed for mixture R4 can be explained with an improved bonding behaviour caused by the polymer addition [9]. A similar failure load for mixtures R0 and R1 indicates similar bonding characteristic for these cementitious binder systems.
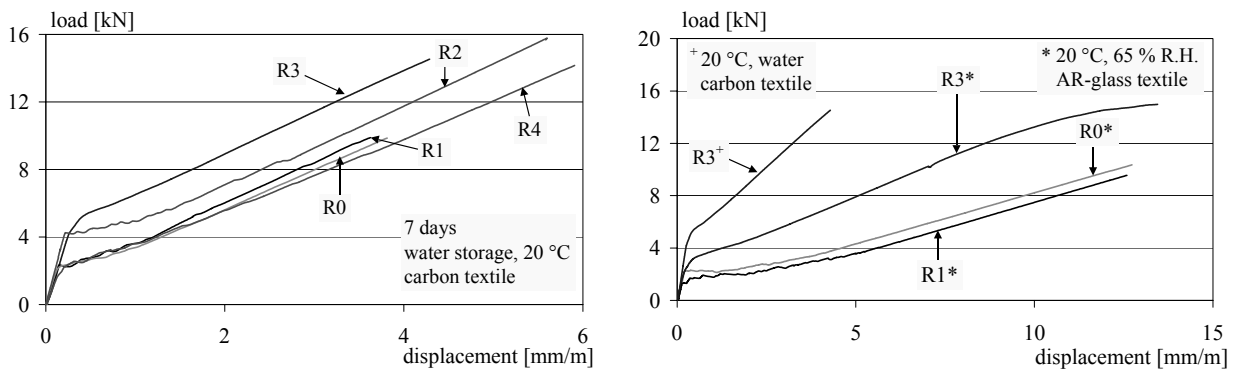
Figure 6: Results of tensile test on textile reinforced elements (left: carbon textile, 7 days, water storage at 20 °C; right: AR-glass textile, 7 days, 20 °C, 65 % R.H.)

Figure 6 (right) shows the load-displacement curve for mixture R3 (7 days, carbon textile, water storage) as already described for Figure 6 (left) in direct comparison with tensile tests using an AR-glass textile as reinforcement material. It shows that the use of carbon textile leads to a reduced stiffness in the composite under tensile load. However, the test also shows that approximately the same maximum load is reached during the test which presumably indicates similar bonding characteristics of the two textiles. Comparing specimens of the mixtures R0, R1, and R3, reinforced with AR-glass textiles again the use of short fibres leads to a significant increase in service load similar to the results of carbon reinforced specimens. Nevertheless also an increase in stiffness between the mixtures R1 and R3 can be observed, possibly on account of a higher overall degree of reinforcement

(AR-glass textile + AR-glass short fibres). As carbon has a significantly higher Young´s modulus compared to AR-glass this effect is not observed for the tensile test shown in Figure 6, left, (carbon textile + AR-glass short fibres). Similar to the elements reinforced with carbon textile the different matrix composition of R0 and R1 has no significant influence on the load carrying behaviour and load capacity of a composite reinforced with AR-glass textile (Figure 6, right).

3.4   4-point bending test on permanent formwork elements

The results of the 4-point bending test on the permanent formwork elements are shown as load versus mid-span deflection curves in Figure 7. In case of the R0 composition, the presented curve refers to the average of 3 test results, in case of the R1 composition to the average of 2 test results. A comparison between both progressions outlines that the principle load carrying behaviour of both composites is very similar. The first cracks are initiated in the flange at a flexural load of about 1.7 kN. The stiffness of the system decreases significantly and the load carrying behaviour in the tensile zone is dominated during the further loading process by the interaction of textile and cementitious matrix. The ultimate load is reached for composition R0 at a load level of 5.2 kN and for composition R1 at a 19 % higher load level of 6.3 kN. In both cases the mechanism is a compressive failure in the ribs, i.e. the compressive strength of the concrete is reached. Therefore higher strengths to reach bending failure are needed. In principle UHPC mixtures are suitable for the use in formwork elements.
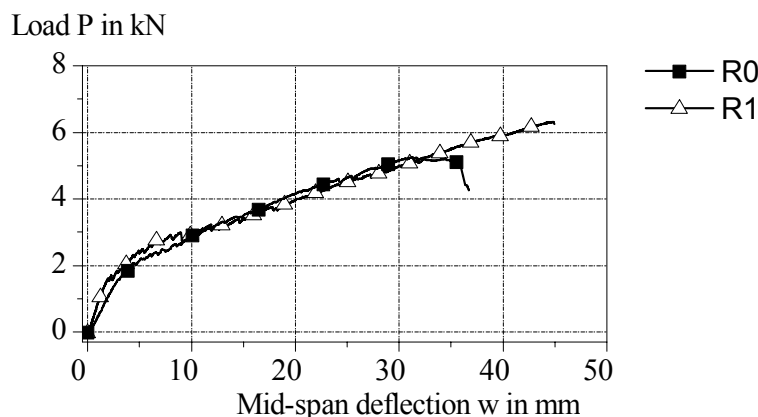
Figure 7:   Results of 4-point bending tests on permanent formwork elements.

4   Conclusions

Within this research project UHPC mixtures are developed which show, in comparison to the reference mixture R0, an increased compressive strength, and especially higher tensile strengths when short AR-glass fibres are added. The fracture energy and the characteristic length are determined by 3-point bending tests on fine grained concrete specimens. These parameters indicate a high brittleness of the unreinforced UHPC (no short fibres) mixtures and a ductile fracture behaviour of short fibre reinforced UHPC mixtures compared to the reference mixture. The tensile tests of the textile reinforced elements show that the adding of

AR-glass short fibres also leads to a change in loading capacity and fracture behaviour. A higher service load and a continuous load carrying behaviour due to a finely distributed crack development are observed, i.e. higher loads are achieved at same displacements. The changes in the matrix composition of the UHPC mixtures (no short fibres) probably do not influence the bonding characteristic significantly and hence no significant differences in the progression of the load-displacement curves obtained by the tensile tests are observed. These findings are verified with the 4-point bending test on structural elements of the mixtures R0 and R1 as they show the same progression of the load versus mid span deflection curve until a compressive failure in the ribs. In case of the R1 composition a brittle failure is observed in the structural 4-point bending test, which is in accordance with the significantly lower fracture energy compared to the reference mixture. Mixture R0 shows a more quasi ductile failure as the structure starts yielding at ultimate load level (Figure 7).

As the compressive failure of the concrete in the ribs is so far dominating the failure of the structure, a modification of the R0 composition by short glass fibres which rather leads to an increase in tensile strength will have no significant effect on the load carrying capacity of the formwork elements. Still, the results show that the increase in compressive strength of about 24 % for mixture R1 compared to mixture R0 also leads to increase ultimate load in the 4-point bending test. If the rib geometry is strengthened and such the failure of the system transferred in the tensile zone, an altogether higher ultimate load probably would be reached in combination with the R3 mixture. It can be expected, that in case of a carbon textile which features a significantly higher Young's modulus, the compressive zone is extended because the neutral axis wanders towards the stiffer reinforcement. In that case the dominating failure mechanism may not be any more the compressive failure of the ribs but the tensile failure of the composite in the flange. As it is found in the present study that the results of the compressive tests on concrete and tensile tests on textile reinforced specimens allow a good estimation of the overall structural behaviour of the composite, it can be expected that a carbon textile composite with the mixture R3 would feature a considerably increased load carrying capacity compared to mixture R0, or even mixture R3 in combination with AR-glass textile. In future investigations these findings will be verified with further experiments.

5 Acknowledgement

6 References

[1] Brameshuber, W. ; Brockmann, T.: Development and Optimization of Cementitious Matrices for Textile Reinforced Elements. London : Concrete Society, 2001. - In: Proceedings of the 12th International Congress of the International Glassfibre Reinforced Concrete Association, Dublin, 14-16 May 2001, S. 237-249.

[2] Brameshuber, W. ; Brockmann, T. ; Hegger, J. ; Molter, M.: Untersuchungen zum textilbewehrtem Beton. In: Beton 52 (2002), Nr. 9, S. 424-426,428-429

[3] DIN EN 196-1, 05.95, Prüfverfahren für Zement, Teil 1: Bestimmung der Festigkeit

[4] DIN 18555-2, 09.82, Prüfung von Mörteln mit mineralischen Bindemitteln, Teil 2: Frischmörtel mit dichten Zuschlägen, Bestimmung der Konsistenz, der Rohdichte und des Luftgehalts

[5] DIN 18555-3, 09.82, Prüfung von Mörteln mit mineralischen Bindemitteln, Teil 3: Festmörtel, Bestimmung der Biegezugfestigkeit, Druckfestigkeit und Rohdichte

[6] DIN 1048-5, 06.81, Prüfverfahren für Beton, gesondert hergestellte Probekörper

[7] Brameshuber, W. ; Brockmann, T.: Textilbewehrter ultrahochfester Beton. Berlin : Bauwesen, 2003. - In: Ultrahochfester Beton: 3. Leipziger Fachtagung Innovationen im Bauwesen, Leipzig, 27./28.11.2003, (König, G. ; Holschemacher, K. ; Dehn, F. (Ed.)), S. 153-164

[8] Wesche, K.: Baustoffe für tragende Bauteile. Bd.: 2: Beton, Mauerwerk. 3.Aufl. Wiesbaden: Bauverlag, 1993

[9] Dilger, K. ; Mund, F. ; Dilthey, U. ; Raupach, M. ; Walk-Lauffer, B. ; et al: Einsatz einer polymeren Phase zur Verbundverbesserung. Dresden : Lehrstuhl für Massivbau, 2003. - In: Textile Reinforced Structures, Proceedings of the 2nd Colloquium, Dresden, 29.9.2003-1.10.2003, (Curbach, M. (Ed.)), S. 133-144

Teutsch, Manfred
Dr.-Ing., Akademischer Direktor
Institute for Building Materials, Concrete
Structures and Fire Protection
Technical University Braunschweig
Braunschweig, Germany

Grunert, Jens
Dipl.-Ing., Wissenschaftlicher Mitarbeiter
Institute for Building Materials, Concrete
Structures and Fire Protection
Technical University Braunschweig
Braunschweig, Germany

Bending design of steel-fibre-strengthened UHPC

Summary

Ultra high performance concrete (UHPC) differs from normal- and high strength concrete by having a more compact material structure. The UHPC components show a higher resistance against mechanical abrasions and freeze-thaw-stress as well as a greater impermeability for fluids and gases. Furthermore the mechanical qualities of UPHC are superior to those of normal or high strength concrete. Without adding steel fibres UHPC is a very brittle material, which fails abruptly. A ductile material behaviour can be reached by using steel fibres. This article describes how to design a UHPC for bending by generating stress-strain-relations Therefore two different kinds of stress-strain-rises will be presented and discussed by the authors.

Keywords: s*teelfabric concrete, bending design*

1　　　General

Regarding compression strength concrete can be divided in a normal, high or ultra high strength concrete. Normal and high strength concrete is specified according to DIN 1045 [1] by the supervising authority. Whereas there are no design regulations for UHPC in Germany. For buildings or components consisting of UHPC a qualification design approval or agreement of individual case is required. Recommendations of designing these UHPC components are developed in [2] and [3].

According to the grain-size UHPC can be subdivided in fine-grained and coarse-grained UHPC. Fine-grained UHPC already exists protected by patents and is utilized by the company Lafarge under the label Ductal®.This UHPC was used sporadically for construction projects [4]. For most tests and applications so far fine-grained UHPC was utilized (Ductal®).

Both sorts of UHPC have their brittle behaviour in common in the compressive as well as in the tensile area. Along with rising strength a more and more brittle behaviour is present. A ductile material can be generated by adding steel fibres. But then both sorts of UHPC differ. To the fine-grained UHPC huge amounts (>200 kg/m³) of short steel fibres (l_f ca. 10 mm) can be added without leading to undesired fibre concentrations ("Igelbildung") during manufacturing. In the coarse-grained UHPC undesired fibre concentrations are formed already when adding fibre amounts < 200 kg/m³ independent to the length of fibres. Tests at the Institut für Baustoffe, Massivbau und Brandschutz im Fachgebiet Massivbau (iBMB) showed that a very efficient UHPC can be created by using ca. 80 kg/m³ of long fibres (l_f = 30 mm)

2　　　Tests

For the design of ultra high performance steel fibre reinforced concrete (UHPSFRC) components the knowledge of the material qualities is required which were determined by material tests. For recording the compression strength usually cylinder or cubic blocks are examined. Because of minor differences between the crushing test of UHPC and normal or high strength concrete these tests are not mentioned in this report. Rather it will be described how the material tension behaviour can be determined by performing tests.

2.1　　　Centric tension tests

Using centric tension tests is the best way of directly determining the tension bearing behaviour. However centric tension tests are carried out rarely because the undisturbed force introduction cannot be realized without high efforts. Figure 1 shows the set-up of a centric tension test.
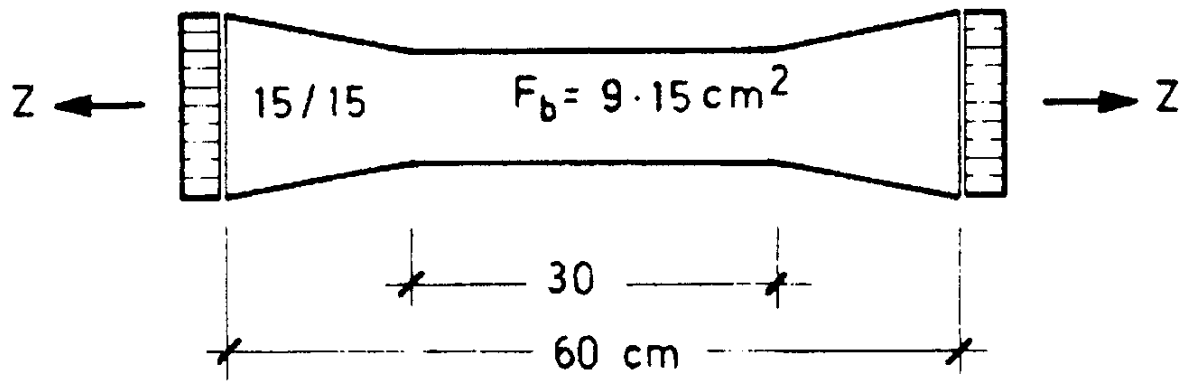
Figure 1: Axial tension test [5]

2.2   Bending tension test

The direct determination of the tensile strength is very hard as described under 2.1. Therefore usually the tensile strength is calculated indirectly using bending tension tests. For coarse-grained UHPSFRC tests on beams are recommended. In Germany flexural beams with dimensions of 15/15/70 cm (w/h/l) are mainly used for the normal and high strength concrete. To determinate the bending tensile strength the so-called 4-point-tests is used. The test set-up is shown in Figure 2. This test is also suitable to determinate the bending tensile strength of UHPSFRC.
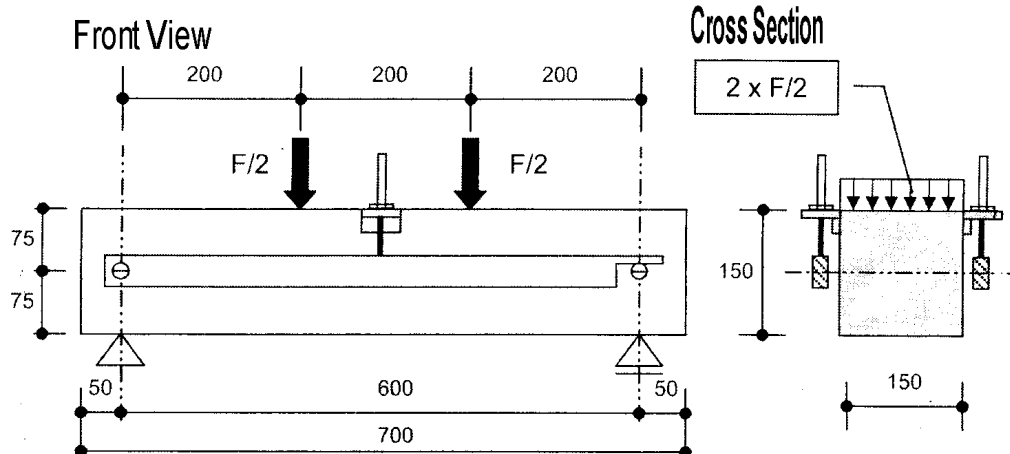
Figure 2:   Bending tension test after the DBV-instructional "Stahlfaserbeton" – „Steelfabric concrete" [6]

Other countries use partly different dimensions and load arrangements. In France the Association Francaise de Génie Civil (AFGC) [7] asks for a determination of the bending tensile strength by utilizing a 3-point-test. Beside beams prisms are also scheduled as test pieces. Prisms are mainly employed for testing fine-grained UHPSFRC.

Based on the 4-point-bending-tension-test a not yet existing guideline for the design of UHPSFRC components should be created. In the 3-point-test the maximum stress is beneath the point where the load is applicated. And the first crack will occur at this point and will increase with higher loads. Based on the chosen load arrangements no further cracks will occur. Unlike with the 4-point-test the maximum stress occurs in the area between both concentrated point loads. Thus the first crack will occur in this area where the material is the weakest. An inhomogenous fibre arrangement along the beam can be recorded with this testing method. Therefore the 4-point-bending-test leads to results which reflects the material behaviour of steel fibre reinforced components the best way.

2.2.1 Evaluation of bending-tension-tests

The DAfStb-Standard „Stahlfaserbeton" – "Steelfabric concrete" (15. draft) [8] outlines to divide steelfabric concrete into classifications of capacity. These classifications of capacity are defined by using the acceptable bending stress of the steelfabric concrete in the range of small (0.5 mm) and big (3.5 mm) crack widths and bending respectively. Figure 3 shows the result of a bending tension test of a UHPSFRC and the crack width for designing the classes of capacity.
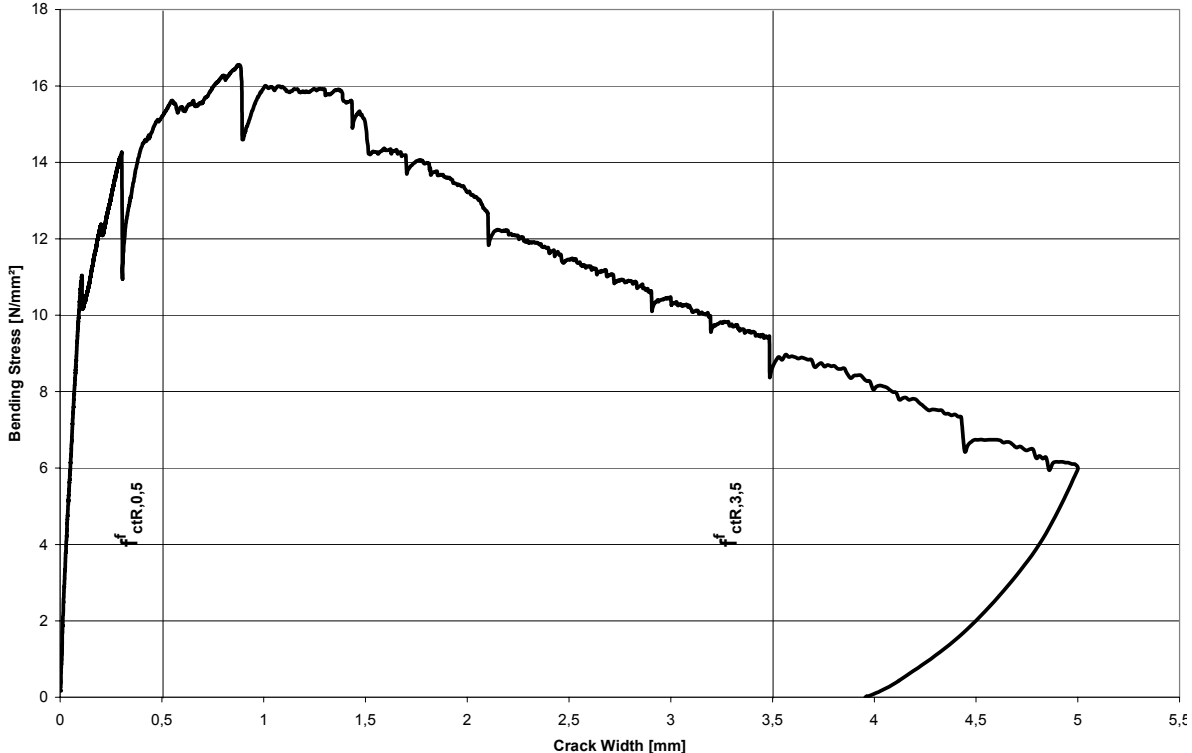
Figure 3:   Results of a bending tension test

With the bending stress $f^f_{ct,fl,0.5}$ and $f^f_{ct,fl,3.5}$ a stress-strain-rise for the area of tension can be defined for designing UHPSFRC components (q.v. 3.2).

3   Design application

3.1   Application France (AFGC)

For France the AFGC supplies design applications [7] for ultimate limits of serviceability (SLS) and of load-bearing capacity (ULS). These applications are shown in Figure 4.
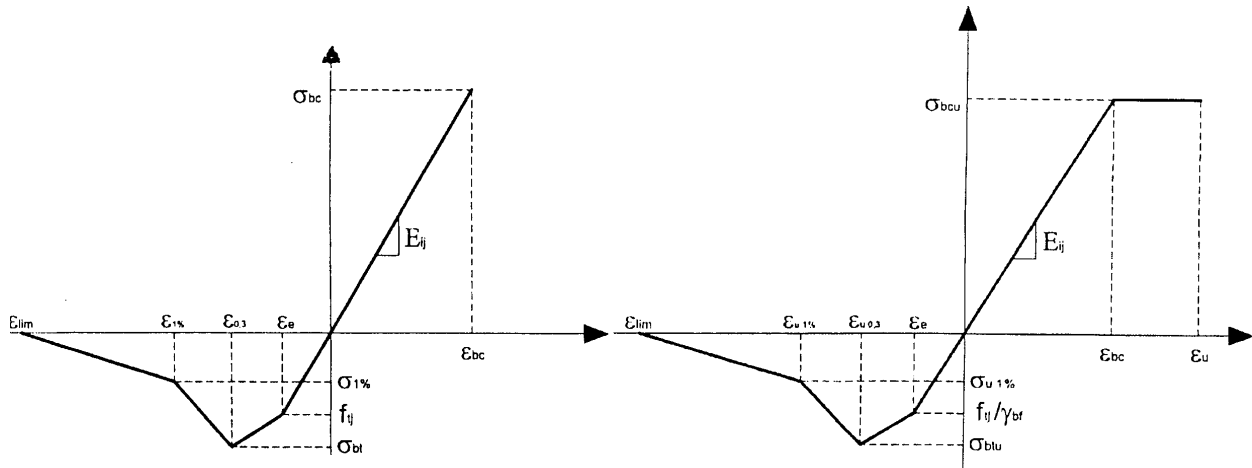
Figure 4: Diagrams for the SLS (left) and ULS (right) regarding the AFGC

In the AFGC-standard the area of tension in SLS and ULS is equally considered. Regarding the ULS solely the concrete tensile strength is divided by the load factor γ (1.5 for concrete and 1.3 for steelfabric concrete) in the elastic area. Other than the Progress report [3] (q.v. 3.2) the AFGC-standard does not give any fixed value for the ductility limit ε_{lim} . It can be calculated with the fibre length and component height.

$$\varepsilon_{lim} = \frac{\ell_f}{4 \cdot \ell_c} \qquad (1)$$

With: ℓ_f = fibre length
         ℓ_c = characteristically length = ⅔ • h

Like shown in equation (1) the maximum crack width is thus about a quarter of the fibre length.

In the compressed range the stress-strain-diagram shows a bi-linear rise in the ULS. In the SLS it shows a linear rise up to the elastic limit. The limit of compressive strength σ_{bc} differs only marginally from the SLS to the ULS one another.

3.2   Application Germany (Progress report of the DAfStb)

3.2.1   General

The suggested design application (Progress report [3]) is generally based on the authors elaborations. The aim of these suggestions is to combine the design with the standards DIN 1045 [1] and the Eurocode [9] respectively. A reinforced UHPC could then be designed

based on these applications. Thus for the design of the cross section the linear strain distribution is relevant. The ductility limit of 25 ‰ on the tensile side and a compression strain of ε_{c2u} = -2.2 ÷ -3.5 ‰ on the compressive side has to be observed.

3.2.2   Compressive strength

So far the standard DIN 1045 [1] includes high strength concrete up to a strength classification of C100/115. For the design of the cross section the stress-strain-rise of Figure 5 is to be used.
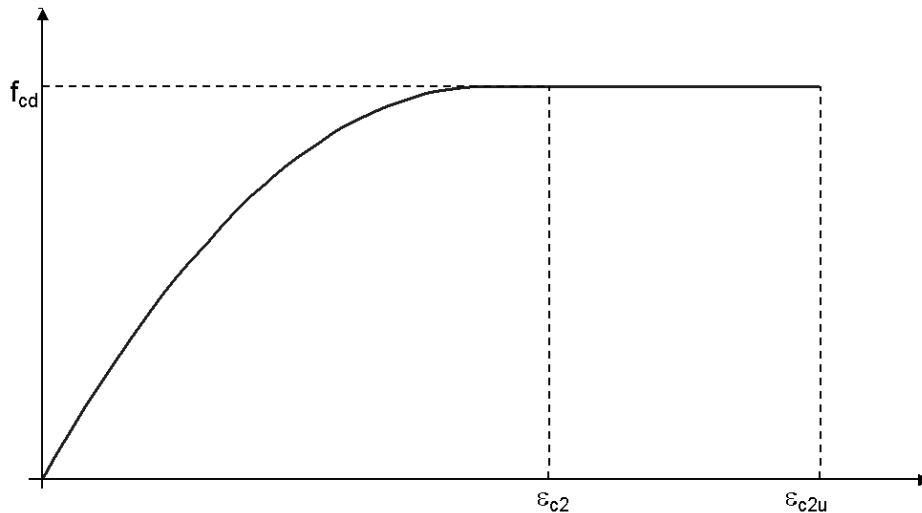
Figure 5: Stress-strain-rise for the cross section design

With: $f_{cd} = \alpha \cdot f_{ck}/\gamma_c$ (2)

From strength classification C55/67 it has to be calculated with γ_c' instead of γ_c.

$$\gamma_c' = \frac{1}{1.1 - \dfrac{f_{ck}}{500}} \cdot \gamma_c \geq 1 \qquad\qquad f_{ck} \text{ in } [N/mm^2] \qquad\qquad (3)$$

To determinate of γ_c' UHPC is subdivided into concrete with or without added fibres. In the german guideline Progress report [3] for UHPC without fibres the application is kept up to a strength classification up to C150. For concrete with higher strength the load factor γ_c' is limited to 1.25 which complies with the value of C150.

$$1.0 \leq \gamma_c' \leq 1.25 \qquad\qquad\qquad\qquad\qquad\qquad\qquad\qquad\qquad\qquad (4)$$

For a UHPC with fibres the application according to DIN 1045 [1] is also used with γ_c' limited to 1.1.

The values of ε_{c2} and ε_{c2u}. show a similar behaviour. According to table 9 of the DIN 1045 [1] it is ε_c=-2.0 ‰ for strength classifications of $f_{ck} \leq 50$. This value decreases to –2.20 ‰ for the strength classification of 100. Unlike that the value ε_{c2u} increases with higher strength

528

classifications. Up to f_{ck} = 50 N/mm² it is ε_{c2u} = -3.5 ‰. With f_{ck} = 100 N/mm² it is ε_{c2u} = ε_{c2} = -2.2 ‰.

For the UHPC no restrictive ductility limits are published in the Progress report [3]. Therefore the authors recommend to limit ε_{c2} to -2.6 ‰ to strength classification f_{ck} = 200 N/mm². For UHPC without fibres it is ε_{c2u} = ε_{c2} similar to high strength concrete. For UHPC with fibres ε_{c2u} is limited to -3.0 ‰. According to Figure 5 the stress between ε_{c2} and ε_{c2u} remains constant at the value of the stress at ε_{c2} . For the above suggested ductility limit, it has to be remarked that their value is only important for the design of components with compressive reinforcement.

With the previously described stress-strain-diagram of the compressive area a design is possible if a regarding rising of the tensile side is known (q.v. 3.2.3).

3.2.3 Tensile stress

As previously explained the bending tests and its results should enable to generate a tensile-stress-strain-diagram. For UHPC referring regulations of the standards DIN 1045 [1] and the DAfStb-guideline „Stahlfaserbeton" – "Steelfabric concrete" [8] are utilized. The guideline includes the following stress-strain-diagram.
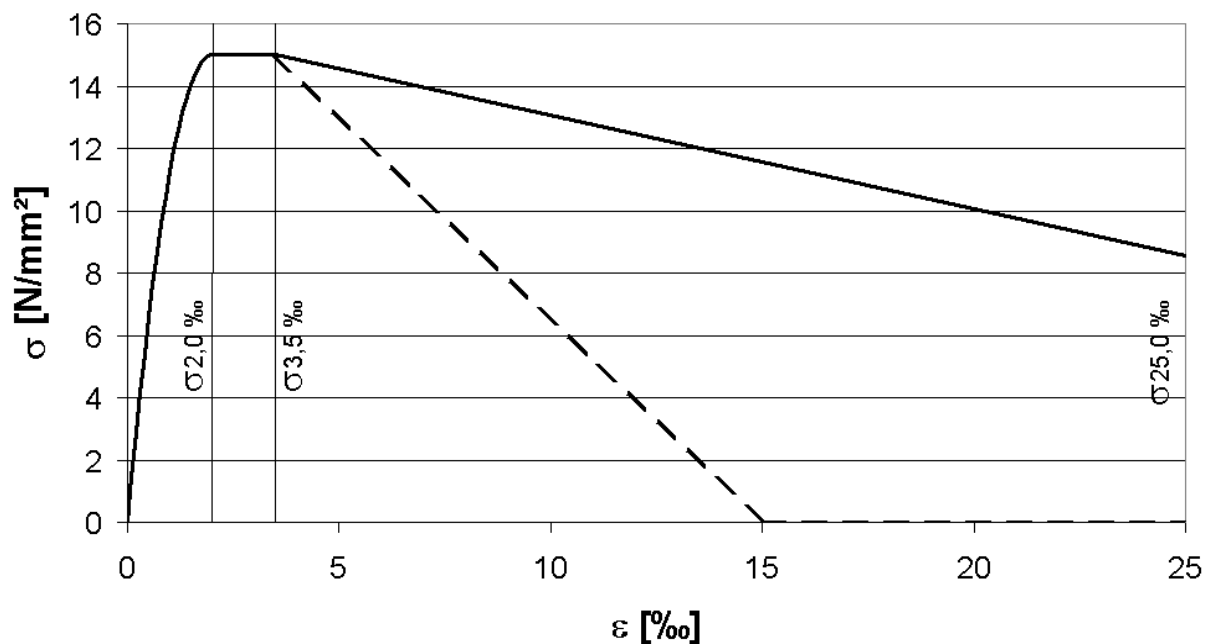
Figure 6: Stress-strain-diagram for steelfabric concrete

This diagram could also be used for UHPSFRC. Whereas $\sigma_{2.0‰}$ is determined based on the bending tensile stress of the test pieces on a crack width of 0.5 mm and $\sigma_{25‰}$ is based on a crack width of 3.5 mm. The dashed line is valid for certain stress-relations which are

explained later. The centric stress at $\sigma_{2.0\text{-}3.5\text{‰}}$ can be determined incorporating bending stress with the following calculation:

$$\sigma_{2.0\text{-}3.5\text{‰}} = f_{0.5} \cdot 0.37 \tag{5}$$

For the relation $f_{3.5}/f_{0.5} \geq 0.7$ follows:

$$\sigma_{25\text{‰}} = f_{3.5} \cdot 0.25 \tag{6}$$

Reinforced concrete components consisting of normal concrete usually complies with this ratio. Components consisting of UHPSFRC show a ratio of $f_{3.5}/f_{0.5} \leq 0.7$ mainly when using short fibres. Based on the results of previous investigations the conversion factor of bending tension to centric tensile stress has to be reduced in the range of 0.5 – 0.7. This reduction is shown in Figure 7.
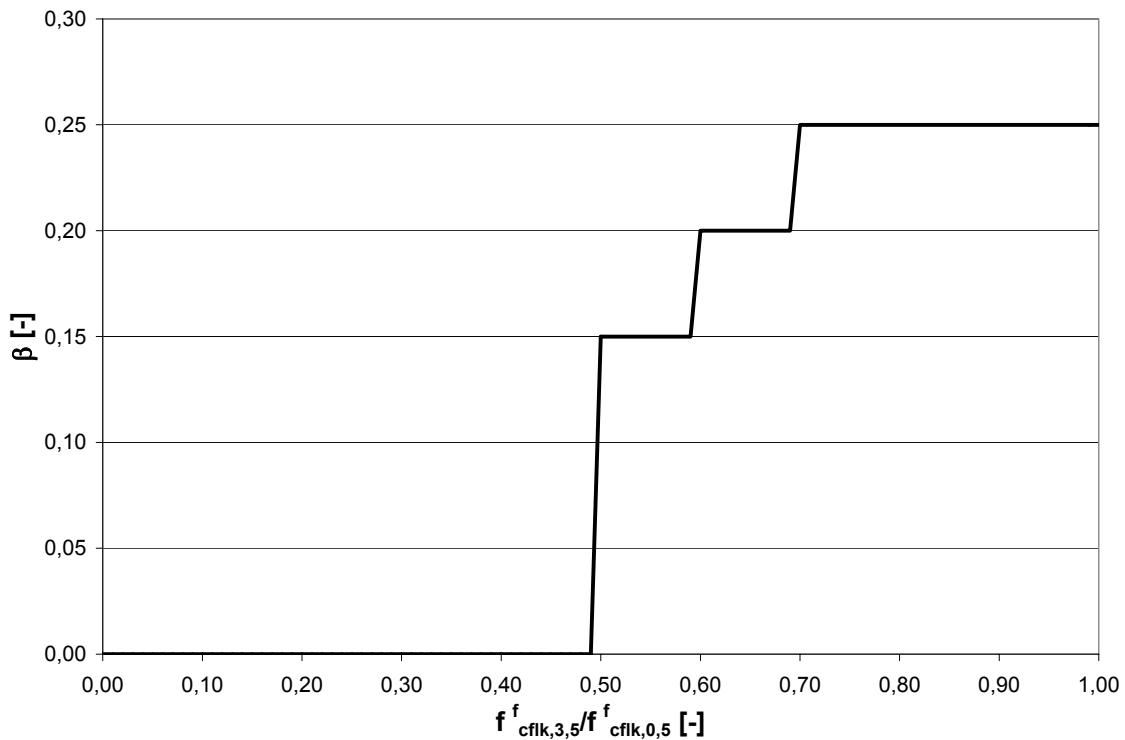
Figure 7: Reduction of the factor for the conversion of bending tension stress to centric tensile stress

With a ratio of $f_{3.5}/f_{0.5} \leq 0.5$ the dashed line from Figure 6 has to be taken, which results in $\varepsilon_{u1} \leq 25$ ‰.

The application Progress report [3] provides the following advantage for the engineer. With only two values of the bending tension test the material behaviour can be described accurately enough for designing purposes. As shown in Figure 8 very good accordance with

the results can be achieved for coarse-grained UHPSFRC in the ULS by applying the rules of the Progress report [3].
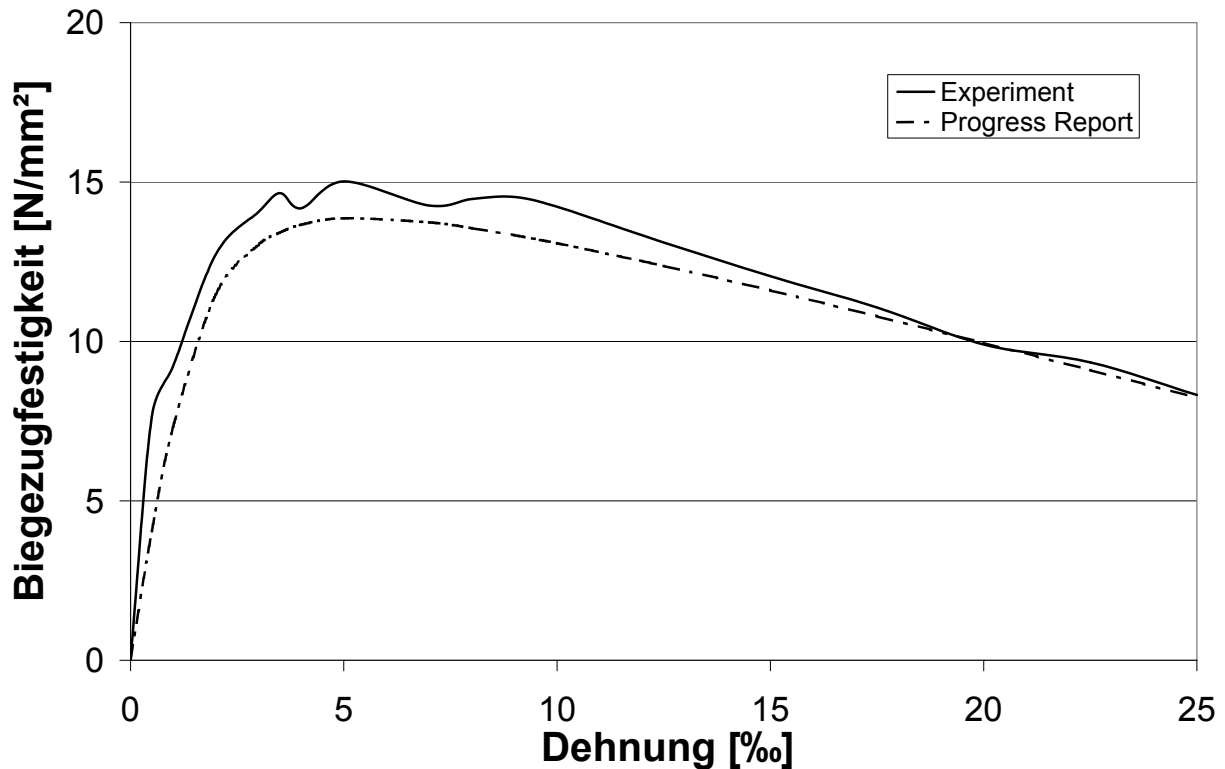
Figure 8:   Comparison test results with the application Progress report [3]

Based on the application Progress report [3] the accordance for the fine-grained UHPSFRC is not as good as for the coarse-grained UHPSFRC.

4   Conclusions

This article introduces design applications for bending stressed components of UHPDFRC. The design recommendations of the Progress report [3] complies well with the design concept of the standard DIN 1045 [1] and the Eurocode [9] respectively. With the recommendation for coarse-grained UHPSFRC a very good accordance with the test results could be shown. This design application can only be used partly for fine-grained UHPSFRC. Therefore further research is required.

The application of the AFGC-standard [7] also complies with the design concept of the Eurocode [9] although it differs in some items. In the tension range the recommended stress-strain-rise is significantly more complex than the application Progress report [3].

5   References

[1] DIN 1045-1: Tragwerke aus Beton, Stahlbeton und Spannbeton. Teil 1: Bemessung und Konstruktion, Berlin, 2001.

[2] Fehling, E.; Bunje, K.: Bemessung für Biegung und Querkraft bei Bauteilen aus UHFB, in Ultrahochfester Beton – Innovationen im Bauwesen- Beiträge aus der Praxis und Wissenschaft, Seite 183-198, Berlin, 2003.

[3] Deutscher Ausschuss für Stahlbeton: Sachstandbericht Ultrahochfester Beton, Berlin unveröffentlicht.

[4] Teutsch, M.: Selbstverdichtender und Ultrahochfest Beton – Baustoffe und Konstruktionen für die Zukunft?, in Braunschweiger Bauseminar 2003, 13. und 14. November, Bauforschung und – praxis in schwierigen Zeiten, Seite 91-100, Braunschweig, 2003.

[5] Leonhardt, F.: Vorlesungen über Massivbau, Erster Teil: Grundlagen zur Bemessung im Stahlbetonbau, Berlin, 1973.

[6] Deutscher Beton- und Bautechnik-Verein e.V.: DBV-Merkblatt Stahlfaserbeton, Fassung 2001,Berlin, 2001.

[7] Association Francaise de Génie Civil: Documents scientifiques et techniques – Bétons fibrés à ultra-hautes performances, 2002.

[8] Deutscher Ausschuss für Stahlbeton: DAfStb-Richtlinie Stahlfaserbeton (15. Entwurf), Ergänzungen zu DIN 1045, Teile 1 bis 4 (07/2001), Berlin, unveröffentlicht.

[9] DIN V ENV 1992-1: Eurocode 2, Planung von Stahlbeton- und Spannbetontragwerken, Grundlagen und Anwendungsregeln für den Hochbau, 1995

Jörg Jungwirth
Dipl. Ing., Doctoral Student
Structural Concrete Laboratory
Swiss Federal Institute of Technology (EPFL)
Lausanne, Switzerland

Aurelio Muttoni
Prof. Dr.
Structural Concrete Laboratory
Swiss Federal Institute of Technology (EPFL)
Lausanne, Switzerland

Structural Behavior of Tension Members in UHPC

Summary

The paper presents a study on the tensile behavior of UHPC conducted at the structural concrete laboratory at the Swiss Federal Institute of Technology in Lausanne (EPFL). Material tests and tests on structural members with reinforcement bars have been performed. A schematic representation of the material behavior allows a general description of the behavior of structural members in tension. The mechanical behavior for tension members and a simple model are presented.

Keywords: UHPC, tensile behavior, bond, structural members, conventionally reinforced UHPC elements, large scale testing

1   Introduction

The high performance concrete project currently under way at the Structural Concrete Laboratory (IS-BETON - EPFL) aims at examining new concept and design approaches to design statically efficient and economically viable structures using ultra high performance concrete.

In this scope, the scientific approach chosen is first to characterize and understand the behavior of UHPC by means of various laboratory experiences on material specimens and structural elements [1, 2]. On this basis, physical models are subsequently developed to describe the observed behavior. Finally, design concepts are proposed, with a perspective on potentially efficient structures.

The present paper focuses on the study of the behavior of UHPC in tension with and without conventional reinforcement. A series of tests on the tensile behavior of UHPC and the behavior

Jörg Jungwirth
Dipl. Ing., Doctoral Student
Structural Concrete Laboratory
Swiss Federal Institute of Technology (EPFL)
Lausanne, Switzerland

Aurelio Muttoni
Prof. Dr.
Structural Concrete Laboratory
Swiss Federal Institute of Technology (EPFL)
Lausanne, Switzerland

Structural Behavior of Tension Members in UHPC

Summary

The paper presents a study on the tensile behavior of UHPC conducted at the structural concrete laboratory at the Swiss Federal Institute of Technology in Lausanne (EPFL). Material tests and tests on structural members with reinforcement bars have been performed. A schematic representation of the material behavior allows a general description of the behavior of structural members in tension. The mechanical behavior for tension members and a simple model are presented.

Keywords: UHPC, tensile behavior, bond, structural members, conventionally reinforced UHPC elements, large scale testing

1   Introduction

The high performance concrete project currently under way at the Structural Concrete Laboratory (IS-BETON - EPFL) aims at examining new concept and design approaches to design statically efficient and economically viable structures using ultra high performance concrete.

In this scope, the scientific approach chosen is first to characterize and understand the behavior of UHPC by means of various laboratory experiences on material specimens and structural elements [1, 2]. On this basis, physical models are subsequently developed to describe the observed behavior. Finally, design concepts are proposed, with a perspective on potentially efficient structures.

The present paper focuses on the study of the behavior of UHPC in tension with and without conventional reinforcement. A series of tests on the tensile behavior of UHPC and the behavior

of bar reinforced tension members in UHPC have been carried out and the main results are presented.

2   Material

The UHPC used for the tests is the CERACEM (BFM – Millau), provided as a premix. Its composition is given in table 1. The CERACEM (BFM – Millau) belongs to the BSI[®]/CERACEM range developed by SIKA and EIFFAGE [3]. The material is characterized by a relatively coarse composition compared to other UHPCs. Aggregates up to 7 mm are included in the matrix. The diameter of the added fibers of 0.3 mm is also relatively thick.

Table 1: Composition of the UHPC

Components		Quantity
Premix (cement, silica fume, sand and granular 0 - 7 mm)	kg/m³	2355
Steel fibers (l_f = 20 mm, $\varnothing_f$ = 0.3 mm, ρ_f = 2.5 vol. %)	kg/m³	195
SIKA specific superplasticizer	kg/m³	44.6
Water	kg/m³	195

To obtain a reliable performance, a strict mixing procedure has to be followed. The batches are mixed in a high performance vertical axis mixer. For curing, the specimens are covered with a plastic foil after casting to avoid drying out. The formwork is taken off after 3 days and the specimens are stored under water until testing. Quality controls on hardened concrete were performed systematically in order to guarantee constant performance of the UHPC. All the tests were performed at 28 days.

3   Material behavior

To take into consideration the local effects of the crack opening, the tensile behavior of the material was analyzed through two different test series. Specimens with constant sections are used to study the uniformly distributed behavior until the crack opening. The local effects of the crack opening are investigated with notched specimens.

3.1   Distributed deformation

The tension tests are carried out on dogbone shaped specimens, with a length of 700 mm, a thickness of 45 mm and a width of 160 mm in the measurement zone (figure 1). The test is performed as a tension test on a clamped specimen. The specimen is fixed with glue in the support to avoid eccentricity and rotation [4]. The test is conducted at a constant deformation speed of 0.33 mm/min. The deformation is measured by 4 LVDT (linear variable differential transformer) on the front side and 5 strain gages on the back side.

In order to analyze the contribution of the two components (cement matrix and fibers), both fiber reinforced specimens and non fiber reinforced specimens are tested.

a) front view   b) side view   c) specimen during testing
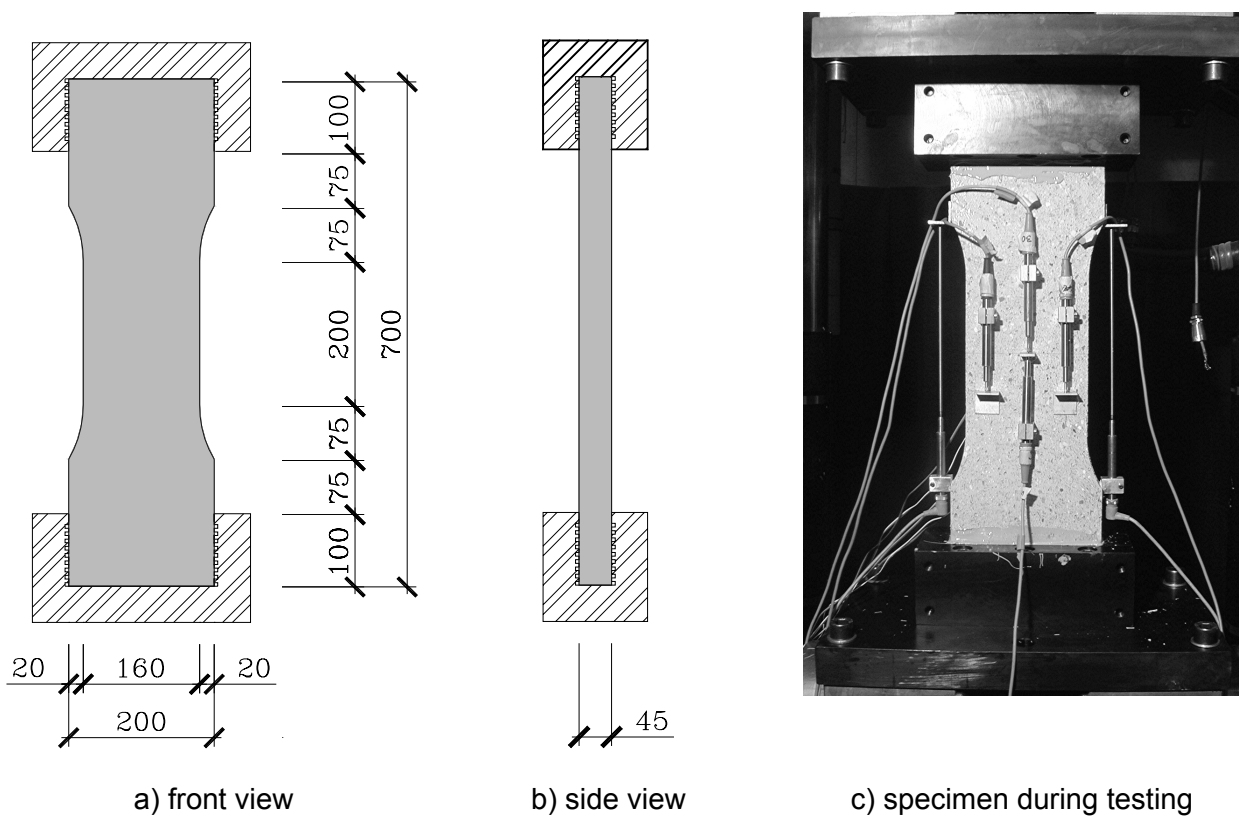
Figure 1: Dogbone shaped specimen for the tensile test (dimensions in mm)

Two test series, with and without fibers, were carried out. Figure 2 shows the resulting stress-strain diagram. Both, the fiber reinforced specimens 1 & 2 as well as the specimen 3 (without fibers) show initially a linear elastic behavior with a Young's modulus of about 60 GPa (secant modulus 0 to 1/3 f_{ct}). At this stage, the fibers have almost no influence and the behavior is governed by the cement matrix. When the mean stress reaches a value of about 8.5 MPa, an initial crack appears. For the specimen without fibers (specimen 3), this leads to brittle failure. However, the stress of the fiber reinforced specimens 1 and 2 slightly increases up to 10 MPa. This effect is due to the high fiber ratio. The fibers crossing the crack have in total a higher strength than the cement matrix. The behavior is similar to the traditional reinforced concrete, characterized by an increase of the capacity after cracking. During this stage multiple cracks are created. This multi cracking effect is regularly distributed over the whole length of the specimen, so it can be assumed as smeared. The very small crack opening (micro-cracks) is just large enough to activate the fibers allowing the transfer of the stresses from the matrix. At a strain of about 2.5 ‰, all cracks have been formed and the bond strength of the fibers crossing the crack is reached in one of the cracks. The deformation localizes in this crack, which opens to become a macro-crack. Finally the fibers are progressively pulled out.
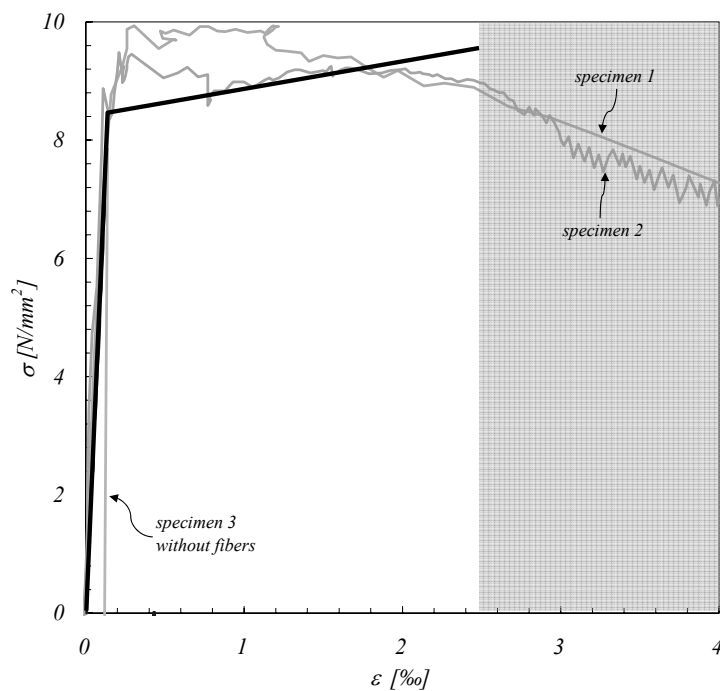
	E [GPa]	$f_{ct,matrix}$ [MPa]	ε_{matrix} [‰]	f_{ct} [Mpa]	ε_t [‰]	note
1	63	8.8	0.16	9.9	2.5	
2	66	8.9	0.11	9.5	2.5	
3	60	7.8	0.14	-	-	no fibers

a) stress – strain diagram   b) results

Figure 2: Pre-peak behavior of the tested UHPC

Several authors propose a bi-linear relation as shown in figure 2 to approximate the behavior of UHPCs [5, 6]

1. The elastic behavior of the matrix described by the Young's modulus and the tensile strength of the matrix.
2. A linear approximation of the multi-cracking phases up to the ultimate bond strength of the fibers crossing the crack.

For the tested UHPC, where the difference between the matrix strength and the ultimate strength is quite small, a linear approach in the multi-crack stage may not be ideal. As the small number of specimens doesn't allow a detailed analysis, the bi-linear relation is adopted as a first approach.

The crack spacing in the multi-crack stage can be estimated by the approach used for traditional reinforced concrete. With the assumption that the force in the fibers (length $l_f = 20\,mm$) crossing the crack is completely transferred to the matrix over the distance of $l_f/2$, the maximal crack spacing is $s_{max} = 2 \cdot l_f/2 = 20\,mm$. If there are two cracks with a spacing larger than the maximum distance, another crack will appear. Thus, the minimal crack spacing is $s_{min} = l_f/2 = 10\,mm$. So the average crack spacing can then be estimated as

$$s_r = \frac{3}{4} l_f = 15 \; mm \qquad\qquad (1)$$

which corresponds well to the crack-spacing observed on the specimens.

3.2   Crack opening

The crack opening behavior of the UHPC after the formation of the macro crack can be observed by means of a notched tensile test (see figure 3). The cross section of the specimen is weakened to a width of 160 mm by a sawed notch in order to control the crack formation. Otherwise, the rest of the test setup is the same as for the previous test. The development of the crack is observed with strain gages on the backside and the crack opening is measured with two LVDTs on the front side of the specimens. The crack is initiated over the whole width of the section by several pre-loading cycles. The pre-loading cycles were started with a nominal stress of 5 MPa. At every subsequent cycle the peak force was increased by 0.5 MPa until the strain gage located over the crack on the backside of the specimen showed the initiation of the crack opening. Subsequently, the crack opening was conducted in one load cycle with a constant deformation speed of 0.08 mm/min.

a) front view   b) side view   c) specimen during testing, opened crack
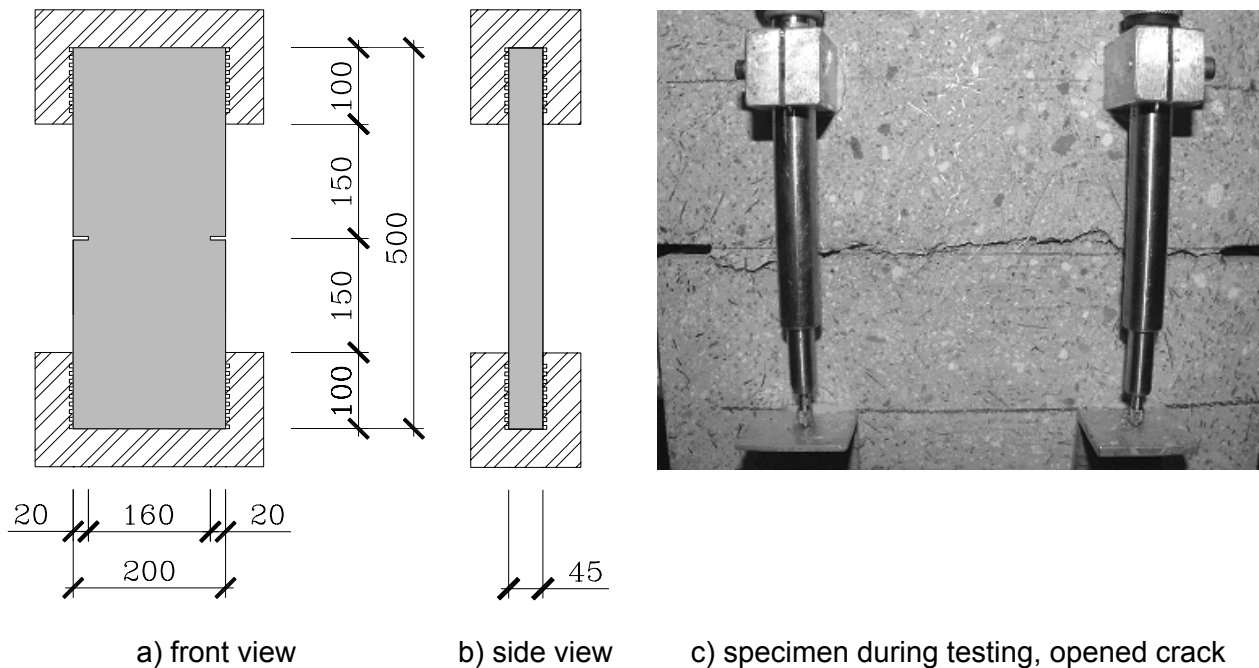
Figure 3: Notched specimen for the tensile test (dimensions in mm)

In order to obtain the actual crack opening from the measurement, which covers a length of 100 mm, the contribution from the uncracked parts of the specimens must be deducted. Elastic uncracked behavior can be assumed, because the stress level remains below the strength of the matrix in the intact part of the specimen. Figure 4a shows, for the three tested specimens (specimen 4, 5, 6), the average stress versus crack opening diagram inserted in the stress – displacement diagram of the test.
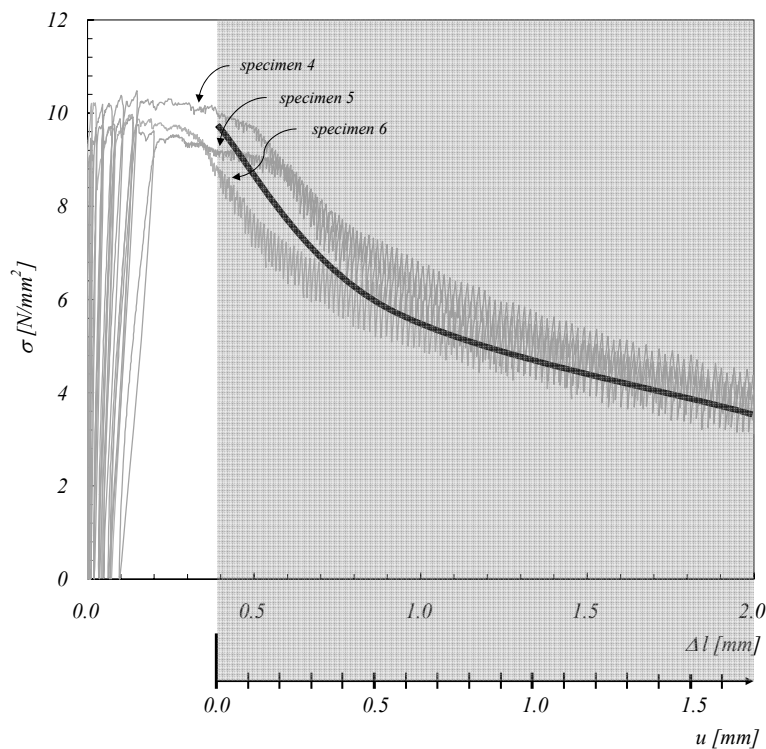
a) crack opening behavior   b) pulled out fibers

Figure 4: Crack opening behavior of the notched specimens

The crack opening is accompanied by a decrease of the mean axial stress. The decrease of the stress is initially large and becomes smaller for larger crack openings. The fracture surface shows that all the fibers are pulled out and that none of them breaks by reaching its ultimate strength (figure 4b).

3.3   Tensile behavior of an UHPC element

The tensile behavior of a tensile element of arbitrary length can now be derived from the distributed pre-peak behavior and the local crack-opening behavior. In a stress-strain diagram (figure 5) the elastic phase (phase 1) and the multiple micro-cracking phase (phase 2) are independent from the length of the specimen. The multi-cracking is a well distributed phenomenon assumed to be smeared over the length. During the multi-cracking phase the fibers are activated when the micro-cracks open. When the ultimate bond stress of the fibers crossing the crack is reached in one crack, the fibers are progressively pulled out. This results in a concentration of the deformation in this particular crack. The nominal strain of the element due to the crack opening (phase 3) thus depends on the length of the element.

a) stress-strain diagram   b) schema of the multi-cracking
                                   phase and crack localization
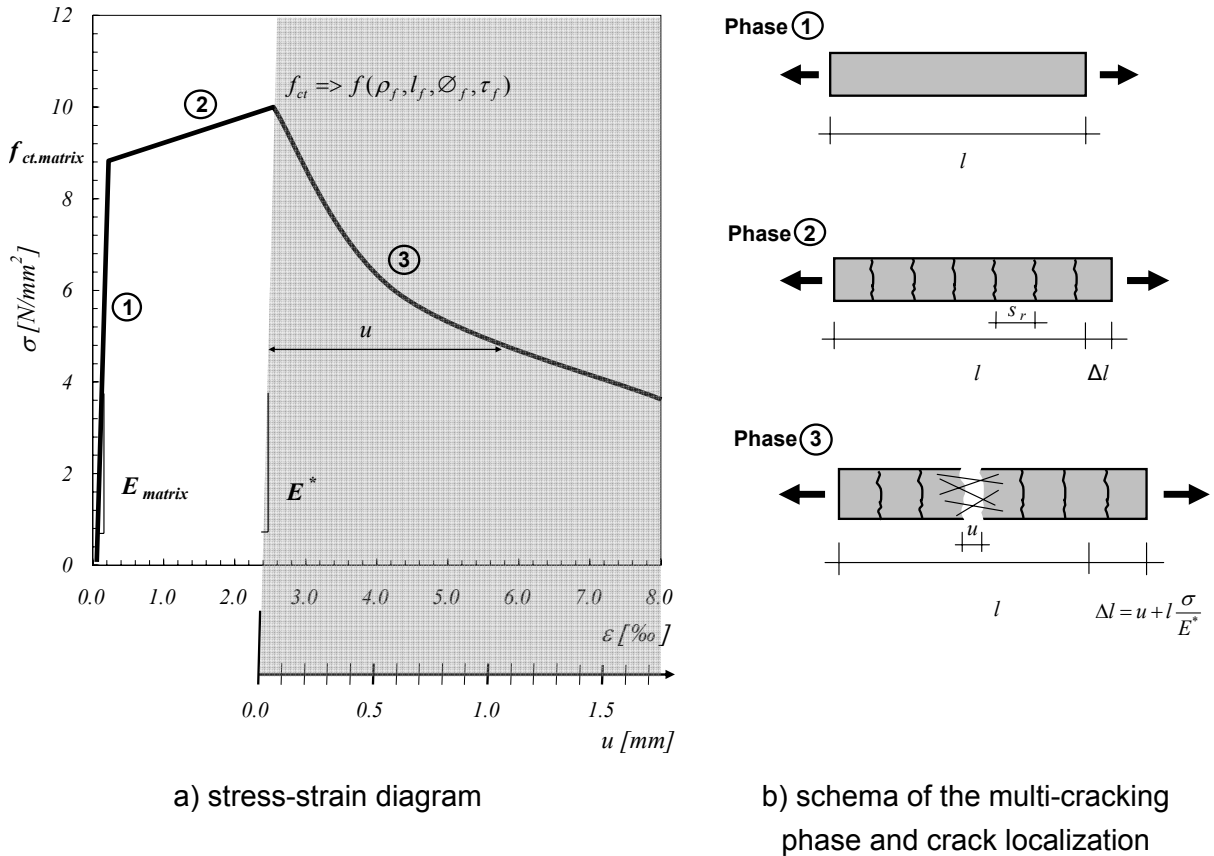
Figure 5: Schematic behavior of a UHPC tensile element

The deformation can be calculated according to the fictive crack model by Hillerborg [7] as the sum of the crack opening u and the elastic deformation of the rest of the element (equation 2). E^* is the unloading modulus, depending on the stiffness of the matrix and the total elastic deformation of micro cracks (not discussed in this paper).

$$\Delta l = u + l \frac{\sigma}{E^*} \tag{2}$$

For various types of UHPC, the shape of the graph is basically the same [4, 5, 6, 8]. The gradient and the length of the different phases vary slightly depending on the composition of the UHPC. The elastic phase is governed directly by the characteristics of the cement matrix ($f_{ct,matrix}, E_{matrix}$). Phases 2 and 3 are governed by the length, the diameter and the ratio of the fibers and by the bond behavior between fibers and the matrix.

4   Structural members

The characteristics of a structural member in tension can be analyzed based on the material behavior illustrated above. In order to obtain an efficient and reliable tie element, it might be reasonable to use fiber reinforced UHPC in combination with steel reinforcement. This is why the bond between reinforcement and the UHPC is analyzed next.

4.1   Bond of reinforcement bars

The bond between reinforcement bars and the fiber reinforced cement matrix is investigated by means of a reinforcement bar pullout test. Knowledge of the bond strength enables to determine the development length and the crack spacing.

The specimen consists of a 160 mm cube with a reinforcement bar (GEWI) positioned in the center (figure 6a). Six specimens with different bond lengths l_b ranging from 20 to 50 mm and two different bar diameters (12 and 20 mm) are tested.

The specimen is loaded by pulling on the reinforcement bar. A metal plate with a central hole serves as support. The slip is measured on the upper side of the specimen as the relative displacement of the bar's end and the concrete surface.
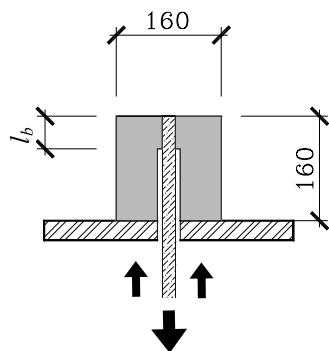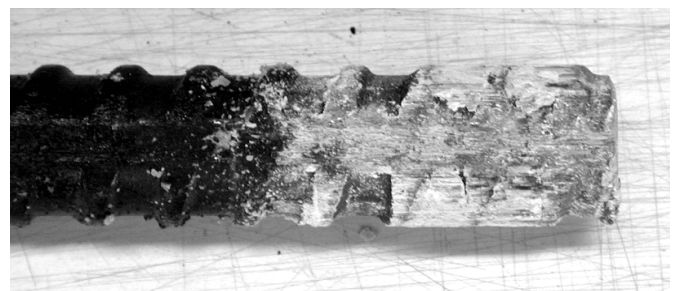
a) test setup   b) pulled out bar

Figure 6: Pullout test (dimensions in mm)

As one can see in figure 6b, the fracture occurs by shearing of the cement matrix. The sheared concrete still sticks between the ribs.

Figure 7 shows the bond-slip-relationship for two different bar diameters ($\varnothing$12 mm and $\varnothing$20 mm). Further, the yield stress and the tensile strength of the bars are indicated.
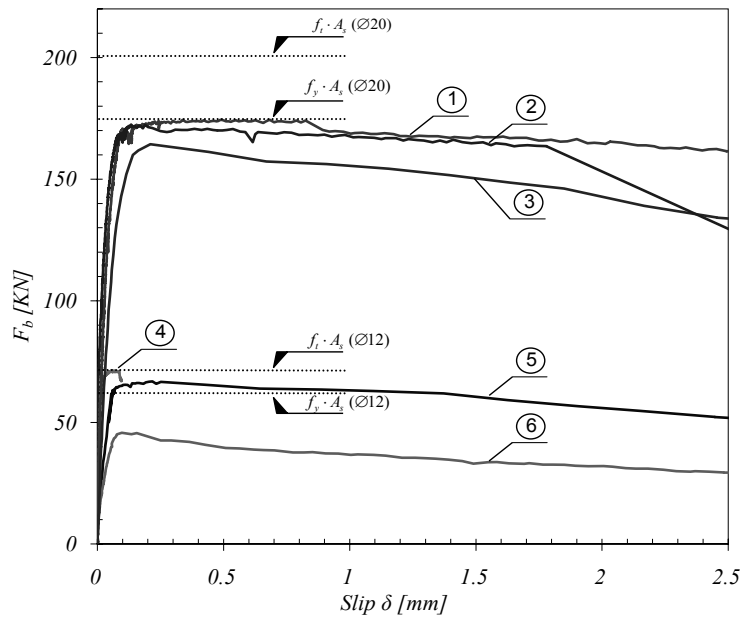
a) force – slip diagram

	Ø [mm]	l_b [mm]	A_b [mm²]	F_b [KN]	τ_b [MPa]	note
①	20	50	3140	174	55	yielding
②	20	50	3140	171	54	-
③	20	40	2512	165	66	-
④	12	50	1880	>71	>38	bar strength
⑤	12	30	1128	67	59	yielding
⑥	12	20	752	46	61	-
average bond strength (without 4):					59	

b) results

Figure 7: Results of the pullout tests (slip at the unloaded end)

In a first phase the behavior is almost linear. Once the bond strength is reached, the slip increases while the force decreases due to the reduced bond length and a non ductile behavior. In the specimen 4 ($\varnothing = 12\ mm,\ l_b = 50\ mm$) the bar strength of the reinforcement has been reached because of a very long anchorage length.

Assuming a constant bond stress distribution, the bond strength can be calculated as the ratio of the pullout strength and the bond surface:

$$\tau_b = \frac{F_b}{\varnothing \pi l_b} \tag{3}$$

The average value of the tested specimens is: $\tau_b = 59\ MPa$

This bond strength is about 10 times higher than the bond strength of conventional concrete. The theoretical development length is thus much shorter and can be calculated as:

$$l_b = \frac{f_y \varnothing_S}{4\tau_b} = 2.4 \cdot \varnothing_S \tag{4}$$

4.2 Tensile behavior of bar reinforced members

In order to understand the behavior of structural members in UHPC, large scale tests simulating the condition in actual structures have been carried out.

Three specimens with different reinforcement ratios between 1 % and 4.8 % (ribbed steel, f_y = 556 MPa) have been tested. The dimensions of the specimens are 160 x 160 x 1500 mm with a measurement length of 1000 mm (figure 8a/b). The strain is measured all along the measurement zone with extensometers spanning over 100 mm.

| a) test setup | b) front view | c) specimen after testing |
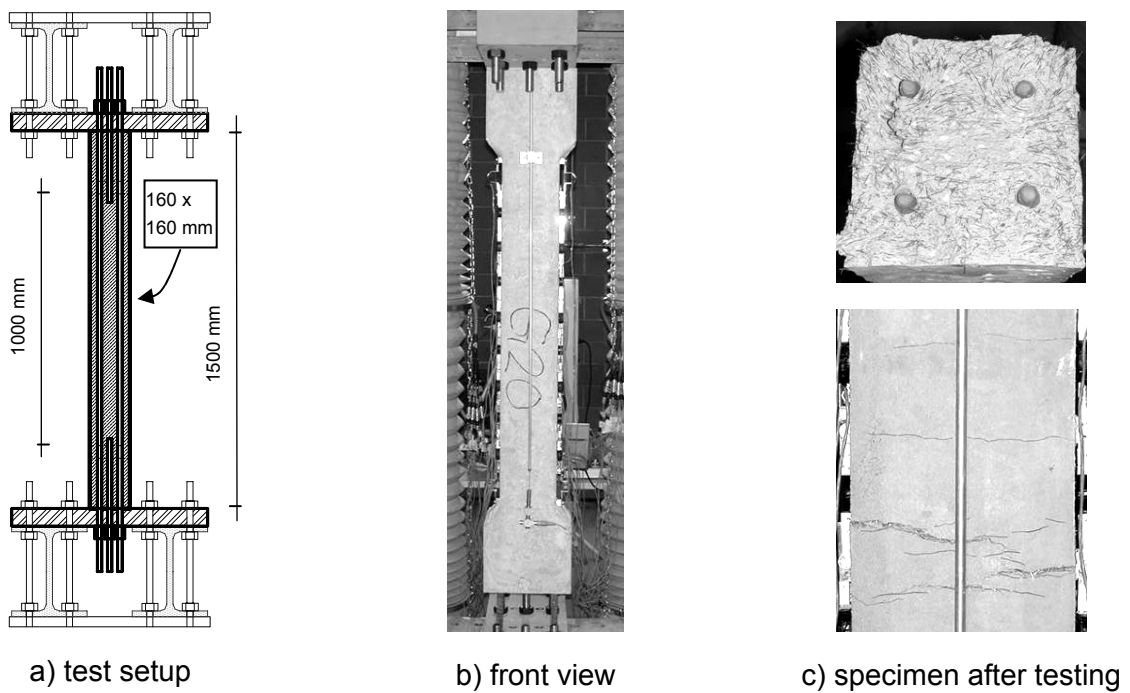
Figure 8: Tensile test of structural members

The tested specimens show a multi cracking behavior (figure 8c). On the fracture surfaces, the fibers that have been pulled out and the plastic deformation of the reinforcement bars can be observed.

a) different reinforcement ratios

b) comparison with model for ordinary reinforced concrete (4∅16)
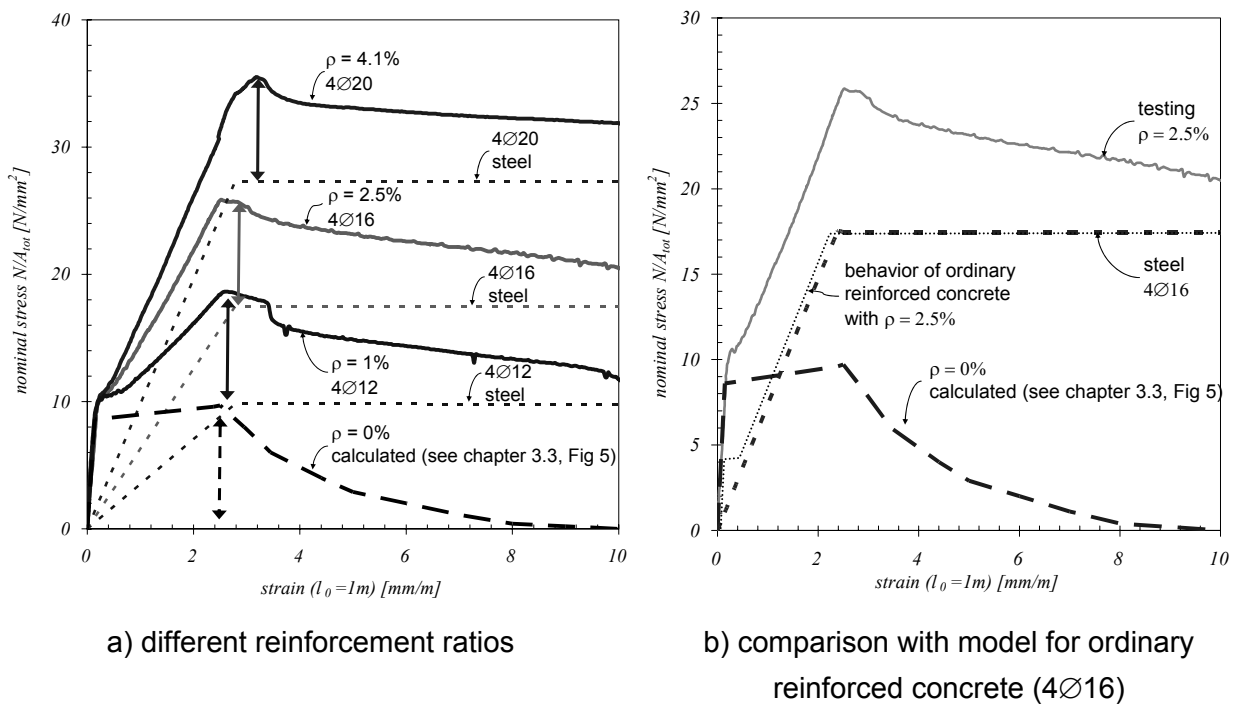
Figure 9: Stress – strain diagram of the tests on bar reinforced structural members in UHPC

The nominal stress - strain diagram for the three different reinforcement ratios (ρ = 1 %, 2.5 % and 4.5 %) is shown in figure 9a (measurement length 1000 mm). The steel behavior for the three cases and a calculated curve for an unreinforced specimen are given for comparison. Figure 9b focuses on the specimen reinforced with 4∅16 and compares the measured behavior of the UHPC with the model for the behavior of ordinary reinforced concrete.

It can be observed, that unlike in the case of ordinary concrete, the strength is composed of the steel strength and a contribution of the UHPC. The contribution of the concrete to the stiffness of the element (tension stiffening) is very high due to the very high bond and tensile strength.

5 Conclusion

Due to the fibers and their contribution to the behavior in tension UHPC shows a different tensile behavior than ordinary concrete. This has an important influence on the design of structures in UHPC. It can be concluded that:

- Major tension stresses should be taken by reinforcement bars or pre-stressed steel to guarantee a reliable and efficient tension bearing.
- The strain hardening effect caused by the fibers leads to a well distributed multi cracking. This eliminates the need of minimal reinforcement for crack distribution.
- The good bond between reinforcement and the matrix leads to a short development length. This should make connection of precast elements very easy.
- Shear reinforcement and reinforcement for the punching zones are not needed for minor shear stresses due to the high tensile strength respectively the high shear strength.

This means that structures can be designed only with UHPC and pre-stressing cables or passive reinforcement carries the major tensile stresses. No further reinforcement is needed.

One possible application of UHPC in tension is its utilization as tendon in underspanned girders (figure 10) [9]. Due to high compression strength of the UHPC a high pre-stress ratio with a high pre-stress force can be employed. This tendon has a very high cracking limit and will remain very stiff after cracking due to the fiber reinforcement. The small crack spacing and the small crack opening should make this tendon also very durable.
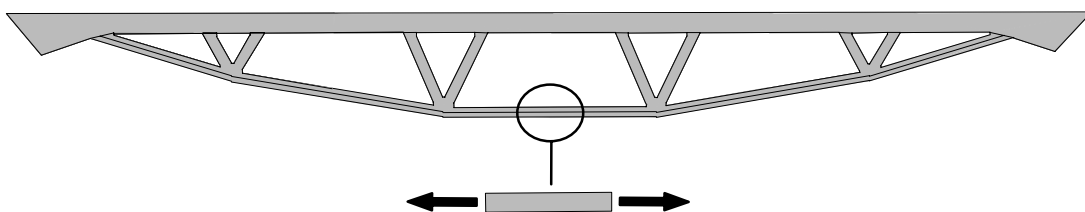
Figure 10: Tensile members for underspanned structures (longitudinal section)

6　　　　Acknowledgements

7　　　　References

[1] **Jungwirth J., Muttoni A.,** *Versuche an Bauteilen aus ultrahochfesten Beton – Teil 1 Material,* EPFL-IS-BETON, Lausanne, **2004**

[2] **Jungwirth J., Muttoni A.,** *Versuche an Bauteilen aus ultrahochfesten Beton – Teil 2 Bauteile*, EPFL-IS-BETON, Lausanne, **2004**

[3] **Maeder U., Lallemant – Gamboa I., Chaignon J., Lombard J.P.,** *CERACEM a new high performance concrete : characterization and applications*, Conference on the UHSC, Kassel, **2004**

[4] **Habel K., Gysler R., Denarié E., Brühwiler E.,** *A Uniaxial Tensile Test for Advanced Cementitious Materials*, internal report, 8 p., **2002**

[5] **Behloul M.**, *Analyse et modélisation du comportement d'un matériau à matrice cimentaire fibrée à ultra hautes performances*, E.N.S. Cachan, doctoral thesis, 182 p., Cachan, France, December, **1996**

[6] **SETRA, AFGC** , *Béton fibrés à ultra-hautes performences*, recommandations provisoires, p. 152, France, **2002**

[7] **Hillerborg A.**, *Analysis of a single crack*, Fracture mechanics of concrete edited by F.H.Wittmann, Elsevier science Publishers B.V., pp 223-249, Amsterdam, Hollande, **1983**

[8] **Plumey S., Jungwirth J., Muttoni A.**, *Comportement des éléments en béton à ultra hautes performances*, EPFL-IS-BETON, Lausanne, **2002**

[9] **Muttoni A.,** *Innovationen im Brückenbau am Beispiel der unterspannten Tragwerke*, Internationales Brückensymposium, Darmstadt, **2003**

J.Aronoff

Ph.D. Student, Consultant Engineer
Technion - Israel Institute of Technology
Faculty of Civil and Environmental Engineering,
Structural Engineering and Construction
Management Department
Haifa, ISRAEL

A. Katz

Senior Lecturer
Technion - Israel Institute of Technology
Faculty of Civil and Environmental Engineering,
Structural Engineering and Construction
Management Department
Haifa, ISRAEL

Y. Frostig

Professor of Structural Engineering
Technion - Israel Institute of Technology
Faculty of Civil and Environmental Engineering,
Structural Engineering and Construction
Management Department
Haifa, ISRAEL

The behavior of very high strength concrete structures with CFRP reinforcing bars

Abstract

The performance of very high strength fiber reinforced concrete beams reinforced with carbon fiber reinforced polymer.(CFRP) re-bars are described. The study is part of a comprehensive research, aimed at determining their mode of failure, their resistance and capacity in flexure and shear, crack pattern, strains in concrete and re-bars, deflections as well as anchorage insufficiencies of the CFRP re-bars. Two beams out of the nine use steel reinforcement, identical to the CFRP ones. They have been tested up to failure for reference.

Three phenomena of special importance have been observed:
-   The mode of failure in beams with CFRP re-bars is different from the mode of failure in beams with steel re-bars.
-   The slip of CFRP re-bars at failure, due to bond failure, plays a major role in the failure mode.
-   The ductility of beams, flexure and shear capacities and crack suppression is remarkable when steel fibers are used.

Keywords: *HPC/High Performance Concrete, VHSC/Very High Strength Concrete, NSC/Normal Strength Concrete, steel Fibres, anchorage, transducers, sliding of bar, deflection, strain.*

1   Introduction

Recently, structures made of concretes whose strength ranges between 120-200 MPa known as VHSC, and in some rare cases ultra high strength concrete known as UHSC, have emerged as new outstanding projects mainly in hi-rise buildings and bridges. There are two main reasons urging the use of such type of concretes today:

- The need for structures which are capable of resisting heavier loads and with larger spans due to the "endless" increasing congestion of the populated metropolitan regions.
- Green concrete demands – smaller cross section of concrete elements which require less concrete volume along with increased durability. It yields improvements in the sustainability of the structures.

Today there is an increase in the need for using HPC/VHSC structures. However, this development depends on concentrated and profound research works, new codes and design guides and rules. This research follows these steps.

This work presents one part of a comprehensive research which deals with beams made of VHSC of 150MPa, as a part of structural systems consisting of prefabricated elements integrated together. The elements are made of fibrous concrete with CFRP (Carbon Fiber Reinforced Polymer) reinforcing bars.

The response of a structure made of this combination of materials is rare and unavailable in the open literature, see example [1-12]. Most of the research works focuses on structures made of NSC with FRP re-bars or HPC with steel re-bars, plain or fibrous concretes but not the combination used here.

Structures made of VHSFC concretes with CFRP re-bars provide a solution to the problems mentioned before. The structural elements, in such structures, are designed as thin walled sections with CFRP bars. Steel re-bars are not used due to their corrosion problems and low strength f_{sy}=500 MPa related to concrete, $f_c\geq150$ MPa. On the other hand, CFRP re-bars don't corrode and their strength is very high, $f_{PB}\geq1600$ MPa. However, notice that their modulus of elasticity is lower than that of steel and they lack an adequate anchoring capacity which may lead to inability to exploit the strength potential of the CFRP re-bars.

The paper presents the results of nine beams which have been tested at the National Building Research Institute at the Technion.

The major goals of the beam tests include:
- Feasibility of casting beams made of fibrous VHSC and CFRP re-bars, with very low water-binder ratio (ω=0.24), without using special measures, such as compacting or steam-curing.
- Ultimate capacities and modes of failure.

- Deflections, strains in concrete and re-bars, crack propagation during the tests and anchorage capabilities.

The tests in this work have been performed in order to be acquainted with the various material characteristics, their mutual behavior and to detect any possible weak spots.

The paper briefly describes the characteristics, preparations, curing and loading of the beams. It also presents the tests results of the ultimate capacities, re-bars anchorage problem, references to cracks, deflections and strains in concrete and reinforcing CFRP re bars. It ends with some conclusions.

2   Materials and test layout

Nine beams 2400/300/150 mm, seven of them reinforced with CFRP re-bars and two with steel re-bars have been prepared for the tests. The one span beams have been tested with four point loading scheme (see table 1) and all of them have been cast with the same concrete mix.

The beams have been prepared in three series. The first one with bottom 12.5 mm CFRP re-bars and 8 mm steel stirrups (Beams: B-1, B-2, B-5, B-9, B-10, B-12); the second one, same as the first one but without stirrups (Beam B-3) and the third ones with bottom 20 mm steel re-bars and 8 mm steel stirrups, for reference (Beams: B-4, B-6). The geometrical and material properties appear in Fig. 1.

2.1   Preparation of beams and test set-up

A heavy duty mixer type Zyklos ZK-150E has been used to prepare the concrete. The mix is relatively flowable despite the high fiber volume and low water/cement ratio and a vibrating table is has been used to ensure proper compaction. After dismantling the molds the beams have been cured by water and polyethylene sheets for one week at temperature of 20-25°C. Four types of detectors, attached to a computer, have been installed in all beams to monitor the deformations at top and bottom of the beam, deflections at various points, strains of concrete and reinforcement and loads. For details on the detection devices and locations see Fig. 1.

Eight beams out of nine have been tested in a MTS-500 testing machine, with a maximum capacity of 500 kN, loaded in a rate of 0.5 mm/minute. Beam #12 was tested in an Amsler testing machine with a 5000kN capacity, in a rate of 5kN per minute.

2.1.1   Test results

The data has been collected by a computer and part of the test results appear in Table 1 and Figs. 2 to 4.

The failure load, P_{max}, see Table 1, describes the maximum load that the beam has reached at failure, see also Figs. 2, 3 and 4. The calculated failure designed loads, P_d, takes into account the contribution of the steel fibers. The strain in the re-bars, $\varepsilon_{(T)}$, is actually the average strain of two strain-gauges which have been installed at mid-span on one of the main re-bars prior to the casting. The maximum strain in concrete, $\varepsilon_{(c)}$, describes the strain in the concrete at mid-span and not under the load. The "slope" describes the average slope of the beam between the location of the load and the support (a=800mm) and is equal δ_{max}/a. "Sliding of bar" refers to the slip displacement monitored at the end of the bar at failure. The slip of the re-bars through the test appears in Figs. 2 to 4. The mode of failure is described in the last column of the table.

2.1.2   Ultimate flexural capacity

All beams, except B-3, have been designed with a moment capacity of 157.58 kNm that corresponds to an external load of 394 kN. Beam B-5 and B-12 have been designed using the balanced reinforcement concept where the concrete and the re-bars fail simultaneously. Actually beam B-5 has reached 86% of the designed capacity and B-12, 87%. Both beams have failed at the same location through a wide diagonal crack with an angle of 60°-70° in the vicinity of one of the loads. At failure, the two 12,5 mm CFRP re-bars in beam B-5, have slide 8.20 mm and 5.72 mm over the supports of the beam. In the vicinity of the wide crack the re-bars have been disintegrated and the concrete in the vicinity of the load has crushed. A "pseudo" plastic hinge develops in the vicinity of the load. The mode of failure can be explained through the sliding of the re-bars that appear in Fig. 2. The flexural capacity does not increase, denoted by R.P.2 in Fig. 2, occurs when the first re-bars starts to slide, R.P.1, until the second bar start to slide (inelastic range), R.P.3. At that instance the flexural capacity of the beam starts to decrease, R.P.4.

The structural behavior of beam B-12 follows the same trends as those of beam B-5 but with a large strain in the re-bars of B-12 that equals 1.3%, which is much higher than that is B-5, and with a slide of the re-bars of 3.5 mm. After the test the re-bars at wide crack have been exposed revealing a total disintegration of the bars, see Fig. 5. This disintegration is a result of the wide crack along with the steep slope of 0.067 rad. A sudden drop of the load has been observed when the load has reached 343.6 KN recorded and a residual deflection of 24 mm is detected when the load is removed.

Beams B-1, B-2, B-9, B-10 have been designed with three 12.5 mm bottom CFRP re-bars for a maximum strain of 0.8% in order to cause a brittle failure of the concrete prior to collapse of the re-bar.

In beam B-1 (the first tested) the CFRP re-bars have slide over the support of the beam and it has been detected through low strains of 0.4%, measured at some of the re-bars. It has been validated by removing the re-bar concrete cover at the end of the beam. The slip of the edges of the bars has been monitored through special indicators attached to the ends of the

re-bars after removal of their edge concrete cover. The amount of the slip in the re-bars appears in Table 1 at failure, and during the tests in Figs. 2 to 4.

In beams B-9 and B-10 special anchorages have been installed at the edges of the bottom re-bars and embedded in the concrete. In this case, the strains in the re-bars have reached higher values of ε_T=1.01% in B-9 and ε_T=0.9% in B-10 along with failure loads of 446.7 kN and 406.7 kN, respectively. Failure has occurred due to slip of the re-bars but at a higher load level as compared with beams B-1 and B-2. All four beams have failed as a result of the formation of "pseudo" plastic hinges. A total disintegration of the re-bars in the crack zone along with a steep slope of the beam of 0.086 rad has been observed in these cases similar to that of beams B-5 and B-12,. The reference beams, beams B-4 and B-6, with steel bottom re-bars, have been designed for the same ultimate flexural capacity as the other CFRP beams (B-1; B-2, B-9, B-10). These two beams have failed due to the formation of plastic hinges in the middle of the beams. There are two main differences between the reference beams and the other ones. The first one refers to the anchorage capacity of steel re-bars that is superior to that of CFRP re-bars and the second one is that the steel re-bars have not disintegrate at failure. Beam B-4 has reached 97% of the designed capacity and in beam B-6 110% of this capacity.

2.1.3 Ultimate shear capacity

The ultimate shear capacity has been tested in beam B-3 which is designed similar to that of beams B-1 and B-2 but without the stirrups. The design shear capacity of beam B-3 reached 351.2 kN and has been determined using the following contributions [12]:
- Shear capacity of the concrete in the compression zone.
- Shear capacity of the fiber concrete in the cracked part of the section.
- Shear capacity due to the friction within the crack and it depends on the size and type of aggregate in the concrete matrix.
- Dowel action of the re-bars.

The beam failed in shear at 92% of the designed capacity in the form of a main diagonal crack, which has widen in the inelastic region, in the vicinity of the load inelastic stage. The shear capacity of the beam is mainly due to the contribution of the steel fibers and the friction which developed in the cracks. The additional shear capacity, ΔP, that beams B-1 and B-2 exhibited is due to the contribution of the steel stirrups in these beams and they equal; ΔP=25kN in beam B-1 (+15.4%); ΔP=38.5kN in beam B-2 (+23.7%). Notice that the existence of the steel fibers shifts the crack angles from the 45° to 50^0 - 70^0. The slip of three of the bars which has initiated the failure of the beams and it can be seen in Fig. 3 at points R.P.1 to R.P.4.

2.1.4 Anchorages at edges of CFRP re-bars

As previously mentioned, the lack of anchorage capacity of the re-bars near the supports has been detected by the very low value of 0.4% monitored at the re-bars of beam B-1. In the next identical beam B-2, the edges of all the lower re-bars have been exposed and the movement of the bars has been recorded, showing a clear slip of the re-bars. The strains in the re-bars in beam B-2 have reached a value of 0.75% and a load capacity of 398.7 KN, higher than those of beam B-1. The same phenomenon has been observed in beams B-3 and B-5 where maximum sliding of 9.4 mm and 8.2 mm developed when the strain reached the maximum value of 0.70% and 0.9%, respectively. The slip has always occurred on the same side of the beam where the "pseudo" plastic hinge develops. Notice that the lower CFRP re-bars totally disintegrates in the vicinity of the the "pseudo" plastic hinges.

The anchorage of the bottom re-bars of beam B-9, B-10 has been improved by means of anchors attached to the end of the re-bars. Another new beam, B-12, similar to B-5, has been cast to investigate the effect of the improved anchorage capacity. The result of this improvement yields higher strain values tin the re-bars and they equal ε_T=1.0% in B-9; ε_T=0.9% in B-10; ε_T=1.3% in B-12. However, the last beam failed while reaching only 87% of the maximum designed capacity due to lower concrete strength, f_c'=148 MPa instead of f_c'=160 MPa. Another reason for the premature crash is the total disintegration of the CFRP re-bars section at the wide crack. The slip of the bar at their edges has reached a value of 3.5mm only, much smaller than that of beam B-5 (8.2mm). Notice, that in this case, the weak link in the chain of the anchorage mechanism is located at a depth of approximately 1 mm below the surface of the bar, within the carbon fibers. This indicates that bonding shear stresses have been transferred from the surface into the bar and failure of the external layer of fibers in the form of fibers breakage has led to bond failure. Notice that contrary to the CFRP re-bars, the anchorage of the steel re-bars is excellent. This has also been proved in previous pullout tests which have been performed in both types of re-bars [13].

2.1.5 Crack patterns and development

The cracks, in most of the beams, have started when the tensile strength of the concrete has been reached at average value of 16.3 MPa (equivalent to external load of 91.4 kN). At this stage a dispersed pattern of cracks in the middle zone between the two loads has developed. The width of the first crack has been considered to be a few microns (10÷15 μm). The starting point of the visible cracking correlates well with the load-deflection (P-δ) diagram. At the onset of cracking the slope of the diagram changes and becomes less steep due to crack formation and as the load is increased the width of the cracks gradually widens to 100-200 μm their length increase. This process proceeds until the stage of the inelastic or quasi inelastic behavior of the beam - increasing the deformations while keeping the load at a constant level, occurs. Once, within the inelastic range, one or two main cracks widens significantly. At this stage the external energy is dissipated through widening of the main

cracks by slippage and breakage of the steel fibers while the pattern of all other cracks remain unchanged with a maximum width of about 200 μm.

3 Deflections

The beams, with the CFRP re-bars, yield larger deflections in the elastic – inelastic range as compared with the reference beams with the steel re-bars. The maximum deflection in beams B-1, B-2 loaded at 200kN is 16.7mm while that of B-4, at the same load level is only 5.4 mm, which is 2.9 times smaller. This difference is a result of the lower value of modulus of elasticity of CFRP relative to that of the steel. For some of beams with both types of re-bars, have developed almost the same range of deflections at failure, see Table 1.

3.1 Strains in concrete at mid-span

The strains in the concrete have been monitored at mid-span in the upper fiber of the concrete section. The largest strains, in the concrete, occur in the near vicinity of the load and not necessarily at mid-span which due to physical obstacles cannot be monitored with devices used in this experimental investigation. The range of strains that has been detected for the nine beams start 0.17% in beam B-3 up to –0.35% in beam B-6. Crushing of the concrete has been observed at the locations of the loads and not at mid-span due to the "pseudo" plastic hinge that develops at theses locations.

3.2 Strain in CFRP re-bars

The strains in the CFRP and steel re-bars have been monitored through strain-gauges attached to the surface of the re-bars at mid-span prior to casting. In B-1, the first tested beam, as mentioned previously, a very low strain of 0.4% has been detected instead of the expected one of 0.8%. It means that the re-bars have not been elongated during the test as a result of the slip, at the anchoring zone, above the supports of the beam. In the second beam, beam B-2, which has followed the test of Beam B-1, six indicators has been installed at the ends of the lower re-bars. The measurements have clearly revealed that slip actually occurred (see column $\varepsilon_{(T)}$ in Table 1 and Figs. 2 to 4).

The strains in the CFRP re-bar in beams B-9, B-10 and B-12, with the improved anchorage capacity, is higher then in previous tests which yielded a higher flexural capacity. The three beams failed in the same mode as the other beams but at a higher load levels.

4 Summary and conclusions

An experimental study of nine beams made of fibrous VHSC reinforced with CFRP re-bars is presented. The research has been performed in order to get a general overview of these new elements, an acquaintance with the various material characteristics, mutual behavior of all components in the beam and to reveal the weak spots of this composite structure. It includes the typical section, geometry layout, material properties and the results in the form of load

versus displacements and slip. The important results at failure are presented in a table. A brief discussion on the failure capacity in flexure and shear along with the crack pattern, deflections and strains in the concrete and the re-bars is presented.

The following conclusions can be drawn from this investigation:

- Casting VHSC beams with very low water-binder ratio is feasible without using any special tools and measures.
- Failure flexural capacity of beams B-1, B-2, B-5, B-9, B-10 and B-12 reinforced with CFRP re-bars has reached an average of 97.5% of the design one. Failure occurred in the near vicinity of the load.
- Failure occurred as a result of combination of de-bonding in the anchorage zone of the re-bar, along with the disintegration of the re-bars in the wide crack. The disintegration of the bars is due to the bent of the beam at this location along with the shear effect at the same location.
- Two identical beams (B-4; B-6) reinforced with steel re-bars have reached on average of 105.5% of the designed flexural capacity. The failure has occurred at mid-span with the formation of a plastic hinge.
- Beam B-3 that has been reinforced with CFRP re-bars without any stirrups has reached 92% of the designed shear capacity. Failure has occurred in the vicinity of one of the loads as a result of the combination of maximum main stresses.
- The concrete has crushed in the vicinity of the load and not at mid-span when CFRP re-bars are used.
- The range of CFRP re-bars strains with an ordinary bonding is 0.7-0.9% while in those with the improved bond they have been raised to 0.9-1.3%.
- There is a deficiency in the bonding mechanism of the CFRP-re-bars. In the first test a slip of 11.3 mm has been detected. Notice that the slip of the re-bars always occurs in the same side where the "pseudo" plastic hinge developed.
- The slip of the well anchored CFRP-bars is associated with breakage of the carbon fibers at a small distance below the surface.
- The beams start to crack when the average tensile strength of the fibrous concrete reaches 16.3 MPa which is equivalent to external load of 91.1 kN.
- The deflections of beams with CFRP re-bars are larger then those with steel re-bars due to the lower modulus of elasticity. At failure, in some of the beams with both types of re-bars, the deflections are similar.
- The steel fibers play an important indispensable role in the structural capacity of the beams. They improve the flexural and shear capacities of the elements as well as suppressing the size and dispersion of the

cracks. The ductility of the VHSC beams, in the inelastic range, is totally attributed to the existence of the steel fibers. Also, notice that their contribution in increasing the concrete strength is about 25% while their contribution to the increase of the modulus of elasticity is only about 4%-6% , see [13].

- The unique noise which is heard during the loading of the beams in the inelastic range (due to frictional work done by the fibers in the concrete) may serve, through the use of acoustic emission devices, as a detector of the health of the concrete beam.

5   Acknowlegements

6   References

1. F.A. Al-Jahdali, F.F. Wafa and S.A. Shihata, "Development length for straight deformed bars in H.S.C." SP 149-29 Proceedings ACI international conference, Singapore, 1994, pp 507-521.
2. M. Theriault, B. Benmokrane – "Effects of FRP reinforcement ratio and concrete strength on flexural behaviour of concrete beams" Jouranl of Composites for Construction, February, 1998, pp 7-16.
3. R. Masmoodi, M. Theriault and Brahim Benmokrane – "Flexural Behaviour of concrete beams reinforced with deformed fiber reinforced plastic reinforcing rods" – ACI structural journal, November-December, 1998, pp 665-676.
4. Q. Chungxiang, I. Patnaikuni – "Properties of high – strength steel fiber-reinforced concrete beams in bending" – Cement & concrete composites 21 1999, pp 73-81.
5. P. Casanova and P. Rossi – "High-strength concrete beams submitted to shear: steel fibers versus stirrups" – ACI international SP-182, 1999,pp 53-67.
6. M. Imam, L. Vandewalle and F. Mortelmans – "Shear capacity of steel fiber HSC beams" – HPC proceedings ACI internatioanl conference, Singapore, 1994, SP 149-13, pp 227-242.
7. S. Mochizuki, Y. Matsuzaki and M. Sugita – "Evaluation items and methods of FRP reinforcement as structural elements" – FRP reinforcement for concrete structures – international symposium sp-138, ACI 1993, pp117-131.
8. E. Sueoka, K. Yasuoka, O. Kiyomiya, M. Yamada, M. Shikamori – "Mechanical properties of composite beams by FRP" – FRP reinforcement for concrete structures" – international symposium SP-138 ACI, 1993, pp 133-148.
9. T. Kakizawa, S. Ohno, T. Yonfzawa – "Flexural Behavior and Energy Absorption of carbon FRP reinforced concrete beams" – FRP reinforcement for concrete structures – international symposium SP-138 ACI 1993, pp 585-598.
10. SS. Faza and H.V.S Ganga Rao – "Theoretical and experimental correlation of behaviour of concrete beams reinforced with fiber reinforced plastic rebars". – FRP reinforcement for concrete structures" international symposium SP-138 ACI 1993, pp 599-614.
11. G. Bernier, M. Behloul, and N. Roux – "Structural Applications Using Ultra High-Strength Fiber Reinforced Concrete", ACI SP-182-5, 1999 , pp 69-85.

12. B. OH, D. Lim, K. Hong, S. Yoo and S. Chae – "Structural behavior of steel fiber reinforced concrete beams in Shear" – ACI SP. 182-2, 1999, pp 9-27

13. J. Aronoff, A. Katz, Y. Frostig – "The behavior of VHSC Structures with Fibers and Reinforced with FRP, Part II – National Building Research Institute No. 017-693-2, December 2003, pp 65-71 (In Hebrew).
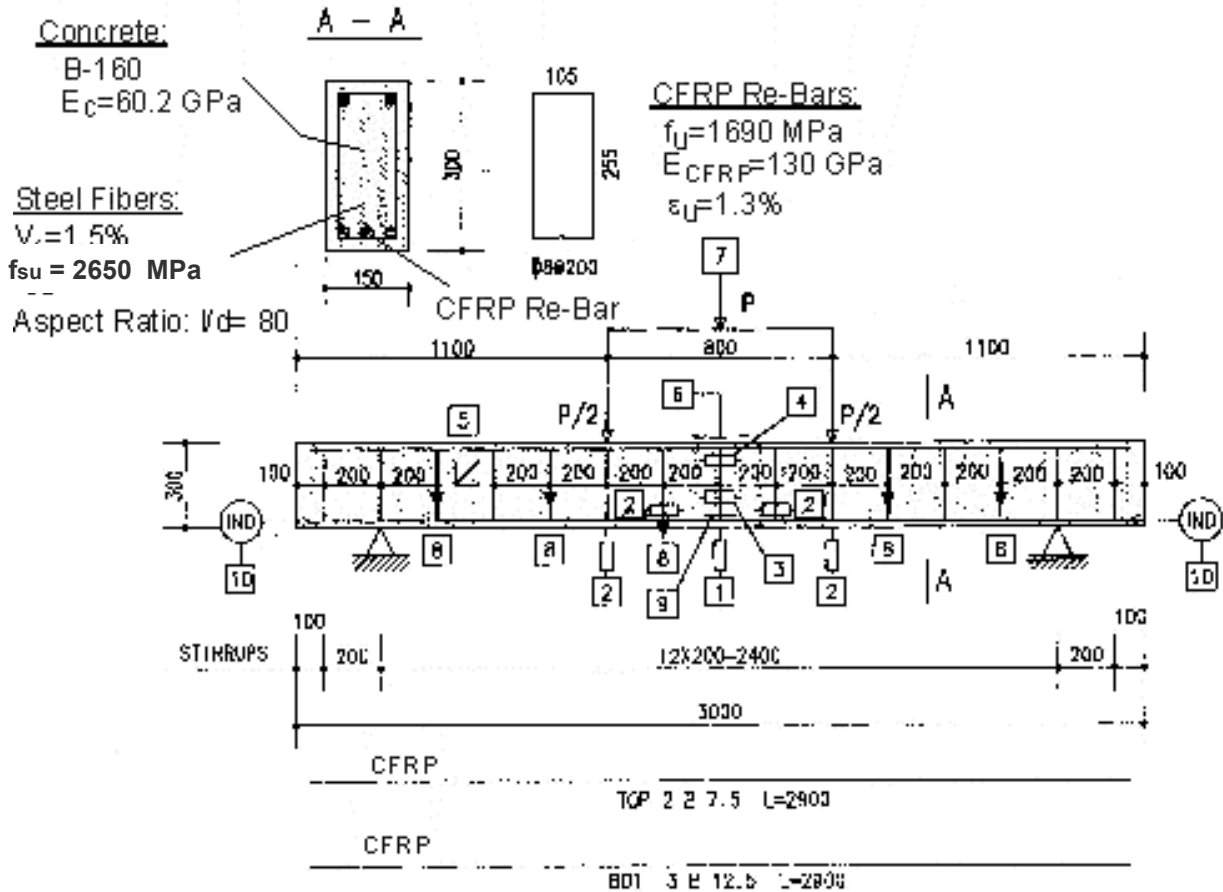
Fig. 1: Geometry, Set-Up Detectors and Reinforcement Layout of a Typical Beam.

FIG 2: BEAM B-5. LOAD VERSUS DEFLECTION AND SLIDE OF BARS. [50,51]

FIG 4: BEAM B-2. LOAD VERSUS DEFLECTION AND SLIDE OF BARS. 50,51,52

FIG 3: BEAM B-3. LOAD VERSUS DEFLECTION AND SLIDE OF BARS 50,51,52
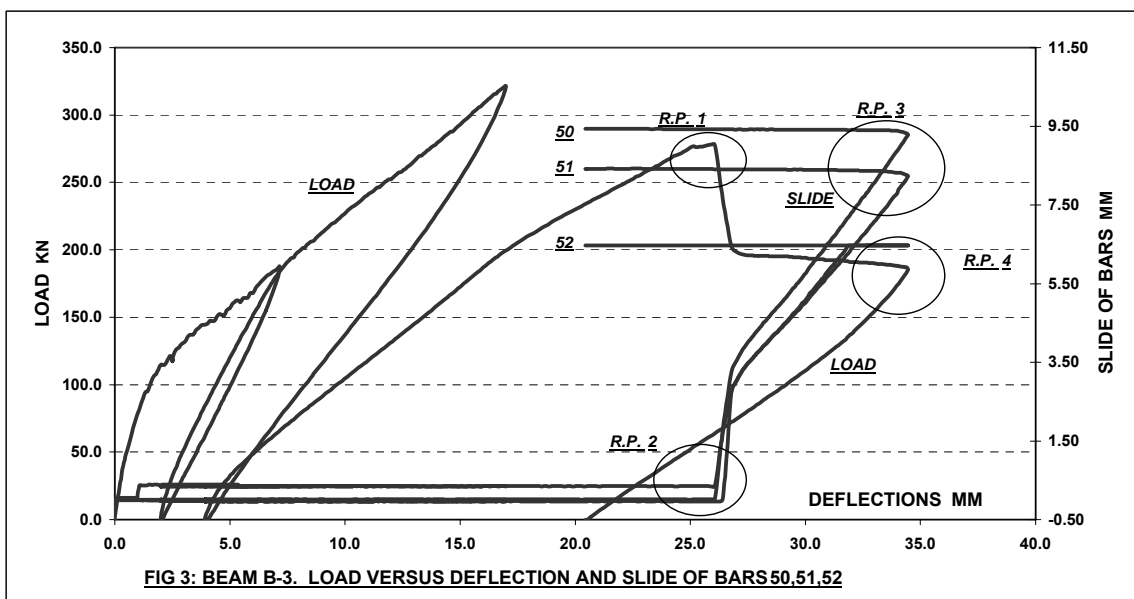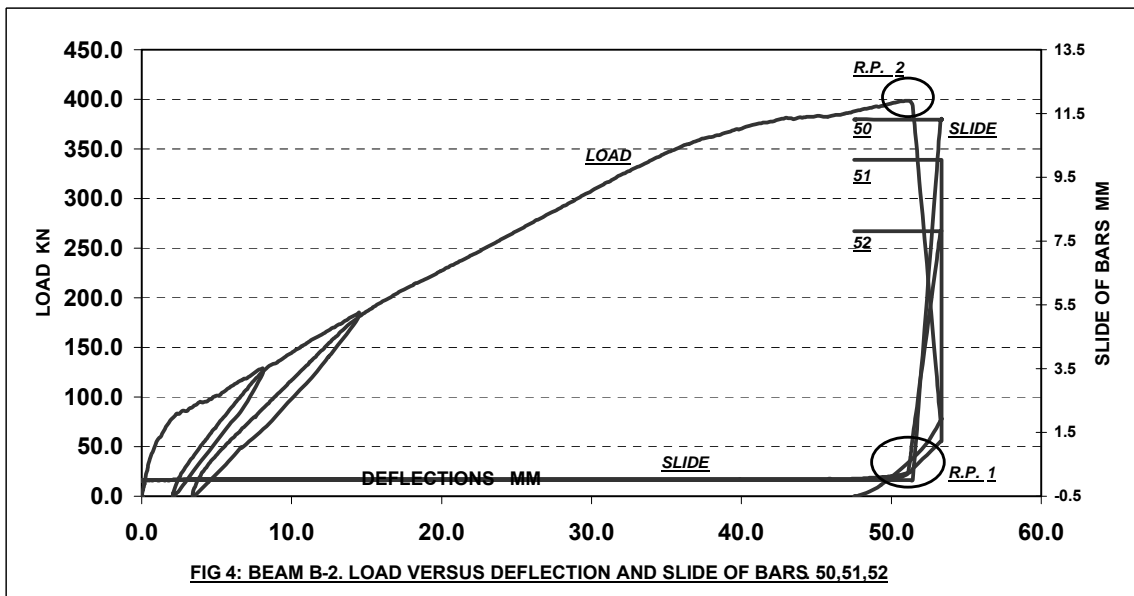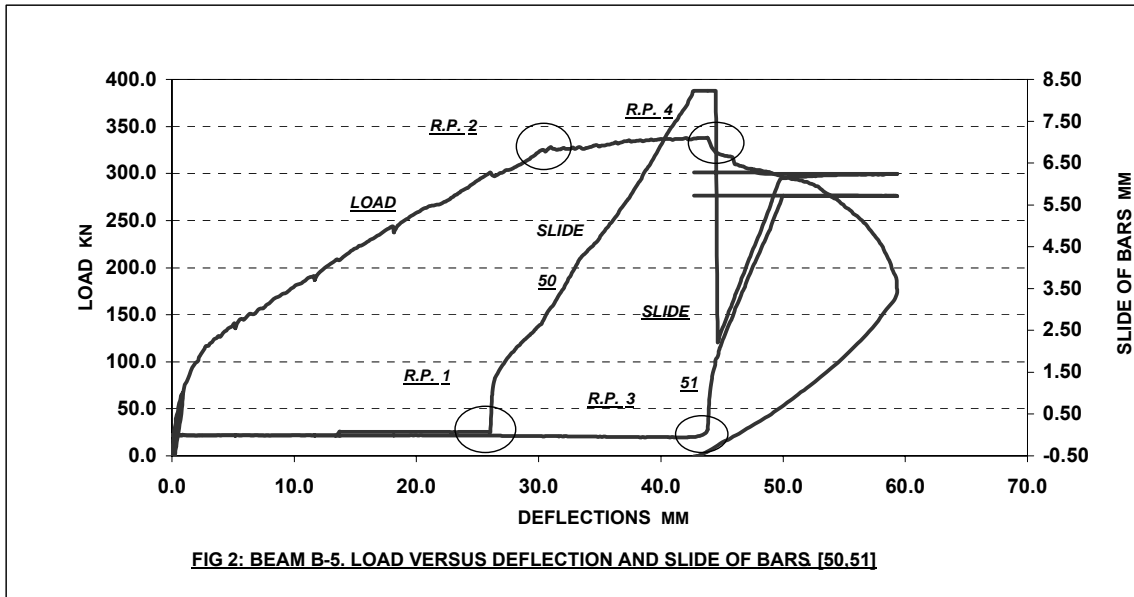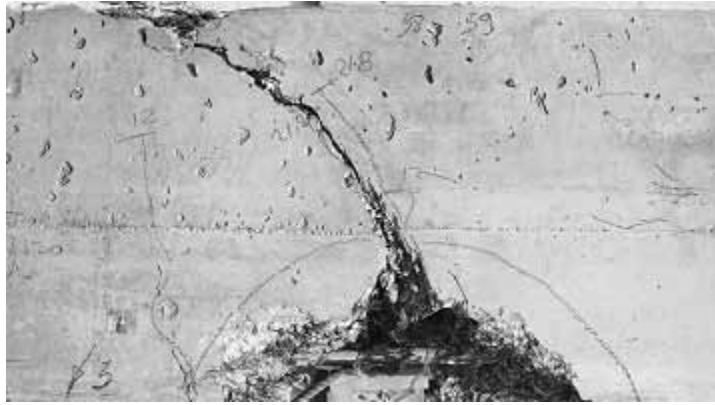
FIG. 5: DISINTEGRATION OF CFRP RE-BARS

Table 1: Test results

No.	Beam No.	Failure Load			Strain in bars		Max. strain in concrete	Deflec. under the load	Ratio	Slope	Sliding of bars	Failure mode & Pattern
		Actual	Designed		Designed	Actual						
		Pmax	Pd	Pmax/Pd	epsilon(D)	epsilon(T)	epsilon(C)	delta(P)	delta(P)/L	delta(P)/a	s	
		kN	kN		%	%	%	mm'			mm'	
1	B-1	371.6	394.0	0.94	0.8	0.40	-0.24	50.0	1/48.0	0.062	11	flexure &shear [1]
2	B-2	398.7	394.0	1.01	0.8	0.75	-0.32	52.0	1/46.1	0.059	11.3	flexure &shear [1]
3	B-3	321.7	351.2	0.92	0.8	0.70	-0.17	34.0	1/70.6	0.047	9.4	shear [1]
4	B-4	383.7	394.0	0.97	0.2	0.20	-0.29	52.3	1/45.9	0.065	none	plastic hinge [2]
5	B-5	337.9	394.0	0.86	1.3	0.90	-0.18	43.0	1/55.8	0.057	8.2	flexure&shear [1]
6	B-6	450.0	394.0	1.10	0.2	0.21	-0.35	34.4	1/69.8	0.043	none	plastic hinge [2]
7	B-9	446.7	394.0	1.14	0.8	1.00	-0.26	69.7	1/34.4	0.086	9.5	flexure&shear [1]
8	B-10	406.1	394.0	1.03	0.8	0.90	-0.30	65.0	1/36.9	0.081	10.2	flexure&shear [3]
9	B-12	343.6	394.0	0.87	1.3	1.30	-0.22	53.9	1/44.5	0.067	3.5	flexure&shear [4]

Failure Cause

[1]   Sliding of re-bars edges

[2]   Ultimate state

[3]   Anchorage

[4]   Disintegration of re-bars.
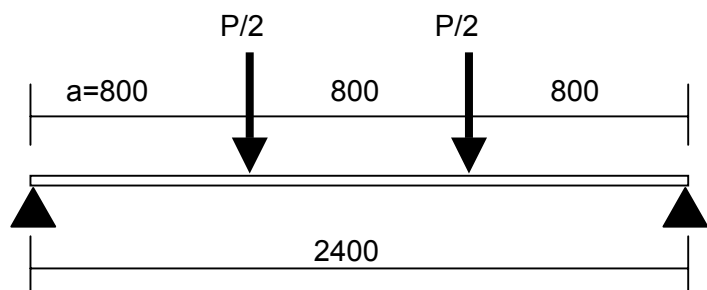
Bernhard Freytag
Dr., Univ.-Ass.
TU Graz
Graz, Austria

Joachim Juhart
Dipl.-Ing.
FH Technikum Kärnten
Spittal/Drau, Austria

Lutz Sparowitz
Dr., Univ.-Prof.
TU Graz
Graz, Austria

Erwin Baumgartner
Dr., FH-Prof.
FH Technikum Kärnten
Spittal/Drau, Austria

The Use of UHPC in Composites
- Ideas and Realisations -

Summary

This paper deals with those beneficial properties of UHPC which are needed for the realisation of composites. It is explained how bond works and why UHPC is well capable for that. Experimental data of bond tests between pre-treated glass panes and UHPC provide the cognitions. Promising composite systems, which are based on the bond between UHPC and other materials, for bridge construction as well as for building construction are presented.

Keywords: *UHPC, steel, glass, concrete, bond, composites, adhesion, friction, interlocking*

1   Introduction

The excellent advantages of Ultra High Performance Concrete (UHPC) are durability and strength. Thus, various possibilities for new developments in structural concrete arise. The enormous compressive strength, about five times stronger than Normal Strength Concrete (NSC), allows slender and light building elements, which almost reach the aesthetic occurrence of steel structures. Like NSC also UHPC can be cast without heating, which allows totally free shaping. For instance, large-span free-formed surfaces (realised by cantilever erected shells) can get a fascinating lightness and transparency when they are combined with structural glass. Furthermore, the property that concrete is initially liquid can easily be utilised in order to get effective bond to other materials. Hence, mixed building technologies can be developed, where each material contributes its beneficial properties. The following chapters deal primarily with the mechanical interaction of different materials. But one must also keep in mind that certain materials also contribute their climatic and acoustic properties.

2 Composites and Bonding Effects

A composite material is defined as a combination of at least two chemically and mechanically distinct materials with a definite interface separating the components. In particular, dissimilar materials are able to combine oppositional properties in one building component. Reinforced concrete is a well known example for that.

In composite construction building components of different materials are joined. They can be joined during the erection so that certain components can be prefabricated. The connecting devices and load transfer zones have a special significance. Usually tension concentrates in these zones.

The possible types of composite actions are shown by means of the example reinforced concrete [1] (see also Figure 1):

2.1.1 Adhesion

Between the binding matrix of concrete and the bonding partner adhesion takes place. Adhesion is *the state in which two surfaces may consist of valence forces or interlocking forces or both* according to "American Society for Testing and Materials (ASTM)". One can differentiate between specific adhesion and mechanical adhesion [2] (see also Figure 1 on the right).

As a rule the phases of the bonding partners do not interact by genuine chemical bond – ionic bond, covalent bond or metallic bond. In the case of specific adhesion they interact by non- covalent bonds, electrostatic forces and other relatively weak forces. For effective adhesion a close and continuous contact of the phases is necessary. Therefore properties as the wettability of the surface of the adherent and the viscosity of the adhesive are decisive [2]. Impurities that worsen the direct contact should be removed by roughening the surface. An appropriate roughness of the surface of the adherent in combination with a well fitting adhesive also provides interlocking on a fine scale which means mechanical adhesion.
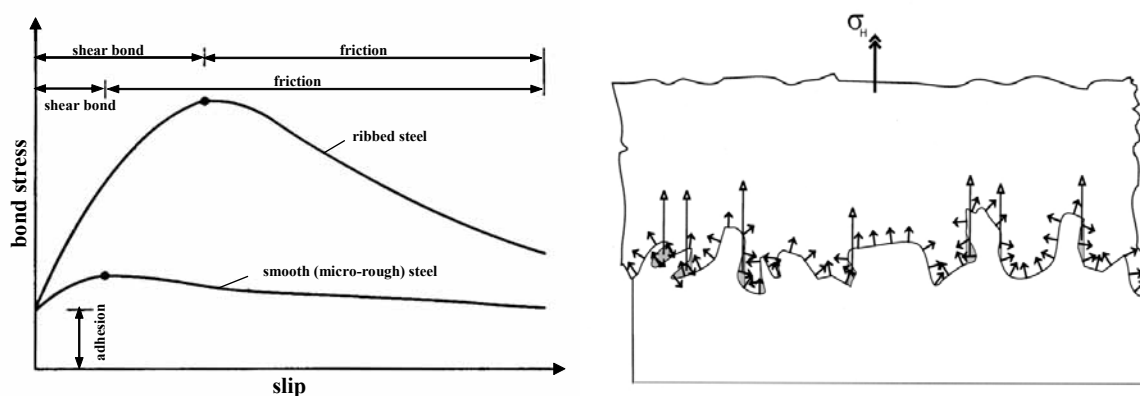
Figure 1:   on the left: The three types of composite action in reinforced [1]
                 on the right: Composite action by adhesion: specific adhesion (short arrows), mechanical adhesion / interlocking (long arrows) [2]

2.1.2 Friction

Friction is activated when the bonded components begin to displace each other and when there is a transverse pressure on the bonding surface. Transverse pressure can either be caused by loads or it can come from shrinkage or swelling actions of one of the components.

2.1.3 Shear Bond

The most effective bond action, for example in reinforced concrete, is shear bond. A mechanical interlocking on a macroscopic level between the ribs of reinforcing steel and the corresponding concrete teeth in between the ribs provides a bond failure determined by the shear strength of the concrete. According to [1] the shear resistance also depends on the geometry of the ribs as well as their spacing (related rib area).

In the case of high strength concrete a new type of ribbed reinforcing steel with an optimised design of the ribs is being developed, as mentioned in [3]. The higher compressive strength and bigger Young´s modulus of high strength concrete in comparison with normal concrete leads to a stiffer bond with ribbed bars. The stiffer bond causes a higher risk for longitudinal cracking. Therefore, such an effect is also expected for the use with UHPC.

3 Beneficial Properties of UHPC in Composites

Fluid UHPC adapts well to its bond partner, so that a flat-spread connection is possible. Thus for example the idea of glass-concrete composites could be realised (see chapter 4.3). In this case mechanical adhesion and interlocking respectively are detected as the primary bond effects.

UHPC distinguishes itself by its well balanced size distribution of the ultrafines and by its high content of ultrafines, which are for the most part hydraulically effective. The viscous mixture of UHPC is very homogeneous and is able to fill up microscopical indentations and to enclose exaltations of a micro-rough surface. Because of the dense structure after hardening and the little porosity of the matrix an effective interlocking with the surface of the bond partner is realized. It is expected that an accurate tuning of the components of UHPC, especially the content of ultrafines and their size distribution, to the roughness of the surface lead to a shear bond on a small scale. Assuming that, the bond failure changes to a shear fracture of UHPC or its bond partner. The visual assessment of the fracture surfaces of glass-UHPC specimen confirms this statement [5]. Predictions about the bond strength due to mechanical adhesion depending on the roughness of the adherent and on material characteristics of UHPC should be possible.

The fibres in UHPC make an essential contribution to ensuring the effect of mechanical adhesion in UHPC composites after crack initation. They are well embedded and increase the tensile strength as well as the fracture toughness [4]. Cracks that develop due to autogeneous shrinkage are well distributed and their opening is minimized.

The bond effect due to mechanical adhesion evokes the use of new composite materials with UHPC or new forms of preparing surfaces of composite materials. An important fact in developing new bond connections is the geometric arrangement of the UHPC. So, one must consider that the shrinking behaviour can generate additional pressure on the connection

when enclosing one bond partner (friction by clamping), but can also decrease the adhesion when filling up an element with UHPC.

Even the use of UHPC as the connecting material between two other materials is possible (see chapters 4.3 and 4.4).

4   Several Applications

The following applications are ordered by the bond partners of UHPC.

4.1   UHPC-Concrete

Because of the high demands made on the fabrication of UHPC, it is mostly used in precasting works. Compared to NSC thin-walled and light elements are fabricated. Often these pre-cast elements are completed with in-situ concrete after their assembling. For this purpose self-compacting concrete is well capable. The final structural behaviour of the construction depends highly on the bond action between UHPC and the in-situ concrete. Considering these aspects, various traditional bridge construction methods can be modified in order to utilise the beneficial properties of UHPC.

4.1.1   Hybrid Segmental Construction Method

The pre-cast elements (Figure 2 on the left) are designed as thin-walled as possible. Their small self-weight requires only few prestressing steel for the assembling. The temporary carrying system changes to the final structure by completing it with in-situ concrete (HPC), reinforcing steel and additional tendons (Figure 2 on the right). All these additional components, including shear reinforcement, run also across the joints between the segments. In this way, the joints, which traditionally are the weakest parts of segmental bridges, become strong and robust. Apart from the reduction of the total demand of prestressing steel, the pre-cast elements are extremly resistant against environmental actions like aggressive fluids and atomised spray.
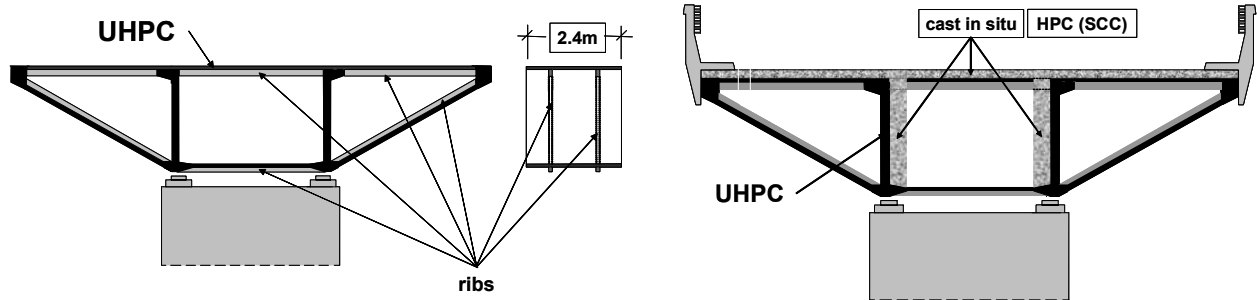
Figure 2:   Light-weight cross section and the supplementary completions

4.1.2   Modified Incremental Launching Technique

Traditionally one increment is cast in a stationary place at one abutment of the bridge. Here the same place is used for the assembling of one increment consisting of multiple pre-cast elements (Figure 3). Caused by the light weight of the structure, the launching procedure can be realised without launching nose and some cables of the centric pre-tension can be saved. When the light-weight structure reaches its final position, the completion with all the required members (Figure 3 on the right), can start. The final composite beam also has "a hard skin and a weak core". The construction of one launching-section is supposed to take one or two days, which brings an essential shortening of the construction period versus the traditional method.
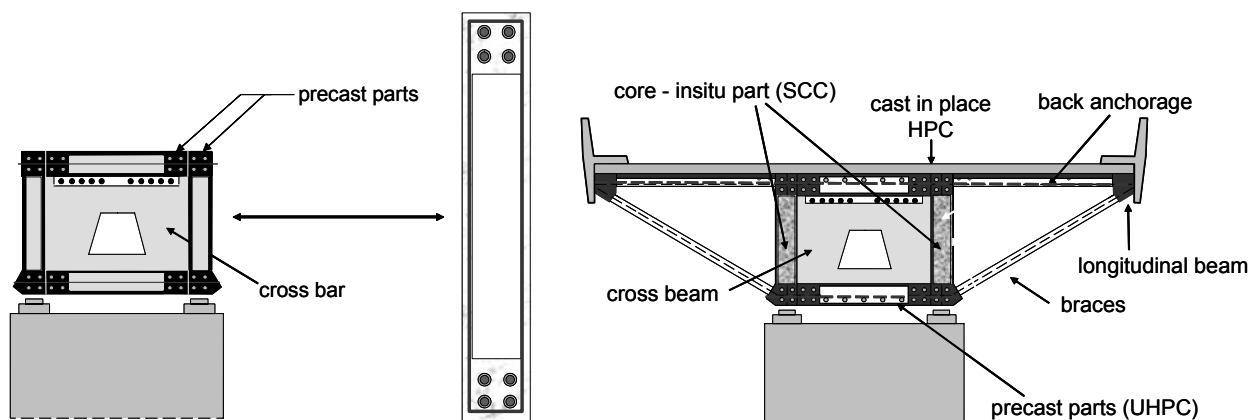
Figure 3:   Built-up cross section for incremental launching on the left, pre-cast component in the middle and the final cross section on the right

4.1.3   The Swivel-In-Method of Arch Construction

In this construction each half of the arch is assembled almost vertically at the springings. The arch halves are built up by pre-cast elements, which are linked by pre-tensioning. The very light arch halves can easily be swivelled in and jointed at the crown. Because of the little weight, also the costs of the required equipment for the swivel-in process are small. That is the reason why this method can get a great revival and can become competitive. In order to carry the deck girder and the traffic load, the hollow space of the arch is filled with in-situ concrete.

4.1.4 Modified Cantilever Erection of Arch Bridges
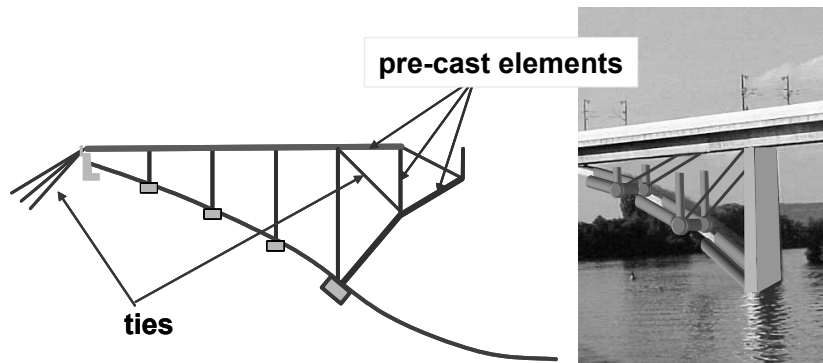
Figure 5: Modified cantilever erection of trussed arch bridges

Using a cantilever erection method for constructing arch bridges, always triangular trusses must be added step by step, starting at the springing (Figure 5). The bars can be thin-walled tubes made of centrifugally cast UHPC. If required, they are filled again with in-situ concrete.

4.1.5 Flat Slabs with Improved Punching Shear Resistance

Figure 6 shows an element working like a mushroom head which is hidden in the depth of the flat slab. Because of the use of UHPC, a very high punching shear resistance can be achieved. Furthermore, intended deviators offer the possibility for easy installation of tendons in two directions. The dimensions of the mushroom element have to be adapted to the static requirements and to the basic grid of the formwork respectively.

564
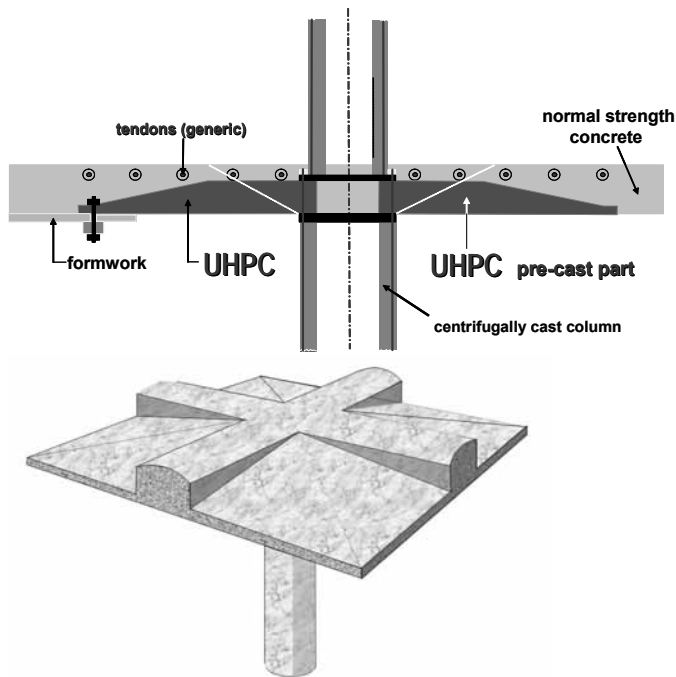
Figure 6:   Hidden mushroom head for improved punching shear resistance in flat slabs

4.2   UHPC-Timber

There are many meaningful applications of composites with timber and concrete. But mostly the much cheaper NSC is more capable. Caused by the strongly differing of E-Moduli a satisfactory exploitation of UHPC is rarely possible. Timber-UHPC composite slabs in building- as well as in bridge construction show very good properties. The advantages concerning oscillations, acoustics and fire are caused by the bigger mass and the high bending stiffness versus plain timber slabs. In the case of poorly insulated slabs the risk of condensation at the interface increases.

4.3   UHPC-Glass

Figure 7:   Glass-concrete composite beam

Glass is one of the most fascinating building materials. It combines transparency, brightness, and reflectance with excellent mechanical properties such as stiffness and strength. Only its

brittleness is a negative fact concerning the safety requirements. Hence, much effort has been spent on developments like tempering or lamination of glass. It ends in a residual capacity for a short time after glass breakage, whereby the residual capacity is much lower than the actual capacity. It is obvious, that brittleness can only be eliminated by composition with non brittle materials. Reinforced concrete is the best example for demonstrating this.

As it is infeasible to connect glass and reinforcing steel directly, another material must be used in between. Apart from organic adhesives concrete can be used as the connecting material. It can easily be formed and fitted to each shape of other materials (see chapter 3). These ideas led to the development of the glass-concrete composite technology [5].

Glass-concrete composites consist of laminated safety glass, UHPC and reinforcement- and/or prestressing steel. Figure 7 shows a simple structural element, which consists of concrete flanges and a glass web. Its cross section is drawn in Figure 8 on the right. Loading tests have shown that the failure of the beam is always indicated by many cracks in the glass. They occur at load levels between 55% and 90% of the ultimate load. So, the brittleness of glass is satisfactorily overcome.

The key to this success is the strong bond between the glass web and the concrete flanges. It can be achieved by a very simple connection. The edge of the glass to be connected is pre-treated and placed in the formwork during concreting (see Figure 8).

Figure 8:   Mounting of the pre-treated glass and the reinforcement in the formwork on the left, cross section of the glass-concrete composite beam on the right

In [6] a test series is presented which focuses on improving the bond strength between glass and concrete. Several methods of pre-treatment of the glass surface in contact are studied: sand blasting, gluing of quartz grains, under-water epoxy and enamelling of corundum. The latter yields the best results. Furthermore, the concrete quality was varied from normal concrete (C50/60) to high performance concrete (compression strength=130 N/mm^2) containing a big amount of silica fume (220 kg/m^3). It turned out, that aside from the pre-treatment of the glass the quality of concrete as well as the amount of fibres in the concrete control the bond strength.

Based on these cognitions additional glass-concrete bond tests are carried out using UHPC. Two types of ductal® (grey and white) with 190 N/mm^2 compressive strength are tested. A short excerpt of the results is shown in Figure 9. The most important conclusions are: The connections with roughly sand-blasted and corundum-enamelled glass surfaces are 30% stronger than those of the tests in [2]. The reason can be found in the well balanced size distribution of the ultrafines. The soft post failure behaviour can be explained by the big content of steel fibres (160 kg/m^3) which keep up the clamping force. The fact that grey ductal® does not yield as good results as the white one, confirms the importance of the size distribution of the ultrafines but also poses the question what role the chemical structure of cement (white and grey cement) plays. The comparison of the strength of roughly and finely sand-blasted specimen (Figure 9 on the right) impressively shows that even the roughness of the surface must carefully be attuned to the characteristics of the binder. This interpretation is based on elder results, where low quality concrete is used and the bond strengths of the finely sand-blasted specimens are better than here. One more reason could probably be found in the type of the superplasticiser in use. However, the visual assessment of the contact surface after the test awakes the feeling that a phobia exists between liquid white ductal® and the finely sand-blasted glass surface.
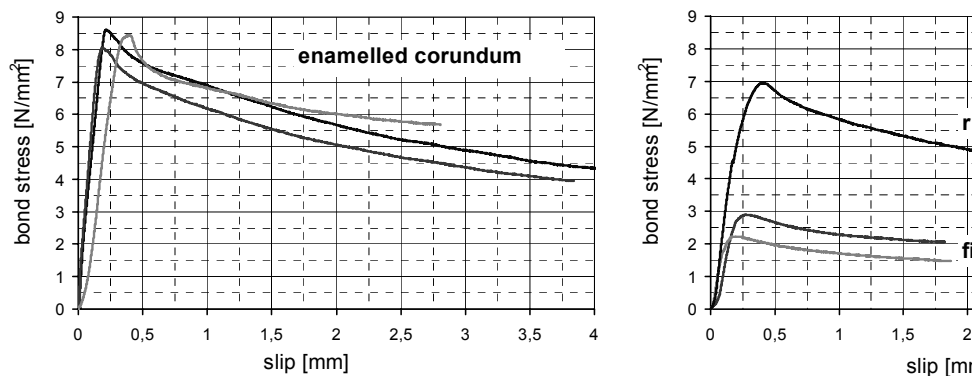
Figure 9:   Selected results of glass-UHPC bond tests

From bond tests mentioned above it can not be seen how much load is carried by each physical mechanism. However, a clamping effect, caused by the shrinking concrete part which clamps the glass, enormously improves the shear strength of the connection.

In order to get more detailed information about the actual clamping force, finite element analyses are carried out for two different connections which were also realised in test beams [5]. The first model considers UHPC 150 with its specific material parameters [7] (axial tensile strength=8,5 N/mm^2). The second one (connection of the beam in Figure 7) involves a high quality UHPC with 16 N/mm^2 axial tensile strength.

The models reproduce cross sections through the connection considering the specific penetration geometries. Based on the relation between length and width of the connection, plane strain is assumed. The interaction of various processes requires the consideration of the following time dependent phenomena in the material model: shrinkage, evolution of the strength (tension and compression) and the evolution of the elastic behaviour. Non linear

springs represent the contact behaviour, which means very big stiffness in compression and almost no stiffness in tension.
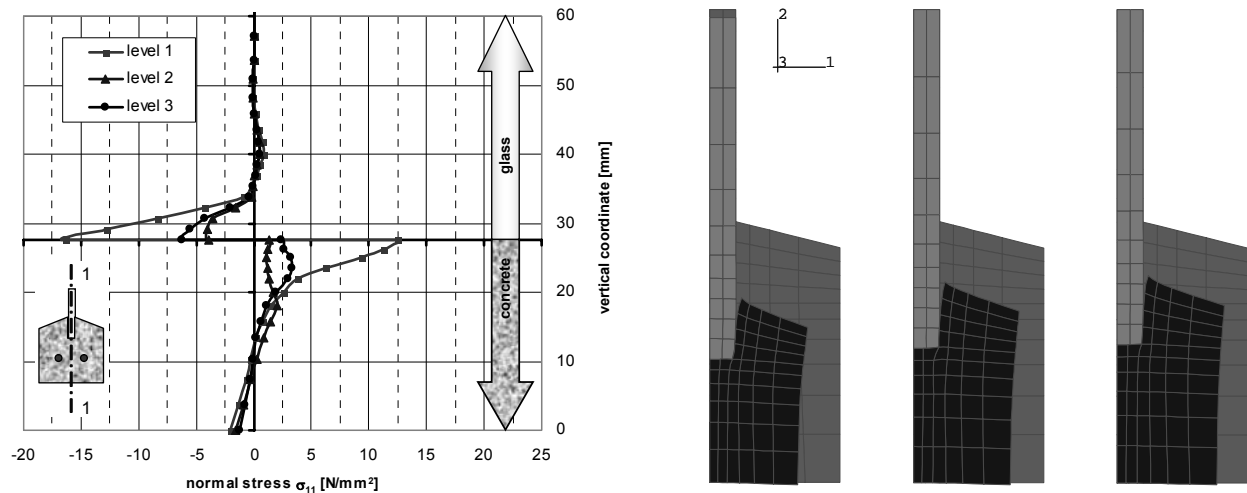
Figure 10: Finite element results of model 1:
Normal stress on the left and deformed figures (400 times heightened) on the right

Important information about the influence of the level of sophistication of the concrete material model is shown in Figure 10. Level 1 means linear elastic behaviour. Cracking and a time dependent increase of the tensile strength is considered in level 2. The E-Modulus is constant. Level 3 agrees with level 2 but also the E-Modulus develops with the course of the time. The curves in Figure 10 show horizontal normal stress along the section line 1-1. These results can be seen as an approximation of the contact stress avoiding the singularity at the edge of the glass pane. The linear elastic analysis yields 12,5 N/mm^2 tensile stress in the concrete. This tension decreases to less than 2 N/mm^2 when level 2 is applied. Considering the increasing E-Modulus during shrinkage (level 3) leads to two times higher tension. Assuming that level 3 brings the most realistic results, the clamping force related to the length of the connection, determined by integration of the compressive stress, amounts 24 N/mm. Due to the two rough surfaces which the clamping force acting is on, 48 N/mm may be taken into account, if the focus is on the friction mechanism.

The second model has a groove in the glass, which is also filled with concrete. The stress distribution is illustrated in two section lines (see Figure 11). Because of the stronger concrete and the thicker glass the tensile stress amounts up to 6,5 N/mm^2 and consequently the sum of the normal forces acting on the glass surface is 168 N/mm.

In order to find a mathematical function describing how the shear strength of the connection depends on the normal force calculated above, further tests must be carried out. Several pull-out tests of connections with various geometries have to be completed with shear bond tests where any contact pressure is eliminated.
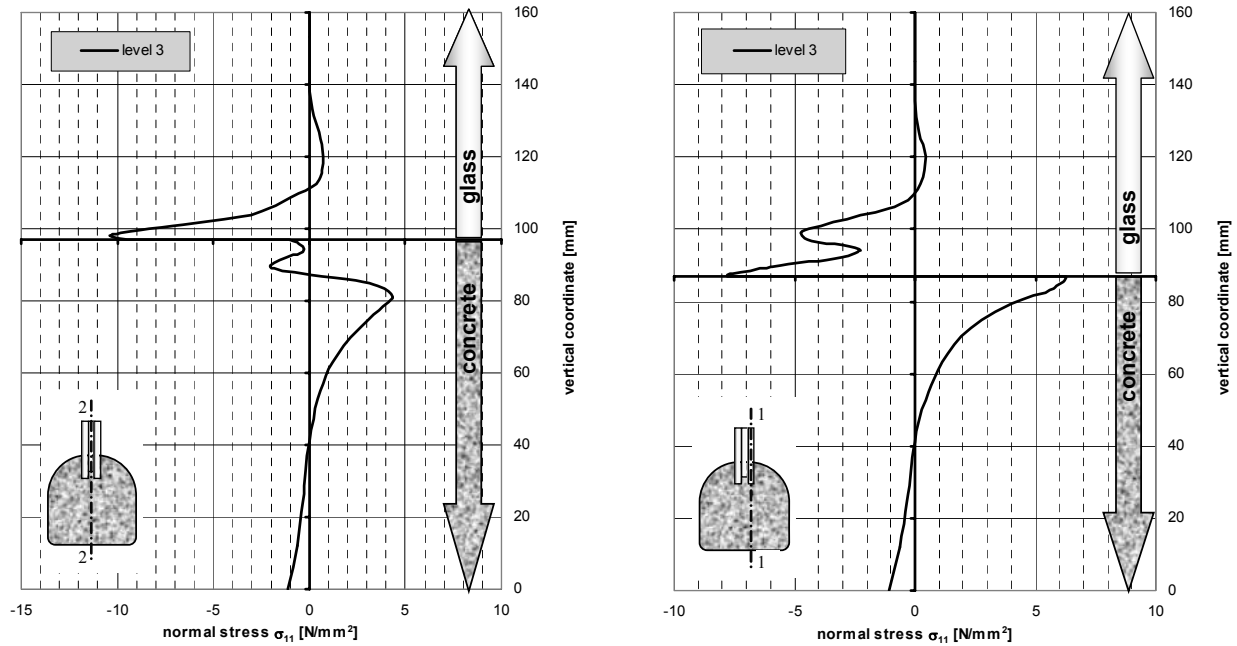
Figure 11: Finite element results of model 2

4.4   UHPC-Steel

The most important and classical composite construction is that of steel and concrete. The shear action in the interface is primarily carried by steel dowels. Probably that kind of construction can be improved by the use of UHPC by one of the following ways: The traditional shear bond is rather weak, because the dowels are heavily displaced in NSC. The stiff and strong UHPC could improve that behaviour. Furthermore, it is imaginable that the good mechanical adhesion of UHPC, which was observed from glass-UHPC bond tests, can also be achieved with roughened steel. Assuming that, one can do without dowels. These speculations must be studied separately in the future.
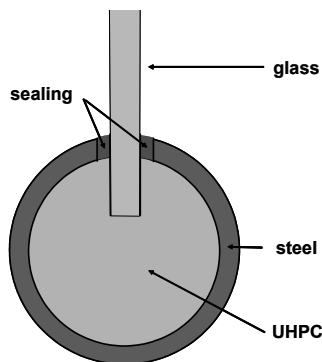
Figure 12: Steel-UHPC-glass composite

However, one idea regarding to chapter 3 and considering the thoughts above is shown in Figure 12. The connecting material between the glass web and the slotted steel tube is UHPC. As said in chapter 3, one must mind for the negative effect of the shrinkage

deformation on the bond behaviour to the steel tube. The development of swelling UHPC could probably solve that problem.

4.5   UHPC-UHPC

It is self-evident to exchange the glass pane of the beam in Figure 7 for a thin-walled pre-cast UHPC plate. Such composites do not totally agree with the definition in chapter 2 , as the material is the same, but it only works, if the adhesion between already hardened UHPC (old) and hardening UHPC (new) is satisfactory. This method is being supposed to simplify the fabrication of built-up sections like folded structures.

5   Conclusion and Outlook

Composite constructions are induced by the attempt of combining different good properties of at least two materials. They only work if a satisfactory load transfer between the components can take place. The well known bond effects are adhesion, friction and shear bond. Especially mechanical adhesion is very stiff and should therefore to be aimed for. Bond tests of glass-UHPC specimens show that UHPC is a good adhesive in view of mechanical adhesion. Its size distribution of the ultra fines must be properly attuned to the roughness of the contact surface. Thus, it is expected that other materials like concrete, steel and timber can also well cooperate with UHPC. In order to come forward in the development of several composite methods of construction an ongoing research project focuses on the bond behaviour between UHPC and the materials mentioned above. Theoretical approaches should be derived from various experiments, which should make possible to predict the bond capacity based on certain parameters like surface roughness as well as adequate characteristics of UHPC.

The variety of possibilities to realise composites with UHPC is shown by means of diverse applications. Concerning bridge construction it can be concluded that both economical and structural advantages can be reached. On the one hand the shortening of the construction periods due to pre-casting the elements and the cheaper equipment (cranes, jacks, scaffolds) due to the lightness of the elements reduce the costs. On the other hand the structures are durable because of the outstanding resistance of the "skin" made of UHPC.

The development of the glass-concrete composite technology makes clear how important UHPC in view of composites is. In that case it allows at the first time the design of transparent, vitreous structural elements, which combine a high load capacity, ductility and aesthetics.

6   References

[1] Leonhardt, F.; Mönnig E.: Vorlesungen über Massivbau, Teil 1, Kapitel 4 Verbundbaustoff Stahlbeton, Springer Verlag, 3.Auflage 1984

[2] Poggel, H.: Untersuchungen zur mechanischen Haftung in Verbundsystemen, Dissertation Universität Siegen, 2001

[3] König et al.: Hochleistungsbeton, Kapitel 4 Verbund zwischen Bewehrung und Hochleistungsbeton, Verlag Ernst & Sohn, 2001

[4] Bornemann, R.: Ultrahochfester Beton,
http://www.uni-kassel.de/fb14/baustoffkunde/deutsch/Forschung/UHPC%20Uni%20Kassel.pdf

[5] Freytag, B.: Die Glas-Beton-Verbundbauweise, Dissertatation, Graz University of Technology, 2002

[6] Freytag, B.; Sparowitz, L.: Glass-Concrete-composite Members. In: Proceedings of the 3rd International PhD Symposium in Civil Engineering, Bergmeister K. (ed.), Vienna, 2000, vol. 2, pp 163-173

[7] Greunz, G.: Experimentelle Untersuchungen zur Druckfestigkeit von ultrahochfesten Betonen mit Basaltzuschlag, Diplomarbeit am Institut für Betonbau, Graz University of Technology, 2000

Part 10:

Processing and Early Age Behavior

Schachinger, Ingo
Dipl.-Ing.
Projektleiter Entwicklung
Fa. Schöck Bauteile GmbH
Steinbach / Baden-Baden, Germany

Schubert, Jürgen
Dipl.-Ing.,
wissenschaftl. Mitarbeiter am cbm der TUM;
München, Germany

Mazanec, Oliver
Dipl.-Ing. (FH)
Student of MSc civil ingeneering
Hannover, Germany

Effect of Mixing and Placement Methods on Fresh and Hardened Ultra High Performance Concrete (UHPC)

Summary:

In order to achieve sufficient ductility and fire resistance, ultra high performance concrete (UHPC) is produced with w/b-ratios near 0.25 and silica fume contents up to 30 wt.% w.r.t. cement. Between 1.0 and 3.5 vol.% steel fibres and up to 0.65 vol.%. PP fibres are added to the mix. This necessitates high mixing energies for UHPC. For example, the specific mixing energy for a UHPC made with 2.5 vol.% steel fibres and 0.3 vol.% PP fibres was 5.81 kW/h. Air bubbles with diameters between 0.1 and 1 mm formed in this highly viscous mortar leading to loss of strength of the hardened concrete.

In this contribution practical methods to reduce the air content of hardened UHPC are introduced and their advantages und disadvantages discussed. Usually, UHPC is produced by compacted a highly fluid concrete with internal or external vibrators so that as much air as possible is removed. This can cause fibre orientation or even sedimentation of the fibres. Tests showed that when the concrete was placed by pumping the fresh concrete temperature increased from 20°C to 40°C while the air content decreased by as much as 2 vol.%. Air removal from the fresh concrete by pressure reduction down to 50 or 70 mbar within a closed mixing system was found to be an very effective, but technologically complicated method.

Keywords: *ultra high performance concrete, mixing energy, mixing procedure, evacuation, air void content, steel fibres, PP fibres*

1 Introduction

The research at the cbm of the TU Munich on ultra high strength concrete began towards the end of the 1990s when the new generation of super plasticizers based on polycarboxylates had not yet reached their current effectiveness. The production of UHPC requires intensive mixing of concrete with the following characteristics:

- Maximum aggregate size < 1mm
- Low w/c ratio
- High silica fume contents > 25 wt.% w.r.t. cement
- Steel fibre contents between 2.5 and 3.5 vol.%

This lled to the introduction of air bubbles which even after prolonged vibration could only be partially removed.

This publication reports on the research results and experience with regard to the reduction of the air bubble content of UHPC using appropriate mixing technology, mixing procedures and placement methods. The work focuses the development of suitable procedures for practical application.

2 Mixing Technology - Effect of Mixer Type on the Fresh Concrete Properties

2.1 General Remarks

Conventional mixer types can be used to produce UHPC in the laboratory or in precast concrete plants. However, a reduction in compressive strength due to enhanced air void content must be accepted if unsuitable mixing and placement procedures are used.

2.2 Compulsory Mixer (Volume 75 l)

The laboratory mixes were made with a 75 l ZZ 75 HE mixer manufactured by Zyklos. The eccentrically mounted turning and dividing paddles, which were very near the bottom of the drum, as well as the drum wall scraper resulted in three dimensional turning of the mix, see Fig. 1. The mixer speed was between 2 and 3 m/s so that the superplasticizer was evenly blended into the mix. Toward the end of mixing (approximately 7 min) the fresh UHPC had a very sticky consistency so that lumps of fresh concrete stuck to the paddles lowering the efficiency of mixing. Due to the sticky consistency the air void content of the fresh concrete was approximately 4.3 vol.%. The fresh concrete temperature was between 20 and 23°C.
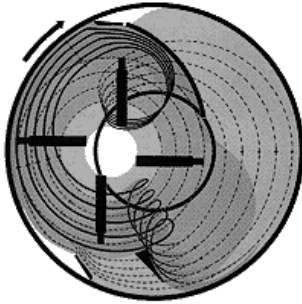
Figure 1:   Mixing method of ZZ 75 HE (Zyklos; Mix volume 75 l)

2.3   Ring Mixer (Volume 1000 l)

In order to produce a UHPC strut (cross section 40×40 cm²) 400 l of fresh concrete were prepared with a 1000 l ring mixer at a precast concrete plant. The ring mixer hat three star-shaped satellites driven by a multiple-stage planetary gear which rotated around the vertical axis, Fig. 2. The speed of mixing was between 1 and 2 m/s. The high shear forces applied by this technique yield an intensive mixing and highly effective distribution of the cement in the mix. After a mixing time of approximately 12 minutes the air void content of the fresh concrete was 3.2 vol.% at 19°C.

Figure 2:   Ring mixer (mix volume 1000 l)

2.4   R-Intensive Mixer with Vacuum Periphery

The following requirements are placed on the on the mixer for UHPC production:

- Short mixing duration
- Homogeneous blending of small quantities of additives and admixtures
- Homogenization of materials having different densities

These requirements and the practice-relevant volume (up to 7 m³) appeared to be fulfilled by the R-intensive mixer produced by Eirich, Fig. 3.
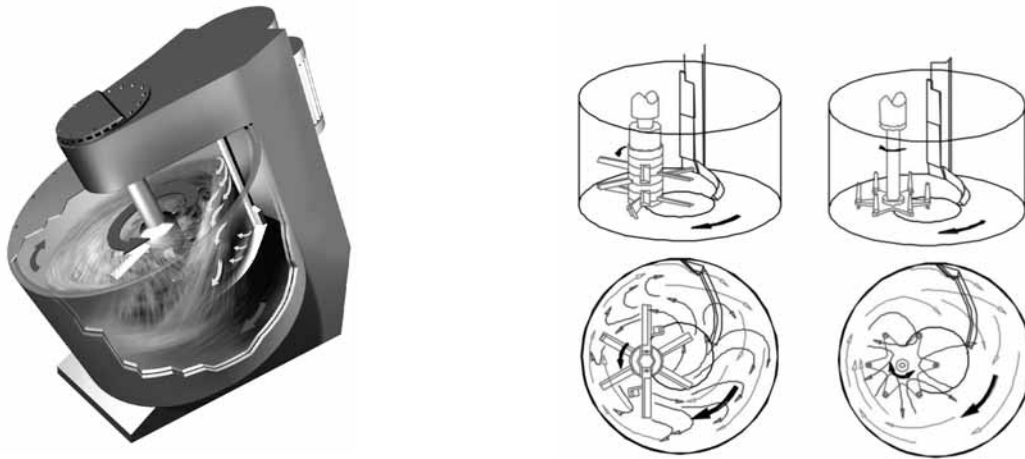
Figure 3:   Mixing method of the R-intensive mixer (Eirich) and turning geometry
(left: star turner; right: rod turner)

Due to the optimum combination of drive and geometry which enables high mixt speeds of up to 40 m/s (opposed currents) and the tilt of the drum this mixer produces optimum homogenization of materials with large differences in density. The vacuum accessory permits evacuation down to pressures of 50 mbar in a closed system. Depending on the required performance the turning geometry can be varied. While the star turner is mainly used to homogenize the dry materials, the rod turner is used to distribute water and superplasticizer and homogenize the final mix.

3   Effect of Air Voids on the Fresh Concrete Properties

During mixing air bubbles find their way into the mix. This effect increases with poor workability and stickiness of the fresh concrete. Air voids with a diameter of 0.1 to 1 mm are similar to the aggregate size and are effectively defects in the concrete which can initiate cracks at high loads.

Usually, UHPC is produced at a fluid consistency similar to self-compacting concrete so that the air void content can be reduced to roughly 2 to 2.5 vol.%.

Since the density of the steel fibres is three times higher than the density of fresh concrete, soft consistencies lead to sedimentation of the steel fibres. On the other hand, PP fibres are very fine ($\varnothing$ < 20 μm) which causes stiffening and reduces air removal from the fresh concrete.

Earlier, when the mixing procedure had not been fully optimized and the superplasticizer was less efficient, the air void content of the fresh concrete was above 4 vol.% on account of the

sticky consistency. By using the vacuum accessory with pressure of 50 mbar during the last mixing phase it was, despite of the sticky consistency, possible to reduce the air content to values below 1 vol.%. This resulted in an increase in concrete density and correspondingly compressive strength from 150 to 230 N/mm^2, Fig. 4.
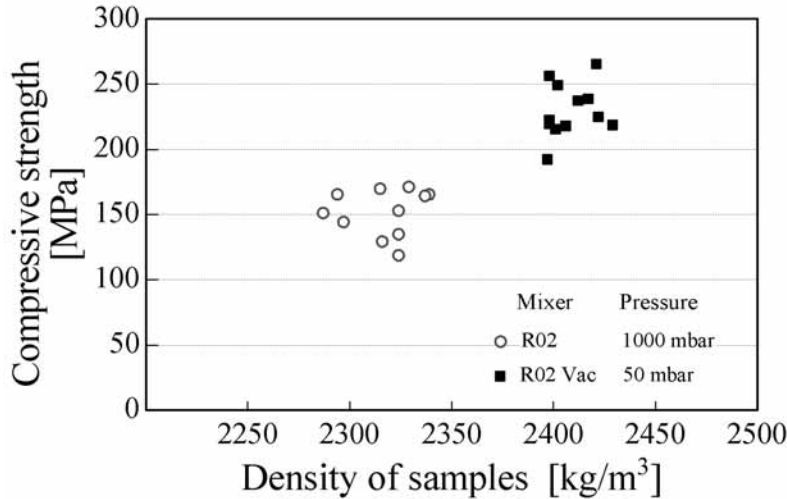
Figure 4: Effect of pressure in the mixer on density and compressive strength of samples

4   Optimization of Mixing Procedure

The following mixing procedure which is divided into 6 steps (Fig. 5) is the result of extensive optimization investigations with the R-intensive mixer in the laboratory. The procedure proved to be effective for the production of UHPC with high fibre contents. A mix speed of 8 to 9 m/s was found to be sufficient and was used for all the mixing steps.

- Step 1:Homogenization of all dry materials (excluding steel fibres) in under 1.5 min.

- Step 2: Addition of water and wetting of the surface of the materials within 1.5 min. Half of the superplasticizer is added with the water in order to avoid agglomeration of the silica fume.

- Step 3: Sufficient contact duration between the cement and the water is necessary to improve the effectiveness of the remaining superplasticizer. This is provided by a 2 minute break. Accordimng to [1] the addition of superplasticizer at the beginning of the dormant period gives the best liquidation and good stiffness behaviour. This could be confirmed by the present investigations.

- Step 4: Continuous addition of steel fibres over 1.5 minutes. The fibres can be added in Step 1 to reduce the total mixing time.

- Step 5:Addition and blending in of the remaining superplasticizer 5 minutes after the first contact between water and cement.

- Step 6: Finally, the system is evacuated to 50 mbar to remove air from the fresh concrete (1.5 min).
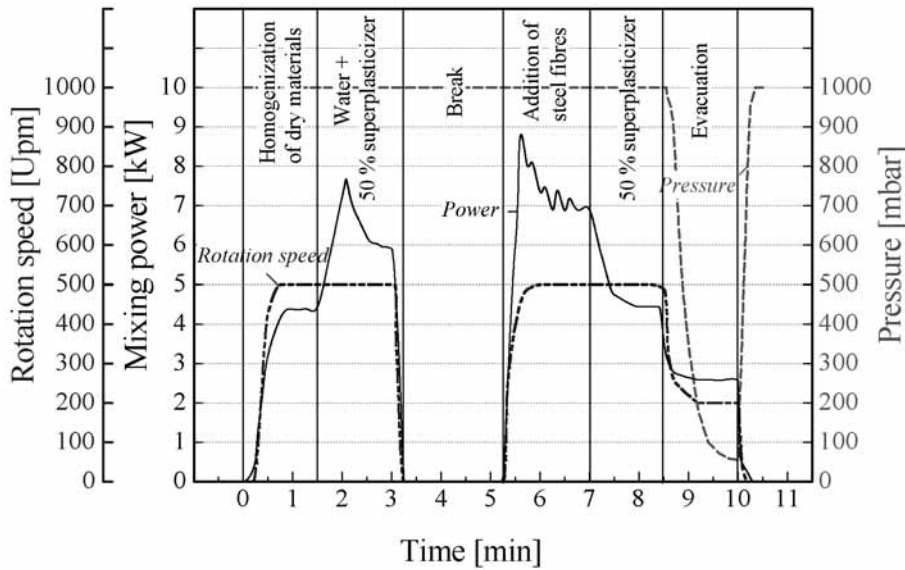
Figure 5: Optimized mixing procedure for fresh concrete preparation with the R08 VAC (Charge: 110 kg)

The parameters shown in Fig. 5 for the rotational speed of the turner and the power applied were measured during the preparation of an UHPC with a fibre cocktail comprising 2.5 vol.% steel fibres and 0.33 vol.% PP fibres.

A specific mixing energy totalling 5.81 kWh/t (Plate: 2.15 kWh/t; Turner: 3.66 kWh/t) was needed for the whole procedure. The necessary mixing time for other types of mixers can be derived from this. Thus a mixing time of 12 min results for a compulsory mixer with a specific mixing energy of 30kW/t. Since thorough mixing is achieved at high degrees of drum filling, the ratio between mixing energy and mixer capacity should be as high as possible.

An even colour of the mix was observed after mixing the dry materials such as quartz sand, cement, silica fume and PP fibres for one minute. In step 2 the mixing power increased to 7.7 kW due to the increase of the cohesive forces on wetting the surfaces. It then fell significantly once the water had been evenly distributed, see Fig. 5.

When the mixer was switched on after the 2 minute break in step 4 the highest power was measured at 9 kW. This can be explained by agglomeration due the start of cement hydration. The fresh concrete had a porridge-like consistency during this mixing phase which enabled a high input of mixing energy. This yielded a good distribution of the steel individual fibres during the subsequent addition of steel fibres to the mix. After homogenization and attainment of a constant power of 7 kW, the remaining superplasticizer was added 5 minutes after the first contact between water and cement. A fluid consistency at a power of 4.3 kW followed.

In the final step of the mixing procedure, air was almost completely removed from the homogeneous, fluid fresh concrete by application of a pressure of 50 mbar. The pressure was chosen so that the water loss from the fresh concrete was minimized. Moreover, the pressure in industrial scale mixers can only be roughly set to this level. In order to minimize further addition of air bubbles, the rotational speed was reduced.

The mixing procedures for the compulsory and ring mixers were adapted from the optimum mixing procedure for the R-intensive mixer. Somewhat more than half of the superplasticizer was added 5 min following the first contact between water and cement to enhance the effectiveness of the superplasticizer and produce better setting behaviour.

Table 1:   Mixing times and steps for the compulsory mixer (75 l)

time [min] begin- end	to do
	Dry homogenisation or quartz sand and silica fume over 1 min
0 – 1.0	Addition of water
1.0 – 1.75	Addition of mixture of cement and quartz powder
1.75 – 2.5	Addition of 40% superplasticizer within 15 s followed by homogenization
2.5 – 6.0	Break
6.0 – 7.0	Addition of remaining (60%) superplasticizer and homogenisation
6.0 – 8.0	Continuous addition of steel fibres

Owing to the controlling system it is not possible to pause the ring mixer (1000 l). The second addition of superplasticizer followed nevertheless 5 minutes after the first contact between water and cement. This was preceded by an extended homogenization period. The total mixing time was 12 min on account of the time needed to handle the large quantities of material.

In both cases, as opposed to the R-intensive mixer, it was not possible to achieve a porridge-like consistency after first addition of the superplasticizer. The reason for this was the low mixing energy which led to lower fresh concrete temperatures of 19 to 23° compared with 28 to 30°C for the R-intensive mixer.

5 Measures to Reduce the Air Content of Concrete Components

5.1 Conventional Methods

5.1.1 Adjustment of a Fluid, Self-Compacting Consistency

The removal of air from UHPC is usually improved by a suitable choice of superplasticizer, cement and silica fume in combination with an optimized mix composition and mixing procedure. A fluid almost self-compacting consistency can be obtained.

Based on extensive investigations with the R-intensive mixer without use of the vacuum accessory, fresh concrete with a mortar flow of 26 to 28 cm proved to be optimal regarding workability, air removal and stability, Fig. 4.
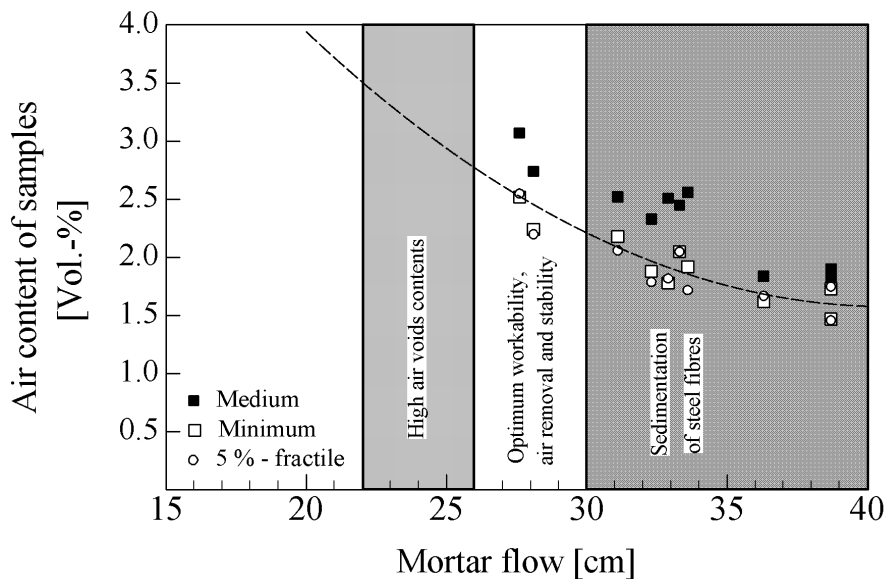
Figure 6: Effect of mortar flow (no hits, mortar cone according to DIN 1060 T.3 (D/d/h = 100/70/60 mm) of fibre-free ultra high strength fresh concrete on the air content of the samples (Compaction 60 s at 70 Hz with formwork fixed to compaction table)

The data in Fig.6 are the result of statistical evaluation of roughly 30 samples per mix. The 5% fractile value for the air void content is in good agreement with the minimum value measured confirming the use of a sufficient number of samples.

Mortar flows below 26 cm led to higher air void contents, but resulted in a lower scatter in bending and post-fracture behaviour [5]. This effect is very important in practice and must according to [1] be determined at a realistic scale during the design of concrete components. The reason for the higher scatter at softer consistency lies in the poor joint between fibre and matrix as well as the different fibre orientation - and even sedimentation - due to the

582

particular placement method and form geometry. Sedimentation of fibres was observed in the laboratory for spreads of 28 to 30 cm and more.

5.1.2   Concrete Placement by Pumping

To reduce the air content, the fresh concrete was pumped into the formwork with a spiral pump with an operating pressure of 25 bars. During pumping the air content of the fresh concrete was reduced on average from 1.3 vol.% to 2.9 vol.%.

The degree of air removal depended on the length of the pipe. On account of the viscous consistency friction resulted, depending on pipe length and concrete quantity, in an increase in fresh concrete temperature from initially 20 to 23°C to roughly 40°C at the end of the pipe.

5.1.3   Air Removal by Vibration

It was not possible to effectively remove air from the concrete for the test struts (cross section 40/40 cm) using the table vibrator at the precast concrete plant. Cores taken from the stuts contained air void as large as 4 mm. It was observed that the air voids introduced during mixing did not rise up through the fresh concrete. This behaviour was obviously caused by the use of an inappropriate combination of vibration frequency and amplitude for the UHPC.

According to the recommendations of Bresson [1] the vibration speed at w/c ratios below 0.3 should be about 0.2 m/s. Fig. 7 indicates which equipment is able to provide this high vibration speed.
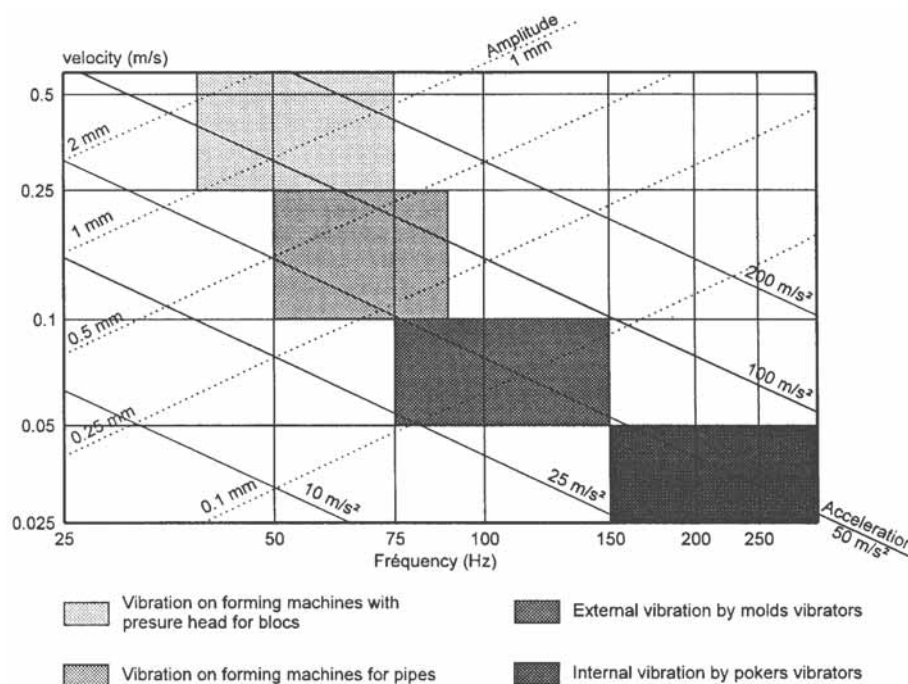
Figure 7:   Characteristic values for the vibration and modes of concrete vibration [3]

Furthermore, as well as the properties of the cement paste the aggregate size affects the optimum vibration frequency. According to [1] the best compaction is reached when the vibration frequency corresponds to the resonant frequency of the mean grain size. Thus in the case of a mean grain diameter of <1 mm a frequency of 200 Hz should be chosen giving an acceleration of 100 to 120 m/s^2 and an amplitude of 0,12 to 0,15 mm. On comparing these values with the data in Fig. 7 it can be seen that such vibrators are not usual in concrete construction.

5.2 Complete Air Removal from Fresh Concrete with Vacuum Accessory

As already mentioned in Section 4, it was possible to reduce the air content of the fresh concrete to values under 1 vol.% irrespective of the steel fibre content (up to 10 vol.%) through the application of pressures of 50 to 70 mbar in the closed mixing system of the R-intensive mixer Fig. 5. The spread of these mixes was between 22.6 and 30.8 cm. To avoid orientation or sedimentation of the fibres the concrete was not vibrated. The post-fracture behaviour of the samples in a displacement-controlled bending test has already been published in [1].
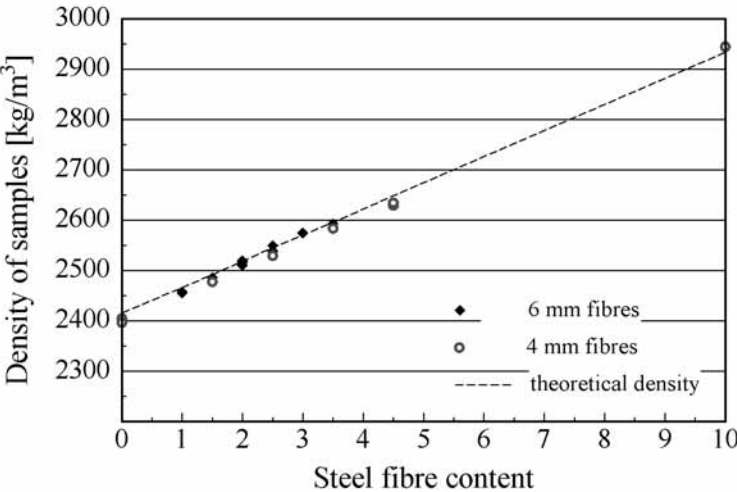
Figure 8: Density of samples as a function of steel fibre content

The air content of fresh concretes with 0.33 or 0.65 vol.% fine PP fibres ($\varnothing$ = 16 μm) added to improve fire resistance were as much as 2.0 vol.% after evacuation. This significantly higher air content was attributed to the fineness of the PP fibres. However, this value is well below the values in the literature for UHPC made with PP fibres in conventional mixers.

6 Conclusions and Recommendations

It is certain that in the near future UHPC will be manufactured exclusively in precast concrete plants. With regard to the practical use of UHPC technology two cases must be considered:

Since the use of UHPC is still at the beginning it may be assumed that UHPC will, at first, find a small number of applications and be produced in a well-equipped precast plant using the available equipment there. In this case a high level of expertise and experience with UHPC is especially important. An optimum combination of the conventional methods described in Section 5.1 to reduce the air content should be chosen. Quality control (monitoring variations the materials etc.) is necessary to avoid production errors. The mixing times should be adapted to the efficiency of the mixer according to Section 4. The production of UHPC with high contents of steel fibres (> 3.0 vol.%) or with PP fibres to improve fire resistance (0.3 to 0.65 vol.%) is very difficult. Conventional mixing methods are expected to result in void contents of 3 to 4 vol.% for cocktail mixes with steel and PP fibres. A highly fluid consistency (spread >30 cm) should be avoided since it will cause a large scatter in the post-fracture behaviour.

An economically viable solution for precast concrete plants lies in the production of large numbers of UHPC components which make the investment in the special vacuum mixing technology worthwhile. The R23 Vac. has a mix volume of 3 m^3 and is suitable for the production of precast concrete. Evacuation down to pressures of 50 to 70 mbar during the last mixing step can yield workable fresh concrete with an acceptable consistency (spread 24 to 27 cm) and an air bubble content below 1 vol.%. The following advantages for the production would be gained:

- Low sensitivity of the hardened concrete properties with respect to quality variation of the mix components on account of the low air void content
- Highly homogeneous concrete microstructure throughout the concrete member
- Good post-fracture behaviour due to an even distribution of fibres.

7   **References**

[1]   Chiocchio, G.; Mangialardi, T.; Paolini, A.E.: Effects of Addition Time of Superplasticizers on Workability of Portland Cement Pastes with different Mineralogical Composition. il cemento, 1986, Heft 2, p. 69-79

[2]   Interim Recommendations for Ultra High Performance Fibre-Reinforced Concretes. Association Francaise de Genie Civil (AFGC) / Service d´ètudes techniques des routes et autoroutes (SETRA), working group on Ultra-High Performance Fibre-Reinforced Concrete.

[3]   Bresson, J.: Mixing and Compacting Techniques fort he Production of Very High Performance Precast Concrete Products. Proccedings of the 4th International Symposium on Utilization of High-strength/High-performance concrete, Paris, 1996, p. 269-272.

[4]   Riker, Rudolf: Maschinentechnik im Betonbau. Ernst & Sohn Verlag, Berlin 1996, ISBN 3-433-01286-5.

[5]   Schachinger, I., Stengel, Th., Heinz, D.: Einsatz von Fasern zur Verbesserung des Nachbruchverhaltens von ultrahochfestem Beton im Biegezugversuch. 15. Internationale Baustofftagung „ibausil", September 2003, Weimar.

Stéphanie Staquet,

PhD student

Department of Civil Engineering

University of Brussels

Brussels, Belgium

Bernard Espion,

Professor

Department of Civil Engineering

University of Brussels

Brussels, Belgium

Early-age autogenous shrinkage of UHPC incorporating very fine fly ash or metakaolin in replacement of silica fume

Summary

This research focuses on the development of the autogenous shrinkage of UHPC since casting time. One of the purposes of this research was to analyse the possibility to substitute the silica fume normally used in UHPC by another pozzolan in order to minimize the autogenous shrinkage. Three optimal mix proportions were tested: the first one was based on the Reactive Powder Concrete mix proportion; 2/3 of the silica fume used in RPC was replaced by a very fine fly ash coming from South Africa in the second one and by a metakaolin in the third one. For each mix proportion, the evolution of the activation energy in function of the concrete strength was determined as well as the thermal expansion coefficient. Two different curings were applied: at 20°C or a heat curing at 42°C during two days after casting. The autogenous shrinkage curves were obtained from the measurements after having eliminated the thermal strains. For UHPC cured at 20°C, the mix proportion containing metakaolin shows an autogenous shrinkage significantly lower than the other mix proportions. For UHPC cured at 42°C, the total shrinkage measured for the mix proportion containing metakaolin is negligible by comparison with the others mix proportions.

Keywords: *autogenous shrinkage, thermal dilation coefficient, heat curing, metakaolin, very fine fly ash, reactive powder concrete.*

1   Introduction

Self-desiccation develops in any concrete that is not water cured because it is a direct consequence of hydration reactions, but the magnitude of autogenous shrinkage varies with the mix proportions. High levels of autogenous shrinkage could have important implications such as dimensional incompatibility between concrete elements and cracking that is partially or wholly induced by restraints to autogenous movements. In trying to understand the mechanisms that govern autogenous shrinkage, it is necessary to understand the real effects existing in structural elements cast in situ as well as in precast elements subjected to heat curing. Whilst there is an increasing body of data on the autogenous behavior of HPC, there is currently only limited knowledge on the impact of early age temperature development on the autogenous behavior of UHPC. There are at least two aspects related to this issue. The first is the accelerated consumption of free water due to an increase in hydration rate caused

by temperature rise. The other is the thermal expansion, which counteracts the hydration-induced autogenous shrinkage. The effect of both factors may significantly influence the concrete deformations under realistic in situ conditions. In this paper, emphasis is placed on the competing effects of autogenous shrinkage and thermal expansion occurring since casting for three optimal mixture proportions of UHPC based on the RPC mix composition [1]. The pozzolan used traditionally in RPC is silica fume. Moreover, the heat curing reported until now for these UHPC is a steam curing at 90°C during two days. This temperature is not so easy to apply in the precast industry. Hence, the purpose of this research was to minimize shrinkage at very early age and to maximize the workability and the early-age strength of UHPC based on Reactive Powder Concrete mixture proportions by changing the type of curing and by replacing a part of silica fume by other pozzolans: a very fine fly ash and a metakaolin.

2 Tested materials

The properties of the silica sand, the crushed quartz and the straight steel wire fibers used in the tests are given in [2]. Polycarboxylate superplasticizer was used. Three different high strength portland cements have also been selected: CEM I 52.5 R LA; CEM I 52.5 HSR LA and CEM I 52.5 R. Their Bogue composition, their alkalis equivalent content in percentage of weight and their Blaine fineness are given in Table 1.

Table 1: Bogue composition and characteristics of three cements CEM I 52.5

* = % of weight	C3S*	C2S*	C3A*	C4AF*	Alkalis*	Blaine (m²/kg)
R LA	64.80	9.02	7.12	10.5	0.36	540
HSR LA	68.56	7.36	2.1	12.4	0.50	401
R	60.11	12.85	8.11	7.14	0.67	495

Three pozzolans have been used: a silica fume coming from the zirconium industry in France; a very fine fly ash coming from South Africa and a metakaolin. Their characteristic parameters are listed in Table 2. In a previous research [2], four different silica fumes were tested. Selection criteria for the silica fumes were derived from the tests. In this part of the research, only one of the best silica fumes in terms of workability and strength for RPC was chosen as the reference pozzolan for the present tests. The same work was done for the metakaolin. Hence, only one of the best metakaolins in terms of workability for RPC is used for the tests presented in this paper.

Table 2: Characteristic parameters of the tested pozzolans

* = % of weight	SiO_2 *	Al_2O_3*	CaO*	Fe_2O_3*	Alkalis	ZrO_2*	BET (m²/g)
Silica fume	93.5	3.5	0.02	0.15	0.14	2.4	12.79
Very fine fly ash	50.20	30.32	8.06	3.82	0.95	-	1.17
Metakaolin	55	40	<0.1	0.6	1.58	-	12

3 UHPC mixture proportions

Tables 3 and 4 summarize the mix compositions of the three UHPC tested. The first mixture proportion (Mixture 1) was based on RPC mixture proportions. In the others, 2/3 of the silica fume used in Mixture 1 was replaced by the very fine fly ash in Mixture 2 and by metakaolin in Mixture 3. In our tests, this percentage of replacement of the silica fume by another pozzolan was the largest allowable in order to keep a good workability for an UHPC. Otherwise, it was necessary to increase significantly the quantity of water and/or the quantity of superplasticizer in the mixture.

Table 3: Tested UHPC mixtures

	Mixture 1	Mixture 2	Mixture 3
Cement	CEMI 52.5 R	CEMI 52.5 R LA	CEMI 52.5 HSR LA
Pozzolans	Silica fume (SF)	SF + Very fine fly ash	SF + Metakaolin

Table 4: Tested UHPC mixtures proportions

Mixtures proportions	Mixture 1	Mixture 2	Mixture 3
Cement	0.996 kg	0.996 kg	0.996 kg
Silica sand	1.425 kg	1.425 kg	1.425 kg
Crushed quartz	0.295 kg	0.295 kg	0.295 kg
Steel fibers	0.218 kg	0.218 kg	0.218 kg
Silica fume	0.324 kg	0.125 kg	0.125 kg
Very fine fly ash	0 kg	0.199 kg	0 kg
Metakaolin	0 kg	0 kg	0.199 kg
Superplasticizer	0.066 kg	0.066 kg	0.066 kg
% in dried up	2%	2%	2%
Net water	0.153 kg	0.1825 kg	0.2025 kg
Water/Cement ratio	0.20	0.23	0.25
Water/Binder ratio	0.15	0.17	0.19

Two different cures were applied: a curing at 20°C and a heat curing at 42°C during two days after casting as is usually done in the precast industry. Table 5 summarizes the results obtained for the compressive strength at 28 days for the concretes cured at 20°C and at 42°C.

Table 5:   Tested UHPC mixtures

	Average compressive strength (MPa) on cubes 50x50x50mm					
Age (day)	1 day		2 days		28 days	
Curing	20° C	42°C	20° C	42°C	20° C	42°C
Mixture 1	3.4	115.6	102.8	143.8	155.3	153.1
Mixture 2	1.6	53.7	35.3	124	156.5	148.7
Mixture 3	55	113	89.6	143	155.5	154.2

4   Testing method

The experimental work is based on the use of a concrete dilatometer (Figure 1) where the free length change of a prismatic specimen (60mmx60mmx240mm) is measured. In order to measure shrinkage at very early age, the specimens have to stay in the mould during testing. However, the friction between the specimen and the mould may, in combination with the low stiffness of the concrete in this phase, hinder the movement of the specimen. In order to eliminate the restraint by the mould, Teflon sheets 1mm thick were disposed [3]. For measurements at room temperature, the steel plates of the mould are insulated on the inside with polystyrene boards. For measurements at 42°C, the steel plates of the mould are not insulated. The specimens were sealed to prevent from drying during the test period. When the fresh concrete is placed in the mould, it is completely covered with a plastic watertight foil. A steel plate finally covers the top of the specimen. The ability of the equipment to prevent moisture loss during the experiments was checked by measuring the evolution of mass with time with an accuracy of 0.5g. The maximum change in mass of tested specimens was less than 0.01% during the test periods. Therefore, influence of moisture movements to or from the specimens could be ignored.

At each end of the specimen, an inductive displacement transducer measures the length change. The signals are recorded separately and added to obtain the total length change. The transducers are connected to the specimen by thin invar rods reaching 20mm into the specimen and, hence, the active length of the specimen is 200mm. At the end of each invar rod, a thin steel disc is fixed as anchorage. A thermo-couple measures the temperature in the center of the specimen. Shrinkage must be measured immediately after casting in a mould that permits constant readings without disturbing the concrete. Registrations of both length change and temperature start within 5 minutes after concrete mixing.
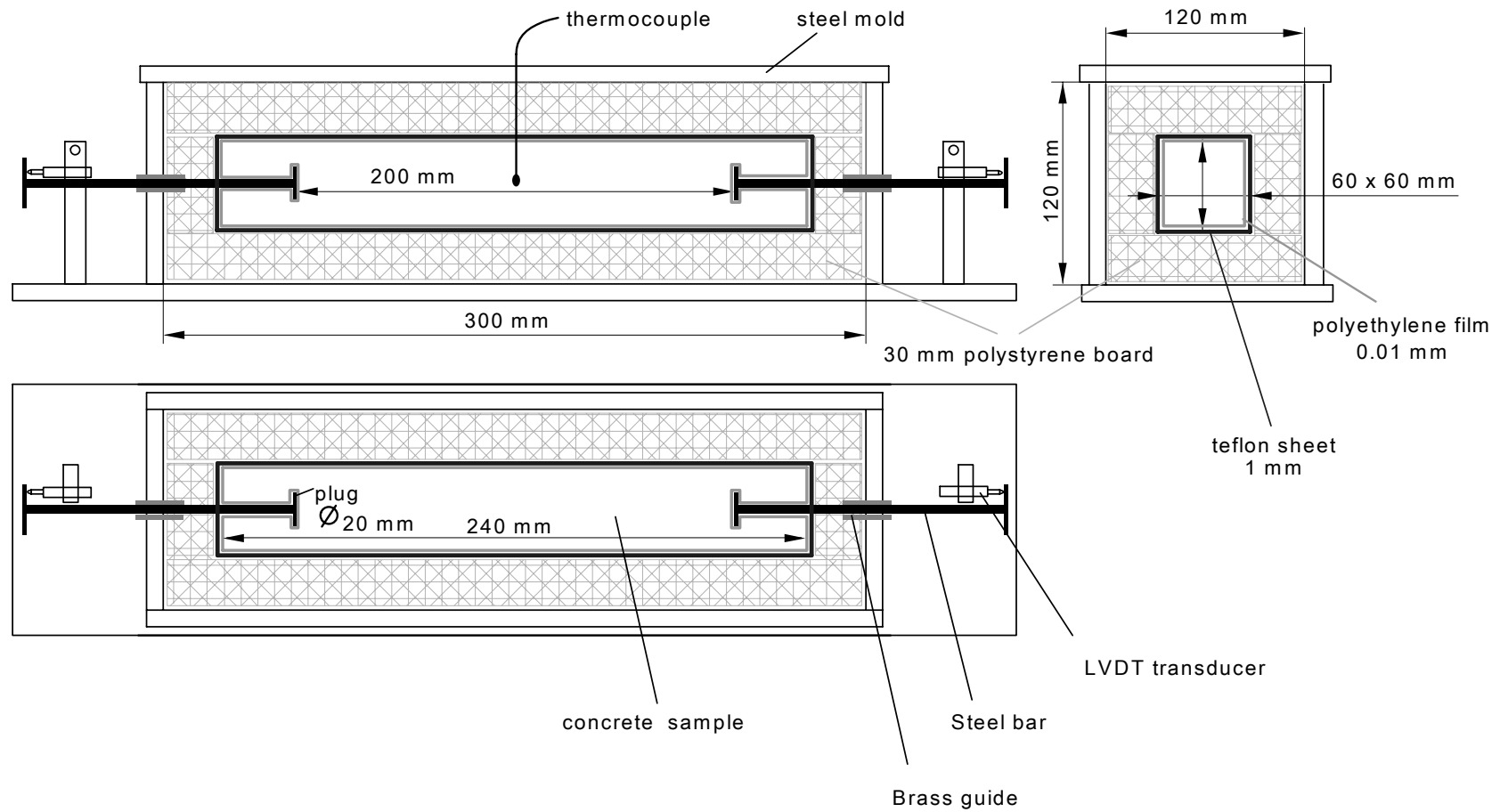
Figure 1:   Concrete dilatometer for measuring the strains since 5 minutes after the casting time

5   Discussion of recorded data

Figures 2 to 4 show the total measured strains (black lines) of the three concrete mix proportions along with the temperature (grey lines) recorded in concrete, with and without heat curing. It is observed that, during the very first hours after casting, concretes submitted to a heat curing swell as long as the thermal expansion is larger than autogenous shrinkage. Usually, autogenous shrinkage overtakes the initial thermal expansion quite rapidly, so that low water/cement ratio concretes shrink after the initial swelling phase. In ultra high performance concrete, the increase in the temperature of concrete by heat curing is very helpful as it delays the development of shrinkage. The thermal expansion that accompanies the temperature rise of 20°C is shown to substantially reduce the shrinkage in particular for Mixture 3.
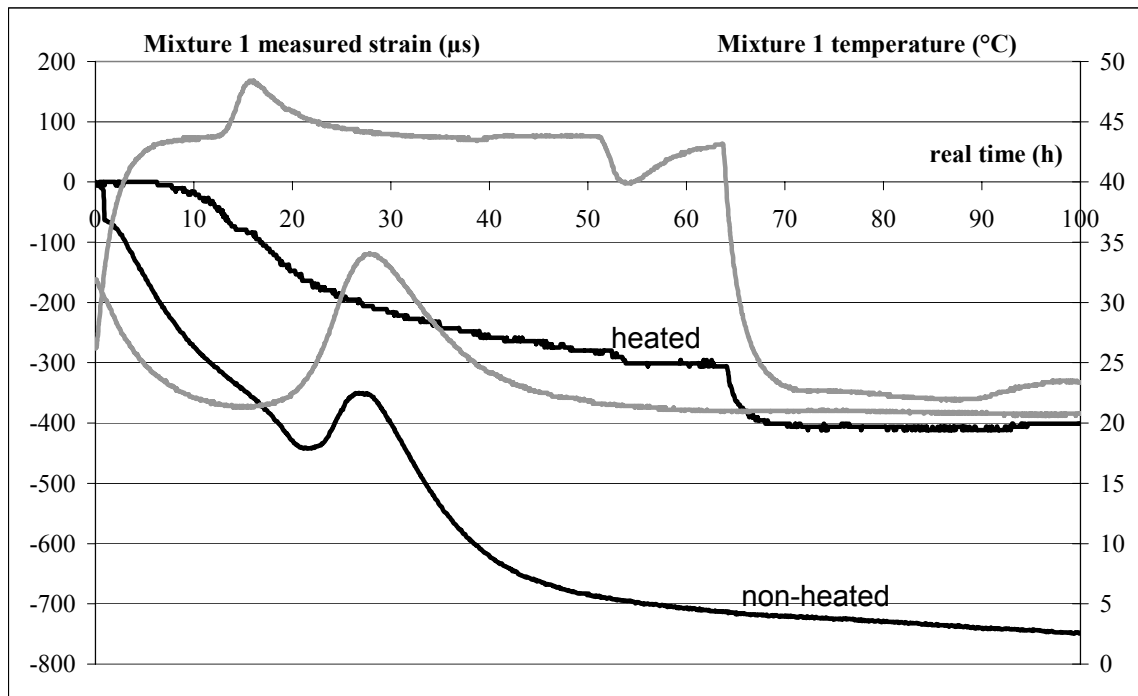
Figure 2:   Evolution of the measured strain and temperature in Mixture 1 with real time
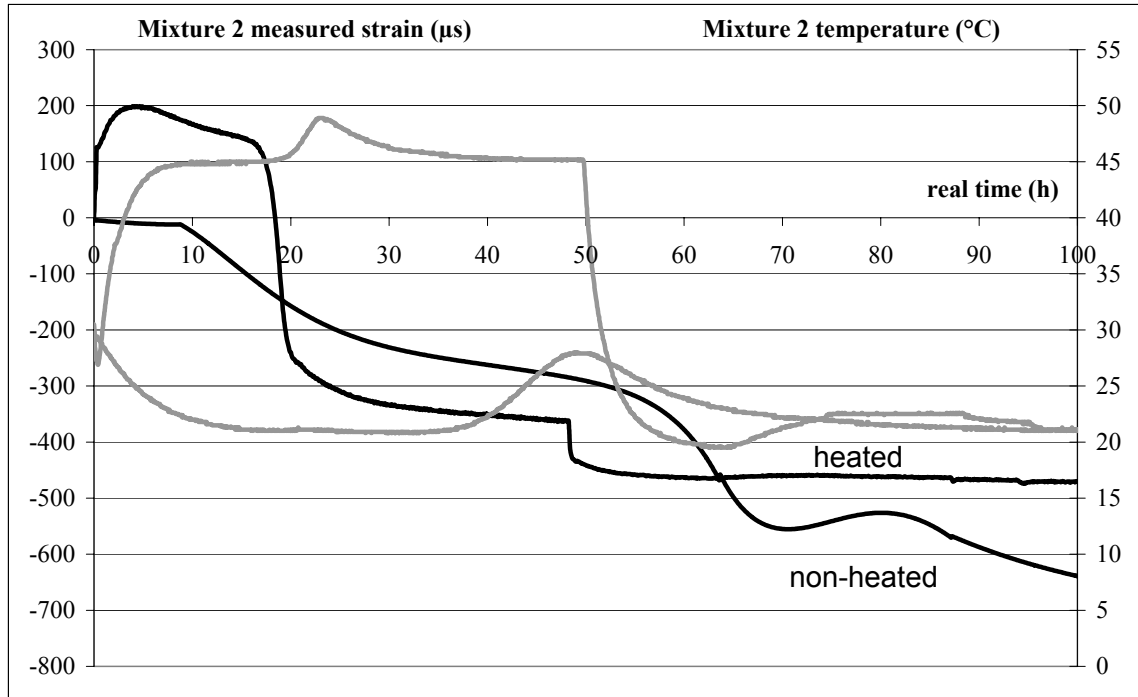
Figure 3:   Evolution of the measured strain and temperature in Mixture 2 with real time
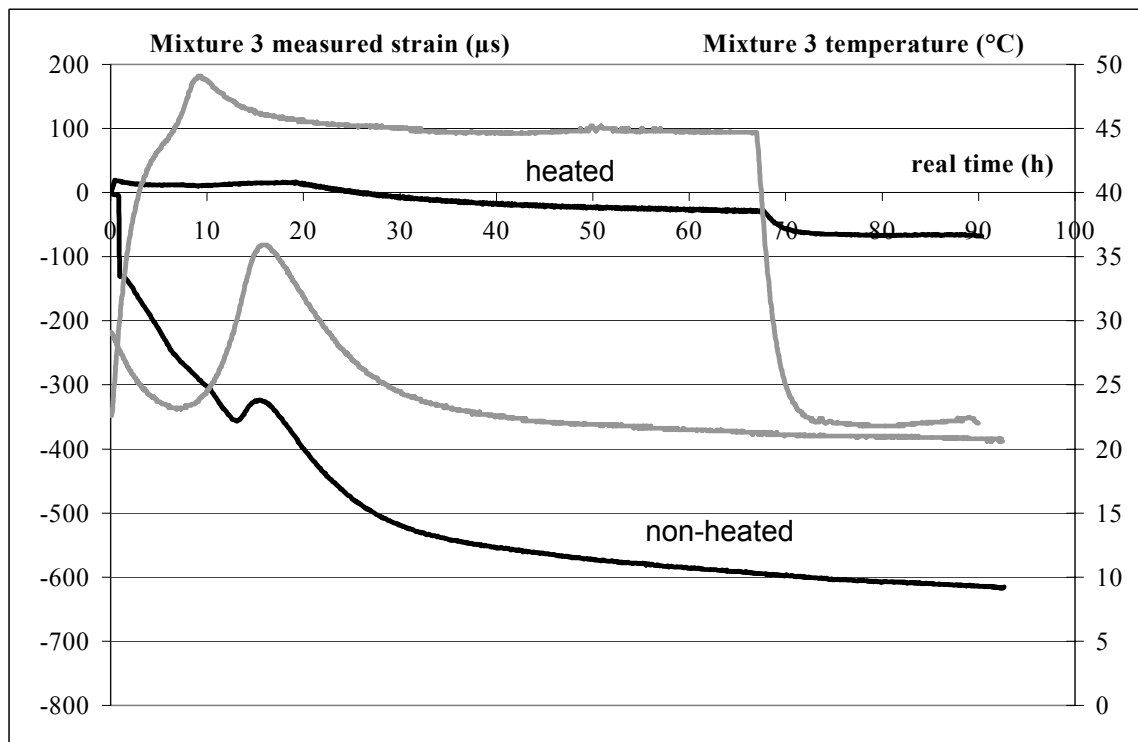
Figure 4:   Evolution of the measured strain and temperature in Mixture 3 with real time

6　　　Activation energy and thermal expansion coefficient

As the hydration process produces heat, the reaction becomes self-accelerating because the rate of hydration increases with increasing temperature. The setting time can clearly be identified on Figures 2,3 and 4 by the peak of temperature that occurs after a long dormant period. The strength development of UHPC is closely linked to the progress of cement hydration. This leads to the idea that the strength development can be expressed as a function of a time-temperature combination. Fig. 5 shows the early-age compressive strength results measured on cubic specimens with 50mm sides for the concrete mixtures cured at 20°C (grey lines) and at 42°C (black lines). From these experimental data, the evolution of the activation energy with compressive strength was determined for each mix by using the Arrhenius law [4].
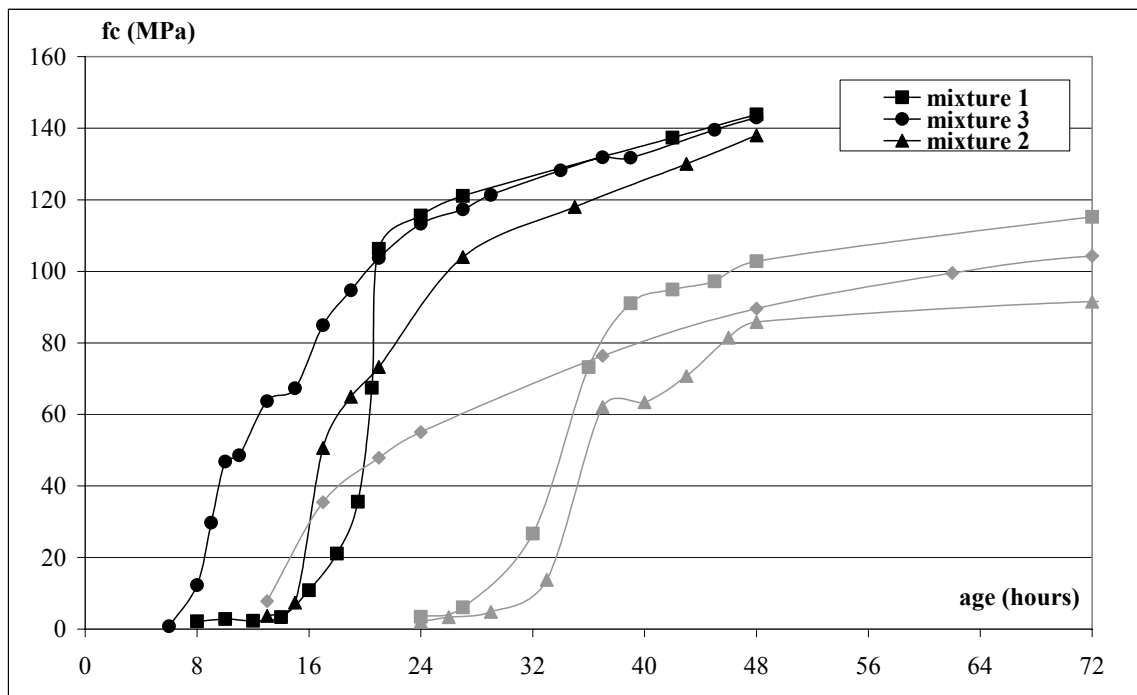
Figure 5:　　　Early-age compressive strength for samples cured at 20°C and 42°C

Figure 6 shows that the activation energy can reach very high values for these UHPC. Then, by using the maturity principle, the equivalent time to 20°C and the evolution of the thermal expansion coefficient was computed for each mix by taking into account the variation of the activation energy with compressive strength [5]. In figure 7, the evolution of the thermal expansion coefficient (TEC) with equivalent time to 20°C of each mix is detailed. The first value of TEC given in these figures corresponds to an age from which the Arrhenius law is supposed to be valid: it is assumed that a minimum value of 1MPa in compression is required. The determination of TEC before this age - when the concrete is still in a fresh state - is very difficult and depends strongly on experimental conditions and rate of temperature change.
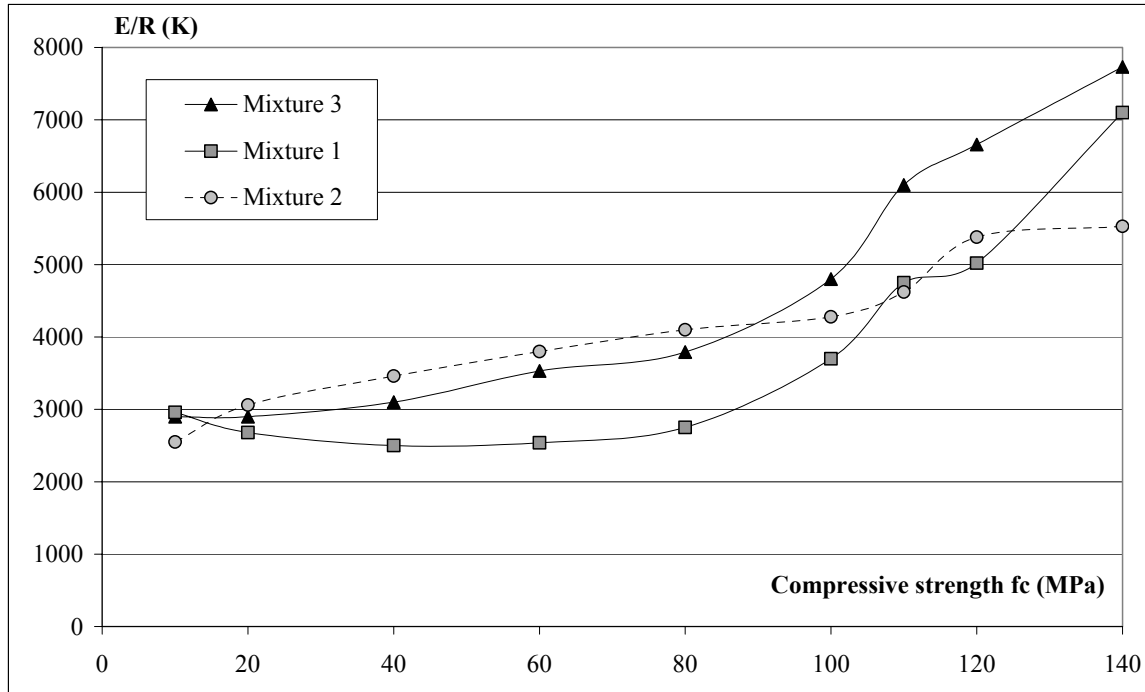
Figure 6:   Evolution of the activation energy with the compressive strength
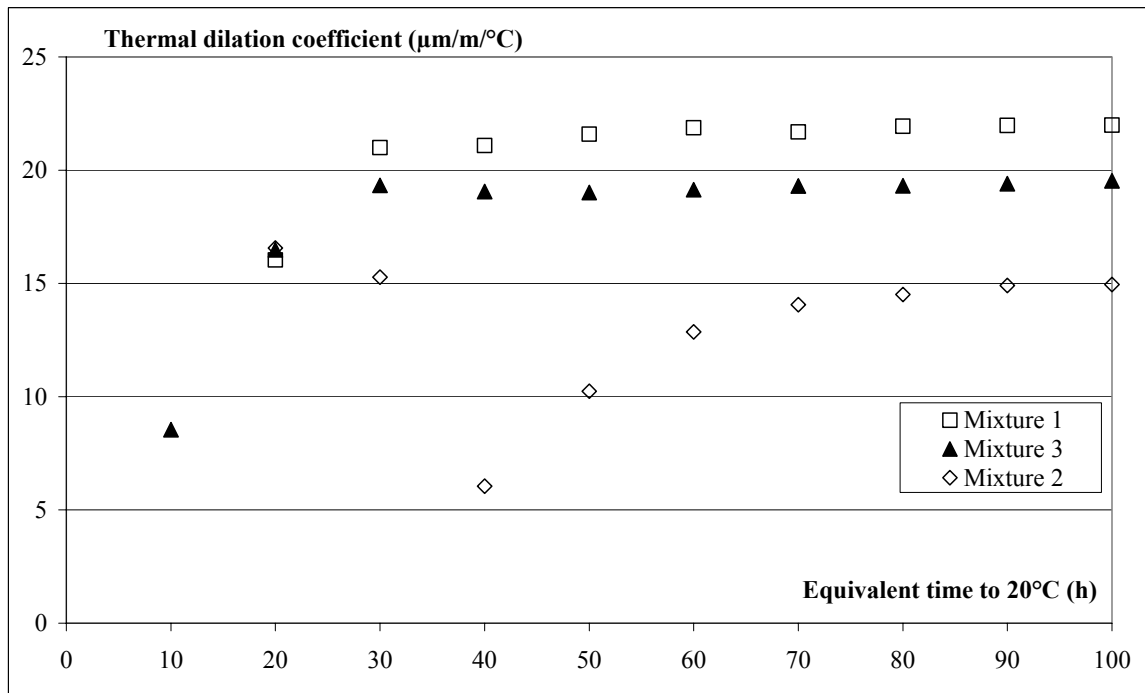
Figure 7:   Evolution of the thermal expansion coefficient of the mixtures with equivalent time

After a strong initial decrease, a minimum value for the thermal expansion coefficient is expected after setting followed by a gradual increase with time due to increased hydration and reduction of the internal relative humidity by self-desiccation. In Figure 7, the time for the minimum value of the TEC corresponds to the age after the dormant period when the temperature begins to increase. Then, the TEC seems to stabilize quickly.

7   Zero time of autogenous shrinkage

Knowing the evolution of the TEC, the autogenous shrinkage can be obtained very easily from the measured strains but a zero-time for the beginning of autogenous shrinkage has to be chosen. After mixing, the temperature of concrete is higher than 20°C. So, for the tests without heat curing, the concrete temperature decreases during the first hours and the thermal effects are dominant. Measurements at very early age represent a combination of concrete movements not necessarily due to autogenous shrinkage. Since autogenous shrinkage is generally used for prediction of cracking, the strain generated in the period before concrete setting should be excluded. The moment of interest is the hardening phase when restrained autogenous shrinkage leads to stresses. So, the zero-time for the equivalent time is chosen when an important chemical activity takes place and the Arrhenius law can be used, which corresponds to the time chosen for the first value of TEC. Figures 8 to 10 show the evolution of the autogenous shrinkage for the three mixes without heat curing from the chosen zero-time. Mixture 3 incorporating metakaolin seems to be very promising since its autogenous shrinkage is the lowest among the tested mixes. Figure 11 shows the evolution of the autogenous shrinkage in function of the equivalent time for Mixture 1 with and without heat curing. The introduction of a simple time shift by using the equivalent time is not enough to obtain the two curves coinciding at early age. The autogenous shrinkage is not directly proportional to the equivalent time [6]. For samples with heat curing, the rate and the magnitude of the autogenous shrinkage at very early age is higher than those for samples without heat curing. From the chosen zero-time (1d in equivalent time), the two curves seem to coincide, which confirms the assumption that, for the range of temperatures in these tests, the autogenous shrinkage and thermal strains can be uncoupled.
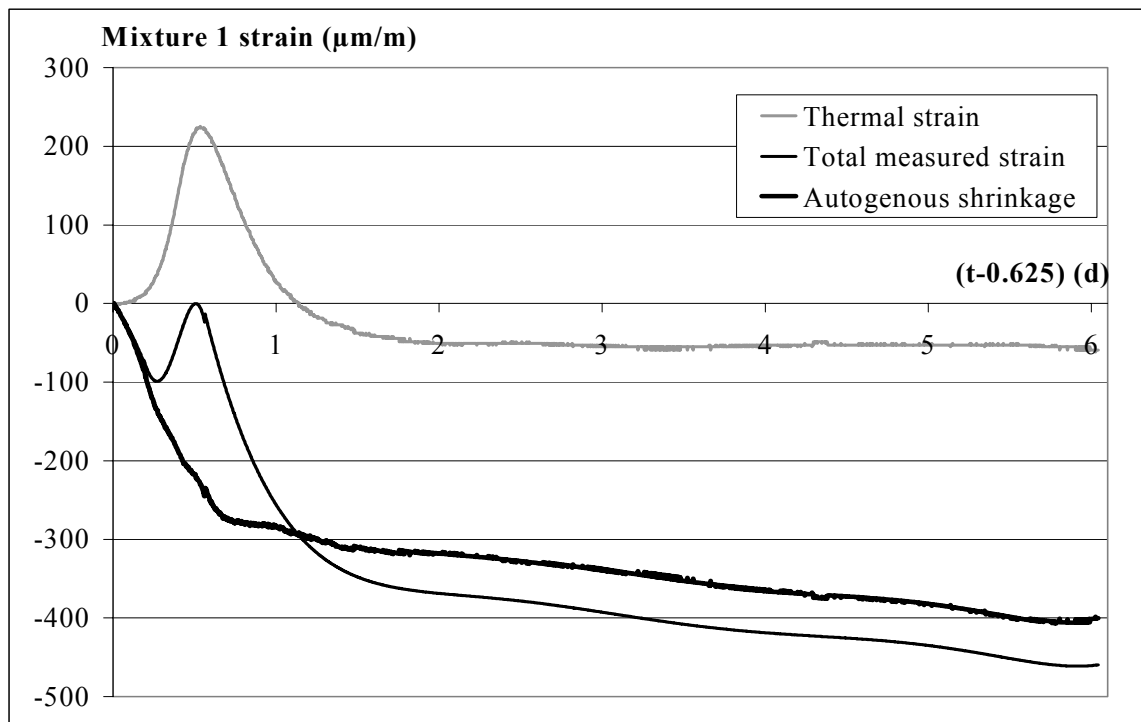
Figure 8:   Evolution of the autogenous shrinkage in Mixture 1 cured at 20°C from t = 0.625d
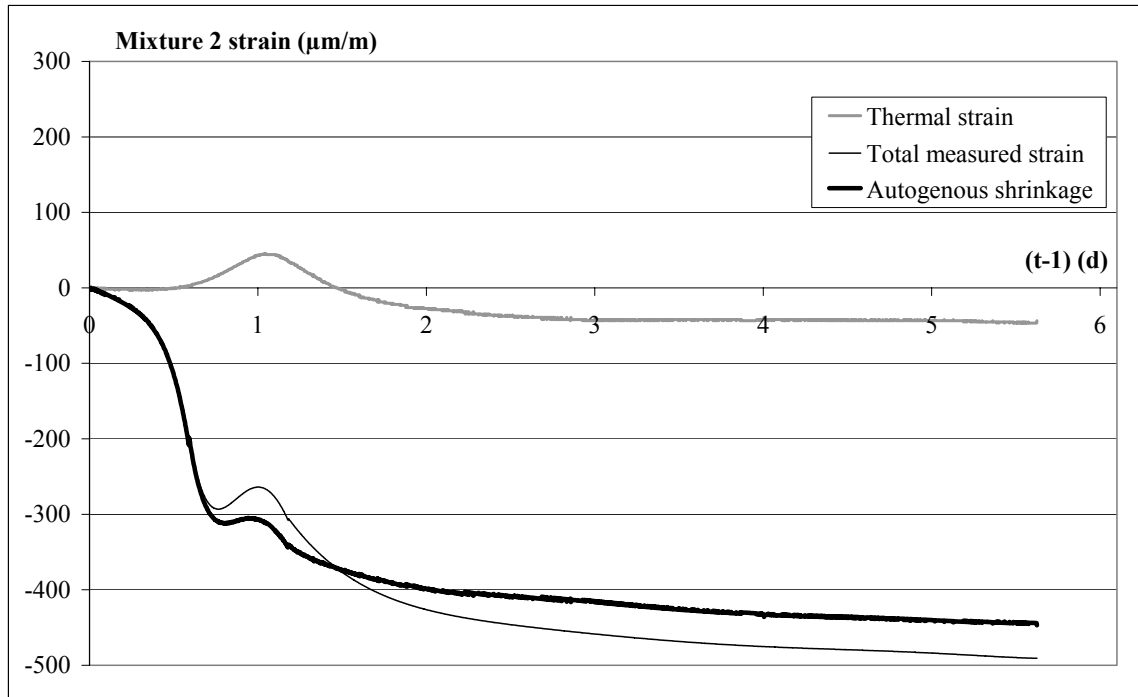
Figure 9:   Evolution of the autogenous shrinkage in Mixture 2 cured at 20°C from t = 1d
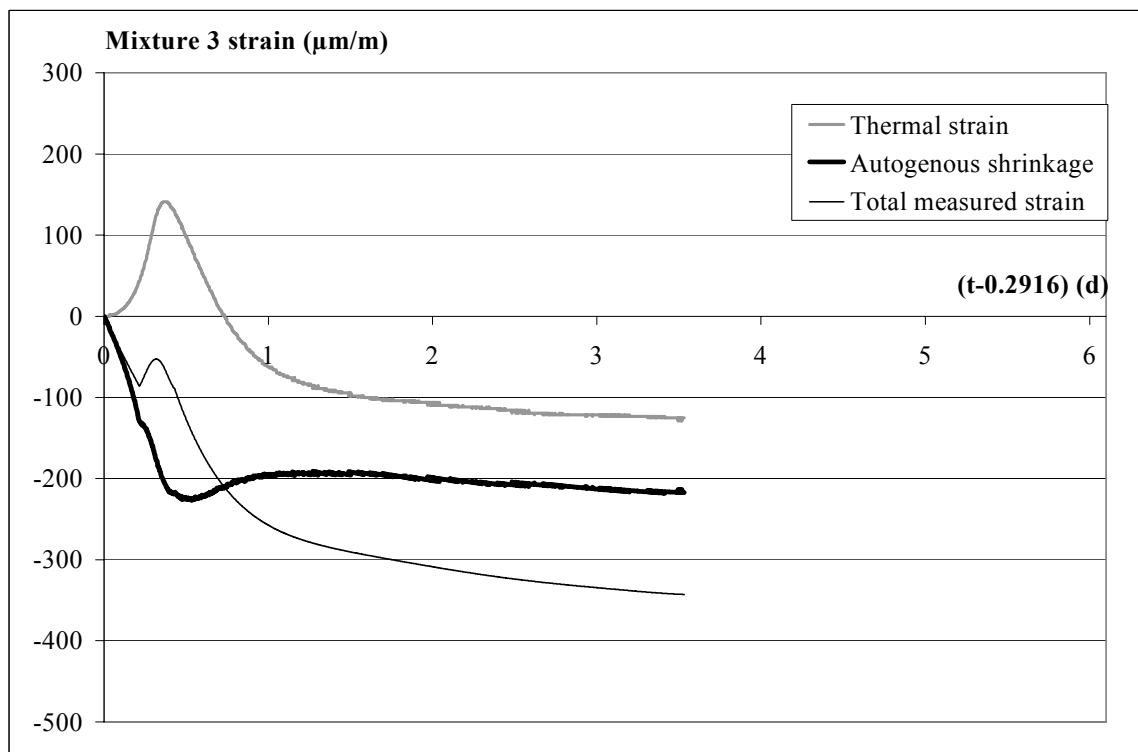
Figure 10:   Evolution of the autogenous shrinkage in Mixture3 cured at 20°C from t =0.2916d
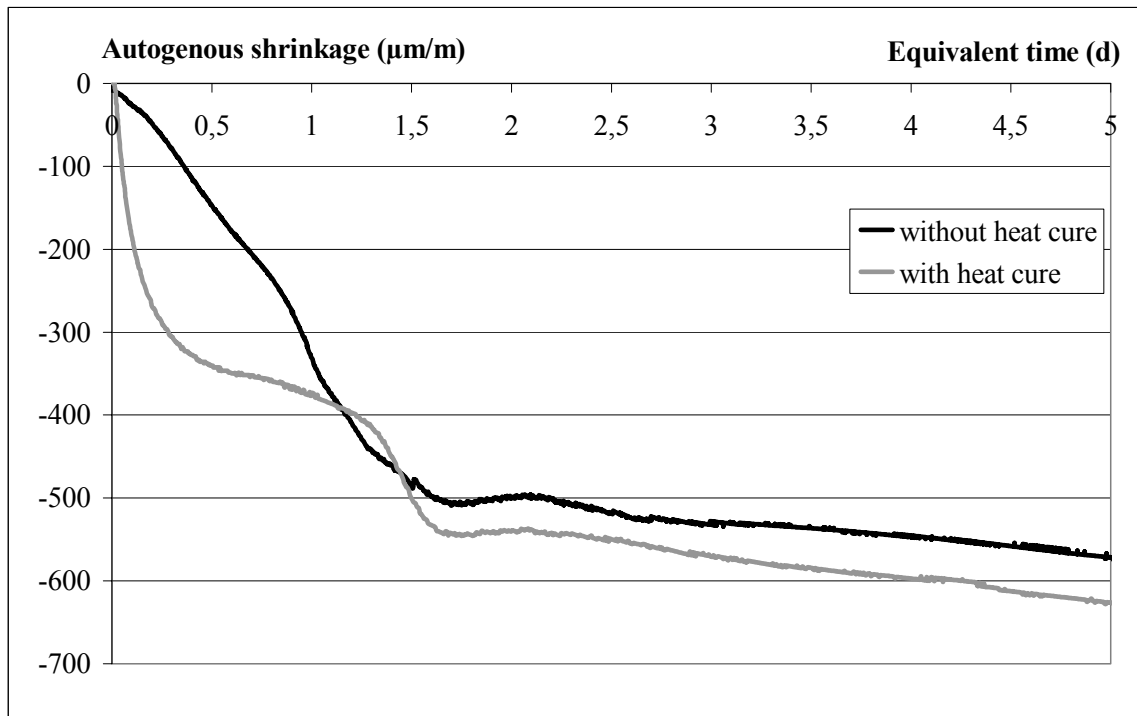
Figure 11: Evolution of the autogenous shrinkage in Mixture 1 with and without heat curing

8 Conclusions

This research has shown that at early-age, the mixture incorporating metakaolin exhibited the lowest autogenous shrinkage development in comparison with the other mixtures. The heat curing at 42°C applied to UHPC during two days after casting was shown to substantially reduce the effective strain (thermal strain + autogenous shrinkage) in particular for the mixture incorporating metakaolin. For a range of temperatures from 20°C to 42°C, the application of an equivalent time to 20°C seems to be valid from the setting time corresponding to the age at which a minimal value of compressive strength of 1 MPa is reached. Before setting, the results show that the autogenous shrinkage is not directly proportional to the equivalent time.

9 References

[1] Richard, P.; Cheyrezy, M.: Composition of reactive powder concrete. In: Cement and Concrete Research 25, No. 7, S.1501-1511, 1995.

[2] Staquet, S.; Espion, B.: Influence of cement and silica fume type on compressive strength of RPC. In: Proc. High Strength/High Performance Concrete, Leipzig, S.1421-1436, 2002.

[3] Tazawa et al.: Test method for autogenous shrinkage and autogenous expansion of cement paste, mortar and concrete. In: Autogenous shrinkage of Concrete, E&FN Spon, London, S.56-59, 1999.

[4] Laplante, P.; Boulay, C.: Evolution du coefficient de dilatation thermique du béton en fonction de sa maturité aux tout premiers âges. In Materials and Structures 27, S. 596-605, 1994.

[5] Piérard, J.: Early-age shrinkage characterization of high and ultra-high performance concretes. Civ.Eng.grad.thesis, Dept. of Civil Engineering, University of Brussels, Brussels, 2003 (in French).

[6] BjØntegaard, Ø.; Sellevold, E.J.: Interaction between thermal dilation and autogenous deformation in high performance concrete. In Proc. Shrinkage 2000, RILEM, Paris, S.43-55, 2000.

Ippei Maruyama

Research Associate

Hiroshima University

Hiroshima, Japan

Hidetoshi Ito

Associate Professor

Hiroshima Institute of Technology

Hiroshima, Japan

Ryoichi Sato

Professor

Hiroshima University

Hiroshima, Japan

Expansive behavior of expansive high strength concrete and its induced stress

Summary

In this contribution, effect of concomitant use of expansive admixture and/or shrinkage reducing admixture and/or low heat Portland cement on high-strength concrete deformation experimented, and it is concluded that it is possible to produce expansive high-strength concrete using expansive admixture. Additionally this contribution formulates the 3-dimensional finite element method as well as a practical calculation method based on beam theory, both of which consider the principle of superposition and liner stress-strain relationship on creep, in order to evaluate the early-age shrinkage/expansion-induced stress in reinforced high-strength concrete members. Applicability of the proposed methods is evaluated by comparing computed values with experimental values on shrinkage/expansion-induced stress in RC beam specimens.

Keywords: *expansive high strength concrete, expansive additive, 3-D FEM, beam theory*

1   Introduction

High Performance Concretes, characterized by low water-binder ratio, are particularly sensitive to self-desiccation of the cement paste during the hydration process, which leads to autogenous shrinkage. If a restraint is present, autogenous shrinkage, added to temperature–induced deformations, may lead to high self-induced stresses, possibly causing surface and even through cracks and potentially jeopardizing the durability of the concrete structure [1,2].

Recently, experimental investigations on controlling the autogenous shrinkage have been carried out comprehensively from the material point of view [3]. These studies revealed that expansive additive [4], shrinkage-reducing chemical agent [4,5], as well as Portland cement containing higher C2S content and lower contents of C3A or C4AF [6] were effective for reducing autogenous shrinkage. Additionally, the effect of the combination of above-mentioned materials on reducing autogenous shrinkage and stress has been investigated, and HSCs with lower risk of early-age cracking have been developed [7].

The present study aims to evaluate the effect of shrinkage-reducing materials on control of autogenous shrinkage induced stress in RC members, and also to propose a relevant numerical analysis method based on step-by-step procedure [8] considering the principle of superposition and the age at application of load on creep for calculating early-age shrinkage/expansion-induced stress. For this purpose, RC beam specimens made of various HSCs with low water-cement ratio, using expansive additive and/or shrinkage reducing chemical agent and/or C2S-rich Portland cement, subjected to early-age induced stresses are experimentally evaluated. At the same time, Young's modulus, and creep coefficients are measured, and modeled based on CEB-FIP Model Code (MC90) in order to apply the numerical analysis. The applicability of the proposed method is demonstrated by comparison with the experimental values.

2 Analysis method

2.1 Finite Element Analysis

2.1.1 Basic equation for superposition principle of creep strain

The sum of elastic and creep strain in concrete is proportional to a sustained load under ordinary service stress level. The strain by volume change is superposed on the stress-induced strain. Hence, an uniaxial strain-stress relationship of concrete with deformation and stress history can be obtained as:

$$\varepsilon_x(t_{i+1/2}) = \sum_{j=1}^{i}\left[(\Delta\sigma_{x,c})_j J(t_{i+1/2},t_j)\right] + \varepsilon_{x,\Delta T,as,ds}(t_{i+1/2},t_{1/2}) \qquad (1)$$

where, $t_{i+1/2}, t_i$: middle and beginning of i-th time interval, $\varepsilon_x(t_{i+1/2})$: strain in the x-axis at the end of i-th time interval, $(\Delta\sigma_{x,c})_j$: incremental stress in the x-axis at j-th time interval, $J(t_{i+1/2},t_j) = \dfrac{1}{E_c(t_j)} + \dfrac{\phi(t_{i+1/2},t_j)}{E_{c,28}}$:Compliance function, $E_c(t_j)$: Young's modulus at t_j in temperature adjusted concrete age, $E_{c,28}$: Young's modulus at 28 days in temperature adjusted concrete age, $\phi(t_{i+1/2},t_j)$: creep coefficient at $t_{i+1/2}$ caused by a constant load applied at t_j, $\varepsilon_{x,\Delta T,as,ds}(t_{i+1/2},t_{1/2})$:difference of free strain in the x-axis due to temperature change and shrinkage or expansion of concrete from $t_{1/2}$ to $t_{i+1/2}$. And Temperature adjusted concrete age is calculated by:

$$t = \sum_{i=1}^{n}\Delta t_i \exp\left[13.65 - \frac{4000}{273 + T(\Delta t_i)/T_0}\right] \qquad (2)$$

where, t : temperature adjusted concrete age, Δt_i : number of days where a temperature T °C prevails, T_0 =1 . The difference of strain at i-th time interval and (i-1)-th time interval introduced by Eq. 1 is given by:

$$\left(\Delta\varepsilon_{x,c}\right)_i = \varepsilon_x(t_{i+1/2}) - \varepsilon_x(t_{(i-1)+1/2})$$

$$= (\Delta\sigma_{x,c})_i J(t_{i+1/2},t_i) + \sum_{j=1}^{i-1}\left[(\Delta\sigma_{x,c})_j \frac{\Delta\phi(t_i,t_j)}{E_c,28}\right] + \left(\Delta\varepsilon_{x,\Delta T,as,ds}\right)_i$$

$$\Delta\phi(t_i,t_j) = \phi(t_{i+1/2},t_j) - \phi(t_{(i-1)+1/2},t_j) \qquad (3)$$

where, $\left(\Delta\varepsilon_{x,c}\right)_i$: incremental strain in the x-axis at *i*-th time interval, $(\Delta\sigma_{x,c})_i$ incremental stress in the x-axis at *i*-th time interval, $\left(\Delta\varepsilon_{x,\Delta T,as,ds}\right)_{xi}$ incremental free strain due to temperature change and shrinkage or expansion of concrete in the x-axis at *i*-th time interval. According to Eq. 3, under the condition that the stress and the strain until (*i-1*)-th interval are known and an incremental strain $\left(\Delta\varepsilon_{x,c}\right)_i$ at *i*-th interval is given, the incremental stress $(\Delta\sigma_{x,c})_i$ at *i*-th interval is obtained as:

$$(\Delta\sigma_{x,c})_i = \frac{E_c(t_i)}{1+\dfrac{E_c(t_i)}{E_c,28}\phi(t_{i+1/2},t_i)}\left\{\left(\Delta\varepsilon_{x,c}\right)_i - \sum_{j=1}^{i-1}\left[\frac{(\Delta\sigma_{x,c})_j}{E_c,28}\left(\Delta\phi(t_i,t_j)\right)\right] - \left(\Delta\varepsilon_{x,\Delta T,as,ds}\right)_i\right\} \quad (4)$$

Consequently the stress at *i*-th interval $\sigma_{x,c}(t_i)$ is calculated:

$$\sigma_{x,c}(t_i) = \sigma_{x,c}(t_{i-1}) + (\Delta\sigma_{x,c})_i \tag{5}$$

Based on the superposition principle of strain, Eq. 4 leads to the 3-dimensional expression assuming isotropic property:

$$\{\varDelta\boldsymbol{\sigma_c}\}_i = \left[\boldsymbol{D_c}\right]_i\left[\{\varDelta\boldsymbol{\varepsilon_c}\}_i - \sum_{j=1}^{i-1}\left[\frac{(\varDelta\boldsymbol{\sigma_c})_j}{\left[\boldsymbol{D_{c,28}}\right]}\left(\Delta\phi\left(t_i,t_j\right)\right)\right] - \{\varDelta\boldsymbol{\varepsilon_{\Delta T,as,ds}}\}_i\right] \tag{6}$$

where, $\{\varDelta\boldsymbol{\sigma_c}\}_i$: incremental stress vector at *i*-th interval, $\{\varDelta\boldsymbol{\varepsilon_c}\}_i$: incremental strain vector at i-th interval, $\{\varDelta\boldsymbol{\varepsilon_{\Delta T,as,ds}}\}_i$: incremental strain vector due to temperature change and shrinkage or expansion of concrete, $\left[\boldsymbol{D_c}\right]_i$:stress-strain matrix of concrete at *i*-th interval, $\left[\boldsymbol{D_{c,28}}\right]$ stiffness matrix of concrete at 28 days in temperature adjusted concrete age.

2.1.2 Formulation of incremental finite element equation

Based on the principle of virtual work, following equation is obtained:

$$\{\varDelta\boldsymbol{P}\}^T\{\delta\varDelta\boldsymbol{v}\} = \int_V\{\delta\varDelta\boldsymbol{\varepsilon}\}^T\{\varDelta\boldsymbol{\sigma}\}dV \tag{7}$$

where, $\{\varDelta\boldsymbol{P}\}$:load vector, $\{\delta\Delta\boldsymbol{v}\}$: virtual displacement vector, $\{\boldsymbol{\sigma}\}$: stress vector according to the load $\{\varDelta\boldsymbol{P}\}$, $\{\delta\varDelta\boldsymbol{\varepsilon}\}$: virtual strain vector by virtual displacement.
Displacement and strain have a following relationship:

$$\{\delta\varDelta\boldsymbol{\varepsilon}\} = \left[\boldsymbol{B}\right]\{\delta\varDelta\boldsymbol{v}\} \tag{8}$$

$$\{\varDelta\boldsymbol{\varepsilon_c}\}_i = \left[\boldsymbol{B}\right]\{\varDelta\boldsymbol{v_c}\}_i \tag{9}$$

where, $\{\varDelta\boldsymbol{v_c}\}_i$: displacement at *i*-th interval. $\left[\boldsymbol{B}\right]$: strain-displacement matrix which are derived from the assumption of isoparametric 8-nodes, 6-hexaheron element with one dimensional shape function. Substituting Eq. 7 into Eqs. 6, 8, and 9 leads to:

$$\{\delta\varDelta\boldsymbol{v}\}^T\{\varDelta\boldsymbol{P}\} = \int_V\left([\boldsymbol{B}]\{\delta\varDelta\boldsymbol{v}\}\right)^T\left[\boldsymbol{D_c}\right]_i\left\{[\boldsymbol{B}]\{\varDelta\boldsymbol{v_c}\}_i - \sum_{j=1}^{i-1}\left[\frac{\{\varDelta\boldsymbol{\sigma_c}\}_j}{\left[\boldsymbol{D_{c,28}}\right]}\Delta\phi_{i,j}\right] - \{\varDelta\boldsymbol{\varepsilon_{\Delta T,as,ds}}\}_i\right\}dV \tag{10}$$

Creep, shrinkage and temperature parts in the right side of Eq. 10 can be expressed as equivalent nodal force. Hence the following equation is obtained:

$$\{\varDelta\boldsymbol{P}\} + \{\varDelta\boldsymbol{f}\} = \int_V\left[\boldsymbol{B}\right]^T\left[\boldsymbol{D_c}\right]_i\left[\boldsymbol{B}\right]dV\{\varDelta\boldsymbol{v_c}\}_i \tag{11}$$

$$\{\varDelta\boldsymbol{f}\} = \int_V\left[\boldsymbol{B}\right]^T\left[\boldsymbol{D_c}\right]_i\times\left\{\sum_{j=1}^{i-1}\left[\frac{\{\varDelta\boldsymbol{\sigma_c}\}_j}{\left[\boldsymbol{D_{c,28}}\right]}\Delta\phi_{i,j}\right] + \{\varDelta\boldsymbol{\varepsilon_{\Delta T,as,ds}}\}_i\right\}dV \tag{12}$$

where, $\{\varDelta\boldsymbol{f}\}$:equivalent nodal force vector of creep, shrinkage, and temperature strain.

With local stiffness matrix $\left[\boldsymbol{K}_e\right]$, Eq. 11 is expressed as:

$$\{\Delta P\} + \{\Delta f\} = \left[\boldsymbol{K}_e\right]\{\Delta \boldsymbol{v}_c\}_i \qquad (13)$$

where, $\left[\boldsymbol{K}_e\right] = \int_V [\boldsymbol{B}]^T \left[\boldsymbol{D}_c\right]_i [\boldsymbol{B}] dV$: local stiffness matrix. The global stiffness matrix is constructed for finite element (FE) method from local stiffness matrices according to the assembly principle, and nodal force and nodal displacement are obtained by solving following simultaneous linear equations:

$$\{\Delta F\} + \{\Delta F'\} = \left[\boldsymbol{K}\right]\{\Delta V_c\}_i \qquad (14)$$

where, $\{\Delta F\}$: global incremental load vector, $\{\Delta F'\}$: global incremental equivalent nodal force vector of creep, shrinkage, temperature strain, $\left[\boldsymbol{K}\right]$: global stiffness matrix, $\{\Delta V_c\}_i$: global incremental displacement vector.

2.2 Beam theory

In this section, as a practical calculation method for stress analysis in a beam specimen, the model based on beam theory is proposed. This proposed model deals with a beam which has two different depths of reinforcing bars. The basic concept for creep strain is the same as that of the FE analysis mentioned in former section.

Eq. 3 can be expressed with compliance function:

$$\left(\Delta \varepsilon_c\right)_i = \left(\Delta \sigma_c\right)_i J(t_{i+1/2}, t_i) + \sum_{j=1}^{i-1} \left[\left(\Delta \sigma_c\right)_j \Delta J(t_i, t_j)\right] + \left(\Delta \varepsilon_{\Delta T, as, ds}\right)_i \qquad (15)$$

where, $\Delta J(t_i, t_j) = \dfrac{\phi(t_{i+1/2}, t_j) - \phi(t_{(i-1)+1/2}, t_j)}{E_c, 28}$: difference of compliance function.

The concrete strain at upper (compressive side) and lower (tensile side) reinforcing bar is obtained by following equation:

$$\Delta \varepsilon_{cc,i} = \Delta \sigma_{cc,i} J\left(t_{i+1/2}, t_i\right) + \sum_{j=1}^{i-1} \Delta \sigma_{cc,j} \Delta J\left(t_i, t_j\right) + \Delta \varepsilon_{sh,i} \quad (16)$$

$$\Delta \varepsilon_{ct,i} = \Delta \sigma_{ct,i} J\left(t_{i+1/2}, t_i\right) + \sum_{j=1}^{i-1} \Delta \sigma_{ct,j} \Delta J\left(t_i, t_j\right) + \Delta \varepsilon_{sh,i} \quad (17)$$

where, $t_{i+1/2}, t_i$: end and middle of i-th time interval, $\Delta \varepsilon_{cc,i}$:incremental strain of concrete at the same depth of compressive reinforcing bar i-th time interval, $\Delta \varepsilon_{ct,i}$: incremental strain of concrete at the same depth of tensile reinforcing bar at i-th time interval, $\Delta \sigma_{cc,i}$: incremental stress of concrete at the same depth of compressive reinforcing bar at i-th time interval, $\Delta \sigma_{ct,i}$: incremental stress of concrete at the same depth of tensile reinforcing bar at i-th time interval, $\Delta \varepsilon_{sh,i}$: incremental free strain of concrete at i-th time interval.

The incremental stress of concrete is obtained by the force in reinforcing bars with the assumption of linear strain distribution:

$$\Delta \sigma_{cc,i} = -\alpha_{cc} \Delta \varepsilon_{sc,i} - \alpha_{tc} \Delta \varepsilon_{st,i} \quad , \quad \Delta \sigma_{ct,i} = -\alpha_{tt} \Delta \varepsilon_{sc,i} - \alpha_{ct} \Delta \varepsilon_{st,i} \quad (18)$$

$$\alpha_{cc} = \frac{A_{sc} E_s}{A_c}\left(1 + \frac{\left(d' - C_g\right)^2}{I_c / A_c}\right), \ \alpha_{tt} = \frac{A_{st} E_s}{A_c}\left(1 + \frac{\left(d - C_g\right)^2}{I_c / A_c}\right) \qquad (19)$$

$$\alpha_{tc} = \alpha_{ct} = \frac{A_{st}E_s}{A_c}\left(1 + \frac{\left(d - C_g\right)\left(d' - C_g\right)}{I_c / A_c}\right)$$

where, d, d': distance from extreme top fiber to centroid of tension and compression reinforcement, A_c: Cross sectional area of concrete in section of beam, A_{sc}: Cross sectional area of compressive reinforcing bar in section, A_{st}: Cross sectional area of tensile reinforcing bar in section, $\Delta\varepsilon_{sc,i}$: incremental strain in compressive reinforcing bar at *i*-th interval, $\Delta\varepsilon_{st,i}$: incremental strain in tensile reinforcing bar at *i*-th interval, C_g: centroid of section, I_c: geometrical moment of inertia.

On the other hand, conformity principle of strain is given by:

$$\Delta\varepsilon_{cc,i} = \Delta\varepsilon_{sc,i}, \quad \Delta\varepsilon_{ct,i} = \Delta\varepsilon_{st,i} \qquad (20)$$

Hence, combining Eqs. 16, 17, 18, and 19 leads to following equation with matrix form:

$$\begin{bmatrix} 1 + \alpha_{cc}J\left(t_{i+1/2}, t_i\right) & \alpha_{tc}J\left(t_{i+1/2}, t_i\right) \\ \alpha_{ct}J\left(t_{i+1/2}, t_i\right) & 1 + \alpha_{tt}J\left(t_{i+1/2}, t_i\right) \end{bmatrix}\begin{Bmatrix} \Delta\varepsilon_{sc,i} \\ \Delta\varepsilon_{st,i} \end{Bmatrix} = \sum_{j=1}^{i-1}\begin{Bmatrix} \Delta\sigma_{cc,j}\Delta J\left(t_i, t_j\right) \\ \Delta\sigma_{ct,j}\Delta J\left(t_i, t_j\right) \end{Bmatrix} + \begin{Bmatrix} \Delta\varepsilon_{sh,i} \\ \Delta\varepsilon_{sh,i} \end{Bmatrix} \qquad (21)$$

According to Eq. 21, the incremental stress of concrete and reinforcing bars at the i-th interval is obtained, when the histories of the incremental stress, the incremental deformation until (*i-1*)-th interval, and the incremental deformation at *i*-th interval are given.

3   Experiments and materials

3.1   Materials and mixture proportions

The materials used for the experiments are is listed in Table 1. And the mixture are listed in Table 2 as well as their air content, slump flow, and temperature just after mixing.

NC1 and NC2 represent the reference high strength and highly-flowable concrete using ordinary Portland cement. The difference among these are aggregate quality and water-to-cement ratio. NE-CSA represents the concrete with expansive additive which is calcium-sulfoaluminate type (E-CSA). NS represents the concrete with shrinkage reducing agent (S). NES-CSA represent the concrete containing both E-CSA and S. On the other hand, LC represents the concrete with low-heat Portland cement (L). And LE-CSA, LS, and LES-CSA are corresponding to the concrete consist of L with E-CSA, S, and both E-CSA and S respectively. NC1, NE-CSA, NS, NES-CSA, LC, LE-CSA, LS, and LES-CSA are using the same quality of aggregate and are denominated as B1 series. NES-LIME represents the concrete with expansive additive which is lime type (E-LIME) and shrinkage reducing agents. NES-LIME has the same quality of aggregate as that of NC2. These NC2 and NES-LIME are denominated as B2 series. HC has the water-to-binder ratio of 0.25 with silica fume whose content is 60 kg/m^3.

Table 1: Materials

Material (Designation)	Type (Designation) / Characterastics
Cement (C)	Normal Portland cement (N) / specific gravity: 3.16g/cm^3, blaine: 3500cm^2/g
	Low-heat Portland cement (L) / specific gravity: 3.22g/cm3, blaine: 3310cm^2/g
	High-early strength Portland cement (H) / specific gravity: 3.14g/cm^3; blaine: 4420cm^2/g
additive (Ad)	Silica fume (SF) / specific gravity: 2.20g/cm^3, blaine: $2 \cdot 10^5$cm2/g, SiO_2: 91%
Expansive additive (EX)	Calcium-sulfoaluminate (E-CSA) / specific gravity: 2.96g/cm^3, blaine: 3050cm^2/g
	Lime type (E-LIME) / specific gravity: 3.15g/cm^3, blaine: 3490cm^2/g
Shrinkage reducer agent (SRA)	Lower alcohol alkyleneoxide adduct
High-range water reducing agent (SP)	Polycarboxylic acid based high-range water-reducing agent (SP1) / density 1.07g/cm^3
	Polycarboxylic acid based high-range water-reducing and air-entraining agent (SP2)
Fine aggregate (S)	Land sand (S1) / density: 2.62 g/cm^3 , absorption: 1.66%, F.M.: 2.84
	Land sand (S2) / density: 2.61 g/cm^3 , absorption: 1.44%, F.M.: 2.82
	River sand (S3) / density: 2.61 g/cm^3, F.M.: 2.69
Coarse aggregate (G)	Crushed sand stone (G1) / maximum: 20mm, density: 2.64 g/cm^3 , absorption: 0.85%, F.M.: 6.61
	Crushed sand stone (G2) / maximum: 20mm, density: 2.65 g/cm^3 , absorption: 0.74%, F.M.: 6.52
	Crushed sand stone (G3) / maximum: 20mm, density: 2.63 g/cm^3, F.M.: 6.68

Table 2: Mixture proportions

	W/B	W	C	EX	SRA	SF	S	G	SP/B*	Slump flow	Air content	Temp.
		(kg)	(kg)	(kg)	(kg)	(kg)	(kg)	(kg)	(kg)	(mm)	(%)	(^{o}C)
NCl	0.3	175	583 (N)	-	-	-	800 (S1)	832 (G1)	0.90 (SP1)	625	1.0	19.0
NE-CSA	0.3	175	543 (N)	40 (CSA)	-	-	798 (S1)	832 (G1)	0.93 (SP1)	425	0.6	21.2
NS	0.3	169	583 (N)	-	6	-	800 (S1)	832 (G1)	1.00 (SP1)	630	1.5	18.0
NES-CSA	0.3	169	543 (N)	40 (CSA)	6	-	789 (S1)	832 (G1)	1.15 (SP1)	625	1.3	19.0
LC	0.3	175	583 (L)	-	-	-	809 (S1)	832 (G2)	0.50 (SP1)	580	2.1	18.7
LE-CSA	0.3	175	543 (L)	40 (CSA)	-	-	806 (S1)	832 (G1)	0.58 (SP1)	580	1.3	16.9
LS	0.3	169	583 (L)	-	6	-	809 (S1)	832 (G1)	0.51 (SP1)	555	1.3	18.3
LES-CSA	0.3	169	543 (L)	40 (CSA)	6	-	806 (S1)	832 (G1)	0.60 (SP1)	665	1.2	16.6
NC2	0.3	175	583 (N)	-	-	-	797 (S2)	835 (G2)	0.70 (SP1)	550	2.9	14.3
NES-LIME	0.3	169	543 (N)	40 (LIME)	6	-	797 (S2)	835 (G2)	0.60 (SP1)	475	1.6	15.3
HC	0.25	150	540 (H)	-	-	60	766 (S3)	940 (G3)	2.2 (SP2)	685	2.7	13.5

606

3.2 Experiments and results

3.2.1 Mechanical properties of concrete

Compressive cylinder strength whose specimen size of ϕ100 mm × 200 mm of concrete are determined. Young's modulus of concrete is determined at the same time of testing of compressive strength. All these tests are conducted at the age of 0.42, 0.5, 0.67, 1, 3, 7, 14, and 28 days and averaged values among three specimens are evaluated at each age. After demolding at a concrete age of one day, the specimens are cured with two conditions: 20 ^{o}C water curing and sealed curing in room temperature with aluminum adhesive tape to prevent the evaporation of water.

Compressive strength of sealed concrete under room temperature as well as Young's modulus, and Poisson's ratio are given in Table 3. In addition, for comparison with development of cement hydration, the compressive strength of concrete saturated under 20 ^{o}C condition are listed in Table 3 as well. Development of Young's modulus of each concrete is modeled as a function of temperature adjusted concrete age [9]:

$$Ec(t) = E_{c,t28} \exp\left(s\left(1 - \left(\frac{t_{e,28} - a}{t - a} \right)^{0.5} \right) \right) \quad (22)$$

where, $t_{e,28}$: temperature adjusted concrete age at 28 days, $E_{c,t28}$: Young's modulus of sealed concrete at 28 days, a, s: material parameters.

Table 3: Mechanical properties of sealed and saturated concrete at 28-days

	Compressive strength (saturated) (N/mm^2)	Compressive strength (seal) (N/mm^2)	Young's modulus (seal) (kN/mm^2)	parameter a	parameter s	$t_{e,28}$	Poisson ratio
NC1	85.3	77.0	35.5	0.20	0.14	24.2	0.20
NE-CSA	74.4	64.0	33.4	0.20	0.11	24.1	0.19
NS	81.2	84.6	39.2	0.15	0.17	24.3	0.20
NES-CSA	82.4	87.2	37.7	0.20	0.14	24.0	0.17
LC	73.5	66.8	37.0	0.32	0.17	22.1	0.16
LE-CSA	83.3	69.8	37.3	0.30	0.15	22.1	0.18
LS	70.5	65.8	34.7	0.35	0.16	22.8	0.20
LES-CSA	76.1	66.6	36.4	0.35	0.21	21.7	0.15
NC2	91.4	80.3	39.6	0.23	0.15	15.9	0.19*
NES-LIME	83	76.3	37.3	0.16	0.18	16.0	0.21*
HC	121.7	106.5	37.5	0.12	0.15	17.4	-

*: value of concrete specimen curing in water at 20 ^{o}C at 28th day

According to results of regression, the parameters of modeling as well as $t_{e,28}$ are listed in Table 3. Regarding the parameter a, which corresponds to the initial setting time effect, the time that stress is measured in self-induced stress test is used for regression curves.

Figure 1: Details of deformation specimen.

3.2.2 Deformation

Figure 1 shows the details of specimens for measurement of autogenous shrinkage. All the specimens have the same cross-section as the beams used for self-induced stress (see further). After demolding at a concrete age of one day, all the specimens are sealed with aluminum adhesive tape to prevent the evaporation of water and set at room temperature. Embedded strain gauge whose size is $\phi 20$ mm × 104 mm and reference length is 100 mm with low elastic modulus of 39 N/mm^2 and a thermocouple are equipped in the center of the specimens. Autogenous deformation as well as drying shrinkage of concrete are determined by subtracting thermal strain from measured strain. The thermal expansion of concrete coefficient is assumed to be 10 × 10^{-6} /^{o}C. The commencement of measurement is just after pouring the concrete.

Experimental results of autogenous deformation concerning B1 and B2 series are shown in Figure 3. The data are plotted as a function of temperature adjusted concrete age from the point of view of the hydration process. Using low-heat Portland cement, shrinkage reducing agent, expansive additive, and combination of them is effective upon a compensation for autogenous shrinkage. All the concrete that has expansive additive and/or shrinkage reducing agent shows smaller autogenous shrinkage, and especially, some concrete (NC2, LE-CSA, and LES-CSA) using expansive additive shows expansion rather than shrinkage, even they are high strength concrete. A concomitant effect of using both expansive additive and shrinkage reducing agent, is observed for the concrete with low-heat Portland cement, i.e., the compensation quantity of LES-CSA, which is 384 × 10^{-6}, is more than the summation of those of LE-CSA and LS corresponding to 305 × 10^{-6} and 12 × 10^{-6}, respectively. The compensation quantity of NES-LIME is much larger than that of NES-CSA, and
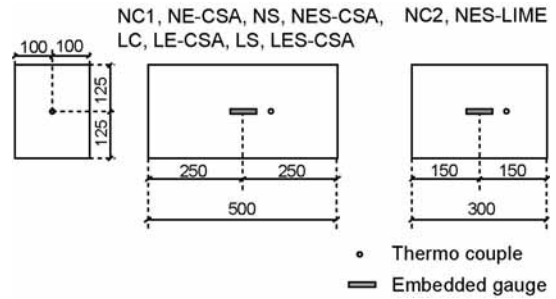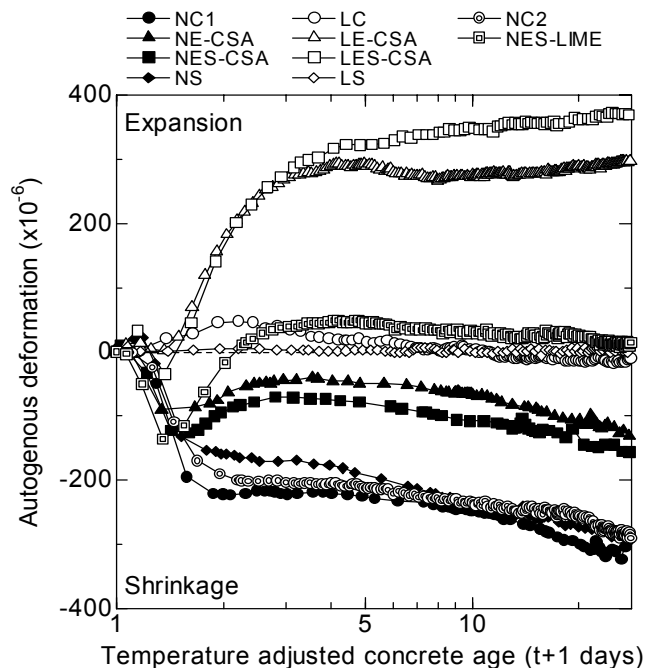

Figure 2: Autogenous deformation of Concretes.

NES-LIME shows an expansion at 28 days in temperature adjusted concrete age.

3.2.3 Uniaxial compressive creep

Uniaxial compressive creep test focusing an early age behavior is conducted with NC2, NES-LIME, and HC. These three mixture proportions are selected in order to evaluate a final creep coefficient and a rate of creep development with disregard to cement type and additive. The loading ages are 1.24, 2.26, and 16.6 concrete age for NC2 and NES-LIME, and 0.44, 0.85, and 1.74 concrete age for HC. Specimens whose size

Figure 3: Creep Coefficient

is 200 × 250 × 300 mm3 are prepared, and after demolding at a concrete age of one day, all the specimens are sealed with aluminum adhesive tape to prevent the evaporation of water and set at room temperature. The load during the creep test is fixed at a stress/strength ratio of 20%. The strength of the concrete is tested at loading age. The stress fluctuation of the accumulation is controlled within ±5% of the targeting stress. The results of creep coefficients are shown in Figure 3. For NC2, NES-LIME, HC, the value of creep coefficient is determined by a ratio of creep strain to elastic strain represented by Young's modulus of sealed concrete at 28-days in temperature adjusted concrete age. The development of the creep coefficient is modeled for analysis by following equation whose concept is based on CEB-FIP MODEL CODE 1990 [10]:

$$\phi(t,t_0) = \phi_0 \left[\frac{(t-t_0)/t_1}{\beta_H + (t-t_0)/t_1} \right]^{0.3} \tag{23}$$

$$\phi_0 = 5.31 \cdot \left(E_c(t_0)/E_{c,28} - 1.0 \right)^2 + 1.11 \tag{24}$$

$$
\begin{aligned}
& 0 \le E_c(t)/E_{c,28} < 0.346 \qquad \beta_H = 0.000001 \\
& 0.346 \le E_c(t)/E_{c,28} < 1.0 \quad \beta_H = 40.5 \cdot \left(E_c(t)/E_{c,28} - 0.346 \right) + 0.485
\end{aligned} \tag{25}
$$

where, $\phi(t,t_0)$: basic creep coefficient, ϕ_0: ultimate basic creep coefficient, β_H: coefficient representing the effect of loading age on rate of creep development, t: temperature adjusted concrete age (days), t_0: temperature adjusted concrete age of loading age, t_1: 1 day, $(E_c(t)/E_{c,28})$: relative Young's modulus, i.e., the ratio of Young's modulus of sealed concrete at t to that of sealed concrete at 28 days in temperature adjusted concrete age.

The value of $E_{c,28}$ is obtained by extrapolating the regression curve of Eq. 22. And ϕ_0 and β_H of each experimental result are calculated by regression with Eq. 23.

3.2.4 Self-induced stress in reinforced concrete beam

The reinforced concrete (RC) beam specimens for measuring the self-induced stress are prepared for each mixture proportion. The beams for B1 series have dimension 200 mm in width, 250 mm in height, and 2700 mm in length and the used reinforcing bars (RBs) whose

size is 19 mm in diameter and Young's modulus is 190 kN/mm^2 are set at the depth of 210 mm from the extreme compressive fiber with a hook bended at both ends. Wire strain gauges are attached on the upper and bottom side of RBs at mid-span.

The beams for B2 series have a size of 200 mm in width, 250 mm in height, and 2400 mm in length. The used RBs for B2 series have a size of 19 mm in diameter (D19) and Youngs's modulus of 197 kN/mm^2 and are grooved along their length at two opposite sides for

attaching wire strain gauges. These RBs are set at the depth of 210 mm from the extreme compressive fiber, without using hooks. Teflon sheets 1.0 mm thick at the bottom of the mold, polystyrene board 3 mm thick on the both ends of the mold, and polyester film 0.1 mm thick on all the sides and bottom of

Figure 4: Stress in concrete at extreme bottom fiber.

the mold are applied to reduce the friction between the mold and the specimen. After demolding, all the specimens are sealed with aluminum adhesive tape to prevent the evaporation of water and cured under room temperature. The demolding time of LS and LES is 2-days and the others are 1-day after mixing.

Self-induced stress of concrete is obtained from the measured strain of the RBs. The averaged strain of RB (upper and bottom measurement B1 and both sides measurement B2 series) is corrected by subtracting the thermal strain that is measured by a dummy steel bar in the beam. Self-induced stress in concrete at the extreme bottom fiber due to restraint of RBs is determined by considering equilibrium of force among the concrete and the RBs as well as the assumption of linear strain distribution. The results of self-induced stress at extreme bottom fiber are shown in Fibure 4. NE-CSA, NES-CSA, LE-CSA, LES-CSA, and NES-LIME shows compressive stress at concrete age of 18.5 days.

4   Analysis

Proposed FE analysis needs modeling of development of Young's modulus, history of temperature and autogenous deformation, Poisson's ratio, Thermal coefficient, and creep coefficient behavior. With regards to the history of autogenous deformation and temperature, analysis is carried out with experimental data. And creep model, which is shown in 3.2.3, is assumed to be applicable to the case of tensile creep. Poisson's ratio of concrete is assumed to be constant as a value of sealed concrete at 28 days, which are shown in Table 3, and a value of 0.30 is adopted for Poisson's ratio of RB. Values of thermal coefficient are assumed to be constant as well. The value of 10.0×10^{-6} for concrete and the value of 11.8×10^{-6} for RB are adopted. Isoparameteric elements with 8 nodes is adopted for FE analysis, and 2792 elements and 3474 nodes are used for beam specimen with B1 and B2 series. The

experimental results of the beam specimens are evaluated with the proposed FE analysis and the proposed beam theory. With input data of temperature history as well as deformation history, stress in RBs and stirrups, and concrete at extreme bottom fiber are presented. The better case of LES-CSA and the worse case NE-CSA are shown in Figure 5. The simulation results by the proposed beam theory are plotted as well.

The FE analysis as well as the beam theory follows precisely the behavior of all the specimens, even the behavior of concrete strain from shrinkage to expansion. But in few cases, namely the case of NES-CSA, NE-CSA, and NES-CSA-S2, the FE analysis results divagate from the experimental results after 10 days and there remains about 5 N/mm^2 difference in the tensile RB at 28 days. These three specimens have similar behavior of deformation. The deformation of these specimens show a sudden drop and the minimum value of the shrinkage strain is obtained at about 0.5 day followed by slight expansion until 3 days. After the peak at 3 days, they show a second mild shrinkage behavior. This deformation behavior brings the steep increase of tensile stress in concrete at about 0.5 days followed by gradually decrease. In this case, under the shrinkage process, cement particles with expansive additive are hydrating and forming the optimum matrix at the vicinity of reinforcing bar under shear stress. This compacted structure, however, may be injured by E-CSA reaction and may result in micro-cracks. This phenomenon does not apply to the cases of concrete using E-CSA with low-heat Portland cement. In this case, the slow process of hydration may absorb the shock of reaction by E-CSA, resulting in a more sound matrix. The evidence of this explanation and micro-cracking remains to be an issue of future study. The
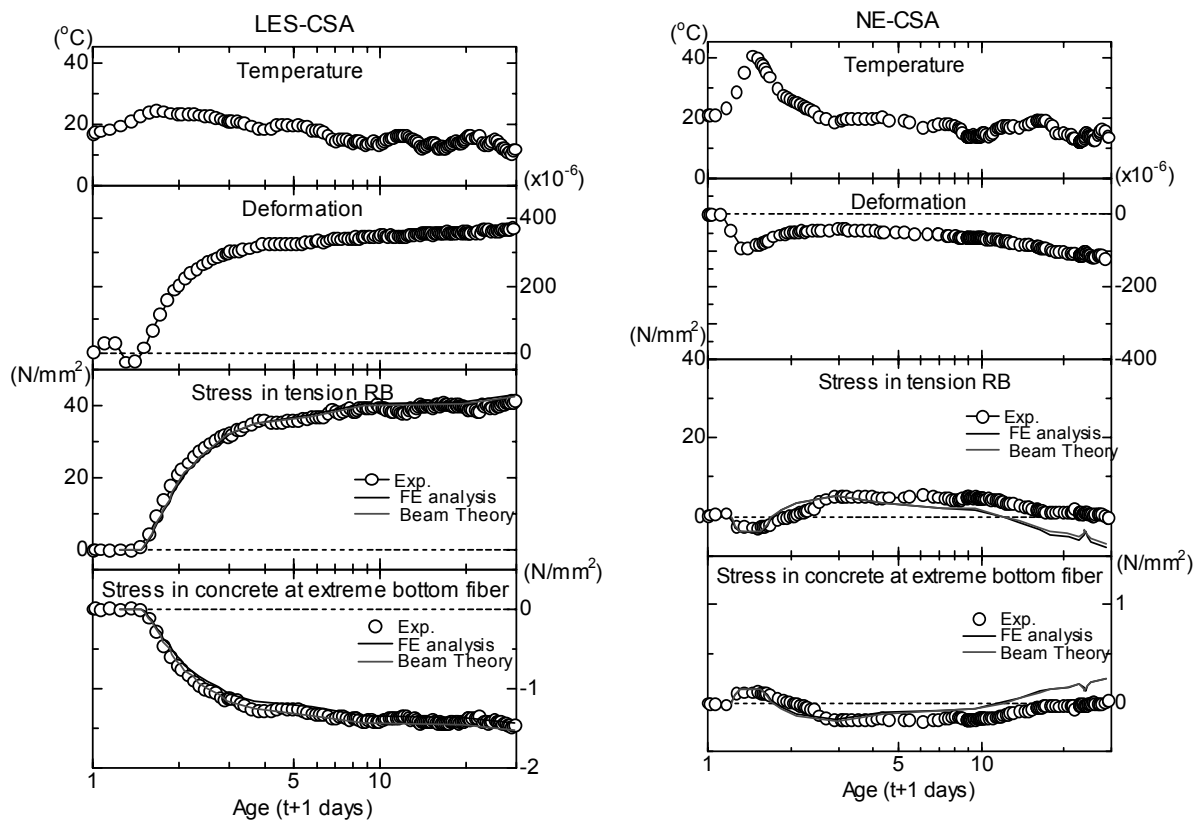

Figure 5: Comparison of experimental results with the FE analysis and the beam theory good agreement of experimental data with the FE analysis as well as beam theory results

indicates that the concrete with expansive additive, which is considered to have non-linear properties in stress-strain relation on normal strength level, has the same linear stress-strain relationship as that of normal concrete when it is low water-to-binder ratio. For evaluating the accuracy of the the FE analysis, comparisons are plotted in Figure 6 choosing three inflection points of each concrete that are seen at about 1, 4, 28 days.
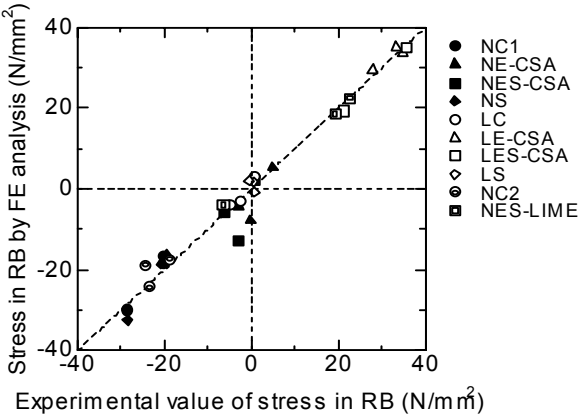
Figure 6: Comparison of FE analysis results with experiment with regard to stress in RB.

5   Conclusion

1. Expansive-high strength concrete providing compressive stress in reinforced concrete can be produced by using low-heat Portland cement, shrinkage reducing agent, and expansive additive.

2. Incremental creep analyses based on 3-D FE technique as well as beam theory, to which the principle of superposition is applied, show fairly good agreement with experimentally obtained not only stress but also strain in concrete restrained by steel bars using Young's modulus, creep coefficient, autogenous deformation and temperature varying with time.

3. The fairly good agreement of experimental data with the FE analysis results leads to the conclusion that the concrete with expansive additive has the same linear stress-strain relationship as that of conventional high strength concrete.

6 References

[1] Paillere, A.M., Buil, M. and Serrano, J.J.: Effect of fiber addition on the autogenous shrinkage of silica fume concrete. In: ACI Materials Journal, 86(2), S. 139-144, 1989

[2] Tazawa, E. and Miyazawa, S.:Autogenous shrinkage of cement paste with condensed silica fume. In: Fourth CANMET/ACI International Conference on Fly Ash, Silica Fume, Slag, and Natural Pozzolans in Concrete, Istanbul, Turkey, SUPPLEMENTARY PAPERS, S. 875-894, 1992

[3] JCI.: Autogenous Shrinkage of Concrete. In: E. Tazawa, Ed. London: E & FN SPON, S. 21-26, 1999

[4] Tazawa,E. and Miyazawa,S.: Autogenous shrinkage caused by self desiccation in cementitious material. In: 9th International Congress on the Chemistry of Cement, Vol.4, New Delhi, India, S. 712-718, 1992

[5] Weiss, W.J., Borichevsky, B.B. and Shah, S.P.: The Influence of a Shrinkage Reducing Admixture on Early-Age Shrinkage Behavior of High Performance Concrete. In: 5th International Symposium on Utilization of High Strength/High Performance Concrete, Vol.2, Sandefjord, Norway, S. 1339-1350, 1999

[6] Tazawa,E. and Miyazawa,S.: Influence of Cement and Admixture on Autogenous Shrinkage of Cement Paste. In: Cement and Concrete Research, 25 (2), S. 281-287, 1995

[7] Sato, R., et. al.: Experimental Studies on Reduction of Autogenous Shrinkage and Its Induced Stress in High Strength Concrete. In: Proceeding of the 2nd Int. Research Seminor on Self-Desiccation and Its Importance in Concrete Technology, Lund, Sweden, S. 163-171, 1999

[8] Neville, A.M., Dilger, W.H. and Brooks, J.J.: Creep of Plain and Structural Concrete. In:Construction Press, S. 246-255, 1983

[9] JCI.: Autogenous Shrinkage of Concrete. In: E. Tazawa, Ed. London: E & FN SPON, S. 31, 1999

[10] CEB.: CEB-FIP MODEL CODE 1990, Thomas Telford, S. 2-29 - 2-34, 1999

Boudewijn M.Piscaer
Omya Concrete Minerals
Köln, Germany

Fertilizations from the Refractories industry

Introduction

Especially for the people not familiar with an unusual word, an explanation. Refractories are high temperature resisting products used for the heat enclosing industries such as blast furnaces, known from slag for cement, as well as power stations fly ash thermal known from the fly-ashes. Also Portland cement clinker could not be made without the use of refractories as well as other basic products such as petrol, glass, ferrous and non-ferrous metals etc. Refractories were in the past mostly ceramically bonded by high temperature firing in kilns. Some were chemically, clay and hydraulically bonded which only took a small market share.

High temperature resisting low cement concrete was without any doubt the first Ultra High Performance Concrete. It was patented and developed early 70th in France by Lucien Prost. The objective was to reduce cement, not for cost reduction, but in order to reduce the free lime present in the Aluminate cement. This free lime was the cause for lower melting temperature of the lining. Therefore the old high cement content unburned refractory concrete was still inferior to ceramically bond burned brick.

The consequence of the low cement concrete innovation was exciting. We discovered not only higher temperature resistance but also lower permeability and higher physical strength. The main part of the cement was replaced by a micro silica addition.

Patent circumvention motivated a French competitor to develop yet other binders such as reactive pure micronized Alumina. The race for better concrete had started and created exciting opportunities for the whole cement bonded refractories branch. While we all know the advantages of molding the desired shape using concrete, the refractory users, being used to brick, had to develop other application techniques and design.

Keywords: *fertilization, refractories industry*

1 Background of companies and people involved

"Luck is when opportunity meets with preparedness" (Pierre Elliot Trudeau).
Early 80th a key French researcher, who was involved with the second wave of low cement concrete innovations met up in France with an international market developer, the writer, plus a team of competent sales engineers. Repetion of success and internationalization plus taking care of reducing the disadvantages of concrete applications while continuing R & D

were the fundamentals for success. Know-how licenses could be sold world wide and application technology was received in return.

When the large French building group, to whom the refractory division belonged at the time decided to develop civil UHPC it was logical that the same researcher was leading this task.

It is encouraging to know that this researcher and the writer still share the same viewpoints today about how we could make the civil concrete industry innovate successfully and share some of these viewpoints as elements for innovation.

2   Differences between Refractories and Civil Concrete

- Mechanical strength of a cold demolded refractory concrete is seldom of interest. It will get its best properties after the working temperature is obtained by additional ceramic bond.

- Durability will be depending of the application, from 15 minutes from a steel pouring element till 15 years for a blast furnace lining.

- Pore size distribution, related to permeability of gases and liquid metals and aggressive slag, is a key aspect.

- Mineralogical changes happen fast under high temperature and form a basic part of the knowledge of even sales engineers.

- Cost / ton is less important. Mid 80th French iron and steel producers started to pay according to the performance that means how much liquid iron went over the lining before it needed repair and how much material was needed for the repair. The price per ton or m3 was not relevant for the customer but its performance.

- Application ; a refractory concrete is cast or poured with or without vibration, rammed with little moisture. But what need more attention are shotcreting, gunning and spraying.

- Customers of refractories are an industry that has gone trough some high tech development since the 80th. Compare the weight reduction and safety improvements of a car in the last 20 years and you can imagine the technological demand on iron, steel and glass. And refractories are strategically key materials for all of this, including the fuel of the car.
  Also the cement industry, which went through important fuel reductions per ton of cement thanks to new installations could improve the process for a part to better refractories.

The producers of refractory concretes are few and operating international. The performance cost of materials could justify high transportation cost. Products made in France would go to Japan and Australia.

- <u>The Research, Development and Quality Control budget</u> in the refractory industry is rather high, compared with many other industries. It is shamefully low in civil concrete. Even when one large civil cement and concrete group discovered the Reactive Powder Concrete, they discovered they had no real concrete lab to speak of. Only chemical admixture companies, in open competition, have adapted R & D facilities and take care of progress in civil concrete.

3   Differences II

When we look more into detail about the concrete mix compositions we notice following:

- Refractories raw materials are mostly synthetic and processed materials.

- Aggregates can come from all over the world, since the price of refractory concrete is often more than 10 X the price of civil concrete. Only the admixtures travel further than other products.

- Particle and grain size distribution for mechanical packing purpose is very accurate. While most aggregates are 5 till max 10 mm only, we notice a large number of different sizes.

- Also the number of powders under 500 µ is noticeably high.

- A large number of admixtures are used to provide the right rheology. Since almost always the refractory concretes are supplied in bagged material, the admixtures in the composed material are in dry powder form.

- Speed of installation is seldom required which works out well with the complex ingredients. Rather long mixing times are applied for the field mixers.

4 Typical refractory UHPC's

Below you will find some technical properties of some high tech refractory concretes.

Name	Phlowcast M 28	Pliflow FT 70	Monrox AX	Units
Main component	fireclay/Chamotte	calcin.bauxite	andalusite/zircon	
Installation methods	rodding/easy comp.	self compact.	self compacting	
Max.grain size	10	7	5	mm
Material required	2,25	2,58	2,8	T/m3
Water required	5,5-7	6-6,4	5,5-6,5	L/100 kg
Composition				
est. cement content	7-8	4,5-5,5	4-5	%
Al2O3	46	70	52	%
CaO	3	1,4	1,5	%
Cold crush. strength after 110 C	110	120	110	N/mm2

5 (Alumina) cement reduction   Technological consequences

Again, cement reduction was done not for cost or CO2 emission reductions. Refractory fines to replace cement are often more expensive. Classic low performance refractory concrete contained appr.20 % cement per ton. The new low cement concretes were first between 5 and 8, then 2 and 5 %. cement. Late 80th cement reduction for certain expansive concretes went down to 1,5 % and even less.

The alumina cements were considerably improved and reactive micro silica and later micronized alumina were applied in a free market mechanism without regulations. Even though raw material producers and refractory producers belonged to the same group, the use of materials was free flowing and purchasing outside the group took freely place.

Accurate packing, from the coarse aggregates to the micro packing of the powders resulted also in higher strength thus less cement was needed.

Due to the often-special behavior of the few cement types available, several different admixtures were needed in order to obtain the right rheology and maintain proper workability. With pouring other rheology is required than with shotcreting, gunning and spraying were flash setting was even encouraged.

The result of the cement reduction and replacement by other fines was ;
- increased mechanical cold and high temperature strength
- lower permeability,
- higher volume stability and other physical properties

- engineered mineralogical modifications.

6 Alumina cement reductions   Cultural economical consequence

Technology could move in an environment without regulations imposed. Only test methods were synchronized with competition via the PRE (Producteurs Refractaires Europeenes) and ASTM.

Fierce competition, both between high tech refractory concrete suppliers themselves as well as conceptual between concrete and refractory bricks, was the fuel for progress.
This resulted in :

- improved technical sales, installation supervision and training of the people installing the concrete. Especially the shotcrete spraying technique needed special attention.
- R & D would use fast feed back from the installers and adapt the product to practical use such as larger ranges of water dosages,
- customers would adapt design and practices to the new products developed,
- a healthy supplier - customer relation, in which performance responsibility was essential,
- despite the reduction of cement per ton of refractory concrete, the total volume of cement and certainly not the financial contributions were reduced. The increased demand on properties resulted in increased prices for cement. The increased market share due to better performance of the concrete over brick resulted in increased market share for concrete and alumina cement.

7 Inspiration I   Raw Materials

Fines

One of the most important inspirations from the refractory industry is the use of fines for micro-packing and reactivity.

- Quality control on stable Particle Size Distribution of all fines which influences micro packing and water demand should become routine and takes little time,
- Selection of possible Portland cements compatible with admixtures and other fines , both in micro-packing and chemical compatibility,
- Besides the proven micro silica, investigate other cost effective and reactive fines such as calcium carbonates. These are now also available in slurry form that should also be investigated. A recent test using this micro fine slurry for UHPC was encouraging.
- Develop micro packing know-how, which becomes more complicated when using chemical admixtures. We have to enter nano-technology, fashionable or not.

Aggregates

- Investigate the most cost effective aggregates available in the refractory market, based on hardness, permeability/adhesion, elasticity and color. Maybe some can be

cost effective in your country. While bauxite is already in application in UHPC, maybe high iron content bauxite can be cheaper.

- Utilize more fractions, even for regular concrete, in order to obtain best engineered packing, e.g. 0-0,5 0,5 -1, 1-2, 2-3,5, 3,5-5 etc.

8 Inspiration II Manufacturing

When using very small amount of ingredients, they can be easily sucked up by dust extraction. Premixing of these fines, including especially admixtures, has been practiced in the refractory industry since the mid 80th.

Separate binders, as practiced in the refractory industry on certain products, can avoid aging of ingredients due to uncontrolled moisture content of the aggregates.
The use of separate binders has also been an interesting method of selling confidential ingredients to a licensee or someone not interested or not capable of controlling the performance of its end product.

Mixing dry, moist and wet ingredients can be most cost effective for civil concrete, used to this. Storage, dosing and mixing facilities should be adapted for the larger amount of products, also for handling bagged goods.

Personnel should be selected and trained to deal with high tech concrete. For this reason, the gradual introduction of Self Compacting Concrete in e.g. the precast industry in the Netherlands has provided a smooth introduction towards UHPC.

9 Inspiration III Application Technology

Self Compacting Concrete originated from the refractory in Japan in the early 80th, but was based on European basic research and European patents. It was clearly the difficult installation of blast furnace runners for iron and slag that speeded up this technology. Homogeneously installed concrete was a must for performance, in this application already detectable after a few weeks.

In Japan it was the transfer in the 80th from the refractory industry to earth quake resistant civil concrete constructions for a bridge with heavy reinforcement and no chance for vibrating compacting.
In the Netherlands we also got most of the SCC technology from Japan but here it was the working environment, which made the use of SCC in, precast popular despite the unnecessary material cost increase.

The refractory industry introduced also the Easy Compacting Concrete densified by simple rodding. This was a conscience step back from the SCC. For cost and error margin UHPC could also get inspired on this.

The link with homogeneity and durability between refractories and civil concrete should also be made. This is possible when we dare to face errors being made on the job site in this respect when applying ordinary vibrated concrete. We can state that ordinary concrete is, in general, poorly homogenized and thus less durable than possible. UHPC cannot afford to be applied the same way.

From the refractory industry we learned the expression that a poor concrete well mixed and installed is better than a good concrete badly mixed and installed. The aim is thus a good concrete well mixed and installed. Training and supervision is a key for performance.

In the mid 80th we set up a special training center for supervisors and customers, accelerating new application techniques and partnerships.

SCC should be supervised by the supplier and paid for by the reduction of site personnel.

10 Inspiration IV Gunniting and Shotcrete rehabilitation

Shotcrete is applying a wet mix by pneumatic means and gunniting is transporting a dry mix pneumatically and mixing it at the nozzle. Especially in gunniting several mixes existed but were poor in density and had a high loss of material due to rebound. The mix you designed was not the mix you got on the surface. In the mid 80th UHP refractory concrete was utilized to rehabilitate gunniting applications. This coincided with the discovery of a super technician, George Trumann, from a US refractory supplier.

Besides a better mix design training, having the right equipment is essential for this exciting application. With this new approach properties similar of cost concrete can be obtained with little or no rebound loss.

In the 90th a new shotcrete technique was developed for refractories, again in the US, by means of mixing a flash setting material at the nozzle. Densities equivalent to vibrated or SCC mixes are obtained, opening again a new way to new applications, especially were form work is time consuming.

Modifying the ingredients but applying the same UHPC technology for civil purposes can be developed. It will have its place in more than tunneling and mountain slopes retainment. Attention has to be made again to equipment and supervision. How about developing this technology in precast factories for fast demoulding ?

11 Inspiration V Design

Refractory design, supply and installation supervision are often in one hand, optimizing use and stimulating innovations. The interaction in civil UHPC with the designer is essential.

The use of several layers of different materials, for cost and thermal conductivity in the case of refractories, can also be looked at. This should especially be interesting in precast were surface concrete could be different than mass back up material. If we can combine brick with concrete, why not UHPC with lower grade or lightweight concrete as a core or back up ?

In refractories throughout running steel reinforcement or prestressing does not exist. Instead refractory Steel V,Y and ceramic anchors are used, spaced on 10 to 20 cm distances. Especially in combination with fibers in the concrete these should be investigated in connection with volume stability of the concrete. Anchors instead of steel webbing could maybe save a lot of cost in design and placing time.

12   Inspiration VI   Miscellaneous

The contacts with refractory consuming industry should also be a form of inspiration, especially looking at the changes in manufacturing, which have taken place at their customers.
Pouring technologies of steel, which went from batch big ingots to continues casting in 30 years worldwide. The glass industry went from vertical to horizontal casting.

With the possibilities of total control over viscosity and setting time behavior we can imagine changes, especially in the precast industry.

The most important inspiration is the absence of regulations in the refractory sector and this is vital for cost effective UHPC development, acceptance and bringing the regular concrete industry on the technological level it deserves. Performance and responsibility towards customers are the only valid guidelines.

Refractory concrete technology has proven to be an inspiration for High Tech civil concrete in the past in a rather passive accidental way. Let's look at this more in an active way. Events such as concrete canoe races should be enlarged and truly become international to create awareness for UHPC, the best locomotive for improving all civil concrete . Lets brainstorm about some ideas here about international promotion.

Part 11:

Fibre Reinforcement

Ludger Lohaus

Prof. Dr.-Ing., Managing Director
Institute of Building Materials,
University of Hannover
Hannover, Germany

Steffen Anders

Dipl.-Ing., Scientific Assistant
Institute of Building Materials,
University of Hannover
Hannover, Germany

Effects of polymer- and fibre modifications on the ductility, fracture properties and micro-crack development of ultra-high performance concrete

Summary

In the present study ultra-high performance concrete was modified using polymer dispersions and reinforced using alkali-resistant-glass (AR-glass) fibres. The objective was to investigate the effects on ductility in general and on micro-cracking in particular. Furthermore different parameters describing the fracture properties and micro-crack development were calculated and evaluated.

It is shown, that the effects of fibres and polymer dispersions on the properties of ultra-high performance concrete differ significantly from what is known for normal strength concrete.

Generally speaking only slight increases in ductility using AR-glass fibres and polymers in ultra-high performance concrete could be observed. In the case of particular polymers even losses in ductility were measured. The characteristic length, ductility length and correlated crack-formation energy show similar results for the different concretes, but general tendencies cannot be predicated at present. Only in the case of the crack-formation energy significant tendencies were observed. The experiments will be extended to the effects of polymer modifications and fibre reinforcement on the dynamic behaviour of ultra-high-performance concrete.

Keywords: *Polymer modification, fibre reinforcement, ductility, fracture properties, micro-crack development*

1 Introduction

Ultra-high performance concrete is increasingly being used in structures or structural elements subjected to dynamic loads, for instance in offshore applications or bridge constructions. Due to the extraordinarily high compressive strength the dead weight of the concrete decreases whereas the rate of the live loads may be increased. Therefore the effects of live loads respectively dynamic loads on the microstructure are more pronounced in comparison with commonly used normal strength concrete.

Due to the well known relation between the fracture properties of concrete and its behaviour under cyclic loading, ultra-high performance concrete reinforced using AR-glass fibres and

steel fibres as well as concrete modified using polymer dispersions was examined with regard to the ductility, fracture properties and especially micro-crack development.

The analysis was also focused on the expressiveness of different parameters which have been proposed in the literature to describe the ductility in general and the micro-crack development in particular.

2 Experimental programme

In order to determine the effects of fibre reinforcement and polymer modifications on the fracture properties of ultra-high performance concrete different types and contents of fibres as well as polymers were used.

In the case of the AR-glass fibres the varied parameters were the fibre length (13 mm and 25 mm), the fibre content (1 kg/m³ to 6 kg/m³) as well as the fibre type (dispersible fibres and fibre bundles). The content of the dispersible fibres was varied from 1 kg/m³ to 3 kg/m³ whereas the content of the fibre bundles ranged between 3 kg/m³ and 6 kg/m³. The tests on steel fibre reinforced mixes are not finished yet. In the case of polymers three types namely styrene-acrylate, styrene-butadiene and epoxy resin were chosen. The polymer contents were specified to 2.5 %, 5.0 % and 10.0 % by cement mass. According to Schorn and Lohaus [1, 2, 3] the amount of the cement paste was kept constant throughout the tests, because the different mixes would not be comparable if the cement paste/aggregate ratio has been changed.

The reference concrete was designed as follows.

Cement (CEM I 52,5R)	603 kg/m³
Microsilica	100 kg/m³
Water content (total)	178 kg/m³
Superplasticizer (PCE)	34 kg/m³
River sand 0/2 mm	612 kg/m³
Crushed basalt 1/5 mm	916 kg/m³

The compressive strength of the reference concrete was about 150 N/mm² at the age of 28 days. Due to the demanded on-site applicability of the concrete for instance in offshore applications the specimens were not heat cured. They were demoulded one day after casting and stored in climate 20°C and 65 % relative humidity until testing.

For the different mixes the compressive strength, the flexural strength, the slump flow up to 60 min after mixing as well as the air content were determined.

The fracture properties were derived from 4-point-bending tests using notched beams of 100 mm×100 mm×500 mm with a span of 400 mm. These tests were stopped at a mid-span deflection of 0.25 mm. The test set-up is displayed in figure 1. From these tests different parameters describing the ductility, fracture properties and micro-crack development were calculated. These parameters are defined and evaluated in the following.
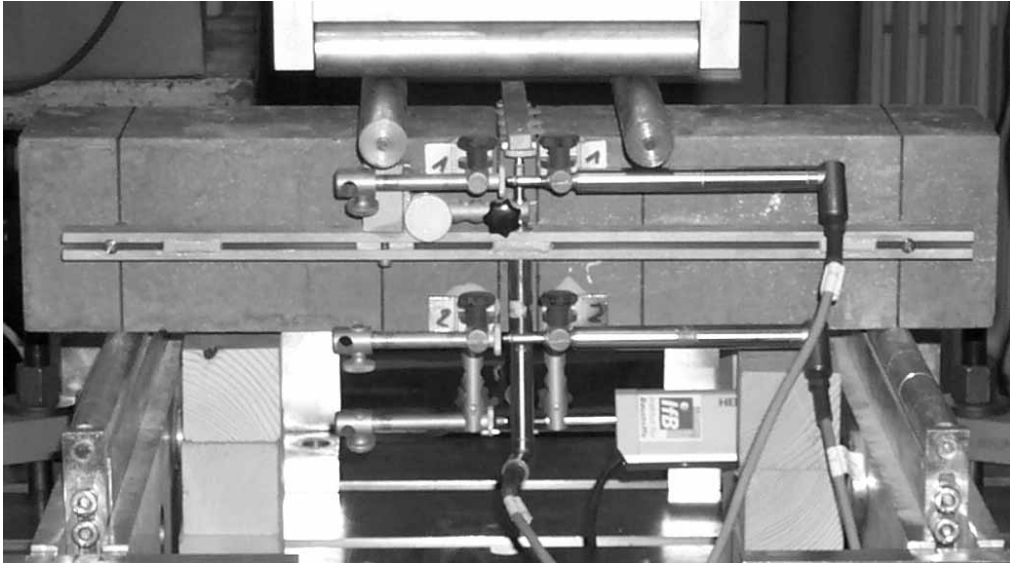
Figure 1:   Test set-up for 4-point-bending tests.

3   Tensile behaviour of concrete and its characterization

3.1   Tensile behaviour of concrete

It is recognized, that the development of micro-cracks starts well before the tensile strength is reached. According to e.g. Kopp [4] the stress-strain respectively load-deflection curve of concrete in uniaxial tension can be divided into four different parts according to figure 2.

In the first part (1) of the stress-strain curve only load-independent, stochastically distributed micro-cracks can be found in the cement stone. Already in the second part (2) the load-induced micro-cracking starts. These micro-cracks are orientated perpendicular to the tensile stresses. This second part overlaps with part three (3), which is characterized by the accumulation of load-induced micro-cracks. This accumulation starts before the tensile strength is reached, and causes a significantly decreasing slope the of stress-strain curve. The accumulation of the micro-cracks is limited to a very small part of the specimen and merges into the macro-crack opening in the fourth part (4) of the curve.

Even if this model of the tensile behaviour of concrete has been derived for normal strength concrete subjected to uniaxial tension the fundamental mechanisms are supposed to be similar for high- and ultra-high performance concrete.
From these load-deflection curves different parameters can be calculated, which are said to describe the ductility and micro-crack development of concrete.
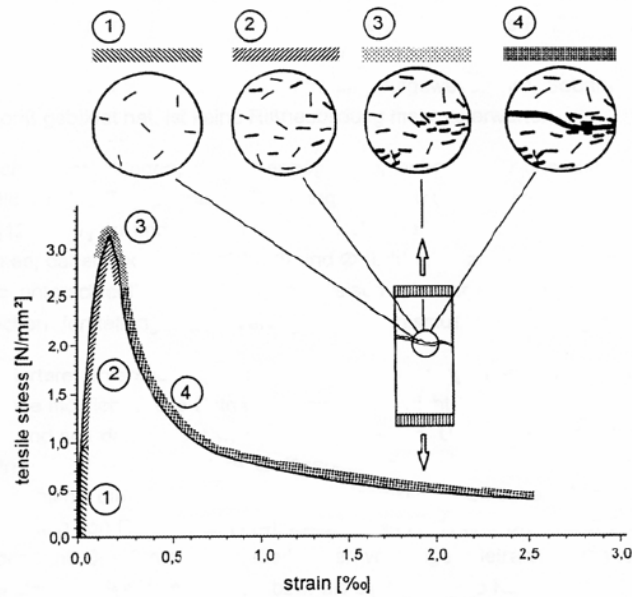
Figure 2:   Micro-crack development of concrete loaded in uniaxial tension [4].

3.2   Ductility Parameters

In the literature a lot of parameters can be found to describe the ductility of concrete or building materials in general. The most common parameters are the fracture energy and the characteristic length [5]. Apart from these two parameters the ductility length [6], the crack-formation energy as well as the correlated crack-formation energy [4] were calculated and will be defined in short.

Further parameters such as the toughness indices and the residual strength factors according to ASTM C 1018-97 or the equivalent flexural strengths [7] were not taken into consideration yet as they are especially determined for steel fibre reinforced concrete with pronounced load-bearing capacity in the descending branch.

Fracture Energy

The fracture energy defines the energy which is needed to separate a specimen completely. Often a high fracture energy is said to indicate a ductile material. Nevertheless the fracture energy does not distinguish between the energy dissipated in the pre- and post-peak part of a load-deflection curve.

The fracture energy is defined as the area under the stress-strain-curve or load-deflection curve respectively until the specimen is completely separated. As described in chapter 2 the 4-point-bending tests were stopped at a mid-span deflection of 0.25 mm. Even if the resulting value is not the fracture energy according to its definition, it will nevertheless be referred as fracture energy in the following.

Characteristic length and ductility length

The characteristic length is a means of describing the ductility of materials. According to Hillerborg's definition it is half the length of a tensile bar, being able to store the same amount of elastic energy as dissipated in the fracture process. Therefore brittle materials are described by a short characteristic length, ductile materials by higher values for the characteristic length. If materials are to be compared with respect to ductility the characteristic length is a better means than the fracture energy. The characteristic length is calculated according to equation 1:

$$l_{ch} = \frac{G_f \cdot E}{f_{ct}^2} \qquad \text{(eq. 1)}$$

Where l_{ch} equals the characteristic length, G_f the fracture energy, E Young's modulus and f_{ct} the tensile strength. It has to be considered, that the characteristic length is calculated from the fracture energy and thus contains the energy needed for the micro-crack development and the macro-crack opening.

The ductility length (D_l) is similar to the characteristic length. According to Kopp [4] it is calculated as follows:

$$D_l = \frac{G_f}{f_{ct}} \qquad \text{(eq. 2)}$$

As a result, the statements concerning the characteristic length are also true for the ductility length.

Crack-formation energy

The crack-formation energy describes the amount of energy that is dissipated in the specimen for the micro-crack development (G_{ci} in figure 3). As can be seen in figure 3 only irreversible deformations are taken into account.
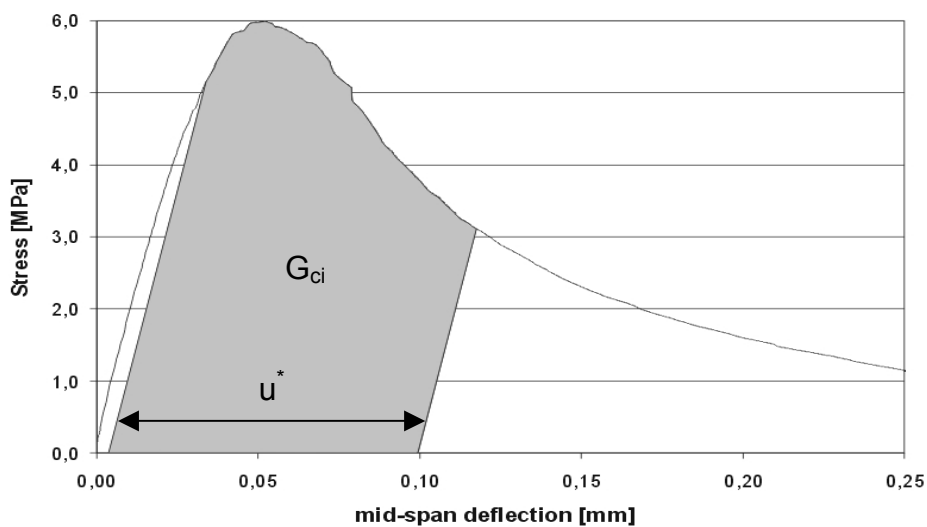

Figure 3: Definition of the crack-formation energy according to Kopp [4].

It is rather difficult to calculate the crack-formation energy, because of difficulties in defining the points where the increased micro-cracking and the opening of the macro-crack start. According to [4] these points localize the beginning and the end of the crack-formation respectively.

Apart from the mid-span deflection of beams loaded in flexure Kopp [4] also measured the deformations in the compressive and tensile regions on the top and at the bottom of the specimen. This method has been adapted to the present conditions for the fibre reinforced mixes only. These deformations were measured using the horizontal gauges 1 and 2 in figure 1.

Kopp defined, that the increased micro-cracking starts, as soon as the tensile deformations exceed the compressive deformations and hence the linear elastic behaviour ends. This point is comparable to the first crack strength according to ASTM C 1018-97. The opening of the macro-crack is defined to start as soon as the stress at the bottom of the specimen respectively the notch vanishes. Hence, this point is a calculated one depending on the assumptions for the non-linear stress distribution in the cross-section.

By dividing the crack-formation energy by the corresponding mid-span deflection (u^*) the correlated crack-formation energy is calculated (eq. 3). According to Kopp this parameter can be interpreted as mean stress during the micro-crack development.

$$G_{ci}^* = \frac{G_{ci}}{u^*} \qquad \text{(eq. 3)}$$

For more detailed information the reader is referred to [4]. In the present study the assumptions concerning the stress-distribution were adapted to ultra-high performance concrete following the regulations of Model Code 90 [8]. The major difference between the fracture energy and the crack-formation energy is that the latter does not include the energy of the fourth part (4) of the load-deflection curve according to figure 2, which is governed by the macro-crack opening.

4 Results

4.1 Load-deformation behaviour in flexural tests

As examples for the stress – mid-span deflection curves in bending tests the reference concrete, a mix reinforced using 13 mm, dispersible fibres (content = 2.0 kg/m³ - 13 D 2.0), a mix reinforced using 25 mm, fibre bundles (content = 3.0 kg/m³ - 25 B 3.0), a mix using hooked steel fibres, a mix containing 10 % by cement mass of epoxy resin and finally a mix modified using 10 % by cement mass of styrene-acrylate are shown in figure 4. Each curve represents the average of three tested specimens.
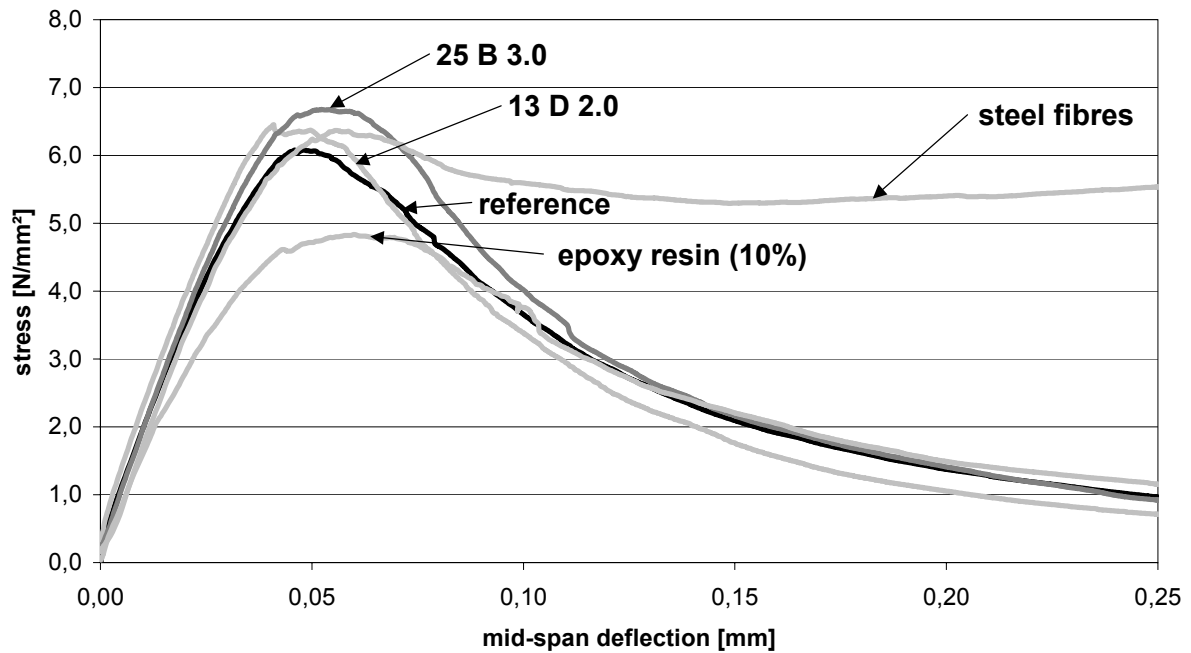
Figure 4:   Stress – mid span deflection curves of selected mixes
13 D 2.0   AR-glass fibre, 13 mm, dispersible fibres (D), 2.0 kg/m³
25 B 3.0   AR-glass fibre, 25 mm, fibre bundles (B), 3.0 kg/m³

As can be derived from figure 4 AR-glass fibres cannot compete with steel fibres in preventing brittle failure of ultra-high performance concrete. Minor differences can be observed as long as the mid-span deflection does not exceed 0.1 mm. Using fibres seems to increase the bending strength and the linear elastic behaviour compared to the reference concrete. Secondly AR-glass fibres seem to increase the energy needed for micro-crack development up to a mid span-deflection of about 0.1 mm.

In the case of the polymer modified mixes, the styrene-acrylate shows a brittle behaviour which is comparable to the reference concrete. As expected from normal strength concrete, Young's modulus and the bending strength decrease using epoxy resin. Nevertheless the post-peak behaviour remains the same compared to the reference concrete in any case except for the steel fibre reinforced mix.

In order to quantify the ductility and micro-crack development the parameters described in chapter 3.2 were calculated.

4.2   Ductility parameters

In this section the previously described parameters were compared and evaluated. Two tendencies can be derived from figure 5, which displays the fracture energy. Firstly the fracture energies of the AR-glass fibre reinforced mixes tend to be higher than the fracture energy of the reference mix whereas most of the polymer modified concretes show a decreasing fracture energy.
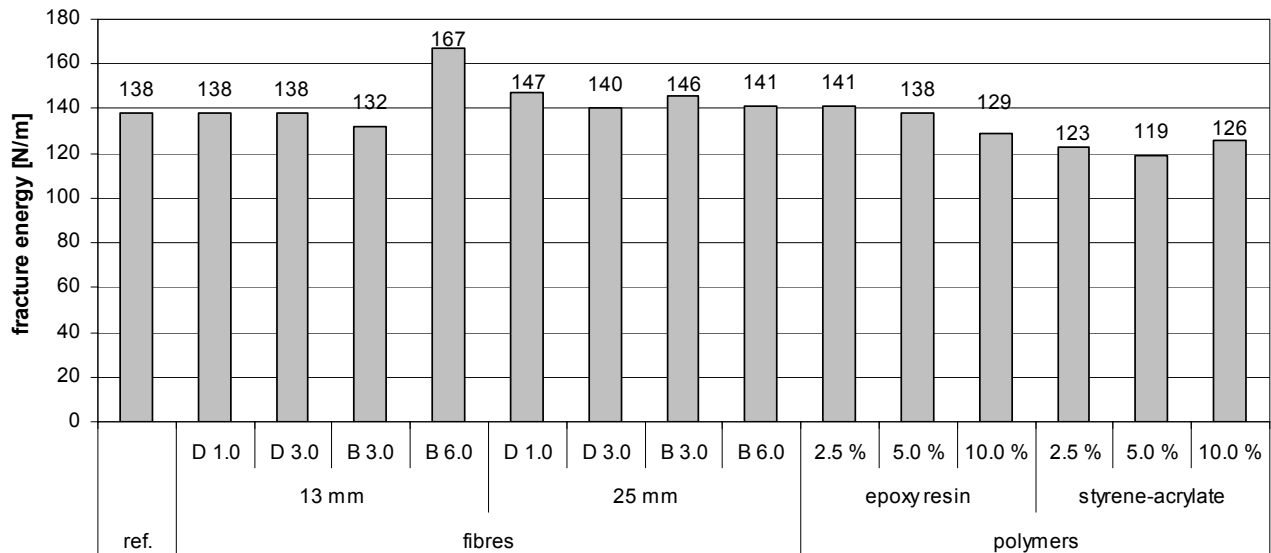
Figure 5: Fracture energies of the concrete mixes.

The reason for the effects of AR-glass fibres not being more pronounced is that they have a stronger effect on the micro-crack development than on the macro-crack opening. Apart from the general slight increase in fracture energy it can only be stated, that the 25 mm long fibres perform little better than the 13 mm long fibres, except for the 13 mm fibre bundles with a content of 6 kg/m³. Generally it is not possible to distinguish different AR-glass fibre reinforced mixes only taking the fracture energy into consideration.

In the case of the polymer modified mixes the fracture energy tends to decrease with an increasing content of epoxy resin. In comparison the steel fibre reinforced concrete reaches a fracture energy of about 250 N/m.

Because of the fracture energy being an absolute value it should be compared to the crack-formation energy which is shown in figure 6.

In general the statements concerning the fracture energy of the AR-glass fibre reinforced mixes can be transferred to the crack-formation energy. Moreover the crack-formation energy seems to be more selective than the fracture energy. Again the longer fibres perform little better than comparable short fibres, even if the number of fibres per unit mass is halved.

The dissipated energy increases with an increasing fibre content. The only exception is the mix using 25 mm long fibre bundles with a content of 6.0 kg/m³.

To what extent for example the increase in the crack-formation energy of the 13 mm long fibre bundles with a content of 6 kg/m³ affects the resistance to dynamic loads is to be answered in further investigations.
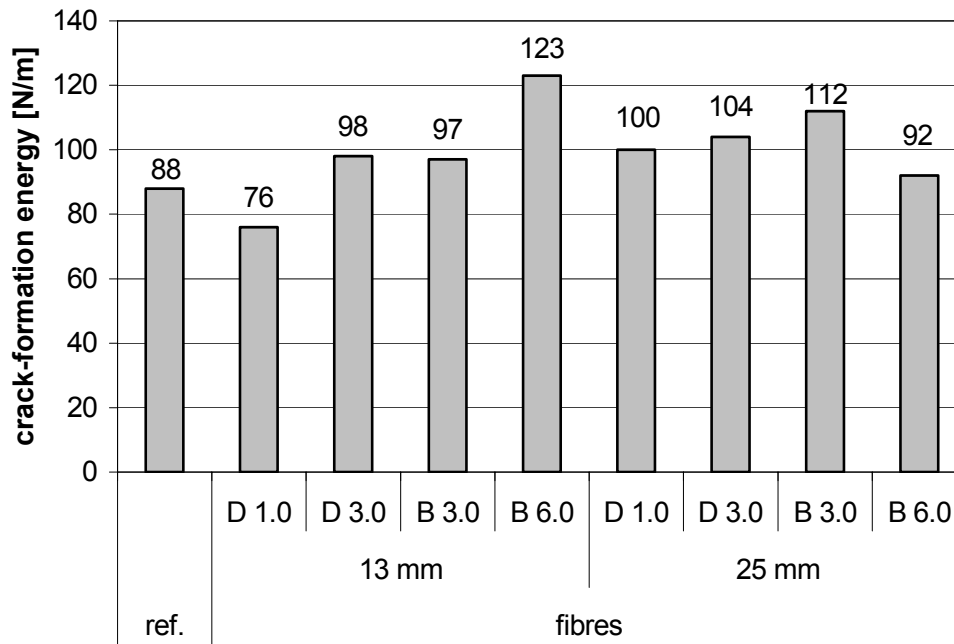
Figure 6:   Crack-formation energies of the AR-glass fibre reinforced mixes.

The second set of parameters that are to be compared are the characteristic length, the ductility length and the correlated crack-formation energy. It was desisted from showing the ductility length, for the tendencies are similar to the characteristic length with significantly reduced differences between the mixes. The characteristic length as well as the correlated crack-formation energy are shown in figures 7 and 8.

In figure 7 in analogy to the trend of an increased fracture energy, a general increase in ductility in terms of characteristic length can be observed with respect to the fibre reinforced mixes. For single concrete mixes, for instance 13 D 1.0 or 25 D 1.0 the increase in characteristic length is more pronounced than the increase in fracture energy.
In comparison the steel fibre reinforced concrete results in a characteristic length of about 440 mm.

In general the expectation of a significant increase in ductility of UHPC with increased contents of AR-glass fibres cannot be confirmed from the performed tests.
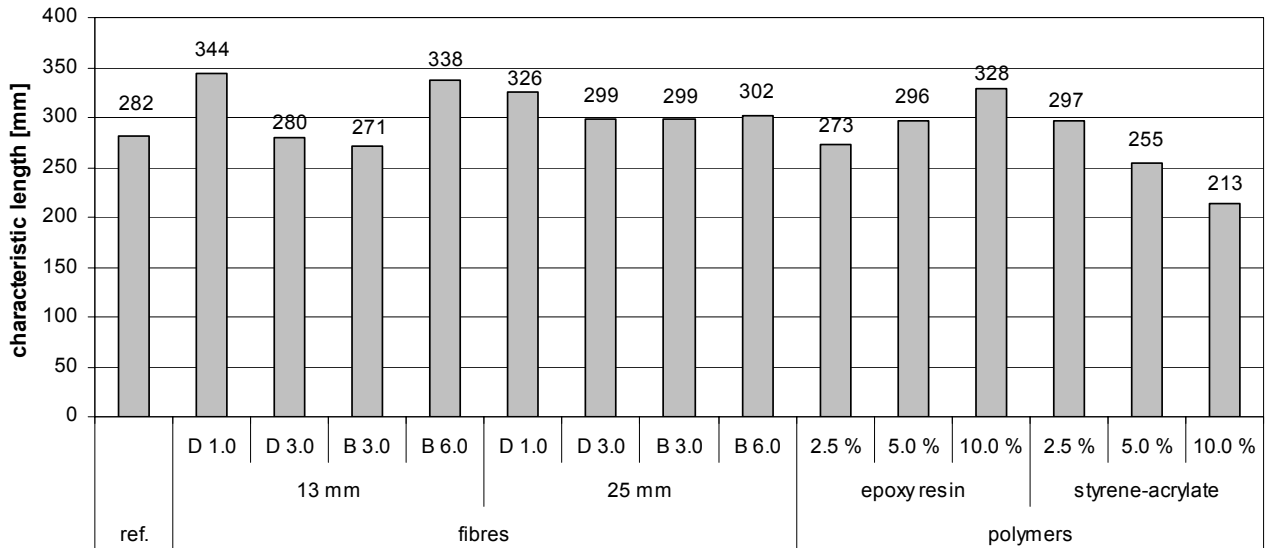
Figure 7:   Characteristic lengths of the different concrete mixes.

In the case of the polymer modified mixes no significant increase in ductility can be observed compared to the reference concrete, even if the epoxy modified mixes show an increased ductility with an increased polymer content. The opposite is true for concrete modified using the styrene-acrylate. The reason for the fracture energy and the characteristic length working in opposite directions with reference to the polymer content is that the addition of polymers also affects the tensile strength and Young's modulus. In this case the strength is significantly reduced adding epoxy resin to the concrete mix whereas an increase in strength was observed for the mixes using styrene-acrylate.
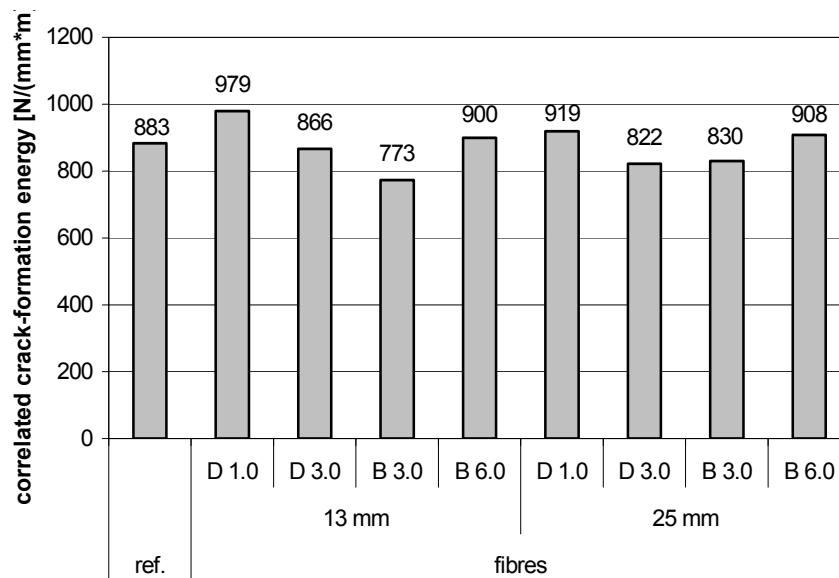

Figure 8:   Correlated crack-formation energies of the AR-glass fibre reinforced mixes.

634

As can be seen in figure 8 the tendencies already stated for the characteristic length can be transferred to the correlated crack-formation energy. The only difference is, that the relation between particular concrete mixes may differ comparing characteristic length and correlated crack-formation energy. Furthermore, the results of the correlated crack-formation energy seem to be more pronounced compared to the characteristic length.

5 Evaluation of the ductility parameters

As already described in section 4.1 the differences between the load-deflection curves are rather small. Furthermore, the ductility of the AR-glass fibre reinforced and polymer modified mixes cannot stand comparison with a steel fibre reinforcement in terms of fracture energy or characteristic length.

For this reason and the fact, that special attention was drawn to the micro-crack development very selective parameters describing ductility and micro-crack development were demanded.

As described in the previous sections, the only parameter showing selective results concerning the micro-crack development is the crack-formation energy. The results for the crack-formation energy seem to be acceptable, because the correlated crack-formation energy and the characteristic length show similar results even if they are differently calculated.

The reason for the results of the crack-formation energy being more pronounced than the fracture energy is that the latter does not distinguish between the energy dissipated in micro-crack development and macro-crack opening.

A comparison between the characteristic length, ductility length and correlated crack-formation energy shows that the ductility length is the least selective parameter. Characteristic length and correlated crack-formation energy show similar results even if the results of the correlated crack-formation energy are most pronounced.

It has to be taken into consideration, that the calculation of the crack-formation energy requires considerably higher effort compared to the fracture energy. Firstly more gauges are required and secondly the calculation is more complex.

6 Conclusions

In the present study ultra-high performance concrete was reinforced using AR-glass fibres of different length, type and content as well as modified using polymers of different type and content for comparison reasons. In both cases the effects on the ductility were less pronounced compared to polymer modification and fibre reinforcement of normal strength concrete.

Generally speaking the increase in ductility using AR-glass fibres and polymers in ultra-high performance concrete is small compared to the performance of steel fibres. In the case of particular polymers even losses in ductility were observed.

With regard to the fracture energy and characteristic length, apart from a slight increase in ductility in the case of AR-glass fibres no significant changes could be observed in ultra-high performance concrete.

If special attention is drawn to the micro-crack development the crack-formation energy is the most promising and selective parameter to describe the different concrete mixes. With regard to fracture energy, characteristic length, ductility length and correlated crack-formation energy no significant tendencies can be found comparing different ultra-high performance concretes.

Compared to polymer modified concrete, AR-glass fibres appear to be a more promising means to control the micro-crack development.

Further tests are to be performed in order to investigate, whether and in which way the observed differences can be transferred to the dynamic performance of the different concrete mixes. Furthermore the experimental programme will be extended to for instance further types of fibres, fibre cocktails and additional parameters describing the ductility and the micro-crack development of concrete.

7   References

[1]   Schorn, H.: Betone mit Kunststoffen und andere Instandsetzungsbaustoffe. Ernst & Sohn Verlag, Berlin, 1991.

[2]   Schorn, H.: How to test efficiency of polymers in cement concrete, in: Polymers in Concrete – Proceedings of the 6th International Congress on Polymers in Concrete. Shanghai: 1990, pp. 799 – 805.

[3]   Lohaus, L.: Festigkeits- und Verformungsverhalten epoxidharzmodifizierter Betone. Dissertation, Ruhr-Universität Bochum, 1984.

[4]   Kopp, S.: Nachweis, Beurteilung und Quantifizierung von Gefügeveränderungen im Beton mit energetischen Kenngrößen. Dissertation, Ruhr-Universität Bochum, 1998.

[5]   Hillerborg, A.; Modeer, M.; Petersson, P.E.: Analysis of Crack Formation and Crack Growth in Concrete by means of Fracture Mechanics and Finite Elements. In: Cement and Concrete Research. Vol. 6; S. 773-782, 1976.

[6]   Budnik, J.: Bruch- und Verfomungsverhalten harzmodifzierter und faserverstärkter Betone unter einachsiger Zugbeanspruchung. Dissertation, Ruhr-Universität Bochum, 1985.

[7]   Deutscher Beton- und Bautechnik-Verein E.V. (Hrsg): DBV-Merkblatt Stahlfaserbeton. Berlin, 2001.

[8]   Comité Euro-International du Béton : CEB-FIB Model Code 1990. Thomas Telford Services Ltd., London, 1993.

Marko Orgass
Dipl.-Ing.
University of Leipzig, MFPA Leipzig
Germany, Leipzig

Yvette Klug
Dipl.-Ing. (PhD Student)
Leipzig University of Applied Sciences Leipzig,
Germany

Fibre Reinforced Ultra-High Strength Concretes

Summary

This paper describes the influence of short steel fibres and a fibre mix of short and long fibres on the mechanical properties of Ultra-High Performance Concrete (UHPC) especially regarding the ductility and the size effect. In this regard the fibre contents changed between 0, 1 and 2 Vol.-%. The results of numerous tests show the capacity of the investigated concretes with maximum grain sizes of 0.8 mm (Reactive Powder Concrete, RPC) and 5.0 mm (UHPC), represented by the flexural strength and the post crack behaviour. Otherwise the compressive strengths of specimens with different geometries are shown. A specific characterisation of the interfacial transition zone of matrix and fibre was made by means of microscopically inspections.

Keywords: *post crack behaviour, microscopically inspections, ultra high hybrid fibre concrete*

1   Introduction

To class the construction material fibre reinforced concrete (FRC) regarding its design engineering application range, it should be accentuate, that FRC has to range between plain concrete and reinforced concrete and not to put FRC on a par with reinforced concrete. Independent on the compressive strength of a concrete, FRC offers advantages over plain and reinforced concrete such as an increase of tensile strength and mechanical load capacity and an improvement of ductility and fire resistance as well. Just in today's time high performance concrete becomes more important and the applications continue to be pushed higher and higher, the improvements to conventional concrete concerning the durability and reliability of construction are of particular importance. However, in this connection possible disadvantages of FRC should be mentioned as well. First the impairment of the workability, complicating the compaction and the post-processing, furthermore the increase of material costs and the extra risk of corrosion of steel-fibres at the edge layer of the concrete, in view of penetration of water and oxygen, merely a matter of aesthetic without consequences for bearing capacity.

Because of the increased performance mentioned before in the last years conventional fibre reinforced concrete has established and it is common practice to use FRC as construction material, especially with industrial floor constructions and domestic constructions as well. Whereas considering the application of fibre reinforced ultra-high strength concrete (FRUHPC) presently only some projects and visions exist. That way some components of

bridges were built by means of FRUHPC as pilot projects, like the well-known precast, prestressed pedestrian bridge in Sherbrooke (Canada), erected in 1997. Further on, the company Schöck uses an element of fibre reinforced Reactive Powder Concrete as thrust bearing and structural measures in respect of tunnelling repair were carried out using FRUHPC.

2 State of the art

2.1 Bearing capacity of Fibre Reinforced Ultra-High Strength Concrete

Even though UHPC features high compressive strength, impermeability and surface abrasion resistance UHPC show very brittle failure behaviour and therefore a limited post-crack behaviour. Linear-elastic material behaviour characterises UHPC, so the elements fail explosively without any omen.

Under addition of fibres the load-displacement behaviour and consequently the ductility and fracture toughness can be improved. This can be traced back to the fact, that the fibres are able to transfer emerging loads by bridging the cracks. Here the fibres make an impact not until the appearance of cracks. That means after reaching the maximum load the descending arm of the load-displacement curve doesn't drop down at once. Depending on the kind of fibre, fibre length especially, and the fibre content, slow and even reduction of loads appear, coming along with increasing deformations. Otherwise it is possible to increase the compressive and tensile strength of the concrete, due to the absorption of notch stresses within the crack process zone by means of the fibres. Thus the crack process may be hindered.

2.2 Types of Fibres

To reach the desired load-bearing behaviour according to the respective application, the different types of fibres have to be used purposeful. Thus, the steel fibres, polypropylene fibres and glass fibres will be used in respect of the following effects:

- Steel Fibres:
  - Increase of fracture energy, subsequent improvement of ductility
  - Increase of strength (compressive strength, tensile strength)
  - Reduction of tendency for cracking

- Polypropylene Fibres (PP fibres):
  - Decrease of microscopic crack growth with high loading
  - Gain in fire resistance
  - Decrease of early shrinkage

- Glass Fibre:
  - Reduction of internal stresses within young concrete

As a result of the usage of fibre cocktails, mostly combination of different steel fibres or polypropylene fibres in addition, the advantages may be affected more tightly focused. That is, that by means of a fibre cocktail of short and long steel fibres for instance, a directed increase of compressive strength or tensile strength and improvement of the post crack behaviour as well is possible, caused by the interaction of the fibres both at micro (short fibres) and at macro (long fibres) levels (see Figure 1).
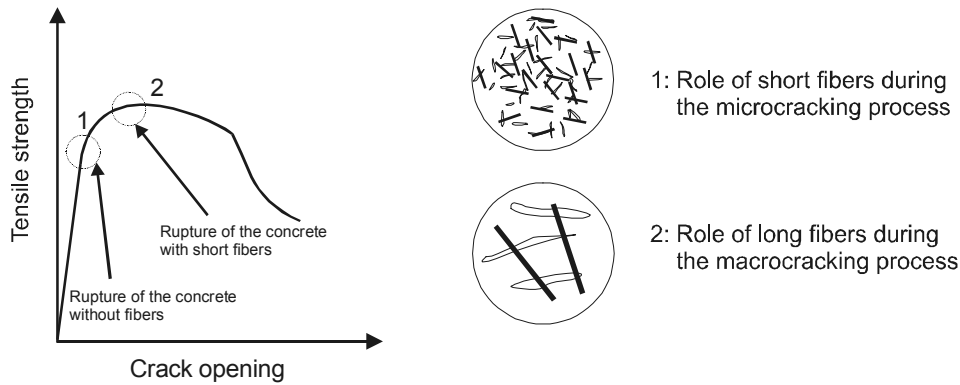
Figure 1: The role of fibres in different stages of concrete tensile cracking [1]

2.3 Effects and mode of actions of fibres

As mentioned before the modes of functioning of the several fibres differ.

To increase the **ductility** and to improve the **fracture toughness** of the concrete the best effect can be achieved by fibre cocktails or steel fibres, in several cases by means of polypropylene fibres as well. Basic requirement to develop the full potency of the used fibres is a good embedding within the binder matrix. In consequence of the bond between fibre and surrounding matrix the resistance to fibre pull-out is given, whereby the fibre decreases the transferability of tensile stresses within the crack and great crack opening can be avoided, decelerated respectively. Thereby the bridging of the cracks is controlled by the fibre lengths. Due to the ductile material behaviour implicated by means of the fibres an abrupt and explosive failure of structural members can be avoided.

The best way to **increase** the **mechanical properties** is the addition of short plain steel fibres on condition of even distribution of these fibres within the matrix. To reach higher ultimate loads, microcracking has to be prevented and consequently the absorption of tensile stresses has to be increased. That means the function of the fibres is the prevention of intergrowth of microcracks and therefore the prevention of the development of macrocracking.

Regarding the grain size of UHPC and the geometry (diameter, length) of short steel fibres, these fibres fit excellent into the concrete structure and therefore optimum conditions concerning an even fibre distribution and 3-dimensional fibre orientation are given. Thus the structure of the uncracked concrete will be improved. The fine distributed fibres absorb stresses developing at the crack tip by which the inner crack propagation will be minimised and the structure will be stabilised. Therefore the advantage by using short steel fibres is the improvement of tensile and compressive strength.

Another important reason to use fibre reinforced concrete is the improvement of the **durability**. This change of material behaviour may be achieved by polypropylene fibres. The principle is based on the fact that during the production of the concrete water molecules accumulate to the surface of the fibre. Therefore the evaporation of water at young concrete will be reduced and consequently the crack widths, shrinkage cracks especially, will be reduced too. The advantage of using polypropylene fibres is reflected in a decreased early shrinkage and a better durability to water penetration.

The **fire resistance** may be increased by addition of polypropylene fibres or fibre cocktails. In the case of fire the concrete warms and the water vapour developing by heating the water which is not hydrated, wants to escape by capillary pores. However, UHPC well known for the high impermeability is characterised by the very low proportion of capillary pores and therefore the water vapour can not escape and water vapour pressure builds up resulting in flaking of the surface of the concrete. Polypropylene fibres have the property to melt by temperatures of approximately 160°C. That implies that in the event of fire polypropylene fibres produce a channel system. Thus liquid and steam can expand into these pores and the water vapour pressure can relax. By the use of polypropylene fibres explosive flaking can be limited and the flaking depths can be reduced [2].

3   Experiment

By the realization of the experiments we aimed to investigate the improvement of the ductility of ultra-high performance concrete by application of short high strength steel fibres on the one hand and long normal strength steel fibres on the other hand. Referring to this the influence of fibre volume fraction, fibre length and concrete composition on the flexural strength and the post fracture behaviour was analysed. Furthermore, the influence of specimen geometry on the mechanical properties was reviewed.

In the first test series the influence of the fibre volume fraction and the maximum grain size was investigated. These experiments were carried out on ultra-high performance concrete without (C-RPC - reactive powder concrete) and with coarse aggregates (C-UHPC). The maximum grain size of C-RPC was 0.8 mm and 5 mm with C-UHPC. High strength steel fibres, 13 mm long and 0.16 mm in diameter, were used. The fibre volume fraction was 0, 1, and 2 Vol.-%. All concretes were compacted by a poker vibrator. The second test series was performed on self-compacting RPC (S-RPC), which had almost the same proportion as the RPC of the first series. The concrete for this series was not mixed in a laboratory mixer, but in a dual shaft mixer with the capacity of 2.5 m³ in a concrete plant. The fibre volume fraction with S-RPC was 0 and 2 Vol.-%, whereas the fibre reinforced concrete contained a fibre cocktail of 1 Vol.-% short and 1 Vol.-% long steel fibres mentioned above. On the basis of similar proportions of C-RPC and S-RPC, the results of both series could be compared with one another, especially the effects of the fibre mix of short and long fibres on the concrete properties.

The fracture surface and some special areas of the fibre were observed with an ESEM (Environmental Scanning Electron Microscope).

3.1   Concrete composition

In both concretes of the first test series the powder was composed of ordinary Portland cement CEM I 42.5 R, grey silica fume and quartz powder. The fineness of this quartz powder is between the silica fume and the cement and was used as a micro filler to optimise the packing density of the powder mixture. According to the suggestions in [3] coarse aggregate was eliminated in C-RPC (see Table 1). Only quartz sand in the range of 0.3 to 0.8 mm was used as aggregate. With C-UHPC also quartz sand was used and basalt splits with particles from 1 to 3 and 2 to 5 mm as coarse aggregate in addition. Superplasticizer

(SP) on the basis of polycarboxylateether ensured the flowability of the investigated compacted UHPC.

In contrast to the first test series the powder of the self compacting RPC of the second test series was composed of Portland cement CEM I 42.5 R, white silica fume and the same quartz powder. Anymore, the superplasticizer was different.

Table 1 Proportion of compacted / self compacting UHPC with and without coarse aggregates

Materials	C-RPC[1]	C-UHPC[2]	S-RPC[3]
Cement CEM I 42.5 R (c)	1,00	1,00	1,00
Water to cement ratio (w/c)	0,27	0,29	0,27
Water to binder ratio (w/b)	0,21	0,24	0,21
Volumetric water to powder ratio	0,43	0,47	0,43
Quartz sand (0.3-0.8 mm)	1,54	0,81	1,54
Basalt split (1-3 mm)	0,0	1,13	0,0
Basalt split (2-5 mm)	0,0	0,79	0,0

[1] Compacted – Reactive Powder Concrete
[2] Compacted – Ultra High Performance Concrete
[3] Self compacting – Reactive Powder Concrete (ready-mixed concrete)

3.2 Properties of fresh Concrete

The consistency of all fresh UHPC was evaluated with the slump flow test [4], executed immediately after mixing. It was observed that in UHPC without coarse aggregate (RPC) the incorporation of steel fibres had no significant influence on the consistency, while in UHPC with coarse aggregates the slump flow decreased for about 10 cm (Table 2).

Table 2 Properties of fresh concrete

	Containing fibres [Vol.-%]	Slump flow [mm]
Without coarse aggregate	0	530 / 830[1]
(RPC)	1	560
	2	560
	2 (Mix)	770[1]
With coarse aggregate	0	600
(UHPC)	1	540
	2	500

[1] ready-mixed concrete

3.3 Properties of hardened concrete

3.3.1 Compressive Strength and Splitting Tensile Strength

The dependence of the compressive strength (f_c) on the specimen geometry was determined on specimens with the following four geometries:

- Prisms, b/h/l = 4/4/16 cm³,
- Cubes, b/h/l = 10/10/10 cm³,
- Cylinder, Ø = 10 cm, h = 30 cm,
- Cylinder, Ø = 15 cm, h = 30 cm.

The splitting tensile strength was tested on 15x15x15 cm³ cubes.

The compressive strength and the splitting tensile strength were tested at the same concrete age. In Tables 3 to 5 the compressive strength, the vibrating method, the specimen geometry, as well as the fibre volume fraction was combined. Also the increase in compressive strength was tabled.

Table 3 Compacted RPC: Compressive (f_c) and splitting tensile strength (f_{tk})

Specimen geometry [cm]		Fibre concentration		
		0 Vol.-%	1 Vol.-%	2 Vol.-%
Cube, b/h/l = 10/10/10	f_c [N/mm²]	144	150	160
	increase	---	4,2%	11,0%
Cylinder, Ø = 15, h = 30	f_c [N/mm²]	138	148	154
	increase	---	7,7%	11,5%
Cylinder, Ø = 10, h = 30	f_c [N/mm²]	123	133	134
	increase	---	7,6%	9,0%
Prism, b/h/l = 4/4/16	f_c [N/mm²]	128	160	188
	increase	---	24,6%	46,6%
Cube, b/h/l = 15/15/15	f_{tk} [N/mm²]	8,3	11,4	12,1
	increase	---	37,4%	45,8%

Table 4 Compacted UHPC: compressive (f_c) and splitting tensile strength (f_{tk})

Specimen geometry [cm]		Fibre concentration		
		0 Vol.-%	1 Vol.-%	2 Vol.-%
Cube, b/h/l = 10/10/10	f_c [N/mm²]	137	142	151
	increase	---	4,3%	10,8%
Cylinder, Ø = 15, h = 30	f_c [N/mm²]	129	132	129
	increase	---	2,6%	0 %
Cylinder, Ø = 10, h = 30	f_c [N/mm²]	109	126	129
	increase	---	15,8%	18,6%
Prism, b/h/l = 4/4/16	f_c [N/mm²]	130	152	165
	increase	---	17,2%	26,8%
Cube, b/h/l = 15/15/15	f_{tk} [N/mm²]	9,1	10,0	11,5
	increase	---	9,9%	26,4%

Table 5 Self compacting RPC: compressive strength (f_c)

Specimen geometry [cm]		Fibre concentration	
		0 Vol.-%	2 Vol.-% (Mix)
Cube, b/h/l = 10/10/10	f_c [N/mm²]	160	160
	increase	---	0%
Cylinder, Ø = 15, h = 30	f_c [N/mm²]	162	144
	increase	---	-11,6%
Prism, b/h/l = 4/4/16	f_c [N/mm²]	154	181
	increase	---	17,6%

Regarding the fibre volume fraction it was observed that with increasing fibre proportion the compressive strength of the investigated compacted concretes increases with each specimen geometry, especially in case of prisms, with self compacting concrete just in case of prisms. Furthermore the variation of the compressive strength of vibrated concretes is stronger than that one of self-compacting concrete.

By analysing the fibre reinforced concretes, the highest compressive strength was obtained on the smallest specimen (here prism). Concerning the size effect the decrease in compressive strength with increasing slenderness was only observed on vibrated specimens. In the case of self-compacting concrete the influence of specimen slenderness can be ignored.

3.3.2 Flexural strength

The Flexural strength of the concretes was ascertained by 3-point or 4-point bending tests with beams of the following geometries:

- Three-point bending test, b/h/l = 4/4/16 cm³,
- Four-point bending test, b/h/l = 10/10/50 cm³ (see Figure 2a),
- Four-point bending test, b/h/l = 15/15/70 cm³ (see Figure 2b).
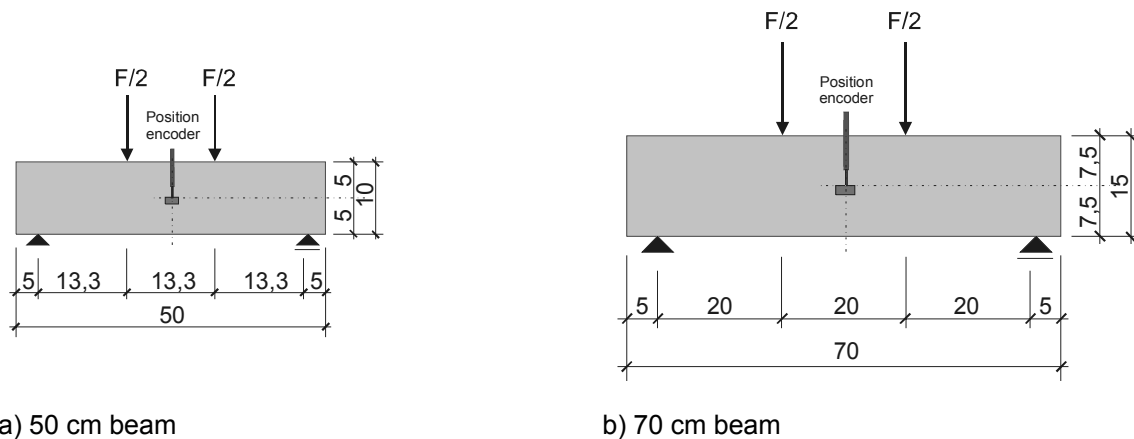

a) 50 cm beam   b) 70 cm beam

Figure 2: Four-point bending test

In case of 4-point bending tests the loading rate was controlled by the displacement, 0.2 mm/min following [5]. The deflection was recorded with LVDT located on opposite sides of the tested beam.

The plain concrete failed abruptly at the end of linearity. With the increase of the fibre volume fraction the flexural strength increased almost proportionally. In the case of RPC we can establish that the higher the fibre volume fraction, the greater the influence of specimen geometry on the flexural strength. For example, the flexural strength of fibre free concrete was almost the same independent of the specimen geometry, while at 2 Vol.-% fibre content the increase of the flexural strength obtained on prisms was up to tree times higher than that obtained on large 15x15x70cm beams (Tables 6 to 8). This may result from the obviously stronger fibre orientation in the smaller prism. With UHPC this establishment can not be reflected.

Table 6 Compacted RPC: flexural strength ($f_{ct,fl}$)

Specimen geometry [cm]		Fibre concentration		
		0 Vol.-% (C-RPC-0%)	1 Vol.-% (C-RPC-1,0%)	2 Vol.-% (C-RPC-2,0%)
Beam, b/h/l = 15/15/70	$f_{ct,fl}$ [N/mm²]	10,6	11,9	13,0
	increase	---	12,3%	22,6%
Beam, b/h/l = 10/10/50	$f_{ct,fl}$ [N/mm²]	9,8	11,2	14,7
	increase	---	14,3%	50,0%
Prism, b/h/l = 4/4/16	$f_{ct,fl}$ [N/mm²]	9,9	11,6	18,3
	increase	---	17,2%	84,9%

Table 7 Compacted UHPC: flexural strength ($f_{ct,fl}$)

Specimen geometry [cm]		Fibre concentration		
		0 Vol.-% (C-UHPC-0%)	1 Vol.-% (C-UHPC-1,0%)	2 Vol.-% (C-UHPC-2,0%)
Beam, b/h/l = 15/15/70	$f_{ct,fl}$ [N/mm²]	7,1	8,1	9,9
	increase	---	14,1%	39,4%
Beam, b/h/l = 10/10/50	$f_{ct,fl}$ [N/mm²]	7,7	9,2	9,8
	increase	---	19,5%	27,3%
Prism, b/h/l = 4/4/16	$f_{ct,fl}$ [N/mm²]	12,2	11,9	14,1
	increase	---	-2,5%	15,6%

Table 8 Self compacting RPC: flexural strength ($f_{ct,fl}$)

Specimen geometry [cm]		Fibre concentration	
		0 Vol.-% (S-RPC-0%)	2 Vol.-% (Mix) (S-RPC-Mix)
Beam, b/h/l = 15/15/70	$f_{ct,fl}$ [N/mm²]	9,0	12,1
	increase	---	34,6%
Beam, b/h/l = 10/10/50	$f_{ct,fl}$ [N/mm²]	9,4	16,4
	increase	---	73,9%
Prism, b/h/l = 4/4/16	$f_{ct,fl}$ [N/mm²]	9,6	21,3
	increase	---	122,3%

Regarding the post crack behaviour, ductile material behaviour was observed till at a fibre volume fraction of 2 Vol.-%. The combination of the short high strength steel fibres with the long normal strength steel fibres at this concentration affected the post fracture behaviour quite positively. The suspected deterioration of the workability due to the incorporation of long steel fibres was not observed. At corresponding fibre content, the results of the smaller beams (10/10/50 cm) indicate a slightly higher ductility than that one of the bigger ones (15/15/70 cm). This phenomenon can also be explained with the relative stronger fibre orientation within the smaller specimen. The fracture behaviour of the concrete with coarse aggregates (UHPC) is similar to that ones without coarse aggregates (RPC), whereas the load displacement curve of the UHPC points out the clearly steeper descending branch.
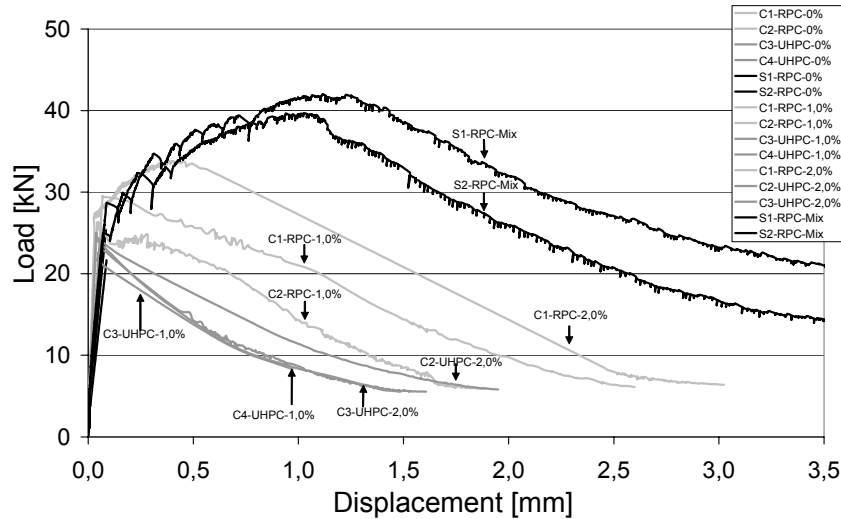
Figure 3: Deformation behaviour of beams 50 cm; compacted RPC (C_-RPC-_%), compacted UHPC (C_-UHPC-_%), self-compacted RPC (S_-RPC-_%)
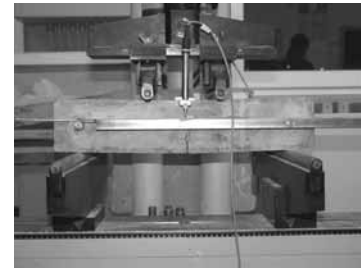
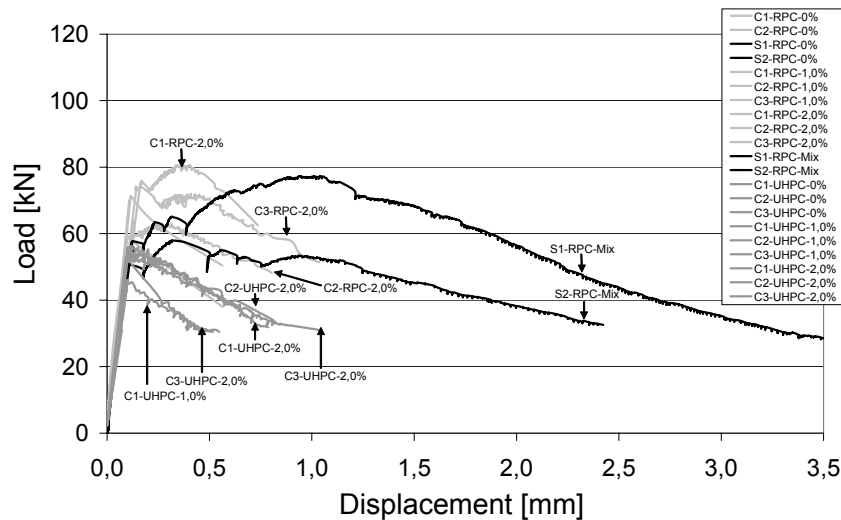Figure 4: S1-RPC-Mix, beam 50 cm

Figure 5: Deformation behaviour of beams 70 cm; compacted RPC (C_-RPC-_%), compacted UHPC (C_-UHPC-_%), self-compacted RPC (S_-RPC-_%)
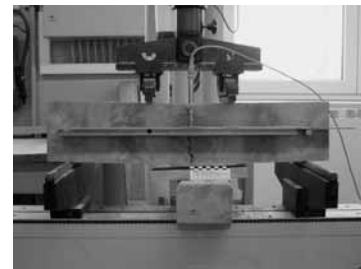
Figure 6: S1-RPC-Mix, beam 70 cm

If we focus the failure mode it was shown that at the fibre volume fraction of 1 Vol.-% the concretes failed quite brittle. The failure was controlled by a single vertical crack. At the fibre volume fraction of 2 Vol.-% the failure was characterized with a main vertical crack and many small cracks (see Figures 3 to 6).
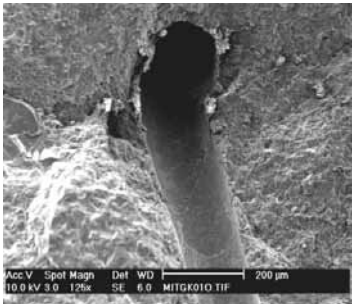
3.4 Microscopy

By developing a crack with increasing tensile stress, fibres bridging the crack flanks take part in the load transfer and will be pulled out. In normal strength concrete fibres are usually pulled out without any concrete residue on their surface. By means of some specimens from the crack surface of our tested bending beams the fibres were analysed microscopically. Some what different from the fibres embedded in conventional concrete, concrete residues

on the fibres pulled out from ultra-high performance concrete could be ascertained. This indicates a good bond between matrix and fibre with UHPC/RPC and therefore the fibre reinforced UHPC/RPC has the potency to transfer higher stresses between the crack flanks. The ESEM-Image in Figure 7a shows the good matrix/aggregate bond in UHPC. Just caused by differences in the shrinkage behaviour of matrix and aggregates the microstructure show interferences within the interfacial transition zone of the matrix and the coarse aggregate by a crack of about 0.1 µm. With the inspection of the fracture surface it was shown that the stressed fibres didn't crack, they were pulled out. Figure 7b shows the surface of the channel of a fibre pulled out from the UHPC. An example of the concrete residue on the fibre surface mentioned above can be seen in Figure 7c.
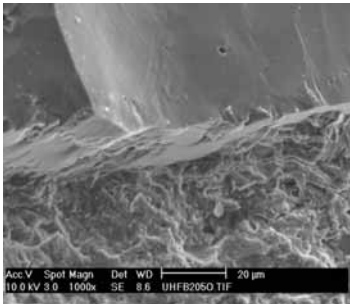
a) bond between matrix and aggregate

b) fibre pulled out from UHPC
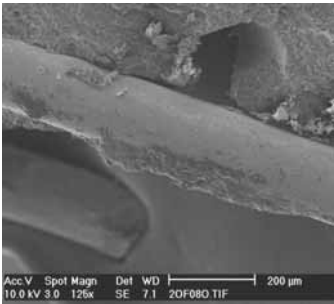
c) concrete residue on the fibre surface

Figure 7:   Microscopy

Conclusion

The paper presents the influence of the short and long steel fibres in respect of ductility and size effect on the mechanical properties of ultra-high performance concrete. Experiments were carried out on specimens with different geometries. The influence of steel fibres was evaluated with the flexural strength and the post crack behaviour. The characteristics of the internal transition zone between matrix and fibre were documented with the ESEM-Image.

It was observed, that highest compressive and flexural strength was obtained on smallest specimens (prism). In vibrated concrete the compressive strength decreased with the increase of the specimen slenderness. This phenomenon was not observed in self-compacting ultra-high performance concrete.

The flexural strength of ultra-high performance concrete without coarse aggregates is higher than that of ultra-high performance concrete with coarse aggregates. Flexural strength increased almost proportionally with the increase of the fibre volume fraction. Ductile post fracture behaviour was observed till at the fibre volume fraction of 2 Vol.-%, especially with the use of the fibre cocktail composed of 1 Vol.-% short fibres and 1 Vol.-% long fibres.

4   References

[1]   Rossi, P.: Ultra-High-Performance – A French perspective on approaches used to produce high-strength, ductile fiber reinforced concrete. In: Concrete International, pp. 46-52, 12. 2001.

[2]   Hertel, C.; Orgass, M.; Dehn, F.: „Brandschutztechnische Aspekte bei Faserbeton", In: Innovationen im Bauwesen-Faserbeton, Bauwerk-Verlag, Berlin 11.2002.

[3]   Richard, P.; Cheyrezy, M.: Composition of reactive powder concrete. In: Cement and Concrete Research 25, No. 7, S. 1501-1511, 1995.

[4]   DAfStb-Richtlinie: „Selbstverdichtender Beton", Beuth-Verlag, Berlin 11.2003.

[5]   Deutscher Beton-Verein e.V.: DBV-Merkblatt „Stahlfaserbeton", Wiesbaden, 10.2001.

Gözde Güvensoy
Istanbul Technical University
Istanbul, Turkey

Fikret Bayramov
Istanbul Technical University
Istanbul, Turkey

Alper Ilki
Istanbul Technical University
Istanbul, Turkey

Cengiz Sengül
Istanbul Technical University
Istanbul, Turkey

Mehmet Ali Tasdemir
Istanbul Technical University
Istanbul, Turkey

A. Necip Kocatürk
Iston Concrete Products and Ready Mixed Concrete Company
Istanbul, Turkey

Mehmet Yerlikaya
Beksa Steel Cord Industry and Trading Company
Kocaeli, Turkey

Mechanical Behavior of High Performance Steel Fiber Reinforced Cementitious Composites under Cyclic Loading Condition

Summary

Within the past five years, High Performance steel Fiber Reinforced Cementitious Composites (HPFRCCs) which have compressive strengths over 200 MPa have been developed by the authors of this work. These high performance concretes allow remarkable flexural strength and very high ductility. Under cyclic loading conditions, there is no significant loss in the initial compliance of HPFRCCs, the slopes of the unloading-reloading loops are almost the same as the slope of the initial ascending part of the load-deflection curve. Although the residual strength decreases gradually after the peak stress in HPFRCCs, the stiffness degradation is not significant under cyclic loading condition.

Keywords: *steel fibres, reactive powder concrete, fracture energy, cyclic loading, focal point*

1 Introduction

The high performance cement based composites, so called RPCs have been first developed in the early 1990's by the researchers at the laboratories of Bouygues in Paris. RPCs represent a new generation of concretes with cube strengths between 200 and 800 MPa, the tensile strengths between 25 and 150 MPa, and unit weights of 2500 – 3000 kg/m^3. The fracture energy of these materials can reach up to 40000 J/m^2, as compared to 100 to 150 J/m^2 for ordinary concretes [1-4]. The fracture energies of RPCs, thus, are about 300 times that of normal strength concrete or even 1350 times for Slurry Infiltrated Fiber Reinforced Concrete (SIFCON) [5]. The RPC microstructure has a more compact particle arrangement

and is enhanced by the presence of the strongest cementitous hydrates as compared to high performance concrete (HPC). RPCs are produced by using very fine sand, cement, silica fume, superplasticizers, and short cut steel fibers. Their very low porosity gives them important durability and transport properties and makes them potentially suitable materials for storage of industrial wastes. These features are achieved by i) precise gradation of all particles in the mixture to yield a matrix with optimum density, ii) reducing the maximum size of the particles for the homogeneity of the concrete, iii) reducing the amount of water in the concrete, iv) extensive use of the pozzolanic properties of highly refined silica fume, v) optimum composition of all components, vi) the use of short cut steel fibers for ductility, vii) hardening under pressure and increased temperature, in order to reach very high strengths [1,4].

Since HPFRCCs have excellent impact resistance properties, they can be employed for; i) military structures, ii) strategic structures against earthquake, and iii) retrofitting of reinforced concrete structures. They are also used for small or medium size prefabricated elements. The main objective of this work is to determine fracture energies and strengths of these new generation HPFRCCs, and their mechanical behavior under cyclic loading condition.

2   Classification of Cementitious Composites

From the strength point of view, the classification of high strength concretes can be made as: i) normal strength concrete (NSC) up to grade 60 MPa, ii) high strength concrete (HSC), grades 60-90 MPa, iii) very high strength concrete (VHSC), grades 90-130 MPa, iv) reactive powder concrete (RPC), grades 200-800 MPa, and v) high performance lightweight concrete (HPLC) greater than 55 MPa [6].

From the mechanical behavior point of view, SFRCs can be divided into two categories based on their performances: i) conventional SFRCs, and ii) HPFRCCs such as RPCs. The conventional SFRCs exhibit ductile behavior compared to the brittle matrix, but their flexural and tensile strengths are not very high, and especially the compressive strengths of these materials do not practically change with the fiber volume fraction. The HPFRCCs, however, exhibit large strain hardening before peak stress, and their tensile and compressive strengths are very high compared to those of conventional SFRCs [7]. Ductile Fiber Reinforced Cementitious Composites (DFRCCs) show deflection hardening and multiple cracking in bending with significant ductility in tension and compression. DFRCC is a class of Fiber Reinforced Cementitious Composite (FRCC) that exhibits multiple cracking. Multiple cracking leads to improvement in properties such as ductility, toughness, fracture energy, and strain capacity under tension, compression, and bending. As seen in Figure 1, DFRCC is a broader class of materials than HPFRCC. FRCC includes the entire class of FRCCs, where DFRCC as well as other composites such as fiber reinforced concrete (FRC) and fiber reinforced mortar (FRM) are sub-sets. Engineered Cementitious Composites (ECCs), make up a particular type of HPFRCC, whose composition is optimized in a cost-effective way on the basis of micromechanics. ECC typically has a tensile strain capacity of greater than 3%.

Microstructure optimization limits the fiber content of ECC to be less than 2-3% [8]. HPFRCC also includes SIFCON and SIMCON (Slurry-Infiltrated Mat Concrete).
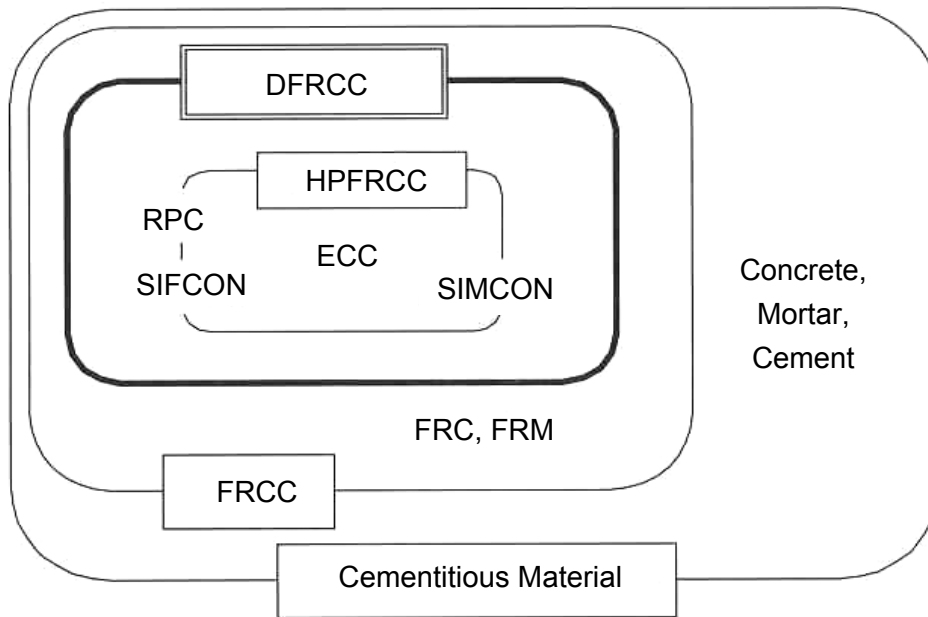

Figure 1:   Classification of cementitious composites [8]

3   Effect of Hot Curing on the Mechanical Properties of HPFRCCs

According to Ozyurt et al. [9], as shown in Figures 2 and 3, hot curing regime enhances the microstructure of HPFRCCs; as a result, the net bending strength and specific fracture energy can be greatly improved by curing at high temperature. It is also shown that high temperature curing regime activates pozzolanic reaction in HPFRCCs resulting in reduced curing period [9].
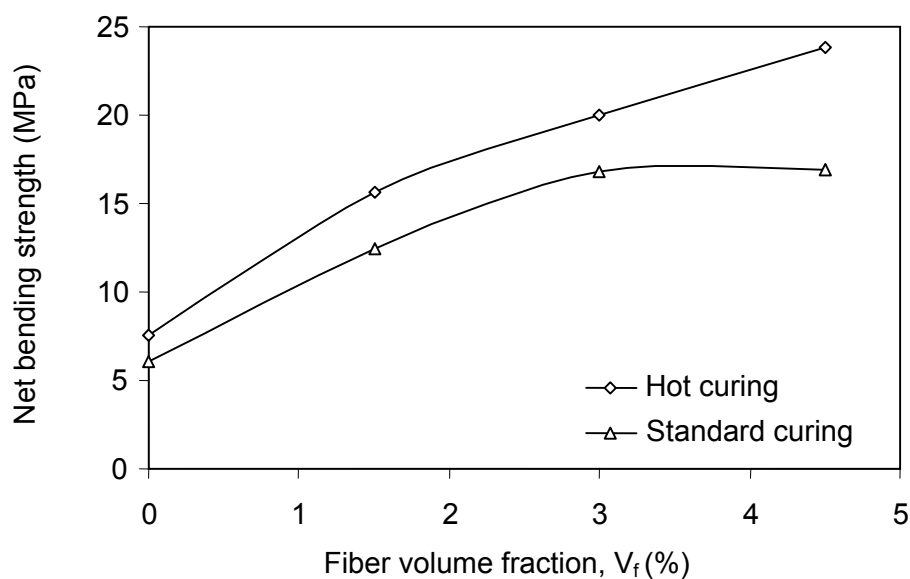

Figure 2:   Effects of fiber volume fractions and curing conditions on net bending strength [9]
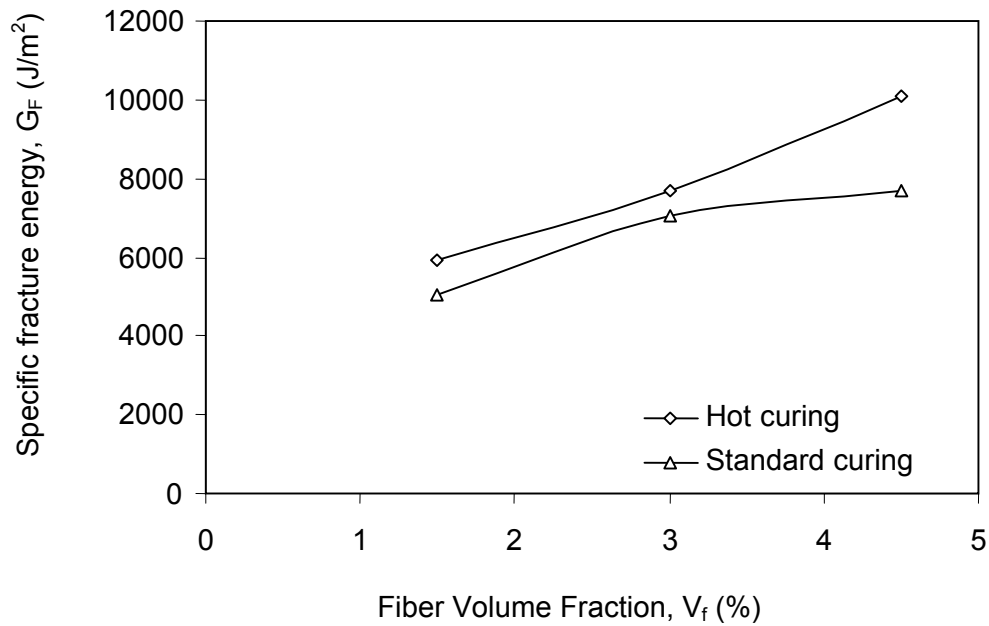
Figure 3: Effects of fiber volume fractions and curing conditions on specific fracture energy [9]

4 Experimental Work

4.1 Materials and Mix Proportions

Five HPFRCC mixtures were cast for this investigation. Cement used was ordinary Portland cement with a density of 3.17 g/cm^3. Silica fume was used in the amount of 25 % of the cement by weight. Silica fume was grey-blue colored and very fine-grained with a specific area of 22130 cm^2/g. Siliceous sands (sand 1: 0-0.5 mm and sand 2: 0-0.25 mm), sea sand (sand 3: 0-0.25 mm), and round siliceous sea sand (sand 4: 0-2 mm) were used as aggregate; their densities were 2.65, 2.63, and 2.65, respectively. Straight, short cut and brass coated steel fibers (OL 6/15) commercially available from Beksa were used. Aspect ratio (L/d=length/diameter) of steel fibers was 40 (i.e., L=6 mm and d=0.15 mm). The density and tensile strength of the steel fibers were 7.85 g/cm^3 and 2250 N/mm^2, respectively. The volume fractions of steel fibers were varied between 5.0 % and 7.8 %. HPFRCC mixtures produced that contain different aggregate type were coded as M1, M2, M3, M4, and M5 as shown in Table 1. Three types of high-range water reducing admixture (HRWRA) were used; HRWRA 1 in M2, M3, and M5 mixtures, HRWRA 2 in M1 mixture, and HRWRA 3 in M4 mixture. The aim of producing trial mixtures (M1, M2, M3, and M4) was to obtain a compressive strength over 200 MPa. In all mixtures, because the efficiency of HRWRA was low, over dosage was required. For reaching the target values of strength, cement and silica fume content were slightly increased, the water/binder ratio was decreased while the steel fiber content was significantly increased. Based on the fact that 60 % of the HRWRA is composed of water, water/cement and water/binder ratios were re-calculated and expressed with the names of total water/cement and total water/binder ratios. The details of the mixtures, mixture proportions and properties of fresh concretes are given in this table.

Table 1:   Mixture codes of the HPFRCCs

Mixture code/Aggregate type	M1	M2	M3	M4	M5
sand 1 (siliceous sand: 0-0.5 mm)	x	x	x	x	-
sand 2 (siliceous sand: 0-0.25 mm)	x	x	x	x	x
sand 3 (sea sand: 0-0.25 mm)	-	x	x	x	-
sand 4 (round siliceous sea sand: 0-2 mm)	-	-	-	-	x

Table 2:   Mix proportions and properties of fresh concretes

		M1	M2	M3	M4	M5
cement	kg/m^3	945	889	839	865	1015
silica fume	kg/m^3	236	222	210	217	254
sand 1 (siliceous sand: 0-0.5 mm)	kg/m^3	331	311	182	146	-
sand 2 (siliceous sand: 0-0.25 mm)	kg/m^3	331	222	297	319	345
sand 3 (sea sand: 0-0.25 mm)	kg/m^3	-	89	242	319	-
sand 4 (round siliceous sea sand: 0-2 mm)	kg/m^3	-	-	-	-	230
HRWRA 1	kg/m^3	-	85	131	-	99
HRWRA 2	kg/m^3	86	-	-	-	-
HRWRA 3	kg/m^3	-	-	-	96	-
water	kg/m^3	211	273	181	184	228
steel fiber (OL 6/15)	kg/m^3	444	418	394	428	609
	(%)	(5.7)	(5.3)	(5.0)	(5.4)	(7.8)
water / cement		0.22	0.31	0.22	0.21	0.22
total water / cement		0.28	0.36	0.31	0.28	0.28
water/ binder		0.18	0.25	0.17	0.17	0.18
total water / binder		0.22	0.29	0.24	0.22	0.23
unit weight	kg/m^3	2584	2509	2476	2574	2780

4.2   Specimen Preparation

In mixing, cement, silica fume, siliceous sands, sea sand and round siliceous sea sand were blended first in dry condition. Half of the high-range water reducing admixture and of the water were mixed in a pan and added to the mixture. The remaining of the high-range water reducing admixture and the water were added to the mixture gradually to provide homogeneity in the mixture. Steel fibers were scattered in the mixture and carefully mixed to achieve a uniform distribution. The specimens were cast in steel moulds and compacted on a vibration table. All the specimens were demoulded after about 24 hours, stored in water saturated with lime, at 20 ± 2^0C until 7 days of age. Then, hot water curing was applied to the specimens at 90 ± 2^0C for 2 days. After thermal treatment, all the specimens were restored in water saturated with lime at 20 ± 2^0C until 28 days of age. At least three beam specimens were prepared for the fracture energy tests in the dimension of 280 mm in length and 70x70

mm in cross section. For compressive tests, it was aimed to use the broken parts of the beams, 70 x 70 mm in cross section, after completion of the bending tests.

4.3 Test Procedure

For all the beams, the tests for the determination of the fracture energy (G_F) were performed according to the recommendation of RILEM 50-FMC Technical Committee [10]. The effective cross section, however, was reduced to 42x70mm by sawing. The notched beam specimen tested is shown in Figure 4. HPFRCC beam specimens were tested at the loading rate of 0.075 mm/min up to a deflection of 0.5 mm, and then at 0.25 mm/min up to a 10 mm deflection. As schematically seen in Figure 4, the deflections were measured simultaneously by using a linear variable displacement transducer (LVDT). The load was applied by Instron 5500 R closed-loop testing machine of 100 kN capacity. The load versus mid span deflection curve for each specimen was obtained by recording the measurement taken at the mid span. The load-deflection curves were used for evaluating the fracture energy. The area under the load versus deflection at mid span curve (W_0) was described as a measure of the fracture energy of the material.
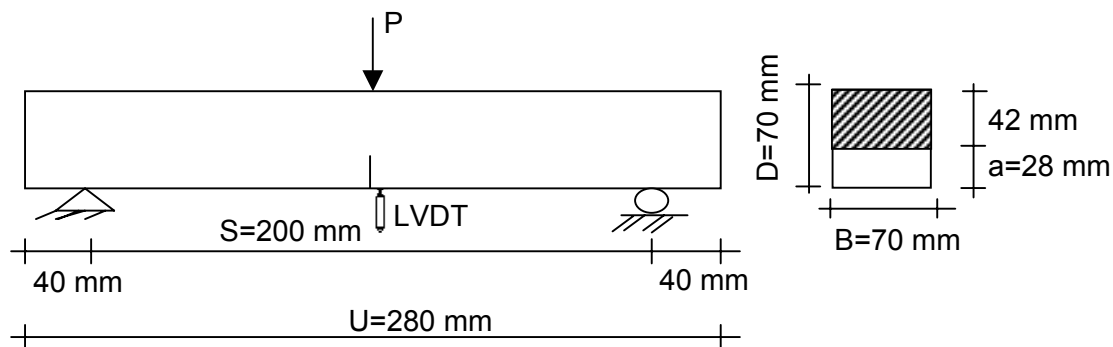

Figure 4: Schematic representation of the test setup

The results obtained here are based on the area under the complete load-deflection curve up to a specified deflection. This cut-off point was chosen as 10 mm deflection. It is seen from the schematic curve that, the energy at this specified deflection (i.e. 10 mm), however, is not totally dissipated. This property was determined using the following expression [10]:

$$G_F = \frac{W_0 + mg\frac{S}{U}\delta_s}{B(D-a)}$$

(1)

Here, B, D, a, S, U, and m are the width, depth, notch depth, span, length, and mass of the beam, respectively. W_0 is the area under the load-mid span deflection curve, which is shown in the inset of Figure 5. g is the gravitational acceleration and δ_s is the specified deflection of the beam (i.e. 10 mm).

654

4.4 Experimental Results

The experimental results are shown in Table 3. As seen in the table, the addition of steel fibers results in net bending strengths ranging from 22 to 54 MPa, splitting tensile strengths from 21 to 38 MPa, compressive strengths from 117 to 220 MPa, and fracture energies from 8560 J/m^2 to 23500 J/m^2. Figure 5 shows the mechanical behavior of a conventional mortar, conventional SFRC, and HPFRCC under three point monotonic bending test. The measured average fracture energy was 23500 J/m^2 for HPFRCC and 108 J/m^2 for the conventional mortar [11]. It can be concluded that the fracture energy of HPFRCC is almost 220 times that of the conventional mortar.

Table 3:   Mechanical properties of HPFRCCs

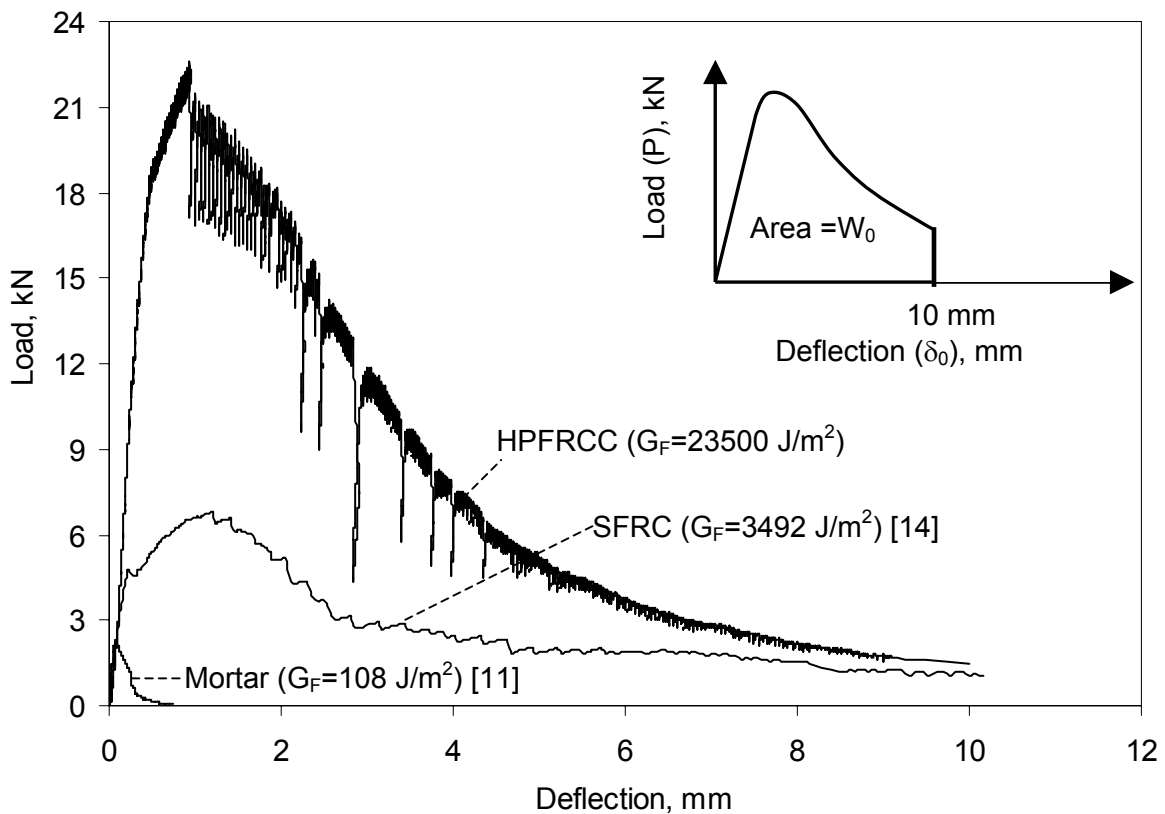| Mechanical properties		M1	M2	M3	M4	M5
compressive strength, f_c	MPa	162	156	117	146	220
net bending strength, f_{net}	MPa	54	49	30	22	37
splitting tensile strength, f_{st}	MPa	30	24	20	21	38
fracture energy, G_F	J/m^2	23500	18740	9840	8560	17220

Figure 5:   Comparison of the load-mid span deflection curves of HPFRCC (for mixture M1), SFRC and conventional mortar

4.4.1 Degradation Properties

The determination of a unique focal point of stiffness degradation in concrete has been defined by Lee et al. [12] for compression, and used by Tasdemir et al. [13] for three point bending, as shown in Figure 6. In the later one, the first three unloading-reloading cycles has been used to locate the focal point; when the postpeak load dropped to about 40 percent of the maximum value, further cycles proved to be inappropriate to use. The normalized stiffness as a measure of degradation of stiffness and the focal point had been determined by Tasdemir et al. [13] using unloading-reloading cycles, in both the load-Crack Mouth Opening Displacement (CMOD) and the load-deflection curves. The normalized stiffness had been correlated to the normalized local fracture energy, to the normalized permanent CMOD and δ, and to the normalized load (strength degradation). Thus, the focal point has been employed as a measure of concrete brittleness.
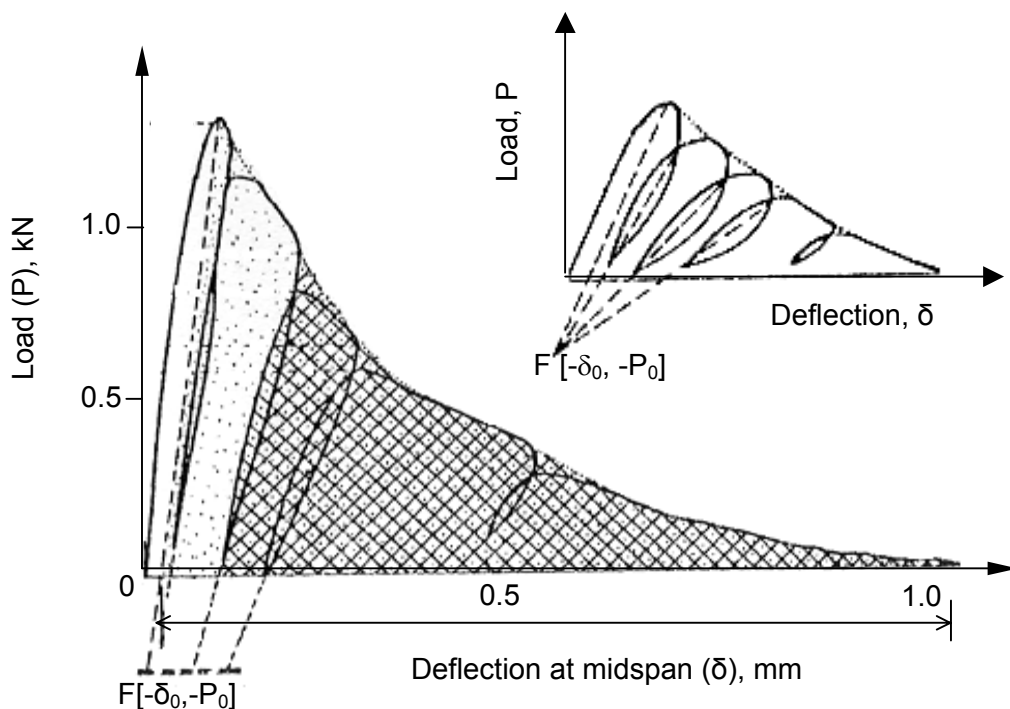

Figure 6: Typical results of unloading-reloading cycles for a plain concrete beam [13]

Figure 7 shows load-mid span deflection curves obtained from the bending tests under cyclic loading on HPFRCC beams. As seen in the figure, there is no significant loss in the initial compliance of HPFRCCs, the slopes of the unloading-reloading loops are almost same as the slope of the initial ascending part of the load-deflection curve. This is an evidence of the ductility of HPFRCCs. Although, the residual strength decreases after the peak stress, stiffness degradation in HPFRCCs is not significant. Under cyclic actions, steel fibers efficiently bridge the cracks and no significant loss of stiffness is observed even when high levels of deflections are reached. As seen in the inset of Figure 7, similar results were obtained in conventional steel fiber reinforced concretes depending on the steel fiber volume fraction (V_f) and the aspect ratio (L/d) by Bayramov et al. [14], and also in steel fiber reinforced lightweight concretes depending on aggregate type by Campione et al. [15].
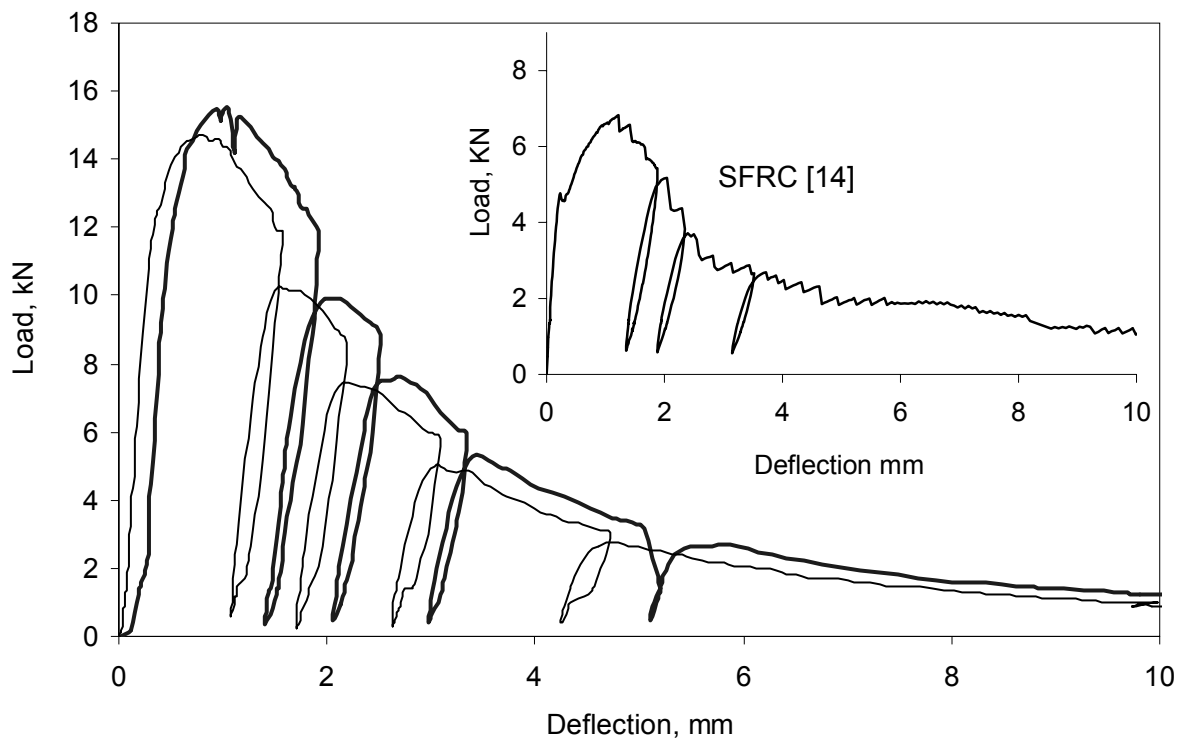
Figure 7:   Typical load-mid span deflection curves of HPFRCCs (mixture M5)

5   Seismic Retrofitting Non-Ductile Reinforced Concrete Columns

As a new technique for retrofitting damaged and/or understrength reinforced concrete beams, CARDIFRC® as a new high-performance class of materials developed at Cardiff University are physically and mechanically compatible with the material of the structure being retrofitted [16-19]. As a similar application, Ilki et al. [20] have investigated the behavior of non-ductile column confining zones with and without adequate lap splices using HPFRCC panels with mechanical characteristics close to M3. As seen in Figure 8, their specimens are composed of the upper half of a column of the lower story, the beam-column connection and the lower half of a column of the upper story. Longitudinal reinforcing bars of the 2 of the specimens were continuous, while the other 2 specimens had lap-splices of 40 times the diameter of longitudinal bars, opposing the fact that the lap-splice lengths should have been around 90 times the diameter of longitudinal bars considering the yield strength of plain bars and concrete quality. As seen in Figure 9, higher energy absorption and more stable hysteresis loops were recorded, despite of the insufficient transverse reinforcement in the confinement zone. It can be concluded that the investigated retrofitting technique significantly improved for both the strength and particularly the ductility. The details of the testing program, the retrofitting technique and the test results can be found in Reference 20.
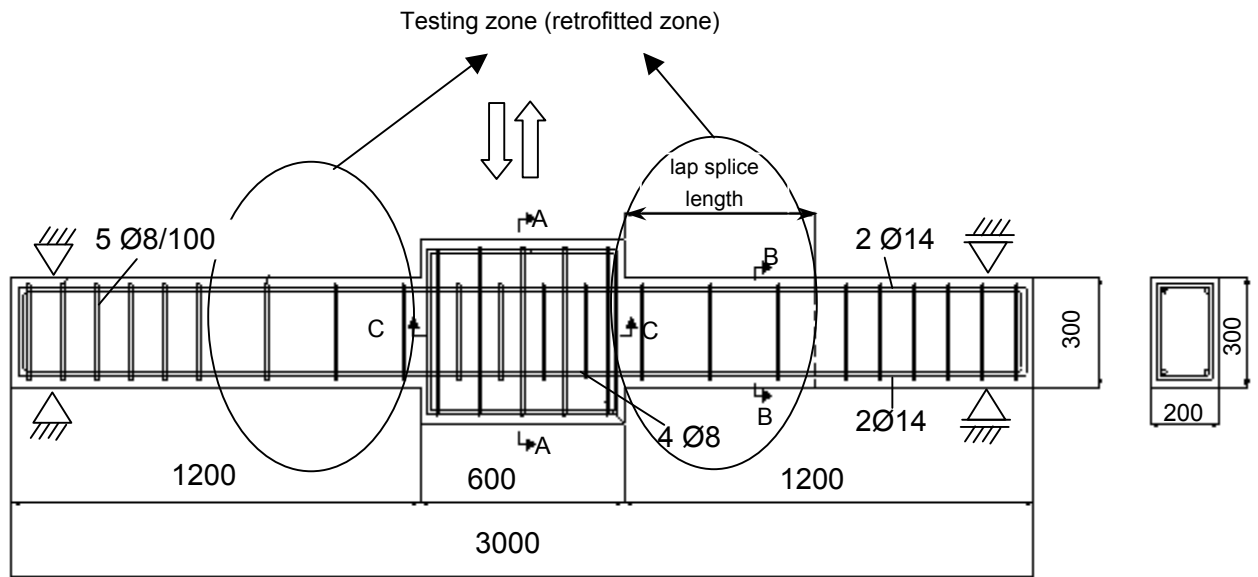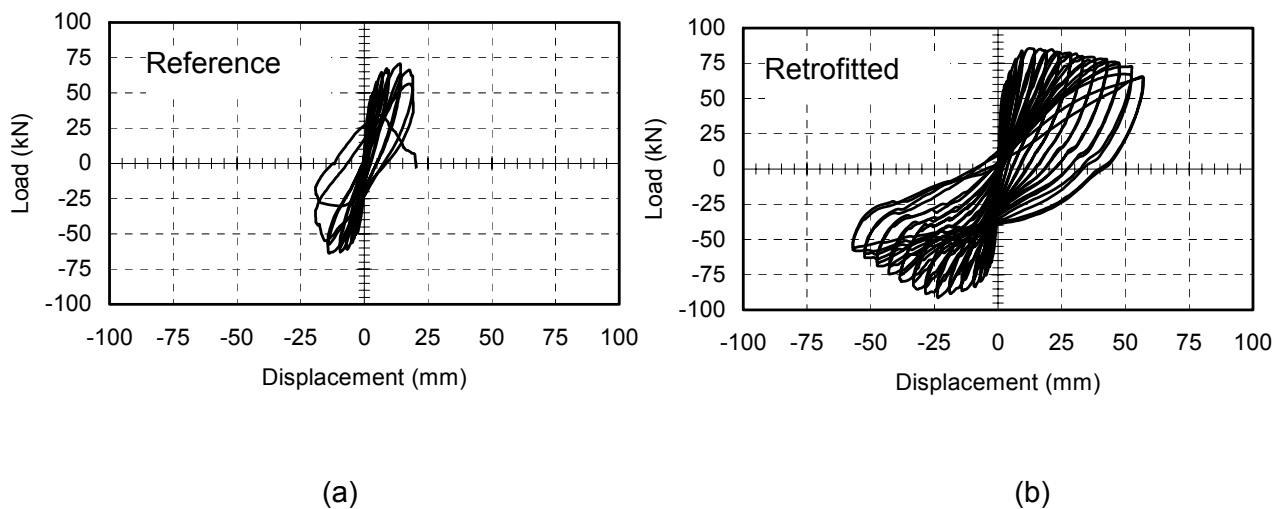
Figure 8: Reinforcing details of the specimen

(a)   (b)

Figure 9: Hysteresis loops of column-beam sub-assemblages under cyclic loading conditions: (a) Reference, and (b) Retrofitted

6   Conclusions

Based on the available data on HPFRCC, which is potentially suitable for being used in several applications the following conclusions can be drawn:

1. The fracture energy of HPFRCC is almost 220 times that of the conventional mortar and the compressive strength of this cementitious composites reaches up to 220 MPa.
2. There is no significant loss in the initial compliance of HPFRCCs, the slopes of the unloading-reloading loops are almost the same as the slope of the initial ascending part of the load-deflection curve.

3. In HSCs without steel fibers, the focal point defined can be taken as a measure of concrete brittleness. In HPFRCCs, however, this point is far from the origin or does not exist, in contrast to that of HSCs without steel fibers. Although, the residual strength decreases gradually after the peak stress in HPFRCCs, the stiffness degradation is not significant under cyclic loading condition.

4. A new retrofitting technique based on high performance fiber reinforced cementitious composites (HPFRCCs) with high tensile strength and high energy absorption capacity, which is designated as CARDIFRC$^®$s, has been developed at Cardiff University. HPFRCC overcomes some of the problems associated with the current techniques based on the externally bonded steel plates and FRP (Fiber Reinforced Polymer) laminates which arise due to mismatch between their tensile stiffness and strengths and those of the concrete structure being retrofitted. The potential application of these new generation cement based materials in retrofitting of concrete structures damaged by earthquakes or by unexpected loads will be a sufficient contribution. It is hopefully expected that the laboratory findings can be transferred to the engineering practice. On the other hand, these materials can be used at some strategic structures and also for building containers for industrial waste materials.

Acknowledgement

7   References

[1]   Richard, P.; Cheyrezy, M.: Reactive Powder Concrete, Bouygues Corporation, France, 1994.

[2]   Richard, P.; Cheyrezy, M.: Composition of reactive powder concrete. In: Cement and Concrete Research 25, No. 7, pp.1501-1511, 1995.

[3]   Dugat, J.; Roux, N.; Bernier, G.: Mechanical properties of Reactive Powder Concretes. In: Materials and Structures 29, pp.233-240, 1996.

[4]   Walraven, J.: Evolution of Concrete. In: Structural Concrete: Journal of fib, Vol. P1, No.1, pp.3-11, 1999.

[5]   Fritz, C.: Tensile testing of SIFCON. In: Proc. 1st International Workshop on HPFRCCs, June 23-26, Mainz, RILEM, Eds. H.W. Reinhardt and A.E. Naaman, pp. 518-528, 1991.

[6]   Kmita, A: A new generation of concrete in civil engineering. In: Journal of Materials Processing Technology 106, pp.80-86, 2000.

[7]   Alaee, F.J.: Retrofitting of concrete structures using High Performance Fiber Reinforced Cementitious Composite (HPFRCC). PhD Thesis, University of Wales, Cardiff, 2002.

[8]   JCI-DFRCC Committee: DFRCC terminology and application concepts. In: Journal of Advanced Concrete Technology 1, No.3, S. 335-340, 2003.

[9] Ozyurt, N.; Ilki, A.; Tasdemir, C.; Tasdemir, M.A.; Yerlikaya, M.: Mechanical behavior of high strength steel fiber reinforced concretes with various steel fiber contents. In: Proc. 5th International Congress on Advances in Civil Engineering, September 25-27, Istanbul Technical University, Istanbul, pp.885-894, 2002.

[10] RILEM Technical Committee 50-FMC: Determination of the fracture energy of mortar and concrete by means of three-point bend test on notched beams. In: Materials and Structures 18, No.106, pp.287-291, 1985.

[11] Aldikacti, K: Meso-mechanical modeling of hardened cement paste, mortar and concrete. MSc Thesis, Institute of Applied Sciences and Technology, Istanbul Technical University, Istanbul, 2004.

[12] Lee, Y.; Willam, K.; Kang, H.D.: Experimental observations of concrete behavior under uniaxial compression. In: Proc. FramCos-2, July 25-28, Vol.1: S.397-414, ETH Zurich, Switzerland, 1995.

[13] Tasdemir, C.; Tasdemir, M.A.; Mills, N.; Barr, B.I.G.; Lydon, F.D.: Combined effects of silica fume, aggregate type, and size on post peak response of concrete in bending. In: ACI Materials Journal 96, pp.74-83, 1999.

[14] Bayramov, F.; Ilki A.; Tasdemir, C.; Tasdemir, M.A.: An optimum design of steel fiber reinforced concretes under cyclic loading. In: Proc. FraMCos-5, April 12-16, Vol.2: pp.1121-1128, Vail, Colorado, 2004.

[15] Campione, G., Miraglia, N.; Papia, M.: Mechanical properties of steel fiber reinforced lightweight concrete with pumice stone or expanded clay aggregates. In: Materials and Structures 34, pp.201-210, 2001.

[16] Alaee, F.J.; Benson, S.D.P.; Karihaloo, B.L.: A new technique for retrofitting concrete structures. In: Proc. ICE, Structures and Buildings 152, pp. 309-318, 2002.

[17] Alaee, F.J; Benson, S.D.P.; Karihaloo, B.L.: High-performance cementitious composites for retrofitting. In: International Journal of Materials and Product Technology 17, No. 1/2, pp.17-31, 2002.

[18] Alaee, F.J.; Karihaloo, B.L.: Retrofitting RC beams with CARDIFRC. In: ASCE Journal of Composites for Construction 7, pp.174-186, 2003.

[19] Alaee, F.J.; Karihaloo, B.L.: Fracture model for flexural failure of RC beams retrofitted with CARDIFRC. In: ASCE Journal of Engineering Mechanics 129, pp.1028-1038, 2003.

[20] Ilki, A.; Yilmaz, E.; Demir, C.; Kumbasar, N.: Prefabricated SFRC jackets for seismic retrofit of non-ductile reinforced concrete columns. Accepted for publication in the Proceedings of the 13th World Conference on Earthquake Engineering, Vancouver, Canada, 2004.

A. Si-Larbi
Student
University Lyon 1
France

E. Ferrier,
Associate Profesor
University Lyon 1
France

P. Hamelin
Professor
University Lyon 1
France

Flexural behaviour of Ultra High Performance Concrete reinforced with mixed short fibers and CFRP rebars

Summary

The high performances fibers reinforced concretes (HPFRC) (compressive strength higher than 150 MPa) or the ultra-high performances fibers reinforced concretes (UHPFRC) have been developed these last years. These materials present a particular interest for the civil engineering because of their high mechanical properties in compression and because of their best durability (AFGC, [1]). The addition of metallic short fibers to this concrete permits to get a ductile material with increased properties in traction. The ductility of the material is the consequence of a micros and macros cracks fiber bridging (G. Chanvillard, [2]). Nevertheless the use of active or passive rebar is even necessary for structural applications (P. Rossi, [3]). Concerning structural applications, the main objective concerning the use of the HPFRC or UHPFRC is to lighten the structures, to increase the bearing capacity and the durability. Several structures made of prestressed concrete have been achieved thus, but the use of these concretes for steel reinforced applications is limited. Indeed the performances of the concrete in compression (4 times superior to the traditional building concrete) require the increase of the volume ratio of steel rebar. Because of the important diameter of these frameworks, beam mechanical hypothesis must be discussed : the section are plane and remains plane, the non slip of the framework from concrete, the influence of the concrete tensile properties.

On the other hand thanks to the progress achieved recently in the domain of composite materials, it is possible to assess high performance carbon armatures having mechanical properties in traction higher to the one of steel (1900 MPa). The use of these framework would permit to decrease the ratio of steel. The brittleness of these materials requires their use in combination with steel armatures in order to keep a structural ductility. The objective of this survey is to validate the main hypotheses of steel reinforced concrete beam, to

quantify the contribution of the short fibers reinforced concrete and to value the performance of mixed tense reinforcements: steel and composite carbon epoxy.

Keywords: *mixed materials, UHPC, CFRP rebars, High performance structures*

1 Introduction

The objectives are here to outline the possibility to design reinforced concrete beams using mixed steel-CFRP framework and ultra high performance fiber reinforced concrete (UHPFRC) material.

The UHPFRC find numerous applications in the civil engineering field in the cases of architectural elements (flat panels, urban equipment, or of specific works [5]) and of the prestressed structures [6]. The use of a concrete reinforced with short fibers permits to limit the steel rebars numbers used in usual reinforced concrete structure. For structure such as beams, ultra high performance concrete (UHPC) is used with steel prestresses concrete techniques in order to increase the compression level in concrete. The higher cost of the material associated to a complex manufactured method (application of prestressed), limit the development of such material.

The UHPFRC are manufactured with the same conditions to those of the classic concretes but with very small quantities of water (E/C=0.2 to 0.3). They constitute a family of materials whose performances vary according to their methods of manufacture. Numerous possible variants exist for the formulation of the UHPFRC. In any case, the principals constituent are the aggregates, the cement, the silica fume and superplasticizer. The different aggregates are subject of a rigorous selection that aims to optimise the homogeneity of the concrete [De Larrard, 2]. That permits to get high compression strength ranging from 100 to 150 MPa. According to the required applications, a thermal treatment or a pressure appllied during the cure, can permit to modulate the quality of the concrete according to the needs [Richard, 3]. However, in our study, we will limit ourselves to the UHPFRC without thermal treatment.

The main constituents modifications of the UHPFRC influence a significant way the behaviour law of the concrete. The stress-strain relation is linear until the peak stress, the module of elasticity of the concrete is increased of about 30 % compared to an usual concrete (Fig. 1). The yielding strain is nearly insignificant compared to the total strain, so one will note that the strain corresponding " to the peak stress" is a little less important than for a usual concrete. The UHPC tensile strength increases lesser that the compression strength. The ratio of the compression and tensile concrete is about a twentieth for the UHP concretes whereas the ratio is of 1/10 for the classic concretes.

The addition of 2% of short metallic fibers (10 mm) to this UHPC allows getting better mechanical properties and modifying in a significant way the post-peak behavior in tension. The fibers permit to get a ductile material both in tension and bending with improved tensile properties (superior in 10 MPa) and a bending behavior more ductile. This ductility of the material is the consequence of the bridging effect of the macros and micro concrete cracks already observed by many studies (G. Chanvillard, [4]). To summarize, metal fibres can modify both the tensile strength and the ductility.

662

 To reduce the cost, it is necessary to search for classical and technical solutions of reinforced concrete structure. The first studies carrying on reinforced concrete beams using UHPFRC exhibit the performances and the limits of these structures:

- firstly, the addition of metallic fibers to the concrete matrix permits to reduce and above all to eliminate the transverse stirrups [7].

- secondly the gains of performances are important.

- on the other hand, the tests of beams in UHPFRC "over reinforced by steel rebars" [8, 9], failed by concrete crushing in the compressed part with a brittle failure mode.

While reducing the quantity of tensile rebars, it is possible to get a ductile failure by steels yielding but with a weak level of compression of the top fiber (about 40% of the ultimate compression concrete strength). It does not permit to valorise the UHPFRC.

The development of this new kind of concrete for the structures made of reinforced concrete requires an optimisation of the design. It aims at getting "ductile" structures and to reach a level of strain to significant failure of the part compressed of the beam. In this objective, it is possible to use more efficient materials in tension that steel such as high strength CFRP. These rebars reinforcement obtain by pultrusion of carbon fibers in combination with epoxy matrix have very interesting mechanical properties just as well to the level of their rigidity (160 GPa) that of their ultimate strength (2500 MPa). The inconvenience of the carbon fibers for civil engineering structures is a brittle mechanical behavior. This behavior does not correspond to the mechanical behaviors of a steel reinforced concrete beam. Also the combination of CFRPs framework and steel rebars will permit to get a set of tensile longitudinal reinforcements more effective presenting a yielding mechanical behavior. The beams obtained finally present a ductile and safety behavior. The addition of short metallic fibers in the UHPC permits to remove the transverse steel rebars and contribute to the reduction of the cost of production of these structures.

In order to optimise the behavior of the beams in UHPFRC reinforced by mixed armatures, it is first necessary to identify the mechanical behavior of these structures and to compare them with reference beams made of usual reinforced concrete. In order to differentiate the effect of the rebar's material and the addition of short metallic fibers, we first design à UHPC beam reinforced by steel rebars. Then, the study of a UHPC reinforced by short metallic fibers permits to identify the influence of the fibers on the behavior of the structure. The following step corresponds to the introduction of mixed armatures with the aim to evaluate the relevance of this association.

The crack bridging effect by the short metallic fibers is especially studied opposite the normal and shear stress. Besides the modifications brought to the structural behavior by the use of steel-CFRP mixed armatures are commented. The criteria to evaluate the gains and the levels of performance of the multi-material beams are the analysis of the ultimate behavior (gains of load, mechanisms of failure…) and the moment-curvature response of the

structure. The variations of bending stiffness and the internal moments equilibrium is studied according to the nature of the beam's constituents.

2   Material and tests specimens description

2.1   Properties of the concrete high performance

The UHPFRC retain for this study is formulated by Lafarge®. The beams have been cast in moulds by the team of the Central Laboratory of Research of Lafarge. The concrete was placed in three layers and was vibrated internally and externally. All beams and control specimens were cast and cured under similar conditions. The beams and specimens were kept covered under polyethylene sheets for 28 days until 24 hours before testing.

Axial compressive tests have been done on 12 specimens and an 28 days average compressive strength of 140 Mpa is obtained.

2.2   Mechanical properties of the armatures

The steels used for rebars present an average yield strength of 550 MPa and a Young modulus of 210 GPa). The CFRP armatures have a brittle elastic behavior with an ultimate strength of 2500 MPa and a young's modulus of 160 GPa.

2.3   Beams characteristics

A design according to the rules of the Eurocode 2 permits to define the areas of armatures kept by this survey (Fig. 1).
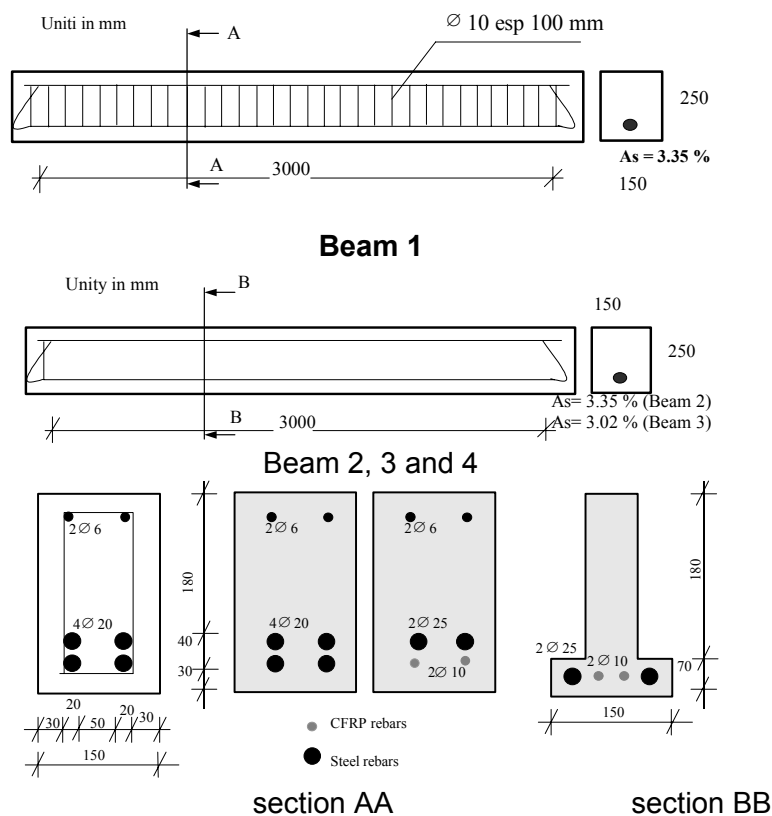

Figure 1: Beams description

3 meter span beams have been designed according to the EC2 with a required failure of the steel/composite rebars and a structural dead load of 200 kN, leading to an ultimate moment of 115 kN.m. Four 20 mm in diameter steel rebars are necessary for beam 1 and two 25 mm in diameter steel rebars are mixed with two 10 mm CFRP rebars for beam 2, 3 and 4. The shear resistance is verified while keeping a concrete tensile strength of 10 MPa and according to Rilem recommendations [10].

Four beams based on this prior design have been tested (Fig. 2). The first beam permits to verify the design and to identify the bending behavior of the UHPC beams. The mechanical test done on the second beam in UHPFRC allows evaluating the contribution of the short metallic fibers. In this case, no shear steel framework is display. The last two beams have been tested in order to observe the efficiency of CFRP rebars. Especially, the fourth beam shows a reduced concrete area in the upper part (Fig. 2) in order to increase the compression ratio of the concrete and then the contribution of the rebars.

The four-point loading is made of two equally concentrated loads, acting each to 35 cm of the middle span i.e to 1.15 m of the supports (Fig. 3). The tests are driven while achieving a loading by successive loadings all 250 daN.
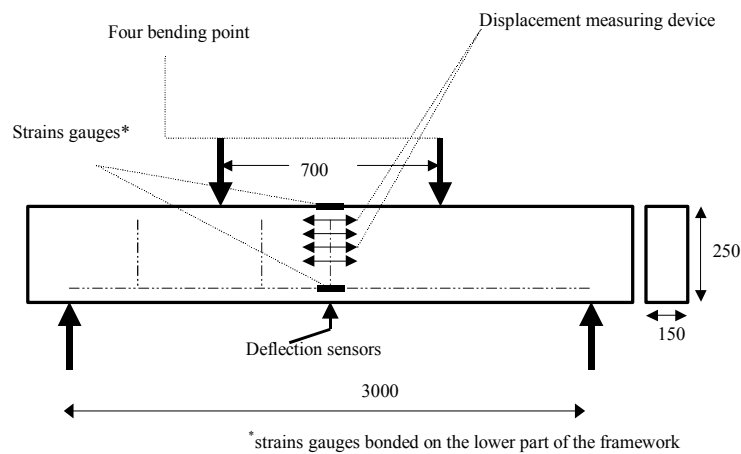

Figure 2: Experimental device

3   Experiment and results analysis

3.1   Instrumentation of the beams

Electrical strains gauges of 120 ohms and a 10 mm grid length have been bonded on the concrete as well as on the longitudinal steel rebars at the mid-span of the beam. Besides, displacement measurement device are bonded on the concrete with one regular interval of 200 mm in width and 20 mm in height to the level of the central area compressed (Fig. 3). The analysis of these set of data permits to obtain the Navier diagrams and the moment-curvature curves. A 100 mm LVDT displacement sensor is placed at the mid-span to

measure the deflection. For each level of loading, the values of the displacements and the strains gauges are monitored. The tests are carried out to failure.

3.2 Experimental results

The table 2 gives the values of the tests results obtained. Severals analysis can be done in order to evaluate the effects of the short metallic fibers and of the mixed rebars. First, the evolution of the mid-span displacement will give information about stiffness and structure ductility. Then the analysis of material strain allows to focus on the efficiency of each. The last part concerns the survey of the failure mode of each of the beams. For each of these parts a comparison of the different mechanical behaviors is achieved.

Table 2: Beam tests result

	Cracking load (kN)	Yielding load (kN)	Failure load (kN)	Mid-span deflection (mm)	Failure mode
Beam 1	20.3	183	199	31.0	Tensil rebars
Beam 2	24.7	153	173	34.8	Tensil rebars
Beam 3	27.8	201	270	51	Tensil rebars
Beam 4	15.0	180	200	32.3	Concrete in compression

3.2.1 Evolution of the mid span displacement

The different load-displacement curves don't present any significant discepencies all along the loading (Fig. 4). Indeed, the evolution of the mid span displacement corresponds to the three stages of behavior of a reinforced concrete structure. A first stage correspond to the behaviour of a beam non cracked. The second stage drives to the cracking of the beam. Indeed, the cracking decreases the inertia and therefore the bending stiffness of the area. The last stage of behavior corresponds to the yielding of the tense longitudinal armatures. Concerning the beam 3 (mixed armatures), it is important to note that the third stage of behavior is modified. The armatures made of steel yielded and the CFRP rebars are elastic, they bare a supplementary effort. The analysis of the stress-strain curves confirms, thereafter, this observation. A gain of load of 50% is gotten then for the beam 3. The use of steel-CFRP mixed armatures permits to get a structural behavior therefore is equivalent to strain hardening material.
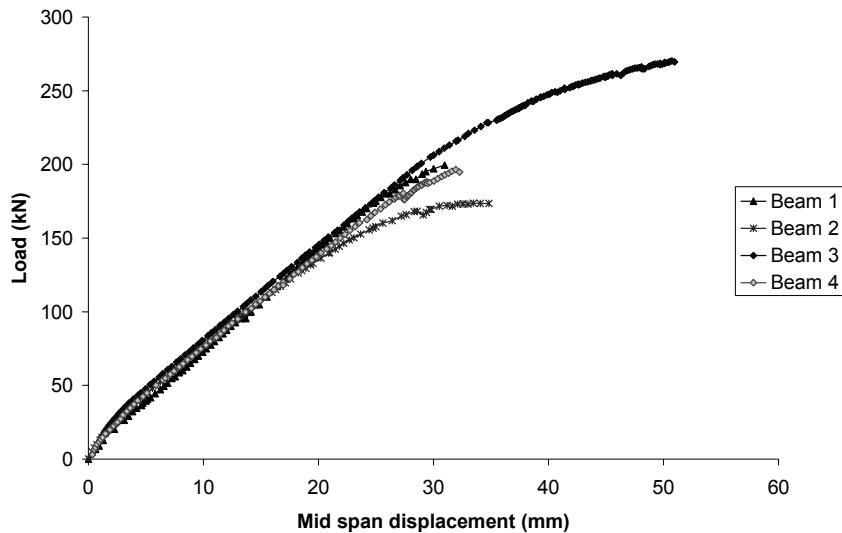
Figure 3: Evolution of mid-span deflection as a function of loading

3.2.2　　　**Evolution of strains**

The table 3 represents the evolution of the strains of the top fiber and the lower armatures all along the loading. The table 3 gives the strains values for 3 load levels corresponding to the occurring of cracks in the concrete in tension, to the steel rebars yielding and to the failure.

The load-strain curves of the Fig. 4 illustrate the linear behavior until failure for the concrete or for the steel rebars. It is also important to note that for the beams 1 and 3 the maximal strains recorded on steel have a value superior to the 10 ‰ conventional allowable strain. For the beam 1 a strain of 14 ‰ has been recorded for example before the failure of steel in tension. It is again important to note that for the beam 3, the answer in load-strain is of elastic-yielding-hardening type. It permits the increase of the beam area moment. Concerning the strains of the top fiber of the concrete compressed, a significant difference exists between the concrete UHPBF of the beam 2 and the UHP concrete non-reinforced of the beam 3. Indeed for the same level of loading, the strain of the top fiber is raised more for the UHPFRC (beam 2) that for the UHP concrete (Fig. 4). This difference is probably explained by a structural effect (position of the neutral axis, beam section equilibrium) corresponding to a modification of the tensile mechanical law of the concrete. The analysis of the diagrams of Navier confirms this observation subsequently. In order to analyse the origin of the behavior differences noted between the different beams, it is important to calculate the evolution of the position of the neutral axis and the beam curvature.

Table 3: Beams materials strain values for several level of loading

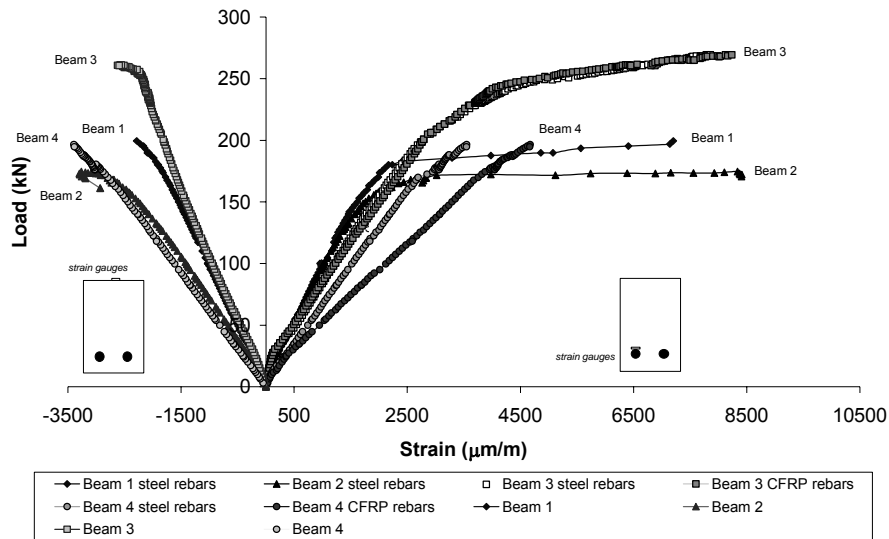|		Beam 1	Beam 2	Beam 3	Beam 4
Upper strain value (µm/m)	craking	-233	-254	-212	-229
	yielding	-1540	-2310	-1810	-2780
	Failure	-2470	-3260	-3160	-3400
Rebars strains (µm/m)	craking	200	287	160	147
	yielding	2850	2870	2910	2820
	Failure	14600	12500	13500	3540

Figure 4: Evolution of material strain during the loading

3.3 Diagrams of Navier-Position of neutral axis

Displacement measurement device placed on the side of the beams in the compressive part allows to assess the variation of length and therefore the compressive strains in several points of the beam height. The measures of strains for the top beam fiber and to the armatures position permit to complete the Navier diagram. This analysis allows to assess the curvature and the position of the neutral axis according to the applied load.

$$\chi = \frac{\varepsilon_{topfiber}}{(h - z_u)} \qquad (1)$$

$$z = \frac{1}{\chi} \cdot \varepsilon + (h - z_u) \qquad (2)$$

The position of the neutral axis (z_u) and the value of the curvature (χ) are obtained for every level of loading (Fig. 5). It is possible to notice that the curve is linear through the beam

668

height that is in conformity with an ideal beams bending behavior. The diagrams defined for every level of loading, the position of the neutral axis and the value of the curvature.
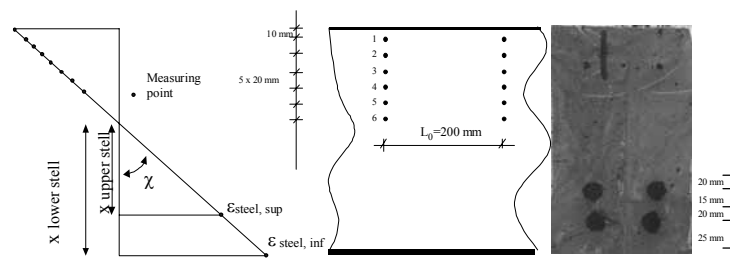

Figure 5: Calculated curvature

For every beams, this curvature is identical in the compression and tension parts that permits to verify that the classic assumption of the reinforced concrete, when the mixed armatures (steel-carbon) or the UHPFRC are used, are kept. As far as the evolution of the curvature is concerned, we can note similarities between the beams 1 and 3. The curvature of the beam 2 follows the one of the beams 1 and 3 up to 30 kN.m (corresponding to 52,2 kN). Beyond this value the curvature of the UHPFRC beam increases more rapidly than the one of the UHPC beams without short metallic fibers and of the UHPFRC beams with mixed armatures. This can be explained by the lower neutral axis in the case of the beam 2. Indeed, the results analysis permits to observe the variation of the position of the neutral axis (z_u, Fig. 6).

This position stabilizes quickly around 164 mm for the first UHPRC beam. This phenomenon corresponds to a brittle materials behavior where cracks grow quickly. Thereafter the balance of the section is ensured thanks to the armatures in beams and to the compressed part. The neutral axis position stabilizes rapidly toward a height of 146 mm. Behaviour of beams 2, 3, 4 present difference with the beam 1.

he behavior of the tense UHPFR concrete is more ductile due to its tensile mechanical behaviour law; the crack propagation is controlled by short metallic fibers. The effect on the structure is to modify the neutral axis position. The neutral axis position stabilizes itself for a load of 70 kN to a position of 166 mm. The fibers are therefore particularly efficient and contribute to make lower the position of the neutral axis of 146 mm toward a height of 166 mm. The efficiency of the metallic short fibers on the flexural bending behaviour of the beam is put in evidence and must be quantified.

The contribution of the fibers in tension part is valued precisely thereafter. It is important to note that the ultimate load value are in conformity with the design value for the beam 1, but weaker for the UHPFRC beams. The conventional balances of section should be reconsidering. Indeed, the position of the calculated neutral axis does not take into account the tensile behaviour law of the short-fiber reinforced concrete, that modifies the position of the neutral axis.
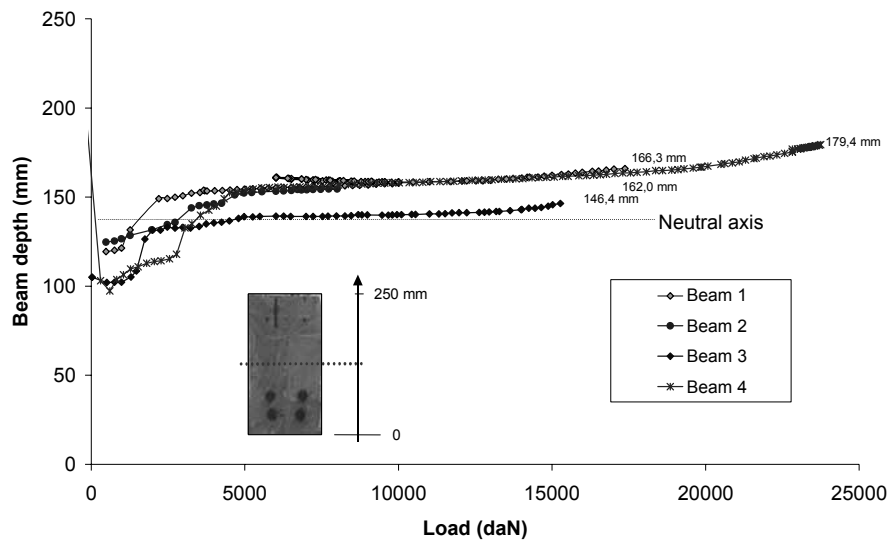
Figure 6: Neutral axis position in function of loading

3.3.1   Failure mode and cracking pattern of the beams

Concerning the beam 1, the behaviour is nearly linear with a low ductility; its failure results from the yielding of steels rebars. The rate of maximal concrete stress in compression (superior fibers) is of 50% of the ultimate concrete stress. A failure in compression of the concrete is observed then, but it is subsequent to the failure of the steel rebars. All along the loading, vertical cracks regularly spaced (in the zone of vertical stirrups) are observed for the beam 1. The beam 2 does not present any shear concrete cracks pattern. The set of the cracks develops itself vertically; a high crack number does not reach the height corresponding to the position of the steel rebars. The observation of the cracking, confirms that the position of the neutral axis is lower than for the beams 1. The numbers of cracks is higher with a weaker spacing (3 to 5 cm). The failure occurs in the tension part following the apparition of one macro cracks in central zone of constant moment. This macro cracks occurs when the lower bed of armatures is broken. The strain rate is then of 80 % of the ultimate concrete strain. The failure of the armatures induces a drop of the load until a value of 100 kN, but the load maintains itself under the effect of the bridging effect of crack by the metallic fibers. The same observations are made for the beam 3, with a superior cracking height corresponding to a higher position of the neutral axis. Concerning the beam 4, section reduction of the compression of the area in part compressed permits to get the crushing of the concrete in compression. The UHPFRC is used then to the maximum of its performances in compression. It is then possible to consider an optimised area in order to get a failure of the concrete in compression associated to a yielding of the armatures. In conclusion, the ductility and the failure mode of the UHPFRC beam can be obtained by a suitable design (rate of reinforcement, geometry)

4   Conclusion

The tests on structures done in this paper put in evidence the possibility to use ultra high performance fiber reinforced fibers concrete for the design of reinforced concrete structure. The main hypotheses of the steel reinforced concrete may be applied to this kind of structures.

The use of CFRP-steel mixed rebars permits in an elastic stage to keep a bending stiffness comparable to the beams reinforced by traditional armatures. On the other hand the use of mixed armatures increases by 50% the failure load. The ductility of the structure is also increased thanks to the strain yield hardening behavior due to the combination of the mixed armatures.

The presence of short metallic fibers in the concrete contributes really to the internal balance of the beam section, the sum of the internal moments of the tensile part is increased by 10%. The tensile stress undertaken by the short fibres embedded in the concrete decrease the position of the neutral axis. The lever arm of the moment took by steel rebars is decreased whereas, in a same time, the moment undertaken by the concrete in compression is increased. On the other hand, it is important to note that the metallic fibers permit to suppress all transverse armatures in the shear zone.

Finally the results of this sstudy confirm the potentiality of this kind of structure. Indeed while using a traditional concrete (with a compressive strength of 40 MPa), a beam section of 190x315 mm^2 is necessary to reach one moment of failure of 115 kN.m (beam 1, 2 and 4) and a beam section of 210x350 mm^2 to reach 150 kN.m (beam 3). The use of UHPFRC permits to decrease of 40 % the weight of the structure whereas its association with CFRP armatures in carbon permits to reduce the same weight of 50 %. The use of UHPFRC contributes to decrease the weight of the structures therefore. The performance of the material permits to consider the optimisation of the section in order to improve the performances of it and get lighter structures with higher performances.

5   References

[1]   P. Rossi, Ultra-High Fibre reinforced concretes (UHPFRC): An overview, Proceeding of the fifth International Rilem Symposium,PRO 15, Rilem Publications p. 87-100

[2]   De Larrard, Le Roy F. Relation entre formulation et quelques propriétés mécaniques des BHP. Matériaux et construction 1992 ; 25 : 464-475.

[3]   Richard P. Reactive powder concrete : a new ultra-high-strength cementitious material. 4th international symposium on utilisation of high-strength/high performance concrete Paris. 1996.

[4]   Chanvillard G., Characterisation of fibre reinforced concrete mechanical properties : A review. Proceeding of the fith International Rilem Symposium PRO 15. Rilem Publications : 29-50

[5]   Chong Hu. Casanova P. Delalande F. Mix design of very high strength steel fiber reinforced concrete (VHS SFRC for tunnel liner. Proceeding of the fith International Rilem Symposium PRO 15, Rilem Publication :129-138

[6] Aïtcin P C. Richard P., The pedestrian/bikeway bridge of Sherbrooke. Proceeding of 4th international symposium on utilisation of high-strength/high performance concrete Paris. : 1996.

[7] Casanova P. Rossi P. Scaaller I. Can steel fibers replace transverse reinforcement in reinforced concrete beams. ACI Materials Journal 1997; 94 (5): 341-354

[8] Qian C. Patnaikuni I. Properties of high-strength steel fiber-reinforced concrete beams in bending, Cement and Concrete Composites 1999; Vol. 21: 73-81

[9] Ashour S., Wafa F.F. Flexural behaviour of high-strength fiber reinforced concrete beams. ACI structural Journal 1993 ; 90 (3) :79-287

[10] Final recommendations of Rilem TC 162-TDF. Materials and structures 2003 ; Vol 36 : 560-567

6   Acknowledgements

Roland Bornemann
Dipl.-Ing.
University of Kassel
Department of Structural Materials
Kassel, Germany

Silvan Faber
Dipl.-Ing.
University of Kassel
Department of Structural Materials
Kassel, Germany

UHPC with steel- and non-corroding high-strength polymer fibres under static and cyclic loading

Abstract:

Fine steel fibres with a high aspect ratio (l/d) can be used in order to reduce steel fibre content of common ultra high performance concretes from 196 kg/m³ to 78 kg/m³. Mechanical properties, i.e. bending and compressive strength, can almost be maintained. An addition of high strength polyvinylalcohol fibres is a way, to increase strength and ductility of UHPC despite of a low steel fibre content. Due to a low steel fibre content, corrosion on concrete surfaces could be reduced. Furthermore high strength polyvinylalcohol fibres are capable to replace steel fibres in thin concrete beams. In this case corrosion can completely be avoided.

1   Targets

Ultra high performance concretes usually contain high amounts of fine steel fibres [1-6]. The content varies between 2,0 – 2,5 vol%. High amounts of equally distributed steel fibres lead to a significant increase of flexural and tensile strength but also improve material´s ductility. Apart from the positive effect on mechanical properties, a high amount of steel fibres may causes stains on surfaces. Fibres close to the concrete´s surface may corrode due to enviromental conditions.

Additionally a reduction of steel fibre content saves money, because the production of fine steel fibres is very costly.

In order to solve/minimize corrosion problems and to enhance both economy and mecanical performance, 3 strategies had been developed which should lead to a reduced fibre content:

- utilization of long and fine steel fibres (length = 17 mm; diameter = 0,15 mm)
- utilization of high strength polyvinylalcohol fibres (PVA) as a steel fibre substitute
- utilization of a fibre"cocktail" containing both fine steel and polyvinylalcohol fibres

2 Materials and mixtures

For the study a ultra high performance mortar had been selected with a maximum grain size of 0,5 mm. The mix composition can be taken from table 3. On the basis of this composition, fibre contents and types were varied. We studied 5 different mixtures. Type and amount of fibres can also be taken from table 3.

	Specific density [kg/dm³]	Main constituent	Blaine [cm²/g]
CEM I 52,5 R HS/NA	3,1	-	4.600
microsilica	2,2	>98 vol% SiO_2	>200.000
quartz powder	2,65	>99 vol% SiO_2	3.800
Sand (0,125 – 0,5mm)	2,65	>99 vol% SiO_2	-

Table 1: Properties of the mineral constituents

The used steel and PVA fibres both have a high tensile strength. However the PVA fibres show a significantly lower moduls of elasticity than steel fibres. The workability was tested according to DIN EN 1015-3. We decided to allow a minimum spread of 20 cm in oder to ensure good workablility. Steel fibres with a very high aspect (l/d) ratio usually tend to agglomeration in concrete and mortar. Due to the very sticky consistency of ultra high performance concrete and mortar, it is possible to disperse fibres with very high aspect ratios. This was the reason why we obtained workable mortars (table 3) with steel fibres of 17 mm length and 0,15 mm diameter (aspect ratio l/d =115).

	Geometrie	Material and specific denisity	Modulus of elasticity [N/mm²]	Tensile strength [N/mm²]
Steel fibre 1	Length = 9mm Diameter = 0,15mm	Steel, 7,85 kg/dm³	210.000	2.300
Steel fibre 2	Length = 17mm Diameter = 0,15mm	Steel, 7,85kg/dm³	210,000	2.300
PVA 1	Length = 30mm Diameter = 0,66mm	Polyvinylalcohol, 1,3 kg/dm³	29.000	1.000
PVA 2	Length = 15mm Diameter = 0,31mm	Polyvinylalcohol, 1,3 kg/dm³	29.000	800

Table 2: Types and properties of fibres

Mixture 1 with a high amount (196 kg/m³) of short steel fibres served as a reference mix (l/d = 60). Mixture 2 contained 78 kg/m³ of long steel fibres with a very high aspect ratio (l/d = 115). Mixtures 3 and 4 did not contain steel fibres, instead 52 kg/m³ (4 vol%) of PVA fibre types

PVA 1 (l/d = 45) and 2 (l/d = 48) were added. Mixture 5 finally represents a combination of long steel fibres (78 kg/m³; l/d = 115) and PVA fibres (26 kg/m³; l/d = 48).

		Mixture 1	Mixture 2	Mixture 3	Mixture 4	Mixture 5
CEM I 52,5 R HS/NA	kg/m³	733	744	722	722	729
Sand 0,125/0,5	kg/m³	1.008	1.023	993	993	1.003
Microsilica	kg/m³	230	234	227	227	229
Quartz powder	kg/m³	183	186	180	180	182
HRWRA	kg/m³	28,6	29	28,2	28,2	28,5
Water	kg/m³	161	164	159	159	160
Steel fibre 9mm	kg/m³	196	-	-	-	-
Steel fibre 17mm	kg/m³	-	78	-	-	78
PVA 1	kg/m³	-	-	52	-	-
PVA 2	kg/m³	-	-	-	52	26
Spread	cm	25	28	20	20	27

Table 3: Mix design

3 Test procedure

In order to investigate the bond of steel fibres in UHPC, single fibre pull out tests were performed (Fig. 1). The embedded length of the fibres in UHPC varied between 5 to 15 mm. By the variation of the embedded length we were able, to measure both the maximum tensile and bond strength of the steel fibres.
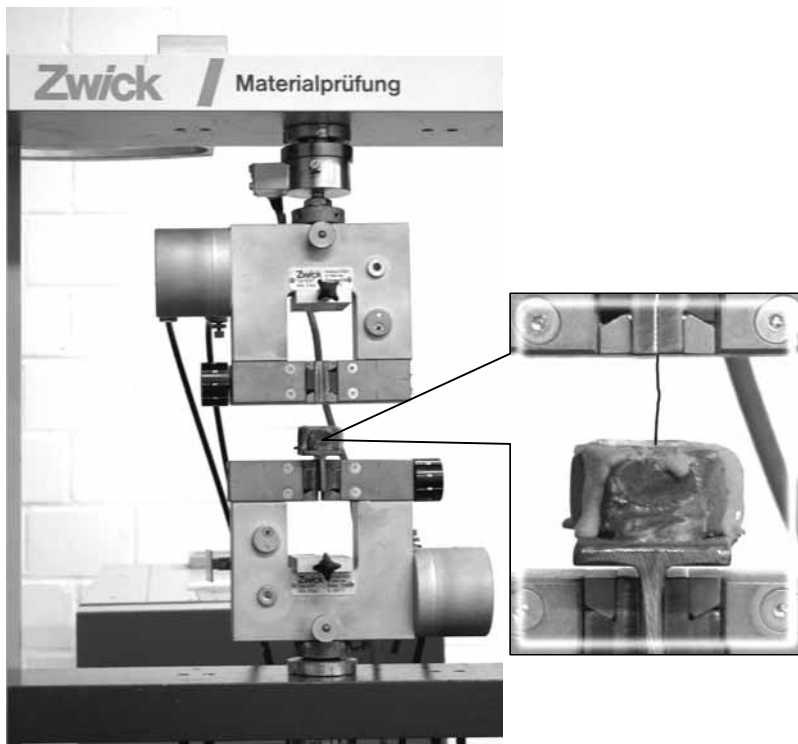

Fig. 1: Test set up for single fibre pull out tests

The bending strength of prisms (160x40x40 mm) and beams (700x150x150 mm) had been determind according to DIN EN 196-1 and [7]. The tests had been carried out deflection controlled, in order measure the ductility of the different mixtures, depending from fibre content, length and type.

Finally we made 4 point dynamic load tests with beams (700x150x150mm). The test set up corresponds to [7]. Samples containing different fibre types were loaded till the first crack appeared. The crack width was in all cases about 0,5 mm. Subsequently, the cracked beams were subjected to cyclic loading (5Hz). The minimum bending strength was 2 N/mm², the maximum was determinded with approximatly 40 - 45% of the maximum bending strength of the material. In nearly all presented cases 10 N/mm². This assumption corresponds to the maximum design load that this material has to bear in service.

4   Results and conclusions

The fibre pull out tests gave results in reference to the maximum bond strength and tensile strength of the steel fibres (Table 4). The information given by the producer concerning tensile strenght of the steel fibres (2.300 N/mm²) could be confirmed in test series with an embedded length ranging from 10 – 15mm (table 4).

The bond strength could be calculated with the measured tensile force P_{max} and the embedded length of the fibres (l_F = 5 mm). Under the assumption of an equal distribution of the bond strength τ_m all over the surface of the fibre (diameter d = 0,15 mm) values can be calculated (equation 1).

$$\tau_m = \frac{P_{max}}{d \cdot \pi \cdot l_F} \quad \text{(equation 1)}$$

In the studied cases generelly the fibres were pulled out. The calculated bond strength reached maximum values of 13,6 N/mm² (table 4).

No.	Embedded length l_E [mm]	Max. force P_{max} [N]	Failure mode	Bond strength τ_m [N/mm²]	fibretension [N/mm²]
1	5,0	32,1	Pull out	13,6	1.817
2	5,0	27,7	Pull out	11,8	1.568
3	5,0	20,4	Pull out	8,7	1.154
4	10,0	48,1	Rupture	10,2	2.722
5	10,0	38,1	Rupture	8,1	2.156
6	15,0	38,3	Rupture	5,4	2.167
7	15,0	41,6	Rupture	5,9	2.354

Table 4: Results of pull out tests of steel fibres

From the results a reasonable fibre length can be derived. A sudden failure of a fibre due to overload would reduce the ductility of such a ultra high performance concrete. With a maximum tensile strength of approximatedly 2.300 N/mm² and a bond strenght τ_m which ranges between 8,7 – 13,6 N/mm², a critical length can be derived which shouldn´t be exceeded (equation 2):

$$l_F = \frac{P_{max}}{d \cdot \pi \cdot \tau_m} \quad \text{(equation 2)}$$

Following this equation, fibres start to rupture with an embedded length between 6,3 – 9,8 mm. If one wants to exploit most of the fibre´s tensile strength capacity, then the steel fibre length should be close to 13 mm. In order to guarantee ductility, a length of 20 mm shouldn´t be exceed. As a compromise we chose a fibre length of 17 mm with a diameter of 0,15 mm (l/d = 115) for our experiments.

4.1 Static load tests of prisms and beams

In previous test with prisms (160x40x40 mm) the bending strength and deflection behaviour of the mixtures 1–5 had been examined (Fig. 2 and appendix, table 5). Mixture 2 with a steel fibre content of only 78 kg/m³ (length = 17 mm; diameter = 0,15 mm) showed nearly the same performance as mixture 1 with shorter steel fibres (length = 9 mm; diameter = 0,15 mm) and a content of 196 kg/m³.

Comparable bending strength and ductility could also be reached by the substitution of steel fibres by PVA fibres of type 1 and 2 (Mixtures 3 and 4). Differences between mixtures 1, 2 and 3, 4 occurred in reference to their deflection. After leaving the linear elastic range with the formation of cracks, the mixtures with PVA fibre addition showed a significantly bigger increase in deflection. The lower modulus of elasticity of the PVA-fibres in comparison with steel fibres, could be the reason for this behaviour.

Highly favourable properties showed mixture 5 with a combination of steel and PVA fibres. In comparison to the other discussed mixtures a significant increase of bending strength was achieved.
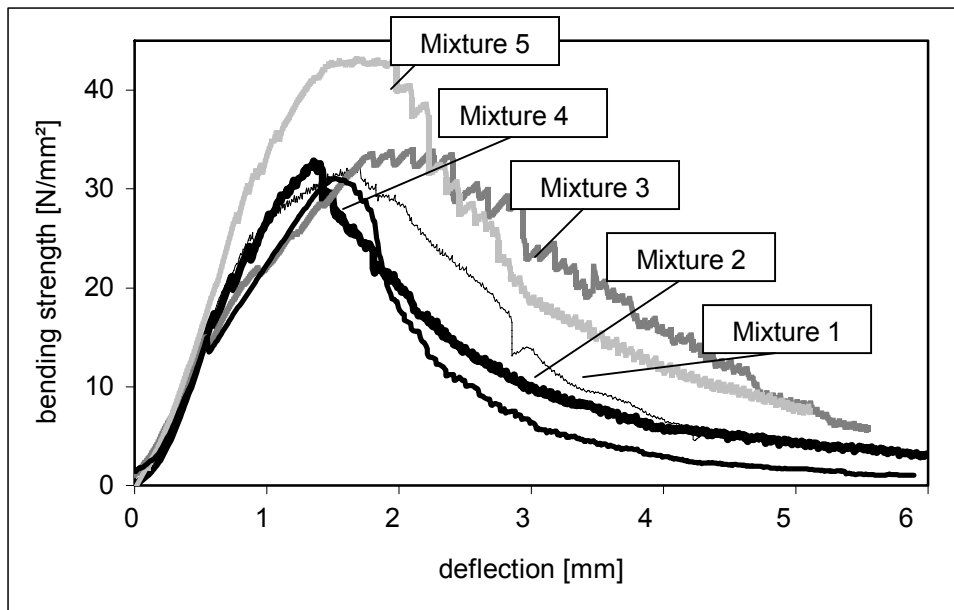
Fig. 2: Characteristic patterns of load-deflection curves of prisms (mixtures 1 – 5)

Both bending strength and deflection of beams (700x150x150 mm) showed the same trends like the results obtained with prisms. Additionally, it could be shown that ultra high performance concretes generelly show a pronounced scale effect concerning bending strength. With increasing heigth of the UHPC-specimens, strength decreases. The highest loss of bending strength generally showed mixtures with PVA fibres only (Fig. 3 and appendix, table 6).
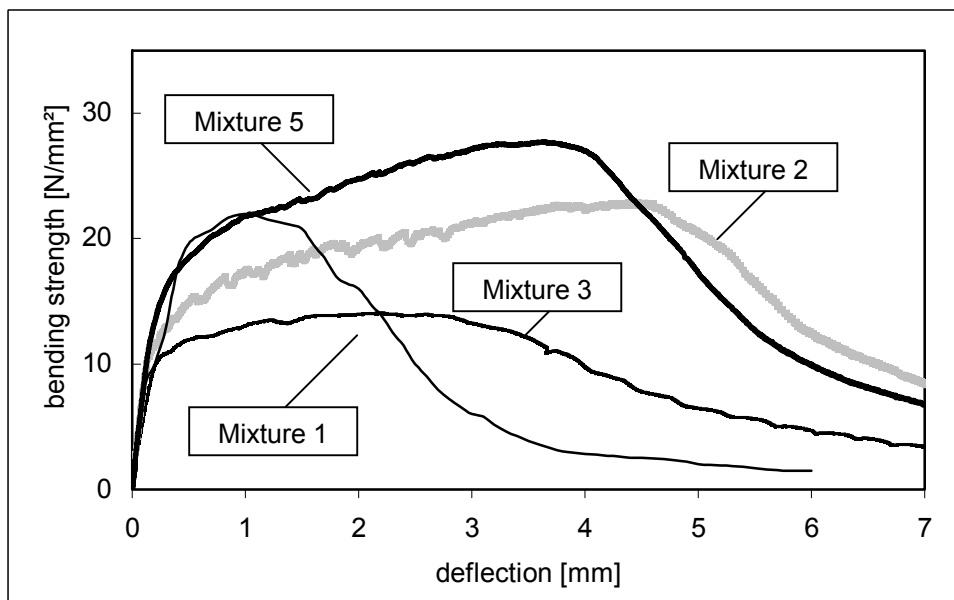
Fig. 3: Characteristic patterns of load-deflection curves of beams (mixtures 1, 2, 3 and 5)

4.2 Dynamic load test of beams

Finally we tried to find out, if the durability of precracked (crack width 0,5 mm) ultra high performance concrete beams (700x150x150 mm) under cyclic loading could be improved by the addition of PVA fibers. In a first step, the bearing capcitiy under cyclic loading of an uncracked UHPC-beam had been determind (Fig. 4). The test stopped after 10^6 load cycles, the beam showed no signs of failure. Subsequently, precracked beams of the mixtures 1,2 and 5 were tested with the same test prodedure, with an ocillating bending strength between 2 – 10 N/mm². The results showed, that ultra high performance concrets with a steel fibre reinforcement do not behave like a conventionally reinforced one with steel bars. A anticipated and gradual failure of the concrete structure occures. Mixture 1 failed after 25.000 load cycles, mixture 2 after 27.000 cycles. An improvement of durability under cyclic loading can be achieved by the addition of PVA fibres. In the presented case (Fig. 4) the number of cycles could nearly be doubled and the failure occurred more gradually. Although the PVA fibres habe a significantly lower modulus of elasticity, they seem to be able to have a very beneficial influence on load bearing capacity. The stresses which act on the steel fibres seem to be reduced, the failure comes later and more gradually.
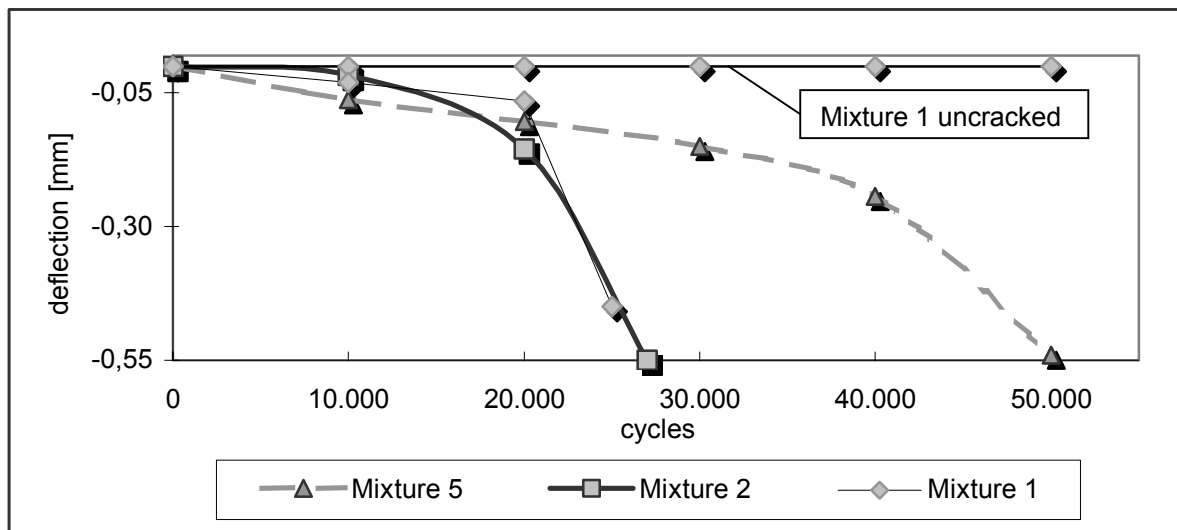

Fig. 4: Deflection growth under cyclic loading (bending strength: min.= 2 N/mm² max.= 10 N/mm²; cracked specimen, crack width 0,5 mm)

Similar trends showed the dynamic test of mixture 5 (52 kg/m³ of PVA fibre 1) in fig. 5. In this case the maximum bending strength only reached values of about 14 N/mm² (Fig. 3 and appendix, Table 6). So the dynamic bending tests were carried out with a minimal strength level of 2 N/mm² and a maximum of 6 N/mm². The sample showed a higher level of deflection, probably because of the significantly lower modulus of elasticity of the PVA fibres. As noted before, the failure occurred also in this case more gradually. PVA-fibres seem to have a good connection with the surrounding UHPC-matrix.
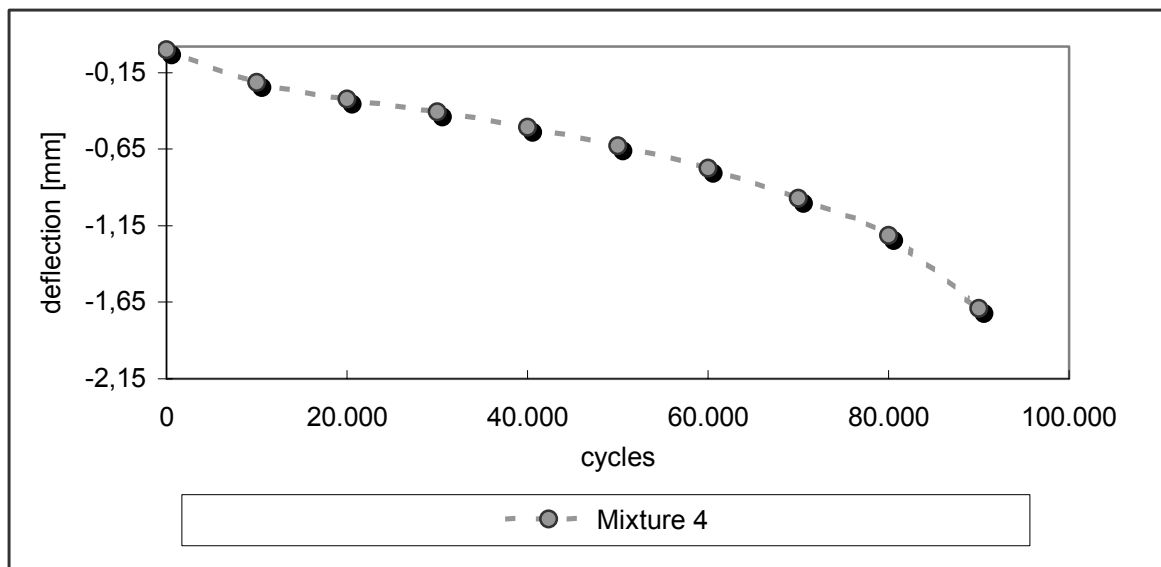
Fig. 5: Deflection growth under cyclic loading (bending strength: min.= 2 N/mm² max.= 6 N/mm²; cracked specimen, crack width = 0,5 mm)

5   Summary

The test results showed that equally good ultra high performance concretes can also be produced with a reduced steel fibre content of only 78 kg/m³ instead of 196 kg/m³. The lower amount of fibres can contribute to a reduction of rost-stains on the concrete surface and improved economy.

Concrete beams and prisms showed during the test series a clear scale effect on bending strength. The scale effect was very pronounced in the case of PVA fibres. Small specimen showed during the tests the same bending strength as specimen with steel fibre addition. However, much lower bending strenght were obtained for beams.

The combination of PVA and steel fibres increased the bending strength of prisms and beams significantly. Additionally this combination improved the behaviour under cyclic loading. A disadvantage of PVA fibre additions is the reduction of compressive strength (appendix, table 5).

6   References

[1] Bornemann, R.; Schmidt, M.; Fehling, E.; Middendorf, B.: Ultra-Hochleistungsbeton UHPC – Herstellung, Eigenschaften und Anwendungsmöglichkeiten; Beton- und Stahlbetonbau, Heft 7, 2001, S. 458-467.

[2] Richard, P.; Cheyrezy, M.: Composition of reactive powder concrete. In: Cement and Concrete Research, Vol.25, No.7, 1995, S.1501-1511.

[3] Bornemann, R.; Schmidt, M.: The role of powders in concrete. In: Proceedings of the 6th International Symposium on Utilization of high strength/high performance concrete, Vol. 2, S. 863-872, Leipzig 2002.

[4]   Schmidt, M.; Fehling, E.; Bornemann, R.; Bunje, K.; Teichmann, T.: Ultra-Hochfester Beton: Perspektive für die Betonfertigteilindustrie; In: Beton - Fertigteil Jahrbuch 2003.

[5]   Schmidt, M.; Fehling, E.; Bornemann, R.; Bunje, K.; Teichmann, T.: Ultra-Hochfester Beton: Perspektive für die Betonfertigteilindustrie; In: Betonwerk + Fertigteil - Technik 03/2003 (german/englisch)

[6]   Schmidt, M., Fehling, F., Teichmann, T., Bunje, K.: DFG –Forschungsbericht: Entwicklung, Dauerhaftigkeit und Berechnung Ultra-Hochfester Betone. Universität Kassel 2003.

[7]   Bemessungsgrundlagen für Stahlfaserbeton im Tunnelbau. Deutscher Beton- und Bautechnik-Verein, Ausgabe 2001.

7   Appendix

Type of mixture	Bending strength of prisms [N/mm²]	Spread [cm]
Mixture 1	32,5 32,2 34,9	23
Mixture 2	27,7 38,1 32,8	26
Mixture 3	28,4 33,8 30,9	20
Mixture 4	30,6 30,6 26,6	20
Mixture 5	43,3 44,0 45,8	22

Table 5: Strength of prisms (160x40x40 mm) and spread of mixtures

Type of mixture	Bending strength of beams [N/mm²]	Compressive strength of cylinders [N/mm²]
Mixture 1	22,1 22,3	180,4 179,6
Mixture 2	23,1 22,9	175,4 174,9
Mixture 4	14,6 14,7	-
Mixture 5	24,3 27,7	154,7 167,2

Table 6: Strength results of beams (700x150x150 mm) and
cylinders (300x150 mm)

Part 12:

Durability

Herold, G.

Dr.-Ing., Dr. rer. nat.

University of Karlsruhe

Karlsruhe, Germany

Müller, H. S.

Prof. Dr.-Ing.

University of Karlsruhe

Karlsruhe, Germany

Measurement of porosity of Ultra High Strength Fibre Reinforced Concrete

Summary

The durability of concrete is determined to a great extent by its porosity and the related pore radius distribution. These two characteristics have very small values in ultra high strength concrete compared to concrete with the usual strength classes. In the framework of a more extensive research project on the durability and fatigue behaviour of ultra high strength concrete, initial investigation results on porosity by mercury intrusion porosimetry (MIP), gas adsorption and scanning electron microscopy (SEM) are presented.

Keywords: *porosity, mercury intrusion, gas adsorption, scanning electron microscopy*

1   Introduction

High strength concretes have been developed within recent years, and strength classes up to B 115 belong to the status of contemporary concrete technology. For concretes of even higher strength classes (ultra high strength concrete, UHSC) ranging between 150 – 200 N/mm^2 fabrication techniques and production engineering are either available or already far-advanced [1]. But developments in mixture composition (increasing packing density by addition of micro grain size fractions, improvement of workability by high water-reducing admixtures, increasing the cement content) also have an important negative consequence: the increase of cracking tendency because of increased chemical shrinkage due to the high quantity of cement used [2]. One possible approach to decrease cracking of the rigid material consists in using metallic fibres within the mixture (ultra high strength fibre reinforced concrete, UHSFRC) [3].

Still little is known about the structural performance of such construction materials. Particularly the lack of knowledge associated with fatigue and durability behaviour [4] is one of the obstacles to a wider application of these ultra high strength concretes. In fact, the potential in durability of this new material is rather unknown so far.

Based on this particular gap in our knowledge a joint research project was initiated. Within the working plan, the fatigue behaviour of these concretes will be investigated by TU Delft in The Netherlands, and the University Karlsruhe will carry out experiments on durability. The samples of the same concrete mixes will be used, and in addition an exchange of tested concrete specimens between the project partners will be realized. In particular, samples

already tested for durability in Karlsruhe are going to be examined in Delft with regard to their fatigue behaviour and vice versa.

For the investigation in this work, concrete with compressive strength values of approx. 150 N/mm^2 are produced. Because the pore volume and pore distribution of the material have an overwhelming influence on concrete durability, the first step of the investigations includes examinations of the material's microstructure and pore volume by mercury intrusion porosimetry, gas adsorption and SEM.

2   Mixing, curing and characterization of concrete

A representative ultra high strength fibre reinforced concrete (UHSFRC) was designed. It is a powder concrete with a maximum aggregate size of 0.5 mm, consisting of quartz sand, quartz powder, cement and microsilica. The proportions of these constituent materials have been chosen in order to optimize the packing density of the mixture. The admixture is a modified acryl polymer, which causes a strong increase of the setting time. The water to cement ratio (w/c) is equal to 0.25. The concrete was reinforced with steel fibres (fibre content 2.5 Vol.-%) to improve the ductility. Table 1 gives details on the composition of the concrete mixture.

Table 1:   Composition of ultra high strength reinforced concrete (fibre content 2.5 Vol.-%)

Constituent material	Unit	Amount
cement CEM I 42,5 R-HS or cement CEM III 42,5 N-NW/HS/NA	kg/m³	824
quartz powder	kg/m³	100
quartz sand	kg/m³	1098
microsilica	kg/m³	160
superplasticizer	kg/m³	66
fibres (l = 8 mm, d = 0.175 mm)	kg/m³	179
water	kg/m³	160

The slump flow of the fresh concrete was determined to be 74.5 cm. The values of compressive and flexural tensile strength of the specimens (prisms 40 x 40 x 160 mm^3, tested at an age of 7 days) of the above mixtures, depending on the type of concrete, can be seen in Table 2.

Considering the 7 day strength values, the exchange of CEM I for CEM III of the same strength class has a comparatively marginal effect, whereby the mixture with Portland cement shows, as expected, the greater compressive and tensile strength values after storage in damp boxes. After heat treatment, however, the subsequent hardening potential of the CEM III cements exerts its effect and the strength values are above the comparative values of the mixture with CEM I cement.

Table 2: Compressive and flexural tensile strength of the same mixture with CEM I and CEM III cement (7 days damp box or 2 days heat treatment at 90 °C)

Strength	Treatment	Unit	CEM I	CEM III
Compressive strength	damp box	N/mm^2	92	84
Compressive strength	heat treatment	N/mm^2	138	151
Flexural tensile strength	damp box	N/mm^2	11	7
Flexural tensile strength	heat treatment	N/mm^2	21	24

For the mixture with Portland cement the fibre content was varied between 0 and 4.0 Vol.-%. The respective strength values of these concretes, depending on the fibre content, after storage of the specimens in the damp boxes or resp. after heat treatment at 90°C are given in the subsequent table 3.

Table 3: Compressive and flexural tensile strength of UHSFRC depending on fibre content and subsequent treatment (age 7 days)

Strength	Unit	Fibre content (Vol.-%)			
		0	0.5	2.5	4.0
Compressive strength (damp box)	N/mm^2	92	106	133	133
Compressive strength (heat treatment)	N/mm^2	138	195	214	234
Flexural tensile strength (damp box)	N/mm^2	11	11	27	28
Flexural tensile strength (heat treatment)	N/mm^2	21	25	34	46

3 Measurement of porosity of UHSFRC

Measurements of porosity on UHSFRC were performed by the mercury intrusion method (MIP) and the gas adsorption method (adsorbate: nitrogen and krypton).

Nitrogen surface areas were calculated from adsorption measurements using the BET method [5]. Nitrogen adsorption was contacted at 77 K using a volumetric method with 0.162 nm^2 as the molecular area for nitrogen. The adsorption of krypton at 77 K has come into widespread use for the determination of relatively small surface areas because its saturation vapour pressure is rather low (p ~ 266.6 Pa). Therefore also krypton adsorption was measured by a volumetric method with 0.210 nm^2 as the molecular cross-section for krypton. The maximum pressure of mercury intrusion porosimetry used was about 420 MPa. A contact angle of 141° and the recommended surface tension value of mercury of 485 mNm^{-2} were used to calculate the pore size distribution.

Both the gas adsorption measurements as well as the mercury intrusion porosimetry measurements were carried out on granulate material with particle sizes of 2 – 4 mm from the respective concrete. The fibres were separated correspondingly before the measurements, so that the obtained results actually refer to the bulk concrete. BET surface areas as well as mercury intrusion porosity measurements of hardened cement paste and concrete are sensitive to the drying procedure (oven drying at 105°C in this work). There is a tendency towards the reduction of the specific surface size with the increasing drying of the hardened cement paste [6].

Figure 1 shows the full adsorption-desorption isotherm (N_2) of the heat-treated UHSFRC in comparison to an ordinary concrete. The basic features of the curve of UHSFRC corresponds to the one for ordinary concrete, i.e. the adsorption and desorption branch shows a wide hysteresis loop for relative pressures $p/p_0 > 0,45$ (gas adsorption isotherm of type II b, formerly termed H3). These types of isotherms are obtained with aggregates of plate-like particles, which therefore possess non-rigid slit-shaped pores [7].
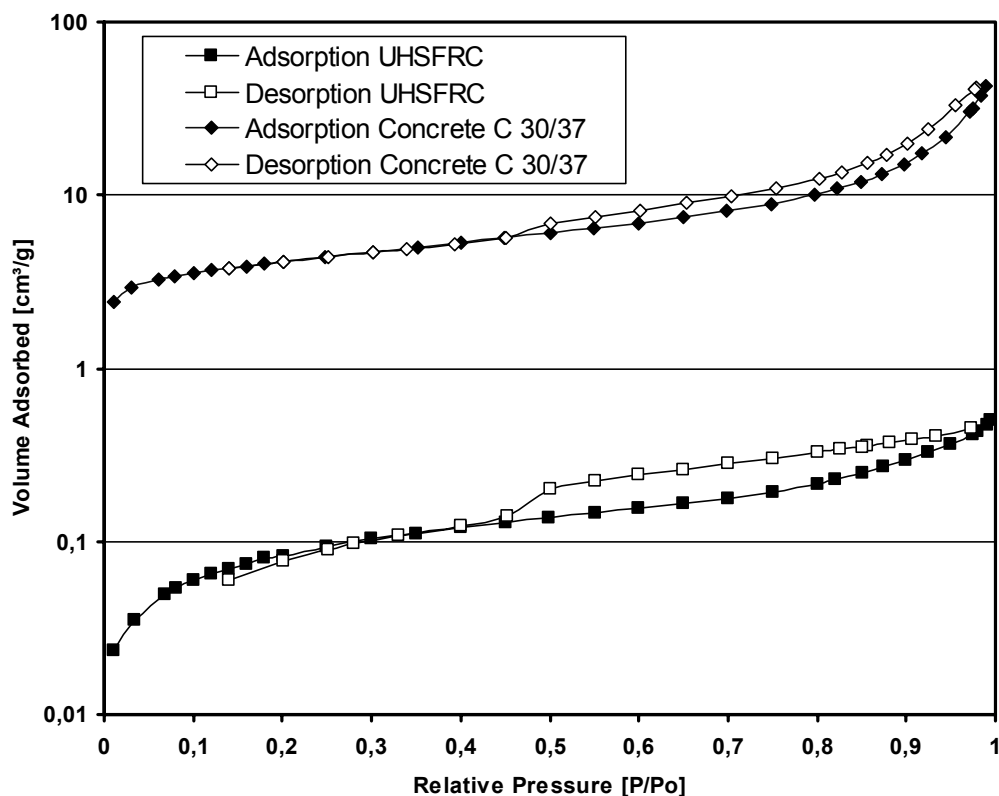
Figure 1: Adsorption and desorption isotherms (N_2) of concrete class C 30/37 and of ultra high strength fibre reinforced concrete

The BET method for calculation of specific surface A involves two steps [5]: evaluation of the monolayer capacity n_m from the isotherm, and conversion of n_m into A by means of the molecular area a_m. A useful check on the validity of n_m is that the value of C (BET constant) should be neither too low nor too high. If C < 50, point B, indicating the completion of the

monolayer, is not sufficiently sharp and the BET monolayer cannot be determined with high accuracy. If C > 200, there is either a significant micropore filling contribution or localized adsorption on specific sites. A "normal" value of C (50 – 150) for low temperature adsorption indicates a well-defined localized monolayer. Surface areas between 2.5 and 150 m^2/g have been reported on hardened cement pastes. The BET constant C mainly falls within the range of 70 to 110 [8].

The specific surfaces calculated from the nitrogen isotherms according to BET resulted in values of about 3 m^2/g for the concrete stored at room temperature independent of cement type. Very similar values were obtained for the specific surfaces when evaluating the krypton isothermes. Due to the heat treatment, the specific surface was obviously considerably reduced. Here the BET surfaces obtained from the krypton adsorption are clearly above the corresponding values from the nitrogen measurements (approx. factor 3). An assessment and detailed interpretation of these measurement results has still to be made. Overall, however, the adsorption measurements give clear evidence of the very low specific surfaces of the ultra high strength concretes, particularly after heat treatment.

Table 4: Results of gas adsorption method and mercury intrusion porosimetry of UHSFRC

Concrete sample		CEM I 42,5 R	CEM I 42,5 R	CEM III/A 42,5 R	CEM III/A 42,5 R
Curing temperature		20°C (28 d)	20°C (2 d) 90°C (2 d)	20°C (28 d)	20°C (2 d) 90°C (2 d)
BET nitrogen	m^2/g	2,88	0,360	2,91	0,64
BET krypton	m^2/g	3,30	1,15	3,35	1,94
Average pore radius (N_2)	nm	5,8	3,5	6,4	3,5
Hg-porosity (420 MPa)	%	10,2	6,2	10,5	6,4
Hg-porosity (200 MPa)	%	8,5	1,6	9,8	2,6
Average pore radius (420 MPa)	nm	7,3	2,8	12,9	3,6
Bulk density	g/cm^3	2,211	2,241	2,258	2,285

If the total porosies measured by MIP are compared to each other at a pressure of 200 und 420 MPa, then the following may be ascertained: the doubling of the applied pressure results only in a comparatively low increase in porosity of the samples stored at room temperature, while for the heat-treated samples there was a significant increase in porosity of around 4 % - 5 %. After the heat treatment a considerable reduction of the pore volume accessible for mercury occurs, which can be attributed to a densifying of the matrix becoming also evident in the in crease in the bulk density. In addition to the decrease of the recordable total pore volume, the average pore diameter is also significantly decreased.
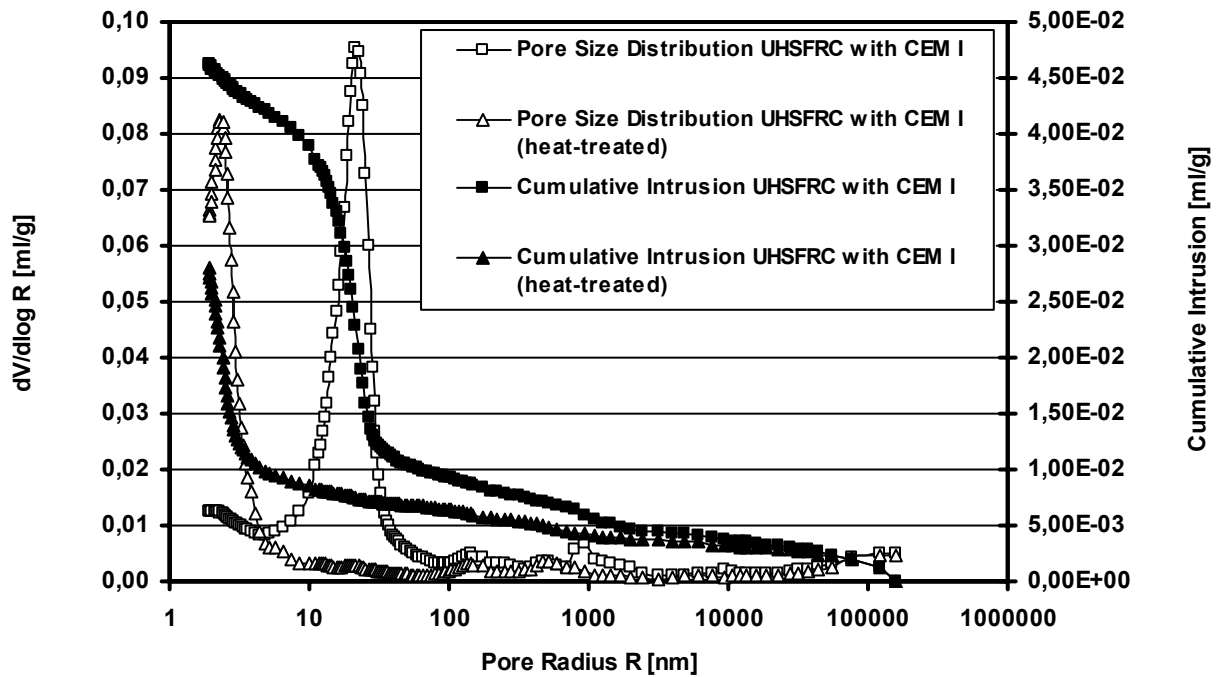
Figure 2: Comparison of the pore size distributions and pore volumes (measured by MIP) of UHSFRC with and without heat treatment (pressure 420 MPa)

The MIP value measured at 420 MPa amounts to about 10 % for the two ultra high strength concretes with CEM I or resp. CEM III. After heat treatment of both concretes their density increases while at the same time there is a significant reduction of the MIP value to about 6 %. The calculated average pore radius is more than halved after heat treatment and corresponds in its magnitude with the average pore radius obtained from the gas adsorption measurements.

In Fig. 2 both the pore radius distribution as well as the cumulative pore volume are shown for UHSFRC with and without heat treatment. After heat treatment there is a distinct shift of the maximum of the monomodal pore radius distribution to considerably smaller pore radii. In addition, the total pore volumes recorded are almost halved.

The measurement scope of the mercury pressure porosimetry mainly includes the mesopore area (pore size 2 – 50 nm). The pore radius distribution recorded using this method indicates pore sizes, which comply practically exclusively with the mesopore area. For this reason the gas adsorption measurements were also evaluated according to a method for recording the mesopore space, even if the form of the gas adsorption isotherms indicates considerable restrictions due to the application to the mesopore range. Considering the various classical procedures proposed for mesopore size analysis, the Barrett, Joyner and Halenda (BJH) method [9] appears to remain the most popular one with a widespread use. The BJH method involves among others the assumption of rigid pores of cylindrical shape (like the mercury intrusion method). Generally in this method, the desorption branch of the hysteresis loop is

favoured for pore size analysis and used to relate the amount of adsorbate lost in a desorption step to the average size of pores emptied in the step.
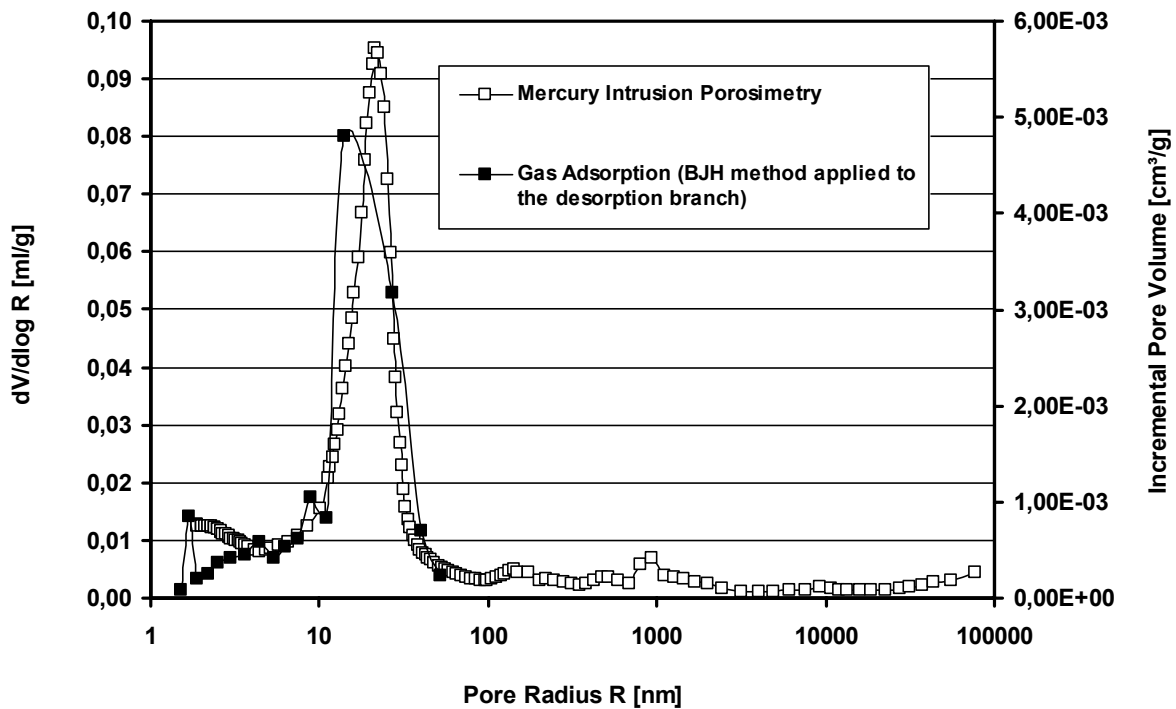

Figure 3: Pore size distribution measured by gas adsorption (BJH method applied to desorption branch) and by MIP (UHSFRC with CEM I without heat treatment)

The range of pores covered by MIP extends from r ~ 1.5 nm (corresponding to the maximum pressure of about 420 MPa) to r ~ 7.5 µm, the size of pore penetrated at atmospheric pressure. There is thus a remarkable overlap of the mercury intrusion porosimetry with the gas adsorption method. But nevertheless the two methods are best regarded as complementary, as each becomes increasingly uncertain when its scope is extended. The gas adsorption method shows uncertainty at the upper end of the mesopore range and the mercury intrusion method at the lower end.

Since in practice the lower limit of pore sizes accessible to mercury porosimetry is about 1.5 nm, and the upper limit of the gas adsorption method is between 10 - 20 nm, the two methods have to be used in conjunction if the complete curve of total pore volume against pore radius is under consideration. To bring the two curves into correspondence it is necessary to choose some reference point on the mercury intrusion curve, not too close to the lower limit of the MIP method (Joyner took r = 4 nm) and then to assume that the total pore volume at that point is given by the cumulative volume from the gas adsorption method. It is expected that the two methods will support each other as far as pore size distribution is concerned, but the agreement of the total pore volumes themselves is merely a consequence of the mode of normalization [7].
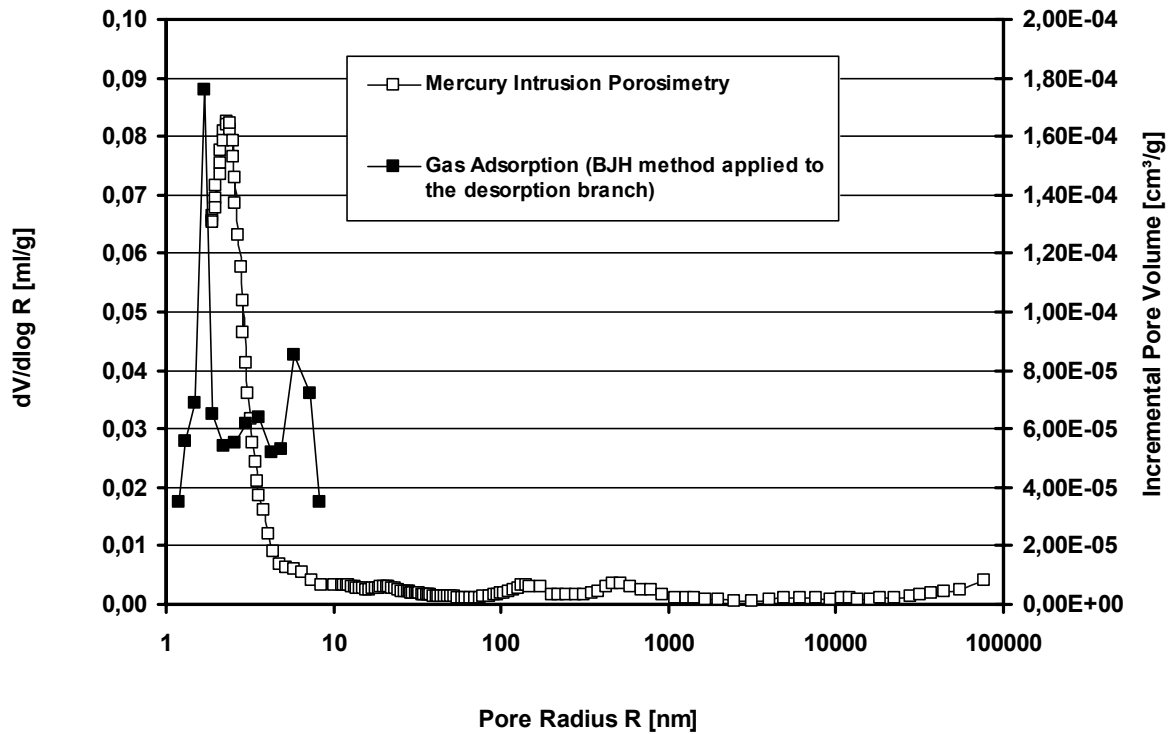
Figure 4: Pore size distribution measured by gas adsorption (BJH method applied to desorption branch) and by MIP (UHSFRC with CEM I and heat treatment)

Figure 3 compares the pore radius distributions obtained for UHSFRC from gas adsorption and MIP, while Fig. 4 gives this comparison of methods for the mesopore area of the heat-treated UHSFRC. Both methods agree in revealing a clear shift of the maximum of the pore radius distribution in the mesopore area to smaller pores as a result of heat treatment.

At the lower end of its range of validity the mercury porosimetry overlaps not only with the gas adsorption method, but also with the scanning electron microscopy method.

The following photograph (Fig. 5) conveys an impression of the structure of ultra high strength concrete mediumly magnified. The carbonated concrete at the surface seems porous to a great extent. The measurement of single pores on this surface seems unrealistic, especially if photographs of the next stages of magnification are taken into account. A greater magnification may well reveal that the sides of the "hills" in Fig. 5 are themselves composed of a series of additional, irregular features on a finer scale. If this finer detail is observed at all levels of magnification, such a surface has an infinite area. Checking the pore diameter determined by gas adsorption and MIP in the lower mesopore area by means of SEM is probably more or less futile for this reason.

Therefore the approaches of fractal geometry [10] seem better suited for obtaining a more realistic description of the inner structure of these cement-bonded materials than the often used inner surface determined by sorption measurements according to BET.

Nevertheless, MIP and gas adsorption measurements are and remain valuable tools in the quantitative recording of structural changes in these materials, even if they are unable to show the actual material structure due to model-based assumptions (e.g. cylindrically shaped pores).
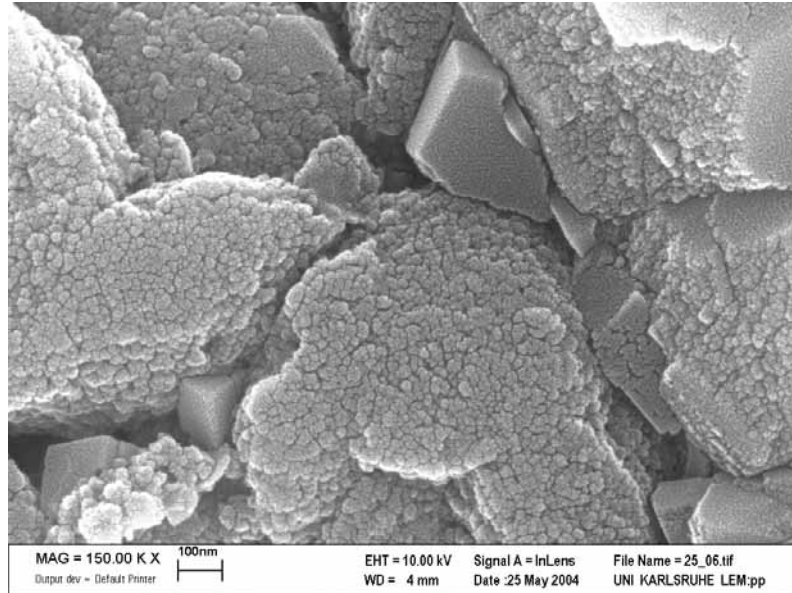

Figure 5: Carbonated surface of UHSFRC with medium magnification (SEM)

4 Discussion and conclusions

The pore space of cement-bonded materials greatly influences its durability. Thus the pore volume and the pore radius distribution of ultra high strength concretes (UHSFRC) were investigated using gas adsorption and mercury intrusion porosimetry. At a pressure increase of 200 to 420 MPa, the intruded mercury volumes rise strongly, indicating very small pore radii which are normally accessible only with gas adsorption measurements. The nitrogen desorption isotherms evaluated according to the BJH method support the mercury porosimetry measurements and show a pore radius maximum of about 1.5 nm.

Considerable differences result in the pore radius distribution and the total porosity between heat-treated and non-heat-treated ultra high strength concrete made with the same constituents. While for the concrete without heat treatment a maximum of about 10 nm can be observed in the pore radius distribution, which is also supported by the gas adsorption measurements, for the concrete treated with heat this pore area disappears, and only the singular pore radius maximum at 1.5 nm can still be observed. In addition, the low specific surface of the ultra high strength concrete is further reduced by the heat treatment. The question, how far the microstructure of the non-heat-treated concrete approaches the heat-treated concrete at a higher age with regard to total porosity and pore radius distribution cannot yet be finally answered.

5   References

[1]   Schmidt, M.: Ultra-Hochleistungsbeton – Ausgangsstoffe, Eigenschaften und Leistungsfähigkeit. Schriftenreihe Baustoffe und Massivbau, Heft 2, Universität Kassel, 2003

[2]   Schachinger, I.; Schmidt, K.; Heinz, D.; Schießl, P.: Early-Age Cracking Risk and Relaxation by Restrained Autogenous Deformation of Ultra High Performance Concrete. Proceedings of the 6th International Symposium on High Strength / High Performance Concrete, Leipzig 2002

[3]   Schwartzentruber, A.; Philippe, G.; Marchese, G.; Laurence, O.: Cracking Tendency of UHSC - Influence of Fibers and Expansive Admixtures. Proceedings of the 6th International Symposium on High Strength / High Performance Concrete, Leipzig 2002

[4]   Schmidt, M.; Fehling, E.; Teichmann, Th.; Bunje, K.: Durability of Ultra High Performance Concrete (UHPC). Proceedings of the 6th International Symposium on High Strength / High Performance Concrete, Leipzig 2002

[5]   DIN 66131: Bestimmung der spezifischen Oberfläche von Feststoffen durch Gasadsorption nach Brunauer, Emmett und Teller (BET). Ausgabe Juli 1993

[6]   Lawrence, C. D.: An examination of possible errors in the determination of nitrogen isotherms on hydrated cements. Cement and Concrete Association; Technical Report 42.520, 1978

[7]   Gregg, S. J.; Sing, K. S. W.: Adsorption, Surface Area and Porosity. 2nd edition, Academic press, 1982

[8]   Lawrence, C. D.: The interpretation of nitrogen sorption isotherms on hydrated cements. Cement and Concrete Association; Technical Report 530, 1980

[9]   DIN 66134: Bestimmung der Porengrößenverteilung und der spezifischen Oberfläche mesoporöser Feststoffe durch Stickstoffsorption – Verfahren nach Barrett, Joyner und Halenda (BJH). Ausgabe Februar 1998

[10] Kriechbaum, M.; Tritthart, J.; Degovics, G.; Laggner, P.: Direkte Bestimmung der fraktalen inneren Struktur von erhärtendem Zement durch Röntgenkleinwinkelstreuung. Zement und Beton, 34. Jahrgang, Heft 4, 1989

Lutfi Ay
PhD, R&D and bridge design engineer
Skanska / Royal Institute of Technology, KTH
Stockholm, Sweden

Curing tests on ultra high strength plain and steel fibrous cement based composites

Summary

Plastic shrinkage is not usually a problem in Ordinary Concrete (OC) since there is normally enough bleeding water. Due to lack of bleeding water UHPC can crack if the surface is not protected from drying. Self-desiccation develops within the whole mass of concrete, while drying begins to develop at the surface of concrete. This can create tensile stress gradients at the surface. The curing membrane that is adequate for OC may not help because it does not prevent UHPC from self-desiccation. The objective of this test was to investigate the performance of plain concrete and Steel Fibrous Cement Based Composite (SFCBC) when they are cured in different curing conditions. Both plain and SFCBC cubes were exposed to three different curing regimes; water, standard and sealed curing. The water-cured specimens had the lowest compressive strength, while the standard cured had the highest compressive strength. It can be concluded that UHPC should not be water cured as much as possible. It should not be expected that the water curing might create an open system in the whole body. A partially open system can harm the balance between inner and the outer part of the concrete. This can result in pre-stressing in the body and on the fibers.

Keywords: *Curing, Hydration, Degree of hydration, Self-desiccation, UHPC*

1   Introduction

According to Aitcin [1], the main component of shrinkage in normal strength concrete is the drying shrinkage. Plastic shrinkage is not usually a problem since there is normally enough bleeding water. Due to lack of bleeding water HPC can crack if the HPC surface is not protected from drying. Aitcin notices also that the rapid development of self-desiccation shrinkage is important during cement hydration. Self-desiccation develops within the whole mass of concrete, while drying begins to develop at the surface of concrete, creating tensile stress gradients at the surface. The curing membrane that is adequate for the usual concrete does not help HPC because it does not prevent HPC from self-desiccation. An external source of water must be available as soon as the hydration begins. According to Aitcin, the sooner and the longer this initial water curing, the better. In addition, when water curing stops desiccation shrinkage begins.

El-Sakhawy et al. [2] investigated the effect of the method and the duration of curing on the concrete durability. The methods of curing were freshwater, wet burlap, plastic film, liquid membrane and air curing (no curing). Their study considered different curing durations of 3, 7, 14, 21 and 28 days. Specimens were exposed to various conditions of deterioration such as sulfate attack, cycles of wetting and drying, temperature change, high temperature, fire and corrosion of reinforcing steel. The concrete had $400 \, \mathrm{kg/m^3}$ cement content, no silica fume and the water-cement ratio was $w/c = 0.45$. They studied the performance of these different curing conditions by comparing the results of compressive and tensile strengths. The water curing gave always the highest compressive and tensile strengths for all conditions of deterioration. The relative performance of the curing methods, listed in decreasing order, was found to be, water curing, wet burlap curing, plastic film curing, liquid membrane and air curing.

Kovler et al. [3] studied the effect of curing conditions on compressive and splitting tensile strength of high strength concretes. They applied two curing regimes: water curing at $20 \, \mathrm{^\circ C}$ and sealed curing at $30 \, \mathrm{^\circ C}$. The mixes were based on low water-binder ratios in the range of 0.25 to 0.35 and the silica content were between $5\,\%$ to $15\,\%$ of the cement content. Autogenous shrinkage was induced in the sealed curing and largely eliminated in the water curing. The effect of autogenous shrinkage on the tensile strength was much greater than on the compressive strength.

Atlassi [4] observed that water does not penetrate into the concrete specimens with low w/c ratios. A reversed moisture gradient (lower relative humidity in the interior of the specimens) is created when they are water cured. The reversed moisture gradient causes internal stresses. The wet exterior part tries to swell but the inner part restrains this expansion. Thus,

tensile stresses on the exterior part and the compressive stresses in the interior part are developed. Thus, the least internal stresses occur in a concrete that is sealed. The compressive stresses due to axial test plus the internal compressive stresses cause decrease in the compressive strength in a wet curing.

Persson [5] did one of the most comprehensive investigations (650 specimens) on the effect of curing conditions on autogenous shrinkage, relative humidity change and strengths of concrete. Persson studied compressive and splitting tensile strength of concrete, which was air cured, sealed and water cured. The study was carried out over a period of 2700 days. The measurements were done at 28, 90, 450 and 2700 days. He investigated six different mixes, which had different compositions and water-cement ratios. The water-cement ratios were between 0.22 and 0.58. The behavior of the mix, which had the lowest water-cement ratio $w/c = 0.22$ at 28 days, is interesting for this unvesigation. This mix had cement content $c = 484 \, \text{kg}/\text{m}^3$ and silica-cement ratio $s/c = 10 \, \%$. The compressive strength of water-cured, sealed and air-cured specimens were $110 \, \text{MPa}$, $112 \, \text{MPa}$ and $119 \, \text{MPa}$, respectively, after 28 days. These values were $139 \, \text{MPa}$, $138 \, \text{MPa}$ and $142 \, \text{MPa}$, respectively, after 2700 days. The water-cured and sealed specimens had lower value than the air-cured at 28 days. The compressive strengths of the three curing regimes were very close to each other after 2700 days.

2   Objectives and description

The objective of this test was to investigate the performance of plain concrete and SFCBC when they are cured in different curing conditions. The questions that will be answered by help of this test program are,

1- Should a concrete, which has very low w/c ratio should be cured as long as possible?

2- Can water curing increase the degree of hydration so that it will contribute to the compressive strength?

3- What is the effect of self-desiccation shrinkage on the compressive strength in a sealed curing, a closed system?

4- Is the standard curing good enough or can we get any benefit by curing SFCBC longer than what the codes require?

5- How does plain concrete and SFCBC behave under the similar curing conditions?

6- Are there other mechanisms during curing, which influence the composites with very low water-cement ratio?

Two series of cubes $(100 \, \text{mm} \cdot 100 \, \text{mm} \cdot 100 \, \text{mm})$ were tested under compression when they were about 34 days old. The first series was of plain concrete and the second series was of SFCBC. Both of the series were cured with three different curing conditions. Three cubes were tested for each curing condition. The first curing condition was so that the cubes were submerged in the water until one hour before they were tested. The second curing condition was water curing for five days according to Swedish standard before the cubes were air

cured until the test. The third one was sealing the cubes by plastic sheeting and keeping them in a climate chamber that has 80 ± 5 %RH and 20 ± 2 °C until the test. Both plastic sheeting and the climate chamber were supposed to prevent the moisture exchange of the specimens from the environment.

Both plain concrete and SFCBC had the same matrix. In other words, they had the same water-cement ratio $w/c = 0.19$, water-binder ratio $w/(c+s) = 0.16$ and silica-cement ratio $s/c = 0.16$. The volume fraction of steel fibers of SFCBC was $V_f = 3.5$ %. Ingredients of these mixes are given in Table 1.

Table 1:   Ingredients of plain concrete and SFCBC

	Amount [kg/m^3]	
	Plain	SFCBC $V_f = 3.5$ %
Water	206	206
Cement	1083	1083
Silica fume	173	173
Fine aggregate, FA2-4	275	247
Fine sand FS20	482	432
Fine sand FS25	161	144
Superplasticizer	38	38
Fibers	-	273

According to the model of Jensen [6] following set of volume fractions V_i [m^3/m^3 cement paste], the hydration products of a cement paste with silica fume, can be described as

Chemical shrinkage	$V_{cs} = k(0.2 + 0.7(s/c))(1-p)\alpha$	(1)
Capillary water	$V_{cw} = p - k(1.4 + 1.6(s/c))(1-p)\alpha$	(2)
Gel water	$V_{gw} = k(0.6 + 1.6(s/c))(1-p)\alpha$	(3)
Gel solid	$V_{gs} = k(1.6 + 0.7(s/c))(1-p)\alpha$	(4)
Non-reacted silica fume	$V_s = k(1.4(s/c))(1-p)(1-\alpha)$	(5)
Unhydrated cement	$V_{uc} = k(1-p)(1-\alpha)$	(6)

where α is the degree of hydration, p is the initial porosity of the paste $p = (w/c)/(w/c + \rho_w/\rho_c + (\rho_w/\rho_s)(s/c))$, s/c is the silica-cement ratio and k is defined as

$k = 1/(1 + 1.4(s/c))$. The density of cement, water and silica are assumed as, $\rho_c = 3150 \text{ kg}/\text{m}^3$, $\rho_w = 1000 \text{ kg}/\text{m}^3$ and $\rho_s = 2200 \text{ kg}/\text{m}^3$ respectively.

The volume of capillary water in Equation (2) must be zero for the hydration stops. The maximum degree of hydration for a sealed system can be derived as

$$V_{cw} = 0 \rightarrow \alpha_{max} = \frac{p}{k(1.4 + 1.6(s/c))(1-p)} \tag{7}$$

And for an unsealed hydration,

$$V_{cw} + V_{cs} = 0 \rightarrow \alpha_{max} = \frac{p}{k(1.2 + 0.9(s/c))(1-p)} \tag{8}$$

According to the model above, this mix has a maximum degree of hydration $\alpha_{max} = 0.36$ in sealed hydration and the maximum degree of hydration is $\alpha_{max} = 0.44$ in an open system. Volume fractions in the sealed and the open systems are given in Table 2. The pore volume due to chemical shrinkage is $V_{cs} = 0.06$ in the sealed hydration. In an open system, the external water causes further hydration and the pore volume vanishes $V_{cs} = 0.00$. To provide an open system only by water curing is impossible. However, water curing may help the concrete to reach higher degree of hydration.

Table 2:   Volume fractions of hydrates in sealed and open systems according to Jensen´s Model

	Sealed	Open system
Max. degree of hydration	0.36	0.44
Chemical shrinkage	0.06	0.00
Capillary water	0.00	0.00
Gel water	0.17	0.21
Gel solid	0.34	0.42
Non-reacted silica fume	0.35	0.31
Unhydrated cement	0.08	0.07
$\sum V_i$	1	1

3   Results and discussions

The weight, the density and the compressive strengths of the two series are given in Table 3 and Table 4. The weight and the density of the specimens vary depending on the curing type in the plain concrete. The water-cured specimens have the highest weight and density while

the sealed specimens have the lowest values. This indicates that a certain amount of water absorption has occurred in the standard and the water curing.

Table 3:   Results of plain concrete specimens, which were cured under different conditions

	Mass [g]	Density [kg/m³]	f_c [MPa]
Water-cured	2465.3 (9.0)*	2394.3 (15.6)	140.1 (6.0)
Standard	2417.3 (3.1)	2384.7 (8.3)	158.8 (6.1)
Sealed	2390.0 (8.0)	2362.3 (18.8)	149.9 (1.9)

(*) The values in the parentheses are the standard deviations of three test results

Table 4:   Results of SFCBC specimens, which were cured under different conditions

	Mass [g]	Density [kg/m³]	f_c [MPa]
Water-cured	2635.3 (12.7)*	2554.7 (21.2)	177.2 (1.8)
Standard	2592.0 (11.1)	2552.0 (9.2)	180.5 (2.8)
Sealed	2605.7 (9.7)	2549.3 (12.1)	173.2 (4.4)

(*) The values in the parentheses are the standard deviations of three test results

The water-cured specimens have the lowest compressive strength $f_c = 140.1 \, \text{MPa}$. The highest value is the compressive strength of the standard curing which is $f_c = 158.8 \, \text{MPa}$. In both cases, the standard deviations are almost $6 \, \text{MPa}$. The difference in the compressive strength is $18.7 \, \text{MPa}$, which is not negligible. The specimens of SFCBC, which were cured by standard method has also the highest compressive strength $f_c = 180.5 \, \text{MPa}$ in comparison with the others. The differences in the compressive strength of SFCBC are not as high as the plain concrete.

It is a well-known fact that, the impermeability of the concrete increases as the compaction increases. This composite, which was tested, is such a material. The hydration reactions of the Ultra High Performance Concrete (UHPC) may differ from the reactions in HPC. One of the possible explanations of why water cured specimens have less strength is that the skin of them hydrated more than the internal core. This caused a denser material at the skin and softer material in the core. The differences in the compressive strength of inner and the outer part of the specimens may have caused the lesser strength. Another explanation may be that during this kind of hydration (water curing) it is very probable that more micro cracks occurred than for the two other curing regimes. The micro fibers that were used in this test may have prevented the micro crack occurrence. This is why the differences in the strengths of SFCBC are not as high as in the plain concrete.

4   Conclusions

From the results of this test, it can be concluded that UHPC should not be water cured as much as possible. It should not be expected that the water curing might create an open system in the whole body. A partially open system can harm the balance between inner and the outer part of the concrete. This can result in pre-stressing in the body and on the fibers.

Self-desiccation influences the compressive strength negatively. The standard curing is better than the two other curing conditions in the short term. However, there must be an optimal duration for curing of UHPC. This may be longer or shorter than the standard requires. This can be mentioned as further investigation for this test. The SFCBC may be less sensitive to moisture gradient and be influenced less by the different curing conditions.

The performances of water-cured samples should not be compared with the other curing regimes in compression. If the benefit of the water curing will be analyzed, the specimens must be dried for a long time before the test.

5   References

[1]   Aitcin P.C.: The use of high-performance concrete in bridge construction, The network of centers of Excellence on High-performance Concrete, Canada, November 1996.

[2]   El Sakhawy N. R., El-Dien H. S., Ahmed M. E., Bendary K. A.: Influence of curing on durability performance of concrete, Magazine of Concrete Research, vol. 51, no. 5, pp 309-318, 1999.

[3]   Kovler K., Schamban I., Igarashi S., Bentur A.: Influence of mix proportions and curing conditions on tensile splitting strength of high strength concretes, Materials and Structures, vol. 32, pp 500-505, 1999.

[4]   Atlassi E.: Effect of moisture gradients on the compressive strength of high performance concrete, Symposium Utilization of High Strength Concrete, Lillehammer, June 20-23, Norway, Proceedings, vol. 2, pp 646-653,1993.

[5]   Persson B.: Hydration and strength of high performance concrete, Advanced Cement Based Materials, no. 3, pp 107-123, 1996.

[6]   Jensen O. M.: Autogenous deformation and RH-change-self desiccation and self-desiccation shrinkage, Ph.D. thesis, $TR\,284\,/\,93$, ISSN $0907-7073$, Building Materials Laboratory, Technical University of Denmark, Lyngby, 1993.

Heinz, D.
Prof. Dr.-Ing.
University of Technology
Munich, Germany

Dehn, F.
Dr.-Ing.
University of Leipzig
Leipzig, Germany

Urbonas, L.
Dr.-Ing.
University of Technology,
Munich, Germany

Fire Resistance of Ultra High Performance Concrete (UHPC) – Testing of Laboratory Samples and Columns under Load

Summary

This study was focussed on the behaviour of UHPC samples with different compositions and dimensions under fire load. For the investigations of the fire resistance, cylinders with $\varnothing$/H = 100/200 mm and columns of practical dimensions - cross section of 120 x 240 mm² and a length of 2 m were made. The concretes were made with steel fibres or with fibre cocktails containing steel and polypropylene. The sample testing followed the standardized "ETK" – temperature curve according to DIN 4102-2. The columns were heated under static load. The temperature distribution in the cylindrical samples and the compression of the columns during the test were determined. Furthermore porosity, pore size distribution (mercury intrusion porosimetry), and microstructure (SEM) of samples were investigated.

Keywords: *ultra high performance concrete, fire resistance*

1   Introduction

Fire resistance of building elements is an important consideration in building design. Building elements from UHPC show different behaviour during fire treatment in comparison with ordinary concrete. Due to its dense microstructure UHPC is more sensitive to fire. The use of steel fibres and especially fibre cocktails from steel fibres and polypropylene fibres (PP-fibres) improve the fracture behaviour of HPC [1, 2]. Hertel et al. [2] doped the UHPC with 0.4 vol.-% steel fibres, 0.4 vol.-% Polypropylene fibres or, a fibre cocktail of 0.2 vol.-% steel fibres and 0.2 vol.-% polypropylene fibres. Despite the destruction of all samples during the fire test, some improvement of fire resistance was observed in concretes with polypropylene fibres or fibre cocktail. Schneider et al. [3] tested the UHPC with steel fibres and 6 mm spliced polypropylene fibres (3.6 and 7.3 kg/m³). In this case no positive effect on the fire resistance was observed.

The aim of this study was to test the influence of steel-polypropylene fibre cocktails on the UHPC behaviour under fire load.

2 UHPC Samples for the Fire Tests

The concretes were made from blast furnace slag cement CEM III B 42,5 NW/HS, silica fume, fine quartz and doped (reinforced) with steel fibres or steel – polypropylene fibre cocktails. Steel fibres with a diameter of 150 µm and a length of 6 mm were used as well as polypropylene fibres with a diameter of 16 µm and length of 4.9 mm. A superplasticizer of polycarboxylate type was used to achieve a low water-cement-ratio. The concrete mix designs are presented in Table 1.

A high intensity pilot vacuum mixer (R 08 VAC. Fa. EIRICH) was used for the production of fresh concretes. The workability of mixtures decreased with increasing amount of PP-fibres at the same water-cement-ratio. Especially concrete 3 with 0.66 vol.-% PP-fibres showed a low workability.

For the investigations of the fire resistance, cylinders with Ø/H = 100/200 mm and columns of practical dimensions - cross section of 120 x 240 mm² and a length of 2 m were made. After 24 hours, the concrete specimens were removed from the mould and heat-treated in water at 90 °C for 24 hours. After heat-treatment, the concrete samples were stored at approximately 20 °C and 50 % relative humidity. After 5 months, the compressive strength and Young's modulus of elasticity were determined. The compressive strength of the concrete cylinders was higher than that of the columns: roughly, 180 compared with 125 MPa. The Young's modulus of columns with PP-fibres was about 47,000 N/mm².

Table 1:   The mix designs of UHP concretes

Components	Mass [kg/m³]	Volume [dm³/m³]	Ratios
Concrete 1			
Quartz sand	925	349	sand/CEM = 0.97
CEM III B 42,5 NW/HS	953	318	sf/CEM = 0.21
Silica fume (sf)	204	87	w/c = 0.22
Steel fibres	197	25	w/(c+sf) = 0.18
PP-fibres	-	-	
Superplasticizer (sp)	28	25	
Water	196	196	
Total	2502	1000	
Concrete 2			
Quartz sand	922	348	sand/CEM = 0.97
CEM III B 42,5 NW/HS	950	317	sf/CEM= 0.21
Silica fume (sf)	203	87	w/c = 0.22
Steel fibres	197	25	w/(c+sf) = 0.18
PP-fibres	3	3	
Superplasticizer (sp)	28	25	
Water	196	196	
Total	2498	1000	
Concrete 3			
Quartz sand	916	345	sand/CEM = 0.97
CEM III B 42,5 NW/HS	943	319	sf/CEM = 0.21
Silica fume (sf)	202	86	w/c = 0.22
Steel fibres	273	35	w/(c+sf) = 0.18
PP-fibres	6	6.6	
Superplasticizer (sp)	20	19	
Water	194	194	
Total	2554	1000	

3.   Fire Resistance of Cylindrical Concrete Specimens.

The cylindrical samples were tested in a small test facility. The sample testing followed the standardized "ETK" – temperature curve according to DIN 4102-2. The duration of testing was 90 min. Between 950 – 1050 °C, during the first burning test, the measured temperature was about 50 °C above the standard ETK curve. During the second burning test the measured temperature conformity with "ETK" was better (Figure 1).

Already after a few minutes the sample without polypropylene fibres exhibited spalling (Figure 2, a). After 90 minutes this sample was destroyed beyond recognition. The spalling behaviour of concrete during the fire load was clearly reduced by the addition of PP-fibres (Figures 2 and 3). For the concrete samples with 0.3 vol.-% PP-fibres only small spalling

could be observed. After 90 min. none of the concrete cylinders with 0.66 vol.-% PP-fibres showed any signs of spalling. However, cracks with width of 0.3-0.5 mm appeared distributed over the whole sample surface.
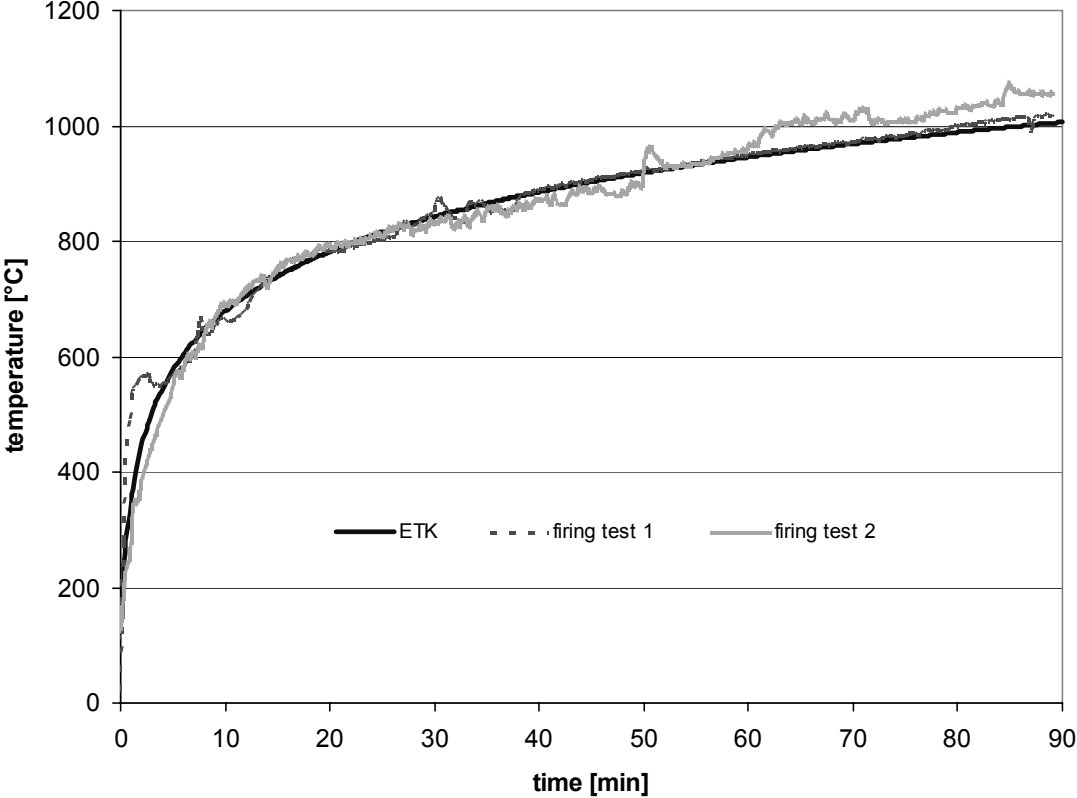
Figure 1:   Temperature development in the burning chamber during fire tests in comparison to standardized temperature curve according DIN 4102-2 (ETK)
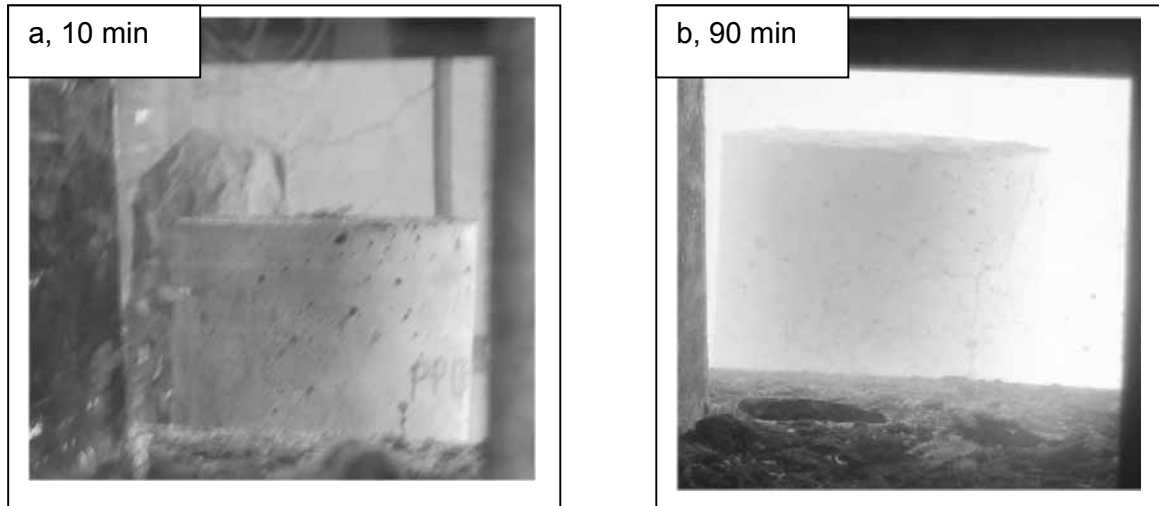
Figure 2:   Concrete samples during fire test (with 0.66 vol.-% PP-fibres in the front; without PP-fibres – left in background)
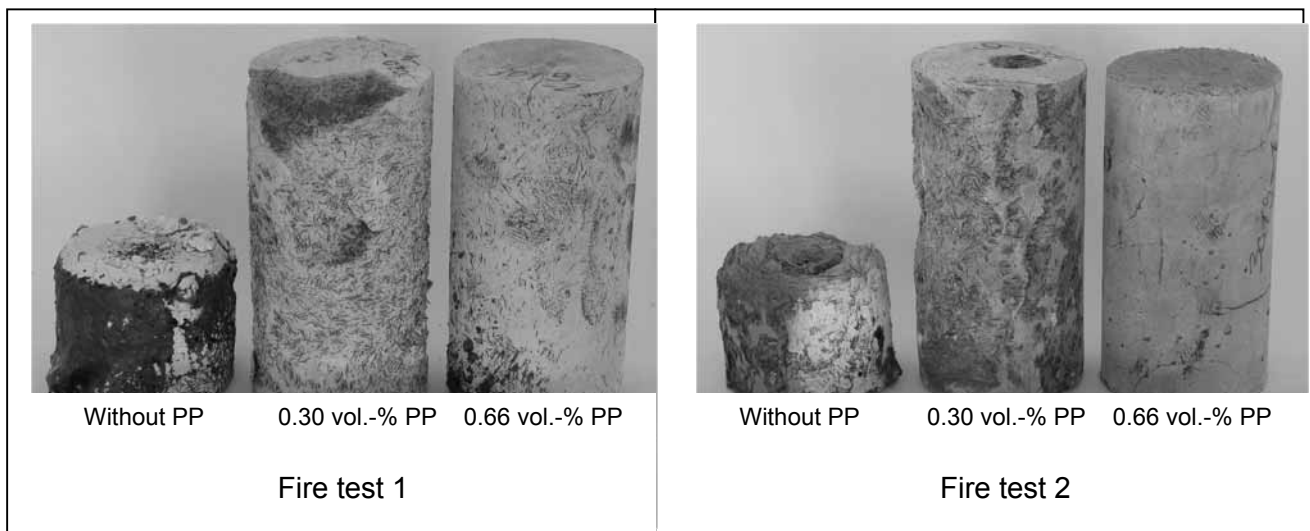
Figure 3:   Effect of polypropylene fibres on the spalling behaviour of concrete samples during the fire test

A high weight loss due to high spalling was measured for the control samples without PP-fibres. The physical and chemical bound water, destruction of PP-fibres and possibly dissociation of carbonates was the reason for 8.7 wt.-% weight loss by concrete cylinders with 0.66 >vol.-% PP-fibres.

Table 2:   Weight changes of concrete samples during the firing test

Concrete sample No.	Without PP-fibres	With PP-fibres 0.30 vol.-%	With PP-fibres 0.66 vol.-%
		Weight loss [wt.-%]	
1	60.6 (1)	14.4 (1)	8.7 (1)
2	62.7 (2)	10.6 (2)	8.9 (1)
3	78.8 (1)	11.4 (2)	8.4 (2)

(1)   Fire test 1

(2)   Fire test 2

During the first firing test (as already mentioned, the temperature was about 50 °C higher as required) a dark brown melt on the surface of concrete was formed (Figure 3). According to the results of an energy dispersive x-ray analysis the resulting slag is composed essentially of FeO, SiO_2 and CaO and small amounts of SO_3, MgO, Al_2O_3 and K_2O (Table 3). Thermodynamic calculations have been carried out for this system by using of program FactSage. The results of the calculations showed that due to oxidation of steel to FeO the melt formation in small amounts already at approx. 800 °C is possible.

Table 3:   Chemical composition of concrete and slag

Component	Concrete	Slag
	[wt.-%]	
SiO_2	61.5	53.0
CaO	20.6	16.9
Fe	8.5	-
Fe_2O_3	0.7	-
FeO		20.1
MgO	2.8	1.1
Al_2O_3	4.1	4.4
SO_3	1.5	3.0
K_2O	0.3	0.5

Four temperature sensors were inserted in to the concrete cube (150 mm) with 0.66 vol.-% PP-fibres to record the development of the temperature distribution in the concrete during the fire test (Figure 4). After 90 min the temperature at 15 mm depth reached 950 °C, in a depth of   75 mm – 700 °C.
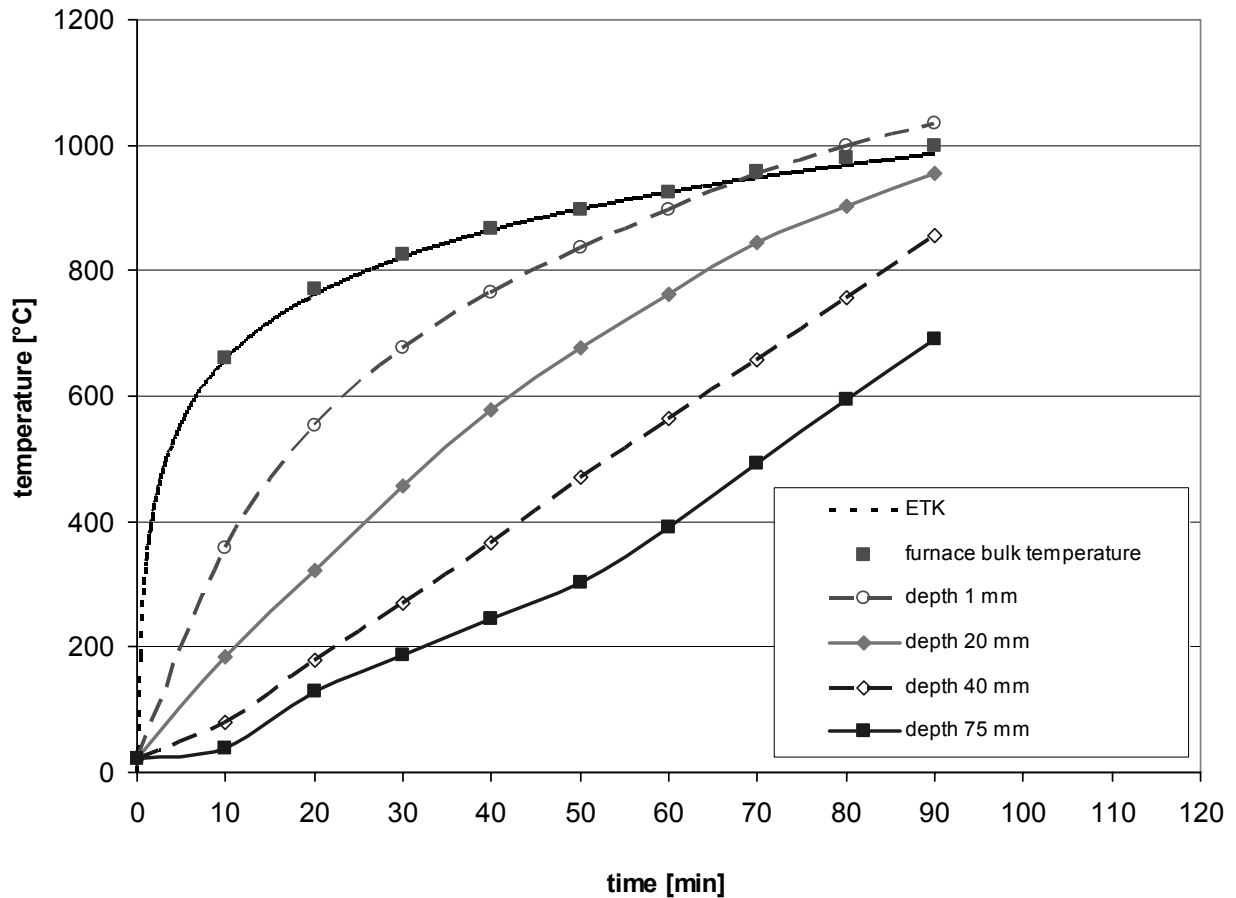
Figure 4: The temperature in different depths of the concrete sample as a function of the duration of the fire test

4.   Fire Resistance of Column Blocks under Mechanical Load

A column with a cross section of 120 x 240 mm² was tested in a large testing facility at MFPA Leipzig (Figure 6). The 2m column was cut in to two blocks with approximately 100 cm length. Each block was placed in the loading facility of the firing chamber before the testing. The narrow side of each concrete block was oriented to a burner (Figure 5). The loading facility as well as the bottom and the head of concrete block were protected against heat using gas concrete slabs. About 70 cm of the sample was located unprotected in the burning chamber. The heating of the burning chamber took place according to the ETK. During firing the blocks was not directly exposed to flames. The temperature of the burning chamber was measured with five thermocouples. The concrete stumps were loaded with 90 (0.52 f_{ck}) and 103 MPa (0.60 f_{ck}) during the fire tests according to [6].

The direct measurement of the block deformation during the test was not possible with the available testing facility. The distance sensor was fixed on the hydraulic cylinder in order monitor the deformation behaviour of the concrete stump.

The observations during the test are noted in the Table 4

Side 2

Flame →   Side 1   Concrete block   Side 3

Side 4

Observation window
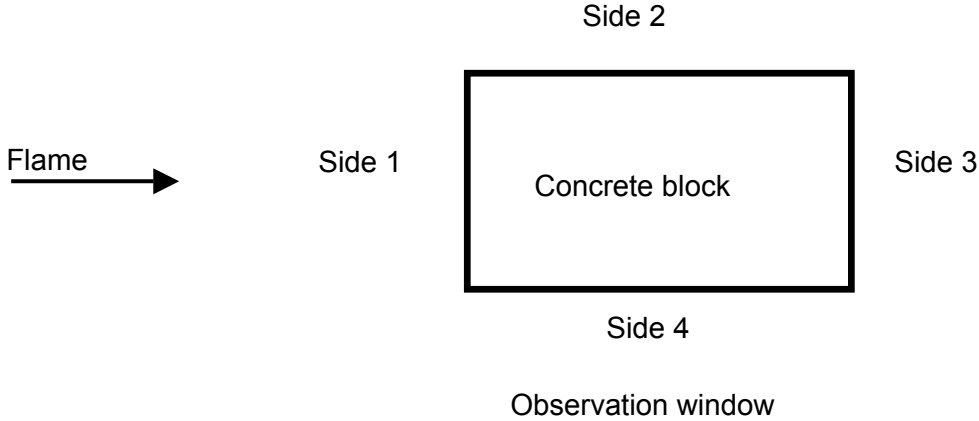
Figure 5:   Position of flame and concrete stumps during the firing test.

The observations during the fire tests showed that spalling of concrete samples started after a relatively short time of test duration (Figure 7). A "spalling period" with relatively short duration was followed by a dormant period without visible propagation of destruction. A short time before failure a small flame on the back part of the concrete block was observed. This phenomenon was caused by combustion of polypropylene fibre decomposition products. No length changes were observed up to 20 min of test duration. During the following test run until failure, contractions of approx. 5 mm/m at 90 MPa load and 6 mm/m at 103 MPa load were measured.

Figure 6: Testing facility

Figure 7: Spalling of concrete during the fire test

The load bearing capacity of concrete block 1, loaded with 90 MPa lasted for 59 min, the stump 2 loaded with 103 MPa – 52.5 min.

Table 4:   Observations during the firing test

Time, min.	Tempe- rature °C (side 4)	Results of observation
Concrete block load with 90 MPa		
-5	20	loading with test load
0	20	test begin
3.5	540	horizontal crack in the middle of stump on the side 4
9	686	crack is dark coloured, repeated noises may be caused by cracking and spalling
11	728	spalling on the bottom of side 4, vertical crack on the side 3
12	735	increasing spalling, however with just a small depth (few millimetres)
17	784	concrete becomes dark coloured
57	955	small flame on the side 3
59	958	abruptly failure of concrete stump
Concrete block load with 103 MPa		
-5	20	loading with test load
0	20	test begin
10	651	spalling on the lower third of side 4
17	757	spalling on the lower third of side 3 (approx. 3 cm)
20	781	more spalling on the side 4
52.5	929	abruptly failure of concrete stump

The porosity, pore size distribution (mercury intrusion porosimetry), and microstructure (SEM) of the samples taken from the destroyed columns were investigated.

As expected the porosity of the parts of the column stressed by fire was higher. So the porosity on the side 4 of the column after fire test ranged from 9.3 to 19.2 %, in the middle of the fire loaded column - about 8.3 %. The porosity of the column part not exposed to fire remained at 7.3 %. The analysis of the pore size distribution showed an increase of the pores with a diameter of approx. 8-20 µm in the fire loaded parts of the column (Figures 8 and 9).
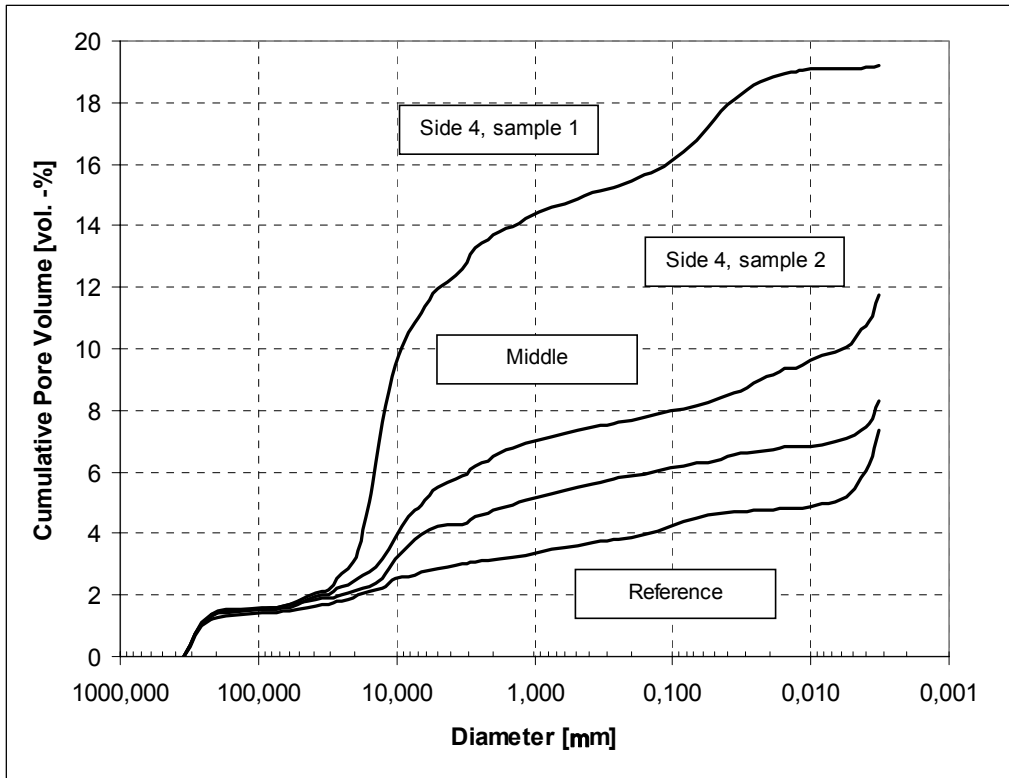
Figure 8:   Cumulative pore size distribution of UHP concrete samples after fire test
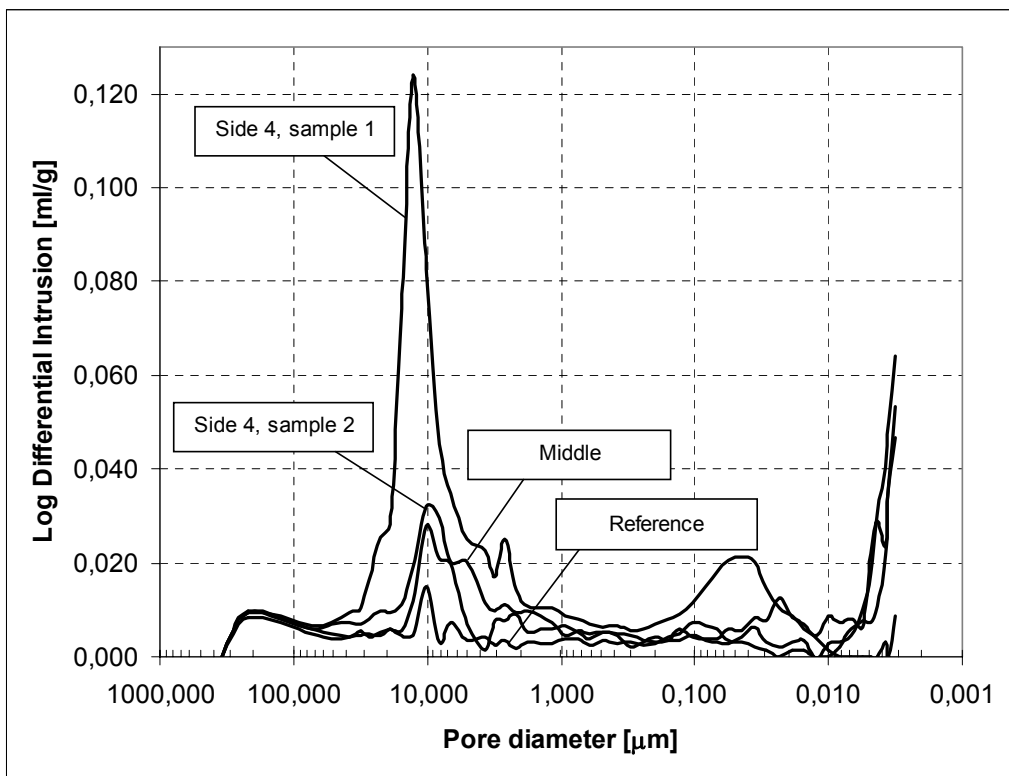
Figure 9:   Differential pore size distribution of UHP concrete samples after fire test

The following figure 10 shows some selected SEM images which indicate the influence of the decomposition of PP-fibres on the microstructure of fire exposed UHPC.
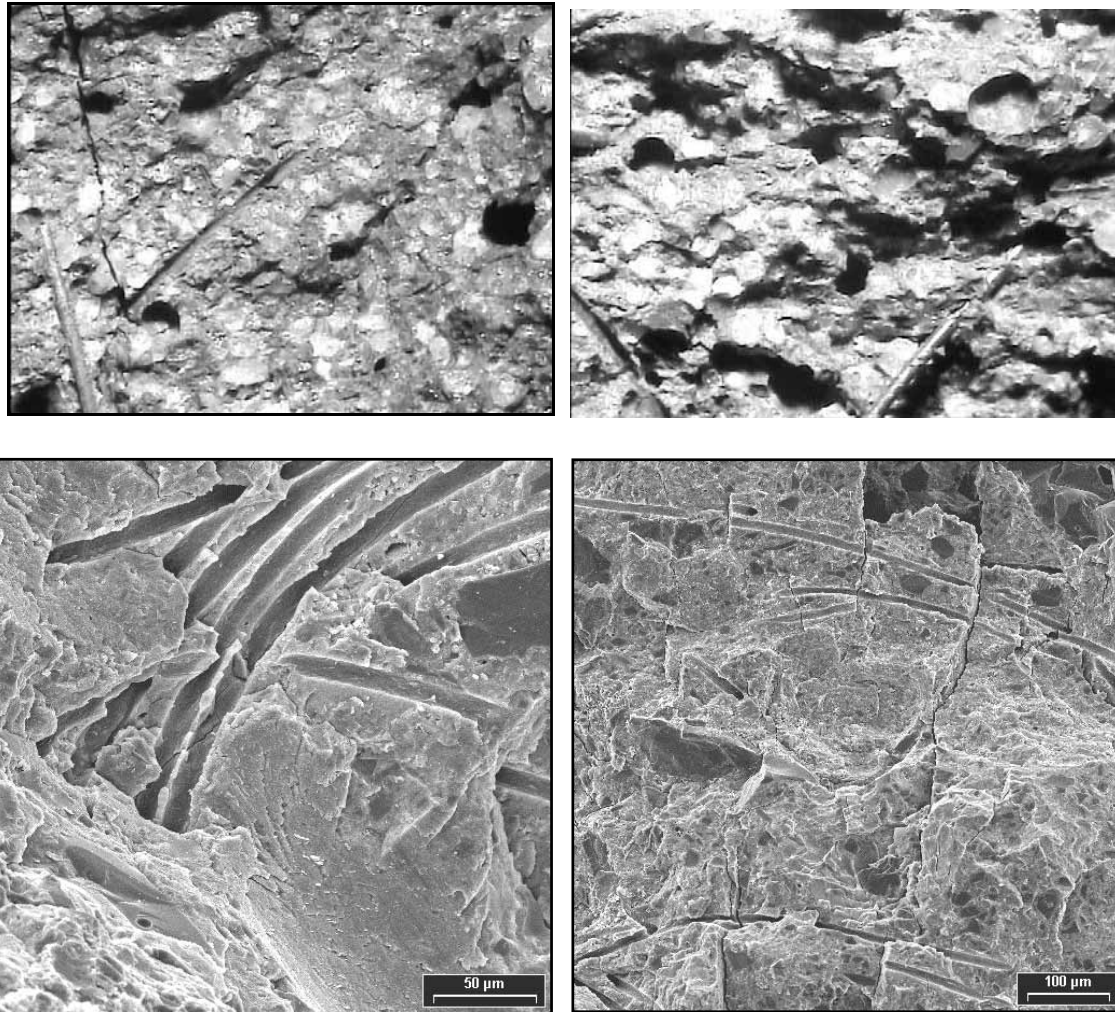
Figure 10: SEM images of the fire exposed UHPS mixtures

5. Discussion of Results

The fire resistance of concretes depends on several factors. The most important are the type, the size, and the content of aggregates, the nature and the content of hydrated phases, the additions of different sorts of fibres, the strength and the porosity of the concrete. The former investigations showed a relatively unfavourable fire resistance of UHPC [2,3]. The main reason is the very dense, brittle structure. According to [3], the spalling of UHPC during the fire load occurs due to high steam pressure in the concrete leading to high internal stresses. The use of appropriate types and amounts of polypropylene fibres improves the spalling behaviour of UHPC. Above 150 °C, polypropylene fibres begin to melt, above 200 °C to volatilize and provide additional capillary pores. In this investigation the measured pore diameter was in the region between 8 and 20 µm, comparable with the diameters of polypropylene fibres. For a successful improvement of the fire resistance, the quality and the amount of the PP-fibres are important. The best behaviour under fire load was shown by the concrete mix with the best fracture behaviour [5]. The concrete specimens with 3.5 vol.-%

steel fibres and 0.66 vol.-% PP-fibres showed no spalling after fire test duration of 90 min according to ETK curve. The attempts to improve the fire resistance of UHPC with spliced PP-fibres or with lower PP-fibre amount were less successful [2, 3].

At higher temperatures of about 1000 °C a melt formation was observed. The chemical and thermodynamical investigations showed that due to oxidation of steel to FeO a melt formation in small amounts already at approx. 800 °C is possible. This phenomenon affects negatively the behaviour of concretes made with steel fibres at high temperatures.

During the fire test on the mechanically loaded columns, in contrast to unloaded cylinders, some spalling in the first 20 min was observed. During this time the temperature in 1 mm concrete depth reached about 550 °C, in 20 mm depth – 320 °C. At these temperatures dehydration of calcium silicate hydrates and calcium aluminate hydrates will have taken placed. The α–β quartz conversion takes place at a higher temperature - at 573 °C. It is possible that mechanical load caused additional stresses and strains in the structure of UHPC that rose the spalling. The load bearing capacity of concrete columns at 90 MPa and 103 MPa was maintained for 52 and 58 min respectively. Behloul et al. [4] found that columns made from UHPC with PP-fibres stayed intact 82 to 89 min during the fire test by using an ISO fire curve (identical with ETK). In this case, however, the mechanical load of the columns was with 50 MPa relatively low.

6.   Conclusions

- Additions of suitable amounts of steel and polypropylene fibres permit the improvement the fire resistance of ultra high performance concrete. The best results were achieved with 3.5 vol.-% steel fibres and 0.66 vol.-% PP-fibres

- Possibly the use of higher mechanical loads reduces the achievable fire resistance class

- Additionally, fire resistant surface coatings are advisable for a satisfactory fire resistance of UHPC containing steel and PP-fibre cocktails

714

7 References

[1] Kützing, L.: Fire Resistance of High Performance Concrete with Fibre Cocktails. In: Leipziger Annual Civil Engineering Report, LACER Nr. 4, 1999, S. 185 – 192

[2] Hertel, C., Orgass, M., Dehn, F.: Brandschutztechnische Aspekte bei Faserbetonen. In: König, G., Holschemacher, K., Dehn, F.: Faserbeton - Innovationen im Bauwesen, Bauwerk-Verlag, Berlin 2002

[3] Schneider, U., Horvath, J., Dehn, F.: Abplatzverhalten von ultrahochfestem Beton (UHPC) unter Brandbeanspruchung In: Leipziger Annual Civil Engineering Report, LACER Nr. 6, 2001, S. 1 – 9

[4] Behloul, M., Chanvillard, G., Casanova, P., Orange, G.: Fire Resistance of Ductal Ultra High Performance Concrete. In: Proceedings of First fib Congress, 13-19 Oct. 2002, Osaka, Japan, pp. E278 1-10

[5] Schachinger, I., Stengel, Th., Heinz, D.: Einsatz von Fasern zur Verbesserung des Nachbruch verhaltens von ultrahochfestem Beton im Biegezugversuch. In: ibausil, Internationale Baustofftagung, 24.-27. September 2003, Weimar, S.2-0313 – 2-0322

[6] Association Française de Génie Civil (AFGC): Bétons fibrés à ultra-hautes performances – recommandations provisoires, Janvier 2002

Detlef Heinz

Prof. Dr.-Ing.

cbm centre for building materials, TU Munich

Munich, Germany

Horst-Michael Ludwig

Dr.-Ing.

Schwenk Zement KG

Karlstadt, Germany

Heat Treatment and the Risk of DEF Delayed Ettringite Formation in UHPC

Summary

Heat-treatment is one stage of processing during the production of ultra-high performance concrete (UHPC). This treatment is necessary to achieve the high compressive strengths of > 200 N/mm² characteristic of UHPC. In most cases treatment temperatures of 90 °C or above are applied. For conventional concretes made with cements, susceptible to heat-treatment, it is well established that temperatures above 70 °C can cause delayed ettringite formation (DEF) as a disruptive process during the service life of the concrete.

This paper discusses the theoretical background and the parameters affecting the risk of a DEF in UHPC and describes the strength development, the microstructure and the phase composition of heat-treated UHPC. The results from laboratory testing of UHPC confirm the hypothesis, that DEF should be no risk for UHPC.

Keywords: *UHPC, delayed ettringite formation, phase composition, microstructure, compressive strength*

1   Introduction

Ultra-high strength concrete or more accurately ultra-high performance conrete UHPC is a very compact, fine or coarse grained type of concrete which has been developed as a new type of construction material during the past decade. The concretes considered here are of the fine grained type with a maximum grain size of 0.5 mm and a compressive strength between 150 and 270 MPa. Heat curing at 90 °C is common method to produce such high strengths. The application of this temperature raises the question whether there is any danger of DEF during the subsequent service life with corresponding negative effects on the performance of the UHPC components.

Since the end of the seventies of the past century, a number of cases have been reported of damaging expansion and map cracking of precast concrete products which were heat treated during production. The damage observed in railway sleepers made of prestressed concrete and cured at temperatures as a high as 100 °C is well known. This provoked intensive research efforts [1,2]. Today it is well established that the deterioration process only occurs when the treatment temperature exceeds ~ 70 °C and that the reason for expansion and cracking is delayed ettringite formation, which is in fact a type of internal sulphate attack (ISA) [3].

The following contribution discusses the relevant parameters potentially affecting volume stability of heat treated UHPC and describes the strength development, the porositiy and the phase composition of heat-treated UHPC.

2   DEF – State of Knowledge

During heat-treatment of concrete at early ages high temperatures lead to specific alterations in the formation of hydrate phases. Heat-treatment of cement of normal compositions (OPC) at temperatures up to 100 °C causes primarily formed ettringite as well as monosulphate to disappear [3,4]. Small amounts of a hydrogarnet can be found at higher temperatures. The early hypothesis that with increasing temperature an increasing part of the alumina and the sulphate is incorporated in the CSH-phases was confirmed by the investigations of [3]. Beside the reversible incorporation of sulphate in the CSH, monosulphate is found in very small pores of the CSH paste directly after the heat treatment. Depending on the cement composition and the environmental conditions (humidity, temperature etc.) sulphate and monosulfate react to form ettringite and create expansion. Only concrete that has experienced temperatures above 70 °C show deterioration under some circumstances [3,4]. The expansion occurs typically after 1 to 4 months under laboratory conditions but in field concretes it can be much later.

During the past 20 years many parameters affecting DEF have been investigated [3,4]. The most important chemical parameters are the SO_3 and the C_3A content of the cement, the molar ratio SO_3/Al_2O_3 and the content of alkalies. At present there is no satisfying description of the complex relationship between cement composition and damaging DEF [6]. For a specific cement clinker there is a threshold value for the sulphate content. In all cases values < 3 wt.-% SO_3 do not result in expansion [4,6]. Cements with medium C_3A content show expansion only with medium and high alkali content. Most important for UHPC is that cements with low or no C_3A are less susceptible to DEF and that blends with > 30 wt.-% siliceous fly ash or > 30 wt.-% slag (ggbs) show no expansion [2,6,7]. Results for binders with comparable silica fume contents are not available.

DEF needs water for the necessary transport processes in the paste. Normal concretes and mortars show expansion only when there are periods of sufficient water uptake by direct water contact or the concrete is exposed to an ambient humidity of > 95 % r.h..
Decreasing w/c-ratios lead to dense pastes with low capillary porosity. This prolongs the start of the DEF. Even with a w/c as low as 0.4 DEF started after 2 years and finished after 8 years in water stored laboratory mortar samples, which had been heat treated at 90 °C [7].
Low ambient temperatures accelerate DEF and the expansion process [4].

3   Composition of UHPC

The investigations on the influence of an early heat-treatment on the properties of UHPC were made with Duracrete products of Schwenk. Basis of the UHPC-systems of Schwenk are two cements, a CEM I 42,5 R-HS and a CEM III/B 42,5 NW/HS, with a high sulphate

resistance. The cements are chosen according to different applications. The benefits of these cements for the application in UHPC are generally the low water demand, the low heat of hydration, the good workability and the favourable characteristic of hardening. The other cements used, especially for the investigations of the risk of a damaging DEF after a heat-treatment, are shown in table 1.

Table 1: Selected properties of the used cements

		CEM I 42,5 R-HS	CEM III/B 42,5 NW/HS	CEM I 42,5 R	CEM I 42,5 R white	CEM I 42,5 R
		1	2	3	4	5
SO_3	wt.-%	2.7	3.5	3.73	2.7	3.2
C_3A	wt.-%	1.9	-	9.5	10.2	10.6
SO_3/Al_2O_3	mol.ratio	0.93	-	0.82	0.84	0.7
Na_2O_e	wt.-%	0.73	0.69	1.23	0.43	0.72
ggbs	wt.-%	-	69	-	-	-

Reactive and inert additions are used, which give an optimized grain size distribution in combination with the cements. These additions are a special quality of silica fume, finely ground granulated blastfurnace slag (GGBS) and quartz with a grain size < 0.5 mm. The dosages of silica fume adjusted in the experiments described here expressed as sf/c-ratio are ~ 0.25 for the CEM I and ~ 0.12 for the CEM III.

The w/c-ratio of the UHPC systems is ~ 0.22. For the adjustment of consistency a superplastiziser on polycarboxylatic ether basis is used, especially designed for low water concretes. The dosage depends strongly on the applied fibre cocktail and lays between 1.0 and 1.5 % of the cement content.

The fibre cocktail is individually optimized for every application. For better comparable results the investigations on the heat treatment of UHPC described here were made without fibre addition. Basically the results are also valid for UHPC with fibres, because fibre addition doesn`t affect the durability of the matrix and the compressive strength only to a small extent.

4   Heat-treatment

The heat treatment was carried out at temperatures between 65 and 180 °C. Following placement the specimens were left in the formwork for 24 h in a moist atmosphere at 20 °C and a relative humidity of 93 %. The UHPC specimens were then heat-cured according to the procedures in Table 1. The relative humidity was 93 % during the heat-treatments.

Table 2: Heat-treatment procedures with different maximum temperatures

	65 °C	90 °C	105 °C	120 °C	180 °C
1st heating	up to 65 °C in 1h	up to 90 °C in 1h	up to 90 °C in 1h	up to 90 °C in 1h	up to 90 °C in 1h
1st constant temperature	22 h 21 min	22 h	10 h	10 h	10 h
2st heating	-	-	up to 105 °C in 1h	up to 120 °C in 1h	up to 180 °C in 1h
2st constant temperature	-	-	10 h 47 min	10 h 34 min	9h 43 min
cooling (1.17 K/min, 65 % r.h.)	down to 20 °C in 39 min	down to 20 °C in 1 h	down to 20 °C in 1h 13 min	down to 20 °C in 1 h 26 min	down to 20 °C in 2 h 17 min

5   Compressive Strength

Figs 1 and 2 show the development of compressive strength for the two UHPC systems with the cements 1 and 2 over the range of different heat-treating temperatures. The optimum addition of fibres can result in a further strength increase. It is apparent that at 20 °C the UHPC systems achieve 28d strengths of approximately 170 MPa and 180 MPa, respectively. As expected, better results were obtained for the 1d strength of concrete made with CEM I 42,5 R-HS compared with the concrete containing ground granulated blastfurnace slag, 51 and 36 MPa, respectively. Contrasting this behaviour, UHPC made with Portland blastfurnace cement exhibited a well-defined delay in strength development (190 MPa after 56 d) whereas UHPC with CEM I 42,5 R-HS had almost reached its strength potential after 28 d.

The different heat-treatments led not only to an increase in compressive strength compared with the 20°C storage, but also caused the final strength to be available immediately after completion of curing.

The compressive strength increased with the temperature of heat-treatment between 65 and 120 °C continuously and reached 230 to 240 MPa. A sudden increase in strength was observed on further increasing the heat-treatment temperature to 180 °C. In this case strengths between 270 and 280 MPa were reached.

The slight reduction in strength measured for the heat-treated-specimens at 28 d compared with 1 d values is due to relaxation following the heart-treatment. The compressive strength measured after longer periods of time did not decrease further.
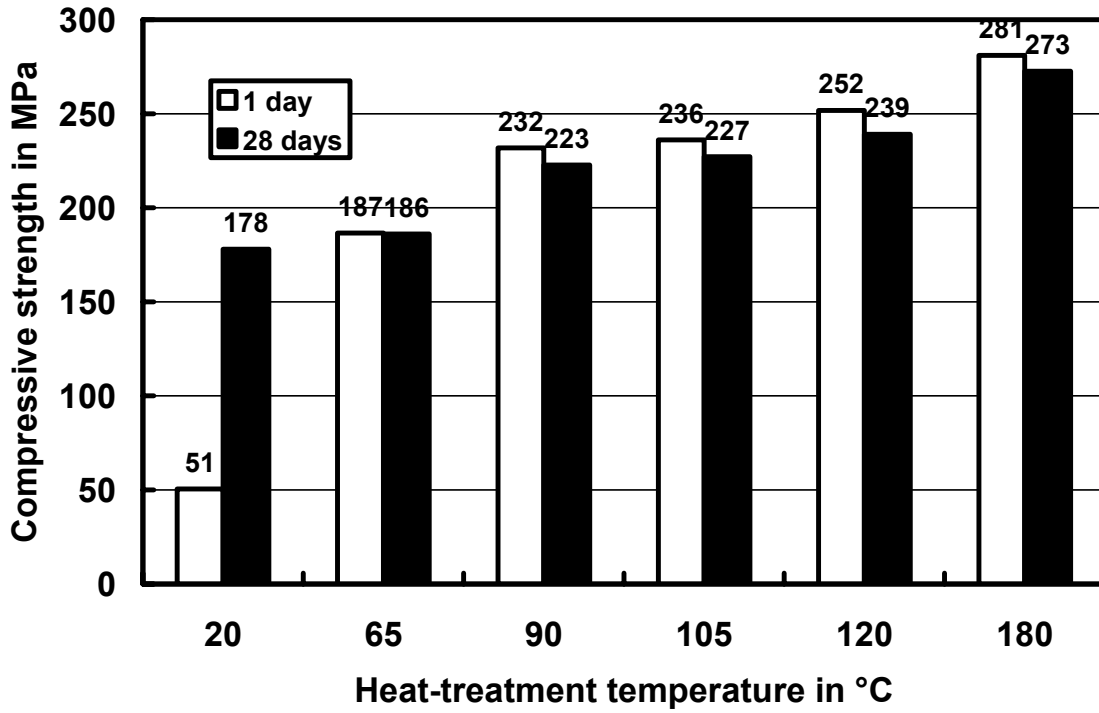
Fig. 1   Compressive strength of UHPC made with CEM I 42,5 R-HS and heat-treated at various temperatures
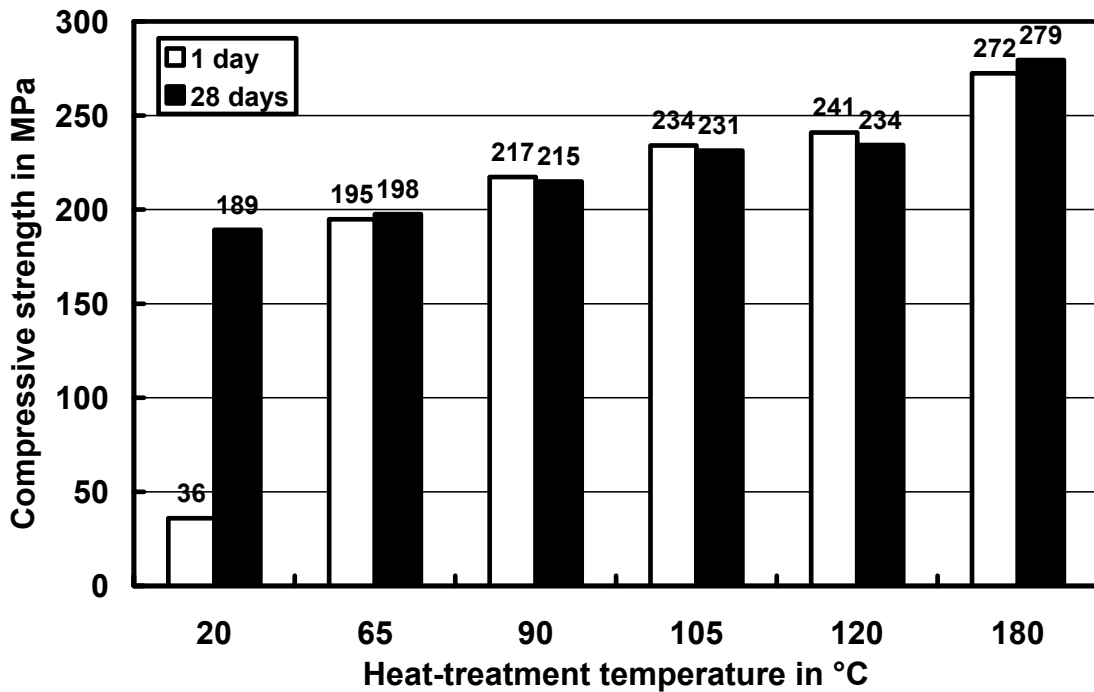
Fig. 2   Compressive strength of UHPC made with CEM III/B 42,5 NW/HS and heat-treated at various temperatures

6 Development of Microstructure

As well as high strength, the highly compact microstructure UHPC is an important property. The size and number of capillary pores determine the degree of compactness of the micro-structure. They also control the transport of aggressive media from the environment into the concrete.

In Fig. 3 pore size distributions obtained with mercury intrusion porosimetry are compared for the concretes C 20/25, C 35/45, C 70/85 and UHPC (without heat-treatment). It is apparent that the capillary porosity (pore diameters > 10 µm) is lower at higher strength classes. Whereas the capillary porosity of the two normal concretes C20/25 and C 35/45 are 15.6 vol.-% and 12.7 vol.-%, respectively, the porosity of the high-performance concrete C70/85 is lower at 8.5 vol.-%. The greatest compactness was achieved by the UHPC with a capillary porosity of only 5.0 vol.-%.
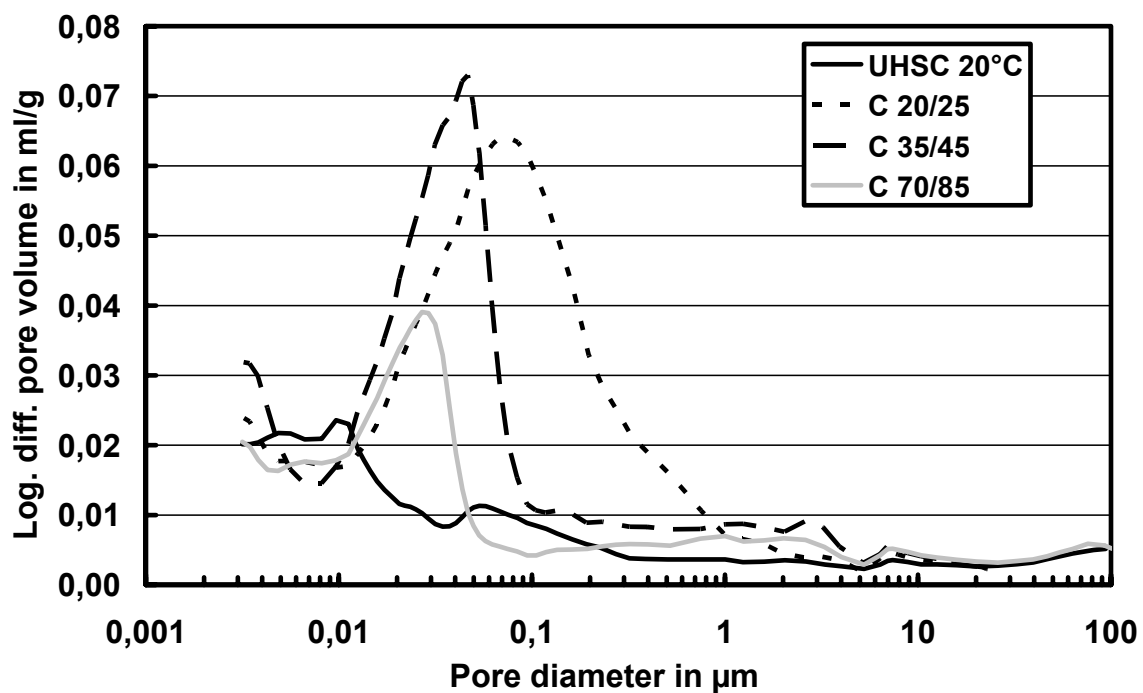
Fig. 3   Pore size distribution of UHPC and concretes of various strength classes

Fig. 4 shows the total and capillary porosity measured with mercury intrusion porosity for UHPC heat-treated at various temperatures. The results indicate that heat-treatment above 90 °C enables the reduction of capillary porosity to values around 2 vol.-%.
As well as reducing of the total and capillary porosity, heat-treatment leads to modification of the C-S-H microstructure. This is characterized by, for example, the ratio of coarse gel pores (>3 nm) determined by mercury intrusion porosity to fine gel pores (< 3 nm) determined by helium pycnometry, Fig.5. The proportion of finer gel pores increases steadily as the temperature of heat-treatment is raised to 120 °C. At the same time the amount of coarser

gel pores decreases. Above 180 °C the trend reverses and the amount of finer gel pores decreases.
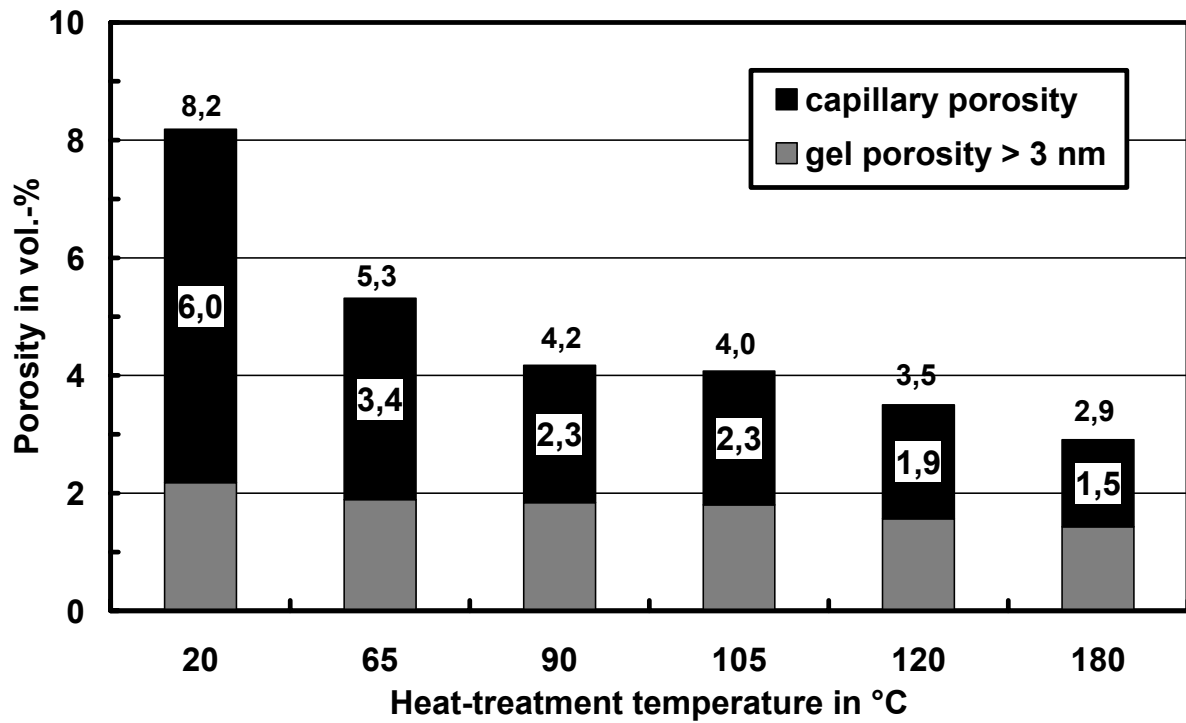
Fig. 4   Capillary and total porosity of UHPC made with CEM I 42,5 R-HS and heat-treated at different temperatures
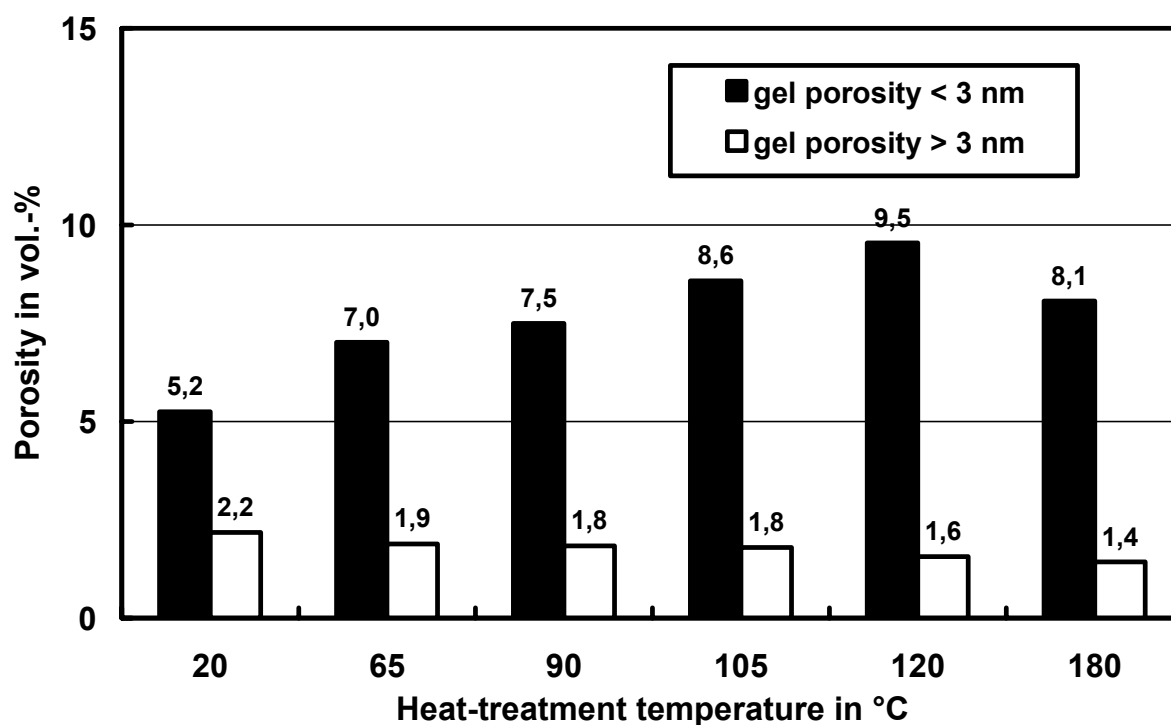
Fig. 5   Contribution of finer and coarser gel pores to porosity of UHPC made with CEM I
          42,5 R-HS and heat-treated at different temperatures

The above observations are in good agreement with the results of chemical and mineralogical investigations performed with hardened cement pastes. As the temperature of heat-treatment increases to 120°C the C/S-ratio for the C-S-H phases becomes smaller. However, crystalline C-S-H phases do not form. The lower C/S-ratio leads to stronger bonding within the C-S-H phases and thus increased strength and compactness of the solid matrix. Above 180 °C quantities of crystalline C-S-H were detected.

7   Phase Composition

In order to obtain information on phase composition and the effect of heat-treatment, the UHPC systems were investigated using X-ray diffraction (XRD) and thermal analysis (DSC/TG). In addition, scanning electron microscopy was used to investigate the morphology of the phases present.

The results of the X-ray diffraction measurements with UHPC made with CEM I 42,5 R-HS - corrected for quartz - are presented in Fig. 6. The data were analysed using the Rietveld method. However, the values in Fig. 6 indicate the relative rather than absolute changes in phase composition caused by the different heat-treatments.
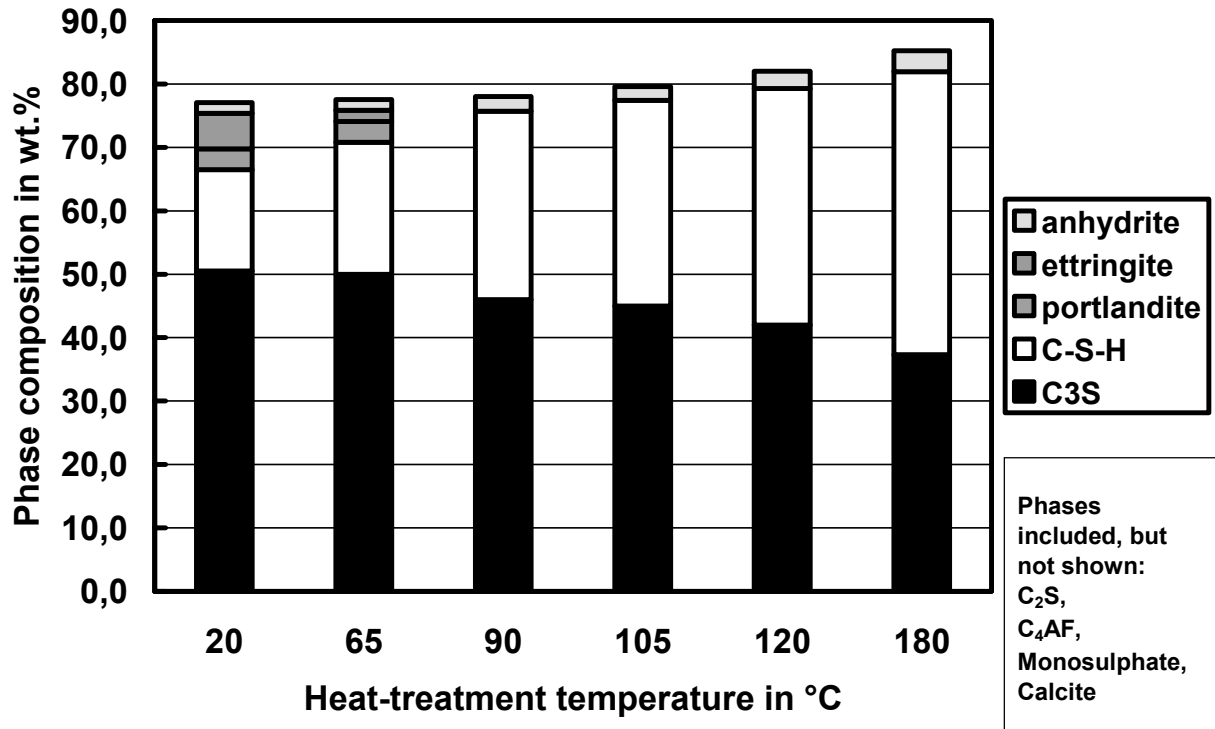
Fig. 6   Phase composition of hardened cement paste in UHPC made with CEM I 42,5 R-HS and heat-treated at various temperatures

The data obtained did not permit an exact quantitative assessment of the phases because, for example, it was not possible to determine directly the contribution of the X-ray amorphous C-S-H phases. A model calculation was used to estimate the amount of amorphous C-S-H.

The thermal analysis provided additional information on the effect of heat-treatment. The corresponding DSC curves are presented in Fig. 7.
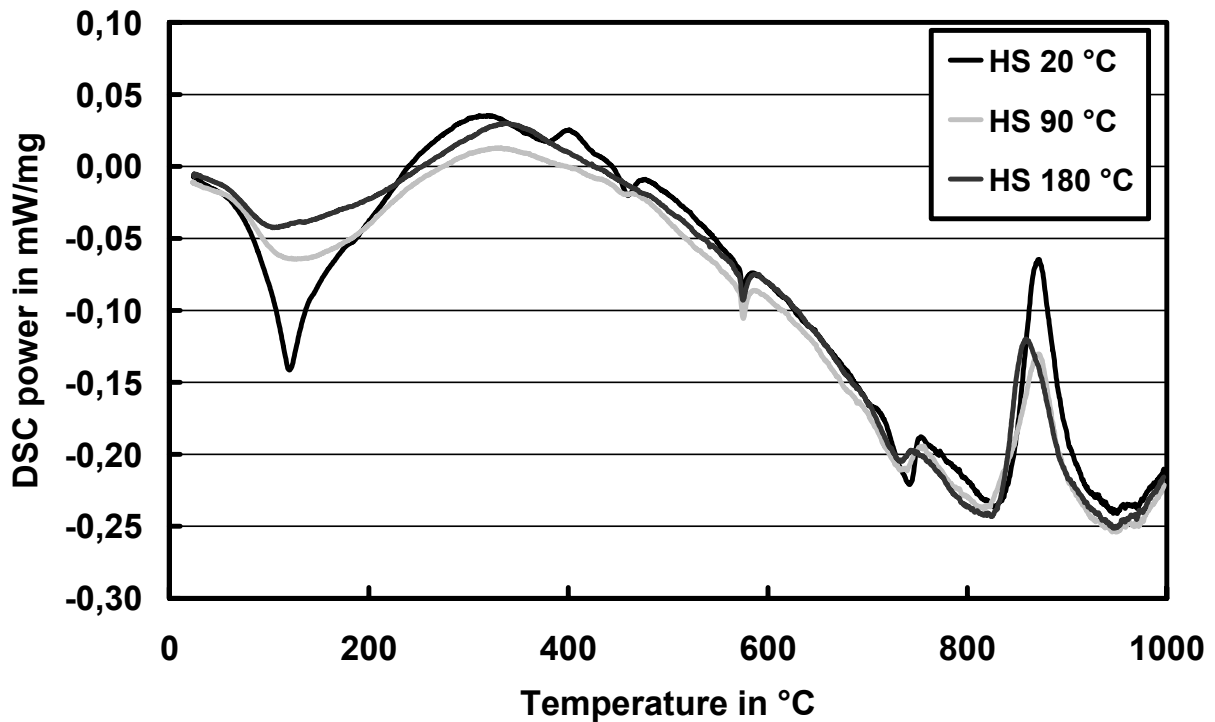
Fig. 7   DSC curves for UHPC made with CEM I 42,5 R-HS and heat-treated at various temperatures

The following statements may be made based on the analyses of the phases and in view of the results obtained using scanning electron microscroscopy:

All specimens contain considerable quantities of unhydrated clinker phases C_3S, C_2S and C_4AF. The amount of these phases decreases with the temperature of heat-treatment.

The sulphate added to the cement to govern its setting behaviour did not completely react. Residual anhydrite was found in all specimens.

In all cases the C_3A phase reacted completely. This is due to the high chemical reactivity of this phase and the use of CEM I 42,5 R-HS cements with low C_3A contents.

As expected, ettringite was not present in specimens subjected to heat-treatment at temperatures above 65 °C. This conforms to the well-known behaviour of normal concrete cured at this temperature.

Calcium hydroxide (portlandite) is not present after heat-treatment at 65 °C and above. This can be explained by the enhanced reactivity of the silicate additives which bind more calcium hydroxide at higher temperatures. This effect was also apparent in the the scanning electron micrographs.

At higher heat-treatment temperatures a heightened reaction rate leads to more intensive C-S-H formation from the clinker phases as well as from the fine additives (silica fume, ground granulated blastfurnace slag). Whereas at 120 °C the C-S-H phases are completely

amorphous to X-rays, crystalline C-S-H phases develop during heat-treatment at 180 °C. A mineralogical classification of these phases is not currently possible. However, it can be excluded that they are Xonotlite (C_6S_6H) which can form in UHPC at temperatures above 230 °C. The morphology of the C-S-H phases obtained at 90 and 180 °C is compared in Figs 8 and 9.

More silicon is incorporated in the C-S-H phases as the temperature of the heat-treatment increases, i.e. the C/S-ratio for the C-S-H phases becomes smaller. The lower C content of the C-S-H phases results in a more compact gel structure (see section 5).
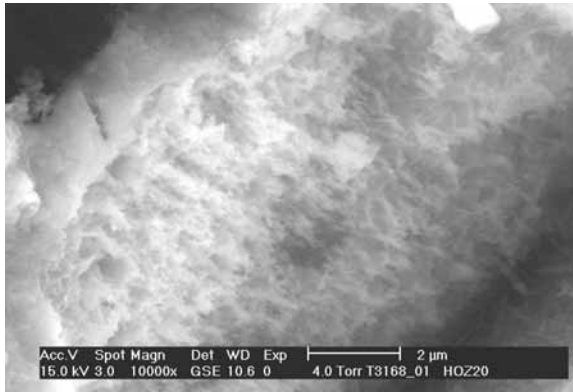
Fig. 8   SEM micrograph of C-S-H phases in UHPC made with CEM I 42,5 R-HS and heat-treated at 90 °C
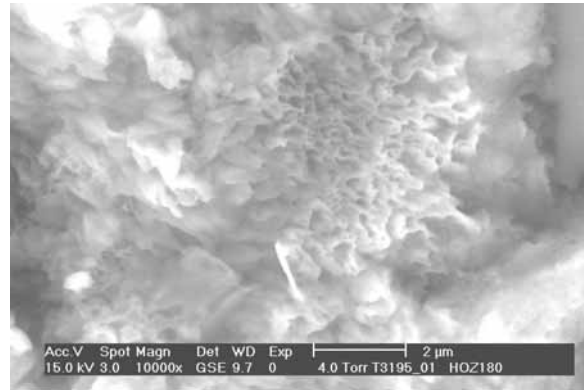
Fig. 9   SEM micrograph of C-S-H phases in UHPC made with CEM I 42,5 R-HS and heat-treated at 180 °C

8   Likelihood of Damage due to Delayed Ettringite Formation

The Duggan test [9] was used to ascertain whether the restriction of the initial sulphate bonding (s. 6) by the heat-treatment can lead to later damage on account of delayed ettringite formation. In variance with the original test procedure, flat prisms (1*4*16 cm3) fitted with gauge pins to monitor changes in length were used. Following standard test procedure, the heat-treated specimens were subjected to alternating cycles in temperature and moisture (in water at 21°C and dry at 82°C). Afterwards, the samples are stored in water and the length changes continuously recorded. The Duggan test stipulates a maximum expansion of 0.5 mm/m after 21d as an acceptance criterion. In the present case the test duration was extended to 400d.

Only the specimens heat-treated at 90°C were investigated using the Duggan test. Higher heat-treatment temperatures are rarely applied in practice and were thus not investigated here. Furthermore, precast UHPC components are usually treated at 90°C. The components of the first bridge made of UHPC (the pedestrian bridge in Sherbrooke, Canada) were heat-treated at this temperature.

Fig. 10 shows the development of the expansion for UHPC made with CEM I 32,5 R-HS and CEM II/B 42,5 NW/HS. The expansion of standard mortars according to DIN EN 196 made with CEM I 42,5 R and with white Portland cement C$_3$A (cements 3 a. 4 in tab. 1) are included for comparison. These mortars were also heat-treated at 90°C before testing.
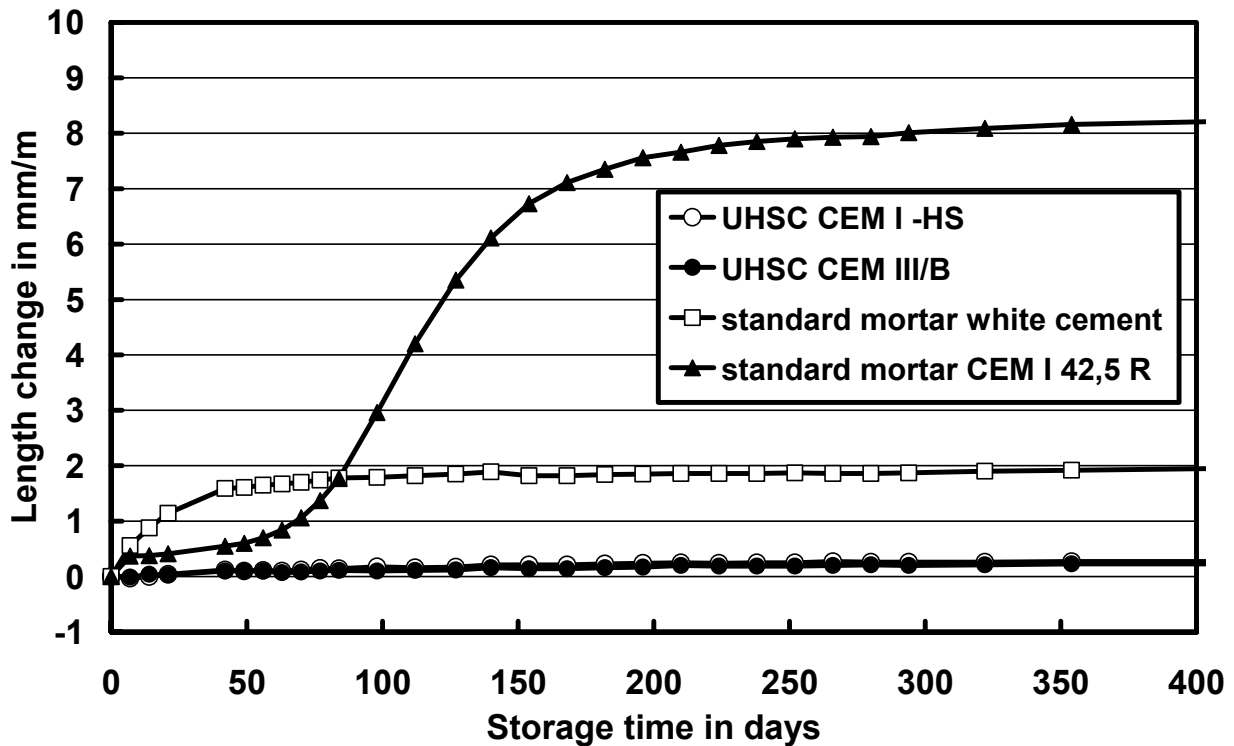
Fig. 10   Expansion of different mortar and concrete specimens during the Duggan test. The specimens were heat-treated at 90°C

The following expansions were measured following storage in water for 21 d

UHPC with CEM I 42,5 R-HS	0.04 mm/mm
UHPC with CEM III/B 42,5 NW/HS	0.04 mm/mm
Standard mortar with CEM I 42,5 R	0.41 mm/m
Stand mortar with Portland white cement	1.14 mm/mm

The standard mortar made using white Portland cement did not fulfil the Duggan test criterion but showed only little expansion during subsequent water storage. The standard mortar with CEM I 42,5 R is a borderline case. Although the expansion at 21d marginally fulfils the acceptance criterion, the expansion continues and reaches 8.2 mm/m after 400 d water storage. These results confirm the need of longer storage periods even after the initial stress due to the Duggan test procedure.

Both types of UHPC exhibited virtually no expansion after 21 d water storage. As can be seen in Fig. 10, the relatively moderate expansion of these concretes did not appreciable change between 21 and 400 d. It may therefore be assumed that, in spite of a heat-treatment

temperature of 90°C and the phase composition after the heat-treatment, the use of CEM I 42,5-HS in UHPC presents no danger of damage caused by delayed ettringite formation.

The results of investigations on the long-term stability of heat-treated UHPC with a CEM I 42,5 R (cement 5, Tab. 1) are given in Fig. 11 [9]. The samples were heat-treated at 90 °C for 24 h after different periods of storage between 1 and 25 d. The development of elastic modulus during water storage at 5 °C was monitored up to about 3 years after the heat-treatment . The results give no indication of damaging reactions during this time.
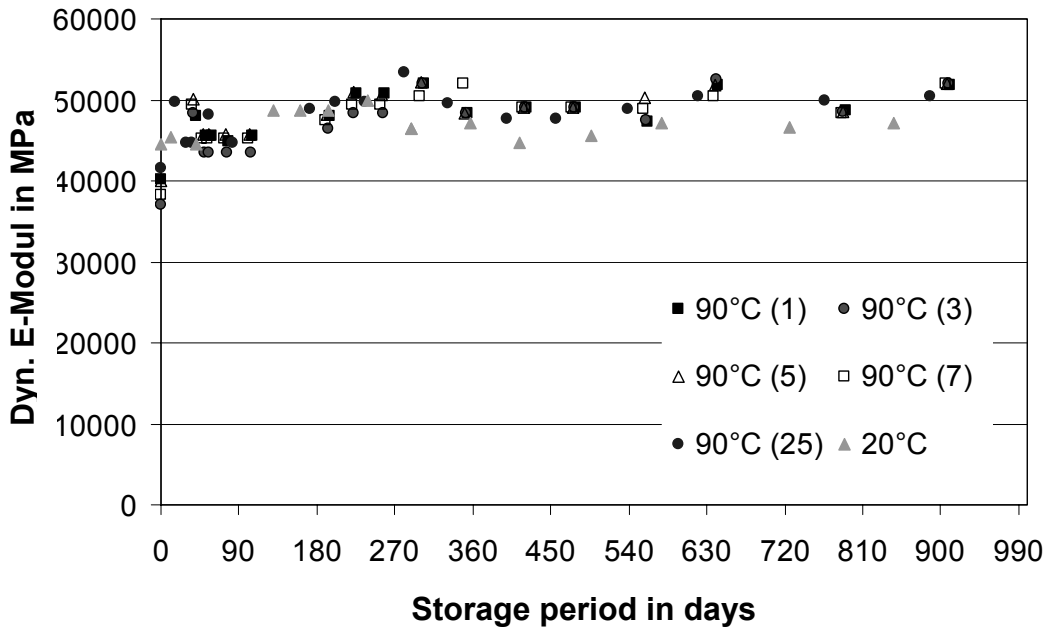
Fig. 11 Development of elastic modulus of heat-treated UHPC samples with cement 5 during water storage at 5 °C. Figures in brackets: duration of storage in days

9   Conclusions

The following conclusions may be drawn:

- Heat-treatment of UHPC made with CEM I HS and CEM III HS at temperatures up to 180 °C increases the compressive strength up to 280 MPa. As well as strength, the compactness of the microstructure increases.

- The phase composition analysis of these two cements after heat-treatment showed considerable amounts of unhydrated C_3S, C_2S and C_4AF, but no C_3A. Portlandite was not present at 65 °C and above, ettringite above 65 °C. Residual anhydrite was found in all samples.

- A 90 °C heat-treatment of UHPC with a CEM I HS or a CEM III HS with 69 % of ggbs did not lead to a damaging DEF although some anhydrite was detectable after the heat-treatment. This agrees with results of investigations on the effect of binder composition and microstructure for heat-treated normal concretes. In addition, a heat-treated UHPC with a CEM I with 10.6 % C_3A remained stable during prolonged water storage at 5 °C.

10 References

[1] Ghorab, H.Y.; Heinz, D.; Ludwig, U.; Meskendahl, T.; Wolter, A.: „On the Stability of Calcium Aluminate Sulphate Hydrates in Pure Systems and in Cements", VII. Int. Congr. Chem. Cem., Vol. IV, Paris 1980, pp. 496 - 503

[2] Heinz, D.; Ludwig, U.; Nasr, R.: „Modellversuche zur Klärung von Schadensursachen an wärmebehandelten Betonfertigteilen, Teil II: Wärmebehandlung von Mörteln und späte Ettringitbildung", TIZ 106, H. 3 (1982), pp. 178 - 183

[3] Taylor, H.F.W.; Famy, C.; Scrivener, K.L.: "Delayed Ettringite Formation", Cem.Concr.Res., 31, 2001, pp. 683 - 693

[4] Heinz, D. and Ludwig, U.: „Mechanism of Secondary Ettringite Formation in Mortars and Concretes Subjected to Heat-Treatment", Concrete Durability, Katherine and Bryant Mather, Int. Conf. (SP-100), Vol. 2, J.M. Scanlon (ed.), American Concr. Inst., Detroit, pp. 2059 (1987)

[5] Famy, Ch.; Scrivener, K. and Brough, A.: "Role of microstuctural characterisation in understanding the mechanism of expansion due to delayed ettringite formation", Internal Sulfat Attack and Delayed Ettringite Formation, Proc. of the international RILEM TC 186-ISA Workshop, K.Scrivener, J.Skalny (ed.) RILEM Public. S.A.R.L.,PRO 35 pp.197 (2004)

[6] Kelham, S.: "Effects of Cement Parameters on Expansion Associated with DEF", Internal Sulfat Attack and Delayed Ettringite Formation, Proc. of the international RILEM TC 186-ISA Workshop, K.Scrivener, J.Skalny (ed.) RILEM Public. S.A.R.L.,PRO 35 pp.197 (2004)

[7] Heinz, D.; Kalde, M.; Ludwig, U. and Ruediger, I.: Present State of the Investigation on Damaging Late Ettringite Formation (DLEF) in Mortars and Concretes, in Ettringite – the sometimes host of destruction, (SP 177), B. Erlin (ed.), ACI Int. Farminton Hills, Michigan, (1999)

[8] Duggan, C.R. et al.: Rapid Test of Concrete Expansivity Due to Internal Sulfate Attack – ACI Materials Journ. Vol. 89 (1992)

[9] Forschungsbericht F 10005/00: Hochleistungs-Feinkorn-Beton, cbm centre for building materials, TU Munich, (2004) unpublished

Frank Dehn
Dr.-Ing.
MFPA Leipzig / University of Leipzig
Leipzig, Germany

Temperature Behaviour of Ultra High-Performance Concrete (UHPC) - A Micro Analytical Reflect

Summary

The development of cement based materials has reached a permanent upside trend within the former decades. From the point of time the last step in this development row is ultra high-performance concrete (UHPC). To be able to use the high efficiency of this material additional concepts for the application and construction explanation are necessary. The concrete recipes have to be developed according to the application case if the high effectiveness and the costs shall be considered together. One aspect which is not sufficiently cleared for such cementitious materials is the behaviour during rising temperatures resulting in spalling and decomposition. One passable way to improve this specific behaviour is to use fibres. However, up to now only phenomenological characterisations exist which back up the positive impact of fibres with regard to fire exposed UHPC.

This paper will give a general survey on the spalling mechanisms due to temperature exposure as well as an overview on test results from literature and own investigations which were focused on micro analytical considerations on the effect of fibres in fire exposed UHPC.

Keywords: *Temperature behaviour, Ultra high-performance concrete, Decomposition, Fibres*

1   Ultra high-performance concrete

Ultra high-performance concrete is indicated as a cementitious material with outstanding strength and durability properties. This peculiar behaviour results from a modified approach in the conceptual design of concrete mixtures. Instead of normal concrete UHPC consists of fine reactive filler, large amounts of cement and concrete admixtures. Along with a extremely reduced water-cement ratio the matrix includes hardly no pores and micro defects as starting points of concrete failure.

This leads to a very dense cement and concrete matrix which has an enhanced sensitivity to vapour formation within the pores resulting in a spalling of the concrete surface if the temperature exceeds a certain range. In the following chapters the main kinds and mechanisms of concrete spalling are explained.

2 Concrete behaviour at higher temperatures

Because concrete contains water which changes its aggregation state when heated the temperature behaviour of concrete is a complex phenomenon. Free water behaves different from physically and chemically bound water.

The aggregates may change their crystal structure, as e.g. quartz, or loose weight, as e.g. limestone which releases its carbon dioxide (CO_2). During fire load, temperature gradients occur, leading to internal stresses in the cross-section, or the edge conditions obstruct thermal strains, so that restraining forces are developed. In this case, thermal creep and relaxation, which are both increased by heating, play an important role.

Hardened cement paste consists of hydrated and still not hydrated cement, of chemically bound and physically bound water, and of free water. The portions differ in dependence on the level of hydration and the state of concrete moisture. Up to approx. 105 °C, the free water, the physically bound as well as parts of the chemically bound water are released. The concrete permeability increases rapidly. This first stage could be defined as the hydrothermal reactions of concrete. The second stage is indicated by the cement gel decomposition at 180 °C. This correlates with the beginning of first strength losses which could be observed by definite crack formation on the concrete surface. Calcium hydroxide ($Ca(OH)_2$) (Portlandite) is decomposed by dehydration at 500 °C (triple point of water), the decomposition of the calcium silicate hydrate (CSH) occurs at 700 °C, and from 1,150 °C hardened cement paste may smelt.

Initially, the thermal strain of hardened cement paste develops as expected for mineral materials: a positive strain occurs to approx. 150 °C. Afterwards there is a shortening. At approx. 250 °C, the initial length is reached again. From those temperatures, the shortening continues up to approx. 600 °C, then a differentiation depending on the different binders occurs. The concrete additives silica fume and fly ash stop the shortening between 600 °C and 800 °C, to re-start again at higher temperatures. The hardened cement paste of common Portland cement is shrinking by 1.5 % up to 500 °C, and by 3.8 % up to 800 °C. The hardened cement paste with silica fume and fly ash is shrinking by 1.6 % up to 800 °C. The deformation of the hardened concrete paste caused by shrinkage causes incompatibilities with the aggregates and so to a separation of aggregates and cement matrix within the interfacial transition zone.

Aggregates are expanding when heated, but with strong differences. The coefficient of thermal strain is not constant either from room temperature to 100 °C, on the contrary the coefficient of thermal strain increases with increasing temperature. The values given in Table 1 were measured in a large-scale investigation of Canadian stones [1]. It can be clearly seen that the values may vary between 3 and $47.5 \cdot 10^{-6}$ °C^{-1}. The values indicate that the thermal strain does not develop uniformly with the temperature. The quartz transformation at 550 to 600 °C is characterised by an increase of the strain of quartzitic sandstone and quartz granite. In limestone, the strain is rapidly decreasing at 800 °C and more, by the elimination of carbon dioxide.

Table 1   Linear coefficient of thermal strain of stones [1]

Temperature range (°C)	Coefficient of thermal strain a ($\cdot 10^{-6}$ °C^{-1})			
	Sandstone	Limestone	Granite	Anorthosite
20 - 100	10.0	3.0	4.0	4.0
100 - 300	15.0	9.0	13.5	8.5
300 - 500	21.5	17.0	26.0	10.0
500 - 700	25.0	33.0	47.5	12.5

The thermal strain of concrete is the consequence of the thermal strain of the aggregates, which cover approx. 70 % of concrete's volume, and of the hardened cement paste. As long as two components expand synchronously, the strain can be determined from their portions in volume. This can be successfully done up to approx. 200 °C, when the hardened cement paste and the aggregates show an approximately similar behaviour. At higher temperatures, the hardened cement paste is shortening, and the aggregates expand. An internal restraint is developed in the structure, in which the matrix is exposed to tensile strains, and the aggregates to compressive strains.

It depends on the grain size of the aggregates and the rupture strain of the matrix until cracks occur. When approximately assuming that the rupture strain of the matrix is 10^{-4}, de-strengthening begins at that little strain already. Thus, if furthermore assuming that the de-strengthening ends at approx. 150 μm, a visible crack would occur at such a differential thermal strain. For a quartz grain with a diameter of 8 mm this happens at a heating to approx. 400 °C, for a grain of 32 mm to approx. 250 °C. When the cracks have occurred in the matrix the internal restraint is released, and the concrete will approach to the thermal strain of the aggregates. Comparing the thermal strain of the aggregates with the thermal strain of concretes a general similarity is obvious. Depending on the type of aggregates normally the thermal strain is growing in a non-linear way up to approx. 600 °C. This behaviour comes to an end sooner or later.

Other parameters as type of cement, water-cement ratio, cement content, humidity, age of the concrete, are of minor importance. A higher cement content and a lower water-cement ratio which have to be considered in UHPC slightly reduce the thermal strain, also a high humidity of the concrete. These influences cause approx. 1 to $2 \cdot 10^{-6}$ K^{-1} and can be neglected in many cases.

Table 2 summarises the basic reactions inside a cement matrix which is subjected to higher temperatures.

Table 2   Reactions inside cement matrix during temperature rise

	Temperature range [°C]	Process	Consequences
1. Phase (hydrothermal reactions)	20 - 100	Increase of saturation vapour pressure	Increased moisture absorption, evaporation of free and phys. bound water
	100 ± x	Evaporating of free and physically bound water	Rapid rise of permeability, strength loss
2. Phase (decomposition of cement matrix)	100 - 200	Removal of water (pores, products)	Strength loss, release of additional water which has to be removed inside the cement matrix
	100 - 300	Decomposition of cement matrix	
	450 - 550	Dehydration (1)	Release of Portlandite
	600 - 700	Dehydration (2) (CSH, β-C_2S)	Strong strength loss and release of water
3. Phase (melting of cement matrix)	1200 - 1300	Start of cement matrix melting	Complete loss of texture
	> 1400	Cement matrix is melt Total destruction of concrete	

3   Spalling behaviour of concrete

Thermal processes are initiated inside a structural concrete element by temperature exposure which, having a homogenous and dense concrete matrix, may lead to damages at the concrete surface exposed to the flames up to explosive spalling. Causes for explosive spalling are [2]:

- thermal processes (thermal stresses, elastic incompatibilities due to different elongations between aggregates and hardened cement paste);
- thermo-hydraulic processes (vapour pressure).

Besides aggregate spalling and sloughing off of small or large concrete layers the explosive spalling should be considered as the most important cause by the development of vapour pressures and, resulting from this, the occurrence of tensile stresses. They are generated, for example, during the efflux of vapour by the friction on the pore walls in temperature exposed concrete, and may lead to the spontaneous formation of cracks. At a heating-up to 300 °C already, i.e. after a relatively short time of fire beginning, tensile stresses of 8 MPa may occur in the concrete which may increase to double the value at the further increase of the temperature to 350 °C, and by far exceed the tensile strength of the concrete.

The bound water, and to a certain extent also the water bound in the gel pores, as well as crystal water from the aggregates, are physically desorbed. Part of the evaporated water tries to penetrate through the pores out of the concrete. The other part of the vapour diffuses into the concrete body. This vapour reaches a colder zone where water is generated again by condensation. In this zone - depending on the factors indicated above - the pores will be saturated sooner or later. It forms a spatial barrier for diffusion, and so causes an increase of the generating vapour pressure. Then the exceeding of the tensile strength of the concrete causes a "floe"-like spalling of the concrete.

For UHPC the saturated zone is located nearer to the surface exposed to the flames because of the denser structure of the concrete. This causes a quicker heating-up of the condensed water and a quicker rise of the vapour pressure.

The processes during the explosive failure of concrete under fire loading are as follows (Figure 1).
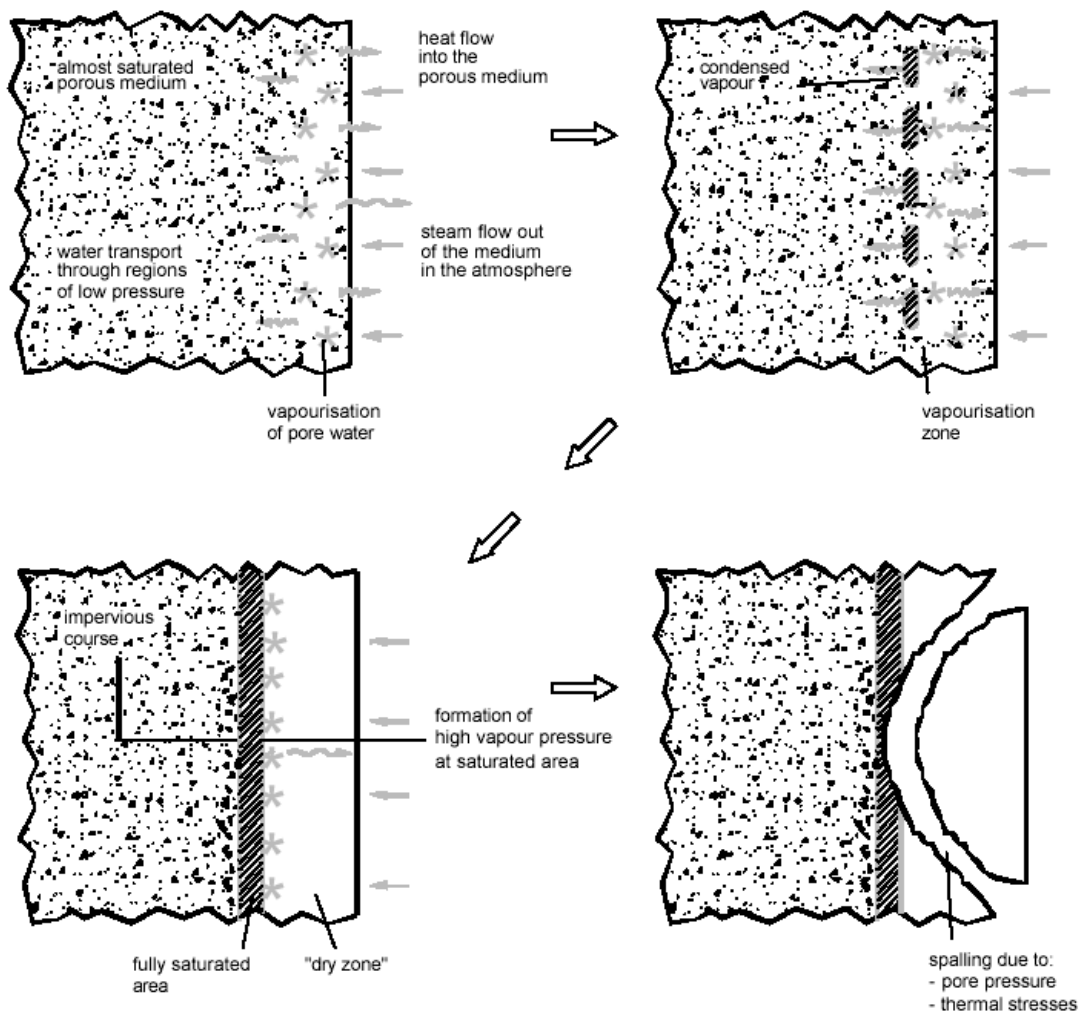
Figure 1   Explosive spalling of concrete due to fire exposure [2, 3]

It is necessary to reduce the moisture content in the concrete and to provide a sufficient pore structure so that the vapour can escape in due time before the vapour pressure approaches the tensile strength of the concrete. Thus, additional pores have to be provided which are generated in the case of fire only.

An effective reduction of explosive spalling for UHPC can be reached by a pore system which leads to a sufficient release of the high vapour pressure. This could be achieved by the addition of plastic fibres, e.g. polypropylene fibres [4, 5]. These fibres may lead to the following effects:

1)   Improvement of permeability due to formation of capillary pores which are composed during melting and burning of fibres. This effect is generally mentioned to describe the efficiency of fibres.

2)   Improvement of permeability due to creation of transition zones (TZ) which are open for diffusion (Figure 2). Considering the structure in TZ between aggregates and cement matrix additional pores are formed. The thickness of these TZ are mainly influenced by w/c-ratio, cement type and additives. The TZ allow for a higher substance transportation (moisture diffusion). By addition of fibres TZ will be connected. The system will get open for filtration and permeability.

3) Improvement of permeability due to additional micro pores which are gained by structural aeration while mixing the fibres in the concrete. This effect may exists as there is a decrease in strength when using a high content of fibres.
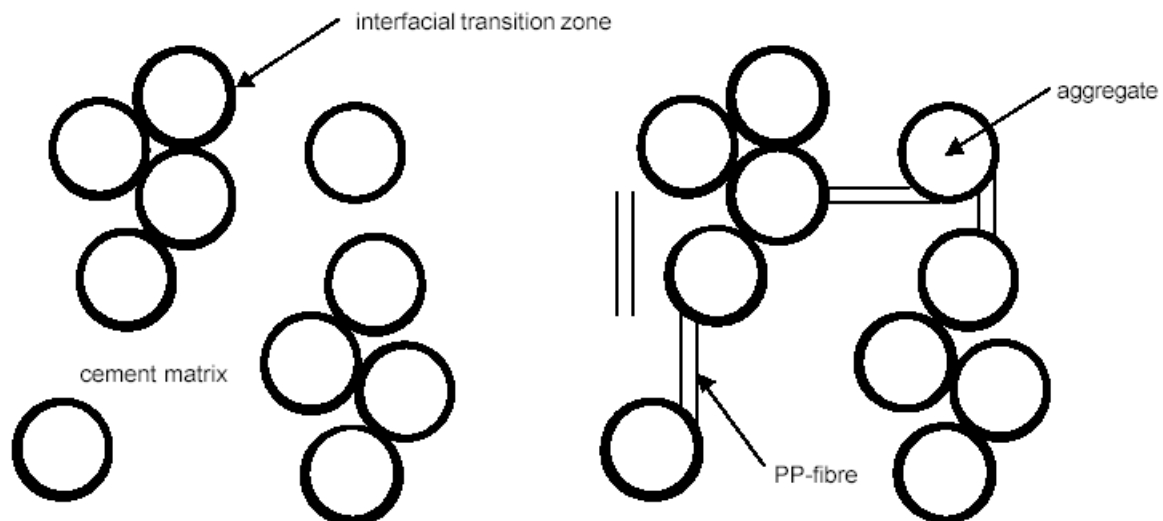
Figure 2   Illustration of fibre effectiveness with regard to interfacial transition zones (TZ) [3]

4   Thermal behaviour of fibres

Under normal conditions polypropylene fibres are described to change their chemism at a temperature of 165 °C. In order to confirm this specific behaviour the melting of fibres was observed visually (Figure 3). From the following pictures the different stages of melting, fluidising and decomposing could be seen.

| max. temp. 27 °C | max. temp. 150 °C | max. temp. 165 °C | max. temp. 200 °C |

| max. temp. 250 °C | max. temp. 350 °C | max. temp. 400 °C | max. temp. 600 °C |
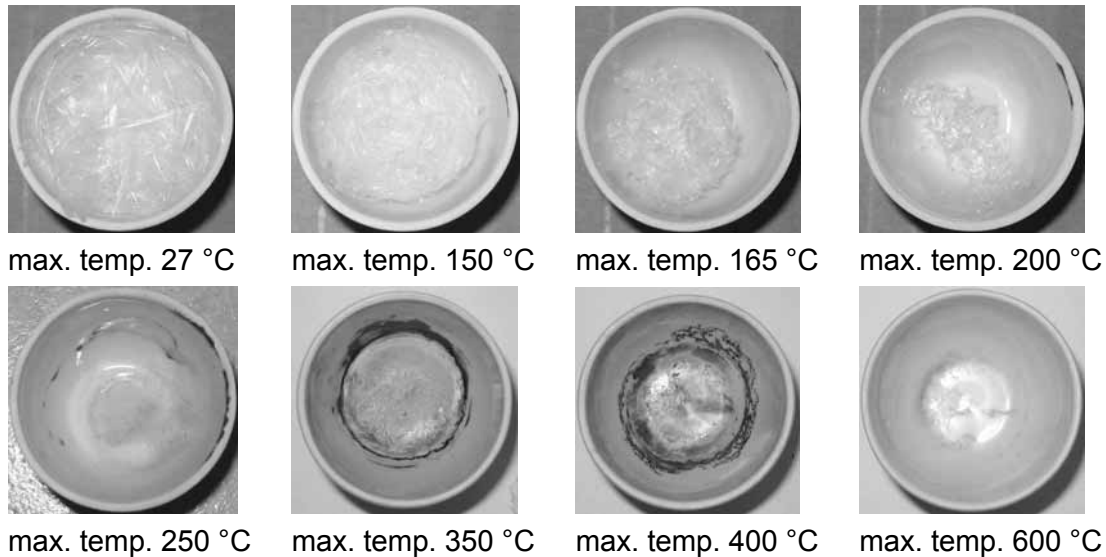
Figure 3   Behaviour of pp-fibres at rising temperatures

| max. temp. 27 °C | max. temp. 180 °C | max. temp. 200 °C | max. temp. 400 °C |
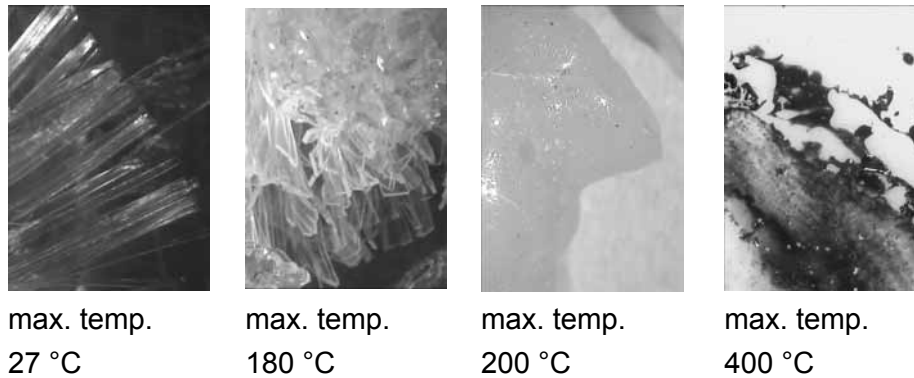
Figure 4   Stereo microscopy images of pp-fibres at different temperature stages

Figures 3 and 4 point out the melting process and the residue at 400 °C respectively. In addition the rectangular shape of non-melted pp-fibres is seen.

The following diagram (Figure 5) shows test results of the differential thermal analysis (DTA) and thermal gravimetry (TG) of pp-fibres (ppf).
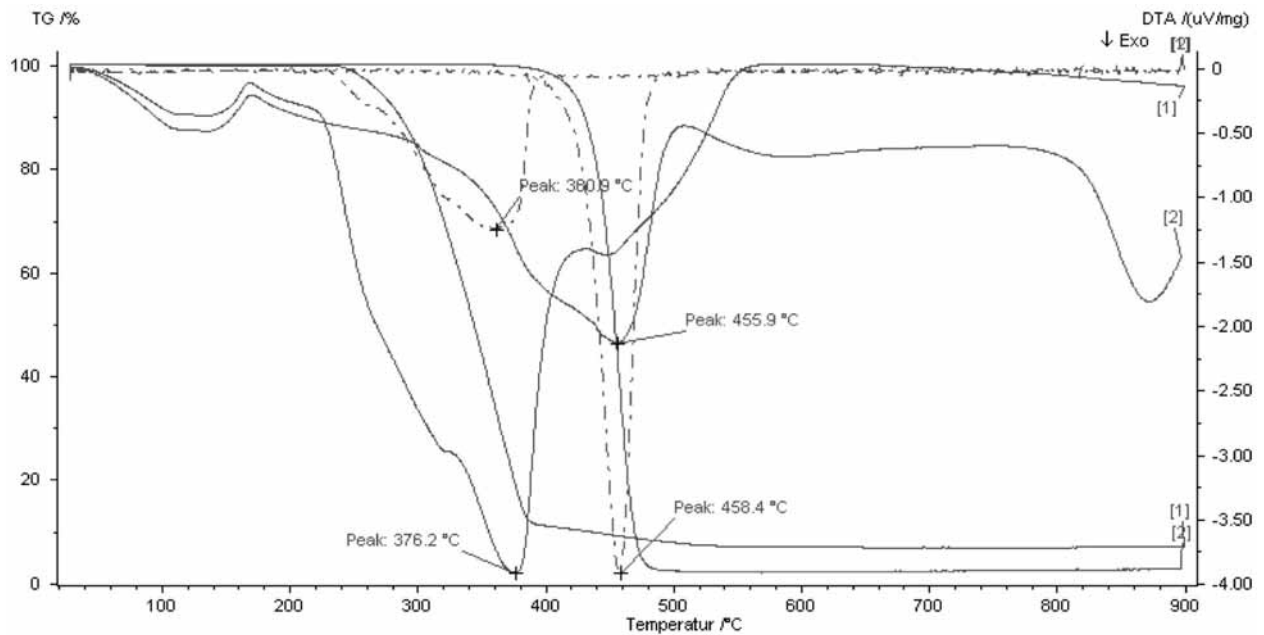
Figure 5   DTA and TG of ppf under oxygen (curve I1I) and nitrogen (curve I2I) exposure

Curve I1I confirm the melting point and the phase of decomposition. In comparison to this the pp-fibres exposed to nitrogen atmosphere show a different thermal behaviour. The pp-fibres are to be pyrolyzed. The decomposing process, which can be clarify with the derivative function (dotted dashed curve) of TG has another characteristic behaviour and is shifted in a higher temperature range with a maximum of approx. 460 °C.

It has to be stated that the above mentioned description is only veritable for idealized conditions. The real behaviour of pp-fibres within the concrete matrix is different and something between these two extreme atmospheres.

5   Behaviour of fibres within the concrete matrix

Preliminary tests with a light optical microscope have approved the thermal behaviour of pp-fibres and showed the initiated cracking (Figure 6). Unfortunately the light optical microscopy sets boundaries when covering the temperature dependent changes exactly.

The following explanations are only significant for cement matrixes. The use of aggregates was disclaimed in order to neglected these negative influences:

- Formation of internal stresses and cracking due to different thermal expansion coefficients of matrix and aggregates.
- Crack formation due to excursive volume changes of aggregates at higher temperatures (e.g. quartz inversion).
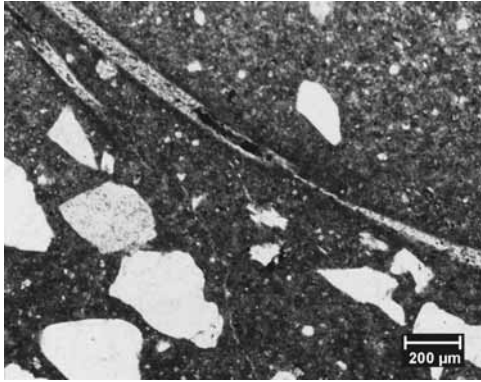
Figure 6   Thin section (thickness 35 µm)
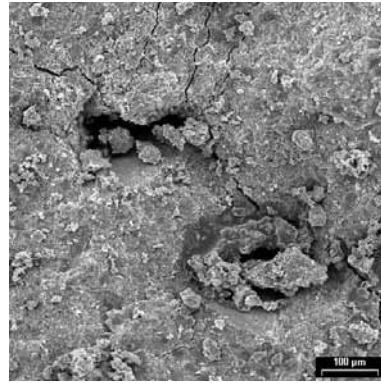
Figure 7   SEM 200 °C (200 x)

Figure 6 shows a thin section with a cast of melted polypropylene fibres in a 300 °C exposed UHPC. A comparable SEM image (Figure 7) gives an impression of the mentioned crack growth, e.g. from the holes generated by the melted pp-fibres and between them.
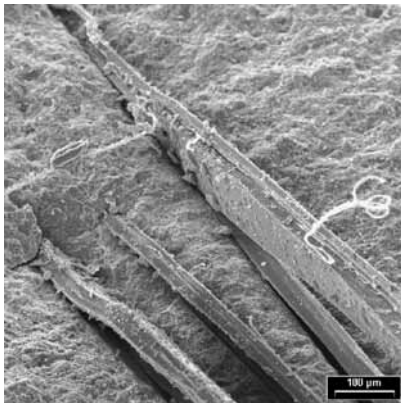
a) max. temp. 105 °C (200 x)
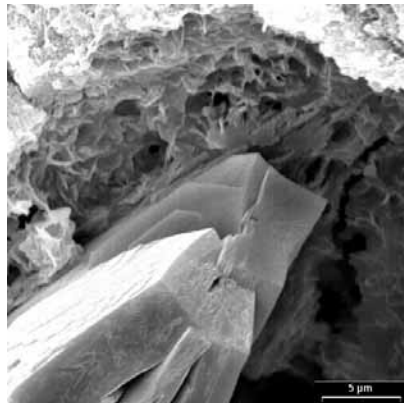
b) max. temp. 200 °C (5,000 x)

Figure 8   SEM images of pp-fibres embedded in cement matrix

In comparison Figure 8a where the pp-fibres at 105 °C is still intact Figure 8b illustrates fibres which start to decompose.
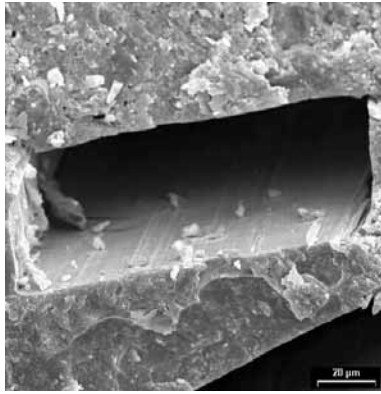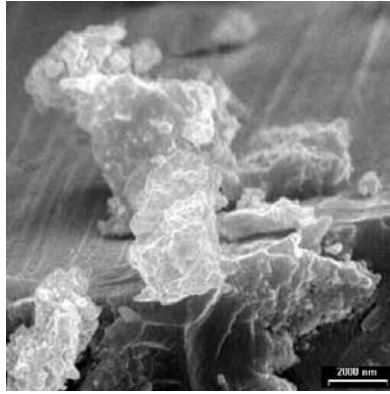
max. temp. 200 °C (1,000 x)   max. temp. 200 °C (10,000 x)

Figure 9   SEM images of pp-fibres melting products in cement matrix

For a temperature of 200 °C rectangular voids are formed depending on the shape of ppf. The magnification approves that the pp-fibres are melted. At higher temperatures (400 - 600 °C) almost no pp-fibres or products are recognizable.

As a result of the investigation it was found that the liquefied pp-fibres products penetrate into the surrounding concrete matrix even when there are no cracks. This is a result of the increased porosity of cement matrix at higher temperatures (Figure 10).
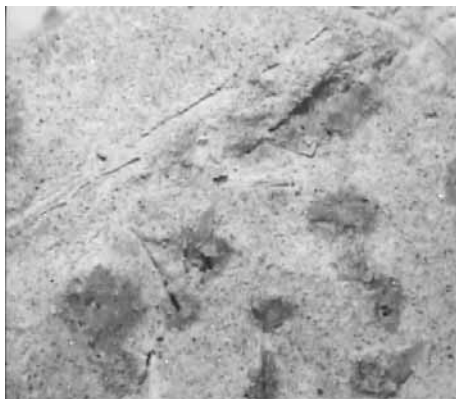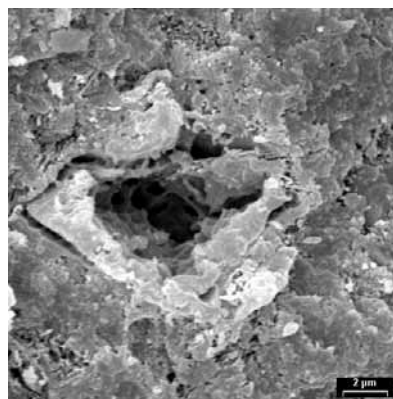
a) max. temp. 200 °C   b) max. temp. 200 °C (7,500 x)

Figure 10   Images of liquefied pp-fibres

Both images collected with a stereo microscope (Figure 10a) and the SEM (Figure 10b) exemplify the liquefying process at a temperature of approx. 200 °C.

740
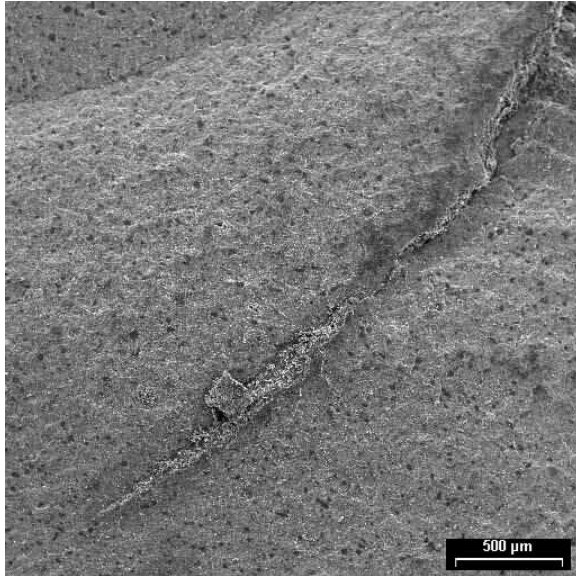
Figure 11   Channel filled with liquefied pp-
fibres, max. temp. 350 °C (50 x)
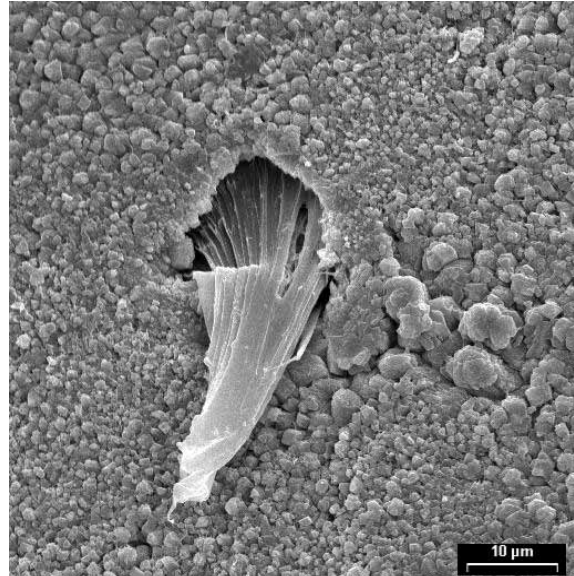
Figure 12   Surface of melted pp-fibres max.
temp. 200 °C (2,000 x)

In addition to the demonstrated micro analytical methods the orientation of the pp-fibres was investigated by a digital analysis (Figure 13, 14).
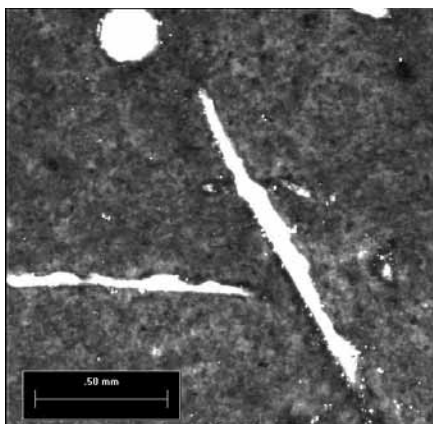
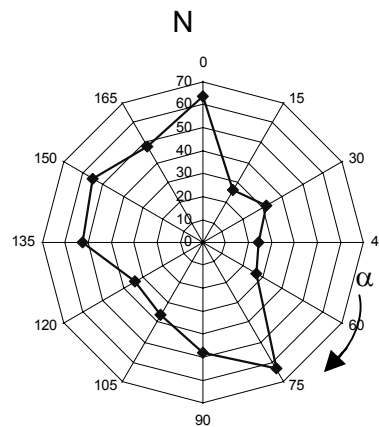Figure 13   Microscopic image of
specimen surface

Figure 14   Orientation of voids on prepared
surface

In Figure 13 oblong voids as a kind of pp-fibres characterisation can clearly be seen. The orientation of all counted oblong voids of the specimen surface is shown in Figure 14. The homogeneous mixture of pp-fibres within the cement matrix could be verified.

6 Conclusions

In this paper a general overview was given concerning the temperature behaviour of ultra high-performance concrete (UHPC). It was pointed out that for a deeper understanding of the reactions within the dense UHPC matrix micro analytical and solid state physical methods are necessary. Resulting from these investigations concrete technological and constructive improvements could be derived leading to a reduced spalling and a better performance of exposed UHPC structures [6, 7].

7 References

[1] Soles, J.A.; Geller, L.B.: Experimental studies relating mineralogical and petrograhic features to the thermal piercing of rocks, Mines Branch Techn. Bull. TB 53, Dept. of Mines and Techn. Surveys, Ottawa 1984, Canada

[2] Schneider, U.; Horvath, J.; Dehn, F.: Abplatzverhalten von ultrahochfestem Beton unter Brandbeanspruchung, Leipzig Annual Civil Engineering Report (LACER), No. 6, 2001 (in German) (*Spalling behaviour of UHPC under fire loading*)

[3] Dehn, F.; König, G.: Fire resistance of different fibre reinforced high-performance concretes, Proceedings Workshop HPFRCC 4 (Naaman, A.; Reinhardt, H.-W.), University of Michigan, Ann Arbor USA, RILEM publications 2003

[4] Dehn, F.: Fasern im Beton zur Erhöhung des Brandwiderstandes, 9. HOLCIM Betontagung, ETH Zürich, Schweiz (in German) (*Fibres in concrete to increase the fire resistance*)

[5] Dehn, F.; Wille, K.: Micro analytical investigations on the effect of polypropylene fibres in fire exposed high-performance concrete (HPC), Proceedings 6. RILEM Symposium on Fibre Reinforced Concrete (FRC), BEFIB 2004, September 2004, Varenna, Italy

[6] Wille, K.; Dehn, F.; Kützing, L.: Fibre resistance of high-strength concrete (HPC) columns with fibre cocktails under loading, Leipzig Civil Engineering Report (LACER), No. 8, 2003

[7] Heinz, D.; Dehn, F.; Urbonas, L.: Fire resistance of ultra high-performance concrete (UHPC) – Testing of laboratory samples and columns under Load, Proceedings International Symposium on Ultra High-Performance Concrete (UHPC), September 2004, Kassel, Germany

Part 13:

Applications

B. Middleton

Graduate Student

Dept. of Civil Engineering, University of Calgary

Calgary, Canada

R. Day

Professor

Dept. of Civil Engineering, University of Calgary

Calgary, Canada

L. Cowe Falls

Assistant Professor

Dept. of Civil Engineering, University of Calgary

Calgary, Canada

Durability and Mechanical Properties of High Performance Concrete for Ultra-Thin Whitetopping Pavements

Summary

Increase in truck and bus traffic and vehicle sizes across North America has resulted in a consequent increase in asphalt pavement rutting and loss of performance. As agencies struggle to rehabilitate and maintain pavements with minimum disruption to traffic, Ultra Thin Whitetopping (UTW) has emerged as a viable new technical and economic alternative. The use of a high performance concrete under highly-restrained geometric and very-severe exposure conditions constitutes the necessity for ultra-high performance. UTW is a pavement maintenance and rehabilitation strategy in which a 50 to 100 mm layer of concrete is placed over and bonds to an underlying asphalt pavement. UTW was initially intended for use on highways, streets, at intersections and at bus stops where severe rutting of the original asphalt pavement had developed. With the development of higher performance concrete materials, however, the potential exists to use UTW on high volume, heavily-loaded, roads exposed to severe winter environments. The use of UTW in Canada and the U.S. has grown since its first application in 1991. Many of these applications have occurred within the last 5 years and the majority have been fast-tracked in order to achieve a high early strength "fix" within 24 hours of placement. The number of UTW applications in cold climates is small; however, with further investigation of the response of UTW to freeze-thaw and scaling conditions, the potential for use is large.

The paper outlines an investigation of the mechanical and durability properties of high early strength concrete for potential application in fast-tracked UTW construction in cold climates. An evaluation is made of the impact of different cement materials, synthetic fibre types, and curing procedures on compressive strength, flexural strength, shrinkage and scaling durability. High early-strength concrete containing ordinary or rapid-hardening cement in conjunction with a low water cementing-materials ratio (w/cm) gave excellent 1-day compressive and flexural strengths, and was highly resistant to scaling from de-icing agents. The use of a Class C fly ash at a 30% replacement level gave acceptable strengths for use in UTW applications, but as expected, early strengths were below those mixes without fly ash.

This lower strength is offset by findings that the shrinkage of fly-ash concrete was significantly smaller than that of other mixes – an important consideration in maintenance of the concrete-asphalt bond in UTW application. The fly ash concrete showed poor scaling resistance. Discussion centres around possibilities to improve the performance of the fly ash performance by modifying mixing and curing specifications and employing other pozzolans, such as silica fume.

Keywords: *concrete, pavements, ultra-thin whitetopping, durability, scaling, fly ash*

1   Introduction

Ultra Thin Whitetopping (UTW) has shown significant promise in alleviating pavement deformation and distress at intersections, airports, interchange ramps and bus stops [1-4]. UTW consists of a 50-100mm thick Portland cement concrete pavement that is placed over a deteriorated asphalt pavement that has been milled and cleaned prior to concrete application. The dependence upon the bond between the asphalt and concrete allows the structure to be designed as a composite section. More concrete is in compression and the need for steel reinforcement is eliminated, although synthetic fibres are often used to mitigate plastic and shrinkage cracking. A few hours after placement – just at the time the concrete can support the weight of concrete saws –control joints are "soft-cut" into the pavement. The joint grid-spacing is usually in the range of 0.6-1.8m -- the recommended spacing is 12 times the UTW slab thickness. Thus, a series of small adjoining panels absorb the traffic load more by deflection than bending, and distribute the load into the subgrade more evenly than asphalt.

The critical factor for success of UTW construction is the establishment and maintenance of a good bond between asphalt and concrete. This can be realized by:

- A suitable high-performance mix design to achieve high strength at very-early (18-24 hr) ages, excellent long-term strength, low shrinkage (especially at early ages before the joints are cut), and satisfactory durability for the projected environment;
- assurance of a rough yet clean asphalt surface at the time of concrete application;
- very early soft-cutting of the green concrete into panels before shrinkage and curling effects can damage the bond;
- a sufficiently thick asphalt section that will allow a significant lowering of the neutral axis – and thus place more concrete into compression – guidelines indicate that the asphalt section, after milling, should have a minimum thickness of 75 mm.
- proper curing to realize satisfactory early compressive and flexural strengths of the concrete.

Lack of attention to these details results in concrete panels with early stress-cracking due to traffic; this primarily occurs at the panel corners where the asphalt-concrete bond is inferior, although cracking along the control-joint edges is also observed.

Deterioration can also be due to environmental influences such as excessive drying and freeze-thaw and salt-scaling attack. In Calgary in winter, for example, relative humidity can often be less than 20% while Chinook winds can be responsible for more than 300

freeze-thaw cycles per season. At the same time, the use of chloride de-icing salts is abundant. Accordingly, it is important that the concrete used for UTW construction has assurance of satisfactory performance under freeze-thaw and scaling conditions.

Life Cycle Cost Analysis (LCCA) is an economic procedure that incorporates into the selection of a design strategy consideration of both engineering and economic factors. It allows agencies to estimate the cost involved in maintenance and rehabilitation programs by taking into account different alternatives and all significant costs expected over the economic life of each alternative in equivalent dollars [5]. In order to compare alternatives that require investments at different times during an analysis period, all costs are brought to a point in time that can be used as a baseline period. Typically, this is the design year or the year when the project will be constructed.

A comparison of the LCCA of UTW and traditional Hot Mix Asphalt (HMA) was done to evaluate the feasibility of UTW in a high volume, high truck traffic roadway [6]. Several assumptions were made in the analysis including a construction cost of $40,000/lane-km and maintenance treatments of panel replacements at 7 year intervals (at $5,000/lane-km taking 12 hours) and diamond grinding at 22 years (at $3,500/lane-km to refinish the surface taking 12 hours)[7]. Reconstruction of the road was assumed to be necessary at 40 years. User delay costs were calculated for Average Daily Traffic (ADT) of 10,000 of which 50% are commercial vehicles. Opportunity cost was assumed at $14/hr for passenger cars and $50/hr for trucks and user delay was calculated from posted speeds and queuing analysis. HMA maintenance needs were estimated as crack sealing every two years (at a cost of $250/lane-km), patching every 5 years (at $500/lane-km) and a mill and overlay every 13 years (at $15,000/lane-km).

The total costs for UTW over a 40 year analysis period, converted to present worth using a discount factor of 4%, are presented in Table 1 and Figures 1 and 2. Figure 1 shows that UTW is more economical when user delay is included in the analysis, while if only construction costs are compared, UTW is less economical (Fig. 2). Although the construction cost of UTW is higher here, the difference is more than made up for by the lower user delays incurred. As well, a less pessimistic analysis of UTW maintenance will make the concrete more competitive with the asphalt. Regardless, the lower user delay costs make UTW an attractive option.

Although there have been several successful UTW projects in Canada [8, 9] there are still no major UTW projects in many major Canadian urban centres, including Calgary. The reticence to use UTW appears to be the result of (a) inertia of local authorities to move away from traditional construction, and (b) lack of adequate information concerning the long term performance of UTW pavements -- especially in cold climates [11-12]. When considering the additional initialcosts associated with implementing UTW in comparison with asphalt pavements, it is clear that a performance database for materials, mix proportions and construction methods must be established.

The experimentation reported here contributes towards evaluation of UTW construction by assessing some mechanical and durability properties of types of high early strength concrete that could suitably be used in UTW exposed to severe winter

environments. Specific goals of the project were to assess the impact of (a) type of cementing materials; (b) synthetic fibre type; and (c) curing procedures, on the performance of the fresh and/or the hardened material.

Table 1 - Total Costs of a UTW Treatment, Including User Delay Costs

Yr	Event	Cost	User Delay (hrs)	User Costs	Factor	Lane-km	Future Cost	Present Value Costs	Total Costs (Present Value)
0	Construction	$40,000	24	$160,000	1	2.4	$256,000	$256,0000	$256,000
7	Panel Replace	$4,000	12	$80,000	0.76	2.4	$89,600	$68,088	$324,088
14	Panel Replace	$4,000	12	$80,000	0.58	2.4	$89,600	$51,741	$375,830
21	Panel Replace	$4,000	12	$80,000	0.44	2.4	$89,600	$39,319	$415,149
22	Diamond Grind	$2,500	12	$80,000	0.42	2.4	$86,000	$36,288	$451,438
28	Panel Replace	$4,000	12	$80,000	0.33	2.4	$89,600	$29,879	$481,317
35	Panel Replace	$4,000	12	$80,000	0.25	2.4	$89,600	$22,706	$504,023
40	Reconstruction	$40,000	24	$160,000	0.21	2.4	$256,000	$53,322	$557,345

Figure 1 – Comparison of UTW and HMA: Including User Delay
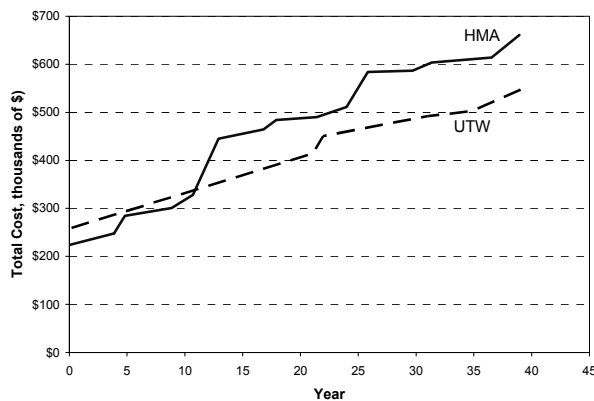
Figure 2 – Comparison of UTW and HMA: Construction Costs only
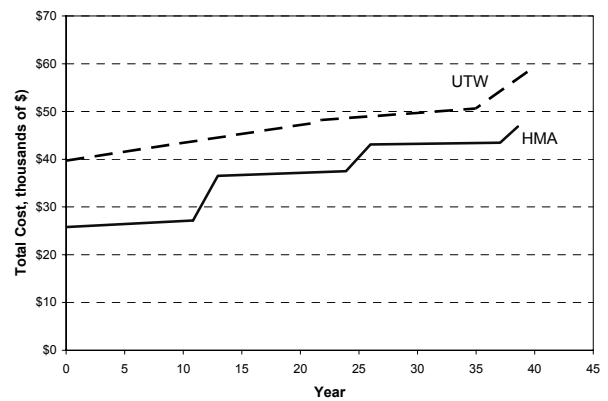
2 Experimentation

2.1 Materials

The materials used in the study are summarized as follows:

Material	Description
Cements	Ordinary Portland (OPC): SiO_2=20.3%, Al_2O_3=4.1%, CaO=64.3%, Fe_2O_3=2.7%, SO_3=2.4%, Blaine = 380 m^2/kg, LOI=2.8%. Rapid Hardening Cement (RHC): SiO_2=20.6%, Al_2O_3=5.3%, CaO=65.5%, Fe_2O_3=2.4%, SO_3=2.4%, Blaine = 380 m^2/kg, LOI=2.8% Both cements meet Canadian Standards Association (CSA) requirements for Types 10 and 30, respectively (ASTM Type I and III).
Fly Ash	An Alberta fly ash derived from subbituminous coal. SiO_2=57.6%, Al_2O_3=21.8%, CaO=11.5%, Fe_2O_3=3.1%, SO_3=0.6%, Na_2O=0.3%, K_2O=0.7%, Passing 45μm sieve=90.1%, 7/28 day strength activity index=87%/101%.
Coarse Aggregate	14mm nominal maximum size crushed limestone, gradation meets Canadian Standards (CSA) specifications.
Fine Aggregate	Screened natural quartzite sand meeting CSA sieve specifications.
Superplasticizer	Rheobuild 1000 from Master Builders. A sulphonated naphthalene formaldehyde polymer complying with ASTM C494, for Types A and F.
Air Entrainer	Micro-Air 100 by Master Builders, conforming to ASTM C260.
Fibres	Two types of synthetic fibres: (1) monofilament polypropylene fibre (MONO), length = 38 mm, nominal diameter = 0.9 mm, tensile strength = 650-800 MPa; (2) fibrillated polypropylene fibre (FIBRILLATED), length = 38 mm, nominal diameter = 0.01 mm; tensile strength = 620-760 MPa.

2.2   Mix Design

Table 2 shows the design mix proportions and the measured slumps and air contents of the fresh concretes. Three of the four concrete (Mixes 1, 2, and 4) were designed from an understanding of general UTW proportioning guidelines [1], a survey of various UTW projects in the U.S., and Canada [3,4,9,10, 13, 14], and the City of Calgary specifications for pavement concrete [15]. The key factor for the fast tracking of UTW applications is a sufficiently reactive cement content, and a low w/cm ratio [16]. For the current work, the cement content and w/cm ratio were chosen to achieve a compressive strength of 30 MPa at 24 hours.

In Mix 3, 30% of the cement was replaced by fly ash. This type of concrete is at the lowest replacement level of "High Volume Fly Ash Concrete" – a new designation in the upcoming 2005 edition of the Canadian concrete standard (CSA A23.1/2-2005). This mix was included to provide an examination of the lower-envelope of performance for fly-ash concrete, and a basis for future examination of the suitability of various ternary cementing blends (e.g. ash + silica fume) in UTW construction. City of Calgary specifications currently do not allow fly ash in flatwork (pavements, sidewalks, curb & gutter). However, previous tests [17] have indicated that fly ash can produce satisfactory concrete in such applications.

Table 2: Mix Proportions and Fresh Properties of Concrete Mixes per m^3

Materials	Mix 1 Fibr.	Mix 2 Mono.	Mix 3 Fly Ash	Mix 4 RHC
Coarse Agg. (kg)	1025	1025	1025	1025
Fine Agg. (kg)	700	700	700	700
Mono Fibre (kg)	1.8	0	1.8	1.8
Fibrillated Fibre (kg)	0	1.8	0	0
Cement (kg)	475, OPC	475, OPC	332.5, OPC	475, RHC
Fly Ash (kg)	0	0	142.5	0
W/CM	0.30	0.30	0.30	0.30
Measured Slump (mm) Target = 65-100 mm	65	65	100	60
Measured Air Content (%) Target = 4-7%	4.8	4.7	6.6	4.5
Measured Density	2306	2278	2264	2278

For the four mixes, the mass of cementing materials, coarse and fine aggregate, fibres, and w/cm (water cementing-materials) ratio were kept constant; the dosages of superplasticizer and air-entrainer were allowed to fluctuate to achieve the target slump and air content. Thus, Mix 1 (Fibrillated) & 2 (Monofilament) differ only in the Type of fibre. Mix 1 (OPC) & 4 (RHC) differ only in the type of cement used, while Mixes 1 and 3 (Fly Ash) differ because Mix 3 has 30 % of the cement replaced by Alberta fly ash.

2.3 Curing Procedures

Mix 1 was chosen to examine the effect of three different curing régimes on scaling performance. The three régimes were (all curing was performed at 23°C):

Régime	Curing 0 to24	Curing 24 h to 14 d	Curing 14 d to 28d
A	Wet burlap and polyethylene sheet	Laboratory	Laboratory
B	Fog room	Fog room	50% relative humidity
C	Polyethylene sheet	Laboratory	Laboratory

For scaling, the other three mixes were subjected to régime B – this is the régime specified in the scaling-test specification that was used (see below). For assessment of the various parameters on mechanical strength, all four mixes were cured in accordance with régime A. Shrinkage specimens were cured in accordance with ASTM C490.

2.4 Testing Procedures

The tests, specimen sizes and replicates are given in Table 3. Except for scaling, tests were performed in accordance with ASTM specifications. The scaling test used was MTO LS-412

[18], Ontario Ministry of Transportation. This test is similar to ASTM C672, but stresses quantitative over qualitative analysis through rigorous sampling of the mass loss from the specimens after every 5 freeze-thaw cycles. A summary of the test procedure follows:

> Concrete prisms are cured for 28 days (curing regime B, above), covered by a 3% NaCl solution, and placed in a freezing environment for 16-18 hrs, at -18 ± 2°C, followed by storage at 23 ± 2°C, 45-55% humidity for 6-8 hrs. This procedure is repeated for 50 freeze-thaw cycles after which the testing is terminated. After every 5 cycles, the de-icing solution along with all the flaked off concrete from the surface is removed; this involves thorough washing of the specimen's surface with water and brushing with a wire brush to simulate the effect of traffic loadings. The solid residue is gathered by straining through filter paper and drying in an oven at 105°C before weighing to the nearest 0.01g. After the washing of each slab, the surface is covered with a new solution of de-icing agent.

Visual rating and photographs of the scaled slab-surfaces were also obtained. These results support the mass-loss vs. time data reported below and thus are not reported here.

Table 3: Specimen Size and Number of Samples for each Test Type

Specimens	Size (mm)	# Specimens / Mix
Compressive Strength Cylinders (ASTM C39)	Φ100 x 200	7
Flexural Strength Prisms (ASTM C78)	100 x 100 x 355	6
Shrinkage Prisms (ASTM C490 & C157)	50 x 50 x 285	2
Air Void Analysis Cylinders (ASTM C457)*	Φ100 x 200	1
Scaling Slabs (MTO LS-417)	300 x 300 x 75	3

* modified point count at a depth of 7 mm from the finished concrete surface

Compressive strength tests, on cylinders with ends ground, were performed at 1, 14, 28 and 56 days; each test is the average of 2 specimens, except for 56 days. Flexural strength was measured at 1, 14 and 28 days. Shrinkage was measured at 1, 2, 4, 7, 14, 21, 28 and 42 days. The analysis was conducted at depth of approximately 7 mm from the finished surface.

3 Results and Discussion

3.1 Fresh Concrete Properties

All of the mixtures had slumps within the desired range of 65 to 100 mm and air contents in the target range of 4 to 7 % (Table 2). The fly-ash concrete (Mix 3) had higher air content and slump than the other mixes – Alberta fly ash is known to improve workability and cohesion and thus is expected to retain air. Mix 4, with rapid-hardening cement, proved very difficult to place, consolidate and form due to rapid setting. This suggests that tight control in the field is necessary if rapid-hardening (high early strength) cement is to be used in UTW construction.

The concretes differing only in fibre-type (Mixes 1 and 2), had similar slumps. However, Mix 2, containing fibrillated fibres, was very hard to finish and upon completion of finishing a large number of fibres still remained protruding from the surface. This difficulty is

believed to be associated with the much larger number of fibrillated fibres per unit volume of concrete when compared to the monofilament fibres – fibrillated fibres had an equivalent diameter 1/10th that of the monofilament fibres.

3.2   Compressive Strength

The compressive strength development for the concrete mixes is shown in Figure 3. Cylinders were moist-cured for 1 day and then placed in the ambient air for the remaining period (Curing regime A). Only Mix 3, with fly ash, did not meet the desired 30 MPa compressive strength at 24 hours. All other mixes greatly exceeded the 1 day target strength – indicating a potential to alter mix designs to lower cement contents and cost. The current mixes could also be used to advantage to provide required strengths earlier times – although research is necessary to examine the reliability of strength gain in the 12-24 hr time period. Because of the termination of water-curing at one day, the rate of strength gain for all mixes after 14 days is minimal. The use of fly ash at a 30% replacement level reduced the overall compressive strength gain by approximately 45 % -- it is actually the fly-ash concrete that comes closest to meeting the original design specification of 30 MPa at 1 day and it is expected that the use of a ternary blend of cement-ash-silica fume would allow the one day target to be met. The use of monofilament fibres gave slightly better compressive strength performance over all ages when compared to the fibrillated fibres.

3.3   Flexural Strength

The flexural strength development for the four mixes is shown in Figure 4. The fly ash mix at one day, again, showed lower strength than the other three mixes. Flexural strengths in the range 6.5-7 MPa at 24 hours for the mixes that do not contain ash are more than adequate for UTW applications. However, from between 1 and 14 days the flexural strength gain of these three mixes is not in proportion to the compressive strength gains (compare Figs 3 and 4); conversely the flexural gains of the fly ash mix (3) is appreciable between 1 and 14 days. This is consistent with the concept that the slower hydration of fly ash produces a more homogenous product that is less prone to microcracking as a result of early drying and thermal gradients. No significant influence of fibre-type on flexural strength is observed.

3.4   Shrinkage

Shrinkage results are shown in Figure 5. Mix 4, with rapid hardening cement, showed substantially higher shrinkage strains than the other mixes. Among the fibre-laden concretes, use of the monofilament fibre leads to slightly reduced shrinkage compared to the fibrillated fibre. The reduction in the cement content as a result of fly-ash use is reflected by the significantly reduced shrinkage of Mix 3 when compared to the other mixes. Since the integrity of the asphalt-concrete bond in UTW applications is critical, the use of supplementary cementing materials to reduce the quantity of cement and early shrinkage is desirable.
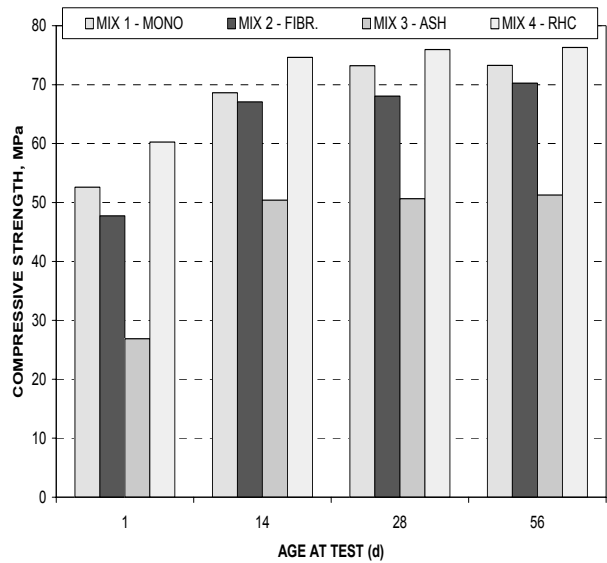
Figure 4: Flexural Strength Development

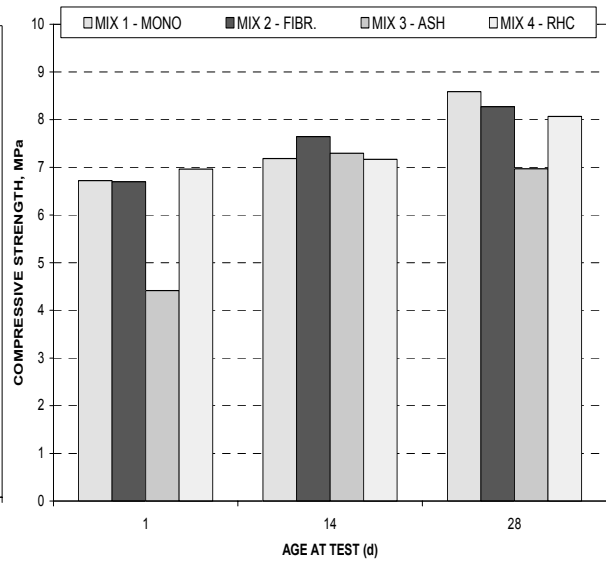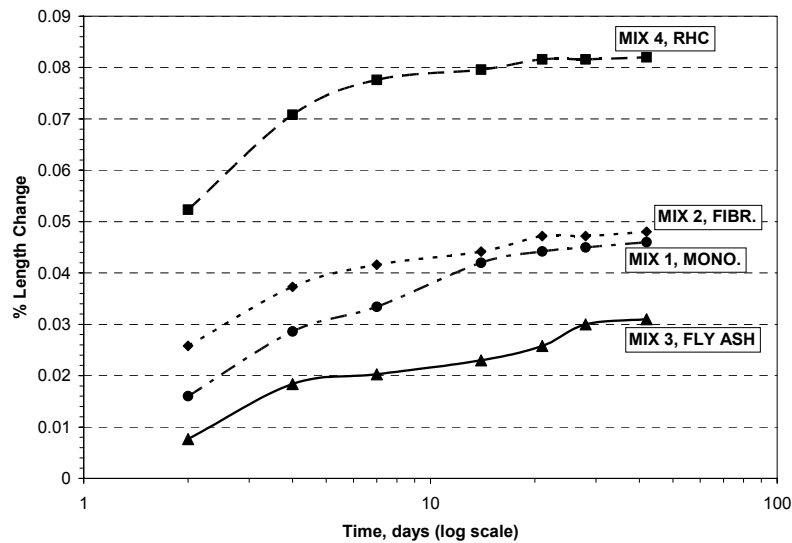Figure 3: Compressive Strength Results, MPa

Figure 5: % Shrinkage of Different Concrete Mix Types

3.5   Air Voids

The results of petrographic air void analyses are given in Table 4. CSA A23.1 specifies a maximum spacing factor of 0.230 mm for regular concrete and 0.250 mm for concrete with a w/cm less than 0.35. Mixes 1, 2 and 3 satisfy CSA requirements. The City of Calgary, however, has a stricter standard for flatwork, requiring a maximum spacing factor of 0.200 mm; in this case only the fly ash mix (3) satisfies the requirement.

Table 4: Results of Air Voids Analysis

Property	Mix 1 Mono	MIx 2 Fibr.	MIx 3, Ash	MIx 4 RHC
Fresh Air Content, %	4.8	4.7	6.6	4.5
Air in Hardened Conc., %	5.0	4.7	7.0	4.1
Paste Content (%)	39.1	38.7	37.8	39.6
Paste-Air Ratio (p/A)	7.8	8.2	5.4	10.0
Specific Surface, mm^{-1}	17.2	16.5	30.6	15.6
Spacing Factor, mm	0.224	0.248	0.157	0.265

3.6 Freeze Thaw Scaling

Figure 5 is a plot of the cumulative scaling mass loss vs. the number of freeze-thaw cycles experienced in the MTO LS 417 test. The results clearly illustrate the susceptibility of the fly-ash concrete (mix 3) to the combined influence of freezing/thawing and de-icier salts. The total cumulative mass loss for Mix 3 after 50 cycles was 2.95 kg/m^3 -- more than three times the MTO limit of 0.8 kg/m^3. If fly ash concretes are to be used in such exposures there is a clear need to either (a) reduce the replacement level; (b) increase the extent of moist curing, or (c) combine the use of fly ash with other pozzolanic materials (e.g. silica fume). Further research is necessary to determine which combination, of these alternatives could lead to an increased use of fly ash in UTW and other flatwork applications. The other three mixes showed minor scaling.

Figure 6 illustrates the significant effect of the curing regime on the scaling of Mix 1, with monofilament fibres. The 14-day moist curing (B) gives the lowest level of scaling. Using wet burlap underneath polyethylene sheet provides additional curing water (cure A) and produces a concrete with better scaling resistance than if polyethylene sheet is used alone. Quality early age curing is important for all classes of concrete, especially those that contain pozzolans. Future research will concentrate upon this aspect.

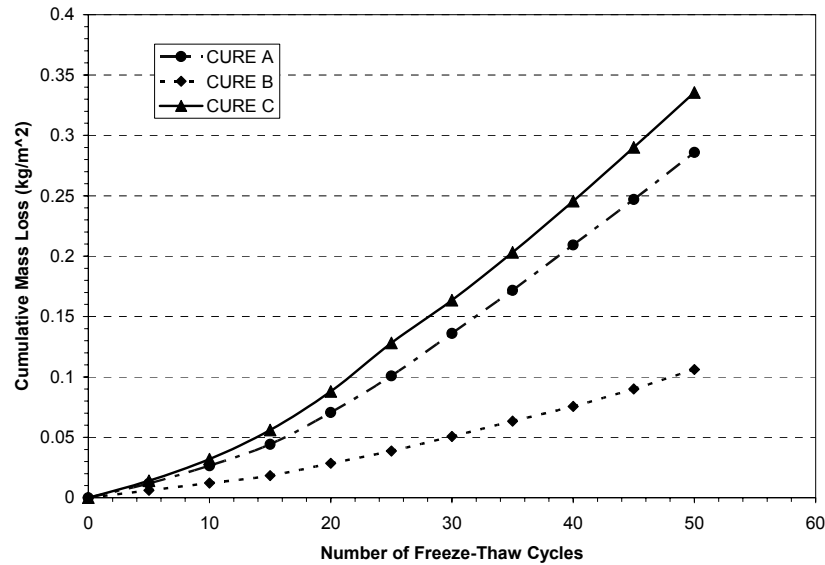Figure 5: Cumulative Scaling Mass Loss for the Different Concrete Mixes
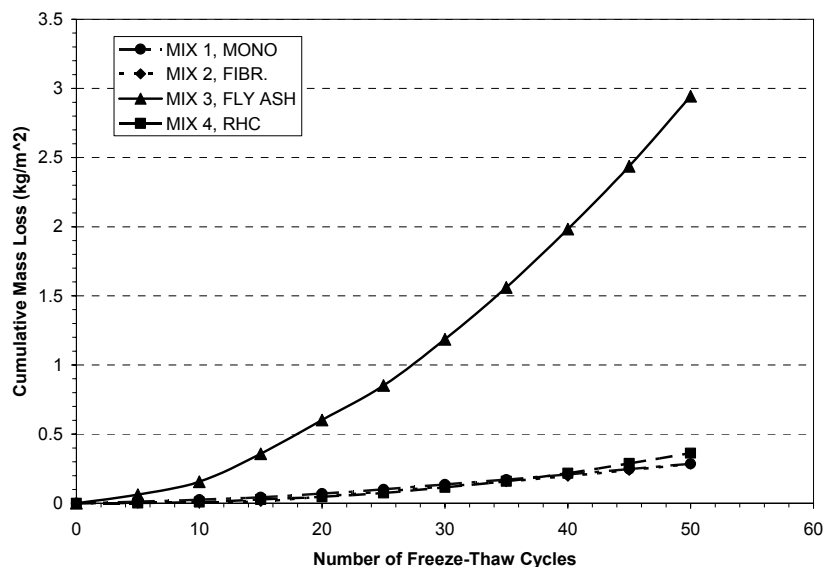
Figure 6: Cumulative Scaling Mass Loss vs. Curing Procedure, Mix 1

4 Conclusions

The tests reported here are from early stages of research into the mechanical and durability performance of UTW concretes subjected to cold climates. Conclusions noted here apply to these research results:

- High ordinary and rapid-hardening cement contents (475 kg/m^3) combined with low water-cement ratios allowed for very high early strength development, and played a key role in providing superior scaling resistance. Shrinkage of these mixes was, however, appreciable. Although the use of rapid-hardening strength yields higher rate of strength gain, it also yields appreciably higher early shrinkage strains.

- Conversely, 30% replacement of cement by Alberta Class C fly ash resulted in 35-45% lower compressive and flexural strengths at 1 day. Fly ash concretes had greatly increased scaling susceptibility, but much lower shrinkage when compared to the non fly-ash mixes. If fly ash is to be used in UTW applications in cold climates other measures – such as extended curing (not practicable in some applications), or the use of combinations of pozzolans (slag, fume and fly ash) need to be thoroughly investigated.

- Scaling testing procedures using quantitative analysis such as mass loss of scaled off particles measured at many incremental cycles as seen in MTO LS 412; is a considerably more sensitive method of laboratory scaling testing for concrete samples than the visual qualitative analysis used by ASTM C 672.

- Monofilament and fibrillated polypropylene fibres when used at small dosages had little influence on workability, strength gain or scaling susceptibility and resistance.

- A 1-day curing procedure of using polyethylene sheets overlying wet burlap provides a sufficient, low-cost method for curing fast-track UTW concrete.

5 References

[1] American Concrete Pavement Association (APCA), "Ultra-Thin Whitetopping – Concrete Information", IS100.02P, 2000.

[2] American Concrete Pavement Association (ACPA), "Construction Specification Guideline for Ultra-Thin Whitetopping", 1999.

[3] Cole, L.W., "Pavement Condition Surveys of Ultrathin Whitetopping Projects", American Concrete Pavement Association, 1997, pp. 175-187.

[4] Delatte, N., and Sehdev, A., "Mechanical Properties and Durability of BCO and UTW Concrete," Transportation Research Board, National Research Council, Washington, 2003.

[5] Pavement Type Selection and Life Cycle Cost Analysis " – Colorado Department of Transportation Pavement Design Manual. http://www.dot.state.co.us/DesignSupport/ PavementDesignManual/New%20Pavement%20Design%20Manual%208-13- 03/Chapter%209.pdf, accessed October 2003

[6] Martin, L. "Innovative Approaches for Preventing Permanent Deformation in Calgary's Pavements" Research Report, Dept. of Civil Eng., U of Calgary, Fall 2003

[7] Kirk, S. J. and Dell, A.J., "Life Cycle Costing for Design Professionals" McGraw- Hill, New York, NY, 1995

[8] Cement Association of Canada (CAC), "An Overview of Concrete Pavements in Canada", PowerPoint presentation – Tim Smith, Cement Association of Canada, 2000.

[9] Fung, R., Corbett, M., Keegan, K., and Richards, M., "Ultra-Thin Whitetopping for Ottawa Transitway Bus Station Rehabilitation", Transportation Association of Canada, Halifax, Nova Scotia, 2001.

[10] Mack, J.W., Hawbaker, L.D., and Cole, L.W., "Ultrathin Whitetopping State-of-the-Practice for Thin Concrete Overlays of Asphalt", Transportation Research Record, No. 1610, 1999, pp. 39-43.

[11] Ghafoori, N., and Mathis, R.P., "Scaling Resistance of Concrete Paving Block Surface Exposed to Deicing Chemicals", ACI Materials Journ., V. 94, No.1, Jan-Feb, 1997, pp. 32-38.

[12] Afrani, I., and Rogers, C., "The Effects of Different Cementing Materials and Curing on Concrete Scaling", Cement, Concrete, and Aggregates, CCAGPD, Vol. 16, No. 2, Dec. 1994, pp. 132-139.

[13] Armaghani, J.M., Diep, T., Rehabilitation of Ellaville Weigh Station with Ultra-Thin Whitetopping, State of Florida,, FL/DOT/SMO/99-429, State Materials Office, 1999.

[14] Rangaraju, P.R., "Development of Some Performance-Based Material Specifications for Minnesota's High Performance Concrete Pavements", Journal of Transportation Research Record, TRB, National Research Council, Washington, D.C., 2003.

[15] The City of Calgary, Engineering and Environmental Services Department, "Standard Specifications for Street Construction, 2002".

[16] Abel, J., Hover, K., Effect of Water/Cement Ratio on the Early Age Tensile Strength of Concrete, Transportation Research Record, No. 1610, 1998, 33-38.

[17] Gifford, P.M., Langan, B.W., Ward, M.A., Day, R.L. and Joshi, R.C., "A Study of Fly Ash Concrete in Curb and Gutter Construction under Various Laboratory and Field Curing Regimes", Canadian Journal of Civil Engineering, V14, No. 5, Oct. 1987, pp 614-620

[18] Ontario Ministry of Transportation (MTO) Laboratory Testing Manual, "Method of Test for Scaling Resistance of Concrete Surfaces Exposed to Deicing Chemicals,", Test Method LS-412, Rev. No. 17, August 1, 1997.

Kaufmann, Josef
Dr., senior researcher
EMPA, Swiss Federal Laboratories for
Materials Testing and Research
Dübendorf, Switzerland

Development of special mortars for an application in centrifugal casting process

Summary

One possible production method for pylons, pipes or columns is the centrifugal casting method. Elements fabricated by this technique often are highly armed with steel bar reinforcement. The laying of this reinforcement is a cost and time consuming process. An economical alternative is the application of ultra high strength, especially in bending and tension, fiber reinforced concrete. Owing to their high density steel fibers are not ideal for an application in centrifugation technique. Relatively expensive high strength and modulus fibers (carbon, PVA, etc.) may be used instead.

To reduce material costs, ultra high performance mortars with no artificial fiber addition, which even improve their strength in the centrifugation process (>200 MPa in compression and > 25 MPa in bending) were developed. Conventional mixing and curing without heat treatment is sufficient to obtain the ultra high performance.

This was realized using an increased packing density of the cement matrix obtained by blending Ordinary Portland cement with microfine cement based on blast furnace slag, rather than a more common addition of pozzolanic micro silica. Prevention from early age cracking and a further improvement of strength performance is realized with acicular additions. Excess water is expelled during the centrifugation process, resulting in very low w/c ratios. The thixotropic character of the fresh mixture is ideal for the centrifugation application, leading to high green body strength.

Keywords: *microfine cement, centrifugation casting, mineral fiber, pipes*

1   Introduction

Centrifugation or spinning at rather high speed is an integral part of the manufacturing process of reinforced or pre-tensioned concrete poles, piles and pipes. A generally cylindrical mould is filled with the fresh mixture, closed and then rotated around its axis. The resulting centrifugal forces press the material against the inner wall of the mould and compacts it. The compaction due to the centrifugation forces can give denser and stronger products as well as a better surface finish. If the process parameters are carefully chosen, segregation effects can be minimized. The centrifugation casting method is mostly used for the production of pipes, columns and pylons [1].

Depending on the application, elements fabricated by this technique often are highly armed with steel bar reinforcement. The protection against corrosion requires a certain thickness of the covercrete layer, which leads to thick, heavy structures and hence to high manipulation and transport costs. Furthermore, the laying of this reinforcement is a cost and time consuming process with few possibilities of automation. It is therefore economically interesting to replace the steel bar reinforced concrete by a non-corrosive fiber reinforced composite (FRC) with ultra high strength, especially in bending and tension.

Fig.1   Centrifugation: production of a concrete pile

A prerequisite for the development of FRC is an appropriate, optimized cement matrix. The matrix should combine properties such as low porosity, high density, and excellent mechanical properties. To improve green body strength of centrifuged products, a thixotropic behavior of the fresh mix is helpful. All this can be achieved by combining two or more binder components with different size distributions [2]. The addition of micro-fine cement to the ordinary Portland cement improves the rheological properties of the fresh mixture and leads to a dense cement matrix with high strength.

For fiber reinforced materials, the spinning may change fiber distribution and lead to a certain orientation along the rotation axis. This effect may further improve advantageous material properties. However, the application of steel fibers is not possible. Owing to their relatively high density, segregation occurs. Relatively expensive high strength and modulus fibers (carbon, PVA) or much more economic mineral fibers may be used instead.

2   Materials and procedures

Fine-grained minerals are frequently added to cementitious materials in order to improve the rheology, matrix strength, and durability. In addition to their ability to contribute to the binding, the fine particles will fill the large spaces of the granular matrix structure and will enhance the packing density [3]. However, depending on the amount and grain size of the ultra-fine particles, additional water may be required to keep the rheology within practical limits, thereby risking the positive effect of the added minerals to get lost [4]. For example, silica

fume and fly ash are commonly used as additives to the cement and are known to enhance the matrix strength by improving the microstructure and durability [5]. The drawback of using silica fume is based on the higher water requirements and the susceptibility of shrinkage. Therefore, a concept replacing silica fume by micro-fine cement was tested. The binder system was composed of Portland cement CEM I 42.5 N according to the European standard EN 197-1, blended with micro-fine cement (Portland cement blended with blastfurnace slag; $d_{50} \cong 2.5$ µm). The chemical composition of the cementitious binders and the particle size distribution is given in reference [6]. A superplasticizer based on polycarboxylatether was used as water reducing agent.
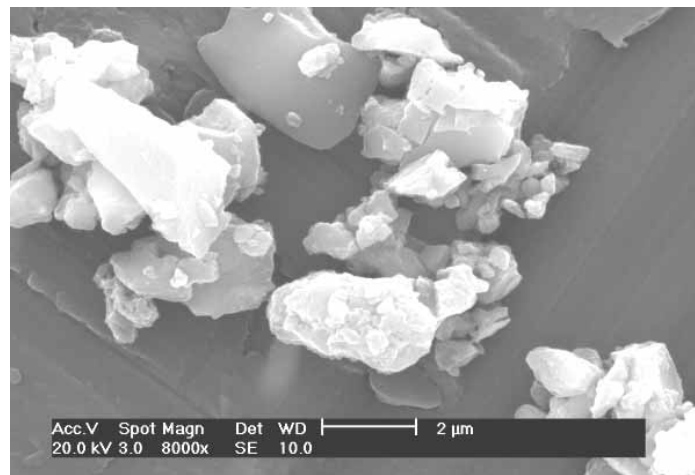
Fig. 2   Micro-fine cement grains of typical size

In order to obtain a further improvement of strength performance (especially bending strength) and to prevent the cement pastes from early age cracking acicular additions were added. Different mineral fibers were tested previously. Very good results were obtained with wollastonite ($CaSiO_3$, see fig.2). Its morphology is bladed, acicular and shard-like cleavage. The aspect ratios vary from <3:1 to> 3:1 depending on processing. This mineral has a low biopersistence and is not classified as carcinogenic to humans [7].
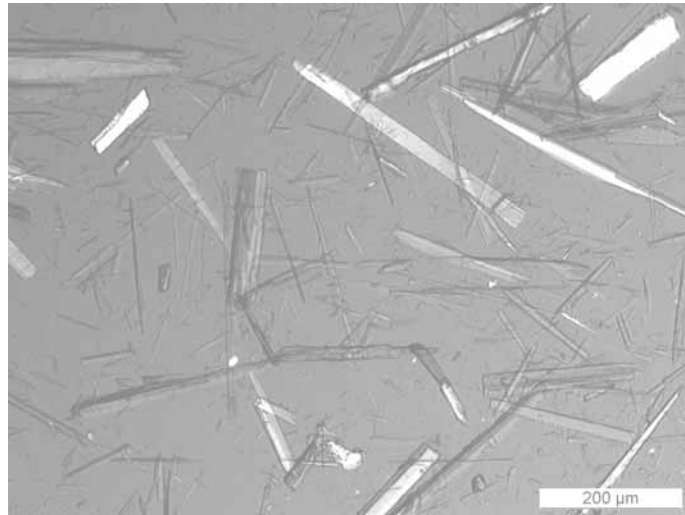
Fig. 3   Wollastonite fibers as observed by conventional light microscope

All pastes were prepared using a conventional lab-mixer at low speed of 62.5 rpm. Rheological parameters (yield stress, viscosity) were determined

Some samples were produced by conventional casting procedure (in mould). The samples (size 15x15x80 mm^3) were cast and then stored during 24 hours at 20°C, 95%RH. After dismantling of formwork, the samples were cured in different relative humidity regimes all at 20°C. Their mechanical properties (flexural and compressive strengths) were measured after 7, 28 and 90 days.

For the centrifugation process, the fresh mixture was transferred into a conical steel form (length 180 mm, diameter varying from 180 mm to 176.5 mm). The spinning speed was at 669 rpm. The samples were dismantled of formwork after 24 hours and then cured in water at 20°C. After five days, samples of 15x15x80 mm^3 were cut. After cutting, the specimens were stored under water at 20°C. After 7 and 28 days, the mechanical properties were measured.

3   Results

Rheology

In a first test series Portland cement CEM I 42.5 N pastes were prepared with microfine cement and, for comparison purposes, limestone filler. The water/binder ratio was 0.20, and 2.0% superplasticizer in respect to the binder was used.

For the rheological measurements a rheometer (Paar Physica MCR 300) in controlled shear rate mode was used. It was equipped with a spherical measuring system, developed especially for cement pastes and mortars [8]. Instead of a laminar flow, as for example in cylindrical geometry, a displacement flow is caused by a sphere rotating concentrically around the test system axis. The sphere performs about 3/4 of a full circle through the cement paste or the mortar during the data acquisition.

This kind of measuring system has several advantages compared to conventional systems (e. g. cylinder or plate-plate), when used for building materials: wall slip and sedimentation

are minimized, the examination of mortars up to an aggregate grain size of about 4 mm is possible.

The pastes were mixed as described above. Immediately after mixing a flow curve with shear rates from 0.01 s^{-1} to 100 s^{-1} was recorded. Apparent yield stress and plastic viscosity were calculated according to the Bingham model. Microfine cement and limestone filler showed the best results concerning workability compared to microsilica and calcined china clay. Figure 4 shows the results.

Pure Portland cement paste shows a yield value of 129 Pa and a viscosity of 105 Pa·s. The replacement of up to 20 % Portland cement by microfine cement leads to a decrease both in yield value and in viscosity. Thus the rheological properties of cement pastes can be improved. Higher dosages of microfine cement cause an increase in yield stress and in viscosity, so the dosage of 20% can be seen as the optimum with a yield value of 20 Pa and a viscosity of 39 Pa·s. Dosages of microfine cement above 50% could not be examined because of their poor workability. The slump flow of this mixture also shows an optimum with 305 mm compared to 235 mm for the pure cement paste. The limestone filler shows a completely different behavior. Increasing limestone content in the binder decreases both the yield value and viscosity, no minimum can be observed. The combination of the microfine cement with Portland cement leads to a bimodal grain size distribution. Because the packing density is improved, the paste shows a better workability at the same w/b-ratio. The optimum is at 20% microfine cement content that seems to be the right amount to fill the voids between the cement grains. Otherwise it is possible to reduce the w/b-ratio by partial replacement of Portland cement without loss of workability.
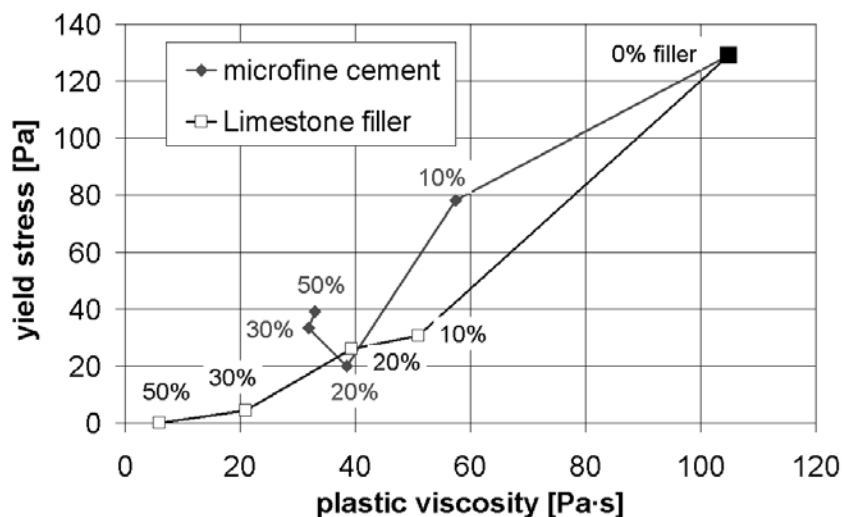
Fig. 4   Bingham parameters of the investigated cement pastes with different filler contents (mass%)

Flexural and compressive strength of conventionally cast prism

First the influence of the addition of the microfine cement on the compressive strength of conventionally cast specimens (40x40x40 mm³) without any fiber addition or acicular reinforcement is presented. The addition of microfine cement increases compressive strength significantly (Figure 5). The slump flow as kept constant at 200 mm meanwhile the w/c ratio was adjusted. 2 mass% of superplasticizer war applied. The greatest increase is found for the batch with the highest amount of microfine cement. Curing condition has a minor influence on the compressive strength as shown elsewhere [8].
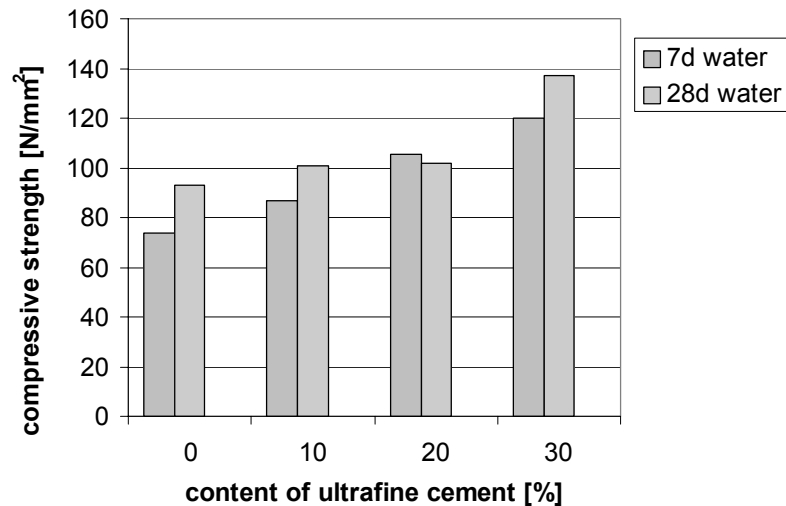
Fig.5   Influence of content of microfine cement (mass%) on the compressive strength of moulded prisms after 7d and 28d (full water immersion)

Further improvement of the performance is obtained when acicular additives are added to the fresh mix. The effect of different amount and type of wollastonite (CaSiO₃) was studied. Wollastonite type W2 and W3 have a higher aspect ratio compared to W1. The mix proportions are given in table 1. Besides some variation in batch 4 and 5) the w/c was adapted to approach a slump of about 200 mm. This however, was not easy owing to a thixotropic character of some mixes. Conventionally mixing and casting process was applied. The specimen were exposed to three different curing regimes; A) 7/28d under water at 20°C, B) 7d at 20°C/98%RH ("humid") then under water at 20°C, C) 7d at 20°C/98%RH then at 20°C/70%RH. After 7d and 28d the flexural strength (3 point, span 45 mm) and the compressive strength (on cubes 15X15X15 mm³) was measured. The results are plotted in Table 2.

batch #	CEM I 42.5 [mass%]	microfine cement [mass%]	Wollastonite [mass%]	Type	Water [mass% **)]	superplasticizer [mass% **)]	w/c*)	slump [mm]
1	80	20	0	-	16	2	0.16	190
2	60	20	20	W1	15	2	0.19	214
3	60	20	20	W2	21.5	2	0.27	207
4	60	20	20	W3	21.5	2	0.27	275
5	60	20	20	W3	20	2	0.25	260
6	60	20	20	W3	18	2	0.23	240

*) c = CEM I 42.5 + microfine cement

**) mass% of dry components (CEM I 42.5 + microfine cement + wollastonite)

Table 1   Mix proportions

The much higher aspect ratio of the wollastonite type W2 and W3 lead to higher w/c ratio to allow the preparation of the mix and to obtain similar workability as with W1. Probably the application of a high shear mixer would have lowered the water demand. Despite the higher w/c much better performance is obtained with high aspect ratio mineral fibers. Very high bending strength of up to 31 MPa is obtained. The curing condition has a significant influence on the bending strength. No heat treatment was applied. However a soft treatment at high relative humidity (> 98%RH) during the first few days is more advantageous than immersion into water with respect to bending strength. Best results are obtained when transferring the specimens after 7 days to a dry (20°C/70%RH) climate. Probably the loss of some excess water and the formation of capillary forces lead to higher strength. With respect to compressive strength samples with full water immersion generally perform better than those of the other curing conditions.

batch #		bending strength [MPa]		Compressive strength [MPa]	
		7d	28d	7d	28d
1	7dwater then water	18.4 ± 0.8	16.3 ± 1.6	120.3 ± 8.4	142.2 ± 15.0
	7d humid then water	15.9 ± 1.1	18.4 ± 0.9	124.3 ± 7.1	151.8 ± 8.6
	7d humid then 70%RH	X	15.7 ± 1.2	X	131.8 ± 10.1
2	7dwater then water	17.4 ± 0.5	17.6 ± 2.6	113.4 ± 19.7	140.1 ± 6.1
	7d humid then water	21.5 ± 2.8	19.8 ± 0.8	117.4 ± 6.9	135.2 ± 9.4
	7d humid then 70%RH	X	20.0 ± 1.1	X	135.6 ± 10.8
3	7dwater then water	24.7 ± 2.2	21.6 ± 3.0	111.9 ± 11.6	146.8 ± 10.3
	7d humid then water	n.a.	24.2 ± 1.5	n.a.	128.5 ± 5.3
	7d humid then 70%RH	X	25.8 ± 3.4	X	131.9 ± 7.3
4	7dwater then water	25.3 ± 3.8	24.1 ± 1.9	120.2 ± 10.4	132.0 ± 17.5
	7d humid then water	22.2 ± 1.7	22.8 ± 4.1	115.2 ± 8.0	129.9 ± 6.4
	7d humid then 70%RH	X	30.9 ± 1.3	X	138.1 ± 4.0
5	7dwater then water	23.1 ± 2.3	23.9 ± 1.4	130.6 ± 9.1	149.1 ± 19
	7d humid then water	24.3 ± 2.9	26.4 ± 1.7	120.1 ± 12.1	135.5 ± 23.3
	7d humid then 70%RH	X	31.6 ± 2.1	X	154.4 ± 9.2
6	7dwater then water	24.1 ± 1.7	20.1 ± 4.3	144.5 ± 11.5	170.0 ± 18.5
	7d humid then water	24.3 ± 1.6	23.3 ± 1.8	124.6 ± 19.5	154.6 ± 15.7
	7d humid then 70%RH	X	28.6 ± 1.6	X	162.7 ± 16.7

Table 2 Bending and compressive strength in function of storage conditions (all at 20°C)

Flexural and compressive strength of centrifuged material

With the above described centrifugation process pipes with wall thickness of 25 mm (diameter 180 mm, length 180 mm) were produced. The mix designs are given in table 3. Slump was kept between 290 mm and 300 mm to guarantee a very good workability. The centrifugation process leads to a further improvement of the mortar. When the centrifugal acceleration exceeds 20 g, a further compaction is observed. Excess water is then expelled, lowering the w/c ratio of the mix. The excess water has a high Ca content and contains some fine cement fractions. The excess liquid was collected and then dried at 110°C to determine its water content. This data was used to calculate the reduction of the w/c ratio caused by the centrifugation process and to obtain an estimate for the effective w/c ratio after centrifugation.

After cutting the specimen they first remained at 20°C/98%RH, followed by two different curing regimes: A) 2d in water then 21d at 70%RH and B) 23d in water, all at 20°C.

Bending strength (3 point, span 45 mm) of cut prisms 15x15x80 mm^3 and compressive strength of cut prisms (15x15x25 mm^3) was determined. Owing to the fact that the grain size of the used particles is relatively small, the size effect on the strength properties is not very big. This was confirmed by measurements on larger (40 x 40 x 160 mm^3) specimens.

The results are plotted in figure 6 and 7. Best results were obtained for medium amount of mineral fibers (20%). Lower strength is observed for higher wollastonite content. The same observations are made for the compressive strength. When no microfine cement is used (batch 5), the bending and the compressive strength are much lower than when this cement component is added.

The batch with the lowest wollastonite content shows much better performance at 7d than at 28d and for curing regime B. It seems that reinforcement with only 15% of mineral fibers of this batch is too low to prevent from shrinkage cracking. In all other cases, curing conditions have no significant influence on the strength properties and very high early strength is observed which increases slightly with age. High bending strength over 30 MPa and very high compressive strength over 220 MPa is measured.

batch #	CEM I 42.5 [mass%]	Microfine Cement [mass%]	Wollastonite [mass%]	Type	Water [mass% **)]	Super-Plasticizer [mass% **)]	w/c *)	w/c eff ***)
1	63.5	21.2	15.4	W3	15.3	2	0.18	0.15
2	60	20	20	W3	21.6	2	0.27	0.21
3	52.5	17.5	30	W3	30	1.9	0.43	0.27
4	47.4	15.8	36.8	W3	31.8	1.8	0.50	0.40
5	80	0	20	W3	30	2	0.38	0.20

*) c = CEM I 42.5 + microfine cement

**) mass% of dry components (CEM I 42.5 + microfine cement + wollastonite)

***) recalculated from expelled water after centrifugation

Table 3   Mix proportions for the production of centrifuged pipes
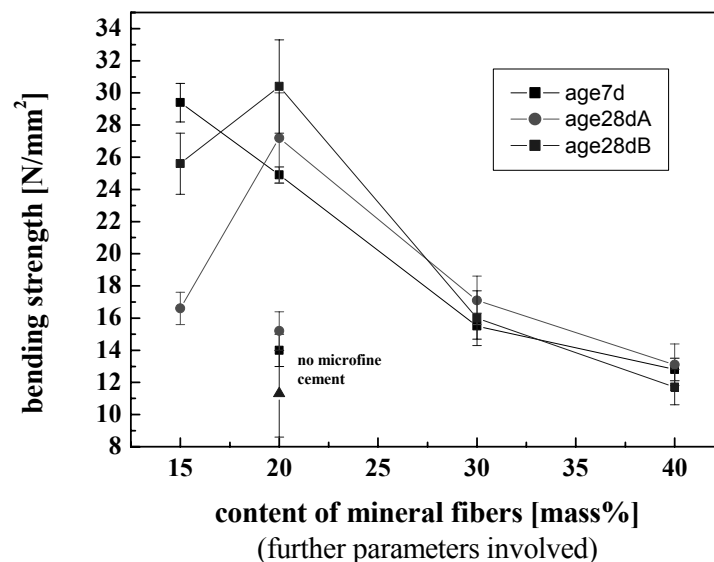
Fig. 6   Bending strength at 28d of prisms cut from centrifuged pipes with curing conditions (all 20°C): 5d 98%RH then   A: 2d water then 21d at 70%RH B: 23d water
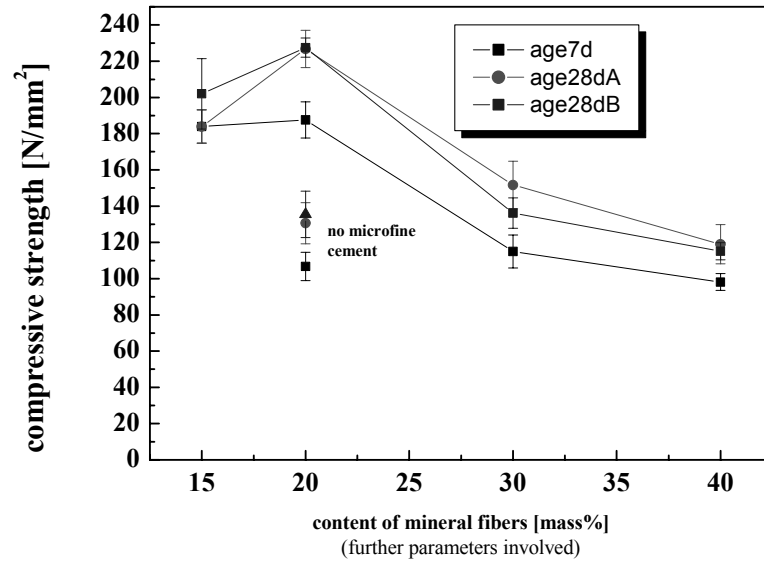
Fig. 7   Compressive strength at 28d of prisms cut from centrifuged pipes with curing
conditions (all 20°C): 5d 98%RH then   A: 2d water then 21d at 70%RH B: 23d
water

Microscopic studies of the presented wollastonite-mortars show a very dense microstructure
with few defects (fig. 8). Centrifuged specimens are free of air inclusions. The bond between
the wollastonite fibers and the cement matrix is good. However, there is no evidence for a
chemical reaction of the wollastonite with the cement clinker. A consequence of the dense
microstructure is the high frost resistance of these materials. Pipes (diameter 180 cm, wall
thickness 1 cm) subjected to 140 frost cycles (+20°C/-20°C, in water during heating period)
showed no loss of strength. First results of strength measurements performed on such pipes
confirm the strength properties as obtained on cut prisms.
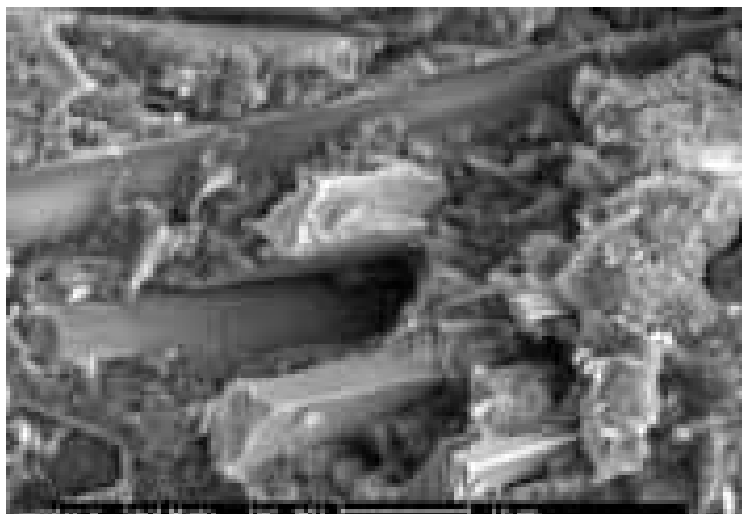
Fig. 8:   ESEM micrograph of wollastonite mortar (batch 1, 28d, broken surface)

4   Conclusions

The addition of microfine cement to ordinary Portland cement has a positive influence on the rheological properties of the fresh cement pastes. This allows a reduction of w/c ratio which leads to very high strength. Further improvement is obtained with an addition of mineral fibers, e.g. wollastonite with high aspect ratio. Conventional mixing and curing at 20°C (no heat treatment) is sufficient to reach bending strength of more than 30 MPa. Further improvement, especially considering compressive strength is possible when applying a special casting technique: centrifugal casting. A further water reduction is possible which leads to ultra high strength materials. Applications in the production of thin elements, pipes, pylons or columns are possible.

## 5	References

[1]	Dilger W.H., Rao S.V.K.M., "High performance concrete mixtures for spun cast concrete poles," *PCI Journal*, vol. 42, no. 4, 1997, S. 82–96.

[2]	German R., *Particle packing characteristics*, Metal powder industries federation, Princeton, (1989).

[3]	Bache H., "Densified cement ultrafine based materials", *Proc. 2nd Int. Conf. on Superplasticizer in Concrete*, Ottawa, 1981, pp. 3-35.

[4]	Neville, A.M., *Properties of concrete*, Longman, Harlow, UK, 1995.

[5]	Lange, F., Mörtel, H., Rudert, V., "Properties of mortars containing fine-ground cements," *Bull. Amer. Ceram. Soc.*, vol. 75 no. 3, 1996.

[6]	Kaufmann J., Winnefeld F., "Influence of addition of ultrafine cement on the rheological properties and strength of Portland cement paste", *Proc. Int. Conf. Innovations and Developments in Concrete Materials and Construction*, Dundee, UK, Sept. 2002, 827-836.

[7]	World Health organization IARC Monographs on the evaluation of carcinogenic risks to humans: Silica, some Silicates, coal dust and para-Aramid fibrils, Volume 68 (1996)

[8]	Kaufmann J., Matschei Th., Hesselbarth D., „Effect of the addition of ultrafine cement on the properties of fiber reinforced composites", Proc. 11th int. Conference on the Chemistry of Cement ICCC *Conference, Durban South Africa, 2003, pp. 1683-1691.*

Carsten Vogt
Dipl.-Ing.
CBI
Stockholm, Sweden

Björn Lagerblad
PhD
CBI
Stockholm, Sweden

Torbjörn Hugo-Persson
Manager Investigation Technology
SKB
Äspö, Sweden

Optimization of UHPC for selective stabilization of deep boreholes

Summary

This report concern the use of optimized fiber reinforced UHPC for stabilization of deep boreholes. In the concept an extended borehole is filled with UHPC and drilled again with the original drill diameter. This will give a remaining tube that stabilizes weak rock. The concrete has high demands on pumpability, workability and strength. Moreover it must contain silica fume to lower the impact on pH in the ground water. The concrete that can fulfill these demands is a modified reactive powder concrete. It contains more silica fume, somewhat higher w/b and the steel fibers are replaced with glass fibers. This concrete has been tested in field and it gives the desired properties. The modified UHPC gives only slightly less strength both with steel and glass fibers. The glass fibers works well and may be long-time durable, as the pH in the UHPC is lower due to the high contents of silica fume.

Keywords: *selective stabilization of boreholes, UHPC, steel fibres, glass fibres, low pH concrete*

1   Introduction

In Sweden spent nuclear waste will be deposited in canisters in crystalline granitoid bedrock at depth of around 500 meters. To find suitable rock types two areas have been selected for a close geological analysis. This demands an extensive drilling program and bore holes that will be measured and monitored. The drill holes will pass different deformation and transmissive zones that will endanger the equipment and measurements. Thus the holes that may go to a depth of more than 1000 meters must be stabilized.

Swedish Cement and Concrete Research Institute (CBI) have been asked by Swedish Nuclear Fuel and Waste Co (SKB) to formulate different concepts of how to stabilize the boreholes. Traditional injection with cement grouts did not work well. One of the concepts is to widen the critical section of the drill hole, fill this extended hole with concrete and then drill with the original drill size again. This will result in a remaining "tube" that will stabilize the rock. It is expensive and difficult to widen the hole thus it is favorable to have very strong

concrete for thin tube thickness. In the concept a widening and thickness of 10 mm of the remaining tube is assumed. The concrete must be possible to transport to a fairly deep position in water filled holes, which apart from strength also puts high demands on equipment, rheology and D-max of the aggregates. The concrete should have a compressive strength of 30 MPa after 24 hours considering the fact that the concrete may be diluted with ground water when cast. Moreover, the cementitious material must be formulated in such a way that the contamination to the ground water is minimal. The amount of cementitious material in the rock shall be small. To avoid a pH plume the cement paste shall be difficult to dissolve and the amount of organic material shall be at a minimum. From earlier investigations we know that if the binder contains more than 20 wt. % silica fume the mix will not give a pH of more than 12 and with more than 30 wt. % silica fume the pH will be less than 11 in the ground water.

The demands on the properties of the concrete can not be fulfilled with normal concretes, thus ultrahigh performance concrete is needed. Reactive powder concrete can fulfill many of the demands. This concrete has small size aggregates and it is very strong both as regard compressive and flexural strength. Moreover, already in its basic concept this concrete contains rather large amounts of silica fume. The application method also requires UHPC with high flowability, long opening time, high stability against separation in water and fast hardening. Field tests and simulation in laboratory were performed to test material properties as well as application technique. The effect of casting trough water in the boreholes was especially studied. Separation, textures and microstructure were investigated on polished sections in SEM and by other means.
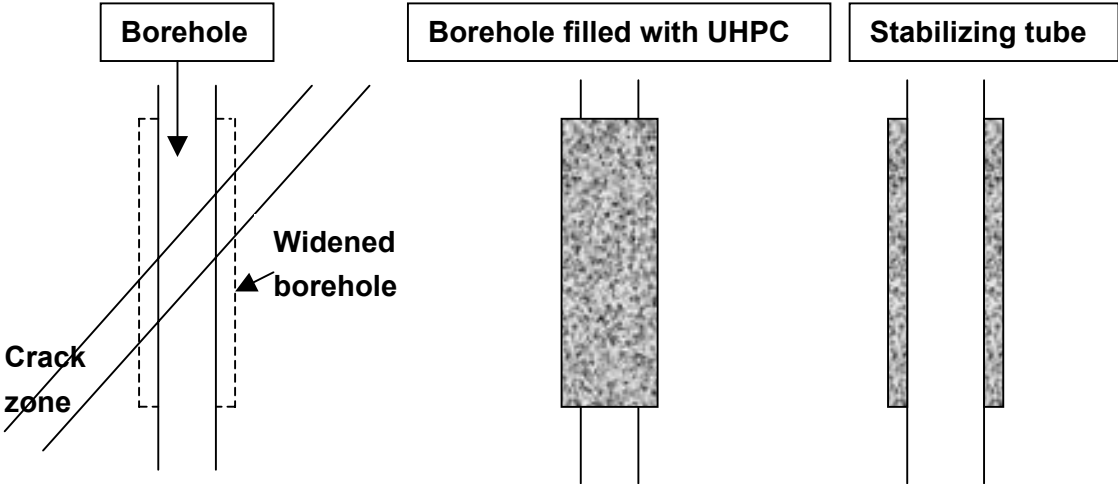
Figure 1:   Sketch showing the concept with a tube of UHPC stabilizing the borehole.

2   Materials and methods

The recipe was based on a basic recipe used for reactive powder concrete. To lower the pH the amount of silica fume was increased to 23-wt % of amount of binder. Preliminary test have shown that it is possible to increase the amount of SF to 30 wt. % of the binder to get a pH of less than 11. To get a good flowability 6-mm steel fibers (Bekaert) was used in the first

instance. The steel fibers caused problems both during casting and drilling, thus in another set we tested glass fibers (CEM-FIL, Saint-Gobain). Glass fibers may lose their physical properties with time but the stabilization only needs to be effective during some years. Moreover, the low pH inside the concrete will presumably give a longer durability time to the glass fibers.

2.1 Materials and mix design

The following materials and proportions were used for the production of the UHPC in laboratory investigations and for the field tests:

Table 1: Composition of the UHPC. -SF = steel fibers, -GF = Glass fibers.

Component	UHPC-RPC	UHPC-SF	UHPC-GF
White OPC CEM I 52,5 (SR/LA) (Aalborg)	788 kg/m^3	788 kg/m^3	788 kg/m^3
Undensified silica fume (Elkem)	142 kg/m^3	236,4 kg/m^3	236,4 kg/m^3
Quartz flower M500 (Sibelco)	107.5 kg/m^3	107,5 kg/m^3	107,5 kg/m^3
Fine quartz sand (<250 µm)	533 kg/m^3	391,3 kg/m^3	403,6 kg/m^3
Coarse quartz sand (<500 µm)	533 kg/m^3	391,3 kg/m^3	403,6 kg/m^3
Polycaboxylate Superplasticizer (dry)	16.2 kg/m^3	3,5 kg/m^3	3,5 kg/m^3
Water	186 kg/m^3	249,6 kg/m^3	249,6 kg/m^3
Steel fibers (l = 6mm) (Bekaert)	228 kg/m^3 (Volume 2.9 %)	228 kg/m^3 (Volume 2.9 %)	-
Glass fibers (l = 6mm) (CEM-FIL, Saint-Gobain)		-	53,6 kg/m^3 (Volume 2.0 %)
Water-binder-ratio	0.20	0.25	0.25

The concrete was mixed in a forced mixer. The concrete was designed to be self-compacting, as no vibration is possible in the boreholes. The laboratory samples were cured in 100% humidity at 20˚C. No heat-curing was used as this is impossible in the boreholes. To simulate the conditions in deep boreholes, samples were also stored at 5˚C.

2.2 Methods

One of the big problems was to fill the boreholes with concrete of sufficient quality. In field the boreholes are filled with water and the concrete must push this water away. This must be done carefully as the water may mix with the concrete and dilute it, which will result it lower quality. Thus we have tested the concretes in both laboratory and in field conditions to find out the effect of water interaction. No organic compounds, often used in under water casting, were allowed. Moreover, in the rock the temperature will vary between 5 and 15 ˚C depending on depth.

2.2.1 Fresh concrete properties

Spread flow tests and flowing time were used to evaluate the workability of the concretes. The tests were similar to the ones used to evaluate the flowability of self-compacting mortar

recommended by OKAMURA [1]. A set cone according to DIN EN 459-2 was used to determine the spread flow after mixing and up to 4 hours later. The plastic funnel that was used to determine the flow time was different from the one used by Okamura. The opening in our tests had a diameter of one centimeter as this is what we will get in the field tests.

The hardening time, influence of different types of plasticizer and influence of casting in water were determined by isothermal calorimetry. The heat released by paste samples of 60 g was measured over a period of 36 hours.

2.2.2 Hardened concrete properties

The compressive strength of the laboratory samples was tested on 100x100x100 mm cubes. For measurement of flexural strength 40x40x160 mm prisms were used. Autogenous shrinkage was tested on sealed samples in flexible plastic tubes according to JENSEN [2]. These samples were stored at both 20˚C and 5˚C. The durability of glass fibers was tested on samples after 28 days curing at 20˚C and 100% RH according to GRAM [3], using a climate box with four heat/moisture cycles per day. The samples are heated to 105˚C for 5.5 hours and then sprayed with water of 10˚C for 0.5 hours.

2.2.3 Laboratory simulation

To simulate the effects on the hardening time of casting concrete in water filled boreholes, concrete was casted in 80- mm plastic tubes filled with water. The concrete sample was removed 4 hours after casting in the tube and heat of hydration was measured, using isothermal calorimetry.

2.2.4 Field tests

In two areas two holes with a diameter of 76 mm and up to 7m deep were drilled in granitic rocks. In one of the areas the rock had normal cracks while it in the other area contained wide and open cracks. Different methods of casting were tested. Two days after casting a drill core with a diameter of 45 mm was taken from the concrete. Following this the original borehole was overdrilled with a 102-mm drill core. This resulted in three drill cores, one from the rock, one from the concrete and one that included rock and the "tube".

The massive concrete core was used for investigation of compressive strength, water-cement-ratio and fiber content. Strength tests were done on cylinders with a height of two times the diameter. The fiber content of samples from the field test was measured with different methods. Steel fiber UHPC was milled and the fibers were removed with a magnet and weighted. Glass fiber content was determined on polished samples in SEM investigations, creating a map of the zirconium distribution in the sample. The water-binder ratio of the samples from the field tests was calculated by comparing the measured density with the density of laboratory samples. Analysis of the microstructure, texture and chemical composition was done on polished samples in scanning electron microscope (SEM).

The results from these tests were used to optimize concrete recipe and application technique. In a new test hole 5 of realistic scale and depth, tests were done with the UHPC containing glass fibers and the actual application equipment and methods described in figure

1. So far two transmissive zones in the hole were stabilized using this concept. The drilling was continued after 96 hours the first test and after 28 hours for the second. Compressive strength and density were analyzed for the removed drill cores.

3   Results

3.1   Material properties

3.1.1   Fresh concrete properties

The fresh concrete properties described were evaluated to be sufficient for the demands of the application method in the boreholes. Only small differences are noticeable between the concretes with different fiber types.

Table 2:   properties of fresh UHPC

	UHPC-SF	UHPC-GF
Spread flow of paste without fibers	295 mm (after mixing)	
	255 mm (after 4 hours)	
Flowing time without fibers	38 sec (after mixing)	
	110 sec (after 4 hours)	
Spread flow of concrete with fibers	275 mm (after mixing)	265 mm (after mixing)
	230 mm (after 4 hours)	225 mm (after 4 hours)
Flowing time of concrete with fibers	45 sec (after mixing)	52 sec (after mixing)
	130 sec (after 4 hours)	146 sec (after 4 hours)

The glass fibers make somewhat stiffer concrete even though their content is lower than the steel fiber concrete. Advantages of the glass fibers are though that the concrete is easier to pump.

The type of plasticizer was found out to be the main influencing factor on the hardening time of the UHPC. Thus by changing the type of superplasticizer it is possible to adjust the opening time to the actual situation. Isothermal calorimetry shows the heat development and gives an impression of the influence of the different plasticizers. All types of plasticizers were tested, but only the modern ones based on polycarboxylate give sufficient workability to the UHPC.

Figure 2 shows which influence different kinds of superplasticizers have on the heat of hydration and on the stiffening times. Plasticizer 2 and 3 are products especially for the prefabrication industry. They increase the released heat of hydration of the cement significantly and shorten the dormant period. That might be advantageous for low depths or at cold temperature as concrete strength develops faster and the work can progress earlier but it may be risky if the concrete shall be casted at great depth.

The influence of casting the concrete through water on the heat of hydration was tested (Fig. 3). Basically the concrete becomes diluted and it may lose some soluble products like alkalis and sulphates from the early pore water to the groundwater. The results show that the

dilution mainly results in an extended dormant period but cumulative the heat-development is similar to that of undisturbed samples.
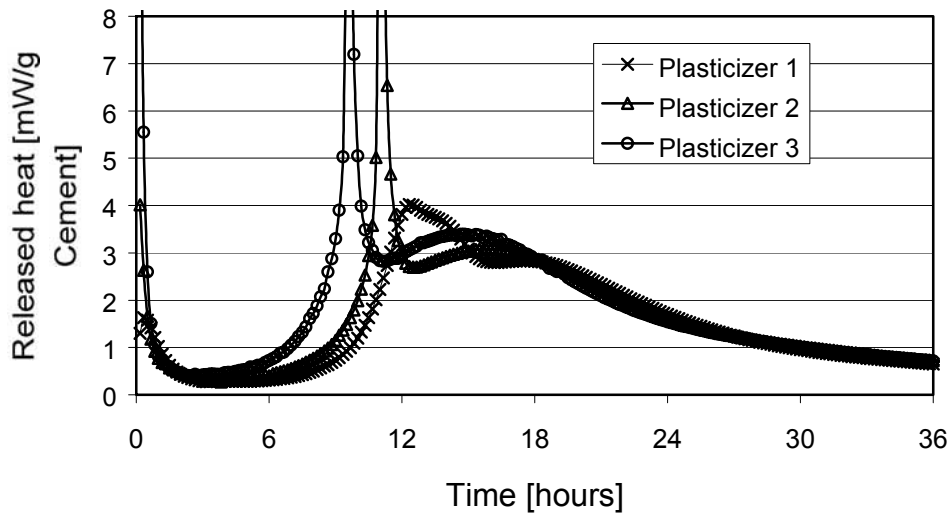
Figure 2:   Influence of type of plasticizer (polycarboxylate) on heat of hydration. The heat peak at the start of the acceleration period with the "fast" superplasticizers is a fact and not an artifact.
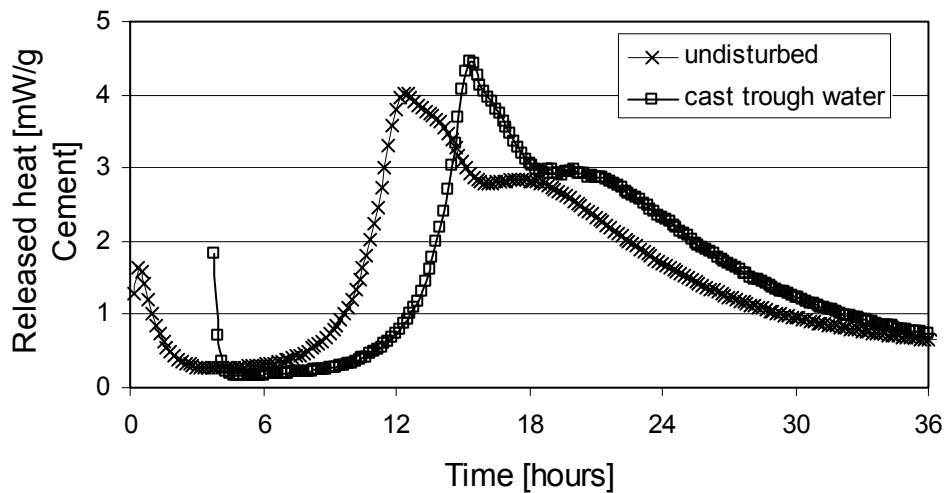
Figure 3:   Influence of casting through water on heat of hydration, the sample was removed from the water filled tube after 4 hours and put into the calorimeter (start of measurement)

3.1.2   Hardened concrete properties

Table 3 shows the summarized properties of the hardened laboratory samples. The compressive strength was 155 and 146 MPa after 28 days at 20°C. This is somewhat lower than for reactive powder concrete that has not been steam cured. This is presumably due to the higher content of SF and the somewhat higher water/binder. Curing at lower temperature mainly delays the strength development but it also seems to lower the final strength

somewhat. The flexural strength of both, concrete with glass fibers and steel fibers is close to equality, even though the volume content of glass fibers is only two third of the steel fibers. The strength of these concretes will fulfill the physical requirements of the application. So far the glass fibers seem to be durable as the flexural strength increases up to 91 days and no loss in flexural strength was observed after 100 cycles in the climate box. The observed increase in flexural strength may be a result of the high temperature treatment in the climate box.

Table 3:   Compressive and flexural strength of laboratory samples. SF = steel fibers GF = glass fibers.

Age	Compressive strength [MPa]				Flexural strength [MPa]		
	RPC	UHPC-SF	UHPC-SF	UHPC-GF	RPC	UHPC-SF	UHPC-GF
	20˚C	5˚C	20˚C	20˚C	20˚C	20˚C	20˚C
1 day		22.7	52.3	53.1		-	-
2 days	52.2	72.3	79.9	78.8		-	-
7 days	113.3	103.7	111.5	102.7		-	-
28 days	158.2	141.4	154.8	145.6	31.6	21.5	24.5
91 days	182.2	161.5	171.7	161.4	31.8	24.1	25.7
Durability test of glass fibers				**Flexural strength [MPa]**			
Reference (cured at 20˚C and 100% RH)				26.0			
After 100 cycles in climate box				29.6			

The concrete in the boreholes will be in wet environment all the time. Therefore the autogenous shrinkage was measured in sealed flexible plastic tubes. In fact drying shrinkage gives the same values as autogeneous shrinkage presumably due to the lack or capillary pores in the UHPC.
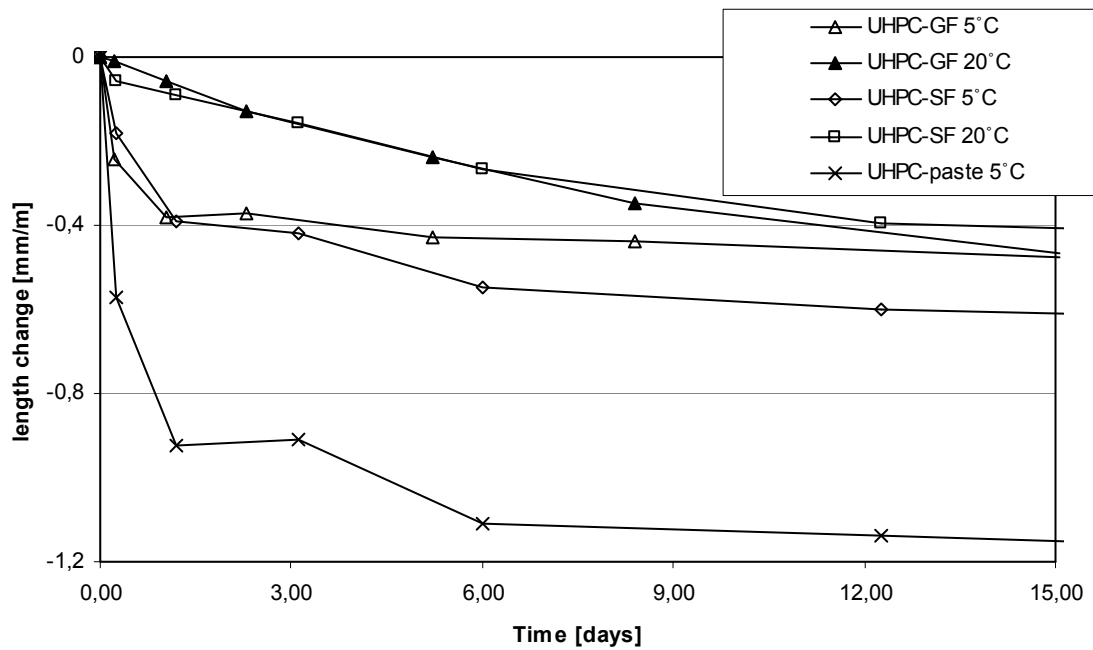
Figure 4:   Early autogenous shrinkage of UHPC stored at different temperatures

Figure 4 shows the autogenous shrinkage of the UHPC with and without fibers at different curing temperatures. The measurements started after the samples had built up enough strength to enable the test, which means between 12 and 18 hours. Of special importance for the autogenous shrinkage are the first 24 hours after setting. Approximately 70-80 % of the final shrinkage occurs during this period of time. All samples cured at 5°C showed an increased shrinkage in the early state compared to 20°C. Later the shrinkage of the samples stored at 20°C increases and the values get more even. The plain concretes without fiber reinforcement had much higher shrinkage than with fibers, especially when stored at 5°C. The measurements show that fibers stabilize the concrete and reduce the shrinkage. Long-term tests show that the process with fiber UHPC will continue further to a final value of 0.7-0.9 mm/m.

3.2   Field tests

So far, 5 test holes with different application techniques and concrete compositions have been tested. All holes were full of water. Hole 1 was filled with steel fiber UHPC from the bottom, using a hand pump and a hose. The analyzed cores showed that the concrete had filled cracks with a width over 0.5 cm. The inner core had a good bound to the surrounding rock. The steel fibers separated to a noticeable degree, the concrete core at the top 100 cm was nearly free from fibers, fibers that settled in the lower parts. This is presumably due to dilution of the concrete made is less stable, which allowed sedimentation of the heavy steel fibers. Nevertheless, the concrete below the first 100 cm seemed fine and could fulfill the requirements.

Hole 2 was filled from the top, just pouring the steel fiber concrete trough a funnel in the water filled hole. The concrete ran up to 7 m free through water. This casting method

resulted in much difficulty for the drilling crew and basically no inner concrete core could be obtained. Only some parts of heavily separated steel fibers in the lower part of the hole were found.

Table 4:   Compressive strength, steel fiber content and calculated water-cement-ratio of UHPC-SF from test-hole 3, samples taken from different depths

UHPC-SF (Hole 3 measured 34 days after casting)			
Depth [m]	f_{cc} [MPa]	Fibers [%]	w/c [-]
1.30	87.9	0	0.55
2.20	105.0	1.45	0.44
3.20	147.5	1.46	0.34
4.28	141.1	3.21	0.35
6.50	146.1	1.72	0.33
Reference (laboratory mix, 28 days)			
	154.8	2.9	0.325

Hole 3 was filled with another technique. The steel fiber UHPC was pumped in the hole from the bottom, using a pressure vessel and air pressure. The removed core showed similar properties to core 1, which means fiber separation in the top 100 cm and increased fiber content in the bottom. Strength, water-cement-ratio and fiber content were measured on this sample (see table 4). With increasing depth the water-cement-ratio decreases while the fiber content increases. Therefore higher strength values were obtained. It was noticed that the steel fibers complicated the drilling remarkably. The drilling tools were consumed much faster than normal and drilling progress was slow. That fact and the observed fiber separation was the motivation to test glass fibers.

Hole 4 was filled with UHPC-GF with a screw pump and a plastic tube from the bottom. Basically it is the same filling method as in hole 1 and 3 but the screw pump gives a higher pressure and a thinner tube could be used. The concrete was drilled out after 3 days and analyzed. The results are shown in table 5. Fiber separation was much less than in the samples with steel fibers due to that the glass fibers have a lower density (similar to the paste) than the steel fibers.

The overcoring also showed that the concrete filled cracks from 0.5 cm up to 15 cm. The drilling was much easier than with steel fiber concrete and the inner shell was stable and bound to the rock (figure 4). The fiber distribution was more even than with steel fibers, even in the top part fibers were observed. The samples from the deeper parts of the hole have lower porosity, lower water-cement-ratio and higher strength. This indicates that also this concrete is somewhat diluted with ground water. Thus in a real case the bore holes must be filled to above the cracked zone to compensate for the diluted upper part. The Ca/Si and the w/c increases upwards in the core. The increase in w/c indicates dilution. This would, however, not influence the Ca/Si. Thus there must be a separation where cement accumulates in the lower parts and silica fume in the higher more diluted parts. Moreover,

the low Ca-Si-ratio in the paste indicates a low maturity of the paste, which is logical after only 3 days of hydration, the Ca/Si ratio will increase when more cement becomes hydrated. The UHPC do not contain any portlandite and the Ca/Si ratio will determine the pH of the pore solution. The SEM investigations showed that the glass fibers are evenly distributed and well bound to the paste (figure 6)

Table 5: Compressive strength, glass fiber content (vol. %), calculated water-cement-ratio, porosity and Ca-Si-ratio of UHPC-GF from test-hole 4, samples taken from different depths. The Ca/Si-ratio was determined by energy dispersive analysis on spots on flat polished samples.

UHPC-GF (Hole 4) (measured 3 days after casting)					
Depth [m]	f_{cc} [MPa]	Fibers [%]	w/c [-]	Porosity [%]	Ca-Si-ratio (mean value)
1.43	30.9	1.36	0.55	14.1	0.564…0.928 (0.704)
1.78	38.3	2.02	0.54	10.3	0.593…0.763 (0.704)
3.74	66.5	2.61	0.31	7.3	0.638…0.987 (0.856)
5.67	62.1	2.83	0.35	6.7	0.646…1.087 (0.846)
Reference (laboratory mix, 2 days)					
	78.8	2.00	0.325		

Hole 5 is a full scale borehole to test different stabilization methods. The hole has a diameter of 76 mm and so far a depth of 110m. The equipment, concrete and application method are tested under practical circumstances. Experience from the four other holes lead to the decision to design the application tool with a removable top piston that will follow the concrete into the hole and expand above the concrete to protect it from water. The removed concrete cores were analyzed and showed a very even fiber distribution. The density of samples from the upper and lower part of the core was close to equality but the strength differs. The concrete seems to be diluted somewhat with water, especially at the top.

Table 6: Compressive strength and density of UHPC-GF from test-hole 5, the tests were done at 17m (test1) and 105m (test2) depth.

Position within the core	Compressive strength [MPa]		Density [g/cm^3]	
	Test 1 (6days)	Test 2 (2 days)	Test 1 (17m)	Test 2 (105m)
Top	92.9	58.4	2.028	2.228
Middle	-	72.9	-	2.256
Bottom	112.9	55.0	2.256	2.281
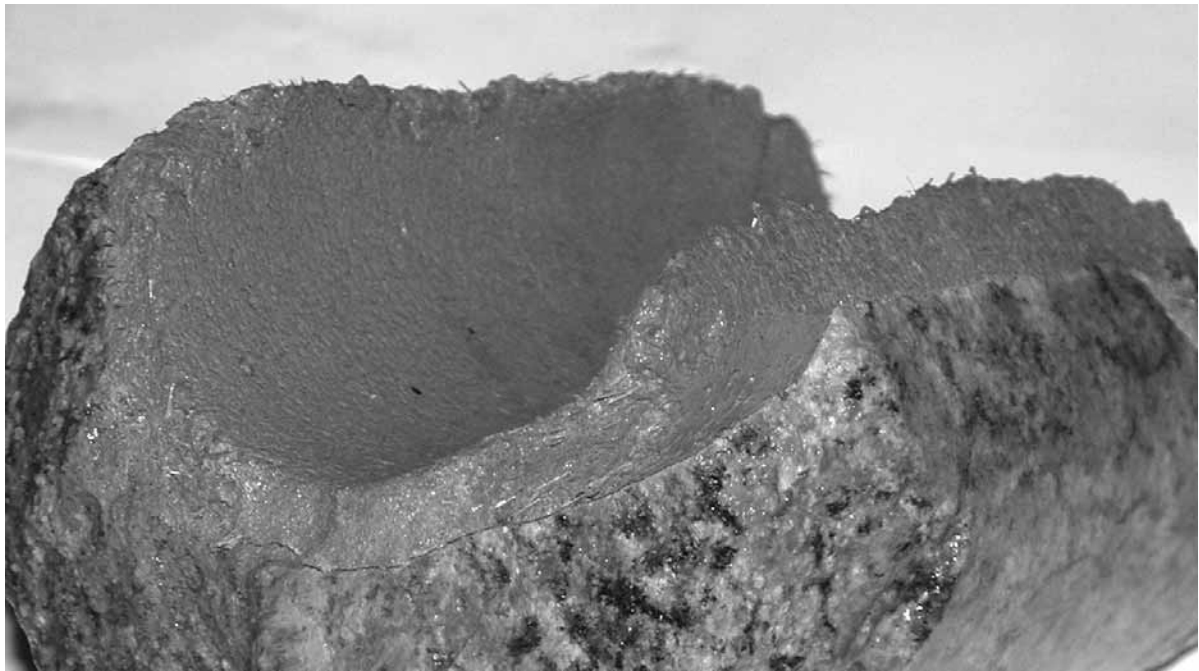
Figure 5:   Sample from borehole 4 with glass fiber UHPC. Thickness of tube/shell is 0.6 mm. Overcored after 3 days.
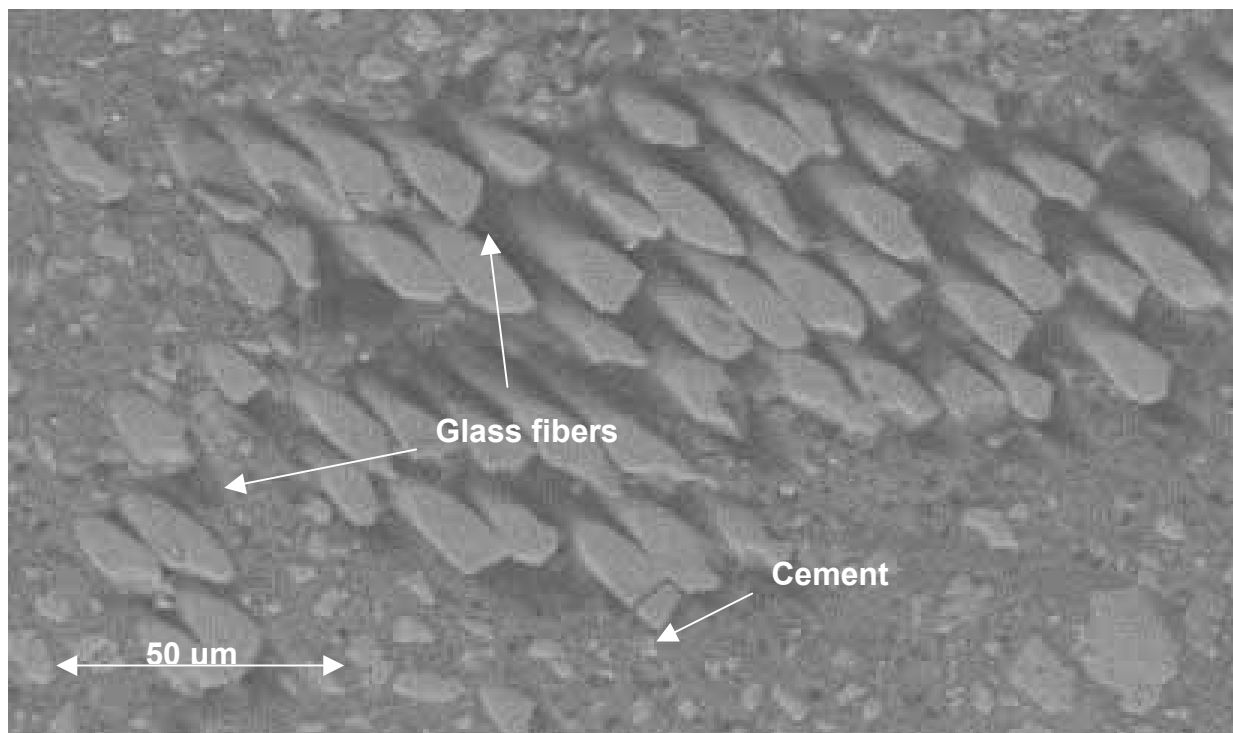
Figure 6:   SEM picture of glass fibers in sample from bore hole 4. Observe the dense paste around and partly in the glass fiber bundle. The light grey particles are unhydrated cement grains, the dark ones pores. Overcored after 3 days.

4   Discussion

The application with borehole stabilization by forming a tube in the rock demands special concrete properties. The concrete shall be cast in water, have high strength and fulfill certain chemical properties. This requires a special application technique and specially designed concrete. The concrete that could fulfill these requirements is a modified reactive powder concrete. This concrete is in principal based on densely packed particles of fine quartz sand, quartz flour, cement, silica fume and fibers. With the help of superplasticizers the water binder ratio is very low. The fine grain size of the aggregate allows short and thin fibers.

In the designed concrete the amount of silica fume is increased and the steel fibers are replaced with glass fibers. It is not possible to steam cure and thus the strength will be less but it will still be a very strong concrete. The high contents of silica fume will give a matrix with low pH and thus the glass fibers will last longer before they become brittle. The difference between steel fibers and glass fibers is only noticeable in compressive strength, flexural strength is nearly equal. The fresh concrete properties were designed for the planned application technique. The concrete has an open time of more than 4 hours and the flowability allows pumping. The setting time and early hardening can be influenced by the choice of plasticizer. The stability in water is satisfying, especially if glass fibers are used.

The obtained flexural and compressive strength was not extremely high but sufficient for the planned application. The concrete has a fast hardening even at 5°C; principally only the one-day strength is influenced by the lower temperature. The final strength is also somewhat lower but the difference will not have any influence on the efficiency. The special composition of the concrete may have positive influence on the durability of glass fibers. The pH in the paste is much lower than in normal concrete. Investigation done on laboratory samples after 91 days show a Ca-Si-ratio of 0.9 to 1.1 of the paste. This Ca-Si-ratio will give a pH of less than 12 in the paste. Normal cement paste has a Ca-Si-ratio of about 1.8-2.1 and a pH of above 13 and thus the glass fibers loose their physical properties within short time. Theoretically the glass fibers may be durable in the UHPC and so far the test results verify that.

The field tests showed that it is necessary to pump concrete from bottom of the hole. It is not possible to simply pour the concrete into the water filled holes. That would lead to extreme fiber separation as the concrete is not stable enough in water. Underwater compounds might increase the stability but are not allowed in this application. The tests also demonstrated that glass fibers are superior to steel fibers. Glass fibers make it easier to handle the concrete and do separate less when cast into water filled bore holes. Glass fiber reinforced concrete is much easier to drill than steel fiber concrete. The UHPC has the ability to fill cracks and forms a stable inner tube in the bore holes.

5   Conclusions

It was possible to design UHPC recipes which have the requested properties in fresh and hardened state. It is possible to increase the content of silica fume and still keep the properties of a reactive powder concrete. High contents of silica fume will lower the impact on ground water chemistry and make glass fiber more durable. The high flowability and small

grain size of the aggregates allows application in boreholes with diameters of 56 or 76 mm and also enables the concrete to penetrate cracks. The high cement content and low water-cement-ratio gives the concrete a fast hardening and satisfying stability in water. Incorporation of fibers increases the flexural strength and abrasion resistance. Glass fibers make a better concrete than steel fibers. The physical properties of glass fiber and steel fiber concrete are similar. The low pH of the paste may increase the durability of glass fibers.

6 Acknowlegdements

7 References

[1] Okamura, H Ozawa, K.: Mix Design for Self-Compacting Concrete, Concrete Library of JSCE, (25) (June 1995) 59-75.

[2] Jensen, O.M.; Freiesleben Hansen, P.: A dilatometer for measuring the autogenous deformation in hardening Portland cement paste, Materials and Structures 28, 1995

[3] Gram, H.-E.: Durability of natural fibers in concrete, CBI forskning/research 1-83, 1983

Xincheng Pu

professor

Chongqing Univ.

Chongqing,China

Yongwei Wang

graduate student

Chongqing Univ.

Chongqing,China

Chong Wang

assistant professor

Chongqing Univ.

Chongqing,China

Chaojun Wan

assistant professor

Chongqing Univ.

Chongqing,China

Huaijing Pu

engineer

Chongqing Univ.

Chongqing,China

Kilometer Compressible Material and Its Preparation

Summary

Application and required properties of kilometer-compressible material (KCM) were discussed after it was defined. The performance of tubular ultra high strength concrete encased in steel tube (UHSCST) was reported, which is regarded as the basic way to get KCM. The results show that the tubular UHSCST has great load bearing and significantly improved ductility. New formula was established to evaluate the load bearing of concentrically loaded short columns filled with tubular UHSC. Different yield strengths of the steel and different axial compressive strengths of the concrete were selected to form 40 kinds of simulated tubular UHSCST with different outside diameters and different thickness. The load bearing of the 40 kinds were calculated and compared with the reckoned load bearing of KCM deduced from a real project in China.

Keywords: *kilometer compressible material, kilometer building, ultra high strength concrete, tubular ultra high strength concrete encased in steel tube, load bearing capacity*

1   Introduction

Compression is a kind of force status which material may bear. Different from other force status (tension, bend, shear, twist etc.), the compressive load bearing capacity of a shaft always partly depends on its longitudinal bending, that is, the more the length of a shaft is, the more its longitudinal bending is, the less its compressive load bearing capacity is. In order to reduce the effect of the longitudinal bending and raise the stability of the structure, crosswise supporting or division board are often installed to decrease the reckoned length of the shaft bearing compressive load. Even though, while the height of the building rises as a greater scale, the load which the bottom material bears will become bigger and bigger until

the strength cannot meet the require of the load, therefore, the material with higher strength and greater load bearing capacity is required.

KCM is defined as a kind of material which has the capacity of bearing compressive stress when extending its dimension as far as one kilometer or more along the direction of compressive stress, for example, materials in the columns of super skyscrapers with the height of no less than 1,000 meters which bear the tremendous load of the building, materials in the load bearing columns and shear walls of the oceanic structures with the depth of more than one kilometer, materials in the arch ring of an arch bridge with no less than 1,000 meters long span. However, materials in the pavement of road or tracks of railway, as well as other wire rod and tubing can not be regarded as KCMs because their directions of load bearing are obviously different from their directions of length or the compressive loads along the directions of length are almost zero although their length is possibly more than 1,000 meters; And as for the main load bearing cables of the ultra long span suspending bridge, their length is possibly more than 1,000 meters, and the directions of the load bearing are the same as that of the length of the main load bearing cables, for example, Akashi-Kaikyo Bridge in Japan and Jiangyin Changjiang Bridge in Jiangsu of China, but the force they bears is tensile stress, therefore, it also can not be thought as KCMs.

Because of the above characteristics of compression of materials, it is very difficult to prepare KCMs. Up to now, no actual KCMs have been used in the practical projects. However, the development of human society has gradually shown its great demand for KCMs.

2 Application Prospects And Demands Of Kilometer Compressible Materials

2.1 Erecting Super Skyscrapers

At present, the world population has been more than 6 billions and is forecasted to be up to 8 billions till 2050. The quickly increasing population makes the per capita cultivated land decrease to a great extent. In order to solve the residence problem of the extra population as well as other living problems, it is necessary to build lots of housing, kinds of traffic installation, types of cultural and educational facilities, a great deal of industrial bases of production, large quantities of business and medical health service centres, many entertainment and playing places and so on, all of which cause great occupation of land unexpectedly. Therefore, in the future, the contradiction between population and land will be sharp-pointed extremely, and land resource will become more and more precious. So it is the inevitable developing tendency to extend our living space even producing place to sky and ocean.

Actually, it is the fact that more and more skyscrapers have been extended to sky space and the height record of the highest building has been broken again and again. For instance, the original Equitable Building in New York, which was established in 1870 and won the highest and the only one with elevator of the time, has only 7 stories, and is only about 25 meters, while the Taipei International Financial Center at Taipei, which will be completed in 2004, has already been 508 meters high (see Table 1).

As we know, skyscrapers met well the mankind's requirements of the living and developing. The highest one is often regarded as the symbol of the city where it located and the show of the city progress. It was also a kind of reveal of art of the time. It suggested the technological improvements, particularly the construction technology. It was carrier of mankind civilization. Furthermore, it was demonstration of economic strength. So it can be anticipated that the present height record of 450 meters will be broken and the more than 1,000 meters high super skyscraper will be established. Actually, many designing ideas and plans have already been put forward. For example, "super skyscrapers research association" with 97 Japanese companies put forwarded a super skyscraper plan named Sky City-1000 with the height of 1,000 meters, the total area of 1000 hectares, the service life of 1,000 years. The Taisei corporation in Japan raised a greater super skyscraper idea called X-SEED4000 which is designed as a three-dimensional compound sky city and will be 4,000 meters high and its diameter of foundation will be 6000 meters broad. The Bionic Building in Hong Kong, China was planed to be 1180 meters high.

Table 1:   The height of the world highest building of the time

Year	Name of the edifice	Stories	Height(m)
1870	The original Equitable Building, New York, New York, USA	7	~25
1885	Home Insurance Building, Chicago, Illinois, USA	10	55
1913	Woolworth Building, New York, New York, USA	59	241
1930	Chrysler Building, New York, New York, USA	77	319
1931	Empire State Building, New York, New York, USA	102	381
1973	World Trade Center, New York, New York, USA	110	417
1974	Sears Tower, Chicago, Illinois, USA	109	442
1997	Petronas Towers, Kuala Lumpur, Malaysia	88	450
2004	Taipei International Financial Center (Taipei 101), Taipei, Taiwan, China	101	508

There are two kinds of key difficulties to build super skyscraper: one is how to develop and apply new kinds of structural materials; the other is how to select proper structural plans and systems. So if there are no new structural materials of types with excellent properties, particularly tremendous load bearing capacity, it is difficult to realise above ideas and plans.

2.2   Constructing Super Long Span Bridges

Some super bridges with over 1,000 meters long span have been built, for example, Jiangyin Changjiang Bridge, Jiangyin, Jiangsu Province, China and Tsing Ma Bridge, Hong Kong, China. It is noted that all of them are not arch or cable-stayed but suspension types.

In 1997, an arch bridge was completed at Wanzhou District in Chongqing, China, which is named Wanxian Yangtze River Bridge and is a world record-breaking design for a reinforced concrete arch bridge with a main arch span of 420 m. The arch of this bridge was set below the deck. Its stiffened framework was made from tubular high strength concrete encased in steel tube. The strength grade of the high strength concrete is C60 measured by Chinese standards. The bridge takes its stride over the river, that is, there is no pier in the water. It is out of ordinary that an innovative self-shoring staged construction method was developed

during the construction of the bridge although the bridge span is up to 420 meters long. As the first step of construction, the cable crane spanning the river hoisted and installed the empty steel tube truss frames, each of which was prefabricated with steel tubes. Every steel tube truss frame is made up of five top tubes and five bottom ones. Each tube's diameter is measured by 402 mm and thickness of wall is measured by 16 mm. The completed steel tube frame performed the dual role of arch falsework and arch main reinforcement. All the 36 sections of frames were put together side by side through foot to top of the arch from both river sides symmetrically to form box arch ribs by the conventional cantilever launching technique which is often adopted in the construction of the main girder of the cable-stayed bridge until the two sides of the bridge joined at the bridge top. The second step of construction is to form the rigid framework lattice arch after the C60 concrete was pressed into the tubular steel tubes by pump through foot to top of the arch from both river sides symmetrically and synchronously until the steel tubes were fulfilled. At last, depending on the ready-formed framework, the moulds can be hung on the frames. The C60 high strength concrete was cast into these moulds to wrap the frames in which a 16 meters wide and 7 meters deep three-cell reinforced concrete box section was designed for the arch rib to form reinforced-concrete arch ring [1]. This is an innovative breakthrough of bridge construction technology [2]. In authors' opinion, the span of arch bridge can be lengthened more if this advanced bridge construction technology is combined with KCMs.

There are many great rivers, numerous deep gullies between high mountains, and lots of channels between thousands of islands in the world. It is necessary to construct a great number of bridges if roads, highways and railways are built to stride across these rivers, gullies, and channels. Increasing the span length of the bridges is a good way to decrease even completely avoids the hardship when piers are necessary to build under deep water of these rivers and channels. It is the developing trend of bridge construction technology to construct long span and super long span bridges to stride over the rivers, gullies, and channels without stops. KCMs will play great role in the construction of super bridges with over 1,000 meters long span.

2.3   Building Deep Ocean And Ocean Floor Structures

Ocean occupies about three quarters of the earth surface. It provides potential place for the living and developing of mankind. In order to explore the natural resources storing in the ocean, such as oil, natural gas and other mineral resources, many countries have built a great deal of offshore drilling rigs and mining platforms. These kinds of oceanic buildings are expected to extend to deeper water, for example, through 1,000 meters to 3,000 meters deep. Under this circumstance, KCMs will be the very important materials for developing the deep ocean resources.

Plans have been conceived to construct ocean floor buildings as well as other ocean floor projects in the ocean bottom deeper than 200 meters. These ocean floor buildings will bear tremendous pressure of seawater. In this case, there is ample scope for the abilities of KCMs.

2.4   Raising Super High Rise Structures

Mineral fuels, such as coal, oil, natural gas etc., will be ultimately used up; waterpower also will be eventually exhausted. However, solar energy is a kind of inexhaustible energy in supply and use. The sun radiates its energy outwards and projects one 2.2 billionth to earth, that means the energy the earth receives from the sun every second equals the energy which 6 millions standard coals output after burning. But the clouds and aerosphere reflect most of the energy the sun projects to the earth. The solar energy are not effectively utilized until the collection device and power plant of solar energy are built in the sky even deep sky some day. Only KCMs provide the possibility of this case.

Hot wind generation of electricity is a new type of power production system in which the ground hot wind drives turbine engine to yield electricity. It has several advantages, for example, no fuel is needed, no pollution to environment, perfectly clean energy, installed capacity up to 0.2 million kilowatts. This generation system needs building an about 1,000 meters high tower that is like a chimney and is very suitable to construct in the desert area. The KCM has its very good application prospects in the 1-kilometer high tower construction of the hot wind power station.

The KCM also has its broad application prospects in the constructions of the deep into sky television towers, high-altitude sightseeing buildings, and other installations needing constructions in high-altitude.

2.5   Other Applications

Besides above mentioned applications with good prospects, owing to its tremendous load bearing capacity, the KCM also can be used in the constructions of the super long span underground cave depots, the super long span sports buildings, the explosion-proof doors and some other special buildings.

The KCM also has ample scope for its abilities in the common industrial and civil architectures. It can greatly reduce the section area and self-weight of the structural units and then lighten the whole building, increase the floorage of the building.

3   The Properties Requirements Of The Kilometer-Compressible Material

(1) Very high strength and tremendous load bearing capacity

The completed skyscrapers have lost some useful floor area because the strength of their materials is relatively low and the structural section area is unexpected great. The materials in the kilometer high buildings will bear more tremendous load, while the areas which are occupied by the structures are expected to be limited within an acceptable range. So very high strength is required for the KCM, thus its load bearing capacity can meet the demand.

(2) Great elastic modulus

Only the great elastic modulus can make the KCM deform no more than acceptable when undergoing tremendous loads.

(3) Good ductility

The good enough ductility can prevent the material from brittle failure when suffering dynamic load caused by the cyclone, ocean wave, earthquake etc.

(4) Relatively low self-weight

The relatively low self-weight of the building materials can reduce the self-weight of the buildings.

(5) Durable under different service conditions

The super skyscrapers, super long span bridges, and super deep oceanic structures can be durable only in which the durable materials are used.

(6) Sufficient supply and wide-ranging resources of raw materials

The construction of super buildings is a gigantic project; large quantities of materials are required. So the resources of the raw materials which are used to prepare the KCM are expected to be wide-ranging and sufficient supply is needed. And the relatively simple process and preparation as well as relatively low cost of production are requested.

4   Preparing Methods Of The Kilometer-Compressible Materials

At present, the materials in use can be divided into three main types: organic materials, metal, inorganic and non-metallic materials. Most of the materials which are used as structural materials are metal, inorganic and non-metallic materials; Most of the building structural materials, which are widely used and have great quantities, are many kinds of steels and all types of cements and concretes with different strength grades. For instance, the steels were used as the main structural materials in some skyscrapers with more than 100 stories, such as Sears Tower at Chicago, World Trade Center and Empire State Building at New York, that were mentioned in Table 1, while the concretes were used as the main structural materials in other high-rises, for example, Water Tower Place at Chicago (74 stories), Ryugyong Hotel in Pyongyang, North Korea (105 stories), Central Plaza at Hong Kong (78 stories), Jin Mao Tower (88 stories) at Shanghai, Petronas Towers (88 stories) at Kuala Lumpur.

The steel is characterized by high strength, good ductility. So the super high-rise steel structures buildings have lightweight but are lack of rigidity.

On the other hand, the super high-rise steel reinforced concrete buildings have good rigidity, low cost, but great self-weight. With the strength of the concrete raised, the load bearing capacity of the concrete is increased greatly thus decreases the self-weight of the building.

The successful preparation of the UHSC [3], which compressive strength is 100 to 150 MPa, greatly contributed to the decreasing of the concrete structure's self weight and the increasing of the load bearing capacity. However, as the concrete strength increased, its brittleness rises, its ductility decreases, so the stress-strain curve of the UHSC seems to be linear, and no post-peak segment. The brittleness of UHSC is unexpectedly great, so explosive spalling often takes place when destroyed by compressive load [4]. This is regarded as the natural defect of UHSC. In authors' opinion, it is unreasonable that UHSC is used by means of traditional steel reinforcement.

As to a new type of carbon nano-material, its strength is 100 times more than that of the steel. Its Young's elastic modulus is high up to 1 TPa (10^{12} Pa). And its coefficient of

elongation reaches percentages [5]. Moreover, it is lighter than steel. So theoretically speaking, this kind of new nano-material is a strong candidate of KCM. But at present, this kind of material can only be produced in the lab and in very small amount. It is very expensive, that is, times more than gold. There is no possibility of applying it into practically manufacturing KCM right now.

From the aspect of material strength, the strength of reactive powder concrete can reach 200 MPa up to 800 MPa. However, it is also impossible for this kind of ultra high strength material to be used in kilometer high buildings. It is because the production of this material is based on the special technique by means of heat-press process, and its raw material need to be refined (removing coarse aggregate), so the producing cost rises greatly.

As a result, considering the resource of the present bulk building structural materials, and the accumulated experience in engineering applications, it can be summed up that the preparation of KCM seems to be only based on the steel and concrete right now. However, each of them has its own weakness, and cannot completely meet the six requirements mentioned above, so cannot be used alone. Thereby, two conclusions can be drawn. First, it is necessary to compound these two materials effectively to overcome their individual weakness and give play to their strong points. Second, the increasing strength of both is needed. So the expected technological method to prepare KCM is the effective compound of ultra high strength steel and UHSC.

The concrete which is encased in steel tube will be in three-direction-compressed state because of the full restrain from the steel tube when the concrete encased in steel tube undergoes the compressive load. This kind of compounding is the effective one which overcomes the individual weakness of the steel and concrete and give play to their strong points. Particularly, UHSC encased in ultra high strength steel tube will possibly be the KCM which is applicable in practical use. The properties of this kind of material can fully meet the six requirements of KCM which are put forwarded above. The reasons are:

1) The problem of very high brittleness of the UHSC will be solved with complete satisfaction. The steel tube restrains UHSC encased in it during the compression until close to fail when it undergoes compressive load. In this case, sudden fracture of the concrete does not happen. The whole compound material will great ductilely deform with the plastic deformation of the steel. That is, by means of encasing UHSC, which is very brittle, in steel tube, this effectively compounding material turns from the brittle material of UHSC into a kind of ductile one. This overcomes the defect of great brittleness of the UHSC. Literature [6] and the authors' experimental results confirm this completely.

2) The steel has very high strength and very good ductility, but the steel tube is still easy to fail by means of lose the stability of the steel tube wall because of the wall is very thin when undergoing very high compressive stress. After the steel tube is filled by the concrete, the core concrete gives very strong support to the steel tube wall, so increases its stability. Therefore, by means of this perfect compounding, both steel tude and UHSC mutually make up their deficiencies.

3) The strength of ultra high strength steel tube and UHSC is already very high. After compounding, UHSC encased in the steel tube bears three-direction-compressed stress because its lateral deformation is strained, this causes the strength of the concrete is increased, that is, more than that when the concrete bears uniaxial compression. During bearing the compressive load, the stress state of the steel tube wall turns gradually from the axial compression into circular tension. In this case, the concrete bears most axial compression, while the steel tube bears the tensile stress which is caused by its restrain to the crosswise expansion of the concrete, thus the advantage of high tensile strength of the steel material is brought into full play. So the load bearing capacity of the compounding material is more than the simple total load bearing capacity of the steel tube and the concrete, that is, one plus one is more than two.

Furthermore, when the concrete strength is increased from 30 MPa in common concretes to 150 MPa of UHSCs, its weight per volume increases very slightly from 2,400 kg/m^3 to 2,600 kg/m^3.

Hence a conclusion can be drawn that no matter what is considered, such as strength, stiffness, ductility, self weight, the resource of the material and so on, UHSCST is the very ideal candidate of the KCM.

5   The Preparation Of The Kilometer-Compressible Material Which Comes From Ultra High Strength Concrete Encased In Steel Tube

In order to practically get KCM, in the concrete technology lab at Chongqing University, authors prepared 29 UHSCST short columns with the confinement index of 0.416~1.249 using UHSCs, the cubic compressive strength of which is 156.7 MPa and 164.9 MPa and axial compressive strength is 134.5 MPa and 141.0 MPa respectively at the age of 90 days, compounded by the steel tubes, the yield strength of which is 313~345 MPa and the diameters are 138~140 mm [4]. The coarse aggregate of the concrete is the crashed limestone, the maximum grain size of which is 20 mm. The fine aggregate is intermediate river sand. Portland cement with Chinese Grade 625#, silica fume, and superplasticizer were used. The water to cement and mineral admixture ratio is 0.20 and 0.18. The fluidity of the fresh concrete is very good. The slumps are 258 mm and 228 mm, and the slump flowing diameters are 629 mm and 438 mm, the flow-up time of the upside-down slump tube is 15 second and 24 second respectively. Its workability is good enough to operate by present construction technology.

The experimental results suggest:

(1) The brittleness of these UHSCs is so great that it exploded suddenly and violently when failed under compressive load. However, the UHSCST becomes a kind of compound with very good plasticity if encasing this UHSC in steel tube. The compression test can be continued until the strain of the specimens reached up to 7.87%~20.77%. Although the displacement of the specimens is very large, the specimens did not disintegrate and spall. When the tests stopped, the residual load

bearing capacity is as high as 75.3%~135.2% of the peak strength of the specimens depending on the confinement index.

Furthermore, although in experiment the diameter to thickness ratios of most steel tubes are no less than 20, there doesn't appear yield phenomenon even locally among the thicker steel tubes of the UHSCSTs.

(2) Regarding the load bearing capacity of the UHSCST has the same form of computing equation as $N_c = A_c f_c (1 + K\theta)$ which was established by Shaohuai Cai for high strength concrete encased in steel tubes [7], according to the authors' 29 columns' experimental results, it can be deduced that K=1.21 [4]. Hereafter, K is modified reasonably to 1.20 in this literature. So the load bearing capacity of the UHSCST can be calculated by the following equation:

$$N_c = A_c f_c (1 + 1.2\theta) \qquad (1)$$

In the equation, N_c means the load bearing capacity of the UHSCST short columns (N); A_c refers to the section area of the core concrete (mm^2); f_c is the axial compressive strength of the UHSC (MPa); θ refers to the confinement index, which is defined as $\theta = \dfrac{A_a f_a}{A_c f_c}$, in which A_a represents section area of the steel tube (mm^2), f_a refers to the yield strength of the steel (MPa).

With the increase of the strength grade of concrete, the crosswise deformation of the concrete decreases, which means the confinement effect of steel tube to the concrete decreases, that is, K in the equation decreases. According to CECS104: 99 (Technological regulations for high strength concrete structures) in China, for the high strength concrete encased in steel tube, K equals 2.00 when the core concrete belongs to C50 grade, K equals 1.70 when the core concrete belongs to C80 grade, that is, K decreases 0.05 when the strength grade increases C5. The strength of authors' concrete is as high as 156.7~164.9 MPa, so it is reasonable that K is determined as 1.20. This K value, at the same time, suggests that the confinement effect of the steel tube to the core concrete is still obvious.

Compared with the decrease of K, f_c increases more. So the load bearing capacity for UHSCST calculated by equation 1 is tremendous. Giving the outside diameter D of the steel tube fulfilled with UHSC, for example, D equals 2,500 mm which is acceptable since the real biggest outside diameter D of the steel tube fulfilled with concrete, that is, the concrete encased in steel tube columns in the Union Square at Seattle, has been 3,000 mm, f_a equals 345 MPa, f_c equals 140 MPa, θ equals 0.72, A_c equals 3801336 mm^2, calculating by equation 1, the load bearing capacity of this UHSCST is determined as N_c, and N_c equals 9.92×10^{5}kN, that is, 99.2 kiloton (see also item 3 in Table 2). At present, the world highest building among those buildings which were built by concrete encased in steel tube is the SEG Plaza at Shenzhen, China, which was completed in 1997. SEG Plaza has 76 stories (72 stories above ground), and 291.6 meters high, in which the largest axial force which a single column bears is 9 kiloton [8]. Compared with this real project, it can be seen that the above designed UHSCST which has tremendous load bearing capacity as big as 99.2 kiloton can possibly be used as columns to build kilometer(s) high super skyscrapers which has more than 300

stories and more than 1,000 meters high. Therefore, the above designed UHSCST can be named KCM. It is noted that this kind of KCM has the best advantage regarding its easy getting of raw materials.

6   Further Optimisation

As for the KCM prepared above, its most weak point is that compared with the strength of the concrete, the strength of the steel tube is too low, the f_a to f_c ratio equals 2.2~2.6. In the completed buildings which were built by concrete encased in steel tube in China, the f_a to f_c ratio equals 5.9~11.8. So ultra high strength steel tube seems to be required. In order to get enough confinement index, the steel tube wall need to be thickened. But the steel tube is difficult to be produced, processed and welded after being thickened. So further development of the KCM requires the compound of the UHSC with the ultra high strength steel tube which matches the strength of the concrete. At present, low alloy super steel has already been developed successfully and produced in enormous quantities in China, which yield strength is as high as 800 MPa. This kind of steel not only has very high strength, but also has very good coefficient of elongation and easy to be welded. It provides material basis for the KCM from UHSCST using UHSC and ultra high strength steel tube.

Furthermore, the yield strength of alloy structural steel is up to 1,000 MPa (20SiMnVB). And according to the literature [9], if the carbon content and alloy elements are adjusted, and the producing technology is improved, the yield strength of ultra high strength steel is able to be up to 1,380 MPa or more. It is easier to prepare KCM by means of compounding UHSC with ultra high strength steel with the strength f_a of 800, 1,000, 1380 MPa. The load bearing capacity of this KCM will be more tremendous.

Now giving f_a equals 345, 800, 1,000, 1380 MPa; f_c equals 140 MPa; D equals 1,500, 2,000, 2,500, 3,000 mm (In authors' opinion, in kilometer high building, the diameter of the column as large as 3,000 mm is not beyond acceptance, in the Shimizu Tower in Japan which is planned to build as high as 121 stories and 550 meters, the cross section area of the columns is 4,000 times 2,400 mm [10]) and θ equals 0.72~1.51, according to equation 1, the load bearing capacity of UHSCs encased in steel tubes in forty plans is calculated as shown in Table 2.

It can be seen from the data in Table 2 that with the increase of fa, D, and θ, the reckoned load bearing capacity is increased up to 3.57~23.72×105 kN, that is, 35.7~237.2 kiloton. The 41st item in Table 2 is about the concrete encased in steel tube column in SEG Plaza, its reckoned load bearing capacity is up to 1.68×105 kN, that is, 16.8 kiloton, here K is determined as 1.9. Kilometer high building is 3.44 times higher than SEG Plaza, so it can be roughly estimated that the column which load bearing capacity reaches up to 3.44 times 1.68×105 kN equals 5.78×105 kN can possibly be used as column in the construction of the kilometer high super skyscraper. Among the forty plans in Table 2, there are thirty-one plans which can reach the load bearing capacity, and more than half among the thirty-one plans are 2 to 4.1 times more than this load bearing capacity. So there is no worry to adopt these plans to build kilometer high skyscrapers. Certainly, the load of the building does not simply rise in proportion to the height of the building because besides vertical loads, the toppling

force moment caused by the lateral wind load will be increased sharply while the increasing height of the building. But this problem can be solved by the aid of the building structure design, that is, the cross section area of the building can be increased gradually from the top to the bottom to increase the force moment resistance, or large-scale supporting tube structure system can be used.

It also can be seen from the data in Table 2 that when confinement index is given, with the increasing strength of the steel tube, the wall thickness of the steel tube decreases. So it is more reasonable to use ultra high strength steel tube to produce KCM than use normal strength one. Regarding the convenient processing of the steel tube, the maximum thickness of the steel tube wall should not be more than 50 mm which was put forward by the literature [11]. Most steel tube thickness of the plans presented in Table 2 cannot meet the requirement except four plans.

Table 2:   The reckoned load capacity of the kilometer compressible material-concrete filled steel tube

Yield strength of the steel f_a/MPa	Axial compress strength of the concrete f_c/MPa	Outside diameter of the steel tube D/mm	Confinement index θ	Wall thickness of the steel tube t/mm	Diameter/thickness ratio D/t	No.	Section area of the steel tube A_a/mm^2	Section area of the concrete A_c/mm^2	Percentage of steel content ρ/%	Reckoned load bearing capacity N_c/10^{5}kN
345	140	1500	0.72	90	16.7	1	398669	1368481	22.56	3.57
345	140	2000	0.72	120	16.7	2	708745	2432855	22.56	6.35
345	140	2500	0.72	150	16.7	3	1107414	3801336	22.56	9.92
345	140	3000	0.72	180	16.7	4	1594676	5473924	22.56	14.19
800	140	1500	0.75	45	33.3	5	205696	1561454	11.64	4.15
800	140	1500	1.00	58	25.9	6	262751	1504399	14.89	4.60
800	140	1500	1.45	80	18.8	7	356886	1410264	20.20	5.14
800	140	2000	0.75	60	33.3	8	365682	2775918	11.64	7.40
800	140	2000	0.98	76	26.3	9	459377	2682222	14.62	8.17
800	140	2000	1.47	108	18.5	10	641942	2499658	20.43	9.66
800	140	2500	0.75	76	32.9	11	578364	4329992	11.78	11.59
800	140	2500	0.99	96	26.0	12	725031	4183719	14.77	12.82
800	140	2500	1.46	134	18.7	13	996025	3912725	20.29	15.07
800	140	3000	0.75	87	34.5	14	822785	6245815	11.64	16.61
800	140	3000	0.99	115	26.1	15	1042304	6026296	14.75	18.46
800	140	3000	1.45	160	18.8	16	1427543	5641057	20.20	21.64
1000	140	1500	0.78	38	50.0	17	174535	1592625	9.88	4.32
1000	140	1500	1.01	48	31.3	18	218957	1548193	12.39	4.79
1000	140	1500	1.47	67	22.4	19	301628	1465522	17.07	5.67
1000	140	2000	0.77	50	40.0	20	303306	2835294	9.75	7.64

(Table 2 continued)

Yield strength of the steel f_a/MPa	Axial compress strength of the concrete f_c/MPa	Outside diameter of the steel tube D/mm	Confinement index θ	Wall thickness of the steel tube t/mm	Diameter/thickness ratio D/t	No.	Section area of the steel tube A_a/mm²	Section area of the concrete A_c/mm²	Percentage of steel content ρ/%	Reckoned load bearing capacity N_c/10⁵kN
1000	140	2000	1.01	64	31.3	21	389257	2752343	12.39	8.52
1000	140	2000	1.48	90	22.2	22	540041	2601559	17.19	10.11
1000	140	2500	0.76	62	40.3	23	474872	4433878	9.67	11.89
1000	140	2500	1.01	80	31.3	24	608214	4300536	12.39	13.32
1000	140	2500	1.51	114	21.9	25	854528	4054222	17.41	15.96
1000	140	3000	0.75	73	41.1	26	671269	6397331	9.50	17.02
1000	140	3000	1.00	95	31.6	27	867003	6201597	12.27	19.10
1000	140	3000	1.47	134	22.4	28	1206512	5862088	17.07	22.68
1380	140	1500	0.75	27	55.6	29	124945	1642205	7.07	4.37
1380	140	1500	0.99	35	42.9	30	161086	1606064	9.12	4.92
1380	140	1500	1.49	51	29.4	31	232161	1534989	13.14	5.99
1380	140	2000	0.75	36	55.6	32	222124	2919476	7.07	7.77
1380	140	2000	0.97	46	43.5	33	282380	2859220	8.99	8.68
1380	140	2000	1.44	66	30.3	34	401006	2740594	12.76	10.48
1380	140	2500	0.75	45	55.6	35	347068	4561682	7.07	12.13
1380	140	2500	1.00	59	42.4	36	452450	4456300	9.22	13.73
1380	140	2500	1.49	85	29.4	37	644892	4263858	13.14	16.64
1380	140	3000	0.76	55	54.5	38	508861	6559739	7.20	17.56
1380	140	3000	1.00	71	42.3	39	653324	6415276	9.24	19.76
1380	140	3000	1.46	100	30.0	40	911064	6157536	12.89	23.72
345	140	1600	0.60	28	57.0	41	138281	1872343	6.90	1.68

So the authors suggest multi-confinements structure, that is, core concrete→steel tube→concrete→steel tube→concrete→steel tube, or mother-and-son structure, that is, certain numbers of smaller steel tubes are installed in the biggest steel tube, then all the rest free space is fulfilled by concrete, to solve this problem. Under the guarantee of no change to confinement index and total load bearing capacity, the wall thickness of all the compositive steel tubes can be thinned until the process with present technology can easily go ahead.

7   Conclusions

It can be summarized from above that it is the basic technique to get KCM by means of compounding UHSC with steel tube, especially ultra high strength steel tube. The naissance of the KCM can be regarded as the new starting point of the building structure materials, even the whole technology of construction. This new kind of structural material which is characterized by its tremendous load bearing and very good ductility can provide powerful support to architectural masters and structural masters when designing the more than one kilometer high super skyscrapers, super high-rise structures and many other special buildings. Without its aids in the designing of the Sky City-1000 in Japan, the gigantic columns as big as about 75 m times 25 m and very large-scale tubes have to be taken into account.

The structural plan and system are also very important in the construction of the kilometer high buildings. If the structural system is appropriately designed, it is possible to build super buildings with the height of 4,000 kilometers even more using this KCM with tremendous load bearing by means of UHSC encased in ultra high strength steel tube.

It also can be looked into the future that KCM will greatly promote the development of our human society.

8   References

[1]   Liu, Z., Li, F., Roddis, W., M., K., Analytic model of long-span self-shored arch bridge, In: Journal of Bridge Engineering 7, No. 1, S. 14-21, 2002.

[2]   Cai, S., The application of high strength concrete encased in steel tubes in the civil engineering in China, In: The Guidelines of Design and Construction of High Strength Concrete Structures (the second edition, in Chinese), China Architecture and Building Press, Beijing, 2001.

[3]   Pu, X., Yan, W., Wang, C., Wan, C., Bai, G., He, G.: The preparation technology of the ultra high strength high performance concretes with strength range from 100 MPa to 150 MPa. In: China Concrete and Cement Products (in Chinese) , No. 6, S. 3-7 , 1998.

[4]   Pu, X., et al, Study on the deformation properties and load bearing capacity of kilometer compressible material made from ultra high strength concrete encased in the steel tubes, In: Proceedings of the national high strength and high performance concrete workshop, Fuzhou, China, 2002.

[5]   Zhang, L., Mou, J., Nanomaterial and Nanotechnology, Science Press (China), 2001.

[6]   Tan, K., Pu, X., Cai, S., Study on the mechanical properties of steel extra-high strength concrete encased in steel tubes. In: Journal of Building Structures (in Chinese) 20, No. 1, S. 10-15 , 1999.

[7]   Cai, S., The computing for the structures of concrete encased in steel tubes and its application. China Architecture and Building Press,.Beijing, 1989.

[8]   Cai, S., The late progress of structure technology of concrete encased in steel tubes. In: Tumu Gongcheng Xuebao (in Chinese) 22, No. 2, S. 16-26 , 1999.

[9]   Zhou, H., Yan, H., New Materials Dictionary, Shanghai Scientific and Technological Literature Publishing House, Shanghai, 1996.

[10] Han, L., Structures of Concrete Encased in Steel tubes, Science Press (China), 2000.

[11] Zhong, S., High-rise Structures made from concrete encased in steel tubes, Heilongjiang Science and Technology Press, Harbin, 1999.

Peter Racky
University Professor, Head of the Department of Construction
Management
University of Kassel
Kassel, Germany

Cost-effectiveness and sustainability of UHPC

Summary

Ultra High Performance Concrete – UHPC is examined in the following with regard to its cost-effectiveness and sustainability. It is the intention of this paper to provide a qualitative and quantitative statement on the behavior of UHPC regarding those two criteria. The behavior of normal-strength and high-strength concrete serves as comparison size. The energy and raw material consumption of UHPC is examined with a design example for a compound unit (column under pressure). A relevant economic advantage of the UHPC is obvious regarding the life-cycle which exceeds the construction process of a building. Because of the smaller cross-section of columns being necessary now with the same loadbearing capacity, the useable floor space can be increased.

Keywords: *cost-effectiveness, sustainability, energy and raw material consumption, life-cycle costs.*

1   Introduction

In the design, planning and construction of buildings the principle of cost-effectiveness has long been one of the principal demands made of civil engineers. Since the 1990s this demand has been extended further and further to include the increasingly widespread social requirement of sustainability. While the cost-effectiveness factor is concerned purely with economic optimization, the principal concern of sustainability also embraces ecological and social factors. Cost-effectiveness and sustainability are by no means mutually exclusive. On the contrary, cost-effectiveness is an integral component of the concept of sustainability.

Among the ecological objectives that aim at more sustainability are the minimal use of non-renewable resources, the guarantee of renewable resource regeneration and the minimization of environmental impact from waste disposal and residues [1]. In view of the fact that construction produces approx. 70% of all material-flow in Germany, it is understandable that sustainability must be one of its particular concerns in order to achieve a higher success rate in sustainability objectives [2]. Accordingly, the decision as to which materials are to be used for the construction project is particularly important.

The increasing demand for sustainability in construction invariably extends the time frame which has to be analysed. In addition to the classical life-cycle of the structure, a comprehensive sustainability analysis has to take account of the production process of building materials as the waste disposal after demolition.

With this in mind, Ultra High Performance Concrete (UHPC) will be investigated with respect to its cost-effectiveness and sustainability. The aim of this paper is to make a qualitative and quantitative statement about the behaviour of UHPC with regard to both of these criteria. A comparison will be made between the behaviour of UHPC and normal and high-strength concrete.

2   Energy and raw material consumption in the operational use of UHPC

The energy and raw material consumption associated with the operational use of UHPC will be investigated by means of a design example for a compound unit, subjected to high pressure. Tab. 1 shows the energy and raw material consumption required to gather and/or produce the principal materials of reinforced concrete [3].

	Energy consumption [MJ/to]	Raw materials consumption [to/to building materials]
Cement PC	4,693	1.5
Gravel, Sand	137	1.0[*]
Reinforcement steel	10,875	6.4

[*] Estimated

Tab.1:   Energy and raw material consumption required to gather and/or produce the building materials. Source: [3]

On this basis the energy and raw material consumption together with building material requirement per m³ of concrete are investigated for concretes of strength classes C 40/50 and C 80/95 as well as for UHPC with a cylinder compressive strength > 180 N / mm² (hereinafter called simply C 180). It is clear from tab. 2 that energy consumption, in particular, increases considerably the higher the compressive strength of the concrete. Among the reasons for this are the higher cement content and the necessary addition of steel fibres at a volume of 2.5 Vol.-% in C 180 [4]. But no conclusions about the degree to which the sustainability requirement is satisfied can be drawn from this. This only becomes possible from the design example carried out.

Concrete strength class		C 40/50	C 80/95	C 180
Cement content	kg/m^3	370	490	760
Aggregates	kg/m^3	1,866	1,642	1,521
Steel fibres	kg/m^3	-	-	194
Energy consumption	MJ/m^3	1,992	2,525	5,885
Raw material consumption	kg/m^3	2,421	2,377	3,903
Building material requirements	kg/m^3	2,236	2,132	2,475

Tab.2:   Composition, energy and raw material consumption as well as building material requirement per m³ of the concrete types considered. Sources: [3], [4]

A 3.50 m high reinforced concrete column with square cross-section is designed for design load N_{Ed} = 40 MN. The reinforcement content μ amounts to 4 %. For concrete strength class C 40/50 these specifications produce a lateral length of 1.00 m and thus a column cross-section of 1.00 m² (fig. 1). If the design load and the reinforcement degree are retained, a required lateral length of 0.82m (column cross-section = 0.67 m²) for concrete strength class C 80/95 is obtained. If C 180 is used, the required lateral length is reduced to 0.66 m (column cross-section = 0.44 m²).
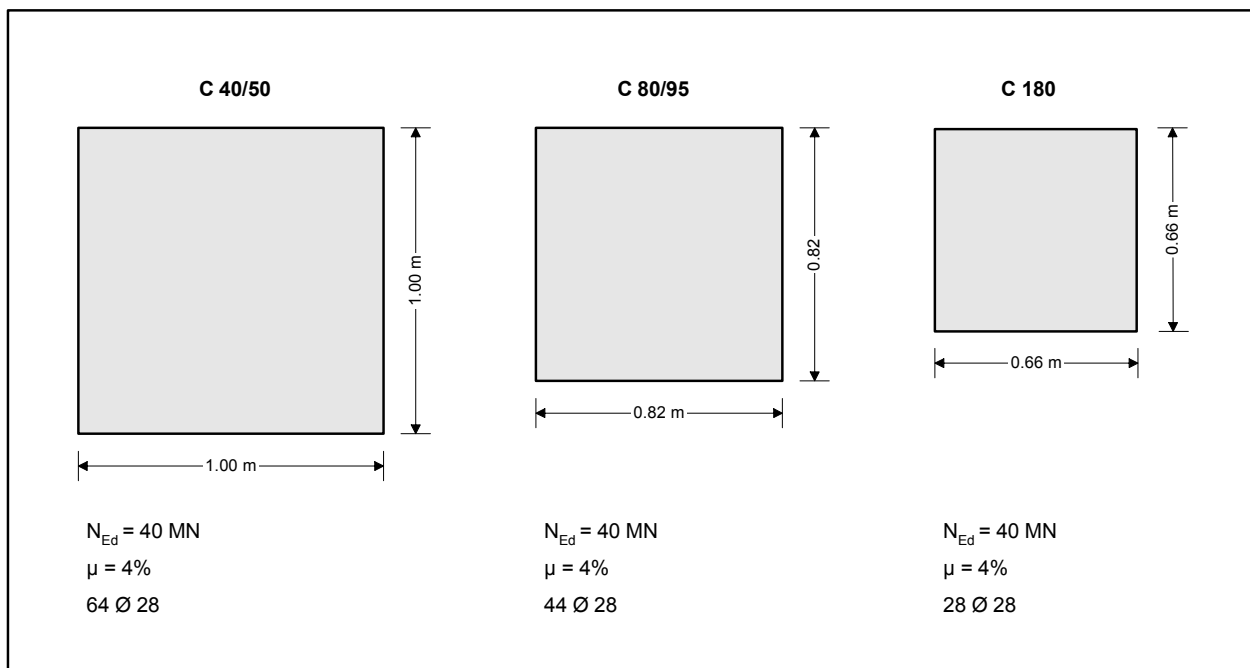
Fig. 1:   Column cross-section and compression reinforcement of a reinforced concrete column according to concrete strength class

The energy and raw material consumption for reinforced concrete columns according to concrete strength class at equal load bearing is shown in tab. 3. It is clearly recognizable that

UHPC best satisfies sustainability requirements. Energy consumption for the column falls with the use of C 180, compared with C 40/50, by approx. 26 %, raw material consumption by as much as 42 %. UHPC thus demonstrates the best results vis-à-vis the ecological objective "minimization of use of non-renewable resources". Furthermore, environmental impact through building waste in the event of demolition at the end of the building's life-cycle is minimized as a result of the leaner compound units dimensions that are possible.

Concrete strength class		C 40/50	C 80/95	C 180
Cross-section concrete column	m^2	1.0	0.67	0.44
Volume concrete	m^3	3,360	2,258	1,464
Cross-section reinforcement steel	cm^2	400	270	174
Volume steel	m^3	0.140	0.095	0.061
Weight steel	to	1.08	0.74	0.47
Energy consumption				
Concrete	MJ	6,693	5,701	8,616
Reinforcement steel	MJ	11,745	8,048	5,111
Total	MJ	18,438	13,749	13,727
Raw materials consumption				
Concrete	to	8.13	5.37	5.71
Reinforcement steel	to	6.91	4.74	3.01
Total	to	15.04	10.11	8.72

Tab. 3: Energy and raw material consumption for a reinforced concrete column according to concrete strength class (N_{Ed} = 40 MN, l = 3,50 m)

It should be noted in this example that energy and raw material consumption in UHPC might be reduced significantly still further below the values of C 80/95, if it were possible to reduce the necessary content of steel fibres in the concrete mixture.
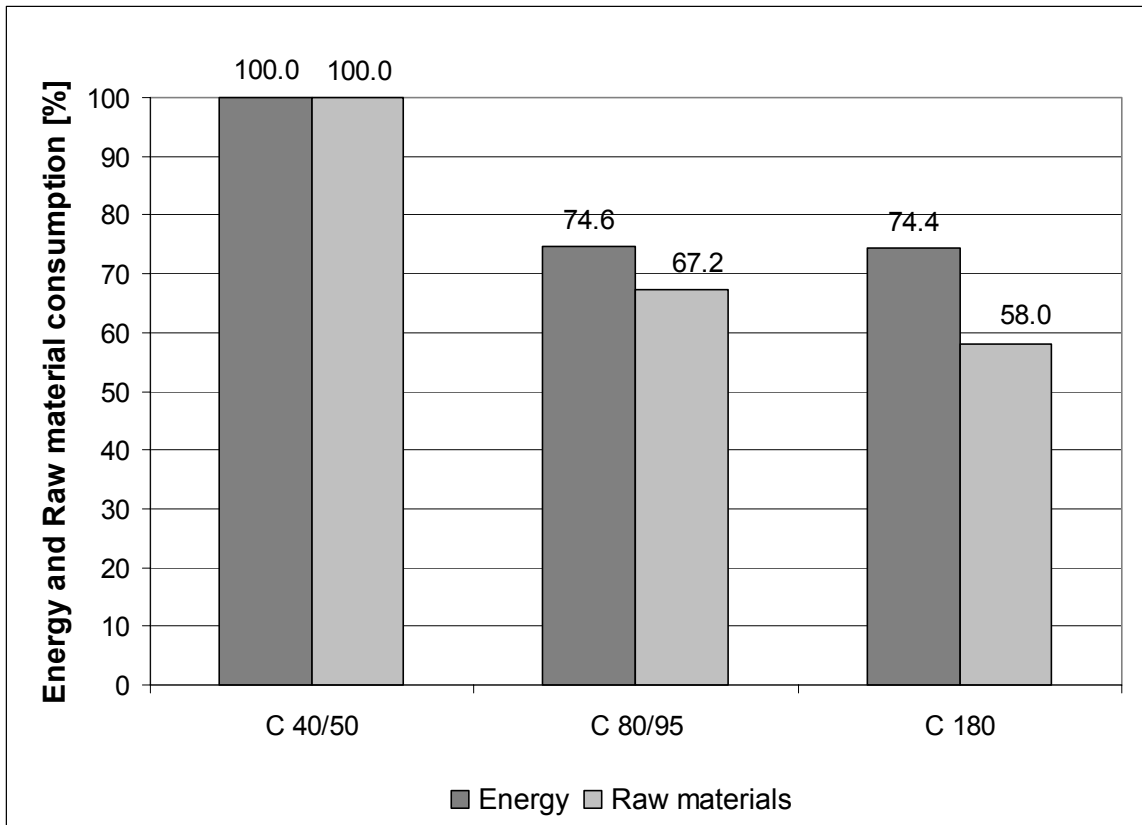
Fig. 2 :   Relative comparison of energy and raw material consumption for a reinforced concrete column according to concrete strength class
(N$_{Ed}$ = 40 MN, l = 3,50 m)

3   Cost-effectiveness benefits through increased floor space

After consideration of the ecological concerns the economic benefits of the use of UHPC will be presented. This, too, will be done by means of the columns considered above. If one compares the net production costs, the higher costs per m³ of concrete with increasing compressive strength, including expenditure on additional quality assurance measures, expert reports and special licences necessitated by the use of non-standard concrete, are offset by lower costs in respect of the following considerations:

1   Lower quantities of concrete to be built in.

2   Lower quantities of reinforcement.

3   Lower quantities of formwork.

These result in a reduction of materials, wages, transport costs, and the necessary lifting and moving capacities (cranes, concrete pumps) on the building site. This is true not only of the columns considered. Because of the reduced compound unit measurements the load assumptions for the design of the foundation are reduced. Thus, here too there are possibilities for cost reductions similar to those for the columns mentioned above. In view of a possible reduction in foundation measurements, there may also be lower excavation costs as a result of reduced excavated material. Quantitative comparison of production costs in

individual cases must take into account current market prices.

UHPC proves to be economically beneficial in terms of both production costs and the utilization phase. The smaller columns cross-section necessary with the same load-bearing capacity increases the rentable floor space. In the design example carried out the increase of usable floor space with C 180 compared with C 40/50 per column and storey amounts to 0.56 m². Supposing that the target for the building in question is a monthly net yield rent of 25 €/m² over a period of 50 years, which is accumulated over the complete period and annually capitalized with 4 %, the result after 50 years is a final value of approx. 25,850 € per column and storey. If one reduces the life-cycle in a maximum risk scenario to 20 years and the monthly net yield to 15 €/m², this gives a final value of approx. 3,025 € per column and storey. If one discounts the final values in both cases to a one-off payment at the beginning of the life-cycle, there is a present value of approx. 3,637 € per column and storey and 1,381 € per column and storey respectively. This means that the column made of C 40/50 would have to cost less by this amount in order to compensate for the multiple yields because of the increase in usable floor space. And this in consideration of the above-mentioned reasons for additional costs.
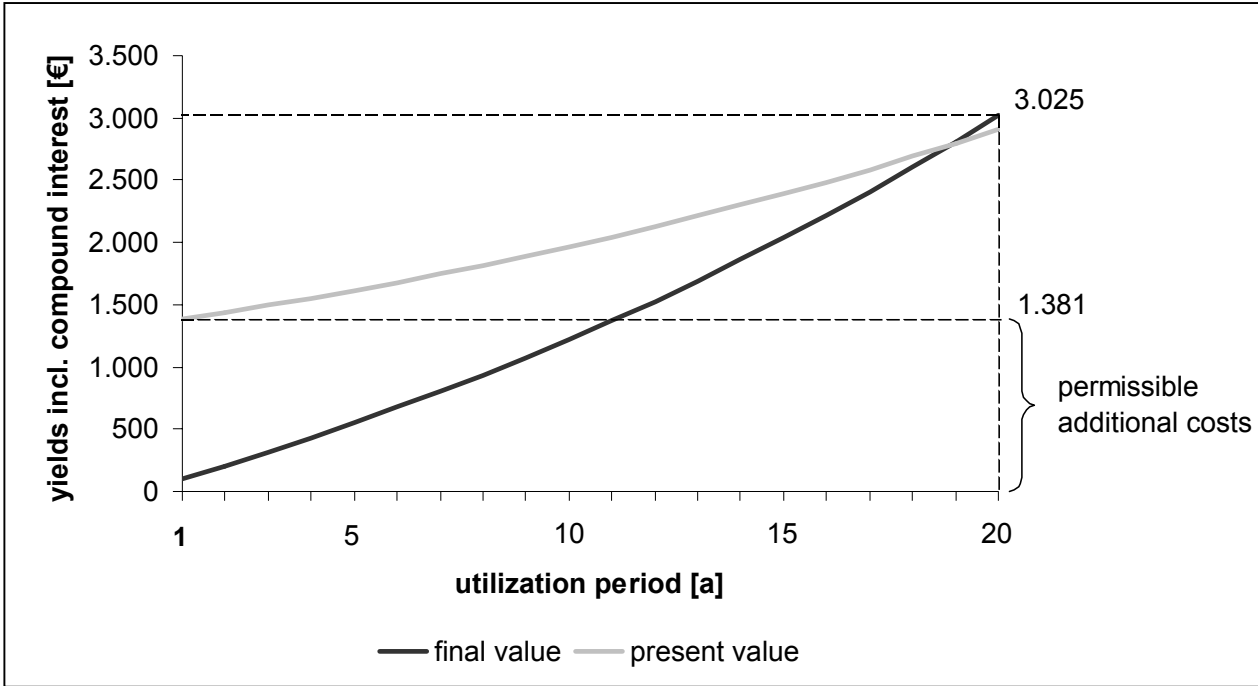
Fig. 3:   Maximum permissible additional costs of a UHPC column offset by the advantages of increased floor space.

Estimating the current market price for a column of C 40/50 at approx. 2,000 € reveals that, in the worst possible scenario, the column made of C 180 would have to be a maximum of 1.7 times more expensive in order not to be offset by the advantages of the increased floor space. On the basis of this result, the economic advantage of UHPC as compared with normal strength concrete is clearly shown, in the opinion of the author, by the example provided.

4 Economic aspects with respect to the life-cycle costs of a structure

In addition to the production costs, the costs incurred during the life-cycle of a structure also have to be assessed in terms of cost-effectiveness. These include the repair and maintenance costs to keep the structure functional as well as the costs incurred by demolition at the end of the life-cycle of the structure. Together with the production costs they make up the sum total of the life-cycle costs. Fig. 4 shows the qualitative course of the life-cycle costs of a bridge. Investigations carried out in Austria reveal that the average replacement costs for the raw bearing structure of a bridge that had reached the end of its life-cycle with a effective span of up to 40 m were approx. 640 €/m² of bridge area [5]. The costs for repair of the bearing structure thus amount to 28 % of this value.
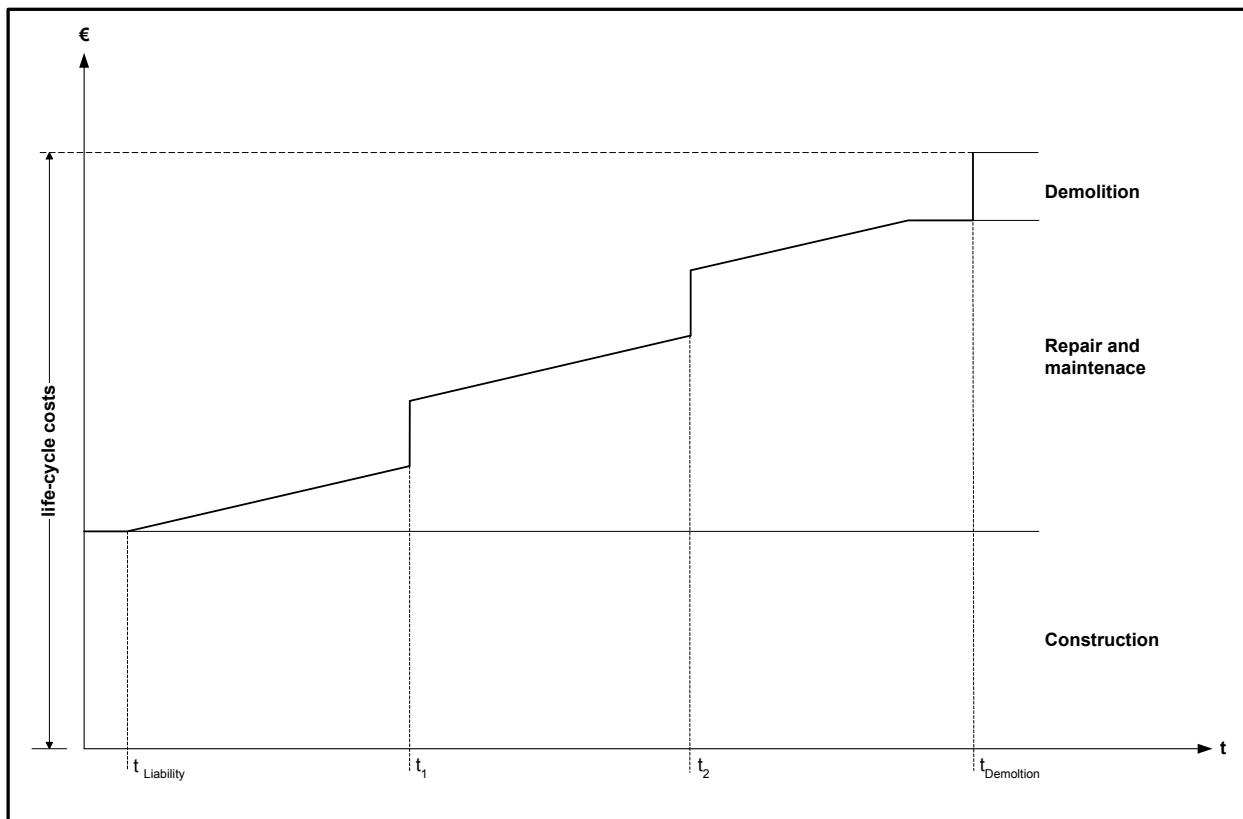
Fig. 4: Qualitative progress of life-cycle costs of a bridge. Source [5]

In order to be able to evaluate alternative construction designs with respect to their life-cycle costs for a cost-effectiveness comparison, use has to be made of the present value method [6]. By means of this method all costs to be incurred in the future are discounted to the current time of consideration. The present value thus specifies the amount which has to be invested at the time of consideration, and then has to produce interest in order to be able to settle all future costs.

The above-mentioned cost analysis helps to show how large the present value is in terms of new building costs, in order to clarify its importance for a cost-effectiveness evaluation of a construction design. For this the following assumptions will be made:

- production costs of the bearing structure = 650 €/m² bridge area,
- repair costs for the bearing structure per repair measure = 30 % of the production costs,
- the total of the maintenance costs for the bearing structure between two repair measures = 30 % of the production costs,
- demolition costs of the bearing structure = 30 % of the production costs,
- liability period of the building contractor = 4 years,
- period between repair measures = 25 years.

If one takes the calculation interest rate as 4 %, the result for the costs of building maintenance and demolition is a present value of approx. 251 €. This corresponds to just under 39 % of new building costs. If the costs proposed for maintenance, repair and demolition are reduced from 30 % to 20 %, the present value amounts to approx. 167 €, which is still just under 26 % of the new building costs assumed. The size of the present values shows that the life-cycle costs in a cost-effectiveness comparison between alternative construction designs must be taken into account in order to generate a comprehensive decision-making basis.

On the long-term behaviour of UHPC in practice and the resulting maintenance and repair costs, the shortage of actual buildings using it means that the existing data is insufficiently comprehensive. Thus, no comparative present value calculation for bearing structures of normal-strength concrete and UHPC can be made at present. Available research results, however, show that UHPC displays greater frost / de-icing salt resistance, lower rate of carbonization progress and greater chloride resistance compared with normal- and high-strength concrete [7]. It can therefore be concluded that structures from UHPC will also show comparatively lower maintenance and repair costs in future. Accordingly, research is urgently needed to gather the appropriate data and experience values. In this context close co-operation between universities, construction contractors, architects, structural engineers, investors and owners is desirable.

5   Conclusions and prospects

Increasing social demand for sustainability in construction requires an appropriate engineering evaluation of UHPC. By means of a design example the lower energy and raw materials consumption of UHPC required for a column is compared with that of normal and high-strength concrete. This shows the relatively high degree of success in achieving the ecological goal of sustainability. The economic benefits are shown by citing the example of the increase in floor space that can be achieved in a building, as a result of smaller compound units. There is also the factor of the optimized durability of UHPC, which generates altogether lower life-cycle costs than the existing standard concretes. In short, UHPC can be characterized as the more sustainable building material.

The above-mentioned considerations make clear and also explain that the two criteria of cost-effectiveness and sustainability are increasingly important to the engineering evaluation of a structure because they give rise to further developments with respect to the shaping of the contractual arrangements between contractor and client. If, as shown, not only the net construction costs, but also the total life-cycle costs and yields are taken into consideration, then it becomes clear why, in practice, the utilization period is increasingly included in the period of validity of construction contracts. The building contractors, in these cases, are also liable for functional maintenance and optimizing the maintenance costs of the building during the utilization. Evidence of this development can be found in new contract models drawn up by public bodies in infrastructure projects, e.g. "function construction contracts" in federal highways construction [8]. This underlines the fact that the construction industry will, in future, be increasingly faced with more extensive and more complex social demands. The emphasis is less on the mere provision of production capacity and much more on sustainable solutions to the construction problems at hand. The possible practical use of UHPC, also seen in a wider context, can make a very valuable contribution to construction technology.

6   References

[1] Bundesamt für Bauwesen und Raumordnung (Hrsg.): Leitfaden Nachhaltiges Bauen. 2001

[2] Graubner, C.-A.; Hüske, K.: Nachhaltigkeit im Bauwesen. Verlag Ernst & Sohn 2003

[3] Böing, R.; Schmidt, M.: Rohstoff- und energiesparendes Konstruieren mit Beton. In: Beton Heft 7/1997

[4] Bornemann, R.; Schmidt, M.; Fehling, E.; Middendorf, B.: Ultra-Hochleistungsbeton UHPC. In: Beton- und Stahlbetonbau, Heft 7/2001

[5] Wicke, M.; Kirsch, P.; Straninger, W.; Scharitzer, B.: Kostenmodell für den Funktionserhalt von Straßenbrücken. In: Bauingenieur Heft 2/2001

[6] Schelle, H.: Wirtschaftlichkeitsrechnungen für die Angebotswertung im Bauwesen. Werner-Verlag 1992

[7] Schmidt, M.; Fehling, E.; Teichmann, T.; Bunje, K.; Bornemann, R.: Ultra-Hochfester Beton: Perspektive für die Betonfertigteilindustrie. In: Betonwerk + Fertigteil-Technik Heft 3/2003

[8] Knoll, E.: Konzeption und Inhalt von Funktionsbauverträgen. In: Straße + Autobahn Heft 1/1999

Tue, Nguyen Viet
Prof. Dr.-Ing. habil.
Universität Leipzig
Leipzig, Germany

Schenck, Gunter
Dipl.-Ing.
Universität Leipzig
Leipzig, Germany

Küchler, Michael
Dipl.-Ing.
Universität Leipzig
Leipzig, Germany

Jürgen Reinhardt
Dr.-Ing.
Bilfinger Berger AG
Leipzig, Germany

Application of UHPC filled Tubes in Buildings and Bridges

Summary

UHPC filled tubes are structural members with high bearing capacities and sufficient ductility. Their general application to buildings and bridges, however, requires solutions for the joint between the UHPC filled tube and the connected members, e.g. connection between the slab made of normal strength concrete and the UHPC filled tubes as columns.

In this paper some proposals for the joints in tall buildings and truss bridges are presented. Experiments with theses proposals show encouraging results.

Keywords: *UHPC, tubes, joints, perforated steel plate*

1 Introduction

Ultra high performance concrete (UHPC) with a compression strength up to 300 MPa represents the latest concrete-technological development on strength. Using UHPC both the range of application of the century building material concrete is extended and architecturally superior buildings can be erected. The durability of the buildings can be increased also by improved material properties.

In this paper it is reported of some application possibilities by steel tubes filled with UHPC. Results of experimental investigations are presented to solve the problems in the joint region in such constructions.

2 UHPC Filled Steel Tubes

The behaviour of concrete with different compression strengths under compression is presented in fig. 1. It has to be realized that with increasing compression strength the brittleness of the concrete increases. For stresses below approx. 70 % of the compression strength, UHPC yields hardly plastic deformations. Beyond that the lateral strain of UHPC is likewise small because of missing micro cracks.

However, if the UHPC is confined sufficiently, members with high load bearing capacity and sufficient ductility can be build, despite the brittleness of the material. It is well known that circular cross sections yield the best confinement effect.

Basing on this consideration, the bearing behaviour of steel tubes filled with UHPC is examined currently at the Institute for Structural Concrete and Building Materials at the University of Leipzig.

The compression strength of the concretes lies between 150 and 180 MPa.
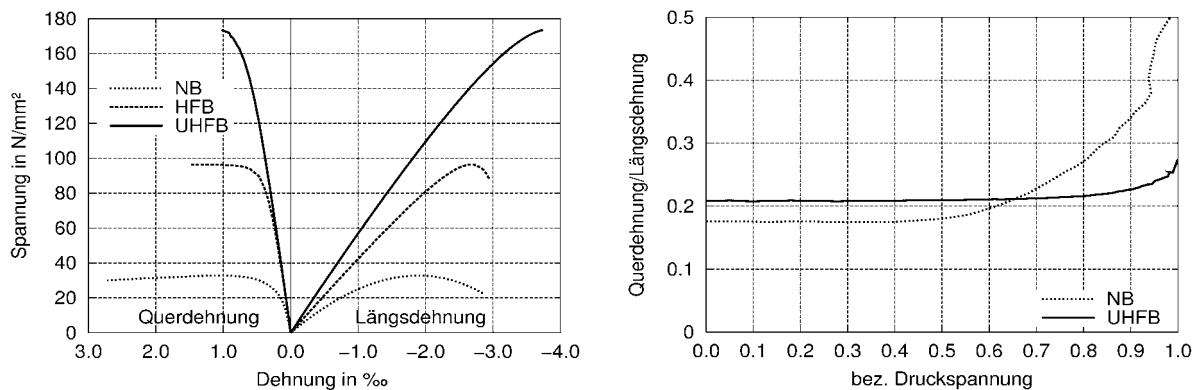
Figure 1:   Behaviour of concrete under compression

A hybrid member can be used as an element for buildings and bridges. Fig. 2 shows the behaviour of such an element under predominant compression load. The load is applied on the concrete cross section only.
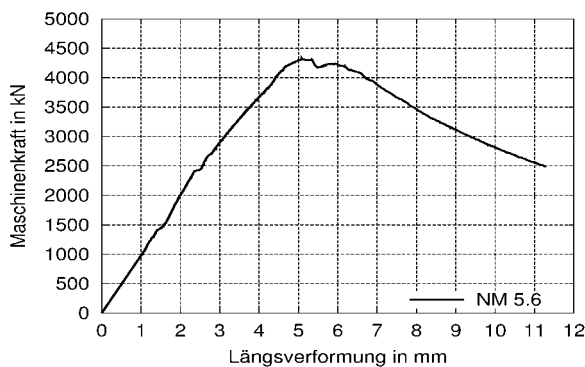
Figure 2:   Behaviour of a UHPC filled tube under predominant compression stress
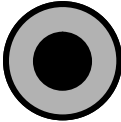
Basing on the tests, conclusions for detailing can be derived or members made of UHPC. It is observable that very high ultimate loads can be attained. Due to the sufficient confinement by the steel tube, an abrupt load drop can be impeded. The structural member fails very ductile.

Despite a high shrinkage of the concrete and the loading on the concrete cross section, the bond behaviour between steel tube and the concrete is able to carry the bending moment. The longitudinal force is mainly borne by the concrete cross section.

3 Applications in Buildings and Bridges

Because of its high compression strength, it is favourable to apply UHPC tohighliy loaded bearing members columns in multi-storeyed buildings. Table 1 shows a comparison of e.g. with different types of columns.

Table 1: Comparison of a conventional composite column with steel core and a column with UHPC filling

			Column 1	Column 2
Concrete strength	f_{ck}	**MPa**	60	180
	$f_{cd} = 0,85 \cdot f_{ck} / (\gamma_c \cdot \gamma')$	*MPa*	34	81,6
Tube strength	$f_{ak,t}$	*MPa*	360	360
	$f_{ad,t} = f_{ak,t} / \gamma_a$	*MPa*	327,3	327,3
Steel core strength	$f_{ak,c}$	*MPa*	320	- -
	$f_{ad,c} = f_{ak,c} / \gamma_a$	*MPa*	290,9	- -
Tube	D_t x t	*Mm*	406,4 x 8,8	406,4 x 8,8
Steel core diameter	D_c	*Mm*	167,4	- -
Bearing capacity	$N_{pl,d}$	**MN**	13,29	13,29
Quantity of steel		*Kg/m*	259,1	86,3
Price of steel		*Euro/kg*	1,00	0,90
Quantity of concrete		*m³/m*	0,0967	0,1187
Price of concrete		*Euro/m³*	500	500
Material costs		**Euro/m**	259	137

UHPC filled steel tubes are a good alternative to the steel composite columns concerning the dimensions of the column. The costs per load unit are substantially smaller. With the high load-carrying capacity, the realization of transparent building is possible.

However, carrying the column load through the joint, which is generally made of NSC, is critical. Because of the difference of the compression strength between the column (UHPC) and slab (NSC), a sufficient bearing capacity of the joint cannot be achieved only by the confinement effect due to the surrounding slab (Ospina and Alexander [1] and Shah [2]). A conventional steel composite column is usually not ideal for arranging the rebars in the joint area, in particular at columns with large sections.

In order to solve this problem, a steel mounting element was developed shown in fig. 3. The advantage of this element is that the conventional reinforcement rebars can be arranged inside the joints. The installation of the special mounting element is simple and can be realized after laying the bottom reinforcement of the slab.
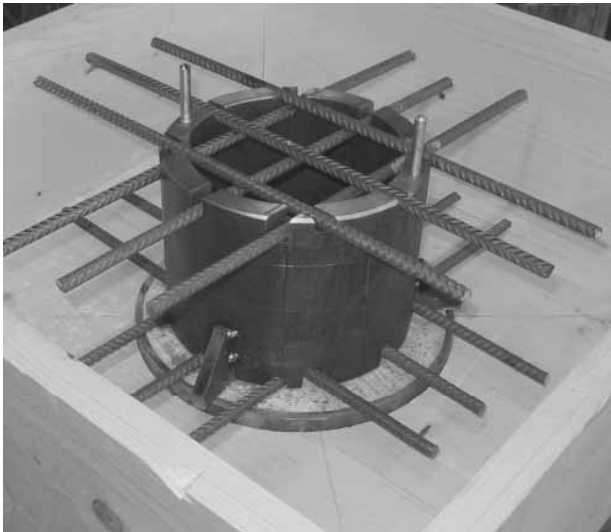
Figure 3: Special mounting element

The shear force of the slab can be carried into the lower column by reducing the diameter of the special mounting element without any additional element.

The increase of compression strength required for a safe transferring of the column load can be adjusted by the wall thickness of the special mounting element.

The first test results using this special mounting element are assembled in section 4 of this paper.

For hybrid truss, frame or arch structures (fig. 4) the application of the element presented here is also possible and useful.
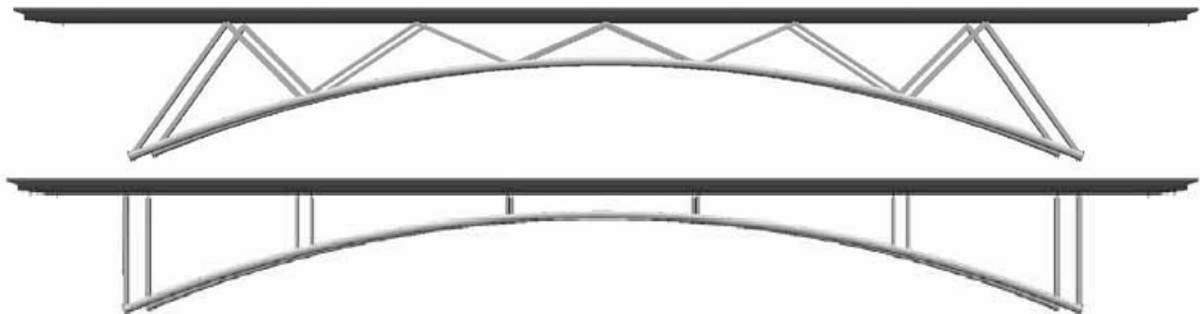
Figure 4: Hybrid bridge constructions

Not only the high compression strengthis used at hybrid cross-sections, but also the improved durability characteristics by UHPC can be utilized. Potential tension forces in such structures can be equalized by an appropriate pre-stressing. The high compression strength and the good confinement allow the application of high initial forces on a small surface.
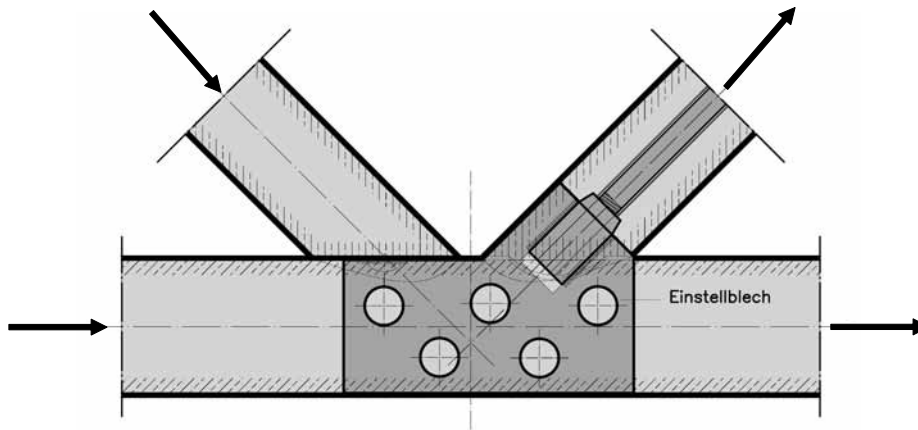
Figure 5:   Compression-tension-joint with perforated steel plate

Using UHPC in prefabricated steel tube structures may be a good substitute for cast-iron joints and avoid great wall thickness at the joint area as it is often needed for normal steel tube structures. Thereby, the manufacturing costs can be reduced. Beyond that also the sensitivity of such structures to manufacturing tolerances is reduced. In fig. 5 an example of such an construction is presented.

A force transfer between steel and concrete is a decisive point. Tests were performed, therefore, to investigate the load transfer between tube and core. The results can be taken from section 5.

4   Slab Joint Tests with Special Mounting Elements

Several tests on the transfer of the column load through the slab were conducted for the determination of the load-bearing capacity of a confined slab joint made of normal strength concrete. The experimental setup of the tests D4 and D5 is shown in fig. 7. The tests D1, D2 and D3 were performed without surrounding slab and without slab reinforcement. The concrete strength of the core concrete of all specimen exceeded f_{cm} = 150 MPa, while the concrete strength in the joint region was about $f_{cm} \approx$ 40 MPa.

If was observed that the bearing capacity of the column was never limited by the capacity of the special mounting element.

Table 2:   Overview joint/slab tests

test	type	slab reinforcement	maximum load in kN	failure	remark
D1	joint	--	4860	column	thick gap
D2	joint	--	4700	column	slitted
D3	joint	--	5560	column	not slitted
D4	joint/slab	ρ=0,37%	5170	column	excentric columns
D5	joint/slab	ρ=0,67%	5730	--	limit of testing machine

While the ultimate load was newer the decisive point, the limitation of the deformation in the gaps below and above the special mounting element inside the column-slab joint may be critical under service loading. Since these gaps were always filled with normal strength concrete, the concrete there was squeezed out from the gap laterally (fig. 6). The resulting deformations were about the size of the gap thickness.

concrete squeezed out of the gap
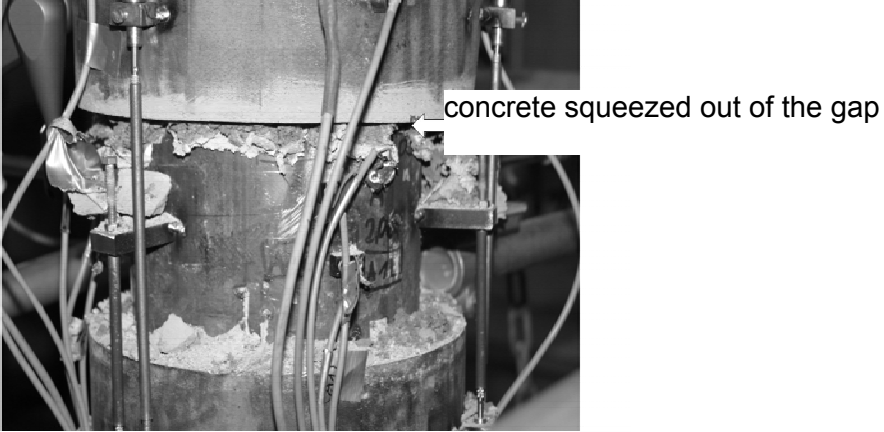
Figure 6: Failure of concrete in the area of the gap

For the optimisation of the bearing behaviour of the tests D2 and D3, the joint thickness was reduced and a reduction of deformation of approximately 50 % could be attained.
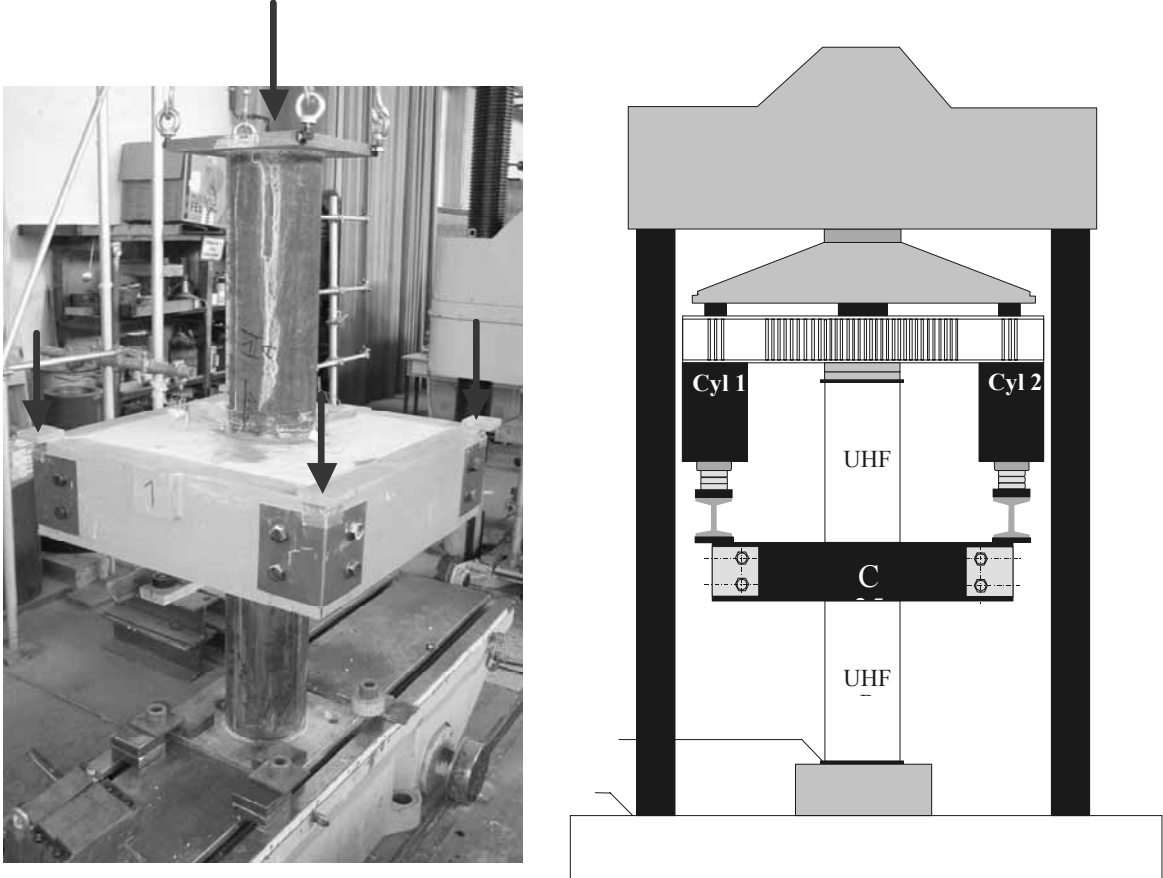
Figure 7: Test setup

The tests D4 and D5 were conducted to examine the influence of the surrounding slab.

For the test D4 the slab reinforcement was designed to reach the yield stress before the column was loaded. The effect of the confinement of the joint region is reduced due to the cracking of the tensile zone of the surrounding slab.

In the specimen D5 the reinforcement quantity was increased so that the slab (under the same slab loading as in test D4) remained uncracked. The aim was to activate the confinement of the slab completely.

The test results can be found in fig. 8. It is obvious that the deformations are reduced from the test D 1 to the test D 5. The influence of the confinement due to the surrounding slab (tests D4 and D5) is evident. The influence of the reinforcement ratio of the slab test D4 and D5 is small if the tests are compared with the tests D1, D2, and D3 without slab reinforcement.

Table 2:   Deformation of the gaps with a load of F=4500 kN

Test	D1	D2	D3	D4	D5
Deformation in mm	16	9	7,5	3	2
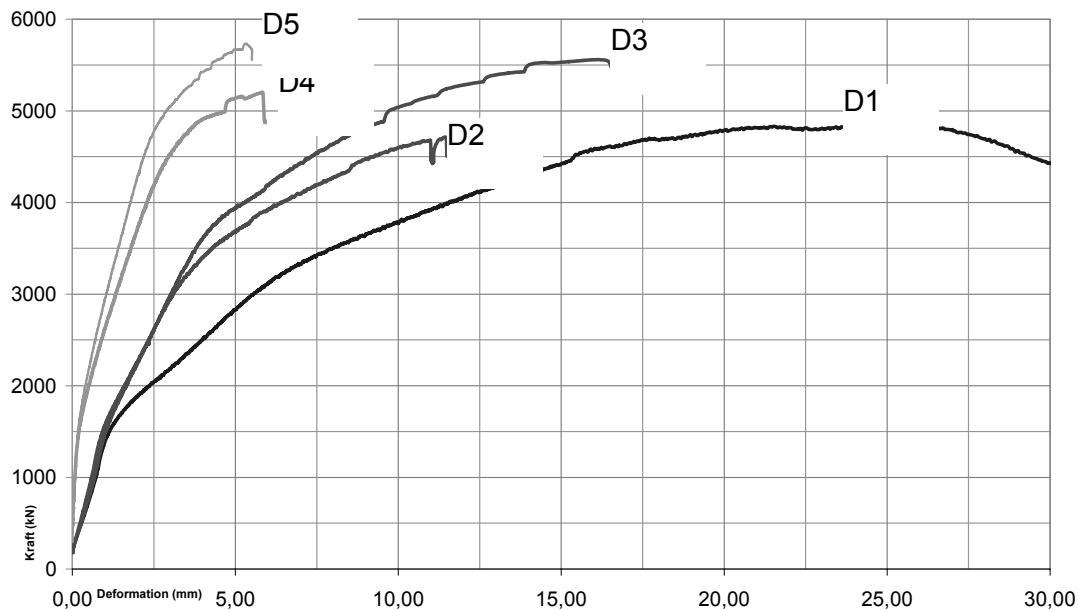
Figure 8:   Test results

5   Tests for Determining Bond Effect of perforated steel Plate

This test series were performed to determine the load-bearing capacity of the concrete dowel made of UHPC, which goes through the holes of a special mounting element consisting of perforated steel plate. This experimental investigation should yield some perceptions on the slip and deformation behaviour in interaction with the confined steel tube. The essential question can be formulated: Is the capacity of the concrete dowel sufficient to bear the forces increasing or is an additional reinforcement needed, e.g. greater wall thickness, with appropriate weld seam thickness.

In the first step the series covered six sample test specimens with different hole shapes within the steel plate.

In order to increase the ductility and, thus, to be able to defect a group effect on the UHPC dowels, new considerations were made (fig. 9). At two of the six plates (Po-02 and Po-04) a appropriate cross section attenuation was made by milling out the slots. The deformation capacities of the steel can be controlled according to the requirements and the demanded ductility. In order to exclude a force transfer within the groove, the slots were closed with a material of low strength and low stiffness before concreting (fig. 10, on the right side).
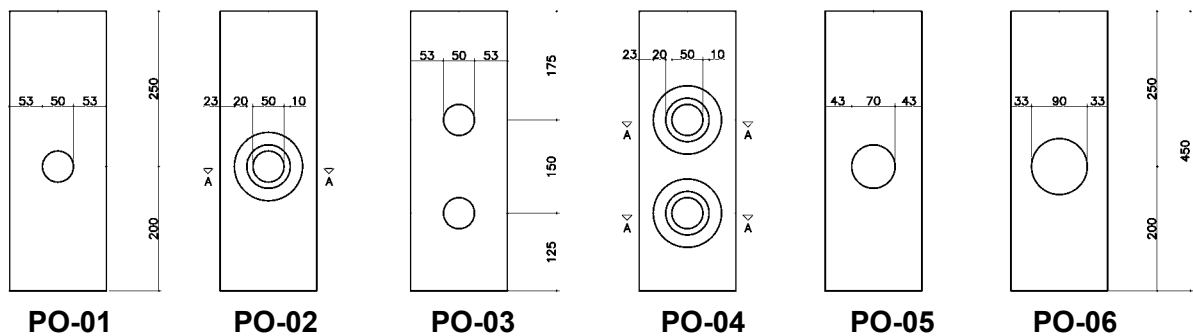
Figure 9:   Perforated steel plates (test series 1)

The experimental setup can be seen in fig. 11. The 20 mm thick perforated steel plates were placed into a 450 mm long steel pipe with an external diameter of 219.1 mm and a wall thickness of 4.5 mm. To guarantee a shifting way, a 20 mm strip made of strong expanded polystyrene was glued on the lower edge of the perforated steel plate. This strip was removed after casing the test specimens.
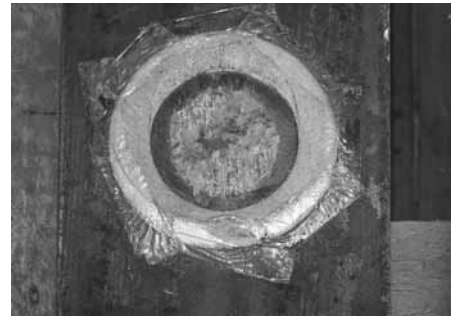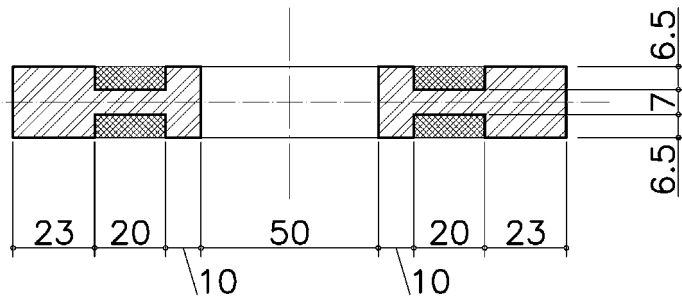
Figure 10: Section and top view of a perforated steel plate (PO-02)

The pipes were cleaned before casting to remove loose particles. Beyond that, the inner surfaces of the pipes, without further pretreatment, remained in their rolling skin condition. The perforated plates, however, in order to exclude friction influences to a large extent, were coated with formwork wax. The pipes were casted finally with UHPC with a maximum aggregate size of 5 mm.

In fig. 12 the results of some tests are presented. High load-bearing capacities and great ductility could be attained. The load droped only after a very large deformation. It is interesting that the stiffness of the UHPC dowels decreases hardly after the cracking along the shear section of the concrete dowels. Only during the cracking at the external concrete ring between the plate and the pipe wall, a clear reduction of stiffness was registered. Afterwards, the confinement effect of the steel tube ensured that the load remained on a high level. The reason for this positive behaviour is, among other things, the small plastic deformation of the UHFB. It leads also to the fact that the stress of the external concrete ring increases only slowly with the increase in longitudinal deformation. These perceptions are very valuable for the development of the bond element, since it is very difficult to detect a group effect of head bolts within constructions made of high-strength concrete.
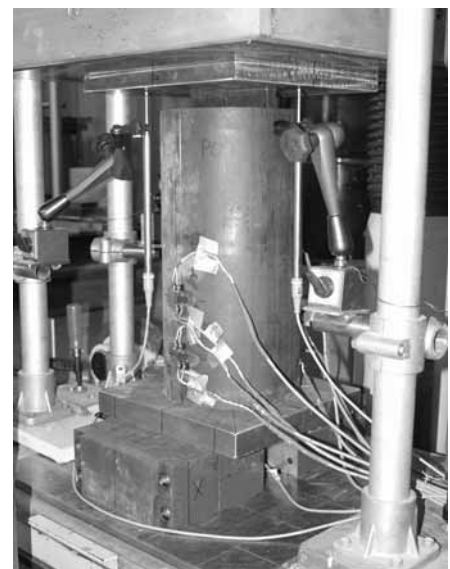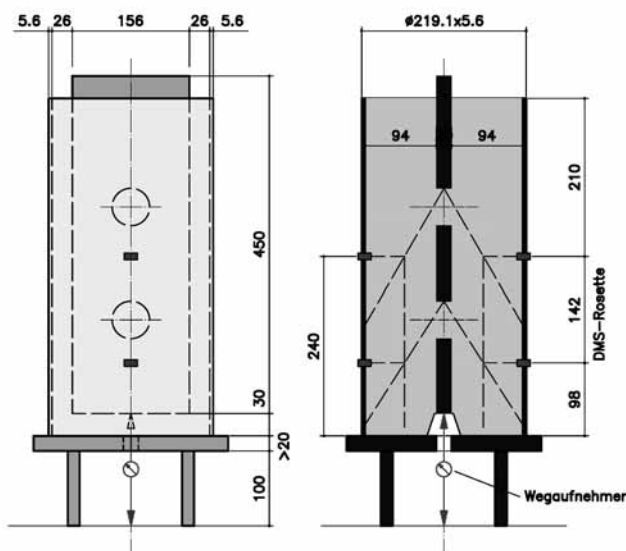
Figure 11: Section and top view of a perforated steel plate (PO-02)

In fig. 13 the increase of the steel tensile stress in tangential direction is presented as a function of the applied load. It should be made clear that a considerable increase of stresses occures only after the cracking at the outside concrete ring. Further tests are planned, in order to get a safe prediction of the ultimate load for design.
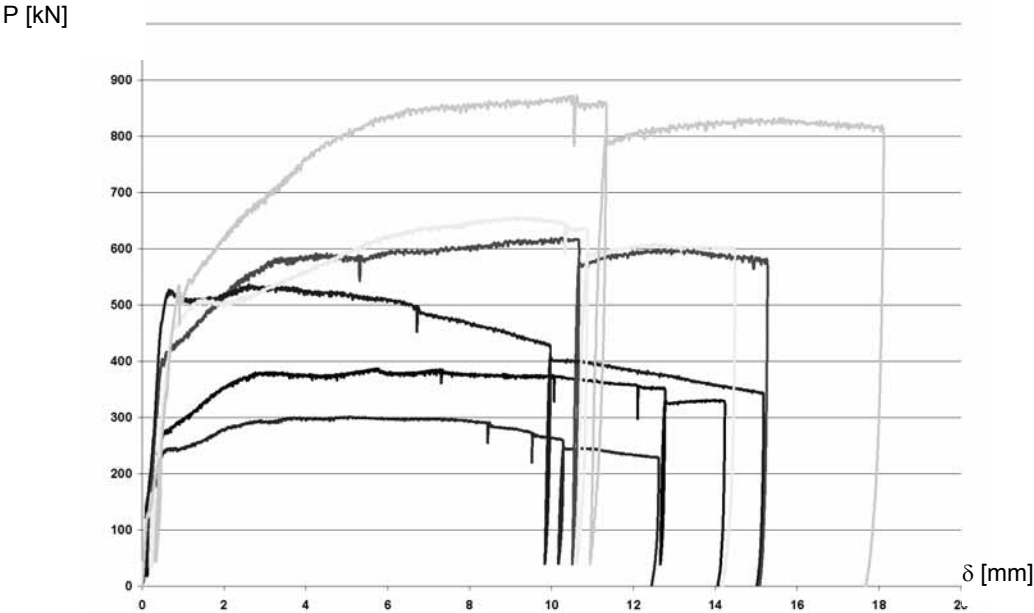
Figure 12: Test results
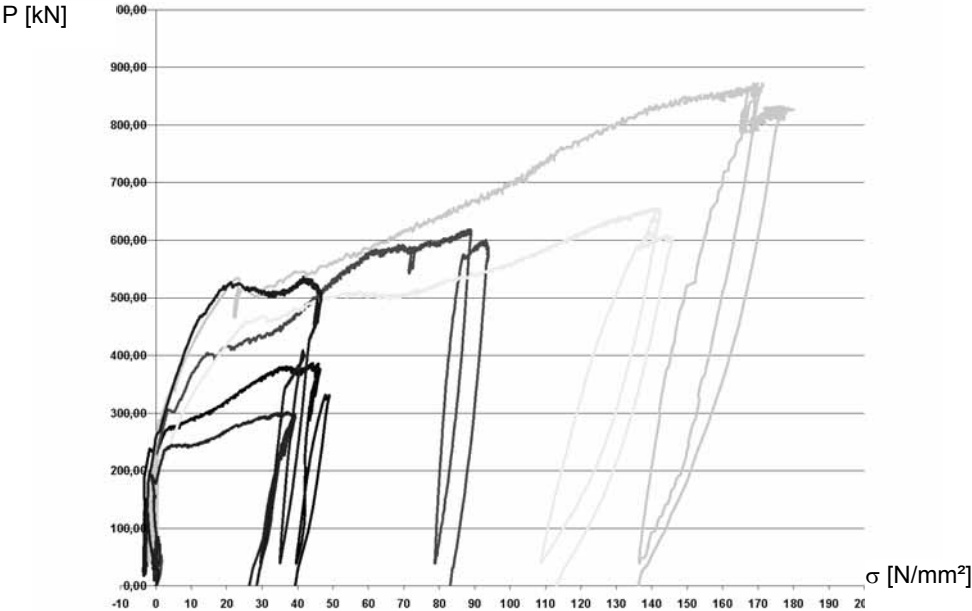
Figure 13: Steel stress in tangential direction of the steel pipe

6 Outlook and Conclusions

UHPC filled tubes are structural members with high bearing capacity and sufficient ductility. They have special properties due to the interaction between steel and concrete which should be considered in the design. Furthermore, for the application of these structural members in buildings special solutions for the joints are necessary. Some proposals are presented in this paper. The test results with these proposals are encouraging. More investigations are necessary in order to develop the design rules for this structural members.

For a general application of the perforated steel plates in buildings and bridges, calculation models will be developed basing on the test results obtained so far. Therefore, the tests are evaluated and the results are described in detail. A parallel FE-calculation is carried out, in order to understand the bearing behaviour of the members, in particular the reciprocal effect between filling concrete and confining steel.

7 References

[1] Ospina, C.; Alexander, S.: Transmission of Interior Concrete Column Loads Through Floors. In: Journal of Structural Engineering, vol. 124, June 1998.

[2] Shah, S. A. Ali: Experimental Investigation of High Performance / High Strength Concrete Columns with Intervening Normal Strength Concrete Slabs, Dissertation, Universität Leipzig, 2004

Ultra High Performance Composite Bridge across the River Fulda in Kassel
– Accompanying investigations according to the required
agreement by the authorities –

Ekkehard Fehling

Prof. Dr.-Ing.

Universität Kassel

Kassel, Germany

Michael Schmidt

Prof. Dr.-Ing. habil.

Universität Kassel

Kassel, Germany

Kai Bunje

Dipl.-Ing.

Fehling + Jungmann GmbH

Kassel, Germany

Nguyen Viet Tue

Prof. Dr.-Ing. habil.

Universität Leipzig

Leipzig, Germany

Ultra High Performance Composite Bridge across the River Fulda in Kassel
– Accompanying investigations according to the required agreement by the authorities –

Summary

Since no provisions concerning the new material UHPC exist in the German building codes, a so called "Zustimmung im Einzelfall" (Special Case Approval) for the realisation of the design of the Gärtnerplatzbrücke using UHPC has to be given by the authorities. This means that specific tests have to be performed on the material and on the main structural elements. The results of the tests need to be examined by an independent expert.

Keywords: *UHPC, material tests, special case approval, Zustimmung im Einzelfall*

1   Introduction

The departments of Concrete Structures (Prof. Dr.-Ing. Ekkehard Fehling) and Building Materials (Prof. Dr.-Ing. habil. Michael Schmidt) at the University of Kassel have worked for some years on the investigation and further development of Ultra High Performance Concrete. On the one hand, questions of the mixture optimisation, the durability and the mechanical qualities of the material were examined and on the other hand design models for the ultimate limit state and the serviceability state were developed [1-3]. Therefore the time is ready to build the first greater bridge construction made of the new material in Germany.
As the first project of a UHPC-bridge in Germany, it is intended to build a pedestrian and cycle track bridge across the Fulda river by the City of Kassel as a client. The planned bridge is a hybrid construction made of steel and Ultra High Performance Concrete. This bridge shall replace an existing wood bridge which shows severe damage.

Since there are no provisions concerning the new material UHPC in the German building regulations, a so called "Zustimmung im Einzelfall" (Special Case Approval) has to be given by the authorities. This means that specific tests have to be made on the material and on the main construction elements. The results of the tests need approval from an independent

expert. Prof. Dr.-Ing. habil. Nguyen Viet Tue from the University of Leipzig has been appointed as independent expert for this project.

2 Expert opinion

In the framework of an initial report on the requirements with regard to the material properties and to the design concept of the new Gärtnerplatzbrücke, guidelines for the required tests have been set up by the independent expert [4]. The Special Case Approval (Zustimmung im Einzelfall) will be based on the results of those tests and the following expert judgement. As far as possible, requirements defined by the relevant design codes and design guidelines shall be observed. Open questions, which cannot be answered by existing regulations, have to be answered with the help of experimental investigations.

3 Material tests of the hardened concrete

In context of the design and the Special Case Approval, the concrete quality has been defined. It is intended to use a concrete with an average strength f_c = 165 N/mm² with a steel fibre content of 0.99 vol.-%. The following material tests have to be carried out:

- The compressive strength is to be tested on cylinders with a geometric ratio from d/h = 1/2. The cylinders must have at least a diameter of 10 cm. Two series with five test specimens, each from a different batch have to be tested according to DIN EN 12390. The average compressive strength f_c has to reach at least 165 N/mm² and the lowest single value is not allowed to be below 145 N/mm².

- The flexural strength is to be tested on beams 15 *15 * 70 cm on UHPC with steel fibres. Prisms 4 * 4 * 16 cm are not allowed for the initial type tests. 2 series with 5 test specimens, each from a different batch are to be tested. The tests have to follow the German regulations for steel fibre concrete (Merkblatt für Stahlfaserbeton [5]). The average flexural strength for the proposed conceptual design with transverse prestressing has to reach at least 15 N/mm² and the lowest single value must not fall below 10 N/mm². The ultimate load is defined as the flexural strength.

  In order to take the size effect into account, additional flexural tests on specimens with the real element thickness have to be performed. For this reason, test slabs (plates) must be produced under real production conditions. The test beams have to be sawed out of the plates. The crack width and the deflection have to be measured.

- The freeze thaw and the freeze thaw de-icing salt resistance is tested by using the CIF

  and CDF-test (Capillary suction of De-icing salt and Freeze-thaw test).

Ultra High Performance Composite Bridge across the River Fulda in Kassel
– Accompanying investigations according to the required
agreement by the authorities –

- The resistance against sulphate attack will be tested over a short period of time by the Duggan-test [6] and by the Wittekind-method with and without a pre-damage of the specimens [7].

- The degree of shrinkage has to be quantified by measurement of the autogenous shrinkage and the complete shrinkage. [3] (Research report of the University of Kassel on UHPC) shows the storage test conditions.

- The creep behaviour is to be tested on cylinders with a geometric ratio from d/h = 1/2.

- The pore-size distribution – especially the amount of the capillary-pore content – is measured using mercury pressure porosimetry.

- The development of carbonation will be observed under normal climatic conditions (20°C/55-65% rel. humidity). The examination will be performed by light microscopy using thin slices.

4   Construction element tests

4.1   Precast bridge deck plates

The load resistance capacity of the precast bridge deck plates will be tested in a full scale test. The major question is the transverse load carrying capacity of the deck plate elements. Therefore three loading positions will be simulated:

- Bending load resistance of the cantilever and local resistance of the anchorage of the railing post → vertical loading on the cantilever and horizontal loading on the railing post
- Bending load resistance at midspan → vertical loading in the middle of the bridge deck
- Shear force resistance of the bridge deck → vertical loading near to the supporting beam

Figure 1 shows the test specimen with the different load positions.
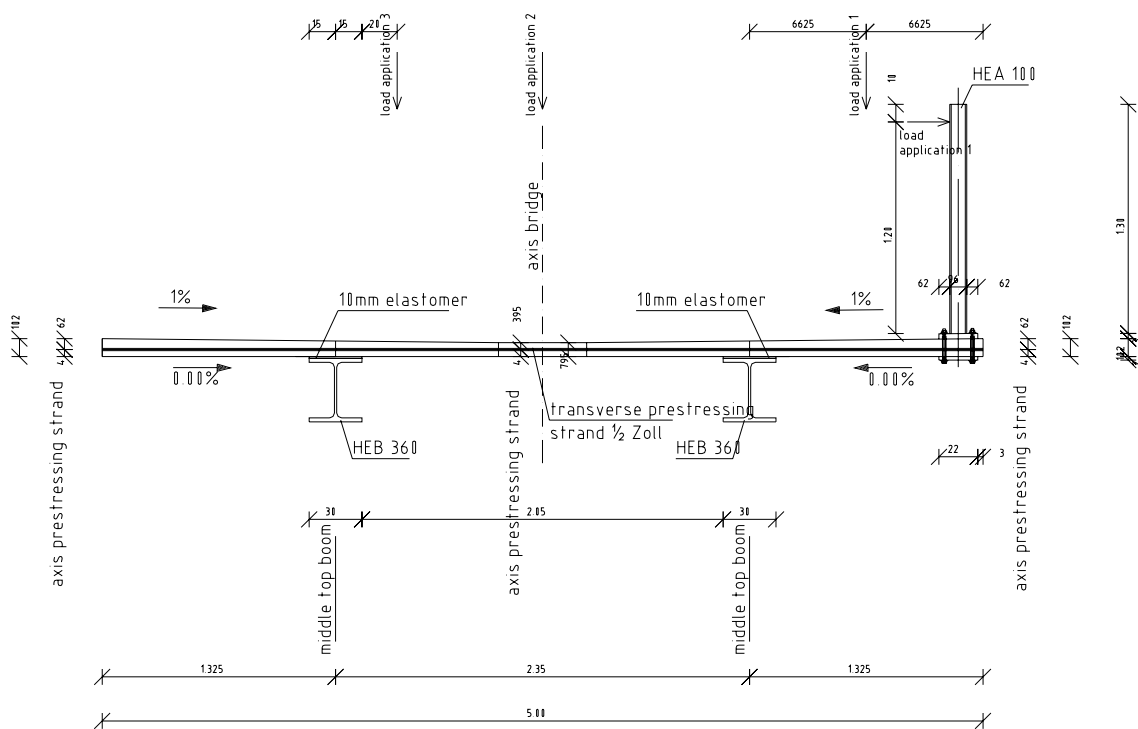
Figure 1:   Tests on precast bridge deck elements

4.2   Connections steel diagonals to the UHPC booms

In the connection points of the steel diagonals to the UHPC booms very high shear forces have to be transferred into the UHPC booms. The maximum forces in the 36 m span are around 600 kN (characteristic value). Therefore special tests on these connecting points are planned. Figure 2 and 3 show the connection detail. The diagonals are connected with so called perfobond bond connectors to the UHPC booms.
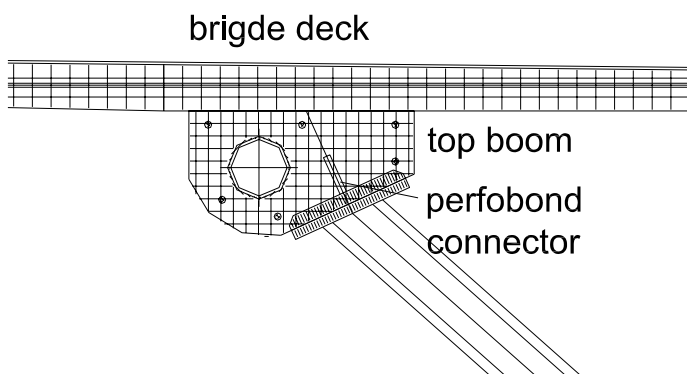
Figure 2:   Cross section connecting detail

Ultra High Performance Composite Bridge across the River Fulda in Kassel
– Accompanying investigations according to the required
agreement by the authorities –
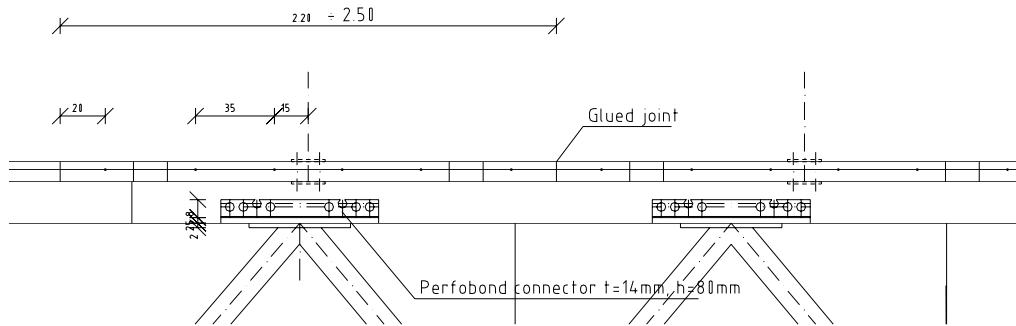
Figure 3:   Connecting detail

4.3   Glued UHPC connections

The mechanical durability and the strength of the glued connections have to be tested. Therefore a comprehensive test program has been developed in cooperation with the independent expert. In the following a short overview from the planned tests are given.

4.3.1   Pre-tests on prisms:

In order to find the best parameters for the preparation of the surface of the Ultra High Performance Concrete elements for the glued connection pre-tests on glued prisms (160 * 40 * 40 mm) have to be done. It is supposed to carry out 4-point flexure tests (Figure 4) and centric tensile load tests. The following parameters are of interest:

- Required time for the hardening of the glue
- Curing of the concrete (heat treated, water stored, air stored)
- Surface condition of the concrete (shot blasted, brushed and non-treated)
- Temperature at the gluing procedure
- Joint shape
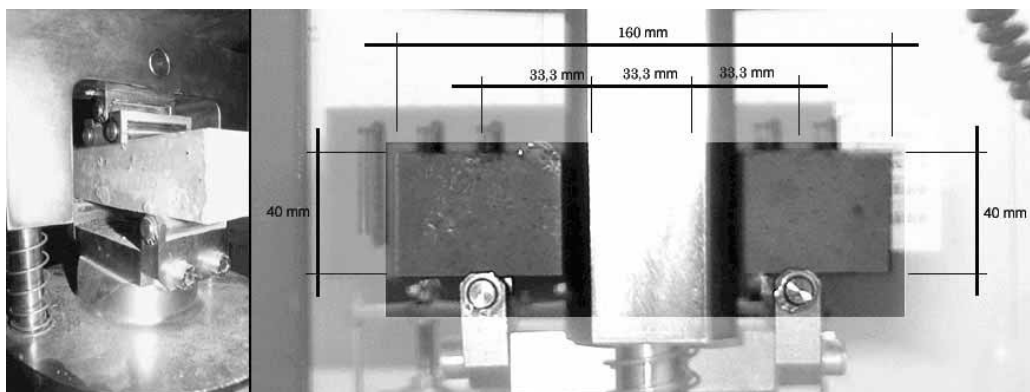
Figure 4:   4 – point bending tests

4.3.2   Test plates

On test plates with real element heights it is supposed to do 4-point flexure tests and centric tensile load tests under static and dynamic loads. For the tests on small plates the best surface conditions resulting from the pre-test on prisms should be used.
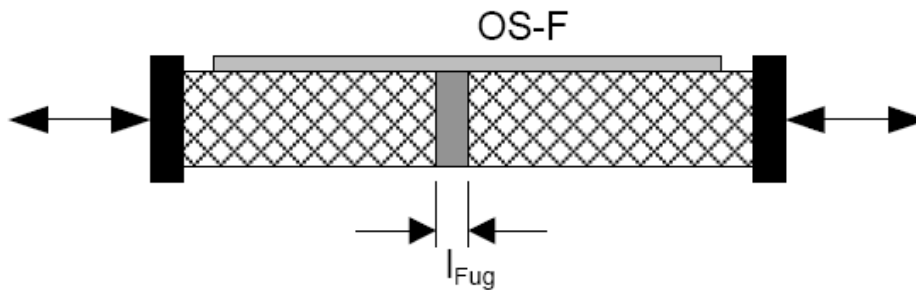
Figure 5:   Test geometry

4.3.3   Shear force

In accordance to [8], tests on prisms and cylinders under combination of shear and compression have been performed at the University of Kassel in order to evaluate the shear resistance capacity in glued connections (see Figure 6).
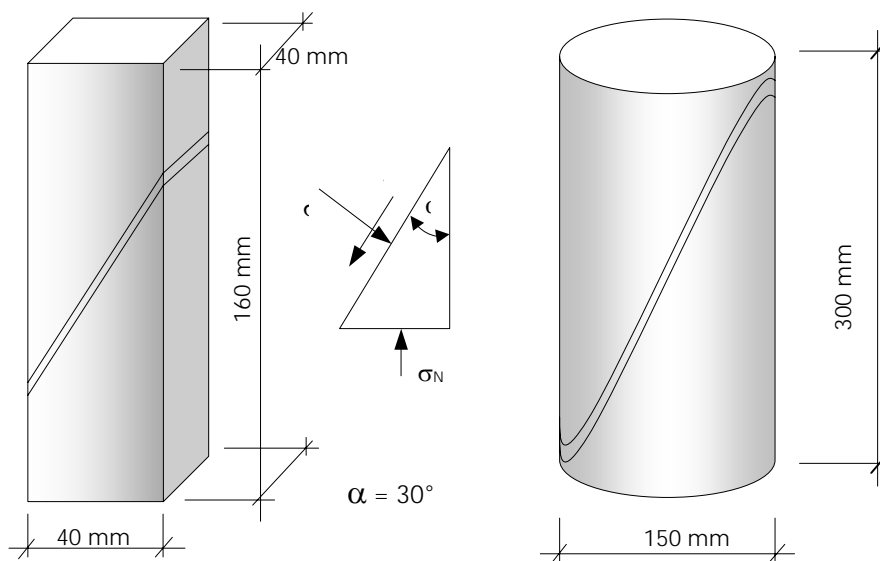
Figure 6:   Pressure shear tests on prism and cylinders with saw cut joints

After 72 hours the shear strength in the glued joints was between 20 and 25 N/mm². In order to take the influence from additional tensile stresses into account, additional test specimens are planned. Three plates as showed in Figure 7 are glued together. The thickness of the glued joint and the thickness of the middle plate are kept variably, in order to study the effect of moments resulting from eccentricities.

Ultra High Performance Composite Bridge across the River Fulda in Kassel
– Accompanying investigations according to the required
agreement by the authorities –
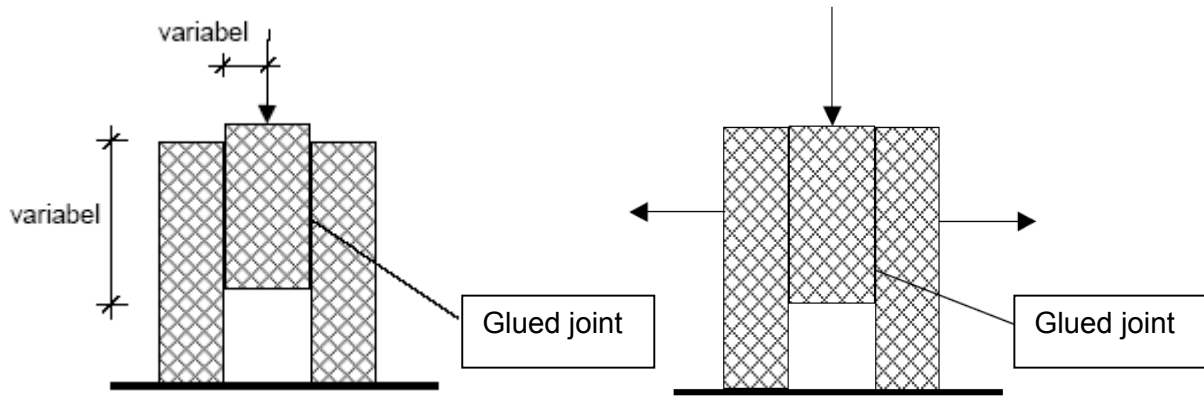
Figure 7:   shear + tensile strength test specimens

5   Conclusions

To build a safe structure using a new material, it is very important to gain experience with the use of the material. This holds true for the optimisation of the manufacturing and erection process, the behaviour of the material itself as well as for the behaviour of special structural elements. The tests on material, structural elements and connection details as they will be used in the structure of the Gärtnerplatzbrücke, give the information required for a safe design of such a structure using innovative materials.

6   References

[1]   Bornemann, R., Fehling, E., Schmidt, M., Middendorf, B.: "Entwicklung und Verhalten von Ultrahochfestem Beton (UHPC)", In: Beton- und Stahlbetonbau, 2001.

[2]   Schmidt, M., Fehling, E., Teichmann, T., Bunje, K., Bornemann, R.: "Ultra-Hochfester Beton: Perspektive für die Betonfertigteilindustrie", In : Betonwerk + Fertigteil - Technik, Heft 3 (2003), S. 16

[3] Fehling, E.; Schmidt, M.; Teichmann, T.; Bunje, K.: Entwicklung, Dauerhaftigkeit und Berechnung Ultra-Hochfester Beton (UHPC), Forschungsbericht an die DFG, Universität Kassel, 2003

[4]   Stellungnahme zu den Anforderungen an Baustoffeigenschaften und zum Bemessungskonzept der Gärtnerplatzbrücke aus UHFB, Universität Leipzig, Institut für Massivbau und Baustofftechnologie, Prof. Dr.-Ing. habil. N. V. Tue

[5]   Deutscher Beton- und Bautechnik Verein e.V.: DBV-Merkblatt Stahlfaserbeton, 2001

[6]   Duggan, C. R. et al: Rapid Test of Cencrete Expansivity due to Internal Sulfate Attack – ACI Material Journal Vol.89 (1992)

[7]   Tang, L.; Nilsson, L. O.: Rapid determination of the chloride diffusifity in concrete by applying an electrical field. ACI Materials Journal 89; S. 49-53; 1992

[8]   FIP Fédération Internatioal de la Précontrainte: Proposal for a standard for acceptance tests and verification of epoxy bonding agents for segmental construction, Cement and Concrete Association, Wexham Springs 1978

Achim Lichtenfels
Dipl.-Ing.
Ingenieurbüro Lichtenfels
Keltern, Germany

Ultra-High Performance Fibre Reinforced Concret for shells

Summary

Shells are elegant and efficient structure, but also expensive to construct and therefore very few are being built currently. This paper will present a procedure to produce shells made of ultra-high performance fibre reinforced concrete (UHPFRC). Deformation is used to turn plane elements into shells. Since many UHPFRC-elements are prefabricated, a joining method will be introduced which is suitable for this material. In order to cover stresses beyond the tensile strength of the fibre reinforced concrete, results of tests with prestressed elements will be presented. This paper will also address sandwich-elements with UHPFRC top layers for the increase in stability of shells under compression and for incorporating the required heat insulation. Finally, examples of pre-deformed shells will be presented.

Keywords: *UHPFRC, Shells, Hot-Water-Storages, Construction Joints, UHPFRC and reinforcement, Sandwich-elements, ductile shells*

1   Objective

Shells are elegant and efficient structures with concrete as the ideal material. Concrete may be poured into any form, it is durable and, when reinforced, safely supports any load. Unfortunately, the number of shells built has steadily declined over the past years and decades. This trend will have to be counteracted, or this part of the building culture will be lost. UHPFRC is an innovative material with a multitude of possibilities to be applied in the construction of shells. Besides its suitability for shells in general, UHPFRC is especially suited for the construction of hot water storage tanks. Hot water tanks serve as storage for solar heat used for the hot water supply of urban housing areas. By such a storage from summer to winter a considerable amount of fossil fuel is saved. Further details about longterm hot water storage tanks are described in [1], in this Symposium volume by Reineck and Greiner [2] and in [3] to [12].

2   Introduction

Aesthetics as well as economics are major factors to be considered not only in view of the construction but also with respect to the maintenance of a structure. Since the basic ingredient for UHPFRC is rather expensive minimizing the material expenditure has to be closely adhered to during the design process. This is an essentiel characteristic of shell structures. However, the considerable amount of formwork involved in the construction of

shells also causes high costs. UHPFRC will only be successfully in structures if the gain from minimizing the material is not consumed by the considerable construction costs. Since prefabricated elements are mostly used for UHPFRC-shells it is essentiel that the joints are suited for the material used. Therefore joints are also described in this article, as well as UHPFRC-elements reinforced with steel bars and the use of sandwich-elements.

3 Joints

3.1 Requirements for the Joints

UHPFRC-elements are mainly prefabricated, and in the following a method for joining is described where fibres are used, which complies best with the material. The main requirement for joints between UHPFRC-elements is that the loadbearing capacity of the structure may not be dictated by the loadbearing capacity of the joint because this would greatly inhibit the proper use of the material or require extensive strengthening of the structure at the joints. Another factor to be considered is that prefabricated parts are frequently exposed to temperature treatment, whereas temperatur treatment of the in-situ joints will be highly difficult and costly. Further requirements, especially for shell structures are the impermeability of the joint, no temperature treatment, favourably no reinforcing bars due to their large dimensions and the stress concentrations, and the free form in plan.

3.2 Fibre Joints

Fibres would be best for joining UHPFRC elements, but the fibres added to the concrete are not suitable due to their small dimensions of only a diameter of approx. 0.2 mm and a length

of 15 to 20 mm. Therefore, fibres with a diameter of 0.7 mm were selected and were inserted into a supporting ribbon as described in Fig. 1, and for this joint tests were carried out [1].This procedure may easily be conducted mechanically and at almost any angle; therefore, forces oblique to the joint can also be transferred. In addition to carrying the fibres, the supporting ribbon also serves as a flexible formwork at the edges.
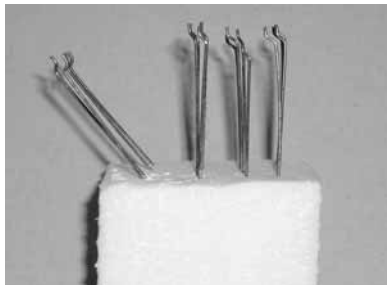
Fig. 1: Supporting ribbon with fibres

3.3 Test Program

Several test of the bonding behaviour of fibres were conducted to determine the loadbearing capacity of the joint. A fibre content of 0.26 to 1.3 % was chosen. During this deformation controlled test the forces were measured at the press. Three transducers were arranged around the circumference to determine the opening of the joint. Fig. 2 depicts the test setup. The following describes the production: First the fibres were inserted into the support element and concreted into the bottom of the specimen. The supporting element was removed after hardening of the concrete and a thin layer of grinded quartz, mixed with water was poured into the formwork, thus separating the bottom part from the top. After drying of

the separating layer, the top part of the specimen was concreted. Due to the separating layer only the fibres transmit the forces. Fig. 3 shows the behaviour of bond stress and joint opening for smooth fibres without end hook, with a bond length of 12 mm (left) and for fibres with end hook, with a bond length of 28 mm (right). The fibre content was 1.3 %. This results in a maximum bond stress of 8 MPa.
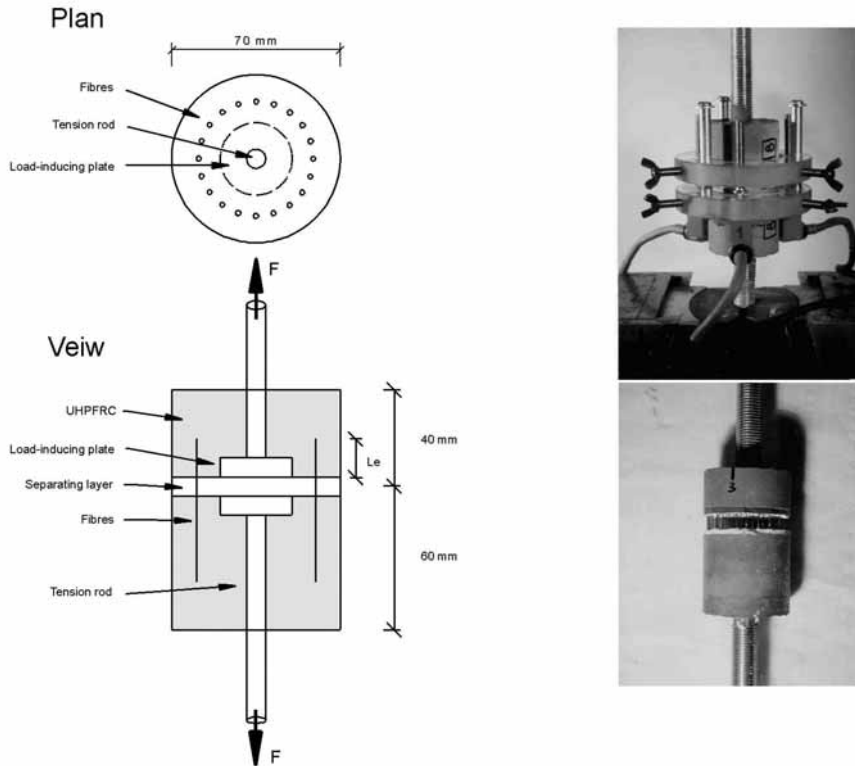
Fig. 2.: Test set-up and specimen of the bond-stress-tests
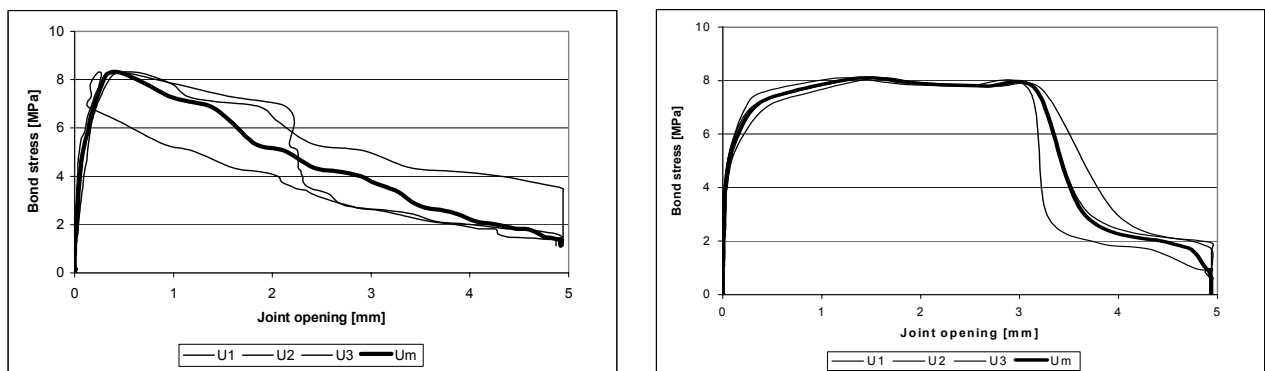
Fig. 3: Graph of bond stress and joint opening, with l_e = 12 mm and 28 mm and 1.3 % fibres

U_1 to U_3 represent the longitudinal joint opening. U_m is the mean joint opening derived from U_1 to U_3. This shows that with longer fibres and end hooks a distinct plateau may be reached.

Plan

Fibres
Tension rod
Load-inducing plate

70 mm

F

View

UHPFRC
Load-inducing plate
Construction joints
Fibres
Tension rod

40 mm
28 mm = Lü
40 mm

F
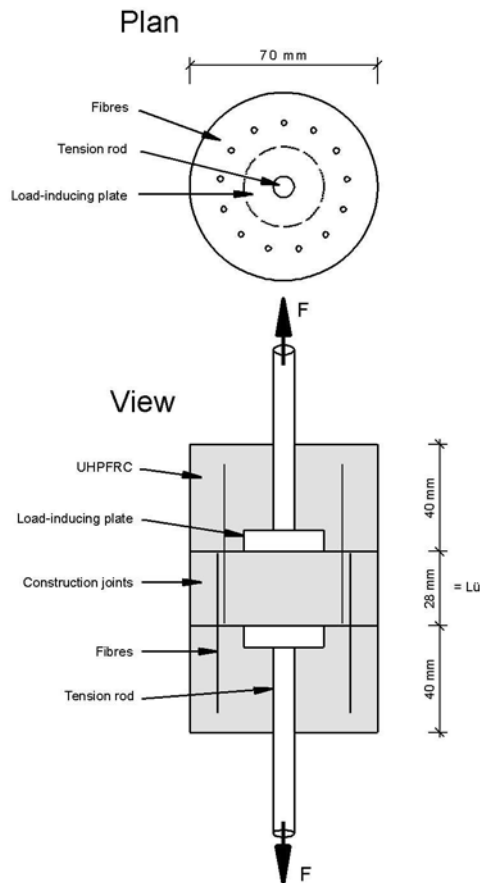
Furthermore, construction joints with a fibre content of 0.26 % and 1.3 % were tested, as depicted in Fig. 4. For this purpose, specimens with a concrete height of 40 mm were produced, joined after hardening and concreted. The fibre overlap measured 28 mm. Wire fibres 0.7 mm in diameter and 60 mm in length with end hooks were used. The tensile strength of the fibres amounted to 2.400 MPa.

Fig. 5. described the results of a test with 0.26 % (left) and 1.3 % (right) fibre content. This proves the positive congruity of the applicable bond stresses between the test of the construction joint and the bond stress at equal fibre content. With a lower fibre content the applicable bond stress increases which results from the reduced damage to the concrete due to a decrease in stress. The larger applicable bond stress coincides with a rather large deformation.

Fig. 4: Test set-up for the tests of the construction joints
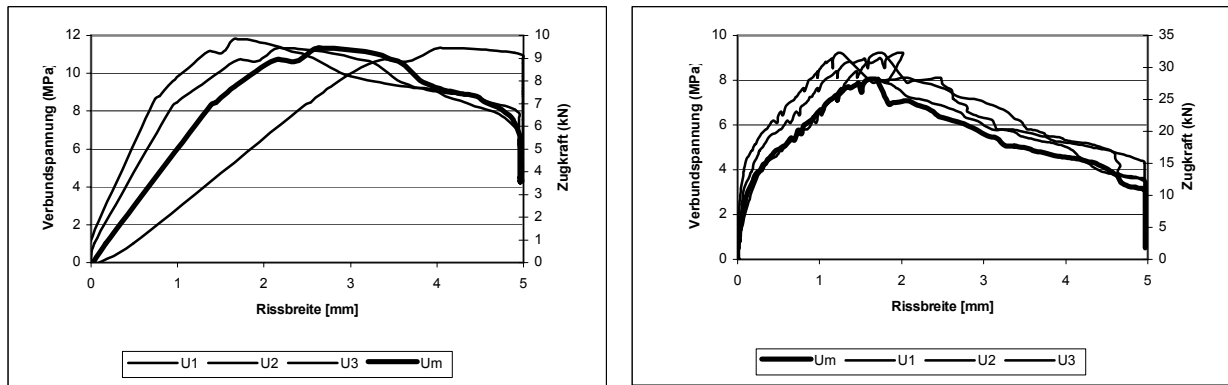
Fig. 5: Applicable forces and bond stresses in construction joints with a fibre content of 0.26 % and 1.3 %

The applicable tensile force in the construction joint under ultimate stress is derived according to eq. (1):

$$F_u = f_{bu} \cdot l_b \cdot U_f \cdot n_f < f_{y,f} \cdot A_f \cdot n_f \tag{1}$$

A required fibre content of 0.87 % is derived based on these first tests, with an applicable bond stress of 8 MPa and an overlap of 30 mm for a UHPFRC with an axial tensile strength $f_{ct,ax}$ of 12 MPa.

3.4   Prospect

On the basis of these primary tests further tests have to be conducted with regard to specimen geometry, anchoring length and anchoring type, as well as fibre content in the joint.

4   Reinforced UHPFRC-Elements

4.1   Introduction

If UHPFRC is to be used for any type of shell an increased and above all a guaranteed tensile strength of the material is desireable to transfer tensile forces without enlarging the cross-section. For this purpose flexural tests were conducted [1] investigating the behaviour of UHPFRC-elements reinforced with profiled prestressing strands. The results showed that the loadbearing capacity increased significantly compared to elements without reinforcement.

4.2   Tests and Results

Several 3-point bending tests on slab strips were conducted as graphically depicted in Fig. 6. The degree of reinforcement selected for the specimens did not exceed ρ = 1.5 % to prevent the concrete compression zone from failing before the tension zone. Higher degrees of reinforcement are only significant when tensile stresses prevail. Ribbed prestressing wires St. 1570/1770 with a diameter of 4 mm are applied as reinforcement. The fibre content was 2.5 %. Fig. 7 shows the material models used for the analysis of the tests.

Fig. 8 reflects two test results and proves that test results and the analysis agree well. At the ultimate limit state the check results generally show larger deflections, whereas the loadbearing capacity is on the safe side. The agreement of the test results with the results of the analysis at the limit state of serviceability depends mainly on the decline in stress of the concrete under tension after cracking. Here the tests produced values from 25 % to 50 %. The analysis is based on a mean value of 37.5 %.
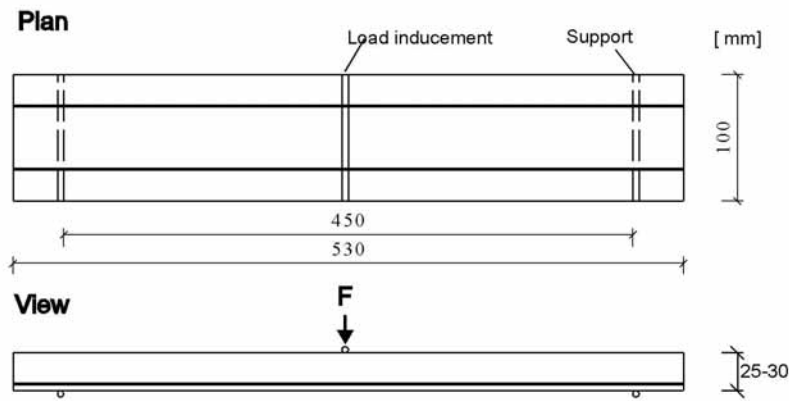
Fig. 6: 3-points bending test to determin the behaviour of UHPFRC-elements reinforced with steel bars
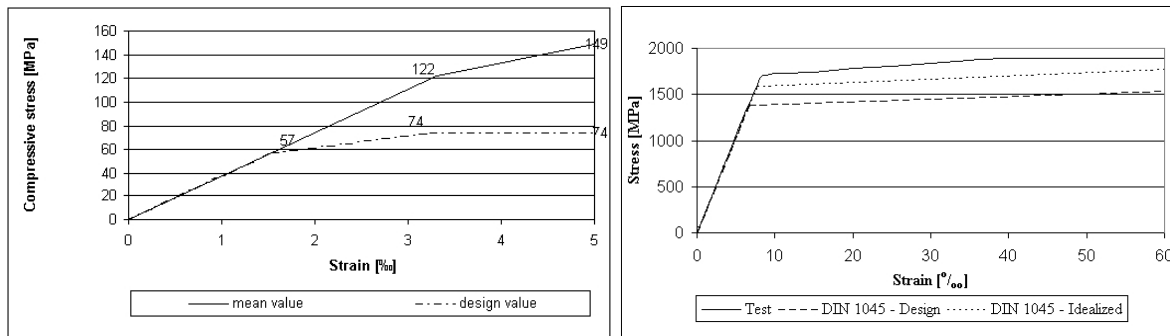
a) UHPFRC   b) Steel
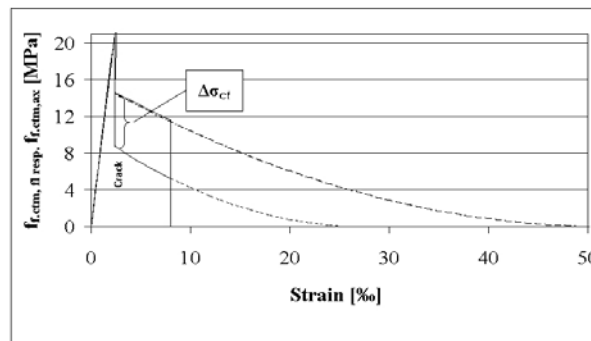
c) Tension Stiffening

Fig. 7: Material models for the check
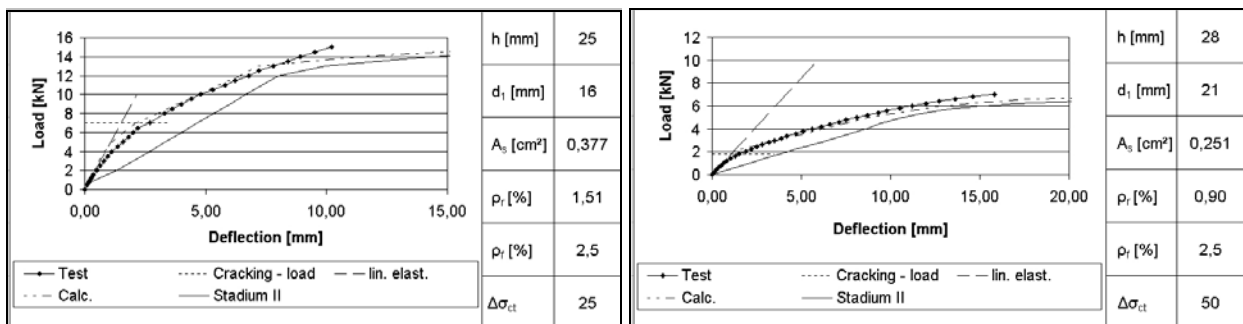
a) Reinforcement 1.51 %   b) Reinforcement 0.90 %

Fig. 8: Test results and analysis of flexural test beams reinforced with steel bars

Assuming a maximum tensile strength in bending of 30 MPa for thin UHPFRC-elements, the following maximum loadcapacities and load increases were attained for specimen a) and b):

a)   F = 2.77 kN   Load increase = 5.4 (with $\rho = 1.51$ %)
b)   F = 3.5 kN   Load increase = 2.8 (with $\rho = 0.90$ %)

This proves that adding non-prestressed high-strength reinforcement significantly increases the loadbearing capacity of UHPFRC. In addition to tests of the bending strength, tests of the shear strength and the joint configuration were also conducted [1].

4.3   Prospect

Besides the tests of the bending strength further tests of the centric tensile stress are to be conducted. Also, testing the variation and determination of the required fibre content might prove interesting.

5   Sandwich-Elements for Shells

5.1   Introduction

Thin UHPFRC-structures under compression are in danger of stability failure far below the admissible concrete compression stress. Sandwich-elements are one possibility to improve the use of the material. They consist of two UHPFRC top layers and a thin core layer. Polyurethane and polystyrene heat insulation, shaped at the surface, are especially suited for the core layer. The advantage of sandwich-elements is that the top layers determine the loadbearing capacity of the structural element in its plane and the core layer transfers the loads laterally to the plane. The core layer also strengthens the top layers against local buckling (creasing) and guarantees the required spacing.

5.2   Selection of Stiffness for the Core Layer

The cross-section of the sandwich-element and the choice of core stiffness depend on several factors. The four major factors are:

- increase in stiffness, e. g. in cae of stability problems.
- reduction of stiffness in certain areas, e. g. to reduce the interferential influence at the edges or to reduce the effects of restraint
- structural system, e. g. the span and the support.
- type of loading.

In Eq. (2) the example of a flexure test beam is used to determine the required shear modulus of the core layer to provide the cross-section of the sandwich-element with the same bending stiffness as a solid cross-section with twice the thickness of the top layer.

$$G_K = \frac{2 \cdot f_V}{9 \cdot f_M} \cdot \frac{E_c \cdot h_D^3 \cdot \left(4 \cdot h_D^2 + 6 \cdot h_K \cdot h_D + 3 \cdot h_K^2\right)}{l^2 \cdot h_K^2 \cdot \left(2 \cdot h_D + h_K\right)}$$

(2)

where   the indices D represent the UHPFRC top layer,

the indices K the core layer and h the layer thickness.

The Factor f_V expresses a value for the shear deformation depending on the support and the type of stress, and f_M stands for the deformation due to bending. It is essential that the required shear modulus of the core layer decreases in the square with the length. This is highly benefitial for wide-span structure with their jeopardized stability since some stiffness of the core layer significantly increases the overall stability. This will be described below with the bifurcation load of a flat arch as an example.

5.3   Bifurcation Load of a Flat Sandwich-Arch

The efficiency of sandwich-elements will be demonstrated by the example of a flat circular arch (Fig. 9). The analysis is based on the assumed maximum overall height of 50 mm. Each top layer of the sandwich-elements is 25 mm thick and 1.0 m wide. The thickness of the core layer is chosen at 50 mm and the elastic modulus varies. Fig. 10 shows the dependency of the possible stress on the elastic modulus of the core layer. The marginal points represent the absence of the core layer causing the loadbearing capacity to decrease to one quarter of the solid cross-section and the stiff core allowing for a sevenfold increase in stress in this example.
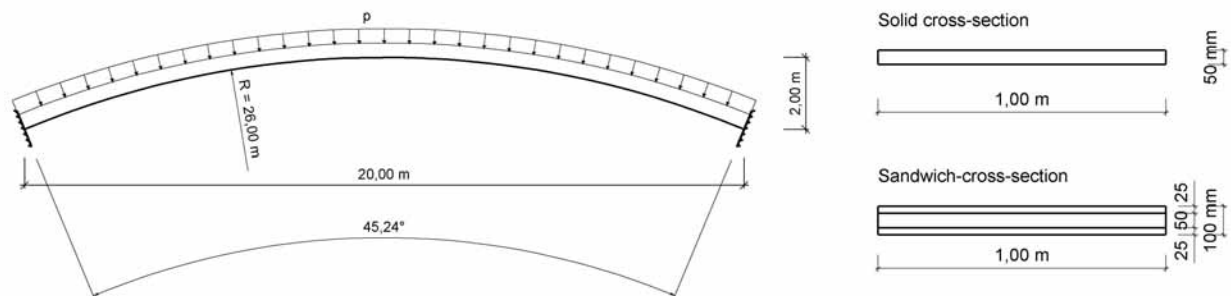
Fig. 9: Structural system of the flat sandwich-arch

According to Petersen [13] the bifurcation load for a 50 mm thick solid cross-section amounts to p_{ki} = 2.87 kN/m² . The respective compression is σ_{ki} = 1.5 MPa, thus far below the possibilities of UHPFRC. Finite elements are applied to determine the bifurcation load of the sandwich-elements, using an 8-node plane-stress-element with deformations. To avoid locking-effects EAS-attachments are added to the deformations.
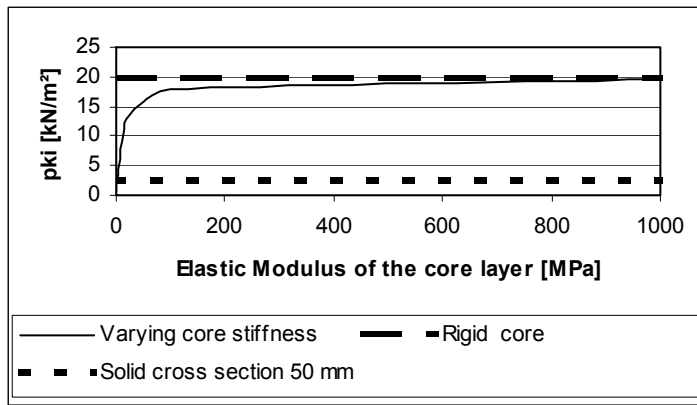
Fig. 10:   Load capacity depending on the elastic
modulus of the core layer

Fig. 10 clearly shows that in the case of stability problems even a low elastic modulus of the core layer significantly increases the load capacity.

Viable PUR- resp. PS-core-layers possess an elastic modulus of 20 to 100 MPa. This allows for an increase in load of 4.5 to 6.2.

6   Pre-Deformed Shells

6.1   Introduction

Contrary to plane surfaces curved surfaces are extensive and expensive to produce. The polygonal assembly of curved surfaces from plane elements results in a multitude of small parts depending on the shape and the curvature of the shell. The automotive industry uses punch presses to produce chassis parts and with the existing plastic deformation almost any shape is possible. This procedure may not be applied to concrete elements since deformation is limited and only very few identical structural elements are required. However, the reduced thickness of UHPFRC-elements provides a limited possibility to use pre-deformed structural elements, as the two following examples will describe.

6.2   Example 1: Roof for a Hot Water Storage Tank

The first example describes a roof intended for a hot water tank, to be built as a research project in cooperation with the University of Stuttgart on the university campus. This research project entails two laboratory storage tanks measuring 9 x 9 m for the testing of various linings. One of the two laboratory storage tanks is to be equipped with a floating cover, the other with a supporting UHPFRC-roof. After the testing of the various lining materials both laboratory storage tanks will be deconstructed and enlarged to a size of 12 x 20 m for continuous use over several years as research storage tank with the most suited materials. Fig. 11 shows the possible cover of the research storage tank, planned as a strut-and-tie structure. The one-dimensional tie allows for easy pre-deformation as long as the material used retains sufficient strength.

Cross-section

Tie and heat insulation
Heat insolation
UHPFRC

Varying, depending on the imposed load

15,00

Plan

20,00

12,00

0,50 1,00   12,00   1,00 0,50

15,00
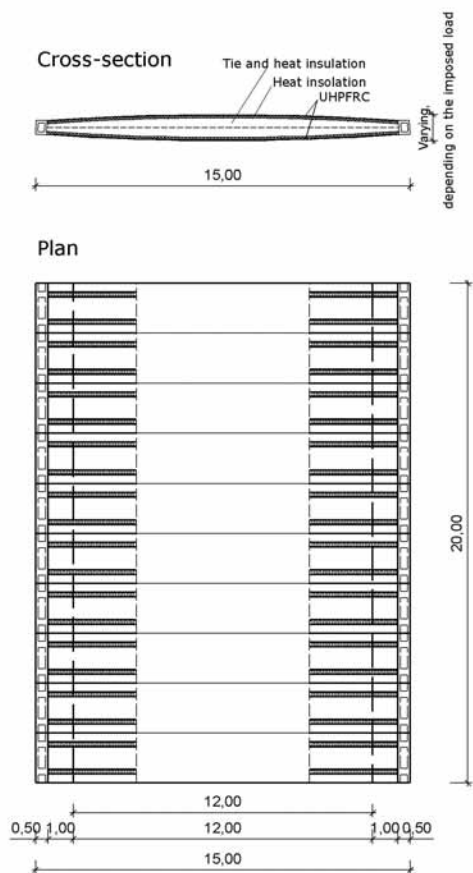
Fig. 11:   Cross-section and view of the basic roof structure

Fig. 12 shows a graphic depiction of the manufacture and pre-deformation-procedure. First the 20 mm thick tie is placed on a plane formwork. The formwork already contains a steam barrier to prevent any contact between the concrete and the water inside the storage tank. In a second step the two end girders are concreted. The pre-deformation-procedure of the plane tie is the third step. In this procedure the formwork beneath the tie is lowered to the desired measurement f and simultaneously the tie is positioned. After reaching the desired deflection, tie and strut form a self-stiffening structure. The tie as UHPFRC-element will be equipped with additional reinforcement; the strut will be UHPFRC-sandwich-element. This ensures an optimum use of the material.

UHPFRC   Formwork

①

②

Tie

③
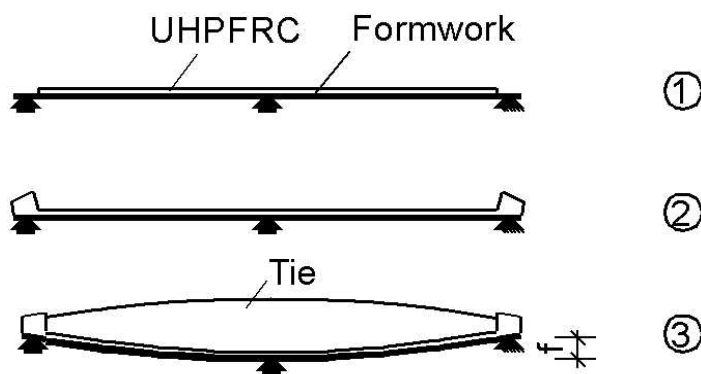
Fig. 12: Basic manufacture procedure of the pre-deformed tie

6.3   Example 2: Spherical Cap as a Roof of a Hot Water Storage Tank

The second example examines a pre-deformed spherical cap as suspended shell for the roof of a Hot water storage tank with a diameter of 33 m and cylindrical in plan. Contrary to the structural member of the first example, plane elements, even without constraint, experience

membrane stress, which stiffens the structure. This causes smaller deformations. A two-step-procedure is recommended also for plane structural elements. First the necessary pre-deformation is activated and then the deformation is blocked, using for example a ring girder. The blocking may be omitted for small loads such as dead load and snow since the loadbearing capacity will suffice. However, Fig. 13 clearly shows that high variations in deformations occur. Fig. 13 describes the non-linear load-deformation-behaviour of a roof without blocking (1), as well as a roof with blocking after reaching the deformation due to dead load (2) and a completely blocked system (3). The respective maximum membrane stresses are depicted in Fig. 14. They increase after blocking due to the smaller sag. Such a roof requires wire-reinforced UHPFRC for realization as may easily be derived from the described maximum stresses.
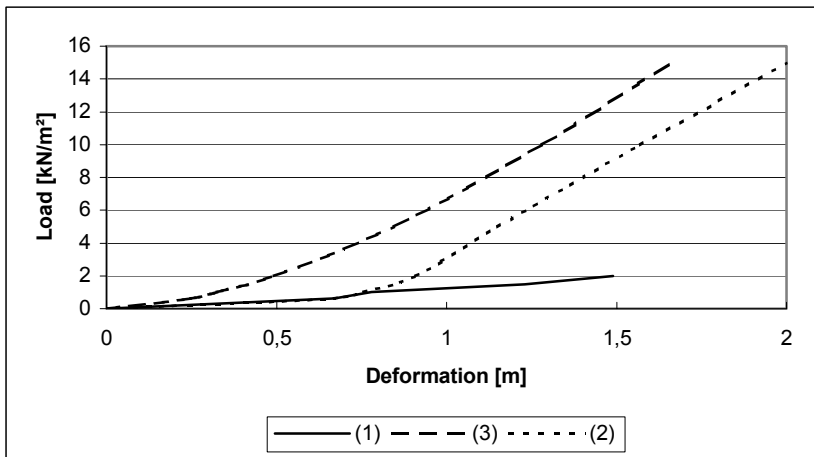
Fig. 13: Load-deformation-behaviour of the UHPFRC spherical cap
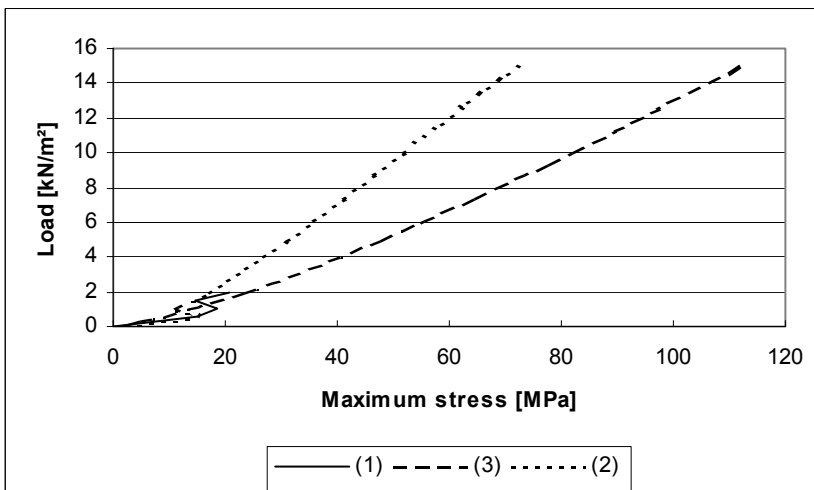
Fig. 14: Load-maximum stress-behaviour of the UHPFRC spherical cap

6.4　Prospect

Currently this procedure is expanded to include also structures under compression, sandwich-elements and additional shapes and geometries.

7　References

[1] Lichtenfels, A.: Schalentragwerke und Wärmespeicher aus Ultra-Hochleistungs-Beton. University of Stuttgart (in German, in preparation)

[2] Reineck, K.-H.; Greiner, S. (2004): Tests on ultra-high performance fibre reinforced concrete designing hot-water tanks and UHPFRC-shells. Symposium of Ultra High Performance Concrete, Kassel, 13 – 15 September 2004

[3] Hahne, E.; Fisch, M.N. (1992): Einsatz von solarunterstützten Nachwärmeversorgungssystemen mit saisonalem Wärmespeicher. Forschungsbericht zum BMFT-Vorhaben 0328867A, Institute of Thermodynamics and Thermal Engineering (ITW), University of Stuttgart, June 1992 (in German)

[4] Hahne, E.; Fisch, M.N. (1995): Solarunterstützte Nahwärmeversorgung mit und ohne Langzeit-Wärmespeicherung. Forschungsbericht zum BMFT-Vorhaben 0328867C, Institute of Thermodynamics and Thermal Engineering (ITW), University of Stuttgart, June 1995 (in German)

[5] Fisch, N.; Möws, B.; Zieger, J. (2001): Solarstadt: Konzepte, Technologien, Projekte. W. Kohlhammer, Stuttgart, 2001 (in German)

[6] Reineck, K.-H.; Lichtenfels, A.; Greiner, S. (2001): Seasonal storage of solar energy in hot-water tanks made out of high performance concrete. in: Session A6: Energy and Conservation, Environmental Aspects in Operation, Aspects of Health and Working Environment, Proceedings fib Symposium "Concrete and Environment"Berlin 2001, 3-5 October. Ed. by: DBV - Deutscher Beton- und Bautechnik Verein E.V. Berlin, 2001 (in English)

[7] Reineck, K.-H.; Lichtenfels, A.; Greiner, S. (2002): HPC hot-water tanks for the seasonal storage of solar heat. p. 739 - 752 in: V. 1 Proceedings 6th International Symposium on Utilization of High strength / High Performance Concrete, Leipzig June 2002. (Edtrs. König, G.; Dehn, F.; Faust, T.). Leipzig University, Institute for Structural Concrete and Building Materials, 2002 (in English)

[8] Reineck, K.-H.; Greiner, S.; Lichtenfels. A. (2003): Wasserspeicher aus UHFB - Bemessung. S. 257 - 268 in: König, G.; Holschemacher, K.; Dehn, F. (Hrsg.): Ultrahochfester Beton - Innovationen im Bauwesen, Beiträge aus Praxis und Wissenschaft. Bauwerk Verl., Berlin 2003 (in German)

[9] Reineck, K.-H.; Lichtenfels, A. (1997): Entwurf und Bemessung von Heißwasser-Wärmespeichern aus Konstruktionsbeton, study within the research project BMBF 0329606C, Institute for Structural Design II, University of Stuttgart, 1997 (in German)

[10] Lichtenfels, A. (2004): Doctor thesis, University of Stuttgart (in German, in preparation)

[11] Schlaich, J. (1982): Neue und erneuerbare Energiequellen. Festschrift 75 Jahre DAfStb. DAfStb H. 333, 115-130, 1982 (in German)

[12] Schlaich, J. (1997): Bauen für eine solare Energieversorgung. Vortrag in Fachsitzung 2, Deutscher Betontag. 10. April 1997, Berlin. DBV-Tagungsband, 306-321, Wiesbaden, 1997 (in German)

[13] Petersen, C. (1982): Statik und Stabilität der Baukonstruktionen. Verlag Vieweg, Braunschweig, (1982)

Gregor Zimmermann

Dipl. Ing., PhD Student

University of Kassel

Kassel, Germany

Thomas Teichmann

Dipl. Ing., PhD Student

University of Kassel

Kassel, Germany

Membrane Concrete Grid Shells – UHPC Grid Shells

Abstract

Not at least the membrane constructions of Frei Otto's widespan lightweight structures [1][2] are well-known. Since then, the research for new, more efficient lightweight structures has continued. Research groups engage in constructions using membranes, cable nets or shells. However, the combination of building materials is not new nor is the combination of concrete and membranes. Nevertheless, to achieve the ideal utilisation of concrete and membranes, it is necessary to adjust the construction to the special material properties. The patent "membrane concrete composite construction" (Fig.1) takes a step forward towards the further development of structure combinations. With this method not only the different materials complement one another, but also does the structural design of the complete construction.

The construction results from the special manufacturing. A two-part membrane shell is made which provides an integrated chamber system between both membranes. The shell is fixed to the floor and inflated by air pressure, similar to pneumatic buildings. When the form of the building is completed, the chamber system is inflated by overpressure. Finally the chamber system is filled with concrete e.g. UHPC (Ultra High Performance Concrete).

After the UHPC is compressed, a grid shell is formed which primarily is stressed by compressive forces. Then the air pressure inside the building can be reduced which results in a lightweight structure made of "membrane concrete". With this method, the membrane system could fulfill several functions which do not only serve for sheeting but under special circumstances also for statical structures. Preferably new materials, for example, UHPC (Ultra High Performance Concrete)[3] should be used which allow a well-optimized lightweight wide span construction.

To investigate the suitability of ultra-high performance concrete (UHPC) for membrane concrete grid shells, first tests with a powder concrete UHPC C200 with a 1.5 v. -% share of fibres were already done.

The present outline illustrates the idea of "membrane concrete composite constructions" and first results of the concrete investigations. It will provide an insight into the basics and presents possibilities for research and further development of the invention.

Keywords*: Membrane, concrete, UHPC, air-inflated hall, shell, grid, pneumatic controlling, connecting details, form finding, two-part shell construction, grid shell structure, BIONIK structure.*

1 Membrane Concrete Grid Shells – The Idea

The main idea was to combine different construction or assembly types to get a new structure. Main focus was the use of new materials and technologies to point out their technical advantages as well as the development of cost-effective construction systems. Secondarily an architectural appealing system should be the result of the new construction system.

In the last decade some new technologies in the building industry had been developed but not often used jet. New concrete types like UHPC (Ultra High Performance Concrete) that could absorb large pressure and tension forces or Membranes with new surface coatings that are more resistant against environmental influences.

The Idea of combining pneumatic moulds and concrete shell structures is not new. Innovative is the use of UHPC that includes the reinforcement in combination with inflated double layered membrane structures which are connected to each other directly or with membrane flaps. Those are arranged in a special way that continuous chambers are created which could be filled with UHPC. The result is a "Membrane Concrete Grid Shell", particularly a thin wide spanning concrete grid shell with a nearly arbitrary grid respective mesh.

The following paragraphs will describe the components, the construction system as well as details and the first concreting test series.

Figure 1:   Sample of "Membrane Concrete Grid Shell"

1.1 Basic Components and Constructions

The MBG system consists of different independent constructions and materials which will fulfil different static tasks during the assembly of the building and the completion. As there are:

1.1.1 Membrane

PTFE Foils, PTFE coated fibre fabrics, PVC coated Polyester fabrics and ETFE Foils are used in textile architecture. For large inflatable structures with high loads PVC coated Polyester fabrics are the common membrane types. Five classes, from TYP I with low permissible stress (3000 N/5cm) up to TYP V with high permissible stress (9800 N/5cm) are available.

Regarding to MBG structures, the internal pressure, the concrete load and the resulting tensile stress is very low. Depending on the size of the structure it is possible to use membranes TYPE II or TYPE III. The connection respective membrane details are easy to manufacture. High frequency weldings or clamping plates are very simple and cost-effective. In combination with hook and loop fasteners or other zip connections the membrane could be removable. [4]

1.1.2 Concrete

Concrete in a large variety is obtainable. Relating to MBG structures, concrete with integrated reinforcement should be used. The reduction of weight respective concrete load during the assembly of the MBG inflated system and the minimization of concrete for structural, architectural and design aspects are the main idea. For this, the UHPC (Ultra High Performance Concrete) which is developed and adapted for the MBG structures by a research cooperation of the University Kassel, is the best choice [5]. UHPC is a self-compressing concrete with a high Young's module and a high permissible strength. Among other things, the integrated steel fibres achieve this property. The compressive strength of UHPC could be between 200N/mm² and 400N/mm². The Young's module is about 55000 N/mm². Splitting tensile strength is up to 17 N/mm² and bending stiffness 39 N/mm². Further values are W/b=0.2 and w/z=0.28. These are approximately given specifications that could be changed for the needs of MBG structures. The material could be pumped with a piston pump, thus allows a simple handling.
First tests on concreting membrane tubes with a special developed UHPC are described in chapter 3.

1.1.3 Inflated Structures & airforms

Inflated structures in the building industry are known since 1918. F.W.Lanchester developed a patent >> An Unproved Construction for Field Hospitals, Depots, and like purposes << [6]. Since than a lot of pneumatic structures had been build. Pioneers like Frei Otto and Walter Bird evolved a lot of forms and membrane materials. With the introduction of new technologies and computer aided design totally new pneumatic structures and shapes are possible.

Figure 2:   NouvelleDestination ipl © ;
                 portable inflatable exhibition environment | inflate design ©

The first concrete domes with the use of airforms had been built by Wallace Neff in 1940 [7], [8], [9]. It was a single layer dome membrane. The reinforcement had to be fixed from outside and was covered with shotcrete. This kind of construction method is not substantially changed till today. In 1987 Werner Sobek developed mathematical methods to calculate inflatable structures under concrete load and form finding air supported concrete shells [10].

1.1.4   Theory on Concrete Grid Shells

Steel, wood or bamboo is often used to build grid shell structures [11], [12]. Concrete is an exception, finally not of the material itself, but because of the complex formwork. The cost of a concrete grid shell is out of all proportion to the structure .

So there is nearly no experience with monolithic concrete grid shells. A lot of questions are open and interesting research topics could be defined. An important question is the stability of such an concrete grid shell under dynamic loads during assembly like dynamic wind loads and   the stability after completion through e.g. earth quakes. Especially because of the atypical shape and mesh of architectural designed concrete grid shells that could be found with special optimization algorithms as there are structure optimization, CAO (computer aided optimization), SKO (Soft Kill Option), evolutionary design or generative design. The result could be optimized shells that are not comparable with the typical steel or wooden beam gird shells.

1.1.5   Assembly Method

Figure 3 shows assembling the MBG system on side. The double-layered membrane is outspread on the ground and the edges fixed at the circumferential foundation. The System will be erected by inflating the airform. After the inner maximum pressure is achieved, the second membrane chamber system could be inflated. This will simplify the handling and reduces deformations through wind. Concreting sections from the foundations to the top or pole will be defined and filled with UHPC in an special order and given time steps. The

dimensions on these concreting sections are depending on the size of the whole MBG construction.

This remark represents the simple idea behind the construction. In further paragraphs you will see the complexity of the interdependencies for airforms, concrete grid shells and structures.

Figure 3:   Construction assembly scheme of a simple MBG dome.

1.2   Airform and Concrete Gird Interdependency

Several physical states of the construction will appear. Particularly the UHPC will change his properties during time extremely, from a very fluent to a high compressed material. These Properties must be considered for designing airforms and concrete grid structures. Also the airform itself demands a special geometry and construction to work as concrete mould. The Gridshell must fulfil several static functions to be stable, which depends on the geometry of the grid mesh and the airform. So every construction part or detail is associated with other parts or functions as shown in Figure 4. To understand all these effects, some construction topics will be explained roughly.
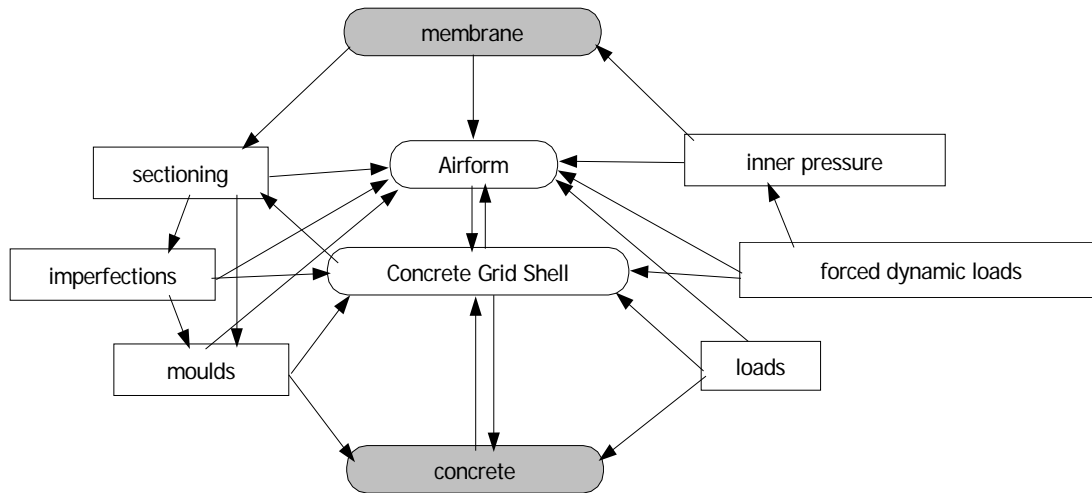
Figure 4: Sketch: Interdependencies of airform, concrete grid shell, materials…

1.2.1   Mould Geometry

The airform or mould exists out of two layers membrane, connected via direct welding or flap (Figure 5). Space between those weldings will act as concrete chambers. The mesh could vary on the surface and generate different patterns. Those patterns are arbitrary. Depending on the curvature of the surface, the mesh could be adapted. With this simple concept it is possible to generate concrete grid shells within a large solution space. The final geometry of the concrete chambers respective membrane moulds must be recognized for the patterning of the airform. Wrikels could weaken the concrete profile extremely.
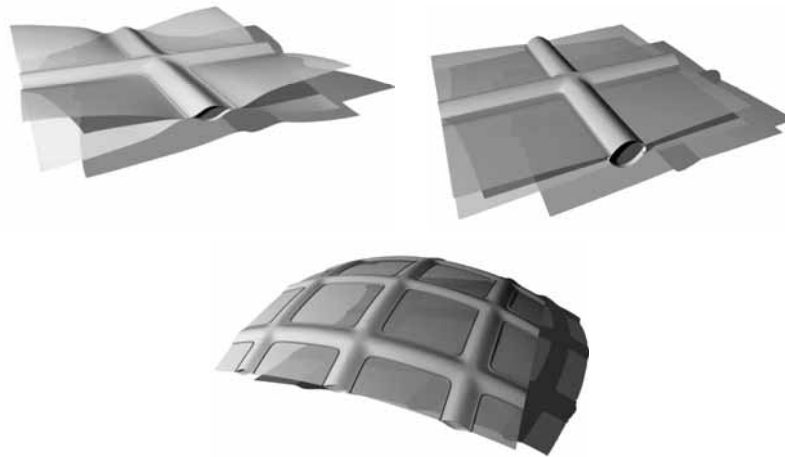
Figure 5: Two welded membrane layers (left) and with membrane flaps (middle) filed with concrete; double curved MBG mould structure (right)

To produce that complex double-layered membrane moulds demands a high technical understanding and production facilities are required. Generally it is possible to build almost every pneumatic supported form.

844

1.2.2 Forced deformations and vibrations on UHPC

Normally concrete must be compressed. UHPC is a self-compacting material and concrete vibrators could be dispensed. Interesting are the first hours after concreting. The material will pass through different phases:

· Unset concrete

· Solidifying concrete

· Hardening concrete

Forced deformations or vibrations on unset UHPC could be beneath notice. Quite the contrary the UHPC properties could be improved through additional compression.

Phase transformation from solidifying to hardening concrete under forced deformations or vibrations could be disadvantageous.

Squalls, wind or snow loads on the airform will cause deformations in geometry. Those deformations will be assigned to the hardening concrete structure. If those additional forces are high, the permissible stresses of the UHPC could be reached and the structure could be damaged before completion. This depends on the dimensions, inner pressure of the airform and must be considered during dimensioning the MBG structure.

The strength of UHPC as a function of time and forced vibrations in combination with concreting geometry must be researched to allow pre-dimensioning of UHPC grid shell structures.

1.2.3 Friction between airform and UHPC

UHPC and membrane are in direct contact. The concrete is placed between membrane-chambers. So the direct friction between membrane and UHPC is not a very important characteristic value for static reasons.

Some boundary conditions must be defined for the process of concreting. Advantage of using UHPC is the possibility to create very thin grid shell structures. So the concrete chambers could be very flat. In this case, the friction between UHPC and Membrane must be very low otherwise the concrete will clump because of the included reinforcement steel fibres and plugs the chamber system.

PVC coated polyester fabrics do have a roughness density of 29 μm under normal conditions. If the membrane is under strong pretension, the roughness density increases up to 128μm [10].

The concrete must not stick at the membrane because concreting starts from foundations to the top in sections.

1.2.4 Theory on Concreting in Sections

A major aspect is the classification or sectioning of concreting zones in vertical or horizontal direction. The size of those zones will depend on the size of the airform, the grid of the concrete structure and handling.

Remark 1: Concreting will start from foundations to the top. To guaranty a uniform allocation of concrete in the champers and to prevent large death load deflection it is necessary to provide spaced valves in horizontal and vertical direction.

Remark 2: Deformations caused by death load must be avoided. Concreting the complete structure in one step will cause large deformations on top and at the foundations. This could have fatal negative effects to the final concrete grid structure. High stressed areas and moments could destruct the structure. Implementing this knowledge in the dimensioning of the structure could solve this problem in a dowdy way.
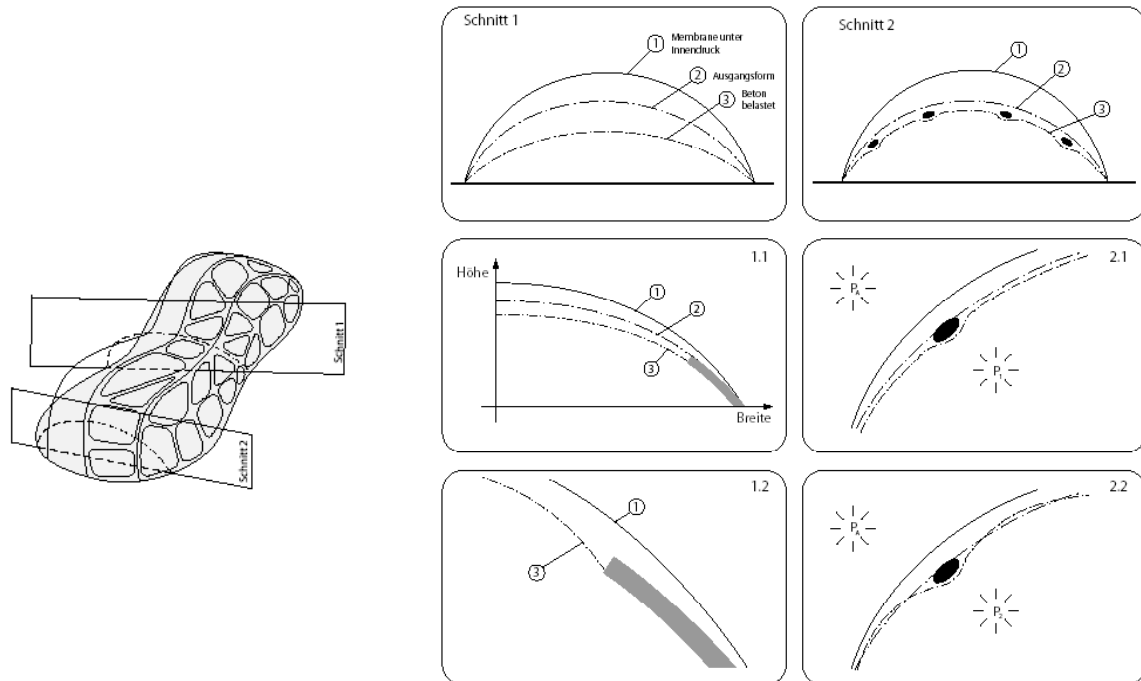
Figure 6:   Sections with the concrete structure under construction

Remark 3: Small concreting zones could effectuate reducing deformations. Therefore the complete structure will be build of several dependent concrete systems. Figure 3 shows the schematic of the system.

After concreting the first section, the death load of the concrete will deform the airform. The intensity depends on the inner pressure and other forced loads. A small deflection to the pre-set position will be implemented. To reduce the total deflection of the structure, changing the inner pressure must regulate the deformation during the second concreting phase. If this will not be considered, the concrete structure will have buckles and the static properties are enervated.

Remark 4: The segregation of UHPC during concreting could be a problem. Steel fibres are integrated pro rata to the volume of concrete. Ideally the fibres are allocated consistent in the volume after preparing the UHPC. Unclear is the allocation of fibres after concreting. A segregation in the injection pump as in the membrane chambers is possible. Concreting in sections will reduce this segregation effect in the total system.

1.2.5   Contributing static UHPC properties during further concreting steps

The previous paragraphs are showing the advantages of concreting in sections. With this, the grid structure will be produced out of several single grid structures, which are connected

rigid. Also the single grid shell structures have to work as stiffening systems during the subsequent concreting steps.

Depending on the section concreting speed the hardening even solidifying UHPC structure has to handle with forces from changing inner pressure, further forced loads or the death load of the subsequent grid structure. The dimensioning of the concrete profiles have to be coordinated to this aspect.

2 UHPC Test Series for Membrane Moulds

To implement all the parameters of geometry, deformations, forced loads, death loads, mesh and structure it is necessary to know the properties of UHPC, but not only the properties itself. Rather the behaviour of UHPC in the injection pump, the handling of pumping into a membrane chamber. Also the material properties during pumping, filling the concrete chamber, solidifying and hardening in the chamber have to be evaluated. The material interaction of UHPC and membrane and steel fibres could be interesting. To get some information on those topics, a test series for concreting in membrane chambers was accomplished.

2.1 Assembly of Test Series

To prove a couple of interdependencies and parameters we arranged an UHPC-Membrane test series. Thus a 3m membrane tube with 12cm diameter and filler neck was assembled. The tube was directly connected to a concrete spiral pump type PFT N 2V. A crane suspended the tube during concreting and hardening.

Figure 7: Spiral pump type PFT N 2V and filled 3m membrane tube $\varnothing$12cm

2.2 Mixing and Pumping

In pumping investigations a fine particle concrete M1Q with a maximum aggregate size of 0.5 mm, consisting of quartz sand and 733 kg/m³ cement was used. To increase the tensile strength the concrete was reinforced with 1.5 vol.-% steel fibres (D/L=0.15/9 mm). The mixing proportions are shown in table 1.

The cement used was a CEM I 52,5 R HS/NA, being advantageous for UHPC because of its low C$_3$A and alkali content. The superplastiziser used for plastification was based on polycarboxylate ether. Slump test result of 65 $\pm$ 2 cm shows that the consistency was flowing to almost self compacting.

After mixing the fresh concrete, it was filled in a spiral pump and was pumped in the tube from bottom opening. The total pumping time at this test was 25 minutes. After pumping was finished, the opening was closed and the column with the concrete was leaved at 20°C vertically for 7 days.

Table 1: mixing proportions [13]

concrete		powder concrete M1Q
cement	kg/m³	733
silica fume	kg/m³	230
quarz powder	kg/m³	183
quarz sand	kg/m³	1008
coarse aggregates	kg/m³	-
steel fibres	kg/m³	118
w/c-ratio		0,24
w/f-ratio		0.44
resulting w/c-ratio		-
calc. packing density for 0-125 m		0.76 (Schwanda [14])
curing		at 20°C in tube

2.3 Strength

At 28 day age, the concrete column was demoulded and cutted to 16 cylinders of 12 cm hight. After every second cylinder a plate of 1 cm thickness was cutted (figure 8). From this plate two 4x4 cm samples were taked, in which steel fibre direction and content were determined at the centre and at the edge (figure 9). From down (cylinder 1), middle (cylinder 8) and upper (cylinder 16) four 4x4x12 cm prisms were cutted. In these prisms the fibre direction and flexural strength longitudinally and compressive strength laterally with respect to the concrete column were measured.
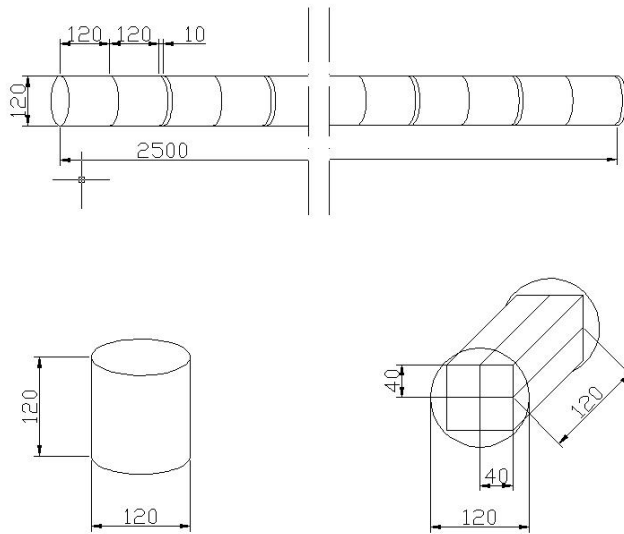
Figure 8: membrane, cylinders and prisms dimensions

The compressive and flexural strengths of all specimens were tested after 28 days, according to DIN 1048 and EN 196 (table 2). The specimens were cylinders (D/L = 120/120 mm) and prisms (W x H x L = 40 x 40 x 120 mm³).

Table 2:   compressive strength in longitudinal direction, compressive and flexural strength in transversal direction, spec. density

cylinder	compr. strength cylinder	compr. strength prism	flexural strength prism	spec. density	fibre share centre	fibre share edge
	N/mm²	N/mm²	N/mm²	g/cm³	a.-%	a.-%
1 (bottom)		190	17.8	2.484		
2 *	151			2.474	1.40	1.20
3	161			2.492		
4	148			2.505		
5	150			2.507		
6	156			2.504		
7	161			2.491		
8*		218	38	2.519	1.50	1.22
9	162			2.494		
10	166			2.520		
11	162			2.522		
12	144			2.531		
13	152			2.469		
14*	142			2.471	1.78	1.64
15	152			2.554		
16 (top)		218	17.6	2.489		

*at these cylinders the volume of fibres was determined

The average compressive strength was 155 N/mm² in the longitudinal direction. In middle of the concrete column (cylinder 6 to 11) compressive strength of the cylinders was 6 N/mm² higher. In transversal direction, at bottom (cylinder 1) compressive strength was 190 N/mm² while at middle and top (cylinder 8 and 16) compressive strength was similar and equal 218 N/mm².

The investigation of fibre direction illustrated that fibre direction was parallel to column axis, this is parallel to the flow of the fresh concrete. This reduces the compressive strength in longitudinal direction of the concrete column because they can´t take over lateral forces. Compressive strength of prisms laterally were at least 35 N/mm² higher. This increase not only depend on smaller sample dimension but also on fibre direction, which take over part of lateral force. The flexural strength of prisms was in middle of column 38 N/mm² and about 18 N/mm² at the bottom and top.
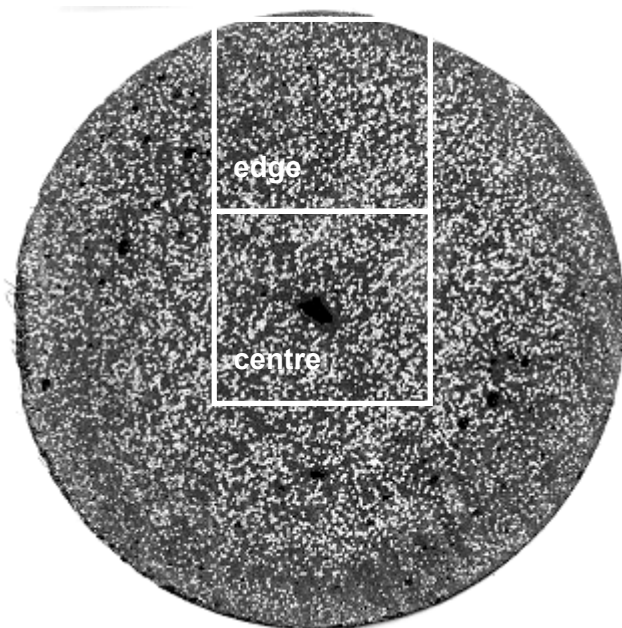
Figure 9: Cross-section of the cylinder 14, saw-cut, unpolish

The investigation of fibre content in lateral direction show that the amount of fibre in outer area is less than in the centre, figure 9. After polishing the 4x4 cm samples from edge and centre (figure 10) fibre content was analysed by picture analysis software. Until preparing this paper only the plates from cylinders 2, 8 and 14 were investigated.
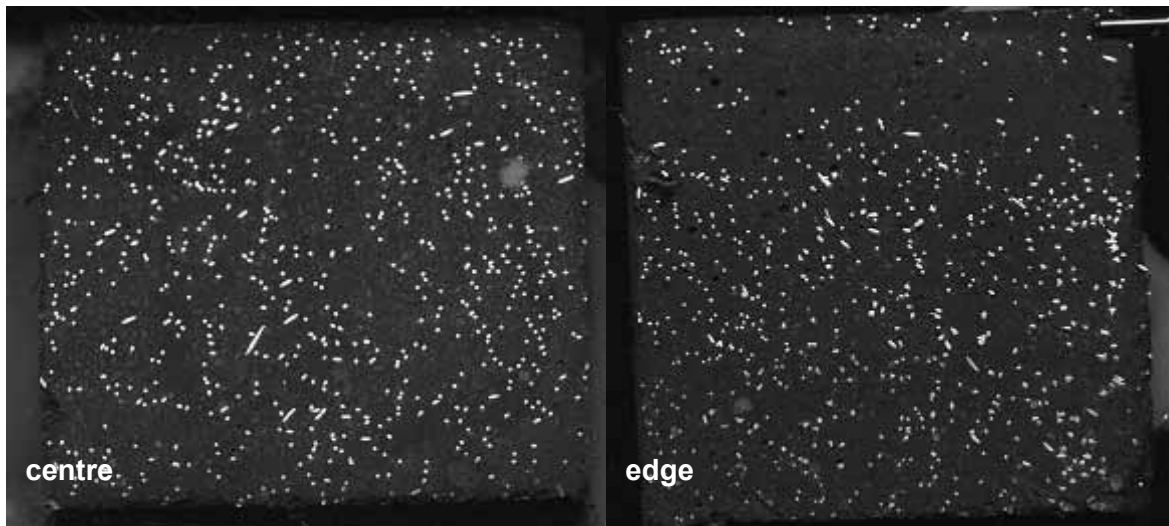
Figure 10: scan section for fibre distribution of cylinder 8; left: centre section, right: edge section, polished surface

The average fibre content in edge was 0.21 a.-% lower than in centre. At bottom part of the column the average fibre content was 1.30 a.-% while it increased to 1.36 a.-% and 1.71 a.-% in middle and top parts respectively.

3   Conclusions

With this brief description of the "membrane concrete grid shell" research project you grasp the complexity of membrane grid shell structures. The ideas behind this system are simple and realizable. UHPC allows a very minimal dimensioning of those structures. Airforms and moulds could be form-fined and patterned with special software. The technologies to manufacture and build those structures are given.

The biggest challenge consists in the calculation of optimal respective minimal structures and their adaptation to the airform. For this computing and optimization methods are found and have to be improved. The return calculation of the structure's UHPC loads onto the geometry of the airform during assembly and its patterning will be complicated. Secure is, that these in theory determined findings must and will be tested with preproduction models. For more determination of the performance of UPHC used in membrane constructions more investigations are required.

At the best, a construction method is enhanced, which allows the realization of cost-effective large wide spanning light weight structures out of concrete grid shells with an very short construction time because of the few amount of concrete and the simple air supported membrane mould.

5   References

[1] Bach, K.; Burkhardt, B.; Otto, F.: Seifenblasen - Forming Bubbles; IL 18: Karl Krämer, Stuttgart: ISBN -3-7828-2018-5

[2] Otto.F.: Lufthallenhandbuch, Air Hall Handbook; IL 15: Karl Krämer, Stuttgart: ISBN -3-7828-2015-0

[3] M. Schmidt: Ultra-Hohfester Beton, Ultra Hochleistungsbeton - Ausgangsstoffe, Eigenschaften und Leistungsfähig: university press, Kassel (2003); ISBN 3-89958-518-6

[4] Koch,Klaus-Michael,: Prestel, München (2004) : ISBN -3791330489

[5]   Bornemann, Schmidt, Fehling, Middendorf: Beton- und Stahlbetonbau :Ernst und Sohn, Berlin; ISBN 2001458-467

[6] Lanchaster: Improvements in the construction and roofings of buildings for Exhibitions and like Purposes : Patent GB000000145193A (1919)

[7] Wallace Neff, Building construction : Patent US000002335300A (1941)

[8] Wallace Neff, Verfahren zur Herstellung von schalenförmigen Baukonstruktionen: Patent DE000001052103B (1959)

[9] Wallace Neff, Improved method of erecting shellform concrete structures : Patent S000002892239A (1952)

[10] Sobek, Werner: Dissertation: Universität Stuttgart; Verlag G. Sobek, Stuttgart (1987); ISBN 3-9801085-1-1

[11] Chilton, John: Architectural Press, Oxford: ISBN -0 7506 3275 5

[12] Bulenda, Knippers, Sailer: Finite Elemente in der Baupraxis, Modellierung, Berechnung und Konstruktion; Untersuchung zum Tragverhalten von Netzkuppeln; Beiträge der Tagung FEM '95: Ernst und Sohn, Berlin (1995): ISBN 3-433-01289-X: 201-211

[13] Bornemann, R.; Schmidt, M.; Fehling, E.; Middendorf, B.: "Ultra-Hochleistungsbeton – Herstellung, Eigenschaften und Anwendungsmöglich-keiten"; Beton- und Stahlbetonbau, Jahrg. 96 (2001), Heft 7, S. 458 – 467

[14] Schwanda, F.: Das rechnerische Verfahren zur Bestimmung des Hohlraumes und Zementleimanspruches von Zuschlägen und seine Bedeutung für den Spannbetonbau; Zement und Beton 37, 1966, S. 8-17

J. C. Walraven
Professor of Concrete Structures
Delft University of Technology
The Netherlands

Designing with ultra high strength concrete: basics, potential and perspectives

Summary

Ultra High Performance Concrete is a very recent development. Although the cost of this material is higher than the cost of conventional concrete per m^3 it is nevertheless competitive, because of the much lower volume of material that is needed/ to realise structural elements. Additional advantages are lower transportation costs, lower maintenance costs and a longer service life. Furthermore UHPC has a high potential for upgrading and extending existing structures. It should be realised that the large area between B100 and B200 offers particular chances and should not be ignored. Attention should be given to practical code recommendations, covering the whole possible spectrum of possibilities in a consistent way. UHPC offers a wide and promising perspective.

Keywords: *Ultra high strength concrete, future, perspective*

1   From FRC to UHPFRC

Fibre reinforced concrete has been a promising material for many decades. Substituting traditional reinforcement by fibres is an attractive idea from the viewpoint of labour efficiency. Adding fibres to a concrete mixture is much easier than fabricating and placing reinforcement, especially if particular shapes are required. The disadvantage of fibres, however, is that they are basically oriented in all directions. If centric tension is concerned, a considerable overdose of fibres would be necessary in order to meet the structural demands. Therefore fibre concrete is much more suitable for cases where redistribution of forces and stresses can occur. This is already the case for simple bending. It can easily be shown that a hardening type of behaviour - that means that the ultimate bearing moment is larger than the flexural cracking moment - is obtained if the residual "plastic" tensile strength of the fibre concrete is higher than about 1/3 (0,37) of the flexural tensile strength of the plain concrete, Fig. 1.
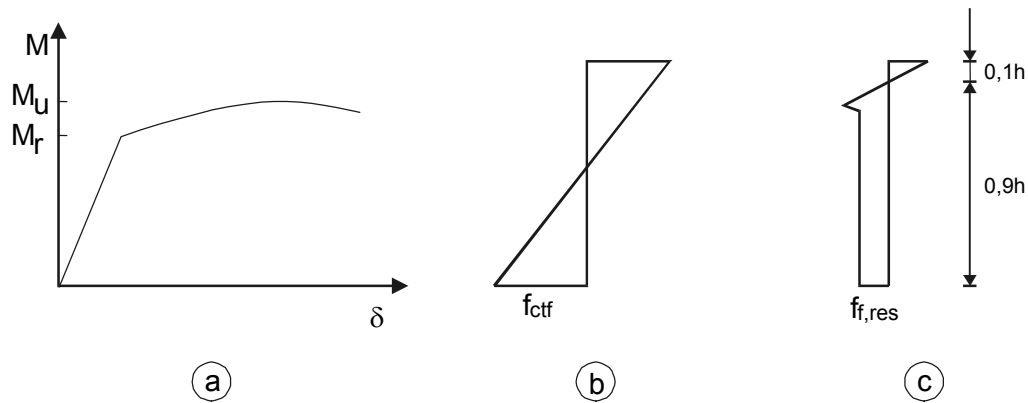
Fig. 1. Description of minimum conditions for hardening behaviour of FRC.

    a. Load-deflection curve of FRC beam

    b. Cross-sectional stress distribution at cracking moment

    c. Cross-sectional stress distribution at ultimate moment

For this comparison the flexural cracking moment of the plain concrete is formulated as:

$$M_r = 0,67h \, (0,25bh \, f_{ctf}) \tag{1}$$

and the ultimate moment as:

$$M_u = 0,5h \, (0,9bh \, f_{f,res}) \tag{2}$$

where f_{ctf} is the flexural tensile strength of the plain concrete and $f_{f,res}$ is the residual "plastic" tensile strength of the fibre reinforced concrete. From Eq. 1 and 2 it follows that M_u is larger than M_r if $f_{f,res} > 0,37f_{ct}$. Depending on the fibre type used, this condition is met at a minimum fibre content of about 30-40 kg/m^3. From a technological point of view such a content is no problem, even for conventional concrete mixtures. The three-dimension fibre orientation needs not always to be a disadvantage. In the case of for instance tunnel segments, about 100 kg/m^3 traditional reinforcement is necessary in order to cope with the effects of bending moments and splitting forces. However, the location, the direction and the magnitude of splitting- and spalling forces is hard to predict, because they depend on fabrication- and placement inaccuracies of the elements. Furthermore, for durability reasons, the cover to the reinforcing bars is mostly larger than 35 mm. It is remarkable that in this case more cover means more damage to the element in the construction stage, because spalling effects concern especially the cover region, Fig. 2. Fibres, however, are present anywhere and in any direction and are thus highly efficient in order to cope with such structural actions. This was confirmed by a pilot project, involved in the construction of the 2nd Heinenoordtunnel, the first bored tunnel in The Netherlands [1]
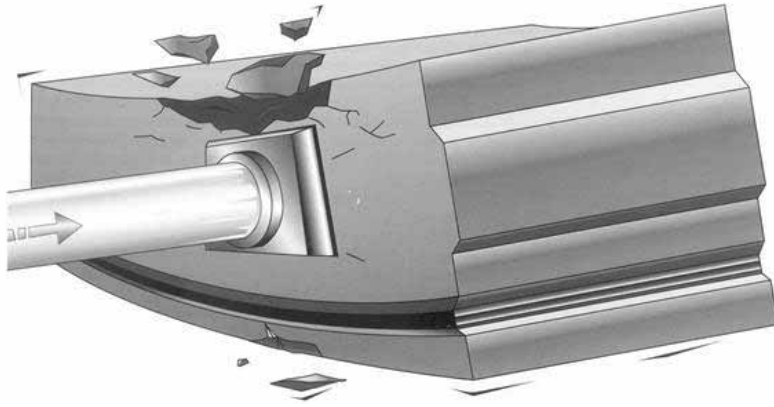
Fig. 2.   Spalling in a lining element of a bored tunnel: a case for fibre reinforced concrete

In this case 60 kg/m^3 hooked-end fibbers were successfully applied. Those fibres had a high carbon content and consequently a yield strength, which was nearly double that of traditional fibres. This was necessary because of the relatively high strength of the lining concrete.

Fibre contents over 80 kg/m^3 were, for reasons of concrete technology, hardly possible because of the reduction of workability of the concrete and the occurrence of "fibre-balling". So, by this practical upper limit to the fibre concentration, it was not possible to enter the area where fibre reinforced concrete would really be a practical and economical solution to many structural problems.

Normally in technical sciences "moving the borders of knowledge" is a gradual process. However, not in this case. After years of research had been invested in extending the concrete strength classes from B65 to B105 (newest Eurocodes), especially French researchers showed that B200 could be made, and even produced on an industrial basis. This was based on a new, revolutionary way of thinking about the technology of concrete. In order to obtain
not only an ultra high strength concrete, but rather ultra high performance concrete (ductility), four principles were defined:

1. The size of the maximum particle should be drastically reduced to obtain better homogeneity.
2. The highest possible particle packing should be obtained be combining fractions of various types of aggregate.
3. The amount of water should be kept as low as possible.
4. Short fibres should be added to guarantee excellent ductility

Especially step 3 was revolutionary, because this was contrary to classical thinking. Traditionally, so much water should be added that all the (expensive) cement would hydrate. The additional water was considered to be necessary for workability. However, after the

invention of high performance superplasticizers, the last argument could be omitted. Further it was realised that residual water might have a very negative effect on the concrete microstructure: the porosity and the permeability are increased and, by moisture gradients occurring during water migration, which is inevitable in concrete, internal pressures occur which can lead to microcracking and loss of favourable properties.

Fig. 3 shows the casting of a precast beam for the first European UHPC bridge in Bourg-les-Valence, France, by the Dutch firm Hurks Beton. The material was quite tough (highly viscous) during casting, but it appeared to be nearly self-compacting.

Fig. 3. Casting a UHPFC beam by Hurks Beton, the Netherlands, for the viaduct Bourg-les-Valence (France).

2 The long way to design recommendations for FRC

In order to design in fibre reinforced concrete of any type, design recommendations are necessary. It is remarkable that it appears to be extremely difficult to agree on the basics of designing with fibre reinforced concrete in general. This has different reasons. On the one hand there is certainly a commercial aspect. Different fibres have different characteristics and therefore a different behaviour. There has always been a rather lively discussion on which properties are needed for design. An important aspect is, however, most and for all, the representivity of the test results. There have been many propositions, such as the centric tensile test, the three- and the four points bending tests with or without notch, the splitting test and the circular slab test. From a scientific point the most objective test seemed to be the centric tensile test on a cylinder, drilled from the structure. However, centric tensile tests are difficult to perform. Furthermore, since the size of the cylinder is limited for practical reasons, the aspect of scatter of fibre content, distribution and orientation cannot be ignored. Moreover, there is a boundary effect: at the edges the fibres are sawn-through and not

anchored.   All the other tests have the practical disadvantage, that they show an "integral" behaviour. The basic stress-displacement relation or stress-strain relation has to be found by inverse modelling. Finally RILEM [2,3] choose the three point bending test with a notch as the basis for deriving the basic stress displacement (strain) relation.   The stress-strain relation has to be calculated from the load-deflection relation with a prescribed procedure. The resulting basic stress-strain relation is shown in Fig. 4. In order to get
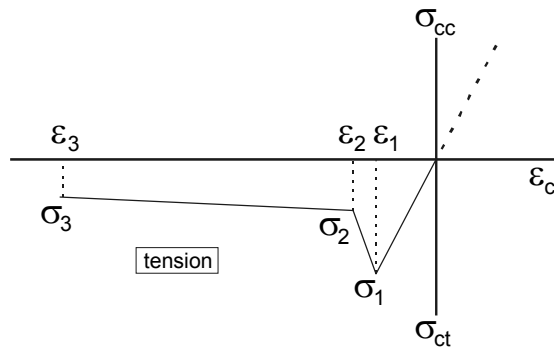
Fig. 4.   Basic stress-strain relation for conventional FRC, according to RILEM [2,3]

consistency in test results, the procedure of filling the mould and compacting the concrete has been prescribed very strictly. It is known that otherwise a too large scatter would occur, because of variations in fibre concentration, orientation and as such effectivity. However, if this is recognised for the basic test, it should be kept in mind that casting and compaction in a real structure is not accurately described. Therefore it might be wondered how representative the apparently accurate stress-strain relation, obtained under laboratory conditions, is for FRC cast at the building site. In large structures, with for instance long yield lines, the behaviour will be averaged, but in for instance linear structures with small cross-sectional dimensions, there might be a preference orientation, which can be both favourable and unfavourable. A questionable aspect in the RILEM recommendation is the definition of a size factor, which deviates only slightly from that for plain concrete [4]. Theoretically the size effect should tend to disappear with increasing ductility of a material. It was shown in Kooiman [5], that ignoring the effect of fibre distribution could lead to misinterpretation of the size effect. This is certainly an area to be further considered. For UHSFC meanwhile a French recommendation is available [6]. Also here a basic stress-strain law is defined. Fig. 5 shows the simplified version. Contrary to the RILEM relation for traditional fibre reinforced concrete, in this case the influence of mixing and placement of the concrete is regarded. Therefore characterisation tests are defined depending on the type of structure studied (thin slabs, thick slabs, beams, shells) and depending on the type of action exerted on it (centric tension, bending). The recommendation gives for any test procedure the conversion factors to obtain the basic-stress strain relation. Furthermore the recommendations give instructions for taking into account the effect that the placement method has on the real strength values to be considered in calculations. This correction of the basic (intrinsic) strength curves

consists of applying a reduction coefficient 1/K representing the difference between the intrinsic curve and what would have been obtained on specimens taken from an actual structural element. To determine the K-factor, the recommendations impose suitability tests conducted on a representative model of the actual structure.
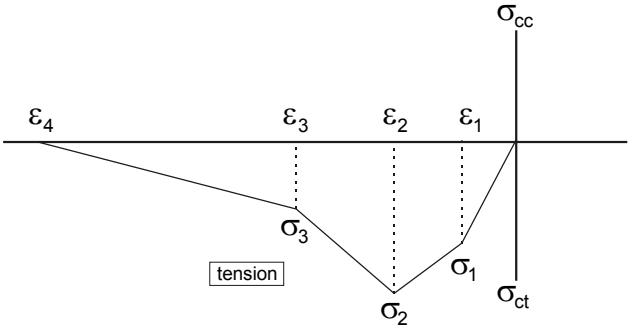
Fig. 5.　　Stress-strain law for UHSFC according to French Regulations [6].

The recognition of this important phenomenon makes the French proposal very valuable. Nevertheless further research in this area is certainly useful.

The significance of fibre orientation was recently demonstrated at a number of experiments at TU Delft [7]. As an example fig. 6 shows the fibre orientation at various positions in a tunnel-lining element, which was cast with a self-compacting fibre concrete (f_{ccm} = 65-70 MPA, 65 kg/m^3 of steel fibres). The element was cast in a horizontal position, with lower and upper formwork. The concrete was mixed in a truck-mixer and cast into the mould through a gutter, consisting of a half-open pipe. Afterwards cylinders were drilled out and slices of them were investigated with Röntgen photography. The differences in orientation were remarkable. The orientation numbers varied between 0,24 and 0,91.
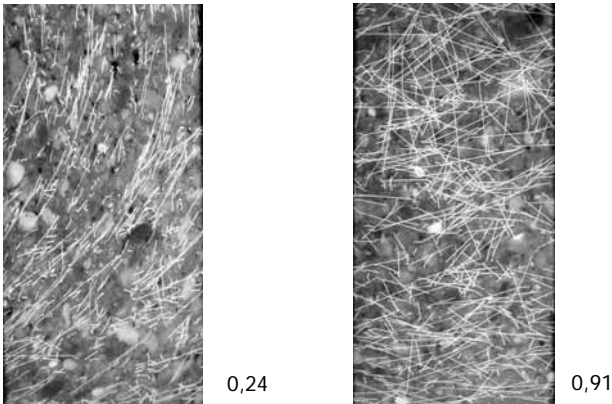
Fig. 6.　　Fibre orientation in a tunnelling element cast with self-compacting fibre concrete

3 Considering the strength region between B100 and B200

It was shown before, that the development to ultra high strength fibre concrete developed shockwise. The long history of achieving concrete with strength of B100 was followed by a jump to B200. However, it should be investigated whether what the range in-between could offer to the building industry. An example is the production of sheet piles of HPFC, Fig. 7. The

Fig. 7.   Production of a prestressed sheet pile of UHSFC

Piles are prestressed in longitudinal direction by strands, but have no further reinforcement, apart from the fibres in the mixture. The concrete mixture consisted of 913 kg cement, 61 kg. microsilica, 207 litres of water, 1098 kg of aggregate with a maximum diameter of 1 mm, 125 kg of straight steel fibres (13 mm length) and 21 litres of superplasticizer. The cube compressive strength after 24 ours was already 74 Mpa. Hence, the elements could be demoulded very quickly, After 28 days the cube compressive strength was 120 Mpa. The centric tensile strength was 6 MPA after 1 day, 12 Mpa after 1 week and 13,5 Mpa after 28 days. The price of this concrete was about 445 Euro/m^3. This seems quite high at first sight, but it should be realised that the piles have a thickness of only 45 mm in stead of 120 mm for traditional concrete B65. So the volume of concrete necessary is only about 1/3. Because of the much smaller cross-sectional area less prestressing steel is necessary, and because of the fibres no further reinforcement is required. Another advantage is that the UHPFC piles, contrary to the B65 piles, can be stacked on one another and can therefore very economically be stored and transported. At the site they can be handled more easily. So, finally, the price of a UHPC element is hardly higher than that of a classical concrete pile. It should be noted that the price of the steel fibres was a very substantial part of the total price. 63% of the m^3 price of 445 Euro was consumed by the fibres. So, if UHPFC could reach the

level of bulk-application, design and construction with such elements would become more economic than traditional concrete, if calculated on the realistic basis of integral cost.

It was remarkable, that the fibres tended to orientate into the axial direction of the sheet piles. The casting procedure and the flow of the concrete caused this. The formwork for the element was placed in longitudinal direction, Fig. 6. The concrete was cast from the top, and could flow between the formwork for the flanges and so reach the lower flange. After filling the formwork locally, the concrete could flow into the longitudinal direction. Because of the small wall-thickness of the element, a substantial part of the fibres orients into the longitudinal direction by touching the formwork or the prestressing strand. This is favourable for the behaviour in bending but less for the shear capacity of the keys between the piles, which are loaded in transverse direction. Tests showed, however, that the shear capacity of the keys was still sufficient.

In a later step it was studied whether it is possible to make the mixture cheaper by using aggregate fractions available on the market, in stead of carefully composing the particle gradation in the laboratory. The study showed that nearly equivalent mortars could be developed with different particle size distributions [7].

Another interesting application of a concrete, which is in-between the more conventional high strength concrete and the ultra high strength concrete, is the repair of bridge decks. In the Netherlands a substantial number of bridges has been built with orthotropic steel decks with an asphalt layer on the top. This type of bridges, however, often shows problems, related to flexural deformations of the deck plate under traffic loads and their effect on the ribs or stiffeners, crossbeams and girders. Due to the increase of both the traffic intensity and the axle loads, which was not foreseen in the initial design, premature fatigue cracks occurred. Repairing the cracks and applying a new asphalt layer can give a solution for a new number of years, but it is not satisfactory, also because of the shutdown time for the traffic necessary for this repair. Another solution that was proposed was the replacement of the asphalt layer by a reinforced high performance concrete overlay, which is bonded to the bridge deck. Tests have been carried out into the effect of concrete overlays, which contained one ore more layers of welded reinforcement (bar diameter 8 mm and bar spacing 50 mm). The concrete contains both steel fibres and acrylic fibres. The average concrete cube strength is 120 Mpa. The concrete contains about 70 kg/m^3 of steel fibres (12 x 0,4mm). The thickness of the overlay is about 50-60 mm. The connection to the steel beams is made by at first applying an epoxy-layer (2 mm) on the steel surface, on which split (4-6 mm) is sprayed in order to obtain an interface layer with sufficient bonding capacity. Fig. 8 shows a steel beam with overlay, subjected to a fatigue test at TNO, the Netherlands [8]. The replacement of the asphalt layer by the high performance fibre concrete results in a substantial reduction of the stresses. Stress amplitudes of 124 Mpa are reduced to only 28 Mpa. This means that the mass of the concrete plays an important role. Of course, the layer thickness could be smaller by increasing the strength of the concrete, but then the stress amplitudes would become proportionally larger as well. Tests have been carried out with regard to the time dependent behaviour of the concrete, the adhesion capacity, the frost-thaw resistance in combination

with de-icing chemicals and on chloride penetration [9]. These tests confirmed the durability of the solution.

Fig. 8.   Fatigue tests on a bridge deck with high performance fibre concrete [8]

4   Ultra high strength: high potential or academic toy?

Ultra high strength concrete offers a combination of favourable properties. The high strength in combination with the high toughness gives already the possibility to design light structures with adequate stiffness. This could lead to more slender cross-sections or to larger spans. However, it should be realised, that a substantial task of engineers in future would be to repair and upgrade structures and to increase the capacity of existing structures. An actual case is the problem of increasing traffic congestion. Meanwhile the Dutch government has decided to extent many of the existing main roads with an additional lane. This means, however, that also existing bridges should be widened. The problem is that those existing bridges have not been designed for future extensions. Therefore the bridges have to be strengthened in order to be able to carry an additional load. In order to keep the increase of the dead weight to the lowest possible value, UHPC is a logic material. Fig. 9 shows a design for the extension of an existing bridge with an additional lane for traffic class 30 [10].
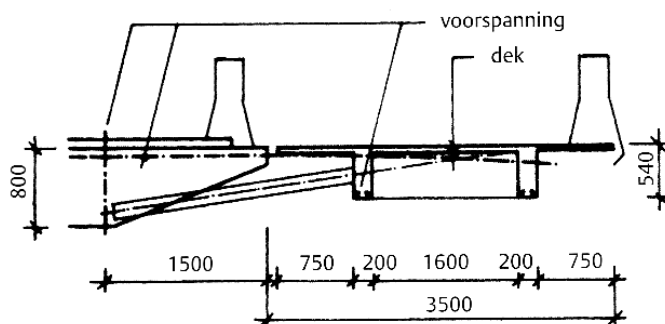
Fig. 9.   Widening of an existing bridge with UHPC [10].

Another example of a potential application concerns the steel doors of the large storm surge barrier "Oosterscheldekering" in the Netherlands, which was built 1980-1986 in order to avoid in future a flood disaster like the one which occurred in 1953. This is a semi-open barrier with 65 lifting doors made of steel, which are closed when a storm tide is announced. The doors have a width of 45 m and a height of about 15 m. Because of the very aggressive marine environment the steel doors have been provided with a coating in order to protect them against corrosion. However, inspection in the early nineties showed that nevertheless substantial corrosion developed. So the coating had to be replaced, which increased the maintenance costs significantly. Two MSc studies [11,12] at TU Delft were devoted to the question whether a door made of UHSC (Strength class B200) would be an alternative (Fig. 10). From the point of view of durability this might be an excellent solution. The design showed that the weight of a door in UHSC is 640 tons, whereas the weight of a steel door is 450 tons. However, an exchange is still possible because the lifting equipment was substantially overdesigned and nowadays new, low friction materials are available, reducing the force on the lifting machines during operation. The cost for fabricating one UHPC door and replacing one steel door is estimated at 3,7 million Euro. The State Department of Infrastructure Rijkswaterstaat has meanwhile further optimised the design and tends to make a pilot with one door, in order to further explore the potential of the material. A final decision has not yet been taken.
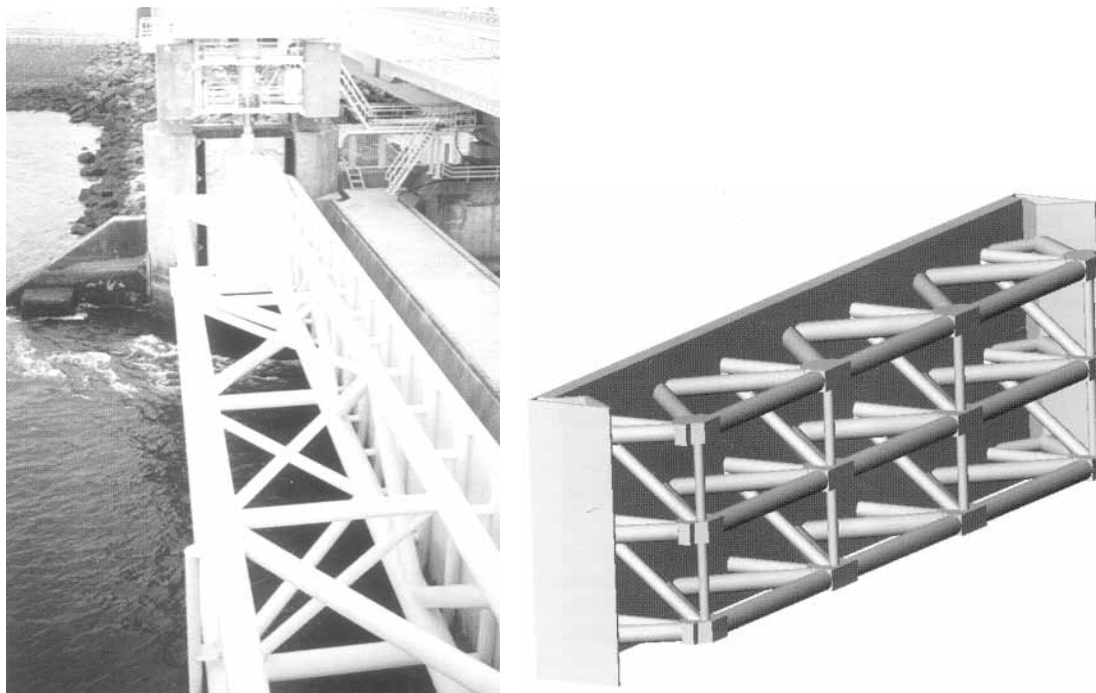
Fig. 10.   Design of a UHPC door for the storm surge barrier
            Oosterschelde in The Netherlands

It is quite sure that the potential of high and ultra high performance concrete for structural applications is considerable. The challenge is to take full profit of its advantages in design, considering not only the high strength, but also the high ductility and the excellent durability. In comparing UHPC with conventional concrete it is essential to make a cost comparison on an integral basis. Although the price of one m^3 of UHPC is considerably larger than that of a conventional concrete it should be realised that much less of this material is needed for a structure, and that this structure may show much lower maintenance costs. This will be a significant criterion in future, because future codes will place design for life cycle on the same level as design for structural safety and serviceability. This is at least one of the main points of attention in the new fib Model Code for Concrete Structures, which is in preparation now.

5   Conclusions

1. UHPC offers large possibilities for application, many of which have not yet been recognised.
2. For showing the competitiveness of UHPC it is necessary to make cost calculations on an integral cost basis, including the cost of the structure and its maintenance costs.
3. The large area between B100 and B200 can offer many interesting possibilities as well.
4. A consistent code should be developed, crossing the bridge between conventional fibre concrete, high and ultra high strength concrete.

6   References

[1] Kooiman, A.J., Walraven, J.C.,"Steel fibre reinforced high performance for the application in shield tunnel linings", Proceedings of the world tunnel congress 98 on tunnels and metropolises, Sao Paulo, April 1998, pp. 721-726.

[2] L. Vandewalle et al. (2000): Recommendation of RILEM TC 162-TDF: Test and design methods for steel fibre reinforced concrete: bending test", Materitals and Structures, 2000, Vol. 33, pp. 3-5 [3]

[3] Vandewalle et al. (2002): "Recommendations of RILEM TC 162-TDF: "Test and design methods for steel fibre reinforced concrete: final recommendations for bending test", Materials and Structures, 2002, Vol. 35, pp. 579-582

[4] Vandewalle, L., "Design with σ-ε method", Proceedings of the RILEM TC 162-TDF Workshop on Testing and Design Methods for Steel Fibre Reinforced Concrete – Background and Experiences, Bochum, 20-21 March 2003, pp. 31-46

[5] Kooiman, A.J., "Modelling Steel Fibre Reinforced Concrete for Structural Design" PhD-Thesis, TU Delft, Oct. 2000.

[6] Petitjean, J., Resplendino, J., French Recommendation for Ultra-High Performance Fiber-Reinforced Concrete", Proceedings of the conference

[7] Lappa, E., van der Veen, C., Walraven, J.C., „Self-compacting high strength steel fiber reinforced mortar for precast sheet piles", Proceedings of the 3rd International RILEM Symposium „Self-compacting concrete", Reykjavic, Aug. 2003, pp. 732-740.

[8] Boersma, P., Kaptijn, N., Nagtegaal, G., „Extension of het life time of orthotropic steel bridge decks", Cement 2004, Nr. 4, pp. 56-61 (in Dutch).

[9]   Braam. C.R., Buitelaar, P., Kaptijn, N., „Reinforced high performance concrete overlay system for steel bridges", "High strength concrete for bridge deck repair", Cement 2003, No. 1, pp. 86-91 (in Dutch)

[10] Blokland, G. van, "Widening of bridges with RPC", MSc-Thesis, TU Delft 1997.

[11] Tol, H., "B200 steel doors for the Storm Surge Barrier Oosterschelde", MSc thesis TU Delft 2000.

[12] Cheung, C.K., "Detailing the B-200 concrete doors for the Storm Surge Barrier Oosterschelde", MSc-thesis, TU Delft, 2002

Subject Index